ΔΕΛΤΙΟ ΤΗΣ ΕΛΛΗΝΙΚΗΣ ΓΕΩΛΟΓΙΚΗΣ ΕΤΑΙΡΙΑΣ
BULLETIN OF THE GEOLOGICAL SOCIETY OF GREECE
ΤΟΜΟΣ
VOLUME
XXXX



11° Διεθνές Συνέδριο της Ελληνικής Γεωλογικής Εταιρίας
11th International Conference of the Geological Society of Greece

Γεωπεριβάλλον
χθες, σήμερα, αύριο

Geoenvironment
past, present, future

ΠΡΑΚΤΙΚΑ
PROCEEDINGS

ΤΕΥΧΟΣ 1	PART 1
ΠΑΛΑΙΟΝΤΟΛΟΓΙΑ	PALAEONTOLOGY
ΣΤΡΩΜΑΤΟΓΡΑΦΙΑ	STATIGRAPHY
ΙΖΗΜΑΤΟΛΟΓΙΑ	SEDIMENTOLOGY
ΤΕΚΤΟΝΙΚΗ	TECTONIC
ΔΥΝΑΜΙΚΗ	DYNAMIC
ΕΦΑΡΜ. ΓΕΩΛΟΓΙΑ	APPLIED GEOLOGY

ΑΘΗΝΑ 24-26 Μαΐου 2007 ATHENS 24-26 May 2007



ΕΘΝΙΚΟ ΚΑΙ ΚΑΠΟΔΙΣΤΡΙΑΚΟ
ΠΑΝΕΠΙΣΤΗΜΙΟ ΑΘΗΝΩΝ
NATIONAL AND KAPODISTRIAN
UNIVERSITY OF ATHENS

1837-2007
170 ΧΡΟΝΙΑ
YEARS

ΕΘΝΙΚΟ ΚΑΙ ΚΑΠΟΔΙΣΤΡΙΑΚΟ
ΠΑΝΕΠΙΣΤΗΜΙΟ ΑΘΗΝΩΝ
NATIONAL AND KAPODISTRIAN
UNIVERSITY OF ATHENS

1837-2007
170 ΧΡΟΝΙΑ YEARS

11° Διεθνές Συνέδριο της Ελληνικής Γεωλογικής Εταιρίας
11th International Conference of the Geological Society of Greece

Γεωπεριβάλλον
χθες, σήμερα, αύριο

Geoenvironment
past, present, future

ΠΡΑΚΤΙΚΑ PROCEEDINGS

ΑΘΗΝΑ 24-26 Μαΐου 2007 **ATHENS 24-26 May 2007**

ΕΛΛΗΝΙΚΗ ΓΕΩΛΟΓΙΚΗ ΕΤΑΙΡΙΑ
GEOLOGICAL SOCIETY OF GREECE

ΟΡΓΑΝΩΤΙΚΗ ΕΠΙΤΡΟΠΗ

Πρόεδρος	Καθηγητής Μιχαήλ Δ. Δερμιτζάκης
Γενική Γραμματέας	Αναπλ. Καθηγήτρια Αλεξάνδρα Ζαμπετάκη-Λέκκα
Ειδικοί Γραμματείς	Επικ. Καθηγήτρια Μαρία Τριανταφύλλου Λέκτορας Ασημίνα Αντωναράκου
Υπεύθυνοι Εκδρομών	Καθηγητής Σπύρος Λέκκας Καθηγητής Μιχαήλ Σταματάκης Δρ. Δημήτριος Γαλανάκης
Υπεύθυνοι Ειδικών Συνεδριών	Καθηγητής Βασίλειος Καρακίτσιος Δρ. Σωκράτης Ρουσιάκης Θεοδώρα Τσουρού
Ταμίες	Αναπλ. Καθηγητής Απόστολος Αλεξόπουλος Ευγενία Μωραΐτη Δρ. Κατερίνα Κούλη
Γραμματεία Εκδόσεων	Επικ. Καθηγήτρια Χαρά Ντρίνια Δρ. Μαργαρίτα Δήμιζα
Υπεύθυνοι Παρουσιάσεων poster	Αν. Καθηγητής Πάρις Παυλάκης Δρ. Χρυσάνθη Ιωακείμ Λέκτορας Ευτέρπη Κοσκερίδου
Υπεύθυνοι Εκθέσεων	Επικ. Καθηγητής Νικόλαος Βούλγαρης Δρ. Νικόλαος Τσαπάρας Γεώργιος Λύρας
Υπεύθυνοι Ιστοσελίδας	Επικ. Καθηγητής Νικόλαος Βούλγαρης Χαράλαμπος Βασιλάτος

ORGANIZING COMMITTEE

President	Professor Michael D. Dermitzakis
General Secretary	Assoc. Professor Alexandra Zambetakis-Lekkas
Executive Secretariat	Assist. Professor Maria V. Triantaphyllou Lecturer Assimina Antonarakou
Field Trip Committee	Professor Spyros Lekkas Professor Michael Stamatakis Dr. Dimitrios Galanakis
Workshop Committee	Professor Vassilios Karakitsios Dr. Sokratis Roussiakis Theodora Tsourou
Treasurers	Assoc. Professor Apostolos Alexopoulos Eugenia Moraiti Dr. Katerina Kouli
Publishing Secretariat	Assist. Professor Hara Drinia Dr. Margarita Dimiza
Poster Secretariat	Assoc. Professor Paris Pavlakis Dr. Chrysanthi Ioakim Lecturer Efterpi Koskeridou
Exhibition Secretariat	Assist. Professor Nikolaos Voulgaris Dr. Nikolaos Tsaparas George Lyras
Web Site	Assist. Professor Nikolaos Voulgaris Charalambos Vassilatos

ΔΙΟΙΚΗΤΙΚΟ ΣΥΜΒΟΥΛΙΟ ΤΗΣ ΕΛΛΗΝΙΚΗΣ ΓΕΩΛΟΓΙΚΗΣ ΕΤΑΙΡΙΑΣ

Πρόεδρος	ΜΑΡΙΝΟΣ Παύλος	*Καθηγητής Εθνικού Μετσοβίου Πολυτεχνείου*
Αντιπρόεδρος	ΠΑΥΛΙΔΗΣ Σπύρος	*Καθηγητής Αριστοτελείου Πανεπιστημίου Θεσσαλονίκης*
Γεν. Γραμματέας	ΑΛΕΞΟΠΟΥΛΟΣ Απόστολος	*Αν. Καθηγητής Εθνικού και Καποδιστριακού Πανεπιστημίου Αθηνών*
Ταμίας	ΜΩΡΑΪΤΗ Ευγενία	*Γεωλόγος Ι.Γ.Μ.Ε.*
Ειδ. Γραμματέας	ΓΑΛΑΝΑΚΗΣ Δημήτρης	*Δρ. Γεωλόγος Ι.Γ.Μ.Ε*
Έφορος	ΦΟΥΝΤΟΥΛΗΣ Ιωάννης	*Επικ. Καθηγητής Εθνικού και Καποδιστριακού Πανεπιστημίου Αθηνών*
Μέλος	ΓΕΩΡΓΙΟΥ Χαρ/μπος	*Γεωλόγος Ι.Γ.Μ.Ε*
Μέλος	ΙΩΑΚΕΙΜ Χρυσάνθη	*Δρ. Γεωλόγος Ι.Γ.Μ.Ε*
Μέλος	ΠΑΠΑΒΑΣΙΛΕΙΟΥ Κων/νος	*Αν. Καθηγητής Εθνικού και Καποδιστριακού Πανεπιστημίου Αθηνών*
Μέλος	ΚΙΛΙΑΣ Διαμαντής	*Καθηγητής Αριστοτελείου Πανεπιστημίου Θεσσαλονίκης*

COUNCIL OF THE GEOLOGICAL SOCIETY OF GREECE

President	MARINOS Paul	*Professor, National Technical University of Athens*
Vice-President	PAVLIDES Spyros	*Professor, Aristotle Uvinersity of Thessaloniki*
Secretary General	ALEXOPOULOS Apostolos	*Assoc. Professor, National and Kapodistrian University of Athens*
Treasurer	MORAITI Eugenia	*Geologist, I.G.M.E.*
Ex. Secretary	GALANAKIS Dimitris	*Dr. Geologist, I.G.M.E.*
Trustee	FOUNTOULIS Ioannis	*Assist. Professor, National and Kapodistrian University of Athens*
Member	GEORGIOU Charalambos	*Geologist, I.G.M.E.*
Member	IOAKIM Chrysanthi	*Dr. Geologist, I.G.M.E.*
Member	PAPAVASSILIOU Konstantinos	*Assoc. Professor, National and Kapodistrian University of Athens*
Member	KILIAS Adamantios	*Professor, Aristotle Uvinersity of Thessaloniki*

ΠΡΟΛΟΓΟΣ

Η Γη αποτελεί ένα σύνθετο και δυναμικό σύστημα, του οποίου η γνώση και η κατανόηση μπορεί να συμβάλει όχι απλώς στην αναβάθμιση της ποιότητας της ζωής μας αλλά ακόμη και στην πρόβλεψη του μέλλοντος του πλανήτη μας. Η μελέτη της ιστορικής εξελίξεως του γήινου συστήματος εμπίπτει στο γνωστικό αντικείμενο της Γεωλογίας και την διακρίνει από τις άλλες Φυσικές Επιστήμες. Παράλληλα όμως, η ίδια η γεωλογική έρευνα απαιτεί τη συνεργασία όλων των Φυσικών Επιστημών για την αρτιότερη εξαγωγή συμπερασμάτων, γεγονός που καθιστά τελικά τη Γεωλογία ένα ιδιαίτερα διαδραστικό τομέα, που μπορεί και πρέπει να παράγει έρευνα αιχμής σε θεωρητικό αλλά και εφαρμοσμένο επίπεδο. Η Γεωλογία, όπως και κάθε επιστήμη, έχει τους δικούς της στόχους και τα δικά της μεθοδολογικά εργαλεία, τα οποία, ωστόσο, διευρύνονται σήμερα, μέσω της διεπιστημονικής προσεγγίσεως που κερδίζει όλο και περισσότερο έδαφος στις σύγχρονες τάσεις της έρευνας, σε διεθνές επίπεδο.

Ο Γεωλόγος-Γεωεπιστήμονας ερευνά τη Γη, τους ωκεανούς, την ατμόσφαιρα. Ανησυχεί και προβληματίζεται για τη Γη και το μέλλον της. Καλείται σήμερα, πέρα από τη διερεύνηση των κλασσικών γεωλογικών διεργασιών, να δώσει πειστικές απαντήσεις σε ερωτήματα που απασχολούν πολύ σοβαρά την ανθρωπότητα. Γιατί και πώς αλλάζει το παγκόσμιο κλίμα; Πώς λειτουργούν και αλληλεπιδρούν τα γήινα συστήματα; Πώς πρέπει να διαθέτουμε τα βιομηχανικά μας απόβλητα; Πώς θα πρέπει να αντιμετωπισθούν οι ενεργειακές ανάγκες της ολοένα και πιο απαιτητικής σύγχρονης κοινωνίας; Πώς θα ικανοποιηθούν οι ανάγκες για νερό και τροφή;

Ο Γεωλόγος του 21^{ου} αιώνα διαθέτει όλη την ιστορική γεωλογική γνώση που έχουν αποκομίσει οι προηγούμενες γενιές αλλά και ένα πλήθος ερευνητικών και επαγγελματικών επιλογών. Μπορεί να:

- ψάχνει για ζωή στον Άρη και άλλους πλανήτες
- εξερευνά τον ωκεάνιο πυθμένα
- παρακολουθεί τη δραστηριότητα των μεγάλων ηφαιστείων
- κάνει μουσειακή έρευνα
- συμμετέχει στο χωροταξικό-πολεοδομικό σχεδιασμό
- μελετά τρόπους περιβαλλοντικής απορρυπάνσεως και να διαμορφώνει τη λήψη αποφάσεων για τη διαχείριση του γεωπεριβάλλοντος
- μελετά και συμβάλλει στη μείωση του βαθμού επικινδυνότητας για την ανθρώπινη ζωή και περιουσία από φυσικές καταστροφές
- κατανοεί και εξηγεί γιατί αλλάζει το κλίμα
- παρέχει γεωλογική γνώση σε μικρά και μεγάλα τεχνικά έργα
- εξερευνά τους πιθανούς φυσικούς πόρους και να τους διαχειρίζεται με περιβαλλοντικά ασφαλείς τρόπους
- εξασφαλίζει ποιοτικούς υδάτινους πόρους
- διασφαλίζει την εδαφική ποιότητα για τη γεωργική παραγωγή

Ωστόσο, παρά το γεγονός ότι ο γεωλόγος αποκτά όλο και πιο υπεύθυνη θέση στην κοινωνία, τα στοιχεία δείχνουν ότι η ανεργία και η υποαπασχόληση συνιστούν πλέον βασικά γνωρίσματα του συγκεκριμένου κλάδου, τόσο στον ιδιωτικό όσο και στον δημόσιο τομέα, και αυτό δεν είναι ένα αποκλειστικά ελληνικό φαινόμενο. Ήδη οι επιπτώσεις τους έχουν επηρεάσει το διεθνή χώρο την τελευταία δεκαπενταετία. Πολλά πανεπιστημιακά Γεωλογικά Τμήματα σε Ευρώπη και Αμερική έχουν περιορίσει τις δραστηριότητές τους ή

έχουν υποστεί διοικητικές μεταβολές. Αρκετά έχουν αλλάξει τον τίτλο τους στην προσπάθεια να προσεγγίσουν με επιτυχία τις σύγχρονες τάσεις.

Στην Ελλάδα λειτουργούν σήμερα τρία γεωλογικά Τμήματα, στα Πανεπιστήμια Αθηνών, Θεσσαλονίκης και Πατρών, με υψηλό επίπεδο προπτυχιακών και μεταπτυχιακών σπουδών, από τα οποία αποφοιτούν κάθε χρόνο περίπου 300 γεωλόγοι.

Για να φτάσει η διδασκαλία των Γεωγνωστικών μαθημάτων στο σημερινό της επίπεδο έχει διανύσει μία μακρά πορεία σε βάθος χρόνου, τις απαρχές της οποίας θα πρέπει να αναζητήσουμε στην πρώτη φάση λειτουργίας των Πανεπιστημίων Αθηνών, Θεσσαλονίκης και Πατρών.

Συγκεκριμένα, στον Οργανισμό λειτουργίας του **Εθνικού και Καποδιστριακού Πανεπιστημίου Αθηνών** του 1839, μεταξύ των άλλων μόνιμων τακτικών εδρών οριζόταν και η έδρα της Φυσικής Ιστορίας με γνωστικά αντικείμενα Ζωολογία, Ορυκτολογία, Γεωλογία και Βοτανική. Επίσης, με διάταγμα του ιδίου έτους, τα μαθήματα της Ορυκτολογίας και της Γεωλογίας χαρακτηρίζονταν υποχρεωτικά μαθήματα.

Το 1932 ιδρύθηκε το πέμπτο κατά σειρά Τμήμα της Φυσικομαθηματικής Σχολής, το Φυσιογνωστικό το οποίο έδιδε πλέον πτυχίο Φυσιογνωσίας και Γεωγραφίας, συνδυάζοντας τις κατευθύνσεις των Βιολογικών και Γεωλογικών επιστημών.

Το 1970 το Τμήμα Φυσιογνωσίας και Γεωγραφίας διαχωρίστηκε στα αυτοτελή Τμήματα Βιολογίας και Γεωλογίας, με απονομές αντίστοιχων πτυχίων.

Το 2004 το Τμήμα Γεωλογίας μετονομάστηκε σε Τμήμα Γεωλογίας και Γεωπεριβάλλοντος καλύπτοντας με αυτόν τον τρόπο και όλα εκείνα τα αντικείμενα των Γεωεπιστημών που σχετίζονται με το Περιβάλλον.

Στο **Αριστοτέλειο Πανεπιστήμιο Θεσσαλονίκης** ιδρύθηκαν ήδη από το 1926 τα Εργαστήρια Γεωλογίας, Πετρολογίας και Ορυκτολογίας και Μετεωρολογίας και Κλιματολογίας, τα οποία άρχισαν τη λειτουργία τους το ακαδημαϊκό έτος 1928-1929, στο πλαίσιο της Σχολής των Φυσικών και Μαθηματικών Επιστημών.

Το 1943 άρχισε η λειτουργία του Φυσιογνωστικού Τμήματος, του οποίου τα βασικά αντικείμενα ήταν οι γεωλογικές και οι βιολογικές επιστήμες. Το τμήμα αναπτύχθηκε τα επόμενα τριάντα χρόνια μέχρι το 1973, οπότε διασπάστηκε και δημιουργήθηκαν τα Τμήματα Γεωλογίας και Βιολογίας.

Το Τμήμα Γεωλογίας του **Πανεπιστημίου Πατρών**, το νεώτερο από τα τρία Γεωλογικά Τμήματα της χώρας, ιδρύθηκε το 1977 στη Σχολή Θετικών Επιστημών (τότε Φυσικομαθηματική Σχολή) του Πανεπιστημίου Πατρών και λειτούργησε από το 1978.

Ωστόσο, οφείλουμε να ομολογήσουμε ότι η ανάπτυξη των Γεωεπιστημών δεν είναι αποκλειστικά πανεπιστημιακή υπόθεση. Αφορά το σύνολο της γεωλογικής επιστημονικής κοινότητας σε τοπικό αλλά και διεθνές επίπεδο.

Είναι απαραίτητο να δημιουργήσουμε μια προσεκτικά τεκμηριωμένη, ευρέως υποστηριζόμενη και αυστηρά πιστοποιημένη καταγραφή και μια αντίστοιχη βάση δεδομένων σε εθνικό αλλά και διεθνές επίπεδο, με έμφαση στους τομείς όπου η Γεωλογία μπορεί να συνεισφέρει στη σύγχρονη κοινωνία.

Η προοδευτική πορεία της επιστήμης της Γεωλογίας είχε πάντα άμεση σχέση με την υλική ανάπτυξη της κοινωνίας αλλά και με τη διανοητική εξέλιξη που ήταν αναγκαία ώστε να αποκτήσουν οι άνθρωποι περιβαλλοντική συνείδηση. Η Γεωλογία έχει ήδη αποτελέσει αναπόσπαστο μέρος της βιομηχανικής επαναστάσεως, ενώ κατόπιν, η ραγδαία τεχνολογική εξέλιξη συντέλεσε ώστε ο άνθρωπος να δρα ως ένας «γεωλογικός» παράγοντας που υπεισέρχεται στο ρυθμό της φύσεως και η συμμετοχή του καθίσταται

καθημερινά εντονότερη, με επιπτώσεις είτε θετικές, είτε αρνητικές για τον ίδιο και το φυσικό του περιβάλλον.

Η πιστοποιημένη καταγραφή των τομέων της σύγχρονης Γεωλογικής δραστηριότητας, όπως η μελέτη του Γεωπεριβάλλοντος και η ανάπτυξη των Βιογεωεπιστημών, θα συμβάλει στη διείσδυση της εφαρμοσμένης Γεωλογικής επιστήμης στον κοινωνικό ιστό και στην κατανόηση και αποδοχή των δυνατοτήτων που αυτή προσφέρει στην ελληνική και παγκόσμια κοινωνία.

Για να είναι ο πτυχιούχος γεωλόγος έτοιμος να αντιμετωπίσει τις προκλήσεις της σύγχρονης κοινωνίας απαιτούνται εκσυγχρονισμένες και υψηλού επιπέδου σπουδές, γι' αυτό και είναι απαραίτητο η πολιτεία να στηρίζει τα γεωλογικά τμήματα, όσον αφορά την αναβάθμιση του διδακτικού ερευνητικού προσωπικού αλλά και της υλικοτεχνικής υποδομής.

Η συνεχής μέριμνα για την προώθηση της έρευνας και η δημιουργική αγωνία για το φωτισμό μιας ακόμη πτυχής της αλήθειας είναι το κίνητρο που βρίσκεται πίσω από κάθε επιστημονική προσπάθεια και ακριβώς αυτή η πλευρά τονίζεται στο πλαίσιο του παρόντος 11ου Διεθνούς Συνεδρίου της Ελληνικής Γεωλογικής Εταιρείας, το οποίο εντάσσεται «τύχη αγαθή» στον εορτασμό των 170 χρόνων από την ίδρυση του Εθνικού και Καποδιστριακού Πανεπιστημίου Αθηνών.

Η Γεωλογία και τα σημεία στα οποία η γεωλογική έρευνα «τέμνεται» με τα ενδιαφέροντα άλλων επιστημονικών πεδίων οριοθετεί τις εργασίες που παρουσιάζονται εδώ και έχουν ως βασικό κίνητρο την ατέρμονα πορεία του επιστήμονα προς την έρευνα και την αλήθεια, σε συνάρτηση με την προσέγγιση των πορισμάτων της γεωλογικής επιστήμης προς το ευρύτερο κοινό.

Στο 11^{ο} Διεθνές Γεωλογικό Συνέδριο «Γεωπεριβάλλον: Χθες – Σήμερα – Αύριο» της Ελληνικής Γεωλογικής Εταιρίας, το οποίο οργανώνεται από το Τμήμα Γεωλογίας και Γεωπεριβάλλοντος του Εθνικού και Καποδιστριακού Πανεπιστημίου Αθηνών και πραγματοποιείται στα κτήρια του Τμήματος Γεωλογίας και Γεωπεριβάλλοντος, από τις 24 έως και τις 26 Μαΐου 2007 έχουν δηλώσει συμμετοχή πολλοί διακεκριμένοι επιστήμονες από την Ελλάδα και το εξωτερικό καθώς και νέοι επιστήμονες και ερευνητές, οι οποίοι έχουν την ευκαιρία να παρουσιάσουν τις μελέτες τους πάνω σε θέματα αιχμής που σχετίζονται με το Γεωπεριβάλλον. Συμμετέχουν περισσότεροι από 500 σύνεδροι, 250 αξιολογητές, 500 συγγραφείς με 151 προφορικές και 41 αναρτημένες παρουσιάσεις από 22 χώρες. Τα Πρακτικά που παραδόθηκαν σήμερα αποτελούνται από 4 τόμους των 2.500 σελίδων συνολικά.

Οι εργασίες του Συνεδρίου χαρακτηρίζονται από ποιότητα και πρωτοτυπία και καλύπτουν όλα τα αντικείμενα των γεωεπιστημών. Επίσης στο πλαίσιο του συνεδρίου οργανώνονται εννέα «Στρογγυλές τράπεζες» *(Οικονομική Γεωλογία-Γεωχημείας, Τεχνική Γεωλογία, Διδακτική των Γεωεπιστημών, Γεωμορφολογία & Περιβάλλον, Διατήρηση Γεωλογικής-Γεωμορφολογικής Κληρονομιάς, Υδρογεωλογία, Παλαιοντολογία-Στρωματογραφία, Τεκτονική, Νανογεωεπιστήμες,)* όπου παρέχεται η δυνατότητα για συζήτηση και προβληματισμό σε ενδιαφέροντα αντικείμενα των Γεωεπιστημών.

Επίσημες γλώσσες του συνεδρίου είναι η ελληνική και αγγλική, ενώ οι εργασίες δημοσιεύονται στην αγγλική γλώσσα με εκτεταμένη περίληψη στα ελληνικά, προσδίδοντας στην Ελληνική Γεωλογική κοινότητα τη δυνατότητα οργανωμένης και άμεσης πρόσβασης στο διεθνές «γεωλογικό γίγνεσθαι».

Σκοπός του συνεδρίου είναι η παρουσίαση και ανάπτυξη ζητημάτων που έχουν σχέση με τα σύγχρονα γεωπεριβαλλοντικά προβλήματα και ειδικότερα με τη βελτίωση και διαχείριση της γνώσης του παρελθόντος, την καταγραφή και μελέτη των διεργασιών που

επιδρούν στο Γεωπεριβάλλον καθώς και τις προοπτικές της βασικής και εφαρμοσμένης έρευνας στον τομέα των Γεωεπιστημών.

Οποιαδήποτε όμως πρόοδος και αν πραγματοποιείται πρέπει να βρίσκεται πάντοτε εντός του πλαισίου της διατήρησεως του φυσικού περιβάλλοντος και γενικότερα προστασία της φύσεως. Το πλαίσιο αυτό είναι ο ζωτικός χώρος επιβιώσεως του κοινωνικού ανθρώπου της εποχής μας. Το αντικειμενικά τεράστιο ενδιαφέρον που παρουσιάζει η γεωλογία καθώς και η διαρκώς εντεινόμενη προσπάθεια για ανεύρεση πρώτων υλών, κατέστησαν τη γεωλογία πεδίο καίριας σημασίας για την ανθρωπότητα. Δεν πρέπει όμως να λησμονούμε αυτό που αναφέρει ο Πίνδαρος «Αλλά κέρδει και σοφία δέδεται».

Θεωρούμε υποχρέωσή μας να ευχαριστήσουμε όλους τους συντελεστές της διοργανώσεως αυτού του συνεδρίου. Τα μέλη της οργανωτικής επιτροπής, τους αξιολογητές, τους φοιτητές και τους χορηγούς.

Ιδιαίτερα οφείλουμε να ευχαριστήσουμε τις Πρυτανικές Αρχές του Πανεπιστημίου Αθηνών, και ιδιαίτερα τον αρμόδιο Αντιπρύτανη καθηγητή κ. Ιωάννη Καράκωστα, που ενέταξαν τις εργασίες του 11^{ου} Διεθνούς Γεωλογικού Συνεδρίου της Ελληνικής Γεωλογικής Εταιρίας στο πλαίσιο του επίσημου εορτασμού των 170 χρόνων από την ίδρυσή του.

Το Πανεπιστήμιο Αθηνών, με αναφορές στο ιστορικό του παρελθόν, αντιμετωπίζει με αίσθημα ευθύνης το παρόν και ατενίζει με αισιοδοξία το μέλλον. Ένα μέλλον άρρηκτα συνδεδεμένο με το μέλλον του πλανήτη. Η ακαδημαϊκή οικογένεια δεν μπορεί και δεν θέλει να μείνει ουδέτερη ή αδιάφορη μπροστά στην αγωνία της ανθρωπότητας για την προστασία του βιοτικού της χώρου.

Το 11^{ο} Διεθνές Γεωλογικό συνέδριο *«Γεωπεριβάλλον: χθές-σήμερα- αύριο»* δίνει το στίγμα της ελληνικής γεωεπιστημονικής πραγματικότητας και των διεθνών της προεκτάσεων μέσα από το θεσμό του Εθνικού και Καποδιστριακού Πανεπιστημίου Αθηνών που συμπληρώνει πλέον εκατόν εβδομήντα χρόνια γόνιμης λειτουργίας και αδιάλειπτης προσφοράς.

Ο Πρόεδρος της Οργανωτικής Επιτροπής

Μιχαήλ Δ. Δερμιτζάκης
Καθηγητής Γεωλογίας & Παλαιοντολογίας
τ. Αντιπρύτανης Πανεπιστημίου Αθηνών

PREFACE

The Earth constitutes a compound and dynamic system, and better and broader knowledge of our planet and the processes that are in progress on it might enable us to better understand our past as well as foresee our future. The research of historic development of the Earth system as a total deep in time distinguishes Geology from any other Natural sciences. However, this research as such requires the inter-relation of all Natural sciences for its comprehension, thus rendering Geology a particularly interactive sector that can and should produce top research at theoretical as well as at applied level. Finally, Geology, just as every other science, has its own objectives and its own methodological tools, which, though, are being currently broadened through inter-scientific approaches – a process that is constantly gaining ground at the international level among the modern research tendencies.

A geologist-geoscientist researches the Earth, the oceans, the atmosphere, but also conducts research beyond that level. He is concerned about the Earth and its future. He/She is currently summoned, apart from the classic geological activities, to provide persuasive answers to the questions that puzzle all the human beings. Why and how does the world climate change? How do the Earth systems function and inter-relate? How should we allocate our industrial waste? How are we supposed to face the energy needs of all the more demanding modern society? How should we cover the needs for water and food?

A geologist of the 21st century accumulates all the historic geological knowledge that has been acquired by the previous generations but also a big selection of research and professional options. He/she is able to:

- Look for life existence on Mars and other planets
- Research the ocean bottom
- Monitor the activities of big volcanoes
- Conduct museum research
- Participate in land and urban planning
- Study ways of environmental pollution control and shape the decision-making for the Earth environment management
- Research and contribute to the reduction of degree of risk for the human life and fortune from natural disasters
- Comprehend and explain why the climate changes
- Provide geological knowledge for the benefit of small and large scale technical projects
- Research the potential natural resources and manage them in environmentally safe way
- Ensure qualitative aquatic resources
- Ensure the surface quality for the needs of agricultural production

However, although a geologist acquires more and more responsible position in the society, the evidence shows that unemployment and underemployment henceforth constitute the basic traits of the particular sector so much in the private as in the public sector, which is not an exclusively Greek phenomenon. Its repercussions have already influenced the international domain for the last 10 years. A lot of academic Geological Departments in Europe and America have limited their activities or have suffered

administrative changes. A considerable number of them have changed their title in an attempt to successfully approach modern tendencies.

In Greece, the three geological departments that function at the Universities of Athens, Thessaloniki and Patras at the high level of modern under and postgraduate study, annually provide roughly 300 graduates with specialised high level training, who are ready to offer the Greek society the best possible services in the domain of Geosciences.

In order to reach its current level, the teaching of Geosciences has followed a long course of time development, the principles that we should seek in the first phase of operation of the Universities of Athens, Thessaloniki and Patras.

In particular, in 1839, in the operation Organization of **National and Kapodistrian University of Athens**, among the other permanently operating departments, there was created a department of Natural History aimed at the scientific subjects of Zoology, Mineralogy, Geology and Botanic. Furthermore, as a mandatory subjects, in compliance with the same year issued decree, there were defined the subjects of Mineralogy and Geology.

In 1932, in accordance with the law requirements, there are founded the fifth department of the School of Physics and Mathematics and the Natural History Department and thus the Faculty grants, among the others, the degree in Natural History and Geography, combining the streams of Biological and Geological sciences.

In 1970, the Department of Natural History and Geography is divided into independent departments of Biology and Geology, granting the corresponding degrees.

In 2004, the Department of Geology is renamed into the Department of Geology and Geoenvironment covering all the subjects of Geosciences related to the Environment.

In 1926, following the foundation of **Aristotelian University of Thessaloniki,** there were founded the Laboratories of Geology, Petrology and Mineralogy and Meteorology that started operating in the academic year of 1928-1929, in the framework of the former School of Physics and Mathematics.

In 1943, there started the operation of Natural History Department, basically aimed at studies in the domain of Geological and Biological Sciences. In the duration of the following 30 years, the Department was further developed as until 1973, when it was split into the Departments of Geology and Biology.

The Department of Geology of the **University of Patras**, the newest one out of the three Departments of Geology of the country, was founded in 1977 in the School of Sciences (the former School of Physics and Mathematics) of the University of Patras and started operating in 1978.

One thing is certain. The rescue of Geological Science is not an exclusively academic matter. It concerns the total of Geological Scientific community at both - local and international level.

What can and what should we do?

It is essential to create a carefully documented, widely supported and certified recording and a corresponding data at both – national and international level - of the sectors where Geology can contribute to the modern society.

The progressive course of Geological science has always had direct relation as much to the material development of the society, as to the mental development that was necessary so that the people should develop effective relations with their environment.

Geology already constitutes an integral part of industrial revolution. Afterwards, the human being acted and is still acting as a geological factor that enters into the rhythm of nature and his/her participation is rendered more and more intense day by day, with either positive or negative repercussions for himself and his natural environment.

The certified recording of the sectors of modern Geological activity, just as the study of Geoenvironment and the development of Biogeosciences, is going to contribute to the penetration of applied Geological science into the social structure and the comprehension and acceptance of possibilities offered to the modern humanity and in particular, to the Greek society.

So that a graduate geologist should be ready to face the challenges of the modern society, he/she is required to have conducted modern and high level studies, thus it is essential that the state should permanently support the geological departments so much with regard to the upgrading of the educational and research personnel as to the upgrading of the material and technical infrastructure.

The on-going concern for the promotion of research and this creative anxiety for the enlightening of one more aspect of truth constitute the motive that is found behind each scientific effort and it is precisely this aspect that is outlined in the framework of the present 11th International Conference of the Geological Society of Greece which is fortunately included in the celebration of the 170 anniversary of the foundation of National and Kapodistrian University of Athens.

Geology and the points at which the geological research "intersects" with the subjects of other scientific domains define the projects presented here that are mainly motivated by the interminable course of science aimed at research and truth, in tandem with the approach of the geological science conclusions concerning the broader public.

The 11th International Geological Conference "Geoenvironment: past-present-tomorrow" of the Geological Society of Greece that is organized by the Faculty of Geology and Geoenvironment of National and Kapodistrian University of Athens and which takes place at the premises of the Faculty of Geology and Geoenvironment from 24th to 26th May, 2007 has attracted the participation of a lot of distinguished scientists from Greece and overseas as well as the young scientists and researchers who have the opportunity to present their studies on the top subjects related to Geoenvironment. There participate more than 500 congress members, 250 reviewers, 500 authors making 151 oral and 41 poster presentations from 22 countries.

The work of the congress is characterized by quality and originality and covers all the subjects of Geosciences. Also, in the framework of the congress, there are organised nine "Round Tables" (*Economic Geology-geochemistry, Technical Geology, Didactics of Geosciences, Geomorphology and Environment, Geological-geomorphological Heritage, Hydrogeology, Paleontology-stratigraphy, Tectonics, Nanogeoesciences,)* that provide the possibility for discussion and insight into the interesting subjects of Geosciences.

The official languages of the congress are Greek and English, while the presentations are published in the English language with extensive summary in the Greek language, providing the Greek Geological community with the possibility of organised and direct access to international geological "sphere of activities".

The aim of the Conference is the presentation and development of the subjects that are related to the modern Geoenvironmental problems and, in particular, to the improvement and management of knowledge of the past, the recording and study of the activities that affect Geoenvironment as well as the prospects of the basic and applied research in the domain of Geosciences.

However, any progress that has been achieved, should be always found within the frame of maintenance of natural environment and, more generally, the nature. This frame is the vital space of survival of the social human being of our era. The objectively enormous interest that geology presents and the constantly intensified effort aimed at the discovery of raw materials have rendered Geology the domain of vital importance to the mankind. We should not, though, forget what Pindar mentioned: "Even wisdom has to yield to self-interest".

We regard it as our obligation to thank all those who participated in the organisation of this Conference. The members of the organisational committee, the reviewers, the students and the sponsors.

In particularly, we would like to thank the National and Kapodistrian University of Athens and especially the Vice-Rector professor Ioannis Karakostas who included the works of the 11th International Geological Conference of the Geological Society of Greece in the frame of the official celebration of its 170 foundation anniversary.

The University of Athens with references to its historic past, faces the present with the feeling of responsibility and looks into the future with optimism. And that is the future that is indissolubly connected with the future of our planet. The academic family cannot and does not want to remain neutral or indifferent in front of the anxiety of the mankind for the protection of its biotic space.

The 11th International Geological Conference "Geoenvironment: past-present-future" reflects the Greek Geoscientific reality and its international extensions through the institution of National and Kapodistrian University of Athens that henceforth concludes a hundred and seventy years of productive operation and sustainable offer.

The President of the Organizing Committee

Michael D. Dermitzakis
Professor of Geology & Paleontology
f. Vice-Rector of the University of Athens

ΚΡΙΤΕΣ/REVIEWERS

AGARWAL, V., Ocean Sciences Division, Space Applications Centre, Ahmedabad, India

AKBULUT, H., Afyon Kocatepe University, TEF

ALLISON, R. J., University of Sussex

AL-ORAIMI, S., Sultan Qaboos University, Sultanate of Oman

ALTHERR, R., University of Heidelberg, Germany

ANASTASAKIS, G., National and Kapodistrian University of Athens, Greece

ARIKAS, K., Universitat Hamburg, Germany

BABA, A., Canakkale Onsekiz Mart University, Canakkale/Turkey

BAISE, L., Tufts University, Medford

BALITSKY, V.S., Russian Academy of Sciences, Moscow, Russia

BALTATZIS, E., National and Kapodistrian University of Athens, Greece

BANERJEE, R., National Institute of Oceanography, Goa, India

BARBA, S., Istituto Nazionale di Geofisica e Vulcanologia, Roma, Italy

BARROCU, G., University of Cagliari, Italy

BARTOLINI, C., Universita di Firenze, Italy

BAUM, R. L., U.S. Geological Survey, Denver,

BAYRAM, A., Dokuz Eylül Üniversitesi, Turkey

BEESON, R.C. Jr., University of Florida, USA

BELLATRECCIA, F., Università degli Studi Roma Tre, Roma, Italy

BENAVENTE GONZALEZ, J., Universidad de Cadiz. Poligono Rio San Pedro

BERGER, J., Isotope Geology-Africamuseum, Tervuren, Belgium

BERSEZIO, R., Università di Milano, Italy

BITNER, M.- A., Polish Academy of Sciences, Warszawa, Poland

BODENAN, F., Environment & Process Division, Orléans cedex 2, France

BORGES, J.- F., Universidade de Évora, Portugal

BOUCOT, A., Oregon State University, Oregon

BOYCE, J., University of Hawaii, Honolulu, Hawaii

BOZKURT, E., Middle East Technical University, Ankara, Turkey

BRADY, P.V., Sandia National Laboratories, Albuquerque, New Mexico

BRAUNMILLER, J., Swiss Seismological Service, Zurich, Switzerland

BRIDEAU, M.-A., Simon Fraser University, Canada

BROSKA, I., Geological Institute SAS, Bratislava, Slovak Republic

BRUNETTI, B.G., Universita' di Perugia, Italy

BURCHFIEL, B. C., Massachusetts Institute of Technology (MIT), USA

CALABRIA, C.R., GeoSystems Consultants, Inc., Fort Washington

CALCATERRA, D., Federico II University of Naples, Italy

CALONGE, A., Universidad de Alcalá, Madrid, Spain

CAPO, S., Université Bordeaux 1, France

CAPUTO, R., University of Ferrara,Ferrara, Italy

CARMINATI, E., Universita' degli Studi di Roma "La Sapienza", Roma Italia

CASAS, A., University of Barcelona

CASTELLI, D., Università degli Studi di Torino, Italy

CASTRO, S., Universidad de Concepción, Chile

CAVINATO, G.-P., Universita di Roma "La Sapienza", Rome, Italy

CHAPMAN, R., The University of Leeds, UK

CHIU, J.-M., University of Memphis, Memephis, USA

CHOPIN, E., University of Reims Champagne-Ardenne, Reims – France

CLARK, I., University of Ottawa, Canada

COLELLA, C., Università di Napoli "Federico II", Italy

DEBNATHM, N.-C., Univerisity of Mumbai, India

DENIS, A., Université Bordeaux I, France

DI STEFANO, A., Universita' di Catania, Italy

DIEDERICHS, M., Queen's University, Kingston, Ontario

DIETRICH, V. J., Eidgenössische Technische Hochschule (ETH), Zurich, Switzerland

DILL, H., Federal Institute for Geosciences and Natural Resources, Hannover, Germany

DOHRMANN, R., Rheinisch-Westfälische Technische Hochschule Aachen, Germany

DONER, H., University of California, USA

DRAHOR, M.G., Dokuz Eylül University, Buca-Izmir, Turkey

EBEL, J., Boston College, USA

EINSTEIN, H.H., Massachusetts Institute of Technology (MIT), USA

ENEOGWE, C.I., ExxonMobil Mobil Producing Nigeria, Geochemistry Laboratory

FAIRHEAD, J.D., University of Leeds, UK

FEATHERSTONE, W., Curtin University of Technology, Perth, Australia

FERNANDEZ-TURIEL, J.L., Institute of Earth Sciences J. Almera - CSIC, Barcelona

FIDELIBUS, D., Politecnico di Bari, Italy

FILIPPI, A., College of Geosciences, Texas A&M University, USA

FISHER, J., University of Plymouth, Denver, UK

FOUNTOULIS, I., National and Kapodistrian University of Athens, Greece

FRANCISKOVIC-BILINSKI, S., Rudjer Boskovic Institute, Zagreb, Croatie

FREY, M.-L. , World Heritage Site Messel Pit, Messel, Deutschland

FROGLEY, M.R., University of Sussex, UK

GANERØD, G., Geological Survey of Norway

GARFUNKEL, Z., Hebrew University of Jesusalem

GAUTIER, P., Equipe Lithosphere, Geosciences Rennes, France

GENTILI, S., Istituto Nazionale di Oceanografia e di Geofisica Sperimentale - Udine, Italy

GEORGE, S., Macquarie University, Sydney, Australia

GERMAIN, D., University of Moncton, Nouveau-Brunswick, Canada

GIOVAMBATTISTA, R.Di , Istituto Nazionale di geofisica e Vulcanologia, Roma, Italy

GLENN, N. F., Idaho State University, USA

GOFAS, S., Universidad de Ma'laga, Spain

GOKARN, S.G., Indian Institute of Geomagnetism, Colaba, Mumbai, India

GOLOSOV, V., Moscow State University, Russia

GRAEFE, K.-U., Geosciences Department, University of Bremen

GRAHAM, I., University of New South Wales, Sydney, Australia

HARZHAUSER ,M., Natural History Museum of Vienna, Austria

HERMANN , J., The Australian National University, Canberra, Australia

HIGGITT, D.L., National University of Singapore

HORNE, D., Queen Mary University of London, UK

HUGHES, D., Rhodes University, Grahamstown, South Africa

HURNI, L., ETH Hönggerberg, Zürich, Switzerland

IAMANDEI, S., Geological Institute of Romania, Bucharest, Romania

ICHINOSE, G., United Research Services (URS) Group, Inc., Pasadena, California

JABOYEDOFF, M., University of Lausanne, Suisse

JACKSON, J., Bullard Laboratories, Cambridge, UK

JOYNER, L., Cardiff University, UK

KAHLE, H.-G., ETH Hoenggerberg, Zurich, Switzerland

KARAKITSIOS, V., National and Kapodistrian University of Athens, Greece

KARAMAN, A., Istanbul Technical University, Istanbul, Turkey

KATERINOPOULOS, A., National and Kapodistrian University of Athens, Greece

KELEPERTZIS, A., National and Kapodistrian University of Athens, Greece

KIKUCHI, R., Polytechnic Institute of Coimbra, Portugal

KILBURN, C., University College London, UK

KIRZHNER, F., Israel Institute of Technology, Haifa, Israel

KLUSMAN, R.W., Colorado School of Mines Golden, Colorado, USA

KOEPKE, J., Universitaet Hannover, Hannover, Germany

KOMATSU, T., Kyushu University, Japan

KOPER, K.D., Saint Louis University, Missouri, USA

KOUKOUVELAS, I., University of Patras, Greece

KRAUS, I., Comenius University, Bratislava

KROH, A., Natural History Museum Vienna, Austria

KROONENBERG, S., Delft University of Technology, Netherlands

KRUEGER, F., Institute of Geosciences in Potsdam, Germany

KYRIAKOPOULOS, K., National and Kapodistrian University of Athens, Greece

LEEDER, M., University of East Anglia, Norwich Norfolk, UK

LEMEILLE, F., Institut de Radioprotection et de sûreté nucléaire (IRSN) France.

LEUCCI, G., University of Lecce, Italy

LEVIN, N., The University of Queensland, Australia

LIRER, F., Istituto Ambiente Marino Costiero (IAMC)-CNR Napoli

LONGHITANO, S., University of Basilicata, Potenza, Italy

LÜNING, S., University of Bremen, Bremen, Germany

LYKOUSSIS, V., National Centre for Marine Research, Attica, Greece

MADEJON, P., Instituto de Recursos Naturales y Agrobiologi'a de Sevilla, Spain

MAGKANAS, A., National and Kapodistrian University of Athens, Greece

MAHDI, H., University of Arkansas at Little Rock, Little Rock, USA

MALIVERNO, E., University of Milano-Bicocca, Italy

MANZANO, M., Technical University of Cartagena, Spain

MÄRKER, M., Università di Firenze, Italy

MARTENS, P.N., RWTH Aachen University, Germany

MARTIN, J., NC State University, Raleigh, USA

MATSUOKA, A., Niigata University, Japan

MATTEI, M., III Università di Roma, Italy

MELFOS, V., Aristotle University of Thessaloniki, Greece

MICHEL, F., Carleton University, Canada

MICHETTI, A.M., Università dell'Insubria, Como, Italia

MIGIROS, G., Agricultural University of Athens, Greece

MIKSA, E., Desert Archaeology Inc., Tucson, USA

MITASOVA, H., Dept. of Marine, Earth and Atm. Sciences, Raleigh, USA

MITROPOULOS, P., National and Kapodistrian University of Athens, Greece

MOISSETTE, P., Université de Lyon I, France

MOLINAROLI, E., Università Ca' Foscari di Venezia, Italy

MOLSON, J., Ecole Polytechnique, Montreal, Canada

MONROS, G., Universitat jaume I, Castelló, Spain

MONTEIRO SANTOS, F. A., University of Lisbon, Portugal

MORENO, C., Universidad de Huelva, Spain

MORETTI, I., Institut Français du Petrole, Paris, France

MORO, M., Istituto Nazionale di Geofisica e Vulcanologia, Rome, Italy

MORTENSEN, J., Roskilde University Center, Denmark

MOTTERSHEAD, D., University of Portsmouth, UK

MOUYAN, I., Univesity Med V, Rabat, Morocco

MUSSON, R., British Geological Survey, Edinburgh UK

NASIR, S., Sultan Qaboos University, Oman

NAVA, A., Centro de Investigación Científica y Educación Superior de Ensenada, Ensenada, México

NAVAS, A., Estación Experimental de Aula Dei, Zaragoza, Spain

NEIGE, P., Université de Bourgogne, Dijon, France

NERAUDEAU, D., Université de Rennes 1, France

NGUYEN, F., Forschungszentrum Jülich GmbH, Jülich, Germany

NICOLETTI, P.G., Consiglio Nazionale delle Ricerche , Roges di Rende CS, Italy

NOCETE, F., University of Huelva, Huelva, Spain

OHMINATO, T., Earthquake Research Institute, Tokyo Univ.

OLDOW, J. S., University of Idaho, Moscow, Idaho

ORLANDO, L., University of Rome 'La Sapienza', Italy

ORLOVSKY, L., Ben Gurion University of the Negev, Israel

PACE, B., Universita` degli Studi "G. d'Annunzio", Chieti Scalo, Italy

PAGE, A., University of California, Riverside, USA

PALMSTROM, A., Sandvika, Norway

PALOMBO, M.R., Dipartimento di Scienze della Terra - CNR, Roma, Italy

PAPADOPOULOS, T., National and Kapodistrian University of Athens, Greece

PAPADOPULOS, S., S.S. Bethesda, Maryland

PAPAGEORGIOU, Ch., National and Kapodistrian University of Athens, Greece

PAPAGIANNI, D., University of Southampton, UK

PARRIAUX, A., Ecole polytechnique fédérale de Lausanne, Switzerland

PATRO, P.K., National Geophysical Research Institute, Hyderabad, India

PAVLIDES, S. B., Aristotle University of Thessaloniki

PAVLIS, G., College of Arts and Sciences, Indiana University

PAVLOPOULOS, K., Harokopio University, Athens, Greece

PEJON, O., University of São Paulo, Brazil

PE-PIPER, G., Saint Mary's University, Halifax, Canada

PEREZ-ARLUCEA, M., Universidad de Vigo, Spain

PESSAGNO, E., The University of Texas at Dallas

PICCARDI, L., C.N.R. - Istituto di Geoscienze e Georisorse, Firenze - Italy

PIPER, D., Bedford Institute of Oceanography in Halifax, NS

PLATZMAN, E., University Southern California, Los Angeles, USA

PLOMEROVA, J., Czech Academy of Sciences, Prague, Czech Republic

POMONI, F., National and Kapodistrian University of Athens, Greece

POSTMA, G., Utrecht University, The Netherlands

POWER, I.M., The University of Western Ontario, Canada

PREMOLI SILVA, I., Dipartimento di Scienze della Terra, Milano

PUTNIS, A., Institut fur Mineralogie, Correns, Germany

QUEROL, X., Instituto de Ciencias de la Tierra "Jaume Almera", Barcelona

QUINN, R., University of Ulster, UK

RAITH, J.G., Montanuniversität Leoben, Austria

RIAZA, A., Instituto Geológico y Minero de España (IGME), Spain

RINAUDO, C., Università degli Studi del Piemonte Orientale "A. Avogadro", Italy

RING,U., Johannes Gutenberg Universität, Mainz, Germany

ROBERTS, G., University of London, UK

ROBERTSON, A., University of Edinburgh, UK

ROELAND, M., TNO Science & Industry, Apeldoorn, The Netherlands

ROSENBERG, P.E., Washington State University, Pullman, USA

ROSSMAN, G.R., California Institute of Technology, Pasadena, USA

ROYDEN, L., Massachusetts Institute of Technology, USA

RUIZ-ORTIZ, P.A., Universidad de Jaén, Spain

SAINT MARTIN, S., Muséum National d'Histoire naturelle, Paris, France

SARDA, R., Centre d'Estudis Avancxats de Blanes (CSIC), Girona, Spain

SCHÖNER, R., Friedrich-Schiller-Universität Jena, Jena, Germany

SILENY, J., Academy of Sciences, Praha, Czech Republic

SLAYMAKER, O., University of British Columbia, Vancouver BC

SPEZZAFERRI, S., Université de Fribourg

SPROVIERI, M., Istituto Ambiente Marino Costiero (IAMC)-CNR Napoli

STAMATAKIS, M., National and Kapodistrian University of Athens, Greece

STAMMLER, K., Seismologisches Zentralobservatorium, Erlangen, Germany

STEBBINS, J., Stanford University

STEENBRINK , J., Universiteit Utrecht, the Netherlands

STETLER, L.D., Geological Engineer, SDSM&T, Rapid City

STILLE, H., Royal Institute of Technology, Stockholm, Sweden

STUYFZAND, P.J., Vrije Universiteit, Amsterdam, Netherlands

SUCHA, V., Comenius University, Bratislava, Slovakia

SUZUKI, N., Hokkaido University, Japan

SYLVESTER, Z., Shell International Exploration and Production Inc., Houston, Texas, USA

TALMON, A., Delft University of Technology, the Netherlands

TATTERSALL, I., American Museum of Natural History, New York, USA

TAYMAZ, T., Istanbul Technical University, Turkey

TEN VEEN, J., Ruhr-Universität Bochum, Germany

TIBERT, N. E., University of Mary Washington, Virginia, USA

TOPAL, T., Middle East Technical University, Ankara, Turkey

TRIANTAPHYLLOU, M.,National and Kapodistrian University of Athens, Greece

TSIAMBAOS, G., National Technical University of Athens, Greece

TUCKER, M., University of Durham, UK

TULIPANO, L., Universita degli Studi di Roma "La Sapienza"

UKAWA, M., Volcano Research Department, Japan

UNCLES, R., Plymouth Marine Laboratory, UK

VAIOPOULOS, D., National and Kapodistrian University of Athens, Greece

VALLIANATOS, F., Technological Educational Institute of Crete, Greece

VANDERPOST, C., Harry Oppenheimer Okavango Research Centre, Maun, Botswana

VANNUCCI, G., INGV-Istituto Nazionale di Geofisica e Vulcanologia, Bologna ITALY

ΘΕΜΑΤΙΚΕΣ ΕΝΟΤΗΤΕΣ – TOPICS

ΤΟΜΟΣ 1 - VOLUME 1

Παλαιοντολογία - Στρωματογραφία - Ιζηματολογία	Paleontology - Stratigraphy - Sedimentology	1
Τεκτονική - Δυναμική - Εφαρμοσμένη Γεωλογία	Tectonic- Dynamic- Applied Geology	251

ΤΟΜΟΣ 2 - VOLUME 2

Υδρογεωλογία	Hydrogeology	523
Ορυκτολογία - Πετρολογία -Γεωχημεία- Οικονομική Γεωλογία	Mineralogy-Petrology-Geochemistry-Economic Geology	641

ΤΟΜΟΣ 3 - VOLUME 3

Γεωφυσική-Σεισμολογία	Geophysics- Seismology	1032
Φυσικό Περιβάλλον και Ανθρωπογενείς Παρεμβάσεις	Natural Environment and Anthropogenic Activities	1331

ΤΟΜΟΣ 4 - VOLUME 4

Φυσική Γεωγραφία- Γεωμορφολογία	Physical Geography- Geomorphology	1513
Τεχνικά έργα και Γεωεφαρμογές	Engineering Works and Geological Applications	1634
Γεωεπιστήμες και Πολιτισμός	Geosciences and Culture	1759
Νέες τεχνολογίες στη Γεωφυσική και Γεωλογική έρευνα	New Technologies in Geophysical and Geological Research	1892

ΠΕΡΙΕΧΟΜΕΝΑ/CONTENTS

Παλαιοντολογία - Στρωματογραφία – Ιζηματολογία
Paleontology - Stratigraphy - Sedimentology

Bellas, S., Frydas, D. and Keupp, H. 1
Late Miocene calcareous nannofossil stratigraphy and intra-Mediterranean bioevents correlation: Kalidonia Case section (NW Crete, Greece)

Caus, E., Albrich, S., Berástegui, X., Bernaus, J.M., Boix, C. and Villalonga, R. 14
Biotic and Abiotic events in a shallow carbonate platform (Upper Cretaceous, South Pyrenean margin)

Codrea, V., Barbu, O. and Bedelean, H. 21
Middle Miocene Diatomite-bearing formations from western Romania

Danelian, T., Galoyan, G., Rolland, Y. and Sosson, M. 31
Palaeontological (Radiolarian) late Jurassic age constraint for the Stepanavan ophiolite (Lesser Caucasus, Armenia)

Drinia, H., Antonarakou, A., Kontakiotis, G., Tsaparas, N., Segou, M. and Karakitsios, V. 39
Paleobathymetric evolution of the early Late Miocene deposits of the Pre-Apulian zone, Levkas island, Ionian Sea

Getsos, K., Pomoni-Papaioannou, F. and Zelilidis, A.*A* 53
Carbonate ramp evolution in the transition from the Apulia platform to the Ionian basin during Early to Late Cretaceous (NW Greece)

Iatrou, M., Papatheodorou, G., Piper, D.J.W., Tripsanas, E. and Ferentinos, G.*A* 64
Debate on the similarity of particle sizing results derived from the analysis of fine-grained sediments by two different instrumentations

Karakatsanis, S., Koukouzas, N., Pagonas, M. and Zelilidis, A. 76
Preliminary sedimentological results indicate a new detailed stratigraphy for the Florina sedimentary basin and relate them with CO_2 presence

Karakitsios, V. and Agiadi-Katsiaouni, K. 85
Regional correlation and cyclostratigraphy in the Mid-Cretaceous formations of the Ionian zone

Kati, M., Zambetakis-Lekkas, A. and Skourtsos, E. 101
Carbonate succession of Tripolitza platform in Mari area, Parnon mountain, SE Peloponnesus, Greece

Konstantopoulos, P., Maravelis, A., Nikolaidou, D., Pantopoulos, G. and Zelilidis, A. 113
Application of bed thickness distributions in turbidite deposits of Mavri Miti area, SW Greece.

Koskeridou, E. 121
Pliocene Brachiopods from Rhodes island (Cape Vagia section)

Kostopoulos, D. S. and Koufos, G. D. 134
Similarity relationships among Greek Middle Miocene to Early-Middle Pleistocene mammal assemblages

Krassilov, V. and Shuklina, A. 142

Terrestrial biotic crises: paleobotanical record and interpretation

Maravelis, A., Konstantopoulos, P., Pantopoulos, G. and Zelilidis, A. 154
Application of bed thickness distributions in turbidite deposits of Lemnos island, NE Greece

Metaxas, A., Karageorgiou, D. E., Varvarousis, G., Kotis, T., Ploumidis, M. and Papanikolaou, G. 161
Geological evolution – stratigraphy of Florina, Ptolemaida, Kozani and Saradaporo graben

Pantopoulos, G., Konstantopoulos, P., Maravelis, A. and Zelilidis, A. 173
Application of bed thickness distributions in Late Eocene-Oligocene turbidite deposits of Greece: some preliminary results

Photiades, A., Carras, N., with, i. c., Bortolotti, V., Fazzuoli, M. , and Principi, G. 182
The *late Early Cretaceous transgression on the Laterites in Vourinos and Vermion massifs (western Macedonia, Greece).*

Sofikitis, E., Siavalas, G., Chatziapostolou, A., Kalaitzidis, S. and Christanis, K. 191
Greek coastal mires: A preliminary study of the Agoulinitsa peatland, Western Peloponnese

Theodorou, G.E., Roussiakis, S.I., Athanassiou, A., Giaourtsakis, I. and Panayides, I. 201
A Late Pleistocene endemic genet (Carnivora, Viverridae) from Aghia Napa, Cyprus

Triantaphyllou, M. V., Antonarakou, A., Kouli, K., Dimiza, M., Kontakiotis, G., Ziveri, P., Mortyn, G., Lykousis, V. and Dermitzakis, M.D. 209
Plankton ecostratigraphy and pollen assemblage zones over the last 14 000 years in SE Aegean Sea (core NS-14)

Tsaparas, N., Drinia, H., Antonarakou, A., Marcopoulou-Diakantoni, A. and Dermitzakis, M.D. 225
Tortonian Clypeaster fauna (Echinoidea: Clypeasteroida) from Gavdos island (Greece)

Voudouris, P., Velitzelos, D., Velitzelos, E. and Thewald, U. 238
Petrified wood occurrences in western Thrace and Limnos Island: mineralogy, geochemistry and depositional environment

Τεκτονική – Δυναμική – Εφαρμοσμένη Γεωλογία
Tectonic- Dynamic- Applied Geology

Al-Zoubi, A. S. 251
The basement fault system in the Northwestern Arabian Plate, Jordan

Diamantis, K., Karamousalis, Th., Antoniou, V. and Migiros, G. 264
Uniaxial compressive strength, dry unit weight and fracture patterns of ultrabasic rocks in Othrys

Fountoulis, I., Mavroulis, S. and Theocharis, D. 275
The morphoneotectonic structure of the transitional zone between the Gortynia Mt. horst and the Pyrgos-Olympia basin (Central - western Peloponnese, Greece)

Ganas, A., Drakatos, G., Bosy, J., Petro, L., Kontny, B., Stercz, M., Melis, N. S., Cacon, S., Papanikolaou, M., Pirentis, A. and Kiratzi, A. 287

Ganas, A., Spina, V., Alexandropoulou, N., Oikonomou, A. and Drakatos, G. 297
The Corini Active Fault in Southwestern Viotia region, central Greece: segmentation, stress analysis and extensional strain patterns

Georgiadis, G.A., Tranos, M.D. and Mountrakis, D.M. 309
Late- and Post-Alpine tectonic evolution of the southern part of the Athos peninsula, northern Greece

Gkarlaouni, C., Papadimitriou, E. E., Kilias, A., Falalakis, G. and Gemitzi, A. 321
The evolution of the stress field in Eastern Macedonia and Thrace

Khoshravan, H. 333
Caspian Sea geodynamical evolution effect on the sea level changing along the Quaternary Period

Kondopoulou, D., Zananiri, I., Michard, A., Feinberg, H., Atzemoglou, A., Pozzi, J.-P. and Voidomatis, Ph. 343
Neogene tectonic rotations in the vicinity of the North Aegean Trough: new palaeomagnetic evidence from Athos and Samothraki (Greece).

Kranis, H. 360
Neotectonic basin evolution in central-eastern mainland Greece: an overview

Lekkas, E., Danamos, G. and Skourtsos, E. 374
Implications for the correlation of the Hellenic nappes in SW Aegean: the geological structure of the Archangelos region, Rhodes island

Messini, A.D., Papadimitriou, E.E., Karakostas, V.G. and Baskoutas, I. 386
Stress interaction between thrust faults along the SW Hellenic Arc (Greece)

Mposkos, E., Krohe, A., Diamantopoulos, A. and Baziotis, I. 399
Late- and post-Miocene geodynamic evolution of the Mesogea basin (east Attica, Greece): Constraints from sediment petrography and structures

Palyvos, N., Sorel, D., Lemeille, F., Mancini, M., Pantosti, D., Julia, R., Triantaphyllou, M.V. and De Martini, P.M. 412
Review and new data on uplift rates at the W termination of the Corinth rift and the NE Rion graben area (Achaia, NW Peloponnesos)

Papanikolaou, D. and Papanikolaou, I. 425
Geological, geomorphological and tectonic structure of NE Attica and seismic hazard implications for the northern edge of the Athens plain

Rondoyanni, T., Galanakis, D., Georgiou, C. and Baskoutas, I. 439
Identifying fault activity in the central Evoikos gulf (Greece)

Sakellariou, D., Rousakis, G., Kaberi, H., Kapsimalis, V., Georgiou, P., Kanellopoulos, Th. and Lykousis, V. 451
Tectono-sedimentary structure and Late Quaternary evolution of the north Evia gulf basin, central Greece: preliminary results

Skourtsos, E. and Lekkas, E. 463
The tectonic setting of the October 8th 2005 earthquake in Kashmir, north Pakistan

Skourtsos, E., Pope, R. and Triantaphyllou, M.V. 475
Tectono-sedimentary evolution and rates of tectonic uplift of the Sfakia coastal

zone, southwestern Crete

Tranos, M.D., Plougarlis, A.P. and Mountrakis, D.M. 488
A new consideration about the Almopia-Paikon boundary based on the geological mapping in the area of Nerostoma-Lakka (central Macedonia, Greece).

Tsimi, Ch., Ganas, A., Soulakellis, N., Kairis, O. and Valmis, S. 500
Morphotectonics of the Psathopyrgos active fault, western Corinth Rift, central Greece.

Zouzias, D., and St. Seymour, K. 512
Magma intrusion in 'Proto-caldera caldera' systems: example from the Nisyros volcano

Υδρογεωλογία
Hydrogeology

Nikas, K., Antonakos, A., Lambrakis, N. and Kallergis, G. 523
The use of "Antecedent Precipitation Index" and "Delay Factor" to estimate runoff from rainfall; a case study from eight drainage basins - Achaia, Peloponessos, Greece

Pliakas, F., Mouzaliotis, A., Kallioras, A. and Diamantis, I. 536
Hydrogeological assessment of the salinization problem of Xilagani – Imeros aquifer system in SW plain area of Rhodope prefecture, Greece

Sotiropoulos, P., Tzanis, A. and Sideris, G. 548
Watertool™: An automated system for hydrological investigations with application at the area of Kato Souli (NE Attica, Greece).

Soulios, G., Voudouris, K., Kalfountzos, D., Kaklis, T., Sotiriadis, M., Alexiou, J. and Kotsopoulos, S. 560
Preliminary results of groundwater recharge experiments in Larisa prefecture

Stamatis, G., Parpodis, K., Lambrakis, N. and Zagana, E. 570
Origin and quality of thermal groundwaters in the region of Farsala (E. Thessaly/Greece)

Tsourlos, P., Vargemezis, G., Voudouris, C., Spachos, T. and Stampolidis, A. 580
Monitoring recycled water injection into a confined aquifer in Sindos (Thessaloniki) using Electrical Resistivity Tomography (ERT): Installation and preliminary results

Vargemezis, G. 593
Interpretation of VLF measurements related to hydrogeological surveys

Vargemezis, G., Tsourlos, P. and Stamoulis, K. 605
Application of Geophysical methods to the study of mechanism of springs

Voudouris, K., Alexopoulos, A., Antonakos, A. and Kallergis, G. 616
Water resources in the wider area of the Aposelemis basin, Crete island, Greece

Zarris, D., Lykoudi, E. and Panagoulia, D. 629
Sediment yield estimates in north-western Greece and analyses with hydrologic and geomorphologic factors

Ορυκτολογία - Πετρολογία -Γεωχημεία- Οικονομική Γεωλογία
Mineralogy-Petrology-Geochemistry-Economic Geology

Aurisicchio, C., Bartolomei, A., Kyriakopoulos, K. and Magganas, A. 641
An unusual tourmaline composition from Sithonia Peninsula (northern Greece)

Baziotis, I., Mposkos, E., Palikari, S. and Perraki, M. 653
Geochemistry of ultramafic rocks from the ultrahigh-pressure metamorphic Kimi Complex in East Rhodope (NE. Greece)

Bedelean, H., Codrea, V. and Barbu, O. 666
Geological and mineralogical characterization of some zeolitic tuffs from NWrn Transylvania, Romania

Boudi D., Prophitis E., Zachariadis P., Kostopoulos D., Baltatzis E., and Chatzitheodoridis E. 676
Petrology, Geochemistry and Geotectonic setting of the Titaros ophiolite and associated Pelagonian basement rocks in the area NW of Mt. Olympos, Greece

Christidis, G.E. 690
Layer charge and charge distribution of smectites: a parameter which controls important physical properties of bentonites

Christofides, G., Koroneos, A., Liati, A. and Kral, J. 700
The A-type Kerkini granitic complex in north Greece: geochronology and geodynamic implications

D'Alessandro, W., Brusca, L., Kyriakopoulos, K., Margaritopoulos, M., Michas, G. and Papadakis, G. 712
Fluid geochemistry investigations on the volcanic system of Methana

Filippidis, A., Kantiranis, N., Stamatakis, M.G., Drakoulis, A. and Tzamos, E. 723
The cation exchange capacity of the Greek zeolitic rocks

Gamaletsos, P., Godelitsas, A., Chatzitheodoridis, E. and Kostopoulos, D. 736
Laser μ-Raman investigation of Greek bauxites from the Parnassos-Ghiona active mining area

Georgiadis, I.K., Tsirambides, A., Kassoli-Fournaraki, A. and Trontsios, G. 747
Petrology and provenance study of the Neogene and Quaternary clastic sediments from: Herso Kilkis (Macedonia, Greece)

Kalafati, K. and Christidis, G.E. 759
Replacement of TiO_2 pigment by $CaCO_3$ from Cefalonia in emulsion paints

Kantiranis, N., Filippidis, A., Stamatakis, M.G., Tzamos, E. and Drakoulis, A. 769
A preliminary study of the Colemanite-rich tuff layer from the Sourides area, Karlovassi basin, Samos Island, Hellas

Kantiranis, N., Filippidis, A., Vouta, S., Drakoulis, A., Koutles, T. and Tzamos, E. 775
The cation exchange capacity of industrial minerals and rocks of Milos island

Kapsiotis, A., Tsikouras, B., Grammatikopoulos, T., Karipi, S. and Hatzipanagiotou, K. 781
On the metamorphic modification of Cr-spinel compositions from the ultrabasic rocks of the Pindos ophiolite complex (NW Greece)

Karampelas, S., Fritsch, E., Sklavounos, S. and Soldatos, T. 794
Identification of treated-color freshwater cultured pearls

Karampelas, S., Fritsch, E., Zorba, T., Paraskevopoulos, K.M. and Sklavounos, S. 805
An update in the separation of natural from synthetic amethysts

Karipi, S., Tsikouras, B. and Hatzipanagiotou, K. 816
Petrology and geochemistry of granitic pebbles in the Parnassos flysch at Iti Mountain, continental Central Greece

Katsikopoulos, D., González-Fernández, Á. and Prieto, M. 829
Preliminary results upon crystallization of the Calcite-spherocobaltite solid solution

Kiomourtzi, P., Pasadakis, N. and Zelilidis, A. 839
Geochemical characterization of satellite hydrocarbon formations in Prinos-Kavala basin (North Greece)

Kitsopoulos, K. 851
Mg-Fe-rich amphiboles associated to pyroclastics from Santorini island, south Aegean Sea volcanic arc, Greece

Koukouzas, N., Hämäläinen, J., Papanikolaou, D., Tourunen, A. and Jäntti, T. 859
Mineralogical and chemical composition of CFB fly ash derived from co-combustion of xylite and biomass

Koukouzas, N., Ziock, H., Ziogou, F. and Typou, I. 872
Mineral carbonation as a potential carbon dioxide storage option for the region of Western Macedonia, Greece.

Magganas, A. 884
Pla*giogranitic rocks of Evros Ophiolite, NE Greece*

Mariolacos, K. 899
Empirical thermochemical values for higher order oxides – an uncritical consideration

Oikonomopoulos, I., Perraki, T., Kaouras, G. and Antoniadis, P. 906
Mineralogical study of inorganic intercalated seams at Achlada lignite deposits (NW Greece)

Papavassiliou, C. T. 918
Geochemical-mineralogical and metallogenetical aspects concerning the origin of sediments from Leg. 22 D.S.D.P drilled sites 212 and 213 in Eastern Indian Ocean

Papoulis, D. 936
^{29}Si and ^{27}Al CPMAS NMR qualitative and quantitative analysis of kaolinite and dickite in Kos island kaolins, Greece

Pomonis, P., Rigopoulos, I., Tsikouras, B. and Hatzipanagiotou, K. 947
Relationships between petrographic and physicomechanical properties of basic igneous rocks from the Pindos ophiolitic complex, NW Greece

Rigakis, N., Nikolaou, K., Marnelis, F. and Pakos, T. 959
The utility of oil shows usefulness in hydrocarbon exploration of Western Greece

Stamatakis, M.G., Renaut, R.W., Kostakis, K., Tsivilis, S., Stamatakis, G. and Kakali, G. 972
The hydromagnesite deposits of the Atlin area, British Columbia, Canada, and

their industrial potential as a fire retardant

Theodosoglou, E., Koroneos, A., Paraskevopoulos, K. M., Christofides, G., Papadopoulou, L. and Zorba, T. 984
Comparative infrared spectroscopic study of Ca-amphiboles

Tombros, S. and St. Seymour, K. 996
Hermione, evolution of a Te-bearing epithermal mineralization, Argolis, Hellas

Tsipoura-Vlachou, M. 1009
Diagenesis of the marly-gypsum formations, Igoumenitsa area, N.W. Greece

Tsirambides, A., Georgiadis, I.K., Papadopoulos, A.A., Ziafetis, A.A. and Giouri, A.N. 1022
Mineralogical and geochemical study of Neogene red beds from Moudania and Potidea, Chalkidiki (Macedonia, Greece)

Γεωφυσική-Σεισμολογία
Geophysics- Seismology

Agalos, A., Papadimitriou, P., Voulgaris, N. and Makropoulos, K. 1032
Source parameters estimation from broadband regional seismograms for earthquakes in the Aegean region and the Gorda plate

Athanasiou, E., Tsourlos, P., Vargemezis, G. and Tsokas, G. 1045
Nondestructive 2-D geoelectrical surveying into a building's basement

Baskoutas, I., Papadopoulos, G.A., Karakostas, V.G. and Papadimitriou, E. E. 1055
Recent 2005-2006 strong seismic activity in Greece under the aspect of seismicity parameters temporal variation analysis

Chailas, S., Tzanis, A. , and Lagios, E. 1063
Structure of the Marathon basin (NE Attica, Greece) based on gravity measurements

Daskalaki, E. and Papadopoulos, G.A. 1074
The 26th December 2004 Indian Ocean tsunami: the intensity field

Di Fiore, B., Chianese, D., Loperte, A., Conte, G., Dibenedetto, A., Vitti, P., Voza, O. and Greco, E. 1080
First geophysical results in the Archeological sites of Θουρια (Peloponnese, Hellas) and Sibari-Thurii (southern Italy)

Karamanos, C.K., Karakostas, V.G., Papadimitriou, E.E. and Sachpazi, M. 1091
Earthquake relocation in the wester termination of the North Aegean Trough

Kassaras, I., Louis, F., Magganas, A., Makropoulos, K. and Kaviris, G. 1103
Anelasticity beneath the Aegean inferred from Rayleigh wave attenuation

Kaviris, G., Papadimitriou, P. and Makropoulos, K. 1114
Magnitude Scales in Central Greece

Kiratzi, A., Benetatos, C. and Roumelioti, Z. 1125
Distributed earthquake focal mechanisms in the Aegean Sea

Kokinou, E., Panagiotakis, C. and Vallianatos, F. 1138
Earthquake/noise discrimination and estimation of P-S phases based on wave characteristics

Kolaitis, A., Papadimiriou, P., Kassaras, I. and Makropoulos, K. 1150
Seismic observations with broadband instruments at Santorini volcano

Kougoulis, Ch., Arvanitis, A., Kolios, N., Koutsinos, S. and Kougoulis, J.-S. 1162
Geothermal exploitation in the Sani-Afytos area of the Kassandra peninsula (Chalkidiki peninsula, Northern Greece)

Moshou, A., Papadimitriou, P. and Makropoulos, K. 1177
Teleseismic body wave inversion

Nikolintaga, I., Karakostas, V. G., Papadimitriou, E.E., Vallianatos, F. and Panopoulou, G. 1187
Velocity models inferred from p–waves travel time curves in south Aegean

Orfanogiannaki, K., Karlis, D. and Papadopoulos, G.A. 1199
Identification of temporal patterns in the seismicity of Sumatra using Poisson Hidden Markov models

Papadopoulos, T.D., Goulty, N., Voulgaris, N., Alexopoulos, J.D., Fountoulis, I., Kambouris, P., Karastathis, V., Peirce, C., Chailas, S., Kassaras, I., Pirli, M., Goumas, G. and Lagios, E. 1207
Tectonic structure of Central-Western Attica (Greece) based on geophysical investigations-Preliminary results

Papageorgiou, E., Lagios, E., Vassilopoulou, S. and Sakkas, V. 1219
Vertical & horizontal ground deformation of Santorini island deduced by DGPS measurements

Papathanassiou, G., Valkaniotis, S. and Pavlides, S. 1226
Applying the INQUA scale to the Sofades 1954, Central Greece, earthquake

Pirli, M., Pirlis, E. and Voulgaris, N. 1234
Mislocation vectors for the Tripoli seismic array, Greece, and structural effect implications from backazimuth and slowness residual analysis

Pirli, M. and Schweitzer, J. 1246
Regional and teleseismic event detection capability of the small-aperture Tripoli seismic array, Greece

Roumelioti, Z., Ganas, A., Sokos, E., Petrou, P., Serpetsidaki, A. and Drakatos, G. 1257
Toward a joint catalogue of recent seismicity in western Greece: preliminary results

Segou, M. and Lozios, S. 1267
Seismogenic sources and related active faults in the gulf of Corinth; a combined approach

Stampolidis, A., Tsokas, G., Kiratzi, A. and Pavlides, S. 1279
Major tectonic structures in northeastern Greece deduced from geophysical and seismological data

Tzanis, A. 1292
Critical-point behaviour in self-organizing systems: the September 1999 Athens earthquake and Stock Market correction

Tzanis, A. and Drosopoulou, E. 1304
The electric structure of the schizosphere in SE Thessaly, Greece, and its correlation with active tectonics

Zamba, I. and Kouskouna, V. 1318
Seismic history of Pella and the 1st century B.C. earthquake

Φυσικό Περιβάλλον και Ανθρωπογενείς Παρεμβάσεις
Natural Environment and Anthropogenic Activities

Argyraki, A., Plakaki, A. and Godelitsas, A. 1331
Characterization of garden soil pollution in the mining village of Stratoni, N. Greece

Arikas, K. 1343
Mineralogical and geochemical study of the Kirki mining wastes, Evros region, Greece –determination of the environmental impact by toxic and heavy metals

Bathrellos, G.D. 1354
An overview in urban geology and urban geomorphology

Bathrellos, G.D., Skilodimou, H.D., Livaditis, G. and Verikiou-Papaspiridakou, E. 1365
Geomorphological study of Kleinovitikos stream drainage network (Trikala prefecture – western Thessaly)

Boev, B. 1377
Trace elements in the soils of the Tikves region

Daci, A., Kaza, G., Deda, T. and Hoti, S. 1387
The environmental impact of the Copper industry in the Fani River Valley (Repsi "Hot spot") Mirdita, Albania

Dimitrova, D., Cholakova, Z., Velitchkova, N., Kotsev, T., Mladenova, V., Kerestedjian, T. and Antonov, D. 1397
Heavy metal and metalloid concentration dynamics in mine and surface waters in the vicinity of Chiprovtsi and Martinovo mines, Northwestern Bulgaria

Giannoulopoulos, P. and Poulovassilis, A. 1409
In situ estimation of actual evapotranspiration. A case study in Argos plain

Iordanidis, A., Buckman, J., Triantafyllou, A.G. and Asvesta, A. 1421
Atlas of airborne particles from Kozani area, Northern Greece

Kadetova, A.V., Kozyreva, E.A. and Rybchenko, A.A. 1433
Degradation of shores in the urban area of Irkutsk city under the influence of man-made reservoir

Kadetova, A.V., Rybchenko, A.A. and Trzhtsinsky, Yu. B. 1440
Technogenic change of the geological environment of urban areas (by the example of Irkutsk town)

Khak, V.A., Kozyreva, E.A. and Trzhcinsky, Yu.B. 1449
Eolation dynamics in the shore of artificially impounded bodies (by the example of Bratsk water reservoir, Russia)

Mariolakos, D., 1457
Comparative evaluation of water collection methods using multicriteria decision making analysis

Mazaeva, O. A. and Khak, V. A. 1469
Development of linear erosion forms under the influence of technogenic conditions

Mimides, T., Psomiadis, E. , and Trikili, I. 1476
Monitoring land use changes and soil degradation using spot and temporal aerial photograph data – the case of Vathy basin (Kalymnos island – Dodecanese Greece)

Mitta V.V., and Bogomolov Yu.I. 1485
Late Jurassic of the Russian platform: Ammonite evolution and paleoenvironments

Papastergios, G., Filippidis, A., Christofides, G., Kassoli-Fournaraki, A., Fernández-Turiel, J. L., Georgakopoulos, A. and Gimeno, D. 1491
Trace element contents in uncultivated surface soils in the Kavala area, northern Greece

Stefanova, M., Marinov, S. P., Gonsalvesh, L., Mastral, A., Callen, M. and Gadjanov, P. 1499
PAHs in fly ash from lignite combustion

Zotiadis, V. and Kollios, A. 1505
Assessment of hydrocarbons subsoil and groundwater pollution in a refinery occupied property at the old industrial zone of Athens - Pireaus, Greece

Φυσική Γεωγραφία- Γεωμορφολογία
Physical Geography- Geomorphology

Alexouli–Livaditi, A., Vouvalidis, K., Livaditis, G. and Pechlivanidou, S. 1513
Drainage network characteristics of Athens plain at the end of the 19th century

Foutrakis, P., Poulos, S., Maroukian, H. and Livaditis, G. 1522
A study of the deltaic coast morphometry of river Pinios in relation to its hydro- & sediment dynamics

Karamousalis, Th., Poulos, S., Maroukian, H. and Ghionis, G. 1530
Geomorphological characteristics of the sand-dune field of the central Kyparissiakos Gulf

Karymbalis, E., Gaki-Papanastassiou, K. and Maroukian, H. 1538
Recent geomorphic evolution of the fan delta of the Mornos river, Greece: natural processes and human impacts

Kontou, A., Gaki-Papanastasiou, K. and Maroukian, H. 1552
Comparative geomorphological observations in two groups of alluvial fans of Sperchios and Eurotas regions, Greece

Lykoudi, E. and Antoniou, M. 1566
Study of natural mechanisms for the supply of transported materials to the Ag. Varvara coast (Lesvos island)

Pagonas, M. and Kontopoulos, N. 1578
Morphometric and hydrographic characteristics of torrents of NW Peloponnese, Greece

Palyvos, N., Pantosti, D., Stamatopoulos, L. and De Martini, P.M. 1586
Geomorphological reconnaissance of the Psathopyrgos and Rion-Patras Fault zones (Achaia, NW Peloponnesus).

Papadopoulou, K. and Vriniotis, D. 1599

Quality of soil and water in deltaic deposits of Louros and Arachthos rivers related to karstic rocks of the wider area

Pehlivanoglou, K.G. and Martsoukou, M. 1609
The foreshore zone determination according to the Greek legislation, using geologic and oceanographic data

Sambaziotis, E. and Fountoulis, I. 1621
Estimation of flash flood hazard in the Pidima-Arfara area (Messinia, SW Greece), based on the study of instantaneous unitary hydrographs, longitudinal profilesand stream power

Τεχνικά έργα και Γεωεφαρμογές
Engineering Works and Geological Applications

Chatziangelou, M. and Christaras, B. 1634
Influence of the geometric characteristics of wedges on the safety of Vrasna tunnel in Egnatia highway, N. Greece

Douveas, N., Kavadia, D. and Papadopoulou, P. 1644
Geotechnical foundation conditions of Mesologion swimming pool center

Georgiadis, G.A., Tranos, M.D., Makedon, T.K. and Dimopoulos, G.C. 1652
Contribution of geological mapping in road construction: an example from Veria – Kozani National road, Kastania area

Konstantopoulou, G. and Vacondios, I. 1664
Engineering geological map of the urban area of Kastoria, NW Greece

Kosiari, S. 1674
Study of northern Evia's ultramafic rocks as skid-resistant aggregates in pavement construction mountain (central Greece): correlations and evaluation

Koukis, G., Sabatakakis, N. and Lainas, S. 1683
Soil suitability estimation for housing purposes in landslide-prone areas. The case of Karya village, Patras, W. Greece

Koukis, G., Sabatakakis, N. and Papanakli, S. 1695
Laboratory testing properties of sandstones

Loupasakis, C. and Karfakis, J. 1703
Preservation of villages constructed on sliding areas – a case study from Karditsa Prefecture, Greece

Matziaris, V., Ferentinou, M., Agelopoulou, O., Karanassiou, S. and Sakellariou, M. 1710
Landslide hazard analysis – a case study in Kerasia village (prefecture of Karditsa)

Pyrgiotis, L., Koukis, G. and Sabatakakis, N. 1722
Rainfall and landslides in Karditsa county (Greece): a statistical approach

Tsatsanifos, C., Kontogianni, V. and Stiros, S. 1733
Tunneling and other engineering works in volcanic environments: Sousaki and Thessaly

Vacondios, I., Konstantopoulou, G. and Karadassi, S. 1741
The contribution of clay minerals in the landslides occurrence within Pindos flysh

formation

Vargemezis, G., Gerolymatos, E. and Aggelopoulos, A. 1749
Elecrical Tomography and VLF methods contribution to underground wastewater pipe construction

Γεωεπιστήμες και Πολιτισμός
Geosciences and Culture

Bathrellos, G.D., Skilodimou, H.D. and Chrysanthaki, I. 1759
Building and constructive materials as an urban geological resource in Trikala prefecture

Dierckx, H. M. C. and Tsikouras, B. 1768
Petrographic characterization of rocks from the Mirabello bay region, Crete, and its application to Minoan archaeology: the provenance of stone implements from Minoan sites

Fassoulas, C., Paragamian, K. and Iliopoulos, G. 1780
Identification and assessment of Cretan geotopes

Iordanidis, A., Garcia-Guinea, J. and Karamitrou-Mentesidi, G. 1769
Characterisation of Mycenaean and matt-painted pottery from Aiani, ancient upper Macedonia, Greece

Loupasakis, C. and Nikolaou, N. 1808
Safety assessment and protection of monuments located in caves – a case study from the city of Volos, Greece

Meléndez, G., Fermeli, G. and Koutsouveli, A. 1819
Analyzing Geology textbooks for secondary school curricula in Greece and Spain: Educational use of geological heritage

Mertzanis, A., Karetsos, G., Smyrni, V., Efthimiou, G. and Zakinthinos, G. 1833
National Park of Iti: Environmental and geomorphological impacts from the mining activity (Greece)

Sakellariou, D. 1845
Remote sensing techniques in the search for ancient shipwrecks: how to distinguish a wreck from a rock in geophysical recordings

Tsipoura-Vlachou, M. and Michopoulos, K. 1859
Characterization and causes of the building stone decay at the Artemis temple, Brauron, E. Attica, Greece

Zambetakis-Lekkas, A. and Elefanti, P. 1874
Micropaleontology and biostratigraphy efficient tools in archaeological research. Raw material provenance in the upper Palaeolithic Kastritsa cave, Ioannina region (Greece)

Zouros, N., Velitzelos, E., Valiakos, I. and Labaki, O. 1880
The Plaka petrified forest park in western Lesvos – Greece

Νέες τεχνολογίες στη Γεωφυσική και Γεωλογική έρευνα
New Technologies in Geophysical and Geological Research

Alexopoulos, J.D., Tomara, V., Vassilakis, E., Papadopoulos, T.D., Dassenakis, 1892

M., Poulos, S., Voulgaris, N., Dilalos, S., Ghionis, G., Goumas, G. and Pirlis, E.
A contribution to environmental research of the Korissia coastal wetland (Corfu isl., Greece), with the application of combined geological and geophysical methods supported by Geographic Information Systems

Bathrellos, G.D. and Skilodimou, H.D. 1904
Using the analytic hierarchy process to create an erosion risk map. A case study in Malakasiotiko stream, Trikala perfecture

Bedini, E. 1916
Use of GIS and Remote Sensing to detect change along the coastline segment between Shkumbini and Semani rivers, central Albania

Beqiraj, A., Alikaj, P., Lamaj, M., Muceku, Y., Çanga, B. and Leka, G. 1925
Geological-geophysical study for the disign of a hazardous waste landfill in Albania

Charalambous, S. and Sakellariou, M. 1934
Estimation of rockfall hazard using a GIS-based three-dimensional rockfall simulation model

Fakiris, E., Papatheodorou, G. and Panagiotopoulos, P. 1947
An innovative data mining procedure, using clean algorithm and factor analysis, for irregularly sampled temporal environmental data sets

Kokkalas, S., Jones, R. R., McCaffrey, K. J. W. and Clegg, P. 1959
Quantitative fault analysis at Arkitsa, Central Greece, using Terrestrial Laser-Scanning ("LIDAR")

Ladas, I., Fountoulis, I. and Mariolakos, I. 1973
Using GIS & Multicriteria Decision analysis in landslide susceptibility mapping – a case study in Messinia prefecture area (SW Peloponnesus, Greece)

Marinos P.G., Novack M., Benissi M., Stoumpos G., Panteliadou M., Papouli D., Marinos V. and Korkaris K. 1986
Evaluation of ground information with respect to EPB tunnelling for the Thessaloniki metro, Greece

Nikolakopoulos, G.K., Vaiopoulos, D.A. and Skianis, G.A. 1998
A preliminary approach on the use of satellite hyperspectral data for geological mapping

Paradisopoulou, P.M., Papadimitriou, E.E., Karakostas, V.G. and Kilias, A. 2008
Application for source parameters calculations as input for static stress changes studies

Parcharidis, I., Foumelis, M. and Lekkas, E. 2020
Vertical tectonic motion in Andaman Islands detected by multi-temporal satellite radar images

Rontogianni, S., Clarke, P., King, M., Lavallée, D., England, P., Parsons, B. and Floyd, M. 2032
Strain rates in Greece using GPS measurements from 1994-2000

Skianis, G.A., Vaiopoulos, D.A. and Nikolakopoulos, G.K. 2048
A study of the performance of the MSR vegetation index, using probabilistic and geostatistical methods

Vargemezis, G., Tsourlos, P., Papazachos, C. and Kostopoulos, D. 2060
Application of Electrical Resistivity Tomography to the detection of the Ermakia

(Northern Greece) cavity system

Vassilopoulou, S., Chousianitis, K., Sakkas, V., Damiata, B. and Lagios, E. 2070
GIS development for ground deformation data management. A case study in Cephallonia island (western Greece)

Δελτίο της Ελληνικής Γεωλογικής Εταιρίας τομ. XXXX, 2007
Πρακτικά 11ου Διεθνούς Συνεδρίου, Αθήνα, Μάιος 2007

Bulletin of the Geological Society of Greece vol. XXXX, 2007
Proceedings of the 11th International Congress, Athens, May, 2007

LATE MIOCENE CALCAREOUS NANNOFOSSIL STRATIGRAPHY AND BIOEVENTS CORRELATION: KALIDONIA CASE SECTION (NW CRETE, GREECE)

Bellas S.[1], Frydas D.[1], and Keupp H.[2]

[1] *University of Patras, Department of Geology, 26500 Rion/Patras, drbellas@zedat.fu-berlin.de, Dfrydas@upatras.gr*

[2] *Free University of Berlin, Department of Geosciences, Institute of Paleontology, Malteserstr. 74-100, D-12249 Berlin, keupp@zedat.fu-berlin.de*

Abstract

Calcareous nannofossils are widely used for biostratigraphic correlations. Quantitative approaches enable better understanding of reliability of bioevents. In order to refine the late Miocene stratigraphy of NW Crete, the deposits of Kalidonia basin along its type section are here investigated. It was possible to distinguish the Tortonian/Messinian boundary by NN11a & NN11b, CN9a & CN9b, MNN11a & MNN11b biozones. Reticulofenestra pseudoumbilicus PB (Paracme Beginning) and R. rotaria FO (First Occurrence) proved to act as additional significant biohorizons improving the stratigraphic evolution of the studied paleobasin and providing a tight biochronologic framework. The Kalidonia section fully covers an undisturbed marine depositional cycle from the upper Tortonian to upper Messinian, where a predominant deep water facies (DWF) is followed by transitional sediments (TF) and the sequence closes at the top by a reefal-bioclastic facies (RF) relative to the 'Calcare di Base' in Italy indicating the 'Messinian Salinity Crisis Event'.

Key words: *Calcareous nannoplankton, biostratigraphic correlations, Tortonian, Messinian.*

Περίληψη

Τα ασβεστολιθικά ναννοαπολιθώματα χρησιμοποιούνται ευρέως για βιοστρωματογραφικούς συσχετισμούς. Η καλύτερη κατανόηση των βιογεγονότων βελτιώνεται με τη χρήση ποσοτικών δεδομένων. Μελετήθηκαν οι αποθέσεις της ιζηματογενούς λεκάνης Καλυδώνια στην τυπική της τομή, με σκοπό τη λεπτομερέστερη στρωματογραφία του ανώτερου Μειόκαινου της ΒΔ Κρήτης. Προσδιορίστηκε το όριο του Τορτονίου/Μεσσηνίου με τη χρήση των βιοζωνών NN11α & NN11β, CN9a & CN9b, MNN11a & MNN11b. Επιπρόσθετα σημαντικοί βιοορίζοντες που βελτιώνουν τη στρωματογραφική εξέλιξη της μελετηθείσας παλαιολεκάνης και παρέχουν ένα ισχυρό βιοχρονολογικό πλαίσιο, αποδείχθηκαν η αρχή της παρακμής της Reticulofenestra pseudoumbilicus (PB) και η πρώτη παρουσία της R. rotaria (FO). Η τυπική τομή Καλυδώνια περιλαμβάνει θαλάσσια ιζήματα ενός αδιατάρακτου ιζηματογενούς κύκλου που καλύπτει απόθεση από το ανώτερο Τορτόνιο έως και το ανώτερο Μεσσήνιο, όπου κύρια φάσεις βαθιάς θάλασσας, ακολουθούνται από μεταβατικές φάσεις ιζημάτων, ενώ η ακολουθία ολοκληρώνεται στην κορυφή της τομής με υφαλογόνες-βιοκλαστικές

φάσεις που σχετίζονται με τους επονομαζόμενους 'Ασβεστολίθους Βάσης' της Ιταλίας και προσδιορίζουν και την έναρξη της 'Κρίσης Αλμυρότητας του Μεσσηνίου'.
Λέξεις κλειδιά: *Ασβεστολιθικό ναννοπλαγκτό, βιοστρωματογραφία, συσχετισμοί, Τορτόνιο, Μεσσήνιο.*

1. Introduction

The Hellenic Arc System, has been since long the subject of intensive research (McKenzie 1970, Makris 1978, Angelier 1979 Dewey and Sengör 1979 Mascle *et al.* 1982, Dixon and Robertson 1984). Generally it is believed, that southward retreat of the trench system induced migration of the arc itself, and gave birth and shape to the present-day Hellenic Arc System configuration (Wortel and Spakman 1992). The extension in the Aegean Sea (especially at the southern part of it) and the southward movement of Crete Island was caused by the rollback effect of the slab and the broad subduction zone (Le Pichon 1982, Meulenkamp *et al.* 1988, 1994). This rollback process of the Hellenic subduction zone started about 12 my ago (Meulenkamp *et al.* 1994). Furthermore, the active tectonics deformation of the Aegean region itself is dominated not only by extensional but by combined strike-slip motions and compressional tectonics as well (Jackson 1994, Meulenkamp *et al.* 1988). The concentration of slab pull forces causes a pattern of subsidence (combined with depocenters development) and uplift migrating along strike. Subsequently prevailed a maximum crustal thinning and subsidence in the region of Cretan Sea produced the back-arc basin(s) at the north of Crete as it was firstly suggested by studies of Makris (1978) and Angelier *et al.* (1982) and recently by Wortel and Spakman (2000).

The Neogene basins of northwestern Crete are generally considered the result of the prementioned subsidence. NNE- and WNW- trending fault systems, which were developed during the middle Miocene, represent the dominant structural feature controlling the configuration of these basins. Sedimentary deposition commenced at most if not at all of them during either the middle or the early late Miocene interval, usually at the Serravallian or the lower Tortonian respectively (Freudenthal 1969, Meulenkamp *et al.* 1979, Keupp and Bellas in collab. with Frydas and Bartholdy 2000).

Based on recently published integrated bio-, cyclo- and magnetostratigraphic schemes dealing with the late Miocene deposits of Mediterranean, this work aims firstly to present a tight biostratigraphy of the Kalidonia section located between Kolymbari and Kastelli town at the northwestern Crete Island. A refinement of the existing biostratigraphy will be further discussed. The Kalidonia section is considered the "type section" of Kalidonia basin (Keupp and Bellas in collab. with Frydas and Bartholdy 2000, this work). In addition to the Potamida section ("representative section" of Kissamou Formation after Freudenthal 1969) and due to the good material quality, exposure possibilities (easy access, undisturbed sequences) and preservation of the microfossils and nannoflora, Kalidonia is also considered as a subtypus locality for the Deep Water Facies (DWF), former "Kissamou Formation". The variability of paleodepositional environmental conditions prevailed in Kalidonia basin during the late Tortonian to late Messinian time span is lithostratigraphically demonstrated. Furthermore, the reliability of some known biohorizons of calcareous nannofossils has been evaluated along the studied section and their applicability concerning the biochronological correlation in the eastern Mediterranean Sea has been discussed and commented. For this purpose, we have used semiquantitative data of calcareous nannofossils.

2. The study area in the Neogene

The Kalidonia Basin is a small sedimentary basin (or subbasin), located on the NW Crete and situated directly on the foot of Rodopou peninsula (Fig. 1). Geologically, the Kastelli and Maleme (or Voukolies) Basins bound this basin to the west and to the east respectively (Keupp and Bellas in collab. with Frydas and Bartholdy 2000). Pre-Neogene strata, mostly represented by the P-Q

Group (Phyllites-Quartzites) separate the neogene successions of Kalidonia Basin, by those of the other basins. Remnants of neogene littoral deposits of Kalidonia have been mapped along the Rodopou peninsula at various altitudes. It has been postulated that syngenetic formation of horst (uplifted blocks where erosion predominates) and graben structures (downfaulted areas where sediments accumulate) modified an initially rather uniform depositional area of NW Crete (Frydas *et al.* 1999). Despite this isolation and the small size, the Kalidonia basin and its Neogene strata present a similar to the other Cretan basins lithostratigraphic facies and biostratigraphic history (i.e. Meulenkamp *et al.* 1979), pointing to a rather common development of them all.

Four sedimentary formations of Neogene age have been recognized in the broader area of Plakalona, namely the Mesonisi, Roka, Cherethiana and Kissamou (*sensu* Freudenthal 1969). In general the Neogene strata have been distinguished into two major groups based on their depositional environment, a) the non-marine and b) the marine facies. The Mesonisi Formation belongs to the terrestrial-fluviatile facies, which was not encountered in the studied section. Miocene and Pliocene age deposits firstly recognized in NW Crete by means of foraminifera by Christodoulou (1963) and later on were studied by Dermitzakis and Markopoulou-Diakantoni (1979), Meulenkamp *et al.* (1979) and Schmidt (1979). According to Kontopoulos *et al.* (1996) the Neogene strata of NW Crete were distinguished in two depositional sequences, the Miocene Sequence A and the Pliocene Sequence B, or the so-called First Miocenic Cycle and the Second Pliocenic Cycle (Frydas and Keupp 1996). The present study allows us to affirm that the sediments of the Kalidonia basin belong to the first and older depositional sequence (i.e. the Miocenic Cycle).

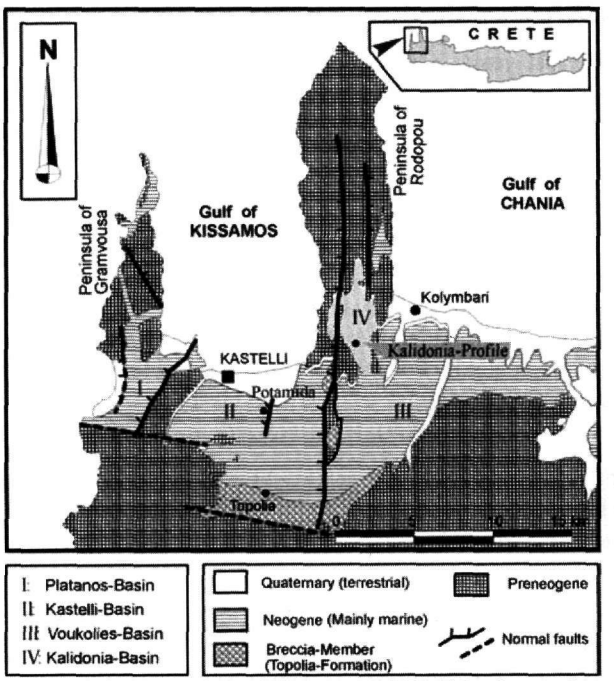

Figure 1 - Location of the studied Kalidonia section in NW Crete Island

3. Material and Methods

Kalidonia section is located on the new national road connecting Kolymbari village and Kastelli town (Fig. 1). Samples of soft sediment were collected for biostratigraphic analyses at an average distance of 0.90 meters. In other studies of ODP for similar purposes, considering biostratigraphy and palaeoecology, resolution of ca. 1.0-1.5m was judged good enough. In our case decompaction was not taken into account. Micropaleontology was mainly based on the calcareous nannofossils identification under both the normal light (at magnifications of ca. 1000x) and the scanning electron microscope (SEM.). Smear slides preparation followed standard techniques. In a preliminary publication, the planktonic foraminifera of Kalidonia section were also studied and some of the key species were reported and illustrated, but as subordinates to the nannoflora (compare Plate 2 in Frydas *et al.* 1999). The biostratigraphic schemes used are the "standard" zones of Martini (1971) and Okada and Bukry (1980). Additional useful bioevents and their biochronological calibration are based on Theodoridis (1984), Martini and Müller (1986), Young

et al. (1994), Raffi and Flores (1995), Fornaciari (2000), Lourens *et al.* (2004) and Raffi *et al.* (2003, 2006). A quantitative and subsequently semiquantitative study using the calcareous nannoplankton has been also performed. Quantification of species presented in Table 1, based on the following pattern: **A** (Abundant)= >20 individuals (measuring 100 specimens), **C** (Common)= 11-20, **F** (Few)= 6-10, **R** (Rare)= 2-5 and **P** (Present)= 1 individual/smear slide.

4. Results

4.1. Lithostratigraphy and biofacies

In the last years, a new concept concerning facies and sedimentary architecture for the neogene deposits of NW Crete has been developed. Therefore, facies terminology of the present work and their subdivision in broad follows that of Frydas and Keupp (1996), Bellas *et al.* (1998, 2000) and Keupp and Bellas in collab. with Frydas and Bartholdy (2000).

According to this concept three mainly depositional lithofacies, which compose the ca. 32 meters thick Kalidonia section, are recognized in the studied section (Fig. 2):

Unit-1. (Deep Water Facies or **–DWF-**). At the base, grey, amorphous, homogenous, slightly sandy marls about 17 meters thick, are overlain by 8 meters of slightly laminated marls and claystones of middle/outer shelf to slope or mesopelagic environment. When alternate, the former marls are generally considered to correspond to insolation minima, while the later one to insolation maxima (Krijgsman, *et al.* 1999). This facies is correlated to the former "Kissamou Formation" after Freudenthal (1969). It is followed upwards by:

Unit-2. (Transitional Facies or **–TF-**). Yellowish sandy marls (~2 meters thick) and a sandstone bank (1 meter thick), point to the transition from shelf sediments to shallow-water, neritic environment. The **TF** is correlated to the former "Cherethiana Formation" after Freudenthal (1969).

Lithofacies of Unit-2 exhibits important fossil elements, like Brachiopods of the Genus *Terebratula* sp., abundant Pectenidae and a significant biohorizon of the benthic foraminifer *Heterostegina* sp.. Freudenthal (1969) firstly reported on the *Heterostegina* massive banks of the former "Roka Formation". However, the later occurrences are referred to the transgressive littoral facies **LF-A (LF-At, t** for transgressive) and characterize the basal neogene sediments (in our case of Tortonian age) deposited in the NW Crete basins, while the frequent occurrences of *Heterostegina* bioevent recorded in Unit-2 of Kalidonia section, are referred to the regressive littoral facies **LF-A (LF-Ar, r** for regressive) or to the **TF** of the above basins and depict a pre-commence of the so-called "Messinian Event" of middle-upper Messinian age.

Unit-3. (Reefal-bioclastic Facies or **–RF-**). The section closes at the top with a caprock consisting of the recently described reefal-bioclastic limestones facies, which is placed in the upper, regressive, littoral facies Type A (part of **LF-A**, in Bellas *et al.* 1998).

The **RF** in Kalidonia (Unit-3) is about 3.5m thick and it is partly correlated to the former "Roka Formation" after Freudenthal (1969). It is rich in macrofossils like Corallinaceae (*Lithothamnium*), scleractinian Corals (*Tarbellastraea* sp., *Porites* sp.), Tentaculats (cyclostome Bryozoa, *Terebratula sinuosa*), Cirripeds (*Pyrgomma* sp.), Molluscs (*Glycimeris* sp., *Lithophaga* sp., diverse pectinids and molds of gastropods), and Echinoids (*Schizechinus* sp., *Clypeaster* sp.). The **RF** is characteristic for deposition during onset of the well-known Mediterranean Messinian Salinity Crisis, which mainly affected the margins and the highly uplifted blocks (Plakalona case) of the basins in the studied area. Similar marine algal limestones were reported from the marginal Late Messinian Sea in Spain, Tunisia, western Sinai and central Crete (Sonnenfeld 1985, our unpublished data).

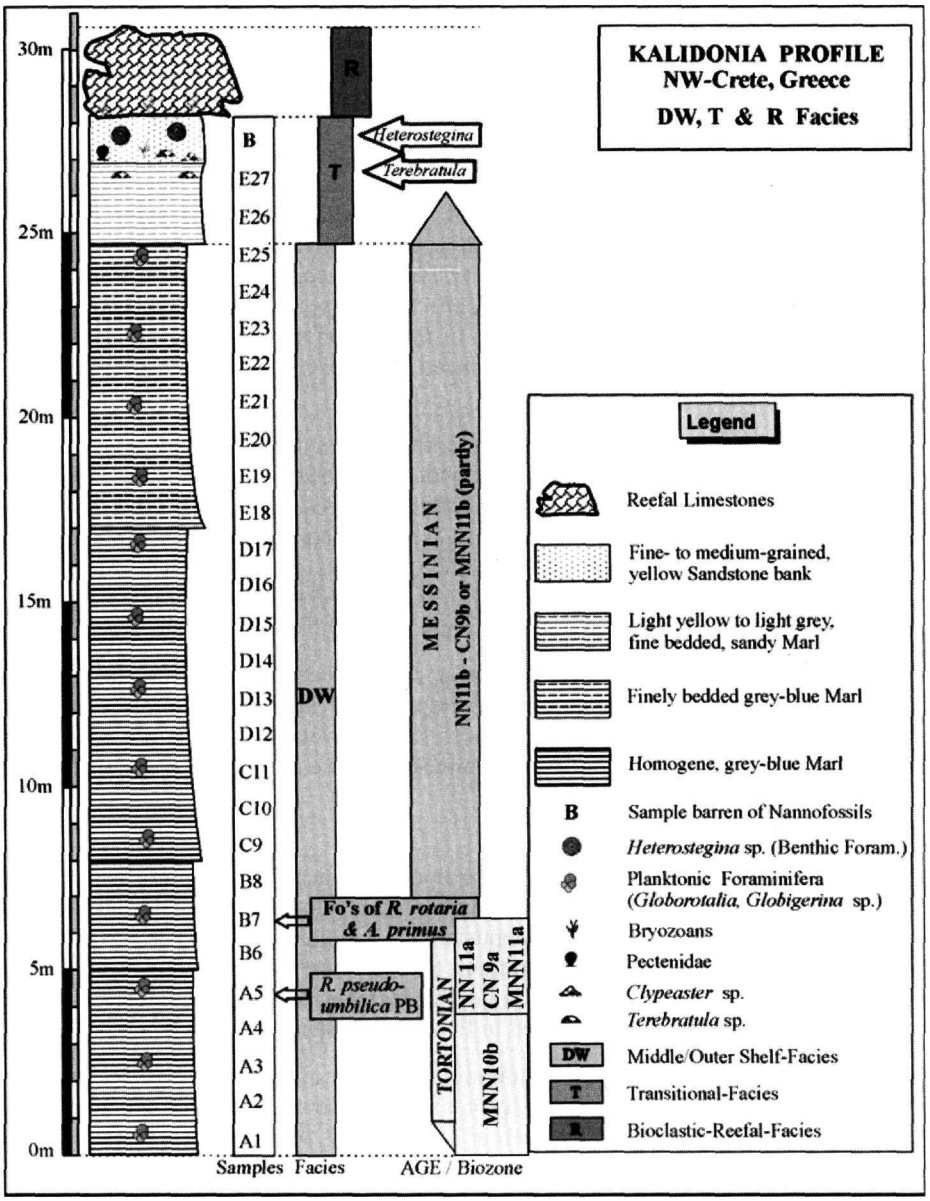

Figure 2 – Lithostratigraphy, facies and key biostratigraphic events of calcareous nannofossils along Kalidonia section

The whole succession of the three above-mentioned litho-biofacies generally points to a regressive sequence, developed from deep marine at the base (Unit-1), to shallow-water (Unit-2) and further to pure littoral deposits at the top (Unit-3). It belongs to the first sedimentation cycle (A) of Late Miocene age (Frydas and Keupp, 1996; Kontopoulos *et al.* 1996).

4.2. Calcareous nannofossils biostratigraphy

4.2.1. Late Miocene calcareous nannofossil biozones

According to the preliminary study (based on a first set of five samples) of the calcareous nannofossils of Kalidonia section (Frydas *et al.* 1999, Keupp and Bellas in collab. with Frydas and

Bartholdy 2000), their association was placed in the **CN9** biozone (= *Discoaster quinqueramus*) sensu Okada and Bukry (1980) "Low-latitude biostratigraphic zonation", or to the equivalent and homonymous of it **NN11** zone of "Standard Nannofossil Zonation" (Martini 1971). The latter zone was primary defined on the basis of the total range of *D. quinqueramus*.

Okada and Bukry (1980) subdivided the CN9 Zone in CN9a and CN9b by use of *Discoaster berggrenii* and/or *Discoaster surculus* occurrences. Martini and Müller (1986) also subdivided the NN11 in NN11a and NN11b, by the presence of *Amaurolithus delicatus* at the base of the last subzone. Theodoridis (1984) developed another biozonation scheme for the Mediterranean Miocene CN9 Zone, where three zones (*Coccolithus pelagicus*, *Amaurolithus primus* and *Reticulofenestra rotaria*) and one subzone (*Calcidiscus leptoporus* Zone MA) were distinguished. First Occurrence of *A. primus* defined the base of the homonymous species Zone, while a small interval (that of *R. rotaria* Zone) was introduced by presence/disappearance of this species (base/top of homonymous Zone).

A further attempt to biostratigraphically refine the important stratigraphic period of Late Miocene was made by Raffi and Flores (1995). They subdivided the CN9b into three parts; CN9bA, CN9bB and CN9bC, by using the FO and LO of *Amaurolithus amplificus* (now *Nicklithus amplificus* sensu Raffi *et al.*, 1998) as defining the base and top of CN9bB. According to recent studies by Hilgen *et al.* (2000), the *Amaurolithus amplificus* s.s. FO postdates the Tortonian/ Messinian (T/M) boundary. Since this species was not identified in the studied samples (compare also Fornaciari, 2000), the above tripartite subdivision of CN9b is not applicable in this paper.

Recently, Raffi *et al.* (2003) proposed for the upper Miocene five out of seventeen selected biohorizons of calcareous nannofossils as easily reproduced in the Mediterranean and out of it, which as they stated, were also considered useful for correlations to worldwide stratigraphy. Among them, four could be incorporated and commented in the present study.

4.2.2. Biostratigraphic results

The calcareous nannofossils of the Kalidonia section are generally well preserved, comprising a total of 47 different species, but are represented in low abundances. In the upper part of the section, due to the littoral character of the deposits (TF; samples E25-E27), the assemblage is not considered original. Late Miocene most important taxa have been identified and reported in Table 1. In the following it will be commented on key biohorizons of selected species from Kalidonia section, as they have been mainly recognized in E. Mediterranean by Raffi *et al.* (2003, 2006).

Discoaster pentaradiatus is exceptionally found common in only one sample by the base of the Kalidonia section; otherwise, this species is sporadically present and generally occurs in very low abundances. Therefore, the proposed by Raffi *et al.* (2003) *D. pentaradiatus* FCO (First Common Occurrence), defining the base of Zone MNN10b, is not recognized in the present work.

Both, *D. berggrenii* and *D. quinqueramus*, the key species of CN9 Zone, are present along the section (samples A1 to E24) although inconsistently.

The *Reticulofenestra pseudoumbilicus* PB is easily recognizable and can be placed at the stratigraphic level of samples interval A4 to A5, where the species after a constant presence from the base of the section upwards (samples A1 to A5), disappears or after a small recover in samples B7 and B8, is simply present as rare specimens to the top of the section.

In Kalidonia section, first *Amaurolithus*, although rare, together with *R. rotaria*, have been both recorded at the level of sample B7 onward (Table 1), therefore indicating the CN9a/CN9b, NN11a/NN11b and MNN11a/ MNN11b subzonal boundary and subsequently the T/M boundary.

These nannofossil events make possible an important assignment of the lower part of Kalidonia section (samples A1-B6) at the upper Tortonian zones NN11a/CN9a, while the sediments which bound sample B7 to the Tortonian/ Messinian boundary and the rest of the succession is placed to

the lower Messinian zone NN11b/CN9b (samples B7 to E24). *R. pseudoumbilicus* size ranged from greater than 8 μm at the base, to less than 7 μm at the top and the scarcity of it upsection, are additional bioevents that also support our previous results (co. also Young 1990, Huang 1997). The T/M boundary coincides with sample level B7. Lithostratigraphically, above sample E24 sedimentation firstly changes to littoral type and later commences a transition (TF) to the RF deposition, pointing to the onset of the salinity crisis Messinian event in the Mediterranean. The RF facies relatively corresponds to the base of the 'Calcare di Base' dated at 5.95 Ma by Hilgen *et al.* (1995) or at 5.96±0.02 Ma by Krijgsman *et al.* (1999).

Summarizing, the following bioevents of calcareous nannofossils are well documented and provide a useful and reliable stratigraphical framework applicable to the Kalidonia section. They are listed from the base of the section onwards below. **a)** Occurrence of both *D. berggrenii* and *D. quinqueramus* (NN11a, CN9a), **b)** common occurrence of *R. pseudoumbilicus*, followed by **c)** PB (paracme beginning) of it (base of MNN11a), **d)** Common FO's at the same stratigraphic level of both *A. primus* and *R. rotaria* (~T/M boundary and NN11b, CN9b, MNN11b) and **e)** almost consistent presence of *D. quinqueramus* to the section upward and possible top occurrences of both *D. berggrenii* and *D. quinqueramus* (E24 sample). It follows an almost barren interval of calcareous nannofossils, prior to the Reefal Facies (RF) development at the top of the section.

5. Discussion

Considering the Kalidonia section, *D. berggrenii* was observed in low abundances at the base of the Kalidonia section and *D. quinqueramus* was simply present in the samples of the section upwards to the top. As Wei (2003) pointed out, major disagreements exist on the taxonomical concepts used by various authors for these species. Both of them characterize the NN11/CN9 zone of calcareous nannofossils. The ages of 8.5 Ma and of 8.2 Ma were assigned to the FO datums of *D. quinqueramus* and *D. berggrenii berggrenii* respectively (EXXON core in the Gulf of Mexico, Wei, 2003). The datum of the top of *D. berggrenii* roughly calibrated at ~6.2 Ma by the previous author. The *D. quinqueramus-berggrenii* intergrade appears slightly later (is relatively younger in age). It is reported by Rio *et al.* (1990) to have gradationally evolved from *Discoaster bellus* (Young *et al.* 1994). The *D. bellus* is inconsistently represented in low abundances along the section. Based on the specimens' rarity and preservation state, we consider at least the uppermost two occurrences of them to be reworked (samples E24 & E25).

Since *D. pentaradiatus* occurs sporadically and in very low abundances along Kalidonia section, its FCO (calibrated at 9.37 Ma by astronomically induced sedimentary cycles by Raffi *et al.* 2003) cannot be identified. Obviously this event stratigraphically predates commence of deposition of the section basal layers in Kalidonia basin.

According to Raffi *et al.* (2003, 2006) and Lourens *et al.* (2004), the event of *R. pseudoumbilicus* PB (Paracme Beginning) characterizes the base of Zone MNN11a, with an absolute age of 8.76 or 8.71 Ma respectively. Young (1998), Fornaciari (2000), Kameo and Bralower (2000) and Marino and Flores (2002) report on this event too. According to the latter, this paracme interval incorporates the base of NN11b, although others place it to the upper part or only the base of CN8b (Fornaciari 2000, Kameo and Bralower 2000). We have also identified the paracme interval of *R. pseudoumbilicus* in the Potamidha section of NW Crete (Schmidt 1979: fig. 1, p. 169, 188), where it is obvious that the abundance of this species dramatically reduces at the upper stratigraphic intervals to the top of the section (late part of II, III and IV). This is well correlated with the interval starting with the so-called *R. pseudoumbilicus* PB by Raffi *et al.* (2003).

The reliability of events related to the genus *Amaurolithus* was confirmed by Negri and Villa (2000) for Cretan sections, as well as by Raffi *et al.* (2003, 2006) on a combined study of various sections and holes. *Amaurolithus* spp. and/or *A. primus* FO (First Occurrence) biohorizon is equivalent to the base of Subzone MNN11b and it is calibrated at 7.46-7.47 Ma (Qued Akrech

section of Morocco; Hilgen *et al.* 2000), at 7.430-7.435 Ma (Faneromeni section of SE Crete; Negri and Villa 2000), or somewhat younger at 7.424 Ma (E. Mediterranean; Raffi *et al.* 2006). These species FO's slightly predate the Tortonian/Messinian (T/M) boundary in Mediterranean Neogene. They are the closest nannofossil bioevents corresponding to the T/M boundary, which is defined by the FAD of the foraminifera grouped as *Globorotalia conomiozea*. The T/M boundary level in Morocco was astronomically dated at 7.251 Ma, found in the middle of the reversed Subchron C3Br.1r (Hilgen *et al.* 2000). According to these authors, all above *Amaurolithus* group events (including the *A. delicatus* FO, not mentioned here), predate the T/M boundary and are considered "extremely useful" to delimit it on a global scale. The T/M datum in the Mediterranean was initially placed at 7.24 or at 7.12 Ma by Hilgen *et al.* (1995) and Krijgsman *et al.* (1995) respectively, but recently it has been dated at 7.246 Ma (Lourens *et al.* 2004, Raffi *et al.* 2006).

Raffi *et al.* (2003) stated that the *R. rotaria* FO and FCO are not reliable events, not improving the biostratigraphic resolution by calcareous nannofossils. Despite that, Negri and Villa (2000) had pointed out the usefulness of this event, especially in onland sections, like that of Faneromeni in SE Crete and considering the nannofossil events across the Tortonian/Messinian boundary. *R. rotaria* is a circular but distinctive variant of *R. pseudoumbilicus*, relatively easy to identify and it is reported from CN9b subzone by many authors like Theodoridis (1984), Flores *et al.* (1992), Young (1994), Bellas *et al.* (1998, 2000), Siesser and Kaenel (1999), Duermeijer *et al.*, (1999), Hilgen *et al.* (2000), Keupp and Bellas, in collab. with Frydas and Bartholdy (2000) and Raffi *et al.* (2003, 2006). It is true that *R. rotaria* may not be always present (or better identified) in all studied sections in the Mediterranean till now, however if it is recognized once, then is very important as biohorizon (proved both in Faneromeni and in present case of NW Crete onland sections). Notably, the FO and the FCO of *R. rotaria* are differently dated at 7.421 and 7.264 Ma respectively (Negri and Villa 2000) or recently at 7.41 and 7.24 Ma (Lourens *et al.* 2004). Therefore, *A. primus* FO predates the occurrence of *R. rotaria* by a difference of ~0.01 Ma. In our samples set, *A. primus* and *R. rotaria* occur both at the same stratigraphic level (sample B7). It seems that the samples resolution interval along Kalidonia section (ca. 0.90 m) was low and not enough to distinguish these events from one another. Hilgen *et al.* (2000) study of the classic Messinian Moroccan Oued Akrech section (Atlantic Morocco), correlated *A. primus* FO with an age ranging between 7.470 and 7.466 Ma, dates which are obviously older than those obtained from eastern Mediterranean (7.424 Ma according to Raffi *et al.* 2006). According to Theodoridis (1984: 48, fig. 44), the occurrence of *R. rotaria* can be in part correlated to the lowermost part of the CN9b subzone of Okada and Bukry (1980), a fact further supporting our data.

6. Conclusions

The Kalidonia section, a type profile of the Neogene Kalidonia sedimentary basin was used for a biostratigraphic study of late Miocene deposits in the eastern Mediterranean Sea. New nannofossil data and development of the science (integration of magneto-, cyclo-, and biostratigraphy) make easier the age calibration of Kalidonia as well as correlations with assignments of bioevents from the Mediterranean and the Atlantic Morocco where major disturbance took place at the entrance of the ocean water to the Mediterranean during most of the upper Messinian.

The calcareous nannofossil distribution pattern is well documented. It shows a high paleo-biodiversity and good preservation but scarcity of the key species in the Deep Water Facies (DWF, Unit-1). Presence from the base upwards of *D. berggrenii* and *D. quinqueramus* defines the NN11 or the equivalent of it CN9 Zones of Upper Miocene age for the studied section. Both species range almost to the top, where due to factors of sensitivity to carbonate dissolution in shallow-waters they disappear (Transitional and Reefal Facies, TF & RF, Units -2, -3).

Table 1 – Semiquantitative distribution and biozones of calcareous nannofossils in Kalidonia section

Samples Number - Species	*Amaurolithus primus*	*Braarudosphaera bigelowii*	*Calcidiscus leptoporus*	*Calcidiscus macintyrei*	*Coccolithus pelagicus*	*Coccolithus miopelagicus*	*Cryptococcolithus takayamae*	*Dictyococcites antarcticus*	*Dictyococcites productus*	*Discoaster adamanteus*	*Discoaster asymmetricus*	*Discoaster bellus*	*Discoaster berggrenii*	*Discoaster brouweri*	*Discoaster calcaris*	*Discoaster challengeri*	*Discoaster intercalaris*	*Discoaster moorei*	*Discoaster pansus*	*Discoaster pentaradiatus*	*Discoaster quinqueramus*	*Discoaster quinqueramus-berggreni*	*Discoaster surculus*	*Discoaster variabilis*	*Geminilithella jafari*	*Geminilithella rotula*	*Hayaster perplexus*	*Helicosphaera carteri*	*Helicosphaera orientalis*	*Helicosphaera pacifica*	*Helicosphaera stalis ovata*	*Helicosphaera stalis stalis*	*Helicosphaera sellii*	*Holodiscolithus macroporus*	*Pontosphaera* spp.	*Reticulofenestra minutula*	*Reticulofenestra pseudoumbilicus*	*Reticulofenestra rotaria*	*Rhabdosphaera clavigera*	*Rhabdosphaera procera*	*Scapholithus fossilis*	*Scyphosphaera* spp.	*Sphenolithus abies*	*Sphenolithus morjformis*	*Sphenolithus verensis*	*Syracosphaera pulchra*	*Syracosphaera* sp.	BIOZONES
E27			R	R	P	P		P	A															A	P		R		P							R				F			P	R	
E26			F	P	C			C	A															A	F		C									P				C				P	
E25			C	R	R			F	A	P		P		P									R	A	C		A	P	P						R			R		R	P	F				P	
E24			R	F	P			R	A	P	P	P	P	R				P	P	P	P	P	P	R	A	F		C	P	R				P	R		R	C		F		C	P		R	F	
E23	P		C	R				R	A	P			P	P		P			P	P	P	P		R	A	A		C							R	P			C		F		C		P		P	
E22			F	R	R	P		F	A	P			P	P		P			R	P		P	P	R	A	A	P	C		R		P			R		P		C				C		P		F	
E21			F	R	R			F	A																A	C		C		R		P			R	R		C				C				R	
E20			F	F	R			C	A	P	P			R		P			P	P	P			P	A	C		F	P					P	R	R		F		F		C				F	
E19		P	F	F	R		R	C	A	P	P			P		P					P			P	A	F	R	C		P					R	R		F		R	P	C			P	R	
E18	P		F	R					A	P			P				P		P	P	P	P	P	P	A	C	P	A	R	R					P			C			P	C				R	
D17			R	F	R			C	A	R			P	R		P			P	P	P			P	A	F		C		P				P	R		R	F		P	F	P	P	R	R	
D16	R		R	C	F			R	A	P				P		P					R	P	P	P	A	F		F	P					R	P			F		R	C		P	P	R	
D15			P	F	C			F	A	P						P								P	A	F	P	C	P					P	R			C			F				F	
D14			P	F	R			A	A	P				R		P		P	P	P			P	P	A	F		F						F	R		P	F		R	P	F				F	
D13			R	R	R		P	A	A	P			P	R		P			P	P				P	A	F	R	C							P			F				F				F	
D12		P	R	F	R				A	P				R	P				P	P	P	P		P	A	C		C	R		P		P		P			C		R	R	C				F	
C11			F	F	R			R	A	P				R		P			P	P	P		P	P	A	C		C		P			P			P	R		R		F	R				R	
C10			R	F	P	P		R	A	P			P	R		P	P		P	P	P		P	P	A	F		C	R	P					P		C		F	P	C	P		P	R	
C9	P		R	C	R				A	P				P		P			R	R				R	A	C		C						R	R			F		C		C			P	R	
B8	P		R	R	F		P	F	A	P	P					P			P	P			P	P	A	F		C	P						R	P	C	C		R		C				R	
B7	P		R	F	R		P	F	A	P			P	P		P		R	P	P		P		R	A	R		C							R		C	P	R		R	R	C		P	P	P	
B6			R	P	R			P	A	P			P	P		P			P	P	P			R	A	C	P	F	P	P			P	R	R		F		F	R	C		R	P	F	
A5			F	R	R			R	A	P			P			P			P	P	P			R	A	R	P	C		R				R	F		F		R	P	C	P	P	R	R	
A4			R	F	F			A	A	P			P	P		P			R	R			P	R	A	R		F							R	C		R		F	R	F			P	R	
A3			R	F	F	P	P	F	A	P				P		R			R	R			P	P	A	F		F	R		P	P		P	R	F		C		R	P	A		P	R	R	
A2			F	R	R			R	A	R		P	P	P		P		P	R					R	A	F		C							R	A		F		P		C				P	R	
A1			P	R	P	P		R	A	P		P	P	P		P	P		P	C	P		P	P	A	C		A							R	C		F	P	R	P	C			P	R	

NN11a - CN9a - MNN11a

MNN10b

NN11b or CN9b or MNN11b (partly)

In Kalidonia section the interval starting with the *R. pseudoumbilicus* PB bioevent (Paracme Beginning) is easily recognizable and can be placed at the stratigraphic interval between samples (s.) A4 and A5 (located at ca. 4-5 meters from the base of the section upwards). This event marks the base of MNN11a subzone. It is dated and astronomically calibrated at 8.761 Ma, well correlated with that proposed by Raffi *et al.* (2003, 2006) for the Mediterranean Sea. Large *Reticulofenestra* (>7 μ) specimens were never fully recovered. Reappearance of this species was rare and inconsistent up to the top of the section (Table 1).

Integrated biostratigraphy correlate the FO of *A. primus* (including the *Amaurolithus* spp.) and that of *R. rotaria*. It is possible to find both events at the same stratigraphic level together, due to close ages of both biohorizons (7.42 and 7.41 Ma respectively, Lourens *et al.* 2004, Raffi *et al.* 2006) if sampling resolution is low as in our case. In the above context, the lowermost part of Unit-1 (s. A1-A4) is placed in the upper part of MNN10b subzone. The calcareous nannofossil assemblage of s. A5 to B6 is biostratigraphically placed in the CN9a (or the equivalent NN11a, MNN11a) subzones, while the upper part of Unit-1 (s. B7 to E24) is placed in the CN9b (or the NN11b, MNN11b) subzones.

The commencement of sedimentation in Kalidonia basin cannot be exactly evaluated but it can be placed in the time interval between 9.37 Ma (*D. pentaradiatus* FCO) and 8.761 Ma (*R. pseudoumbilicus* PB), being closest to the latter datum. Deep water sedimentation in the basin lasted to about 6.1-6.2 Ma (*D. berggrenii berggrenii* top or LO datum, located at level of sample E24).

The caprock of Kalidonia section consists of bioclastic, karstified limestones and coral-reef remnants. Considering the base of this reefal facies (RF), which characterizes the synchronous onset of the Messinian salinity crisis (Krijgsman *et al.* 1999), relatively equivalent to the 'Calcare di Base' in Italy, an age of ca. 5.960±0.02 Ma can be inferred. Subsequently the Units-1 and -2 of Kalidonia section (measuring 28 meters in thickness, including compaction) cover deposition between 3.41 and 2.80 Ma, plus the unknown time demand for development of the RF (regressive Unit-3). An average sedimentation rate of ca. 1.11 cm/kyr is calculated for the deposition of the lower two lithostratigraphic units in Kalidonia basin during the Late Miocene.

7. Aknowledgments

The DFG (Deutsche Forschungsgemeinschaft) is specially thanked for financial support to H.K. and S.B., while the latter was Research Assistant in Berlin. FU-Berlin (Free University, Paleontology Institute) permission was necessary for laboratory and instrumental (S.E.M.) research work. Mrs. A. Hoernig-Pint helped a lot in the field during her Diplom-work. Review comments by M. Triantaphyllou (Athens) and A. Di Stefano (Catania) improved the original manuscript.

8. References

Angelier, J., 1979. Néotectonique de l'arc égéen, *Soc. Géol. Nord, Spéc. Publ.*, 3, 418pp.

Angelier, J., Lyberis, N., Le Pichon, X., Barrier, E., and Huchon, Ph., 1982, The tectonic development of the Hellenic arc and the sea of Crete: a synthesis, *Tectonophysics*, 86, 159-196.

Bellas, S., Keupp, H., and Frydas, D., 1998a. The first Neogene (Upper Miocene) marine Transgressional-Regressional cycle of NW. Crete. Evidence based on sedimentologic and biostratigraphic data, *15th Intern. Sedimentol. Assoc. Conf. (IAS98),* Alicante/Spain, 13-17 April, 182-183.

Bellas, S.M., Keupp, H., and Frydas, D., 2000. Nannofossil biostratigraphy of the Late Miocene marine sedimentary sequences from NW Crete Island, Greece, *Spec. Publ. Geol. Soc. Greece*, 9, 9-18.

Christodoulou, G., 1963. Geologische und mikropalaeontologische Untersuchungen im Neogen der Insel Kreta, *Habilitation*, Athens, University of Athens, 157pp.

Dermitzakis, M.D., and Markopoulou-Diakantoni, A., 1979. Stratigraphy and macrofauna of the Neogene deposits in Kastelli Kissamou district (W. Crete), *VIIth International Congress on Mediterranean Neogene,* Athens 1979, *Ann. Géol. Pays Hell.*, hors série, A, 1, 317-328.

Dewey, J.F., and Sengör, A.M.C., 1979. Aegean and surrounding regions: complex multiplate and continuum tectonics in a convergent zone, *Bull. Geol. Soc. Am.*, 90, 84-92.

Dixon, J.E., and Robertson, A.H.F., 1984. The geological evolution of the eastern Mediterranean, *Geological Society Spec. Publication*, 17, London, Blackwell, 824pp.

Duermeijer, C.E., Krijgsman, W., Langereis, C.G., Meulenkamp, J.E., Triantaphyllou, M.V., and Zachariasse, W.J., 1999. A Late Pleistocene clockwise rotation phase of Zakynthos (Greece) and implications for the evolution of the western Aegean arc, *Earth Planet. Sci. Lett.*, 173, 315-331.

Flores, J.A., Sierro, F.J., and Glacon, G., 1992. Calcareous plankton analysis in the pre-evaporitic sediments of the ODP Site 654 (Tyrrhenian Sea, Wesetrn Mediterranean), *Micropaleontology*, 38(3), 279-288.

Fornaciari, E., 2000. Calcareous nannofossil biostratigraphy of the California Margin. In M. Lyle, I. Koizumi, C. Richter and T.C.Jr. Moore (eds), *Proc. O.D.P., Sci. Results*, 167, 3-40, College Station TX.

Freudenthal, T., 1969. Stratigraphy of Neogene deposits in the Khania province, Crete, with special reference to foraminifera of the family Planorbulinidae and the genus *Heterostegina, Utrecht Micropal. Bull.*, 1, 1-208.

Frydas, D., and Keupp, H., 1996. Biostratigraphical results in Neogene deposits of NW Crete, Greece, based on calcareous nannofossils, *Berliner geowiss. Abh.*, E 18, 169-189.

Frydas, D., Keupp, H., and Bellas, S., 1999. Biostratigraphical research in Late Neogene marine deposits of the Chania Province, western Crete, Greece, *Berliner geowiss. Abh.*, E30, 55-67.

Hilgen, F.J., Krijgsman, W., Langereis, C.G., Lourens, L.J., Santarelli, A., and Zachariasse, W.J., 1995. Extending the astronomical (polarity) scale into the Miocene, *Earth Planet. Sci. Lett.*, 136, 495-510.

Hilgen, F.J., Bissoli, L., Iaccarino, S., Krijgsman, W., Meijer, R., Negri, A., and Villa, G., 2000. Integrated stratigraphy and astrochronology of the Messinian GSSP at Qued Akrech (Atlantic Morocco), *Earth Planet. Sci. Lett.*, 182, 237-251.

Huang, L., 1997. Calcareous nannofossil biostratigraphy in the Pearl River Mouth Basin, South China Sea and Neogene reticulofenestrids coccolith size distribution pattern, *Mar. Micropaleontol.*, 32, 31-57.

Jackson, J., 1994. Active tectonics of the Aegean Region, *Ann. Rev. Earth Planet. Sci.*, 22, 239-271.

Kameo, K. and Bralower, T.J., 2000. Neogene calcareous nannofossil biostratigraphy of Sites 998, 999 and 1000, Caribbean Sea. In R.M. Leckie, H. Sigurdsson, G.D. Acton and G. Draper (eds), *Proc. O.D.P., Sci. Results*, 165, 3-17, College Station TX.

Keupp, H., Bellas, S., in collab. with Frydas, D., and Bartholdy, J., 2000. Neogene development of the sedimentary basins of NW Crete Island, Chania Prefecture, South Aegean Arc System (Greece), *Berliner geowiss. Abh.*, E34, 3-117.

Kontopoulos, N., Zellilidis, A., and Frydas, D., 1996. Late Neogene sedimentary and tectonostratigraphic evolution of northwestern Crete Island, Greece, *N. Jb. Geol. Paläont. Abh.*, 202(3), 287-311.

Krijgsman, W., Hilgen, F.J., Langereis, C.G., Santarelli, A., and Zachariasse, W.J., 1995. Late Miocene magnetostratigraphy, biostratigraphy and cyclostratigraphy in the Mediterranean, *Earth Planet. Sci. Lett.*, 136, 475-494.

Krijgsman, W., Hilgen, F.J., Raffi, I., Sierro, F.J., and Wilson, D.S., 1999. Chranology, causes and progression of the Messinian salinity crisis, *Nature*, 400, 652-655.

Le Pichon, X., 1982. Landlocked oceanic basins and continental collision: the eastern Mediterranean as a case example. In K. Hsü (ed.), "*Mountain Building processes*", 201-211, London, Academic Press.

Lourens, L., Hilgen, F.J., Shackleton, N.J., Laskar, J., Wilson, D., 2004. The Neogene Period. In F.M. Gradstein, J.G. Ogg and A.G. Smith (eds), "*A Geological Time Scale 2004*", 409-440, Cambridge, Cambridge University Press.

Makris, J., 1978. The crust and upper mantle of the Aegean region from deep seismic soundings, *Tectonophysics*, 46, 269-284.

McKenzie, D., 1970. The plate tectonics of the Mediterranean region, *Nature*, 226, 239-243.

Marino, M., and Flores, J.A., 2002. Miocene to Pliocene calcareous nannofossil biostratigraphy at ODP Leg 177 Sites 1088 and 1090, *Mar. Micropaleontol.*, 45, 291-307.

Martini, E., 1971. Standard Tertiary and Quaternary nannoplankton zonation. In Farinacci A. (ed.), *Proc. IInd Planktonic Conference*, Roma (1970), Tecnoscienza, II, 739-777pp.

Martini, E., and Müller, C., 1986. Current Tertiary and Quaternary calcareous nannoplankton stratigraphy and correlations, *Newsl. Stratigr.*, 16 (2), 99-112.

Mascle, J., Jongsma, D., Campredon, R., Dercourt, J., Glacon, G., Lecleath, A., Lyberis, N., Malod, J.A., and Mitropoulos, D., 1982. The Hellenic margin from eastern Crete to Rhodes: preliminary results, *Tectonophysics*, 86, 134-147.

Meulenkamp, J.E., Dermitzakis, M., Georgiadou-Dikeoulia, E., Jonkers, H.A., and Böger, H., 1979. Field Guide to the Neogene of Crete, *Publ. Dept. Geol. Pal. Athens Univ.*, ser. A, 32, 1-32.

Meulenkamp, J.E., Wortel, M.J.R., van Wamel, W.A., Spakman, W., and Hoogerduyn Strating, E., 1988. On the Hellenic subduction zone and the geodynamic evolution of Crete since the late Middle Miocene, *Tectonophysics*, 146, 203-215.

Meulenkamp, J.E., van der Zwaan, G.J., and van Wamel, W.A., 1994. On Late Miocene to Recent vertical motions in the Cretan segment of the Hellenic arc, *Tectonophysics*, 234, 53-72.

Negri, A., and Villa, G., 2000. Calcareous nannofossil biostratigraphy, biochronology and paleoecology at the Tortonian/Messinian boundary of the Faneromeni section (Crete), *Palaeogeogr., Palaeoecol., Palaeoclimatol.*, 156(3-4), 195-209.

Okada, H., and Bukry, D., 1980. Supplementary modification and introduction of code numbers to the low-latitude coccolith biostratigraphic zonation (Bukry, 1973, 1975), *Mar. Micropaleontol.*, 5(3), 321-325.

Raffi, I., and Flores, J.-A., 1995. Pleistocene through Miocene calcareous nannofossils from eastern Equatorial Pacific Ocean. In: N.G. Pisias, L.A. Mayer, T.R. Janecek, A. Palmer-Julson and T.H. van Andel (eds), *Proc. of the O.D.P., Sci. Results*, 138, 233-286pp. College Station, TX.

Raffi, I., Backman, J., and Rio, D., 1998. Evolutionary trends of calcareous nannofossils in the Late Neogene, *Mar. Micropaleontol.*, 35, 17-41.

Raffi, I., Mozzato, C., Fornaciari, E., Hilgen, F.J., and Rio, D., 2003. Late Miocene calcareous nannofossil biostratigraphy and astrobiochronology for the Mediterranean region, *Micropaleontology*, 49(1), 1-26.

Raffi, I., Backman, J., Fornaciari, E., Pälike, H., Rio, D., Lourens, L., and Hilgen, F.J., 2006. A review of calcareous nannofossil astrobiochronology encompassing the past 25 million years, *Quaternary Science Reviews*, 25 (2006), 3113-3137.

Rio, D., Raffi, I., and Villa, G., 1990. Pliocene-Pleistocene calcareous nannofossil distribution patterns in the western mediterranean. In K.A. Kastens, J. Mascle, *et al.* (eds), *Proc. O.D.P. Sci. Results*, 107, 513-533pp, College Station, TX.

Schmidt, R.R., 1979. The calcareous nannofossils of the Potamidha section. In C.W. Drooger, *et al.*, Problems of detailed biostratigraphic and magnetostratigraphic correlation in the Potamidha and Apostoli sections of Cretan Neogene, *Utrecht Micropal. Bull.*, 21, 167-191.

Siesser, W.G., and de Kaenel, E.P., 1999. Neogene calcareous nannofossils: Western Mediterranean biostratigraphy and paleoclimatology. In R. Zahn, M.C. Comas and A. Klaus (eds), *Proc. O.D.P. Sci. Results*, 161, 223-237pp, College Station TX.

Sonnenfeld, P., 1985. Models of Upper Miocene Evaporitic genesis in the Mediterranean Region. In D.J. Stanley and F.-C. Wezel (eds), *Geological Evolution of the Mediterranean Basin.* 323-346pp, New York Berlin Heidelberg Tokyo, Springer-Verlag.

Theodoridis, S., 1984. Calcareous nannofossil biozonation of the Miocene and revision of the Helicoliths and Discoasters, *Utrecht Micropal. Bull.*, 32, 1-271.

Young, J.R., 1990. Size variation of Neogene *Reticulofenestra* coccoliths from Indian Ocean DSDP Cores, *J. Micropalaeontology*, 9(1), 71-86.

Young, J., 1998. Neogene. In P. Bown (ed.), *Calcareous Nannofossil Biostratigraphy*. 225-265, London, Br. Micropaleontol. Soc. Publ.

Young, J.R., Flores, J.-A., and Wei, W., 1994. A summary chart of Neogene nannofossil magnetobiostratigraphy, *Journal of Nannoplankton Research*, 16, 21-27.

Wei, W., 2003. Upper Miocene nannofossil biostratigraphy and taxonomy of EXXON core CH30-43-2 from the Gulf of Mexico, *Journal of Nannoplankton Research*, 25(1), 17-23.

Wortel, M.J.R., and Spakman, W., 1992. Structure and dynamics of subducted lithosphere in the Mediterranean region, *Proc. K. Ned. Akad. Wetensch.*, 95, 325-347.

Wortel, M.J.R., and Spakman, W., 2000. Subduction and slab detachment in the Mediterranean-Carpathian region, *Science*, 290, 1910-1917.

Δελτίο της Ελληνικής Γεωλογικής Εταιρίας τομ. XXXX, 2007
Πρακτικά 11ου Διεθνούς Συνεδρίου, Αθήνα, Μάιος 2007

Bulletin of the Geological Society of Greece vol. XXXX, 2007
Proceedings of the 11th International Congress, Athens, May, 2007

BIOTIC AND ABIOTIC EVENTS IN A SHALLOW CARBONATE PLATFORM (UPPER CRETACEOUS, SOUTH PYRENEAN MARGIN)

Caus E.[1], Albrich S.[1], Berástegui X.[2], Bernaus J. M.[3], Boix C.[1], and Villalonga R.[1]

[1] *Universitat Autònoma de Barcelona, Department of Geology (Paleontology), 08193-Bellaterra, Spain. esmeralda.caus@uab.es, sergi.albrich@campus.uab.es, carme.boix@campus.uab.es, raquel.villalonga@campus.uab.es*

[2] *Institut Geològic de Catalunya, Balmes, Barcelona-08006, Spain. xberastegui@igc.cat*

[3] *Oolithica Geosciences LTd., Lower Ground Floor 53/57 Rodney Rd. Cheltenham GL50 1HX. United Kingdom(present address: Statoil ASA, GEX N-AFR D5-FH, N-4035, Stavanger, Norway. JMBE@statoil.com*

Abstract

A detailed sedimentological and paleontological study of the Late Santonian-Late Campanian carbonate platform deposits of the Serres Marginals area (South margin of the Pyrenean Basin) has been performed. Three depositional shallow carbonate sequences have been distinguished (C1, C2 and C3). Within the shallow platform sequences moderate energy subtidal to intertidal, high energy sand-shoal, protected lagoon and restricted lagoon to lacustrine facies have been identified.
Key words: *Carbonate platform, larger foraminifera, Upper Cretaceous, South Pyrenean margin.*

Περίληψη

Πραγματοποιήθηκε μία λεπτομερής ιζηματολογική και παλαιοντολογική μελέτη των αποθέσεων ανθρακικής πλατφόρμας της περιοχής Serres Marginals (νότιο περιθώριο της λεκάνης των Πυρρηναίων) και αναγνωρίσθηκαν τρεις ακολουθίες ρηχών ανθρακικών αποθέσεων (C1, C2 και C3). Εντός των αποθέσεων ρηχής πλατφόρμας περιγράφονται ενδιάμεσης ενέργειας υποπαλιρροιακές έως ενδοπαλιρροιακές φάσεις, αβαθείς άμμοι υψηλής ενέργειας καθώς και λιμνοθαλάσσια έως λιμναία περιβάλλοντα.
Λέξεις κλειδιά: *ανθρακική πλατφόρμα, μεγάλα τρηματοφόρα, Ανώτερο Κρητιδικό, Νότιο περιθώριο των Πυρρηναίων.*

1. Introduction

Throughout most of the Cretaceous period, the area occupied nowadays by the Pyrenees was a deep and narrow furrow that extended between the Iberian and European plates. The palaeogeography of the Pyrenean gulf shows a basin with an east-west oriented axis (Pyrenean Basin), which extended from off-shore (Galicia, NW Spain) to the "Bassin de Beausset" (SE

France), and opened into the Atlantic Ocean (Bay of Biscay). Shallow carbonate and siliciclastic carbonate platforms developed on both sides of the deep basin within the neritic domain.

As the result of the collision between the Iberian and European plates (Pyrenean-Alpine Orogeny), that occurred from the late Cretaceous to Oligocene period the materials deposited in these platforms were deformed, fragmented, detached from their substrate and displaced northwards and southwards, respectively along the Pyrenean axis. Nowadays, they form a puzzle of small units separated by tens or hundreds of kilometres, which are sometimes unrelated to their neighbours.

In this scenario, the control of biotic and abiotic events occurring in the shallow carbonate platform of each unit makes it possible to reconstruct the stratigraphic sequences, and calculate the temporal and spatial setting of each unit in the Pyrenean Basin during the Upper Cretaceous period. The work has been restricted to the central part of the south Pyrenean margin (Serres Marginals thrust-sheet).

2. Geological setting

The Serres Marginals thrust sheet, together with the Bòixols and Montsec thrust sheets, constitute the south verging thrust sheets of the Upper Thrust Sheets unit (Muñoz *et al.* 1984) from the south-central Pyrenean unit (Seguret 1972) (Fig. 1). The main tectonic units are oriented almost in parallel to the Pyrenean basin axis, and document different palaeoenvironmental settings.

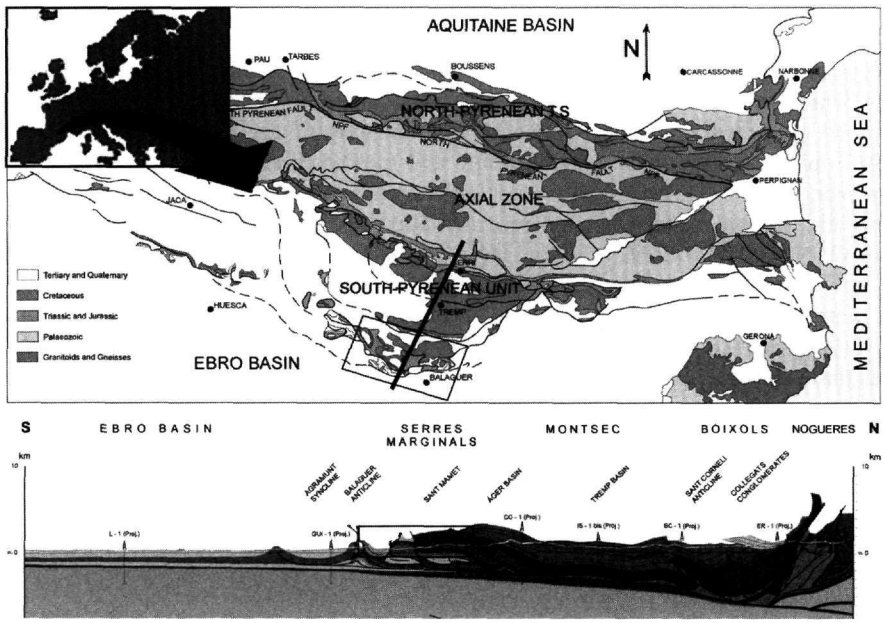

Figure 1 - General geological map of the Pyrenees. Black line indicates the ECORS profile, represented below. The squares indicate the Serres Marginals Unit, the studied area. (from Berástegui *et al.* 1993)

In the Pyrenees, the late Cretaceous deposits belong to two main tectonostratigraphic cycles (Berástegui *et al.* 2002). The lower cycle (late Cenomanian-early Santonian) corresponds to a transition phase, in which the Upper Cretaceous deposits reflect homogeneous and moderate subsidence, related to lithostratigraphical thermal contraction, after the initial extensional episodes that occurred during the Lower Cretaceous. During the upper cycle (late Santonian-Maastrichtian), the northern edge of the Iberian plate became a convergent margin, and the south margin of the Pyrenean basin registered a major change: the generation of a rapidly subsiding, terrigenous basin at the north of the studied area coeval with the growth of hanging-wall anticlines related to the

emplacement of early thrust sheets (Bòixols thrust sheet, Fig. 1). In the shallower areas of the basin (Montsec and Serres Marginals thrust sheets, Fig. 1), the sedimentary response started with a coastal onlap of platform carbonates, which developed into a shallow carbonate platform system that extended landwards beyond the former basin margins. A shift from the early convergence to more widespread compression provoked a shallowing-upwards, regressive tendency in the study area, which is reflected by marsh lignitiferous black marls and continental red beds ("Garumnian facies": late Campanian to middle Palaeocene), the base of which has deposits very rich in dinosaur bones and nests.

3. Material and methods

An interdisciplinary study where mapping, and detailed stratigraphical and sedimentological analysis were integrated with paleontological data derived mainly from larger foraminifera was made. Several regionally spaced sections, covering all palaeoenvironmental settings within the Serres Marginals thrust sheet have been measured. The section exemplified in Fig. 2, made in the Coscoll cliff (Fig. 3) is one of the best exposed and most representative.

The use of larger foraminifera instead of other groups of fossils or microfossils is for the following reasons: 1. Larger foraminifera are abundant and diverse in the studied platform sediments. They are represented by large discoidal and conical agglutinated foraminifera, porcellaneous foraminifera such as fabulariids and meandropsinids, and lamellar-perforated siderolitids, rotaliids and orbitoidids. 2. Larger foraminifera are huge unicellular organisms, whose shells, which were obtained by growth-steps, reflect the complex morphology and structures through ontogeny. Therefore, an accurate analysis of such microfossils makes it possible to separate time dependent characters, which can be used in biostratigraphy, from characters with an environmental meaning, which can be used to interpret the paleoenvironment (Hottinger 1978). 3. Larger foraminifera occupy all tropical to subtropical oligothrophic and mesotrophic neritic paleoenvironments from the littoral zone to the lower limit of the photic zone (limit of the larger foraminifera bearing symbionts), and the palaeogeographical reconstruction of the Western Tethys placed the studied area in the 32° N (Dercourt *et al.* 1985). 4. Most of the genera and/or species of larger foraminifera replaced each other over a short period of time. 5. The larger foraminifera are the only larger group of sallow-water fossils whose shells have sufficient diagnostic to be identified in thin sections to a taxonomic level of high-resolution biostratigraphic significance, and many shallow-water limestones that cannot be disaggregated by means of common methods.

4. Facies, Palaeoenvironment and Age

Lithologically, in the studied sections within the Serres Marginals thrust sheet, from bottom to top, the following units are distinguished: Les Serres Marginals sandy beds, Les Serres Marginals limestones and the "Garumnian" beds (Fig. 2).

4.1. Les Serres Marginals sandy beds

This unit overlies Jurassic sediments and is of a thickness varying from 55 to 76 m. It consists of yellow sandy limestones, sands, clays and sandstones interbedded with marly limestones, marls and calcarenites, which can be partially dolomitized. The faunal content is represented by some irregularly distributed rudists (radiolitids) and oyster banks, fragmented echinoids and a rich fauna of larger foraminifera (*Cuneolina cylindrica* Henson, *Pseudocyclammina sphaeroidea* Gendrot, *Dicyclina schlumbergeri* Munier-Chalmas, *Dictyopsella kiliani* Munnier-Chalmas in Schlumberger, *Accordiella conica* Farinacci, *Nezzazatinella picardi* Henson, *Meandropsina vidali* Schlumberger, *Nummofallotia cretacea* Schlumberger, *Lacazina elongata* Schlumberger, *Fascispira* sp., *Orbitokathina vonderschmitti* Hottinger). Caus and Gómez-Garrido (1989) suggested a Late Santonian age for this unit. It is interpreted to have been deposited in a shallow platform area with major important terrigenous input.

4.2. Les Serres Marginals limestones

The thickness of the unit varies from 100 to 300 m, and four types of facies have been recognised in every measured section.

4.2.1. Open marine carbonate facies

Light grey limestones and marly limestones (packstone-wackestone) organised on a decimetre to metre-scale. Marly interbeds of thickness of a few centimetres are commonly observed. The faunal content is composed of bryozoa, echinoids, larger and smaller foraminifera, some fragmented bivalves and red algae, and locally sponge spicules. Larger foraminifera are represented by three successive assemblages: Op-1) *Cuneolina cylindrica* Henson, *Pseudocyclammina sphaeroidea* Gendrot, *Dictyopsella* sp. (small and flat forms), *Fascispira* sp., *Nummofallotia cretacea* Schlumberger, *Praestorsella roestae* Visser, *Pararotalia tuberculifera* (Reuss), *Rotorbinella* sp., and *Praesiderolites douvillei* Wannier. Op-2) *Dictyopsella* sp. (small and flat form), *Fascispira* sp., *Nummofallotia cretacea* Schlumberger, *Praestorsella roestae* Visser, *Pararotalia sp., Praesiderolites dordoniensis* Wannier, *Orbitoides*? *concavatus* Rahaghi, *Lepidorbitoides* cf. *minima* Douvillé. Op-3) *Dictyopsella* sp. (small and flat form), *Fascispira* sp., *Praestorsella roestae* Visser, *Pararotalia sp., Praesiderolites sp., Pseudosiderolites* aff. *vidali* Douvillé, *Orbitoides*? cf. *concavatus* Rahaghi, *Neumannites granulosus* Rahaghi, *Vanderbeeckia* sp., *Lepidorbitoides* cf. *bisambergensis* Jaeger. These facies are interpreted as deposited in a subtidal to intertidal environment near fare weather wave base, with a moderate energy.

4.2.2. Sand-shoal, high energy facies

Grey and brown thick-bedded to massive bioclastic limestones that are highly rich in bryozoa, echinoids, rudists, red algae and larger foraminifera. Some fragmented corals are also present. Larger foraminifera are represented by three assemblages: Sh-1) *Abrardia catalaunica* Bilotte, *Orbitoides tissoti* Schlumberger, *Pseudosiderolites vidali* Douvillé (small forms). Sh-2) *Abrardia catalaunica* Bilotte, *Adrahentina iberica* Bilotte, *Biloculina fragilis* Hofker, *Orbitoides media* d'Archiac and *O. megaloformis* Papp and Küper (replaced each other in time), *Pseudosiderolites vidali* Douvillé, *Siderolites* aff. *calcitrapoides* Lamarck (primitive form), *Siderolites denticulatus* Douvillé (primitive form). Sh-3) *Orbitoides* cf. *gruembachensis* Papp, *Orbitoides*? *concavatus* Rahaghi, *Siderolites calcitrapoides* Lamarck, *Siderolites denticulatus* Douvillé, *Omphalocyclus macroporus* (Lamarck) (rare). The limestones correspond to grainstones and packstones, and they present large-scale cross-bedding. This kind of facies is the most wideespread in the studied area, and the biological and lithological features of the sediments indicate a deposition under moderate to high energy shallow water with an important reworking the bioclasts.

4.2.3. Protected lagoon, low-energy facies

These consist of well stratified grey to pale brown and commonly bioturbated marly limestones. Lithologically, they are formed by wackestones-packestones with abundant larger foraminifera, dasycladacean algae, rudists and some corals indicating a protected marine area. Larger foraminifera are represented by three successive assemblages: L-1) *Ilerdorbis decussatus* Hottinger and Caus, *Calveziconus lecalvezae* Caus and Cornella, *Abrardia catalaunica* Bilotte, *Cyclopsinella* aff. *steinmanni* Munnier-Chalmas, *Cyclolina* aff. *cretacea* D'Orbigny, *Broeckinella* sp., *Dicyclina schlumbergeri* Munnier-Chalmas, *Orbitokathina* sp., L-2) *Abrardia catalaunica* Bilotte, *Dicyclina schlumbergeri* Munnier-Chalmas, *Accordiella conica* Farinacci, *Nezzazatinella* sp., *Daviesina*? L-3) Nezzazatinella sp., conical agglutinated foraminifera with exoskeleton (beams), *Fascispira colom* Silvestri, *Omphalocyclus macroporus* (Lamarck), *Laffiteina* sp., *Daviesina* cf. *fleuriasi* Hofker. These facies are interpreted as deposited in a protected area (lagoon) behind the sand-shoal facies (4.2.2).

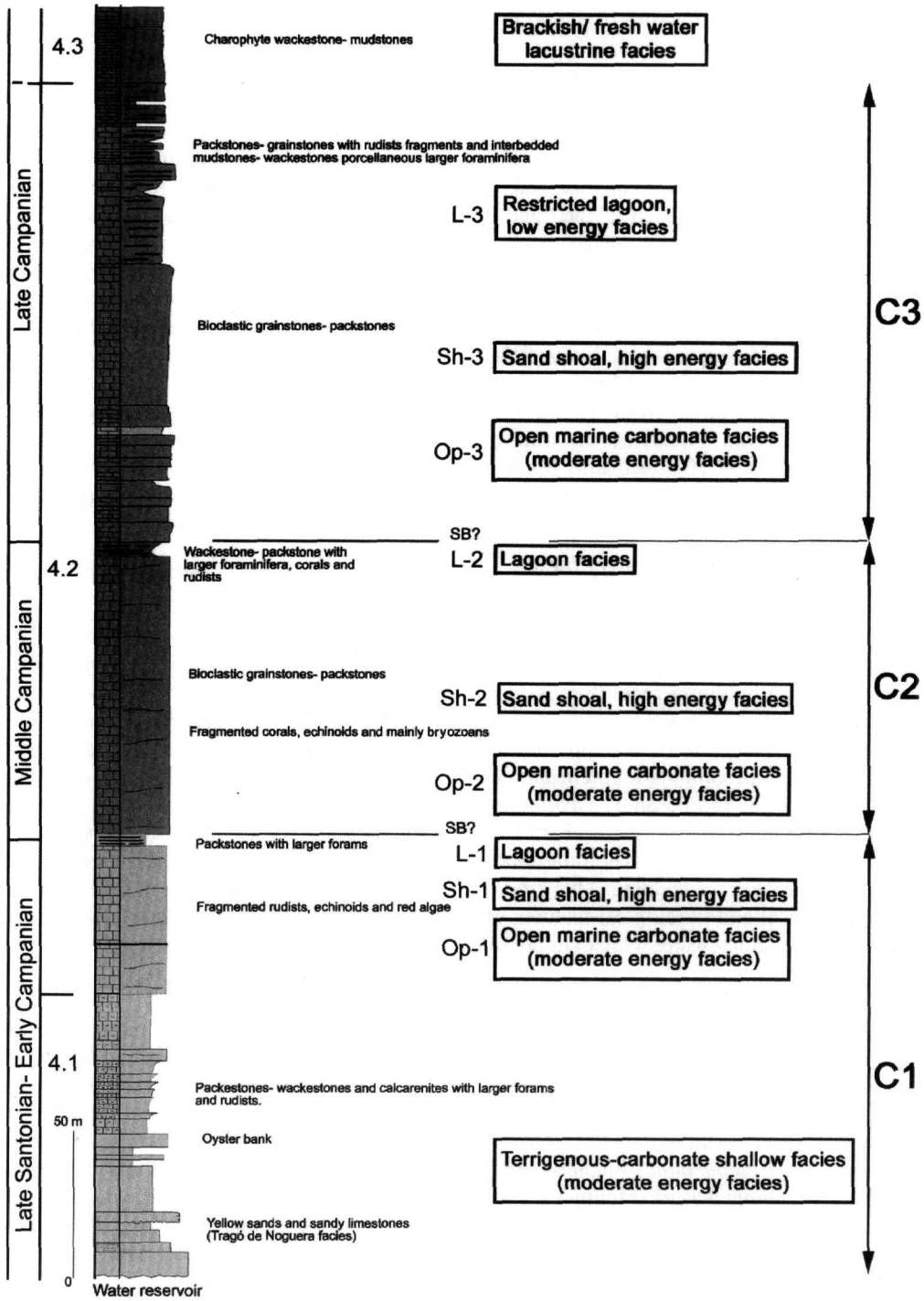

Figure 2 - The Coscoll section. See the distribution of facies and Larger Foraminiferal assemblages in the stratigraphic sequences C1, C2 and C3

4.2.4. Restricted shallow-water, low energy facies

Medium well bedded grey limestones and marly limestones (wackestones-packestones) with rudists and miliolids grading successively to "discorbid" and charophyte limestones. A continuous rudist biostrome is regularly distributed in all of the measured sections and can be used for correlation. The foraminiferal distribution indicates the passage from littoral marine to brackish lacustrine environment.

The temporal distribution of the larger foraminifera from each facies assemblages enables us to suggest that the Les Serres Marginals limestones date to the Early to Late Campanian.

4.3. The "Garumnian" beds

These consist of decimetric-thick grey micritic limestones with mainly charophyte remains, ostracods and fresh-water molluscs. Some packstones appear as formed by accumulations of charophytes, probably due to the storm reworking. They are interpreted as being brackish/fresh water lacustrine deposits.

5. Stratigraphic sequences and events

The spatial and temporal distribution of larger foraminifera together with the characteristics of the rocks enabled us to recognise three main stratigraphic sequences (see Fig. 2 and 3): the lowest one (carbonate platform 1) is composed of a terrigenous-carbonate shallow facies, moderately deep open marine carbonates, little developed sand-shoals and very well developed protected lagoonal facies. It belongs to the Late Santonian-Early Campanian. The middle sequence (carbonate platform 2) is characterised by well developed sand-shoal and protected lagoonal facies, and it is date . The upper one (Carbonate platform 3) includes well developed sand-shoal, protected lagoon, restricted shallow water and continental lacustrine deposits.

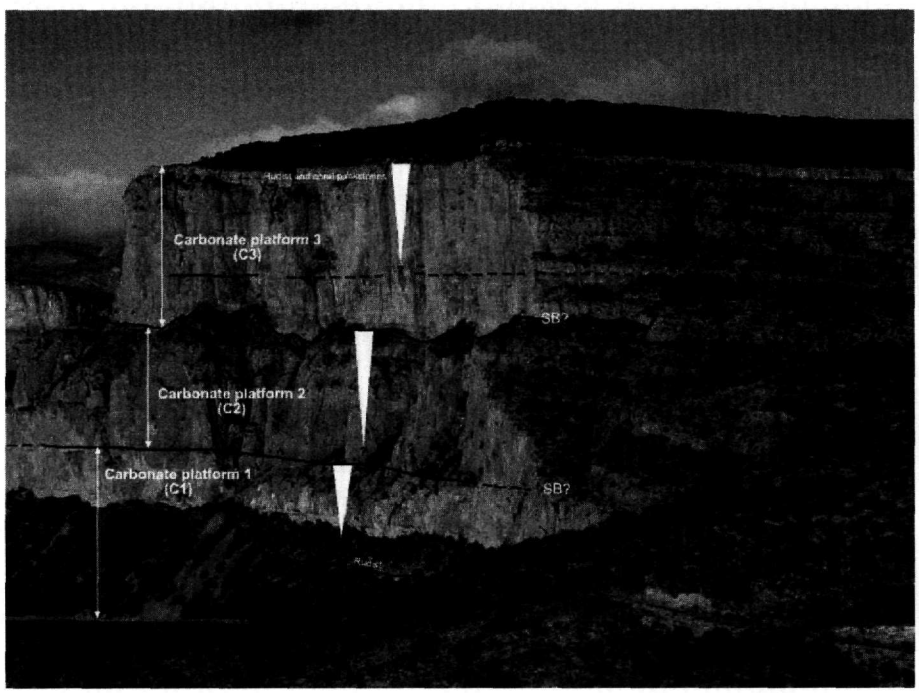

Figure 3 - Field view of the Coscoll section. Compare with Fig. 2

This homogeneous distribution of facies (and palaeoenvironments) in the whole of the studied area (central part of the south Pyrenean margin) suggests that the main agent responsible for the

development of the three sequences is the relative change in the sea level, which increases or decreases the accommodation space. However, sequences one and three show evidence of tectonic activity. The terrigenous input at the base of the first sequence coincides with the beginning of the compressional phase in the Pyrenean (Alpine) Orogeny, whereas the generalised regression at the end of the third sequence is due to the intensification of the deformation. Therefore, the abiotic events controlling the growth and demise of the carbonate platforms were the eustatic cycles and tectonic activity mainly at the end of the third sequence.

The fossil distribution through the carbonate packages of the three sequences show the environmental and age constrains.

6. Acknowledgments

We are grateful to Joan Rosell (Universitat Autònoma de Barcelona) for help with the field-work. The study was financed by the Spanish Ministry of Education and Science, projects: BTE2000-0158 and BTE2003-04101.

7. References

Berástegui, X., Caus, E., and Puig, C., 2002. Pyrenees.In W. Gibbons and M.T. Moreno (eds), *The Geology of Spain, Geological Society London*, 265-272pp., London.

Berástegui, X, Losantos, M., Munoz, J.A., and Puigdefábregas, C., 1993. Geològic del Pirineu Central 1: 200.000, *Institut Cartogràfic de Catalunya*, Barcelona.

Dercourtm, J., Zonenshain, L.P., Ricoum, L. E, Kazminm, V.G, Le Pichonm, X, Knipper, A., Grandjacquet, C., Sorocktin, O., Geyssant, J., Lepvrier, C., Sborshchikov I.V., Boulin, J., Biju-Duval, B., Sibuet., J.C., Savostin, V., Westphal, M., and Lauer, J.P., 1985. Présentation de 9 cartes palóegeographiques au 1/20.000.000, s´étendant de l'Atlantique au Pamir pour la période du lias à l'actuel, *Bulletin Societé Géolique de France* 8/1, 5, 637-652.

Hottinger, L., 1978. Comparative Anatomy of Elementary Shell Structures in Selected Larger Foraminifera. In Hedley and Adams, *Foraminifera,* 3, 203-266.

Muñoz, J. A., Puigdefábregas, C., and Fontboté, J.M., 1984. Orógenos alpinos III. El Pirineo. In *Geología de España. Instituto Geológico y Minero de España*. 161-205.

Seguret, M., 1972. Etude téctonique des nappes et series décollés de la partie centrale du versant sud des Pyrenees. "Caractère synsedimentaire, ròle de la compression et de la gravité", *PhD Université de Montpellier, Ustela*, sér. Geologie structurale, 2, 155pp.

Δελτίο της Ελληνικής Γεωλογικής Εταιρίας τομ. XXXX, 2007
Πρακτικά 11ου Διεθνούς Συνεδρίου, Αθήνα, Μάιος 2007

Bulletin of the Geological Society of Greece vol. XXXX, 2007
Proceedings of the 11th International Congress, Athens, May, 2007

MIDDLE MIOCENE DIATOMITE- BEARING FORMATIONS FROM WESTERN ROMANIA

Codrea V.[1], Barbu O.[1], and Bedelean H.[1]

[1] Babeş-Bolyai University of Cluj-Napoca, Faculty of Biology and Geology, Department of Geology - Paleontology, vcodrea@bioge.ubbcluj.ro, obarbu99@yahoo.com , 1 Kogălniceanu Str., 400074 Cluj-Napoca, Romania

Abstract

In Western Romania diatomite occurs only in the Lower Sarmatian (Middle Miocene) formations, as a consequence of intense volcanism developed in Apuseni Mountains and evolution of peculiar sedimentary basins connected to the Pannonian realm. The main basins with diatomite successions are Zarand and Vad Borod. The diatomite preserves besides diatoms (centric and pennate) and other microfossils (dinoflagellates, ebriidinas, silicoflagellates, phytolites) assemblages a lot of macrofossils as plants (mainly foliar imprints), fish, reptiles and mammals. Several taxa are indicative for environment reconstruction. The Lower Sarmatian climate is estimate as wet warm temperate to subtropical. A tentative of both aquatic and land environments reconstruction is done.
Key words: *Sarmatian, diatomite, fossils, environment reconstruction.*

Περίληψη

Στη δυτική Ρουμανία διατομίτες εμφανίζονται μόνο στους σχηματισμούς του κατώτερου Σαρματίου (Μ. Μειόκαινο), ως αποτέλεσμα της έντονης ηφαιστειότητας που αναπτύχθηκε στα όρη Apuseni και της εξέλιξης των ιδιόμορφων ιζηματογενών λεκανών που συνδέονται με την ευρύτερη περιοχή του Παννόνιου. Οι κύριες λεκάνες με διατομιτικές αποθέσεις είναι η λεκάνη του Zarand και η λεκάνη του Vad Borod. Ο διατομίτης περιέχει εκτός από διάτομα και άλλα μικροαπολιθώματα (δινομαστιγωτά, πυριτιομαστιγωτά, φυτόλιθοι), πολλά μακροαπολιθώματα όπως φυτά (κυρίως αποτυπώματα φύλλων), ψάρια, ερπετά και θηλαστικά. Πολλά από τα περιγραφέντα taxa είναι κατάλληλα για την αναπαράσταση του χερσαίου και υδάτινου παλαιοπεριβάλλοντος καθώς και του κλίματος το οποίο, για το κατώτερο Σαρμάτιο, προκύπτει υγρό θερμό εύκρατο έως υποτροπικό.
Λέξεις κλειδιά: *Σαρμάτιο, διατομίτης, απολιθώματα, αναπαράσταση περιβάλλοντος.*

1. Introduction

In Western Romania, several geological events occurred in the Middle Miocene: a new generation of sedimentary basins was born and an intensive magmatic activity begun, with a paroxysmal period between 14.8-10 My (Săndulescu 1984, Roşu *et al.* 2000).

A peculiar interest concern the sedimentary basins located on the western rim of the Apuseni Mountains, due to accurate data recorded into their Badenian and Sarmatian successions. Among these "gulf-basins" the Zarand Basin had a peculiar evolution: although the epoch of its genesis is nearly the same as in the other coeval basins (Şimleu, Vad-Borod, Beiuş, Mureşului passage way etc.), specific environments developed there in Sarmatian. Such an environment reffers to the Lower Sarmatian (Volhynian) tuffaceous/diatomite-bearing successions which occurred due to the intense Sarmatian volcanic activity. Sarmatian diatomites are not completely missing from the other analogous Neogene basins (*e.g.* Vad-Borod, Beiuş) but there one can observe only short diatomitic episodes interbedding into various other lithologies.

This contribution deals with the peculiar Lower Sarmatian depositional environments, indicating the diatom assemblages which lead to the diatomite accumulations from the Middle Miocene sedimentary basins from Western Romania.

2. Geological setting

The Neogene basins from Apuseni Mountains were born as eastward extensions of the Pannonian Basin since Badenian. These basins evolved as margins of the Pannonian Basin realm, where the different eustatic events marked better vestiges than elsewhere. Excepting the Şimleu Basin, the other ones are trended NW-SE or W-E, betraying older fractures inherited from the Laramian tectogenesis. Their basements involve Paleozoic and Mesozoic rocks belonging to the Inner Dacides (Săndulescu 1994, Săndulescu and Dimitrescu 2004). Over the basement, Neogene molass fills all these basins (Fig. 1).

In the Zarand Basin the Neogene deposits are of both sedimentary and volcanic origin (Istocescu 1971). The succession begin with Badenian formations (Botfei, Minişu de Sus and Mocrea; Codrea *et al.* 1999), followed by Sarmatian ones (Cărand, Camna, Urviş-Beliu and Paulian; Pestrea 1999). Pannonian *s.str.* and Pontian formations (Beliu, Hăşmaş, Prunişor, Mărăuş) remain extremely poor outlined due to the unsuitable manner of definition and scarcity of data published by Marinescu *et al.* (1998).

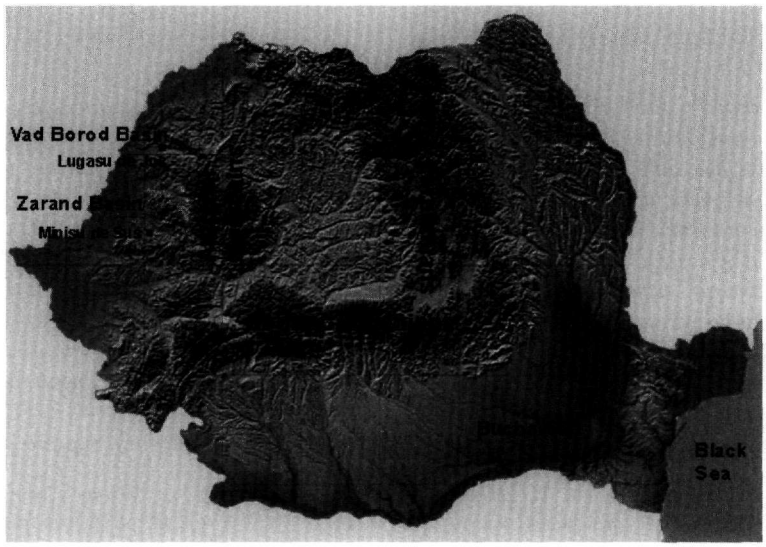

Figure 1 – Locations of the Vad-Borod and Zarand Neogene Basins in Western Romania

The Vad-Borod Basin in located northerly from Zarand. There, the Lower Sarmatian diatomite occurs only on restricted surfaces. The diatomite belongs to the Cornițel Formation (Popa 2000). However, one worth to be pointed out that the eastern sector of the Vad-Borod Basin, where Cor-

niţel Formation is originating from, can be somehow different form the western sector, where the diatomite occur.

3. Middle Miocene diatomite-bearing environments

3.1. Zarand Basin

The diatomite occurs into the Cărand Formation as a distinct facies, which Săsăran *et al.* (1999) described as FA1 ("the diatomite facies") into the "diatomite-tuffaceous facies associations" (FA). The diatomite is laying unconformity on Mesozoic basement. The best diatomite exposures can be followed in the former diatomite open-pits, once mining this rock at Bârzăviţa, Pârâul Nemţului or Stupii Surdului, all located in Minişu de Sus village neighbourhood. The diatomite occurs always next to the pyroclastic facies associations (FB), *i.e.* different tephra (lapillistones and andesite tuffs), pyroclastic breccia flows and lahar facies (Fig. 2).

In his papers Pantocsek (1886, 1889, 1905) illustrated several diatom species and genera from different sites belonging to Cărand Formation: Minişu de Sus, Camna, Cărand and Nermiş. For Minişu de Sus, Camna and the Bremia Valley (Volume II, 1889) he referred more thoroughly to diatomites. He considered two diatomite successions to belong to brackish-water environment (Minişul de Sus, Camna) and one deposit related to a marine basin (Bremia Valley, Camna).

Later, Krestel (1970) focused her study on the Minişul de Sus diatomite and redescribed the regions previously studied by Pantocsek, but new areas too: Stupii Surdului, Dealul Râtului, Bârzăvicioara, Drânovăţ, Pârâul Neamţului and Câmpul Lat. She stressed that the diatoms assemblages comprise centric mostly planktonic and generally pennate benthyic epiphytic forms. In addition to diatoms, there are also ebriidians, chrysomonads, silicoflagellates, sponge spicules and phytolites. She was considering that the diatomite from Minişu de Sus had a neritic zone genesis, in temperate climate, in Early Sarmatian (Volhynian).

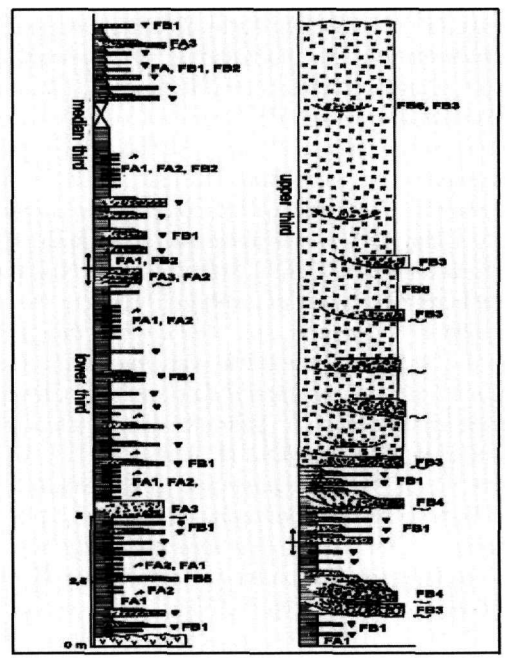

Figure 2 – Facies distribution of the Sarmatian deposits in Cărand Formation (according to Săsăran *et al.* 1999)

Another study on the same diatom assemblages has been recently carried out by Pestrea (1996, 1999), describing 240 species in 66 genera. There is a preponderance of pennate forms as to the centric ones. For the Cărand profile she also established three types of associations with biostratigraphic importance from the Volhynian – Bessarabian interval.

The last contributions on the diatom assemblages belong to Barbu (2002) and Barbu and Codrea (2002).

The study we carried on stressed the following list of taxa:

DIATOMS (109 taxa: 47 centric and 62 pennate)- *Melosira ambigua* (Grunow) O. Muller, *Melosira arenaria* Moore, *Melosira clavigera* Grunow, *Melosira rieufii* Heribeaud, *Melosira undulata* (Ehrenberg) Kutzing, *Paralia sulcata* (Ehrenberg) Kutzing, *Podosira hyalina* Jouse, *Hya-*

lodiscus constrictus (Pantocsek) Kanaya, *Hyalodiscus frenguellii* Hanna, *Hyalodiscus scoticus* (Kutzing) Grunow, *Endictya oceanica* Ehrenberg, *Stephanopyxis schulzii* Stein, *Thalassosira decipiens* (Grunow) Jorgensen, *Coscinodiscus lineatus* Ehrenberg, *Coscinodiscus marginatus* Ehrenberg, *Coscinodiscus nitidus* Gregory, *Coscinodiscus oculus-iridis* Ehrenberg, *Coscinodiscus radiatus* Ehrenberg, *Coscinodiscus sarmaticus* Pantocsek, *Coscinodiscus subtilis* Ehrenberg, *Liradiscus rugulosus* Forti, *Xanthiopyxis leguminiformis* Jouse, *Xanthiopyxis ovalis* Lohman, *Actinoptychus reinholdii* Hajos, *Actinoptychus senarius* (Ehrenberg) Ehrenberg, *Actinoptychus splendens* (Schadbolt) Ralfs, *Actinoptychus undulatus* (Bailey) Ralfs, *Actinoptychus* sp., *Asteromphalus loczyi* Pantocsek, *Auliscus caelatus* Bailey, *Actinocyclus ehrenbergii* Ralfs, *Actinocyclus ehrenbergii* var.*tenella* (Brebison) Hustedt, *Rhizosolenia* sp., *Chaetoceros aculeatus* Makarova, *Chaetoceros affinis* Lauder, *Chaetoceros dentatus* Korotkevicz, *Chaetoceros muelleri* Lemmerman, *Chaetoceros subtilis* Cleve, *Chaetaceros* sp.1, *Chaetoceros* sp.2, *Triceratium formosum* f. *pentagonale* A. Schmidt, *Biddulphia tuomeyi* (Bailey) Roper, *Cerataulus* sp., *Pseudopyxilla capreolus* Forti, *Pterotheca* sp., *Anaulus minutus* Grunow, *Anaulus simplex* Hajos, *Gephyria media* Arnott, *Gephyria media* f. *rinnboeckii* Jurilj, *Rhabdonema adriaticum* Kutzing, *Grammatophora arctica* Cleve, *Grammatophora marina* Kutzing, *Grammatophora hamulifera* Kutzing, *Grammatophora robusta* Dippel, *Plagiogramma truanii* Pantocsek, *Plagiogramma* sp., *Dimerogramma marinum* (Gregory) Ralfs, *Cymatosira* sp., *Opephora pacifica* (Grunow) Petit, *Fragilaria brevistriata* Grunow, *Fragilaria brevistriata* var. *elliptica* Heribeaud, *Fragilaria construens* (Ehrenberg) Grunow, *Fragilaria construens* var. *subsalina* Hustedt, *Fragilaria construens* var. *venter* (Ehrenberg) Grunow, *Rhaphoneis debyi* Pantocsek, *Rhaphoneis amphiceros* Ehrenberg, *Rhaphoneis obesula* Hanna f. *trigona* Hajos, *Synedra parasitica* (W.Smith) Hustedt, *Synedra tabulata* var. *obtusa* Pantocsek, *Synedra tenera* W.Smith, *Synedra ulna* (Nitzsch) Ehrenberg, *Eunotia* sp., *Cocconeis placentula* Ehrenberg, *Cocconeis placentula* Ehrenberg var. *euglypta* (Ehrenberg) Cleve, *Cocconeis scutellum* Ehrenberg, *Cocconeis* sp., *Achnanthes baldjikii* var. *podolica* Missuna, *Achnanthes brevipes* Agardh, *Achnanthes brevipes* var. *intermedia* (Kutzing) Cleve, *Rhoicosphenia curvata* (Kutzing) Grunow, *Mastogloia splendida* (Gregory) Cleve, *Mastogloia aquilegiae* Grunow, *Dictyoneis* sp., *Dilponeis vacillans* (A. Schmith) Cleve, *Dilponeis chersonensis* (Grunow) Cleve, *Dilponeis* sp., *Anomoeoneis spaerophora* (Kutzing) Pfitzer, *Navicula distans* (W. Smith) Ralfs, *Navicula hennedyi* W.Smith, *Navicula humerosa* Brebisson, *Navicula latissima* var. *elongata* Pantocsek, *Navicula lyra* Ehrenberg, *Navicula placentula* f. *rostrata* A. Mayer, *Navicula pennata* A.Schmidt, *Pinnularia* sp., *Caloneis* sp., *Amphora gibberula* Missuna, *Cymbella helvetica* Kutzing, *Cymbella ventricosa* Kutzing, *Gomphonema ventricosum* Gregory, *Deticulopsis hustedtii* Simonsen & Kanaya, *Epithemia* sp., *Rhopalodia gibberula* var. *magana* (Missuna) I. Kiss, *Rhopalodia musculus* (Kutzing) O. Muller, *Nitzschia navicularis* (Breb. ex. Kutzing) Grunow, *Nitzschia punctata* var. *aralens* Borszczow, *Nitzschia spectabilis* (Ehrenberg) Ralfs, *Suriella baltjiskii* var. *podolica* Missuna, *Camylodiscus* sp.;

DINOFLAGELLATES ENDOSKELETONS - *Calicipedinium quadripes* Dumitircă, *Carduifolia gracilis* Hovasse;

EBRIIDIANS - *Ammodochium rectangulare* (Schultz) Deflandre, *Hermesinum schultzii* Hovase, *Parathranium* sp., *Podamphora* sp.;

SILICOFLAGELLATES - *Distephanus crux* Ehrenberg, *Deflandriocha* sp.; chrysomonads - *Archaeomonas* sp.1, *Archaeomonas* sp.2; sponge spicules (which are very frequently found and are 3-4 mm in);

PHYTOLITES - *Lithostylidium* parasp., *Lithomestites clepsammidium* (Ehrenberg) Deflandre, *Lithomestites* parasp.1, *Lithomestites* parasp.2, *Lithostylidium biconcavum* Ehrenberg, *Lithodontiumum* parasp.

Out of the total number of taxa, 58.1 % originated from marine environments, 16.2 % from marine-brackish ones, 4.1% from brackish ones, 8.1 % from both brackish and fresh water ones and 13.5 % from fresh water.

Although the presence of different diatom taxa is not uniformly distributed within the profiles, two large types of assemblages can still be pointed out.

The first one involves the preponderance of pennate diatoms with dominance of *Fragilaria* and *Navicula* genera, next to *Cymbela, Cocconeis, Synedra.* The centric diatoms that can be mentioned are mainly *Melosira ambigua* and *M. arenaria.* This assemblage is indicative for brackish environment. It includes not only diatoms but also: chrysomonads and numerous sponge spicules.

The second assemblage is completely different from the first one, comprising other genera of centric and pennate diatoms. Its peculiarity involves the following taxa: *Paralia sulcata, Coscinodiscus, Actinoptycus, Chaetoceros, Grammatophora, Plagiograma, Mastogloia* and *Navicula,* all indicating a marine-brackish environment. There are many *Coscinodiscus* and *Chaetoceros* species - the latter being extremely abundant – as well as *Navicula* ones too. In addition to diatoms, there are also new groups of siliceous representatives such as: silicoflagellates, ebriidians and dinoflagellates.

The distribution of these assemblages along the succession is irregular: the brackish water diatom assemblage is dominating almost in the whole sequence, with some qualitative and quantitative variation from one level to another, whereas the marine-brackish diatom one occurs only in four restricted levels within the profile.

Some index species as *Anaulus simplex, Coscinodiscus sarmaticus,* etc. have a wide regional extension, *e.g.* the Czech Republic, Slovakia, Croatia, Hungary, Bulgaria, led to the conclusion that the studied deposits can be included within the *Anaulus simplex* (Hajos 1986, 1990) zone of the Lower Sarmatian (Volhynian).

As compared with the previous studies 15 new genera were identified: *Paralia, Endictya, Auliscus, Cerataulus, Anaulus, Plagiogrammma, Eunotia, Mastogloia, Dictyoneis, Anomoeoneis, Gomphonema, Denticulopsis, Epithemia, Surirella* and *Campylodiscus* with 27 species, forms and varieties.

Two genera were pointed out for the silicoflagellates and erbidians: *Deflandriocha* and *Podamphora.* We should mention a novelty for this area, the presence of dinoflagellates: two species had been identified: *Carduifolia gracilis* Hovase and *Calicipedinium quadripes.*

In addition to the microflora one can mention some other elements allowing the reconstruction of the Lower Sarmatian paleoenvironment. Some of them refer to taxa originating into the basin water assemblages, as fish (mostly clupeids) or dolphins (probably Kentriodontidae representatives) (Codrea *et al.* 1991a, b). Sometimes, during the fresh water episodes, turtles as *Trionyx stiriacus* Peters occurred too (Vremir *et al.*, 1997). The turtle remains could also be buried into diatomite as a result of rework of their carcases from the surrounding areas, carried into the basin by the river streams. A tentative of reconstruction of the Lower Sarmatian water life is illustrated in Fig. 3.

The emerged environments bordering the basin are documented either by macroflora, or by the vertebrates (Fig. 4).

The macroflora, when it occurs is very well preserved, either as foliar imprints or silicified truncks fragments. The following taxa had been collected from the diatomite or pyroclasts: *Cystoseirites partschi* Sternberg, *Fucus* sp.1, *Fucus* sp.2, *Pteris radobojana* Unger, *Glyptostrobus europaeus* (Brongniart) Unger, *Thuja* sp., *Pinus* sp. aff. *Pinus taedaeformis* (Unger) Heer, *Pinus* sp.- ace quaternae, *Pinus* sp., ex. gr. *quinae* Beissner- type 1, *Pinus* sp., ex gr. *quinae* Beissner- type 2, *Daphnogene polymorpha* (Al. Br.) Ettingshausen, *Lindera antiqua* (Heer) Givulescu & Barbu,



Figure 3 – Reconstruction of the Lower Sarmatian aquatic environment at Minişu de Sus (drawing by Flaviu Săsăran)

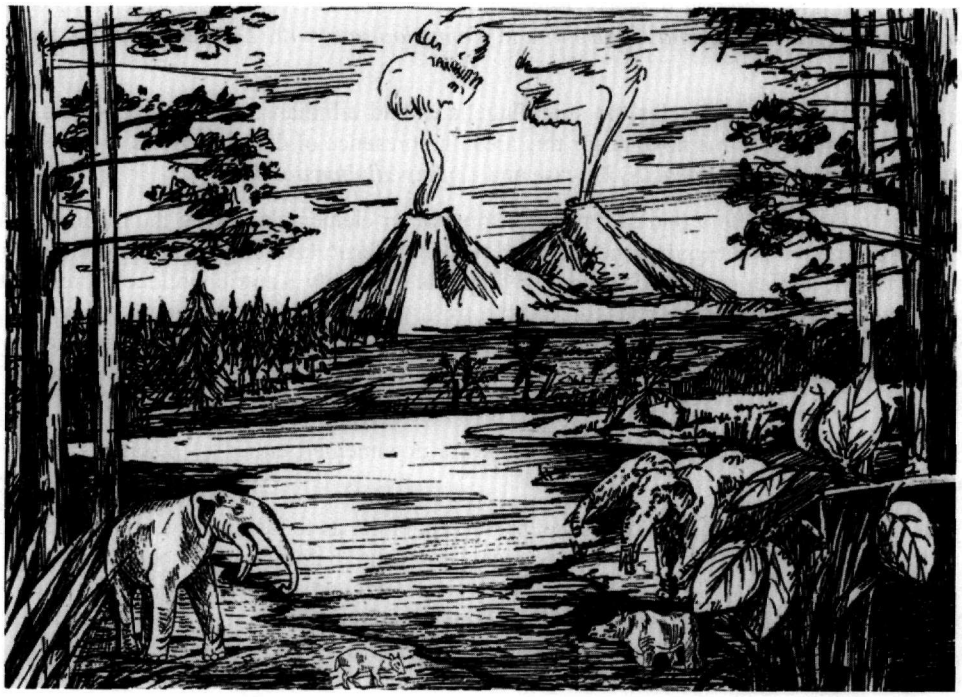

Figure 4 – Reconstruction of the Lower Sarmatian land environment at Minişu de Sus (drawing by Flaviu Săsăran)

Laurophyllum braunii (Heer) Nemejc & Knobloch, *Laurophyllum* ? sp., *Platanus leucophylla* (Unger) Knobloch, *Quercus* cf. *ilex* Linné, *Quercus* sp. or *Castanea* sp., *Myrica lignitum* (Unger)

Saporta, *Myrica vindobonensis* (Ettingshausen) Heer, *Carya denticulata* (Weber) Iljinskaia, *Acacia parschlugiana* Unger, *Cassiophyllum berenices* (Unger) Krausel, *Gleditsia lyelliana* (Heer) Hantke, *Gleditsia knorii* (Heer) Gregor, *Zanthoxylon europaeum* Unger, *Rhus prisca* Ettingshausen, *Populus populina* (Brongniart) Knobloch, *Chamaerops humilis* Linné *fossilis* Kolakovski, *Dicotylophyllum* sp.1, *Dicotylophyllum* sp.2, *Dicotylophyllum* sp.3. (Givulescu *et al.* 1995, 2002).

This typically Sarmatian flora is in complete concordance with the other Early Sarmatian floras from Transylvania. It belongs to the type flora with *Cystoseirites*, but without *Palaeocarya*, an element which has not been stressed up to the present stage of our research (Givulescu 1992).

The taphocaenosis is not very rich. The fossils are made up of having been brought from the surrounding land areas at different moments and, as we shall show later, from various different assemblages.

From a statistic point of view, within this flora there are: 16 families with 20 genera and 24 species + 3 uncertain ones. Therefore, it is a flora with a low number of samples, but still sufficiently rich in families and genera. It is also worth mentioning that, out of the identified forms, 10 are arctotertiary, 6 palaeotropical, *i.e.* 62.50 % : 37.50 %; there are 15 trees and 7 shrubs, *i.e.* 68.18 % : 31.82 %; we found 9 types with dentate leaves and 7 with whole margin leaves, *i.e.* 56.25 % : 42.75 %.

We should point out as a significant fact the presence of a palm tree in the Early Sarmatian, *Chamaerops humilis fossilis* (Givulescu and Barbu 1999). The remaining flora is common for the Early Sarmatian. Anyway, we are also stressing *Lindera antiqua,* and *Quercus* cf. *ilex*, which had their first appearance datum in the Transylvanian floras, just like *Carya denticulata*. On the other hand, *Myrica vindobonensis* and *Acacia parschlugiana* are relicts, because they are peculiar to the Early Miocene and Oligocene. It is very interesting to note the numerous *Pinus* types and the discovery of a *Pinus* with *quaternae* needles.

The foliar remnants belong to several environments. Putting aside the brackish water environment with *Cystoseirites,* two categories can be distinguished on the surrounding basin land: one of flooded swamps with *Glyptostrobus, Gleditsia, Myrica, Platanus*, probably *Pinus taedaeformis* and maybe even *Carya;* another with drier areas with Lauraceae, other vegetables and especially *Chamaerops* and *Quercus* cf. *ilex*., which forms assemblages even in actual occidental Mediterrean region. The shurb *Zanthoxylon* as well as the fern *Pteris* were also present too.

The Early Sarmatian climate had been estimate on the percentage of whole margin leaves. One can presume a subtropical wet climate (Cfa *sensu* Koppen) or according to Dilcher (1973), a wet or even very wet warm temperate one.

For over a decade of field missions a sample of Sarmatian land vertebrate fossils have been collected. It concerns mammals, as water-chevrotain (*Dorcatherium crassum* (Lartet)), listriodon (*Listriodon splendens splendens* Von Meyer), a small rhino (*Alicornops simorrense* (Lartet)), dinothere (*Deinotherium giganteum* Kaup) and mastodon (*Gomphoterium angustidens* (Cuvier)) (Nicorici 1976, Codrea *et al.* 1991 a, b, Codrea 1992, 1996). In addition, an *Anchitherium* calcaneum exists in the collection of the Hungarian Geological Istitute (MAFI) in Budapest (unpublished). The whole assemblage can be related to the MN 7+8 unit, *i.e.* the terminal Astaracian.

In order to understand the context in which diatomite sediments were laid, we should refer to the Volhynian palaeogeography of this area. After the low marine level tendency which happened at the end of the Late Badenian, in Volhynian there were ingressive tendencies due to which the Zarand area turned into an archipelago belonging to the Central Paratethys. The surface covered by the Sarmatian waters overcame the Badenian one. In this manner the Sarmatian happen to lye in unconformity over the Permo-Mesozoic basement.

The large mammals and the macroflora, both are evidence for the processes taking place on land environments. The macroflora remnants show that the coasts were dense forested areas, where *Anchitherium*-type fauna occurred. The presence of *Listriodon* as well as that of *Dorcatherium* is evidence in this respect. Water-chevrotain seems to account for the presence of gallery-forests, just like *Alicornops simorrense* which could even be indicative for swamps, also documented by *Glyptostrobus europaeus*, *Myrica lignitum, M. vindobonensis, Glaeditsia lyelliana* etc.

As a conclusion, mainly the diatomite assemblages indicate that at Minişu de Sus only the Volhynian can be proved, a different situation compared to the Carand site, where Pestrea (1999) found the Bessarabian too.

3.2. Vad-Borod Basin

The small diatomite outcrops we have studied from the Cornițel Formation (Popa 2000) are located near Lugaşu de Jos, ten km westward from Aleşd town. The succession is analogous with the one from Minişu de Sus, with diatomite interbedding in tuff. There, Pantocsek (1886, 1889, 1905) mentioned a list including 104 taxa. Among the peculiar forms, there are: *Clavicula biharenisis* Pantocsek, *Actinocyclus circumdatus Panocsek., Actinoptychus kymatodes* Pantocsek,, *Coscinodiscus biharensis* Pantocsek., *Coscinodiscus martonfi* Pantocsek, *Epithemia biharensis* Pantocsek., *Melosira biharensis* Pantocsek, *Navicula (didyma Ehrbg. var.?) elesdiana* Pantocsek,, *Navicula halionata* Pantocsek, *Navicula pseudofusca* Pantocsek., *Plagiogramma biharense* Pantocsek., *Surirella (striatula Turp.?) antiqua* Pantocsek, *Surirella biharensis* Pantocsek, *Surirella rotunda* Pantocsek, *Triceratium (acutangulum Grev. var.?) grovei* Pantocsek, *Triceratium (antillarum Clev. var.?) laetum* Pantocsek, *Triceratium polygibbum* Pantocsek. As one can observe, all were new species described by Pantocsek.

From the diatomite, leaf imprints as well as fish skeletons had been collected. The macroflora comprises: *Daphnogene polymorphum* (Braun) Ettingshausen, *Tetraclinis salicornioides* (Unger) Kvacek and *Myrica lignitum* (Unger). They prove the same climate as at Minişu de Sus. The fish are represented by skeletons and otoliths belonging to *Blennius* sp., *Gobius* sp., *Dapalis* sp., *Prolebias* sp., *Pomatoschistus triangularis* (Weiler), *Acentrogobius* sp., *Prolebias senesi* Brzobohathy and Stancu. According to the number of fish vertebra, the basin had brackish waters, probably 29 ‰. Considerable amount of fresh water probably come into the basin as an input carried on by the river streams.

4. Conclusions

In the Western Apuseni Middle Miocene sedimentary basins the diatomite occurs as consequence of the Neogene volcanism, in Sarmatian. All this kind of basins was related to the great Pannonian Basin realm, since the Badenian. The main diatomite sequences can be followed in Zarand and Vad Borod basins. However, thiner diatomite episodes can occur also in the other analogous basins from Western Romania.

All this diatom assemblages (centric and pennate) as well as the micro organisms occurring besides (dinoflagellates, ebriidinas, silicoflagellates, phytolites) formed rocks which afforded exceptional fossilisations. Leaf imprints, fragments of siliceous woods, bones and teeth of fish, reptiles or mainly large mammals had been collected from the different outcrops. Several taxa are good markers for the Sarmatian environment reconstructions. The Lower Sarmatian (Volhynian) landscape in both in Zarand and Vad-Borod basins concerned dense forested areas, sometimes with swampy tendencies, in a wet warm temperate climate. The vertebrate fauna belongs to final Astaracian, *i.e.* MN 7+8 unit. The rims of the Sarmatian basin crossed several salinity changes. The brackish water dominance had been interrupted by fresh water episodes, documented by different diatom assemblages.

Several decades, mining had been carried on for the Western Romania Sarmatian diatomite (Brana 1967). The reserves there are still important and would legitimate the continuation of mining mainly in Zarand Basin.

5. Acknowledgements

We address our thanks to our friend ***Flaviu Săsăran*** a full gifted artist who helped us in our tentatives in reconstructing the Sarmatin environment at Minişu de Sus. A lot of colleagues form Babeş-Bolyai University Cluj-Napoca gave us their competence proof in interpreting the Sarmatian from Western Romania: Acad. ***Răzvan Givulescu***, Prof. Dr. ***Iustinian Petrescu***, Senior lecturer Dr. ***Emanoil Săsăran***. We are thankful to all. Special thanks to Prof. Dr. ***László Kordos*** for his hospitality and collegial help during our visits in Budapest at the Hungarian Geological Institute (M.A.F.I).

6. References

Barbu, O., 2002. Asociaţii de diatomee şi alte microorganisme silicioase din depozitele sarmaţiene inferioare din cariera Bârzăviţa II, jud. Arad., *Armonii Naturale,* IV, 65-70.

Barbu, O., and Codrea, V., 2002. Additional taxa within the siliceous microfloristic assemblages from the Bârzâviţa II quarry (Arad county, Romania), *Studia Universitatis Babeş-Bolyai, Biologia,* XLVII, 2, 11-14.

Brana, V., 1967. *Zăcăminte nemetalifere din România.* Editura tehnică, 472pp.

Codrea, V., 1992. New mammal remains from the Sarmatian deposits at Minişu de Sus (Tauţ, Arad county*), Studia Universitatis Babeş-Bolyai, Geologia,* 37/2, 35-41.

Codrea, V., 1996. Additional data concerning the Early Sarmatian Listriodontinae of Minişu de Sus, *Studia Universitatis Babeş-Bolyai, Geologia,* 41/2, 93-101.

Codrea, V., Laslo-Faur, and Al., Dudaş, C., 1991a. Gigantic suid: *Listriodon* aff. *lockharti* (Pomel) from the Sarmatian Diatomitic-Tuffaceous Complex at Minişu de Sus (Tauţ, Arad District). In *The Volcanic Tuffs from the Transylvanian Basin*: 93-102pp.

Codrea, V., Laslo-Faur, Al., Dudaş, C., Hosu, Al., and Barbu, O., 1991b. The first Romanian record of *Deinotherium levius* JOURDAN from the Sarmatian Diatomitic-Tuffaceous Complex at Minişu de Sus (Tauţ, Arad District). In *The Volcanic Tuffs from the Transylvanian Basin*: 103-109pp.

Codrea, V., Barbu, O., and Săsăran, E., 1999. Contributions to the nomenclature of the Badenian succession from the Crişul Alb Depression, *Studia Universitatis Babeş-Bolyai, Geologia,* XLIV (2), 119-124.

Dilcher, D., L., 1973. *Paleoclimatic interpretation of the Eocene floras of Soutestern North America.* In Vegetation and Vegetation History of Northern Latin America, Elsevier, 39-59.

Givulescu, R., 1992. Considerations on the Sarmatian floras of Transylvania, *Romanian Journal of Paleontology,* 75, 47-59.

Givulescu, R., Barbu, O., and Codrea, V., 1995. New Plants from the Volhynian Diatomites at Minişu de Sus, *Studia Universitatis Babeş-Bolyai, Geologia,* 40/2, 63-68.

Givulescu, R., and Barbu, O., 1999. Eine fossile Palmae *Chamaerops hummilis* Linné fossilis Kolakovski aus dem Miozän von Rümanien, *Beitrage zur Paläontologie,* 24, 87-90.

Givulescu, R., Barbu, O., and Codrea, V., 2002. The Sarmatian Flora from Minişu de Sus, Romania. *Documenta naturae,* 144, 35pp.

Hajos, M., 1986. Stratigraphic position of Miocene Diatom and Silicoflagellate Zones in the Central Paratethys. *In 9th Diatom Symposium*, 181-196pp.

Hajos, M., 1990. Succession of the fossil diatom floras in the Carpathian Basin, Hungary, *Nova Hedwigia*, 100, 227-236.

Istocescu, D., 1971. Studiul geologic al sectorului vestic al bazinului Crişului Alb şi ramei Munţilor Codru şi Highiş, *Institutul Geologic, Studii tehnice şi economice, Seria J*, 8, 201pp.

Krestel, S., 1970. Studiul micropaleontologic al diatomitelor din Republica Socialistă România, *Rezumatul Tezei de doctorat*, Universitatea din Bucureşti, 28pp.

Marinescu, Fl., Mărunţeanu, M., Papaianopol, I., and Popescu, Gh., 1998. Tables with the correlation of the Neogene deposits in Romania, *Romanian Journal of Stratigraphy*, 78, 181-186.

Nicorici, E., 1976. *Trilophodon angustidens* (Cuvier) din Sarmaţianul inferior de la Minişul de Sus (bazinul Zarandului), *Dări de Seamă ale Institutului de Geologie şi Geofizică*, 62(3), 77-79.

Pantocsek, J., 1886. Beitrage zur Kenntnis der Fossilen Bacillarien Ungarns. Theil I, 1886: Marine Bacillarien. *Nagy-Tapolcsany, Julius Platzko* 76pp.

Pantocsek, J., 1889. Beitrage zur Kenntnis der Fossilen Bacillarien Ungarns. Theil II, 1889: Brackwasser Bacillarien, *Nagy-Tapolcsany, Julius Platzko*, 123pp.

Pantocsek, J., 1905. Beitrage zur Kenntnis der Fossilen Bacillarien Ungarns. Theil III: Beschreibung neuer Bacillarien welche in der Pars III der "Beitrage zur Kenntnis der Fossilen Bacillarien Ungarns abgebildet wurden", *Pozsony, C.F. Wigand*, 118pp.

Pestrea, S., 1996. Comparative Sarmatian diatom assemblages from Getic and Zarand areas and their paleogeographic and paleoecologic implications, *Anuarul Institutului Geologic al României*, 69 (I), 140-143.

Pestrea, S., 1999. Studiul diatomeelor sarmaţiene din România, *Teză de doctorat*, Universitatea din Bucureşti, 32pp.

Popa, M., 2000. Lithostratigraphy of the Miocene deposits in the Eastern part of Borod Basin (North-Western of Romania), *Studia Universitatis Babeş-Bolyai, Geologia*, 45/2, 93-103.

Roşu, E., Panaoitu, C., Pecskay, Z., Panaiotu, C., E., and Ivăşcanu, P., E., 2000. Neogene magmatism in the Apuseni Mountains. Evolution and geochemical features, *Anuarul Institutului Geologic al României*, 72, Special Issue, 71-72.

Săndulescu, M., 1984. *Geotectonica României*. Editura Tehnică, 336pp.

Săndulescu, M., 1994. Overview on Romanian Geology, *Romanian Journal of Tectonics and Regional Geology*, 75, *2*, 3-15.

Săndulescu, M. and Dimitrescu, R., 2004. Geological Structure of the Romanian Carpathians, *32nd International Geological Congress, Field Trip Guide Book – B12*, 1, 3-18.

Săsăran, E., Codrea, V. and Barbu, O., 1999. Facies assemblages and architecture of the sedimentary environments from the Cărand Formation (Sarmatian) in the Zărand Depression (Western Romania), *Studia Universitatis Babeş-Bolyai, Geologia*, 44 (2), 103-117.

Vremir, M., Codrea, V., and Farkas, B., 1997. *Trionyx stiriacus* Peters, 1855 (Reptilia, Testidines) from the Sarmatian (Middle Miocene) of Minişu de Sus (Romania), *Annales Historium-Naturalis Museis Nationalis Hungarici*, 89, 43-52.

Δελτίο της Ελληνικής Γεωλογικής Εταιρίας τομ. XXXX, 2007
Πρακτικά 11ου Διεθνούς Συνεδρίου, Αθήνα, Μάιος 2007

Bulletin of the Geological Society of Greece vol. XXXX, 2007
Proceedings of the 11th International Congress, Athens, May, 2007

PALAEONTOLOGICAL (RADIOLARIAN) LATE JURASSIC AGE CONSTRAINT FOR THE STEPANAVAN OPHIOLITE (LESSER CAUCASUS, ARMENIA)

Danelian T.[1], Galoyan G.[2,3], Rolland Y.[2], and Sosson M.[2]

[1] *Université Pierre-et-Marie-Curie, UMR 5143, Micropaléontologie, C. 104, 4 place Jussieu, 75005 Paris, France danelian@ccr.jussieu.fr*

[2] *Laboratoire Géosciences AZUR., Université de Nice Sophia Antipolis Parc Valrose, 28 Avenue de Valrose, 06108 Nice Cedex 2, France*

[3] *Institute of Geological Sciences, National Academy of Sciences of Armenia, 24a Baghramian avenue, Yerevan, 375019 Armenia*

Abstract

Micropalaeontological age evidence for the sedimentary cover of ophiolites is important to understand the palaeogeographic and geodynamic evolution of Tethyan realms. The Stepanavan ophiolitic suite of Northern Armenia consists of peridotites, gabbros, plagiogranite and lavas with a radiolarite sedimentary cover. It is regarded as the northern extension of the Sevan-Akera ophiolitic zone and may be considered as the eastern extension of the Izmir-Ankara suture zone. It represents the relics of a slow-spreading mid-oceanic ridge that was active between Eurasia and the South-Armenian Block of Gondwanian origin. Radiolaria extracted from radiolarites of the Stepanavan ophiolite provide for the first time a Late Jurassic (late Kimmeridgian to early Tithonian) age constraint for this part of Tethyan oceanic crust preserved in Lesser Caucasus.

Key words: *Tethys, radiolarites, Mesozoic, Late Jurassic, Caucasus.*

Περίληψη

Η χρονολόγηση με βάση μικροπαλαιοντολογικά δεδομένα, των ιζηματογενών καλυμμάτων των οφιολίθων είναι ιδιαίτερης σημασίας για την κατανόηση της παλαιογεωγραφικής και γεωδυναμικής εξέλιξης των περιοχών της Τηθύος. Η οφιολιθική ακολουθία του Stepanavan στη Βόρεια Αρμενία συνίσταται από περιδοτίτες, γάββρους, πλαγιογρανίτες και λάβες και ιζηματογενή καλύματα ραδιολαριτών. Θεωρείται ως η βόρεια επέκταση της οφιολιθικής ζώνης Sevan-Akera και η ανατολική επέκταση της ζώνης Izmir-Ankara. Αντιπροσωπεύει κατάλοιπο μιας βραδέως εκτεινόμενης μεσο-ωκεάνιας ράχης, που ήταν ενεργή μεταξύ της Ευρασίας και του νότιου Αρμενικού τεμάχους γκοντβανικής προέλευσης. Τα ραδιολάρια που εξετάστηκαν από τους ραδιολαρίτες στην περιοχή της οφιολιθικής ακολουθίας του Stepanavan πιστοποιούν για πρώτη φορά ηλικία Ανώτερου Ιουρασικού (ανώτερο Κιμμερίδιο έως κατώτερο Τιθώνιο) προσδίδοντας ηλικία για αυτό το τμήμα του ωκεάνιου φλοιού της Τηθύος που παρατηρείται στο Lesser Caucasus.

Λέξεις κλειδιά: *Τηθύς, ραδιολαρίτες, Μεσοζωικός, Ανώτερο Ιουρασικό, Καύκασος.*

1. Introduction

The geological history of ophiolite units in Armenia (Lesser Caucasus) is linked to the evolution of the Tethys ocean (Dercourt *et al.* 1986). Radiolarian biochronology has had an enormous impact the last twenty years in unravelling the geodynamic evolution of Tethyan oceanic realms and continental margins (De Wever & Dercourt 1985, De Wever *et al.* 1994, Danelian and Robertson 1997, 2001, Danelian *et al.* 2006). The micropalaeontological dating of the siliceous sedimentary cover of ophiolitic lavas are important to constrain the timing of opening, quiescence and closure of parts of Tethys ocean. Dating radiolarites overlying ancient oceanic crust preserved in Armenia is of much importance for our understanding of the geodynamic evolution of the greater area between Eurasia and the South-Armenian Block (Fig. 1) that originated from Gondwana (Knipper 1975, Knipper and Khain 1980).

Here we will present the first radiolarian evidence for the Stepanavan ophiolite unit, which is part of the Lesser Caucasus ophiolite belt, striking E-W in north Armenia (Fig. 2; Aslanyan 1958, Gabrielyan 1959). We will conclude by discussing the implications of this palaeontological evidence for the evolution of the Mesozoic Tethys in Armenia.

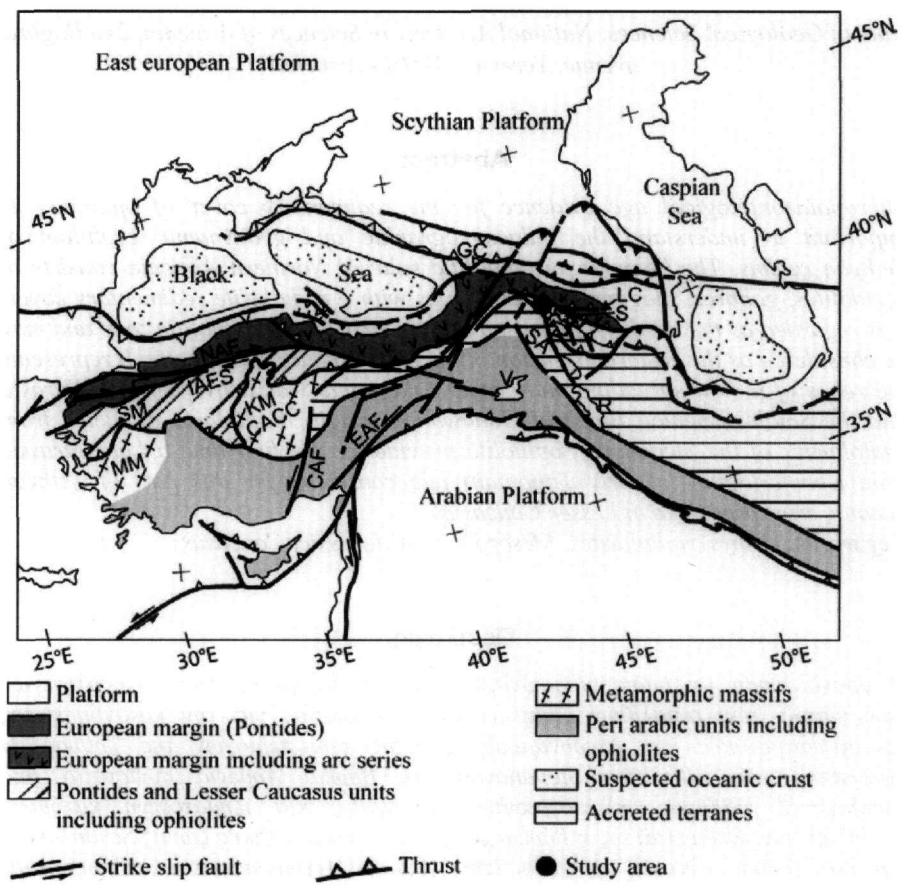

Figure 1 - Structural map of the Arabia-Eurasia collision area, after Avagyan *et al.* (2005). CACC: Central Anatolian Crystalline Complex, KM: Kirsehir Massif, MM: Menderes Massif, SM: Sakarya Massif, IAES : Izmir-Ankara-Erzinchan Suture, NAF : North Anatolian Fault, EAF : East Anatolian Fault, GC : Great Caucasus, LC: Lesser Caucasus, SA: South-Armenian Block, V: Van Lake, S: Sevan Lake, R: Reziyeh Lake

2. Geological setting

Three ophiolite zones are recognized in Armenia (Fig. 2):

1) Sevan-Akera zone, situated in the east and south-east of Lake Sevan, and including the Amassia Stepanavan ophiolites (northwestern part of the Sevan-Akera zone),
2) Vedi, a relatively small outcrop of ophiolitic rocks in the south-east of Yerevan,
3) Zangezur ophiolites, in the southeastern part of the country.

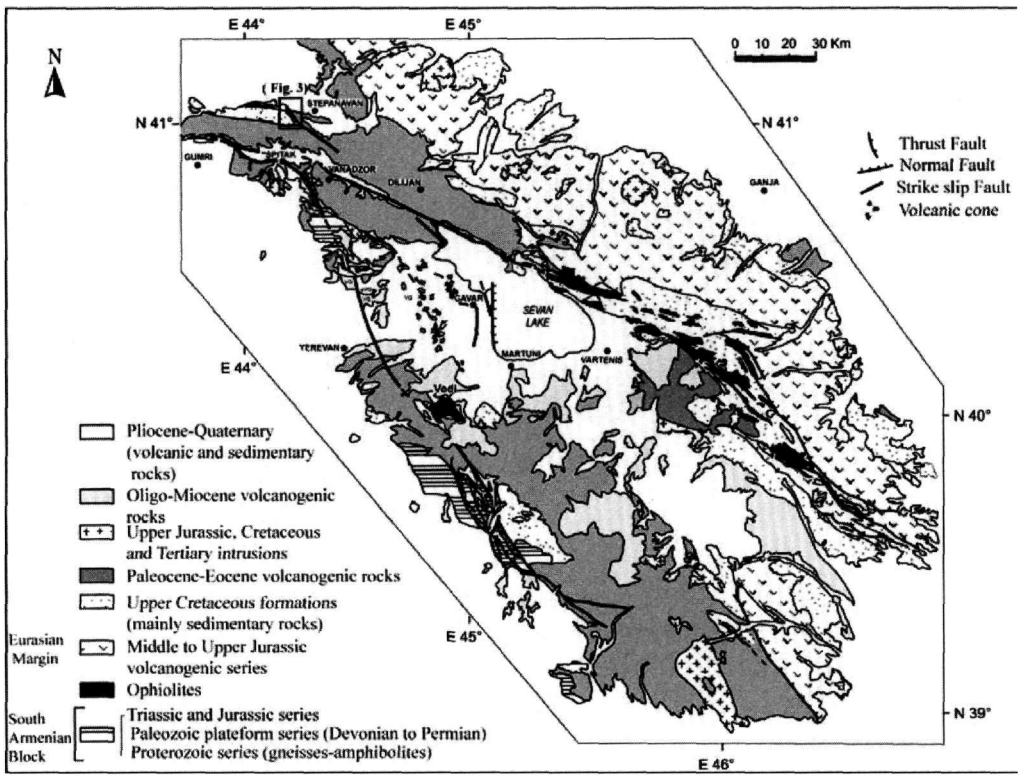

Figure 2 - Geological map of Armenia, showing locations of ophiolitic complexes and of the study area.

Previous work (Aghamalyan 1978) and new structural field observations and cartography south-west of the city of Stepanavan show that a blueschists unit appears in small (~2 km^2-scale) tectonic windows below epidote-amphibolite facies meta-ophiolites. The latter constitutes the tectonic sole of an unmetamorphosed ophiolitic suite covered unconformably by brown siltstones and limestones. The latter passes laterally to pillow lava flows and volcanic tuffs covered uncomfortably in their turn by acidic volcanic rocks assumed of Middle to Upper Eocene age (Figs 3, 4).

The ophiolitic sequence is formed by serpentinized peridotites (lherzolites, wehrlites and websterites) cross-cut by small (100 m-large) intrusive bodies, the composition of which evolved from wehrlites to laminated gabbros and plagiogranites. It is likely that these deep plutonic parts were exposed on the sea-floor and consequently hydrothermalized (occurrence of "listwenites"). They are unconformably overlain by doleritic pillow lavas and radiolarites. Lava flows are scattered, and it is not rare to observe serpentinized peridotites overlain by radiolarites. Diabasic dikes occur also very scarcely.

3. Results

Two radiolarian chert samples (Ar03-51 and 53; Fig. 3) were processed in the laboratory following the hydrofluoric acid treatment described by Pessagno and Newport (1970) and Dumitrica (1970). Only one of them (Sample Ar 03-51) yielded a moderately well-preserved radiolarian assemblage following successive leaching with low concentration acid (HF 4 %).

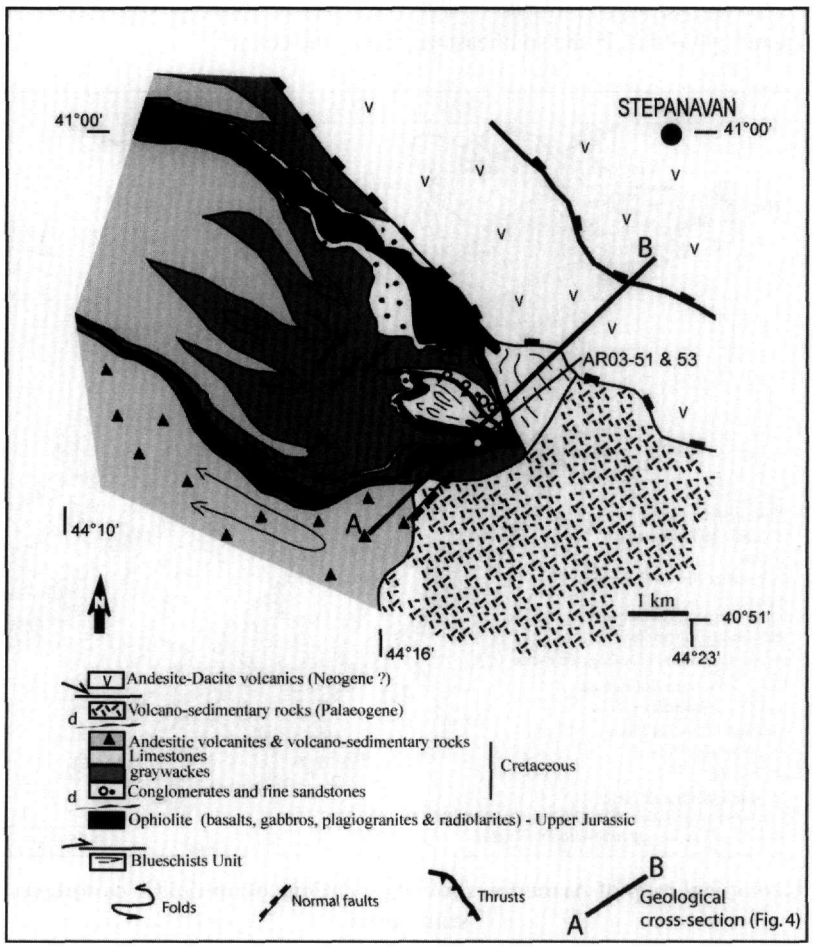

Figure 3 - Simplified geolological map of the Stepanavan ophiolitic complex, with location of the studied samples

Identifiable Radiolaria include the following taxa:

Acanthocircus trizonalis ssp.cf. *A.t.angustus* Baumgartner
Acanthocircus trizonalis trizonalis (Rüst)
Archaeodictyomitra sp.
Cinguloturris carpatica Dumitrica
Emiluvia sp.
Mirifusus dianae (Karrer) *s.l.*
Podocapsa amphitreptera Foreman
Ristola altissima (Rüst) *s.l.*
Sethocapsa simplex Taketani

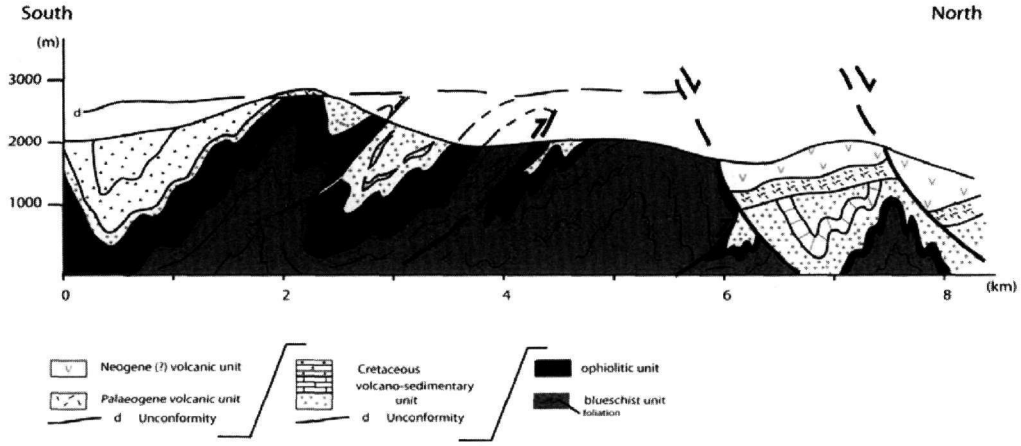

Figure 4 - Simplified geolological section of the Stepanavan ophiolitic complex (see Fig. 3 for its emplacement)

Age-diagnostic Radiolarian species are illustrated in Fig. 5. The assemblage can be correlated with Unitary Association Zones (UAZ) 9 to 11 (mid/late Oxfordian to late Kimmeridgian/early Tithonian) of the biozonation by Baumgartner *et al.* (1995). This is based on the co-occurrence of species *Ristola altissima* (Rüst) *s.l.* (Fig. 5a), *Cinguloturris carpatica* Dumitrica (Fig. 5b) and *Podocapsa amphitreptera* Foreman (Fig. 5c). *Acanthocircus trizonalis angustus* Baumgartner (Fig. 5d) is for the moment identified with some doubts because of its poor preservation. If the presence of this subspecies is confirmed in the future, the age could be restricted to UAZ 9-10 (mid/late Oxfordian to late Oxfordian/early Kimmeridgian).

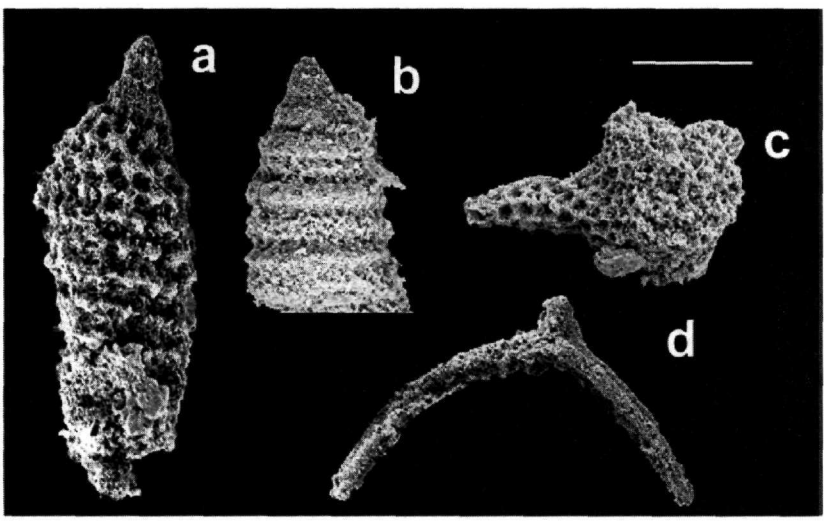

Figure 5 - Scanning electron microphotographs of Radiolaria yielded from sample Ar03/51. Bar scale is common to all species and corresponds to 100 µm. a) *Ristola altissima s.l.*; b) *Cinguloturris carpatica*; c) *Podocapsa amphitreptera*; d) *Acanthocircus trizonalis* ssp. cf. *A. t. angustus*

4. Discussion

The age of Armenian ophiolites is of great importance for understanding the palaeogeographic and geodynamic evolution of the Tethys in Caucasus and for lateral correlations of Tethyan ophiolitic belts in the Middle East.

Previous studies on radiolaria yielded from radiolarites intercalated or overlying ophiolitic lavas from the Sevan zone (Pechaniz river outcrop) pointed to a Late Jurassic-Neocomian age. More particularly, various Lower Cretaceous intervals were recognized, while the presence of Upper Jurassic deposits remained questionable (Zakariadze *et al.* 1983). Although Lower and Middle Jurassic radiolarites appear to exist in Armenia, they seem to be unrelated to ophiolites (Vishnevskaya 1995). More recently, Knipper *et al.* (1997) established the presence of Late Triassic (Carnian) and Early Jurassic (Toarcian) radiolaria in cherts intercalated with ophiolitic breccias in the Zod pass area south-east of Lake Sevan.

The micropalaeontological data presented here provide the first firm evidence for a Late Jurassic formation of Tethyan oceanic crust between the active Eurasian margin (to the North) and the South-Armenian Block (in the South), a microcontinent detached from Gondwana during the Late Palaeozoic –Early Mesozoic time. More particularly, the Stepanavan ophiolite is regarded as part of a slow spreading oceanic ridge that was formed in a back arc position (Galoyan *et al.* submitted).

The Stepanavan ophiolite is considered as the extension to the North of the Sevan-Akera ophiolitic zone and it might be related with the Khoy ophiolite in northern Iran. It also appears to represent an eastern extension of the Anatolian or Izmir-Ankara ophiolitic suture zone (Knipper 1975, Adamia *et al.* 1980), in which the presence of Jurassic, but also Upper Triassic and Lower Cretaceous radiolarites intercalated with ophiolitic lavas were recently documented (Göncüoğlu *et al.* 2000, Tekin *et al.* 2002).

5. Acknowledgments

Funding from the Middle East Basins Evolution (MEBE) project is gratefully acknowledged. Fieldwork was greatly facilitated by the support of the Institute of Geological Sciences of Armenian Academy of Science. This study would not be possibly completed without the travelling funds provided by the French Embassy in Armenia and the French Ministry for Foreign Affairs (ECO-NET program). Constructive remarks by A. Matsuoka (Niigata, Japan) improved the initial manuscript.

6. References

Adamia, Sh., Bergougnan, H., Fourquin, C., Haghipour, A., Lordkipanidze, M., Ozgül, N., Ricou, L., and Zakariadze, G., 1980. The Alpine Middle East between the Aegean and the Oman traverses, *26th International Geololgical Congress*, Paris, C5, 122-136.

Aghamalian, V.A., 1978. The old metamorphic complexes of the territory of Armenian SSR and their tectonic disposition, *Proc. Second Regional Petrographic Symposium on Caucasus, Crimea and Carpathians*, Tbilisi, 109-115.

Aslanyan, A.T., 1958. The Regional Geology of Armenia. Izd.''Haypethrat'', Yerevan. (in Russian)

Avagyan, A., Sosson, M., Philip, H., Karakhanian, A., Rolland, Y.A., Melkonyan, R., Rebai, S., and Davtyan, V., 2005. Neogene to Quaternary stress field evolution in Lesser Caucasus and adjacent regions using fault kinematics analysis and volcanic cluster data, *Geodinamica Acta* 18, 401-416.

Baumgartner P.O., Bartolini A., Carter E.S., Conti M., Cortese G., Danelian T., De Wever P., Dumitrica P., Dumitrica-Jud R., Gorican S., Guex J., Hull D.M., Kito N., Marcucci M., Matsuoka A., Murchey B., O'Dogherty L., Savary J., Vishnevskaya V., Widz D., and Yao A., 1995. Middle Jurassic to Early Cretaceous Radiolarian Biochronology of Tethys based on Unitary Associations, In Baumgartner *et al.* (eds), *Middle Jurassic to Lower*

Cretaceous Radiolaria of Tethys: Occurrences, Systematics, Biochronology, Mém. Géol. (Lausanne), 23, 1013-1048pp.

Danelian, T., and Robertson, A.H.F., 1997. Radiolarian evidence for the stratigraphy and palaeo-oceanography of the deep-water northern passive margin of the Indian plate (Karamba Formation, Indus Suture Zone, Ladakh Himalaya), *Mar. Micropal.* 30 (1-3), 171-195.

Danelian, T., and Robertson, 2001. Neotethyan evolution of eastern Greece (Pagondas Mélange, Evia island) inferred from radiolarian biostratigraphy and the geochemistry of associated extrusive rocks, *Geological Magazine,* 138, 245-363.

Danelian, T., Robertson, A.H.F., Collins, A., and Poisson, A., 2006. Biochronology of Jurassic and Early Cretaceous radiolarites from the Lycian Mélange (SW Turkey) and implications for the evolution of the Northern Neotethyan ocean. In A.H.F. Robertson and D. Mountrakis (eds), *Tectonic Development of the Eastern Mediterranean Region, Geological Society, London, Special Publications* 260, 229-236.

Dercourt, J., Zonenshain, L.P., Ricou, L.E., Kazmin, V.G., Le Pichon, X., Knipper, A.L., Grandjacquet, C., Perchersky, D.H., Boulin, J., Sibuet, J.C., Savostin, L.A., Sorokhtin, O., Westphal, M., Bashrov, M.L., Lauer, J.P., and Biju-Duval, B., 1986. Geological evolution of the Tethys belt from the Atlantic to the Pamirs since the Lias, *Tectonophysics,* 123, 241-315.

De Wever, P., and Dercourt, J., 1985. Les radiolaires triasico-jurassiques marquers stratigraphiques et paléogéographiques dans les chaînes alpines périméditerranéennes: une revue, *Bull. Soc. Géol. France*, 8, I, 5, 653-662.

De Wever, P., Azéma, J., and Fourcade, E., 1994. Radiolaires et Radiolarites: production primaire, diagenèse et paléogéographie, *Bull. Centres Rech. Explor.-Prod. Elf Aquitaine*, 18(1), 315-379.

Dumitrica, P., 1970. Cryptocephalic and cryptothoracic Nasselaria in some Mesozoic deposits of Romania, *Rev. Roum. Géol. Géophys. Géogr., Sér. Géol.,* 14, 45-124.

Gabrielyan, A.A., 1959. The main questions about Armenian Tectonics, *Izd. NAS SSR Armenia.* (in Russian)

Galoyan, G., Rolland, Y., Sosson, M., Corsini, M., and Melkonyan, R., submitted. Evidence for superposed MORB, oceanic plateau and volcanic arc series in the Lesser Caucasus (Stepanavan, Armenia). *C.R. Geoscience.*

Göncüoğlu, M.C., Turhan, N., Sentürk, K., Ozcan, A., Uysal, S., and Yalmiz, K., 2000. A geotraverse across northwestern Turkey: tectonic units of the Central Sakarya region and their tectonic evolution. In E. Bozkurt, J.A. Winchester and J.D.A. Piper (Eds), *Tectonics and Magmatism in Turkey and the surrounding area.* Geological Society, London, Special Publication 173, 139-161.

Knipper, A.L., 1975. The oceanic crust in the alpine belt, Tr. GIN NAS USSR, Edition 267, 207p. (in Russian)

Knipper, A.L., and Khain, E.V., 1980. The structural position of ophiolites of the Caucasus, *Ofioliti*, Special Issue, 2, 297-314.

Knipper, A.L., Satian, M.A., and Bragin, N.Yu., 1997. Upper Triassic-Lower Jurassic Volcanogenic and Sedimentary Deposits of the Old Zod Pass (Transcaucasia), *Stratigraphy, geological correlation,* 3, 58-65. (in Russian)

Pessagno, Jr., E.A., and Newport, R.L., 1972. A technique for extracting Radiolaria from radiolarian cherts. *Micropaleontology,* 18(2), 231-234

Tekin, U.K., Göncüoğlu, M.C., and Turhan, N., 2002. First evidence of Late Carnian radiolarians from the Izmir-Ankara suture complex, central Sakarya, Turkey: implications for the opening age of the Izmir-Ankara branch of Neo-Tethys, *Geobios,* 35, 127-135.

Zakariadze, G.S., Knipper, A.L., Sobolev, A.V., Tsamerian, O.P., Dmitriev, L.V., Vishnevskaya, V.S., and Kolesov, G.M., 1983. The ophiolite volcanic series of the Lesser Caucasus, *Ofioliti*, 8/3, 439-466.

Vishnevskaya, V., 1995. Jurassic-Lower Cretaceous radiolarians from the Caucasus and the Carpathians. In Baumgartner *et al.* (eds), *Middle Jurassic to Lower Cretaceous Radiolaria of Tethys: Occurrences, Systematics, Biochronology*, *Mém. Géol. (Lausanne)*, 23, 915-921pp.

Δελτίο της Ελληνικής Γεωλογικής Εταιρίας τομ. XXXX, 2007
Πρακτικά 11ου Διεθνούς Συνεδρίου, Αθήνα, Μάιος 2007

Bulletin of the Geological Society of Greece vol. XXXX, 2007
Proceedings of the 11th International Congress, Athens, May, 2007

PALEOBATHYMETRIC EVOLUTION OF THE EARLY LATE MIOCENE DEPOSITS OF THE PRE-APULIAN ZONE, LEVKAS ISLAND, IONIAN SEA

Drinia H.[1], Antonarakou A.[1], Kontakiotis G.[1], Tsaparas N.[1], Segou M.[2], and Karakitsios V.[1]

[1] *National and Kapodistrian University of Athens, Faculty of Geology and Geoenvironment, Department of Hist. Geology - Paleontology, cntrinia@geol.uoa.gr, aantonar@geol.uoa.gr, gkontak@geol.uoa.gr, ntsapar@geol.uoa.gr, vkarak@geol.uoa.gr*

[2] *National and Kapodistrian University of Athens, Faculty of Geology and Geoenvironment, Department of Geophysics-Geothermy, msegou@geol.uoa.gr*

Abstract

The Manassi section in Levkas Island belongs to the Pre-Apulian (Paxos) zone, the most external domain of the Hellenic realm. Its Early Tortonian sediments contain a rich foraminiferal fauna dominated, in numbers of individuals, by planktic species. Its benthic foraminiferal assemblage is characterized by a high number of taxa, with low numbers of individuals. Their study provides a basis for interpreting the paleobathymetry of the basin.

The Manassi section represents deposition in upper to lower bathyal depths, during a period of intense tectonic activity. Downslope transport of fauna by turbidity currents partly overprints the signal of paleobathymetrically-diagnostic foraminifera distribution. The recognition of allochthonous taxa is used, together with %P, to identify turbidite beds intercalated with in-situ marly sediments.

The micropaleontological and paleobathymetrical analyses of the studied sediments indicate that these correspond to distal atypical flysch deposited in the foredeep depozone of the most external domain (Pre-Apulian zone) of the Hellenide foreland basin.

Key words: *benthic foraminifera, paleobathymetry, Tortonian, Pre-Apulian zone, Mediterranean.*

Περίληψη

Η τομή Μανάση, (νήσος Λευκάδα) ανήκει στην Προ-Απούλια (Παξοί) ζώνη, η οποία αποτελεί το εξωτερικότερο τμήμα των Ελληνίδων. Τα ιζήματα της τομής, ηλικίας Κατώτερο Τορτόνιο, περιέχουν μια πλούσια πανίδα τρηματοφόρων, όπου επικρατούν σε αριθμό ατόμων, τα πλαγκτονικά είδη. Η υψηλής ποικιλότητας συνάθροιση βενθονικών τρηματοφόρων χαρακτηρίζεται από έναν υψηλό αριθμό ειδών, με μικρό αριθμό ατόμων. Η ανάλυση της κατανομής των ειδών των βενθονικών τρηματοφόρων παρέχει στοιχεία για την παλαιοβαθυμετρική εξέλιξη της λεκάνης. Τα ιζήματα της τομής Μανάση αντιπροσωπεύουν απόθεση σε βάθη της ανώτερης έως και κατώτερης βαθύαλης ζώνης, η οποία έλαβε χώρα κατά τη διάρκεια της μετά του Μέσου

Μειοκαίνου τεκτονικής ανύψωσης της περιοχής. Η κατά μήκος κατωφέρειας μεταφορά της πανίδας εξαιτίας της δραστηριότητας τουρβιδιτικών ρευμάτων επισκιάζει εν μέρει την κατανομή των διαγνωστικών για το παλαιοβάθος βενθονικών ειδών. Η αναγνώριση αλλόχθονων ειδών βενθονικών τρηματοφόρων χρησιμοποιείται, μαζί με την αναλογία των πλαγκτονικών τρηματοφόρων, για να καταδείξει την παρουσία τουρβιδιτικών στρωμάτων μέσα στις μάργες.
Η μικροπαλαιοντολογική και παλαιοβαθυμετρική ανάλυση των αποθέσεων της τομής Μανάσση, έδειξε ότι αυτές αντιπροσωπεύουν έναν μακρινό άτυπο φλύσχη που αποτέθηκε στο κέντρο απόθεσης (depocenter) του πλέον εξωτερικού χώρου (Προ-Απούλιας ζώνη) της προχώρας των Ελληνίδων.
Λέξεις κλειδιά: *βενθονικά τρηματοφόρα, παλαιοβαθυμετρία, Τορτόνιο, Προ-Απούλια ζώνη, Μεσόγειος.*

1. Introduction

A common goal in basin analysis is the assessment of paleobathymetry for use to interpret depositional environments, subsidence history and other aspects of basin evolution. The Middle Miocene foreland basin of Levkas island, Ionian Sea, needs considerable study both for its well-exposed outcrops of deep marine turbiditic strata and as an example of its sedimentary infill. Such studies are considerably hampered, however, by the lack of knowledge of paleobathymetry. The magnitude of uncertainty in paleobathymetric estimates could prevent a correct interpretation of subsidence analysis in such deep-water deposits.

Micropaleontologists have developed several methods to estimate paleodepths, in addition to methods based on the comparative abundance of planktic and benthic foraminifera. For example Culver (1988) documented the bathymetric distribution of some benthic foraminifera in the modern-day Gulf of Mexico, and used these to estimate paleodepths in some Cenozoic sequences in the same region. Murray and Alve (2000) found an overall trend towards an increase in benthic foraminiferal biodiversity with paleodepth. Van der Zwaan *et al.* (1990) determined a regression for the relationship between bathymetry and the percentage of planktic foraminifera with respect to the total fossil foraminiferal population (%P), based on present day bathymetric transects:

$$Depth(m) = e^{3.58718+(0.03534*\%P)}$$

where the plankton fraction %P=100*P/(P+B-S), and P is the amount of planktic foraminifera, B is the amount of benthic foraminifera and S is the amount of environmental stress markers, e.g. species of benthic foraminifera that can tolerate low oxygen concentrations [original list of Van der Zwaan *et al.* (1990) modified by Van Hinsbergen *et al.* (2005)].

However, the most widely applied methodology for assessing paleobathymetry is the analysis of benthic foraminiferal biofacies. In fact, benthic foraminifera have proved to be useful bathymetric indicators. Recent studies on modern faunas demonstrated that the faunal composition is strongly related to organic matter flux rates and dissolved oxygen concentrations in the bottom and pore water (e.g. Corliss 1985, Gooday 1994, Jorissen *et al.* 1995). In oceanic environments both parameters exhibit strong depth-dependent gradients. Consequently, certain benthic foraminiferal faunas are restricted to distinct bathymetric intervals. In particular, continental margins are characterized by a stenobathic distribution of many benthic foraminifera (e.g. Schmiedl *et al.* 1997).

In the present study, the overall nature of the benthic foraminiferal assemblages is examined to prove the validity of paleodepth estimations obtained computed using the percentage of planktic foraminifera, in part of the Miocene age deep sea sediments of Levkas Island.

2. Geological Setting

Levkas Island belongs to the Ionian Islands which are located in the west segment of the Hellenic Arc, the most active plate margin of the Mediterranean region (e.g. McKenzie 1978). The tectonic setting of the wider area is determined by the continental collision between northwestern Greece in the east and the Apulian platform in the west, as well as by the subduction of the African plate under the Aegean microplate along the active Hellenic Arc in the southwest. The Ionian Islands are situated in a transitional zone between the northwestern end of this active subsidence and the continental collision in the north.

The main tectonic structure of this transitional area is the Kephallinia Fault Zone (KFZ), which represents the active boundary between the SW-moving Aegean microplate and the Apulian platform. Based on data from Durmeijer *et al.* (1999) and Gautier *et al.* (1999) the age of the onset of the activity of KFZ could be estimated to a possible maximum age of the Pliocene-Pleistocene boundary. Many neotectonic active faults, striking to the NNE-SSW or E-W direction cross-cut the island (e.g. Cushing 1985).

Levkas island is built up mainly by Alpine Mesozoic-Cenozoic sedimentary rocks belonging to the external units of the Hellenides, the Pre-Apulian (Paxos) zone and the Ionian zone (Fig. 1; Bornovas 1964, IGRS-IFP 1966, Cushing 1985), separated from one another by a major west-directed thrust fault (Aubouin 1957, Jacobshagen 1986). This thrust boundary is marked by evaporite intrusion suggesting that contractional deformation was the most important structural control of orogenesis in Western Greece (Karakitsios and Rigakis in press).

The Pre-Apulian zone corresponds to the most external domain of the Hellenic realm. It has been traditionally considered as a relatively uniform Mesozoic – Cenozoic carbonate transitional domain, between the Apulian platform and the Ionian basin (BP 1971, Karakitsios 1995). The general setting is complicated by strong tectonic deformation, including crustal extension, collision, and flexural subsidence, with undetermined amounts of shortening and block rotation (Karakitsios and Rigakis in press). Indeed, the outcropping successions differ in stratigraphic completeness, sedimentary development and faunal/floral content.

The depositional sequence in the Pre-Apulian zone begins with Triassic to Bajocian limestones, containing intercalations of black shales and anhydrite beds (borehole data, ESSO Hel. 1960). The lowest stratigraphic outcrops, located in Levkas Island, comprise Lower Jurassic dolomites and Middle Jurassic cherts and bituminous shales (Bornovas 1964, BP 1971). The Upper Jurassic consists of white chalky limestones and dolomite intercalations, with rare cherts and organic-carbon-rich black shales, containing planktic foraminifera. Lower Cretaceous limestones and dolomites outcrop only in Kephallonia Island, and are considered less pelagic in comparison to the Ionian facies of the same age. During the Campanian-Maastrichtian the platy limestones gradually become chalky with thin layers of argillaceous schists. They contain planktic foraminifera together with Rudists' fragments indicating the presence of intra-platform basins, characterizing the slope between the Apulian platform and the Ionian basin (Nikolaou 1986, Karakitsios and Rigakis in press).

The Paleocene formations consist of micritic limestones with planktic foraminifera (BP 1971). Intense tectonic activity, resulting in the differentiation of the Pre-Apulian zone, into relatively deep and shallow (sometimes emerged) areas, is deduced by sporadic hiatuses in between Paleocene and Late Cretaceous, described by Mirkou (1974). The Lower Eocene sequence comprises pelagic limestones with marl intercalations, whilst the Upper Eocene formations consist of reefal, unbedded limestones, with Algae, Bryozoans, Corals, Echinoids, and large foraminifera. Oligocene sediments were deposited in small basins (tectonic grabens) in between emerged areas, which were locally eroded. This setting can be attributed to the intense tectonic instability, which persisted throughout the Oligocene. During the Oligocene-Aquitanian, the intense diversification of foraminiferal assemblages (Accordi *et al.* 1998) suggests the presence of flexural subsiding

foreland basins (Karakitsios and Rigakis in press). In the late Early Miocene, progressive deepening ensued, with the demise of the former carbonate slope.

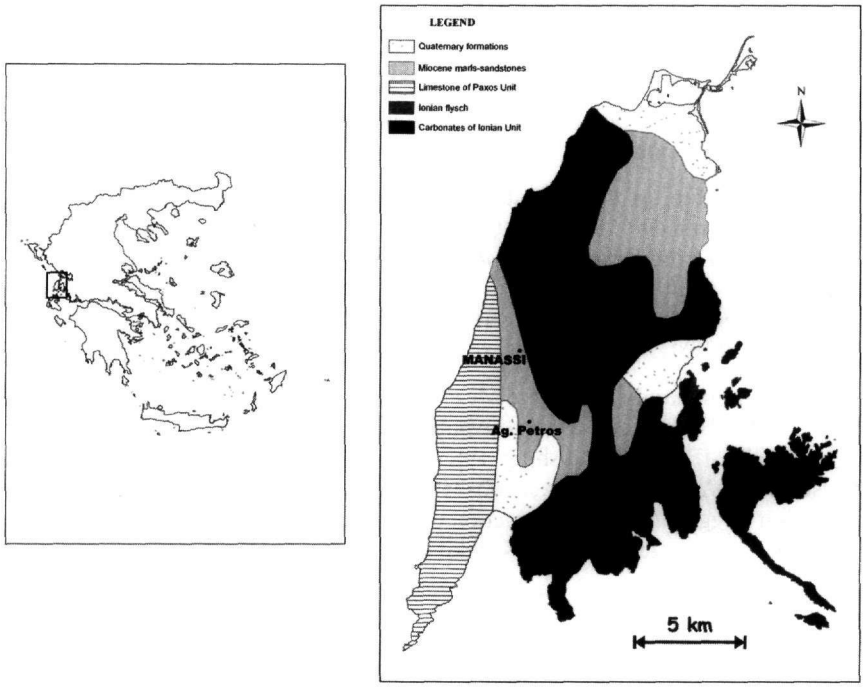

Figure 1 - Simplified geological map of Levkas island indicating the location of the studied section (after Rondoyianni-Tsiambaou 1997)

3. Study Location and Methods

This research deals with a more detailed study on paleobathymetry of a Miocene section (Manassi section) which belongs to the pre-Apulian zone and is located in the southwestern part of Levkas island (Fig. 1).

The Oligocene-Miocene deposits in this area conformably overlie Eocene limestones in the west (de Mulder 1975). Finely-bedded, pelagic limestones of Eocene age are overlain by a relatively thin succession of detrital, neritic limestones, passing upwards into at least 400-500 m of marls and clays, which may reach as high as the Upper Miocene (Bizon 1967).

The Manassi Section is located on the eastern slope of a N-S oriented valley. The studied succession consists of blue grey marls and clays with some fine grained sandstone interbeds. The intercalations of these thin, clastic beds and especially of positively graded sandstones in the studied succession reflect the influence of density currents, which supplied coarser material from a distant hinterland (de Mulder 1975).

The 25 m-thick section was measured and sampled at 0.5 to 1 m intervals. For the faunal analysis 26 samples (391-1 to 391-26) were taken (Fig. 2). Samples were washed over a 63 μm sieve and subsequently the coarse fraction was dry sieved over 125 µm sieve. The fraction >125 μm was then investigated for its benthic foraminiferal content. The picked planktonic specimens were counted and their (%P) was computed. Biostratigraphic attribution is based on the standard biozonal schemes of Iaccarino (1985) according to the absolute ages from Hilgen *et al.* (2000) and Foresi *et al.* (2002).

The total number of planktic (PFN) and benthic (BFN) foraminifera per gram was calculated by extrapolating the number of specimens in the split to the whole residue.

In order to calculate the changing paleobathymetry the following factors were identified:

Diversities were determined following the Shannon-Wiener index (e.g. Buzas and Gibson 1969). In addition, ratios between planktic (P) and benthic (B) foraminifera were calculated applying the formula P/(P+B). The P/B ratios were integrated with marker benthic foraminifera in order to determine paleobathymetry.

To assess the depositional depth of the studied marine sediments, the general relationship between the fraction of planktic foraminifera with respect to the total foraminiferal population (%P) and depth of Van der Zwaan *et al.* (1990) was used, following sample selection and counting procedures described by van Hinsbergen *et al.* (2005).

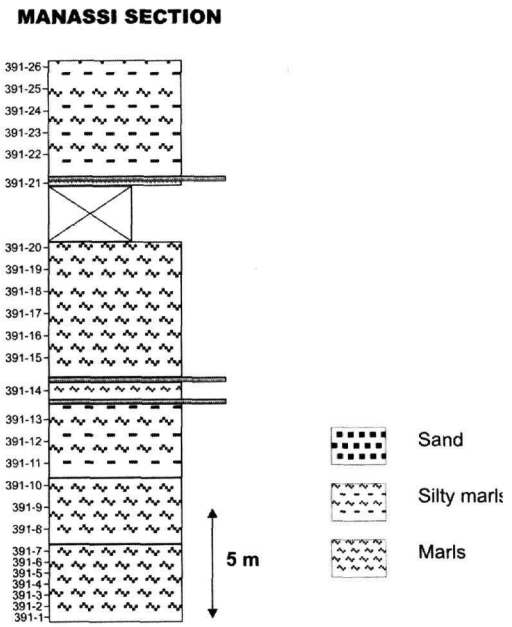

Figure 2 - Lithostratigraphical column of the studied section

The following depth zonation (McDougall, 1985) was used: inner shelf=0-50 m, outer shelf=50-150 m, upper bathyal=150-500 m, upper middle bathyal=500-1500 m, lower middle bathyal=1500-2000 m, lower bathyal=2000-3500 m, >3500 m=abyssal.

4. Biostratigraphy

The planktonic foraminiferal analysis was carried out on the total of samples. Preservation was generally good, although at times was poor. The biostratigraphic results were based on the qualitative analysis of planktonic foraminifera, analyzed at the species level. Their specific identifications were conducted according to reference publications (Dermitzakis 1978, Iaccarino 1985, Hilgen *et al.* 2000, Foresi *et al.* 2002). For the biostratigraphic analysis we only considered the appearance/disappearance of marker species and paracme/acme intervals of selected taxa according to Foresi *et al.* (2002).

The qualitative analysis revealed 14 planktonic foraminifera categories: *Paragloborotalia siakensis, Globigerinoides obliquus obliquus, Globorotalia menardii-preamenardii, Catapsydrax parvulus, Neogloboquadrina atlantica praeatlantica, P. partimlabiata* and *N. acostaensis*. The coiling direction of the neogloboquadriniids was investigated separately because of their biostratigraphic value.

G. obliquus obliquus is present in all the samples and no specimens of *G. subquadratus* were observed. The last common occurrence (LCO) of *G. subquadratus,* has been dated in the Mediterranean at 11.54 and 11.58 Ma (Hilgen *et al.* 2000, 2003, Lirer *et al.* 2002) and at same time (11.54 Ma according to Hilgen *et al.* 2000, 2003, Lirer *et al.* 2002), the first regular occurrence (FRO) of *G. obliquus* is recorded. This event coincides with the end of the first influx of the neogloboquadrinids (FO of neogloboquadrinids 11.78 Ma), (Hilgen *et al.* 2000, 2003, Foresi *et al.* 2002). Above this level *N. acostaensis* occurs in low percentages.

In our record few specimens of *N. acostaensis* are recorded (2-5 %) with random (left and right) coiling direction. *N. antlantica praeantlantica* is also present having the same distributional pattern of *N. acostaensis*. A paracme interval in the distribution range of neogloboquadriniids has been recorded in Mediterranean and dated at 11.54 -11.21 Ma (Foresi *et al.* 2002). These dates coincide with the LCO of *G. subquadratus* and the LO of *P. siakensis* respectively (Iaccarino *et al.* 2004, Foresi *et al.* 2002, Hilgen *et al.* 2003). In the same interval *C. parvulus* is abundant (Foresi *et al.,* 2002). In the studied section the same pattern of *C. parvulus* is observed.

P. siakensis left coiled is abundant from the base of the section upward. The last occurrence of this species has been dated at 11.21 Ma (Hilgen *et al.* 2000, Caruso *et al.* 2002, Di Stefano *et al.* 2002, Foresi *et al.* 2002, Lirer *et al.* 2004, Iaccarino *et al.* 2004). *Catapsydarx parvulus* is present in several samples throughout the section. The last occurrence of this species in Mediterranean is reported at 9.91 Ma (Hilgen *et al.* 2000).

Consequently, according to the biostratigraphical criteria such as the distributional pattern of neogloboquadriniids, the regular occurrence of *G. obliquus obliquus* and the presence of *P. siakensis* in all the samples, the section covers the time interval between 11.54 and 11.2 Ma, having a lower Tortonian age, just above the Serravallian/Tortonian boundary astronomically dated at 11.6 Ma (Hilgen *et al.* 2005).

5. Benthic Foraminifera Species

Of the 26 samples, only one was barren of benthic foraminifera. It is sample 391-26 which contains high fractions of quartz and rock fragments, which probably derived from downslope transport. Four samples yielded fewer than 200 benthics (391-21, 105 total foraminifera only, 391-23, 180 foraminifera only, 391-24, 183 foraminifera only and 391-25, 73 foraminifera only). However, paleodepths for these samples were estimated.

One hundred and sixty nine species and species groups of benthic foraminifera were identified in the 25 samples studied. The primary taxonomic references are given in Ellis and Messina (1940 and supplements).

Fig. 3 shows the frequency of the dominant benthic species in the samples. The most abundant species recovered from the section were *Siphonina reticulata, Cibicidoides kullenbergi, Melonis barleeanus, C. italicus.* These taxa abundantly and persistently occur throughout the section along with *Globocassidulina subglobosa, Gyroidinoides neosoldanii* and *Uvigerina semiornata rutila.* In the upper part of the section, clearly transported shallow water taxa co-occur with deep water species. In these cases it can be clearly inferred that the shallow water taxa have been dislodged downslope into deeper waters, through transport or turbidity activity.

6. Paleobathymetry

6.1. Analysis of %P planktic foraminifera

The result of total planktic foraminiferal (PFN) fauna performed in this study is shown in Fig.4, together with BFN trends. With the exception of samples 391-1 to 391-3 and 391-20, the planktic abundance (P/P+B) in all observed Manassi samples is greater than 90 %. According to Van der Zwaan *et al.* (1990) these data suggest an average water depth of about 1000 m. Moreover, the PFN strongly fluctuates between 1330 specimens per gram and 78.500 specimens per gram; whereas BFN remains relatively stable exhibiting low values (Fig. 4). According to Mendes *et al.* (2004), the BFN is inversely related with water depth. Slightly increased BFN in the lowermost part of the section (sample 391-3) indicates that at this stratigraphic level bottom water conditions have been generally more favorable for the production of benthic foraminifera.

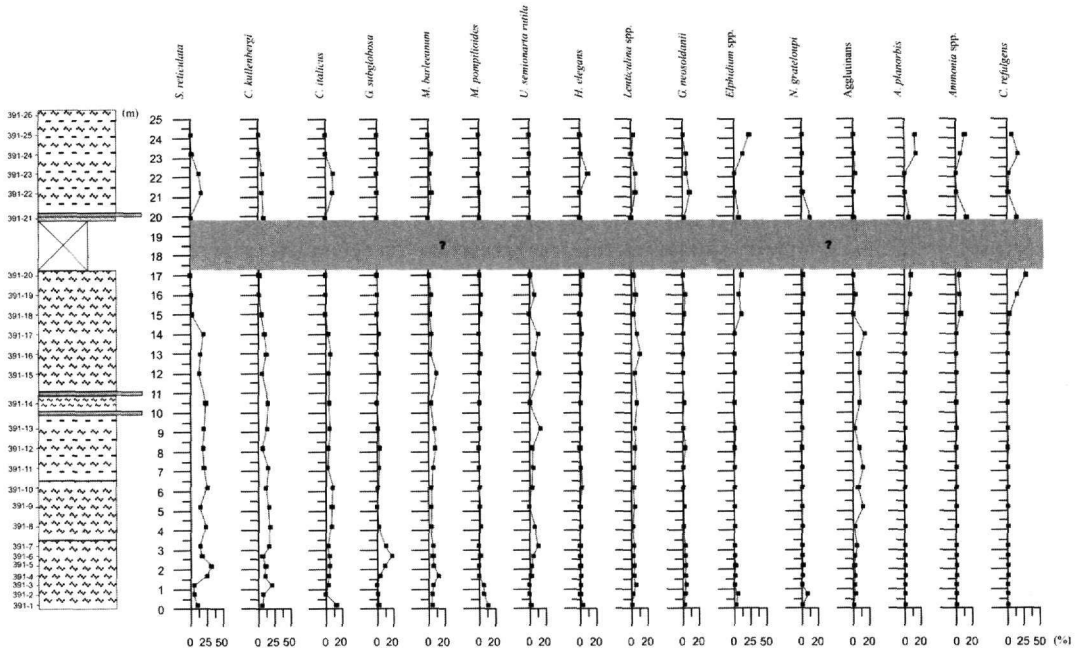

Figure 3 - Abundance pattern of the most significant benthic foraminifera species identified in the studied section

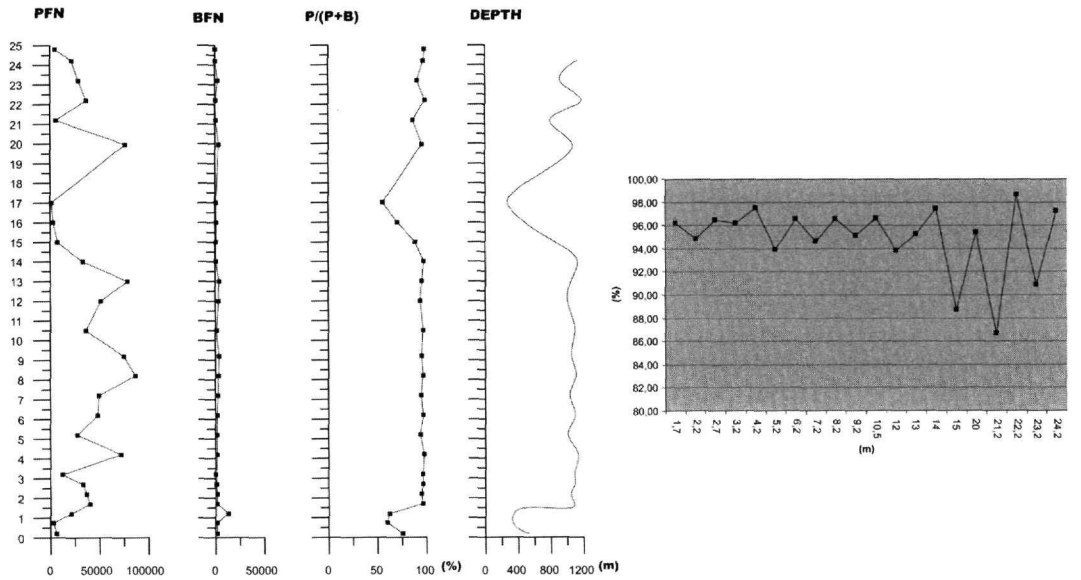

Figure 4 - PFN, BFN, P/B ratios together with the paleodepth curve obtained after the application of the regression of Van der Zwaan *et al.* (1990) of the studied samples. The inlet to the right represents variations in planktic percent above 90 exclusive three samples which show values below 60 %

Fig. 4 also shows planktic percentages of Manassi section samples exclusive of the four aforementioned samples. Several fluctuations are revealed by this graph. There is no relationship between these fluctuations and the sediment grain size as all the samples are from the grey marls. Although the significance of variations in planktic percent above 90 % is problematical, this may

merely reflect periodic dilution of the autochthonous deep-water fauna with transported shallower faunas (e.g. Robertson 1998). It is likely that, in these beds, some degree of faunal reworking has occurred, displacing shallow water taxa into deeper water faunas. This condition suggests that these beds could correspond to turbidite horizons.

In samples 391-1 to 391-3 and 391-20 there is a drop in P/B together with a drop in PFN. According to Speijer and Schmitz (1998), where fluctuations between these records coincide, it is likely that carbonate dissolution has occurred at some step during the generation of the fossil assemblage. In exceptional situations this association of changes may indicate a real paleoenvironmental change. If so, in shelf settings this should be readily discernable from the composition of the planktic and/or benthic foraminiferal assemblages.

Application of van der Zwaan *et al.* (1990) regression indicates that deposition began at ~530 m (deep upper bathyal) during the deposition of sample 391-1 (0.2 m) and regressed to ~340 m (upper bathyal) in sample 391-3 (1.2 m). The sea then transgressed to a paleodepth of ~1130 m (deep lower middle bathyal) during the deposition of sample 391-17 (14 m). An ensuing rapid regression saw sea-levels attain a paleodepth ~270 m (upper bathyal) during the deposition of sample 391-20, then transgress abruptly to ~1100 m (deep middle bathyal) at the time of sample 391-21 and remained relatively constant with short-term fluctuations from sample 391-22 till 391-25.

6.2. Diversity

Shannon-Wiener H(S) values in the Manassi section vary from 2.61 to 3.42 (Table 1). Gibson and Buzas (1973) showed that these values correlate to water depths ranging from 80 to 3200 m in the northeastern Gulf of Mexico. In view of the wide ranges of water depths associated with diversity measure H(S), it is unrealistic to assign absolute water depths to Manassi deposition based on these criteria, although increasing diversity probably indicates increasing water depth in a relative sense. Therefore the variations in diversity may reflect only variations in degree of dilution by shallower water forms.

6.3. Bathymetric significance of foraminiferal assemblages

Any significant trends in palaeobathymetry can be independently checked on the studied samples along the succession, by identifying marker species for selected depth intervals.

The bathymetric preferences of the different foraminiferal taxa were assessed by evaluating their distribution pattern in modern oceans (Table 1). Based on this information the bathymetric evolution at the investigated site can be reconstructed. The paleodepths indicated by the benthic foraminifera in samples 391-4 to 391-18, 391-22 and 391-23 agree with those calculated using Van der Zwaan *et al.* (1990) regression. The benthic assemblages in these samples indicate an upper middle bathyal environment, being dominated by *C. kullenbergi* and *S. reticulata.* For samples 391-18 to 391-21, 391-24 and 391-25, however, the paleodepths calculated from the percentage of planktic foraminiferal fauna differ markedly from those indicated by the benthic one. These samples yielded benthic assemblages that were dominated by *Elphidium* spp. and *C. refulgens* associated with a lesser *A. planorbis* and *Ammonia* spp. The normally shallow-water preferences of *Elphidium* species (Hayward *et al.* 1997) and *C. refulgens* (Murray 1991) suggest that these samples were deposited at neritic paleodepths and not at the bathyal paleodepths as suggested by the abundant planktic foraminifera. Furthermore, benthic foraminifera typical of deep-water habitats, such as were recorded in the lower part of the sequence, were also recovered from these samples, yet in small percentages. Thus the presence of specimens from *Elphidium* species and *C. refulgens* in fossil bathyal assemblages should be explained by sediment displacement (e.g Phleger *et al.* 1953) or rafting of plant material to which cibicidids lived attached into pelagic environments after storms (Sprovieri and Hasegawa 1990).

Table 1- Depth distribution of a selection of benthic marker species based on Parker (1958), Blanc-Vernet (1969), Wright (1978), Parisi (1981), Jorissen (1987), Sprovieri and Hasegawa (1990), Sgarella and Moncharmont Zei (1993), De Stigter *et al.* (1998), De Rijk *et al.* (2000), Seidenkrantz *et al.* (2000), Jannink (2001), Kouwenhoven *et al.* (2003). Note that these studies are all based on the Mediterranean area

Samples	Predominant Species	Abundant Species	Diversity	%P	Depth	Depth (m)
391-1	*C. italicus*	*M. pompilioides* *S. reticulata*	3,17	75,54	Deep Upper Bathyal	532,30
391-2	*C. kullenbergi*	*A. helicinus* *M. pompilioides*	3,41	60,00	Upper Bathyal	332,23
391-3	*C. kullenbergi*		3,07	62,05		342,38
391-4	*S. reticulata*	*C. kullenbergi* *M. barleeanus*	2,88	96,22	Deep Lower Bathyal	1085,11
391-5	*S. reticulata*	*C. kullenbergi* *G. subglobosa*	2,67	94,90		1043,03
391-6	*G. subglobosa*	*S. reticulata* *C. kullenbergi*	2,97	96,49		1094,18
391-7	*C. kullenbergi*	*S. reticulata* *G. subglobosa* *U. rutila*	2,83	96,21		1090,81
391-8	*S. reticulata*	*C.kullenbergi*	2,75	97,50		1131,74
391-9	*C. kullenbergi*	*S.reticulata*	3,03	93,91		1010,36
391-10	*S. reticulata*	*C.kullenbergi*	2,68	96,54		1096,30
391-11	*S. reticulata*	*C.kullenbergi*	3,1	94,65		1033,51
391-12	*S. reticulata*	*C.kullenbergi*	3,12	96,57		1108,00
391-13	*S. reticulata*	*C.kullenbergi* *U. rutila*	2,8	95,17		1053,70
391-14	*S. reticulata*	*C.kullenbergi* *A. helicinus*	2,71	96,63		1095,82
391-15	*S. reticulata*	*U. rutila*	3,32	93,84		1005,78
391-16	*S. reticulata*	*C.kullenbergi,* *Lenticulina* spp.	2,99	95,24		1047,53
391-17	*S. reticulata*	*C.kullenbergi* *U. rutila*	3,18	97,42		1128,66
391-18	*Elphidium* spp.	*Ammonia* spp.	3,42	88,69	Upper Middle Bathyal	848,01
391-19	*C. refulgens*	*Elphidium* spp. *A. planorbis*	3,41	70,54		475,97
391-20	*C. refulgens*	*Elphidium* spp. *A. planorbis*	2,93	55,56	Upper Bathyal	274,82
391-21	*C. refulgens*	*Elphidium* spp.	2,79	95,39	Deep	1063,64

		Ammonia spp.			Middle Bathyal	
391-22	*S. reticulata*	*C. kullenbergi, G. neosoldanii*	3,23	86,70		793,49
391-23	*S. reticulata*	*C. ungerianus, H. elegans*	3,05	98,62		1178,38
391-24	*C. refulgens*	*Elphidium* spp. *A. planorbis*	3,02	90,85		914,46
391-25	*C. refulgens*	*A. planorbis, Ammonia* spp.	2,61	97,20		1128,89

7. Discussion-Conclusions

The present study was undertaken to provide a comprehensive paleobathymetric analysis of a section (Manassi section) located in the central part of the pre-Apulian Zone of Levkas Island. The biostratigraphic analysis based on planktic foraminifera indicated a Lower Tortonian age (between 11.54 and 11.21 Ma). This time interval is considered very crucial for the studied area as it marks the transition from carbonate to clastic sedimentation in western Greece and a phase of compression which affected the external Ionian zone and the pre-Apulian zone of Levkas. This shortening is related to the overriding of the pre-Apulian zone by the Ionian zone.

The paleobathymetric analysis showed that sedimentation occurred in a wide, deep and well-ventilated foreland basin. Deposition occurred on a steep, unstable slope adjacent to a narrow shelf. Periodic downslope transport of shallow-water sediments into deeper water occurred throughout this interval, perhaps related to intense tectonic activity. The prominent occurrence of turbidite horizons can be linked to flysch deposition.

It has so far been generally accepted, that the Pre-Apulian zone lacks typical flysch sediments. However, we consider the post - Oligocene deposits as the distal atypical flysch sediments, deposited in the foredeep depozone of the most external domain (Pre-Apulian zone) of the Hellenides' foreland basin system (DeCelles and Giles 1996). Their partial absence in some areas is due to the fact that these areas correspond to the most external foreland basin forebulge uplifts, which sediments have possibly been eroded, leaving only unconformities.

8. Acknowledgements

This project is co-funded by the European Social Fund and National Resources (EPEAEK II) PYTHAGORAS II (70/3/8020).

9. References

Accordi, G., Carbone, F., and Pignatti, J., 1998. Depositional history of a Paleogene carbonate ramp (Western Cephalonia, Ionian Islands, Greece), *Geol Romana*, 34, 131–205

Aubouin, J., 1957. Essai de corrélation stratigraphique de la Grèce occidentale, *Bulletin de la Societe Geologique de France,* 7, 281–304

B.P., 1971. The geological results of petroleum exploration in Western Greece, *I.G.S.R.,* 10, 1-73.

Bizon, G., 1967. Contribution à la connaissance des foraminifères planctoniques de l'Épire et des îles ioniennes (Grèce occidentale), Publication de l'Institutt Francais du Pétrole, *Edition Technip,* 1–44.

Blanc-Vernet, L., 1969. Contribution a l'étude des Foraminifères de Méditerranée, *Recueil des Travaux de la Station Marine d'Endoume,* 64, 1–281.

Bornovas, J., 1964. Géologie de l' île de Lefkade, *Geol. and Geophys. Research (I.G.S.R.),* 10, 142pp.

Buzas, M.A., and Gibson, T.G., 1969. Species diversity: Benthonic foraminifera in western North Atlantic, *Science,* 163, 72–75.

Corliss, B.H., 1985. Microhabitats of benthic foraminifera within deep-sea sediments, *Nature,* 14, 435-438.

Caruso, A., Sprovieri, M., Bonnano, A., and Sprovieri, R., 2002. Astronomical calibration Serravallian-Tortonian Case Pelacani section (Sicily, Italy). In S.M. Iaccarino (ed.), *Integrated Stratigraphy and Paleoceanography of the Mediterranean Middle Miocene. Rivista Italiana di Paleontologia e Stratigrafia,* 108, 297-306pp.

Culver, S.J., 1988. New foraminiferal depth zonation of the Northwestern Gulf of Mexico, *Palaios,* 3, 69-86.

Cushing, M., 1985. Evolution structurale de la marge nord oust hellénique dans l' île de Levkas et ses environs (Grèce nord occidentale), *Thèse 3me cycle*, Univ. De Paris-Sud.

De Mulder, E.F.J., 1975. Microfauna and sedimentary-tectonic history of the Oligo-Miocene of the Ionian Islands and Western Epirus (Greece), *Utrecht Micropaleontol. Bul.l* 13, 1–139.

De Rijk, S., Jorissen, F.J., Rohling, E.J., and Troelstra, S.R., 2000. Organic flux control on bathymetric zonation of Mediterranean benthic foraminifera, *Marine Micropaleontology,* 40, 151–166.

De Stigter, H.C., Jorissen, F.J., and Van der Zwaan, G.J., 1998. Bathymetric distribution and microhabitat partitioning of live (Rose Bengal stained) benthic foraminifera along a shelf to bathyal transect in the southern Adriatic Sea, *Journal of Foraminiferal Research,* 28, 40–65.

DeCelles, F.G., and Giles, K.A., 1996. Foreland basin systems, *Basin Research,* 8, 105-123.

Dermitzakis, M. D., 1978. Stratigraphy and sedimentary history of the Miocene of Zakynthos (Ionian Islands, Greece), *Annales Geologique des Pays Helleniques,* 29, 47-186.

Di Stefano, E., Bonomo, S., Caruso, A., Dinarés-Turell, J., Foresi, L., Salvatorini, G. and Sprovieri, R., 2002. Calcareous plankton bio-events in the Miocene Case Pelacani section (Southeastern Sicily, Italy). In S.M. Iaccarino (ed.), *Integrated Stratigraphy and Paleoceanography of the Mediterranean Middle Miocene. Rivista Italiana di Paleontologia e Stratigrafia,* 108, 307-324pp.

Duermeijer, C.E., Krijgsman, W., Langereis, C.G., Meulenkamp, J.E., Triantaphyllou, M.V., and Zachariasse, W.J., 1999. A Late Pleistocene clockwise rotation phase of Zakynthos (Greece) and implications for the evolution of the western Aegean arc, *Earth Planet. Sci. Lett.,* 173, 315–331.

Ellis, B.F.S., and Messina, A.R., 1940. Catalogue of foraminifera, *Am. Nat. Mus. N.Y. Spec. Publ.*

Foresi, L.M., Bonomo, S., Caruso, A., Di Stefano, A., Di Stefano, E., Iaccarino, S. M., Lirer, F., Salvatorini, G., and Sprovieri, R., 2002. High resolution calcareous plankton biostratigraphy of the Serravalian succession of the Tremiti Islands (Adriatic Sea, Italy). In S.M. Iaccarino (ed.), *Intergrated Stratigraphy and Paleoceanography of the Mediterranean Middle Miocene. Rivista Italiana di Paleontologia e Stratigrafia,* 108, 257-273.

Gautier, P., Brun, J.-P., Moriceau, R., Sokoutis, D., Martinod, J., and Jolivet, L., 1999. Timing, kinematics and cause of Aegean extension: a scenario based on a comparison with simple analogue experiments, *Tectonophysics,* 315, 31–72.

Gibson, T.G., and Buzas, M.A., 1973. Species Diversity: Pattern in modern and Miocene foraminifera of the eastern margin of North America, *Geol. Soc. Amer. Bull.*, 84, 217-238.

Gooday, A.J., 1994. The biology of deep-sea foraminifera: a review of some advances and their applications in paleoceanography, *Palaios*, 9, 14-31.

Hayward, W.B., Grenfell, R.H., Pullin, D.A., Reid, C., and Hollis, J.C., 1997. Foraminiferal associations in the upper Waitemata Harbour, Auckland, New Zealand, *Journal of the Royal Society of New Zealand*, 27, 21-51.

Hilgen, F.J., Abdul Aziz, H., Krijgsman, W., Raffi, I., and Turco, E. 2003. Integrated stratigraphy and astronomical calibration of the Serravallian and lower Tortonian at Monte dei Corvi (Middle-Upper Miocene, northern Italy), *Palaeogeography, Palaeoclimatology, Palaeoecology*, 199, 229-264.

Hilgen, F.J., Krijgsman, W., Raffi, I., Turco, E., and Zachariasse, W.J., 2000. Integrated stratigraphy and astronomical calibration of the Serravallian/Tortonian boundary Section at Monte Gibliscemi (Sicily, Italy), *Marine Micropaleontology*, 38, 181-211.

Hilgen, F., Aziz, H.A., Bice, D., Iaccarino, S., Krijgsman, W., Kuiper, K., Montanari, A., Raffi, I, Turco, E., and Zachariasse, W.J., 2005. The global boundary stratotype section and point (GSSP) of the Tortonian stage (Upper Miocene) at Monte Dei Corvi, *Episodes* 28 (1), 6-17.

Iaccarino, S. 1985. Mediterranean Miocene and Pliocene planktic Foraminifera. In H.M. Bolli, J.B. Saunders and K. Perch-Nielsen (eds), *Plankton Stratigraphy*. Cambridge Univ. Press, London, 283-314pp.

Iaccarino, S. M., Lirer, F., Bonmo, S., Caruso, A., Di Stefano, A., Di Stefano, E., Foresi, L. M., Mazzei, R., Salvatorini, G., Sprovieri, R., and Turco, E., 2004. Astrochronology of Late Middle Miocene Mediterranean sections. In B. D' Argenio, A.G. Fischer, I. Premoli-Silva, H. Weissert and V. Ferreri (eds), *Cyclostratigraphy: An Essay of Approaches and Case Histories, Society of Sedimentary Geology*, 81, 25-42pp.

IGRS-IFP, 1966. *Etude géologique de l' Epire (Grèce nord occidentale)*, Editions Technip, Paris, 306pp.

Jacobshagen, V., 1986. *Geologie von Griechenland*, Borntraeger, Berlin-Stuttgart, 279pp.

Jannink, N.T., 2001. Seasonality, biodiversity and microhabitats in benthic foraminiferal communities, *Geologica Ultraiectina*, 203, 192 pp.

Jorissen, F. J., de Stigter, H. C., and Widmark, J. G. V., 1995. A conceptual model explaining benthic foraminiferal microhabitats, *Marine Micropaleontology*, 26, 3-15.

Jorissen, F.J., 1987. The distribution of benthic foraminifera in the Adriatic Sea, *Marine Micropaleontology*, 12, 21–48.

Karakitsios, V., 1995. The Influence of Preexisting Structure and Halokinesis on Organic Matter Preservation and Thrust System Evolution in the Ionian Basin, Northwestern Greece, *AAPG Bulletin*, 79, 960-980.

Karakitsios, V., and Rigakis, N., in press. Evolution and Petroleum Potential of the Western Greece, *Journal of Petroleum Geology*.

Kouwenhoven, T.J., Hilgen, F.J., and Van der Zwaan, G.J., 2003. Late Tortonian–early Messinian stepwise disruption of the Mediterranean–Atlantic connections: constraints from benthic foraminiferal and geochemical data, *Palaeogeography, Palaeoclimatology, Palaeoecology*, 198, 303–319.

Lirer, F., Caruso, A., Foresi, L.M., Iaccarino, S., and Iacumin, P., 2004. Paleoclimatic changes in the Serravallian record of the Mediterranean area. In R. Coccioni, S. Galeotti and F. Lirer (eds), *Proceedings of the first Meeting of Environmental Micropaleontology for Young Italian Researcher,* Grybowski Foundation Special Publication, 9, 77-96pp.

McDougall, K., 1985. Miocene to Pleistocene benthic foraminifers and paleoceanography of the Middle America slope, Deep Sea Drilling Project Leg 84, *Initial Reports Deep Sea Drilling Project,* 84, 363-418.

McKenzie, D.P., 1978. Some remarks on the development of sedimentary basins, *Earth Planet. Sci. Lett.,* 40, 23-32.

Mendes, I., Gonzalez, R., Dias, J.M.A., Lobo, F., and Martins, V., 2004. Factors influencing recent benthic foraminifera distribution on the Guadiana shelf (Southwestern Iberia), *Marine Micropaleontology,* 51, 171-192.

Mirkou, R.M., 1974. Stratigraphie et Géologie de la partie septentrionale de l' île de Zante (Grèce), *Ann. Géol.Pays Hell.,* 26, 35-108.

Murray, J. W., 1991. *Ecology and Paleoecology of Benthic Foraminifera*, Harlow, Essex, UK, Longman Scientific and Technical Publishers, 451 pp.

Murray, J.W., and Alve, E., 2000. Do calcareous dominated shelf foraminiferal assemblages leave worthwhile ecological information after their dissolution? In M.B. Hart, M.A. Kaminski and C.W. Smart (eds), Proceedings of the Fifth International Workshop on Agglutinated Foraminifera, *Grzybowski Foundation Special Publication,* 7, 311-331pp.

Nikolaou, C., 1986. Contribution to the study of Neogene and Geological concepts of the Ionian and Preapulian zone and their boundaries in relation to hydrocarbon exploration mainly on Strophades, Zakynthos and Cephallonia, *PhD thesis,* National and Kapodistrian University of Athens, 350 pp., Athens.

Parisi, E., 1981. Distribuzione dei foraminiferi bentonici nelle zone batiali del Tirreno e del Canale di Sicilia, *Rivista Italiana di Paleontologia,* 87 (2).

Parker, F.L., 1958. Eastern Mediterranean Foraminifera, *Reports of the Swedish Deep-Sea Expedition,* 8, 217–293.

Phleger, F.B., Parker, F.L., and Peirson, J.F., 1953. North Atlantic foraminifera. In H. Pettersson, (ed.), *Reports of the Swedish Deep-Sea Expedition 1947–1948., Sediment cores from the North Atlantic*, vol. VII. Fasc. 1, Sweden.

Robertson , B.E., 1998. Systematics and paleoecology of the benthic Foraminiferida from the Buff Bay section, Miocene of Jamaica, *Micropaleontology,* 44, 1-266.

Rondoyianni-Tsiambaou, Th., 1997. Les seismes et les environnement géologique de l' île de Lefkade, Grèce: Passé et futur. In Marinos *et al.* (eds), *Engineering Geology and the Environment,* Balkema, 1469-1474pp.

Schmiedl, G., Mackensen, A., and Müller, P.J., 1997. Recent benthic foraminifera from the eastern South Atlantic Ocean: dependence on food supply and water masses, *Marine Micropaleontology,* 32, 249–287.

Seidenkrantz, M.-S., Kouwenhoven, T.J., Jorissen, F.J., Shackleton, N.J., and Van der Zwaan, G.J., 2000. Benthic foraminifera as indicators of changing Mediterranean–Atlantic water exchange in the late Miocene, *Marine Geology,* 163, 387–407.

Sgarella, F., and Moncharmont Zei, M., 1993. Benthic foraminifera of the Gulf of Naples (Italy): systematics and autoecology, *Bolletino della Societa Paleontologica Italiana,* 32 145–264.

Speijer, R.P., and Schmitz, B., 1998. A benthic foraminiferal record of Paleocene sea level and trophic/redox conditions at Gebel Aweina, Egypt, *Palaeogeography, Palaeoclimatology, Palaeoecology,* 137, 79-101.

Sprovieri, R., and Hasegawa, S., 1990. Plio-Pleistocene Benthic foraminifer stratigraphic distribution in the deep-sea record of the Tyrrhenian sea (ODP LEG 107), *Proceedings of the Ocean Drilling Program, Scientific Results,* 107, 429-459.

Van der Zwaan, G.J., Jorissen, F.J., and De Stigter, H.C., 1990. The depth dependency of planktic/benthonic foraminiferal ratios: constraints and applications, *Mar. Geology,* 95, 1–16.

Van Hinsbergen, D.J.J., Kowenhoven, T.J., and Van der Zwaan, G.J., 2005a. Paleobathymetry in the backstripping procedure: correction for oxygenation effects on depth estimates, *Palaeogeography, Palaeoclimatology, Palaeoecology,* 221, 245-265.

Wright, R., 1978. Neogene paleobathymetry of the Mediterranean basen on benthic foraminifers from DSDP leg 42A. In K.J. Hsü and L. Montadert *et al.*, (eds), *Initial Reports of the Deep Sea Drilling Project*, Scripps. Inst. Oceanogr. 837–846.

Δελτίο της Ελληνικής Γεωλογικής Εταιρίας τομ. XXXX, 2007
Πρακτικά 11ου Διεθνούς Συνεδρίου, Αθήνα, Μάιος 2007

Bulletin of the Geological Society of Greece vol. XXXX, 2007
Proceedings of the 11th International Congress, Athens, May, 2007

A CARBONATE RAMP EVOLUTION IN THE TRANSITION FROM THE APULIA PLATFORM TO THE IONIAN BASIN DURING EARLY TO LATE CRETACEOUS (NW GREECE)

Getsos K.[1], Pomoni-Papaioannou F.[2], and Zelilidis A.[1]

[1] *University of Patras, Department of Geology, k.getsos@upatras.gr, azelilidis@upatras.gr*

[2] *National and Kapodistrian University of Athens, Faculty of Geology and Geoenvironment, Department of Hist. Geology – Paleontology, fpomoni@geol.uoa.gr*

Abstract

Facies analysis of Cretaceous carbonate sequences from the external and central Ionian zone revealed a homoclinal ramp model of evolution. During Berriasian to Valanginian, the carbonate ramp was differentiated to an inner-mid and outer ramp environment, which corresponded to the external and central Ionian zone, respectively, while the main inner ramp environment is assumed that was located in the Pre-Apulian zone. The external Ionian zone (inner-mid ramp) is characterized by mudstones-wackestones with fragmented echinoderms, bivalves, radiolarians and rare aptychus considered to be deposited below the fairweather wave base (FWWB). Locally, thin graded storm deposits intervene, indicating deposition above the storm weather wave base (SWB). Minor occurrences of packstones-grainstones, with fragmented echinoderms, calcareous algae, tubiphytes, lagenid foraminifera and rare ooids occur, as well, considered to be deposited at the lowermost part of the inner ramp, near the constantly agitated fairweather wave base (FWWB). The central Ionian zone (outer ramp) is mainly characterized by mudstones-wackestones with abundant radiolarians and rare calpionellids and calcispheres, considered to be deposited below the storm wave base (SWB). No talus or breccias deposits were observed, during the mentioned time interval, in any part of the studied area. From Hauterivian to Turonian, continual sea-level rise, led to establishment of outer ramp environment in the external Ionian zone, over the previous inner-mid ramp, and outer ramp-basin environment, over the previous outer ramp, in the central Ionian zone. The transition from shallower to deeper conditions is characterized by an overall deposition of mudstones-wackestones with abundant radiolarians rooted in pure micrite.
***Key words**: intercalations, facies zones, ramp, sedimentation rates.*

Περίληψη

Μικροφασική ανάλυση των Κρητιδικής ηλικίας ανθρακικών ακολουθιών της εξωτερική και κεντρικής Ιονίου ζώνης ανέδειξε την ύπαρξη ενός

περιβάλλοντος ράμπας ήπιας κλίσης. Κατά τη διάρκεια του Βερριασίου-Βαλανζινίου η ανθρακική ράμπα ήταν επιμέρους διαφοροποιημένη σε εσωτερική, μεσαία και εξωτερική. Η εσωτερική ράμπα αντιστοιχούσε στην Προ-Απούλια ζώνη, η μεσαία ράμπα στην εξωτερική Ιόνια ζώνη και η εξωτερική ράμπα στην κεντρική Ιόνια ζώνη. Η εξωτερική Ιόνια ζώνη χαρακτηρίζεται από αποθέσεις mudstones-wackestones με θραύσματα εχινοδέρμων, διθύρων, ακτινόζωων και σπάνια aptychus. Η απόθεση των έλαβε χώρα κάτω από τη ζώνη μόνιμου κυματισμού (FWWB). Κατά τόπους εντοπίζονται αποθέσεις κυμάτων καταιγίδας οι οποίες υποδεικνύουν απόθεση πάνω από τη συγκεκριμένη ζώνη (SWB). Μικρές εμφανίσεις packstones-grainstones με θραύσματα εχινοδέρμων, ασβεστολιθικών φυκιών, tubiphytes, lagenid, τρηματοφόρα και σπάνια ωοειδή αποτέθηκαν στο κατώτερο τμήμα της εσωτερικής ράμπας, κοντά στη ζώνη του μόνιμου κυματισμού (FWWB). Η κεντρική Ιόνια ζώνη χαρακτηρίζεται από mudstones-wackestones πλούσια σε ακτινόζωα και σπάνια calpionellids και calcispheres τα οποία αποτέθηκαν κάτω από την ζώνη δράσης κυμάτων καταιγίδας (SWB). Σε κανένα τμήμα των μελετηθέντων αποθέσεων δεν εντοπίστηκαν αποθέσεις κροκαλοπαγών και θραυσμάτων πετρωμάτων. Κατά τη διάρκεια του Ωτεριβιου-Τουρωνίου συνεχής άνοδος της θαλάσσιας στάθμης οδήγησε στη δημιουργία περιβάλλοντος εξωτερικής ράμπας στην εξωτερική Ιόνια ζώνη καθώς και εξωτερικής ράμπας/λεκάνης στην κεντρική Ιόνια ζώνη. Η μετάβαση από ρηχές σε βαθύτερες συνθήκες χαρακτηρίζεται από την απόθεση mudstones-wackestones με ακτινόζωα.

Λέξεις κλειδιά: *παρενστρώσεις, φασικές ζώνες, ράμπα, ρυθμοί ιζηματογένεσης.*

1. Introduction

Ionian zone at the Early to Middle Triassic corresponded to a shallow marine platform, which evolved to a vast basin bounded on both sides by shallow platforms; Apulia platform on the west and Gavrovo-Tripolitza platform on the east (Bosellini and Morsilli 1996). The Ionian zone in general has been studied by Aubouin (1959), IGRS-IFP (1966), Bornovas (1961), Bernoulli and Renz (1970), BP (1971), Karakitsios and Tsaila Monopolis (1988), Karakitsios *et al.* (1988). The Apulian platform has been studied in detail, by Bosellini and Morsilli (1996) and Graziano (2000). Moreover Underhill (1989) suggests that the Pre-Apulia zone in Greece is part of the Apulia platform (Underhill 1989, Fig. 15). The transition from the surrounding Apulia platform to the vast Ionian basin is not clear, yet.

The oldest rocks of the Ionian zone consist of evaporites and dolomites Early to Middle Triassic (Bornovas 1960, Pomoni-Papaioannou 1983, Pomoni-Papaioannou and Tsaila-Monopolis 1983, Pomoni-Papaioannou 1985, Pomoni-Papaioannou *et al.* 2004, Getsos *et al.* 2004). Evaporites are overlain by Late Triassic-Early Jurassic typical internal platform-type limestones, in the upper part of which pelagic limestones have been identified, the so-called Siniais limestones (Renz 1955, IGRS-IFP 1966, BP 1971, Karakitsios and Tsaila-Monopolis 1988). During the Toarcian and on, the pelagic sedimentation continues with the deposition of lower Posidonia shales and filamentous limestones (Karakitsios 1990). The upper Posidonia shales represent deposition during the Callovian-Tithonian interval.

During the Berriasian-Santonian p.p., pelagic sedimentation prevailed, giving rise to the Vigla Limestone Formation (les calcaires de Vigla; Aubouin 1959, Karakitsios and Koletti 1992, Karakitsions *et al.* 2004). Depositional conditions changed during the late Campanian-Maastrichtian interval, when clastic material from the basin margins and the neighbouring zones invaded the basin forming limestone beds, described by Aubouin (1959) as "les calcaires

microbrechiques". During the Paleocene and Eocene, carbonate sedimentation prevailed. Finally, at the end of the Eocene clastic sedimentation was established (Zelilidis *et al.* 2003) (Fig. 1).

The studied Early to Late Cretaceous Vigla's formation appear as extensive outcrops of thin to medium bedded limestones with an average thickness of 200-400 m. Samples were collected from fifteen outcrops and were studied under a polar microscope (Fig. 2). For the description of the samples, the Dunham's (1962) classification was used, whereas for the determination of the depositional environments, the Standard Microfacies Types (SMF) and Facies zones classifications, after Flugel (1972) and Wilson (1975), were used. The present work aims to improve the sedimentological and stratigraphical knowledge of the early to late Cretaceous carbonate sediments of the Ionian zone and consequently the environmental and palaeogeographic evolution of the Mesozoic Ionian basin. Preliminary work was presented at ISC 7 in Neuchâtel (Getsos *et. al.* 2005).

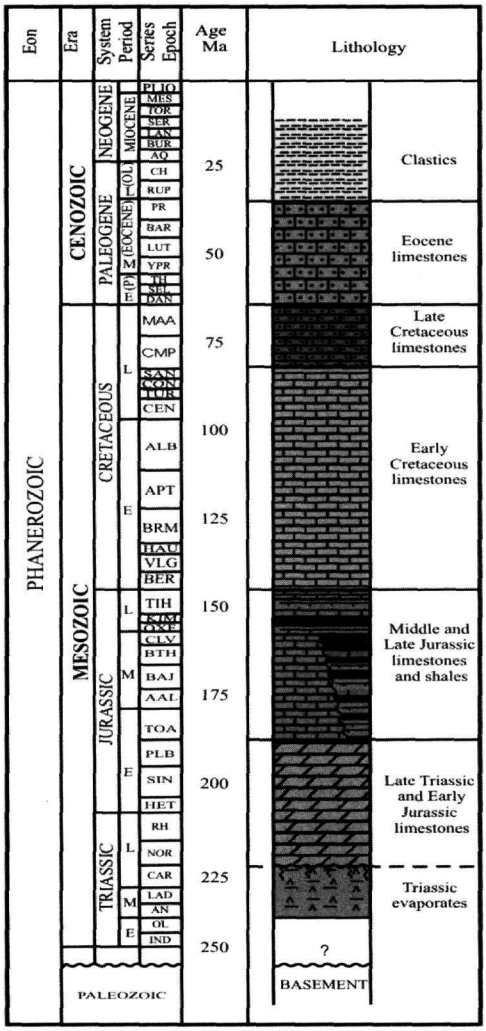

Figure 1 - Stratigraphy of the Ionian zone. The geologic time scale follows the Gradstein *et al.* (2004) time-scale (modification by Zelilidis *et al.* 2003)

2. Age determination

The age determination was contacted using microfossils in combination with nannofossils. The samples were chosen carefully in order any misinterpretation, caused by redeposited fossils, to be eliminated. Aptian and Coniacian-Santonian epochs are not easily detectable due to the absence of important fossils from the study area. According to the studied fossils Vigla's limestones deposition took place in the Berriasian to Turonian time interval.

More precisely Berriasian age was documented by nannofossils, *Nannoconus kamptneri kamptneri, N. dolomiticus, N. broenimanni, Cyclagelosphaera deflandrei, Diazomatolithus lehmanni, Ellipsagellosphaera britannica, Zeugrhabdothus embergeri* and microfossil *Calpionella alpina* studied in wackestones and wackestones-packstones. Valanginian age was documented by nannofossils *Cruciellipsis cuvillieri, Watznaueria barnesiae, Cyclagelosphaera deflandrei, Nannoconus quadratus, Nannoconus bermudezii* (Valanginian-Barremian), *Nannoconus broenimanni* (up to Valanginian), *Nannoconus steinmanni steinmanni, Nannoconus steinmanni minor, Nannoconus colomi, Assipetra infracretacea* and microfossils *Trocholina, Textularid* and *Lenticulina.* Valanginian-Hauterivian age was documented by nannofossils *Conusphaera mexicana mexicana – abundant, Cyclagelosphaera margerelii, Nannoconus bermudezii, Nannoconus cf. Cornuta* and Haterivian-Barremian age by nannofossils *Zeugrhabdotus embergeri, Assipetra infracretacea, Lithraphidites carniolensis, Watznaueria barnesiae.* Albian age was documented by *Rotalipora* and *Planomalina buxtorfi*, Cenomanian by *Globigerinid, Hedbergella* and *Gumbelina* and Turonian by *Globotruncana*

3. Ramps

Carbonate ramps are divided into two groups, homoclinal and distally steepened with a usually offshore slope break between shallow ramp and basin. Ramps and distally steepened ramps have many common characteristics and for that reason it is difficult to be distinguished in the rock record, without the presence or absence of slope or slope apron deposits, respectively. This distinction is additionally hindered due to post-sedimentary tectonism.

Ramp classification is based on two critical interfaces: the fair-weather wave base (FWWB) and the storm wave weather base (SWB). Although these boundaries occur in various depths, in relation to local hydrodynamic and climatic conditions, the sedimentary features that they define are easily distinctive. According to Burchette and Wright (1992), ramps are divided to three parts: the inner ramp, the mid-ramp and the outer ramp.

The inner ramp is located above the fair-weather wave base (FWWB) being dominated by shoals, organic barriers or shoreface deposits. The mid-ramp is located between the fair-weather wave base (FWWB) and the storm wave weather base (SWB), where the sea floor is affected by storm waves. A variety of storm related features occur, such as graded beds and hummocky cross-stratification. Proximal and distal trends can be recognized in mid-ramp deposits (Aigner 1984, Burchette 1987, Faulkner 1988). The outer ramp is located between the lower limit of mid-ramp, where most storms influence the sea floor, and the basin plain. Storm reworking of the sediments is rare, although storm deposits are possible to occur in the upper part (Aigner 1984, Calvet and Tucker 1988). In deeper parts of the zone, restricted conditions may develop, especially in accordance to suboxic basinal sediments. The characteristics of the basinal sediments depend on the depth and nature of the basin itself. They usually lack coarse "tempestites" and turbidites are mostly absent.

4. Sedimentary remarks

Sampling localities are shown in Fig. 2. The studied outcrops were grouped into three areas, based mainly on geographical and sedimentological criteria. The area 1 covers the western part of the study area and contains five outcrops, sites 26, 23, 24, 44 and 21, area 2 is located in the middle part and includes the sites 13, 7, 9 and 10, and area 3 at the eastern part and includes the sites 27, 41, 42 and 43 (Fig. 2).

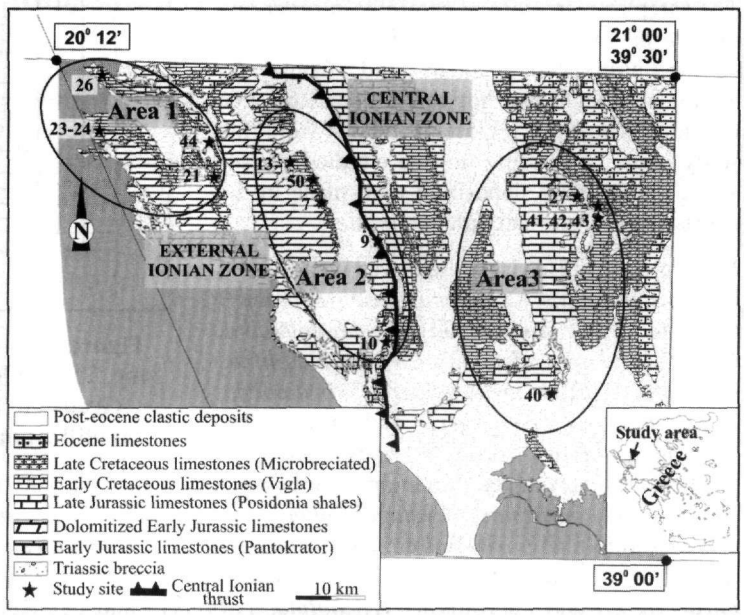

Figure 2 - Geological map of the studied area

4.1. Macroscopic description

A common characteristic found in all studied sequences is that they are consisted of typical pelagic limestones organized in 50-60 cm thick packages. Each package is consisted of five to six thin to

medium bedded limestones. Furthermore there are siliceous rocks usually in lenses and many times in bed-like-form between beds of limestones.

4.1.1. Area 1

In site 26 (locality Liotribia) the Early Cretaceouslimestones were studied in a thick lithostratigraphic column, averaging 280 m in thickness, consisted of thin to medium bedded pelagic limestones, where thin intercalations of coarse-grained packstones intervene. The whole outcrop is characterized by packets of five to six thin beds and varying total packet thickness ranging from 40 to almost 60 centimeters. In the upper part thick-bedded packstones-grainstones occur.

In sites 23, 24 (locality Plataria) the Early Cretaceouslimestones were studied in a lithostratigraphic column of 150 m in thickness. The whole sequence is consisted of 50-60 centimeter thick packets of thin to medium bedded limestones.

In sites 44, 21 (locality Karterion) the typical of E.Cetaceous age, outcrops are consisted of 50-60 centimeter thick packets containing thin to medium bedded limestones. The average thickness do not exceeds 100 meters in both sites.

4.1.2. Area 2

In sites 13, and 10 (localities Karbounarion, Boubopotamon and Skepastos) the typical sequences of Early Cretaceous (Beriassian-Valanginian – Sites 13, 10), are consisted of ordinary packets with medium to thin bedded limestones. The lithostratigraphic column in its locality does not exceed 100 meters in thickness.

In site 9 (locality Skandalon) the Late Cretaceous (Cenomanian-Turonian) sequence is consisted of medium to thin bedded limestones organized in 50-60 centimeters thick packets with five to six 5-10 centimeters thick, internal beds. Total lithostratigraphic column is 100 meters in thickness.

4.1.3. Area 3

In sites 27, 41 & 42 (Berriasian-Valanginian) and 43 (Hauterivian-Barremian) (locality Kouklesi) the Early Cretaceouslimestones were studied in a lithostratigraphic column averaging 150 m in thickness and consisted of typical pelagic limestones organized in 50-60 centimeters thick packages.

4.2. Microscopic description

The prevailing microfacies type in the study area was determined as SMF 3 with interventions of SMF 4.

The main microfacies types in area 1 are consisted of mudstones-wackestones with sparse, whole shelled foraminiferas rooted in pure micrite, determined as SMF 3 (Fig. 3A). The intercalations are commonly consisted of packstones with rare lithoclasts, abundant bioclasts and whole shells of benthic foraminiferas, echinoderms, bivalves and sometimes algae determined as SMF 4 (Figs 3B, C). Under microscope these intercalations are usually observed with a characteristic structure consisted of millimeter-scale packstones at the base passing gradually into wackestones with fine bioclasts and lithoclasts. Finally, the millimeter-scale sequence pass to an end member of mudstones with scattered pelagic foraminiferas. At the top of the outcrop (end of Berriasian) there are grainstones with lithoclasts from older limestones, echinoderms and algae, determined as SMF 4 (Fig. 3C).

The unique microfacies type in the whole sequence studied in area 2 is mudstone-wackestone with scattered pelagic foraminiferas determined as SMF 3 (Fig. 3D). Moreover site 7 has a special characteristic made up from red and grey colored intercalations and cross lamination without any other, distinct lithological differentiation (Fig. 3F).

The prevailing microfacies in area 3 are mudstones-wackestones with scattered pelagic foraminiferas (SMF 3). Within the above mentioned mudstones-wackestones there are thin laminae consisted of packstones with abundant intraclasts. In places a millimeter-thick microsequence consisted of unlaminated intraclastic packstone at the base, unlaminated wackestone in the middle and laminated wackestone at the top, has been observed (Fig. 3E). Furthermore, color differentiated lamination were studied with great similarity to those of area 2.

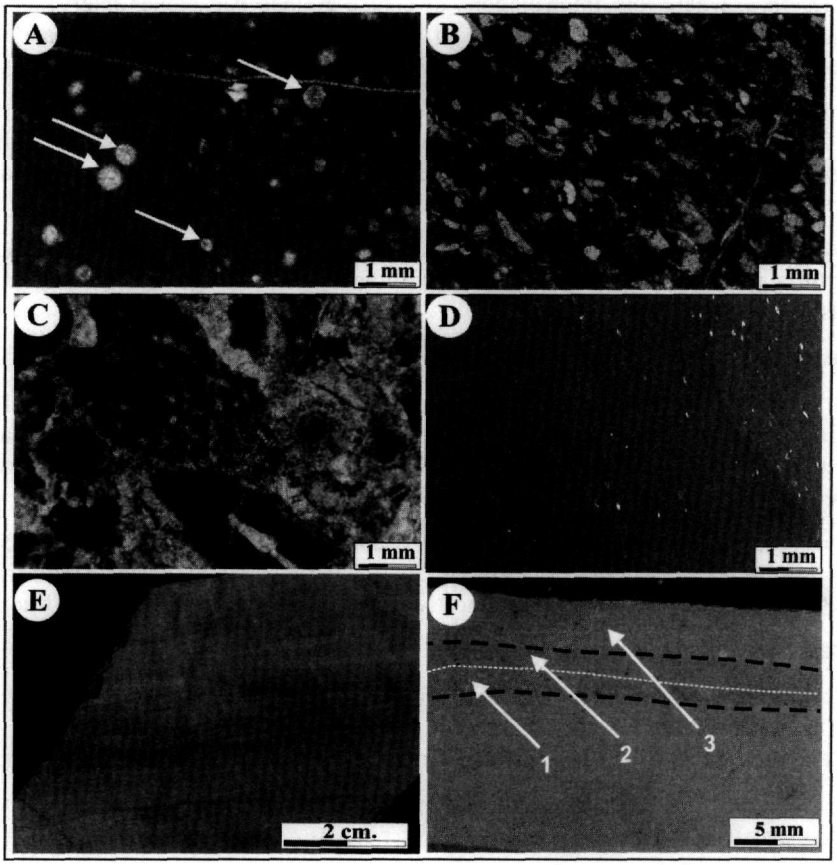

Figure 3 - A) scattered radiolarians rooted in micrite, B) packstone with bioclasts and lithoclasts, C) grainstone-rudstone, D)mudstone – end member of mm scale sequence, E) 1:packstone, 2: laminated wackestone, 3: cross laminated wackestone, E) color differentiated lamination

4.3. Interpretation

The studied rocks in area 1, of Early Cretaceous (Berriasian-Valanginian) age, are typical of a HST ("highstand" system tract) with various short term sea level falls. The intercalations were interpreted as gravity flows with distal and proximal trends, cryptoturbidites or tempestites. The depositional environment of the SMF 3 was interpreted as deep shelf margin (FZ 3) and the SMF 4, consisted of packstones, as distal foreslope (FZ 4), while the grainstones as proximal foreslope. The depositional profile during Early Cretaceous (Berriasian-Valanginian) corresponds to a middle ramp environment with a minor occurrence of inner ramp at the end of Berriasian, while the grainstones were deposited (Fig. 4). The proximal foreslope environment, inner ramp, coincides with an almost 50 m sea level fall (Haq *et al.* 1987). Moreover, grainstone deposition is indicative of the FWWB zone, while the above mentioned intercalations can be determined as deposition

within SWB zone. During Hauterivian-Turonian, rock record shows sedimentation in much more quiet conditions as none resedimented fragment was studied up to Turonian.

The depositional environment in area 2 during Early to Late Cretaceous was interpreted as deep shelf margin or open sea shelf (FZ 3, 2). The color differentiated lamination was correlated with fluctuations of the oxygenation level. The depositional profile corresponds to outer ramp (Fig. 4). The ramp in this area should bear a very gentle inclination towards basin, as no resedimented material was studied.

The depositional environment in area 3 during Early to Late Cretaceous was determined as deep shelf margin (FZ 3) and the lamination was deposited through low density gravity flows, crytpoturbidites, or from distal storm waves, tempestites. The color differentiated lamination was caused by deposition at oxygenation level. The absence of shallow marine material from the coarse lamination (SMF 4) suggests deposition far away from the shelf environment. The depositional profile corresponds to outer ramp (Fig. 4).

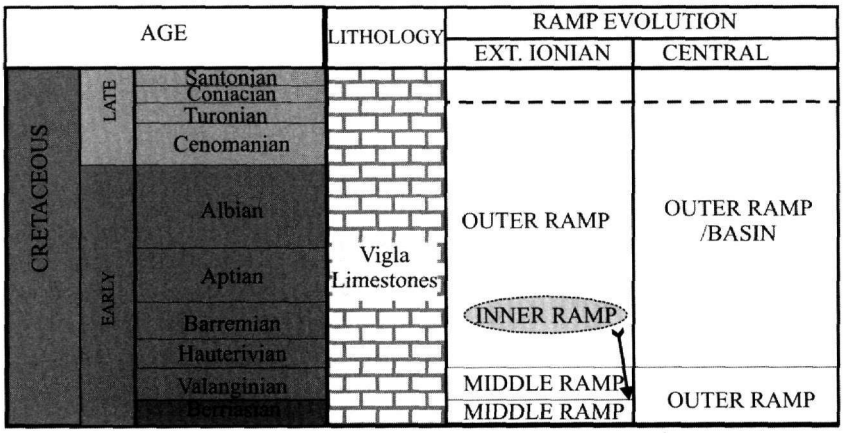

Figure 4 - Ramp evolution during Early to Late Cretaceous

5. Estimation of sedimentation rates

The thickness of the Vigla's limestones in the studied area varies between 50 and 500 m. The strata in general are thickening from the Ionian basin towards the Apulian platform in the west, especially during specific time intervals. For instance, during Berriasian to Valanginian there is a big differentiation in thickness of the strata between external and central Ionian zone. In study area 1 the thickness of the deposited sediments during Berriasian to Valanginian exceeds 300 m while in the same time in study area 2 the thickness is almost 200 m. and in study area 3 the thickness is only 100 m. (Fig. 5). During Hauterivian to Turonian, the difference in thickness is maintained but the values are reduced, 150 m. in area 1 to maximum 50 m. in area 3. Taking into account the above mentioned thicknesses and considering the duration of every epoch in thousands years (Gradstein *et al.* 2004) annual sedimentation rate was estimated. The sedimentation rates during Berriasian – Valanginian time interval are 37 mm/ka, 22 mm/ka and 11 mm/ka for areas 1, 2 and 3, respectively. The sedimentation rates for the Hauterivian – Turonian time interval are 3 mm/ka, 2 mm/ka and 1 mm/ka for areas 1, 2 and 3 respectively. It is obvious that a three times faster sedimentation rate was maintained during the studied time interval, Berriasian-Turonian, between area 1 and area 3. Moreover the sedimentation rate was decreased gently from area 1 to area 3 through area 2. It can be concluded that the sedimentological system had the tendency to become aggradational due to the difference in sedimentation rate between area 1 and areas 2,3. The studied high sedimentation rate in area 1 was probably due to high organic productivity, usual in shallow areas.

6. Discussion

The performed sedimentological study revealed that the Berriasian – Valanginian sediments were deposited on a homoclinal ramp system. The sediments which are nowadays located to the external Ionian zone (area 1) were deposited in middle ramp and less in the lower limit of the inner ramp. Mudstones and wackestones with thin intercalations of packstones correspond to deposition in the middle ramp between FWWB and SWB. The lower limit of the inner ramp probably had occurred for a short period of time in the late Berriasian thus the thickness of the rock record is up to 10-12 meters. This deposit is consisted of grainstones with resedimented clasts of older limestones and benthic foraminiferas. The deposition of these limestone documents a short term eustatic sea level fall occurred in the transition from Berriasian to Vlanginian (Haq *et. al.* 1987). In the same time interval the sediments which are nowadays located in the central Ionian zone (areas 2, 3) were deposited in outer ramp/basin environment as the storm reworking is rare and in much less extent than area 1. During Hauterivian to Turonian the sedimentation pattern was the same for the external and central Ionian zone and it is typical of outer ramp/basin environment as is indicative of the rare storm reworking and the periodically occurrence of red and grey colored lamination. These lamination are in accordance with the suboxic or anoxic conditions which occur in the deeper parts of the outer ramp and basinal environment (Fig. 6). Thus it can be concluded that the ramp system was drowned during the above mentioned time interval.

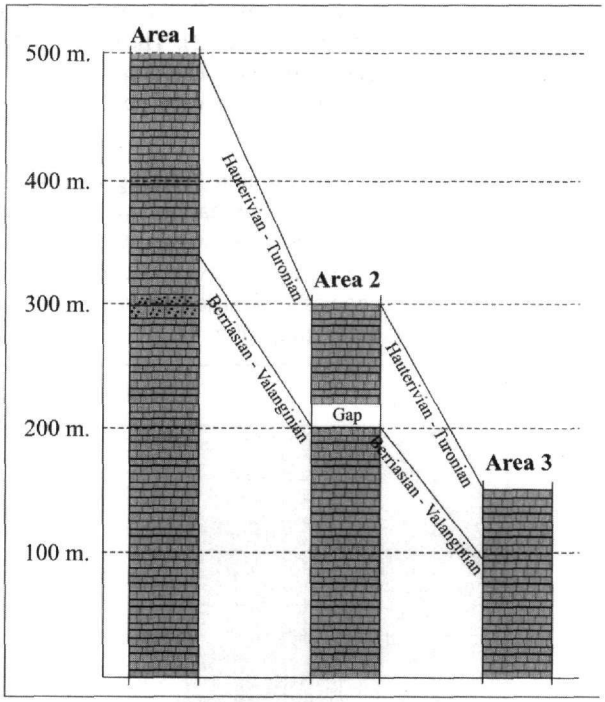

Figure 5 - Stratigraphy of the study area, all the sections are in scale

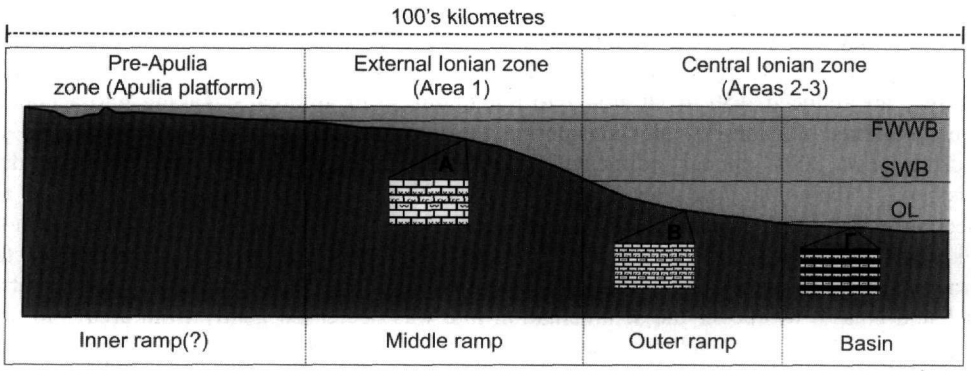

Figure 6 - Two- dimensional figure of the external and central Ionian and pre-Apulian zones during the Cretaceous

The Ionian zone is interpreted as a deep basin adjacent to the Apulia platform. The existence of pre-Apulia zone (Apulian platform) which is characterized by thick platform facies in correlation with the differences in sedimentation studied in this work can prove the presence of a homoclinal ramp system. The absence of any talus deposit from the studied area and presented sedimentological record show that the transition from the Apulia platform to the Ionian basin was a homoclinal ramp.

The high sedimentation rates for the Berriasian – Valanginian time interval are indicative of high organic productivity which show a gradual decrease towards the central Ionian zone (Ionian basin?). In addition to the gentle inclination from the Apulia platform towards the Ionian basin eastwards, the system had the tendency to become aggradational. This gradual decrease is maintained during Hauterivian – Turonian time interval but in much slower rate. The higher sedimentation rate over shallower areas is attributed to the greater organic productivity.

7. Conclusions

During Berriasian to Valanginian the main facies of the external Ionian zone (area 1) were mudstones-wackestones and abundant intercalations of packstones-grainstones with resedimented fragments. Instead, in the central Ionian zone during the above mentioned period mudstones-wackestones with scattered foraminiferas, mainly radiolarians, were deposited with rare intercalations of packstones. During Hauterivian to Turonian the sedimentation pattern was the same for the external and central Ionian zone and the main facies were mudstones wackestones with scattered pelagic foraminiferas and radiolarians. The depositional environment was corresponded to foreslope with proximal and distal trends, deep shelf margin, open sea shelf and basin (den anafereis tetoia perivallonta sto keimeno, oute sto Discussion). The above depositional environments, during Berriasian-Valanginian , correspond to a middle ramp environment with a minor occurrence of inner ramp for the external Ionian zone, (area 1), and to an outer ramp-basin for the central Ionian zone (areas 2 and 3). The transition from the Apulian platform to the adjacent Ionian basin was of a homoclinal ramp type. During Berriasian to Valanginian the sediments were deposited on two different parts of a homoclinal ramp system. It was middle and outer-basin environment which during Hauterivian to Turonian was drowned and outer ramp-basin was established.

The estimated sedimentation rates are much higher in the area 1 than the areas 2 and 3 in the whole time interval. The difference in sedimentation rates between Berriasian – Valanginian and Hauterivian – Turonian time intervals is caused by the differences in organic productivity over the different parts of the ramp. The differences in sedimentation rates for middle and outer ramp show that the homoclinal ramp system was moving towards aggradational settings.

8. References

Aigner, T., 1984. Dynamics of intercratonic carbonate ramps, Upper Muschelkalk, (Middle Triassi c), South-German Basin, *7th Meeting of Carbonate Sedimentologists*, Liverpool.

Aubouin, J., 1959. Contribution a l'etude geologique de la Grece septentrionale: les confins de l'Epire et de la Thesallie, *Annales Geologique des Pays Helleniques*, 10, 870-885.

Bernoulli, D., and Renz, O., 1970. Jurassic Carbonate Facies and New Ammonite Faunas from Western Greece, *Ecl. Geol. Hel.*, 63/2, 573-607.

Bornovas, J., 1961. Observations nouvelles sur la geologie des zones preapulienne et ionienne (Grece occidentale), *Bull. Soc. Geol. France*, series 7, II/4, 410-414.

Bosellini, A., and Morsilli, M., 1997. A Lower Cretaceous drowning uncomformity on the eastern flank of the Apulia Platform (Gargano Promontory, southern Italy), *Cretaceous Research*, 18, 51-61.

British Petroleum Co. Ltd. (BP), 1971. The geological results of petroleum exploration in western Greece, *Instit. Geol. Sub. Res.*, Special report 10.

Burchette, T.P., and Wright, V.P., 1992. Carbonate ramp depositional systems, *Sedimentary Geology*, 79, 3-57.

Calvet, and Tucker, M., 1988. Outer ramp cycles in the Upper Muschelkalk of the Catalan Basin, northern Spain, *Sedimentary Geology*, 57, 185-198.

Dunham, R.J., 1962. Classification of carbonate rocks according to depositional texture, *Memoir, American Association of Petroleum Geologists*, 1, 108-121.

Flugel, E., 1972. Mikrofazielle Untersuchungen in der Alpinen Trias. Methoden and Probleme, *Mitt. Ges. Geol. Bergbaustud.* 21, 9-64.

Getsos, K., Pomoni-Papaioannou, F., and Zelilidis, A., 2004. Triassic carbonate and evaporite sedimentation in Ionian zone (western Greece): palaeogeographic and palaeoclimatic implication, *Bulletin of the Geological Society of Greece*, XXXVI, 699-707.

Getsos, K., Pomoni-Papaioannou, F. and Zelilidis, A., 2005. A carbonate ramp type differentiation of the western Ionian basin during early to late Cretaceous (NWGreece), *7th International Symposium on the Cretaceous*, Abstracts, 132.

Gradstein, F.M., Ogg, J.G., Smith, A.G., Bleeker, W., and Lourens, L.J., 2004. A new geologic time scale with special reference to Precambrian and Neogene, *Episodes*, 27, 83-100.

Graziano, R., 2000. The Aptian-Albian of the Apulia Carbonate Platform (Gargano Promontory, southern Italy): evidence of palaeoceanographic and tectonic controls on the stratigraphic architecture of the platform margin, *Cretaceous Research*, 21, 107-126.

Haq, B.U., Hardenbol, J., and Vail, P.R., 1987. Chronology of Fluctuating Sea Levels Since the Triassic, *Science*, 235, 1156-1167.

IGRS-IFP, 1966. Etude gélogique de l'Epire (Gréce nordoccidentale), *Ed. Technip*, Paris, 306pp.

Karakitsios, V., 1990. Study of Jurassic age paleofaults in Ionian zone (Epirus, Greece), *Proceedings of the 5th international Congress*, XXV/1,307-318.

Karakitsios, V., 1992. Ouverture et inversion tectonique du basin ionien (Epire, Grece). Annales Geologique des Pays Helleniques, 35, 85-318.

Karakitsios, V., and Tsaila-Monopolis, S., 1988. Donnees nouvelles sur les niveaux superieurs (Lias inferieur – moyen) des calcaires de Pantokrator (Zone Ionienne moyen, Epire, Grece contenentale) description des calcaires de Louros (New data from the upper part (early middle Lias) of the Pantokrator limestone (middle Ionian zone, Epirus, continental Greece) description of Louros limestone), *Rev. de Micropaleontologie*, 31(1), 49-55.

Karakitsios, V., Danelian, T., and De Wever, P., 1988. Datation par les radiolaires des Calcaires á Filaments, Schists á Posidonies superieurs et Calcaires de Vigla "zone Ionienne, Epire, Gréce", du Callovient au Tithonique terminal, *Compte Rendu de l'Académie des Sciences*, 306/II, 367-372.

Karakitsios, V., and Koletti, L., 1992. Critical revision of the age of the basal Vigla limestones (Ionian zone, western Greece), based on nannoplankton and calpionellids with paleogeographical consequences. In B. Hamrsmid and J. Young (eds), *Proceedings of the Forth International Nannoplankton Association Conference*, Prague, 1991, Knihovnicka ZPN, 14a, vol. 1, p. 165-177.

Karakitsios, V., Tsikos, H., Van Breugel, Y., Bakopoulos, I., and Koletti, L., 2004. Cretaceous oceanic anoxic events in western continental Greece, *Bull of the Geol. Soc. Greece*, XXXVI, 846-855.

Pomoni, F., 1983. Studiul petrographic si sedimentologic al evaporitelor Triasice din regiunea Epir, *Teza de Doctorat*, Universitatea Bucuresti, 1-190pp.

Pomoni-Papaioannou, F., 1985. The sedimentology and depositional environment of the Triassic dolomite-gyprum facies of western Greece, *Proceedings of the 6th European Meeting of the Inter. Assoc. Sedimentologists*, 367-368.

Pomoni-Papaioannou, F., Karakitsios, V., Kamberis, E., and Marnelis, F., 2004. Chevron-type halite and nodular anhydrite in the Triassic Evaporitic Formation of the Ionian Zone (Western Greece), *Proceedings of the 10th International Congress,Bulletin of the Geological Society of Greece*, XXXVI, 578-586.

Renz, C., 1955. Die vorneogene Stratigraphie der normal-sedimentaren Formationen Griechenlan, *Inst. Geol. Susururf. Res. Athens*, 637.

Underhill, J.R., 1989. Late Cenozoic deformation of the Hellenide foreland, western Greece, *Geological Society of America, Bulletin*, 101, 613-634.

Wilson, J.L., 1975. *Carbonate Facies in Geologic History*, Berlin-Heidelberg-New York (Springer), 471p.

Zelilidis, A., Piper, D. J., Vakalas, I., Avramidis, P., and Getsos, K., 2003. Oil and Gas Plays in Albania: Do Equivalent Plays Exist in Greece? *Journal of Petroleum Geology*, 26, 29-48.

Δελτίο της Ελληνικής Γεωλογικής Εταιρίας τομ. XXXX, 2007
Πρακτικά 11ου Διεθνούς Συνεδρίου, Αθήνα, Μάιος 2007

Bulletin of the Geological Society of Greece vol. XXXX, 2007
Proceedings of the 11th International Congress, Athens, May, 2007

A DEBATE ON THE SIMILARITY OF PARTICLE SIZING RESULTS DERIVED FROM THE ANALYSIS OF FINE-GRAINED SEDIMENTS BY TWO DIFFERENT INSTRUMENTATIONS

Iatrou M.[1], Papatheodorou G.[1], Piper D. J. W.[2], Tripsanas E.[2], and Ferentinos G.[1]

[1] *Laboratory of Marine Geology & Physical Oceanography, Department of Geology, University of Patras, 26500, Rio, Patras, Greece, iatroum@upatras.gr*

[2] *Geological Survey of Canada (Atlantic), Bedford Institute of Oceanography, P.O. Box 1006, Dartmouth, Nova Scotia B2Y 4A2, Canada*

Abstract

A set of grab-sample sediments collected from the basin floor of the Corinth Gulf, Greece, was analysed using two different techniques; LS 230 laser system and Coulter Counter TA II. The present study presents the results derived from the comparison between the two techniques. The correlation between the mean size and the sorting values obtained from the two methods is moderate. Also moderate are the correlations estimated for the fractions of clay and silt obtained from the two methods Furthermore the analysis showed that the Laser Coulter determines coarser grain sizes than the Coulter. The analysis of variation/residuals within individual size intervals showed a higher variability of residuals for the coarser fractions (7-6 and 5-4 phi).

Key words: *electronic particle counting, laser diffractometry.*

Περίληψη

Δύο ενόργανες μέθοδοι κοκκομετρικής ανάλυσης εφαρμόζονται για την ανάλυση θαλάσσιων λεπτόκοκκων ιζημάτων συλλεγμένων από τον πυθμένα του Κορινθιακού κόλπου, για την σύγκριση των αποτελεσμάτων τους. Οι τεχνικές που χρησιμοποιούνται είναι η μέθοδος της περίθλασης της ακτίνας λείζερ (Laser diffraction ή LS) και κοκκομετρική ανάλυση με τη μέθοδο της ηλεκτροαντίστασης (Electroresistance particle counting ή CC). Αν και ικανός αριθμός εργασιών έχουν δημοσιευθεί ως αναφορά στη σύγκριση μεταξύ των ενόργανων και των κλασσικών (κόσκινα-πιπέτα) μεθόδων κοκκομετρικής ανάλυσης, λίγα στοιχεία είναι διαθέσιμα σχετικά με τη σύγκριση των αποτελεσμάτων των ενόργανων μεθόδων και ιδιαίτερος αυτών της παρούσας εργασίας. Η σύγκριση των στατιστικών παραμέτρων με τη μέθοδο των ροπών έδειξε ότι η LS μέτρησε μικρότερες τιμές μέσου μεγέθους (αδρομερέστερα δείγματα) από ότι η CC. Η συσχέτιση των ποσοστών των κλάσεων πηλού και αργίλου κρίνεται ικανοποιητική (R=0.69). Η απόκλιση των μετρήσεων των αδρομερεστέρων κλασμάτων των δειγμάτων είναι αποτέλεσμα του γεγονότος ότι οι δύο μέθοδοι μετρούν το μέγεθος των κόκκων με βάση διαφορετικές ιδιότητες τους (σχήμα,

πυκνότητα). Η απόκλιση των αποτελεσμάτων μεταξύ των δυο μεθόδων αυξάνεται σε δείγματα που χαρακτηρίζονται από την παρουσία ενός κυριάρχου τύπου (mode) με ποσοστό συμμετοχής συνήθως άνω του 6 %.
***Λέξεις κλειδιά**: ενόργανες μέθοδοι κοκκομετρίας, σύγκριση.*

1. Introduction

Particle size is a fundamental property of sedimentary materials providing important information about their provenance, transport history and depositional conditions. So far a variety of traditional technologies have been used for the determination of particle size in clay to sand–sized sediments. These include analysis by settling tube, sieve and pipette (Beuselinck *et al.* 1998). Each technique defines the size of a particle in a different way and thus measures different properties of the same material (Konert and Vandenberghe 1997). The pipette method, suitable only for the finer fractions (less that 63 μm diameter), defines the "Stokes" particle diameter as equivalent to that of a sphere settling in the same liquid with the same speed as the unknown sized particle. The sieve defines a particle diameter as the length of the side of a square hole through which the particle pass and this method is mainly suitable for the analysis of sand and gravel –sized materials (greater than 63 μm diameter). Via sieving methods, the grains are separated and a weight-based size distribution is constructed.

Modern methods involve instrumental techniques which are more rapid than the contemporary ones. In these modern methods are included the particle sizing by electrical sensing (Bianchi *et al.* 1999), X-ray absorption (Singer *et al.* 1988), X-ray attenuation (Stain 1985) and hydrophotometer (Jordan *et al.* 1971). There was also an attempt to apply image-based granulometries to estuarine and marine sediments as a alternative to sieve and coulter counter method (Balagurunathan *et al.* 2001, Frančišković-Bilinski *et al.* 2003). A "Laser diffraction spectrophotometer" which is capable of analyzing a wide range of particles (from clay to sands), measures a particle diameter as equivalent to a sphere that exhibits the same diffraction as the particle. The Sedigraph system senses particle size based on it's settling characteristics. The resistance pulse Counter defines the size of a particle according to its volume. Both the latter two methods are best suited to analyze finer sediments (silt and clay size). The hydrophotometer measures the percentage of transmitting light which passes through a particle suspension and determines the amount of material that has settled. Morphological-granulometric sizing is based on shape area (binary image) or volume (gray scale image).

The application of modern techniques such as Laser diffraction and Electrozone sensing has raised questions about the similarity of the results derived from the above methods. McCave *et al.* (1986), Singer *et al.* (1988), Syvitski *et al.* (1991), Konert and Vandenberghe (1997), Buurnman *et al.* (1997), Loizeau *et al.* (1994), Muggler *et al.* (1997), Beuselinck *et al.* (1999), McCave *et al.* (2006) have compared the above mentioned instrumental techniques with the classical leading occasionally to conflicting results. However it should be mentioned that only a few works have studied the relation between the laser diffractometry and electozone particle counting (e.g.: Singer *et al.* 1988, Loizeau *et al.* 1994).

The present study aims at contributing further in the above studies by comparing two data sets of particle distributions derived from two different analytical techniques; laser granulometry and electroresistance counting. Data sets consist of grain size distributions that occurred in the fine – grained size fraction.

2. Materials and Methods

2.1. The Dataset

A dataset of twenty-eight closely related marine sediment samples, in terms of origin and grain size, were analyzed for particle size determination by two methods: laser diffractometry and

electronic particle counting. The samples come from surface and subsurface sediments collected by Day-grab sampler, from the basin of Corinth Gulf, Greece, at a water depth of 850 m (Iatrou *et al.* 2006). The recent sedimentary cover of the studied area is characterized by the presence of metalliferous tailing disposals derived from an aluminum processing plant and the intercalating natural sedimentation deposits. Structures observed in the sediment samples suggested that the red-mud and the natural mud layers have been deposited by gravity induced flows (Varnavas *et al.* 1986, Papatheodorou *et al.* 2003, Iatrou *et al.* 2006). The dataset consists of subsurface samples which were sub-sampled from six short cores, typical of the sedimentary types composing the modern sedimentological regime (Iatrou *et al.* 2006). They represent all the types of sediments in the area: from natural to red-mud deposits. Previous studies from the study area (Papatheodorou *et al.* 2003, Iatrou *et al.* 2006) showed the fine-grained texture of the sediments and therefore the samples were examined with interest focused on the silt and clay size range.

2.2. Determination of Particle –Size Distribution

2.2.1. Laser Diffractometry

Low angle laser light scattering (LALLS, commonly called laser diffraction) system (LS) pass a laser beam of known wavelength through a suspension of the material to be analyzed and measures the angular distribution and intensity of the forward –scattered (diffracted) light by the particles in suspension. A theoretical model based on diffraction of particles with particular properties and grain-size distribution, is then fitted to the actual diffraction results. (Sperazza *et al.* 2004). The two main diffraction theories which are typically used in the prediction of laser particle results are the Fraunhofer theory and Mie theory.

Particle size analysis was performed with a Beckman-Coulter LS-230 laser granulometer, equipped with a 750-nm laser beam and 126 photodiode detectors. The instrument measures volume % in 92 fractions ranging from 0.4 to 2000 μm corresponding to an interval 0.13 Ø. Fraunhofer mathematical model was used by default to calculate the size of particles based on the concentric ring pattern of light-scatter from the laser beam. Mc Cave *et al.* (1986), Singer *et al.* (1988) and Loizeau *et al.* (1994) argue that the particulate model tends to underestimate particle sizes close to the wavelength of the laser source light.

Each sediment sub-sample was suspended in 10ml of deionized water and was ultrasonically dispersed for less than 5 min. The suspension was afterwards gently poured into the fluid module filled with filtered and degassed water. The fluid circulates through the sample cell during the analysis to make sure that all particles are entrained into the flow and ensuring a random orientation of the particles. The adequate amount of sample was determined by the obscuration percentage of the laser beam through the sample cell and the recommended range was from 8 to 12 %, which equates with 0.2 and 4 gr. for most sediments. Most of the samples in the present study reached the recommended obscuration levels using only a small quantity of material due to the fine texture of the sediments.

2.2.2. Electronic Particle Counting

The Coulter counter (CC) method has been reviewed by various researchers, i.e. Shideler (1976), Singer *et al.* (1988), Bianchi *et al.* (1999), and Molinaroli *et al.* (2000). The Electronic Particle counter volumetrically sizes and counts the particles suspended in a weak electrolyte that pass through a small aperture with electrodes on both sides. Particles moving through the aperture displace the electrolyte and temporarily increase the resistance between the electrodes. A constant current is maintained and the resistance changes produce voltage pulses which are amplified, sorted according to pulse height in a multichannel analyser and counted. The magnitude of the pulses is proportional to particle volume (Milligan and Kranck 1991) and the number of pulses is equal to particle concentration.

The instrument used for the present analysis is a Coulter Counter model TA II. Tubes with 30-μm and 200-μm type apertures were used to cover the analytical range from 0.4 to 80.6 μm. Samples were dispersed with sodium hexametaphosphate solution and ultrasonically treated (bath) for a time not exceeding 10 min. The analysis proceeded in two steps; firstly for the 30-μm and secondly for the 200-μm tube aperture. The suspension of each sample was subsampled by an automatic pipette and was wet-sieved through a 30-μm sieve (or 200-μm in the second stage). Afterwards the subsample was placed in a glass beaker filled with 4 % sodium hexametaphosphate (Calgon) and stirred with a moderate speed. This suspension was counted until a specific number of particles was accumulated in any of the size intervals. The resulting size distributions derived from each of the two steps were combined by matching and re-computing the area under the combined curve to 100 %.

2.2.3. Data Preparation and Statistical Treatment

In this study the upper limit of the size range is different for the two devices; 80.6 μm for the CC and 2000 μm for LS. In order to compare results obtained from the two instrumentations, the distribution results of LS have been recalculated by interpolation in the 24 size classes of CC from 0.4 to 80.6 μm. The particle size results are expressed in volume percent in both analytical techniques, which facilitates the by-instrument comparison.

The method of moments was performed to estimate the mean and sorting of the two datasets. The higher order moments could not present any remarkable correlation between the two methods. The comparison of the results was achieved by: (i) the mean differences of frequency distribution for each of seven grain-size intervals; >10; 10-9; 9-8; 8-7; 7-6; 6-5; and 5-4 Ø (>1; 1-2; 2-4; 4-8; 8-16; 16-32; and 32-63 μm) between the two datasets, (ii) the correlation coefficient between the two bulk datasets and between the silt and the clay fractions measured by the two instrumentations and (iii) the analysis of variation/residuals within individual grain size intervals. Similar approaches have been discussed by Behrens (1978), Konert and Vandenberghe (1997), Loizeau *et al.* (1994) and Molinaroli *et al.* (2000).

3. Results and Discussion

The differences between the mean and sorting measures of Laser Coulter and Coulter Counter were compared using the linear phi scale (Ø) (Table 1, Fig. 1).

In the majority of the samples the mean size values (in phi) calculated by the CC method were overestimated comparing to those determined by LS. Twenty-three samples differed in the mean size by up to 1 Ø (500 μm) with higher overestimation occurred in the fine-grained samples. This overestimation of the mean size is also supported in the grain size frequency distributions curve from the CC analysis which showed a shift towards the fine classes comparing to laser coulter analysis (Fig. 6b). On the contrary, LS method determined larger grain sizes than CC method did up to 1 Ø in five coarse-sized samples. The sorting estimates presented smaller differences between the two methods. However the overestimated sorting values (up to 0.2 Ø or ~870 μm) by the CC method concerned the fine-grained samples. Molinaroli *et al.* (2000) compared the statistical parameters measured by a Galai Cis-1 system (laser based optical analysis), a Coulter Counter and a Sedigraph and showed that the grain size distributions estimated by the laser system had coarser mean size and better sorting in relation to the other two methods.

The mean values of the bulk sediment samples obtained by the two instruments are compared in Figure 1(a). The values are highly scattered around the bisectrix (1:1 line) and the correlation coefficient obtained is 0.7 revealing a moderate interrelation between the laser coulter and coulter counter analysis. This moderate correlation may be due to the very small quantity of sediment involved in the Coulter Counter measurement, which is at least one order of magnitude lower than the quantity used with the laser coulter. Loizeau *et al.* (1994) suggested a similar explanation for the dispersion around 1:1 line. The relationship between Coulter Counter and Laser (Malvern)

Table 1 – Coulter Counter and Laser Coulter mean size and sorting statistics

Sample No	Coulter Counter Mean (phi)	Coulter Counter Mean (μm)	Laser Coulter Mean (phi)	Laser Coulter Mean (μm)	Coulter Counter Sorting (phi)	Laser Coulter Sorting (phi)
1/4	8.306	3.159	7.717	4.751	1.737	1.491
1/5	8.427	2.905	7.804	4.473	1.569	1.501
1/6	8.432	2.896	8.062	3.741	1.574	1.541
12/6	8.457	2.846	7.617	5.093	1.604	1.479
12/7	8.076	3.707	7.575	5.244	1.816	1.432
12/8	8.452	2.855	7.551	5.332	1.667	1.476
12/9	8.199	3.403	7.653	4.968	1.707	1.501
12/11	8.253	3.277	7.609	5.122	1.685	1.451
17/5	7.719	4.745	7.823	4.416	1.657	1.736
17/7	6.448	11.456	7.360	6.088	1.586	1.885
17/8	7.298	6.355	6.378	12.023	1.693	1.848
17/9	7.597	5.167	7.077	7.408	1.774	2.009
17/10	7.882	4.239	7.750	4.646	1.825	1.798
17/12	7.936	4.083	7.997	3.913	1.767	1.599
17/15	7.915	4.144	7.751	4.643	1.801	1.836
20/9	7.879	4.249	7.945	4.059	1.655	1.661
20/10	6.764	9.204	6.143	14.148	1.556	1.748
20/12	7.882	4.238	7.703	4.799	1.854	1.757
20/14	6.224	13.375	6.904	8.349	2.062	2.117
24/6	8.253	3.279	7.803	4.479	1.644	1.515
24/7	7.990	3.934	7.923	4.119	1.760	1.556
24/8	8.037	3.807	7.512	5.478	1.845	1.848
24/20	7.279	6.441	6.815	8.882	1.778	2.030
38/5	8.250	3.285	7.886	4.228	1.737	1.548
38/6	8.031	3.824	7.883	4.235	1.774	1.540
38/7	8.084	3.686	7.716	4.756	1.765	1.542
38/8	8.177	3.454	7.827	4.402	1.740	1.583
38/16	8.350	3.064	7.812	4.449	1.631	1.603

methods was also examined by McCave *et al.* (1986), who compared the modal sizes and reported that in some cases there was little correspondence between the two methods. However it was shown by studies which have compared Coulter Counter with pipette method, that the data presented a satisfactory correlation despite the fact that CC means were coarser than the pipette means in the finer size ranges (Shideler 1976). Furthermore Behrens (1978) which applied

regression equation on the data sets derived from the coulter counter and pipette techniques also showed that the means had high linear correlation (r =0.99. slope = 0.70).

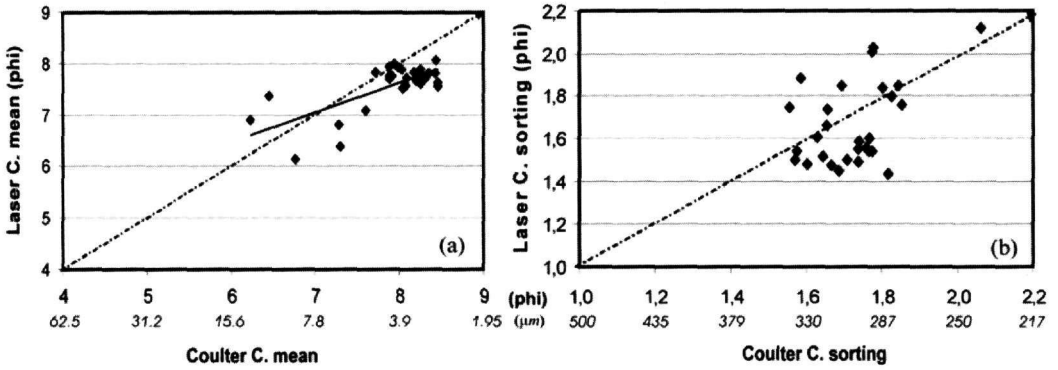

Figure 1 - Comparison of statistical parameters of two data sets (a) mean size and (b) sorting. Dashed line represents 1:1

The distribution of mean values differences of the two methods in specific grain size intervals are presented in Figure 2. The greater dissimilarities obsereved in the finer (>10 Ø), the 10-9 Ø (1-2 μm) and the 8-7 Ø (4-8 μm) intervals. For the finest two intervals (>10 Ø. 10-9 Ø), the Laser Coulter measures are higher than the Coulter Counter by ~ 4 % and ~ 8 %, respectively. The Coulter Counter detects fewer particles than Laser Coulter by almost 7 % for the 8-7 Ø internal. In the 7-6 Ø (8-16 μm) and in the coarsest (5-4 Ø) intervals the frequency distribution of Laser Coulter is overestimated by ~3 %.

The above suggest that the results from the Laser Coulter instrument are shifted towards coarse fractions, and the Coulter Counter overestimates the fine fractions. This could be attributed to particle shape. Jonasz (1991) argued about the influence of particle shape on the grain size analysis and suggested that the projected area of non-spherical particle orientation is larger than that of a sphere with equal volume. Konert and Vanderberghe (1997) compared the Laser Coulter with the pipette-sieve method and also reported that laser method led to coarser results.

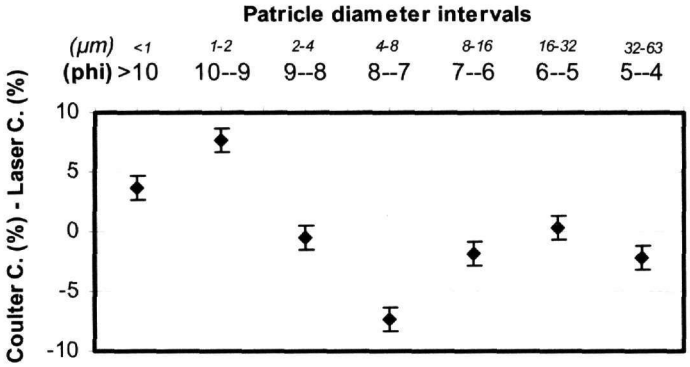

Figure 2 - Mean differences between frequencies for grain size intervals reported in x-axis

The relevance of the data obtained by the two instruments was also examined by treatment of variation/residuals analysis within individual grain-size intervals. The residuals constitute normalized factors which are independent from the magnitude of the frequency in the considered

grain size interval. In the present study the residual values between Coulter Counter and Laser Coulter were derived from the formula applied by Molinaroli *et al.* (2000):

Residual values = (Coulter Counter % - Laser Coulter %)/Coulter Counter %.

Residual values were plotted against Laser Coulter data for seven grain size fractions (>10; 10-9; 9-8; 8-7; 7-6; 6-5; and 5-4 Ø). Linear regression was applied to the scattered plots and correlation coefficient was computed for each size interval. Figure 3 illustrates the correlation between residual values and Laser Coulter data for selected grain size fractions. The >10, 10-9 and 6-5 Ø fractions are not presented here due to the poor correlation observed.

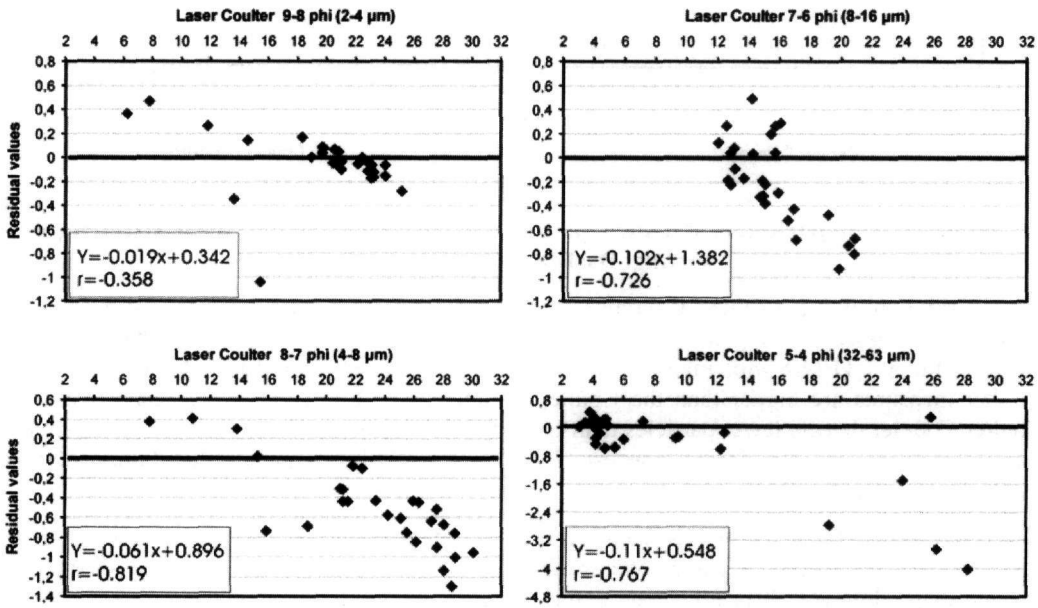

Figure 3 - Residual values plotted vs Laser Coulter selected fractions

In the plots of Figure 3 residual values were almost linearly related to Laser Coulter data in the 8-7 Ø (4-8 μm) (r = -0.819; slope = -0.061). The correlation coefficient decreased in the 7-6 Ø (8-16 μm) (r = -0.726; slope = -0.102) and 5-4 Ø (32-63 μm) (r = -0.767; slope = -0.11) intervals where there was a corresponding increase in the slope which indicated an enhance in the variability of the residuals. Significant correlation was not found in the 9-8 Ø (2-4 μm) interval.

The increase in the variability of the residuals in the coarser grain size intervals (7-6 and 5-4 Ø) may indicate a grater heterogeneity of physical properties (shape and density) of particles. This suggestion is further supported by the findings of Molinaroli *et al.* (2000).

Further comparison between silt and clay fractions obtained by the two methods showed that CC method yield a lower silt fraction than the LS method (Fig. 4). Conversely the clay fraction is overestimated by the CC method. The relationships found between the Laser Coulter and the Coulter Counter derived data for the two size fractions present moderate correlation coefficients (~ 0.69) and a fairly wide scatter of the points around the fitted line. McCave *et al.* (1986) which examined the efficiency of Malvern Laser system to determine clay fraction reported that the Laser method measured only a small fraction of clay present.

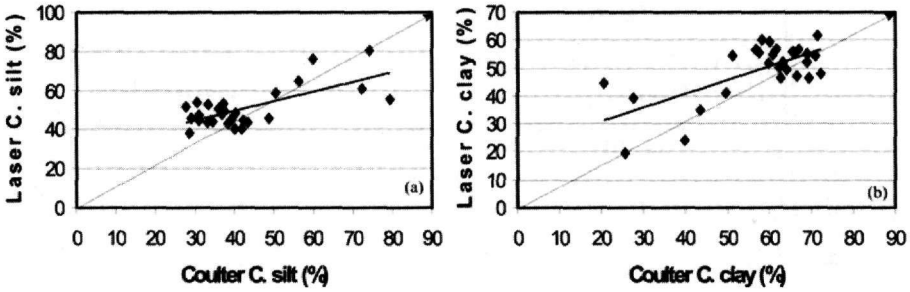

Figure 4 - Comparison of (a) silt and (b) clay fractions

The above mentioned discrepancies between the two methods may be due to the artificial truncation of the size distribution at the higher analytical limit of the tube aperture used by the Coulter Counter technique. As the size percentage data is based only on the analyzed distribution rather than on the total size distribution which is covered by the Laser Coulter method the particles larger than the tube's higher analytical limit are essentially ignored.

The moderate correlation (~0.69) occurred between silt fractions and clay fractions for both methods differs from previously published data which correlate satisfactory the Laser Coulter method with various techniques. Van Donger (1989) obtained a high correlation coefficient of 0.85 (slope = 0.185) for the comparison between the pipette and the Laser Coulter method. In addition Konert and Vanderberghe (1997) also obtained a high correlation coefficient (r = 0.957; slope= 0.361) for the comparison between the clay fractions obtained by Laser Coulter and pipette methods. Moreover, these authors obtained likewise high correlation for the data describing the fine-silt fraction. In a similar work, Beuselinck *et al.* (1998) compared the Laser diffractometry with sieve-pipette technique and showed a satisfactory correlation with $r > 0.9$ in almost all the size fractions. Singer *et al.* (1988) assessed the accuracy of various instrumentations through two sets of standards between 4.0 and 8.0 Ø. After the analysis of polymodal samples, these authors reported that Malvern Laser Sizer showed an overall broadening of individual modes. On the contrary, Coulter Counter delimited correctly the size range of individual modes. According to Singer *et al.* (1988) the disparity in the results for all instruments involved samples with high clay contend, in other words with increased particle-particle interface.

In a further approach of the by-instrumentation comparison, beyond the usual statistical treatment, the total set of particle size data (in volume percent) (24 size classes X 28 samples) from the Coulter Counter analysis was plotted against the results of the Laser Coulter analysis. In Figure 5 the samples that scatter more around the 1:1 line are those which presented the greater differences in the mean size. Due to the wide scattering of the data around the bisectrix a unique linear fit could not be meaningful. A threshold volume percent above which the Coulter Counter relatively underestimates particle diameters was observed. Therefore the data set was divided in two subsets; the first subset contains samples which have volume percent < 6 % in the Coulter Counter and the second consists of samples with volume percents greater than 6 %. It should be mentioned that the selected 6 % volume percent as a critical value is rather arbitrary than based on certain criteria.

On each data subset a linear regression was applied. For the first subset (<6 %) a moderate correlation was found (r = 0.75) between the two techniques. The Laser Coulter method slightly overestimates the volume percent for that subset. On the other hand, the two methods do not exhibit any correlation for the second subset (> 6 %). As a result, the correlation between the two techniques is strongly controlled by the volume percentage distribution of the sediment sample. Figure 6 shows the particle distributions of two sediment samples, representative of the two above subsets.

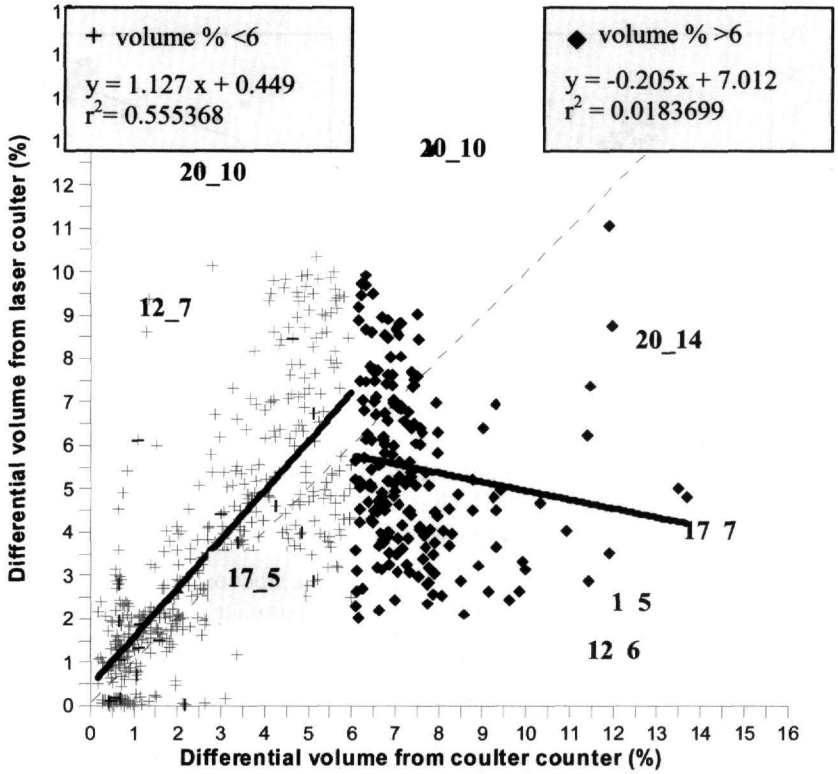

Figure 5 - Particle size distribution volume percents for each sample in each size fraction

The sample 17/5 has a platykurtic distribution without a profound modal size (Fig. 6a). It represents a typical particle distribution for the first data subset containing low percentages (less than 6 %) for each particle size class. The two particle distributions derived from the two techniques present almost the same pattern.

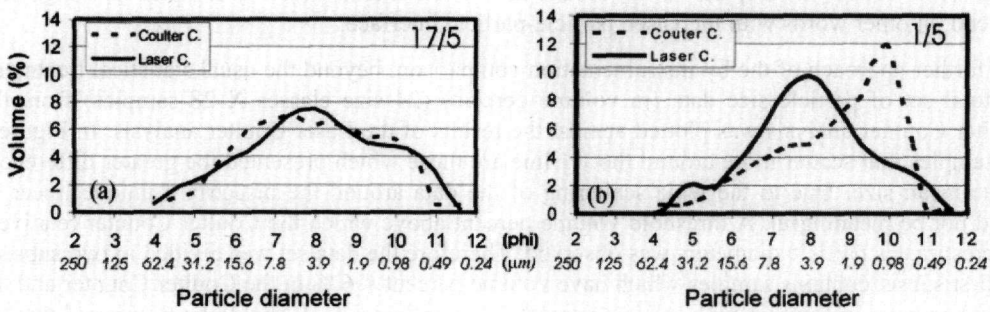

Figure 6 - Typical particle distributions of samples (a) 17/5 and (b) 1/5

The sample 1/5 shows a leptokurtic grain size distribution with a modal size (12 %. 10 Ø for the CC analysis) and it is considered to be a typical member of the second subset. The analysis of sample with both instruments indicated that the Coulter Counter overestimated the high volume percentage size fractions.

The existence of a threshold percentage was also reported by Beuselinck *et al.* (1998). These authors reported that the Coulter Laser method gives greater values than the sieve-pipette method

for most size fractions, but only up to certain percentage, above which fractions are relatively underestimated by the Laser method.

It should be noted that an additional reason for the discrepancy between the two methods may also be the analytical procedure. The Laser Coulter instrument performs measurement in the whole size range of the sample at the same time. On the contrary, the Coulter Counter analysis involves the combination and overlapping of the results derived form the two separate steps, which is sometimes inaccurate. The above suggestion is further considered as a limitation of the electronic counting (CC) method by McCave and Syvitski (1991).

4. Conclusions

The present study compares the particle size distributions measured by the Coulter Counter and Laser Coulter methods applied on 28 fine-grained red-mud tailing and natural sediment samples. The examination of the by-instrument relationship was achieved by (i) comparing the statistical parameters (mean size and sorting), (ii) calculating the mean differences in frequency distributions for specific grain-size intervals between the two datasets, (iii) applying correlation coefficient method between the silt and clay fractions of the two datasets and (iv) performing analysis of variation/residuals within individual grain size intervals.

The relationships between the two techniques for the moment statistical parameters and the silt and clay fractions differed from those appearing in the literature. However, it should be mentioned that previously published works have suggested various levels of relationships between the Laser Coulter and Coulter Counter results, ranging from poor to high correlation. As it is also the case for most comparisons performed between particle sizing techniques. The comparison of statistical parameters was carried out considering only the analytical range common to two instruments, with an interpolation of laser data according to coulter range.

The comparison of moment statistics demonstrated that Laser Coulter determined coarser grain sizes than Coulter Counter, especially in the coarser-grained samples. On the contrary, Coulter Counter instrumentation overrated the clay fraction.

Coarser fraction data present greater variability between the two instruments due to heterogeneity of particles physical properties. The methods reported in this study measure a different property more or less related to particle size. Therefore, the differences in the results are attributed to the sediment property measured by the different instruments.

The full dataset was separated in two subsets due to the fact that it was observed the existence of a more or less arbitrary threshold percentage (6 % in CC). For the first subset (<6 %) a moderate correlation was found ($r = 0.75$) between the two techniques with the Laser Coulter method slightly overestimating the volume percent. On the other hand, the two methods do not show any correlation for the second subset (> 6 %). The great disparity observed between the two methods in the second subset is due to the samples containing silt-clay mixtures, with well-expressed modal sizes.

5. Acknowledgements

The authors would like to thank the geochemical technologist W., Leblanc and sedimentary technician A.O., Brown from the Bedford Institute of Oceanography, Canada, for their great support during the analytical processes. The leading author is supported by the National Scholarships Foundation (NSF) of Greece.

6. References

Balagurunathan, Y., Dougherty, E. R., Frančišković–Bilinski, S., Bilinski, H., and Vdović, N., 2001. Morphological granulometric analysis of sediment images, *Image Analysis and Stereology,* 20, 87–99.

Behnens, E.W., 1978. Further comparison of grain-size distributions determined by electronic particle counting and pipette techniques, *J. Sedim. Petrol.*, 48, 1213-1218.

Beuselinck, L., Govers, G., Poessen, J., Degraded, G., and Frouen, L., 1998. Grain-size analysis by laser diffractometry: Comparison with the sieve-pipette method, *Catena,* 32, 193–208.

Bianchi, G.G., Hall, I.L., McCave, I.N., and Joseph, L., 1999. Measurement of the sortable silt current speed proxy using the Sedigraph 5100 and Coulter Multisizer IIe: precision and accuracy, *Sedimentology*, 46, 1001–1014.

Buurman, P., Pape, T., and Mugger, C.C., 1997. Laser grain-size determination in soil genetic studies: 1. Practical problems, *Soil Science*, 162, 211–217.

Frančišković–Bilinski, S., Bilinski, H., Vdović, N., Balagurunathan, Y., and Dougherty, E. R., 2003. Application of image-based granulometry to siliceous and calcareous estuarine and marine sediments, *Coastal and Shelf Science*, 58, 227-239.

Jonasz, M., 1991. Size, shape, composition and structure of microparticles from light scattering. In J.P.M. Syvitski (ed.), *Principles, Methods and Application of Particle Size Analysis*. 143-162pp, Cambridge, Cambridge Univ. Press.

Jordan, C.F., Fryer, J.R., G.E., and Hemmen, E.H., 1971. Size analysis of silt and clay by hydrophotometer, *J. Sedim. Petrolog.,* 41, 489–496.

Iatrou., M., Piper, D.J.W., Tripsanas, E., Papatheodorou, G., and Ferentinos, G., 2006. Man-made gravitational flow deposits: A useful tool for studying the sedimentation processes in a seismically active graben, the Gulf of Corinth, Greece, *17th ISC, Fukuoka, Japan, 27th August-1st September, Abstracts book P-063,* 279pp.

Konert, M., and Vandenberghe, J., 1997. Comparison of laser grain-size analysis with pipette and sieve analysis: a solution for the underestimation of the clay fraction, *Sedimentology,* 44, 523–535.

Loizeau, J.-L., Arbouille, D., Santiago, S., and Vernet, J.-P., 1994. Evaluation of a wide range laser diffraction grain-size analyser for use with sediments, *Sedimentology,* 41, 353–361.

McCave, I.N., Bryant, R.J., Cook, H.F., and Coughanowr, C.A., 1986. Evaluation of a laser-diffraction-size analyzer for use with natural sediments, *J. Sedim. Petrol.,* 56, 561–564.

McCave, I.N., and Syvitski, J.P.M., 1991. Principles and methods of geological particle size analysis. In J.P.M. Syvitski (ed.), *Principles, Methods and Application of Particle Size Analysis*, 3–21, Cambridge, Cambridge Univ. Press.

McCave, I.N., Hall, I.L., and Bianchi, G.G., 2006. Laser vs settling velocity differences in silt grainsize measurements: estimation of palaeocurrent vigour, *Sedimentology*, 53, 919-928.

Milligan, T.G., and Kranck, K., 1991. Electroresistance particle size analyzers. In J.P.M. Syvitski (ed.), *Principles, Methods and Application of Particle Size Analysis,* 109-118, Cambridge, Cambridge Univ. Press.

Muggler, C.C., Pape, Th., and Buurman, P., 1997. Laser grain-size determination in soil genetic studies: 2. Clay content, clay formation, and aggregation in some Brazilian Oxisols, *Soil Sci.*, 162 (3), 219–228.

Molinaroli, E., De Falco, G., Rabitti, S., and Portaro, R.A., 2000. Stream-scanning laser system, electric sensing counter and settling grain size analysis: a comparison using reference materials and marine sediments, *J. Sedim. Geol.*, 130, 269-281.

Papatheodorou, G., Stefatos, A., Christodoulou, D., and Ferentinos, G., 2003. Small scale present day turbidity currents in a tectonically active submarine graben, the Gulf of Corinth (Greece): Their significance in dispersing mine tailings and their relevance to basin filling. In J. Locat and J. Mienert (eds), *Submarine Mass movements and their consequences*. 459-468, Netherlands, Kluwer Academic Publishers.

Shideler, G.L., 1976, A comparison of electronic particle counting and pipette techniques in routine mud analysis, *J. Sedim. Petrol.*, 46, 1017-1025.

Singer, J.K., Anderson, J.B., Ledbetter, M.T., McCave, I.N., Jones, K.P.N., and Wright, R., 1988. An assessment of analytical techniques for the size analysis of fine-grained sediments, *J. Sedim. Petrol,*. 58, 534–543.

Sperazza, M., Moore, J.N., and Hendrix, M.S., 2004. High-resolution particle size analysis of naturally occurring very fine-grained sediment through laser diffractometry, *J. Sedim. Res.*, 74 (5), 736-743.

Stein, R., 1985. Rapid grain-size analyses of clay and silt fraction by SediGraph 5000D: comparison with Coulter Counter and Atterberg methods, *J. of Sedim. Petrol.*, 55, 590-593.

Varnavas, S., Ferentinos, G., and Collins, M., 1986. Dispersion of bauxitic red mud in the Gulf of Corinth, Greece, *Marine Geology,* 70, 211-222.

Van Dongen, W., 1989. Bepaling korrelgrootteverdelingvan waterbodems en zwevende stof. IJking van de laserbuigingsmethode met de zeef- en pipet methode volgens NEN 5753, Afstudeerverslag HLO-chemie. Rijkswaterstaat/RIZA, Lelystad.

Δελτίο της Ελληνικής Γεωλογικής Εταιρίας τομ. XXXX, 2007
Πρακτικά 11ου Διεθνούς Συνεδρίου, Αθήνα, Μάιος 2007

Bulletin of the Geological Society of Greece vol. XXXX, 2007
Proceedings of the 11th International Congress, Athens, May, 2007

PRELIMINARY SEDIMENTOLOGICAL RESULTS INDICATE A NEW DETAILED STRATIGRAPHY FOR THE FLORINA SEDIMENTARY BASIN AND RELATE THEM WITH CO_2 PRESENCE

Karakatsanis S.[1], Koukouzas N.[2], Pagonas M.[1], and Zelilidis A.[1]

[1] *University of Patras, Department of Geology, 26500 Patras, Greece, A.Zelilidis@upatras.gr, karastyl@gsrt.gr, pagonas@upatras.gr*

[2] *C.E.R.T.H., Attica Technology Park, 15310 Ag.Paraskevi Athens. koukouzas@techp.demokritos.gr*

Abstract

Drill core analysis showed 41 sedimentary cycles in the sedimentary association of the Neogene to Quaternary Florina Basin, with a total thickness up to 560m. The lower part is the Base formation with an up to 297m thick, whereas middle part, Vevi formation is up to 127m thick and the upper part which corresponds to Lophon formation is up to 124m thick. The beginning of sedimentation in the basin, with alternated sand, clay and conglomeratic beds, with presence of xylite, at the lowermost part of Base formation, indicates a weak tectonic activity and low sedimentation rate. Tectonic activity increased and alluvial fans were formed in the rest part of Base formation. The 21 cycles within alluvial fans could be related mostly with 21 episodes of tectonic activity and sedimentation and less with climatic changes or autocyclic events. Depositional environment changed in the Vevi formation from terrestrial to lacustrine, where lacustrine and fluvio-lacustrine deposits were accumulated. Finally, the basin filled up with terrestrial deposits in the Lophon formation. So, the ratio of subsidence rate/sedimentation rate starts with <1, in Base formation, becomes =1 in the case of Vevi's formation and finally becomes again <1 in Lophon formation. Fluvial and alluvial fan environments can be used as CO_2 storage sites, whereas the internal change of stratigraphy in the same environment of sedimentation does not allow the escape of CO_2.

Key words: sedimentary *cycles, alluvial-fans, fluvio-lacustrine environment.*

Περίληψη

Η ανάλυση πυρήνα γεώτρησης στην λεκάνη της Φλώρινας έδειξε την ύπαρξη 41 κύκλων ιζηματογένεσης στην ακολουθία ιζημάτων συνολικού πάχους 560 μέτρων, του Νεογενούς – Τεταρτογενούς. Το κατώτερο τμήμα της ακολουθίας αντιστοιχεί στο σχηματισμό της Βάσης, με συνολικό πάχος 297 μέτρων, ενώ το μεσαίο τμήμα αντιστοιχεί στο σχηματισμό της Βεύης με ένα πάχος 127 μέτρων, και το ανώτερο τμήμα αντιστοιχεί στον σχηματισμό Λόφων με πάχος που φθάνει τα 124 μέτρα. Το ξεκίνημα της ιζηματογένεσης στη λεκάνη, με τις εναλλαγές των στρωμάτων άμμου,

αργίλου και κροκαλοπαγών, με την παρουσία ξυλίτη προτείνει ασθενή τεκτονική και χαμηλό ρυθμό ιζηματογένεσης. Βαθμιαία, η τεκτονική δραστηριότητα αυξάνει και σχηματίζονται αλλουβιακά ριπίδια. Οι 21 κύκλοι μέσα στα αλλουβιακά ριπίδια προτείνουν 21 επεισόδια τεκτονικής δραστηριότητας. Το αποθετικό περιβάλλον αλλάζει σταδιακά από χερσαίο σε λιμναίο όπου συγκεντρώθηκαν λιμναίες και ποταμολιμναίες αποθέσεις. Τελικά, η λεκάνη πληρώθηκε με χερσαία ιζήματα. Έτσι, ο λόγος του ρυθμού βύθισης προς τον ρυθμό ιζηματογένεσης ξεκινάει με <1, στον σχηματισμό της Βάσης, γίνεται =1 στον σχηματισμό της Βεύης και τελικά ξαναγίνεται < 1στον σχηματισμό Λόφων. Ποτάμια περιβάλλοντα ιζηματογένεσης και αλλουβιακών ριπιδίων μπορούν να χρησιμοποιηθούν σαν θέσεις αποθήκευσης CO_2, ενώ οι εσωτερικές αλλαγές της στρωματογραφίας στο ίδιο περιβάλλον ιζηματογένεσης δεν επιτρέπει στο CO_2 να διαφύγει.
Λέξεις κλειδιά: *κύκλοι ιζηματογένεσης, αλλουβιακά ριπίδια, ποταμολιμναίο περιβάλλον.*

1. Introduction – Geological Setting

The studied area is part of the Florina-Amynteon sedimentary basin. It is located in North-West Macedonia (Greece) while is located between the coordinates 40° 42′-40° 54′ latitude and 21° 20′-21° 35′ longitude, and it belongs to Pelagonian geotectonic Zone (Pavlidis and Mountrakis 1987) (Fig. 1). The basement is characterized by the metamorphic rocks of Varnounta and Vorras and Carbonate rocks at the eastern margins of the basin (Kilias 1980).

Metamorphic rocks deposited during the Upper Carbiniferous period constitute two complexes, Vorras and Vernon respectively (Mountrakis 1983). The Vorras complex is composed of orthogneiss with relative homogeneous mass of biotitic gneiss, granular banded muscovitic gneiss, and a layer that is composed of mica and amphibolitic schist and phyllites. The Vernon complex is composed by Vitsi-Nemfeon zone with grey, light coloured and white gneiss, Kleisouras zone with alternations of amphibolitic and schistolithic rock, Gneiss plutonic rocks of Kastorias's zone, Sideroxoriou zone with semi-metamorphic and epimetamorphic rocks and Aposkepou zone with arkoses, conglomerates, pelites, phyllites, tuffic rocks.

The studied basin has been filled up by Neogene and Quaternary sediments (Pavlidis and Mountrakis 1987, Fig. 2). According to Pavlidis (1985), Neogene sediments distinguished in the lower part, Base formation, with an up to 200 m thick, the middle part, Vevi formation up to 50 m thick, and the upper part, Lophon formation, up to 200 m thick. These three parts are characterised by the continuous sedimentation from Late Miocene to Pleistocene. Middle part, according to Pavlidis (1985) is synchronous with Vegora formation from Ptolemais basin, and so, the age of this part is estimated as late Miocene - early Pliocene, but it is equal in lithostromatography with the Ptolemais formation with an early Pliocene age (Pavlidis and Mountrakis 1987, Steenbrink *et al.* 2006). This part is composed of quartz-rich sand, mica layers and grey clay, which at places contains leafs in good condition, followed by layer of lignite which is placed between sand and clay layer. The upper part, due to the presence of some characteristic fossils (e.g. *Planorbis, Neritica, Unio, Lymnaeus*), was formed during Pliocene, synchronous with lignite deposits of Ptolemais basin (Pavlidis 1985) or could be related with the upper part of Ptolemais basin sediments, because they have the same lithology, with an early Pleistocene age (Pavlidis and Mountrakis 1987, Steenbrink *et al.* 2006). Quaternary deposits are mostly terrestrial and were characterized by fluviolacustrine, fluvial and alluvial fan environments that developed during early Pleistocene.

Late Miocene is characterized by NE-SW extension (Pavlidis and Mountrakis 1987) whereas a subsequent Pleistocene episode of NW-SE extension resulted in the fragmentation of the initial basin into several sub-basins, i.e., the sub-basins of Florina, Ptolemais and Servia (Pavlidis and Mountrakis 1987, Steenbrink *et al.* 2006).

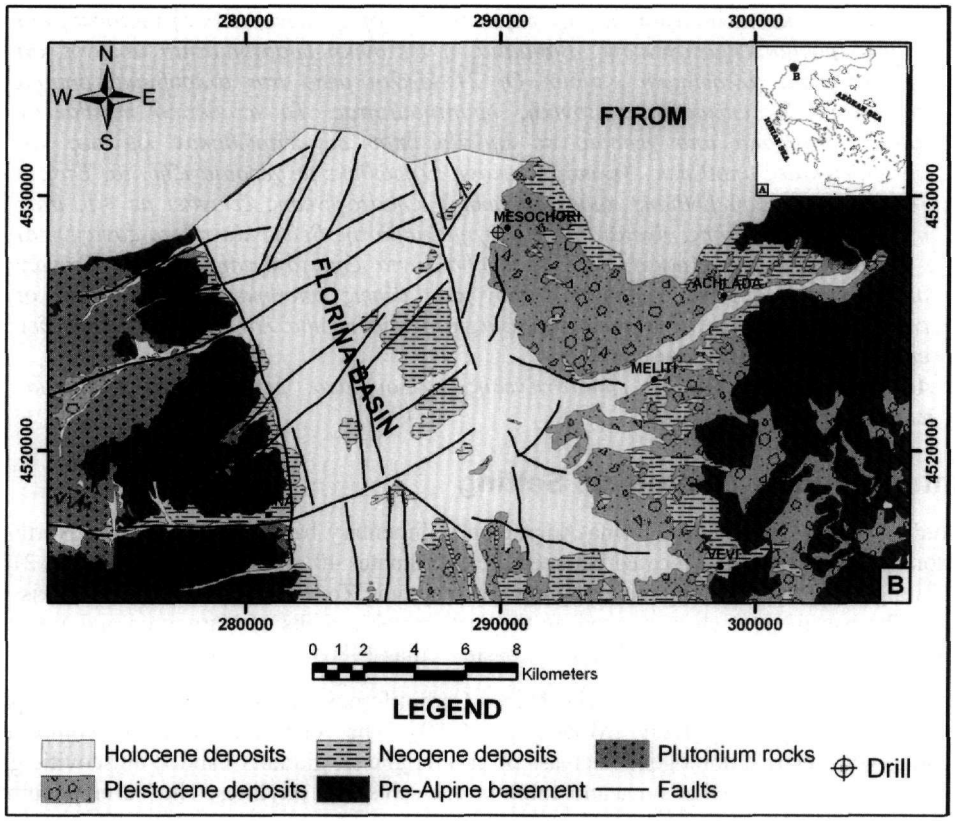

Figure 1 - Geological map of the studied area, modified from I.G.M.E. Florina and Vevi geological maps

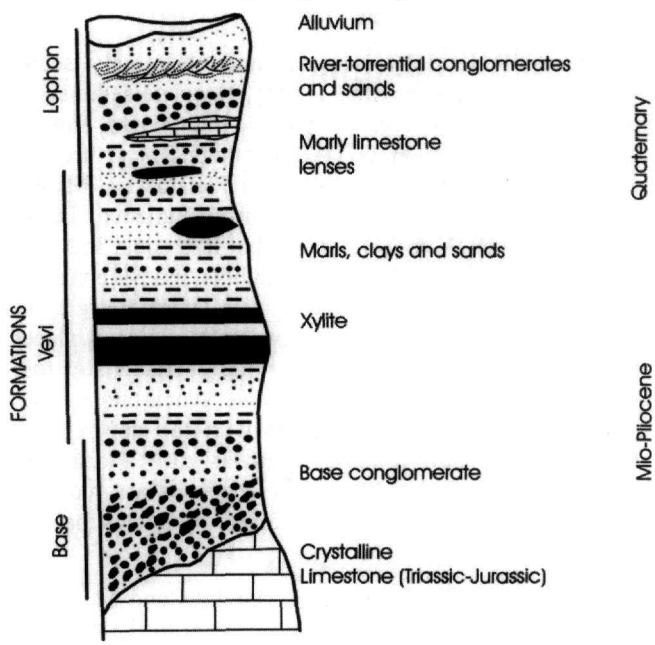

Figure 2 - Stratigraphy of the studied basin, not in scale, according to Pavlidis (1985)

Accrding to Vetoulis (1951), Quaternary deposits occupy a great part of the basin and cover partially or totally the Tertiary formations represented by Pleistocene (Diluvium) and Holocene (Aluvium) deposits while consists of sands, muds, quartz-rich conglomerates and conglomerates. Pleistocene (Diluvium) sediments composed of coarse quartz-rich conglomerates, and mud products as a result of erosion, which was caused by torrents while their thickness varies from 2 up to 5m. Below them there is a 10-30 metres thick layer of muddy sand. Holocene (Aluvium) consist of fluvial deposits and accretions of muddy matter, quartz-rich sand, clays with fluvial fossils such as gasteropods.

The aim of the present work is to present the detailed lithostratigraphy of the sedimentary basin of Florina based on a drill core at the eastern margin of the basin and to introduce a model of the basin evolution from Neogene to present. Age determination of the selected samples and detailed sedimentological analysis of them will establish the exact model of Florina basin evolution, taking into account ages, sedimentological results and published structural data.

2. Sedimentological description of drill core in Mesochori

A drill core, with a length of 570meters, divided into 8 parts (A: 0-124 m., B: 124-152 m., C: 152-251 m., D: 251-376 m., E: 376-430 m., F: 430-548 m., G: 548-560 m., H: >560 m.) (Fig. 3). These divition into 8 parts based on different lithology, from one part to the other, whereas cycles boundary based on the abrupt change from the one lithology to the other. These eight parts show not only their length but also their depth from the surface. The lowermost part, which was met >560 m from the surface, is referred as basement. According to Pavlidis (1985) and our analysis there are three main groups of rocks, the sediments above lignite (0-124 m) which belongs to Lophon formation (Part A), the lignite layers (124-152 m) and the underlying them deposits as far as the depth of 251 m, that belongs to the Vevi formation (Parts B and C), and sediments below them (251-560 m) which related with the Base formation (Parts D, E, F and G). A detailed description (Fig. 3) is given below, from top to bottom.

Part A, 0-124 m: This part is composed of 4 cycles with an upward increase in grain size and decrease in sedimentary thickness of each cycle. At the top third and fourth cycle consists of conglomerates whereas first and second cycle consists of sand. Their thickness from lower to upper cycle is 50.5 m (48 m of mud-2.5 of sand), 36.5 m (33.5 m of mud, 3 m of sand), 30 m (3 m of mud, 8 m of sand, 9 m of conglomerates), 7 m (6 m of sand, 1m of conglomerates).

Moreover, an aquifer appeared between 102-106m from the surface.

Part B, 124-152 m: In this part 11 cycles with alternated clays and sand were recognized. Lignite was detected at the upper part of 5 cycles. Thickness of the cycles, from lower to the upper, are the following: 1m (0.5 m of mud, 0.5 m of lignite), 3 m (1 m of mud – 2 m of sand), 1.5 m (1 m of mud - 0.5 m of sand), 1.5 m (0.5 m of mud – 1 m of sand), 6 m (1.5 m of mud – 4.5 m of sand), 2 m (1 m of mud, 1 m of lignite), 2.5 m (2 m of sand – 0.5 m of lignite), 1.5 m (1.1 m of sand – 0.4 m of lignite), 4.5 m (1.5 m of sand – 3 m of lignite), 1.7 m (1.3 m of sand – 0.4 m of lignite), 2.8 m (2 m of sand – 0.8 m of lignite).

In general, it is noticed an increase of grain size and lignite thickness from the lower to upper cycle of this part.

In last cycle, a CO_2 accumulation was detected. The accumulation was found in sands under the lignite layer. The accumulation has already been exploited.

Part C, 152-251 m: This part it consist by 10 cycles of alternated sand and clay with an upward increase in grain size from the lower to upper cycle. Between 3-24 m is noticed the decrease of cycle thickness and sand's thickness from the lower to upper cycle.

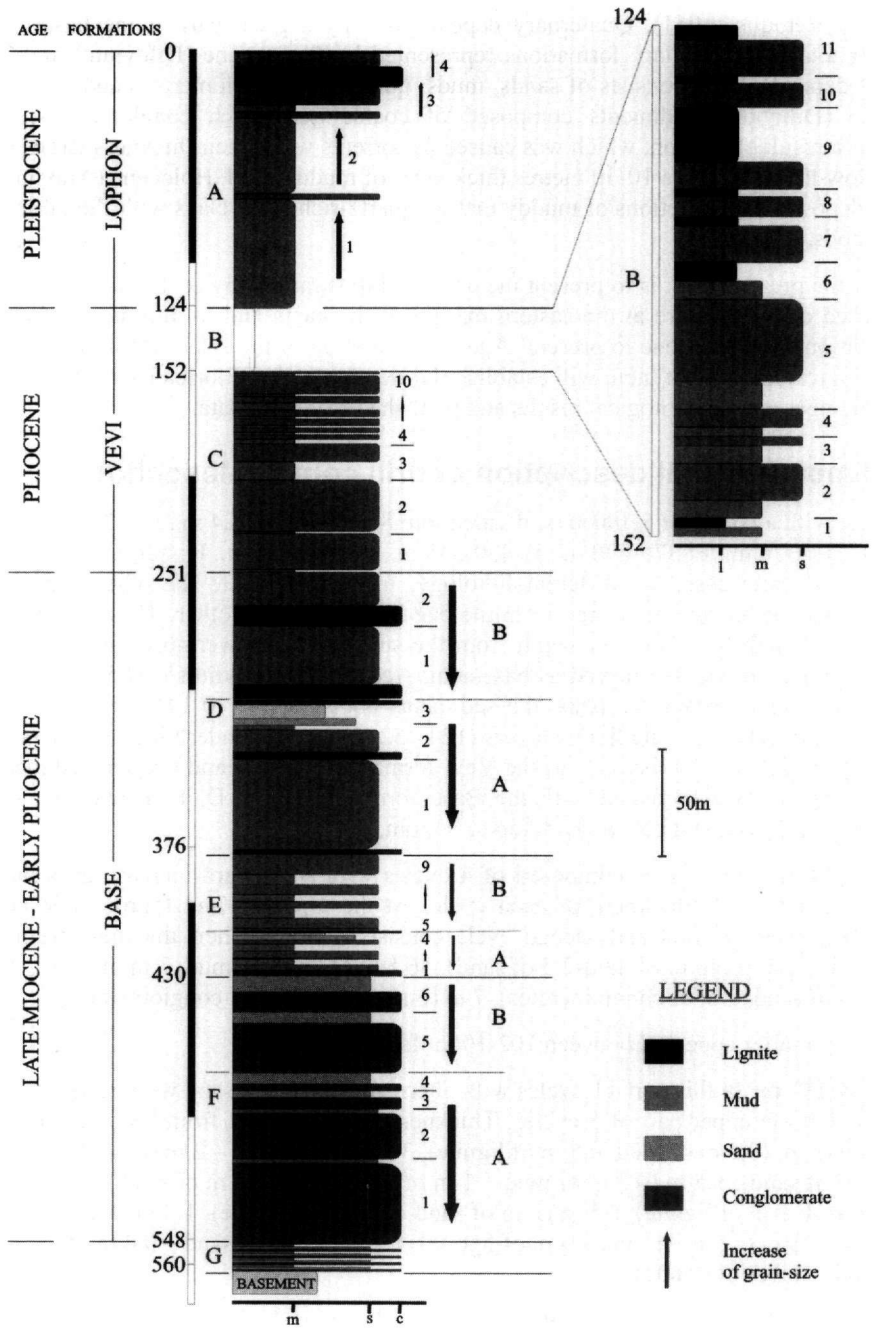

Figure 3 - Stratigraphy of the Florina basin, based on the drill core analysis of this work. Horizontal scale at the base is for lithology, m=mud, s=sand and c=conglomerates. Numbers and letters in each Part show cycles and sequences respectively

The thickness of each cycle, from the lower to upper part, is the following: 17 m (1 m of clay – 16 m of sand), 24 m (1 m of clay – 23 m of sand), 16 m (8 m of clay – 8 m of sand), 4 m (2m of clay – 2 m of sand), 3 m (1 m of clay – 2 m of sand), 4 m (1 m of clay – 3 m of sand), 4 m (1 m of clay – 3 m of sand), 6 m (3 m of clay – 3 m of sand), 9 m (1 m of clay – 8 m of sand), 2 m (1 m of clay – 1 m of sand).

In the sand of the lower cycle, which has thickness of 17 m, an aquifer was detected.

Part D, 251-376 m: 6 cycles which consist of conglomerates and sand were detected while their thickness varies from 3 up to 42 m. These cycles constitute two sequences with decrease in grain size and thickness from the lower to upper sequence of this part.

The cycles and sequences are quoted below. A: 42 m (2m of conglomerates – 40 m of sand), 15 m (3 m of conglomerates – 10 m of sand – 2 m of clay), 9 m (3 m of medium grain size sand – 6 m of fine sand), 3 m (2 m of conglomerates –1 m of sand), B: 32 m (6 m of conglomerates – 26 m of sand), 24 m (9 m of conglomerates – 15 m of sand).

Four natural CO_2 accumulations from depth 296 m up to 334 m (296-306 m, 310-312 m, 322-331 m, 335-338 m) and 2 aquifers (301-304 m, 331-338 m) were detected. An additional CO_2 accumulation exists at 366-372 m depth. These formations appeared in coarse components without an upper layer of fine materials which acts as a cap rock.

Part E, 376-430 m: 9 cycles of alternation of sand and cycle compose this part. Their thickness ranges from 0.5 to 9 m. These cycles constitute two sequences with decrease in grain size from the lower to upper sequence of this part.

The cycles and sequences are quoted below. A: 7.5 m (of conglomerates-sand-clay), 0.5 m (of sand-clay), 6 m (of sand-clay), 5 m (of sand: coarse-medium-fine grain size), B: 2 m (of conglomerates-sand), 9 m (of sand-clay), 6 m (of sand-clay), 9 m (of sand-clay), 9 m (of sand).

Four accumulations of CO_2 in coarse components without an upper rock layer which acts as a cap rock were detected at depths from 380 m up to 409 m.

From 410 m up to the end of this part, a saturated water table layer was recognized.

Part F, 430-548 m: There are 6 cycles which consist of conglomerates and sand. Sand's proportion is greater in the upper than in the lower cycle. These cycles constitute two sequences with decrease in grain size from the lower to upper sequence of this part. The thickness of the cycles and the proportion of conglomerates/sand decreased from the lower to the upper cycle. The cycles from lower to upper are composed of A: 38 m (36 m of conglomerates – 2 m of sand), 22 m (20 m of conglomerates – 2 m of sand), 8 m (5 m of conglomerates – 3 m of sand), 8 m (3 m of conglomerates – 5 m of sand), B: 27m (22m of conglomerates – 5 m of sand), 16 m (9 m of conglomerates – 7 m of sand).

Part G, 548-560 m: Alterations of sand-clay and conglomerates with the presence of xylite is noticed.

Part H, >560 m: At depth 562 m from the surface appears a soil layer which is up to 2 m thick, while under this level appears the basement. The basement consists of gneiss and quartzite.

3. Interpretation

According to Pavlidis (1985) and our analysis Part A belongs to Lophon formation, Parts B and C belongs to the Vevi formation, whereas Parts D, E, F and G belongs to the Base formation. Specially:

Part A from 0-124 m: Sediments of this part were formed in a lacustrine and a fluvial environment. The evolution of the four cycles indicates the activation of the basin four times during the development of the lacustrine environment; two lower cycles which fully deposited and "closed" the lake and two other cycles where the deposition was gradually. The two lower cycles seem to correspond to conditions similar to lake while the two upper cycles correspond to fluvio-lacustrine conditions. Furthermore the variation of cycles' thickness and the decrease of thickness upwards indicate the deactivation of the deposition from older to younger deposits.

Part B from 124-152 m: According to Pavlidis (1985) this is the upper part of Vevi's formation which is of Late Miocene-Early Pliocene age and formed in a lacustrine environment. According to Pavlidis and Mountrakis (1987) and Steenbrink *et al.* (2006) description of this Part seems to be equal with Ptolemais Formation of Ptolemais basin which formed during Early Pliocene.

Part C from 154 to 251 m: According to Pavlidis (1985), this part belongs to the lower part of Vevi's formation. The cycle's structure and thickness, from the lower to upper of this part shows that there are 10 stages of deposition in the basin. Its seems that the dynamic of the deposition was decreased from the lower to the upper parts, while it looks that the basin remains as lake for smaller period of time and was gradually deposited resulted to conglomerates of greater thickness compared to the fine grained sediments.

Part D from 251-376 m: The cycles' structure and their grain size show that correspond to the formation of Base, formed in a terrestrial environment. The two series of sediments indicate that two main events took places which are both related with events of minor importance. It seems that these series correspond to deposits which gradually feed the basin.

Part F from 430 to 548 m: These sediments seem to be deposited by debris flows in alluvial fan environments. The structure of cycles and sequences shows the progressive reduction of tectonic activity but also the renewal of tectonics of the second sequence. Examining this part (430-548 m) together with the overburden part (376-430 m), then probably the overburden sector constitutes the shifted part of a different alluvial fan that was formed in a different place. However, if this part (376-430 m) is related, in terms of genesis, with the overburden part (251-376 m) which was of fluvial origin, then this part (376-430 m) might correspond to sediments of parallel deposition. In both cases immigration of sedimentation process and source of supply from western to eastern parts appears.

Part G from 458 to 560 m: The sediments of this lower stratigraphic part indicate the beginning of sedimentation in a basin where its tectonic activity is weak and the sedimentation rate is low, due to the pure drainage pattern when the basin was formed.

Part H >560 m: Basement with metamorphic rocks

4. Discussion

Florina basin is part of the initial Florina-Ptolemais-Servia basin which formed due NE-SW late Miocene extension (Pavlidis and Mountrakis 1987, Steenbrink *et al.* 2006). Fragmentation of this basin took place during early Pleistocene and due to the NW-SE extension (Pavlidis and Mountrakis 1987). Taking into account the above evolution we could relate sedimentation pattern of the Ptolemais basin to the studied Florina basin. So, the 600 m total thickness of sediments as referred by Steenbrink *et. al.* (2006) for the Ptolemais basin seems to be equal with the 560 m total thickness of the studied Florina basin. In detail, the 300 m thickness of Komnina formation at the lower stratigraphic part of Ptolemais basin seems to be equal with the 297 m thick of Base formation in the Florina basin, whereas the 100 m thick of Ptolemais formation in Ptolemais basin seems to be equal with the 127 m thick of Vevi formation in Florina basin.

According to the above hypothesis we could relate also the time of sedimentation and the depositional environments between the two adjacent basins Ptolemais and Florina. In the case that sedimentation rate is equal in both basins, and this could be indicated due to the fact that from late Miocene to Pliocene the basin was unique, then the Base Formation age of Florina basin could be equal with the age of Komnina formation of Ptolemais basin and it is late Miocene to early Pliocene, whereas Vevi formation in the studied basin could be equal with the Ptolemais formation in Ptolemais basin and it is early Pliocene. Finally, the uppermost Lophon formation is equal with the uppermost formation of Ptolemais basin and it is early Pleistocene. In this case we have a change of the Pavlidis (1985) suggested age for the Vevi formation which was referred as late Miocene-early Pliocene. According to this scenario most of the cycles formed within the

sediments could be related with tectonic activity and tectonic pulses. Tectonic activity produced the relief in order to have an active source.

The second hypothesis is to accept as correct the mentioned age for the Vevi formation and in this case we have different sedimentation rates from one basin to the other and different depositional environments. When we have only 300 m terrestrial deposits in Ptolemais formation during Late Miocene-early Pliocene (Komnina formation), we have 425 m thick sediments with terrestrial and lacustrine deposits in Florina basin (Base and Vevi formations); whereas when we have 100 m thick lacustrine deposits in Ptolemais basin during early Pliocene there is no sedimentation in Florina basin. Taking into account this second hypothesis with different depositional conditions along the unique basin then we could indicate that many of the cycles within the Vevi's formation lacustrine deposits represent autocyclic events such as climatic changes, as this also suggested from Steenbrink *et al.* (2006) for Ptolemais formation in Prolemais basin.

Finally, as the unique basin subdivided into three sub-basins during early Pleistocene, it seems that we have the same sedimentological pattern in the two adjacent basins with the same terrestrial deposits.

5. Conclusions

1. Drill core analysis showed 41 sedimentary cycles in the sedimentary association of the Neogene to Quaternary Florina Basin, with a total thickness up to 560 m.
2. The beginning of sedimentation in the basin, from 548-560 m, with alternated sand, clay and conglomeratic beds, with presence of xylite indicates a weak tectonic activity and low sedimentation rate.
3. From the depth of 251m and up to 548 m, appears the Base formation, with a total thickness of 297 m, formed in a terrestrial environment, probably stacked alluvial-fans, which become fluvial upwards. 21 cycles within alluvial fans indicate 21 episodes of tectonic activity and sedimentation. The upward change from alluvial fans to fluvial deposits indicates the gradual change from more active to less active tectonic activity. Moreover, the Base formation includes the CO_2 accumulations which are found in fine sands and mostly accumulated in the fluvial environment.
4. Between 124 m and 251 m, Vevi formation is present which is developed in a lacustrine environment. 21 cycles within this formation and lignite horizons in the upper part of the sedimentary sequence indicate that sedimentation rate is equal to the subsidence rate and every time when fault activity create space sedimentation filled up the space. Total lignite thickness is up to 6.6 m formed in the upper part of 6 cycles within a total sedimentary association of 28 m thick.
5. The uppermost sediments, between the surface and the depth of 124 m, are the Lophon formation of Pliocene-Quaternary age, accumulated in a fluviolacustrine environment.

Generally, the change from alluvial fans to lacustrine and finally to fluvial deposits could be related with the ratio of subsidence rate/sedimentation rate. So, the above changes could be show that the basin sedimentation started with a ratio <1, becomes $=1$ in the case of Vevi's formation and finally becomes again <1. This results to the covering of the lake with sediments.

CO_2 storage sites mostly referred to fluvial and alluvial fan environments and a detailed study (i.e. porosity) could be relating these environments with future storages of CO_2. Moreover, the internal change of stratigraphy in the same environment of sedimentation does not allow the escape of CO_2. However, it should be a connection between the presence of CO_2 with aquifers and the height of column of water and how much the hydrostatic pressure increases the trapping of gases in the sediments.

6. Acknowledgments

We would like to thank I.G.M.E. for the permission to use the drill core data for detail sedimentological analysis. The authors are indebted the reviewer Dr. Steenbrink for his detailed suggestions and corrections.

7. References

Kilias, A., 1980. Geological and tectonic study of eastern Varnountas area (NW Macedonia), *PhD Thesis*, University of Thessaloniki, 271pp.

Mountrakis, D., 1983. *The geological structure of northern Pelagonian zone and geotectonic evolution of internal Hellenides*. Dissertation for readership, University of Thessaloniki, 289pp.

Pavlidis, S., 1985. Neotectonic evolution of Florina – Vegoritida – Ptolemais basins (W. Macedonia), *PhD Thesis*, University of Thessaloniki, 265pp.

Pavlidis, S.B., and Mountrakis, D.M., 1987. Extensional tectonics of northwestern Macedonia, Greece, since the late Miocene, *Journal of Structural Geology*, 9., 385-392.

Steenbrink, J., Hilgen, F.J., Krijgsman, W., Wijbrans, J.R., and Meulenkamp, J.E., 2006. Late Miocene to Early Pliocene depositional history of the intramontane Florina-Prolemais-Servia Basin, NW Greece: Interplay between orbital forcing and tectonics. *Palaeog. Palaeoc. Palaeoec.*, 238, 151-178.

Vetoulis, D., 1951. The lignitic Amynteon – Vegora basin, *Geol. Anagn., IGEY, Athens, No14*, 1-30.

Δελτίο της Ελληνικής Γεωλογικής Εταιρίας τομ. XXXX, 2007
Πρακτικά 11ου Διεθνούς Συνεδρίου, Αθήνα, Μάιος 2007

Bulletin of the Geological Society of Greece vol. XXXX, 2007
Proceedings of the 11th International Congress, Athens, May, 2007

REGIONAL CORRELATION AND CYCLOSTRATIGRAPHY IN THE MID-CRETACEOUS FORMATIONS OF THE IONIAN ZONE

Karakitsios V.[1], and Agiadi-Katsiaouni K.[1]

[1] *National and Kapodistrian University of Athens, Faculty of Geology and Geoenvironment, Department of Hist. Geology - Paleontology, vkarak@geol.uoa.gr, kagiadi@geol.uoa.gr*

Abstract

The mid-Cretaceous period is characterized by the widespread deposition of organic carbon-rich horizons, documenting oceanic anoxic events (OAEs), which correspond to episodes of major disturbances in the carbon cycle. The causes of these events are still widely debated. In this study, the role of orbital variations in the deposition of black shales in the Ionian Zone (Western Greece), an area already known for documenting OAEs is examined. Cyclostratigraphic data for the Lower Aptian interval are interpreted in a climate change context, and specific mechanisms for the deposition of organic carbon-rich horizons are hypothesized. Field observations, stable isotope and total organic carbon analyses, as well as biostratigraphic data enable a correlation between the Gotzikas section and the Paliambella section, also in the Ionian Zone (Epirus, Greece). In addition, Gotzikas section is also correlated with the Poggio le Guaine - Fiume Bosso composite sequence of the Umbria – Marche region (Italy). Lower Aptian sedimentation in the Ionian Basin seems to be controlled by orbital forcing. The short eccentricity and obliquity rhythms are most prominently recorded. Whilst the presence of amplitude modulation cycles indicates towards a lesser control by the long eccentricity and precession periodicities.

Key words: *Oceanic Anoxic Events, black shales, palaeoclimatology, spectral analysis, orbital forcing.*

Περίληψη

Η περίοδος του Μέσου Κρητιδικού χαρακτηρίζεται από εκτεταμένη απόθεση οριζόντων πλούσιων σε οργανικό άνθρακα, καταγράφοντας ωκεάνια ανοξικά επεισόδια (OAEs), τα οποία αντιστοιχούν σε περιόδους μεγάλων διαταραχών του κύκλου του άνθρακα. Οι αιτίες αυτών των επεισοδίων αποτελούν ακόμη αντικείμενο υποθέσεων. Στη μελέτη αυτή εξετάζεται ο ρόλος των μεταβολών των τροχιακών παραμέτρων στην απόθεση των μαύρων αργίλων της Ιόνιας ζώνης (Δυτική Ελλάδα), μιας περιοχής που είναι ήδη γνωστή για καταγραφές OAEs. Τα κυκλοστρωματογραφικά δεδομένα για το διάστημα του Κατώτερου Άπτιου ερμηνεύονται σε ένα πλαίσιο κλιματικών αλλαγών και γίνονται υποθέσεις για τους ειδικούς μηχανισμούς απόθεσης των πλούσιων σε οργανικό υλικό οριζόντων. Οι παρατηρήσεις υπαίθρου και οι αναλύσεις των σταθερών ισοτόπων και του ολικού οργανικού άνθρακα, καθώς και τα βιοστρωματογραφικά στοιχεία επιτρέπουν το συσχετισμό μεταξύ της τομής Γκότζικα και της τομής Παλιάμπελλα, επίσης στην Ιόνια

ζώνη (Ηπείρος, Ελλάδα). Επιπλέον, η τομή Γκότζικας συσχετίζεται με τη συνθετική ακολουθία Poggio le Guaine - Fiume Bosso της περιοχής Umbria – Marche (Ιταλία). Η ιζηματογένεση του Κατώτερου Άπτιου της Ιόνιας λεκάνης φαίνεται να ελέγχεται από τις μεταβολές των τροχιακών παραμέτρων της Γης. Η περιοδικότητα της σύντομης εκκεντρότητας και της λοξότητας καταγράφονται περισσότερο καθαρά. Ενώ η παρουσία σύνθετης κυκλικότητας δείχνει δευτερεύοντα έλεγχο από τις περιοδικότητες της βραδείας εκκεντρότητας και της μετάπτωσης.
Λέξεις κλειδιά: *Ωκεάνια Ανοξικά Επεισόδια, μαύροι άργιλοι, παλαιοκλιματολογία, ανάλυση φάσματος, τροχιακή επιβολή.*

1. Introduction

The mid-Cretaceous period is characterized by the widespread deposition of organic carbon-rich horizons, documenting oceanic anoxic events (OAEs), which correspond to episodes of major disturbances in the carbon cycle (Jenkyns 1980). The causes of these events are still widely debated. According to the preservation model, decreased ventilation of the sea floor, due to increased detrital input, led to enhanced carbon burial, as a result of low organic matter remineralisation (Tyson 1995). Alternatively, very high primary productivity levels and overwhelming oxic remineralisation of organic matter, may have been the cause of anoxic conditions on the sea floor, through expansion of the oxygen minimum zone (Parrish 1995). Though both resulting in enhanced preservation of organic matter, it appears that the mid-Cretaceous black shales can be separated in two classes, having an either detrital (D-OAEs) or productivity driven origin (P-OAEs) (Erbacher *et al.* 1996).

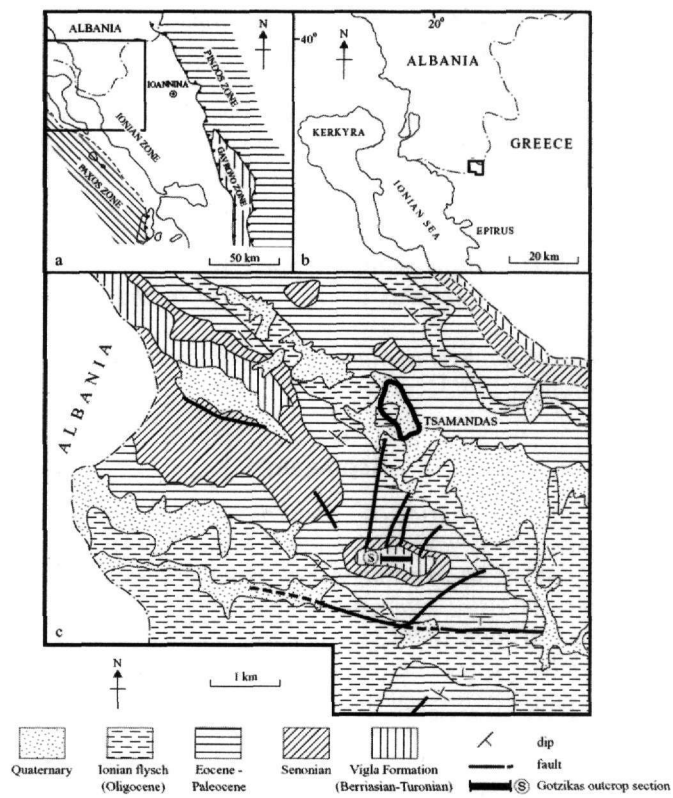

Figure 1 - (a) The zones of NW Hellenides; (b) location of the study area; (c) simplified geological map of the study area (Tsikos *et al.* 2004b)

Recent integrated studies of the mid-Cretaceous basin deposits in the Umbria - Marche region in Italy (Galeotti *et al.* 2003) have confirmed an orbital control on the deposition of bedded cycles and organic carbon-rich facies in this basin. According to these authors, climatic changes, modulated by the orbital forcing, induced changes in the hydrological and atmospheric cycles, led to in enhanced fluxes and preservation of continental-derived organic matter in the black shale horizons.

In this study, the well known Gotzikas section, documenting OAE1b and OAE2 (Tsikos *et al.* 2004, Karakitsios *et al.* 2007) is correlated with the Paliambela section, also in the Ionian zone of Western Greece, and the Poggio le Guaire – Fiume Bosso composite sequence of the Umbria – Marche region (Italy). In addition, the role of orbital variations in the deposition of black shales in the Ionian Zone (Western Greece) is examined. Furthermore, cyclostratigraphic data are interpreted in a climate change context, and specific mechanisms for the deposition of organic carbon-rich horizons are being hypothesized.

2. The Study Section

2.1. Geological Setting

During the Early Jurassic, the Ionian Zone was an area of platform carbonate sediment deposition (Pantokrator limestones) on a base comprising primarily of Triassic evaporites. A period of extensional stress associated with the opening of the Neotethys, from the Pliensbachian to the Tithonian, led to a differentiation of the Ionian realm into discrete palaeogeographic units recording early regional subsidence (Karakitsios 1992). The Lower Cretaceous (Berriasian – Turonian) pelagic Vigla Limestone Formation represents the post-rift formation. This sequence is defined by a Lower Berriasian unconformity at the base of the Vigla Limestone Formation, which largely obscures pre-existing syn-rift structures. Minor off- and on-lap movements along the Ionian Basin margin continued until the Late Eocene, when flysch sedimentation commenced. The evolution of the Ionian Basin constitutes a good example of inversion tectonics in a basin with an evaporitic base (Karakitsios 1995).

The Vigla Limestone Formation s.l. comprise a thick succession of thin-layered (5-10 cm), sub-lithographic pelagic limestones with radiolaria, which are rhythmically interbedded with centimetre- to decimetre-thick radiolarian chert beds. The upper part also contains of a series of intercalated organic carbon-rich marlstones and shales, termed the Vigla Shale Member (Karakitsios 1995, Rigakis and Karakitsios 1998). According to a previous examination of the Gotzikas section, south of the village Tsamandas (NW Epirus; Fig.1) has shown that the Vigla Limestone Formation s.l. has an approximate 100 m thickness (Tsikos *et al.* 2004b). The upper ~ 80 m of this consist of a rhythmically alternating, thinly bedded limestone/black chert succession (Vigla limestones s.s.). Towards the lower 15-20 m of this interval, the limestones become more massive, pinkish-grey in colour and increasingly silicified. Within this portion, Tsikos *et al.* (2004b) have identified an isolated black shale horizon (~ 15 cm thickness), as corresponding to the "Paquier event" (OAE1b). These silicified Vigla limestones continue stratigraphically lower for another 8-10 m below this black shale (Fig. 2). The sediments then pass downwards to the Vigla Shale Member.

According to Tsikos *et al.* (2004b), the Vigla Shale Member, in Gotzikas section, spans the Aptian – Lower Albian interval. However the upper portion of this is not visible in the field. In the lowermost 13,22 m of the succession, 20 individual organic carbon rich marly horizons are seen, ranging in thickness from 10 to 40 cm (Fig.2). These layers are dark grey to black, well laminated and free of any evidence of bioturbation. They are interbedded with reddish-grey, 20-50 cm thick marly limestone beds, silicified in places and containing common intercalations of dark chert layers (5-10 cm thick).

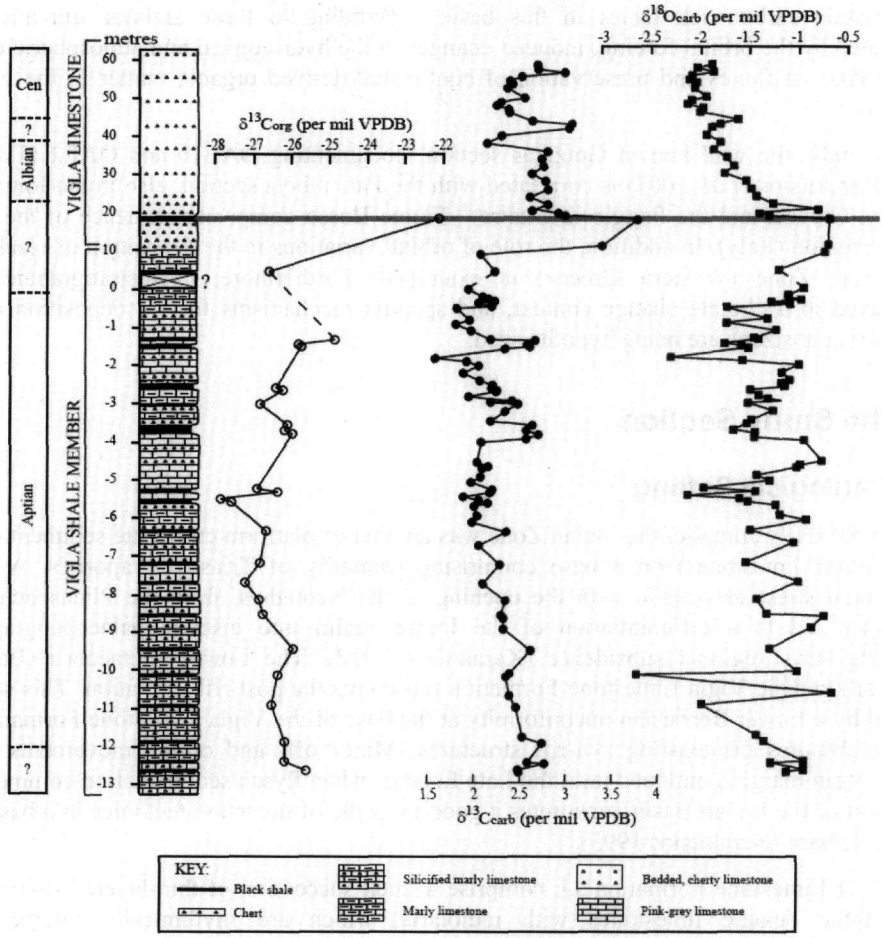

Figure 2 - Lithostratigraphic log and bulk stable (C, O) isotope profiles through the Vigla section in the Gotzikas area (Tsikos *et al.* 2004). The highlighted level corresponds to the 'Paquier' level (OAE1b)

The stratigraphically higher parts of the Vigla Limestone Formation s.l., in this section, lack organic carbon-rich sediments, except for an isolated black shale horizon, about 40 m above the "Paquier" level. This horizon is ~35 cm thick comprising of two distinct, finely laminated sub-units separated by a thin, cherty layer. This horizon has been shown to correspond to the Cenomanian – Turonian "Bonarelli" event (OAE2) (Karakitsios *et al.* 2007).

2.2. Biostratigraphy

Biostratigraphic analyses of planktonic foraminifera and calcareous nannofossils (Tsikos *et al.* 2004b, Karakitsios *et al.* 2007) suggest that the Vigla limestones s.s. in the Gotzikas section span the Albian – Turonian interval. The lowermost 13.22 m of the section comprising of the Vigla Shale Member (i.e. 26.8-14.9m below the OAE1b) may be assigned to the Lower Aptian, based on the presence of the nannofossils *Assipetra infracretacea larsonii*, *Hayesites irregularis*, and *Rucinolithus terebrasletnarius youngii*, as well as the absence of Upper Aptian species (Tsikos *et al.* 2004b).

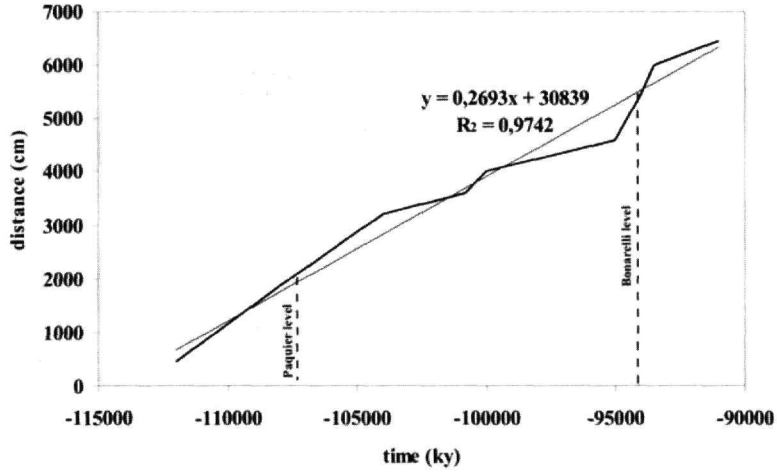

Figure 3 - Age model for the upper part of the Vigla limestones in Gotzikas section. The mean sedimentation rate is 0.2693cm/ky. The trend line was obtained using a linear fit

The black shale corresponding to the "Paquier" event in the lower portion of the section marks the Lower to Middle Albian, as shown by the presence of the calcareous nannofossil *Hayesites albiensis* 3 m below to 10m above this horizon. The ~ 20 m-thick interval above the OAE1b level is assigned to the Middle to Upper Albian period. This is suggested by the first occurrence of the calcareous nannofossil *Quadrum eneabrachium*, and the presence of the planktonic foraminifer *Biticinella breggiensis*, followed by the presence of the planktonic foraminifera *Rotalipora appeninica* and *Planomalina buxtorfi*, and the nannofossil *Eiffellithus turriseiffelii* (Premoli Silva and Sliter, 1995, Karakitsios *et al.* 2007).

A Middle Cenomanian age is given to the 6m of sediments overlying the Upper Albian interval due to the first occurrence of *Rotalipora cushmani* and the continued presence of *R. appenninica*. Also *Praeglobotruncana gibba* occurs 4.5 m higher in the succession. These datum have been used to correlate this black-shale unit with the Cenomanian – Turonian boundary "Bonarelli" level of the Umbria-Marche region (Tsikos *et al.* 2004a, Karakitsios *et al.* 2007). Finally the first occurrence of *Marginotruncana gr. pseudolinneiana* constrains the uppermost part of the succession as Turonian in age (Premoli Silva and Sliter 1995).

2.3. Sedimentation rate

An age model (Fig.3) was contructed, based on the first and last occurrences shown in Table 2, with reference to the biostratigraphic scheme by Bralower *et al.* (1995) and the Geologic Time Scale 2004 (Gradstein *et al.* 2004). The mean sedimentation rate for the upper part of the Vigla limestones s.s. (Albian – Turonian), in Gotzikas section, can be approximated at 0.27 cm/ky (R^2=0.97). Also, there appears to be a substantial relative increase in the sedimentation rate, to 1.10 cm/ky, about 5.5 m (500 ky) prior to the "Bonarelli event". Accumulation of sediment returns to a lower rate (0.30 cm/ky) after this event horizon. Mean sedimentation rate, for the lower part of the Vigla Shale Member in this section, is 0.66 cm/ky.

2.4. Stable isotope and TOC data

The complete stable isotope and TOC data, across the Vigla Limestone Formation in the Gotzikas section (Table 1, 2) are thoroughly described elsewhere (Tsikos *et al.* 2004a, 2004b, Karakitsios *et al.* 2007). Samples 1-7 and 9-42 (Table 1) exhibit TOC (wt%) values between 1-2 %.

Table 1 - Complete dataset for the upper part of the Vigla formation (Albian – Turonian), in Gotzikas section

sample	TOC (wt%)	$CaCO_3$ (wt%)	$\delta^{13}C_{TOC}$ (‰)	$\delta^{13}C$ (‰)	$\delta^{18}O$ (‰)	height (m)	event
1				2.64	-1.50	83.00	LO *Marginotruncana* gr. *pseudolinneiana*
2				2.75	-1.59	77.00	
3				2.73	-1.44	74.50	
4				3.00	-1.90	72.00	
5				2.91	-1.93	70.00	
6				3.02	-2.14	64.50	*LO Praeglobotruncana gibba*
7				2.52	-1.77	62.00	FO *Marginotruncana* gr. *pseudolinneiana*
8	44.5		-22.21			60.00	"Bonarelli event" (OAE2)
9				2.60	-1.83	59.00	FO *Praeglobotruncana gibba*
10				2.70	-2.04	57.50	
11				2.99	-1.87	56.50	
12				2.53	-2.09	55.50	
13				2.40	-2.11	54.50	LO *R.cushmani*, *LO R. appenninica*
14				2.42	-2.05	53.50	
15				2.37	-2.07	52.50	
16				2.31	-2.05	51.00	
17				2.55	-1.94	50.00	
18				2.29	-2.10	49.00	
19				2.25	-2.14	48.00	
20				2.38	-1.99	47.00	
21				2.39	-2.01	46.00	FO *R.cushmani*
22				2.48	-1.72	45.00	
23				2.64	-1.63	44.00	
24				3.07	-1.81	43.00	
25				3.04	-1.89	42.00	LO *P.buxtorfi*
26				2.30	-1.94	40.00	FO *Planomalina buxtorfi*, FO *Rotalipora appenninica*, FO *Eiffelithus ruttiseiffelii*
27				2.14	-1.81	38.00	
28				2.81	-1.87	36.00	LO *B. breggiensis*
29			-25.78			35.00	
30			-26.33			34.50	
31				2.74	-1.74	34.30	
32			-26.12			34.00	
33				2.76	-1.67	32.00	FO *Biticinella breggiensis*
34			-26.49			31.00	
35				2.63	-1.77	30.00	
36				2.78	-1.55	29.00	LO *Hayesites albiensis*
37			-26.40			26.50	

38				2.81	-1.49	25.00	FO *Quadrum eneabrachium*
39				2.61	-1.44	23.50	
40				2.81	-1.27	22.00	
41			-26.86			21.00	
42				2.62	-0.78	20.00	
43	28.87	23.25	-22.14	2.92	-1.32	19.00	"Paquier event" (OAE1b)
44				2.97	-1.42	18.50	
45				3.79	-0.70	16.00	FO *Hayesites albiensis*
46				3.39	-0.72	12.00	
47				2.07	-0.75	9.50	
48	2.33	76.67	-26.61	2.23	-1.21	4.50	

Table 2 - Complete dataset for the lower part of Gotzikas section (Lower Aptian)

sample	TOC (wt%)	$CaCO_3$ (wt%)	$\delta^{13}C_{TOC}$ (‰)	$\delta^{13}C$ (‰)	$\delta^{18}O$ (‰)	height (m)
V1				1.94	-0.96	-0.10
V2				1.88	-0.98	-0.20
V3				2.10	-1.12	-0.30
V4a				2.16	-1.12	-0.36
V4b				2.23	-0.99	-0.42
V4c				2.05	-1.28	-0.48
V4d				2.19	-1.11	-0.54
V4e				1.81	-1.75	-0.60
V7				1.95	-1.34	-0.90
V8				1.80	-1.75	-1.02
V9				1.97	-1.24	-1.20
V11				2.18	-1.46	-1.40
V12a	1.58	76.58	-24.86	2.67	-1.43	-1.43
V12b				2.35	-1.83	-1.52
V12c	2.08	77.92	-25.84	2.58	-1.77	-1.55
V13	2.50	81.17	-25.75	2.61	-1.60	-1.60
V14				2.34	-1.52	-1.65
V16				1.57	-2.31	-1.90
V18				1.92	-1.59	-2.00
V19				2.05	-1.01	-2.10
V20				1.88	-1.18	-2.30
V21				2.06	-1.11	-2.50
V22				2.20	-1.19	-2.60
V23a	1.41	91.33	-26.43	2.19	-1.16	-2.67
V23b	2.34	83.96	-26.25	2.24	-1.50	-2.75
V24				1.94	-1.42	-2.90
V25a				2.41	-1.33	-3.00
V25b				2.18	-1.19	-3.05
V26	3.35	61.67	-26.83	2.48	-1.53	-3.10
V27				2.34	-1.27	-3.30

V28				2.18	-1.49	-3.55
V29a	2.77	74.62	-26.10	2.64	-1.54	-3.65
V29b	2.15	84.67	-26.20	2.57	-1.67	-3.80
V29c	2.64	81.50	-25.97	2.70	-1.45	-3.90
V30				2.57	-1.46	-4.00
V32				2.08	-0.96	-4.10
V33				2.03	-0.78	-4.62
V34a				2.15	-1.00	-4.74
V34b				2.09	-1.03	-4.79
V35a				2.07	-1.44	-4.99
V35b				1.97	-1.31	-5.14
V38	1.88	79.58	-26.91	2.20	-1.97	-5.34
V39	1.08	74.42	-26.79	2.17	-1.45	-5.41
V41a	2.15	75.75	-27.88	2.05	-1.61	-5.61
V41b	3.19	72.92	-27.59	2.15	-1.52	-5.69
V42				2.00	-1.24	-5.79
V43a				2.03	-1.20	-6.04
V43b				1.98	-0.94	-6.19
V45	2.57	54.08	-26.67	2.35	-1.50	-6.44
V46				2.05	1.07	-6.79
V47	4.42	67.83	-26.84	2.28	-1.55	-7.29
V48	1.54	83.42	-27.22	2.10	-1.01	-7.79
V49	2.39	80.08	-26.86	2.34	-1.44	-8.24
V50	3.61	53.35	-26.75	2.29	-1.34	-8.64
V51				2.32	-0.76	-8.70
V52				2.32	-0.89	-9.50
V54	2.43	81.30	-25.96	2.62	-1.31	-10.05
V55				2.39	-1.03	-10.65
V56	1.77	20.00	-26.37	2.35	-2.66	-10.72
V57				2.39	-0.68	-11.22
V58	0.27	41.00	-26.52	2.46	-2.00	-11.52
V59				2.53	-1.44	-12.32
V60	2.29	84.50	-26.20	2.74	-1.37	-12.47
V61				2.58	-0.96	-12.97
V62	6.33	59.92	-26.20	2.77	-1.30	-12.99
V63				2.48	-0.96	-13.17
V64	2.77	81.12	-25.63	2.49	-1.14	-13.22

3. Results

3.1. Regional correlation

The field observation, the stable isotopic and total organic carbon analyses, as well as the biostratigraphic information derived from the samples enabled the correlation between the Gotzikas section and the Paliambella section (Danelian *et al.* 2004) in the Ionian Zone (Epirus, Greece), and the correlation of the study section and the Poggio le Guaine - Fiume Bosso composite sequence (Galeotti *et al.* 2003) of the Umbria – Marche region (Italy), an area with

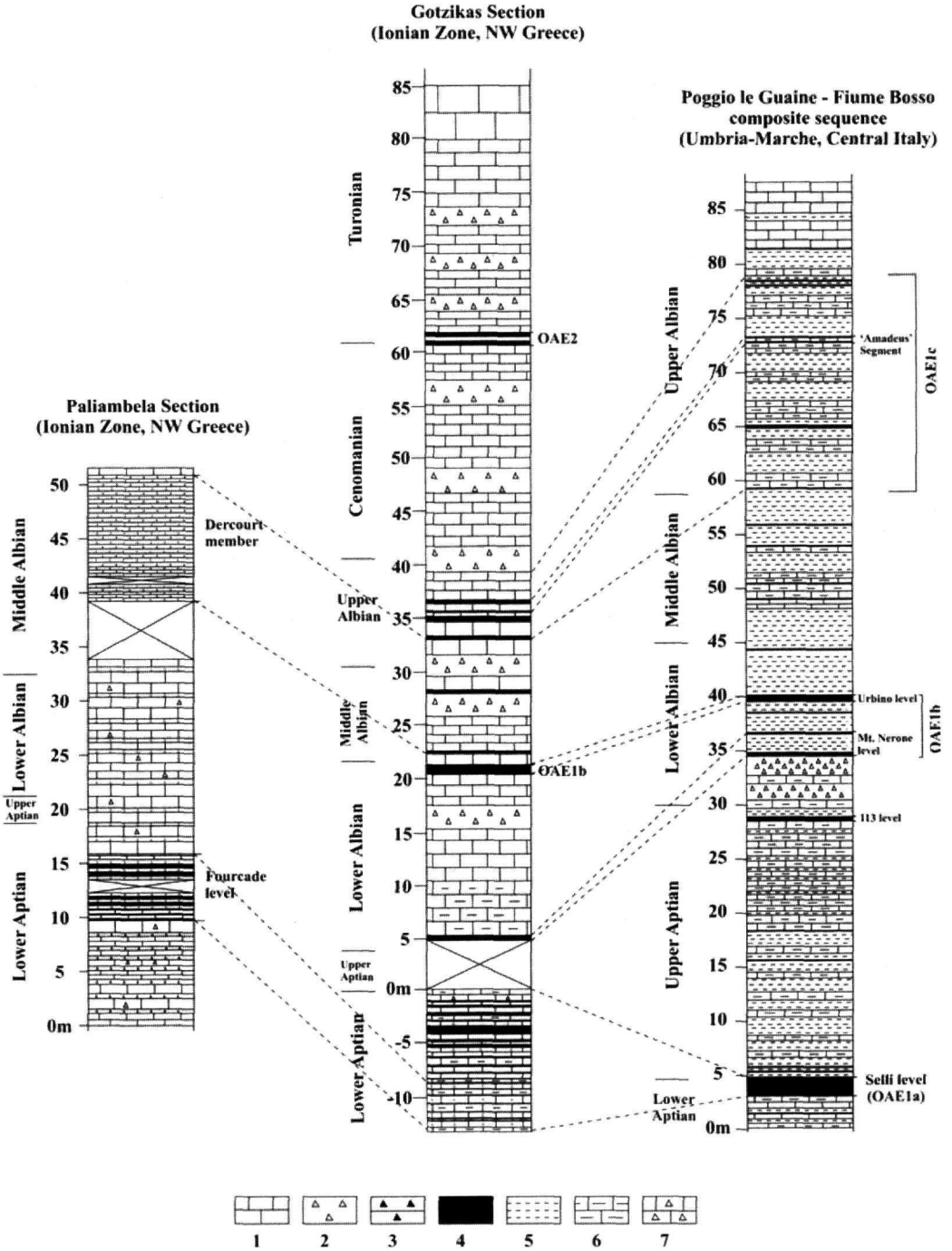

Figure 4 - Regional correlation between Gotzikas section (Tsikos *et al.* 2004b, Karakitsios *et al.* 2007), Paliambela section (based on Danelian *et al.* 2004), and Poggio le Guaine – Fiume Bosso composite sequence (based on Galeotti *et al.* 2003). 1: limestone, 2: cherty layer or nodule, 3: shale & siliceous mudstone, 4: black shale, 5: marl, 6: marly limestone, 7: cherty limestone. Notice that in Gotzikas section, the zero meter level here coincides with the level of the lowermost sample in Table 2 (i.e. V64 at –13.22 m)

sufficiently comparable palaeogeographic and structural evolution to the Ionian realm (Alvarez 1989, Karakitsios 1995). All the correlations can be seen in Figure 4.

The lower part of the Gotzikas section, comprising the Vigla Shale Member, records rhythmic alternations of organic carbon rich/poor horizons, which can be correlated with the Selli event (OAE1a). In the lowermost 4.5 m, cherty/marly limestones alternate with black shale horizons. This is probably an equivalent of the Fourcade siliceous level described by Danelian *et al.* (2004) (Fig.4). However deposition appears to have taken place in a different palaeogeographical setting, allowing for the deposition of carbonate as well as siliceous sediments. This is in agreement with previous studies conducted in this area, which provide evidence for intense sea bottom topography within the Ionian Basin well beyond the syn-rift period, due to the continuation of halokinesis (Karakitsios 1995). It is very probable that carbonate/black shale deposition took place in shallower parts of the basin (e.g. Gotzikas section, especially the upper Lower Aptian part), and chert/black shale deposition in the deeper parts of the Ionian Basin (e.g. Paliambela section).

A single black shale horizon of Early Albian age, ~15 m below the Paquier level (OAE1b), can be correlated with Mt. Nerone level described in the Umbria - Marche region. The OAE1b level is correlated with the Urbino level described in the same sequence (Galeotti *et al.* 2003).

The sediments immediately above the Paquier level (22-33 m; Fig. 4) are most likely to be equivalent to the Dercourt member, described by Danelian *et al.* (2004) in the Paliambela section. The lithology of this part of the section is comprised of limestone and chert interbeds and cherty limestones. Within this unit three black shale horizons have been observed. Whereas field observation of the Paliambela section show shale and siliceous mudstones alternating with cherty layers. The biostratigraphic age of this portion of the Vigla Formation is Middle Albian in both cases.

The upper three black shale horizons, below the Bonarelli level, can be correlated with the OAE1c, which, according to Bralower *et al.* (1993), spans the entire planktic foraminiferal *Biticinella breggiensis* Zone. This event includes the Amadeus Segment described in detail by Galeotti *et al.* (2003), during which black shale deposition appears to be orbitally controlled.

3.2. Cyclostratigraphy

A cyclostratigraphic methodology was applied to the Lower Aptian Vigla Shale Member deposits (lowermost 13.22 m of the section), using field observations and bulk $\delta^{13}C$ data (Table 2). In order to identify periodic patterns in the isotopic content of the deposits, spectral analysis on the $\delta^{13}C$ time-series was applied, using AnalySeries (Paillard *et al.* 1996; Figs 5-7).

Processing of the data, prior to spectral analysis, involved detrending (incorporating mean subtraction), pre-whitening (coeff. = 0.7), and arc sine transformation (Weedon 2003). Linear interpolation was also necessary, since the section was not equally sampled. Following this, a check for stationarity (i.e. a time-series' property of changing its characteristics significantly over the length of the studied interval; Weedon 2003) was conducted by comparing the spectra of several overlapping segments of the dataset.

The spectral analysis employed three different methods; the maximum entropy method (Percival and Walden 1993), the multi-taper method (Thompson 1982), and the Blackman – Tukey method (Priestley 1981) (Figs 5-7). The maximum entropy method (MEM) with a Burg algorithm assumes the presence of multiple autoregressive processes (AR processes). An AR process involves a dependence of each successive value in the dataset, on previous values (Weedon 2003). However, this is probably true for Mid-Cretaceous sediments recording oceanic anoxic events. The processes that seem to trigger and control these events (gas-hydrate release, primary productivity increase, or high detrital input) are evolutionary through geological time. Thus the parameters that record the phenomena (e.g. $\delta^{13}C$, $\delta^{18}O$) can indeed be thought to incorporate a "memory" of sorts, which in essence defines AR processes. As a result the MEM could be considered a valid method of

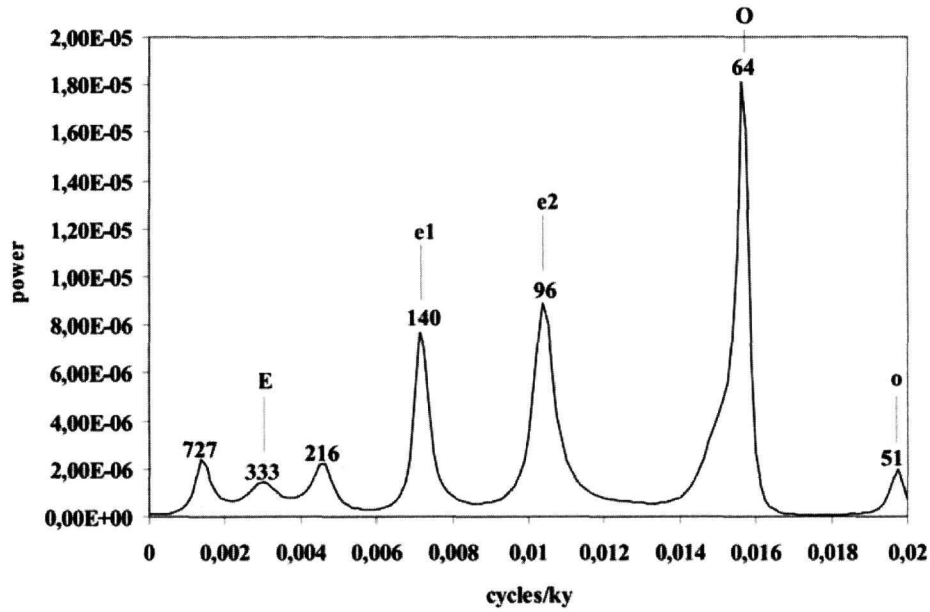

Figure 5 - Power spectrum ($\delta^{13}C$ time-series) for the lower part of the section, produced through the maximum entropy method (MEM), with a length of filter equal to 28 (relatively good resolution and confidence levels). Numbers on the peaks indicate the period (1/frequency). E: long eccentricity rhythm (~404.1 ky distorted), e1: short eccentricity rhythm mode 1 (~123.9 ky according to Laskar, 1999), e2: short eccentricity rhythm mode 2 (~94.8 ky, also by Laskar, 1999), O: obliquity rhythm amplitude modulation of a ~62.5 ky period (Grippo *et al.* 2004), and o: secondary obliquity cycles of ~54 ky periodicity (Grippo *et al.* 2004)

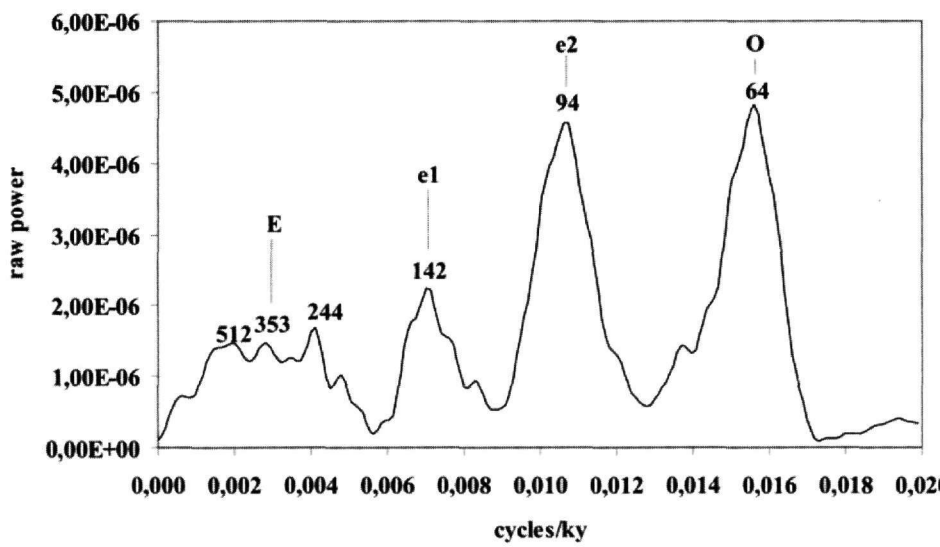

Figure 6 - Power spectrum ($\delta^{13}C$ time-series) for the lower part of the section, produced through the multi-taper method (MTM). The number of tapers was chosen at 3, in order to achieve higher confidence levels. Numbers on the peaks indicate the period (1/frequency)

spectral estimation for this type of cyclostratigraphic data. In order to avoid the slight shift of the frequency, that often occurs with this method, the actual valid peak frequencies were here determined by the use of the multi-taper method (MTM) and the Blackman – Tuckey method (BTM). These two methodologies are non-parametric, and therefore they do not involve any assumptions about the nature of the dataset (Weedon 2003). Also the spectra produced by each different method have a different y-axis scale. Normalization was not considered important since in cyclostratigraphic studies, the form of the spectra is significant and not the power.

Examination of the power spectra produced by all three methods has enabled an estimation of the regular cycles recorded in the sedimentary record, observed in Gotzikas section. The long eccentricity signal (E) is somewhat distorted and exhibits non-linear higher frequency combination tones, probably due to the control of long eccentricity over the sedimentation rate (Weedon 2003). However, the long eccentricity rhythm modulation appears consistently through all three spectra. In addition amplitude modulation cycles of 727 ky period, which appear in both the MEM and the BTM spectra, and 353 ky period, in the MTM spectrum, probably result from the added effect of the precession and eccentricity periodicities (Grippo *et al.* 2004).

As exhibited consistently by all three spectral estimation methods, the black shale deposition during the Lower Aptian interval in the Ionian Basin was strongly controlled by the short eccentricity signal of ~123.9 ky (e1) and ~94.8 ky (e2) (periodicities follow the calculations of Laskar, 1999 for the last 19 My). This e1 mode results from the interactions between the systems of Jupiter, Mars and Jupiter, Earth., whilst the e2 mode is controlled by the Mars, Venus and Earth, Venus systems (Laskar 1999).

The "precession of the equinoxes", which derives from the wobble of the Earth's rotational axis, has an influence on climate depending on its interaction with the ellipticity of the Earth's orbit (essentially eccentricity). Earth and Mars' gravitational attraction forms the precessional periodicity at 19 ky which, combined with the mode of 23 ky formed by the Jupiter and Mercury gravitational fields, provides the precessional cyclicity at 21 ky.

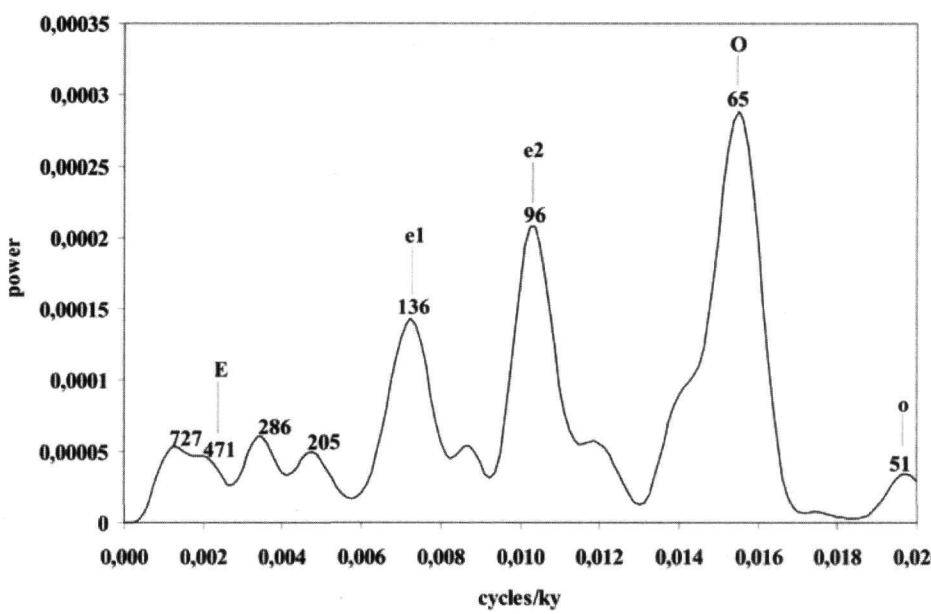

Figure 7 - Power spectrum ($\delta^{13}C$ time-series) for the lower part of the section, produced through Blackman – Tukey method (BTM), with 80% confidence interval. Numbers on the peaks indicate the period (1/frequency). Number of lags = 50

Earth's interactions with Mercury, Venus, Mars and Jupiter also affect the axial inclination, because of the pull exerted on the Earth's equatorial bulge (Laskar, 1999). This effect results in the obliquity cycles, the main period of which is 41 ky. Saturn additionally induces a lesser cycle at 54 ky. Because these periodicities of the orbital rhythm are closely spaced, they produce several amplitude modulations. The size of the sampling interval in the lower part of Gotzikas section did not allow for observation of the high frequency components of obliquity in the spectra produced. However we can observe the 54 ky-period mode in the MEM and the MTM spectra. According to Grippo *et al.* (2004), this peak may be suppressed (as in our case), when observed in low and mid latitudes, because its presence in these records is strongly dependent on the degree of degradation of this signal during transmission (since it is originally generated in the polar region). In all three spectra the 62.5 ky-period amplitude modulation mode of obliquity can be clearly observed. Note that Laskar (1999) estimates that the Earth's obliquity variation, the most unstable of the orbital parameters, is not expected to have remained stable over longer geological times. Nevertheless, consistency in our spectral analysis suggests an indirect estimate of obliquity regular cycles' control on sedimentation, in the lower part of Gotzikas section.

Slight shifts in the periodicities of the orbital cycles, as shown in the spectra (Figs 5-7), relative to those predicted by Laskar (1999), are observed and may be explained in a number of ways. These power spectra are based on a hypothesized age model (assuming constant sedimentation rates), formulated according to the biostratigraphic and field data, and in conjunction with the regional correlation presented. Therefore the expected discrepancies between the above age model and the actual age-depth relationship would tend to shift the regular cyclicity frequencies in the spectra. Furthermore, the calculations of the orbital parameters produced by Laskar (1999) range back to the last 19 My only. It is highly improbable that the same parameters stand true for Mid-Cretaceous time as well. Finally, general limitations of the pre-processing and spectral estimation methods applied herein may have contributed to the shifts in spectral frequencies.

4. Discussion

Orbital eccentricity is responsible for changes in Earth's insolation, especially expressed in seasonality. In general higher eccentricity intensifies the seasons in the hemisphere in which the perihelion occurs during the summer, and the amplitude of these climatic deviations is proportional to the amount of eccentricity. The four eccentricity rhythms, introduced by the gravitational interactions between the planets, in conjunction with the precessional cycles, have a combined effect on climate. This is maximized at the frequencies corresponding to the "difference tone" or the "combination tone" between them (Laskar 1999).

The precession – eccentricity syndrome is thought to be responsible for a decrease in deep-water oxygenation, dysoxia intensifying, at certain times, to the point of anoxia. At these periods, dark marly beds, with elevated organic content and iron sulfide, have been widely deposited (Herbert *et al.* 1986b, Galeotti *et al.* 2003, Grippo *et al.* 2004). These thin precessional anoxic pulsations (PAPs) segment the stratal sequence, into organic-carbon rich and organic-carbon poor horizons. It is proposed here that the lithological alternations observed in the Lower Aptian part of Gotzikas section are caused by such precessional anoxic pulsations, modulated by the precession – eccentricity syndrome.

Comparison between the orbital cyclicities and amplitude modulations calculated by Laskar (1999), and the age model hypothesized for this part of Gotzikas section, allows the conclusion that, when moving backwards within this Lower Aptian segment, the deposition of the black shale horizons was modulated by longer-period precessional amplitude modulations. It can be observed that the duration of time (according to the age model) between consecutive black marls and shales (PAPs) generally increased from ~14-15 ky to ~53 ky through the lowermost part of the section. This phenomenon may be due to an actual change of the modulation mechanism. However, as sedimentation of the lowermost part of the section (equivalent to the Fourcade level of Danelian *et*

al., 2004) took place in a deeper, more siliceous environment, black shale deposition may have been controlled by lower frequency orbital periodicity.

According to Herbert *et al.* (1986a, 1986b), like the precession – eccentricity syndrome, obliquity cycles drove variations in carbonate production and bottom redox conditions. Grippo *et al.* (2004) report thicker and more abundant PAPs and relatively pure limestones in the Piobbico core (Scisti e Fucoidi Fm – Scaglia Bianca sequence, Umbria Marche, Italy) coinciding with strong obliquity signals. According to these authors this observation suggests that primary productivity increased during these times.

There are two main theories regarding the mechanisms triggering black shale formation and PAPs. According to de Boer (1983) carbonate production is a function of primary productivity, meaning that episodes of exceptional organic carbon preservation triggered black shale deposition. On the other hand, Herbert *et al.* (1986a) provided evidence to support increased primary productivity in the carbonate-rich phase, thus suggesting organic hyperproduction as the mechanism responsible for PAPs. Grippo *et al.* (2004) reason that the biotic record favors de Boer's model, and thus assign the PAPs in the Scisti e Fucoidi Formation to the perihelial winter phase of the precessional cycle of low seasonality. Similarly, Galeotti *et al.* (2003) proposed a model for black shale deposition during the Upper Albian, in the Umbria – Marche region. According to these authors, black shale sedimentation occurred during precession minima, in times of increased precipitation, enhanced continental runoff and stratification of the upper water column.

Regarding the Lower Aptian interval in the Ionian Zone, Danelian *et al.* (2004) indicate that the highly siliceous Fourcade level of Paliambela section constitutes a local record of a global ocean eutrophication event during the OAE1a (Baudin *et al.* 1998, Hochuli *et al.* 1999). This is in agreement with observations for the same interval of Gotzikas section. We therefore propose that the Lower Aptian portion of this section (lowermost 13.22 m) is equivalent to the OAE1a event, and the lowermost more siliceous part of these sediments, to the Fourcade level of Paliambela section. Orbital forcing in conjunction with increased upwelling due to the opening of new Mediterranean Tethys gateways, as suggested by Danelian *et al.* (2002, 2004), may have indeed been the cause of the high productivity episode recorded as the OAE1a event in this region.

5. Acknowledgements

This project is co-funded by the European Social Fund and National Resources (EPEAEK II) PYTHAGORAS II (70/3/7950). The authors would also like to thank Professors Dr. A.G. Fishcer and Dr. M. Sprovieri for kindly reviewing the manuscript.

6. References

Alvarez, W., 1989. Evolution of the Monte Nerone seamount in the Umbria-Marche Appenines: 2. Tectonic control of the seamount-basin transition, *Boll. Soc. Geol. Ital.*, 108, 23-39.

Baudin, F., Fiet, N., Coccioni, R., and Galeotti, S., 1998. Organic matter characterization of the Selli Level (Umbria – Marche basin, central Italy), *Cretaceous research*, 151, 701-714.

de Boer, P.L., 1983. Aspects of Middle Cretaceous pelagic sedimentation in southern Europe: production and storage of organic matter, stable isotopes and astronomic influences, *Geologica Ultraiectina*, 31, 112p.

Bralower, T.J., Leckie, R.M., Sliter, W.V., and Thierstein, H.R., 1995. An intergrated Cretaceous microfossil biostratigraphy, In W.A. Berggren, D.V. Kent, M.-P. Aubry and J. Hardenbal (eds), *Geochronology, Time Scales, and Global Stratigraphic Correlation*, SEPM Sp. Publ. 54p.

Bralower, T.J., Sliter, W.V., Arthur, M.A., Leckie, R.M., Allard, D., and Schlanger, S.O., 1993. Dysoxic/anoxic episodes in the Aptian-Albian (Early Cretaceous). In M. Pringle, W.W. Sager, W.V. Sliter and S. Stein, (eds), *The Mesozoic Pacific: Geology, Tectonics, and Volcanism*, *AGU Monograph* 7, 5-37pp.

Danelian, T., Baudin, F., Gardin, S., Beltran, C., and Masure, E., 2002. Early Aptian productivity increase as recorded in the Fourcade level of the Ionian zone of Greece, *C.R.Geoscience*, 334, 1087-1093.

Danelian, T., Tsikos, H., Gardin, S., Baudin, F., Bellier, J.P., and Emmanuel, L., 2004. Global and regional palaeoceanographic changes as recorded in the mid-Cretaceous (Aptian - Albian) sequence of the Ionian Zone (NW Greece), *J. Geol. Soc. London*, 161, 703-710.

Erbacher, J. Thurow, J., and Little, R., 1996. Evolution patterns of radiolaria and organic matter variation: A new approach to identify sea-level changes in mid-Cretaceous pelagic environments, *Geology*, 24, 499-502.

Galeotti, S., Sprovieri, M., Coccioni, R., Bellanca, A., and Neri, R., 2003. Orbitally modulated black shale deposition in the Upper Albian Amadeus Segment (central Italy): a multi-proxy reconstruction, *Palaeo, Palaeo, Palaeo*, 190, 441-458.

Gradstein, F.M., Ogg, J.G., Smith, A.G., et al., 2004. *A Geologic Time Scale 2004*, Cambridge University Press.

Grippo, A., Fischer, A.G., Hinnov, L.A., Herbert, T.M., and Premoli Silva, I., 2004. Cyclostratigraphy and chronology of the Albian stage (Piobbico Core, Italy), *Cyclostratigraphy: approaches and case histories*, SEPM Sp. Publ. 81, 57-81.

Herbert, T.D., and Fischer, A.G., 1986a. Milankovitch climatic origin of mid-Cretaceous black shale rhythms in central Italy, *Nature*, 321, 735-743.

Herbert, T.D., Stallard, R.F., and Fischer, A.G., 1986b. Anoxic events, productivity rhythms and the orbital signature in a mid-Cretaceous deep-sea sequence from Central Italy, *Paleoceanography*, 1, 495-506.

Hochuli, P.A., Menegatti, A.P., Weissert, H., Riva, A., Erba, E., and Premoli Silva, I., 1999. Episodes of high productivity and cooling in the early Aptian Alpine Tethys, *Geology*, 27, 657-660.

Jenkyns, H.C., 1980. Cretaceous anoxic events: from continents to oceans, *J. Geol. Soc. London*, 137, 171-188.

Karakitsios, V., 1992. Ouverture et inversion tectonique du bassin ionien (Epire, Grece), *Ann.Geol.Pays Hell.*, 35, 85-318.

Karakitsios, V., 1995. The influence of pre-existing structure and halokinesis on organic matter preservation and thrust system evolution in the Ionian Basin, Northwestern Greece, *AAPG Bull.*, 79, 960-980.

Karakitsios, V., Tsikos, H., van Breugel, Y., Koletti, L., Sinninghe Damste, J.S., and Jenkyns, H.C., 2007. First evidence for the Cenomanian – Turonian oceanic anoxic event (OAE2, "Bonarelli" event) from the Ionian Zone, western continental Greece, *Int. J. Earth Sci (Geol. Rundsch.)*, 96. 343-352.

Laskar, J., 1999. The limits of Earth orbital calculations for geological time-scale use, *Royal Soc. (London), Phil. Trans.*, series A, 357, 1735-1759.

Paillard, D., Labeyrie, L., and Yiou, P., 1996. Macintosh program performs time-series analysis, *EOS Transactions AGU*, 77, 379.

Parrish, J.T., 1995. Paleogeography of C_{org}-rich rocks and the preservation versus production controversy. In A.Y. Huc (ed.), *Paleogeography, paleoclimate and source rocks*, AAPG studies in geology 40, 1-20.

Percival, D.B., and Walden, A.T., 1993. *Spectral Analysis for Physical Applications. Multitaper and Conventional Univariate Techniques*, Cambridge University Press, Cambridge, 583pp.

Premoli Silva, I, and Sliter, W.V., 1995. Cretaceous planktonic foraminiferal biostratigraphy and evolutionary trends from the Bottaccione section, Gubbio, Italy, *Palaeontogr. Ital.*, 82, 1-89.

Priestley, M.B., 1981. *Spectral Analysis and Time Series*, Academic Press, London, 890pp.

Rigakis, N., and Karakitsios, V., 1998. The source rock horizons of the Ionian Basin (NW Greece), *Mar. Petrol. Geology*, 15, 593-617.

Thompson, D.J., 1982. Spectrum estimation and harmonic analysis. *Proc. IEEE*, 70, 1055-1096.

Tsikos, H., Jenkyns, H.C., Walsworth-Bell, B., Petrizzo, M.R., Forster, A., Kolonic, S., Erba, E., Premoli Silva, I., Baas, M., Wagner, T., and Sinninghe Damste, J.S., 2004a. Carbon – isotope stratigraphy recorded by the Cenomanian – Turonian oceanic anoxic event: correlation and implications based on three key localities, *J. Geol. Soc. London*, 161, 711-720.

Tsikos, H., Karakitsios, V., van Breugel, Y., Walsworth-Bell, B., Bombardiere, L., Petrizzo, M.R., Sinninghe Damste, J.S., Schouten, S., Erba, E., Premoli Silva, I., Farrimond, P., Tyson, R.V., and Jenkyns, H.C., 2004b. Organic-carbon deposition in the Cretaceous of the Ionian Basin, NW Greece: the Paquier event (OAE1b) revisited, *Geol. Mag.*, 141, 401-416.

Tyson, R.V., 1995. *Sedimentary organic matter: organic facies and palynofacies*, Chapman and Hall, London, 615 p.

Weedon, G.P., 2003. *Time-series analysis and Cyclostratigraphy*, Cambridge University Press, 259pp.

Δελτίο της Ελληνικής Γεωλογικής Εταιρίας τομ. XXXX, 2007
Πρακτικά 11ου Διεθνούς Συνεδρίου, Αθήνα, Μάιος 2007

Bulletin of the Geological Society of Greece vol. XXXX, 2007
Proceedings of the 11th International Congress, Athens, May, 2007

SEDIMENTOLOGY AND BIOSTRATIGRAPHY OF AN UPPER TRIASSIC CARBONATE SUCCESSION OF TRIPOLITZA PLATFORM IN MARI AREA, PARNON MOUNTAIN, SE PELOPONNESUS, GREECE

Kati M.[1], Zambetakis-Lekkas A.[1], and Skourtsos E.[1]

[1] *National and Kapodistrian University of Athens, Faculty of Geology and Geoenvironment, Panepistimioupolis Zografou, 154 21, kati@geol.uoa.gr, zambetaki@geol.uoa.gr, eskourt@geol.uoa.gr*

Abstract

The Upper Triassic succession in the base of Tripolitza carbonate platform, in the Mari area of the Parnon Mt. in SE Peloponnesus, mostly consists of dolomites and to a lesser extent of calcitic dolomites. A detailed facies analysis and biostratigraphical study revealed that during Norian – Rhaetian times inter-supratidal and subtidal (shallow lagoonal) facies presenting cyclic development were deposited in the inner platform, similar to those that were formed in most of the Alpine platforms of the southern margin of the Tethys during the same time period. Diagenetic considerations further indicate that this shallow marine carbonate sedimentation was interrupted by subaerial exposure intervals and subsequent early lithification of the recently deposited sediments. The extensive and, mainly, early dolomitization and recrystallization, the presence of meteoric-vadose cements and specifically the repeated appearance of dolocrete horizons in the upper parts of many peritidal cycles, clearly show periodic subaerial exposure of the sediments, as well as the prevalence of semi-arid conditions in the area.

Key words: *Upper Triassic, Tripolitza carbonate platform, peritidal facies.*

Περίληψη

Η Ανω-Τριαδική ανθρακική ακολουθία στη βάση της πλατφόρμας της Τρίπολης, στην περιοχή Μαρί στο όρος Πάρνωνα, Πελοπόννησος, αποτελείται κυρίως από δολομίτες και σε μικρό ποσοστό ασβεστιτικούς δολομίτες. Λεπτομερής ανάλυση φάσεων και βιοστρωματογραφική μελέτη ανέδειξαν ότι κατά τη διάρκεια του Νόριου-Ραίτιου αποτίθεντο μεσο-υπερπαλιρροιακές και υποπαλιρροιακές (ρηχές λιμνοθαλάσσιες) φάσεις με κυκλική ανάπτυξη στο εσωτερικό της πλατφόρμας, παρόμοιες με αυτές που σχηματίζονταν σε πολλές Αλπικές πλατφόρμες του νότιου περιθωρίου της Τηθύος κατά το ίδιο διάστημα. Διαγενετικές παρατηρήσεις υποδεικνύουν περαιτέρω ότι η ρηχή θαλάσσια ανθρακική ιζηματογένεση διακοπτόταν από διαστήματα υποαέριας έκθεσης και επακόλουθης πρώιμης λιθοποίησης των πρόσφατα αποτεθέντων ιζημάτων. Η εκτεταμένη και πρώιμη κυρίως δολομιτίωση και ανακρυστάλλωση, η παρουσία μετεωρικών συγκολλητικών υλικών κατεισδύοντος ύδατος αλλά ιδιαίτερα η επαναλαμβανόμενη εμφάνιση δολοκρητών οριζόντων στα ανώτερα τμήματα πολλών περιπαλιρροιακών κύκλων υποδεικνύουν σαφώς περιοδική υποαέρια έκθεση των ιζημάτων καθώς και την επικράτηση ημίξηρων κλιματικών συνθηκών στην περιοχή.

Λέξεις κλειδιά: *Άνω Τριαδικό, πλατφόρμα Τρίπολης, περι-παλιρροϊκές φάσεις.*

1. Introduction - Geological setting

The development of the carbonate platforms in the peri-Adriatic area is a typical example of shallow sea carbonate sedimentation along the passive margins of southern Tethys, while their evolution is directly connected to the Alpine orogenetic cycle.

In the Hellenides, during Triassic, an outer platform that comprises the Preapulian – Ionian – Gavrovo - Tripolitza area is separated by the Pindos Ocean from the inner Pelagonian platform. In the outer platform the Ionian trough, individualized during Middle Jurassic, separates Preapulian platform from the Gavrovo – Tripolitza one. Two tectonosedimentary units are distinguished in the single Gavrovo – Tripolitza platform. The stratigraphic series of the Gavrovo unit, the outer one, comprises a thick carbonate neritic sequence, known from the Late Jurassic up to Late Eocene, followed by flysch sedimentation. The sedimentary sequence of the Tripolitza unit, the inner one, is more complete. It is constituted by a volcanosedimentary series at the base of Upper Paleozoic – Upper Triassic age, the Tyros beds, followed by a carbonate neritic series of Upper Triassic up to Upper Eocene age, followed by flysch deposits (Fleury 1980, Thiebault 1982, Jacobshagen 1986, Robertson *et al.* 1991). This study presents the results of a detailed sedimentological and stratigraphical investigation on an Upper Triassic carbonate succession, at the base of the Tripolitza platform in Parnon Mountain, southeastern Peloponnesus (Fig. 1a).

Parnon Mountain is built up by several thrust sheets consisting of Upper Paleozoic to Cenozoic sedimentary rocks that detached from their basement, due to the convergence of Eurasian and African plates during the Upper Oligocene-Lower Miocene. These thrust-sheets represent tectonic units derived from different palaeogeographic environments, such as carbonate platforms and deep basins (Fleury 1980, Thiebault 1982, Skourtsos *et al.* 2004). The lower ones exhibit metamorphism and they were uplifted and finally exhumed in Upper Miocene-Lower Pliocene, along low-angle normal faults during an E-W extension. The lowermost of the non metamorphic units, Tripolitza Unit, represents a carbonate platform of Upper Triassic to Upper Eocene age with a volcanosedimentary sequence of Upper Palaeozoic-Upper Triassic at its base, known as Tyros Beds (Lekkas and Papanikolaou 1978, Thiebault 1982, Skarpelis 1982) and a flysch on the top. The original stratigraphic contact between Tyros Beds and the overlain carbonates is in most cases disturbed by later tectonic events (Thiebault 1982, Skourtsos 2002).

Along the eastern flanks of the Parnon Mt., Tripolitza platform extends to thousand square kilometres representing a huge fault block, bound to the west by the Eastern Parnon normal fault and to the east by the Gulf of Argos (Skourtsos 2002). Along the coastal area the volcanosedimentary Tyros Beds and Upper Triassic to Liassic carbonate successions are the dominant formations. An Upper Triassic carbonate succession in the Eastern Parnon Mt, is discussed in this paper.

2. Materials and Methods

Fieldwork included facies analysis, detailed measurements and sampling. Selected and directed samples were taken for microfacies and micropaleontological analysis. Macrofacies analysis was supplemented with the study of structural and textural characteristics in polished slabs as well as with more than one hundred uncovered thin sections, stained with Alizarin red S and potassium ferricyanide to distinguish calcite and dolomite and detect the presence of iron in carbonates. X-ray measurements on most of the samples were carried out in order to determine the percentage of CaO and MgO and also the probable presence of non-carbonate material.

3. Stratigraphy

The study area is situated 2 Km on the northeast of the Mari village, on the eastern flanks of the Parnon Mt. (Figs 1a, b), where the Upper Triassic carbonate facies display significant growth.

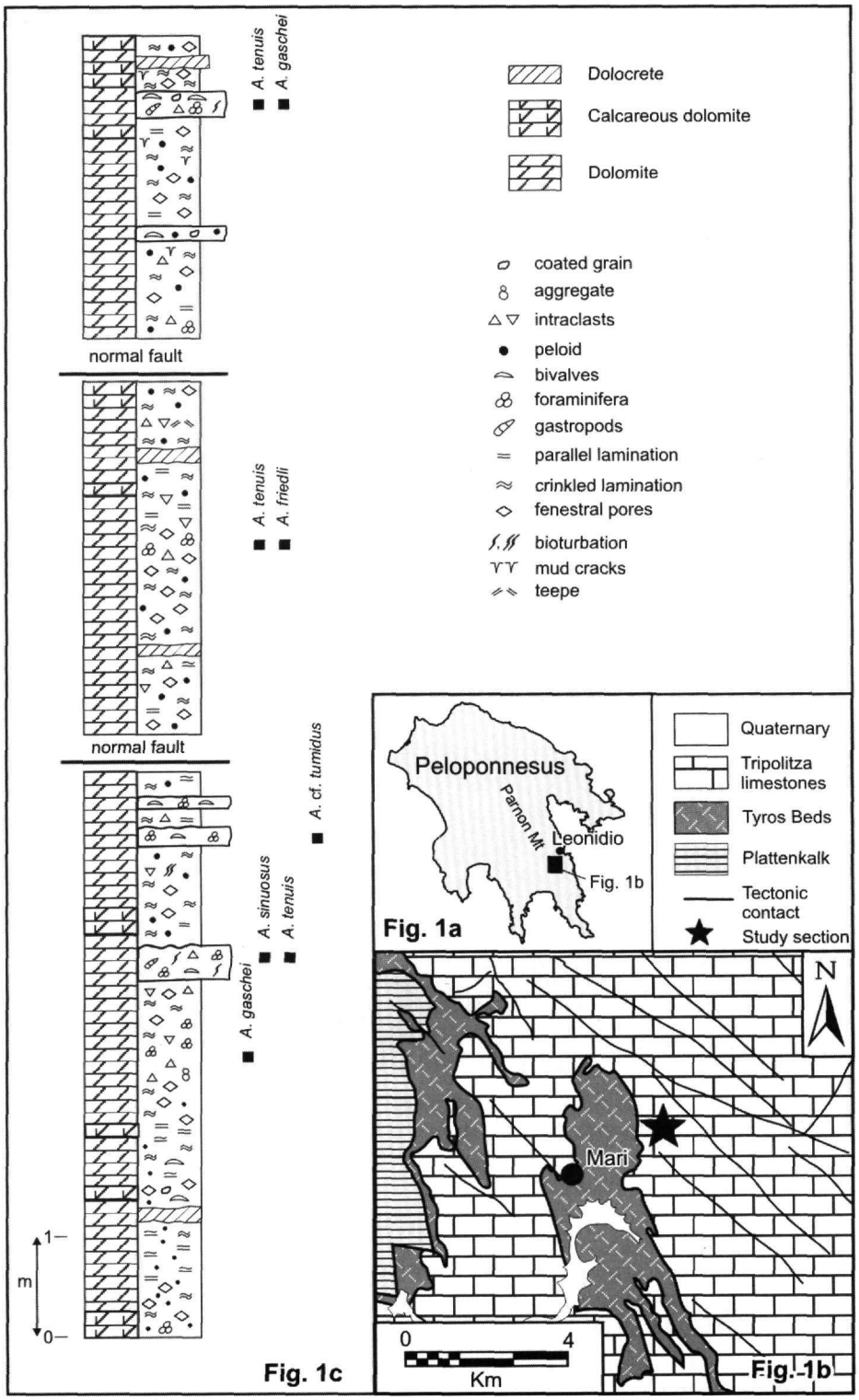

Figure 1 – The study area is situated 2 Km on the northeast of the Mari village, on the eastern flanks of the Parnon Mt. (a, b), Geological map of the study area (b), modified from Skourtsos (2002) (c), Litho-biostratigraphy of the three studied Upper Triassic sections

Three detailed sections are presented in this paper as they are observed in the field, separated by small normal faults. They consist exclusively of dolomites and calcitic dolomites.

Despite the intense dolomitization and the extensive recrystallization, several fossils and microfossils (foraminifera, ostracods, bivalves, gastropods) have been preserved (Fig. 2). Their distribution is presented in figure1c, beside the recognized depositional textural characteristics.

Among the foraminifera the species *Aulotortus sinuosus* WEYNSCHENK, *Aulotortus gaschei* (KOEHN – ZANINETTI & BRONNIMANN), *Aulotortus tenuis* KRISTAN, *Aulotortus* cf *tumidus* KRISTAN – TOLMANN 1964, *Aulotortus friedli* (KRISTAN – TOLLMANN) have been determined. The association of these foraminifera species date the succession as Norian – Rhaetian (Zaninetti 1976, Salaij *et al.* 1983, Ciarapica and Zaninetti 1984).

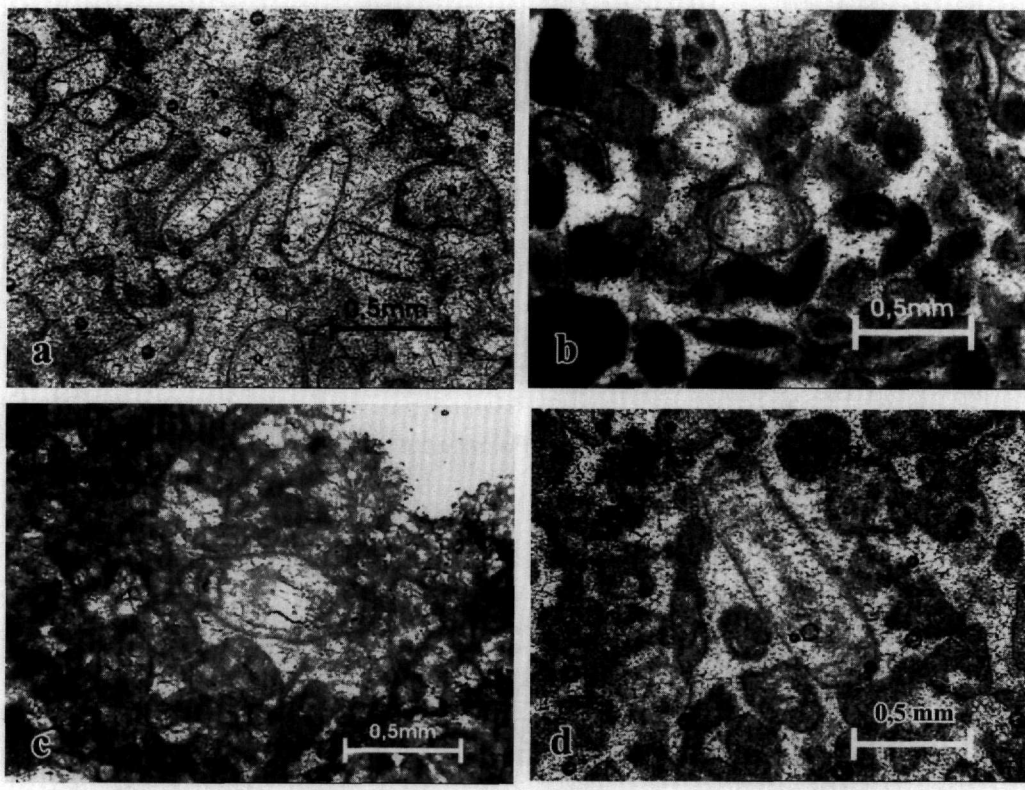

Figure 2 – Facies of recrystallised Aulotortinae (a), *Aulotortus sinuosus* WEYNSCHENK (b), *Aulotortus gaschei* KOEHN – ZANINETTI & BRONNIMANN (c), *Aulotortus tenuis* KRISTAN (d)

4. Lithofacies and environmental interpretation

Facies analysis showed a variety of lithofacies which can be grouped into two main units; the inter-supratidal and subtidal. As shown by the lithostratigraphical column (Fig. 1c) the inter-supratidal facies clearly dominate over the subtidal facies.

The inter-supratidal unit, in the lower parts of the section, consists of alternations of light and dark grey beds of varying thickness, in the range of 30 cm to 1 m, comprising pure dololutite to calcareous dololutite. Locally, the dark grey beds show an internal brecciation, while the light-coloured beds are lightly laminated. Upwards, the lamination becomes more intense and finally the facies are represented by alternations of light-coloured laminated and non-laminated beds of about

35 cm thickness. Although lamination usually appears flat or planar and generally parallel to bedding, locally small-angle cross-laminated layers and also layers with distinct crinkled lamination are observed. In the last two cases, the change in lamination type is marked by a stylolitic surface associated to the pressure-dissolution processes and the accumulation of residual sediment, probably conveyed from vugs and fractures. Unfortunately, sampling from these surfaces, for further examination, was not possible. In the upper parts of the succession, the inter-supratidal unit is represented by an alternation of structureless to lightly laminated beds of 1m thickness with beds of the same thickness but, with intense growth of fenestral fabrics and some internal truncated surfaces. Overall, on the basis of these textural characteristics, the inter-supratidal unit is markedly characterized by the development of stromatolites, typical of the peritidal environments. The subtidal unit comprises a small percentage of the succession and macroscopically is not clearly separated from the former unit. Its study was mostly based on microscopic observation. In the field it is mainly recognized by the presence of arenitic to fine ruditic-sized components. The latter are found either scattered or in distinctive white-grey coloured layers of a few mm to some cm thickness, within the abovementioned structureless beds of the inter-supratidal unit.

XRD analysis and thin sections staining showed that both inter-supratidal and subtidal units are entirely dolomitized, excepting a few parts of the former that become calcareous mostly in the upper parts of the succession (Fig. 1c and following description). It should be noticed, that although this calcitic dolomite was clearly recognized in the X-ray patterns, in the stained thin sections it was difficult to observe such a selective dolomitization.

Detailed microfacies analysis included description and separation of the facies mostly on basis of the textural characteristics (Dunham 1962). Nevertheless, the presence of specific skeletal and non-skeletal grains as well as of sedimentary structures has been used in the discrimination of some microfacies. Finally, eight main microfacies were recognized belonging to the above two units:

MF1 Mudstone / laminated bindstone: This facies is not often observed throughout the sections and mostly constitutes a dolomitic mudstone with very few microfossils, especially ostracods and fragments of thin bivalve shells in a mudstone-wackestone fabric. Sometimes it evolves into a laminated fabric consisting of finer micrite layers of few millimeters thickness alternated with somewhat coarser sparite layers (Fig. 3a). Though the characteristic difference of this facies is the lack of fenestral fabrics, locally where these mudstones become unfossiliferous, they show a few scattered fenestral pores, probably representing shrinkage pores.

This facies is interpreted as tidal-flat deposits, whereas the occurrence of ostracods particularly suggests a tidal-flat pond environment. Similar facies have been described in tidal-flat deposits of the Dachstein-type platforms and inner ramps (Fischer 1964, Flügel 2004, Haas 2004).

MF2 Microbial laminated bindstone: This facies is primarily dolomitic and comprises a significant percentage of the succession. It is made up of very thin planar to wrinkled micritic layers, alternating with sparitic layers in a bindstone fabric (Fig. 3b). The micritic laminae usually exhibit undulate algal structures, while sometimes they consist only of small peloids. The presence of bedding-parallel fenestral cavities, filled with cement and/or internal sediment of dolomitic mud, is quite common. Fossils are not observed.

Thin or thick horizontal laminations, with or without crossbedding, are restricted to the supratidal and upper intertidal area (Shinn 1983) whereas the crinkly lamination, in combination with the presence of fenestral fabrics, suggests additional intermittent exposure and desiccation (Riding 1991). Consequently, this facies was formed in the tidal flat area that was periodically exposed. This facies is comparable to several contemporary analogs (Shinn 1983, Hardie and Shinn 1986) and is also a typical stromatolitic facies of many ancient peritidal carbonates, such as the Upper Triassic carbonates of the Dachstein platform, constituting the algal mat loferites (Fischer 1964).

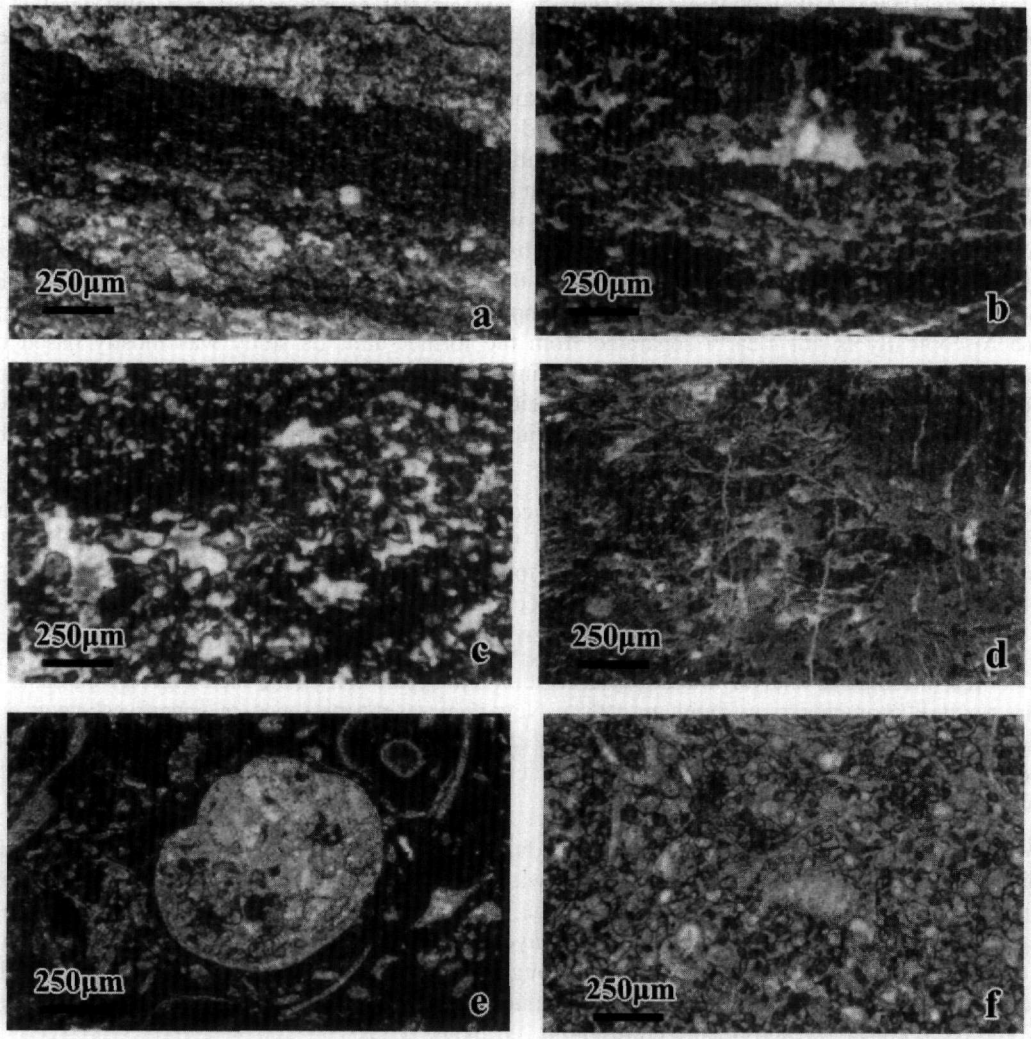

Figure 3 – MF1. Laminated mudstone/bindstone (a), MF2. Microbial laminated bindstone with fenestral fabrics (b), MF3. Fenestral peloidal bindstone/packstone (c), MF4. Intraclastic breccia (d), MF5. Bioclastic floatstone/ wackestone (e), MF6. Coated grainstone (f)

MF3 Fenestral peloidal bindstone: This is the most abundant facies of the succession and is mostly dolomitic, though in its upper part it becomes a calcareous dolomite, as suggested primarily through XRD analysis. It is characterized by intense lamination and large percentage of fenestral pores and larger voids (Fig. 3c). The planar or crinkled to microdomal laminations of millimeter-scale consist principally of very fine and densely packed peloids with microbial contribution; sometimes they are interbedded with finer layers composed of vesicular dolomite, probably representing molds of algae or other organisms which formed the mat. The biogenic grains are relatively few and are represented by recrystallized foraminifers, ostracods and more rarely gastropods and algae. Occasionally the laminations seem to be due to change of size of the peloids. Specifically, very thin layers of coarser peloids or/and small-sized micritic intraclasts, in a packstone fabric and with a distinct reverse grading, are observed. The other main characteristic of this facies are the many and variously sized fenestrae, mostly with laminoid fabrics, obviously representing desiccation structures. Some large prism cracks are also noted. Most of the fenestral cavities are filled mainly with sparite, while a few contain internal sediment in a geopetal fabric.

This facies has many common characteristics with the preceding one, constituting, as well, a typical stromatolitic facies and corresponding to the pellet loferites in Fischer's terminology. Its depositional environment is primarily the intertidal and supratidal area with periods of exposure and desiccation, as suggested by the lamination type and the presence of fenestrae (Shinn 1983, Riding 1991). Moreover, the coexistence of planar-horizontal with crinkled-microdomal lamination indicates an algal origin, although this is suggested with certainty only by the latter form (Shinn 1983). Specifically for the crossbedded laminated layers, a physical origin of the lamination is, however, not excluded but the prevalence of planar lamination against the crinkled and microdomal lamination forms suggests deposition under low energy conditions (Tucker and Wright 1990).

MF4 Intraclastic breccia: This facies takes up a small percentage of the studied sections, in contrast to other settings in the wider area wherein it constitutes a major facies of the Upper Triassic sequence (Zambetakis-Lekkas *et. al.* 2006). In specific, it appears in thin layers consisting of angular clasts in a wackestone to floatstone texture with some vertical desiccation cracks (Fig. 3d). The clasts belong to the microbial stromatolite and/or mudstone/bindstone facies and have calcareous dolomitic composition. The same composition is shared by the micritic to microsparitic matrix, as indicated by XRD analysis. Furthermore, variously sized subangular to subrounded micrite intraclasts are very frequently observed in the fenestral peloidal bindstone facies constituting thin interlayered horizons.

This facies is formed in the supratidal area and is regarded as an indication of desiccation of semi-lithified sediment followed by reworking and redeposition by storms (Shinn 1983). It also corresponds to the "intraformational conglomerate" in Fischer's terminology, making up a typical facies of the loferites of the Dachstein platform and suggesting also supratidal reworking.

MF5 Bioclastic floatstone/wackestone: This -and the remaining- facies, is exclusively dolomitic and is interbedded in the abovementioned supra-intertidal facies, even if the observation of its boundaries, either macro- or microscopically, has not been possible. The bioclasts are represented mainly by gastropods and bivalves, while foraminifers and in a lesser degree echinoderms and algae are also observed (Fig. 3e). The non-skeletal grains are mostly micritic intraclasts and a few coated and aggregate grains. The matrix is a mudstone-wackestone to a fine-grained packstone with variously sized peloids and a few bioclasts mainly of micritized and or recrystallized benthic foraminifera. The most important sedimentary structure is burrowing. Large and distinct burrows are filled with pellets, probably of fecal origin and small bioclasts in a packstone texture. Other characteristics of this facies are the common appearance of geopetal infilling in the internal of the larger skeletal components, particularly of the gastropods, as well as the dissolution of the aragonitic parts of the fossils, leaving molds that filled with sparry dolomite.

The association of the fossils and the composition of the matrix imply a protected shallow subtidal area as the depositional environment. In particular, the presence of the gastropods indicates the area parts with little circulation. Similar facies generally characterize shallow lagoons with relatively restricted conditions (Enos 1983).

MF6 Coated grainstone: This facies is overlain the bioclastic floatstones with abrupt and erosive boundary and consists exclusively of well sorted, sand-sized coated grains in a grain-supported fabric (Fig. 3f). The coated grains are mostly skeletal grains that have been preserved only by their micrite envelopes, corresponding to cortoids, or appear as completely micritized grains. Foraminifera, fragments of molluscs (bivalves) and echinoids were the main bioclasts. Additionally, in this facies the presence of peloids is significant, while some more spherical grains with a poor concentric development are also present, representing probably micritized ooids. The pore space between the grains has been filled mainly with sparry cement.

This facies is formed in shallow marine environment with normal salinity and constant wave action near the platform margin constituting winnowed sands (Tucker and Wright 1990).

Additionally, the aggregation of the fossils characterizes the open-marine parts of platform interior settings (Flügel 2004). The low frequency of this facies, however, and its embedding within the former facies, indicates that it was most probably deposited through periodic storm reworking.

MF7 Aggregate-grain grainstone/rudstone: This facies appears in a small percentage in the succession and is located over the floatstone with gastropods. It consists of arenitic- to ruditic-sized aggregate grains associated with variously sized peloids and many coated grains in a grain-supported fabric (Fig. 4a). The aggregate grains consists mainly of angular to subrounded micritized grains (lumps) and composite grains of cemented peloids and micritized skeletal grains exhibiting a lobate outline (grapestones). To a lesser extent some microbial clasts and a few oncoids are observed. Most skeletal grains are strongly micritized or recognized only from their shape due to the micritic envelopes that they had developed. The main fossils are foraminifera, bivalve fragments, algae and a few gastropods. The sorting is poor and the matrix is completely absent. Many grains show rims of fibrous marine cement while the remaining interparticle pores are mainly occluded by sparry cement.

This grapestone facies is interpreted as shallow subtidal with restricted to open circulation, so as to effect stabilization of grains and also cementation on the sea bottom. It is a characteristic facies of the contemporary deposits of the Great Bahamas Bank, where they are formed in very shallow depth, and also of ancient deposits mostly in rimmed carbonate platforms (Enos 1983, Tucker and Wright 1990, Flügel 2004).

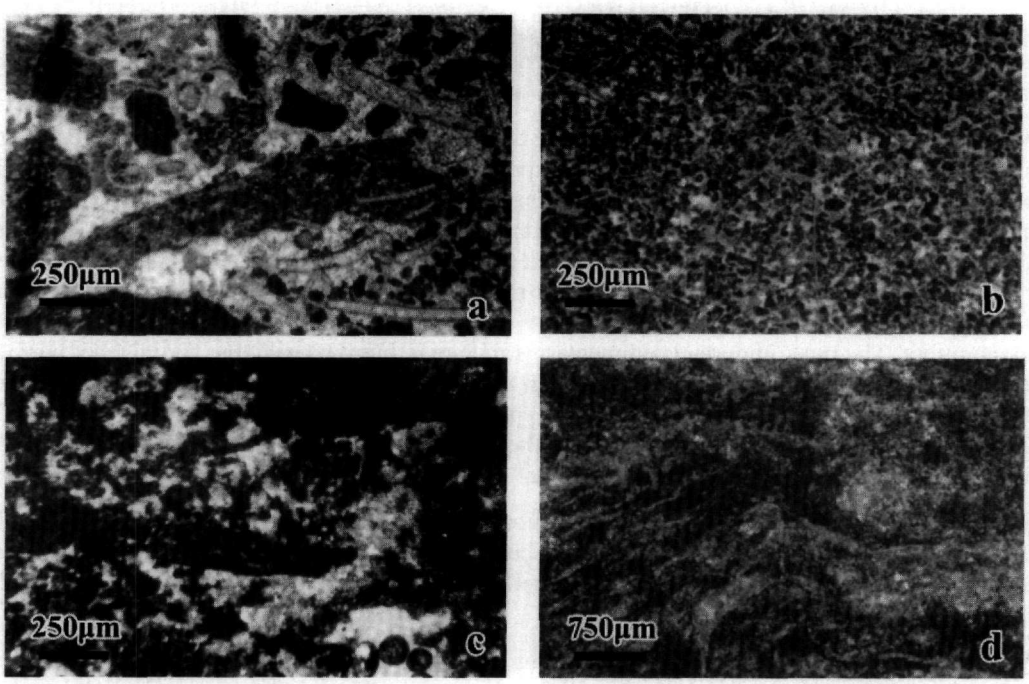

Figure 4 – MF7. Aggregate-grain grainstone (grapestone facies) (a), MF8. Fine-grained peloidal grainstone (b), Vadose cements in dolocrete horizon (c), Microteepe structure (d)

MF8 Fine-grained peloidal grainstone: This facies appears only in the uppermost section and is characterized by the prevalence of very fine, subangular to subrounded peloids in a grain-supported fabric (Fig. 4b). Several of the peloids are fecal pellets and others are very small micritic intraclasts, the latter mainly originating from the reworking of mud. The fossils are very few and are mostly represented by small foraminifera and ostracods. This facies generally displays good sorting. The cement is to some extent microsparite from the recrystallization of micrite. In some cases, very thin pelmicrite layers and/or irregular micritic laminae are observed. In a very few

samples, scattered ruditic-sized, subangular fenestral peloidal intraclasts or fragments of bivalve shells, evidently transported, are noticed. The reworking of these very coarse-grained components is obvious, so much from the irregular shape of intraclasts, as much from the presence of borings on the bivalve shells. The latter clearly indicate the bioturbation of the sediment and, further on, it indirectly interprets the origin of many peloids.

This facies is formed in protected shallow-marine environment with moderate water circulation as in an inner platform lagoon and also in settings with increased salinity, such as in evaporitic arid platform interior (Flügel 2004). Similar facies have been observed in the upper subtidal or lower intertidal area, forming a resistant cemented crust which limits the channel deposition to the intertidal zone (Shinn 1983).

5. Diagenetic features

Though the primary objective of this study is facies analysis and the recognition of the depositional environments of these Upper Triassic rocks, in order to better understand the conditions of their formation, it is worthwhile to make a short reference to the diagenetic alterations. The main reason for this is that the carbonate peritidal sediments, very soon after their deposition, suffer intense early diagenetic modifications, mainly due to an intermediate subaerial exposure interval after the deposition of an individual cycle. As a result thereof, the diagenesis can change the original depositional texture completely. Further on, we shall chiefly deal with the diagenetic features that mainly show the subaerial exposure and early lithification of the sediments.

The most characteristic texture indicating periods of emergence and exposure of the platform is the presence of dolocrete horizons that have been located in the upper parts of some inter-supratidal facies and, more specifically, the peloidal stromatolitic facies. In particular, these horizons show non-homogeneous texture with coarse to very coarse sand-sized subangular to subrounded micritic clasts in a nodular fabric, densely packed peloids in a clotted texture, grains with variously thick coatings which sometimes occur only in one side of the grain, and spar-filled cracks surrounding the micritic clasts. In other horizons micritic grains of similar size or slightly larger are subspherical and show a poor concentric lamination probably constituting small pisoids or vadois (Esteban and Pray 1983). Additionally, these micritic grains are often connected by meniscus cements, while, usually they are also accompanied by gravitational (microstalactitic) cements (Fig. 4c). These types of cement have meteoric-vadose origin (Müller 1971). Finally, most of the horizons display a distinctive reverse graded bedding. All the above textural characteristics reveal typical features of dolocrete, which indicate periods of subaerial exposure and also semiarid climate (Esteban and Klappa 1983, Wright 1994).

As known, another common characteristic structure of the peritidal carbonates is the tepee, which appears as 'pseudoanticlines' with irregular polygonal crests. Although desiccation and related processes can result in such a small polygonal cracking, large peritidal tepees have complicated histories (Kendall and Warren 1987). In the studied area, even if large-scale tepee structures have not been observed, small scale ones have been microscopically recognized inside the intraclastic breccia facies (Fig. 4d). The presence of these microtepee structures, thought it is not a specific diagnostic feature, is usually associated with the formation of caliche facies (in this case dolocretes) indicating subaerial exposure (Esteban and Klappa 1983).

A strong indication of early lithification of the sediments is the preservation of the fenestral pores, desiccation cracks, prism cracks and also of larger vugs through their rapid infilling by cement and/or internal sediment. The filling of the various pores and vugs, however, shows complicated diagenetic history due to the periodical subaerial exposure and the subsequent mixing of meteoric and marine waters. In particular, the overall filling of the larger cavities, originating primarily from dissolution, usually includes: an initial fill with carbonate mud and/or pellets often in geopetal fabric, radiaxial fibrous or bladed cement, probably of marine phreatic origin, lining on the wall of

the cavities and coarse blocky/equant spar, probably of meteoric origin, in the center of the cavities. Further, quite often gravitational cements of meteoric-vadose origin have also been observed to have filled some of the vugs.

Finally the almost complete dolomitization of the studied carbonate succession and also the extensive recrystallization evidently constitute primary diagenetic processes which are connected to the exposure and contributed directly to the early lithification of the sediments. In particular, as far as dolomitization is concerned, two major dolomite generations have been recognized on the basis of textural characteristics: for the most part a very finely to finely crystalline (5-40 μm) replacement dolomite and or cement, and to a lesser extent finely to medium crystalline mosaic (60-160 μm) of anhedral dolomite. The former dolomite generation is considered as an early diagenesis product, during which the textural depositional characteristics have been well preserved, while the latter generally precipitated during a later diagenetic stage. Similar early diagenetic, very fine-grained dolomites are formed even at the present time in intertidal-supratidal sediments of the Bahamas, Florida and Trucial Coast but are also found in many ancient peritidal sequences (Tucker and Wright 1990, Purser *et al.* 1994). In order to further investigate the mechanisms by which the dolomitization fluids moved through the rocks, an additional petrographic and geochemical study is required, something which can be the object of a future work.

6. Conclusions

Sedimentological and stratigraphic study of the Upper Triassic succession of the Tripolitza platform in the Mari area on the eastern flanks of the Parnon mountain indicates that during the Norian-Rhaetian there prevailed conditions of tidal to lagoon sedimentation with cyclicity similar to those of the same time period in nearly all the Alpine platforms on the margins of Neotethys.

Macrofacies and microfacies analysis showed that this Upper Triassic carbonates consist mainly of dolomites and to a lesser extent of calcitic dolomites, which exclusively make up cyclic peritidal facies, deposited in the inner platform. More specifically, the inter-supratidal facies, that are mainly represented by microbial and peloidal stromatolitic bindstones and to a smaller degree by intraclastic breccias, alternate with subtidal, shallow-lagoonal facies consisting mostly of bioclastic wackestones/floatstones. In the latter, a few thin intercalations of grainy facies, such as grapestones and coated grainstones are mainly considered as storm deposits. Overall, the various lithofacies formed in different subenvironments on the tidal flat, such as intertidal and supratidal area and pond, to shallow lagoon with the prevalence of low energy conditions.

This shallow marine sedimentation was, however, periodically interrupted by subaerial exposure intervals, as mainly suggested by the presence of dolocrete horizons within the inter-supratidal facies and also of some diagenetic characters, such as vadose meteoric cements and microtepee structures. More specifically, the repeated appearance of dolocrete horizons mostly implies extended subaerial exposure under semiarid climatic conditions. Consequently, the alternating influence of meteoric and marine waters caused various diagenetic phenomena, which contributed substantially to the early lithification of the sediments. Characteristic of the latter is the preservation of the abundant fenestral pores and larger cavities, through their filling up with multiple types of cements and/or internal sediment. Besides, the recrystallization and especially the dolomitization, which almost completely influenced the succession, played an important role in the lithification of the sediments during early diagenesis.

The studied Upper Triassic succession shows many common characters with cyclic successions of Dolomia Principale of the Southern Alps (Italy) and particularly of the Dachstein Dolomite or Hauptdolomit (Lofer Facies) of the Northern Alps (Austria) Northern Calcareous Alps (Fischer 1964, Bosellini and Hardie 1988, Goldhammer *et al.* 1990, Satterley 1996, Enos and Samankassou 1998). Corresponding shallowing- or deepening- upward cycles in the area of study are, however, hard to interpret, since the position of the subaerial disconformities, which are evidently

represented by the dolocrete horizons, cannot be definitively clarified. Moreover, the rare appearance of the intraclastic breccias (corresponding to Member A of Fischer 1964) in these sections, as well as the presence of some truncated surfaces in the internal of the inter-supratidal unit mostly show incomplete cyclicity. Lastly, the repeated occurrence of subaerial exposure conditions and the vadose alterations may suggest allocyclic (eustatic or tectonic) controls of cyclicity (Wright and Burchette 1996).

7. Acknowledgments

Thanks are due to SARG of National and Kapodistrian University of Athens for financial support.

8. References

Bosellini, A., and Hardie, L.A., 1988. Facies e cicli della Dolomia Principale delle Alpi Venete, *Memorie della Società Geologica Italiana,* 30, 245-266.

Ciarapica, G., and Zaninetti, L., 1984. *Aulotortus pregaschei* (KOEHN-ZANINETTI, 1968): Revision taxonomique et stratigraphique sur la base du matériel type, *Rev. Paléobiol.*, 3 (1) 53-61.

Dunham, R.J., 1962. Classification of carbonate rocks according to depositional texture. In W.E. Ham (ed.), *Classification of carbonate rocks*, *Mem Am Ass Petrol Geol,* 1, 108-121pp.

Enos, P., 1983. Shelf. In P.A. Scholle, D.G. Bebout and C.H. Moore (eds), *Carbonate depositional environments*, *Mem. Am. Ass. Petrol. Geol.,* 33, 267-296pp.

Enos, P., and Samankassou, E., 1998. Lofer Cyclothems revisited (Late Triassic, Northern Alps, Austria), *Facies,* 38, 207-228.

Esteban, M., and Klappa, C.F., 1983. Subaerial exposure environment: In P.A. Scholle, D.G. Bebout and C.H. Moore (eds), *Carbonate depositional environments*, *Mem. Am. Ass. Petrol. Geol.,* 33, 1-54pp.

Esteban, M., and Pray, L.,C., 1983. Pisoids and pisolite facies (Permian), Guadalupe Mountains, New Mexico and West Texas. In T.M. Peryt (ed.), *Coated grains*, *Springer-Verlag, Berlin,* 503-537pp.

Fischer, A.G., 1964. The Lofer cyclothems of the Alpine Triassic. In D.F. Merriam (ed.), Symposium on Cyclic Sedimentation, *Kansas Geological Survey Bulletin,* 169, 107-149pp.

Fleury, J.J., 1980. Les zones de Gavrovo – Tripolitza et du Pinde – Olonos (Grèce continentale et Peloponnése du Nord). Evolution dúne plateforme et d' un bassin dans leur carde alpin, *Soc. Gèol. Nord. Publ.* 4, 651p., *Lille.*

Flügel, E., 2004. Microfacies of carbonate rocks, *Springer-Verlag, Berlin,* 976pp.

Goldhammer, R.K., Dunn, P.A., and Hardie, L.A., 1990. Depositional cycles, composite sea-level changes, cycle stacking patterns, and the hierarchy of stratigraphic forcing: examples from Alpine Triassic platform carbonates, *Geol. Soc. of Amer. Bull.,* 102, 535-562.

Haas, J., 2004. Characteristics of peritidal facies and evidences for subaerial exposures in Dachstein-type cyclic platform carbonates in the Transdanubian Range, Hungary, *Facies,* 50, 263-286.

Hardie, L.A., and Shinn, E.A., 1986. Carbonate depositional environments, modern and ancient, Tidal flats, *Colorado School Mines Q.,* 81, 1–74.

Jacobshagen, V., 1986. *Geologie von Griechenland,* Gebrüder Borntraeger. Berlin-Stuttgart, 363pp.

Kendall, C.G.St.C., and Warren, J., 1987. A review of the origin and setting of tepees and their associated fabrics, Sedimentology, 34, 1007-1027.

Lekkas, S., and Papanikolaou, D., 1978. On the phyllite problem in Peloponnesus, *Ann. Géol. Pays Hell.*, 29, 395-410.

Müller, G., 1971. Aragonite inorganic precipitation in a freshwater lake, *Nature,* 229, 18.

Purser, B.H., Tucker, M.E., and Zenger, D.H., 1994. Dolomites: A volume in honor of Dolomieu, *Spec. Publ. Int. Ass. Sed., Blackwell Science, Oxford,* 451pp.

Riding, R., 1991. Classification of microbial carbonates In *Calcareous algae and stromatolites, Springer, Berlin Heidelberg New York,* 21–51pp.

Salaij, J., Borsa, K. and Samuel, D., 1983. Triassic foraminifers on the West Carpathians, *Geol. Ustav. Dion. Stura,* 1-213.

Robertson, A.H.F., Clift, P.D., Degnan, P.J., and Jones, G., 1991. Paleogeographic and paleotectonic evolution of the Eastern Mediterranean Neotethys, Palaeogeography, Palaeoclimatology, Palaeoecology, 87, 289-344.

Satterley, A.K., 1996. Cyclic carbonate sedimentation in the upper Triassic Dachstein limestone, Asustria: The role of patterns of sediment supply and tectonics in a platform-reef-basin system, *Journal of Sedimentary Research,* 66 (2), 307-323.

Shinn, E.A., 1983. Tidal flat environment. In P.A. Sholle, D.G. Bebout and C.H. Moore (eds), *Carbonate depositional environments, Mem Amer Assoc Petrol Geol,* 33, 173–210.

Skarpelis, N., 1982. Metallogeny of massive sulphides and petrology of the external metamorhic belt of the Hellenides, *PhD Thesis, Univers. of Athens,* 149 pp.

Skourtsos, E., 2002. *Study of the eastern boundaries structure of the Parnon tectonic window*, Phd Thesis, University of Athens.

Skourtsos, E., Lekkas, S., and Alexopoulos, A., 2004. The structural evolution of Mt. Parnon, Peloponnesus, Greece: Implications for synconvergence extension in arc regions, *Proceedings of the 5th International Symposium on Eastern Mediterranean Geology, Thessaloniki, April 2004,* 189-203.

Tucker, M.E., and Wright, V.P., 1990. Carbonate sedimentology, *Blackwell, Oxford,* 482pp.

Thiebault, F., 1982. Evolution géodynamique des Hellénides externes en Peloponnése méridional (Grèce), *Soc. Géol. Nord, Publ.*, 6, 574p.

Wright, V.P., 1994. Paleosols in shallow marine carbonate sequences, *Earth Sci Rev,* 35, 367–395.

Wright, V.P., and Burchette, T.P., 1996. Shallow-water carbonate environments. In H.G. Reading (ed.), *Sedimentary environments: processes, facies and stratigraphy, Blackwell Science Ltd,* 688pp.

Zambetakis-Lekkas, A., Kati, M., and Skourtsos, E., 2006. Stratigraphic and sedimentological investigations on the Upper Triassic base of the carbonate Tripolitza platform (Parnon Mountain, eastern Peloponnesus, Greece), *In Abst. of Geology and Paleontology of the Peri-Adriatic area, May 2006, Napoli, Italy,* 58-59pp.

Zaninetti, L. 1976. Triassic foraminifera from Pakistan, *Riv. It. Paleont. Strat.* 81 (3), 257-280.

Δελτίο της Ελληνικής Γεωλογικής Εταιρίας τομ. XXXX, 2007
Πρακτικά 11ου Διεθνούς Συνεδρίου, Αθήνα, Μάιος 2007

Bulletin of the Geological Society of Greece vol. XXXX, 2007
Proceedings of the 11th International Congress, Athens, May, 2007

APPLICATION OF BEDS THICKNESS DISTRIBUTIONS IN TURBIDITE DEPOSITS OF MAVRI MITI AREA, SW GREECE

Konstantopoulos P.[1], Maravelis A.[1], Nikolaidou D.[1], Pantopoulos G.[1], and Zelilidis A.[1]

[1] *University of Patras, Department of Geology, Division of Physical Geology, Marine Geology & Geodynamics, Laboratory of Sedimentology, 26500 Patras, Greece, tkonstan@upatras.gr, amaravel@upatras.gr, gpantop@upatras.gr, A.Zelilidis@upatras.gr*

Abstract

A physical outcrop, of 100m length and 110 m total thickness studied in combination with sedimentological analysis in detail (stratigraphic sequence, grain size, sedimentological structures) led us to determine the sedimentological environments and the particular subenvironments of each part of the partial stratigraphic sequence which is a proximal depositional environment. The sandstone bed thickness data measured in Mavri Miti area, demonstrates a curved distribution shape in the log-log plots. Where processes such as erosion and bed amalgamation are more significant there was observed a possible deviation from the power-law statistical distributions. The shape of cumulative distribution demonstrates possible proximal fan setting. The above two different approaches shows an agreement in relation to the depositional processes.

Key words: *submarine fans, turbidites, bed thickness analysis.*

Περίληψη

Οι αποθέσεις υποθαλάσσιων ριπιδίων στην περιοχή του Αράξου μελετήθηκαν σε μία τομή μήκους 100m και συνολικού πάχους 110 m. Η λεπτομερής ιζηματολογική μελέτη των αποθέσεων μας οδήγησε στον προσδιορισμό του περιβάλλοντος ιζηματογένεσης, αλλά και των ιδιαιτέρων υποπεριβαλλόντων απόθεσης κάθε τμήματος της ακολουθίας των ιζημάτων. Ένα από τα πλέον αποδεκτά εργαλεία της στατιστικής ανάλυσης των τουρβιδιτικών ακολουθιών, το οποίο χρησιμοποιείται κατά κόρων, είναι η λογαριθμική κατανομή .Σ' αυτή συνήθως προβάλλεται ο δεκαδικός λογάριθμος του πάχους των στρωμάτων στον άξονα χ και ο δεκαδικός λογάριθμος του αριθμού των στρωμάτων που είναι παχύτερα από ένα συγκεκριμένο στρώμα στον άξονα ψ. Μετά τη δημιουργία της κατανομής μελετάται το σχήμα της (ευθεία, καμπύλη) και η μαθηματική εξίσωση που την εκφράζει (λογαριθμική, εκθετική), από όπου εξάγονται συμπεράσματα σχετικά με το περιβάλλον απόθεσης των τουρβιδιτών.

Λέξεις κλειδιά: *υποθαλάσσια ριπίδια, τουρβιδίτες, ανάλυση παχών στρωμάτων.*

1. Introduction- Geological setting

The study area is located in the NW part of Peloponnesus peninsula, is a part of Pindos foreland basin and geotectonically belongs to the Internal Ionian Zone. Pindos thrust activity, during Eocene, formed the Pindos foreland in the pre-existing Ionian and Gavrovo geotectonic zones (Un-

derhill 1985, Clews 1989, Avramidis 2000, Vakalas 2003). The material with which the foreland was supplied, sourced from Eastern, from the forehead of Pindos thrust (Piper *et al.* 1978, Fleury 1980, Clews 1989, Wilpshaar 1995). Mavri Miti sandstone formation represents a turbidite system deposited during early Eocene, in an elongated basin where the major flow was perpendicular and the minor flow was axially, parallel to the Pindos thrust (Fig. 1).

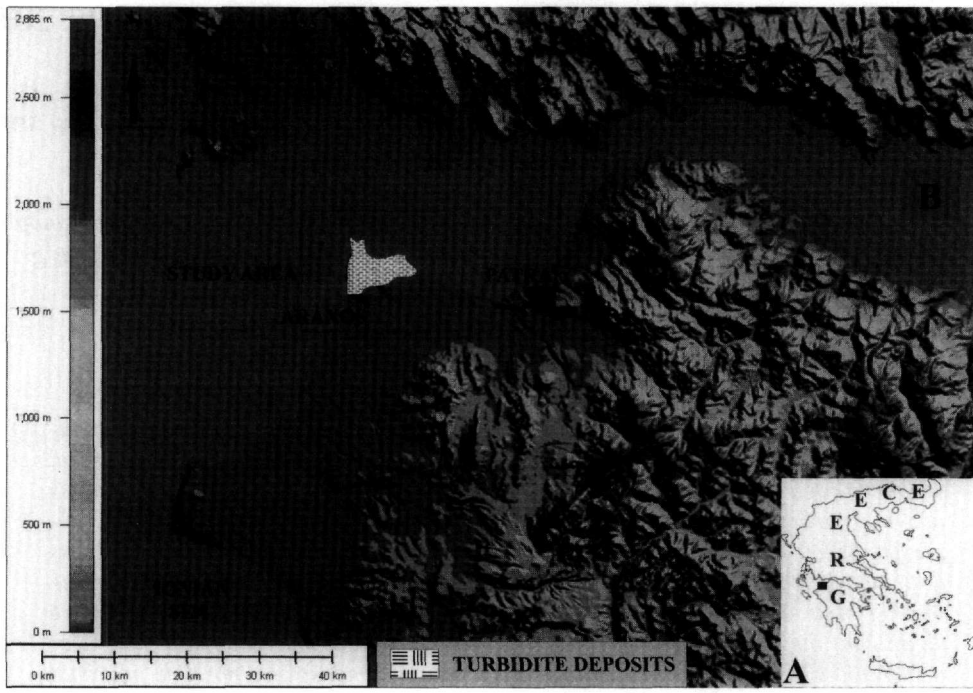

Figure 1 - Geological map of the North-Western part of Peloponnesus. The insert box represents the study area shown in figure

Generally basin analysis provides distinctions between depositional environments, whereas in the case of petroleum reservoirs, this distinction may highlight insight into fluid expulsion, pathways and reservoir geometry. Moreover, turbidite thickness distributions may help to reveal the extent of sand and shale interfingering, which can affect porosity and permeability patterns. The study of bed thickness distributions of various facies can help to identify important reservoir facies within the inner part of fan lobes, where massive and pebbly sandstones are relatively coarse and thick, with fewer and thinner shales between beds (Carlson and Grotzinger 2001).

In turbidites, the frequent interbedding of sand and shale strongly influences the overall heterogeneity of the resulting succession and the distribution of turbidite bed thicknesses is important in modelling and developing hydrocarbon reservoirs that were deposited in deep water (e.g., Flint and Bryant 1993, Tye 2004, Pyrcz *et al.* 2005). Turbidite bed-thickness distributions are often interpreted in terms of power-laws, even when there are significant departures from a single straight line on a log-log exceedence probability plot. It has recently been suggested that turbidite bed thicknesses can be well described by a log-normal mixture model (Talling 2001).

For the present study we used Carlson & Grotzinger methodology who deals mostly with cumulative log-log plots. This was the aim of this paper, a detailed analysis of turbidite bed thickness trend (based on bed thickness distributions using log-log cumulative plots) from the Mavri Miti formation in order to extract information about the geological conditions and the sedimentological characteristics of the turbidite deposits that might generate a power-law distribution, and how departures from it might be used as a guide to prediction of the submarine fan environment.

2. Sedimentological data

2.1. Description

Mavri Miti section consists of alternated fine-grained beds of light brown claystones and sandstones. In its upper stratigraphic part, beds of coarse grained sandstones and grits up to two meters thick appears. In order to approach the best sedimentological analysis of the studied sediments, the whole 110 m thick section (Fig. 2) of Mavri Miti sediments was separated in four parts and from the lower to the upper we have:

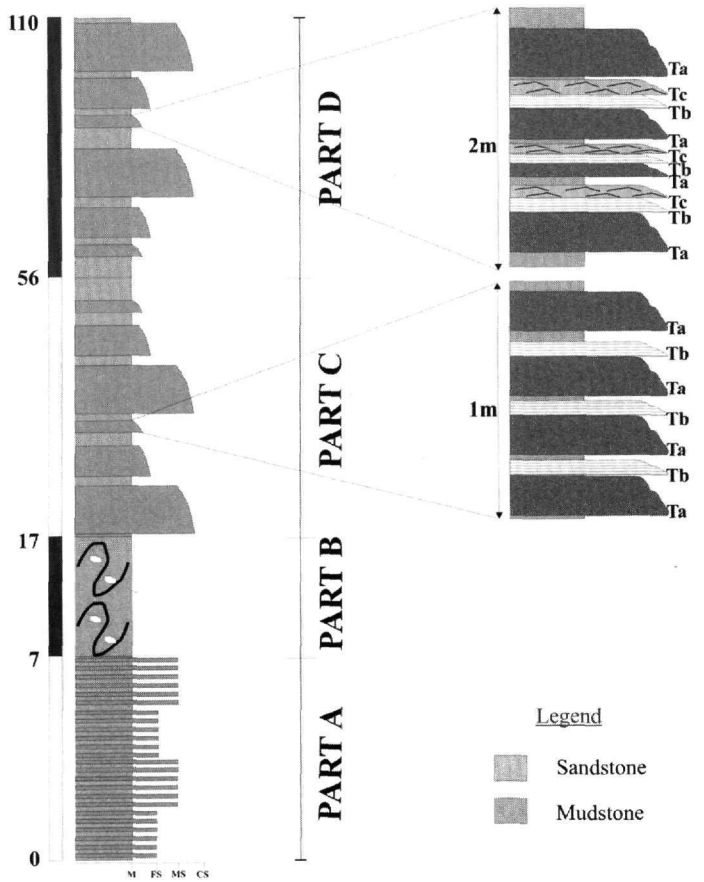

Figure 2 - Stratigraphic column of the studied sediments, not in scale, showing the four parts of the studied area

Part A: The total thickness of the lower part is up to 7m (Fig. 3A). It consists of thin-bedded fine to medium-grained sandstones, 1-7cm thick, with flat bases and very good lateral continuity interbedded with shales. Sandstone/shale ratio is 1/1. Ta Bouma subdivision characterizes sandstone beds, whereas Te Bouma subdivision characterizes claystones.

Part B: A slump horizon with thickness up to10m rests unconformably over the lower part (axis: 160^0, limb: $108^0/82^0$ for the slump) (Fig. 3B). Moreover, within the slump horizon a limestone lence was recognized interbedded with grey coloured mudstone matrix (Fig. 3C). The lence is up to 0.7 m thick and 5m length. This limestone seems to belong to Ionian zone and especially is similar to the Eocene limestones appeared westwards of the studied area.

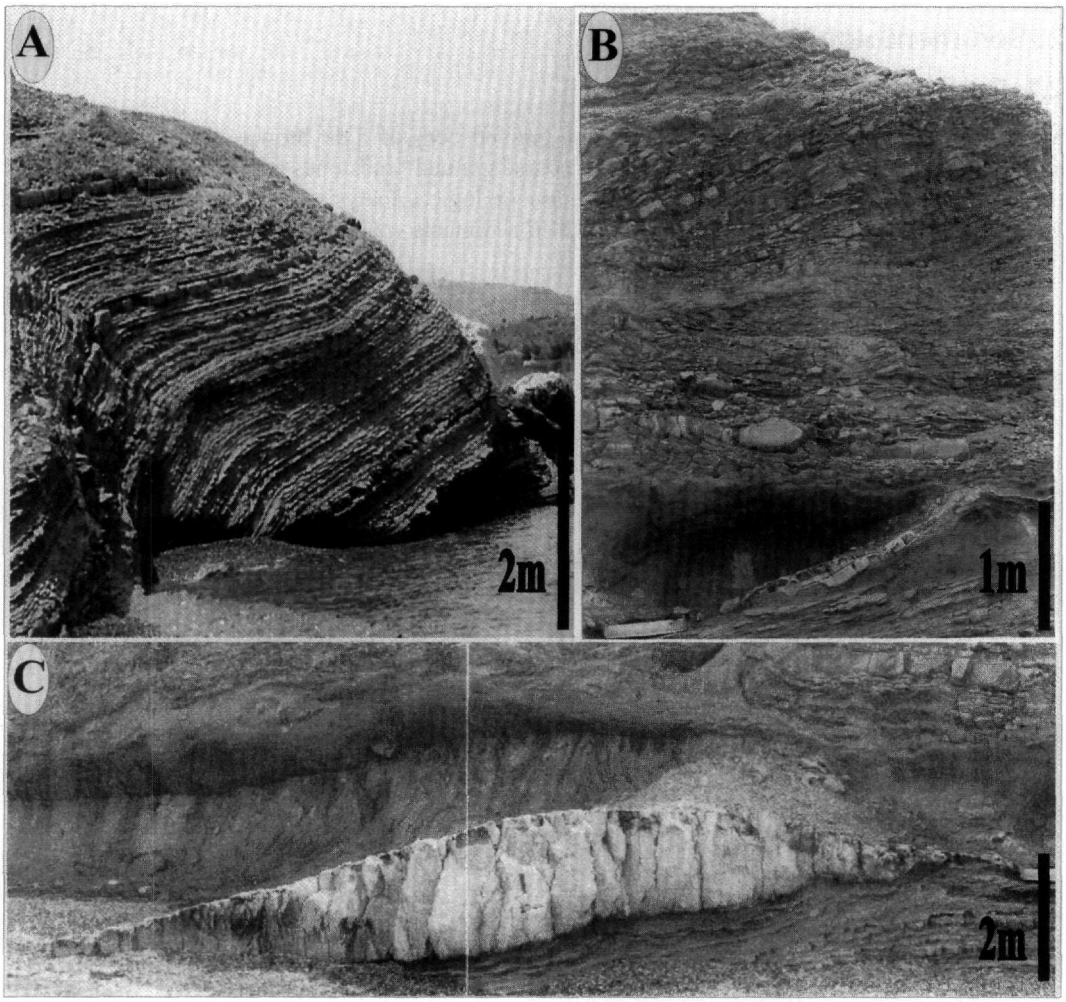

Figure 3 - A) Interchannel deposits in the lower part. B) Slump horizon. C) Limestone lence recognized in a slump horizon, interbedded with grey coloured mudstone matrix

Part C: Medium to thick-bedded sandstones, 10-96 cm thick, interbedded with shales, minimally amalgamated (Fig. 4A). The whole package is up to 40 m thick. Massive Ta units are the most common Bouma subdivisions in the section (70 % of the turbidite subdivisions), whereas Tb units are also common. Sole marks are prominent at the base of sandstone beds and include grooves and scours. The main palaeocurrent trend is WNW-ESE and the minor is ENE-WSW. Packages consisting of laterally continuous interbedded sandstones and shales with an upward-thinning trend. Thick laterally continuous sandy turbidite and slurry beds are also present throughout the section, often containing water-escape structures (dishes, pipes). Generally beds show an ENE dip direction with a dip of 9^0.

Part D: In the upper part of the section sandstones interbedded with shales, with a total thickness up to 55 m and showing an upward thickening trend (Fig. 4B). This stratigraphic part is dominated by Tabc and Ta Bouma sequences (60 % of beds), and which form at places packages up to 10 m thick, whereas Tbc Bouma sequence is common. Complete Bouma cycles and horizons of massive ungrained sand are also present at places in this unit. Toolmarks can easily been seen on the bottoms of thicker deposits, although scourmarks are rare. The main palaeocurrent trend in this part is

NW-SE and NNE-SSW as it results from the measurement of ripples ($308^0/21^0$, $24^0/25^0$). Beds show an E dip direction with a dip of 15^0.

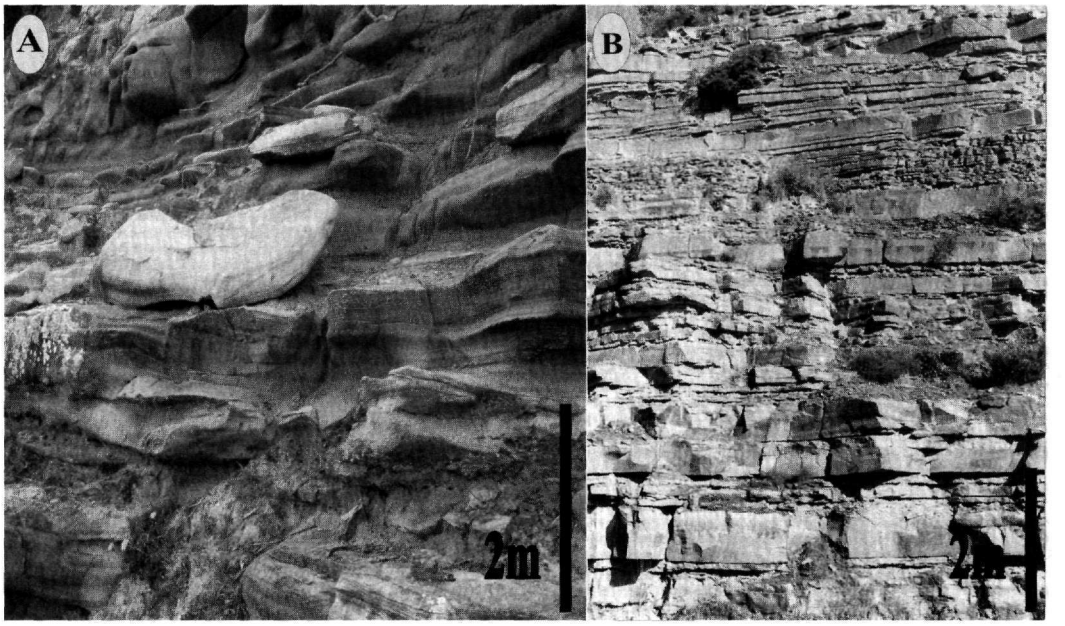

Figure 4 - A) Thick-bedded sandstones minimally amalgamated. B) Tabc Bouma sequences, form packages up to 10 m thick

2.2. Interpretation

The presence of Bouma sequence indicates submarine fans deposits. Ta and Tb Bouma subdivisions in the sandstone beds shows rapid deposition by high-density turbidity current (Bouma, 1962). The deposition of thin-bedded sandstones derived from low-density turbidity currents. Thin-bedded sandstones interbedded with clays derived from middle to low density turbidity currents. Especially, each part of the section is interpreted as:

Part A: The Tae turbidite beds are interpreted as inter-channel deposits from high-density currents involving mass deposition, followed by suspension fall-out with or without later chemical precipitation of chert (Eriksson 1980).

Part B: The slump horizon can be interpreted as a possible submarine rock falls deposit or landslides using as surface of slipping overpressure or liquefied clays. Hemipelagic and turbiditic shale is associated with the thin-bedded intervals. Although it is difficult to separate hemipelagic shale from low-density, dilute turbidite shale, we interpreted these deposits as low-density turbidite shale (Chester 1984).

Part C: This part has been described as close-to-source version of classic turbidites interpreted to have formed within broad channels (Lowe 1982). So, these deposits are interpreted as inner fan deposits. Given that beds extend without substantial changes in thickness for hundred of meters and are also noticeably lenticular, this suggests that the trend of the outcrop is perpendicular to the channel axis. Thick laterally continuous sandy turbidite and slurry beds, containing water-escape structures are interpreted as deposits derived from both debris flows and turbidity currents.

Part D: The Tabc turbidites are interpreted as middle-fan deposits passing west into outer fan deposits in Evinochori area (Pantopoulos *et al.* 2006). Complete Bouma cycles are considered to have accumulated on interchannel reaches of the middle-fan.

3. Statistical analysis

3.1. Methodology

The data sets consist of one measured vertical sequence of continuously exposed turbidites. Because of the inability of distinction between the turbiditic and hemipelagic mud the measurements were restricted to the arenaceous component. Any discernible bed was measured, although bed resolution typically diminished markedly below 1cm. For this reason, a minimum cut-off of 1 cm was established. Where the bed is disrupted and contains preserved bedforms (ripples, etc.) or has been eroded, the determination of the bed thickness becomes complicated and in such cases a number of measurements of the same bed were recorded and the average was used as the bed thickness. In the course of measurement, the thickness of individual sand beds is recorded, regardless of whether or not the beds are inferred to represent a single flow or multiple flows that have been amalgamated to form a single sand bed. This is an important distinction, in that the objectivity of the measurement is increased at the expense of an understanding of the actual distribution of the individual flows. In this manner, the statistical distributions of bed thickness may reflect successions of strata where amalgamation is minimal vs. those where amalgamation is common (Carlson 1998).

3.2. Application

In the studied up to 110 m thick whole section 514 beds were measured, 1 cm up to 150 cm thick (Fig. 5). The cumulative thickness distribution for this stratigraphic part yields a slightly curved shape. According to Carlson and Grotzinger (2001) this shape is consistent with an interpretation for deposition in a proximal environment (channelized, inner fan)

Moreover, we separated the studied section in order to applicate the statistical analysis only in the upper most part (Part D in the sedimentological chapter) with total thickness up to 55 m.In this second distribution data were collected from 132 beds, 1cm up to 140cm thick (Fig. 6). The shape of the cumulative thickness distribution is less curved than the first one, fits slightly better to a power-law and is considered to be diagnostic for turbidites deposited in more distal parts from the source environment(less channelized, middle fan).

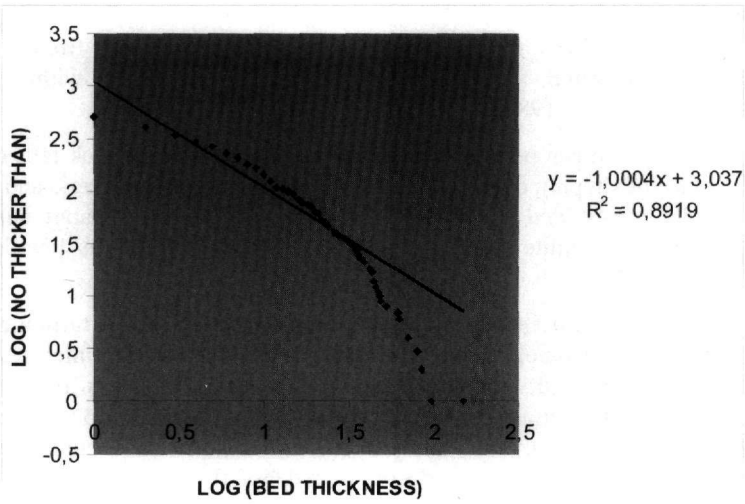

Figure 5 - A cumulative thickness distribution for 514 beds yields a slightly curved shape

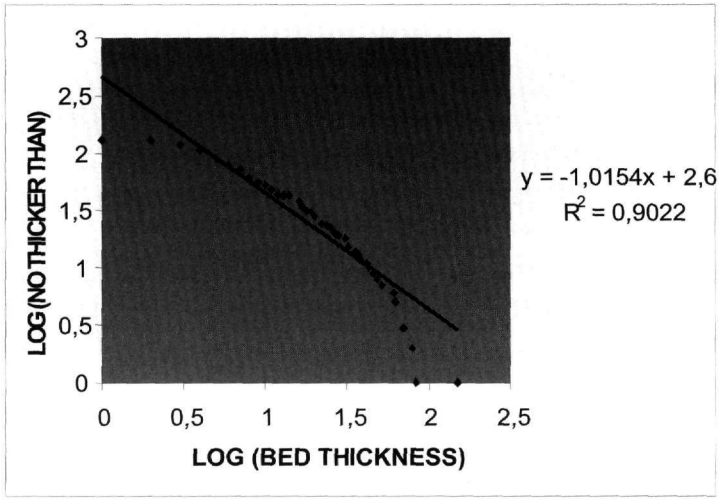

Figure 6 - A cumulative thickness distribution for the one-third of the section, 132 beds

4. Discussion and conclusions

Studied outcrop with a total thickness up to 110 m, composed by submarine fans, subdivided into four parts. In the lower part (Part A) the thin-bedded interval, interpreted as interchannel deposits, is considered to be representative of a different facies from the channel packages of the upper part, part D. The upward thickening trend in the upper part of the section is also considered to be representative of a different facies from the channel deposits, part A.

For statistical analysis we used two different approaches. One with the whole section and a second one only taking into account the upper part of the unit, Part D.

The sandstone bed thickness data measured in Mavri Miti area, demonstrates a curved distribution shape in the log-log plots. Where processes such as erosion and bed amalgamation are more significant there was observed a possible deviation from the power-law statistical distributions. The shape of cumulative distribution demonstrates possible proximal fan setting. The above two different approaches shows an agreement in relation to the depositional processes. Correlation between the statistical results of the whole section and the upper part shows that the upper part has a better fit to a power-law distribution whereas the whole part is more curved with a smooth departure from the power-law distribution, consisted with beds which are more affected by erosion and amalgamation.

From the above we could conclude that this method is in agreement with the sedimentological results and has successfully highlighted usefulness of using cumulative bed thickness distributions in submarine fan deposits.

5. Acknowledgements

This paper is coofounted by E.C., European Social fund and GSRT Greece. EPAN PENED '03ED497.We would like to thank anonymous reviewer for his helpful comments and suggestions.

6. References

Avramidis, P., Zelilidis, A., and Kontopoulos, N., 2000a. Thrust dissection control of deep-water clastic dispresal patterns in the Klematia-Paramythia foreland basin, Western Greece, *Geol. Mag.,* 137.

Bouma, A.H., 1962. The Sedimentology of some flysch deposits: a graphic approach to facies interpretation, Amsterdam, *Elsevier*, 168pp.

Carlson, J., 1998. Analytical and Statistical Approaches toward understanding Sedimentation in Siliclastic Depositional Systems, *PhD Thesis*, Department of Earth, Planetary and Atmospheric Sciences, MIT, Cambridge, MA, 406pp.

Carlson, J., and Grotzinger, J.P., 2001. Submarine fan environment inferred from turbidite thickness distributions, *Sedimentology*, 48, 133-1351.

Chester, T.L., 1994. Analysis of Vertical Cyclicity Patterns in Two Sediment Gravity Flow Sequences, *MSc Thesis*, Stanford University, San Francisco, CA, 169pp.

Clews, J., 1989. Structural controls on basin evolution: Neogene to Quartenary of the Ionian zone of western Greece, *J. Geol. Soc. London*, 146, 447-457.

Eriksson, K.A., 1980a. Hydrodynamic and paleogeographic interpretation of turbidite deposits from the Archean Fig Tree Group of the Barberton Mountain Land, South Africa, *Geol. Soc. Am. Bull.*, 91, 21-26.

Fleury, J., 1980. Les zones des Gavrovo-Tripolitza et du Pinde-Olonus (Grece occidentale et Péloponnèse du Nord): évolution d'une basin dans leur cadre alpin, *Societe Geologique du Nord*, 4, 1-651.

Flint, S.S., and Bryant, I.D., 1993. The geological modelling of hydrocarbon reservoirs and outcrop analogues, *Int. Assoc. Sedimentol. Spec. Publ.*, 15, 269pp.

Lowe, D.R., 1982. Sediment gravity flows: II. Depositional models with special reference to the deposits of high-density turbidity currents, *J. sedim. Petrol.* 52, 279-297.

Pantopoulos, G., Konstantopoulos, P., Maravelis, A., and Zelilidis, A., 2006. Application of bed thickness distributions in turbidite deposits of Greece: Some preliminary results, *Proc. Of the 17th International Sedimentological Congress, Fukuoka, Japan, 27 August-1September, Abstracts Volume B,* 119.

Piper, D.J.W., Panagos, A.G., and Pe, G.G., 1978. Conglomeratic Miocene flysch, western Greece, *J. Sed. Petr.*, 48, 117-26.

Pyrcz, M.J., Catuneanu, O., and Deutsch, C.V., 2005. Stochastic surface-based modeling of turbidite lobes, *AAPG Bulletin*, 89, 177-191.

Talling, P.J., 2001. On the frequency distribution of turbidite thickness, *Sedimentology*, 48, 1297-1331.

Tye, R.S., 2004. Geomorphology: An approach to determining subsurface reservoir dimensions, *AAPG Bulletin*, 88, 1123-1147.

Underhill, J.R., 1985. Neogene and quartenary tectonics and sedimentation in western Greece, *PhD thesis*, University of Wales, Cardiff.

Vakalas, I., 2003. The evolution of foreland basins in Western Greece, *PhD. Thesis,* University of Patras.

Wilpshaar, M., 1995. Applicability of dinoflagellate cyst stratigraphy to the analyses of passive and active tectonic settings, *PhD Thesis*, University of Utrecht, Netherlands.

Δελτίο της Ελληνικής Γεωλογικής Εταιρίας τομ. XXXX, 2007
Πρακτικά 11ου Διεθνούς Συνεδρίου, Αθήνα, Μάιος 2007

Bulletin of the Geological Society of Greece vol. XXXX, 2007
Proceedings of the 11th International Congress, Athens, May, 2007

PLIOCENE BRACHIOPODS FROM RHODES ISLAND (CAPE VAGIA SECTION)

Koskeridou E.[1]

[1] *National and Kapodistrian University of Athens, Faculty of Geology and Geoenvironment, Department of Hist. Geology – Paleontology, ekosker@geol.uoa.gr*

Abstract

Six brachiopod species (5 terebratulids and 1 craniid) from the upper Pliocene sandy and calcareous deposits of the Cape Vagia (Rhodes Island) are described: Gryphus sp., Terebratulina retusa, Megerlia truncata, Megerlia truncata var. monstruosa, Argyrotheca cordata, Megathiris detruncata and Novocrania anomala. This is the first record of Megerlia truncata var. monstruosa from the Pliocene of Greece and of Megerlia truncata from the Pliocene of Rhodes. Megathiris detruncata, Terebratulina retusa and Argyrotheca cordata are described for the first time from the Pliocene of Rhodes. This brachiopod association displays close affinity with those from the Mediterranean province, where assemblages of similar composition are associated with shallow-water, high energy environments. However, the association of Gryphus sp., Terebratulina retusa and Novocrania anomala corresponds to deeper water moderate environments.

Key words: *Pliocene, Mediterranean, Brachiopods, Rhodes, Greece.*

Περίληψη

Στην εργασία αυτή περιγράφονται επτά είδη Βραχιονόποδων (6 terebratulids and 1 craniid) των ανω-Πλειοκαινικών αμμωδών αποθέσεων και ασβεστολίθων της τομής Cape Vagia (νήσου Ρόδου): Gryphus sp., Terebratulina retusa, Megerlia truncata, Megerlia truncata var. monstruosa, Argyrotheca cordata, Megathiris detruncata και Novocrania anomala.

Για πρώτη φορά αναφέρεται το Megerlia truncata var. monstruosa από το Πλειόκαινο της Ελλάδας και το είδος Megerlia truncata από το Πλειόκαινο της Ρόδου. Επίσης τα είδη Megathiris detruncata, Terebratulina retusa και Argyrotheca cordata περιγράφονται για πρώτη φορά από το Πλειόκαινο της Ρόδου. Τα Βραχιονόποδα αυτά αποτελούν βιοκοινότητα η οποία παρουσιάζει πολλές ομοιότητες με την αντίστοιχη συγκέντρωση ειδών στη σημερινή Μεσόγειο, η οποία χαρακτηρίζει ρηχών υδάτων και υψηλής ενέργειας περιβάλλοντα.

Η συνάθροιση των ειδών Gryphus sp., Terebratulina retusa και Novocrania anomala συσχετίζεται με τα ενδιάμεσης ενέργειας βαθιών υδάτων περιβάλλοντα.

Λέξεις κλειδιά: *Πλειόκαινο, Μεσόγειος, Βραχιονόποδα, Ρόδος, Ελλάδα.*

1. Introduction

Pliocene brachiopods of Greece have merely been mentioned or listed by a number of authors in studies dealing with mollusc faunas (Symeonides 1966, Dermitzakis 1969, Mutti *et al.* 1970b, Georgiades-Dikeoulia 1974, Spanopoulou 1997, Steinthorsdottir *et al.* 2006).

Pliocene brachiopods are also described from other Mediterranean regions such as Italy and Spain (see Bitner and Martinell 2001).

The Cape Vagia section in Rhodes Island is an extremely interesting area for the study of Pliocene brachiopods and their environments from shallow to deeper water, yielding a micromorph association. This section is located in a south-facing basin on the eastern coast of Rhodes, in the bay south of Cape Vagia (Fig.1).

In the present work the studied fauna comes from the lower part of the Cape Vagia section that belongs to the upper Pliocene Kolymbia limestone Member.

Even though the existence of brachiopods in the Kolymbia limestone was mentioned by Moissette and Spjeldnaes (1995), Spanopoulou (1997) and Steinthorsdottir *et al.* (2006), this is the first time that a micromorph fauna is described from the Pliocene deposits of Greece. *Megathiris detruncata, Argyrotheca cordata, Megerlia truncata, Megerlia truncata* var. *monstruosa* and *Terebratulina retusa* are described for the first time from the Pliocene of Rhodes and *Megerlia truncata* var. *monstruosa* for the first time from the Pliocene of Greece. The taxonomic position of the specimens described by Steinthorsdottir *et al.* (2006) as *Gryphus vitreus* has been revised.

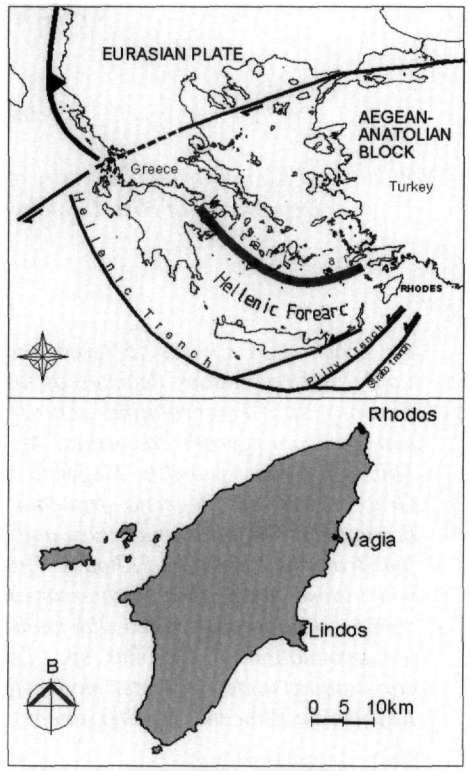

Figure 1 - Position of Rhodes in the Aegean Arc and schematic map of indicating the location of the Cape Vagia area

In this study the collected brachiopod assemblages are analyzed and a paleoenvironmental interpretation is proposed, based on the micromorph fauna through the comparison with recent associations.

2. Geological setting

The Late Pliocene and Pleistocene marine succession of the island of Rhodes, overlies unconformably a metamorphosed Mesozoic limestone which formed a karstic landscape of considerable relief (Mutti *et al.* 1970a-b, Meulenkamp *et al.* 1972, Hanken *et al.* 1996). The infilling sequences are consequently of highly varying thickness.

In the Late Pliocene, a general tilting raised northeastern and lowered southwestern Rhodes. Normal faults separated the island into several tectonic blocks with differential vertical more or less independent and important movements (Mutti *et al.* 1970a-b, Pirazzoli *et al.* 1983, 1989, Hanken *et al.* 1996). These movements persisted during the Pleistocene and continue to the present day (Meulenkamp *et al.* 1972, Benda *et al.* 1977).

Many authors proposed lithostratigraphic subdivisions of the Plio-Pleistocene deposits (Hedenborg 1837, Bukowski 1899, Mutti *et al.* 1970b, Meulenkamp *et al.* 1972, Hanken *et al.* 1996). Cornée *et al.* (2006) revised the tectono-sedimentary organization of these deposits and defined a new formation (the Ladiko-Tsampika Fm) between the Rhodes Formation (now including three Members: Kritika, Kolymbia, and Lindos Bay clay) and the Lindos Acropolis Formation. The Pliocene-Pleistocene boundary was positioned within the Lindos Bay clay (Keraudren 1970, Sissingh 1972, Benda *et al.* 1977, Løvlie *et al.* 1989, Hanken *et al.* 1996). Thomsen *et al.* (2001) assigned an Early Pleistocene age to the whole marine sequence. Cornée *et al.* (2006a-b) established that these three formations range from Late Pliocene (Kritika to base of the Lindos Bay clay) to Middle Pleistocene in age.

The Upper Pliocene Kolymbia limestone on which the present study focuses, is a bryozoan-mollusc-dominated limestone corresponding to a deepening upward sequence (Moissette and Spjeldnaes 1995, Spjeldnaes and Moissette 1997, Steinthorsdottir *et al.* 2006). It consists of a muddy limestone at the base, overlain by a homogeneous limestone intercalated with coarser layers (Fig.2).

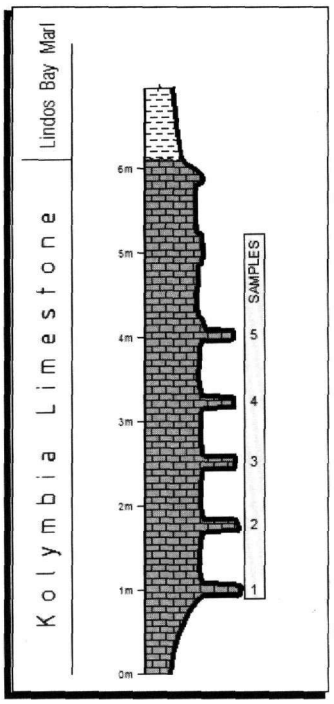

Figure 2 - Log of the brachiopod-yielding beds in the Cape Vagia section. Positions of samples are indicated

3. Materials and Methods

For this study, a total number of 5 samples were collected from the Cape Vagia section (Fig. 2). They were taken from the coarser beds which are characterized by large concentrations of shells and rhodoliths. Bulk samples of 1-1.5 kg were collected throughout the section. Samples 1 and 4 were treated with a solution of Glaubert's salt and then sieved through four mesh sizes (2, 1, 0.5, 0.25 mm). After drying, fossils were picked, and identified to species level whenever possible. Information about their modern ecological characteristics and distribution were used for a paleoenvironmental reconstruction.

Macro and microphotographs of brachiopods were taken with a Jeol JSM 5600. The studied material is housed in the laboratory of the Department of Historical Geology-Paleontology, Section of Geology and Geoenvironment, Athens University.

3.1. Paleontology

The qualitative analysis led to the identification of 7 taxa of Brachiopods: *Gryphus* sp., *Terebratulina retusa* (Linnaeus), *Argyrotheca cordata* (Risso), *Megerlia truncata* (Linnaeus), *Megerlia truncata* var. *monstruosa, Megathiris detruncata* (Gmelin) and *Novocrania anomala* (Müller). *Novocrania anomala* has been already mentioned by Steinthorsdottir *et al.* 2006. However *Gryphus vitreus* identified by these authors is revised herein. The other species are described for the first time from the Pliocene of Greece.

Sample 1 is characterized by the dominance of *Ostrea lamellosa* and the presence of *Argyrotheca cordata, Megerlia truncata,* and *Megathiris detruncata.* Sample 2 is characterized by the abundance of *Gryphus* sp., the presence of *Megerlia truncata var. monstruosa,* and transported pectinids and rhodoliths. Sample 3 is dominated by *Ostrea lamellosa*, *Pecten jacobaeus*, the occurrence of *Gryphus* sp. in great number and the presence of *Terebratulina retusa.* Sample 4 is dominated by *Gryphus* sp. and *Terebratulina retusa* and *Novocrania anomala* is also present.

Sample 5 contains transported rhodoliths, small ostreids and pectinids, *Anomia ephippium* and rare *Gryphus* sp.

SYSTEMATIC PALAEONTOLOGY

A new supra-ordinal classification of the Brachiopoda (Williams *et al.* 1996) has been used here.

Since most investigated species are well known, only some more important and/or recent synonymies are given.

PHYLUM BRACHIOPODA Dumeril, 1806
SUBPHYLUM RHYNCHONELLIFORMEA Williams *et al.*, 1996
CLASS RHYNCHONELLATA Williams *et al.*, 1996
ORDER TEREBRATULIDA Waagen, 1883
SUBORDER TEREBRATULIDINA Waagen, 1883
Superfamily TEREBRATULOIDEA Gray, 1840
Family Terebratulidae Gray, 1840
Subfamily Gryphinae Sahni, 1929
Genus *Gryphus* Megerle von Mühlfeld, 1811
***Gryphus* sp.**
(Plate 1, Figs 1-4)

Morphology. The shell is very large, thick, subpentagonal, strongly biconvex, smooth, with concentric growth lines and has a large foramen. The lateral commissure is curvier than this of *Gryphus vitreus*. The shell is thicker posteriorly and is best preserved at this area. The dimensions of the collected specimens reach about 5 cm in length and 4.5 cm in width. The large size, the shell outline and the type of foramen resemble those of the Pliocene species *Gryphus sphenoideus* that was described by Gaetani and Sacca (1984, 1985). The internal features are unknown and the limited material prevents detailed investigations and identification to the specific level.

The specimens from the Kolymbia limestone attributed by Steinthorsdottir *et al.* (2006) to *Gryphus vitreus* have been re-investigated. It has the characteristics of our specimens and not those of the typical *Gryphus vitreus*.

Occurrence. The genus *Gryphus* is recorded from the Pliocene and Pleistocene of Italy, (Gaetani and Sacca 1984, 1985), of the Pliocene of Spain (Bitner and Martinell 2001) and the Pliocene of north-western Africa (Bitner and Moissette 2003).

The species *Gryphus vitreus* lives in the present day Mediterranean Sea. It is a stenotopic species and is observed on bottoms with moderate to strong currents, low sedimentation, abundance of nutriments and stable temperature and salinity. It has been found on substrates with gravels or shells of the bathyal zone, usually with *Terebratulina retusa* and on the shelf to the bathyal zone with *Novocrania anomala* (Logan 1979). The species found in the Kolymbia limestone is associated with this fauna too.

Superfamily CANCELLOTHYRIDOIDEA Thomson, 1926
Family Cancellothyridae Thomson, 1926
Subfamily Cancellothyridinae Thomson, 1926
Genus *Terebratulina* d'Orbigny, 1847
Terebratulina retusa (Linnaeus, 1758)
(Plate 1, Figs 5-6)

1758 *Anomia retusa*, Linnaeus, p. 701, no.191.
1983 *Terebratulina retusa* (Linnaeus) -Logan, p. 172.
1994 *Terebratulina retusa* (Linnaeus) -Taddei-Ruggiero, p. 209, pl. 2, figs 1-3.

Morphology. Shell biconvex, subpentagonal, longer than wide, slightly auriculate at hinge line. Anterior commissure uniplicate. Externally the valves have numerous, rather coarse, radial ribs,

with smooth rounded tubercules at the postero- lateral margins of both valves. Foramen large, mesothyrid with pedicle collar. The collected specimens reach about 1.1 cm in length and 0.8 cm in width.

Occurrence. Today, *T. retusa* has a wide geographical distribution. It lives in the eastern North Atlantic, eastern Greenland, off Iceland and Mediterranean (Alboran Sea to Greece). Its bathymetric range is from 15 to 450 meters in the Mediterranean (421 m in Greece), deeper in the Eastern Atlantic (15 to 1478 m, off the coast of the British Isles). In the bathyal zone it lives with *Gryphus vitreus* (Logan 1979).

It appeared in the Eocene and has been reported from the Pliocene and Pleistocene of Italy, (Gaetani and Sacca 1984, 1985, Taddei-Ruggiero 1994). In Rhodes, it has been also described from the Pleistocene deposits (Spanopoulou 1997).

In the Kolymbia limestone it has been found in samples 3 and 4 and it is probably coming from deeper water.

SUBORDER TEREBRATELLIDINA Muir-Wood, 1955
Superfamily KRAUSSINOIDEA Dall, 1870
Family Kraussinidae Dal, 1870
Genus *Megerlia* King, 1850
(Syn. Muhlfeldtia Batle, 1880)
Megerlia truncata (Linnaeus, 1767)
(Plate 1, Figs 7-8)

1767 *Anomia truncata*, Linné, p. 1152, no 229.
1927 *Muhlfeldtia truncata* (Linné) -Thomson, p. 226.
1979 *Megerlia truncata* (Linnaeus) -Logan, p. 68, tab. 9, figs 1-23.
1981 *Megerlia truncata* (Linné) -Cooper, p. 36, tab. 3, figs 5-11.

Morphology. Shell small, rounded, biconvex, wider than long. The anterior commissure is sulcate, brachial valve less convex than pedicle valve. Beak suberect, subtruncate, usually abraded. Foramen large, hypothyrid with pedicle collar. The collected specimens reach about 1.3 cm in length and 1.5 cm in width.

Occurrence. Today it is widely distributed in the Mediterranean and the North and East Atlantic, at depths of 15- 200 m. The individuals of *M. truncata* that live in shallow waters have cryptic habits, while the individuals that live in deeper waters exit from their hiding places and attached to small shells or gravels on the bottom of the sea (Logan 1979). In Greece it has been found at depths of 29 to 374 m.

Megerlia truncata appeared in the Miocene. In Crete island it was described by Georgiades-Dikeoulia (1974) from the middle Miocene of St. Asomati, where there had been found the varieties *serravallensis* and *sabata*. Also, Symeonides (1966) mentions *Muhlfeldtia truncata* from the Pliocene of the hill of Vigla, of the village Pachia Amos and Dermitzakis (1969) *Muhlfeldtia truncata* from the Pliocene of St. Haralambos, Peristera and Coutsounari.

In Rhodes, it has been also described from the Pleistocene deposits (Spanopoulou 1997).

Family Kraussinidae Dal, 1870
Genus *Pantellaria* Dall, 1919
Megerlia truncata* var. *monstruosa (Scacchi, 1838)
(Plate 2, Figs 1-2)

1891 *Muhlfeldtia monstruosa* (Scacchi) -Fischer and Oehlert, p. 87, pl. 7, figs 12 a-c.
1927 *Pantellaria monstruosa* (Scacchi) - Thomson, p. 228, figs 70 a-c.
1979 *Megerlia truncata* (Linnaeus) - Logan, p. 68, pl. 9, figs 20-23.
1981 *Pantellaria monstruosa* (Scacchi) - Cooper, p. 17, pl. 3, figs 16-18.

Morphology. Shell has almost smooth dorsal valve, where it has only distinct growth lines, often in clusters. Ventral valve ornamented with delicate radial ribs with nodulose crests. There are many different opinions about the taxonomic position of this taxa (see Logan 2004 and references herein). For the taxonomy I follow the opinion of Logan (1979) and Logan *et al.* (2004) which based on his observations and these of Davidson (1887) and Bitner (1990, 1993), regard *monstruosa* as a variety of *M. truncata* because the shape of the shell and the amphithyrid foramen is influenced by the angle of attachment to the substrate. The foramen is elongated to include the umbonal region of the dorsal valve. The collected specimens reach about 1cm in length and 1.5 cm in width.

Occurrence. The Recent *Megerlia truncata* var. *monstruosa,* in the Mediterranean lives on rocky substrates at depths of 36 to 553 m (Cooper 1981, Logan 1979). In the eastern Atlantic it has been found at depths of 400-2780 m.

Superfamily MEGATHYRIDOIDEA Dall, 1870
Family Megathyrididae Dall, 1870
Genus *Megathiris* d'Orbigny, 1847
Megathiris detruncata (Gmelin, 1790)
(Plate 2, Figs 3-4)

1790 *Anomia detruncata* Gmelin, p. 3347.
1979 *Megathiris detruncata* (Gmelin) -Logan, p.55-59, text-figs 15, 16, pl. 6, figs 1-13.
1985 *Megathiris detruncata* (Gmelin) -Gaetani and Sacca, p. 17, 18, pl. 9, figs 10-12, pl. 6, figs 1-7.
1994 *Megathiris detruncata* (Gmelin) -Taddei Ruggiero, p. 208, pl. 3, figs 6-9.
2003 *Megathiris detruncata* (Gmelin) –Bitner and Moissette, p. 473, fig. 6 (G,H).

Morphology. It is a micromorphic species with a biconvex shell, oval in outline, wide, straight hinge line, large triangular foramen and 10-14 broad ribs. The collected specimens are about 5 mm in length and 6 mm in width.

Occurrence. The Recent *M. detruncata* lives in the Mediterranean at depths of 20 to 160 m (Logan 1979). It also lives in the Lusitanian and Mauritanian regions of the Atlantic Ocean and in the Caribbean Sea (Logan 1983, 1988, 1993, Cooper 1977).

It is very common in the Miocene of the Paratethys (Bitner 1990) and the Pliocene of Italy (Gaetani and Sacca 1985, Taddei Ruggiero 1994) and it was described from the Pliocene of North Africa (Bitner and Moissette 2003). In Rhodes, it has been also mentioned from the Pliocene and described from the Pleistocene deposits by Spanopoulou (1997).

Family Megathyrididae Dall, 1870
Genus *Argyrotheca* Dall, 1900
(Syn. *Cistella* Gray, 1853)
Argyrotheca cordata (Risso, 1826)
(Plate 1, Figs 5-6)

1979 *Argyrotheca cordata* (Risso) -Logan, p.96, pl. 5, figs 1-12.
1994 *Argyrotheca cordata* (Risso) -Taddei Ruggiero, p. 211, pl.3, figs 1-2.
2004 *Argyrotheca cordata* (Risso, 1826) –Bitner and Kaim, p. 197, Tab. 2, figs 2D-K, 3A-E.

Morphology. Two complete and a lot of fragmented specimens. It is small, thin-shelled, subtriangular in outline, smooth covered with almost imperceptible ribs. The anterior commissure is slightly sulcate with a shallow sulcus present in both valves. The sizes of the shell reach the 2 mm in length and 2 mm in width.

Occurrence. As a fossil *A. cordata* is known from the Miocene throughout Europe and from the Pliocene of Italy and Spain. Today it is living in the Mediterranean Sea and the Mauritanian region

of the Atlantic Ocean (see Bitner 1990). It is living in the infra-circallitoral zone no deeper than 100 m and belongs to the "shallow water" group of brachiopods in the Mediterranean sea (Logan 1979). Asgaard and Bromley (1991) confirm the cryptic mode of life of *A. cordata* in shallow water.

SUBPHYLUM CRANIFORMEA
CLASS CRANIATA
ORDER CRANIIDA Waagen, 1885
SUBORDER CRANIIDINA Waagen, 1885
Superfamily CRANIOIDEA Menke, 1828
Family Craniidae Menke, 1828
Genus *Novocrania* Lee and Brunton, 2001
***Novocrania anomala* (Müller, 1776)**
(Plate 1, Figs 7-8)

1888 *Crania turbinata* (Poli) -Davidson, p. 188, pl. 27, figs. 14-23
1981 *Crania anomala turbinata* (Poli) -Cooper, p. 211, pl. 1, fig. 26
1986 *Neocrania anomala* (Muller) -Lee and Brunton, p. 150, figs 32-37.
2001 *Novocrania anomala* (Muller) -Lee and Brunton, p. 5

Morphology. Only the dorsal valve is available for examination. It is roundly elliptical, with conical profile, smooth, exterior ornamented only by concentric growth lines. Its shape is often determined by the shape of its host. The collected specimens are about 4 mm in length and 4.9 mm in width.

Occurrence. N. anomala is recorded from the Middle Miocene of Poland (Popiel-Barczyk and Barczyk 1990), the Pliocene and Pleistocene of Italy (Taddei Ruggiero, 1994) and is still living. It is epifaunal attached to hard substrates, living from the low tide limit in low intensity light (caves), to the bathyal zone.

Today in the Mediterranean it lives at depths from 3 to more than 300 m. It is associated with *Gryphus vitreus* on hard substrates at depths of 120 m to more than 1000 m (Logan 1979, Logan *et al.* 2004).

3.2. Paleoecology

The distribution of brachiopods depends on many factors as the type of substrate, hydrodynamics, temperature and salinity (Emig 1988). They should thus be used with caution as palaeobathymetric indicators (Fisher and Oehlert 1891, Logan 1993).

Steinthorsdottir *et al.* (2006), have given the paleobathymetry of Kolymbia limestone deposits according to which "the limestone comprises two parasequences in a transgressive systems tract and deposition occurred at paleodepths between 30 and 120 m".

These paleobathymetric data are reinforced by the study of the brachiopod and other faunas in each coarser horizon:

The dominance of *Ostrea lamellosa* in the sample 1 at the bottom of the section, indicates an environment of the littoral zone, rich in oxygen and with high turbulence, as this species is attached and generally forms asymmetrical banks in this zone (Pouyet 1984, Ben Moussa 1994). The simultaneous presence of the micromorph brachiopod fauna of *Argyrotheca cordata, Megerlia truncata,* along with the presence of *Megathiris detruncata*, indicates a very shallow-water and high energy environment (Laurain 1984, Asgaard and Bromley 1991).

In sample 2 the presence of *Celleporaria palmata* points to a depth of 30-50 m (Spjeldnaes and Moissette 1997, Steinthorsdottir *et al.* 2006). In this bed *Gryphus* sp. and *Megerlia truncata* var. *monstruosa,* have been found in situ, with transported rhodoliths.

Plate 1 - Figs 1, 2, 3, 4. -*Gryphus* sp. posterior, posterior, lateral and latero-dorsal views.
Figs 5, 6. -*Terebratulina retusa* (Linnaeus) dorsal and ventral views.
Figs 7, 8. -*Megerlia truncata* (Linnaeus) dorsal and ventral views

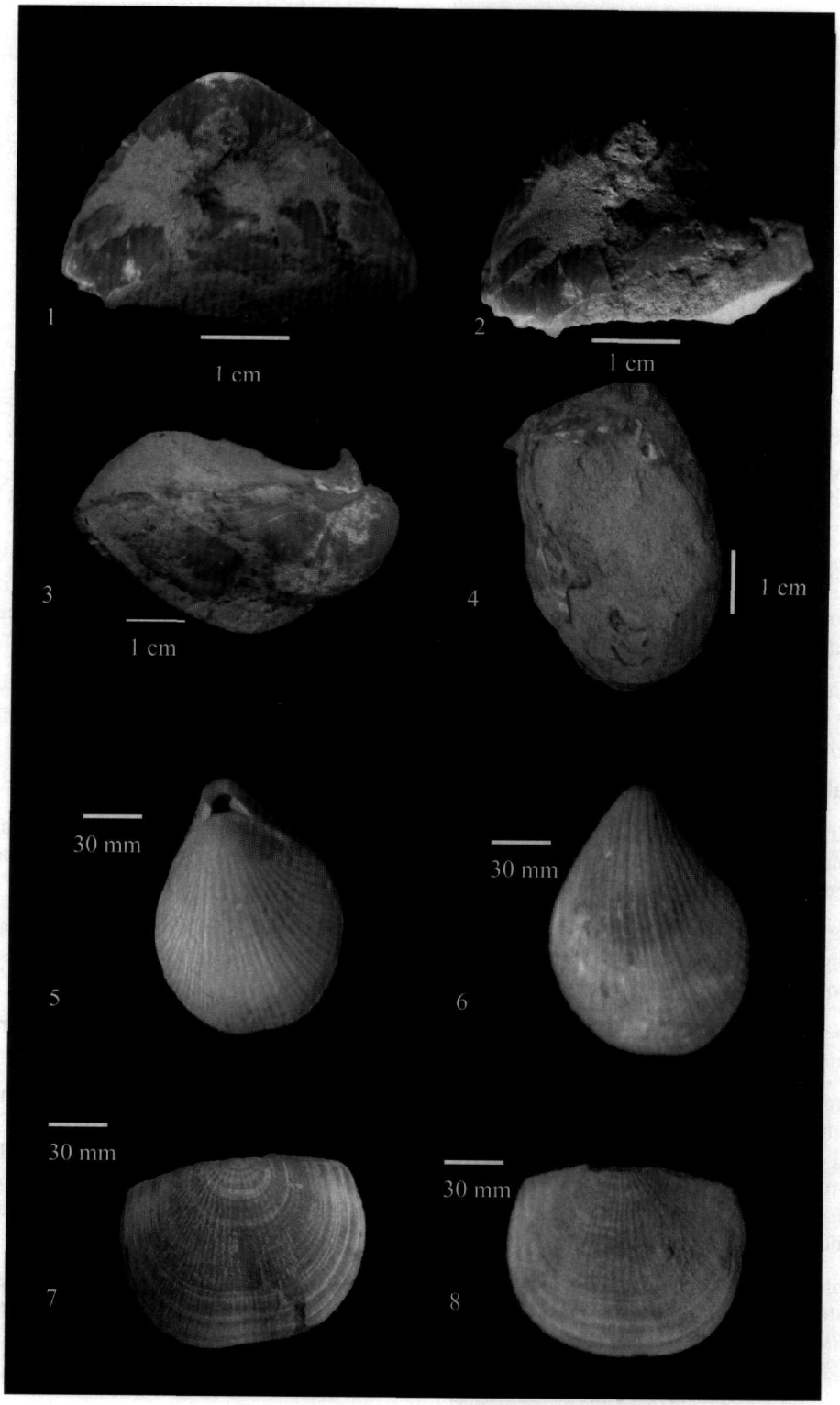

In samples 3 and 4 the association of *Gryphus* sp., *Terebratulina retusa* and *Novocrania anomala* points to a depth of more than 120 m of moderate energy (Logan 1979, Logan *et al.* 2004, Emig 1989a, b). Sample 4 according to Steinthorsdottir *et al.* (2006) represents a tectonic or storm event where fauna mixing dominates and *Gryphus* is coming from deeper water.

Sample 5 resembles sample 2 by its the fauna content.

4. Conclusions

The Pliocene brachiopod assemblages identified in this study have similar composition to some Recent assemblages of the Mediterranean Sea.

For the first time *Megerlia truncata* var. *monstruosa,* is recorded from the Pliocene of Greece and *Megerlia truncata* from the Pliocene of Rhodes. *Megathiris detruncata*, *Terebratulina retusa* and *Argyrotheca cordata* have been first described from the Pliocene of Rhodes. Also the species *Novocrania anomala* and *Gryphus* sp. are described and *Gryphus vitreus* of Steinthorsdottir *et al.* (2006) is discussed to be revised.

The three micromorph species of brachiopods *Argyrotheca cordata, Megerlia truncata* and *Megathiris detruncata,* are present in the assemblage of the sandy, lower part of the Cape Vagia section. This indicates a shallow-water and high-energy littoral environment.

In accordance with previous sedimentological and paleoecological studies based on bryozoans (Spjeldnaes and Moissette 1997, Steinthorsdottir *et al.* 2006), the associations of *Gryphus* sp. and *Megerlia truncata* var. *monstruosa,* and of *Gryphus* sp., *Terebratulina retusa* and *Novocrania anomala*, are interpreted as indicating depths of 30-50 and more than 120 m respectively.

5. Acknowledgements

The author is grateful to Pierre Moissette (University of Lyon 1) for his collaboration during field work. The critical comments and useful suggestions made by Aleksandra Bitner and Pierre Moissette and the help provided by Daphne Lee, were greatly appreciated. Thanks are due to Dimitri Velitzelos for his help with the macrophotographs and the technician Evangelos Michailides for his help during SEM observations. Financial support for this study was provided by Research Project 70/4/5849 of the University of Athens.

6. References

Asgaard, U., and Bromley, R.G., 1991. Colonization by micromorph brachiopods in the shallow subtidal of the Eastern Mediterranean Sea. In D.I. MacKinnon, D.E. Lee and J.D. Campell (eds). Brachiopods through time, 261-269, *Proc. 2nd Int. Brachiopods Congr.* University of Otago, New Zealand, 5-9 February, 1990.

Benda, L., Meulenkamp, J.E., and van de Weerd, A., 1977. Biostratigraphic correlations in the Eastern Mediterranean Neogene. 3. Correlation between mammal, sporomorph and marine microfossil assemblages from the Upper Cenozoic of Rhodos, Greece, *Newsletters on Stratigraphy*, 6, 117-130.

Ben Moussa, A., 1994. Les bivalves Néogènes du Maroc septentrional (façades Atlantique et Méditerranéenne). Biostratigraphie, paléobiogéographie et paléoécologie, *Docum. Lab. Géol. Lyon,* 132, 281.

Bitner, M.A., 1990. Middle Miocene (Badenian) brachiopods from the Roztocze Hills, south–eastern Poland, *Acta Geologica Polonica,* 40, 139–157.

Bitner, M. A., and Martinell, J. 2001. Pliocene brachiopods from the Estepona Area (Malaga, South Spain), *Revista Espapola de Paleontologia,* 16, 177-185.

Plate 2 - Figs 1, 2. -*Megerlia truncata* var. *monstruosa* ventral and dorsal views.
Figs 3, 4. -*Megathiris detruncata* (Gmelin) ventral and dorsal views.
Figs 5, 6. -*Argyrotheca cordata* (Risso) dorsal and ventral views.
Figs 7, 8. -*Novocrania anomala* (Müller) outerl and inner of the dorsal valve.

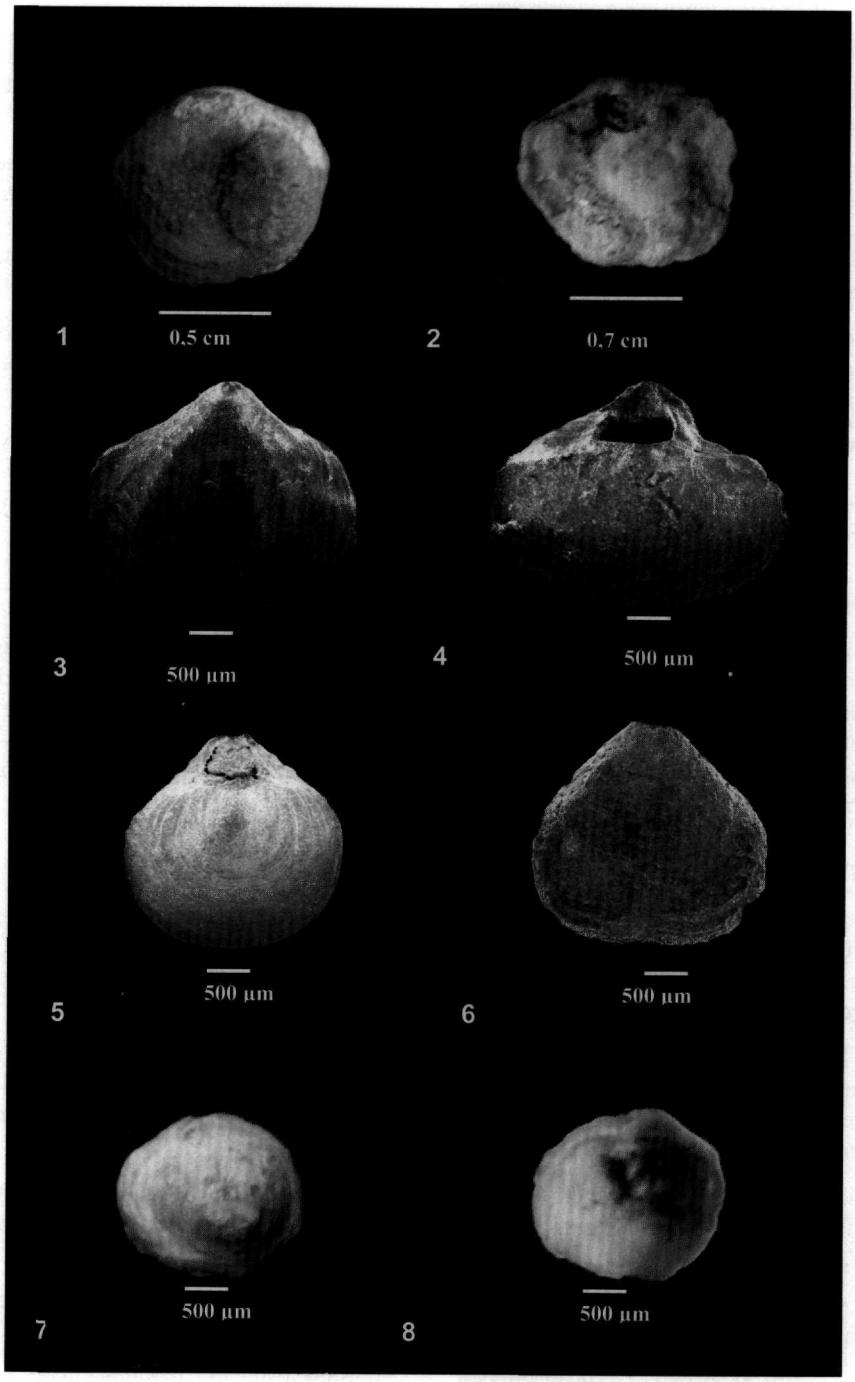

Bitner, M. A., and Moissette, P., 2003. Pliocene brachiopods from north-western Africa, *Geodiversitas,* 25 (3), 463-479.

Bitner, M. A., and Kaim, A., 2004. The Miocene brachiopods from the silty facies of the intra-Carpathian Nowy Sącz Basin (Poland), *Geological Quarterly*, 48 (2), 193–198.

Bukowski, G. V., 1899. Geologische Uebersichtkarte der insel Rhodus, *Jahrb. K. K. Geol. Reichsanst.*, 4, 517-688.

Cooper, G. A., 1977. Brachiopods from the Caribbean Sea and adjacent waters, *Studies in Tropical Oceanography,* 14, 1-211.

Cooper, G.A., 1981. Brachiopoda from the Gulf of Gascogne, France (Recent). *Smithson. Contrib. Paleobiol.,* 44, i-iv, 1-35.

Cornée, J.J., Moissette, P., Joannin, S., Suc, J.P., Quillévéré, F., Krijgsman, W., Hilgen, E., Koskeridou, E., Münch, P., Lécuyer, C., and Desvignes, P., 2006. Tectonic and climatic controls on coastal sedimentation: the Late Pliocene-Middle Pleistocene of northeastern Rhodes Greece, *Sedimentary Geology*, 187, 159-181.

Cornée, J.J., Münch, P., Quillévéré, F., Moissette, P., Vasiliev, I., Krijgsman, W., Verati, C., and Lécuyer, C., 2006b. Timing of Late Pliocene to Middle Pleistocene tectonic events in Rhodes (Greece) inferred from magneto-biostratigraphy and $^{40}Ar/^{39}Ar$ dating of a volcaniclastic layer, *Earth and Planetary Science Letters*, 250, 281–291.

Davidson, T., 1886-1888. A monograph of Recent Brachiopoda, *Linnean Soc. London, Trans.*, ser. 2, 4, 1-248.

Dermitzakis, M., 1969. Geological researches on the Neogene of Ierapetra province of Crete island, *Annales Géologiques des Pays Helléniques,* 1, XXI, 342pp.

Emig, C.C., 1988. Les Brachiopodes actuels sont-ils des indicateurs (paleo) bathymétriques? *Géologie méditerranéenne,* 15(1), 65-71.

Emig, C.C., 1989a. Distribution bathymétrique et spatiale des populations de *Gryphus vitreus* (brachiopode) sur la marge continentale (Nord-Ouest Méditerranée), *Oceanol. Acta,* 12, 205-209.

Emig, C.C., 1989b. Distributional patterns along the Mediterranean continental margin (upper bathyal) using *Gryphus vitreus* (Brachiopoda) densities, *Palaegeography, Palaeoclimatology, Palaeoecology*, 71, 253–256

Fisher, P., and Oehlert, D. P., 1891. *Brachiopodes. Expéditions scientifiques du « Travailleur » et du « Talisman » pendant les années 1880, 1881, 1882, 1883.* Masson, Paris, 140pp.

Gaetani, M., and Sacca, D., 1984. Brachiopodi batiali nel Pliocene e Pleistocene di Sicilia e Calabria, *Rivista Italiana di Paleontologia e Stratigrafia,* 90, 407-458.

Gaetani, M., and Sacca, D., 1985. Brachiopodi neogenici e pleistocenici della provincia di Messina e della Calabria meridionale, *Geologica Romana,* 22 (1983), 1-43.

Georgiades-Dikeoulia, E., 1974. Les Brachiopodes du Miocène moyen de l' ile de Crete (Hangii Assomati, Rethymnos), *Annales Géologiques des Pays Helléniques,* 26, 159-185.

Gmelin, J.F., 1790. Systema naturae, sive Regna tria Naturae systematice proposita per classes, ordines, genera et species, *Regnum animale,* 13 ed., Stockholm, 3021-3910.

Hanken, N. M., Bromley, R.G., and Miller, J., 1996. Plio-Pleistocene sedimentation in coastal grabens, north-east Rhodes, Greece, *Geological Journal*, 31, 271-296.

Hedenborg, J., 1837. (On the Tertiary formations on the Island of Rhodes): Skandia, 10, 238-260.

Keraudren, B., 1970. Les formations quaternaires marines de la Grèce, *Bulletin du Musée d'Anthropologie Préhistorique de Monaco*, 6, 5-153.

Laurain, M., (1984) Bivalves Ostréidés. In: Pouyet S (ed) La faune du faciès "Marnes Bleues", Burdigalien du bassin de Faucon-Mollans-Malaucène (sud-est de la France), *Nouv. Arch. Mus. d'Hist. Nat. Lyon*, 22, 74–78.

Lee, D.E., and Brunton, C.H.C., 1986. *Neocrania* n. gen., and a revision of Cretaceous-Recent brachiopod genera in the family Craniidae, *Bull. Br. Mus. Nat. Hist. (Geol.)*, 40 (4), 141-160.

Lee, D.E., and Brunton, C.H.C., 2001. *Novocrania*, a new name for the genus *Neocrania* Lee and Brunton, 1986 (Brachiopoda, Craniida), preoccupied by *Neocrania* Davis, 1978 (Insecta, Lepidoptera), *Bulletin of the Natural History Museum* (Geology Series), 57(1), 5.

Linnaeus, C., 1758-1767. *Systema Naturae*, 10th ed., Holmiae, 823 pp.

Logan, A., 1979. The Recent Brachiopoda of the Mediterranean Sea, *Bulletin de l'Institut océanographique de Monaco,* 72, 1-112.

Logan, A., 1983. Brachiopoda collected by CANCAP I-III expeditions to the south-east North Atlantic. 1976-1978, *Zoologische Mededelingen Leiden,* 57, 165-189.

Logan, A., 1988. Brachiopoda collected by CANCAP IV and VI expeditions to the south-east North Atlantic. 1980-1982. *Zoologische Mededelingen Leiden,* 62, 59-74.

Logan, A., 1993. Recent brachiopods from the Canarian-Cape Verdean region: Diversity, biogeographic affinities, bathymetric range and life habits, *Courier Forschungsinstitut Senckenberg,* 159, 229-233.

Logan, A., Bianchi, C.N., Morri, C., and Zibrowius, H., 2004. The present-day Mediterranean brachiopod fauna: diversity, life habits, biogeography and paleobiogeography, *Scientia Marina*, 68 (1), 163–170.

Løvlie, R., Støle, G., and Spjeldnaes, N., 1989. Magnetic polarity stratigraphy of Pliocene-Pleistocene marine sediments from Rhodos, eastern Mediterranean, *Physics of the Earth and Planetary Interiors,* 54, 340-352.

Meulenkamp, J.E., De Mulder, E.F.J., and Van De Weerd, A., 1972. Sedimentary history and paleogeography of the Late Cenozoic of the Island of Rhodos, *Zeitschrift der Deutschen Geologischen Gesellschaft*, 123, 541-553.

Moissette, P., and Spjeldnaes, N., 1995. Plio-Pleistocene deep-water bryozoans from Rhodes, Greece, *Palaeontology*, 38, 771-799.

Moissette, P., Koskeridou, E., Cornée, J.J., Guillocheau, F., and Lécuyer, C., in press. Spectacular preservation of seagrasses and seagrass-associated communities from the Pliocene of Rhodes, Greece, *Palaios*.

Mutti, E., Orombelli, G., and Pozzi, R., 1970a. Geological map of Rhodes Island (Greece), *Annales Géologiques des Pays Helléniques*, 22.

Mutti, E., Orombelli, G., and Pozzi, R., 1970b. Geological studies on the Dodecanese Islands (Aegean Sea). IX. Geological map of the island of Rhodes (Greece); explanatory notes., *Annales Géologiques des Pays Helléniques*, 22, 79-226.

Pirazzoli, P.A., Montaggioni, L.F., Thommeret, J., Thommeret, Y., and Laborel, J., 1983. Sur les lignes de rivage et la neotectonique a Rhodes (Grece) a l'Holocene, *Ann. Inst. Océanogr.,* 58, 89–102.

Pirazzoli, P.A., Montaggioni, L.F., Saliege, J.F., Segonzac, G., Thommeret, Y., and Vergnaud-Grazzini, C., 1989. Crustal block movements from Holocene shorelines: Rhodes Island (Greece), *Tectonophysics*, 170, 89-114.

Popiel-Barczyk, E., and Barczyk, W., 1990. Middle Miocene (Badenian) brachiopods from the southern slopes of the Holy Cross Mountains, Central Poland, *Acta Geol. Pol.,* 40 (3-4), 159-181.

Pouyet, S., 1984. La faune du faciès "Marnes bleues". Burdigalien du bassin de Faucon-Mollans-Malaucène (Sud-Est de la France), *Nouvelles Archives du Museum d'Histoire Naturelle de Lyon*, 22, 51-123.

Sissingh, W., 1972. Late Cenozoic Ostracoda of the South Aegean Island Arc, *Utrecht Micropaleontological Bulletins*, 6, 1-187.

Spanopoulou, A., 1997. The Plio-Pleistocene Brachiopods of Rhodes island, *Unpublished Master thesis*, University of Athens. 287pp.

Spjeldnaes, N., and Moissette, P., 1997. Celleporid (bryozoan) thickets from the Upper Pliocene of the island of Rhodes, Greece. In N.P. James and J.A.D. Clarke (eds), *Cool-Water Carbonates*, *SEPM* Spec. Publ., 56, 263–270pp.

Steinthorsdottir, M., Lidgard, S., and Hakansson, E., 2006. Fossils, sediments, tectonics. Reconstructing palaeoenvironments in a Pliocene-Pleistocene Mediterranean microbasin, *Facies*, 52, 361-380.

Symeonides, N., 1966. The Neogene of eastern Crete, *Annales Géologiques des Pays Helléniques,* 1, XVI, 249 pp.

Taddei-Ruggiero, E., 1994. Neogene Salento brachiopod palaeocommunities, *Bollettino della Societa Paleontologica Italiana,* 33, 197-213.

Thomsen, E., Rasmussen, T.L., and Hastrup, A., 2001. Calcareous nannofossil, ostracode and foraminifera biostratigraphy of Plio-Pleistocene deposits, Rhodes (Greece), with a correlation to the Vrica section (Italy), *Journal of Micropalaeontology*, 20, 143-154.

Thomson, J.A., 1927. Brachiopod morphology and genera (Recent and Tertiary), *New Zealand Board Science and Art, Manual,* 7, 338 pp.

Williams, A., Carlson, S. J., Brunton, C. H. C., Holmer, L. E., and Popov, L. 1996. A supraordinal classification of the Brachiopoda. *Philosophical Transactions of the Royal Society of London,* B, 351, 171-1193.

Zezina, O.N., 1985. Living brachiopods and problems of the bathyal zone in the oceans, *Akademiia Nauk. SSSR*, 247 pp.

Δελτίο της Ελληνικής Γεωλογικής Εταιρίας τομ. XXXX, 2007
Πρακτικά 11ου Διεθνούς Συνεδρίου, Αθήνα, Μάιος 2007

Bulletin of the Geological Society of Greece vol. XXXX, 2007
Proceedings of the 11th International Congress, Athens, May, 2007

SIMILARITY RELATIONSHIPS AMONG GREEK MIDDLE MIOCENE TO EARLY - MIDDLE PLEISTOCENE MAMMAL ASSEMBLAGES

Kostopoulos D. S.[1], and Koufos G. D.[1]

[1] *Aristotle University of Thessaloniki, Faculty of Geology, Laboratory of Geology & Paleontology, dkostop@geo.auth.gr, koufos@geo.auth.gr*

Abstract

The Greek fossil record of small and large mammal Local Faunal Assemblages is studied and compared by means of cluster analysis techniques using Jaccard similarity index and unweighted pair-group method. The analysis allow recognizing a good arrangement of the Greek LFAs according to time and a main cluster gap, corresponding to an important faunal renewal that, however, is not synchronous in the large and small mammal community. Minor groupings of large mammal faunas seem also to fit with main climatic trends, whereas the small mammal assemblage appears to undergo longer periods of taxonomic stability.
Key words: *Mammal Faunas, Greece, Biochronology, Neogene-Quaternary.*

Περίληψη

Το Ελληνικό αρχείο Τοπικών Πανιδικών Συνόλων (LFAs) θηλαστικών μελετάται και συγκρίνεται υπό όρους ιεραρχικής ανάλυσης, χρησιμοποιώντας τον δείκτη ομοιότητας Jaccard και τη μέθοδο unweighted pair-group. Η ανεξάρτητη ανάλυση των πανίδων μικρών και μεγάλων θηλαστικών παρουσιάζει καλή χρονολογική ταξινόμηση των ελληνικών LFAs και εμφανίζει, και στις δύο περιπτώσεις, μία βασική ομαδοποίηση σε δύο υποσύνολα. Το παρατηρούμενο διάκενο ερμηνεύεται ως μια σημαντική ανανέωση των δύο πανιδικών συνόλων, η οποία, όμως, δεν εμφανίζεται συγχρόνως στις κοινότητες των μικρών και μεγάλων θηλαστικών. Μικρότερες ομαδοποιήσεις μεταξύ των μεγάλων θηλαστικών φαίνεται να ανταποκρίνονται σε γενικές κλιματικές τάσεις, ενώ το πανιδικό σύνολο των μικρών θηλαστικών εμφανίζεται να διάγει μακρύτερες περιόδους ταξινομικής σταθερότητας.
Λέξεις κλειδιά: *Πανίδες Θηλαστικών, Ελλάδα,, Βιοχρονολογία, Νεογενές-Τεταρτογενές.*

1. Introduction

The Greek Neogene/Quaternary continental record exhibits an important archive of fossil mammal assemblages spanning in time from the middle Miocene up to the late Pleistocene. In the absence of any particular (i.e., local) biochronological/biostratigraphical scheme, both large and small mammal faunas from Greece are usually referred to the well established West European scales, such as the European Mammal Neogene System (MN) of Mein (1975, 1990) and its Quaternary supplements by Guerin (1982, 1990), the Italian Faunal Units (FU) of Gliozzi *et al.* (1997) or the Spanish succession of biozones and continental stages (Agusti *et al.* 2001). Nevertheless, there is

no work till now analyzing the entire Greek biochronological succession of either large or small mammal faunas neither their possible interrelationships.

As each Local Faunal Assemblage (LFA) is a partial record of a particular homogeneous fauna, lived during a definite time span (otherwise of a biochronological unit), multivariate techniques have been proved an efficient tool in the quantification of similarities among LFAs, which could consequently allow the recognition of sequences of non-overlapping and ecologically adjusted assemblages of taxa, living together in a given time and space (Alberdi *et al.* 1997, Azanza *et al.* 2003, Palombo *et al.* 2003, 2006 and literature therein). And in *vice versa*, discontinuities between these "zones" of taxonomical homogeneity might reflect faunal reconstructions through time droved by environmental changes, or structural changes droved by geographical barriers.

The basic aim of this work is to analyse the Greek middle Miocene to early-middle Pleistocene faunal successions of both the large and small mammal assemblages and to contrast their patterns either with the established biochronological schemes, as well as between them with respect to ecological and geographical factors.

2. Materials and Methods

The most important Greek fossil mammalian taxa-gatherings, representing Local Faunal Assemblages (LFAs) of middle Miocene (MN4) to early-middle Pleistocene (MNQ20/21) age have been chosen. Excluding mammal assemblages with less than 3 taxa identified at species level, the case study finally includes 53 large-mammal LFAs and 46 small-mammal LFAs. As a total 99 LFAs were analyzed. The faunal lists used in the analysis are published by Bonis & Koufos (1999), Koufos & Kostopoulos (1997), and Koufos (2001, 2006) with up-to-date records, personal observations and critical reviews. In order to standardize the taxonomy and to increase the taxonomical confidence, forms originally identified as "*conformis*" and "*affinis*" were included within the nominated taxon. Uncertain taxonomical forms (e.g., Bovidae indet., ?Mimomys etc.) were excluded, whereas forms referred to as "sp." were measured as distinct species. 232 species of large mammals and 230 species of small mammals were considered in the analysis. The initial locality-by-taxa datasets are compiled in two "presence/absence" matrices: one for the large and another one for the small mammals. The presence of a taxon in a LFA was coded "1". Both matrices are available on request.

Following previous works (Alberdi *et al.* 1997, Azanza *et al.* 2003, Palombo and Valli, 2004, 2005, Palombo *et al.* 2006) we evaluated similarities among LFAs on the basis of Jaccard binary coefficient (Shi, 1993), performing cluster analysis at species level using unweighted pair-group (UPGMA) method (PAST statistical package, Hammer *et al.* 2001, Hammer & Harper 2006).

3. Results

3.1. Similarities among large mammal LFAs

The Q-mode dendrogram resulting from the clustering of similarities at species level (Fig. 1) divides the large mammal faunas in two main groups, leaving the earliest (early MN4) and poorly known assemblage of Aliveri distantly related to them. The main split reveals a major separation between the middle Miocene to early Pliocene LFAs (Cluster A) from the one hand and the middle Pliocene to early-middle Pleistocene LFAs (Cluster B) from the other. Thus, it appears that the most important break in the faunal composition of the large mammal community occurs at the beginning of Pliocene and not at the Mio-Pliocene boundary, as it would be expected.

The first cluster A includes two main subclusters A1and A2, from which A2 is further divided in two groups A2.1 and A2.2 (Fig. 1). A1 is weakly related to the rest of Cluster A and groups together Thymiana B (MN5) and Antonios (MN4/5) on the basis of the common presence of *Sanitherium slangintweiti* and *Dorcatherium peneckei*. In any case, the serious gap of MN5 to MN9

large mammal faunas certainly obscures the results. Apart from the scanty large mammal assemblage of Kastellios (MN9), A2 groups together the LFAs of late Miocene (A2.1) and early Pliocene (A2.2) age. The latest Miocene (late MN13) LFA of Maramena already shows a separation from the main late Miocene subcluster (A2.1) probably indicating a transitional condition toward A2.2, which is characterized by the association *Sus minor* + *Hipparion* ex. gr. *longipes* or *crassum*.

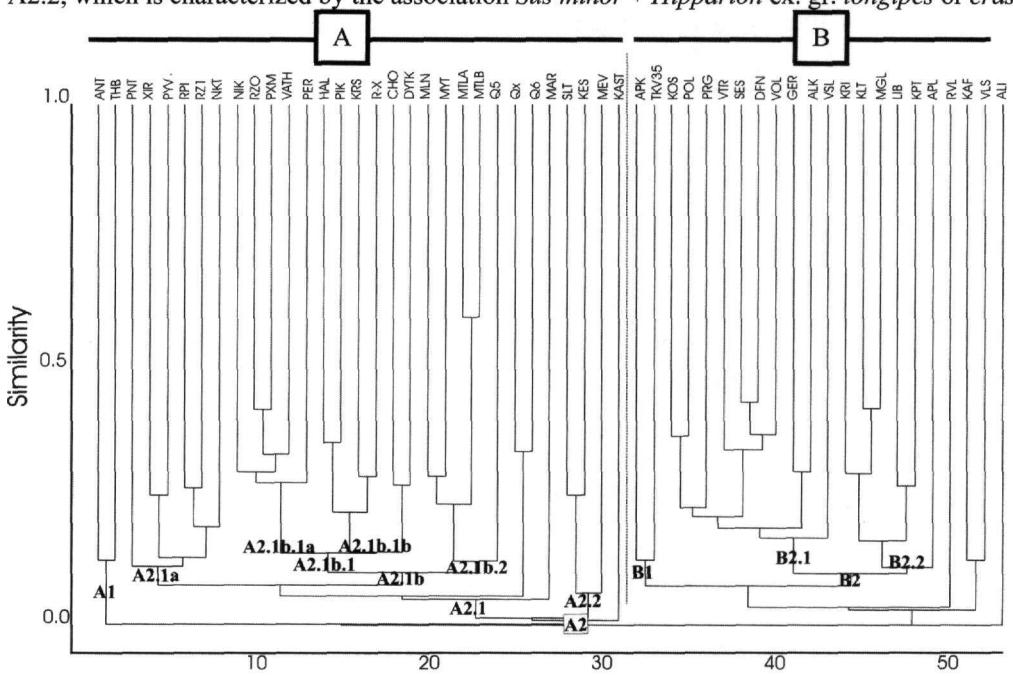

Figure 1 - Q mode dendrogram of 53 Greek large mammal faunas (LFAs). Cophenetic correlation: 0.89

Abbreviations: Aliveri (ALI); Antonios (ANT); Thymiana B (THB); Pentalophos (PNT); Xirochori (XIR); Pyrgos Vassilisis (PYV); Ravin de la Pluie (RPl); Ravin des Zouaves 1 (RZ1); Nikiti-1 (NKT); Nikiti-2 (NIK); Ravin des Zouaves 5 (RZO); Prochoma (PXM); Vathylakkos 1, 2, 3 (VATH); Perivolaki (PER); Halmyropotamos (HAL); Pikermi (PIK); Kerassia (KRS); Ravin X (RX); Chomateres (CHO); Dytiko 1, 2, 3 (DYTK); Mytilinii 4-Samos (MLN); Mytilinii 3-Samos (MYT); Mytilinii 1A (MTLA); Mytilinii 1B (MTLB); Quarry 5-Samos (Q5); Quarry X-Samos (Qx); Quarry 6-Samos (Q6); Maramena (MAR); Silata (SLT); Kessani 1,2 (KES); Megalo Emvolo (MEV); Kastelios-Crete (KAST); Apolakkia (APK); Tourkovounia 3-5 (TKV35); Kos Island (KOS); Polylakkos (POL); Pyrgos (PRG); Vatera (VTR); Sesklo (SES); Dafnero (DFN); Volakas (VOL); Gerakarou (GER); Alikes (ALK); Vassiloudi (VSL); Krimni (KRI): Kalamoto (KLT); Megalopolis (MGL); Libakos (LIB); Kapetanios (KPT); Apollonia (APL); Ravine of Voulgarakis (RVL); Kaiafas (KAF); Volos (VLS)

A2.1 is further divided in two prime subclusters A2.1a and A2.1b with clear chronological meaning. A2.1a gathers late Vallesian (MN9/10, MN10) LFAs with typical faunal association *Ouranopithecus macedoniensis* + *Hipparion macedonicum* + *Samotragus praecursor*, whereas A2.1b subcluster unites Turolian faunas (MN11-13). Inside A2.1b there are also two groups of LFAs. The first one A2.1b.1 includes the MN11-13 LFAs of continental Greece, further segregated chronologically into two subclusters, A2.1b.1a grouping only MN11 assemblages (*Adcrocuta eximia* + *Plioviverops obrigni* + *Hipparion dietrichi* + *Gazella pilgrimi* + *Nisidorcas planicornis* + *Tragoportax rugosifrons*) and A2.1b.1b grouping the MN12-13 assemblages (*Ceratotherium neumayri* + *Hipparion mediterraneum* + *Pliocervus pentelicus* + *Tragoportax amalthaea*), whereas the A2.1b.2 subcluster includes exclusively MN12-MN13 LFAs from Samos (*Hipparion dietrichi* + *Hipparion* ex gr. *forstenae* + *Hipparion brachypus* + *Pachytragus laticeps/crassicornis* + *Samotherium boissieri/major*). This geographical separation is probably strengthened by the isolated placement of the late MN11 assemblages from Samos (Qx and Q6) in to A2.1 subcluster

with typical faunal association: *Samotherium boissieri* + *Criotherium argalioides* + *Majoreas woodwardi*.

Apart from the poor large mammal assemblages of Ravin of Voulgarakis (RVL, MNQ20), Volos (VLS, MNQ20) and Kaiafas (KAF, MNQ20), the second cluster B is separated in two main subclusters B1 and B2 (Fig. 1). B1 unites Appolakia (APK) and Tourkovounia 3-5 (TKV35) both of rather MN 16 age, whereas B2 is further divided in two subclusters. B2.1 includes the middle-late Pliocene to earliest Pleistocene (MNQ17-MNQ19) LFAs and it is characterized by the faunal association: *Mammuthus meridionalis* + *Equus stenonis* + *Eucladoceros ctenoides* + *Metacervocerus rhenanus* + *Gazellospira torticornis* + *Gazella bouvrainae* + *Leptobos* ex. gr. *etruscus*. B2.2 subcluster unites the early to early-middle Pleistocene LFAs with typical faunal association *Canis* ex. gr. *mosbachensis* + *Mammuthus meridionalis* + *Stephanorhinus etruscus* + *Equus stenonis* (last stage) + *Hippopotamus antiquus* + *Praemegaceros pliotarandoides/verticornis* + *Eobison*.

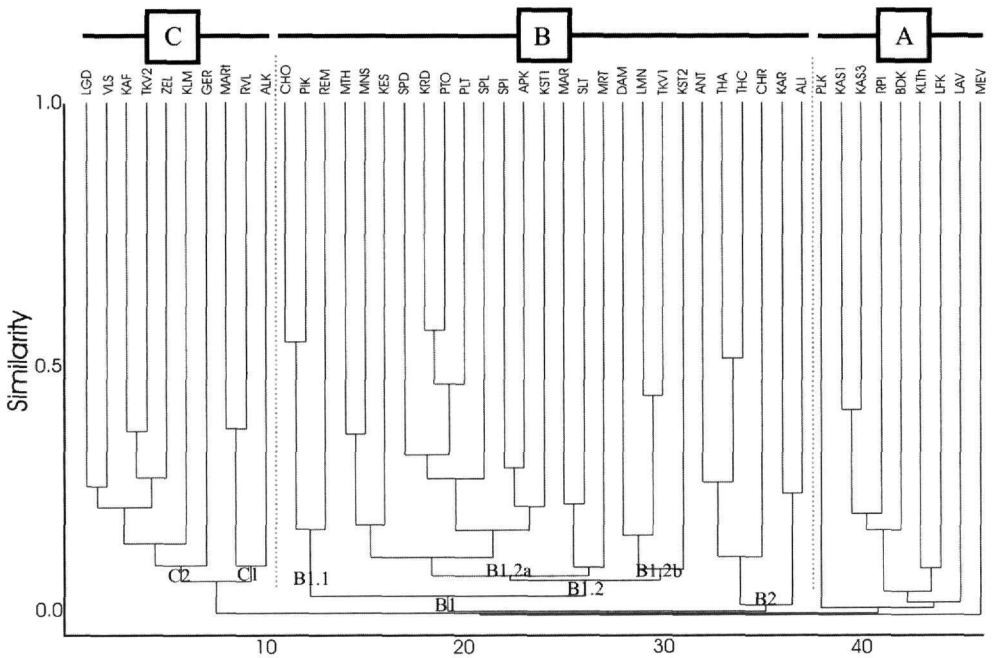

Figure 2 - Q mode dendrogram of 46 Greek small mammal faunas (LFAs). Cophenetic correlation: 0.91

Abbreviations as in Fig. 1 and: Thymiana A (THA); Thymiana C (THC); Chrysavgi (CHR); Karydia I+II (KAR); Plakia (PLK); Kastellios K1 (KAS1); Kastellios K3 (KAS3); Biodrak (BDK); Kalithies (KLTh); Lefkos (LFK); Lava 2 (LAV); Rema Marmara (REM); Ano Metochi 2,3 (MTH); Monasteri (MNS); Spilia 0 (SPD); Kardia (KRD); Ptolemais 1 (PTO); Ptolemais 3 (PLT); Spilia 1 (SPL); Spilia 3,4 (SPI); Kastoria 1 (KST1); Kastoria 2 (KST2); Maritses (MRT); Damartia (DAM); Limni 6 (LMN); Tourkovounia 1 (TKV1); Tourkovounia 2 (TKV2) Lagada (LGD); Kalymnos (KLM); Marathousa (MARt); Zeli (ZEL)

3.2. Similarities among small mammal LFAs

In the species Q-dendrogram of Greek small mammal sites, the LFAs are segregated into three main clusters A, B and C (Fig. 2), whereas the locality of Megalo Emvolo appears as an outlier, evidently because of its extremely poor and specialized small mammal fauna. Unexpectedly, the MN10 LFAs (including the uncertainly dated locality of Kalithies - KLTh) together with some aliens such as Plakia- PLK (MN7-8) and Lava 2 –LAV (MN13) form a separate group (cluster A; Fig. 2) that is distantly related to the main body of Mio-Pliocene faunas (cluster B). Although the

reasons of this situation are not clear, the absence of MN6-MN9 faunas might once again affect the results. The misplacement of Lava 2 (LAV) within cluster A is due to *Leptodontomys catalannicus* present in Lava-2 and Biodrak (BDK; MN10) but the species seems to have a wider distribution, being also present in the late MN 13 locality of Maramena (MAR). Excluding problematic LFAs from the analysis the typical faunal association of cluster A appears to be *Progonomys cathalai* + *Byzantinia* ex. gr. *nikosi* + *Spermophylinus* ex. gr. *bredai.*

Cluster B is divided in two main subclusters (Fig. 2): B1 unites the MN12 to MN16 LFAs plus Kastoria 2 (MNQ18) and B2 unites the MN 4-5 plus Chrysavgi (CHR, MN7-8). Interestingly the only known MN7-8 Greek faunas of Chrysavgi and Plakia (PLK) do not share any taxon. Nevertheless the affiliation of CHR to the group of MN4/5 (B2) faunas is certainly fictitious, as it is based on the common presence of *Schizogalerix* sp. and *Miomimus* sp., both of uncertain specific identification. The typical faunal association of MN4/5 group is *Megacricetodon primitivus* + *Cricetodon aliveriensis-Cricetodon meini* ± *Democricetodon, Alloptox, Schizogalerix.* The LFAs in B1 subcluster are segregated in two groups: B1.1 gathering MN12 LFAs with a quite characteristic association: *Parapodemus gaudryi* + *Byzantinia pikermiensis* + *Kowalskia lavocati* + *Myomimus dehmi* + *Hystrix primigenia* + *Occitanomys brailloni* + *Prolagus michauxi,* and B1.2 which is further divided in B1.2a (MN13-MN15/16 LFAs) and B1.2b (MN16 LFAs plus Kastoria 2). Inside B1.2a subcluster the MN13-MN14 LFAs are split in two groups separated by a group of MN14/15-16 LFAs. The situation is rather representative of the homogeneous small mammal fauna that occurs from the end of Miocene to the end of early Pliocene. The typical faunal association of this period includes: *Apodemus dominans* + *Occitanomys adroveri – brailloni* + *Rhagapodemus hautimangensis* + *Micromys bendai* + *Prolagus michauxi* + *Pseudomeriones,* while more wet elements such as *Castor fiber* characterize the internal group of MN14/15-16 LFAs.

The placement of Kastoria 2 (KST2) inside the B1.2b group of MN 16 LFAs is based on the common presence of *Miomimus roachi* and *Apodemus dominans* and the locality is possibly older than it was previously suggested. The faunal association of this time interval is characterized by the association *Apodemus dominans* + *Mimomys hajnackensis* + *Orientalomys similis* + *Pliomys graecus* + *Rhagapodemus athenensis* + *Dryomimus.*

Cluster C unites the latest Pliocene to early-middle Pleistocene LFAs and although two main groups can be detected (C1 and C2) there is no chronological or other meaning in this division. The typical faunal association of this period is compiled by *Apodemus mystacinus* + *Apodemus sylvaticus /flavicolis* + *Mimomys ex. gr. savini* + *Cricetulus migratorius* + *Allophaiomys* sp. + *Lagurodon arankae.*

4. Discussion and Conclusion

The comparison of mammalian LFAs from Greece by means of multivariate techniques shows a quite good resolution in the cluster definition of higher hierarchical rank. Some minor discrepancies are mostly due to the fossil record biases, as well as to the insufficient taxonomical interpretations at species level. Figure 3 summarizes the basic structure of both the large and small mammal LFAs clustering, excluding unnecessary outliers. It is evident that there is a good arrangement according to time and that the European Biochronlogical framework is broadly respected. The analyses allow recognizing in both cases a main cluster gap, corresponding to an important reorganization of the paleocommutity. These two basic groups of LFAs represent different "Mammal Ages", characterized by a well identified mammal compilation. Although the large and small mammal LFAs show a similar general clustering pattern in the highest hierarchical rank, the lower hierarchical rank groups show several differences between large and small mammal faunas, raising interesting suggestions.

In both the micro- and macro-mammal cases there is a serious change between the MN4/5 and MN9/10 faunas but the misplacement of the MN7-10 small mammal LFAs is hardly appreciable.

Anyway, the small mammal community seems to change more progressively; several small mammals (usually identified at genus level such as, *Megacricetodon, Myomimus, Prolagus, Pliospalax*), that appeared during MN4/5 they are still present in MN13/14 LFAs, though absent from intermediate faunas. Apart from *Deinotherium* no other large mammal appears to be present in later times.

The clear separation of the middle Miocene large mammal association from the Vallesian one might reflect the emergence of drier and more open environmental conditions in the Eastern Mediterranean area (Koufos, 2006) but the poor representation of MN6-MN8 large mammal LFAs might affect the results. The Turolian geographical separation between the large mammal faunas from continental Greece and the eastern coasts is not observable in the small mammal fauna. This severance should be explained by the presence of a geographic barrier in between the two regions that might prevent extensive large mammal interchanges. The absence of *Mesopithecus* in the east and the presence of different but relative large taxa or morphotypes of the same species from every quarter support this hypothesis. Geraads *et al.* (2005) discuss the presence of a humid/forest corridor along the eastern shore of Aegean Sea during Vallesian times, while other authors already suppose the existence of a marine connection between the Aegean Sea and Parathethys in the early Tortonian (Meulekamp and Sissingh 2003). It is quite possible that such kind of barrier or its leftovers was still active in later times (e.g. early-middle Turolian).

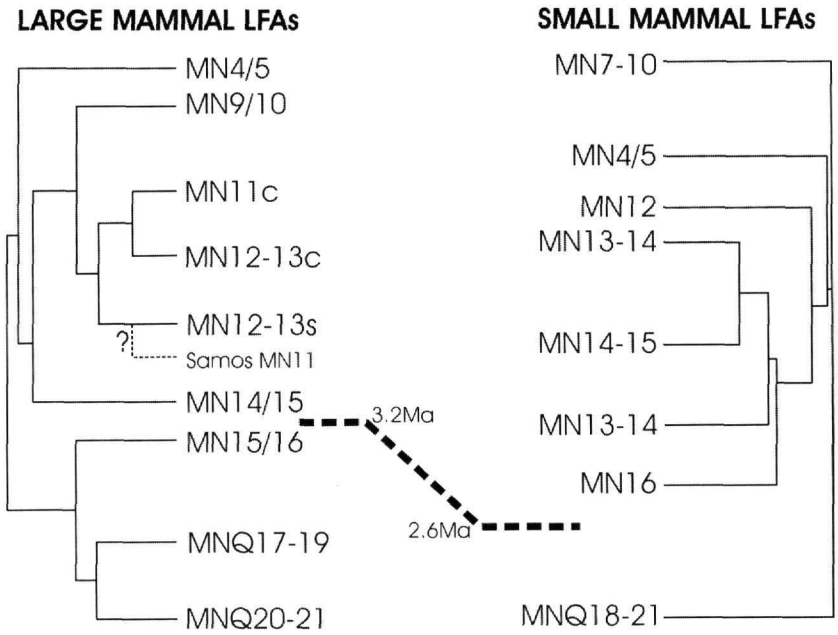

Figure 3 - Comparison of large and small mammal LFAs clustering

Cluster groups are directly referred to the European Mammal Neogene/Quaternary zones, excluding unnecessary outliers. Dashed line indicates the major break in the two LFAs successions. MN 11 and MN12-13 faunas are marked by a "c" for continental and an "s" for insular

In a general way, the large mammal community seems to respond more immediately to broad climatic trends such as the early Pliocene wetness, the mid-Pliocene desiccation and the early Pleistocene deterioration. On the contrary, both the late Miocene – early-middle Pliocene and the latest Pliocene – early Pleistocene small mammal community appear to be rather homogeneous.

The fundamental reorganizations in the faunal composition do not appear to be synchronous in the two communities. The basic renewal into the large mammal fauna takes place at the end of early Pliocene (end of Ruscinian), time which roughly corresponds to the first Pliocene crisis at 3.2 Ma, when the glaciation process emerges in the Northern Hemisphere (Agusti and Antón 2002).

Although, the lack of MN17 small mammal LFAs might alter the results, the main change in the small mammal community seems to take place somewhat later, during middle-late Pliocene (~2.6Ma) as a response to the true establishment of a glacial-interglacial dynamics (Agusti and Antón 2002), which allow the south-eastern part of Europe to enter into a drier phase. On the other hand, the faunal reconstruction of the micromammalian community between middle Turolian and late Turolian/Ruscinian that coincides with the re-establishment of humid conditions in the Balkans, appears slightly later in the large mammal assemblage (at the end of Miocene). The causes of apparent diachrony between small and large mammal faunal renewals are plausibly controlled by several factors and a further analysis is needed. Undersampling and stratigraphic incompatibility between the successions of small and large mammal LFAs seem to play a key role in the present case but biotic reasons such as the different response rate of the two mammal groups in climate changes should also be in consideration.

5. Acknowledgements

The first author is grateful to Prof. M.-R. Palombo (Rome) for collaboration and discussions on the faunal similarity multivariate techniques and problems. Thanks are also due to two anonymous reviewers for valuable comments and suggestions.

6. References

Agusti, J., and Antón, M., 2002. Mammoths, Sabertooths, and Hominids, Columbia University Press, New York. 313p.

Agusti, J., Cabrera, L., Garces, M., Krijgsman, W., Oms, O., and Pares, J., 2001. A calibrated mammal scale for the Neogene of Western Europe . State of the art, *Earth Science Review,* 52, 247-260.

Alberdi, M.T., Azanza, B., Cerdeño, E., and Prado, J.L., 1997. Similarity relationship between mammal faunas and biochronology from latest Miocene to Pleistocene in the Western Mediterranean area, *Eclogiae Geologica Helvetiae,* 90 (1), 115-132.

Azanza, B., Palombo, M. R., and Alberdi, M. T., 2003. Similarity relationaships between large mammal faunas of Spanish and Italian peninsulas from the latest Miocene to the middle Pleistocene, *Neues Jahrbuch für Geologie und Paläontologie Abh.,* 229 (1), 95-127.

Bonis, L. de, and Koufos, G. D., 1999. The Miocene large mammal succession in Greece. In J. Agusti, L. Rook and P. Andrews (eds), *The Evolution of Neogene terrestrial ecosystems in Europe. vol. 1.* 205-237pp. Cambridge University Press.

Geraads, D, Kaya, T., and Mayda, S., 2005. Late Miocene large mammals from Yulafli, Thrace region, Turkey, and their biogeographic implications, *Acta Palaeontologica Polonica,* 50 (3), 523-544.

Gliozzi, E., Abbazzi, L., Ambrosetti, P., Argenti, P., Azzaroli, A., Caloi, L., Capasso Barbato, L., Di Stefano, G., Esu, D., Ficcarelli, G., Girotti, O., Kotsakis, T., Masini, F., Mazza, P., Mezzabotta, C., Palombo, M.R., Petronio, C., Rook, L., Sala, B., Sardella, R., Zanalda, E., and Torre, D., 1997. Biochronology of selected Mammals, Molluscs, Ostracods from the Middle Pliocene to the Late Pleistocene in Italy. The state of the art, *Rivista Italiana di Paleontologia e Stratigrafia,* 103 (3), 369-388.

Guérin, C., 1982. Première biozonation du Pléistocène européen, principal résultat biostratigraphique de l'étude des Rhinocerotidae (Mammalia, Perissodactyla) du Miocène terminal au pléistocène supérieur de l'Europe occidentale. *Geobios,* 15 (4), 593-598.

Guérin, C., 1990. Biozones or Mammal Units? Methods and Limits in Biochronology. In E.H. Lindsay, V. Fahlbusch and P. Mein (eds), *European Neogene Mammal Chronology*, 119-130pp. Plenum Press, New York.

Hammer, O., and Harper, D.A.T., 2005. Paleontological Data Analysis, 368pp. Blackwell.

Hammer, O., Harper, D.A.T., and Ryan, P. D., 2001. PAST: Paleontological Statistics Software Package for Education and Data Analysis, *Palaeontologia Electronica*, 4(1), 9pp. http://palaeo-electronica.org/2001_1/past/issue1_01.htm

Koufos, G.D., 2001. The Villafranchian mammalian faunas and biochronology of Greece, *Bollettino della Societa paleontologica Italiana*, 40 (2), 217-223.

Koufos, G. D., 2006. The Neogene mammal localities of Greece: faunas, chronology and biostratigraphy, *Hellenic Journal of Geosciences*, 41 (1), 183-214.

Koufos, G.D., and Kostopoulos, D.S., 1997. Biochronology and succesion of the Plio-Pleistocene macromammalian localities of Greece. In J.-P. Aguilar, S. Legendre and J. Michaux (eds), *Actes du Congés BiochroM'97, Mémoires et Travaux de l'Institute de Montpellier* 21, 619-634pp, Montpellier.

Lindsay, E.H., and Tedford, R.H., 1990. Development and application of Land Mammal Ages in North America and Europe, a comparison. In E.H. Lindsay, V. Fahlbusch, and P. Mein, (eds), *European Neogene Mammal Chronology,* 601-624pp. Plenum Press, New York.

Mein, P., 1975. Résultats du groupe de travail des vertébrés: biozonation du Néogène méditerranéen à partir des Mammifères, *Report Activity RCMNS working groups*, 78-81, Bratislava.

Mein, P., 1990. Updating of MN zones. In E.H. Lindsay, V. Fahlbusch, P. and Mein, (eds) *European Neogene Mammal Chronology*, 73-90pp. Plenum Press, New York.

Meulekamp, J.E., and Sissingh, W., 2003. Tertiary palaeogeography and tectonostratigraphic evolution of the northern and southern Peri-tethys platforms and the intermediate domains of the African-Eurasian convergent plate boundary, *Palaeogeography, Palaeoclimatology, Palaeoecology*, 196, 209-228.

Palombo, M.R., and Valli, A.M.F., 2004. Similarities between large mammal faunas of the Italian Peninsula and France from the Pliocene to the middle Pleistocene, *Neues Jahrbuch für Geologie und Paläeontologie Abh.,* 233 (1), 69-102.

Palombo, M.R., and Valli, A.F.M., 2005. Highlighting the Early–Middle Pleistocene transition in Italian and French large mammal faunas: similarities and faunal renewals. In M.J. Head and P.L. Gibbard (eds), *Early–Middle Pleistocene Transitions: The Land–Ocean Evidence*. Geological Society, London, Special Publications, 247, 263-276pp.

Palombo, M.R., Azanza, B., and Alberdi, M.T., 2003. Italian mammal biochronology from Latest Miocene to Middle Pleistocene: a multivariate approach, *Geologica Romana,* 36, 335-368.

Palombo, M.R., Valli, A.M.F., Kostopoulos, D.S., Alberdi, M.T., Spassov, N., and Vislobokova, I., 2006. Similarity relationships between the Pliocene to middle Pleistocene large mammal faunas of southern Europe from Spain to the Balkans and the north Pontic region. In R.-D. Kahlke, L.C. Maul and P.P.A. Mazza (eds), "Late Neogene and Quaternary biodiversity and evolution: Regional developments and interregional correlations". Proceedings of the 18th International Senckenberg Conference (VI International Palaeontological Colloquium in Weimar). *Courier Forschungsinstitut Senckenberg,* 256, 392-347pp.

Shi, G.R., 1993. Multivariate data analysis in palaeoecology and palaeobiogeography -A review, *Palaeogeography, Palaeoclimatology, Palaeoecology,* 105, 199-234.

Δελτίο της Ελληνικής Γεωλογικής Εταιρίας τομ. XXXX, 2007
Πρακτικά 11ου Διεθνούς Συνεδρίου, Αθήνα, Μάιος 2007

Bulletin of the Geological Society of Greece vol. XXXX, 2007
Proceedings of the 11th International Congress, Athens, May, 2007

TERRESTRIAL BIOTIC CRISES: PALEOBOTANICAL RECORD AND INTERPRETATION

Krassilov V.[1], and Shuklina A.[2]

[1] *Institute of Evolution, University of Haifa, Mount Carmel, 31905 Haifa and Paleontological Institute of Russian Academy of Sciences, 117997 Moscow*
vakrassilov@gmail.com

[2] *Institute of Biology and Soil Science, 690022, Vladivostok*

Abstract

The controversial problem of biotic crises is considered in relation to the Cretaceous – Tertiary and Permian – Triassic transboundary events in the non-marine sequence of Far East and the Russian platform, respectively. In both cases, the floristic changes across the critical boundaries proceeded in few steps, none of which indicated a catastrophic destruction of plant communities. Rather the vegetational changes were related to a spread of continental climates, downslope migrations of altitudinal belts and deciduousness. Neither the end-Permian "fungal spike", nor the end-Cretaceous "fern spike" are supported by paleobotanical evidence. Incidentally, an increase of ferns in the transboundary plant-bearing sequences can be explained, upon the recent examples, by the rapid fern growth on the ash fallouts. A model of biotic crises is proposed, in which the intracratonic rifting and trap magmatism are causally related to the rise/spheric expansion of continental crust. A concerted impact of environmental changes was manifested at the beta level diversity in the first place, e.g. the reduction of wetlands and eutrophication of aquatic ecosystems, with a consequential loss of their alpha diversity.

Key words: *Biodiversity, crisis, Cretaceous – Tertiary boundary, Permian – Triassic boundary.*

Περίληψη

Διερευνάται το πρόβλημα των βιοτικών κρίσεων στο όριο Κρητιδικού-Τριτογενούς και Περμίου-Τριαδικού, σε χερσαίες αποθέσεις της Άπω Ανατολής και της Ρωσικής πλατφόρμας αντίστοιχα. Και στις δύο περιπτώσεις, οι χλωριδικές μεταβολές κατά μήκος των κρίσιμων ορίων έλαβαν χώρα σύντομα, χωρίς καταστροφική διαταραχή των φυτοκοινωνιών. Είναι πιθανότερο οι χλωριδικές μεταβολές να σχετίζονται με την επέκταση του ηπειρωτικού κλίματος, την μετακίνηση προς χαμηλότερα υψόμετρα των ζωνών του δάσους και των φυλλοβόλων ειδών. Ούτε το «μέγιστο των μυκήτων» στο τέλος Περμίου, ούτε το «μέγιστο των πτεριδοφύτων» στο τέλος του Κρητιδικού υποστηρίζονται από παλαιοβοτανικά δεδομένα. Η αύξηση των Πτεριδοφύτων στις αποθέσεις κατά μήκος των ορίων είναι δυνατό να ερμηνευθεί, σύμφωνα με το σημερινό πρότυπο, από την γρήγορη ανάπτυξη των Πτεριδοφύτων σε αποθέσεις ηφαιστειακής τέφρας. Προτείνεται ένα μοντέλο βιοτικών κρίσεων, στο οποίο οι

ενδοηπειρωτικές κινήσεις και ο πλουτώνιος διαπυρισμός σχετίζονται συνήθως με την ανύψωση και επέκταση του ηπειρωτικού φλοιού. Η συνδυαστική επιρροή των περιβαλλοντικών μεταβολών υπολογίστηκε ως β-ποικιλότητα π.χ. η μείωση των υγροτόπων και ο ευτροφισμός των υδάτινων οικοσυστημάτων, συγκεκριμένα έχει ως επακόλουθο την απώλεια της α-ποικιλότητας.
Λέξεις κλειδιά: *βιοποικιλότητα, βιοτική κρίση, όριο Κρητιδικού-Τριτογενούς, όριο Περμίου-Τριαδικού.*

1. Introduction

Biotic crises of the fossil record are the losses of biological diversity, which take a geologically appreciable time to recover. The losses are often perceived as sharp declines in numbers of species (mass extinctions) of the world faunas and floras. However, the idea of crises, catastrophes or revolutions appeared long before the numerical estimates of species losses with modern statistical methods (Raup and Sepkoski 1968, 1982, Sepkoski 1997) and was somehow related not, or not only, to the numbers, but also, and perhaps to a greater extent, to the roles of the species lost. Incidentally, the end-Cretaceous crisis is associated with extinction of dinosaurs in the first place, although these were not the most numerically species-rich group of animal that became extinct. Extermination of humans would probably impress an extraterrestrial observer as a major crisis, if but involving no more than a single dominant species. In other words, the idea of biotic crises incorporates the notions of dominance or significance as synecological estimates related to the *beta* rather than *alpha* diversity (Whittaker 1975, Sepkoski 1988). The major biotic crises of the fossil record are those, in which the dominant groups of organisms are lost signifying a decline of diversity at the level of biotic communities.

Abrupt faunal/floral changes recorded by paleontologists were for a long time associated with the name of George Cuvier rather than Charles Darwin who endeavoured to represent them as illusory, produced by enormous gaps in the fragmentary record of gradual developments (Darwin 1959). Though this once popular explanation failed in the face of modern geochronological dating methods, many researchers still believed in gradual biotic change until the theory of extraterrestrial impacthas switched the prevailing opinions to the opposite. First intended (Alvarez *et al.* 1980) to explain dinosaur extinction at the Cretaceous – Tertiary boundary (KTB), the impact theory soon involved other organisms and other boundaries, in particular the Permian – Triassic boundary (PTB). It was elaborated that dinosaurs, rather than being directly killed by the impact, died out because of its climatic aftermaths and destruction of forests. A "fern spike" above the KTB "Iridium spike" seemed to confirm the latter (Nichols *et al.* 1992, Vajda *et al.* 2001), and the "fungal spike" at the PTB was interpreted much in the same vein (Visscher *et al.* 1996)

In this paper, the ideas of catastrophic extinctions will be critical assessed and the alternatives will be considered. Our previously published results (Krassilov 1975, 1976, 1979, 1979) will be briefly overviewed in the light of new findings.

2. Examples of floristic change at the critical boundaries

2.1. The terrestrial KTB events in the Far East

The north-eastern sector of circum-Pacific belt has developed as a continuous orogenic structure since the mid-Cretaceous (reviewed in Krassiov 1989). To the end of the period, it included the marginal volcanic ranges of Sikhote-Alin, Okhotsk Coast and Chukchi Peninsula, bordered by the miogeosyncline trough of the Tatar Strait - western Sakhalin, Penzhyn Bay and Anadyr Basin, and further to the east, by the volcanic island arcs, fragments of which are preserved in the nappe belts of eastern Sakhalin, Kuril Islands and eastern Kamchatka (Fig. 1). Terrestrial and paralic coal-bearing deposits with plant remains are known form all these structural zones, as well as form cratonic basins back of the marginal ranges.

The most complete floristic sequences are described from the western coast of northern Sakhalin, a marginal zone of miogeosyncline trough filled with clastic shallow marine deposits intercalated by non-marine horizons in the Coniacian and Santonian. The trough subsided in the Campanian and early Maastrichtian, with a shell horizon of giant ammonites and inoceramids at the base of the transgressive sequence. During the later part of the Maastrichtian, the sign of epeiric fluctuations switched to the opposite and the trough was involved in the general uplift (Krassilov 1979).

In the transitional KTB sequence cropping out on the banks of Augustovka River flowing into the Tatar Strait at 51° N, a marine shallowing upward succession of Late Maastrichtian sandstones and shales with ammonites of *Pachydiscus gollevilensis – P. subcompressus* assemblage is gradually succeeded by a paralic coal-bearing sequence with macrofossil remains of a coastal *Parataxodium – Trochodendroides* plant assemblage. This terminal Cretaceous assemblage shares its dominant taxodioid and broadleaved elements with the regional Santonian – Campanian floras, but differs in the presence of rare allochtonous betulaceous leaf morphotypes *Alnites* and *Corylites* representing a dryland community.

The paralic sequence is conformably overlain by the non-marine volcanomictic Boshnyakovo Formation with a rich *Metasequoia - Corylites* assemblage of Paleocene aspect representing a deciduous upland vegetation sparsely recorded as allochtonous elements in the late Maastrichtian already. The KTB is drawn at the basal coarse-grained tuff marked by the first appearance of *Glyptostrobus nordenskioldii*, a widespread Paleogene species. The floristic change appears rather abrupt, although the Mesozoic cycadophyte relicts *Pterophyllum, Cycadites* and *Nilssonia* still persisted into the basal Paleocene. Ferns are relatively diverse, locally preserved as fern beds in association with thin coals and fine-grained tuffites.

On the Lesser Kuril Islands, the Maastrichtian marine deposits with inoceramids are overlain by the thick pillow basalts, agglomerates and tuffobreccias of a rising island arc. Lenticular shales intercalating the volcanic sequence contain shallow-water marine fossils and terrestrial plants of *Metasequoia - Corylites* assemblage, here accompanied by a rich Early Paleocene palynological assemblage still comprising several *Aquilapollenites* spp. and other Cretaceous relicts (Markevich in Krassilov *et al.* 1988). On evidence of the arboreal plant remains, the island arc must have been emergent at least for several thousand years usually taken by insular forests to develop.

A rifting phase marked by the KTB basaltic volcanism in Sakhalin is evident also over the marginal terrestrial orogenic belt, in which the liparitic volcanism switched to the basaltoid extrusions at about the same time. The downfaulted intermountain basins of transcurrent rift zones were filled with volcanomictic coal-bearing clastics containing the *Metasequoia – Betulites* macrofloral assemblage (Krassilov 1989), similar to, but somewhat more diverse (perhaps on account of its intermountain setting) than the contemporaneous Augustovskian assemblage of Sakhalin.

Sedimentary basins further inland developed as a result of a marginal cratonic subsidence back of the Sikhote-Alin, Lesser Hingan and Bureya Ranges. In the Amur – Zea - Bureya interfluves, they were filled with the fluvial and lacustrine Santonian to Maastrichtian clastics, with the mudflows and slump breccias upsection containing dinosaur remains. A general uplift of the territory above the basis of erosion at the KTB resulted in accumulation of thick conglomerates and gravelitic sandstones, with clayey intercalations. These coarse-grained deposits constitute the basal part of a sedimentary cycle topped by the quarried coal measures.

Rich Campanian to early Maastrichtian fossil plants localities have been recently discovered in the Archara - Boguchan depression near Kundur Village (Markevich *et al.* 1994). In 2005 the Kundur locality was jointly by paleobotanists M. Kodrul, E. Bugdaeva and V. Krassilov, who revealed several sedimentary cycles, each containing the aquatic *Quereuxia – Cobbania* assemblages in the basal members followed by the riparian *Parataxodium – Dryophyllum* assemblages above. No plant remains were found in the coarse-grained dinosaur beds upsection, but the overlying

tuffaceous siltstones still contained the Maasrichtian *Dryophyllum*, disappearing in the next sedimentary cycle of the Tsagajan Formation (Fig. 2).

The Tsagajan flora of Amur Province, collected from outcrops and coal quarries near the mouth of the Bureya River, is considered as the nearest Asiatic equivalent of the Fort Union flora of western North America (Kryshtofovich and Baikovskaya 1966, Krassilov 1976). Current taxonomic studies have revealed both continuity and incipient differentiation of the western North American – eastern Asiatic species ranges during the Late Cretaceous and Paleocene (Manchester 1999, Kodrul and Krassilov 2006). The dominant Tsagajanian *Metasequoia – Tiliaephyllum* assemblage represented a species-poor dryland vegetation of a temperate aspect. The wetland assemblages have lost *Quereuxia* (extremely rare in the Tsagajan localities) and *Cobbania.,* the dominant Late Cretaceous forms. They were succeeded by *Limnobiophyllum*, an araceous angiosperm ranging from the uppermost Maastrichtian to the Paleogene.. Fern leaves are locally abundant in the tuffaceous interbeds.

Thus, all over the vast area of northeastern Asia, floristic changes at the KTB reflected the advent of a more continental climate in turn related to a general elevation of land over the basis of erosion. An increase of dryland elements in the fossil record, temperization and deciduousness are the most conspicuous vegetational features of the basal Paleocene. The fossil plant assemblages are relatively poor and the Mesozoic relicts are shorter lived in the Early Paleocene of Amurland owing to a more pronounced continentality there. Coal accumulation resumed in the Early Paleocene with a subsidence and swamping of the pool-apart basins formed over the expanding rift zones.

Courtesy of Kirk Johnson and Douglas Nichols, Denver Museum of Natural history, Krassilov could have sampled the KTB sequence at Sussex, Powder River Basin, Wyoming consisting of the Maastrichtian black shales with *Proteacidites* palynomorphs, overlain, with a sharp contact, by the "magic layer" of anomalous Iridium concentration, followed by a coal seam with fern spores at the base (Nichols *et al.* 1992). The undulate surface of Maastrichtian shales indicates a non-deposition interval before the "magic layer", a cm-thick bleached tonstein covered with a mm-thick ferruginous precipitate. Since no palynomorphs have been ever found in the tonstein, the exact stratigraphic level of palynological change remains unknown. but the the basinal shales below it and the coal-bearing molassoides above belong to quite different sedimentary environments.

Explanation of the "fern spike" above the boundary tonstein in the piedmonts of the Rocky Mountains (Nichols *et al.* 1992) requires a comparison with the analogous fern spikes elsewhere In both the transboundary sequences of Sakhalin and Amurland (above), fern macrofossils appreciably increased in association with volcanic impact. In the Paleogene sequence of eastern Sakhalin, a prominent fern bed is described in the tuffaceous Tchekhovskaya Formation marking a widespread volcanic fallout event (Krassilov *et al.* 1984).

An instructive palynological example comes form the study of Cretaceous spore – pollen assemblages of Primorye, Russian Far East (Shuklina 2006). The coal-bearing Barremian – Aptian sequence includes two consecutive sandstone/shale cycles followed by the volcanomictic Albian – Cenomanian cycle. The coal measures contain a rich palynoflora of spore plants and gymnosperms, in which a distinctive spore morphotype *Laevigatosporites* constitutes a minor, although persistent, element. At the boundary of the coal-bearing and tuffaceous deposits, the percentages of *Laevigatosporites* sharply increased from about 5 % to about 16 %, making a significant correlation marker. In contrast, the other fern morphotypes decreased at this boundary in conjunction with a drastic reduction of the peat-forming wetlands. Since some extant ferns are colonizers of fresh ash falls, (Kornaś 1978, Spicer *et al.* 1985) we suggest that, through the Cretaceous and later on, edaphic conditions created by volcanic fallouts might have promoted certain fern species and, when covering vast areas, could have invoked the palynological fern spikes.

2.2. The PTB terrestrial events in the Volga – Dvina river basins

The historical stratotypic area for the Late Permian extends from the Fore-Urals over the Volga – Kama Basin to the Dvina Basin in the north, comprising the larger part of the Russian Platform. It was inundated by epeiric seas in the Kazanian (Wardian of the currently adopted international stage scale), after which terrestrial deposition has prevailed through the Tatarian redbed sequence and into the Lower Triassic (Vetlugian). The Tatrian is divided into three horizons, the Urzhumian, Severodvinian and Vyatkian, paleomagnitically correlated to the Capitanian, Uchiapingian and Changhsingian of the international scale, the latter two constituting the Lopingian System, with stratotypes in southern China (Jin *et al* 1998).

The regional stratigraphic correlation is based on ostracods, tetrapods, plant macrofossils and palynomorphs. Plant fossils indicate a floristic turnover at the base of the Severodvinian horizon when the hitherto dominant vojnovskialean assemblages disappeared and were replaced by the *Tatarina* flora of peltasperms and conifers (Meyen in Gomankov and Meyen 1986). The Vojnoskyales, or "Siberian cordaites", as they are often named on account of their *Cordaites*-like ribbon-shaped leaves, were most abundant in the coal measures of Siberian coal basins since the mid-Carboniferous. Their extinction is related to a drastic reduction in the extent and productivity of the peat-forming wetlands, which coincided with the initial stage of Siberian traps (Sadovnikov 1997).

The Tatarian – Vetlugian boundary is marked by erosional unconformities with basal conglomerates over the most part of the Volga – Dvina interfluves, indicating a regional uplift at the PTB, with a considerable part of transboundary sequences lost to the hiatuses (Lozovsky and Esaulova 1998). Early Triassic macroflora remained unknown except for *Pleuromeia*, an Olenekian lycopsid first appearing in the upper Vetlugian. In 1998 a representative mesofossil plant assemblage was found in the Vetlugian of Kitchmenga River near Nedubrovo Village, Vologda Region. Here the fine-grained basal sandstones and variegate clays of the basal Vetlugian are conformable on the Vyatkian pink marls. Fragmentary pteridosperm leaves, conifer needles, ovulate disks of *Peltapemum*, seeds, coaly wood and dispersed leaf cuticles are concentrated in dark grey smectitic clay with pyrite nodules. Smectite is developed over the basaltoid ash particles. Both sedimentary features and the well-preserved plant compressions indicate an anoxic estuarine setting (Krassilov *et al.* 1999a, b, 2000).

Leaf cuticles are identified with scanning electron microscopy as belonging to several species of peltaspemous *Tatarina* and coniferous *Quadrocladus*, all known form the Vyatkian. Another conifer, *Ullmannia bronniii*, although not hitherto reported from the Volga Basin, is typical of the Zechsteinian European floras. The palynological assemblage includes such Zechsteinian forms as *Klausipollenites schaubergeri* (Afonin in Krassilov *et al.* 1999a and elsewhere). On the other hand, the megaspores *Otynisporites eotriassicus* are considered as a palynological marker for the basal Triassic in central Europe and elsewhere.

Another marker of the transboundary deposits is a filamentous green alga *Tympanicysta* previously interpreted as a fungus and considered as a major contributor of the PTB "fungal spike" (Visscher *et al.* 1996). The algal bloom in association with the organic-rich anoxic sedimentary environments is evidence of eutrophic conditions (Krassilov *et al.* 1999b).

Though taxonomic comparisons are hampered by the pronounced provinciality of Permian floras in general, certain vegetational features suggest parallel developments in different floristic realms. Courtesy of the International Stratigraphic Commission and the Nanjing Institute of Geology and Paleontology, one of us has been given an opportunity to study the Lopingian section at Laibin, southern China (Shen *et al.* 1999), with a few plant-bearing horizons intercalated in the prevailingly marine sequence (Leonova *et al.* 1999). Cordaitalean leaves were found, together with impressions of cephalopod shells, in the black shale horizon of the Uchiapingian Stage, roughly

corresponding to the last appearance of such leaves in the Severodvinian of Volga Basin and before the Siberian traps.

The Changhsingian Talung Formation above contains plant remains, mostly allochtonous scale-leaved coniferous shoots, at several levels, also associated with abundant cephalopod shells. Though probably represented by different taxa, scale-leaved conifers also prevail in the European floras of Zechsteinian aspect, including the Vyatkian plant assemblages of European Russia. Two successive plant assemblages were recognized in the uppermost Talung, a regressive sequence overlain by basaltic tuffs: a *Paracalamites* – pecopterid wetlands immediately followed by the *Gigantonoclea* - coniferoid dryland assemblage. This succession complies with sedimentary evidence of land elevation at the PTB. The black-shale horizons at approximately the same level in the marine facies (Yang *et al.* 1995, Jin *et al.* 2000) are indicative of widespread anoxic environments.

3. Discussion

The above comparison of the KTB and PTB events reveals that both are chronologically related to elevation of land, simultaneous over vast areas and perhaps world-wide in extent, for which the most plausible explanation is a global uplift of continental crust. Since, for spherical surfaces, elevation means stretching, an activation of extensional tectonic features is to be expected, and indeed both the KTB and PTB are marked by rifting and profuse basaltic magmatism of cratonic areas (the Deccan traps at the KTB and the Siberian – Emeishan traps at the PTB are familiar examples).

The upheaval of the continents implies a spread of continental climates and of dryland vegetation at the expense of wetlands. Examples of such developments are given above for both the KTB and PTB. The downslope shifts of plant communities indicate a cooling trend at the KTB, and the analogous trend at the PTB is suggested by penetration of Angara species to the northern Cathaysian realm (Huang *et al.* 1998).

At present and even to a larger extent in the past, wetlands were the richest store of *beta* diversity. Reduction of wetlands means a loss of various coastal plain, tidal flat, riparian and aquatic plant communities – a considerable decrease of *beta* diversity, impelling extinction or semiextinction of dominant wetland taxa in such plant groups as arboreal lycopsids, sphenopsids, cordaites, vojnovskians, cheirolepids, and nilssonias, to name a few for which there is strong taphonomic evidence of wetland habitats.

The diversity changes at the *beta* level are mainly qualitatively rather than quantitatively. Since, by taphonomic reasons, wetland vegetation is overrepresented in the fossil record, the *alpha* level losses tend to be exaggerated. The overall estimates of taxonomic turnovers are scarcely precise because of gross underrepresentation of dryland communities.

As is well known from the present day nature conservation experience, devastation of wetlands threatens many groups of animals that depend on their resources. Dinosaurs are commonly considered as dryland animals, which is contradicted by the density and diversity of their tracks abundantly found in wetland facies, in particular, in the tidal flat deposits (Smith *et al.* 2001). The only dryland vegetation types capable of supporting a considerable diversity of herbivores are grasslands and savannas that appeared much later in the geological history. Deciduous dryland forests do not support dense populations of herbivores and there is no evidence that they ever did. A spread of mixed broadleaved forests at the expense of wetlands might have reduced dinosaur (and other large animal) populations below the level of their sustainable densities (Krassilov 1981).

At the same time, terrestrial biota might have been directly, as well as indirectly, impacted by effusions of the giant trap provinces. Gaps in arboreal vegetation inflicted by volcanic eruptions might have been filled by ferns colonizing ash fallouts, as they do today. As our examples show,

"fern spikes" are associated with tuffaceous deposits not only at the KTB, but also at the other levels since the Early Cretaceous.

The indirect impacts of volcanic activity might have been much more devastative. In particular, basaltic effusions are a prolific source of iron, an input of which increases productivity of aquatic ecosystems. Eutrophication is evidenced by a spread of anoxic facies concomitantly with algal blooms, such as the *Tympanicysta* bloom in estuarine settings, from which the eutrophic waters splashed over marine shallows (Krassilov *et al.* 1999). Modern examples of huge diversity losses inflicted by eutrophication can be found in (Nixon 1995) and elsewhere. The PTB evidence of eutrophication is a bloom of opportunistic planktonic forms, such as *Guembelitria* (Keller and Pardo 2005).

Trying to find out how Iridium comes into the picture, we have to consider both extraterrestrial and terrestrial sources of this element. The hypothesis of a solitary giant impact appears less viable with the giant Chicxulub crater discarded as a KTB impact structure (Keller *et al.* 2004) and the probability of finding a more credential candidate for such diminishing with the high resolution satellite imaging of the earth. On the other hand, mantle upheaval into the cratonic rift zones would provides a prolific source of geochemical anomalies. Iridium is brought to the surface with peridotites (a commercial source of this element) and ultramafic extrusions. Large peridotite massifs were exposed to erosion with the uplift of ophiolite nappe belts at about the critical boundaries. Notably, most of Iridium KTB sites in the Mediterranean, Rocky Mountains, New Zealand, Japan and elsewhere are found near ophiolitic nappes. Irridium concentrations in the nodular metallic precipitates over the terrestrial tonsteins and marine bentonites, such as "white clay" of the stratotypic PTB (Yang *et al.* 1995), might have been owing to diagenetic enrichments rather than direct fallouts.

3.1. Figures

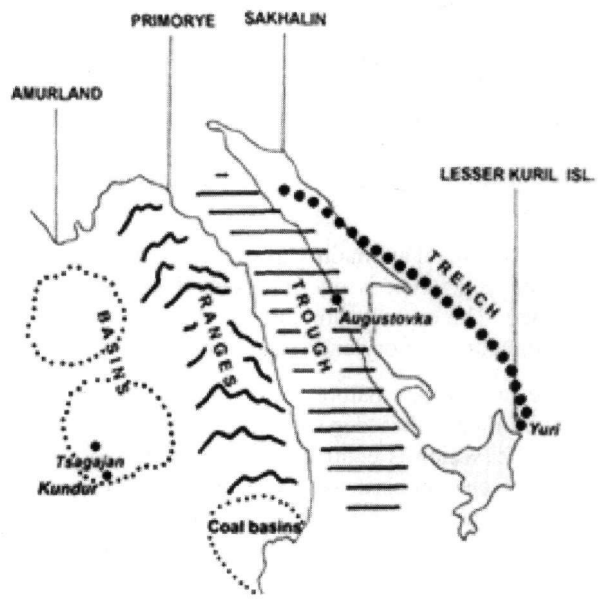

Figure 1 - Site of investigation in the Russian Far East

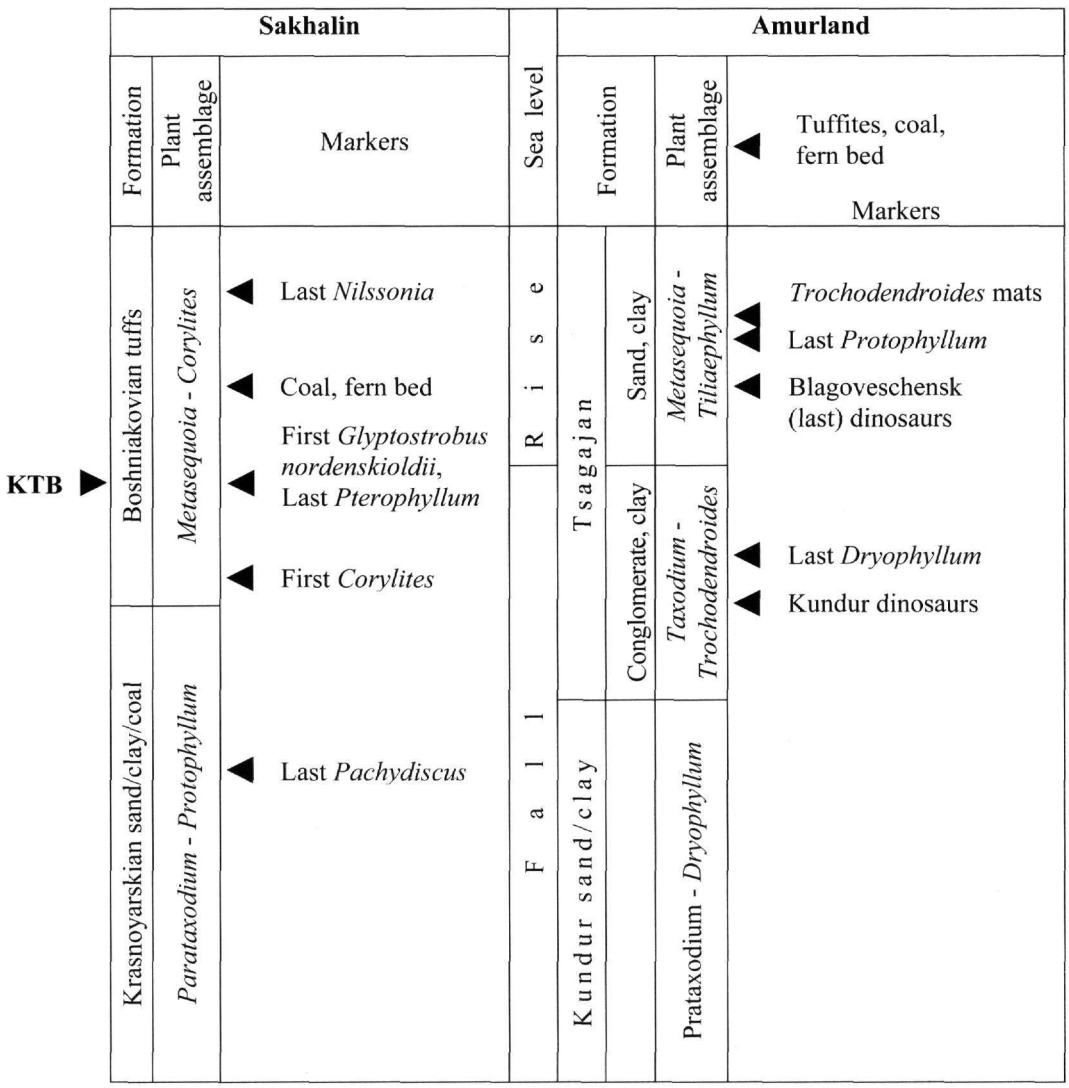

Figure 2 - Scheme of terrestrial KTB events in the Russian Far East

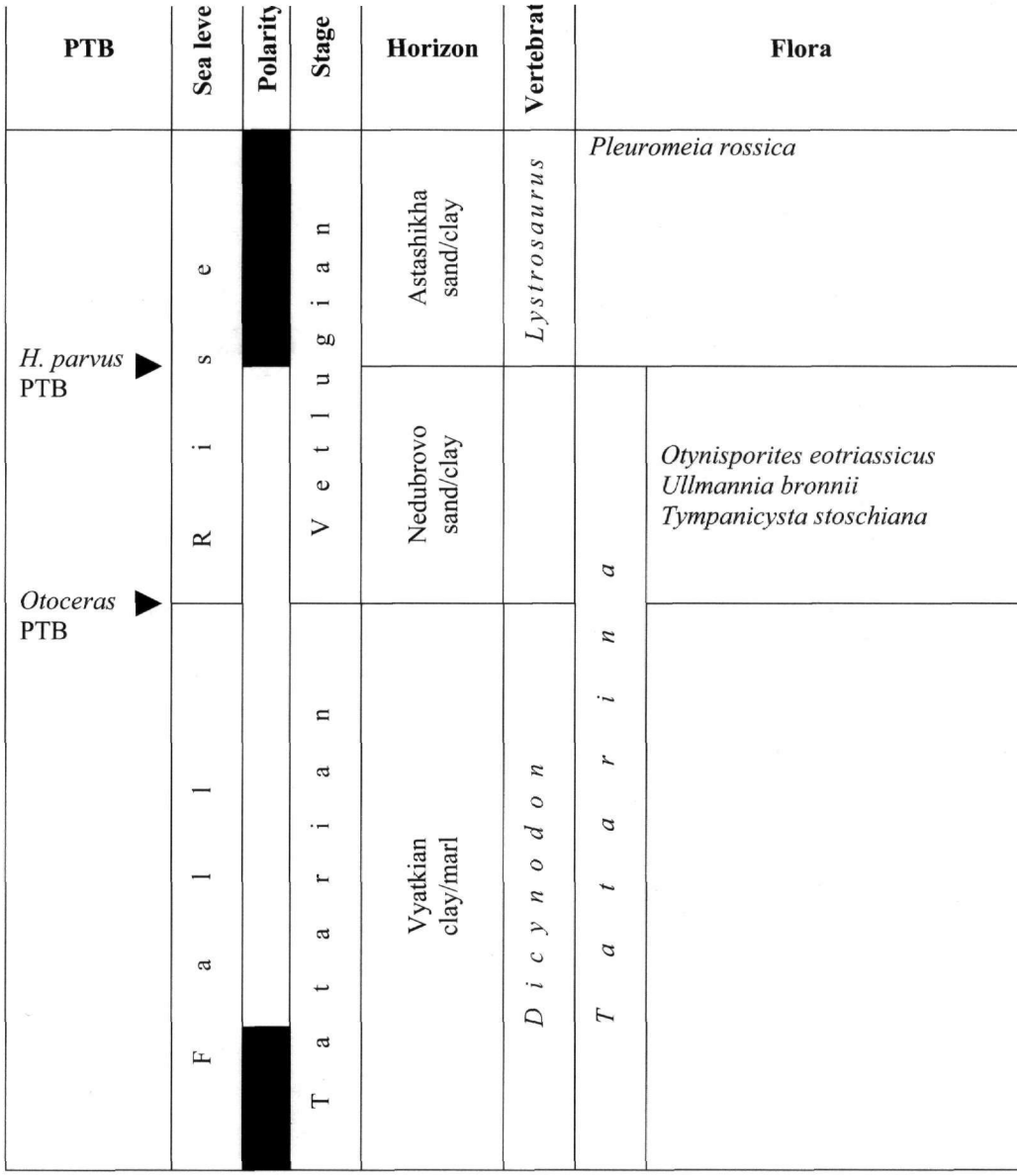

Figure 3 - Terrestrial PTB events in the Volga – Dvina river basins, European Russia

4. Conclusion

Mass extinctions need not be confused with mass mortalities. Mass mortalities can be caused by food shortages, overkill, freezing temperatures, poisoning, etc. Examples of mass mortalities inflicted by cosmic impacts are unknown, but feasible. Yet extinctions of many species of diverse ecologies belonging to different ecosystems are not explicable on the basis of mass mortalities requiring a more general causative model.

A significance of sea level fluctuations for biotic evolution was admitted by Darwin (1859) and was further discussed in relation to biotic crises (mass extinctions) by Newell (1967) and other researchers, who emphasized the loss of habitats for many shallow water marine organisms during the major retreats of epeiric seas. Volcanic impacts on biodiversity including forest fires, sulphur

aerosol and metallic pollution, as well as the climatic effects, are considered in McLaren, (1983); Renne *et al.* (1995) and elsewhere.

Our model establishes a causal link between the major uplifts of continental crust, such as at the KTB and PTB, and the massive magmatic events, such as the Deccan and Siberian – Emeishan traps. Uplift on a sphere is extension culminating in the rifting of continental crust and upheaval of the mantle material. The retreats of epeiric seas resulted in a spread of continental climates, reduction of wetlands, temperization and deciduousness of dryland vegetation. These processes in turn affected the terrestrial phytomass production and availability at the higher trophic levels. The concomitant volcanic activity enhanced eutrophication of freshwater ecosystems and the export of organic matter to marine ecosystems with continental runoff.

The conceivable secondary effects and feedbacks of such concerted impacts are too many to be considered here, but they no doubt contributed to instability of both terrestrial and aquatic ecosystems worldwide. Environmental instability affected the diversity of biotic communities (beta diversity) in the first place, with a consequential drop of alpha diversity - a mass extinction of the fossil record.

5. Acknowledgments

We acknowledge the support by the German – Israeli Foundation, grant 06-555.

6. References

Alvarez, L.W., Alvarez, W., and Asaro, F., 1980. Extraterrestrial cause for the Cretaceous-Tertiary extinction, *Science,* 208, 1095-1108.

Darwin, C.R., 1859. *On the origin of species*, London, Murray, 490pp.

Gomankov, A.V., and Meyen, S.V., 1986. *The Tatarinian flora (composition and distribution in the Late Permian of Eurasia),* Moscow, Nauka , 174pp.

Henderson-Sellers, B., and Markland, H.R., 1987. *Decaying lakes. The origins and control of cultural eutrophication,* Chichester, Wiley, 280pp.

Huang, B., and Ding, Q., 1998. The Angara flora from North China, *Acta Geoscientia Sinica, Geoogica. Sciences,* 19 (48), 97-104.

Jin, Y., Mei, S., Wang W., Wang, X., Shen, S., Shang, Q., and Chen, Z., 1998. On the Lopingian Series of the Permian System, *Palaeoworld,* 9, 1-81.

Jin,, Y., Wardlow, B.R., Glenister, B.F,. and Kotlar, G.V., 1997. Permian chronostratigraphic subdivisione. *Episodes,* 20 (1), 10-14.

Jin, Y.G., Wang, Y., Wang, W., Shang, Q.H., Cao, C.Q., and Erwin, D.H., 2000. Pattern of marine mass extinction near the Permian-Triassic boundary in South China, *Science,* 289, 432-436.

Keller, G., Thierry, A., and Stinnesback, W., 2004. Chicxulub predates the K/T boundary mass extinction,. *Proceedings of the National Academy of Sciences,* 101, 3753 – 3758.

Keller, G. and Pardo, A. 2005. *Gguembelitria* blooms: planktonic proxies for major oceanic environmental catastrophes. In A. Godet, H. Mort, P. Linder and S. Bodin (eds), *7th International Symposium on the Cretaceous.* Neuchâtel, 119 – 120.

Kodrul, T.M., Tekleva M.V., and Krassilov, V.A., 2006. A New Conifer Species, *Mesocyparis rosanovii* sp. nov. (Cupressaceae, Coniferales), and trans-Beringian floristic connections, *Paleontolological Journal,* 40 (3), 328-338.

Kornaś, J., 1978. Fire resistance in the pteridophytes of Zambia, *Fern Gazette,* 11 (6), 373-384.

Krassilov, V.A., 1975. Climatic changes in Eastern Asia as indicated by fossil floras. II. Late Cretaceous and Danian, *Palaeogeography, Palaeoclimatology, Palaeoecology*, 17, 157-172.

Krassilov, V.A., 1976. *Tsagajan flora of Amur Province*. Moscow, Nauka, 92pp. (in Russian)

Krassilov, V.A., 1979. *Cretaceous flora of Sakhalin.* Moscow, Nauka, 182pp. (in Russian)

Krassilov, V.A., 1981. Changes of Mezozoic vegetation and the extinction of dinosaurs, *Palaeogeography, Palaeoclimatology, Palaeoecology,* 34, 207-224.

Krassilov, V.A., 1989. Floristic succession over the Cretaceous–Tertiary boundary in Kavalerovo Region, Primorye, In V. Krassilov, (ed.), *Cenozoic of Far East,* 34-37, Vladivostok, USSR Academy of Sciences, Far Eastern Branch, 248pp.

Krassilov, V.A., Afonin, S.A., and Lozovsky, V.R., 1999. Floristic Evidence of transitional Permian-Triassic deposits of the Volga - Dvina Region, *Permophiles,* 34, 12-14.

Krassilov, V.A., Afonin, S.A., and Barinova, S.S., 1999. *Tympanicysta* and the Terminal Permian Events, *Permophiles,* 35, 16-17.

Krassilov, V.A., Blokhina, N.I., Markevitch, V.S., and Serova, M.Ya., 1988. *The Cretaceous – Palaeogene of the Lesser Kuril Islands,* Vladivostok, USSR Academy of Scences, Far East Branch, 140pp. (in Russian)

Krassilov, V.A., Kundyshev, A.S., Remizovsky, V.I., and Scmidt, I.N., 1984. Flora of the Tchekhov Formation and the Oligocene – Miocene boundary in Southern Sakhalin, *Tikhookeanskaya Geologia (Pacific Geology),* 5, 106-109. (in Russian)

Krassilov, V.A., Lozovsky, Afonin, S.A., and Morkovin, I.A., 2000. First data on the flora of a transboundary Permian – Triassic sequence in Moscow Synclise, *Science Reports of the Russian Academy of Sciences,* 372 (3), 354-355. (in Russian with English translation)

Kryshtofovich, A.N., and Baikovskaya, T.N., 1966. Late Cretaceous flora of Tsagajan in Amur Province. In A.N. Kryshtofovich (ed.), 184-320, *Selected Work, 3.* Moscow, Nauka (in Russian)

Leonova T.B., Krassilov, V.A., and Manankov, I., 1999. Fascination of the South China sections, *Permophiles,* 34, 36.

Lozovsky, V.R., and Esaulova, N.K., 1998. Permian-Triassic boundary in the continental series of East Europe, *International Symposium "Upper Permian stratotypes of the Volga region",* Moscow, GEOS, 246pp. (in Russian)

Manchester, S., 1999. Biogeographical relationships of North American Tertiary floras, *Annals of Missouri Botanical Garden,* 86, 472-522.

Markevich, V.S., Bolotskiy, Ju. L., and Bugdaeva, E. V., 1994. The Kundur locality of dinosaurus in the Priamurie, *Tikhookeanskaya Geologiya (Pacific Geology),* 6, 96-107. (in Russian)

McLaren, D.J. 1983. Bolides and biostratigraphy, *Geological Society of America, Bulletin,* 94, 313-324.

Newell, N.D. 1967. Revolutions in the history of life, *Geological Society of America, Special Paper,* 89, 63-91.

Nichols, D.J., Brown, J.L., Attrep, M. Jr., and Orth, C.J., 1992. A new Cretaceous-Tertiary boundary locality in the western Powder River Basin, Wyoming: biological and geological implications, *Cretaceous Research,* 13, 3-30.

Nixon, S.W., 1995. Coastal marine eutrophication: a definition, social causes, and future concerns, *Ophelia,* 41, 199-219.

Raup, D.M., and Sepkoski, J.J., Jr., 1968. Phanerozoic extinction of families and genera, *Science, 231, 833-836.*

Raup, D., and Sepkoski, J.J., Jr., 1982. Mass extinctions in the marine fossil record, *Science,* 215, 1501-1503.

Renne, R.R., Zhang, Z., Richards, M.A., Black, M.T., and Basu, A.R., 1995. Synchrony and causal relations between Permian-Triassic boundary crises and Siberian flood volcanism, *Science,* 269, 1413-1416.

Sadovnikov, G.N., 1997. Transition from Palaeophytic to Mesophytic in northern and central Asia, *D. Sc. Thesis*, Moscow, 25pp. (in Russian)

Sepkoski, J.A., Ir., 1988. Alpha, beta, or gamma: where does all the diversity go? *Paleobiology,* 14(3), 221-234.

Sepkoski, J.J., Jr., 1997. Biodiversity: past, present and future, *Journal of. Palaeontology,* 71,:533-539.

Shen, S., Wang, W., and Cao, C., 1999. *Permian Stratigraphy in the Laibin-Heshan Area, Guangxi, China. Nanjing: Nanjing Institute of Geology and Palaeontology,* Nanjing, Chinese Academy of Science., 48pp.

Shuklina, A.S., 2005. Correlation of climate and vegetation in the Rasdolninsk Basin through the Early Cretaceous (palynology), *Materials of International Scientific Conference "Rhytms and catastrophes in vegetation cover of Far East, 93-98* Vladivostok, Russian Academy of Sciences, Far East Branch, 232pp.

Smith, J.B., Lamanna, M.C., Lacovara, K.J., Dodson, K.J., Smith, P., Poole, J.R., Giegengack, R., and Attia, Y., 2001. A giant sauropod dinosaur from an Upper Cretaceous mangrove deposits of Egypt, *Science,* 292, 1704-1706.

Spicer, R.A., Burnham, R.J., Grant, P., and Glicken, H., 1985. *Pityrogramma calomelanos*, the primary, post-eruption colonizer of Volcán Chichonal, Chiapas, Mexico, *American Fern Journal,* 75 (1), 1-5.

Vajda, V., Raine, J.I., and Hollis, C.J., 2001. Indication of global deforestation at the Cretaceous-Tertiary boundary by New Zealand fern spike, *Science,* 294, 1700-1702.

Visscher, H., Brinkhuis, H., Dilcher, D.L., Elsik, W.C., Eshet, Y., Looy, C.V., Rampino, M.R., and Traverse, A., 1996. The terminal Paleozoic fungal event: evidence of terrestrial ecosystem destabilization and collapse, *Proceedings of the National Academy of Sciences, 93, 2155-2158.*

Whittaker, R.H. 1975. *Evolution and measurement of species diversity,* New York, Macmillan, 385pp.

Yang, Z., Sheng, J., and Yin, H., 1995. The Permian - Triassic boundary: the global stratotype section and point (GSSP), *Episodes,* 18 (1, 2), 49-53.

Δελτίο της Ελληνικής Γεωλογικής Εταιρίας τομ. XXXX, 2007
Πρακτικά 11ου Διεθνούς Συνεδρίου, Αθήνα, Μάιος 2007

Bulletin of the Geological Society of Greece vol. XXXX, 2007
Proceedings of the 11th International Congress, Athens, May, 2007

APPLICATION OF BED THICKNESS DISTRIBUTIONS IN TURBIDITE DEPOSITS OF LEMNOS ISLAND, NE GREECE

Maravelis A.[1], Konstantopoulos P.[1], Pantopoulos G.[1], and Zelilidis A.[1]

[1]*University of Patras, Department of geology, Division of Physical Geolog, Marine Geology & Geodynamics, Laboratory of Sedimentology, 26500 Patras, Greece, ,amaravel@upatras.gr,, tkonstan@upatras.gr, gpantop@upatras.gr, A.Zelilidis@upatras.gr*

Abstract

The submarine fan deposits in Lemnos Island, of the NE Greece provide a perfect opportunity to investigate the influence of processes such as erosion and bed amalgamation in the alternation of the shape of a power-law cumulative frequency distribution. The bed thickness distribution in two outcrops of late Eocene to early Oligocene turbidite deposits that correspond to different sub-environment, has been assessed statistically. Sediments of the outcrop 1 at the SE parts of the Lemnos Island interpreted as outer fan deposits and sediments of the outcrop 2 located at the NE parts of the island as inner fan deposits show both a good fit to the power-law, amplifying the hypothesis that departures from power-law statistics might be used as evidence of erosion and bed amalgamation. The main difference between these two outcrops is that the power law exponent decreases abruptly from outcrop 1 to outcrop 2, confirming with the aspect that the power law exponent can be considered as a good indicator for the available sedimentary space.
Key words: *submarine fan, turbidites, bed thickness, power-law.*

Περίληψη

Οι αποθέσεις υποθαλασσίων ριπιδίων στο νησί της Λήμνου, στην ΒΑ Ελλάδα, παρέχουν μια πρώτης τάξεως ευκαιρία για την διερεύνηση της επίδρασης διαδικασιών όπως, η διάβρωση και η συμπαγοποίηση στην αλλαγή του σχήματος μιας κατανομής τύπου power-law. Η κατανομή των παχών σε δύο φυσικές τομές τουρβιδιτικών αποθέσεων ηλικίας Αν. Ηωκαίνου- Κ. Ολιγοκαίνου προσδιορίστηκαν στατιστικά. Τα ιζήματα της τομής 1 στα ΝΑ τμήματα του νησιού έχουν ερμηνευθεί σαν αποθέσεις εξωτερικού ριπιδίου ενώ τα ιζήματα της τομής 2 σαν αποθέσεις εσωτερικού ριπιδίου. Οι δύο τομές έχουν καλή συσχέτιση με την κατανομή power-law ενισχύοντας την υπόθεση ότι αποκλίσεις από την power-law κατανομή μπορούν να θεωρηθούν σαν ενδείξεις για διάβρωση και συμπαγοποίηση. Η βασική διαφορά των δύο μελετηθέντων φυσικών τομών είναι ότι ο εκθέτης της κατανομής power-law μειώνεται απότομα από την τομή 1 στην τομή 2 επιβεβαιώνοντας την άποψη ότι είναι ανάλογος με τον διαθέσιμο χώρο ιζηματογένεσης.
Λέξεις κλειδιά: *Υποθαλάσσιο ριπίδιο, τουρβιδίτες, πάχος στρωμάτων, power-law κατανομές.*

1. Introduction-Geological setting

Distinctions between depositional environments are an essential component in basin analysis. The thickness of a turbidite bed in a particular point within a sedimentary basin is determined by the shape of the bed and the distance of the source. The shape of the bed depends upon factors such as initial sediment volume, grain size(s) and flow concentration (Middleton and Neale 1989, Rothman and Grotzinger 1995, Malinverno 1997, Carlson and Grotzinger 2001).

The frequency distribution of turbidite bed thickness provides informations on flow hydrodynamics and is a useful tool for petroleum reservoir modeling, particularly if thicknesses can be related to sediment volumes (Middleton and Neale 1989, Flint and Bryant 1993, Rothman and Grotzinger 1996, Malinverno 1997, Carlson and Grotzinger 2001). The bed thickness values, measured along a vertical succession, follow a power-law trend in their spatial distribution (Hiscott *et al.* 1992, Rothman *et al.* 1994, Rothman and Grotzinger 1996, Malinverno 1997, Carlson and Grotzinger 2001). Departures from power-law statistics between several sub-environments owe to sedimentary processes such as erosion and bed amalgamation (Rothman *et al.* 1994).

The study area is located in the NE Aegean (Fig. 1A). The sedimentological evolution of the Lemnos area is based on the geological mapping that was carried out by Roussos (1993) (Fig. 1B). From upper Eocene to lower Oligocene in Lemnos Island, Greece, submarine fan deposits and shelf deposits were accumulated with shelf deposits overlying the submarine fans (unit 1-4, figs. 1B, 1C) (Maravelis *et al.* 2006). The depositional processes were grain flows, debris flows and low, medium and high-density turbidity currents whereas the recognized sedimentary facies were classified as inner-fan, mid-fan and outer-fan deposits (Maravelis *et al.* 2006).

The aims of this paper are: (i) to highlight on how power-law cumulative frequency distributions can applied both on proximal and distal turbidite deposits and (ii) to use these results in order to establish the basin geometry evolution of Lemnos Island.

2. Methodology

The two data sets consist of measured vertical sequences of continuously exposed turbidites (Fig. 2). On account of the inability of distinction between the turbiditic and hemipelagic mud, the measurements were restricted to the arenaceous component. Each discernible sandstone bed was measured although a minimum cut-off of 1 cm was established. In cases where the determination of bed thickness was intractable on account of erosion, a number of measurements of the same bed were realized in order to evaluate the average bed thickness. Moreover, the thickness of each sandstone bed was measured irrespective of whether or not the beds are inferred to represent a single flow or multiple flows that have been amalgamated to form a single bed.

3. Sedimentological analysis

3.1. Outcrop 1:

This outcrop is located at the SE part of the Lemnos Island near the Skandali village (Fig 1).The deep water sediment deposits consist of monotonous alternations of sandstone and claystone beds (Fig. 2A). The majority of the sandstone beds are thin-bedded (< 10 cm) although a few beds with thickness from 20 cm to 33 cm have been found (Fig. 2B). Regular Tb- and Tc- type turbidites (less than 10 % of the measured sandstones beds contained the Ta subdivision of Bouma sequence) are parallel sided and laterally extensive with a few scours and no channels (Figs. 2C, 2D). Beds are almost always flat based, and tops grade into fine sediment (Fig. 2E). Tool marks can easily be found at the bottom of the thicker deposits although scour marks are very rare. The characteristic features of this outcrop demonstrate deposition from both low and high density turbidity currents. The above sediments, deposited in this particular outcrop, were interpreted as outer fan deposits (Maravelis *et al.* 2006).

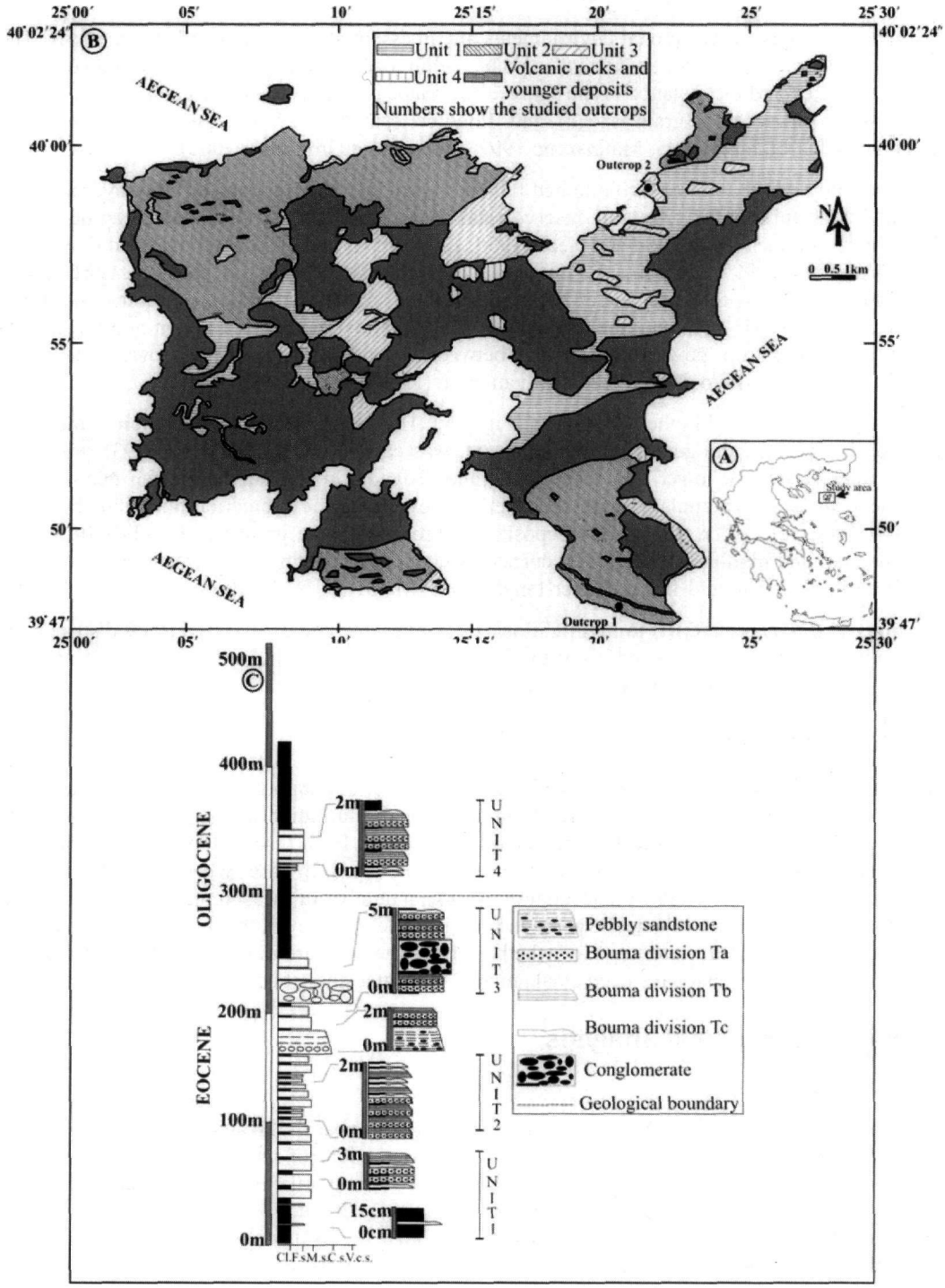

Figure 1 - (A) General location of the study area at the NE Aegean, Greece. (B) Geological map of Lemnos Island. (C) General stratigraphy of the study succession and indication of the main Bouma divisions

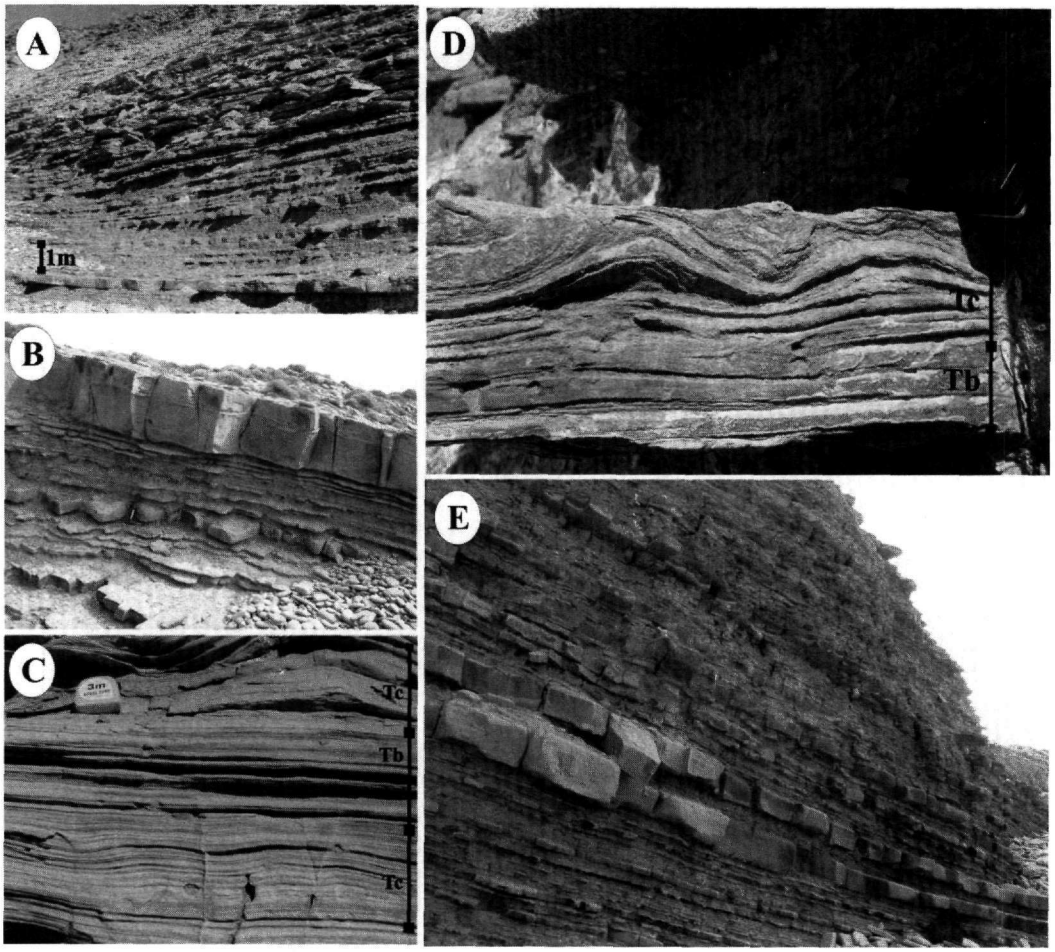

Figure2 - Detailed photographs of the outer fan deposits: (A) Monotonous alternations of sandstone and claystone beds. (B) Medium bedded sandstones in an overall thin bedded succession. (C and D) Regular Tb- and Tc-type turbidites. (E) Sandstones with flat bases in contact with claystones.

3.2. Outcrop 2:

This outcrop is located at the NE part of the Lemnos Island close to the Panagia village (Fig 1). Most of the sandstone beds are thin to medium bedded although a few beds with thickness up to 4 m have been found). Regular Ta- and Tb-type turbidites (less than 10 % of the measured sandstones beds contained the Tc subdivision of Bouma sequence) are parallel sided with bad lateral continuity (Figs 3B, 3C). Beds are almost sharp based although some of the thicker deposits presents erosive bases and tops grade into fine sediment (Fig. 3C). Scour marks can easily be found at the bottom of the thicker deposits. The characteristic features of this outcrop demonstrate deposition from high density turbidity currents. The above sediments deposited in this particular outcrop were interpreted as inner fan deposits and especially channel-fill deposits (Maravelis *et al.* 2006).

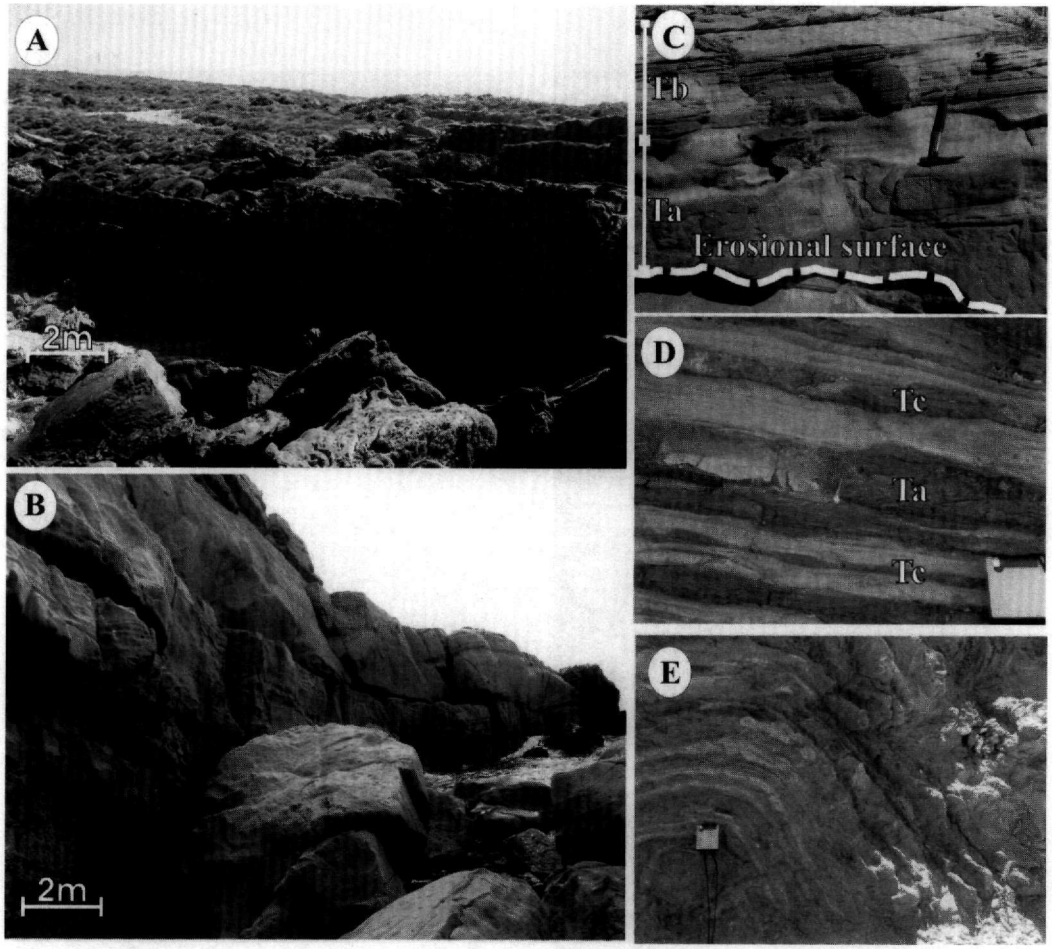

Figure 3 - (A and B) General photographs of the channel-fill. (C) Regular Ta- and Tb-type turbidites and erosional surface at the base of the thicker deposits. (D) Regular Ta- and Tc-type turbidites. (E) Levee deposits

4. Statistical analysis

4.1. Outcrop 1:

In this outcrop, 189 sandstone beds were measured and their log-log values cumulative distribution showed a good fit to the power-law (R^2> 0.9) (Fig. 4) suggesting that erosion and bed amalgamation were not the dominant processes during deposition. Moreover, a high value of power-law exponent (1.33) indicates a broad basin geometry.

4.2. Outcrop 2:

In this outcrop, 58 sandstone beds were measured and the log-log cumulative distribution showed a good fit to the power-law (R^2> 0.9) (Fig. 5) suggesting that erosion and bed amalgamation were not the dominant processes during deposition. Moreover, a low value of power-law exponent (0.73) indicates less broad basin geometry than the outcrop 1. In figure 5 it can be observed that the thickness of two beds is much greater than the rest. This indication could lead to the assumption that excluding these two thick beds, the distribution would be similar to that in outcrop

1. The previous assumption is invalid because if we exclude these two beds the power-law exponent remains low and below unity.

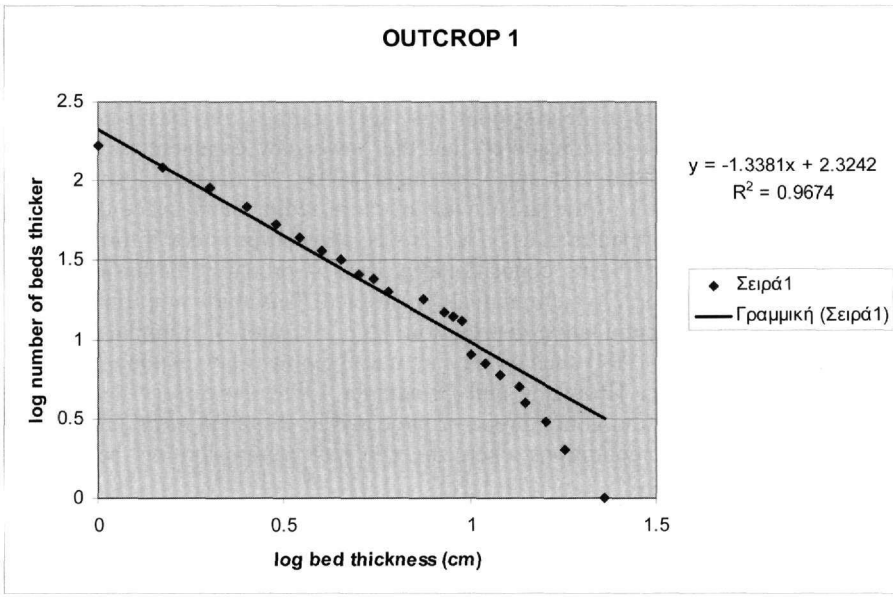

Figure 4 - Log-log bed thickness cumulative distribution of outcrop 1

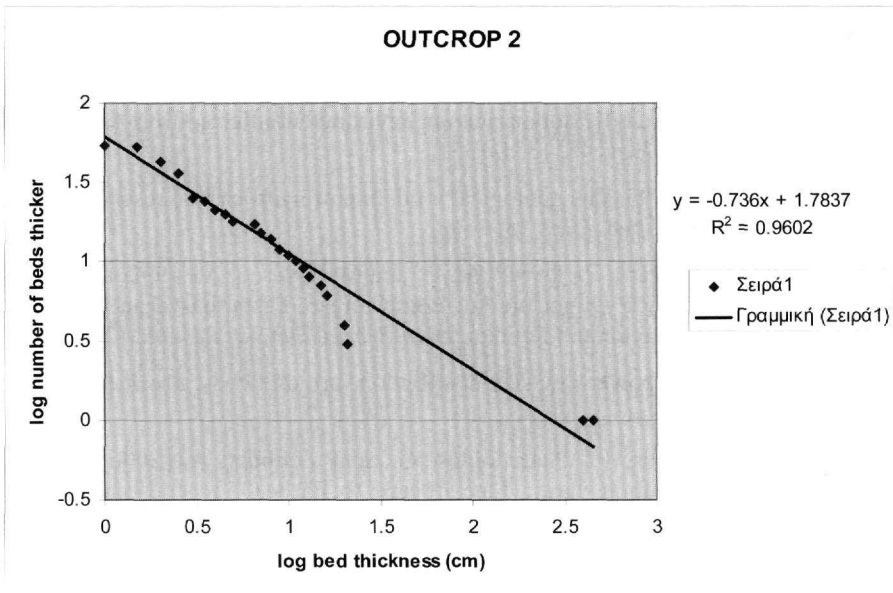

Figure 5 - Log-log bed thickness cumulative distribution of outcrop 2

4. Discussion- Conclusions

The sedimentological analysis in these two outcrops showed that erosion and bed amalgamation were not the dominant factors which controlled the deposition of sediments. Even in the outcrop 2, which has been interpreted as channel-fill deposit, the majority of the sandstone beds presented with flat or sharp bases while the erosion restricted in some of the thicker beds. The statistical analysis showed that the linear fit of the two measured outcrops in the log-log plots show a high

least squares value (R^2= 0.96) thus have a good fit to the power-law (Carlson and Grotzinger 2001) corresponding to minimal erosion (Rothman *et al.* 1994). The main difference between these tow outcrops is that the power-law exponent decreases abruptly from 1.33 at outcrop 1 to 0.71 at outcrop 2. This difference at the power-law exponent can provide useful information about the variation of turbidite deposition from region to region. It has been hypothesized that changes in the power-law exponent are related to depositional variation ranging from basin geometry to flow types (Rothman *et al.* 1994). It is considered that the power-law exponent is analogous to the available sedimentary space (Rothamn and Grotzinger 1995). In outcrop 1 the high value in power-law exponent is the result of the subsistence of more sedimentary space than in outcrop 2 where the turbidity currents formed thicker beds. This conclusion provides information about the basin geometry suggesting that, during depositional processes, probably the basin was broader at the outcrop 1 than at the outcrop 2 which gradually restricted. This study amplifies the theory that the existence of a power-law cumulative distribution is an indicator of minimal erosion and bed amalgamation (Rothman *et al.* 1994) such as the fact that the power-law exponent is analogous to the available sedimentary space (Rothamn and Grotzinger 1995). However, the presence of the power-law cumulative distribution although is not indicated in Rothman *et al.* (1994), this model could be applicable in specific conditions where the effect of the erosion and bed amalgamation was not of great importance.

5. Acknowledgments

This study is confounded by E.C., European Social fund and GSRT Greece. EPAN, PENED ' 03ED497. An anonymous reviewer is acknowledged for his useful comments which improved the manuscript.

6. References

Carlson, J., and Grotziger, J.P., 2001. Submarine fan environment inferred from turbidite thickness distributions, *Sedimentology,* 48, 1331-1351.

Flint, S.S,. and Bryant, I.D., 1993. The geological modeling of hydrocarbon reservoirs and outcrop analogues, *Sedimentol. Spec. Publ.* 15, 269pp.

Hiscott, R.N., Colella, A., Prezard, P., Lovell, M.A., and Malinverno, A., 1992. sedimentology of deep-water volcaniclastics, Oligocene Izu-Bonin forearc basin, based on formation micro-scanner images. In B. Taylor and Fujioka *(eds), Proc. ODP Sci. Results,* 126, 75-96

Malinverno, A., 1997. On the power-law size distribution turbidite beds, *Basin Research*, 9, 263-274.

Maravelis, A., Konstantopoulos, P., Pantopoulos, G., and Zelilidis, A., 2006. North Aegean sedimentary basin evolution during Late Eocene to Early Oligocene time: based on the sedimentological studies at the Lemnos Island, NE Greece, (submitted to *Geologica Carpathica).*

Middleton, G.V., and Neale, W.J., 1989. Experiments on the thickness of beds deposited by turbidity currents, *J. Sed. Petrol.,* 59, 297-307.

Rothman, D.H., Grotzinger, J.P., and Flemings, P., 1994. Scaling in turbidite deposition, *J. Sed. Petrol.,* A64, 59-67.

Rothman, D.H., and Grotzinger, J.P., 1995. Scaling properties of gravity-driven sediments, *Non-Linear Processes Geophy.,* 2, 178-185.

Roussos, N., 1993. Geological map of Lemnos Island, *I.G.M.E., Greece.*

Δελτίο της Ελληνικής Γεωλογικής Εταιρίας τομ. XXXX, 2007
Πρακτικά 11ου Διεθνούς Συνεδρίου, Αθήνα, Μάιος 2007

Bulletin of the Geological Society of Greece vol. XXXX, 2007
Proceedings of the 11th International Congress, Athens, May, 2007

GEOLOGICAL EVOLUTION – STRATIGRAPHY OF FLORINA, PTOLEMAIDA, KOZANI AND SARADAPORO GRABEN

Metaxas A.[1], Karageorgiou D. E.[1], Varvarousis G.[1], Kotis Th.[2], Ploumidis M.[3], and Papanikolaou G.[4]

[1] *Institute of Geology and Mineral Exploration, Messogheion 70, Gr- 11527 Athens, Greece, Geologist dek@igme.gr*

[2] *Dr. Geologist ex director of I.G.M.E.*

[3] *Geologist*

[4] *National & Kapodistrian University of Athens, Geologist & postgraduate student*

Abstract

The purpose of this research is to comprehend the geological and stratigraphical evolution of Florina, Ptolemaida, Kozani and Sarandaporo graben. This graben extends North of the Greek borders and is more than 150 Km long.
The activity of big and profound faults of NW-SE direction, in NW Macedonia, after the end of the Alpine orogenesis cycle and during the Early Miocene was related to the formations' deposition.
A large number of samples were collected from drill cores for the examination of palynology, paleoflora, fossils, and diatoms in order to determine the formations' sequence and age.
The basement and the borders of the depression, belong to the Pelagonian geotectonic zone. The deposition of the ***Early Neogene's series*** *is following. During the Late Pliocene the previous series, is developing into a lacustrine-marshland system, resulting to the deposition of* ***Late Neogene's series*** *formations. In the Quartenary the following formations are deposited:* ***Proastion formation, Perdika formation, terrestrial, fluvial-terrestrial formation, recent formation.***
Four (4) phases of lignitogenesis have been specified, mainly in the Ptolemaida – Amynteo basin.
In this graben they have been deposited the most important lignite deposits of Greece.
Key words: *lignite deposits, NW Macedonia.*

Περίληψη

Μετά το πέρας του Αλπικού ορογενετικού κύκλου και κατά τη διάρκεια του Κατώτερου Μειόκαινου, στην περιοχή της ΒΔ Μακεδονίας –όπως και σε όλο τον Ελλαδικό χώρο– αρχίζει ένας έντονος ρηγματογόνος τεκτονισμός. Αποτέλεσμα αυτού και εξαιτίας της δράσης μεγάλων και βαθιών ρηγμάτων, κύριας διεύθυνσης ΒΔ-ΝΑ, δημιουργείται η Τάφρος Φλώρινας, Πτολεμαΐδας - Αμυνταίου, Κοζάνης-Σερβίων και Νοτιότερα η λεκάνη Σαρανταπόρου. Η τεκτονική αυτή Τάφρος επεκτείνεται πέραν των Ελ-

ληνικών συνόρων προς Βορρά και έχει μήκος μεγαλύτερο των 150 Km. Ένα μεγάλο πλήθος δειγμάτων για την εξέταση παλαιοχλωρίδας, διατόμων, παλυνολογικών εξετάσεων και απολιθωμάτων, με σκοπό τον ακριβή προσδιορισμό της ηλικίας των διαφόρων σχηματισμών, λήφθηκε από τους πυρήνες των γεωτρήσεων.
Το υπόβαθρο και τα περιθώρια του βυθίσματος αυτού, γεωτεκτονικά ανήκουν στην Πελαγονική ζώνη. Ακολουθεί η απόθεση της κατώτερης Νεογενούς σειράς. Κατά τη διάρκεια του ανώτερου Πλειοκαίνου, η παραπάνω σειρά εξελίσσεται σε ένα λιμναίο - ελώδες σύστημα, με αποτέλεσμα την απόθεση των σχηματισμών της ανώτερης Νεογενούς σειράς. Στο Τεταρτογενές αποτίθενται οι παρακάτω σχηματισμοί: Σχηματισμός Προαστείου, Σχηματισμός Περδίκα, Χερσαίοι, Ποταμό - χερσαίοι σχηματισμοί, πρόσφατοι σχηματισμοί.
Τέσσερις (4) φάσεις λιγνιτογένεσης έχουν παρατηρηθεί, κύρια στην λεκάνη Πτολεμαΐδας – Αμυνταίου.
Σε αυτή την τεκτονική τάφρο έχουν εντοπισθεί τα κυριότερα Ελληνικά λιγνιτικά κοιτάσματα.
Λέξεις κλειδιά: *λιγνιτικά κοιτάσματα, ΒΔ. Μακεδονία.*

1. Introduction

This work is the result of a long-lasting research (more than 55 years) carried out by several colleagues who worked in the Geological Institute of Greece, (previously called Geological Service, Institute of Geological Research of Subsoil, National Institute of Geological and Mineral Exploration, Institute of Geological and Mineral Exploration), an Institute which has always been the main center for research in the Energy Resources in Greece.

Some hundred thousands of meters of drill cores were studied and were evaluated, for better determination of the formations sequence and age as well as the tectonic activity in the area. For that purpose a large number of samples were collected from the drill cores for the examination of palynology, paleoflora, fossils, and diatoms.

2. Development – Geological evolution of Graben

After the end of the Alpine orogenesis cycle and during the Early Miocene, an intense tectonic faulting begins, in NW Macedonia, as well as allover Greece. The activity of big and profound faults of NW-SE direction, results to the development of the Florina, Ptolemaida- Amynteo, Kozani– Servia and Sarandaporo graben. This Graben extends North of the Greek borders in F.Y.R.O.M. (Monastiri area), and is more than 150 Km long (Fig. 1).

In this newly created graben some areas, such as Kozani, Xino Nero - Klidi and others, (Fig. 2) are preexistent elevations, which under the influence of faults (NE–SW) vertical to the previous, behave as elevations, or as constant and durable masses in the synizesis, in reference to the other areas of the graben. These elevations separated the graben in many basins (Florina, Amynteo, Ptolemaida, Kozani and Sarandaporo), which some times were autonomous and other times communicated, thus having common geological development. In both cases, we observe during the Neocene and Quaternary, the same or homologous formations along the graben.

The basement and the borders of the depression, belong to the Pelagonian geotectonic zone (Fig. 3). These formations mainly occupy the east and south–southwest borders of the graben. The west and northeast borders consist of by the Paleozoic formations of the crystalline basement of the Pelagonian mass.

During the Late Miocene-Early Pliocene, the graben and mainly the basins in it begin to fill with terrestrial, fluvial, torrential, lacustrine and marshy deposits. Thus we have the deposition of the **Early Neogene's series** (Figs 4, 5), in which we find the large lignite deposits of "xylitic type".

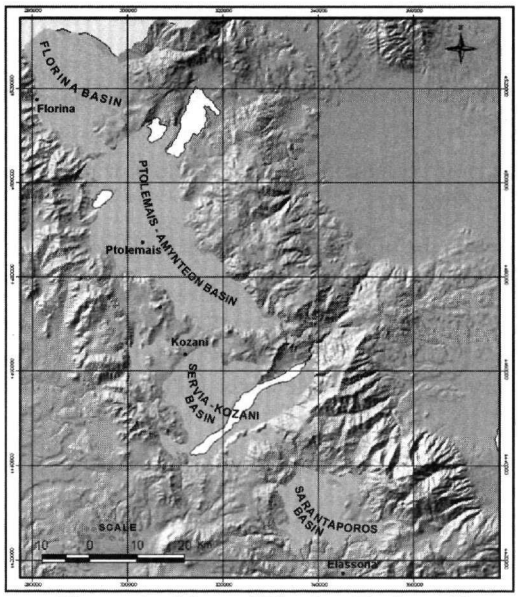

Figure 1 - Map of Florina-Ptolemaida Kozani and Sarantaporo basins

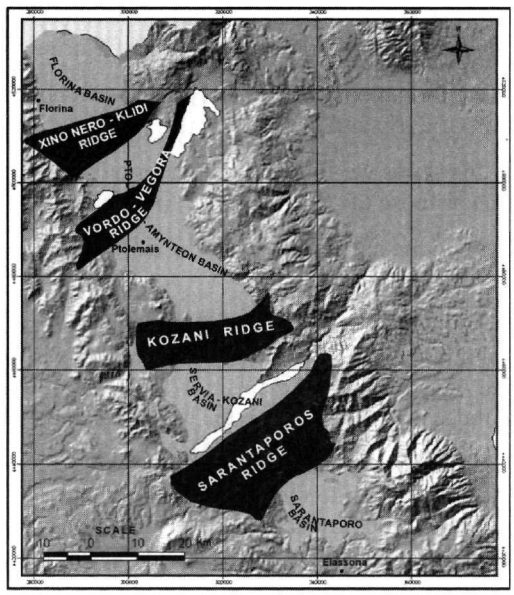

Figure 2 - Map of Graben with ridges

The Early Neogene's series extends in the entire graben. Its main volume is developed in the east borders of the Ptolemaida– Amynteo basin where it exceeds 600m of thickness, in Florina basin, in the south of Kozani-Servia basin, as well as in Sarandaporo basin. As we see in Fig. 6, the lignite bearing formation of the Early Neocene is developing in the east borders of the graben, with the known lignite deposits of Florina, Komnina, Anatoliko, Lava etc. where its thickness declines gradually to the west.

During the Late Pliocene the series that was described earlier, is developing into a lacustrine-marshland system, resulting to the deposition of **Late Neogene's series** formations (Figs 4, 5).

Due to the tectonic activity and the paleogeografical and paleogeomorphological conditions that prevailed this period, this system occupies the entire Ptolemaida – Amynteo basin,

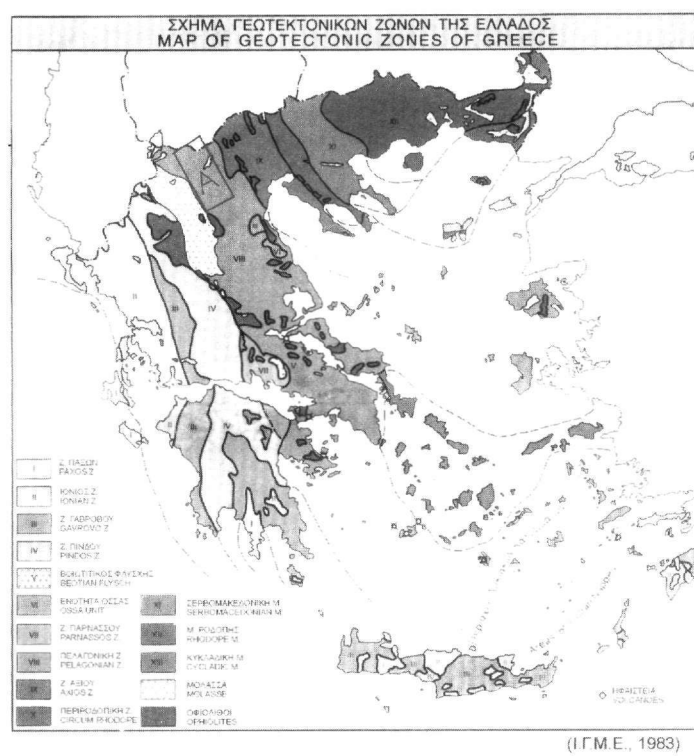

Figure 3 - The position of the Graben ("A" region) in relation to the Greek geotectonic zones

with the exception of the east-northeast section, the Kozani-Servia basin and finally reaches in small endings the southeast section of Florina basin (Fig. 7).

These formations are lake, lacustrine-swampy, and marshy deposits. Their age is determined at the limit of Early and Late Pliocene.

In this series we find the known large lignite deposits of Ptolemaida-Amynteo and Kozani basins, such as those of "South Field", Amynteo, Petrana etc. (Fig. 8).

The houdite and hydromagnesite deposits are locating in the upper formations of the Kozani basin.

The thickest parts of this series, about 500m, were observed in the central and west section of the Ptolemaida-Amynteo basin (Proastion deposit). Also in this area the thickest lignite seam (385 m) and lignite bed (60 m) were observed. This is the result of the ideal conditions concerning the relation of synizesis and deposition. The depositional rate of the vegetable mater followed the rhythm of the synizesis leading to the big Ptolemaida-Amynteo deposits.

A normal transition from the underlying formations of the Early Neogene's series (Late Miocene-Early Pliocene), to the overlying formations of the Late Neogene's series (Early-Late Pliocene) is observed. The absence of these formations in Florina, Sarandaporo basins and the east-northeast section of the Ptolemaida-Amynteo basin, is due to the tectonic activity of this period, which resulted to the rise of these sections of the graben.

After the deposition of the Neogene's formations, begins the deposition of **Proastion formation** (Figs 4, 5) during the Early-Middle Pleistocene (Villafrangian). They are fluvial, fluvial - torrential deposits.

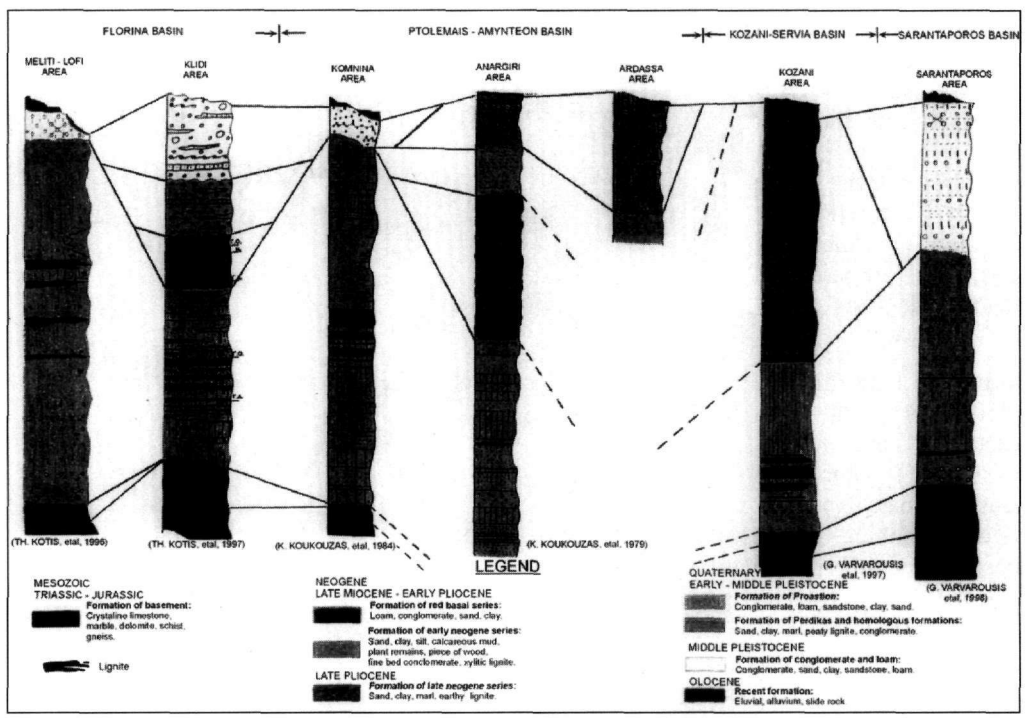

Figure 4 - Stratigraphic correlation between lignite basins of Florina, Ptolemaida – Amynteon, Kozani and Sarantaporo

This formation is limited mainly in the Ptolemaida– Amynteo basin and the southeast section of the Florina basin (Klidi area) (Fig. 9). An unconformity with the underlying Neogene's formations is observed. The main volume of this formation, as well as its stratigraphy, is observed in the ho-

monymous area of Proastion.

After the deposition of the Proastion formation, a strong, fault tectonism, of northeast-southwest and east-west main direction is observed, because of which new smaller basins were created inside the preexistent ones, for example the Ardassa-Vegoritida and Anargyroi-Petron basins. At the same time elevations are formed, or these that already exist amount more. Generally this tectonism along with the preexisting one created the present morphology of the graben.

The deposition of **Perdika formation** follows (Figs 4, 5), mainly in the new basins that are formed within the Ptolemaida-Amynteo basin, after the tectonics that has already been described (Fig. 10). These are fluvial, fluvial- torrential and lacustrine-marshy deposits. A new phase of thick lignitogenesis, with small beds of lignite and thick intermediate wastes is observed. (Fig. 11).

During the Middle Pleistocene we have the deposition of one **terrestrial, fluvial-terrestrial formation** (Fig. 5). This formation is stretching in the southeast section of the Florina basin, in major part of the Sarandaporo basin, in the southeast borders of the Ptolemaida basin and around the Kozani- Servia basin. In most of Sarandaporo basin, this formation is corroding the Early Neocene series formations and acquires its major thickness (Fig. 12).

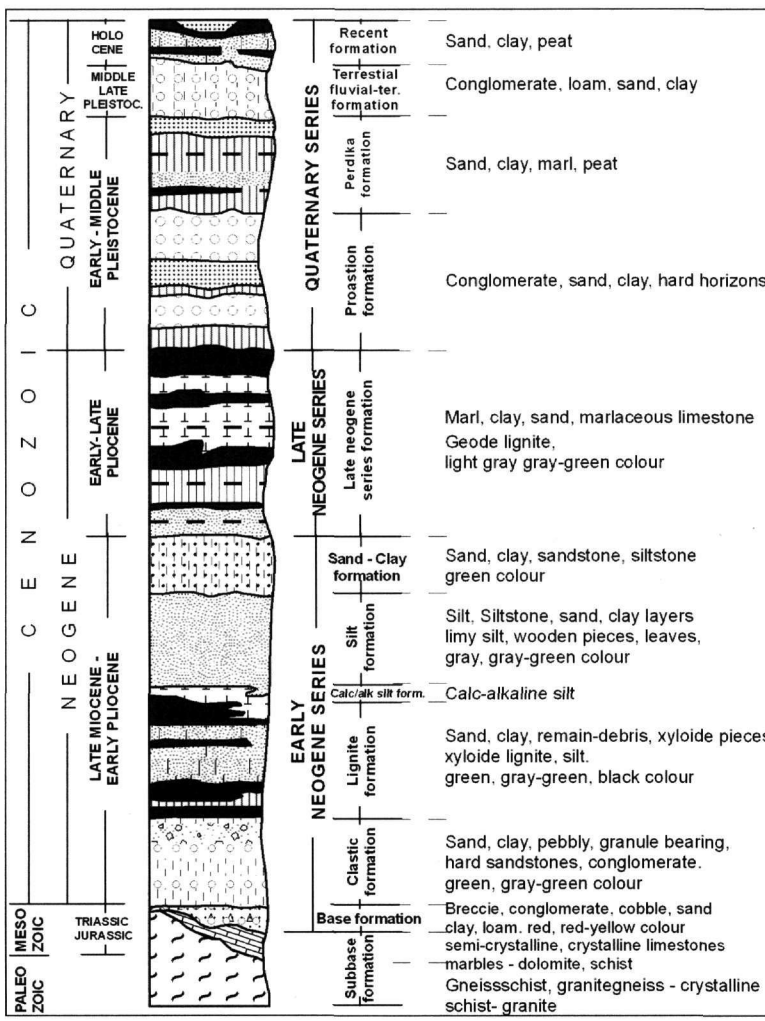

Figure 5 - Synthetic stratigraphic column of the Florina, Ptolemaida – Amynteon, Kozani, Sarantaporo Graben

On the surface we observed contemporary low thickness terrestrial depositions, like **eluvia mantles, alluvial depositions** and **alluvial fans**.

Likewise during the Holocene we have **deposition of peat** in the lakes Chimaditida, Zazari and Vegoritida, where we also observe the last phase of lignitogenesis (Fig. 13).

A schematic representation of the Kozani-Servia basin's paleogeographic evolution is given in Fig. 14, through the different geological periods. The evolution of the entire graben is about the same.

3. Geology – Stratigraphy of the Graben

The basement and the borders of the depression belong, as mentioned above, in the Pelagonian zone and consist of hemi-crystalline to crystalline Triassic-Jurassic limestones, marbles, dolomites and schists. In many places there are lenticular intercalations of phyllites, like in the elevation of Kozani. Also around the city of Kozani and in the west and south of the Kozani-Serbia basin, we observe Jurassic ophiolite rocks. The Pelagonian zone formations also consist of other rocks and occupy mainly the east and south-southwest borders of the graben. The west and northeast borders are composed by formations of the Paleozoic crystalline basement of the Pelagonian mass, and mainly consist, of gneissoschists, granitogneissous and crystalline schists. Similar rocks are also found on the borders of the Sarandaporo basin. We should also mention the known granites that can be observed on the west borders of the Florina basin.

During the Late Miocene-Early Pliocene, the tectonic fault and mostly the basins included in it, begin to fill with terrestrial, fluvial- torrential, fluvial, lacustrine-fluvial, lacustrine and marshy depositions. Thus indicates the deposition of the Early Neogene series (Figs 4, 5, 6). The series age is determined through the diatoms examination (E. Velitzelos), the paleobotany (Schneider and Velitzelos 1973, 1976, 1977) and the palynologic examination (Ioakeim and Vasileiou 1982, Ioakeim 1985), as Late Miocene (;)- Early Pliocene and is comprised, from bottom to top, by the following formations:

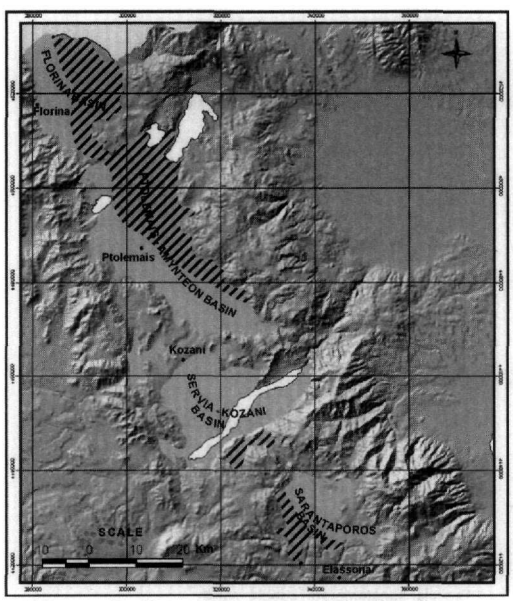

Figure 6 - Location map of lignite formation of late Neogene's series

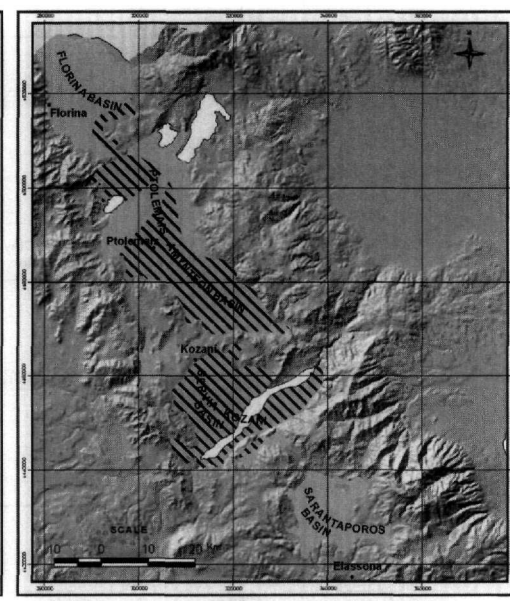

Figure 7 - Location map of late Neogene's

Initially we have the deposition of talus, terrestrial and fluvial- torrential sediments (**Base formation** – Fig. 6) which consist of breccias, whose elements are in proportion to the underlying or nearby basement rocks, conglomerate, disk-shaped stones with varied size elements, in alternation

with sands, clays and mud. The dominating color is red- red brown.

This formation fills and smoothes the irregular surface of the first graben basement. Because of this the formation's thickness varies from one place to the next and sometimes can vary from a certain minimum to several tens of meters. Indicatively we report, that the thickness in the Komnina area is 80m. The base formation expands all over the graben.

Stratigraphically fluvial deposits lie on the previous base formation (Fig. 5); they consist of fine to coarse sands sometimes clayey, and clays in some places sandy. There are interferences of pebbly and granule bearing layers, hard sandstone horizons, as well as conglomerate layers (**clastic formation**) (Fig. 5). Green and green-gray are the prevailing colors. Naturally, in every section of the fluvial system, we find the corresponding sediments.

The lacustrine- fluvial and marshy deposits (**lignite bearing formation**) (Fig. 5) overlying the previous formation, consist of sands, clays with plant remains, xylite pieces and lignite beds of "xylitic type", in alteration with silt and rarely marl. Green and green-gray are the prevailing colors. The biggest "xylitic type" lignite deposits are hosted in this formation, like those of Florina (Kotis *et al.* 1992, 1995, 1996, 1997), Komnina (Koukouzas *et al.* 1984), Lava etc.

This system develops in a clearly lacustrine environment and occupies almost entirely the graben. So, we have the deposition of the silts (**Silt formation**) (Figs 4, 5), with beds of sands and clays in some places. Frequently we observe interferences of calcareous silt - limy silt. In these sediments wood pieces, plant remains, leaves and mineral vivianite are observed. Gray and green-gray are the prevailing colors. On the top of the lignite-bearing stack lies a thin layer of calcareous silt with Ostracodes and operculum (**calc-alkaline silt formation**) is observed (Fig. 5).

This lacustrine system prevails mainly on the Sarandaporo basin, the south-southeast section of the Kozani-Servia basin and the east section of the Ptolemaida – Amynteo basin. On the west of this and the Florina basin, there is the prevalence of a fluvial – fluvial-lacustrine environment with the corresponding sediments. Instead of the silts it is finding fine to coarse sands, with interferences of clays and rarely silts.

Fluvial depositions, overlying the previous formations, consist of alternations of sands, clays with beds of sandstone and siltstone, (**sand-clay formation**) (Fig. 5). The prevailing color is green.

Afterwards and during the Late Pliocene, the previously mentioned lacustrine system is evolving into a lacustrine-marshy system resulting to the deposition of the Late Neogene's series formation (Figs 4, 5).

Due to the tectonic activity and the paleogeographical and paleogeomorphological conditions that prevailed this period, this system occupies the entire Ptolemaida – Amynteo basin, with the exception of the east-northeast section, the Kozani-Servia basin and finally reaches in small endings the southeast section of Florina basin (Fig. 7).

The sediments observed in the Late Neogene's series formation (Figs 4, 5) are marls, clays, sands, marly limestone and earthy lignite, alternated and combined. The prevailing colors are light gray and gray-green.

Fossils of gasteroides (Vetoulis 1956, Gramman 1960) such as *Theodoxus macedonicus* (Neritina), *Valvata piscinalis* etc., lamel gills (Gramman 1960), such as Unio sp. etc, Ostracods such as *Candona neglecta, Iliocypris gibba* e.t.c. and rodents (van de Weerd, 1979) are observed. Traces of paleoflora were specified and pollen was analysed (Ioakim, 1985). From these analyses the age of these formations is set at the limit of Early and Late Pliocene.

In this series the largest known lignite deposits of Ptolemaida-Amynteo and Kozani basins are found, such as these of "South Field" (Anastopoulos and Koukouzas 1972), Amynteo (Koukouzas *et al.* 1979), Perana (Anastopoulos and Brousoulis 1973), etc. (Fig. 8).

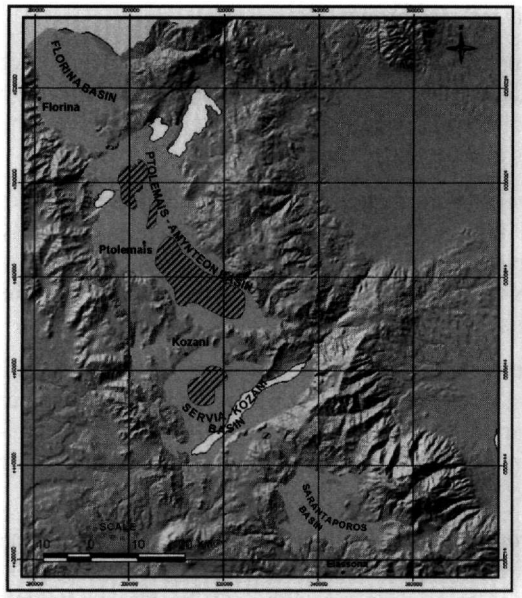

Figure 8 - Map of late Neogene's series deposits (geode lignite deposits)

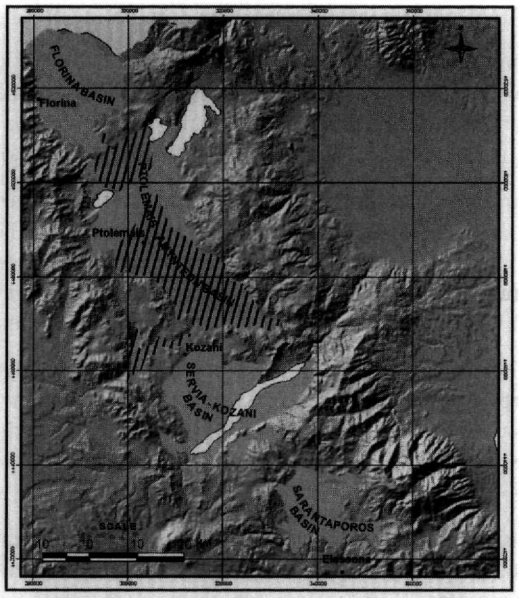

Figure 9 - Location map of Proastion formation

After the Neocene formations deposition, begins the **Proastion formation** deposition (Fig. 5), during the Early-Middle Pleistocene (Villafrangian). There are fluvial, fluvial-torrential depositions that consist of conglomerate, mixed with well-rounded stones of various sizes, with local alternations of sands and clays. These formations are characterised by cross bedding and hard horizons. The formation's maximum thickness is 150 m. During the research, no fossils have been found in the graben, except some Unio at some places. Fine beds of lignite or marshy formations have been observed locally; their extension is small and has no economic interest.

This formation is limited mainly in the Ptolemaida-Amynteo basin and in the southeast section of the Florina basin (Klidi area) (Fig. 9). It is in unconformity with the underlying Neogene formations. The site with the largest volume and presentation of the formation is found in the Proastion area, which actually gave it its name.

Later follows the deposition of **Perdika formation** (Fig. 5), mainly inside the Ptolemaida – Amynteo basin in the newly created sub basins of tectonic origin as previously mentioned (Fig. 10). These depositions are fluvial, fluvial-torrential, lacustrine and marshy. They consist of sands, clays, marls and beds of lignite.

The tectonic activity continued during the Perdika formation deposition, with extended movements, so thick layers of lignite are not observed. On the contrary, many fine beds of lignite with thick interferences of wastes are observed. That is why the lignite deposits of this period have no economic interest (Fig. 11). In the Ardassa area the formation reaches its top thickness at about 350m.

During the middle Pleistocene a terrestrial, fluvial-terrestrial formation is deposited (Fig. 5) and consists of conglomerate with various sized round stones and cobbles, of red loam beds, clays and sands. In some places hard horizons are observed. This formation is spread, as mentioned above, in the Florina basin, as well as in the Sarandaporo basin, where it acquires its maximum thickness (Fig. 12), in the southeast borders of the Ptolemaida – Amynteo basin and on the borders of the Kozani-Serbia basin.

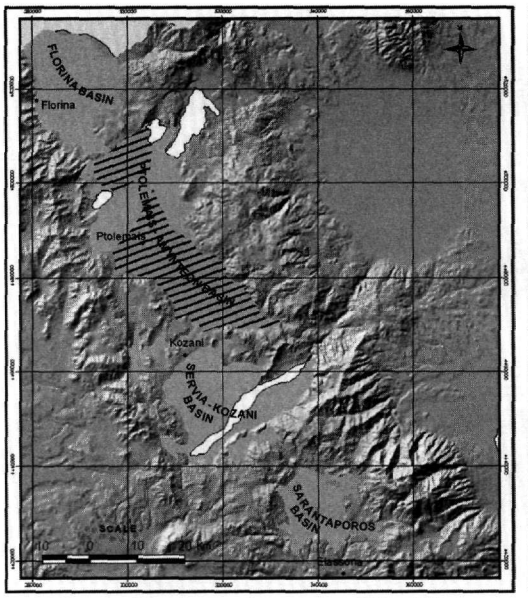

Figure 10 - Location map of Perdika formation

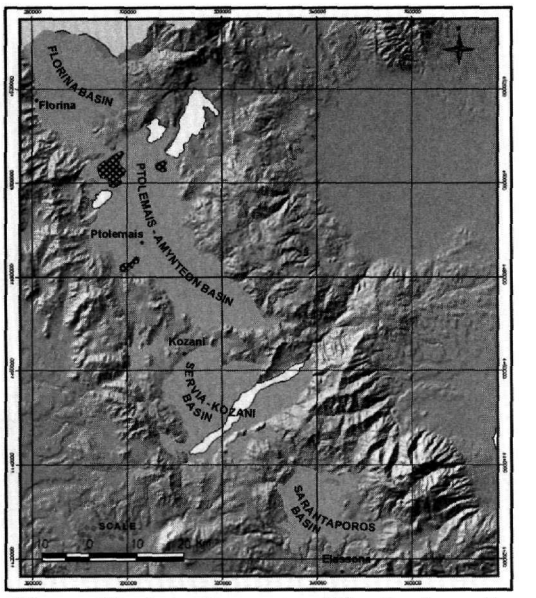

Figure 11 - Location map of lignite deposit in Perdika formation

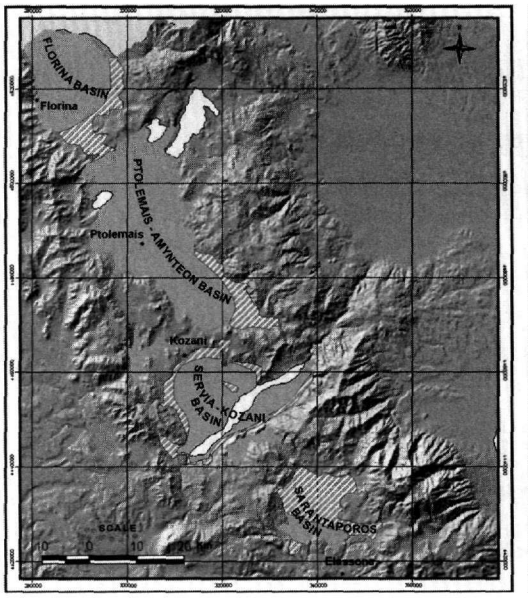

Figure 12 - Location map of Quaternary terrestrial deposit formation

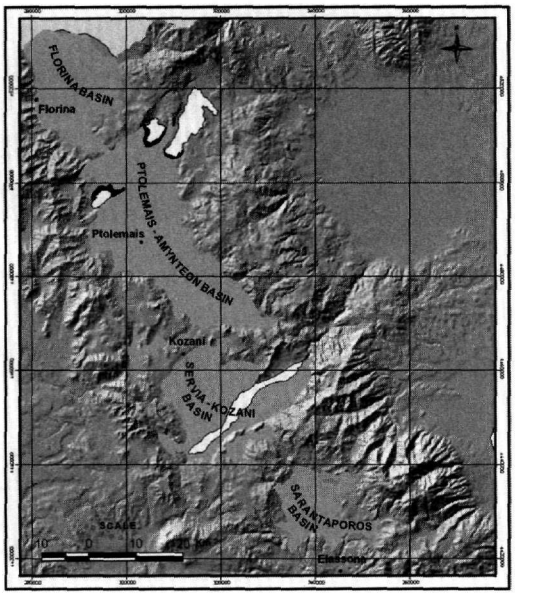

Figure 13 - Location map of recent peat

On the surface lie fine contemporary terrestrial depositions, such as eluvia mantles, alluvial deposits and alluvial fans.

We must also mention that during the Holocene peat is deposited in the remaining lakes Chimaditis, Zazari and Vegoritida, where the last phase of lignitogenesis can be observed (Fig. 13).

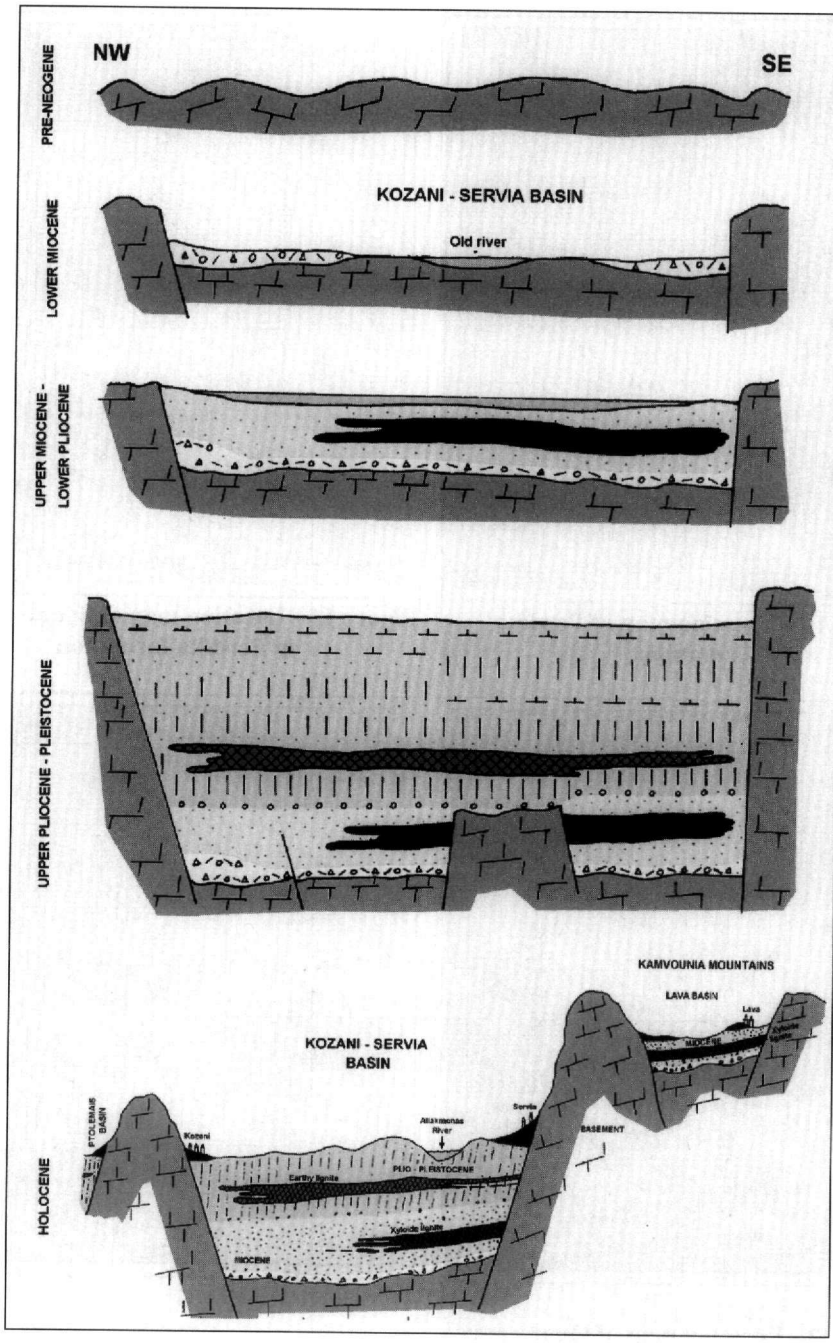

Figure 14 - Evolution of the basin from late Miocene till recently

4. Conclusion

The creation of the graben of Florina, Ptolemaida-Amynteo, Kozani-Serbia, as well as that of Sarandaporo basin, began after the Alpine cycle ended and continues still.

The most important lignite deposits of Greece have been deposited in this graben, developed inside marshy, lacustrine and fluvial-lacustrine depositions whose age is mainly Early Pliocene, Late

Miocene (;).

In the graben and mainly in the Ptolemaida – Amynteo basin, four (4) phases of lignitogenesis have been specified:

- Late Miocene – Early Pliocene (lignite "Xylitic type")
- Early – Late Pliocene (lignite "Geode type")
- Pleistocene (lignite – peat lignite)
- Holocene (peat)

5. Acknowledgments

We would like to thank all our colleague scientists, technologists and technicians who have worked in the area and participated through the results of their research in the synthesis of this paper, and dedicate it to the memory of those who have passed away. Due to limited space we report the Geologists J. Papastamatiou, J. Anastopoulos, K. Koukouzas, Th. Agiotis, D. Dimitriou, the foremen G. Georgopoulos, G. Mitrokostas, Chr. Koutsonas, the technicians J. Anyfantis, K. Christodoulou, Ch. Peglidis.

6. References

Anastopoulos, J.C., and Brousoulis, I., 1973. Lignite bearing Kozani-Servia basin, (Geology – Economic Geology - Drilling study), *N.I.G.M.E.*, 1-77pp., Athens. (in Greek)

Anastopoulos, J.C., and Koukouzas, C.N., 1972. Economic geology of the southern part of Ptolemais lignite basin I.G.S.R., *Geological and Geophysical research*, XVI (1), 1-189. (in Greek)

Barrabe, L., and Feys, R., 1965. Geologie du carbon et des basins Houillers, Mason et cie, Paris.

Ehlers, H., 1960-62. Expertise Ptolemai 21 Bder. (Bericht unverof – fentlicht)

Gersonde, R., and Velitzelos, E., 1978. Diatomeenpalaookologie im neogenbecken von Vegora N-W Mazedonien (vortaufige mitteinlung), *Ann. Geol. Pays Hell.*, 29(1), 373-382.

Gramann, F., 1960. Die Fossilien des Braunkohlenbeckens in Ptolemais – Komanos, Unpublished report. Archive 22625, „Bundesanstalt für Gewissen schafften und Rohstoffe", 1-11, Hannover, Institute of Geology and Mineral Exploration, 1983. Geological map of Greece, Map of Geotectonic Zones of Greece, Echelle 1:500.000.

Ioakim, Ch., 1985. Analyse palynologique des depots lacustres du Pliocene de Ptolemais, Grece septentrionale: un element nouveau dans la reconstitution de l'histoire paleoclimatique des regions méditerranées orientales, *Paleobibliologie Continentale,* XIV(2), 315-332.

Ioakim, Ch., and Vassiliou, D., 1982. Correlation of the drill cores $A\Pi_{14}$, $A\Pi_4$, P_6, P_7, $\Delta\Pi_{21}$ and $\Delta\Pi_{25}$ of the Ptolemaida basin, *Stratigraphy of the Greek lignites*, No 7, 1-48. (in Greek)

Kotis, Th., Metaxas A., Ploumidis M., and Varvarousis, G., 1995. Exploration of lignite deposits in the eastern region of the Florina basin, subarea Achlada- Meliti, I.G.M.E., 1p., Annex I 1-10pp., Athens. (in Greek)

Kotis, Th., Ploumidis, M., Metaxas A., and Varvarousis, G., 1992. Exploration of lignite deposits in the Florina basin, subarea Vevi. (W. Macedonia), I.G.M.E., 1-97pp., Annex I 1-45pp., Annex II p. 1-10, Athens. (in Greek)

Kotis, Th., Ploumidis, M., Metaxas, A., and Varvarousis, G., 1996. Exploration of lignite deposits in the eastern region of the Florina basin, subarea Meliti-Lofi, I.G.M.E., 1-91pp., Annex I

1-11pp., Athens. (in Greek)

Kotis, Th., Ploumidis, M., Metaxas, A., and Varvarousis, G., 1997. Exploration of lignite deposits in the area of Klidi Florina. I.G.M.E., 1-87pp., Athens. (in Greek)

Koukouzas, K., Kotis, Th., Ploumidis M., Metaxas A., 1979. Coal exploration of Anargiri-Amynteon area, *I.G.M.E., Mineral deposit research*, No9, 1-69. (in Greek)

Koukouzas, K., Kotis, Th., Ploumidis M., and Metaxas A., 1981. Coal exploration of "Apophisis" field of Anargiri-Amynteon area, *I.G.M.E., Research for energy resources*, No1, 1-52. (in Greek)

Koukouzas, K., Kotis, Th., Ploumidis M., Metaxas A., and Dimitriou, D., 1984. Coal exploration of Komnina area, Ptolemais district (W. Macedonia). I.G.M.E., *Research for energy resources*, No2, 1-103. (in Greek)

Koukouzas, K., Kotis, Th., Ploumidis M., Metaxas A., and Dimitriou, D., 1985. Lignite deposits of Ptolemaida trench. *Proceedings of the International meeting for the exploitation of low energy solid fuel*, 1-10pp, Deh, Ptolemaida. (in Greek)

Schneider, H., and Velitzelos, E., 1973. Jungtertiare pflanzenfunde aus dem Becken von Vegora in West Mazedonien (Griechenland). Ann. Mus. Goulandris, 1, 245–249pp., 2 pl.h.t., Athens.

Schneider, H., and Velitzelos, E., 1976. Eine Neogenflora im Becken von Vegora 9NW-Mazedonien), *Bulletins de la Société Geologique de France période*, 1971-1980.

Vasiliou, D., 1982. Palynologic research of the drill core $\Delta\Pi_{21}$ of Komnina area, Ptolemais district, Unpublished report. I.G.M.E., 29pp., Athens. (in Greek)

Varvarousis, G., Metaxas, A., Kotis, TH., Ploumidis, M., and Vrettos, K., 1997. Wilfulness report for geological works for the lignite deposits of the Kozani-Servia basin, *I.G.M.E.*, 1-41pp., Athens. (in Greek)

Varvarousis, G., Metaxas, A., Kotis, TH., Ploumidis, M., and Vrettos, K., 1998. Exploration of lignite deposit of the Saradaporo basin. I.G.M.E., 1-30pp., Annex I 10pp., Athens. (in Greek)

Velitzelos, E., and Schneider, H.E., 1977. Jungtertiare Pflanzenfunde aus dem Becken von Vegora in WestMazedonien (Griechenland) In 8vo, offp., 8pp. con 7 figs. Naturama. Italy.

Vetoulis, D.G., 1956. Contribution of the geology knowledge of the Ptolemaida basin, *Ann. Geol. Pays Hell.*, 8 , 48-79. (in Greek)

Weerd Van de, A., 1979. Palynology of some Upper Miocene and Lower Pliocene Sections in Greece. Preliminary results, biostratigraphic implications. *Ann. Geol. Pays Hell.*, Hors series, fasc. 3, 1253-1262pp., Athens.

Δελτίο της Ελληνικής Γεωλογικής Εταιρίας τομ. XXXX, 2007
Πρακτικά 11ου Διεθνούς Συνεδρίου, Αθήνα, Μάιος 2007

Bulletin of the Geological Society of Greece vol. XXXX, 2007
Proceedings of the 11th International Congress, Athens, May, 2007

APPLICATION OF BED THICKNESS DISTRIBUTIONS IN LATE EOCENE-OLIGOCENE TURBIDITE DEPOSITS OF GREECE: SOME PRELIMINARY RESULTS

Pantopoulos G.[1], Konstantopoulos P.[1], Maravelis A.[1], and Zelilidis A.[1]

[1] *University of Patras, Department of Geology, Division of Physical Geology, Marine Geology & Geodynamics, Laboratory of Sedimentology, 265 00 Patras, Greece, gpantop@upatras.gr, tkonstan@upatras.gr, amaravel@upatras.gr, A.Zelilidis@upatras.gr*

Abstract

A simple application of bed thickness distributions was attempted in outcrops of Late Eocene-Oligocene turbidites in three dispersed localities of Greece. The three studied sections are located at Evinohori area (West Greece), Karpathos Island (SE Greece) and Limnos Island (NE Greece). All outcrops show similar sedimentological characteristics. Three types of plots were used: log-log, log-probability and frequency curves. Bed thickness data indicate similarity between West-SE Greece turbidites and discrimination from NE Greece turbidites which is attributed to different basin morphology due to different tectonic processes.
Key words: *submarine fans, turbidites, bed thickness analysis.*

Περίληψη

Μια απλή εφαρμογή των κατανομών πάχους στρωμάτων επιχειρήθηκε σε φυσικές τομές τουρβιδιτών Άνω Ηωκαινικής – Ολιγοκαινικής ηλικίας σε τρεις διαφορετικές περιοχές της Ελλάδας. Οι τρεις τομές που μελετήθηκαν βρίσκονται στο Ευηνοχώρι Αιτ/νίας (Δυτική Ελλάδα), το νησί της Καρπάθου (ΝΑ Ελλάδα) και το νησί της Λήμνου (ΒΑ Ελλάδα). Όλες οι τομές παρουσιάζουν παρόμοια ιζηματολογικά χαρακτηριστικά. Τρία είδη διαγραμμάτων χρησιμοποιήθηκαν: διάγραμμα λογαρίθμου-λογαρίθμου, λογαρίθμου-κλίμακας πιθανότητας και καμπύλης συχνότητας. Οι κατανομές του πάχους των στρωμάτων και στα τρία είδη διαγραμμάτων δείχνουν ομοιότητα ανάμεσα στους τουρβιδίτες Δυτικής και ΝΑ Ελλάδας και διαφορά τους από αυτούς της ΒΑ Ελλάδας. Το γεγονός αυτό πιθανά οφείλεται σε διαφορετική μορφολογία των λεκανών ιζηματογένεσης των τουρβιδιτών, λόγω διαφορετικών τεκτονικών διεργασιών.
Λέξεις κλειδιά: *υποθαλάσσια ριπίδια, τουρβιδίτες, ανάλυση παχών στρωμάτων.*

1. Introduction-Geological Setting

A simple application of bed thickness statistical distributions was attempted in outcrops of late Eocene-Oligocene turbidites in three dispersed localities of Greece (Fig. 1). These localities represent similar depositional environments and cover most of the country's area. The three studied sections are located at Evinohori area (west Greece), Karpathos Island (SE Greece), and Limnos Island (NE Greece). West and SE Greece outcrops belong to Gavrovo and Ionian geotectonic zones respectively (External Hellenides units). Turbidite deposits of west Greece were

deposited in a complex elongated foreland basin system formed by Pindos thrust fault from middle Eocene to late Oligocene (Vakalas 2003). A confined foreland basin model is proposed for Karpathos turbidites (Pantopoulos 2004). Limnos Island turbidites are considered a part of the molassic basins of the North Aegean Area (Internal Hellenides units) (Roussos 1993).

The aim of this work is the use of bed thickness distributions as a quantitative tool of turbidite research (combined with field observations), in order to provide information about sedimentation characteristics of turbidites.

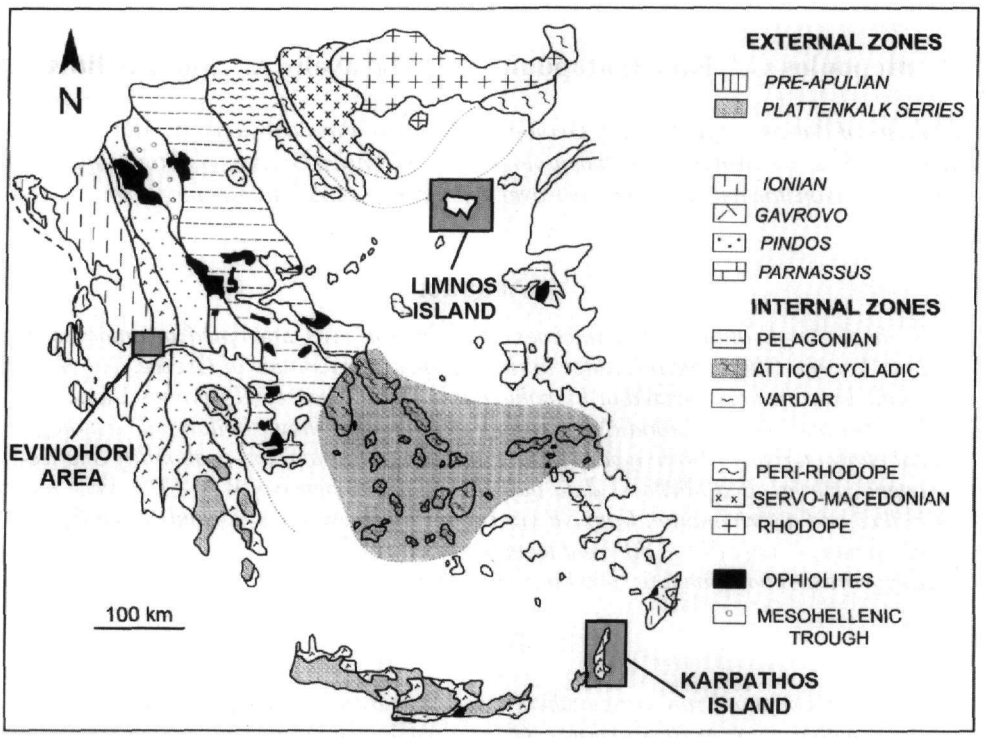

Figure 1 – Geotectonic map of Greece. The studied outcrop areas are shown in boxes

2. Methodology

In total, 470 sandstone beds were measured in the three studied sections. Three types of distribution plots were used for the bed thickness data: an exceedence probability plot in log-log axes, a logarithmic probability plot and a frequency curve plot (a histogram type) of bed thickness. The shape of bed thickness trend in each plot gives information about the type of statistical distribution that fits the data and shows similarities or differences between the data sets. Processing of results was based also on previous studies of turbidite bed thickness distributions made by Rothman and Grotzinger (1995), Carlson and Grotzinger (2001) and Talling (2001). The bed unit that was measured for the bed thickness distributions is the arenaceous component of the turbidite (Bouma divisions Ta-d) (Bouma 1962), which practically represent the sandstones of a turbidite outcrop. The measurement unit is centimetres (cm). A minimal cut-off thickness of 1 cm was established due to measuring difficulties below that thickness. In case of amalgamated or rippled beds, an average thickness was taken after several measures. The thickness of all the sandstone beds above 1 cm was measured in the three studied outcrops (Table 1), normal to bedding, using a tape measure.

3. Outcrop Characteristics

3.1. Limnos Island Outcrop

The studied outcrop (Fig. 2) is located at the southeast part of the island near Skandali settlement. Bed thickness ranges from 1 to 33 cm. The number of beds measured is 189. The outcrop represents a part of the lowest stratigraphic submarine fan unit in the island (Unit 1, Fig. 2). This unit, up to 100 m total thickness is characterized by fine to medium-grained sandstones grading upwards to very fine-grained sandstones interbedded with hemipelagic claystones. Sandstones often exhibit parallel lamination, cross- laminations and/or climbing ripples defining sequence Tb and Tc divisions of Bouma, (1962). The cross-lamination is commonly overlain by convolute lamination. The sandstone beds have flat bases and very good lateral continuity (at least a hundred meters). The claystone facies are brownwish and typically lack internal structure, although beds with silt lamina, with an upward decrease in lamina thickness have been recognized. The characteristic features of this unit demonstrate deposition from both low and high-density turbidity currents. The sandstone and claystones beds are classified as sedimentary facies C2.1, C2.2 and C2.3 and D2.2 in the Pickering *et al.* (1986) nomenclature, respectively. The common occurrence of convolute and climbing ripples clearly indicates rapid deposition of sediments from suspension. Such rapid deposition is related to the dilution of flow associated with the transition from confined, channelized conditions, with high gradients, to unconfined, lateral spreading across more gently sloping depositional lobe areas (Maravelis *et al.* 2007). Those characteristics classify the outcrop deposits as distal from the sediment source and probably outer fan deposits (Mutti and Ricci Lucchi 1972). Limnos Island turbidites have a late Eocene to early Oligocene age (Roussos 1993).

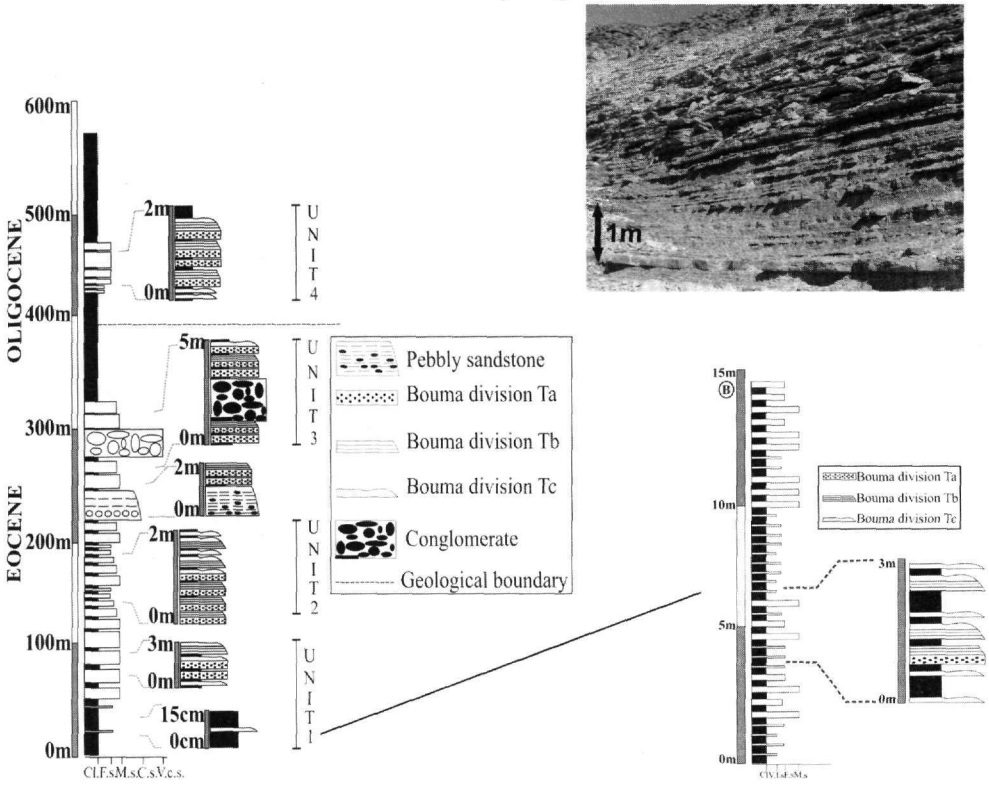

Figure 2 – General stratigraphic framework of submarine fan deposits at Limnos Island (left), with a log and photo of the studied section (right). Modification from Maravelis *et al.* (2007)

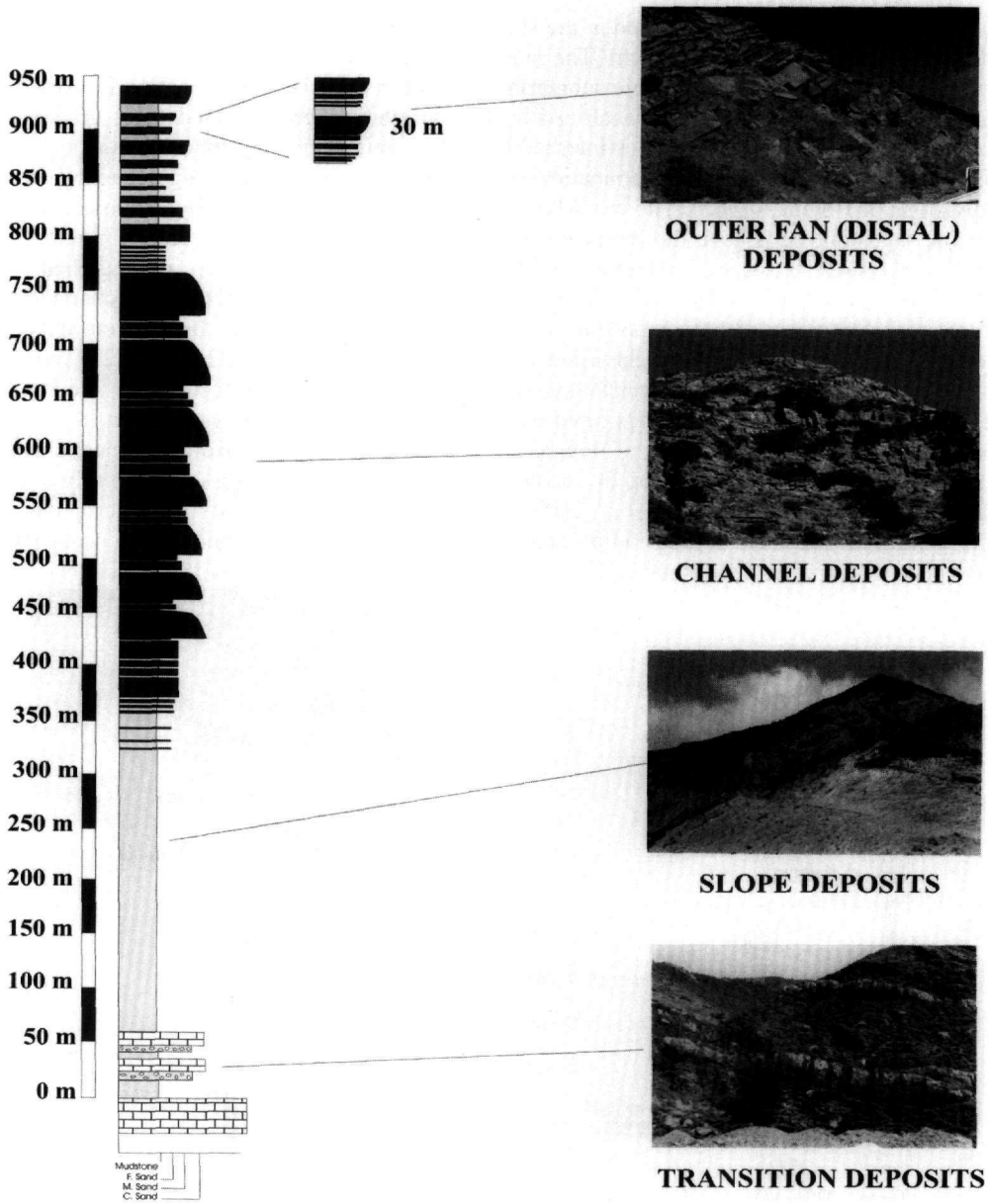

Figure 3 - General stratigraphy of the northern submarine fan basin of Karpathos. The studied section can be observed at the top photo and log. Modification from Pantopoulos (2004)

3.2. Karpathos Island Outcrop

136 beds were measured in the Karpathos Island outcrop (Fig. 3) that is located at the central part of the island, near Spoa settlement. Bed thickness ranges from 1 to 230 cm. The outcrop belongs to the upper stratigraphic units of the northern submarine fan basin of the island (Pantopoulos 2004) and consists of fine-grained sandstone-mudstone alternations which overlie a thick channel-conglomerate submarine fan system which shows evidence of confinement. These sediments

probably were deposited during abandonment of the channels due to the infilling of the topographically confined basin. Sandstone beds consist mainly of Bouma Tabc divisions, are fine-grained and have flat bases. Scarcity of amalgamation surfaces is also observed. These features suggest deposition from both low and high density turbidity currents (Lowe 1982) in a distal from the sediment source submarine fan environment. A late Eocene (Priabonian) to Oligocene age is proposed for Karpathos Island turbidites (Christodoulou 1967, Fytrolakis 1989).

3.3. Evinohori Outcrop

This outcrop (Fig. 4) is located at Antirrio-Agrinio national road, near Evinohori village. Bed thicknesses of the 145 measured beds range from 1 to 140 cm. The outcrop belongs to the lower stratigraphic submarine fan units of the area (southern Pindos foreland basin) and probably is a part of the Ellenika formation (Piper *et al.* 1978, Vakalas 2003). Previous workers give a distal submarine fan depositional setting for the turbidites of the Ellenika formation. Sandstone beds consist mainly of Bouma Tabc divisions, are fine to medium-grained and have flat bases. Amalgamation surfaces are rare. Also a thickening-upward sequence of bed thickness can be observed in the outcrop. These features suggest deposition from both low and high density turbidity currents (Lowe 1982) and classify the outcrop deposits as distal from the sediment source and probably outer fan deposits (Mutti and Ricci Lucchi 1972). A late Eocene to late Oligocene age is proposed for Evinohori area turbidites (Vakalas 2003, Vakalas *et al.* 2004).

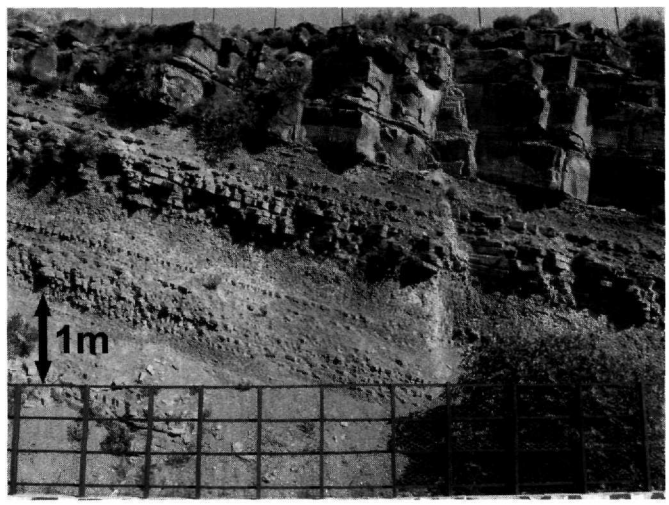

Figure 4 – Evinohori outcrop. A thickening-upward sequence can be observed

Table 1 - Summary of bed thickness data

Outcrop	Number Of Beds	Bed Thickness Range	Average	Standard Deviation
Limnos Island	189	1-33 cm	3.43 cm	3.86
Karpathos Island	136	1-230 cm	14.71 cm	30.31
Evinohori Area	145	1-140 cm	10.78 cm	19.89

4. Bed Thickness Plots

4.1. Log-Log Plot

An exceedence probability plot of sandstone bed thickness was created for each section in a plot with logarithmic values. Straight lines on these plots indicate power law frequency distributions which express scale invariance and self-similarity of a system. Bed thickness data from the three studied sections (Fig. 5) shows a high R^2 value to a linear fit ($R^2 > 0.9$) in the log-log plot. However, nonlinearity can be observed in the log-log plot especially for Evinohori and Karpathos data. A high R^2 value of a linear fit in a log-log plot does not always mean that all data follow a power law distribution but gives a good estimation of the possible power law exponent. Previous studies propose segmentation of the linear fits between thin and thick beds. The latter method gives better fitting and information about the three-dimensional arrangement of the beds (Malinverno 1997). This study attempts a simple fitting application to approximate the power law exponents taking into account the arguments of previous workers. The log-log plot indicates that there is a difference in the power law exponent (linear fit gradient) between the datasets. Turbidites of Evinohori and Karpathos have similar exponents less than unity (approximately 0.8), in contrast with Limnos turbidites which have an exponent more than 1 (approximately 1.3).

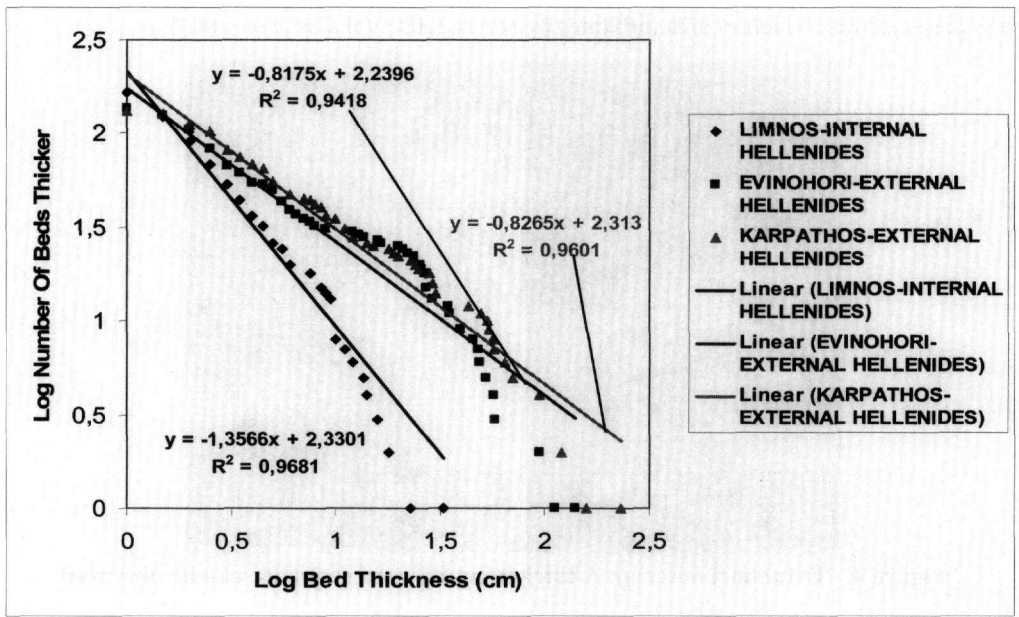

Figure 5 – Log-Log exceedence probability plot

4.2. Log-Probability Plot

A logarithmic probability plot of thickness was also created for each section. Straight lines on these plots indicate log-normal frequency distributions. The logarithmic probability plot (Fig. 6) shows similar segmented trends for west and SE Greece (Evinohori and Karpathos) and a different, more linear trend for NE Greece (Limnos). The stepped trends do not indicate a single log normal distribution but a mixture of log normal distributions (Talling 2001) is possible to be present.

4.3. Frequency Curves

Histograms of the bed thickness data were created, using a logarithmic axis and 5 cm bins. The line that passes from the histogram middle value of each bin forms the frequency curve. Symmetrical (Gaussian) bell-shaped curves on these plots indicate normal or log-normal frequency distributions, depending on the axis scale. In the frequency curve plot (Fig. 7), west and SE Greece data

are again similar and show two symmetrical peaks that are suggestive of a lognormal mixture, in contrast with NE Greece which is showing only one mode, characteristic of a single lognormal population.

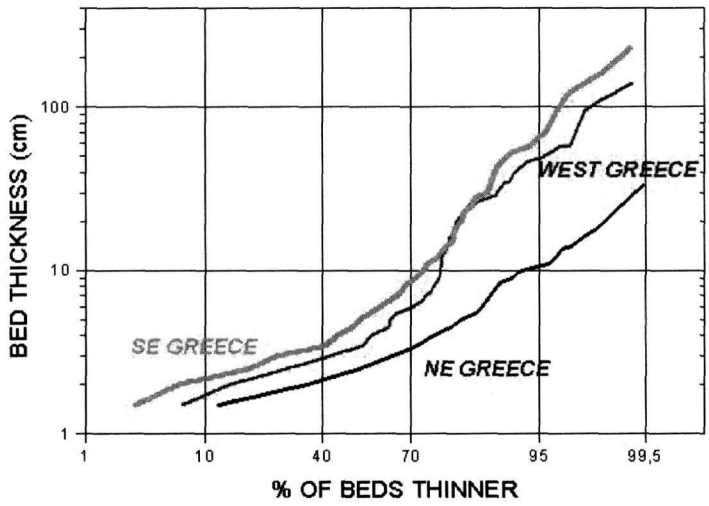

Figure 6 – Log-probability plot

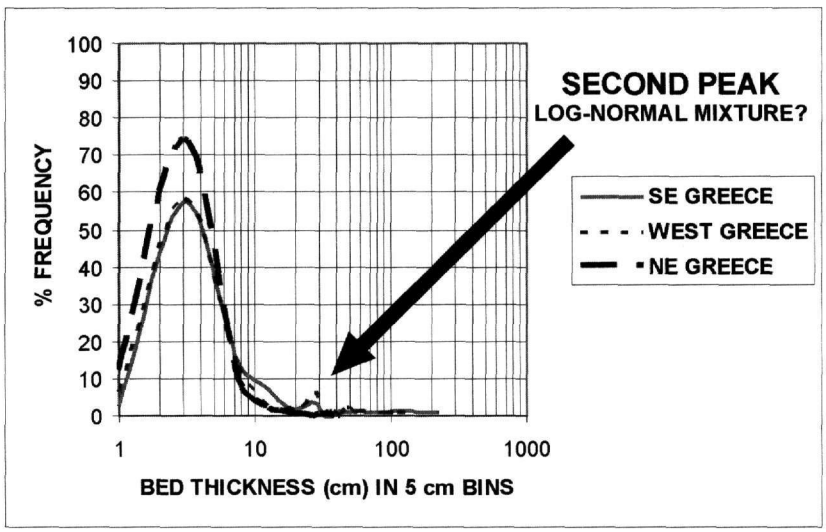

Figure 7 – Plot of frequency curves. West and SE Greece datasets seem to be bimodal

5. Discussion and Conclusions

5.1. Basin Morphology

Rothman and Grotzinger (1995) analyzed bed thickness datasets of turbidites and debris flow deposits of California and South Africa and proposed that variations in the scaling exponent of turbidite power law bed thickness distributions, regional or within the same deposit, are indicative of basin geometry and rheology of the sedimentary gravity flows. They introduced a spreading expo-

nent relative to the bed thickness exponent and the bed volume scaling exponent. In general, deposits with low thickness scaling exponent seem to have lower spreadibility than deposits with higher scaling exponents. The log-log plot of the bed thickness dataset of this study shows two main scaling exponents for three cases of sedimentologically similar turbidites: approximately 0.8 for west and SE Greece turbidites (External Hellenides units), and 1.3 for NE Greece turbidites (Internal Hellenides units). The latter implies that basin geometry played a more important role than flow rheology in the exponent variation and also that west and SE Greece turbidites have a lower speadibility than NE Greece turbidites. This can be expained by the paleogeography of the area at late Eocene-Oligocene: Turbidites of west and SE Greece belong to the external Hellenides units and were deposited mainly in elongated foreland basins (typical in the area in late Eocene-Oligocene), forming thicker beds with low lateral extent. Limnos (NE Greece) turbidites belong to the Internal Hellenides units and were deposited in a tectonically different basin (forearc basin?) in which flows probably were free to spread in wider spaces with lack of topography, forming thinner, laterally extensive beds.

5.2. Type of Bed Thickness Distribution

The log-log plot of the three studied outcrops shows a high R^2 value to a linear fit ($R^2 > 0.9$) indicating a possible power law distribution of bed thicknesses and an agreement between Carlson and Grotzinger (2001) observations and sedimentary characteristics (distal submarine fan turbidites). The log-probability plot and the frequency curves show possible single log-normal or log-normal mixture distributions. The latter is in agreement with Talling (2001) observations. This thickness bimodality could be related with deposition from both dilute and dense flow parts (possibly low and high density turbidity currents) and this is also in agreement with the previous sedimentological results. Further research must be conducted because many types of statistical distributions (power law, log normal, log normal mixtures) can fit the data collected. The type of distribution that characterizes turbidite bed thickness and its relation with submarine fan depositional environments is still a controversial issue. However, depositional information can be extracted from the statistical analysis of turbidite bed thickness data combined with sedimentological observations.

5.3. Concluding Remarks

The observation of different power law bed thickness scaling exponents in sedimentologically similar turbidites of different localities of Greece is useful as a source of depositional information. West and SE Greece turbidite beds seem to have a lower speadibility than NE Greece turbidite beds. Generally, the three plot types used in this research indicate discrimination between west-SE and NE Greece turbidites which is probably due to different basin morphology related to different tectonic processes. Knowledge of differences in sandstone bed thickness and lateral extent is of great importance in hydrocarbon exploration.

6. Acknowledgements

This work was supported by E.C., European Social fund and GSRT Greece, EPAN, PENED `03ED497. Constructive comments by Prof. Riccardo Bersezio and an anonymous reviewer improved the manuscript and are thankfully acknowledged.

7. References

Bouma, A.H., 1962. Sedimentology of some flysch deposits: A graphic approach to facies interpretation, *Amsterdam, Elsevier*, 168pp.

Carlson, J. and Grotzinger, J.P., 2001. Submarine fan environment inferred from turbidite thickness distributions, *Sedimentology*, 48, 1331-135.

Christodoulou, G., 1967. Late Eocene foraminifera from the Karpathos flysch, *University of Thessaloniki Physics-Mathematics Department Review, Thessaloniki,* 10, 163-167. (in Greek with English abstract)

Fytrolakis, N., 1989. Contribution to the knowledge of the pre-Neogene of Karpathos, *Bull. Geol. Soc. Greece,* 23/1, 119-130. (in Greek with English abstract)

Lowe, D.R., 1982. Sediment gravity flows. II: Depositional models with special reference to the deposits of high-density turbidity currents, *J. Sedim. Petrol.,* 52, 279-297.

Malinverno, A., 1997. On the power law size distribution of turbidite beds, *Basin Research,* 9, 263-274.

Maravelis, A., et al. 2007. North Aegean basin evolution during the Late Eocene to Early Oligocene submarine fan deposition: based on sedimentological studies at Limnos Island, NE Greece, *Geologica Carpathica.* (accepted for publication)

Mutti, E., and Ricci Lucchi, F., 1972. Le torbiditi dell'Appennine settentionale: introduzione a11'analisi di facies, *Memoŕe Societa Geologica Italiana,* 11, 161-199. (Translated in English by: Nilsen, T.H., 1978. *International Geology Review,* 20, no. 2, 125-166).

Pantopoulos, G., 2004. Foreland basins evolution in SE Greece: Sedimentological, palaeocurrent and statistical study of submarine fan deposits of Karpathos Island, *Msc. Thesis,* University of Patras.

Pickering, K., et al., 1986. Deep water facies, Processes and models: A review and classification scheme for modern and ancient sediments, *Earth Science Reviews,* 23, 75-174.

Piper, D.J.W., et al., 1978. Conglomeratic Miocene flysch, Western Greece, *Journal of Sedimentary Petrology,* 48(1), 117-126.

Rothman, D.H., and Grotzinger, J.P., 1995. Scaling properties of gravity-driven sediments, *Non-Linear Processes Geophy.,* 2, 178-185.

Roussos, N., 1993. Geological map of Limnos Island, *I.G.M.E., Greece.*

Talling, P.J., 2001. On the frequency distribution of turbidite thickness, *Sedimentology,* 48, 1297-1329.

Vakalas, I., 2003. The evolution of foreland basins in Western Greece, *PhD. Thesis,* University of Patras.

Vakalas, I., et al., 2004. Age determination and palaeogeographic reconstruction of Pindos foreland basin based on calcareous nannofossils, *Bull. Geol. Soc. Greece,* 36/2, 864-873.

Δελτίο της Ελληνικής Γεωλογικής Εταιρίας τομ. XXXX, 2007
Πρακτικά 11ου Διεθνούς Συνεδρίου, Αθήνα, Μάιος 2007

Bulletin of the Geological Society of Greece vol. XXXX, 2007
Proceedings of the 11th International Congress, Athens, May, 2007

THE LATE EARLY CRETACEOUS TRANSGRESSION ON THE LATERITES IN VOURINOS AND VERMION MASSIFS (WESTERN MACEDONIA, GREECE)

Photiades A.[1], and Carras N.[1]
in collaboration with **Bortolotti V.[2], Fazzuoli M.[2], and Principi G.[2]**

[1] *I.G.M.E., Messoghion Str. 70, 115 27, Athens, fotiadis@igme.gr, nicarras@igme.gr*

[2] *Dipartimento di Scienze della Terra, Università di Firenze, ViA La Pira, 4, 50121 Firenze, Italy, milvio@dicea.unifi.it*

Abstract

Three stratigraphical sections from eastern Vourinos (Rhodiani area) to eastern Vermion massifs revealed the same age of the laterite events affecting the serpentinized ophiolite complex after its emplacement on the Pelagonian domain. All of them consist from their base upwards of serpentinized harzburgite slivers with lateritic unconformities on the top, followed by transgressive upper Lower Cretaceous neritic limestones.

At Kteni locality (Rhodiani area), a laterite horizon, lying on top of serpentinites, is covered by transgressive neritic limestones with Salpingoporella urladanasi, assigning a Barremian - Albian age, followed by Orbitolinidae limestones. At Tsimodia locality (NNW to the previous), the laterite horizon, lying on karstified Upper Jurassic reef limestones (which are the top member of a carbonate platform body tectonically lying on the ophiolites), is transgressively overlain by iron-rich pisolith levels and Aptian limestones of the wackestone-mudstone type, also containing Salpingoporella urladanasi, followed by Cenomanian Orbitolina limestones.

Finally, the third examined locality, further north-eastward to the previous, is situated at the eastern slopes of Vermion massif, and more precisely at the NW part of Koumaria village. There, it can again be observed that the lateritized serpentinite slivers are overlain transgressively by neritic limestones with Salpingoporella urladanasi, passing upwards into Upper Cretaceous recrystallized limestones with Orbitolinidae and rudist fragments and, finally, to flysch deposition.

These features allow to recognize that the emersion and the consecutive lateritization of the thrust-emplaced ophiolites in Vourinos and Vermion massifs in the northern Pelagonian domain, starting from the Latest Jurassic, was followed by a marine transgression beginning from the Barremian - Albian, firstly under restricted and brackish carbonate platform conditions, marked by the presence of the dasycladalean alga Salpingoporella urladanasi, followed by normal salinity carbonate platform conditions. The neritic sedimentation was stable until the Early Cenomanian. Subsequently, a deepening, earlier at Vourinos and later at Vermion, resulted in deposition of pelagic and turbiditic carbonates and then of flysch.

Key words: *Stratigraphy, Pelagonian, Salpingoporella urladanasi.*

Περίληψη

Τρεις στρωματογραφικές τομές, από τον ανατολικό Βούρινο (περιοχή Ροδιανής) και το ανατολικό Βέρμιο, απεκάλυψαν την ίδια ηλικία των φαινομένων που σχετίζονται με τις λατεριτιώσεις που προσέβαλαν το σερπεντινιωμένο οφιολιθικό σύμπλεγμα μετά την τοποθέτησή του πάνω στην πελαγονική επικράτεια. Στις τομές παρατηρούνται τεμάχη σερπεντινιωμένων χαρτσβουργιτών που φέρουν λατεριτικές ασυμφωνίες στην κορυφή, καλυπτόμενες από επικλυσιγενείς υστερο-ηωκρητιδικούς νηριτικούς ασβεστολίθους.

Κοντά στο χωρίο Κτένι (περιοχή Ροδιανής), ένας ορίζοντας λατερίτη, που κάθεται στην κορυφή σερπεντινιτών, καλύπτεται από επικλυσιγενείς νηριτικούς ασβεστολίθους με Salpingoporella urladanasi, η οποία προσδιορίζει ηλικία Βαρρέμιο - Άλβιο, ακολουθούμενους από ασβεστολίθους με Orbitolinidae. Στη θέση Τσιμοδιά (ΒΒΔ της προηγουμένης), ο λατεριτικός ορίζοντας, που κάθεται πάνω σε καρστικοποιημένους ανωιουρασικούς υφαλογενείς ασβεστολίθους (οι οποίοι είναι το κορυφαίο μέλος ενός σώματος ανθρακικής πλατφόρμας που κάθεται τεκτονικώς πάνω στους οφιολίθους), καλύπτεται επικλυσιγενώς από ένα σιδηρούχο πισσολιθικό στρωματίδιο και ασβεστολίθους του Απτίου, που έχουν υφή wackestone-mudstone και επίσης περιέχουν Salpingoporella urladanasi, ακολουθούμενους από ασβεστολίθους με Orbitolina του Κενομανίου.

Τέλος, η τρίτη εξετασθείσα τοποθεσία, αρκετά ΒΑ των προηγουμένων, βρίσκεται στις ανατολικές παρυφές του Βερμίου και συγκεκριμένα στα ΒΔ του χωρίου Κουμαριά. Εκεί, ομοίως παρατηρείται ότι τα λατεριτιωμένα τεμάχη σερπεντινιτών καλύπτονται επικλυσιγενώς από νηριτικούς ασβεστολίθους με Salpingoporella urladanasi, που περνούν προς τα πάνω σε ανακρυσταλλωμένους ανωκρητιδικούς ασβεστολίθους με Orbitolinidae και θραύσματα ρουδιστών και, εν τέλει, στο φλύσχη.

Οι παραπάνω χαρακτήρες οδηγούν στο συμπέρασμα ότι η ανάδυση και η επακόλουθη λατεριτίωση των επωθημένων οφιολίθων του Βούρινου και του Βερμίου, στη βόρεια πελαγονική επικράτεια, που έλαβε χώρα αρχής γενομένης από το ύστατο Ιουρασικό, ακολουθήθηκε από μια θαλάσσια επίκλυση που άρχισε μέσα στο διάστημα Βαρρέμιο - Άλβιο, σε συνθήκες ανθρακικής πλατφόρμας, αρχικώς κλειστής και υφάλμυρης, που σημαδεύονται από την παρουσία του φύκους Salpingoporella urladanasi, ακολουθούμενες από κανονικής αλμυρότητας συνθήκες ανθρακικής πλατφόρμας. Η νηριτική ιζηματογένεση έμεινε ακλόνητη μέχρι το κατώτερο Κενομάνιο. Στη συνέχεια, μία βάθυνση, νωρίτερα στο Βούρινο και αργότερα στο Βέρμιο, οδήγησε στην απόθεση πελαγικών και τουρβιδιτικών ασβεστολίθων και στη συνέχεια του φλύσχη.

Λέξεις κλειδιά: *Στρωματογραφία, Πελαγονική, Salpingoporella urladanasi.*

1. Introduction

In the Vourinos and Vermion Massifs (Fig.1) two main tectonic units are present: the metamorphic Pelagonian unit (a), consisting mainly of Upper Triassic-Lower Jurassic marbles and the overlying Jurassic schistose melange and the ophiolitic nappe (b), thrusted during the Late Jurassic, consisting mainly of serpentinized harzburgite and dunite slivers (Photiades *et al.* 1998).

Moreover, on the ophiolites of the Vourinos massif (Rhodiani area), a tectonic wedge-sliver, consisting of limestones of a Middle-Late Jurassic carbonate platform, can also be locally observed. The over-thrusting of this unit on the ophiolites is younger than the Late Kimmeridgian-Tithonian top of the carbonate platform limestones (Bortolotti *et al.* 2004, Carras *et al.* 2004).

Both Jurassic limestones and surrounding ophiolites in the Vourinos area and ophiolites in the Vermion area are locally covered by Fe-Ni laterite lenses, or a thin lateritic, argilo-pelitic bed (Photiades *et al.* 1998).

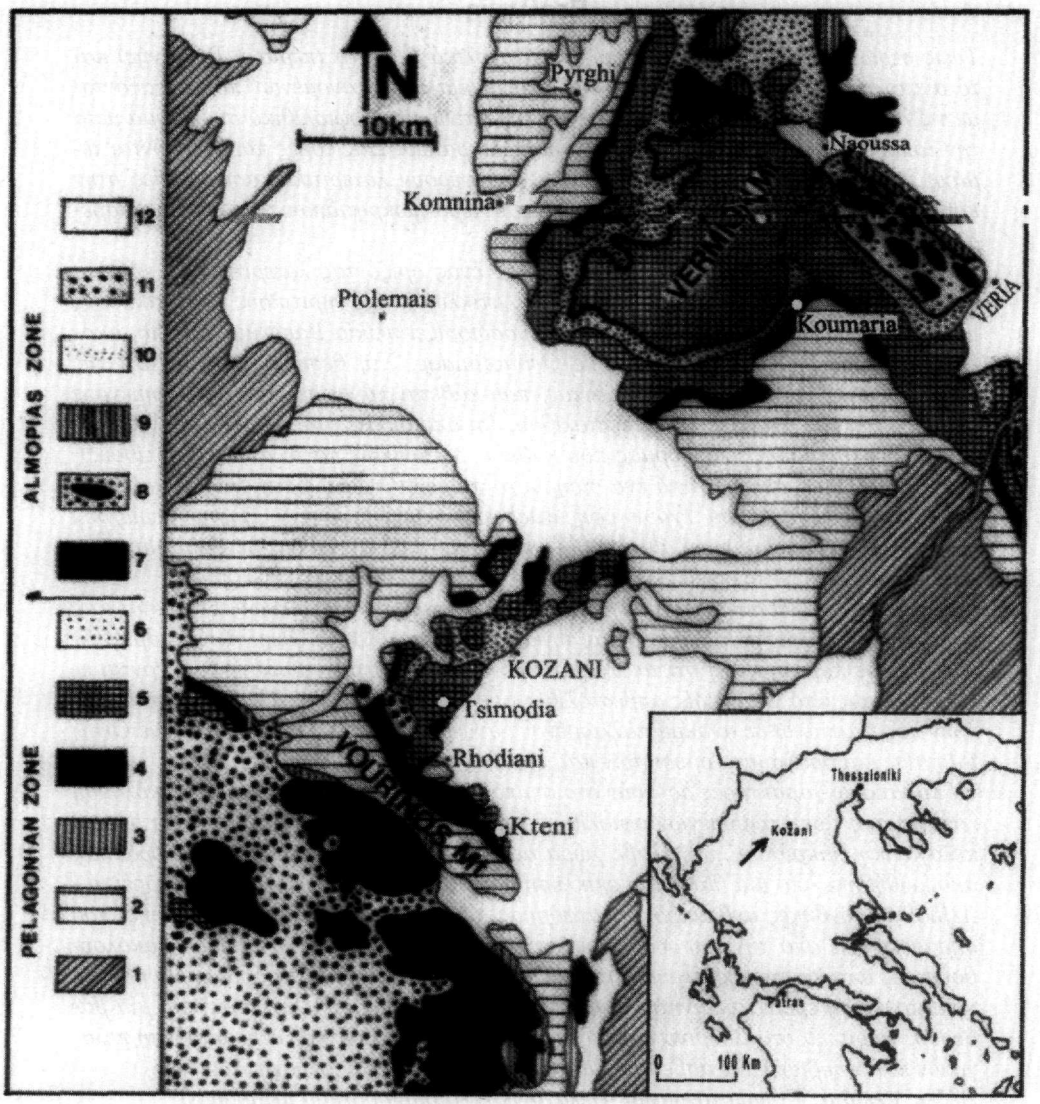

Figure 1 – Geological sketch-map (Brunn, 1956, modified). Key symbols: Pelagonian zone: pre-Alpine basement with gneiss (1); Triassic-Jurassic marble (2); Jurassic schistose melange (3); serpentinite with laterite (4); Upper Jurassic and/or Upper Cretaceous limestone (5); Upper Cretaceous flysch sequence (6); Almopias zone: serpentinite with basic and acidic rock slivers (7); ophiolitic melange formation (8); Upper Cretaceous deep-water limestone (9); Upper Cretaceous flysch sequence (10); molasse formation (11); Neogene and Quaternary deposits (12)

This lateritized substratum in the Vourinos-Vermion area is uncomformably covered by the neritic deposits of a "Mid" Cretaceous transgression, overlain by deep marine, mainly turbiditic, carbonate sediments, during the Late Cretaceous (Photiades *et al.*, 1998; Bortolotti *et al.* 2000 2001, 2002, 2004, Carras *et al.* 2004), followed by Late Maastrichtian flysch deposition.

The aim of this paper is to show that, apart local particularities, the general modalities and timing of the post-ophiolite-emplacement history in both the Vourinos and Vermion areas, i.e. the Latest

Jurassic - Earliest Cretaceous emersion and lateritization event and the consecutive marine transgression, were similar.

2. Stratigraphical data

2.1. The Kteni section

In the Kteni area, at the hill 670 (N 40°9′42,12′′; E 21°47′5,88′′, Vourinos massif, Fig. 1), the serpentinites, bearing lateritic lenses on the top, are overlain by the following transgressive succession, from bottom upwards (Fig. 2):

1. A calcareous conglomerate, 1,5 m thick, with pebbles 8-50 mm in size, coming from Upper Jurassic reef limestones with *Tubiphytes morronensis* Crescenti, *Suppiluliumaella* sp. and coral fragments; the matrix is lateritic.

2. A thin-bedded, black, micritic and brecciated limestone with *Salpingoporella urladanasi* Conrad, Peybernès & Radoičić and ostracods, lying on the conglomerate, or directly on the substratum. The dasyclad alga *S. urladanasi* is known in usually restricted marine to brackish environments of Barremian - Albian age (Carras *et al.* in press).

3. A thick bedded limestone of the rudstone type, with Orbitolinidae and angular fragments of packstones and grainstones of carbonate platform facies. The depositional environment is probably a slope and the age probably Cenomanian.

2.2. The Tsimodia section

In the Tsimodia area (N 40°13′35,4′′; E 21°43′29,94′′, NNW to the previous, Fig. 1), the laterites lie on top of a calcareous body, consisting of Upper Jurassic reef limestones, while the serpentinites crop out downwards in the wider area. The overlying transgressive succession consists, from bottom upwards, of (Fig. 2):

1) A discontinuous level of brown pisolitic limestone, some cm thick, adhered upon the laterite. The microfacies is a bioclastic wackestone, intensely contaminated by lateritic materials forming pisoids, containing *Debarina hahounerensis* Fourcade, Raoult & Vila, Miliolidae, detritus of *Salpingoporella* sp. [*S.* cf. *muehlbergii* (Lorenz)] and mollusk fragments.

2) Above the pisolitic level, or directly on the laterites, a level of brown, thin-bedded, micritic limestones lies, some metres thick. In this level, two types of microfacies have been observed:

- wackestone rich in lateritic mud and *Salpingoporella urladanasi* Conrad, Peybernès & Radoičić (Fig. 3).
- mudstone-wackestone rich in lateritic mud, containing *Debarina hahounerensis* Fourcade, Raoult & Vila, *Palorbitolina lenticularis* (Blumenbach), Miliolidae, and cavities with geopetalic filling.

3) The brown limestones are overlain by dark-gray, thin-bedded, micritic limestones, ca. 10 m thick. The common microfacies is bioclastic wackestone with *Palorbitolina lenticularis* (Blumenbach) (only in the lower part of the level), *Debarina hahounerensis* Fourcade, Raoult & Vila, *Vercorsella laurentii* (Sartoni & Crescenti), *Pfenderina* cf. *globosa* Foury, "*Valvulineria* "sp., *Glomospira* sp., *Salpingoporella dinarica* Radoičić, *Salpingoporella* sp., "*Bacinella*", Miliolidae.

The age of the levels 1, 2 and the lower part of the level 3 is Early Aptian, because of the presence of *Palorbitolina lenticularis* and geometrical considerations. The upper part of the level 3 is generally Aptian.

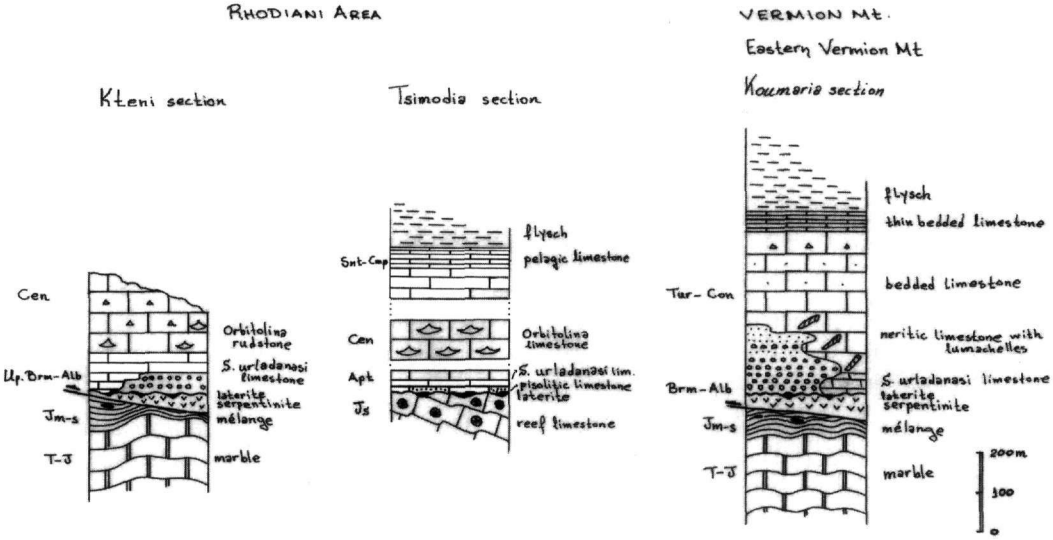

Figure 2 – The stratigraphic columns in the considered sections

4) 30 m upwards, thick-bedded *Orbitolina* limestones are observed. The microfacies consists of ramp bioclastic wackestone with *Orbitolina (Conicorbitolina) conica* (D'Archiac), *Orbitolina* sp. and *"Bacinella"* masses (Early Cenomanian).

5) More upwards along the succession, thin-bedded pelagic mudstones with *Globotruncana linneiana* (D'Orbigny), *Marginotruncana pseudolinneiana* Pessagno, *M. coronata* (Bolli), *Globigerinelloides* sp. and Heterohelicidae (Santonian - Early Campanian) crop out.
This succession reveals the following modalities of the transgression. In the first stage, during the Early Aptian, a carbonate sedimentation environment, contiguous to the still emerged areas and intensely contaminated by lateritic materials, was established; it was composed of various sub-environments, commonly brackish (levels 1 & 2). The connection with the emerged areas was soon interrupted, already during the Early Aptian (lower part of the level 3) and a carbonate platform was stable up to the Early Cenomanian (levels 3 & 4). Afterwards, a deeper environment was established, with pelagic sedimentation (level 5).

2.3. The Koumaria section

In the Koumaria area (N 40°32′17,82″; E 22°4′4,56″, eastern part of the Vermion massif, Fig. 1), the laterites lie directly on the weathered serpentinites (Fig. 2), which are thrust-emplaced on a Pelagonian substratum, consisting (from the base upwards) of a pre-alpine gneiss basement, of detached Triassic-Jurassic marbles, of a chert-bearing bedded marble formation, and of a Jurassic schistose mélange enclosing various sized blocks of amphibolite (Photiades 2004). The transgression on the laterites starts with:

- A body of conglomerates, coarser and wider in the lower part, becoming finer and less extensive upwards. The pebbles originate from the underlying carbonate rocks of the Triassic-Jurassic metamorphic pelagonian substratum.
- Laterally, the laterites are directly overlain by thick-bedded neritic limestones, which overlie gradually also the conglomerates. The base is commonly represented by recrystallized bioaccumulations (*lumachelles*) of gastropods and/or bivalves. Some contaminations by metallic oxides can be interpreted as reworked material of the underlying laterites. A sample from the very base contains a detritus of *SAlpingoporella urladanasi* assigning a Barremian - Albian age.

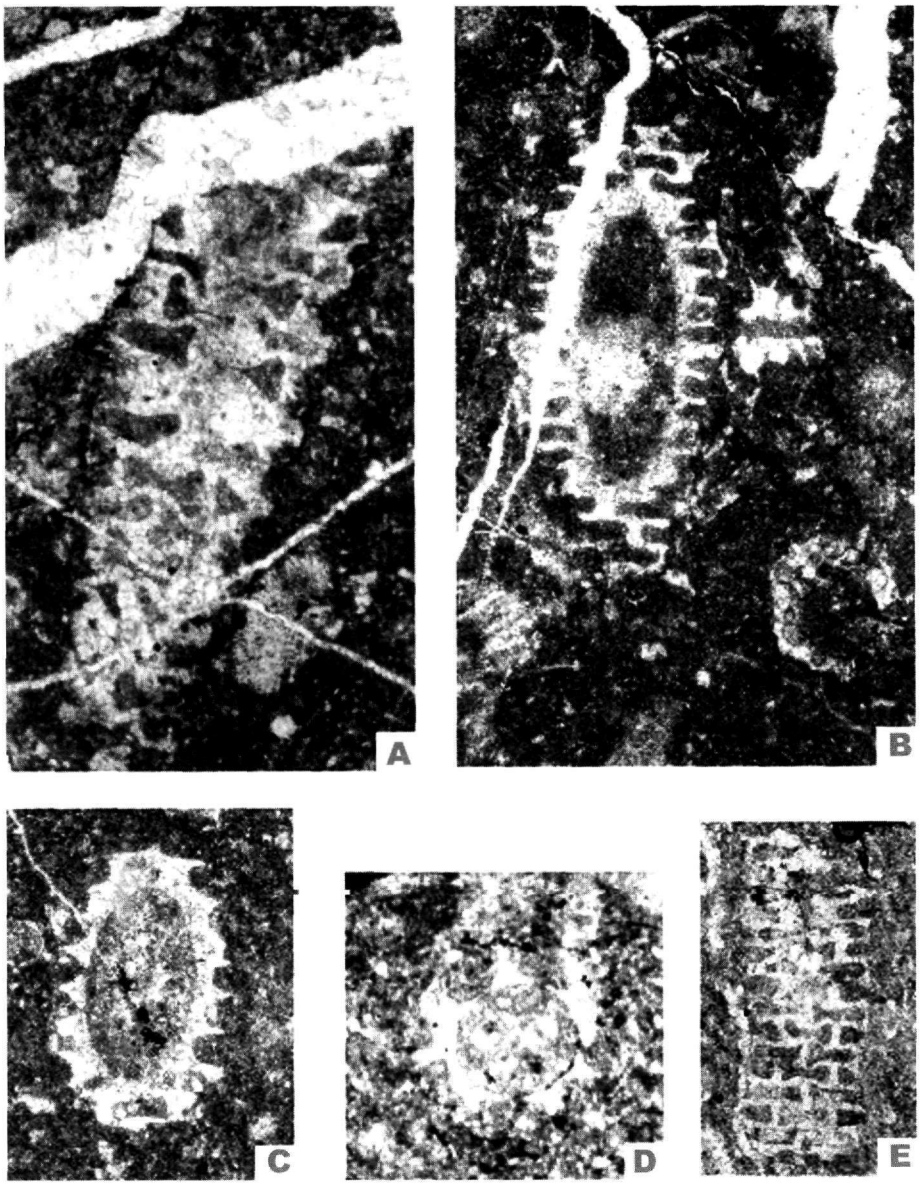

Figure 3 – *Salpingoporella urladanasi* Conrad, Peybernès & Radoičić, tangential-oblique (A), oblique (B, C), horizontal (D) and tangential (E) sections, and charophytes (B), x45. Tsimodia section, level 2, Early Aptian. A-D: sample NK.00.56. E: sample NK.00.66

- On the last conglomerate bed, the overlying thick-bedded neritic limestones contain again *lumachelles* with gastropods and/or bioclastic and fenestral mudstones deposited in a tidal-flat environment. The presence of the dasyclad alga *Likanella? hammudai* Radoičić indicates a Turonian-Coniacian age (Radoičić 1975, Schlagintweit 1993, Ensslin and Schlagintweit 1999).
- Upwards, thin-bedded limestones are exposed, unfortunately recrystallized and not better determined, probably of deep sea environment; they are overlain by the flysch.

3. Discussion- Conclusion

According to Beccaluva *et al.* (1984), the Vourinos ophiolite massif is interpreted as the product of a supra-subduction zone. The outcrops of radiolarites in this area, related to pillow lavas and marking the end of ocean spreading, are of Middle Jurassic age (Middle Bathonian - Early Callovian) on the basis of radiolaria determinations (Chiari *et al.* 2003). On the other hand, radiometric datations of the amphibolites at the base of the same ophiolite body gave 171±4 Ma (Spray *et al.* 1984). This age pertains to a Late Bajocian intraoceanic hot thrust, doubling the oceanic crust/lithosphere (Chiari *et al.* 2003).

The age of the ophiolite nappe emplacement must be younger than Middle Jurassic (the age of the radiolarites). According to Vergely (1984), Photiades *et al.* (1998) and Photiades (2004), it took place probably during the Late Jurassic. Moreover, further information comes from the Middle-Late Jurassic carbonate platform body, tectonically overlying the ophiolites in the Rhodiani (Vourinos massif) area. The over-thrusting of this unit on the ophiolites is younger than the Late Kimmeridgian-Tithonian top of the carbonate platform limestones (Carras *et al.* 2004). In our opinion, both the over-thrusting of the ophiolites upon the pelagonian marbles and the local over-thrusting of the carbonate body upon the ophiolites took place during the same orogenetic event. The local carbonate body, being situated in the course of the ophiolite-nappe-advance, was detached from its substratum and then thrust upon the ophiolites. It is important to say that the detachment surface was not a stratigraphic surface. The first level we can observe upon the ophiolites in the wider Rhodiani area can be one of the four Jurassic levels described by Carras *et al.* (2004). In conclusion, the age of the thrusting seems best defined as Latest Jurassic.

The subsequent emersion of the Vourinos-Vermion area, starting from the Latest Jurassic, gave rise to a land, where the ophiolites, mainly serpentinites, suffered intense *in situ* lateritization, and the carbonates, in some parts of the Vourinos area, were karstified. The laterite materials contaminated the whole area, giving rise to primary or secondary ore deposits upon the erosional or karstic depressions.

The general modalities of the subsequent marine transgression upon the emerged area were substantially similar in the Vourinos and Vermion parts. The transgression started within the Barremian-Albian interval (more precisely Early Aptian at Vourinos), with the deposition of conglomerates and, laterally, with the development of a carbonate platform, firstly restricted, with deposition of brackish facies with *Salpingoporella urladanasi*, and then with normal salinity facies. The neritic sedimentation was stable until the Early Cenomanian. The following sedimentary history is similar, but not coeval, in the two areas: deepening, with pelagic and turbiditic carbonates and then flysch deposition. This deepening appears earlier at Vourinos, within the Cenomanian, just as in the Zyghosti area (see Carras *et al.* 2004) or probably at the Kteni locality, and later at Vermion, after the deposition of the Turonian-Coniacian neritic beds with *Likanella? hammudai* of the Koumaria section.

4. Acknowledgments

This study was financed by I.G.M.E. (Athens) for the Kteni and Koumaria sections and by MIUR 2000 (responsible: G. Principi) for the Tsimodia section. We are grateful to Prof. Dr. Fotini Pomoni-Papaioannou (Athens University) and Dr. Sebastian Lüning (Bremen University) for the critical reading of the manuscript.

5. References

Beccaluva, L., Ohnenstetter, D., Ohnenstetter, M., and Paupy, A., 1984. Two magmatic series with island arc affinities within the Vourinos ophiolite, *Contrib. Mineral. Petrol.* 85, 253-271.

Bortolotti, V., Carras, N., Chiari, M., Fazzuoli, M., Marcucci, M., Photiades, A., and Principi, G., 2000. Decline and fall of an Upper Jurassic - Cretaceous carbonate platform, born (possibly) over wedging ophiolites: Vourinos- Pindos area, Northern Greece- Preliminary results. Abstract and Poster for the *80ª Riunione estiva della Soc. Geol. Italiana, Trieste, 6-8 Setembre*, 93p.

Bortolotti, V., Carras, N., Chiari, M., Fazzuoli, M., Marcucci, M., Photiades, A., and Principi, G., 2001. Characteristics of the Upper Cretaceous transgression in the Kozani area (Pelagonian Domain, Northern Greece), *Geoitalia 2001, 3° Forum Italiano di Scienze della Terra, Chieti, 5-8 September,* Abstracts, 547-548.

Bortolotti, V., Carras, N., Chiari, M., Fazzuoli, M., Marcucci, M., Photiades, A., and Principi, G., 2002. The Late Jurassic carbonate platform of Zyghosti, Vourinos-Pindos Zone, Northern Greece, *VI International Symposium on the Jurassic System, Palermo, 12-22 September,* Abstracts p. 21.

Bortolotti, V., Carras, N, Chiari, M., Fazzuoli, M., Photiades, A., and Principi, G., 2004. Sedimentary evolution of the Upper Jurassic Zyghosti platform, Kozani, Northern Greece, *Proc. Int, Symp. Earth System Sciences 2004, Istanbul-Turkey*, 705-712.

Braud, J., Brunn J.H., Campion, G., Didelot, J., Fourmaintraux, D., Lemaitre, J.-P., Mercier, L., Pichon, J.-F., and Vergely, P., 1984. La chaine du Vermion, ses nappes et sa bande broyée, *Bull. Soc. Geol. France*, (7), 26, 713-717.

Brunn, J.H., 1956. Contribution à l'étude géologique du Pinde septentrional et d'une partie de la Macédoine, *Ann. Géol. Pays Hellén.*, 8, 1-258.

Brunn, J. H., 1982. Geological map of Greece 1:50.000, Piryoi Sheet, *I.G.M.E.*

Brunn, J. H., 1982. Geological map of Greece 1:50.000, Veroia Sheet, *I.G.M.E.*

Carras, N., Conrad, M., and Radoičić, R., *in press*. *Salpingoporella*, a common genus of Mesozoic Dasycladales (calcareous green algae), *Revue de Paléobiologie*, 25(2).

Carras, N., Fazzuoli, M., and Photiades, A., 2004. Transition from carbonate platform to pelagic deposition (Mid Jurassic-Late Cretaceous), Vourinos Massif, Northern Greece, *Rivista Itaiana di Paleontologia e Stratigrafia*, 110(1), 345-355.

Chiari, M., Bortolotti, V., Marcucci, M., Photiades, A., and Principi, G., 2003. The Middle Jurassic siliceous sedimentary cover at the top of the Vourinos ophiolite (Greece), *Ofioliti*, 28(2), 95-103.

Ensslin, R., and Schlagintweit F., 1999. Contributions to the knowledge of Upper Cretaceous calcareous algae from the central Middle Atlas mountains, Morocco, *Z. dt. Geol. Ges.*, 149(4), 473-486.

Pichon, J.F., 1977. Une transversale dans la Zone Pélagonienne, depuis les collines de Krapa (SW) jusqu'au massif du Vermion (NE): Les premières séries transgressives sur les ophiolites), *6th Colloquium on the Geology of the Aegean Region,* Athens, 1, 163-171.

Pichon, J.F., and Lys, M., 1976. Sur l'existence d'une série du Jurassique à Crétacé inférieur surmontant les ophiolites, dans les collines de Krapa (massif du Vourinos, Grèce), *C. R. Acad. Sci. Paris*, 282, 523-524.

Photiades, A., 2004. Geological mapping revision of the Vermion Mountain (Internal Hellenides, Greece), Prodeedings of the *5th International Symposium on Eastern Mediterranean Geology, Thessaloniki, 14-20 April*, 1, 161-164.

Photiades, A., Skourtsis-Coroneou, V., and Grigoris, P., 1998. The stratigraphic and paleogeographic evolution of the eastern Pelagonian margin during the Late Jurassic – Creta-

ceous interval (Western Vermion Mountain – Western Macedonia, Greece), *Bull. Geol. Soc. Greece*, 32(1), 71-77.

Radoičić, R., 1975. On *Likanella hammudai* sp. nov. from the Upper Cretaceous of the Tripoli area (Lybia) and the age of strata containing *Dissocladella ondulata* Raineri, *Ann. Géol. Pénins. Balk.*, 39, 147-152.

Schlagintweit, F., 1993. Kretazische grünalgen aus Flachwassergesteinen der Nördlichen Kalkalpen: Ein Überblick, *Zitteliana*, 20, 123-132.

Spray, J.G., Bébien, J., Rex, D.C., and Roddick, J.C., 1984. Age constraints on the igneous and metamorphic evolution of the Hellenic-Dinaric ophiolites. In J.E. Dixon and A.H.F. Robertson (eds), *The geological evolution of the Eastern Mediterranean*. Geol. Soc. London, Spec. Pap., 17, 619-627pp.

Vergely, P., 1984. Tectonique des ophiolites dans les Hellénides internes. Conséquences sur l'évolution des régions téthysiennes occidentales. *Thèse d'État Sc. Naturelles, Univ. Paris-Sud, Orsay*, 649pp.

Δελτίο της Ελληνικής Γεωλογικής Εταιρίας τομ. XXXX, 2007
Πρακτικά 11ου Διεθνούς Συνεδρίου, Αθήνα, Μάιος 2007

Bulletin of the Geological Society of Greece vol. XXXX, 2007
Proceedings of the 11th International Congress, Athens, May, 2007

GREEK COASTAL MIRES: A PRELIMINARY STUDY OF THE AGOULINITSA PEATLAND, WESTERN PELOPONNESE

Sofikitis E.[1], Siavalas G.[1], Chatziapostolou A.[1], Kalaitzidis S.[1], and Christanis K.[1]

[1] *Section of Earth Materials, Department of Geology, University of Patras, GR-265.00 Rio-Patras, Greece, sailis@otenet.gr, siavalas@upatras.gr, achatzia@upatras.gr, s.kalaitzidis@upatras.gr, christan@upatras.gr*

Abstract

The Agoulinitsa peatland formed on the western shore of the homonymous lake, which was drained in 1969 because of the emerging demand for agricultural land. This study is a preliminary attempt to determine the conditions that prevailed during peat formation. Shallow cores were obtained from the peatland and initial physical, chemical and mineralogical analyses were carried out. High ash yield and pH values indicate that peat accumulated under alkaline conditions with periods of high clastic material influx, while high electric conductivity values indicate increased influx of dissolved solids into the mire. The mineral matter consists mainly of clay minerals, quartz, calcite, halite, sylvite and pyrite. The distribution of these minerals with depth indicates that fresh-water conditions prevailed for a long period during peat accumulation at the central part of the peatland, whereas the sea-water influence was more intense to the south establishing slightly brackish conditions. All data suggest that the Agoulinitsa peatland was developed as a back-barrier mire formed at the southwestern part of the Agoulinitsa Lake, and hence it can be considered as a modern analogue of the Neogene lignite deposits occurring along the west coast of Peloponnese.
Key words: *back-barrier mire, peat, wetland, drainage.*

Περίληψη

Ο τυρφώνας της Αγουλινίτσας σχηματίστηκε στη δυτική ακτή της ομώνυμης λίμνης, η οποία αποξηράνθηκε το 1969, εξαιτίας της αυξανόμενης ζήτησης για καλλιεργήσιμες εκτάσεις. Η παρούσα μελέτη αποτελεί μια πρώτη προσπάθεια για τη διερεύνηση των συνθηκών που επικρατούσαν κατά την τυρφογένεση. Για τις ανάγκες της μελέτης πραγματοποιήθηκαν διατρήματα μικρού βάθους, καθώς και προσδιορισμοί των φυσικών, χημικών ιδιοτήτων της τύρφης, και των ορυκτολογικών συστατικών της. Η υψηλή περιεκτικότητα σε τέφρα και οι υψηλές τιμές του pH υποδηλώνουν πως η τύρφη σχηματίστηκε κάτω από αλκαλικές συνθήκες, ενώ οι υψηλές τιμές της ηλεκτρικής αγωγιμότητας υποδηλώνουν έντονη τροφοδοσία με διαλυμένα στερεά. Στην τύρφη προσδιορίστηκαν αργιλικά ορυκτά, χαλαζίας, ασβεστίτης, αλίτης, συλβίτης και σιδηροπυρίτης. Η κατανομή των παραπάνω ορυκτών με το βάθος υποδηλώνει την επικράτηση συνθηκών γλυκού νερού κατά το μεγαλύτερο διάστημα απόθεσης της τύρφης στο κεντρικό τμήμα της περιοχής, ενώ στο νότιο τμήμα η

επίδραση της θάλασσας ήταν πιο έντονη και οι συνθήκες χαρακτηρίζονται ως ελαφρά υφάλμυρες. Συμπερασματικά ο τυρφώνας της Αγουλινίτσας μπορεί να χαρακτηριστεί ως ένας τυρφώνας που σχηματίστηκε πίσω από αμμώδεις φραγμούς. Παρόμοιες συνθήκες κυριαρχούσαν ήδη από το Νεογενές, στις δυτικές ακτές της Πελοποννήσου και ευνόησαν τη γένεση λιγνιτικών κοιτασμάτων στην ευρύτερη περιοχή.
Λέξεις κλειδιά: *αποξήρανση, παράκτιο έλος, τύρφη, υγρότοπος.*

1. Introduction

In the past decades the wetlands – among them the mires – have attracted the interest of the scientific community as places of high environmental significance, because of the diversity of flora and fauna species living there, as well as due to the fact that they constitute major freshwater deposits. Mires are wetlands of great environmental and economic value, hence in order to preserve these ecosystems it is necessary to study the natural processes that affect mire evolution. Furthermore the study of modern peat-forming environments constitutes the key for better understanding of the various coal-forming processes (Diessel 1992, Lappalainen 1996, Joosten and Clark 2001).

From ancient times up to late 1960's, several mires in Greece, as well as shallow lakes have been drained mainly due to the demand for fertile agricultural land (Psilovikos 1992, Bouzinos *et al.* 1994). Nevertheless, across the territory mires are still developing usually under minerotrophic to weakly minerotrophic conditions. Peat is accumulating mainly under slightly acidic pH values ranging between 4 and 6 (e.g. Christanis 1994, Papazisimou *et al.* 2000, 2002). Minerotrophic mires (fens) are distinguished in those formed in intermontane basins such as the fens of Philippi, Nissi, Chimaditida, Ioannina, Kalodiki, Katouna and Small Prespa (Christanis 1996, Bouzinos *et al.* 2001) and coastal fens like this in Keri, which is the only active one recorded up to now in the country (Papazisimou *et al.* 2000).

The area of the Agoulinitsa Lake with the homonymous mire covers about 46.3 km^2 and is located in western Peloponnese, approximately 7.5 km SSE from the town of Pyrgos (Fig. 1a). After an extended drainage project in 1969 the lake area was converted into urban and agricultural land (Manariotis and Yannopoulos 2004).

The aims of the present preliminary study are to inventorize the main characteristics of the Agoulinitsa peatland and to identify the conditions that prevailed before and during peat accumulation, as well as after the drainage.

2. Geological setting

The Agoulinitsa Lake once covered the central-western part of the Pyrgos Basin, which formed during the post-alpidic extensional phase. The Agoulinitsa sub-basin evolution is controlled by the Pyrgos Fault striking NNW-SSE (Fig. 1a) (Koukouvelas *et al.* 1996). The SE margins of the former lake area consist of limestones of the Gavrovo-Tripoli isopic zone. Pliocene alternations of clay, lignite, sand, silt, sandstone and conglomerate and Pleistocene alternations of clay, sand, conglomerate and breccia of the Pyrgos Basin constitute the eastern margins, while the western margins consist of Quaternary sand dunes (Fig. 1b). The sediments filling the Agoulinitsa Lake, as well as its northern margins are alluvial deposits (sand, gravel and pebble) of the Alpheios River and lagoonal sediments (Kamberis 1987).

The study area has a typical temperate Mediterranean climate, with cold-wet winters and warm-dry summers. According to the data of the Hellenic National Meteorological Service during the last 30 years, the mean annual precipitation is 700 mm unevenly distributed through out the year. Before the drainage the coastal zone of the Agoulinitsa Lake was covered by sand-dune and halophytic vegetation, while helophytes were dominant at the largest part of the lake. The main helophytic species were *Scirpus* spp., *Phragmites australis*, and various Cyperaceae (Natura 2000,

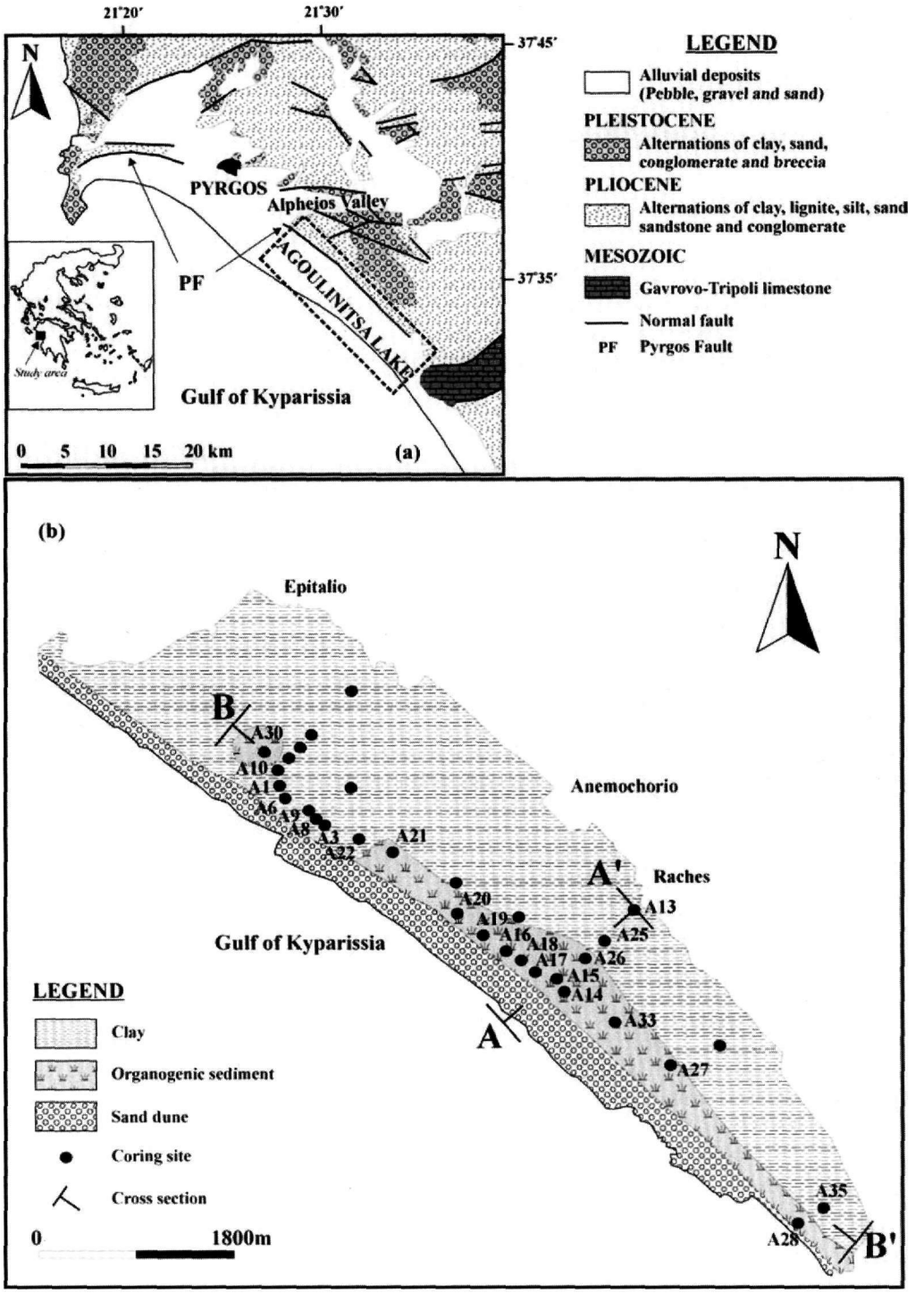

Figure 1 - a) Simplified geological map of the Pyrgos Basin (after Kamberis 1987 and Papazisimou *et al.* 2004). b) Geological map of the study area. Cross sections AA' and BB' are presented in Figure 3

http://natura.minenv.gr). Today the land is mainly used for cotton cultivation and pasture; both activities result in the regression of the helophytic vegetation, except from the SE part of the drained Agoulinitsa Lake.

3. Materials and Methods

Using an Edelman hand-driven corer, thirty-five cores (Fig. 1b) were obtained up to a maximum depth of 3.65 m. The cores were logged at the site and the degree of peat decomposition was determined according to the von Post method (Schneekloth 1981). Samples were picked up from cores A_{33} and A_{35}.

Moisture and ash contents of all the samples were determined according to the ASTM D3173 (1993) and D2974 (Andrejko *et al.* 1983) methods, respectively. The pH and the electric conductivity values were measured in aqueous solution (1:25 sample/water ratio).

The mineralogical analyses of the bulk peat samples obtained from coring sites A_{33} and A_{35}, were carried out using a Philips PW1050 X-Ray diffractometer. The scanning area covered the interval 2θ 3-60°, with a scanning step of 0.02° and a step time of 1 s. The semi-quantitive evaluation was performed according to the method proposed by Papazisimou and Kalaitzidis (2004).

4. Results and discussion

4.1. Lithological data

The stratigraphic features of the peatland were plotted according to the lithological data and the laboratory sample characterization (Fig. 2). It was revealed that the palaeomire developed over a ca. 6 km long, narrow zone along the eastern margin of the sand dune barrier. The maximum width of the palaeomire was c. 800 m (Fig. 1b).

The maximum peat thickness reaches 335 cm at coring site A_{28}. Macroscopically the peat has a light brown to black color. Rhizomes, plant macro-remains and molluscs frequently occur within the peat. The humification degree according to the von Post method ranges from 7 to 8, indicating significant humification of the organic matter. Nowadays the helophytes growing on the surface are mainly *Scirpus* spp. and other Cyperaceae species, along with *Juncus* spp. and *Phragmites australis*.

Apart from peat, other organogenic limnotelmatic facies, like detrital and clayey mud occur at several sites. The surface peat layer is strongly degraded and oxidized because of the drainage. According to local farmers, since the initiation of the cultivation after the drainage, the surface level has subsided approximately 1.5 m, because of the oxidation and the subsequent loss of the uppermost peat layers. Hence it is inferred that before 1969 the peat thickness exceeded 4.5 m. The loss of organic matter because of oxidation and self-ignition of the surface peat layer is common to intensely cultivated peatlands; as an example in Chimaditida fen, the subsidence of the surface peat layer resulted in a loss of the initial thickness between 47.4 % and 77.3 % (Bouzinos *et al.* 1997). Lowering peat surface after drainage also occurs in Philippi peatland, where the upper peat layer subsided 3.5 m within a period of fifteen years only because of the intense cultivation (van der Molen 1962).

Clay and sand layers constitute the inorganic sediments in the area of the palaeomire. The sand layer probably constitutes the substrate of the limnotelmatic environment representing the dune system that developed across the coastline, whereas the clay layers represent the limnic facies that deposited during flooding events; intermediate facies (e.g. clayey sand, sandy clay) occur throughout the sequence.

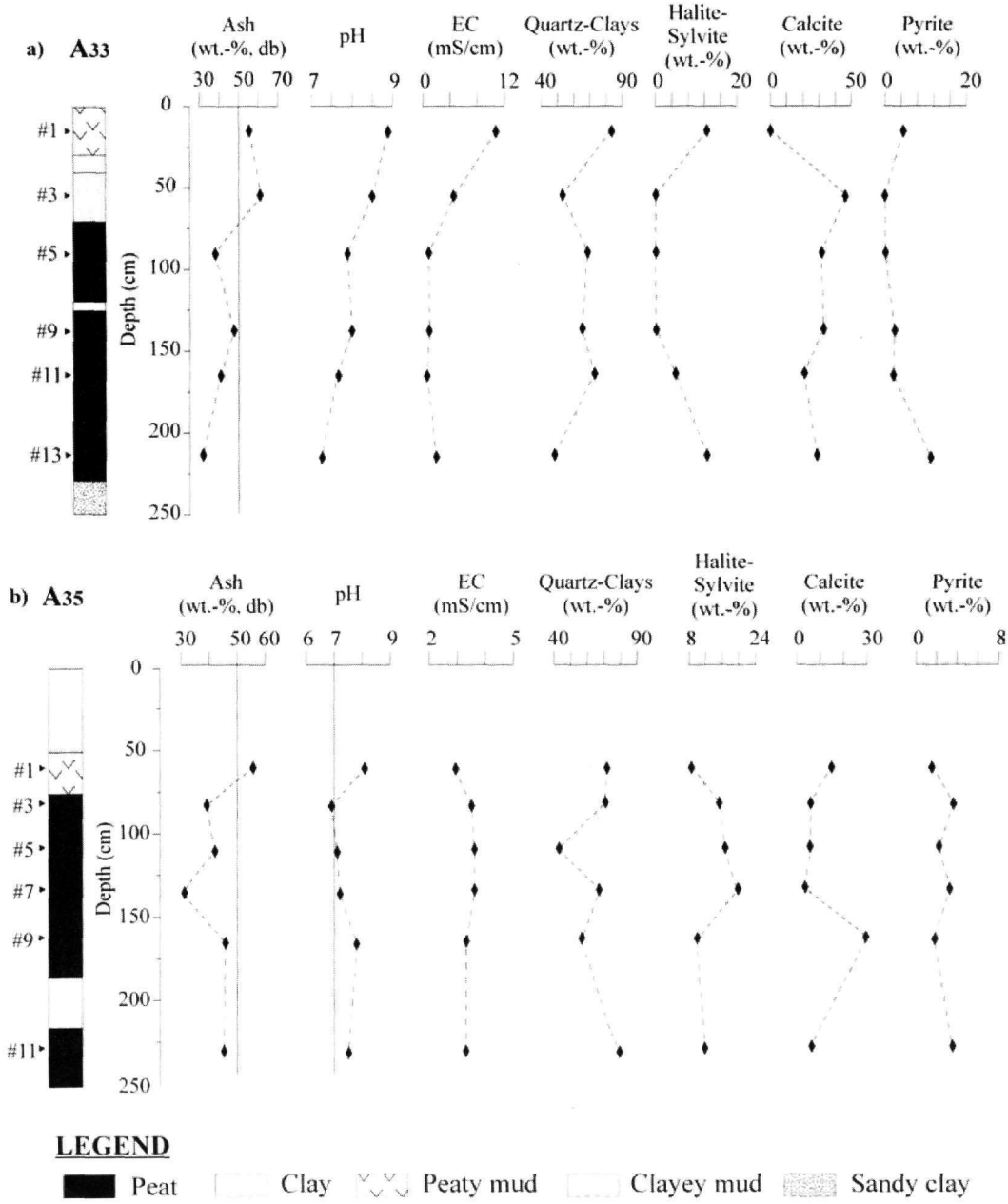

Figure 2 - Ash yield, pH, EC (electric conductivity), and mineral content distribution along the A_{33} and A_{35} cores (db: on dry basis). Organogenic samples with ash content <50 % are regarded as peat, 50-60 % as peaty mud, 60-80 % as mud and 80-90 % as humic clay, silt or sand, depending on the grain size of the sediment (Kearns and Davison 1983)

4.2. Laboratory determinations and peat characterization

Moisture and ash content of the examined organogenic samples range from 67.9 to 86.6 % and 31.5 to 61.6 %, respectively (Fig. 2). The relatively high ash content indicates high inorganic material input during the whole time span of peat accumulation.

The pH values ranging from 6.9 to 8.7, reveal a neutral to alkaline environment at both sites. The relatively high pH values of the Agoulinitsa peat indicate probably seawater influence and/or significant carbonate influx. The establishment of neutral to alkaline conditions apart from neutralizing the organic acids (Shotyk 1988), promotes the biological activity and accordingly the humification of the plant remnants (Moore and Bellamy 1976, Göttlich 1990); this process is reflected in the high humification degree of the studied samples. The electric conductivity values are relatively high (0.6-10.7 mS/cm) revealing high content of dissolved solids (salt), also as an evident of marine influence (Göttlich 1990).

The semi-quantitative determinations of the mineral matter in the bulk peat samples show that quartz, mixed-layer clays (illite-montmorillonite) and calcite constitute the main mineral phases in the Agoulinitsa peat, whereas pyrite, halite and sylvite constitute the minor phases (Fig. 2). In general, both quartz and clays in peat and coal are considered as having a clastic origin, whereas calcite occurs either as clastic grain or as authigenic mineral (Diessel 1992, Ward 2002). Pyrite in coastal mires usually derives from the reduction of the seawater sulphates and the reaction of the H_2S with Fe-ions, which derive from detrital material entering the mire during flood episodes (Delwigg *et al.* 2001). Halite and sylvite usually indicate the sea influence and may be deposited either from seawater solutions or by the wind action (Raymond *et al.* 1983). The mineralogical composition of the Agoulinitsa peat is identical to that of the Keri with the presence of quartz, clay minerals, calcite and pyrite. The existence of halite and sylvite is characteristic for coastal peatlands, while these two minerals are lacking from Greek fen peats deposited in intermontane basins (Kalaitzidis and Christanis 2004).

An interesting feature is the presence of analcime and plagioclase (21.7 and 11.4 wt.-%, respectively) in sample #5 from core A_{35} Analcime in peat is usually related to volcanic ash (Querol *et al.* 2001). Volcanic tuff layers, however, were not identified macroscopically and further investigation on this subject is needed.

4.3. Peat formation in the Agoulinitsa peatland

The activation of the Pyrgos Fault during the Lower Pleistocene caused the subsidence of the western coastal area of Peloponnese (Koukouvelas *et al.* 1996), where the interaction of wind and waves resulted in the formation of sand barriers. Behind them the conditions were favourable for the formation of several lagoons, one of them occurring in the Agoulinitsa area.

According to the stratigraphic features and the laboratory determinations it is evident that the palaeomire was established behind the sand dune zone at low water-table conditions (Fig. 3a). The sand dune barriers acted as obstacles preventing sea intrusion during the lagoon's terrestrialization. Short-term flooding events resulted in the rise of the water table and the establishment of lacustrine conditions, which led to the formation of clay lenses intercalating with peat (Fig. 3b). At later evolutionary stages it seems that peat accumulation was restricted to the central and SE part, while lacustrine conditions were dominant in the NW part.

The high halite, sylvite and pyrite contents at the lower peat layer from core A_{33}, along with the high electric conductivity values (Fig. 2a), indicate that seawater influence was intense at the early stages of peat accumulation in the central part of the palaeomire. Gradually upwards the freshwater contribution to peat formation became more significant. Short-term flooding events caused the transport of clastic material and the interruption of peat formation by the deposition of clay layers. The flooding events were obviously caused by the activity of the Alpheios River.

The uppermost peat horizon at site A_{33} is oxidized due to the drainage of the former lake area. The decline of the water table resulted in the increase of both the halite and sylvite contents and the electric conductivity values.

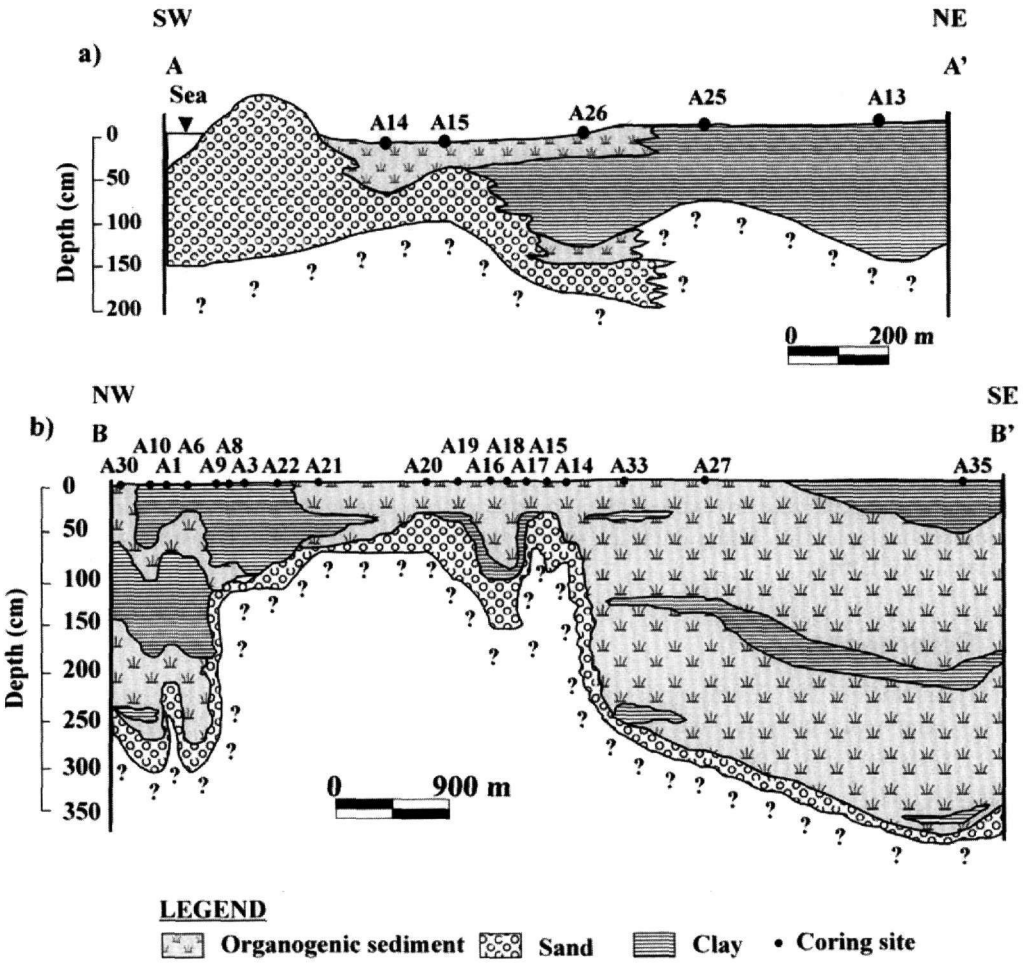

Figure 3 – SW-NE and NW-SE cross sections of the peatland. For the exact locations of both sections see Figure 1b

On the contrary, the high and relatively stable electric conductivity values and the higher contents of halite, sylvite and pyrite in samples from core A_{35} indicate that seawater influence was constant at the southeastern part of the mire throughout peat accumulation (Fig. 2b). Inorganic influx was also significant during peat accumulation with clastic silicate grains constituting the main inorganic fraction, whereas authigenic calcite is a minor mineral phase.

From the comparison of both profiles it is suggested that the central part of the peatland was mainly freshwater-dominated during peat accumulation, whereas seawater was entering the palaeomire from the southeastern margins, where the sand barrier displays its minimum width (Fig. 1b).

The overall data obtained from this study show that the Agoulinitsa peatland can be termed as back-barrier mire similar to those occurring along the eastern coast of Spain (López-Buendía *et al.* 1999). Similar conditions prevailed during Neogene times at several places in western Peloponnese, such as in Magoula, Koumouthekras and Kyparissia, resulting in significant lignite formations (Papazisimou 2002). Thus the Agoulinitsa peatland is considered as a modern analogue of these lignite deposits.

5. Concluding remarks

The former Agoulinitsa Lake with the hosted peatland was a typical lagoonal environment formed behind sand dune barriers. Nevertheless, the results of the present preliminary study suggest that peat accumulated not strictly under brackish conditions, but a major part of the area was fresh-water influenced mainly by the Alpheios River and its flooding events. The only part of the mire affected by seawater seems to be restricted at the south, where the sand dunes appear to be narrow. There maybe existed a seawater entrance into the mire.

In terms of peat geology, the Agoulinitsa peatland can be characterized as coastal back-barrier mire being one of the very few occurring in Greece. Further study concerning the physical-chemical properties and mineralogical composition of the peat is needed in order to reconstruct in detail the palaeoenvironmental conditions that led to the formation of the whole sedimentary sequence.

6. Acknowledgements

The authors would like to express their gratitude for assistance during the fieldwork to Dr. Antonis Bouzinos, Mrs. Tonia Paraschi, and Mr. Aris Liontos, from the Department of Geology, University of Patras.

7. References

American Society for Testing and Materials (ASTM), D3173, 1993. Moisture in the Analysis Sample of Coal and Coke. In 1996 *Annual book of ASTM Standards, Standards Relating to Gaseous fuels; Coal and Coke*. 05.05, 289-290, Philadelphia, PA., ASTM, 495pp.

Andrejko, M.J., Fiene, F., and Cohen, A.D., 1983. Comparison of ashing techniques for determination of the inorganic content of peats. In P.M. Jarrett (ed.), *ASTM Special Technical Publication 820, Testing of Peats and Organic Soils*. 5-19, Philadelphia, PA., ASTM, 241pp.

Bouzinos, A., Broussoulis, J., and Christanis, K., 1994. Conservation and Management of Greek Fens: a "model" to avoid, *Proceedings International Symposium "Conservation and Management of Fens", Warsaw-Biebrza, 6-10 June,* 225-230.

Bouzinos, A., Christanis, K., and Kotis, T., 1997. The Chimaditida Fen (W. Macedonia, Greece): a peat deposit lost, *International Peat Journal,* 7, 3-10.

Bouzinos, A., Papazisimou, S., Christanis, K., and Tzedakis, P., 2001. High rate of peat accumulation in the tectonic depression of Katouna, western Greece, *International Peat Journal,* 10, 85-95.

Christanis, K., 1994. The genesis of the Nissi peatland (northwestern Greece) as an example of peat and lignite deposit formation in Greece, *International Journal of Coal Geology*, 26, 63-77.

Christanis, K., 1996. The peat resources in Greece. In E. Lappalainen (ed.), *Global peat resources*. 87-94, Finland, International Peat Society, 368pp.

Dellwig, O., Watermann, F., Brumsack, H.J., Gerdes, G., and Krumbein, W.E., 2001. Sulphur and iron geochemistry of Holocene coastal peats (NW Germany): a tool for palaeoenvironmental reconstruction, *Palaeogeography, Palaeoclimatology, Palaeoecology*, 167, 359-379.

Diessel, C.F.K., 1992. *Coal-bearing Depositional Systems*, Berlin, Springer Verlag, 721pp.

Göttlich, K., 1990. *Moor und Torfkunde*, Stuttgart, E. Schweizerbart'sche Verlagsbuchhandlung, 529pp.

Joosten, H., and Clarke, D., 2002. *Wise use of mires and peatlands*, Finland, International Mire Conservation Group and International Peat Society, 304pp.

Kalaitzidis, S., and Christanis, K., 2004. Mineral matter in Greek peat – a qualitative approach, *Proc. of the 5th International Symposium on Eastern Mediterranean Geology, Thessaloniki, Greece, 14-20 April,* vol. 3, 1416-1419.

Kamberis, E., 1987. Geological and oil-geology study of NW Peloponnesus, *Ph.D. Thesis*, Athens Polytechnical School, Athens, Greece, 143pp.

Kearns, F., and Davison, A., 1983. Field classification system of organic-rich sediments, *Proc. of Workshop Mineral matter in peat: its occurrence, form and distribution, Los Alamos, New Mexico, 26-39 September,* 147-157.

Koukouvelas, I., Mpresiakas, A., Sokos, E., and Doutsos, T., 1996. The tectonic setting and earthquake ground hazards of the 1993 Pyrgos earthquake, Peloponnese, Greece, *Journal of Geological Society of London,* 153, 39-49.

Lappalainen, E. (ed.), 1996. *Global peat resources*, Finland, International Peat Society, 368pp.

López-Buendía, A.M., Bastida, J., Querol, X., and Whateley, M.K.G., 1999. Geochemical data as indicators of palaeosalinity in coastal organic-rich sediments, *Chemical Geology*, 157, 235-254.

Manariotis, I., and Yannopoulos, P., 2004. Adverse Effects on Alfeios River Basin and an Integrated Management Framework Based on Sustainability, *Environmental Management*, 34, 261-269.

Moore, E.S., and Bellamy, D.J., 1976. *Peatlands*, Berlin Heidelberg, New York, Springer, 221pp.

Natura 2000. http://natura.minenv.gr/natura/server/user/biotopos_info.asp?siteCode=GR2330001.

Papazisimou, S., 2002. Formation and evolution of coastal lignite seams in western Peloponnese. *Ph.D. Thesis*, Dept. of Geology, Univ. Patras, Patras, 226pp.

Papazisimou, S., Bouzinos, A., Christanis, K., and Tzedakis, P.C., 2000. The coastal asphalt fen of Keri, Zakynthos (Hellas), *Proceedings of the 11th International Peat Congress, vol. I, Quebec, Canada, August 6-12,* 58-69.

Papazisimou, S., Bouzinos, A., Christanis, K., Tzedakis, P.C., and Kalaitzidis, S., 2002. The upland Holocene transitional mires of Elatia forest, Northern Greece, *Wetlands*, 22, 355-365.

Papazisimou, S., and Kalaitzidis, S., 2004. Quantitative mineral matter determination in lignites using X-Ray diffractometry and position sensitive detector (XRD-PSD), *Proceedings of the 10th International Congress of the Geological Society of Greece, vol. XXXVI, Thessaloniki, April,* 464-473.

Papazisimou, S., Kalaitzidis, S., Christanis, K., Cressey, G., and Valsami-Jones, E., 2004. Accurate Phase Quantification of Mineral Matter in Bulk Lignite Samples from Western Peloponnese (Greece), *Energy & Fuels,* 18, 547-559.

Psilovikos, A., 1992. Changes in Greek wetlands during the twentieth century: the cases of the Macedonian inland waters and of the river deltas of the Aegean and Ionian coasts, *Proc. of Workshop on Greek Wetlands, Thessaloniki, Greece, 17-21 April 1989*, 175-196.

Querol, X., Alastuey, A., Zhuang, X., Hower, J.C., Lopez-Soler, A., Plana, F., and Zeng, R., 2001. Petrology, mineralogy and geochemistry of the Permian and Triassic coals in the

Leping area, Jiangxi Province, southeast China, *International Journal of Coal Geology*, 48, 23-45.

Raymond, J.R., Andrejko, M.J., and Bardin, S.W., 1983. Techniques for applying scanning electron microscopy to the study of mineral matter in peat. In R.J. Raymond and M.J. Andrejko (eds), *Mineral matter in peat*. 169-179, Los Alamos, Los Alamos Laboratory, NM.

Schneekloth, H., 1981. Kartierung von Mooren. In F. Bender (ed.), *Angewandte Geowissenschaften 1*. 35-37, Stuttgart, Enke.

Shotyk, W., 1988. Review of the inorganic geochemistry of peats and peatland waters, *Earth-Science Reviews*, 25, 95-176.

van der Molen, W., and Smits, H., 1962. *Die Sackung in einem Moorgebiet in Nord-Griechenland (Philippi),* Bremen, Unpubl. Report, 11pp.

Ward, C.R., 2002. Analysis and significance of mineral matter in coal seams, *International Journal of Coal Geology*, 50, 135-168.

Δελτίο της Ελληνικής Γεωλογικής Εταιρίας τομ. XXXX, 2007
Πρακτικά 11ου Διεθνούς Συνεδρίου, Αθήνα, Μάιος 2007

Bulletin of the Geological Society of Greece vol. XXXX, 2007
Proceedings of the 11th International Congress, Athens, May, 2007

A LATE PLEISTOCENE ENDEMIC GENET (CARNIVORA, VIVERRIDAE) FROM AGHIA NAPA, CYPRUS

Theodorou G. E.[1], Roussiakis S. I.[1], Athanassiou A.[1,2], Giaourtsakis I.[3], and Panayides I.[4]

[1] *National and Kapodistrian University of Athens, Faculty of Geology and Geoenvironment, Department of Historical Geology and Palaeontology, 157 84 Athens, Greece, gtheodor@geol.uoa.gr, srousiak@geol.uoa.gr, aathanas@geol.uoa.gr*

[2] *Hellenic Ministry of Culture, Department of Palaeoanthropology–Speleology, Ardittou 34B, 116 36 Athens, Greece*

[3] *Ludwig-Maximilians-Universität München, Department of Geo- and Enviromental Sciences, Section of Paleontology, Richard-Wagner-Str. 10, D-80333 Munich, Germany, i.giaourtsakis@lrz.uni-muenchen.de*

[4] *Cyprus Geological Survey, 1415 Nicosia, Cyprus, ipanayides@gsd.moa.gov.cy*

Abstract

The Pleistocene endemic fauna of Cyprus consists mainly of dwarf hippos and elephants, adapted to the insular environment. Among the rare elements of this endemic fauna is a small carnivore, the viverrid Genetta plesictoides, poorly known from scanty material that comes from two localities. Recent excavations in a rock-shelter site at the area of Aghia Napa yielded —apart from a rich hippo sample— new skeletal remains (a partial skull and a tibia) of the cypriot genet. The dental morphology shows adaptations towards a more carnivorous diet in relation to the extant Genetta genetta.

Key words: *Mediterranean, Cyprus, Genetta plesictoides, Insular Endemism.*

Περίληψη

Η πλειστοκαινική ενδημική πανίδα της Κύπρου περιλαμβάνει κυρίως νάνους ιπποποτάμους και ελέφαντες, προσαρμοσμένους στο νησιωτικό περιβάλλον. Ένα από τα σπανιότερα ενδημικά θηλαστικά της Κύπρου είναι η μοσχογαλή Genetta plesictoides, η οποία είναι γνωστή από πολύ λίγα δείγματα, που προέρχονται από δύο απολιθωματοφόρες θέσεις. Σε πρόσφατες ανασκαφές, που πραγματοποιήθηκαν σε βραχοσκεπή στην περιοχή της Αγίας Νάπας, ανακαλύφθηκαν —εκτός από πολυάριθμα ευρήματα νάνων ιπποποτάμων— νέα σκελετικά λείψανα (τμήμα κρανίου και κνήμη) της ενδημικής μοσχογαλής της Κύπρου. Η μορφολογία της οδοντοστοιχίας υποδηλώνει ότι η μοσχογαλή της Κύπρου, Genetta plesictoides, ήταν προσαρμοσμένη σε περισσότερο κρεοφαγική δίαιτα, συγκρινόμενη προς την αρτίγονη Genetta genetta.

Λέξεις κλειδιά: *Μεσόγειος, Κύπρος, Genetta plesictoides, Νησιωτικός Ενδημισμός.*

1. Introduction

Many Mediterranean islands are renowned for their endemic Pleistocene mammalian faunas. These faunas are usually greatly impoverished and ecologically unbalanced, and include large animals that are able to cross wide sea barriers to reach remote islands. This type of sporadic and highly selective dispersal from a continent to an island has been called a 'Sweepstake Migration' (Simpson 1940, Sondaar 1977, Dermitzakis and Sondaar 1979). The population that reaches an island this way becomes genetically isolated from the parent continental population and undergoes a rapid evolutionary adaptation in the new insular environment, usually affecting the body size and the pattern of locomotion (Sondaar 1977, Lomolino 2005, Palombo in press). The sweepstake migrations and the subsequent evolution of endemic faunas were facilitated during the Pleistocene, as the climatically induced sea-level fluctuations were changing the distance between the mainland and the islands. The low sea levels were making the sea barrier easier and more probable to cross, while the subsequent high levels could make the sea channel crossing practically impossible, causing the isolation of the founding population on an island. The great number of islands in the Mediterranean, especially in the Aegean, made this region highly favourable for the evolution of island endemics (Sondaar and Boekschoten 1967, Dermitzakis and Sondaar 1979, Kotsakis *et al.* 1980, Sondaar *et al.* 1986, Marra 2005, Palombo 2006).

Animals that can migrate using sweepstake routes include mainly those with good swimming capabilities over long distances, i.e. elephants, deer and hippopotamuses, as well as flying animals as birds and bats (Sondaar 1977). Small animals, like rodents and lizards, can also reach a remote island by rafting. Carnivore taxa are normally not expected in insular endemic faunas of 'sweepstake' origin, as they are not long distance swimmers. Therefore, carnivores found on today's islands are probably not colonizers, but insular relics from a time when a mainland–island connection existed (Meiri *et al.* 2004). The usual carnivores of the Mediterranean insular faunas are the otters, which are adapted to aquatic lifestyle (Willemsen 1992). Other occurrences include the canid *Cynotherium sardous* of Sardinia–Corsica (Malatesta 1962, Eisenmann and van der Geer 1999, Lyras *et al.* 2006) and the genet *Genetta plesictoides* from Cyprus (Bate 1903a).

Cyprus, as an oceanic island that was separated from the mainland for a very long time, has yielded a greatly impoverished endemic fauna (Bate 1904, Boekschoten and Sondaar 1972, Reese 1995). The main element is a dwarf hippopotamus, *Phanourios minor* (Desmarest 1822), known from more than 30 sites on the island (Forsyth Major 1902, Bate 1906, Boekschoten and Sondaar 1972, Reese 1995, Reese in Simmons 1999: p.162). Another common endemic species is *Elephas cypriotes* Bate 1903, a dwarf elephant (Bate 1903b, 1905). Some scanty elephant remains of somewhat larger size than *E. cypriotes* may represent another endemic elephant species (Boekschoten and Sondaar 1972). Other, generally quite sparse, findings include the afore mentioned genet *Genetta plesictoides*, as well as some not well known small mammals: one or two species of murid rodents (*Mus* sp.), one or two species of bats and a soricid insectivore (*Crocidura suaveolens*) (Boekschoten and Sondaar 1972, Reese 1995). Endemic fossil deer, a common element in other Mediterranean insular faunas, have not been found on the island.

Recently (2001-2003), the Geological Survey of Cyprus and the Department of Historical Geology and Palaeontology of the University of Athens carried out an excavation in a rockshelter site in the eastern part of the island, near the town of Aghia Napa. The site is situated about 1 km east of the town of Aghia Napa (Fig. 1). It yielded abundant material of the dwarf hippo *Ph. minor*, as well as cranial and postcranial finds of the small carnivore of Cyprus. The new material of this endemic genet is described in the present paper.

2. Geological setting

The basement of the Aghia Napa area is a Late Cretaceous mélange that comprises bentonitic clays, containing blocks of siliciclastic sandstones, lava, pelagic limestones and red radiolarites.

The mélange is overlain by the Late Cretaceous – Early Miocene Lefkara Formation consisting of pelagic chalks with chert intercalations. Patch reefs of the Terra Member (Pakhna Formation) are extensively exposed on the surface overlying Lefkara Formation. The Aquitanian–Burdigalian Terra limestone remnants only rarely reflect reef morphology following Miocene and Pleistocene erosion. The reef facies comprises small frame stone structures made up of massive and branching corals as well as of encrusting organisms such as red algae, foraminiferans, bryozoans and molluscs. Among the coral colonies there is coarse bioclastic debris comprising fragments of bivalves, gastropods, echinoderms, algae, foraminiferans as well as aggregate grains and lime mud. Coral-dominated patch reefs passed outwards into algae-dominated deposits, foraminiferal packstones, grainstones and pelagic carbonates.

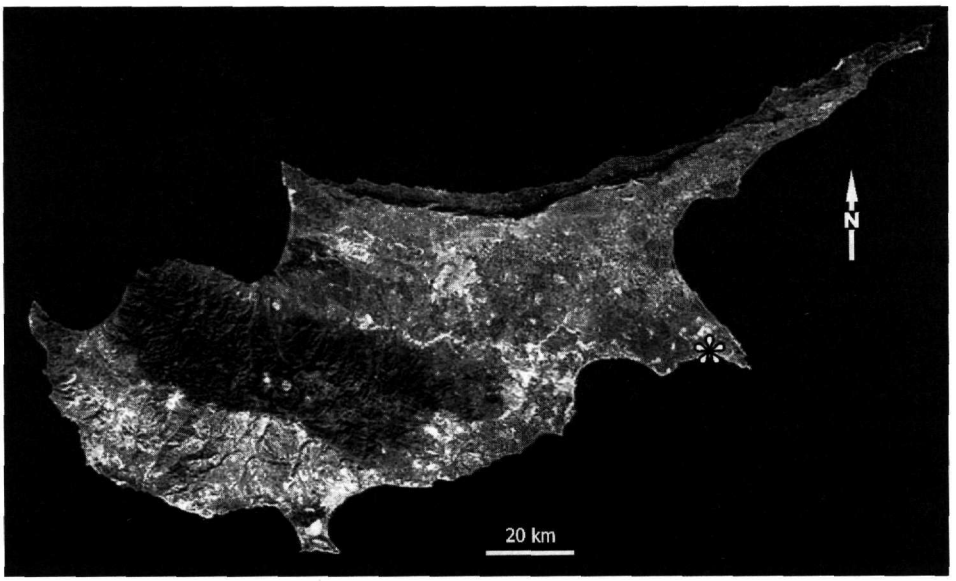

Figure 1 – Satellite image of Cyprus (source: NASA, http://visibleearth.nasa.gov/). The position of the Aghia Napa site is indicated with an asterisk

The rockshelter site of Aghia Napa is filled with clays of terrestrial origin, arranged in horizontal layers. The superficial layers are partly disturbed and the fossil hippopotamus bones are moved and mixed with recent bones. The genet remains were found during the October 2002 excavation, in the square Q8, together with numerous *Phanourios* remains. The sediment at Q8 was completely undisturbed. Due to local erosion, the finds were quite close to the surface (depth: 35 cm). ESR datings carried out on *Phanourios* teeth in the National Centre of Scientific Research 'Demokritos' in Athens, yielded ages of 11.0–13.5 ka for the Aghia Napa site (Bassiakos pers. com.).

3. Taxonomy

Order: Carnivora Bowdich, 1821
Family: Viverridae Gray, 1821
Genus: *Genetta* Oken, 1816

Genetta plesictoides Bate, 1903

Material: Partial skull with the right C–M1 and the left P2–M1 (AN-90.1, Fig. 2); right tibia (AN-90.2). All specimens were found close together in the same pocket and presumably belong to the same individual.

3.1. Description

The skull is narrow and elongated (estimated condylobasal length: 86 mm), with moderately long and low rostrum, which occupies about 1/3 of the skull length. The infraorbital foramen is large and almost circular (3.9×3.4 mm), and opens above the parastyle of P4. The orbital fossa is large and its anterior margin is slightly behind the infraorbital foramen's level.

Due to the deformation of the specimen, the cranial measurements are not accurate. The width of the skull at the supraorbital processes measures approximately 20 mm, while at the constriction behind the postorbital processes it measures approximately 12 mm. The maximal width of the braincase is estimated to 26 mm.

The sagittal crest is very thin, Y-shaped anteriorly, and slightly more developed at the posterior part of the cranial roof. The choanae open 4 mm behind the M1.

The tympanic bulla is elongated, twice as long as it is wide (16.5×8.8 mm). It is characterised by the marked antero-posterior elongation of the entotympanic chamber and the absence of an external auditory meatus tube.

The upper dentition is well preserved on the right side except for the incisors.

The P1 is very small and single-rooted. It is separated by diastemata of 1.5 mm from the canine and the P2. The P2 is elongated and narrow. Its main cusp is located slightly anteriorly in relation to the middle-length of the tooth. The distal crest of the main cusp is more trenchant than the mesial one and exhibits a tiny accessory cusp. The posterior part of the crown is elevated forming a cusp at the distalmost part of the tooth. There is a slightly developed lingual cingulum that extends to the mesial end of the tooth.

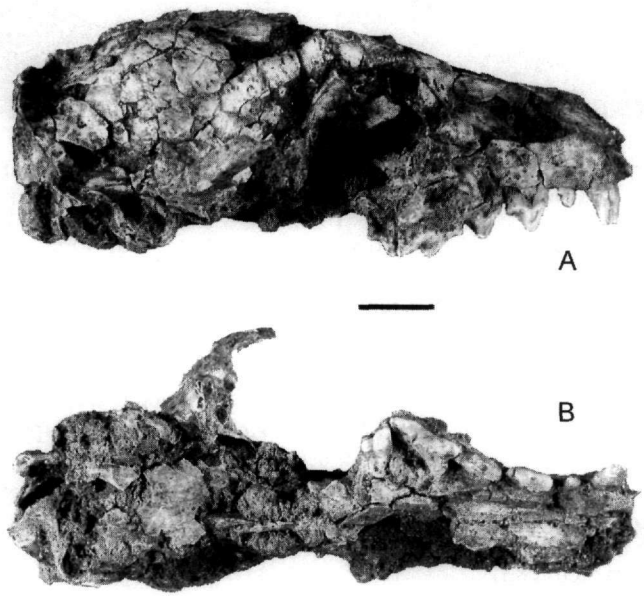

Figure 2 - *Genetta plesictoides* from Aghia Napa, Cyprus; skull: A, right lateral view; B, ventral view. Scale: 10 mm

The P3 is similar to P2 but its main cusp is more symmetrically placed, while there is also a small accessory cusp at the base of the crown and anteriorly. There is no lingual cusp.

The P4 is long and narrow, and has a very small and low parastyle, while the metastyle is clearly smaller in length than the paracone. The tip of the paracone is directed backwards. The protocone is weak, does not protrude significantly lingually, and does not extend mesially beyond the parastyle level. There is a cingulum at the lingual side of the metastyle.

The M1 is subtriangular and transversely elongated. Its mesial margin is convex, while the distal one is slightly concave. The ridge of the paracone is strong, elongated and transversely directed, whereas that of the metacone is very weak and low.

The M2 is lacking and no alveolus is observed behind M1. However, the region posteriorly of M1 is not well preserved and it is possible that a very small M2 did exist.

The tibia has the typical morphology of the family. Its total length is 74.2 mm. The proximal articulation dimensions are DAPprox. = 13.3 mm, DTprox. = 14.5 mm. The distal articulation dimensions are DAPdist. = 6.2 mm, DTdist. = 10.8 mm.

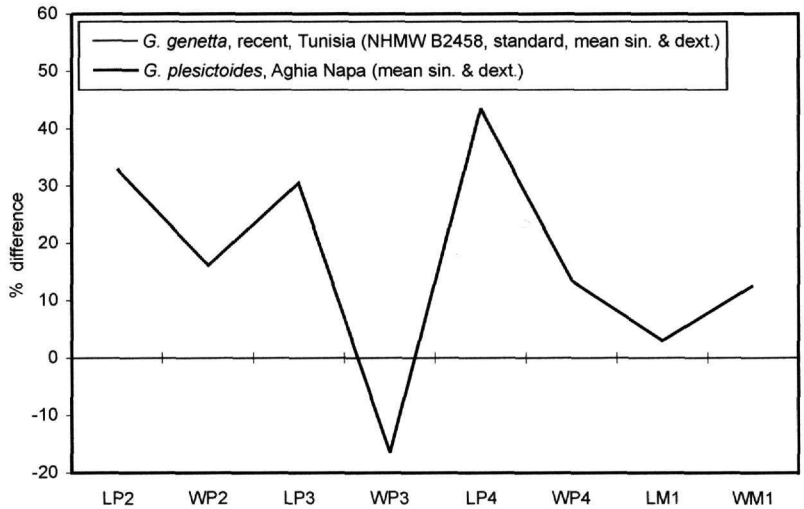

Figure 3 - Diagram comparing the dental dimensions of *G. plesictoides* from Aghia Napa, Cyprus and extant *G. genetta* from Tunisia

4. Discussion

The holotype of the endemic species *Genetta plesictoides* is a mandible found in the cave 'Dikomo Mandra' at Kerynia range in the northern part of Cyprus (Bate 1903a). Later, Steensma and Reese (in Simmons 1999: p.167-169) described a few juvenile carnivore remains from Aetokremnos that they referred to *G.* cf. *plesictoides*. Both samples are not comparable to the material described herein, as they represent different skeletal parts. However, their size —superior in comparison to that of *G. genetta*— is very similar, allowing us to ascribe the studied material to *G. plesictoides*.

In general, the upper dentition of the studied *G. plesictoides* cranial specimen appears to be very similar in morphology to the dentition of the extant *G. genetta.* Nevertheless, it exhibits important differences in some respects. The premolars (P2–P4) of *G. plesictoides* have different proportions, being longer and transversely narrowed. The P3 lacks the internal cusp that characterises the extant *G. genetta*, as well as the extant *G. servalina*, *G. felina* and *G. tigrina*. Contrary to these species, the protocone of P4 does not project lingually so much and is much less developed. Moreover, compared to *G. genetta*, the P4 is longer in relation to the other premolars (especially P3) or the whole cheek teeth series. It is not clear if the M2 is absent in *G. plesictoides*. However, if present,

this tooth must have been diminutive, much smaller than in *G. genetta*, and about as small as in *Osbornictis* (van Rompaey 1988: fig. 3).

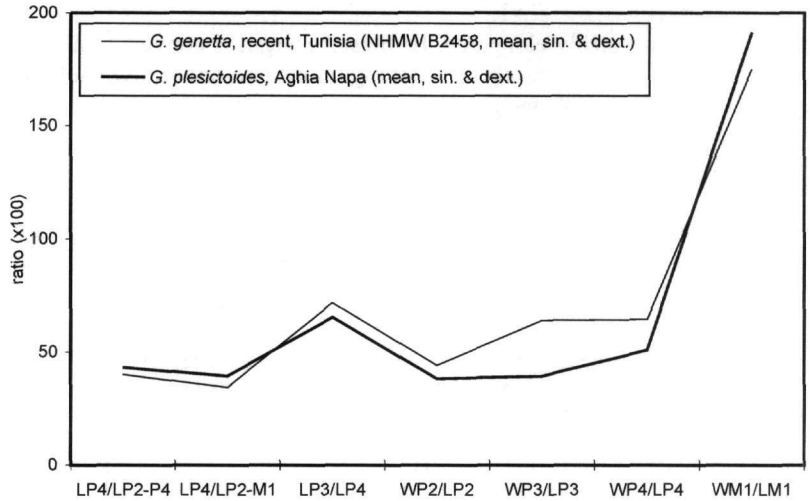

Figure 4 - Diagram comparing the dental proportions of *G. plesictoides* from Aghia Napa, Cyprus and extant *G. genetta* from Tunisia

Table 1 – Teeth measurements (in mm) of *G. plesictoides* from Cyprus, compared to extant *G. genetta*

	Genetta plesictoides **Aghia Napa, Cyprus** sin.	dext.	***Genetta genetta*** **NHMW B2458, Tunisia** (recent, mean sin. & dext.)
(L×W) C	—	4.1×2.9	—
(L×W) P1	—	2.5×1.6	—
(L×W) P2	6.3×2.4	6.2×2.4	4.7×2.1
(L×W) P3	6.6×(2.5)	6.5×2.7	5.0×3.1
(L×W) P4	10.0×5.1	10.1×5.1	7.0×4.5
(L×W) M1	4.1×7.9	4.0×7.6	3.9×6.9
LP2-P4	23.1	23.2	17.4
LP2-M1	25.4	25.5	20.3
(LP4/ LP2-P4)×100	43.2	43.3	40.0
(LP4/ LP2-M1)×100	39.3	39.5	34.3
(LP3/LP4)×100	66.1	64.6	71.9
(WP2/LP2)×100	37.7	38.7	44.2
(WP3/LP3)×100	(37.9)	40.9	64.1
(WP4/LP4)×100	51.4	50.5	64.4
(WM1/LM1)×100	192.7	190.0	175.0

5. Conclusion

The species *G. plesictoides* is a poorly known endemic viverrid. Apart from an adult mandible and scarce limb bones, as well as some scanty juvenile dental and postcranial material, no other skeletal parts of this small carnivore were known until recently. The new material from Aghia Napa is the first adult skull and upper dentition of the species. Its main character is the development of the cutting function of the dentition, probably reflecting a more carnivorous diet, compared to the extant common genet.

The co-occurrence of *G. plesictoides* with *Phanourios minor* in the site of Aghia Napa, positively indicates that the Cypriot genet belongs to the endemic Pleistocene fauna or is at least closely associated with it.

6. Acknowledgments

The excavations were financed by the General Secretariat of Research and Technology of the Greek Ministry of Development (EU project, Code 2013555 – Project of University of Athens 70/3/6050), the Ministry of Agriculture, Natural Resources and Environment of Cyprus, the Cyprus Geological Survey, the Municipality of Aghia Napa – Project UoA 70/3/6017) and the Special Account for Research Grants of Athens University (Project of UoA 70/4/3370). Special studies were financed by the Project on the Palaeontology of Cyprus (70/3/7093).

Special thanks are also owed to Dr Mathias Harzhauser, director of the Geological Department of the Natural History Museum of Vienna (NHMW), Dr Heinz Kollmann (NHMW), Helga Schmitz, librarian at the Geological and Palaeontological Department of the NHMW, Dr Barbara Herzig, Director of the Zoological Department of NHMW, Alex Lukendeker, Alexander Bibl, and Alice Schumacher (NHMW). This study would have been impossible without the help of Adrian Lister (University College London) and Andy Currant, curator of fossil vertebrates at the Natural History Museum London. Acknowledgments are owed to Varvara Perikleous, (Mayor of Aghia Napa), Athos Georgiou (Aghia Napa), George Petridis and Polis Michailidis (former and present Directors of the Cyprus Geological Survey), and Efthymios Tsiolakis (Cyprus Geological Survey) for their support since 2001. Special thanks are also due to Dr I. Bassiakos (NCSR 'Demokritos', Athens), who provided us with the absolute dating of the hippo material.

Last but not least, the authors thank two anonymous reviewers, whose comments and suggestions contributed to the amendment of the manuscript.

7. References

Bate, D.M., 1903a. On an extinct species of genet (*Genetta plesictoides*, sp. n.) from the Pleistocene of Cyprus, *Proceedings of the Zoological Society of London*, 1903(2), 121-124.

Bate, D.M., 1903b. Preliminary note on the discovery of a pygmy elephant in the Pleistocene of Cyprus, *Proceedings of the Royal Society of London*, 71, 498-500.

Bate, D.M., 1904. On the ossiferous cave-deposits of Cyprus, *Geological Magazine*, 1(5), 324-325.

Bate, D.M., 1905. Further note on the remains of *Elephas cypriotes* from a cave-deposit in Cyprus, *Philosophical Transactions of the Royal Society of London*, 197, 347-360.

Bate, D.M., 1906. The pigmy *Hippopotamus* of Cyprus, *Geological Magazine*, 3, 241-245.

Boekschoten, G.J., and Sondaar, P.Y., 1972. On the fossil Mammalia of Cyprus, *Proceedings of the Koninklijke Nederlandse Akademie van Wetenschappen*, 75(4), 306-338.

Dermitzakis, M.D., and Sondaar, P.Y., 1979. The importance of fossil mammals in reconstructing paleogeography with special reference to the Pleistocene Aegean Archipelago, *Annales Géologiques des Pays Helléniques*, 29, 808-840.

Eisenmann, V., and van der Geer, B., 1999. The *Cynotherium* from Corbeddu (Sardinia): comparative biometry with extant and fossil canids, *Deinsea*, 7, 147-168.

Forsyth Major, C.J., 1902. On the pigmy *Hippopotamus* from the Pleistocene of Cyprus, *Proceedings of the Zoological Society of London*, 1902(2), 107-112.

Kotsakis, T., Petronio, C., and Sirna, G., 1980. The Quaternary Vertebrates of the Aegean islands: palaeogeographical implications, *Annales Géologiques des Pays Helléniques*, 30(1), 31-64.

Larivière, S., and Calzada, J., 2001. *Genetta genetta*, *Mammalian Species*, 680, 1-6.

Lomolino, M.V., 2005. Body size evolution in insular vertebrates: generality of the island rule, *Journal of Biogeography*, 32(10), 1683-1699.

Lyras, G.A., van der Geer, A.A.E., Dermitzakis, M.D., and de Vos, J., 2006. *Cynotherium sardous*, an insular canid (Mammalia: Carnivora) from the Pleistocene of Sardinia (Italy), and its origin, *Journal of Vertebrate Paleontology*, 26(3), 735-745.

Malatesta, A., 1962. Il cane selvaggio del Pleistocene di Sardegna, *Geologica Romana*, 1, 173-189.

Marra, A.C., 2005. Pleistocene mammals of Mediterranean islands, *Quaternary International*, 129(1), 5-14.

Meiri, S., Dayan, T., and Simberloff, D., 2004. Body size of insular carnivores: little support for the island rule, *American Naturalist*, 163(3), 469-479.

Palombo, M.R., 2006. Biochronology of the Plio-Pleistocene terrestrial mammals of Sardinia: the state of the art, *Hellenic Journal of Geosciences*, 41(1), 47-66.

Palombo, M.R., in press. How can endemic elephants help us understanding "island rule"?, *Quaternary International*.

Reese, D.S., 1995. The Pleistocene vertebrate sites and fauna of Cyprus, *Bulletin of the Geological Survey of Cyprus*, 9, 1-203.

Simmons, A.H., 1999. *Faunal extinction in an island society: pygmy hippopotamus hunters of Cyprus*, New York, Kluwer, 381pp.

Simpson, G.G., 1940. Mammals and land bridges, *Journal of the Washington Academy of Sciences*, 30, 137-163.

Sondaar, P.Y., 1977. Insularity and its effect on mammal evolution. In M.K. Hecht, P.C. Goodyand and B.M. Hecht (eds), *Major patterns in Vertebrate evolution*. 671-707, New York, Plenum.

Sondaar, P.Y., and Boekschoten, G.J., 1967. Quaternary Mammals in the South Aegean island arc, with notes on other fossil Mammals from the coastal regions of the Mediterranean, *Proceedings of the Koninklijke Nederlandse Akademie van Wetenschappen*, 70(5), 556-576.

Sondaar, P.Y., de Vos, J., and Dermitzakis, M.D., 1986. Late Cenozoic faunal evolution and palaeogeography of the South Aegean island arc, *Modern Geology*, 10(2-3), 249-259.

Van Rompaey, H., 1988. *Osbornictis piscivora*, *Mammalian Species*, 309, 1-4.

Willemsen, G.F., 1992. A revision of the Pliocene and Quaternary Lutrinae from Europe, *Scripta Geologica*, 101, 1-115.

Δελτίο της Ελληνικής Γεωλογικής Εταιρίας τομ. XXXX, 2007
Πρακτικά 11ου Διεθνούς Συνεδρίου, Αθήνα, Μάιος 2007

Bulletin of the Geological Society of Greece vol. XXXX, 2007
Proceedings of the 11th International Congress, Athens, May, 2007

PLANKTON ECOSTRATIGRAPHY AND POLLEN ASSEMBLAGE ZONES OVER THE LAST 14 000 YEARS IN SE AEGEAN SEA (CORE NS-14)

Triantaphyllou M. V.[1], Antonarakou A.[1], Kouli K. [1], Dimiza M.[1], Kontakiotis G.[1], Ziveri P.[2], Mortyn G.[2], Lykousis V.[3], and Dermitzakis M. D.[1]

[1] *National and Kapodistrian University of Athens, Faculty of Geology and Geoenvironment, Department of Hist. Geology - Paleontology,Greece, mtriant@geol.uoa.gr, aantonar@geol.uoa.gr, akouli@geol.uoa.gr, mdimiza@geol.uoa.gr, gkontak@geol.uoa.gr*

[2] *ICTA Autonomous University of Barcelona (UAB) Edifici Cno-Campus UAB, 08193, Bellaterra, Spain, patrizia.ziveri@uab.es, graham.mortyn@uab.es*

[3] *Hellenic Centre for Marine Research, Inst. of Oceanography, 19013 Anavyssos, Greece, vlikou@ath.hcmr.gr*

Abstract

A quantitative analysis of coccolithophores, planktonic foraminifera and pollen assemblages was carried out on core NS-14 (SE Aegean Sea), recovered in the Western Kos Basin. Eleven coccolithophore (ACE1-11) and ten planktonic foraminifera (APFE1-10) ecozones have been recognized during the last 14 000 yrs using calcareous nannofossil and planktonic foraminifera abundances. Additionally eight pollen assemblage zones (PAZ1-8) have been recognised. The established high resolution ecozonal scheme allows a detailed paleoecological reconstruction for the Holocene archive in the SE Aegean Sea, defining two warm and humid phases (9300-8600 yr $_{cal}$ BP and 7600-6400 yr $_{cal}$ BP) associated with the deposition of S1 and a third one between 5200-4200 yr $_{cal}$ BP.

Key words: *coccolithophores, planktonic foraminifera, pollen, ecozones, Holocene.*

Περίληψη

Η ποσοτική ανάλυση ασβεστολιθικών ναννοαπολιθωμάτων, πλαγκτονικών τρηματοφόρων και κόκκων γύρεως που πραγματοποιήθηκε στον πυρήνα NS-14 (ΝΑ Αιγαίο, Λεκάνη Δυτικής Κω), επέτρεψε τον καθορισμό έντεκα οικοζωνών κοκκολιθοφόρων (ACE1-11), δέκα οικοζωνών πλαγκτονικών τρηματοφόρων (APFE1-10) και οκτώ ζωνών συγκέντρωσης κόκκων γύρεως (PAZ1-8). Το υψηλής ανάλυσης οικοστρωματογραφικό σχήμα που αναπτύχθηκε επέτρεψε την λεπτομερή παλαιοικολογική ανασύσταση του Ολοκαίνου στην περιοχή του ΝΑ Αιγαίου και τον καθορισμό δύο θερμών και υγρών περιόδων (9300-8600 yr $_{cal}$ BP and 7600-6400 yr $_{cal}$ BP) που σχετίζονται με την απόθεση του σαπροπηλού S1 και μιας μεταγενέστερης μεταξύ 5200-4200 yr $_{cal}$ BP.

Λέξεις κλειδιά: *ασβεστολιθικά ναννοαπολιθώματα, πλαγκτονικά τρηματοφόρα, κόκκοι γύρεως, οικοζώνες, Ολόκαινο.*

1. Introduction

All the biochemical parameters of the euphotic zone, although relatively increased in the N. Aegean, clearly reflect the highly oligotrophic character of the Aegean Sea (Lykousis *et al.* 2002). Though the modern Aegean Sea is generally characterized by low primary productivity and organic deficient sediments, the late Pleistocene-Holocene deposition of sapropels (dark-coloured organic-rich sedimentary layers) demonstrates that dramatically different conditions periodically occurred and coincided with changes in global and regional climate (Rohling and Hilgen 1991) and / or water circulation and biogeochemical cycling (Anastasakis and Stanley 1986, Van Santvoort and de Lange 1997). The early Holocene sapropel S1 was deposited in the N. Aegean Sea between 9600-6400 yr_{nc} BP (Perissoratis and Piper 1992), in the SW Aegean Myrtoon Basin has lasted between 9000-6900 yr_{nc} BP (Geraga *et al.* 2000), while in the S. Aegean Geraga *et al.* (2005) provided an age of 9000-5500 yr_{nc} BP. Interruptions within sapropel S1, centred roughly at 7000 yr_{nc} BP, have been documented in the Adriatic (Rohling *et al.* 1997) and Aegean Sea (Perissoratis and Piper 1992, De Rijk *et al.* 1999, Geraga *et al.* 2000) and are interpreted as genuine events related to climatic deterioration (De Rijk *et al.* 1999).

The present study aims to high resolution paleoecological reconstruction of the Holocene SE Aegean archive in the shallow, very rapidly accumulated core NS-14 in the Western Kos Basin, SE Aegean. A special effort is being made towards to the detailed investigation of the remarkably thick S1 exposed at the core, and to the establishment of a refined ecostratigraphic scheme based on coccolithophore and planktonic foraminiferal patterns and pollen assemblages.

2. Materials and methods

The 400 cm-long NS-14 gravity core was recovered during the R/V Aegeo-Cruise 1998, in western Kos Basin (SE Aegean Sea; Fig. 1a), from a water depth of 505 m at $36^0 38' 55''$ N and $27^0 0' 28''$ E. A total of 156 samples were collected for coccolithophore analysis every 2 cm in the hemipelagic mud and every 1 cm in the sapropel intervals. Sample preparation followed standard smear slide techniques. Analyses were performed using a Leica DMSP optical polarising light microscope at 1250x magnification by counting at least 300 specimens per sample. Specimens resembling to *Reticulofenestra* spp. were assigned here to EHMC (*Emiliania huxleyi* Moderately Calcified morphotypes) of Crudeli *et al.* (2004, 2006). Additional counts of 15 fields of view (Negri and Giunta 2001) were performed for the species *Helicosphaera* spp., *Rhabdosphaera* spp., *Syracosphaera* spp., *Coronosphaera* spp., *Discosphaera tubifera.* The rare species *Braarudosphaera bigelowii* was counted in a fixed area of 150 fields of view. All results were converted in relative abundances (percentages) of selected species in order to avoid dilution effects such as the input of terrigenous matter.

Foraminiferal analyses were carried out on 67 samples. The sediment was washed through 150 μm mesh sieve and dried at 60^0 C. Quantitative analysis was carried out on each sample, subsampled into aliquots through a microsplitter, in order to obtain at least 300 specimens. Planktonic foraminifera specimens were identified and counted following the taxonomic concept of Hemleben *et al.* (1989). *Neogloboquadrina pachyderma* right and left coiling (d and s) and the two varieties of *Globigerinoides ruber alba* and *rosea* were counted and plotted separately. The species *Globigerinoides sacculifer* includes also *Globigerinoides trilobus*, according to Hemlemben *et al.* (1989) and the species *Globoturborotalita rubescens* and *Globoturborotalita tenella* were counted and plotted together (Capotondi *et al.* 1999). The identified species are expressed as percentages (%) of the total number of planktonic foraminifera. The paleoclimatic curve inferred from planktonic foraminifera assemblages was obtained by the formula (w-c)/(w+c)x100, where w represents the warm-water indicators and c the cold water indicators. *Globigerinoides trilobus-sacculifer*, *Globigerinoides ruber* var. *alba* and *rosea*, *Globoturborotalita rubescens*, *Globorotalia truncatulinoides*, *Orbulina universa* and *Globigerinella siphonifera* were considered warm water species, while *Globorotalia scitula, Globorotalia inflata, Turborotalita quinqueloba*, and *Globigerinita*

glutinata were considered cold water indicators (Hemleben *et al.* 1989, Rohling *et al.* 1993, Pujol and Vergnaud Grazzini 1995).

Pollen analysis was performed on 134 samples of known weight. Samples were treated with 10 % HCl and 38 % HF and sieved over a 10 µm sieve, while *Lycopodium* spores were added in order to check the reliability of quantitative data. Samples were stored and mounted in silicone oil and a minimum of 150 pollen grains was counted in each sample excluding *Pinus*, Pteridophyte spores and aquatics. Percentage diagrams for selected pollen types were constructed, and pollen concentrations were calculated in grains/gram. As no major rivers are draining in western Kos Basin, the main pathway of pollen transport is assumed to be through wind (Muller 1959). Therefore pollen concentration in the sediments reflects changes in wind intensity and pollen production, while concentration of palynomorphs from taxa living in rivers and lakes (like *Sparganium*, *Pediastrum* and Zygnemantaceae) can be used as a proxy of river runoff into the basin (Targarona 1997).

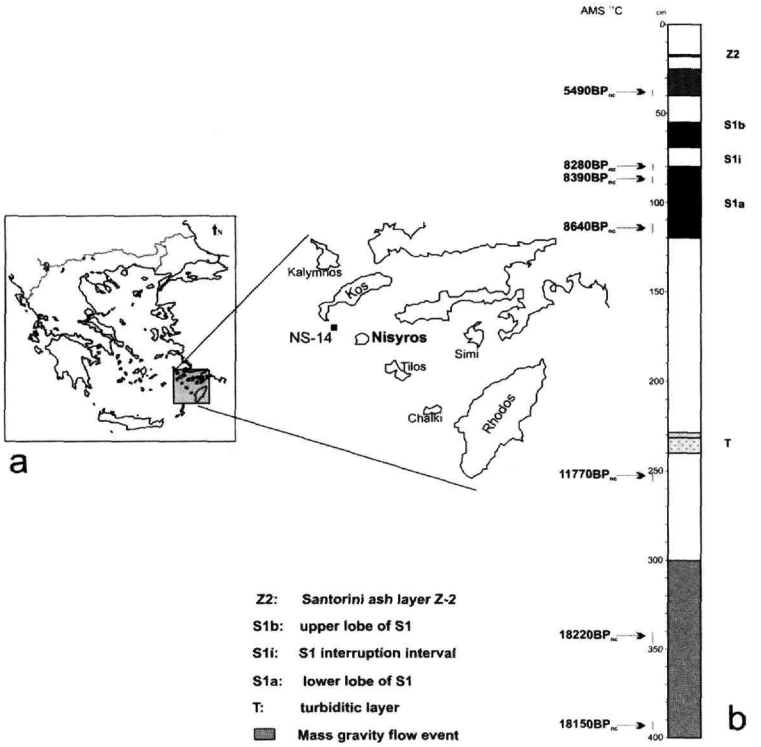

Figure 1 – a. Location of core NS-14 in SE Aegean Sea, b. Core NS-14 stratigraphy and performed AMS datings (after Triantaphyllou *et al.* subm.)

3. Results

3.1. General core lithology and age assessment

From the top to 300 cm, the core lithology mainly consists of grey hemipelagic mud, interrupted by a volcanic ash layer at 17 cm, which represents the most recent Z-2 Santorini ash layer. An additional dark interval is visually detected between 25 and 40 cm. Sapropel S1 is recognised from 55 to 120 cm and is distinctively divided in two units by a lighter grey coloured interval (69-80 cm). A turbiditic layer (T) is located between 231 and 240 cm. Grey clay with pebbles prevail from 300 cm to the bottom (Fig. 1b), representing a gravity flow event.

The base of S1(a) at 120 cm depth is considered to have an interpolated calendar age of 9300 yr $_{cal}$ BP (8800 yr $_{nc}$ BP), whereas the top of S1(a) at 80 cm, corresponds to an interpolated age of 8600

yr $_{cal}$ BP (8300 yr $_{nc}$ BP), (Triantaphyllou *et al.* 2006, Triantaphyllou *et al.* subm.). The top of S1 interruption at 69 cm is calibrated at 7600 yr $_{cal}$ BP (7300 yr $_{nc}$ BP) and the top of S1(b) at 55 cm has an interpolated age of 6400 yr $_{cal}$ BP (6100 yr $_{nc}$ BP). The estimated sedimentation rates (Triantaphyllou *et al.* subm.) indicate rapid accumulation of S1 (an average sedimentation rate of 57 cm/kyr in the lower S1(a) layer; 11 cm/kyr in the interruption and 11 cm/kyr in the upper S1(b) layer). The similar ages provided by AMS ^{14}C datings at 344 and 393 cm (Fig. 1b) indicate that the dark olive grey coarse sediments from 300 cm till the base of the core, represent a mass gravity flow event slightly younger than 18200 yr $_{nc}$ BP, mostly associated with possible seismic activity and landslide phenomena due to the active tectonism of the area (Papanikolaou and Nomikou 2001).

3.2. Coccolithophores

Coccolithophores are generally well preserved in all samples taken from the upper 300 cm of the sediment core. The frequency curves of the most indicative coccolithophore species are shown in Fig. 2a. From 300 cm up to 135 cm depth *E. huxleyi* abundances remain constant above 60 %. Above this level the abundances display a gradual decrease, with minimum values reaching 25 %, during S1 interruption interval. Relative abundances exceeding 60 % reappear from 30 cm towards core top. EHMC morphotypes are restricted mainly in the interval from 300 to 120 cm and reappear at 60 cm; showing the maximum abundance at 15 cm from the top. *F. profunda* shows more or less an inversed pattern to *E. huxleyi* with the highest abundance from 135 to 60 cm. A sharp decrease in the abundance of this species is recorded at 60 cm, during the formation of S1(b). A prominent frequency peak up to 52 % is also recorded at 32 cm. *Rhabdosphaera* spp. increase in relative abundance from 256 cm and upwards. *Syracosphaera* spp. and *Calciosolenia* spp. follow more or less the same trend. On the contrary, *Helicosphaera* spp. start to increase at 135 cm, peaking at the lower part of S1(a), between 120 and 100 cm. A second interval with high frequencies of *Helicosphaera* spp. occurs between 38 and 29 cm. *Gephyrocapsa oceanica* is mainly occuring between 60 and 29 cm with maximum abundance at the upper part of S1(b); outside this interval its presence is only sporadical. *B. bigelowii* is present at 170 cm and 78 cm, but increases at the upper part of S1(b) at 57-55 cm; it occurs with very few representatives up to 29 cm. *Calcidiscus* spp. and *Umbilicosphaera* spp. increase in abundance above 100 cm, but the highest frequencies are recorded above S1. The species *Umbellosphaera tenuis* presents higher values between 300 and 260 cm and above S1 up to 29 cm.

3.3. Planktonic foraminifera

The relative abundance data of 16 planktonic foraminifera species are presented in Fig. 3. *G. ruber alba* and *G. ruber rosea* abundance curves show maximum values at the interval 100-80 cm of the core. *G. ruber rosea* displays also a significant peak in abundance at 54 and 30 cm, whereas the species is almost absent in the lower part of the core. On the contrary *G. ruber alba* shows elevated percentages throughout the core. *G. trilobus/sacculifer* first appears at 130 cm, reaching maximum abundance at the base of S1(a) and between 40-29 cm of the core. It almost disappears between 100-65 cm and then it appears again at 60-20 cm occurring up to the top in small percentages. *O. universa* shows several peaks in abundance during the deposition of S1, while it is almost absent in the lower part of the core. *Neogloboquadrina pachyderma* and *N. dutertrei* totally disappear within S1, existing only in the lower part of the core. However, *N. pachyderma* sinistrally coiled specimens, were found at 125, 80 and 10 cm. *G. bulloides* is continuously present in the core, slightly decreasing in the lower part of S1(a). At 50 cm from the core top the species displays a temporary disappearance but it reoccurs above this level reaching its maximum abundance. The abundance curve of *G. rubescens* and *G. siphonifera* shows a decrease at the interval 120-90 cm; both species are more abundant during 65-50 cm and they abruptly increase at 16-8 cm. *G. glutinata* presents a constant distribution in the core with a gradual decrease from the 54 cm to the top of the core. *T. quinqueloba* displays a sporadic distribution pattern being more abundant in the lower part of the core. The species is absent during S1. Among the minor species, *G. conglobatus*

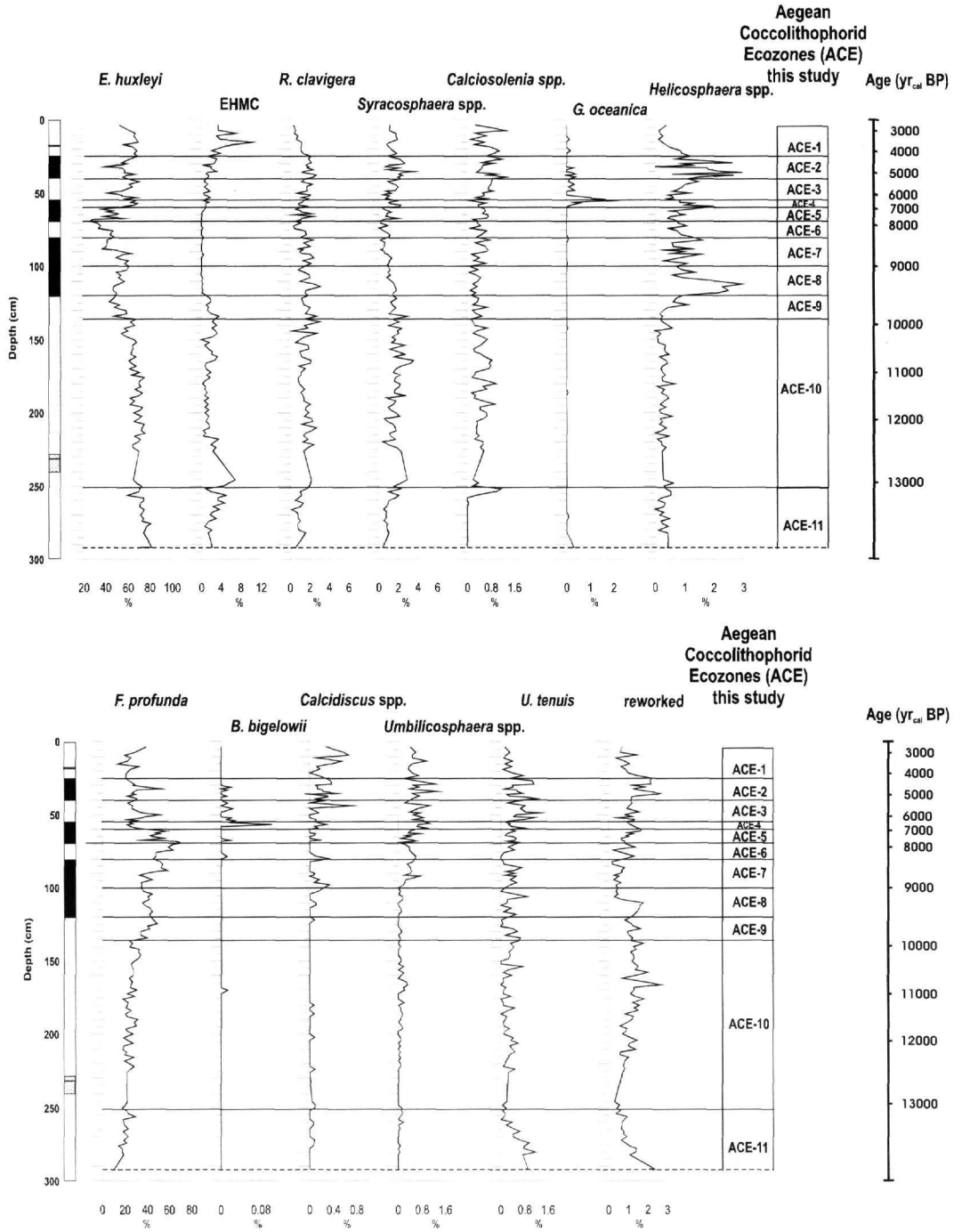

Figure 2 - Frequency curves of the most indicative coccolithophorid species in core NS-14. To the right the established coccolithophoris ecozones (ACE1-11)

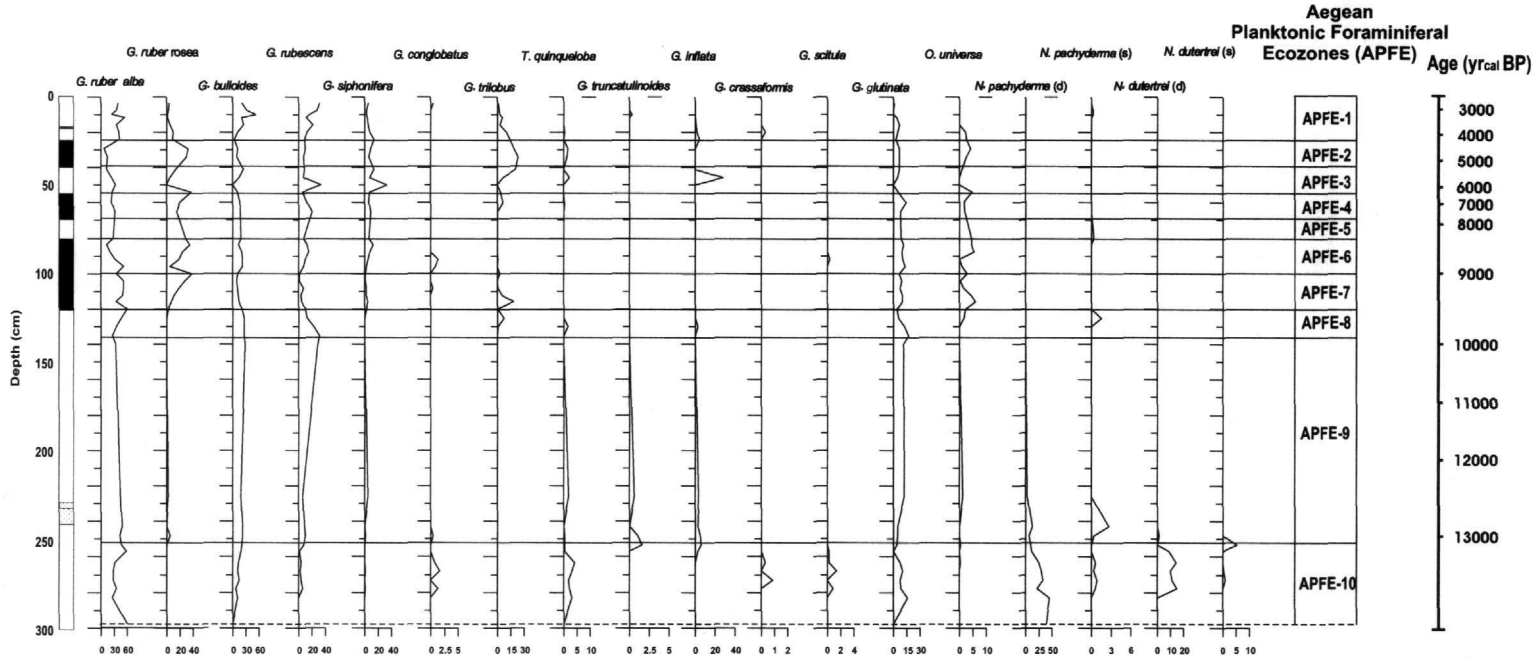

Figure 3 - Frequency curves of the most indicative planktonic foraminifera species in core NS-14. To the right the established planktonic foraminifera ecozones (APFE1-9)

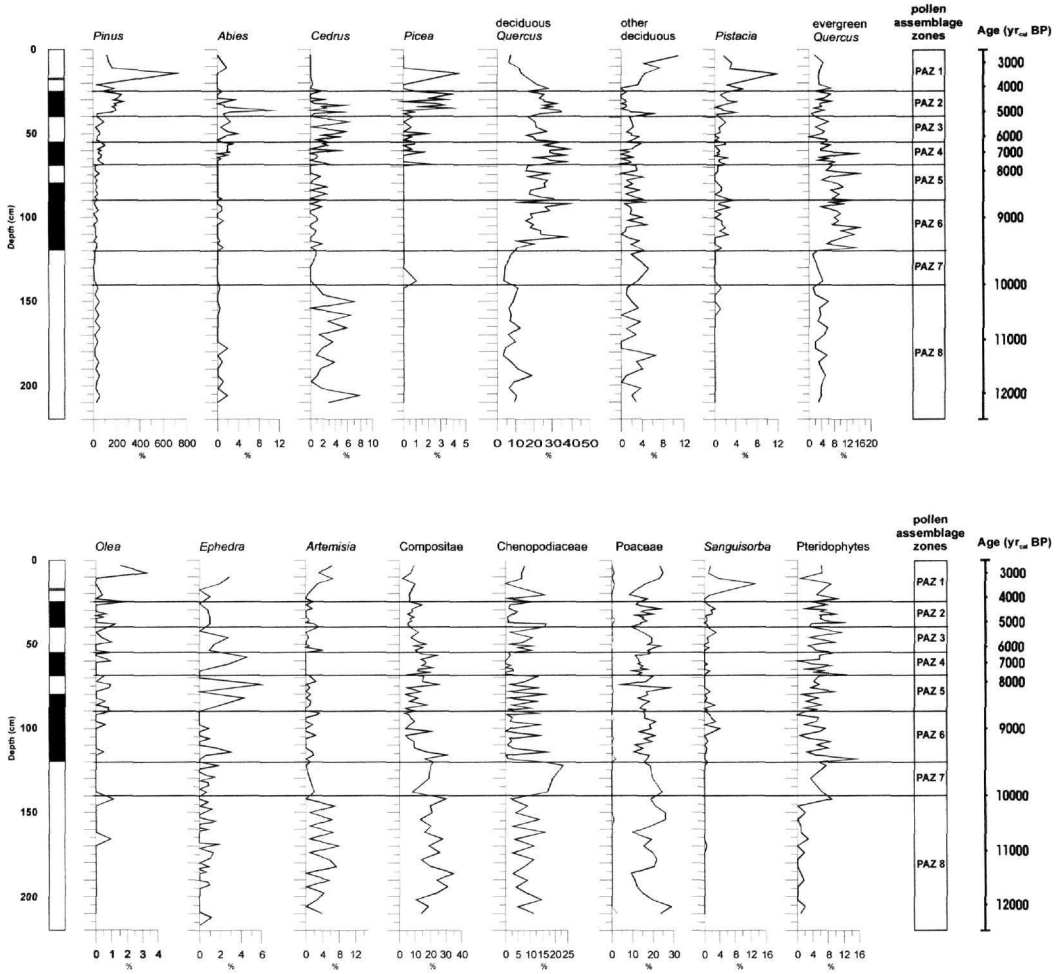

Figure 4 - Frequency curves of the most indicative pollen taxa in core NS-14. To the right the established pollen assemblage zones (PAZ1-8)

and *G. scitula* display the same distribution pattern, existing in small percentages in the lower part of the core; a slight influx is recorded in the upper part of S1(a). *G. inflata* is present in the lower part of the core. Upwards it occurs in low percentages just below S1(a), disappears within the sapropel, and reappears above it reaching its maximum abundance. *G. truncatulinoides* is mainly restricted at the lower part of the core.

3.4. Pollen

Pollen concentrations vary form 10 to 53.000 grains per gram of dry sediment, with the lower concentrations appearing in the lower horizons and the highest within the sapropel and in the 28-40 cm interval. The concentration of aquatic palynomorphs follows the same trend, increasing during the sapropel and showing maximum values in the 28-40 cm interval. No pollen diagram was constructed from 210 cm and downwards due to the extremely low pollen concentrations. Pollen spectra of core NS-14 reflect diversified vegetation ranging from steppe to semi-dessert (*Artemisia*, Chenopodiaceae), mountainous deciduous (*Quercus robur, Sorbus, Acer*) and coniferous forests (*Pinus*, *Abies* and *Cedrus*) representatives (Fig. 4). Arboreal taxa are continuously present in all spectra, though their abundances fluctuate. *Pinus* and *Cedrus* are continuously present while *Abies* appears less abundant and absent in many spectra and *Picea* is mainly represented on the upper 70

cm of the core. *Juniperus* and *Quercus* records continuous presence, the latter shows its highest abundance between 140 cm and 37 cm. Steppe vegetation elements as Compositae, Poaceae, Chenopodiaceae, occur in high values especially below 120 cm. In particular the curve of Chenopodiaceae shows a profound maximum in the 140-120 cm interval. The semi-desert taxa *Artemisia* and *Ephedra* though being almost continuously present in the spectra in low percentages, show relatively higher abundances from 140cm downwards. *Pistacia* appears continuously abundant from 120 cm upwards, becoming an important element of the Mediterranean forest.

4. Ecostratigraphy

4.1. Coccolithophore ecozones

The detailed coccolithophore analysis in the high sedimentation rate NS-14 core reveals a series of abundance fluctuations that permits the documentation and refinement of the regional E. Mediterranean ecostratigraphic scheme (Principato *et al.* 2003, Giunta *et al.* 2003), in particular during the interval of sapropel S1 deposition. Eleven coccolithophore ecozones (Aegean Coccolithophore Ecozones; ACE 1-11) are recognised, documenting the dramatic response of coccolithophore assemblages to environmental changes in SE Aegean (Fig. 2).

ACE-1 (= C1 of Principato *et al.* 2003). Interval: High abundance of *E. huxleyi* and EHCM (*E. huxleyi* moderately calcified morphotypes sensu Crudeli *et al.* 2004), decrease of *Helicosphaera* spp.

ACE-2 (= upper C2 of Principato *et al.* 2003). Top: last common occurrence of *B. bigelowii*. Interval: high abundance of *Helicosphaera* spp., increase of *Syracosphaera* spp., *F. profunda, U. tenuis*.

ACE-3 (= middle C2 of Principato *et al.* 2003). Top: abrupt increase of *Helicosphaera* spp. Interval: increase of *F. profunda*.

ACE-4 (= lower C2 of Principato *et al.* 2003). Top: distinct reduction of *B. bigelowii* and peak of *G. oceanica*. Interval: low abundance values of *Helicosphaera* spp. and *F. profunda*, peak of *B. bigelowii*.

ACE-5 (= C3 of Principato *et al.* 2003). Top: abrupt decrease in abundance of *F. profunda*, decrease of *Syracosphaera* spp. Interval: Peak in abundance of *Rhabdosphaera* spp., *Umbilicosphaera* spp., *Syracosphaera* spp., presence of *B. bigelowii*.

ACE-6 (= upper C4 of Principato *et al.* 2003). Top: peak in *F. profunda*. Interval: presence of *B. bigelowii*.

ACE-7 (= middle C4 of Principato *et al.* 2003). Top: decrease of *Syracospharea* spp. and *R. clavigera*. Interval: high abundance of *F.profunda* and *E. huxleyi*. EHCM morphotypes are absent.

ACE-8 (= middle C4 of Principato *et al.* 2003). Top: increase of *Umbilicosphaera* spp., decrease of *Helicosphaera* spp. Interval: very high abundance values of *Helicosphaera* spp. High values of *R. clavigera*. EHCM morphotypes are absent.

ACE-9 (= lower C4 of Principato *et al.* 2003). Top: increase of *Helicosphaera* spp., decrease of EHCM. Interval: gradual increase of *F. profunda* and *Helicosphaera* spp.

ACE-10 (= C5 of Principato *et al.* 2003). Top: peak in *Syracosphaera* spp., increase of *F. profunda*. Interval: high abundance of *E. huxleyi*, decreased values of *Helicosphaera* spp., peak of EHCM.

ACE-11 (= upper C6 of Principato *et al.* 2003). Top: increase in abundance of *R. clavigera*. Interval: increase of *E. huxleyi* and *U. tenuis*.

4.2. Planktonic foraminiferal ecozones

High resolution analyses performed on planktonic foraminiferal assemblages allowed the recognition of nine bioevents that are used to define ten Aegean Planktonic Foraminiferal Ecozones (APFE1-10), which are well comparable to the ecozones and biozones established in the central and eastern Mediterranean (Jorissen *et al.* 1993, Capotondi *et al.* 1999, Sbaffi *et al.* 2001, Principato *et al.* 2003). We summarise below the principal characters of each APFE in order to explain the high resolution ecostratigraphic scheme recorded in Fig. 3.

APFE-1 (=PF1 of Principato *et al.* 2003). Interval: significant presence of *G. ruber alba* and *G. bulloides*, decrease of *G. ruber rosea* and *O. universa*, presence of *G. trilobus/sacculifer* and *G. rubescens*, slight peak of *G. inflata*.

APFE-2 (=upper PF2 of Principato *et al.* 2003). Top: increase of *G. ruber alba*, decrease of *G. ruber rosea* and *O. universa* , disappearance of *T. quinueloba*. Interval: decrease of *G. ruber alba*, high abundance of *G. ruber rosea*, *G. trilobus/sacculifer* and *O. universa*, significant presence of *G. bulloides, G. glutinata* and *T. quinqueloba*.

APFE-3 (=middle PF2 of Principato *et al.* 2003). Top: disappearance of *G. inflata.* Interval: reappearance and maximum abundance of *G. inflata*, decrease of *G. ruber rosea*, presence of *G. trilobus/sacculifer* and N. *pachyderma*, high *G. ruber alba.*

APFE-4 (=middle PF2 of Principato *et al.* 2003). Top: High abundance of *G. ruber rosea* and *O. universa*, temporary disappearance of *G. trilobus/sacculifer*. Interval: decrease of *G. ruber alba*, positive trend of *G. ruber rosea*, presence of *G. trilobus/sacculifer* and *G. inflata*.

APFE-5 (=lower PF2 of Principato *et al.* 2003). Top: high abundance of *G. ruber alba*, positive trend of *G. ruber rosea.* Interval: decreasing trend of *G. ruber rosea*, *G. ruber alba* and *O. universa*, appearance of *N. pachyderma* (s) and *G. inflata*.

APFE-6 (=PF3 of Principato *et al.* 2003). Top: positive trend of *G. ruber alba* decrease of G. *ruber rosea*. Interval: significant increase of *G. ruber rosea* and high abundance of warm water species such as *O. universa*, *G. rubescens* and *G. siphonifera*, high abundance of *G. ruber alba* followed by a temporary negative trend, increase of *G. bulloides*.

APFE-7 (=upper PF4 of Principato *et al.* 2003). Top: decrease *G. ruber alba*, high abundance of *G. ruber rosea*, peak in abundance of *O. universa*, disappearance of *G. trilobus/sacculifer*. Interval: high abundance of *G. ruber alba* and *O. universa*, gradual increase of *G. ruber rosea* high abundance of *G. trilobus/sacculifer*.

APFE-8 (= lower PF4 of Principato *et al.* 2003). Top: high abundance of *G. ruber alba,* appearance of *G. ruber rosea,* temporary disappearance of *G. trilobus/sacculifer*, positive trend of *O. universa*. Interval: increasing trend of *G. ruber alba*, appearance of *G. trilobus/sacculifer*, presence of *G. inflata* and *N. pachyderma* (s).

APFE-9 (=PF5 of Principato *et al.* 2003). Top: positive trend of *G. ruber alba*. Interval: presence of *G. ruber rosea*, *G. truncatulinoides* and *G. inflata* decrease of *N. pachyderma* (d) and high abundance of *N. pachyderma* (s).

APFE-10 (=PF6 of Principato *et al.* 2003). Top: appearance of *G. inflata* and G. *truncatulinoides,* disappearance of *N. dutertrei* (d). Interval: decreasing trend in abundance of *G. ruber alba* following by an increase at the upper part, fluctuations of *G. scitula*, high abundance of *T. quinqueloba* and *G. glutinata*. The species *N. pachyderma* (d) and *N. dutertrei* (d) show significant abundance values.

4.3. Pollen assemblage zones

Pollen assemblages of NS-14 are organized in the following eight Pollen Assemblage Zones (PAZ 1-8), (Fig. 4).

PAZ-1: High abundance of Poaceae, Chenopodiaceae, *Artemisia, Olea, Pistacia* and *Sanguisorba.* Low values of *Quercus* and *Cedrus.*

PAZ-2: Increase of deciduous *Quercus, Abies, Picea, Pinus* and high pollen concentration. Drop in the values of Chenopodiaceae and *Artemisia.* Aquatic palynomorph concentration reaches its maximum values.

PAZ-3: Increase in steppic elements like Chenopodiaceae and Poaceae and conifers like *Cedrus.* Decrease in *Pistacia*, deciduous *Quercus* and *Picea* in an interval characterised by lower pollen concentration.

PAZ-4: Increase of deciduous *Quercus* and *Pinus.* Sharp decrease in Chenopodiaceae, Poaceae and absence of *Artemisia.* High pollen concentration.

PAZ-5: Increase of Chenopodiaceae, *Artemisia, Ephedra* and *Olea.* Decrease in deciduous *Quercus*, *Pistacia* and *Pinus.* Disappearance of *Abies* and *Picea* pollen.

PAZ-6: Increase of *Quercus* (both deciduous and evergreen), *Pistacia* and *Sanquisorba*, presence of *Abies,* decrease in Chenopodiaceae and high pollen concentration.

PAZ-7: Maximum expansion of Chenopodiaceae, increase in *Artemisia*, *Centaurea* and Poaceae, decrease in most arboreal pollen (*Quercus* deciduous and evergreen, *Abies, Olea*) and absence of *Pistacia.* Low pollen concentration.

PAZ-8: Further increase in abundances of *Artemisia* and Compositae and minor increase of deciduous *Quercus* and Conifers.

5. Paleoecological-paleoclimatic implications

The plankton and pollen abundance patterns and the climatic curve inferred from the planktonic foraminifera assemblages (Fig. 5) enhance the reconstruction of paleoecological-paleoclimatic conditions over the last 14 000 yrs in the SE Aegean Sea.

Warm period. Evidence of climatic fluctuations and seasonality (~14 000-13 100 yr $_{cal}$ BP)

Plankton ecozones ACE-11 and APFE-10 reflect generally warm conditions; the base of the ecozones cannot be defined due to the massive flow event recorded at core NS-14. ACE-11 is characterized by increased abundances of the upper-middle photic zone warm-water species *U. tenuis* (Winter *et al.* 1994) confirming the subtropical features of this interval. However several climatic fluctuations are recorded indicated by the paleoclimatic curve (Fig. 5). Cool and high fertility conditions are recorded by the abundance of *T. quinqueloba, G. glutinata* and *G. scitula* (Thunell 1978, Geraga *et al.* 2005) which dominate the assemblage as well as by neogloboquadriinids which confirm the presence of Deep Chlorophyll Maximum (DCM) and highly productive surface conditions probably due to increased terrestrial input. The warmer periods are reflected mainly by *G. ruber alba* and secondly by *G. rubescens* and *G. conglobatus.*

Temperature decrease. Deep winter mixing related to cooling (13 100-9900 yr $_{cal}$ BP)

The abundance peak of *Calciosolenia* spp. in ACE-10 indicates a shift to wetter period (Amore *et al.* 2004). The presence of *G. inflata* and *G. truncatulinoides* in APFE-9 reveal a well developed deep and cold mixed layer- deep winter mixing related to cooling (Pujol and Vergnaud Grazzini 1995). Peaks in abundance of *N. pachyderma* and *N. dutertrei* sinistral forms show high productivity and cool conditions (Thunell and Sautter 1992). Pollen assemblages are dominated by Gramineae, Compositae and *Artemisia* suggesting dry climatic conditions in PAZ-8 zone. How-

ever the co-existence of deciduous *Quercus, Abies* and *Cedrus* indicate sufficient precipitation for the development of forest vegetation in favourable areas, while the sporadic presence of *Olea*, *Pistacia* and *Sanguisorba* after 10900yr$_{cal}$ BP is indicative of frost-free winters.

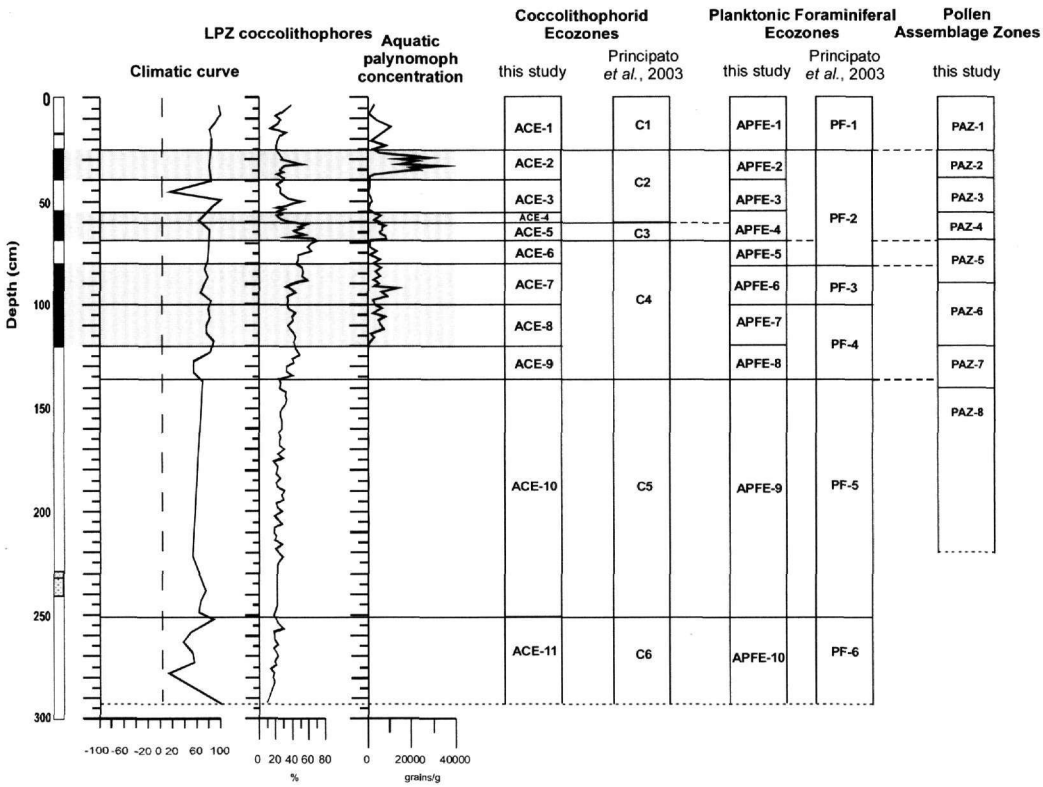

Figure 5 - Paleoclimatic curve inferred from planktonic foraminifera, LPZ coccolithophores relative abundance and aquatic palynomorph concentration and correlation scheme between the assemblage zones defined in SE Aegean Sea (core NS-14) and the correspondent intervals identified by Principato *et al.* (2003).

High primary productivity, increased run off, onset of stratification (9900-9300 yr $_{cal}$ BP)

The gradual increase of *F. profunda* in ACE-9 coccolithophore ecozone supports the establishment of stratified conditions and the onset of nutrient-rich environment in the deep photic zone. Fresh water input and increase in productivity at depth is enhanced by the increase of *Helicosphaera* spp. and *Syracosphaera* spp. (Colmenero-Hidalgo *et al.* 2004, Amore *et al.* 2004). APFE-8 is marked by the appearance of *G. trilobus / sacculifer*, which indicates the occurrence of a shallow pycnocline (Fenton *et al.* 2000), possibly related to strong runoff periods (Rossignol-Strick 1985) and by the abundance of *N. pachyderma* sinistral forms indicating the development of DCM in the lower photic zone. *G. bulloides* is also indicative of high primary conditions and *G. ruber alba,* a warm oligotrophic surface dweller, shows a strong increasing trend indicative of the onset of stratification in the water column at the top of APFE-8. Lowering of SST as indicated by the paleoclimatic curve (Fig. 5) is due to the abundance of cool water indicators (*T. quinqueloba, G. inflata, G. glutinata)* just before the deposition of S1. The expansion of Chenopodiaceae in PAZ-7 zone may reflect the existence of a surrounding arid coastal zone (Geraga *et al.* 2000) and/or prevailing strong SE winds carrying them from the salt marshy areas of N. Africa (Rossignol-Strick 1999).

Increased fresh water input, warm and stratified water column (9300-9000 yr $_{cal}$ BP)

The very high values of *Helicosphaera* spp. followed by the abundance of tropical-subtropical *F. profunda* at the lower part of S1(a) confirm the development of a nutrient-rich environment in the middle-photic zone and further evidence to the lowering of salinity during ACE-8 ecozone. The increase of the paleoclimatic curve towards positive values is the main feature of APFE-7 ecozone due to the high abundance of warm water species (*G. ruber alba* and *O. universa*) as well as *G. ruber rosea* indicative of warmer conditions (Hemleben *et al.* 1989), which suggest enhanced stratification of the water column. Shallow pycnocline and strong run off is evident by the high abundance of G. *trilobus/sacculifer* as well as by the high aquatic palynomorph concentration. Moreover pollen assemblages that reflect the terrestrial response in PAZ-6 indicate the onset of forestation and the development of Mediterranean vegetation belts as a result of the warm and humid conditions.

Warm and stratified water column. Short cooler intervals (9000-8600 yr $_{cal}$ BP)

Warm conditions with negative shifts are suggested by the paleoclimatic curve and the faunal assemblages that prevail in APFE-6 ecozone during the upper part of S1(a). Strong warming of surface waters and stratification of the water column are related to the high values of *G. ruber rosea, G. rubescens* and *G. siphonifera*. Indications of cooler conditions are supported in ACE-7 by the gradual increase of *Umbilicosphaera* spp., a group that has a tendency towards eutrophic adaptation (Young, 1994) and is consistent with the nutrient redistribution in the surface waters (Principato *et al.* 2006).

Slight breaking of stratification, less saline surface waters, on-going productivity in the deep photic zone (8600-7600 yr $_{cal}$ BP)

The prevailing productivity during S1 interruption in the deep photic zone (high *F. profunda*; decreased only at the lower part of the interruption in the ACE-6 ecozone) is co-occurring with relatively less saline surface layer (moderate abundance of *Helicosphaera* spp., sporadic presence of *B. bigelowii* a species suggesting low salinity in surface waters (Negri and Giunta 2001, Giunta *et al.* 2003). A slight breaking of stratification can be attributed to the decrease of *G. ruber rosea*, dramatical reduction of *G. rubescens* and *O. universa* and the presence of *G. glutinata* and *N. pachyderma* dextral specimens in APFE-5 ecozone. The small expansion of steppe vegetation and the cocurrent drop of runoff proxies recorded in PAZ-5 zone indicate a drier period while the presence of *Ephedra* may reflect a drop in temperature (Mudie *et al.* 2002).

Humid conditions. Warm and stratified water column (7600-6900 yr $_{cal}$ BP)

B. bigelowii shows small but clear peak and together with relatively high abundances of *Helicosphaera* spp. and *F. profunda* suggest the constant presence of less saline surface waters and stratified conditions in ACE-5 coccolithophore ecozone during the lower part of S1(b). The expansion of mixed deciduous forests and the increase of aquatic palynomorph concentrations indicate a humid period in PAZ-4 zone. The increase in abundance of *G. ruber rosea*, *O. universa* and *G. rubescens* is indicative for the stratification of the water column in APFE-4 ecozone.

Wet and less warm period. Decline of DCM (6900-6400 yr $_{cal}$ BP)

F. profunda displays a distinct reduction in coccolithophore ecozone ACE-4 during the upper part of S1(b). Additionally an abrupt increase of hyposaline and relatively eutrophic species *B. bigelowii*, less saline *G. oceanica* (Di Stefano and Incarbona 2004) and high nutrient flourishing *E. huxleyi* (Young 1994) is recorded followed by the increase of eutrophic coccolithophore *Umbilicosphaera* spp. Our multiproxy data from NS-14 reveal a series of coolings that resulted to strong fresh water input and the breakage of stratification between 6900 and 6400 yr $_{cal}$ BP implying the decline of DCM at ~ 6500 yr $_{cal}$ BP, that predates the end of the S1 depositional conditions.

Decline of DCM, drop in precipitation (6400-5200 yr $_{cal}$ BP)

The warm and stratified waters continue to occur still for a short period in APFE-3 but they are immediately followed by remarkable vertical mixing as indicated by the peak in abundance of *G. inflata*. The lowering of SST as indicated by the paleoclimatic curve at this level is marked by the presence of cool water indicators (*T. quinqueloba* and *G. glutinata*). Expansion of coniferous forest in lower elevations reflects a temperature fall (Giunta *et al.* 2003) while expansion of steppic elements suggests a drop in precipitation in PAZ-3 zone.

Very humid and warm conditions (5200-4200 yr $_{cal}$ BP)

A warming phase is testified during APFE-2 ecozone by the significant increase of *G. ruber rosea* and *O. universa* and the temporary dissapearence of *G. inflata* (normal marine conditions), whereas strong runoff is evident through high abundance of G. *trilobus/sacculifer*. Moreover the intense fresh water input is documented by the sharp increase of *Helicosphaera* spp. followed by high abundance of *Calciosolenia* spp. and minor peaks of *B. bigelowii* in ACE-2 ecozone. The expansion of mixed deciduous forest together with the maxima of the runoff proxies indicates high precipitation in PAZ-2 zone. The presence of *Picea* in the area is indicative of strong north winds (Mudie *et al.* 2002).

Temperature decrease (4200-2500 yr $_{cal}$ BP)

A cool interval is recognised within coccolithophore ACE-1 due to the increase of *E. huxleyi* and the cool EHCM morphotypes (Crudeli *et al.* 2006). High primary productivity in a cold mixed layer is recorded by the occurrence of *G. bulloides*, *G. inflata* and *G. truncatulinoides,* whereas the presence of *G. glutinata* evidences cooling events in APFE-1 ecozone. PAZ-1 reflects a period with open vegetation cover and indications of human disturbed vegetation.

6. Acknowledgements

This work has been made possible thanks to financial support provided by Pythagoras I project (EU and Greek Ministry of Education, EPEAEK II) and the partial support from the European Science Foundation (ESF) under the EUROCORES Programme EuroCLIMATE, through contract No. ERAS-CT-2003-980409 of the European Commission, DG Research, FP6. The critical comments of Elisa Malinverno and an anonymous reviewer improved significantly the manuscript.

7. References

Anastasakis, G., and Stanley, D.J., 1986. Uppermost sapropel, Eastern Mediterranean: paleoceanography and stagnation, *Nat. Geogr. Res.,* 2, 179-197.

Amore, F. O., Gaffau, M., Massa, B., and Morabito, S. 2004. Late Pleistocene-Holocene paleoclimate and related paleoenvironmental changes as recorded by calcareous nannofossils and planktonic foraminifera assemblages in the southern Tyrrhenian Sea (Cape Palinuro, Italy), *Marine Micropaleontology*, 52, 255-276.

Capotondi, L., Borsetti, A., and Morigi, C., 1999. Foraminiferal ecozones, a high resolution proxy for the late Quaternary biochronology in the central Mediterranean Sea, *Mar. Geology*, 153, 253–274.

Colmenero-Hidalgo, E., Flores, J. A., Sierro, F. J., Bárcena, M. Á., Löwemark, L., Schönfeld, J., and Grimalt, J. O., 2004. Ocean surface water response to short-term climate changes reealed by coccolithophores from the Gulf of Cadiz (NE Atlantic) and Alboran Sea (W Mediterranean), *Pal. Pal. Pal.*, 205, 317-336.

Crudeli, D., Young, J. R., Erba, E., de Lange, G. J., Henriksen, K., Kinkel, H., Slomp, C. P., and Ziveri, P., 2004. Abnormal carbonate diagenesis in Holocene–late Pleistocene sapropel-associated sediments from the Eastern Mediterranean; evidence from *Emiliania huxleyi* coccolith morphology, *Marine Micropaleontology*, 52, 217-240.

Crudeli, D., Young, J.R., Erba, E., Geisen, M., Ziveri, P., De Lange, G. J., and Slomp, C.P., 2006. Fossil record of holococcoliths and selected hetero-holococcolith associations from the Mediterranean (Holocene–late Pleistocene): Evaluation of carbonate diagenesis and palaeoecological–palaeocenographic implications, *Pal. Pal. Pal.*, 237 (2-4), 191-212.

De Rijk, S., Hayes, A., and Rohling, E.J., 1999. Eastern Mediterranean sapropel S1 interruption: an expression of the onset of climatic deterioration around 7 ka BP, *Mar. Geology*, 153, 337-343.

Di Stefano, E., and Incarbona, A., 2004. High resolution paleoenvironmental reconstruction of ODP Hole 963D (Sicily Channel) during the last deglaciation based on calcareous nannofossils, *Marine Micropaleontology*, 52, 241-254.

Fenton, M., Geiselhart, S., Rohling, E.J., and Hemleben, C., 2000. Planktonic zones in the Red Sea, *Marine Micropaleontology,* 40, 277-294.

Geraga, M., Tsaila-Monopolis, S., Ioakeim, C., Papatheodorou, G., and Ferentinos, G., 2000. Evaluation of palaeoenvironmental changes during the last 18,000 years in the Myrtoon basin, SW Aegean Sea, *Pal. Pal. Pal.*, 156, 1-17.

Geraga, M., Tsaila-Monopolis, St., Ioakim, Ch., Papatheodorou, G., and Ferentinos, G., 2005. Short-term climate changes in the southern Aegean Sea over the last 48.000 years, *Palaeogeography, Palaeoclimatology, Palaeoecology*, 220, 311-332.

Giunta, S., Negri, A., Morigi, C., Capotondi, L., Combourieu-Nebout, N., Emeis, K.C., Sangiorgi, F., and Vigliotti, L., 2003. Coccolithiphorid ecostratigraphy and multi-proxy paleoceanographic reconstruction in the Southern Adriatic Sea during the last deglacial time (Core AD91-17), *Palaeogeography Palaeoclimatology Palaeoecology*, 190, 39-59.

Hemleben, C., Spindler, M., and Anderson, O.R., 1989. Modern Planktonic Foraminifera, *Springer-Verlang*, New York.

Jorissen, F.J., Asioli, A., Borsetti, A.M., Capotondi, L., de Visser, J.P., Hilgen, F.J., Rohling, E., J., van der Borg, K., Vergnaud-Grazini, C., and Zachariasse, W.J., 1993. Late Quaternary central Mediterranean biochronology, *Marine Micropaleontology.* 21, 169-189.

Lykousis, V., Chronis, G., Tselepides, A., Price, N.B., Theocharis, A., Siokou-Fragou, I., Wambeke, F.Van, Danovaro, R., Stavrakakis, S., Duineveld, G., Georgopoulos, D., Ignatiades L., Souvermezoglou, A., and Voutsinou-Taliadouri, F., 2002. Major outputs of the recent multidisciplinary biogeochemical researches undertaken in the Aegean Sea, *Journal of Marine Systems*, 33-34: 313-334

Mudie, P.J., Rochon, A., and Aksu, A.E., 2002. Pollen stratigraphy of Late Quaternary cores from Marmara Sea: land-sea correlation and paleoclimatic history, *Mar. Geology*, 190, 233-260.

Muller, J., 1959. Palynology of Recent Orinoco and delta and self sediments. *Micropal.,* 5, 1-32.

Negri, A., and Giunta, S., 2001. Calcareous nannofossil paleoecology in the sapropel S1 of the eastern Ionian sea: paleoceanographic implications, *Pal. Pal. Pal.*, 169, 101-112.

Papanikolaou, D.J., and Nomikou, P., 2001. Tectonic structure and volcanic centres at the eastern edge of the Aegean volcanic arc around Nisyros Island, *Bull. Geol. Soc. Greece,*XXXIV/1, 289-296.

Perissoratis, C., and Piper, D.J.W., 1992. Age, regional variation and shallowest occurrence of S1 sapropel in the northern Aegean Sea, *Geo-Marine Letters.* 12, 49-53.

Principato, M., Giunta, S., Corselli, C., and Negri, A., 2003. Late Pleistocene-Holocene planktonik assemblages in three box-cores from the Mediterranean Ridge area (west-southwest of Crete): paleoecological and palaeoceanographic reconstruction of sapropel S1 interval, *Pal. Pal. Pal.*, 190, 61-77.

Principato, M., Crudeli, D., Ziveri, P., Slomp, C.P., Corselli, C., Erba, E., and de Lange, G.J., 2006. Phyto- and zooplankton paleofluxes during the deposition of sapropel S1 (eastern Mediterranean): Biogenic carbonate preservation and paleoecological implications, *Pal. Pal. Pal.*, 235, 8-27.

Pujol C., and Vergnaud Grazzini, C., 1995. Distribution patterns of live planktic foraminifers as relate to regional hydrography and productive systems of the Mediterranean Sea, *Marine Micropaleontology*, 25, 187–217.

Rohling, E.J., and Hilgen, F.J., 1991. The Eastern Mediterranean climate at times of sapropel formation: a review, *Geol. Mijnb.*, 70-253-264.

Rohling, E.J., Jorissen, F.J., Vergnaud Grazzini, C., and Zachariasse, W.J., 1993. Northern Levantine and Adriatic quaternary planktic foraminifera; reconstruction of paleoenvironmental gradients, *Marine Micropaleontology*, 21, 191–218.

Rohling, E.J., Jorissen, F.J., and de Stigter, H.C., 1997. 200 Year interruption of Holocene sapropel formation in the Adriatic sea, *Journal of Micropaleontology*, 16, 97-108.

Rossignol-Strick, M., 1985. Mediterranean Quaternary sapropels, an immediate response of the African monsoon to variation of insolation, *Pal. Pal. Pal.*, 49. 237-263.

Rossignol-Strick, M., 1999. The Holocene climatic optimum and pollen records of sapropel 1 in the eastern Mediterranean, 9000-6000 BP, *Quaternary Science Reviews*, 18, 515-530.

Sbaffi, L., Wesel, F. C., Kallel, N., Paterne, M., Cacho, I., Ziveri, P., and Shakleton, N., 2001. Response of the pelagic environment to paleoclimatic changes in the central Mediterranean Sea during the Late Quaternary, *Marine Geology*, 178, 39-62.

Sprengel, C., Baumann, K.-H., and Neuer, S., 2000. Seasonal and interannual variations in coccolithophore fluxes and species composition in sediment traps north of Gran Canaria, *Marine Micropaleontology*, 49, 3577-3598.

Targarona, J., 1997. Climatic and oceanographic evolution of the Mediterranean region over the last glacial-interglacial transition, LPP Contribution series, No 7, Utrecht, 155 pp.

Thunell, R.C., 1978. Distribution of recent of planktonic foraminifera in surface sediments of the Mediterranean Sea, *Marine Micropaleontology*, 3, 147-173.

Thunell, R., and Sautter, L. R., 1992. Planktonic foraminiferal faunal and stable isotope indices of upwelling: a sediment trap study in the San Pedro Basin, South California Bight. In C.P. Summerhayes, W.L. Prell and K.C. Emeis, (eds), *Upwelling System: Evolution Since the Miocene, Evolution since the Early Miocene.* Geological Society Sp. Publ. 64, 77–91.

Triantaphyllou, M. V., Gogou, A., Lykousis, V., Bouloubassi, I., Ziveri, P., Rosell-Mele, A., Kouli, K., Dimiza, M., Papanikolaou, M., Gaitani, P., Katsouras, G., and Dermitzakis, M.D., 2006. Primary production trends and response of terrestrial environments in SE Aegean core NS-14. A multiproxy approach, *European Geosciences Union, Vienna, 2-7 April 2006,* Geophysical Research Abstracts, vol. 8, 08347.

Triantaphyllou, M.V., Gogou, A., Lykousis, V., Bouloubassi, I., Ziveri, P., Emeis, K-C., Rosell-Mele, A., Kouli, M., Dimiza, M., Katsouras, G., Nunez, N., Papanikolaou, M., and Dermit-

zakis, M.D. (subm.) Holocene primary production archive and landborne imprints: micropaleontological and biochemical evidence for sapropel formation in the semi-closed Western Kos Basin (SE Aegean Sea), *Paleogeography, Palaeoclimatology, Palaeoecology.*

Van Santvoort, P.J.M., and de Lange, G.J., 1997. Geochemical and paleomagnetic evidence for the occurrence of "missing"sapropels in eastern Mediterranean sediements, *Paleoceanography,* 12, 773-786.

Winter, A., Jordan, R. W., and Roth P., 1994. Biogeography of living Coccolithophores in oceanic waters. In A. Winter and W. G. Siesser (eds), *Coccolithophores*,13-27pp, Cambridge University Press.

Young, J. R., 1994. Functions of coccoliths. In A. Winter and W. G. Siesser (eds), *Coccolithophores*, 63-82pp, Cambridge University Press.

Δελτίο της Ελληνικής Γεωλογικής Εταιρίας τομ. XXXX, 2007
Πρακτικά 11ου Διεθνούς Συνεδρίου, Αθήνα, Μάιος 2007

Bulletin of the Geological Society of Greece vol. XXXX, 2007
Proceedings of the 11th International Congress, Athens, May, 2007

TORTONIAN *CLYPEASTER* FAUNA (ECHINOIDEA: CLYPEASTEROIDA) FROM GAVDOS ISLAND (GREECE)

Tsaparas N.[1], Drinia H.[1], Antonarakou A.[1], Marcopoulou-Diakantoni A.[1], and Dermitzakis M. D.[1]

[1] *National and Kapodistrian University of Athens, Faculty of Geology and Geoenvironment, Department of Hist. Geology - Paleontology, ntsapar@geol.uoa.gr, cntrinia@geol.uoa.gr, aantonar@geol.uoa.gr, mderm@geol.uoa.gr*

Abstract

The Tortonian sediments of Gavdos Island (Greece) contain a rich and diverse echinoid fauna. Clypeasteroid (sand dollars) echinoids are an important component of this fauna and sixteen taxa are recognized. Of these, eleven species are new records for Gavdos Island. The present paper is an annotated species list along with notes on certain aspects of the ecology of the determined echinoderms.
Key words: *Tortonian, Clypeaster, Gavdos, taxonomy.*

Περίληψη

Τα ιζήματα ηλικίας Τορτονίου, της νήσου Γαύδου (Ελλάδα) περιέχουν μια πλούσια και ποικιλόμορφη πανίδα εχίνων με κύριο αντιπρόσωπο το γένος Clypeaster. Από το σύνολο των δεκαέξι ειδών που έχουν αναγνωρισθεί, τα έντεκα αποτελούν καινούριες ανφορές για τη νήσο Γαύδο. Η παρούσα εργασία αποτελεί αναφορά στη συστηματική ταξινόμηση και στην οικολογία των έντεκα αυτών ειδών.
Λέξεις Κλειδιά: *Τορτόνιο, Clypeaster, Γαύδος, Συστηματική ταξινόμηση.*

1. Introduction

Clypeasteroids can be very common in Recent, shallow water environments in a variety of biogeographic settings and represent important members of benthic invertebrate communities. Mass deposits of fossil clypeasteroids are also common and characteristic of many Cenozoic shallow water deposits. Their distribution and formation, however, has received much less attention than molluscan counterparts, although fossil examples are found within all three of the clypeasteroid suborders.

The Neogene deposits of Gavdos Island cover almost half of the island area and have been divided by Anastasakis *et al.* (1995), into two formations: Potamos and Metochia. A good reconnaissance map and description of the formations is given by Anastasakis *et al.* (1995), Drinia *et al.* (2004) and Tsaparas (2005) and need not be repeated here. Antonarakou (2001) and Antonarakou *et al.* (in press) consider that these formations are late Middle and Late Miocene in age respectively, basing their conclusions on the faunas of planktonic foraminifera.

A number of systematic works have been published on the corals, foraminifera and molluscs of the Gavdos Miocene, but until now there has been no work devoted particularly to the echinoids of the island. The most important work is that by Marcopoulou-Diakantoni (1970) who characterized the

skeletal elements of about five genera of echinoids. It is therefore significant to report a second Miocene echinoid fauna from Gavdos Island. This differs from that of Marcopoulou-Diakantoni (1970) in including eleven more taxa. These fossils are preserved in a conspicuous thick marker bed of Middle Toronian age which is characterized by the predominance of the large benthic foraminifer *Heterostegina.*

The present paper is an annotated species list along with notes on certain aspects of the ecology of echinoderms. It supplements the information on echinoderms provided by Marcopoulou-Diakantoni (1970).

2. Material and Methods

The specimens documented herein were collected from throughout a fossiliferous βεδ which provides an excellent marker bed that can be traced almost throughout the basin. Its lithology consists of medium-sized partially cemented sandstone with mottled structure and no visible stratification. In an outcrop scale, endobenthic and epibenthic bivalves, bryozoans, irregular echinoids (including large *Clypeaster*) and large benthic foraminifers (*Heterostegina*) predominate, with minor proportions of gastropods. Because of its typifying large foraminifer fauna and lateral continuity, this bed represents an excellent stratigraphic marker bed. The skeletal content implies a fully marine shelf setting. Skeletal biota are well preserved which points to a rather quiet depositional setting below wave abrasion depth (WAD), (Brachert *et al.* 2003). Large benthic foraminifers have a broad depth range, and their presence fits a depositional environment in the lower segment of the photic zone (e.g. James *et al.* 2001). Their presence implies warm-temperate surface temperatures (Betzler *et al.* 1997).

An adequate number of individuals, from the genus *Clypeaster*, was collected from the above mentioned sandstone marker bed. Most of the specimens' test is covered by attached colonies of membraniporiform type Bryozoans. Taxa were defined almost entirely on the basis of skeletal characteristics, meaning that the same criteria can be used for fossil as for recent echinoderms. Quantitative characters, notably the size of echinoderms were used in order to distinguish between species belonging to the same genus. All given dimensions of specimens are in millimetres. The following abbreviations have been used: Lo= Length, la=width, h=height. Scanning electron microscopy was considered a crucial technique in echinoid taxonomy as small-scale characters are being increasingly applied to differentiate otherwise similar species.

Field observations and material analyses are completed by a more general bibliographic review of the distribution of Late Neogene Mediterranean echinoids. The bibliographic data used are those given by Philippe (1998) for Tortonian echinoids from southeast France; by Montenat and Roman (1970), Roman and Soudet (1990), Néraudeau *et al.* (1999), Lacour and Néraudeau (2000), Saint-Martin *et al.* (2000) for Tortonian to Pliocene echinoids from Spain; by Borghi (1995a, b) and Néraudeau *et al.* (1998) for Pliocene and Pleistocene echinoids from Italy; by Boggild and Rose (1985) for Neogene echinoids from the Maltese islands; by Marcopoulou-Diakantoni (1967, 1972, 1974, 1977); and Heimann and Marcopoulou-Diacantoni (1977) for Late Miocene and Plio–Pleistocene echinoids from Eastern Mediterranean; and by Ragaini (1996) for Pliocene echinoids from Switzerland. Although selective rather than comprehensive in regional coverage, we believe that these most recent accounts of local faunas are taxonomically and stratigraphically more appropriate for our purpose than the sometimes extensive but imprecise older literature.

Because of the important variations in the species concept of the genus *Clypeaster*, we have grouped as much as possible the various species under some great names, such as *C. scillae, C. altus, C .campanulatus* and *C. ventiensis* according to the classification scheme of Marcopoulou-Diakantoni (1985).

3. Results

Even though the preservation state of certain of the studied specimens was not good enough, the following species were determined: *Clypeaster altus, C. calabrus, C. campanulatus, C. crassus, C.* cf. *di-Stefanoi, C. intermedius, C. intermedius* (form *crassicostatus*), *C. lamberti, C. portentosus, C. tauricus, Clypeaster* cf. *ventiensis*. From these species, the following are characteristic for the Miocene of the Mediterranean basin: *C. altus, C. calabrus, C. campanulatus, C.* cf. *ventiensis, C. lamberti.*

3.1. Systematic Paleontology

Phylum: Echinodermata Klein 1734
Subphylum: Echinozoa Haeckel in Zittel 1895
Class: Echinoidea Leske 1778
Subclass: Euechinoidea Bronn 1860
Superorder: Gnathostomata Zittel 1879
Order: Clypeasteroida Agassiz 1872
Suborder: Clypeasterina Agassiz 1872
Family: Clypeasteridae Agassiz 1835
Genus: *Clypeaster* Lamarck 1801

***Clypeaster altus* (Klein, 1734)**

1734. *Scutum angulare altus* Klein, p. 29.
1778. *Echinanthus altus* Leske, p. 189, pl. LIII, fig. 4.
1816. *Clypeaster altus* Lamarck, p. 14, tav. III.
1958. *Clypeaster altus* (Klein).- Imbesi, vol. LIII (n. ser. vol. XXIII), p. 28, tav. X, fig. 1, 1a, 2, 2a, 2b.
1967. *Clypeaster altus* (Klein).- Marcopoulou-Diacantoni, p. 359, Pl. III, fig. 1, 1a, Pl. IV, fig. 2.
1969. *Clypeaster altus* (Klein).-Mitrovic-Petrovic, p. 126, tav. V, fig. 2, 2a.
1985. *Clypeaster altus* (Klein).- Marcopoulou-Diacantoni, p. 103, 105, 108, 159, Pl. I-III.
1998. *Clypeaster altus* (Klein).- Philippe, p. 122
2000. *Clypeaster altus* (Klein).- Marcopoulou-Diacantoni, p. 177.

Specimens: 1 individual ; *Dimensions:* 2004 / P8 :Lo: 135, la: 115, h: 61,,l/L: 0,85, h/L: 0,45

Remarks: Oral face with large infudibulum belonging to the group of *Clypeaster altus.* Ambulacral petals form petaloid open with elevated intermediate region. Ambitus rounded.

Stratigraphical and Geographical distribution. Burdigalian (Algeria, Malta, Italy); Middle Miocene (Algeria, Malta, Sicily, Sardinia, Turkey, France, Greece); Tortonian (Hungary, Greece); Middle Tortonian (Gavdos).

***Clypeaster calabrus* (Seguenza, 1880)**

1880. *Clypeaster intermedius* var. *calabra* Seguenza, Tav. V, fig. 3, 3a, 3b.
1925. *Clypeaster novaresei* Checchia – Rispoli, Tav. IX, fig. 1,1a,1b,1c,2b, Tav. X, Tav. XIII, fig. 1, 1a, 1b, 2.
1925. *Clypeaster calabrus* Seguenza.- Checchia – Rispoli, vol. IX, parte III, p. 18, tav. VII, fig. 2.
1958. *Clypeaster calabrus* Seguenza.- Imbesi, vol. LIII (n. ser. vol. XXIII), p. 17, tav. II, fig. 1,1a, 1b, 2, 2a, tav. III, fig. 1.
1967. *Clypeaster calabrus* Seguenza.- Marcopoulou-Diacantoni, p. 365, Pl. XVI, fig. 1, Pl. XVIII.
1985. *Clypeaster calabrus* Seguenza.- Marcopoulou-Diacantoni, p. 128, 134, 162.

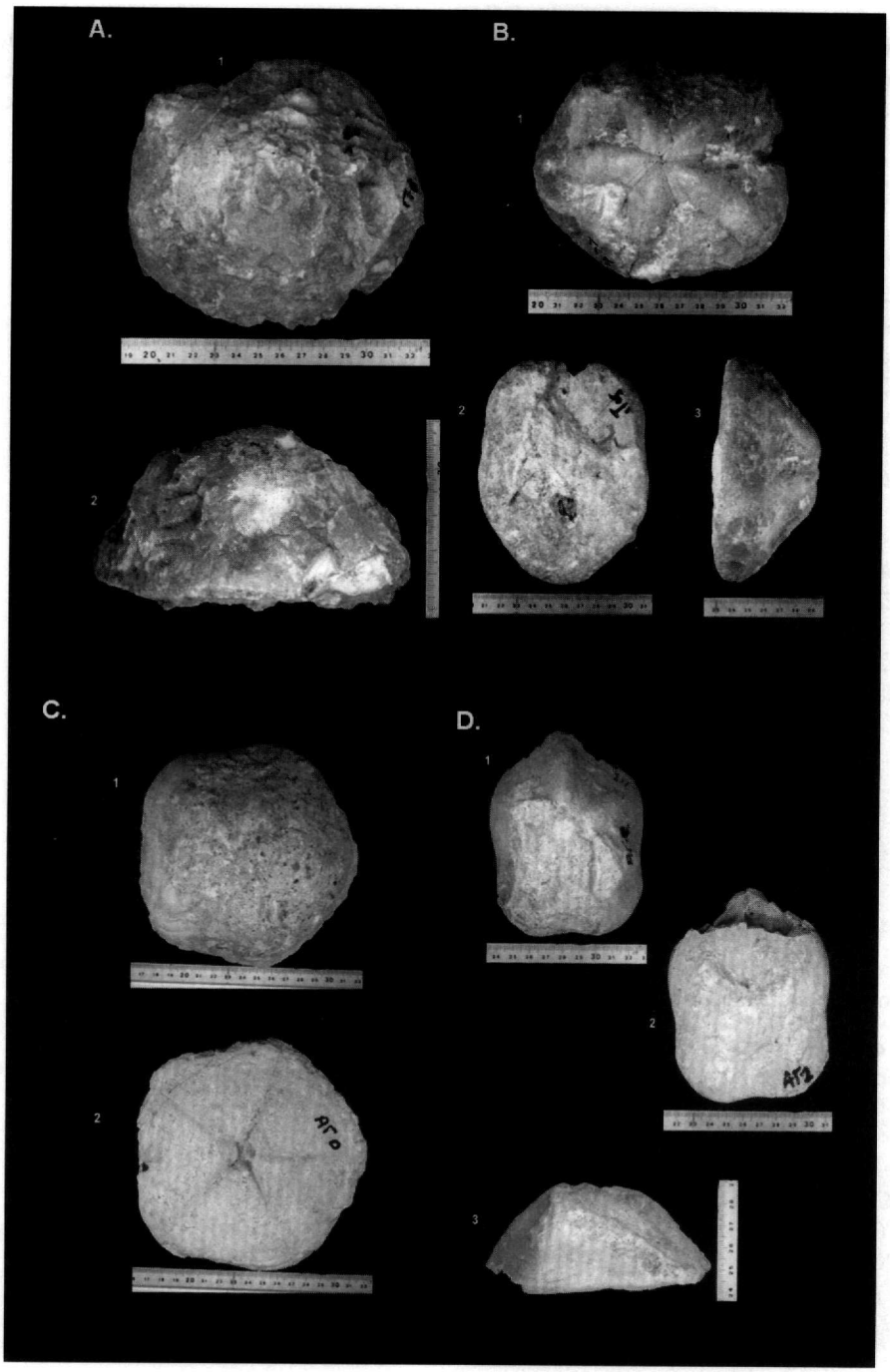

Plate 1 - A. *C. altus*, B. *C. calabrus*, C. *C. campanulatus*, D. *C. crassus*

Specimens: 3; *Dimensions:* 2004 / P5 : Lo:124, la:107, h:56, l / L :0,86, h / L :0,45
2004/G5 : Lo:143, la:122, h:65, l / L :0,85, h / L :0,45
2004/AG3 : Lo:111, la:96, h:44, l / L :0,86, h / L :0,39

Stratigraphical and Geographical distribution: Aquitanian (Italy); Middle Miocene (Italy, Sicily); Middle-Late Miocene (Greece); Middle Tortonian (Gavdos).

Clypeaster campanulatus Schlotheim, 1820

1906. *Clypeaster campanulatus* Schlotheim.- Lambert, p. 14.
1913. *Clypeaster campanulatus* Schlotheim.- Lambert, vol. XXXIX, 3e partie, p. 117.
1967. *Clypeaster campanulatus* Schlotheim.- Marcopoulou-Diacantoni, p. 367, Pl. XII.
1985. *Clypeaster campanulatus* Schlotheim.- Marcopoulou-Diacantoni, p. 104, 116, 118, 119, 162.
1998. *Clypeaster campanulatus* Schlotheim.- Philippe, p. 123.
2000. *Clypeaster campanulatus* Schlotheim.- Marcopoulou-Diacantoni, p. 177, Pl. I, fig. 3a,b, Pl. II, fig. 2a,b, Pl. III, fig. 2a,b.

*Specimens:*3 ; *Dimensions*: 2004/AG0 : Lo:152, la:140, h:47, 1 / L:0,92, h / L:0,30
2004/P9 : Lo:153, la:135, h:60, l / L:0,88, h / L:0,39
2004 / P11 : Lo:156, la:142, h:62, l / L:0,91, h / L:0,39
Remarks: Test pyramidal with large infudibulum and oral face flat belonging to the group of *Clypeaster campanulatus* (Marcopoulou-Diakantoni, 1985). Ambulacral petals form petaloid open with elevated intermediate region. Ambitus rounded.

Stratigraphical and Geographical distribution: Middle Miocene (France, Austria, Spain, Corsica, Valearides, Sardinia, Greece, Turkey); Tortonian (Hungary, Cilice, Syria, Greece); Middle Tortonian (Gavdos).

Cypeaster crassus Agassiz, 1861

1963. *Clypeaster crassus* Agassiz.- Kier, vol. 145, p. 30, Pl. 11, fig. 1-3.
1985. *Clypeaster crassus* Agassiz.- Marcopoulou-Diacantoni, p. 129,132, 166, Pl. XIII,XV,XVI.

Specimens: 1 ; *Dimensions:* 2004 / AG2 : Lo: 109, la : 93, h: 29, l / L: 0,85, h / L: 0,26

Stratigraphical and Geographical distribution: Early Miocece (France, Sardinia, Algeria, Corsica, Egypt); Middle Miocene (France, Turkey); Late Miocece (Florida USA); Tortonian (Hungary); Middle Tortonian (Gavdos).

Clypeaster cf *di–Stefanoi* Checchia – Rispoli, 1916

1916. *Clypeaster di-Stefanoi* Checchia – Rispoli, vol. XXII, p. 238, tav. XXVIII, fig. 2.
1967. *Clypeaster di-Stefanoi* Checchia – Rispoli.- Marcopoulou-Diacantoni, p. 368, Pl. XVI, fig. 2.
1985. *Clypeaster di-Stefanoi* Checchia – Rispoli.- Marcopoulou-Diacantoni, p. 169

Specimens : 1 ; *Dimensions:* 2004 / G2 : Lo: 133, la: 123, h: 50, l / L: 0,92, h / L: 0,37

Stratigraphical and Geographical distribution: Middle Tortonian (Gavdos); Pliocene (Italy, Greece)

Clypeaster intermedius Desmoulins, 1837

1778. *Echinanthus humilis* Leske, pl. XL, fig. 1, pl. XLI, fig. 1.
1837. *Clypeaster intermedius* Desmoulins, p. 73, moules r. 11, r. 12.
1928. *Clypeaster intermedius* Desmoulins.- Lambert, vol. 1, No 2, II partie, p. 13.
1967. *Clypeaster intermedius* Desmoulins.- Marcopoulou-Diacantoni, p. 370, Pl. VI.
1985. *Clypeaster intermedius* Desmoulins. –Marcopoulou-Diacantoni, p. 128, 134, 159, 176, Pl. X-XII.

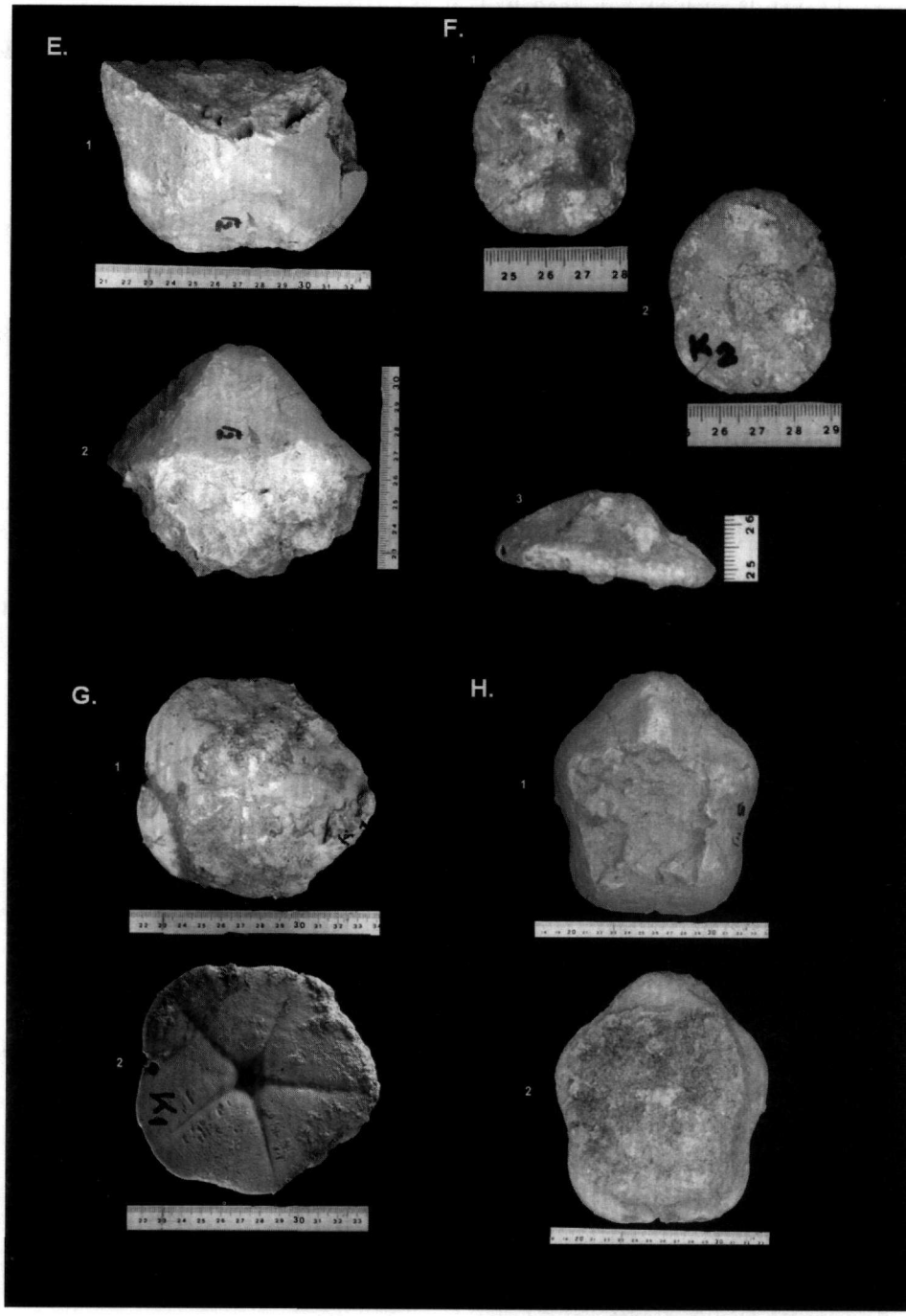

Plate 2 - E. *C.* cf. *di Stefanoi*, F. *C. intermedius* (form *crassicostatus*), G. *C. intermedius*, H. *C. lambert*

1998. *Clypeaster intermedius* Desmoulins. – Philippe, p. 302, pl. 11, fig. 4-6, pl. 12, fig. 1-4.
2000. *Clypeaster intermedius* Desmoulins. – Marcopoulou-Diacantoni, p. 178, Pl. III, fig. 1a,b, Pl. V, fig. 3a,b, Pl. VI, fig. 1.

Specimens : 1 ; *Dimensions:* 2004 / K1 :Lo: 120, la: 103, h: 39, l / L: 0,85, h / L: 0,32

Remarks: In the typical form of this species the impair ambulacral anterior zone is more narrow and elevated than in our specimen. The species belongs to the group of *Clypeaster scillae* (Marcopoulou-Diakantoni, 1985).

Stratigraphical and Geographical distribution: Early-Late Neogene (France, Spain, Corsica, Valearides, Egypt, Algeria, Italy, Middle East); Middle-Late Miocene (Greece); Middle Tortonian (Gavdos).

Clypeaster intermedius (form *crassicostatus*) Desmoulins, 1837

1985. *Clypeaster intermedius* (de la forme crassicostatus) Desmoulins.- Marcopoulou-Diacantoni, pl. XIV, XIX.
1998. *Clypeaster intermedius* (form *crassicostatus*) Desmoulins.- Philippe, p. 117, pl. 12, fig. 4.
2000. *Clypeaster intermedius* (form *crassicostatus*) Desmoulins.- Marcopoulou-Diacantoni, p. 178, Pl. V, fig. 2.

Specimens: 1 juvenile ; *Dimensions:* 2004 / K2 :Lo:51, la:46, h:18, l/L:0,90, h/L:0,35

Remarks: The species belongs to the group of *Clypeaster scillae* (Marcopoulou-Diakantoni, 1985).

Stratigraphical and Geographical distribution: Middle-Late Miocene (Europe, North Africa, Middle East); Middle Tortonian (Gavdos).

Clypeaster lamberti Lovisato, 1905

1905. *Clypeaster lamberti* Lovisato, p. 17.
1907. *Clypeaster lamberti* Lovisato.- Lambert, vol. XXXIV, p. 49, pl. III, fig. 7, pl. IV, fig. 1, 2.
1960. *Clypeaster lamberti* Lovisato.- Roman, No 55, p. 80, pl. IV, fig. 2, 2a.
1967. *Clypeaster lamberti* Lovisato. - Marcopoulou-Diacantoni, p. 372, pl. IV, fig. 1, pl. V, fig. 1, 1a.
1972. *Clypeaster lamberti* Lovisato. -Marcopoulou-Diacantoni, p. 150.
1985. *Clypeaster lamberti* Lovisato. -Marcopoulou-Diacantoni, p. 116, 178, pl. VII.
2000. *Clypeaster lamberti* Lovisato. -Marcopoulou-Diacantoni, p. 179, Pl. I, fig. 1a,b.

Specimens : 4 ; *Dimensions:* 2004 / G1 :Lo:143, la:126, h:58, l / L :0,88, h / L:0,40
2004/G4 :Lo:161, la:142, h:51, l / L :0,88, h / L:0,31
Remarks: The species belongs to the group of Clypeaster campanulatus (Marcopoulou-Diacantoni, 1985).

Stratigraphical and Geographical distribution: Oligocene (Cuba); Miocene (Sardinia); Early-Middle Miocene (Hungary, Sardinia, Turkey); Middle-Late Miocene (Greece); Middle Tortonian (Gavdos).

Clypeaster portentosus Desmoulins, 1837

1837. *Clypeaster portentosus* Desmoulins, p. 218, N° 14.
1843. *Clypeaster agassizi* E. Sismonda, p. 48, pl. II, fig. 5-7.
1861. *Clypeaster portentosus* Desmoulins.- Michelin, 2e serie, tom. VII, p. 125, pl. XXVIII, fig. A-e.
1948. *Clypeaster portentosus* Desmoulins.- Mortensen, Text, p. 7, fig.3.
1958. *Clypeaster portentosus* Desmoulins.- Imbesi, vol. LIII (n.ser.vol. XXIII), p. 21, tav. IV, fig. 2, 2a, 2b, tav. V, fig. 1, 1a, 2, 2a, 3, 4.
1967. *Clypeaster portentosus* Desmoulins. - Marcopoulou-Diacantoni, p. 373, pl. VIII, IX, XIV.

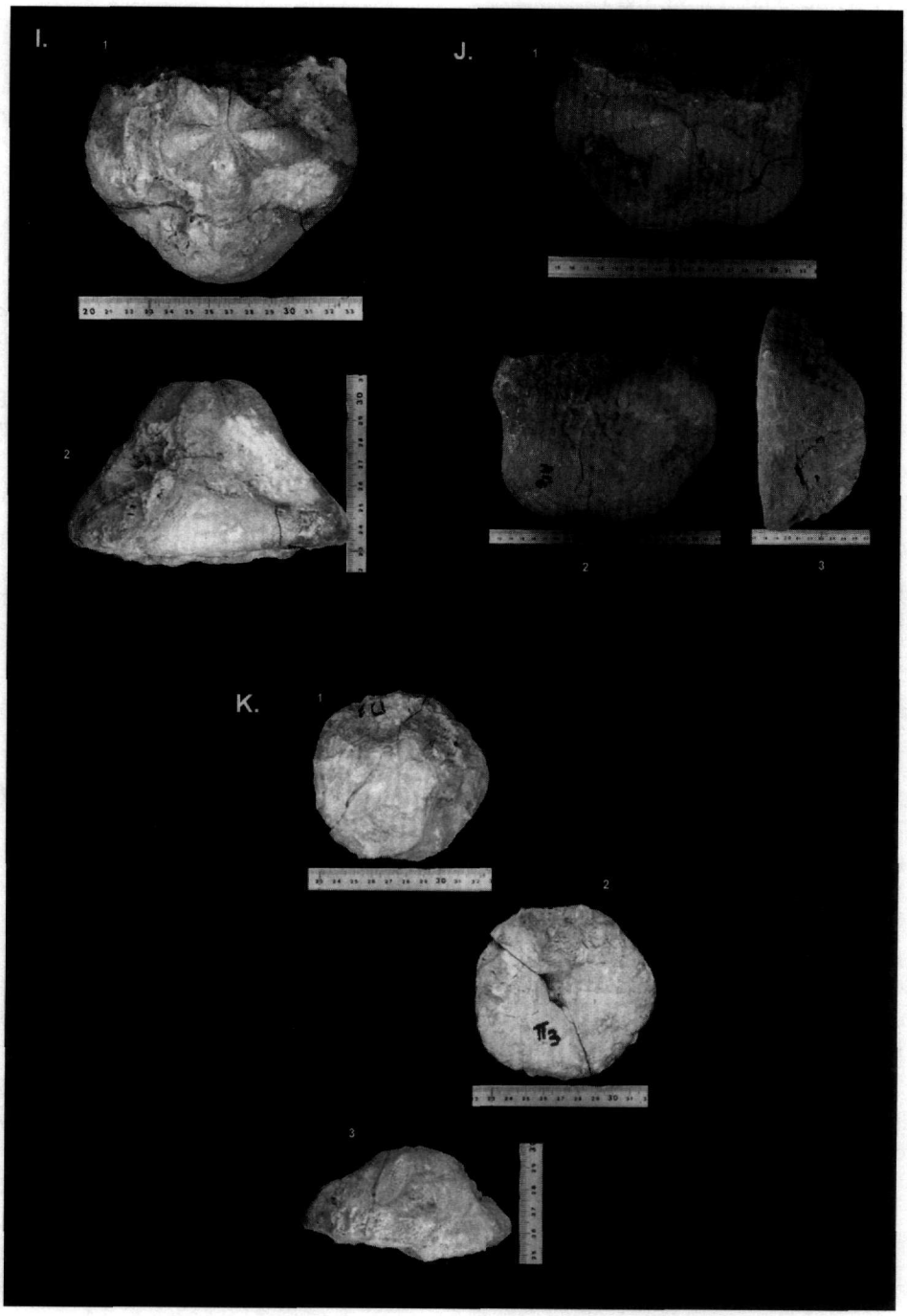

Plate 3 - I. *C. ponterosus*, J. *C. tauricus*, L. *C.* cf. *ventiensis*

1985. *Clypeaster portentosus* Desmoulins. - Marcopoulou-Diacantoni, p. 108,112, 190, pl. IV-VI.

Specimens : 5 ; *Dimensions:* 2004/P4 :Lo:148, la:120, h:86, l / L:0,81, h / L:0,58
2004 / P10 :Lo:142, la:122, h:63, l / L:0,85, h / L:0,44
2004/AG4 :Lo:152, la:131, h:84, l / L:0,86, h / L:0,55
Stratigraphical and Geographical distribution: Middle Neogene (Corsica, Kalavria, Balearics, Malta, Hungary, South France, Algeria, Cyprus); Miocene (Italy); Middle Tortonian (Gavdos).

***Clypeaster tauricus* Desor, 1859**

1861. *Clypeaster tauricus* Desor.- Michelin, p. 108, tav. X, XI, fig. a-e.
1895. *Clypeaster tauricus* Desor.- Cotteau, p. 23.
1958. *Clypeaster tauricus* Desor.- Imbesi, vol. XIII, fig. 2a, 2b.
1967. *Clypeaster tauricus* Desor.- Marcopoulou-Diacantoni, p. 377, pl. XIII.

Specimens : 1 ; *Dimensions:* 2004/AG4 : Lo: 180, la: 152, h: 78, l / L: 0,84, h / L:0,43

Stratigraphical and Geographical distribution: Middle Neogene (Portugal); Middle Miocene (Sardinia, Corsica, Malta, Spain, Syria, Crete); Middle Tortonian (Gavdos).

***Clypeaster* cf. *ventiensis* Tournouer, 1878**

1912. *Clypeaster* cf. *ventiensis* Tournouer. - Lampert
1985. *Clypeaster* cf. *ventiensis* Tournouer. - Marcopouloy-Diacantoni, p. 136, 138, 139, 201, pl. XXIV.

Specimens : 1 ; *Dimensions:* 2004/P3 : Lo: 100, la: 90, h: 35, l / L: 0,90, h / L: 0,35

Stratigraphical and Geographical distribution: Miocene (Sardinia, Katalonia); Middle Tortonian (Gavdos).

4. The irregular echinoid *Clypeaster* as potential paleoenvironmental tool

The irregular echinoid *Clypeaster* is locally common in Oligocene to Quaternary sedimentary deposits in the Mediterranean region, particularly in marine limestones of shallow-water origin. According to Kier and Grant (1965) the major factor influencing echinoid distribution is water depth/shore distance. Other factors (such as light penetration, wave agitation, current direction and food supply) are either functions of these or factors difficult to evaluate. However, Smith (1984) concluded that nine factors affect the distribution patterns of echinoid species: nature of the substratum, hydrodynamic regime, predation, salinity, temperature, food availability, water depth, behaviour and chance.

Paleoenvironments represented by Miocene echinoid assemblages may be interpreted using Recent analogues (e.g. Kier 1972). The significance of such interpretations is that they may be helpfully precise. For example, *Clypeaster altus* is closely similar to Recent species of *Clypeaster* with thick test margins in the Red Sea, such as *Clypeaster fervens*, and *Clypeaster marginatus* is convergent with Recent *Clypeaster* with thin margin from the Red Sea such as *Clypeaster humilis*. The ecological affinities of the Recent representatives of these taxa can therefore be used to interpret quite closely, by morpho-functional analogies, the palaeoenvironmental adaptations of the Miocene species, especially their bathymetrical adaptations

In the present-day Mediterranean and the surrounding marine areas (Red Sea, Atlantic Ocean), the bathymetric range of irregular echinoids can be defined according to the nomenclature proposed by Peres and Picard (1964). These authors define, in the Mediterranean, the infralittoral zone as the inner shelf with photophile seagrass, the circalittoral zone as the outer shelf with sciaphile seagrass and the bathyal zone as the topographical transition to the slope.

Recent *Clypeaster*, with hypermorphic petals, are typical of shallow, high-energy environments in the infralittoral zone thus defined, generally in water depths of about 1–50 m (George and George 1980, Dollfus and Roman 1981, Nebelsick 1992, Roman and Lachkhem 1993). The high subconical *Clypeaster altus*, with a thick test margin, settled in the shallowest environments with high energy, with coarse sediments and lived often epifaunally near coral patches or along the coast (Boggild and Rose 1985, Nebelsick 1992, Roman and Lachkhem 1993).

Thus by analogy with the bathymetric distribution of Recent Mediterranean irregular echinoids, and taking into account the stratigraphical succession of their Miocene representatives, the studied clypeasteroid fauna is indicative of an upper infralittoral environment. Furthermore, the presence of attached colonies of membraniporiform type Bryozoans on the tests of the studied specimens strongly supports the above mentioned conclusion (e.g. Moissette 1988).

5. Acknowledgements

The material of this study has been collected by the senior author during his Phd fieldwork. This project is co-funded by the European Social Fund and National Resources (EPEAEK II) PYTHAGORAS II (70/3/8020).

6. References

Agassiz, L., 1835. Prodrome d'une monographie des Radiaires ou Echinodermes, *Mem. Soc.Sci.nat. de Neufchatel*, t. 1, 1835 et Ann. Sci. Nat., Paris, 7, 257-296.

Agassiz, L., 1839-1840. Description des Echinodermes de la Suisse, *Nouv. Mem. Soc. Helvet. Sc. Nat.*, 1^{e} partie:Spatangoides et Clypeastroides, 101 p., 2^{e} partie:Cidarides, 107pp.

Agassiz, A., 1872-1874. Revision of the Echini, *Mem. Mus. Comp. Zool.*, Part I-III, 764pp.

Anastasakis, G.C., Dermitzakis, M., and Triantaphyllou, M., 1995. Stratigraphic Framework of the Gavdos island Neogene sediments, *Newsl. Stratigr.* 32, 1-15.

Antonarakou, A., 2001. Biostratigraphic and paleoenvironmental implications on Miocene sediments of Eastern Mediterranean (Gavdos Island), *PhD Thesis*, Athens University, 180pp.

Antonarakou, A., Drinia, H., Tsaparas, N., and Dermitzakis, M.D., in press. Assessment of micropaleontological sedimentary parameters as proxies of surface water properties and paleoclimate, in Gavdos island, Eastern Mediterranean, *Geodiversitas*.

Betzler, C., Brachert, T.C., and Nebelsick, J., 1997. The warm-temperate carbonate province—a review of the facies, zonations and delimitations, *Courier Forschungsinstitut Senckenberg*, 201, 83-99.

Boggild, G.R., and Rose, E.P.F., 1985. Mid-Tertiary echinoid biofacies as palaeoenvironmental indices, *Ann. Géol. Pays Hell.* 32, 57–67.

Borghi, E., 1995a. *Paracentrotus lividus* (Lamarck, 1816) nel Pleistocene dell'Emilia. Echinodermi fossili emiliani, *Boll. Soc. Regg. Sci. Nat.*, 15, 1–21.

Borghi, E., 1995b. Segnalazione di una nuova forma affine al *Genocidaris maculata* A. Agassiz, 1869. Echinodermi fossili emiliani. Bibliotheca, Studi Sci. Nat., Tip. Le. Co. ed., 1–14.

Brachert, T.C., Forst, M.H., Pais, J.J., Legoinha, P., and Reijmer, J.J.G., 2003. Lowstand carbonates, highstand sandstones, *Sedimentary Geology*, 155, 1-12.

Bronn, HG., 1860. Die Klassen und Ordnungen der Strah lenthiere (Actinozoa), wissenschlaftliche dargestellt in Wort und Bild. In H.G. Bronn (ed.), *Bronn's Klassen und Ordnungen des Thier-Reiches*, Volume II. Leipzig, 403–404.

Checchia - Rispoli, G., 1916. Gli Echinidi viventi e fossili della Sicilia.Parte terza, *Pal. Ital.,* 12, 221-228.

Checchia - Rispoli, G., 1925. Illustrazione dei Clipeastri miocenici della Calabria, *Mem. per serv. alla descr. della cart. geol. d'Italia*, IX, 1-75.

Cotteau, G., 1895. Description des Echinides recueillis par M. LOVISATO dans le Miocene de la Sardaigne, *Mem. Soc. Geol. Fr.,* Paris, mem. 13, 56p.

Desmoulins, C., 1837. Troisieme memoire sur les Echinides. Synonymie generale, *Actes Soc. Linn. Bordeaux,* N° 49, 45-364.

Desor, E., 1857-1858. Synopsis des Echinides fossiles, *C. Reinwald edit.*,Texte et Atlas, 2 , 490 p.

Dollfus, R.P., and Roman, J., 1981. Les échinides de la Mer Rouge. Monographie zoologique et paléontologique, *Com. Trav. Hist. Sci. Mém. Sect. Sci.,* 9, 1–145.

Drinia, H., Antonarakou, A., Tsaparas, N., Dermitzakis, M.D., and Doukas, C., 2004. Foraminiferal sequence eco-biostratigraphy of the Middle-Early Late Miocene, Potamos Section from Gavdos Island, Greece, In F.F. Steininger, J. Kovar-Eder and M.M. Fortelius (eds), The Middle Miocene Environments and Ecosystem Dynamics of the Eurasian neogene (EEDEN). *Courier Forschungsinstitut Senckenberg*, 249, 29-43.

George, D., and George, J.J., 1980. La vie marine. Encyclopédie illustrée des invertébrés marins. Maloine, Paris, 173pp.

Heimann, K.O., and Marcopoulou-Diacantoni, A., 1977. Sur une faune d'échinides dans la série messinienne de Céphalonie (Grèce) (in Greek), *Ann. Géol. Pays Hell.,* 29, 542–550.

Imbesi, M., 1958. Clipeastri aquitaniani, elveziani e tortoniani della Calabria, *Pal. Ital.,* 53 (n. ser. 23), 1-47.

James, N.P., Bone, Y., Collins, L.B., and Kyser, T.K. 2001. Surficial sediments of the Great Australian Bight: facies dynamics and oceanography on a vast cool-water carbonate shelf, *Journal of Sedimenary Research,* 71, 549 – 567.

Kier, P.M., 1963. Tertiary echinoids from the Caloosahatchee and Tamiami formations of Florida, *Smithsonian Miscellaneus Collections*, 145, n° 5, 63 pp.

Kier, P.M. 1972. Tertiary and Mesozoic echinoids of Saudi Arabia, *Smithsonian Contributions to Paleobiology*, 10, 1–242.

Kier, P.M., and Grant, R.E., 1965. Echinoid distribution and habits, Key Largo Coral Reef Preserve, Florida, *Smithsonian Miscellaneus Collections,* 149, no.6, 68p.

Klein, J.T., 1734. Naturalis dispositio Echinodermatum. Accessit lucubratiuncula de aculeis Echinorum marinorum, cum spicilegio de Belemnitis.Gedani, *Th. J. Schr.*, 8°, 79p.

Lamarck, de M, 1801. Systeme des Animaux sans Vertebres, VIII, 432.

Lambert, J., 1906. Etude sur les Echinides de la molasse de Vence, *Ann. Soc. Lett., Sci. Arts Alpes-Maritimes*, Nice, 20, 1-64.

Lambert, J., 1907. Description des echinides fossiles des terrains mioceniques de la Sardaigne, *Mem. Soc. Pal. Suisse,* Geneve, XXXIV, 1-72.

Lambert, J., 1913. Description des Echinides des terrains neogenes du bassin du Rhone, *Mem. Soc. Pal. Suisse.* XXXIX,.

Lambert, J., 1928. Revision des Echinides fossiles de la Catalogne. 2e partie : echinides du Miocene, echinides du Pliocene et echinides neogenes des Baleares, *Mem. d. Mus. d. Cienc. Nat. de Barcelona*, ser. geol., I, n° 2, 62p.

Lacour, D., and Néraudeau, D., 2000. Evolution de la biodiversité des *Brissopsis* (Echinoidea, Spatangoida) en Méditerranée entre le Messinien et l'Actuel: application paléoécologique aux *B. lyrifera* intragypses de Sorbas (SE Espagne). *Géodiversitas* 22, 509–523 pp.

Leske, N.G., 1778. Jacobi Theodori Klein. Naturalis dispositia Echinodermatum Adita et descriptionibus novisque inventis et synonymis auctorem aucta, *Lipsiae*, 4°, 278p.

Lovisato, D., 1905. Species Fossiles di Bonaria e di Bartolomeo.

Marcopoulou-Diacantoni, A, 1967. La faune des Echinides neogenes des Pays helleniques, *Ann. Geol. des Pays Hell.*, 18, 331-406, Athenes.

Marcopoulou-Diacantoni, A., 1970. Les echinides de l' ile de Gavdos, *Ann. Geol. pays Hellen.*, XXII, 247-255.

Marcopoulou-Diacantoni, A., 1972. Echinides (*Clypeaster, Schizaster, Spatangus, Brissopsis*) de l' Helvetien de l' ile de Crete centrale et orientale, *Ann. Geol. pays Hellen.*, XXIV, 133-178.

Marcopoulou-Diacantoni, A., 1974. Contribution a la connaissance des Echinides neogenes de la region au NW de Sitia (Crete), *Ann. Geol. des Pays Hell.*, XXVI, 251-261.

Marcopoulou-Diacantoni, A., 1977. Les échinides plio-pleistocènes de la région de Neapolis Vion (Péloponèse), *Ann. Géol. Pays Hell.* 29, pp. 436–449. (in Greek)

Marcopoulou-Diacantoni A., 1985. The Morphology and evolution of the genus *Clypeaster* (Echinoidea, Clypeasteroida), *Monography Univ. Thessaloniki.*, 23, no36, 257 p.

Marcopoulou-Diacantoni, A., 2000. The occurrence of Echinoids in the Upper Tortonian sediments of the Plakiotissa region (province of Heraklion, Monofatsiou district, C. Crete). Palaeoenvironmental interpretation, *Proceedings Interim Colloquium R.C.M.N.S.* Special Publications, 9, 173-186.

Michelin, 1861. Monographie des Clypeastres fossiles, *Mem. Soc. Geol. France,* 2e ser., VII, n° 2, 101-147.

Mitrovic–Petrovic, J., 1969. Les Echinides du Miocene moyen dans la Bosnie septentrionale (La vallee de la Save en Bosnie), *Acta geologica,* Zagreb, 6, 113-148.

Moissette, P., 1988. Faunes de Bryozoaires du Messinien d' Algerie occidentale, *Docum. Lab. Geol. Fac. Sci. Lyon*, n° 102, 351p., 23 fig., 6 tabl., 31 pl.

Montenat, C., and Roman, J., 1970. Echinides néogènes d'Espagne (prov. d'Alicante et de Murcia), *Ann. Paléontol.* 56, 39–138.

Mortensen, Th., 1928, 1935, 1940, 1943, 1948, 1950. Monograph of the Echinoidea. I –V_1. Text and Atlas, Copenhagen.

Nebelsick, J.H., 1992. The northern bay of Safaga (Red Sea, Egypt): an actuopalaeontological approach. III Distribution of Echinoids, *Beitr. Paläontol. Österr.* 17, 5–79

Néraudeau, D., Borghi, E., and Roman, J., 1998. Le genre d'échinide *Spatangus* dans les localités du Pliocène et du Pleistocène de l'Emilie (Italie), *Ann. Paléontol,*. 84, 243–264.

Néraudeau, D., Roman, J., and Borghi, E., 1999. Impact of the Messinian crisis on the Mediterranean echinoid fauna. In: Candia Carnevali, M.D., Bonasoro, F. (Eds), Echinoderm Research 1998. A.A. Balkema, Rotterdam, pp. 355–360.

Peres, J.M., and Picard, J., 1964. Nouveau manuel de bionomie benthique de la mer Méditerranée, *Bull. Rec. Trav. Stat. Mar. Endoume,* 31, 1–137

Philippe, M., 1998. Les Echinides Miocenes du bassin du Rhone: Revision systematique, *Nouv. Arch. Mus. Hist. Nat. Lyon,* fasc. 36. premiere and deuxieme partie, 3 – 441.

Ragaini, L., 1996. L'echinofauna pliocencia del canton Ticino nelle collezioni del Museo Cantonale di Storia Naturale di Lugano, *Geol. Insubr.* 1, 47–51.

Roman, J., 1960. Echinides (*Clypeaster, Scutella, Schizaster*) de l'Helvetien du bassin de Karaman (Turquie), *Bull. Min. Res. Expl. inst. Turkey.* 55, 64-96.

Roman, J., and Soudet, H.L., 1990. Les échinides du Néogène récent bétique, *Doc. Trav. IGAL Paris,* 12–13, 53–56.

Roman, J., and Lachkhem, H., 1993. Le bassin sédimentaire de Melilla (Maroc septentrional) et sa faune d'échinoïdes du Messinien (Miocène supérieur), *118° Congr. Nat. Soc. Hist. Scient., 4° Coll. Géol. Afric.*, 445–460pp.

Saint-Martin, J.-P., Néraudeau, D., Lauriat-Rage, A., Secrétan, S., Goubert, E., Babinot, J.-F., Boukli-Hacene, S., Pouyet, S., Lacour, D., Pestrea, S., and Conesa, G., 2000. La faune interstratifiée dans les gypses messiniens de Los Yesos (Bassin de Sorbas, SE Espagne): Implications paléoenvironnementales, *Géobios,* 33,. 637–649.

Schlotheim, E.F. von, 1820. Die Petrefactenkunde, in-8°, texte 437p.

Seguenza, G., 1880. Le formazione terziarie nella provincia di Reggio (Calabria), *Atti d. R. Accad. d. Lincei,*et *Mem. Cl. Sci. fis., mat. e nat.,* Roma, ser. 3, 6, 446 p.

Sismonda, E., 1843. Memoria geo-zoologica sugli Echinidi fossili del Contado di Nizza, *Memoria R. Accad. Sci. Torino,* 6, ser. 2, 1-71.

Smith, A.B., 1984. Echinoid Palaeobiology, London; George Allenand Unwin. 190p.

Tournouer, R., 1878. Sur la mollasse miocene de Forcalquier, *Bull. Soc. Geol. Francaise*, VII.

Tsaparas, N., 2005. Contribution in the history of sedimentation of the marine formations from the Late Cainozoic of Gavdos Island, *Thesis,* 2005, University of Athens. Gaia.

Zittel, K.A. von, 1895, Grundzuge der Paleontologie (Paleozoologie): R. Oldenburg, Munich, 1" edition, 971pp.

Δελτίο της Ελληνικής Γεωλογικής Εταιρίας τομ. XXXX, 2007
Πρακτικά 11ου Διεθνούς Συνεδρίου, Αθήνα, Μάιος 2007

Bulletin of the Geological Society of Greece vol. XXXX, 2007
Proceedings of the 11th International Congress, Athens, May, 2007

PETRIFIED WOOD OCCURRENCES IN WESTERN THRACE AND LIMNOS ISLAND: MINERALOGY, GEOCHEMISTRY AND DEPOSITIONAL ENVIRONMENT

Voudouris P.[1], Velitzelos D.[2], Velitzelos E.[2], and Thewald U.[3]

[1] *National and Kapodistrian University of Athens, Faculty of Geology and Geoenvironment, Department of Mineralogy - Petrology, voudouris@geol.uoa.gr*

[2] *National and Kapodistrian University of Athens, Faculty of Geology and Geoenvironment, Department of Hist. Geology – Paleontology,velitzel@geol.uoa.gr*

[3] *University of Ulm/Germany, Department of Chemistry, Section of "Röntgen und Elektronenbeugung", Ulf.Thewalt@chemie.uni-ulm.de*

Abstract

The present study describes the geology and mineralogy of the main petrified wood occurrences in Evros-Rhodopi and Limnos and integrates them in a volcanic-hydrothermal framework taking into consideration the nature of hydrothermal solutions during the silicification process. In the Lykofi-Fylakto-Lefkymi area, quartz and opal-CT are the main silica polymorph within the wood. The hostrocks exhibit a zeolitic alteration suggesting reduced and slightly alkaline fluids for the silicification of wood. At Kassiteres/Sappes area the presence of silicified wood within kaolinite±alunite altered tuffbreccias indicates that slight acidic fluids were involved in the silicification processes. In Limnos Island the fossiliferous Portianou, Varos-Roussopouli and Moudros-Roussopouli areas occur in the periphery of an eroded volcanic edifice exposed at Fakos peninsula. The silicified wood occurs: (a) within weakly altered pyroclastics and (b) associated to several horizons of sinters interbedded within the pyroclastics. Transformation of amorphous silica to opal-CT and then to quartz is postulated based on XRD and SEM studies. The studied areas represent unique natural monuments, comparable to the petrified forest of Lesvos island.

Key words: *silicified wood, Evros, Limnos, mineralogy, depositional environment.*

Περίληψη

Η παρούσα μελέτη περιγράφει την γεωλογία και ορυκτολογία των κυριώτερων εμφανίσεων απολιθωμένων δέντρων στους νομούς Έβρου-Ροδόπης και τη νήσο Λήμνο, και τις εντάσσει σε ένα ηφαιστειακό-υδροθερμικό πλαίσιο λαμβάνοντας επιπλέον υπόψη την φύση των υδροθερμικών διαλυμάτων που οδήγησαν στην απολίθωση. Στη περιοχή Λυκόφης-Φυλακτού-Λευκίμης, χαλαζίας και οπάλιος-CT είναι τα κύρια πολύμορφα του πυριτίου που εντοπίστηκαν στα απολιθωμένα δέντρα. Τα πετρώματα ξενιστές παρουσιάζουν μια ζεολιθική εξαλλοίωση, υποδεικνύοντας ότι υπεύθυνα για την πυριτίωση των δέντρων ήταν αναγωγικά έως αλκαλικά διαλύματα. Στις Κασσιτερές/Σαππών η παρουσία πυριτιωμένων κορμών εντός τοφφικών λατυποπαγών εξαλλοιωμένων σε καολινίτη±αλουνίτη, αποτελεί ένδειξη ότι στις διαδικασίες πυριτίωσης

των δέντρων συμμετείχαν ελαφρά όξινα διαλύματα. Στη νήσο Λήμνο, οι απολιθωματοφόρες περιοχές Πορτιανού, Βάρος-Ρουσσοπουλίου και Μούδρου-Ρουσσοπουλίου απαντούν στη περιφέρεια ενός διαβρωμένου ηφαιστειακού κέντρου που αναπτύσσεται στην χερσόνησο του Φακού. Στη Λήμνο τα πυριτιωμένα δέντρα απαντούν: (α) εντός ελαφρά εξαλλοιωμένων πυροκλαστικών και (β) σε σχέση με πολυάριθμους ορίζοντες πυριτικού sinter που παρεμβάλλονται μεταξύ των πυροκλαστικών. Μετατροπή αμόρφου πυριτίου σε οπάλιο-CT και στη συνέχεια σε χαλαζία προκύπτει από μελέτες XRD και SEM. Οι περιοχές που μελετήθηκαν αποτελούν μοναδικά φυσικά μνημεία, συγκρίσιμα με το απολιθωμένο δάσος της νήσου Λέσβου.
Λέξεις κλειδιά: *πυριτιωμένοι κορμοί, Έβρος, Λήμνος, ορυκτολογία, περιβάλλον απόθεσης.*

1. Introduction

The northeastern Greece is a very promising district for the development of petrified forests, due to its favourable geological setting and the extensive development of orogenic Tertiary volcano-plutonic arcs. This area is characterized by widespread occurrences of petrified forests, mainly in the volcanic environments of northeastern Aegean (Evros, Limnos island, Lesvos island, Velitzelos and Zouros 1997).

This study was focused on several localities from the two broad areas, Evros and Limnos: In Evros there are several known occurrences east of Alexandroupolis, the Tychero, the Fylakto and also near the Lefkimi areas among them (Fig. 1a). Other newly discovered occurrences are those of Sapes and Perama areas (west of Alexandroupolis) and Aetochori/Pefka (east of Alexandroupolis) indicating the widespread development of petrified forests in the whole region. In Limnos island the main prospective area are the Moudros, Roussopouli, Romanou, Varos and Portianou areas (Fig. 1b).

In order to better understand the processes which resulted in the silicification of wood, this study examines the characteristics of the magmatic-hydrothermal and geothermal systems that were developed during the past in the studied areas. The evolution of these systems was the main factor controlling the circulation of silica-enriched fluids responsible for the silicification of wood. The present study describes the geology and mineralogy of some important petrified wood occcurrences in northeastern Greece and integrates them in a volcanic-hydrothermal framework taking into consideration the nature and chemistry of hydrothermal solutions during the silicification process.

2. Materials and Methods

Laboratory research included optical microscopy, XRD analysis with a SIEMENS type D-500 instrument, SEM analysis using a DSM 962 Zeiss Digital Scanning Microscope, at 5kV, 0.74 nA both performed in the Section of "Röntgen und Elektronenbeugung", Department of Chemistry, University of Ulm/Germany. Selected samples were analyzed for major and trace elements using XRF method with a Phillips PW 1220 instrument in the Institute of Mineralogy and Petrology, University of Hamburg.

3. The geodynamic evolution and volcanic activity in northeastern Greece

The geodynamic evolution in north-eastern Greece includes an early oceanic-continental subduction/collision and post-Alpine extension resulting in the formation of back-arc basins in Rhodope and Limnos island (Krohe and Mposkos 2001). Post-collisional extensional collapse of the orogen resulted in the formation of several supra-detachment basins from the Lutetian (48 – 43 Ma) through the Oligocene up to the Pliocene. Slab break-off and/or slab delamination were principal

mechanisms for the generation of extensive post-collisional magmatism in the area during the Oligocene to Miocene times, which greatly influenced the development of magmatic-hydrothermal systems (de Boorder *et al.* 1998, Pe-Piper *et al.* 1998, Melfos *et al.* 2002). The resulting plutonic-subvolcanic (monzonites, monzodiorites, granodiorites, microgranite porphyries) and volcanic rocks (banakites, trachytes, andesites, dacites, rhyolites) in Evros region show calc-alkaline, high-K calc-alkaline, to shoshonitic affinity (Innocenti *et al.* 1984, Christofides *et al.* 1998). New K/Ar ages of volcanic rocks in this area range from 33.5 to 19.6 Ma, establishing an Oligocene and a Lower Miocene period of magmatic activity (Pecskay *et al.* 2003). An enriched mantle source region for the basic to intermediate magmas and a partial melting of crystal material for the acid magmas has been documented. The magmatic rocks in the island of Limnos are of Lower Miocene age (21-18 Ma) and display an orogenic character and calc-alkaline to shoshonitic affinity (Fytikas *et al.* 1979, 1984, Innocenti *et al.* 1994). The geochemical character of the Limnos magmatic rocks indicates fractional crystallization processes in the boundary between continental crust-mantle related to an enrichment of the melts in K_2O and LILE elements.

4. Description of the petrified wood occurrences in Greece

4.1. Evros region

4.1.1. Regional geology

In Evros region the Cenozoic magmatic activity is closely related to the development of basin-controlled volcano-sedimentary formations which cover discordantly the basement rocks of the Rhodope massif and Circum Rhodope Belt (Papadopoulos 1982). Initial sedimentation started at Lutetian with the deposition of a basal-clastic formation, composed of conglomerates and sandstones overlain by a Priabonian clay-marl formation including marls alternated with sandstones and conglomerates and intercalations of lignitic horizons at the upper levels. The main phase of the Tertiary magmatism took place during the Oligocene (Innocenti *et al.* 1984, Kyriakopoulos 1987, Del Moro *et al.* 1988) and is represented by submarine/terrestrial volcanics and subvolcanic rocks, associated with volcano-sedimentary series composed of marls, sandstones, clays and intercalations of lavas, tuffs and pyroclastics.

4.1.2. Fylakto-Lykofi-Lefkimi-Dadia area

The geology of the area (Skarpelis *et al.* 1987) includes: a) a lower series of marine Priabonian sediments, associated with andesitic lavas, b) pyroclastics and lavas of dacitic to rhyolitic composition with intercalated sediments of Lower-Upper Oligocene age. The volcanics include pyroclastic flows, air fall deposits, as well as lava flows and domes, c) Upper Oligocene shallow marine sediments dominated by sandstones, marls and conglomerates (the Provatonas series), discordantly covering the acid volcanics. The area is also dominated by ignimbrites of several meters thickness.

The Lykofi - Fylakto - Lefkymi area is characterized by numerous occurences of silicified plant fossils, hosted within the Oligocene volcano-sedimentary formations. According to Kopp (1965), Velitzelos *et al.* (2002, 2006), the plant fossils are mainly related to the Rupelian-Chattian lignite-bearing volcano-sedimentary strata of Provatonas series (SE of Fylakto village).

In the present study three fossiliferous localities were mainly investigated: the Vrysi-Pardalos between Lyra and Lagyna (Fig. 2a), the Avgo-Pefkonas, about 500 m west of Fylakto (Fig. 2b) and 3 km north of Lefkimi. In all these localities the petrified wood occurs within the volcano-sedimentary formation of Provatonas series (Fig. 2c) covering discordantly the volcanics. A shallow marine environment is indicated by the presence of coral reefs and also established by the observation of abundant mollusks within the silt layers. In the locality of Vrysi-Pardalos (Fig. 2a) silt strata with abundant leaves are overlain by sandstones and microconglomerates hosting trunks of silicified wood. In the locality of Avgo-Pefkonas near Fylakto village a very similar stratigraphy includes silt layers at the base, overlain by alternations of fine- to very coarse-grained volcano-

sedimentary beds. Several trunks of silicified wood (up to 17 m long) occur within the volcanic agglomerate formation, which is composed of subrounded silicified boulders of acid volcanic rocks within a tuffitic matrix (Fig. 2c).

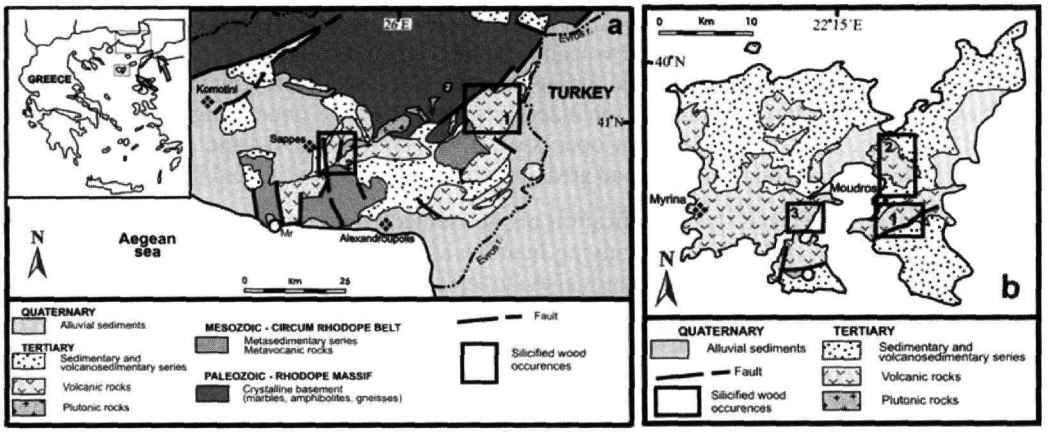

Figure 1 - (a) Geological sketch map showing the geology of the western Thrace (modified after Melfos *et al.* 2002) and location of the petrified-wood occurrences (1, 2); (b) Generalized geologic map of Limnos island (modified after Innocenti *et al.* 1994) and the Moudros (1), Varos-Roussopouli (2), Portianou (3) petrified-wood occurrences

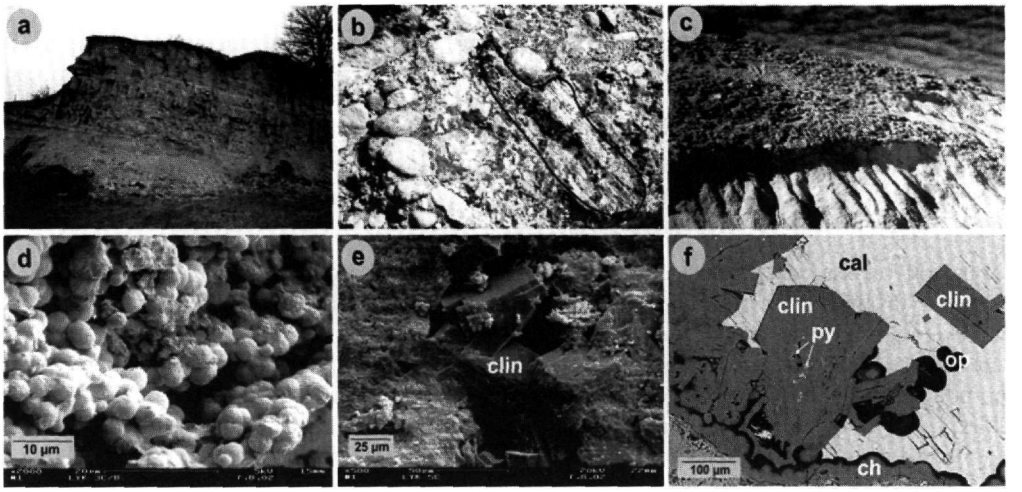

Figure 2 - (a) Location Vrysi-Pardalos: A sedimentary succession from fine-grained stratified silt (bottom) to sandstones and volcanic microconglomerates rich in silicified wood (upper parts); (b) Avgo-Pefkonas locality: Silicified trunk within volcanic agglomerate; (c) Rhyolitic lava overlain by volcano-sedimentary formation of Provatonas series; (d) Locality 3 km west of Lykofi. Spherolites of initial amorphous silica (opal-A) recrystallized to lepispheres of opal-CT, SEM micrograph; (e) Clinoptilolite (clin) crystals filling vugs within silicified coral-reef limestone, SEM micrograph, locality 3 km south of Lykofi; (f) Clinoptilolite (clin), chalcedony (ch), opal (op) and pyrite (py) overgrown by calcite (cal). Wall-rock alteration of dacitic lavas related to amethystine/chalcedonic veining. Kornofolia locality (SEM-BSE image)

In the Lefkimi locality, andesitic hyaloclastites (suggesting a submarine environment of formation) are overlain by coral-bearing reefs and then by fine-grained volcano-sedimentary layers including silicified wood. Volcanic agglomerate strata in the Hills around Lefkimi (similar to those

described above) are very rich in silicified wood and also contain boulders of quartz-chalcedony veins and of alunitic altered rhyolitic rocks.

It should be mentioned that the broad area is also characterized by abundant silicifications indicating intense hydrothermal activity in a shallow submarine to subaerial environment during the Upper Oligocene. The volcanic and volcano-sedimentary rocks (either of acid or intermediate composition) are overlain by opalized coral-bearing limestone reefs outcropping in several localities (e.g. south Lykofi). Both the opalized limestone and the underlying volcanic rock are crosscut by chalcedony-quartz veins. In open spaces well-formed quartz and calcite crystals are observed. The silicified zones in the broad area are accompanied by pyrite and marcasite.

The XRD analysis indicated that silicification of the studied wood material occurs mainly in the form of quartz. Some opal-CT accompanying quartz was detected in the Avgo-Pefkonas locality. A transformation from amorphous silica (opal-A) to lepispheres of opal-CT and finally to quartz is suggested by SEM analysis (Fig. 2d). The hostrock exhibits a zeolitic alteration (including clinoptilolite, mordenite, adularia, calcite, albite, opal-CT) (Figs 3a, b), which seems to be widespread in the broad area (see also Skarpelis *et al.* 1987). Quartz-chalcedony veins within silicified coral reefs as well as within dacitic lavas from the broad area, also exhibit a zeolitic signature (Figs 2e, f). Representative chemical analyses of zeolitic altered hostrocks and one analysis of silicified wood from Fylakto area are presented in Table 1. Besides SiO_2 and H_2O (probably in the form of structural water in opal) the analysis of the wood material indicates depletion in major and trace elements (sample Fy17b, Table 1).

4.1.3. Kassiteres/Sapes area

The Kassiteres represents an intensively hydrothermally altered area, located near Sapes about 20 km NW of Alexandroupolis. It consists mainly of volcanic and intrusive rocks of intermediate to acid composition. A thick volcanic sequence consisting of lava domes, flows and pyroclastics dominates the western and northern part of the Kassiteres area. The close spatial relationship of lava flows, domes, and pyroclastics with intrusive bodies of similar geochemical and petrographical characteristics suggest that the Kassiteres area has been a volcanic centre, probably a single or a composite stratovolcano.

The majority of magmatic rocks in the Kassiteres-Sapes area are intensively altered as a result of repeated hydrothermal activity in the area. Alterations typical of high-sulfidation systems (White and Hedenquist 1995) are characterized by an inner silicic zone (vuggy silica), surrounded progressively by advanced argillic (quartz-alunite-kaolinite) and sericitic (quartz-sericite) alteration (Fig. 4a). Intermediate sulfidation quartz and calcite veins with related K-feldspar (adularia), sericitic and intermediate argillic alteration are developed below the advanced argillic and silicic zones. Intermediate sulfidation quartz veins crosscut the silicic bodies. The veins consist of amethystine/chalcedonic quartz with minor adularia, calcite and barite gangues (Figs 4b, c). These veins are similar to those described from the Lykofi and Lefkimi areas.

Fossilized wood trunks were found on the south of Kassiteres within altered tuffitic material (Fig. 4d). The trunks are hosted in advanced argillically altered (kaolinite alteration) tuff-breccias developed laterally of the silicic and alunitic alteration zone (Figs 4a, e, f). Quartz/chalcedony veins including adularia and calcite crosscut the silicified trunks as well the silicified zones, postdating their formation. Similarly to the results obtained from the Fylakto-Lefkimi area, the silicification in the Kassiteres wood consists almost entirely of quartz. Chemical analyses indicate total SiO_2 contents of 96.2-97.01 wt% whereas small amounts of Al_2O_3 and H_2O are attributed to the presence of kaolinite (samples KassA1-A2, Table 1). Fe_2O_3 up to 0.70 wt% is attributed to the presence of iron oxides.

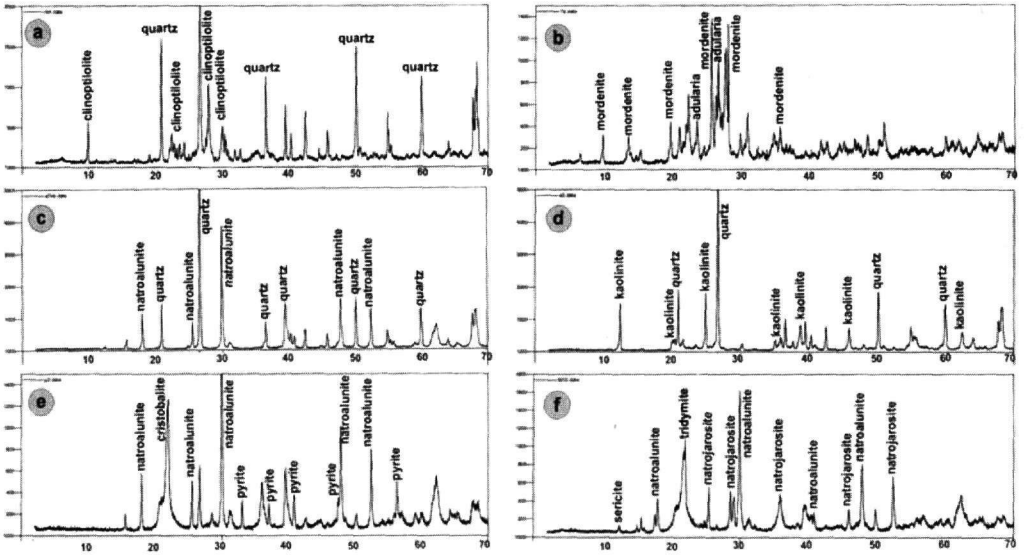

Figure 3 - XRD diagrams indicating various mineral associations within volcano-sedimentary rocks hosting silicified wood. a) Avgo-Pefkonas: Quartz-clinoptilolite alteration of fine-grained volcano-sedimentary layer hosting woods; b) Avgo-Pefkonas: zeolitic alteration (mordenite+adularia) of volcanic fragment from the volcanic agglomerate hosting woods; c) Kassiteres: Advanced argillic (quartz-natroalunite) alteration of tuff-breccia adjacent to the silicified wood; d) Kassiteres: quartz-kaolinite alteration of silicified wood hostrock; e, f) natroalunite in hydrothermaly brecciated silicic and advanced argillic alteration zones from Moudros and Roussopouli areas

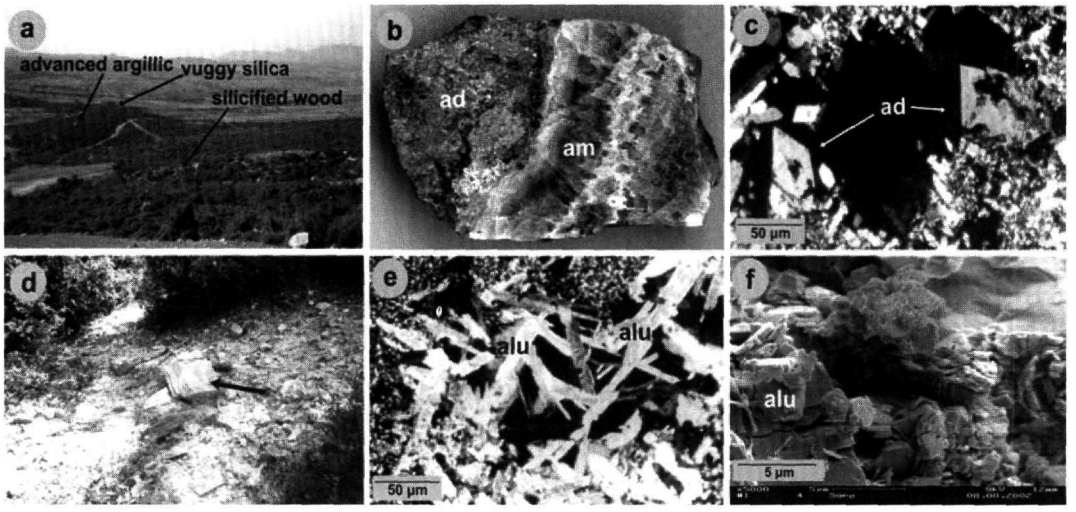

Figure 4 - (a) Silicic alteration (vuggy silica) surrounded and underlying by advanced argillic (quartz-alunite, quartz-kaolinite) and sericitic (quartz-sericite-kaolinite) alteration). Location of silicified wood at Kassiteres area; (b) handspecimen showing colloform banding between amethystine and chalcedonic silica and quartz-adularia rich wallrock alteration (10 cm long); (c) idiomorphic adularia crystals (ad) from the quartz-adularia alteration zone of a dacitic andesite (+ nicols); (d) silicified wood within kaolinite altered tuff-breccia; (e) laminated alunite crystals of replacement origin and quartz, west of Kassiteres (+ nicols); (f) Platy alunite from the wallrock alteration of tuff-breccia hosting silicified wood

4.2. Limnos island

4.2.1. Regional geology

The geology of Limnos island is characterized by a sedimentary basement including molassic deposits of Middle Eocene - Lower Miocene age, covered by volcanic products (lava domes, flows and pyroclastics) of Lower Miocene age and by an Upper Quaternary sedimentary formation (Davis 1960, Roussos 1993, Innocenti *et al.* 1994). A subvolcanic body of quartz monzonitic composition intrudes the volcanics and sediments in the southern part of Fakos peninsula (Fig. 1b). Intense hydrothermal alteration and quartz veining in Fakos area (Voudouris and Skarpelis 1998) are very similar to those described from Kassiteres in Evros region.

Most of the island is covered by volcanic rocks, subdivided (according to Innocenti *et al.* 1994) into three major units: Katalako, Romanou and Myrina Units. The Romanou Unit is the main host of the petrified woods in Limnos island. It consists of up to 160 m thick pyroclastic flow deposits, which extent over broad areas mainly around the Moudros gulf (Fig. 1b). This unit (intercalated between the Katalako and Myrina units) is dominated at the base by white-colored pyroclastic flows, rich in lithic components and pumiceous fragments, followed by intercalations of ignimbrites, volcanic breccias and pyroclastis flows. The pyroclastic rocks of the Romanou Unit are classified as K-rich dacites to latites and are radiometrically dated as 19.8 Ma old (Innocenti *et al.* 1994).

4.2.2. Moudros-Roussopouli-Varos-Portianou

Silicified wood-bearing pyroclastic beds are abundant on the eastern part of Limnos island (Figs 1b, 5). During this study three broad areas were examined, namely those of south Portianou, the Varos-Roussopouli and Moudros-Roussopouli. The stratigraphy in these areas consists of tuffitic layers at the base, overlain by volcaniclastic material (Figs 5a, b, d). In places lava domes and flows penetrate the pyroclastics along the same orientation (NE-SW) as the fault zones in the area.

The broad Moudros-Roussopouli area is characterized by abundant manifestations of hydrothermal activity, similar to those of Evros region. The following hydrothermal alteration zones were distinguished: silicic, advanced argillic and argillic (smectite-kaolinite). The silicic alteration zones (Fig. 5f) are wedge shaped and related to the fault systems developed on the area trending N70E and N40W. It grades outwards to advanced argillic (alunitic), argillic (smectite-kaolinite) alteration and then to fresh rock. The silicification is microcrystalline, massive with colours varying between white, grey and black, the later due to the presence of disseminated pyrite and marcasite. Alunite and anatase are minor constituents of the silicic alteration zone. The silicic zones are crosscut by several hydrothermal breccia bodies, consisting of angular silicified fragments surrounded by an iron oxide-rich matrix (Fig. 5i). In the silicic alteration zone no fossilized wood have been observed. The alunite zone (sample M2, Table 1) is composed of silica polymorphs, natroalunite, natrojarosite, and kaolinite (Figs 3e, f). Acicular alunite crystals (Fig. 5j) occur together with quartz, kaolinite and pyrite as replacements of plagioclase, amphiboles, biotite and pyroxene phenocrysts. Hydrothermal breccias also occur within the alunite zone. The assemblage kaolinite-smectite-pyrte is well developed both laterally, as well as beneath the alunitic zone.

Silicified wood occur in two distinct environments:

A) In slighly altered (argillic alteration) pyroclastics, and typical examples are found in Varos and Portianou. Near Varos village several meters long trunks occur. The Portianou (and also Moudros) localities include in situ silicified wood hosted within the pyroclastics (Fig. 5c).

B) In several layers of opaline, "silica sinter"-similar, silicification extending from Moudros to Roussopouli. The fossiliferous zones [already described by Papp (1953)] are intercallated between the pyroclastic beds and are up to 3 m thick each. At least six silica sinter horizons have been recognized (Fig. 5d). According to Papp (1953) these horizons represent thin bedded lacustrine-

able 1 – Representative XRF analyses of silicified wood and wall-rocks from Evros and Limnos areas

Fyl7a	Fyl7b	Fyl7c	KassA1	KassA2	KassA3	M-2	M7b	M14a	M14b
70.20	96.15	76.41	96.22	97.01	70.21	56.00	93.87	93.20	96.30
11.84	0.00	12.36	0.25	0.03	18.69	14.83	0.05	0.00	0.00
0.92	0.09	0.74	0.70	0.16	0.18	1.18	2.55	1.77	0.04
0.05	0.00	0.01	0.00	0.00	0.00	0.00	0.01	0.00	0.00
0.14	0.01	0.35	0.04	0.01	0.01	0.03	0.01	0.03	0.01
1.78	0.06	0.39	0.06	0.07	0.15	0.27	0.09	0.10	0.05
1.65	0.08	0.49	0.07	0.06	0.10	1.08	0.12	0.08	0.07
4.17	0.00	2.44	0.04	0.00	0.07	2.17	0.03	0.00	0.00
0.12	0.00	0.21	0.01	0.00	0.53	0.65	0.00	0.00	0.00
0.01	0.01	0.01	0.01	0.03	0.32	0.38	0.03	0.00	0.01
0.06	0.02	0.02	0.02	0.01	0.07	16.08	0.04	0.02	0.02
8.2	1.73	5.59	1.4	0.78	7.67	21.03	1.89	2.26	1.05
99.31	98.14	99.13	98.83	98.17	98.33	99.42	98.73	97.48	97.55
798	0	620	47	10	668	2288	197	47	14
56	0	16	0	0	41	164	11	1	0
22	31	7	40	36	7	36	57	111	46
12	0	6	2	2	14	15	3	1	1
32	0	12	0	4	28	100	0	16	7
9	7	10	9	6	0	2	8	5	6
20	0	2	1	0	9	48	0	0	0
52	0	15	0	0	128	80	0	0	0
262	0	94	0	0	14	24	1	0	1
161	1	46	7	4	1964	1637	20	5	4
12	0	11	0	0	10	19	0	0	1
4	0	5	0	0	14	5	3	3	1
16	5	28	6	6	139	119	28	8	1
18	0	12	1	0	9	6	0	0	0
22	0	13	0	0	0	0	26	31	0
85	0	141	2	0	89	466	0	0	0

trace elements in ppm; $Fe_2O_3^*$= total iron as Fe_2O_3; Lyk5b: zeolitic altered acid volcanic rock, Fyl7a: zeolitic altered (mordenite+adularia)
: Avgo-Pefkonas, Fyl7b: silicified wood composed of opal-CT and quartz from Avgo-Pefkonas, Fyl7c: zeolitic altered matrix (quartz+adu
Avgo-Pefkonas. KassA1: silicified wood from Kassiteres, KassA2: silicified wood from Kassiteres, KassA3: advanced argillic altered (qu
;iteres. M2: advanced argillic altered rocks containing quartz+natrolalunite from Moudros, M7b: silicified wood, M14a: Red opal horizon
ored silicified wood from the previous horizon, M21a: black colored silicification with plant material, M21c: silicified wood

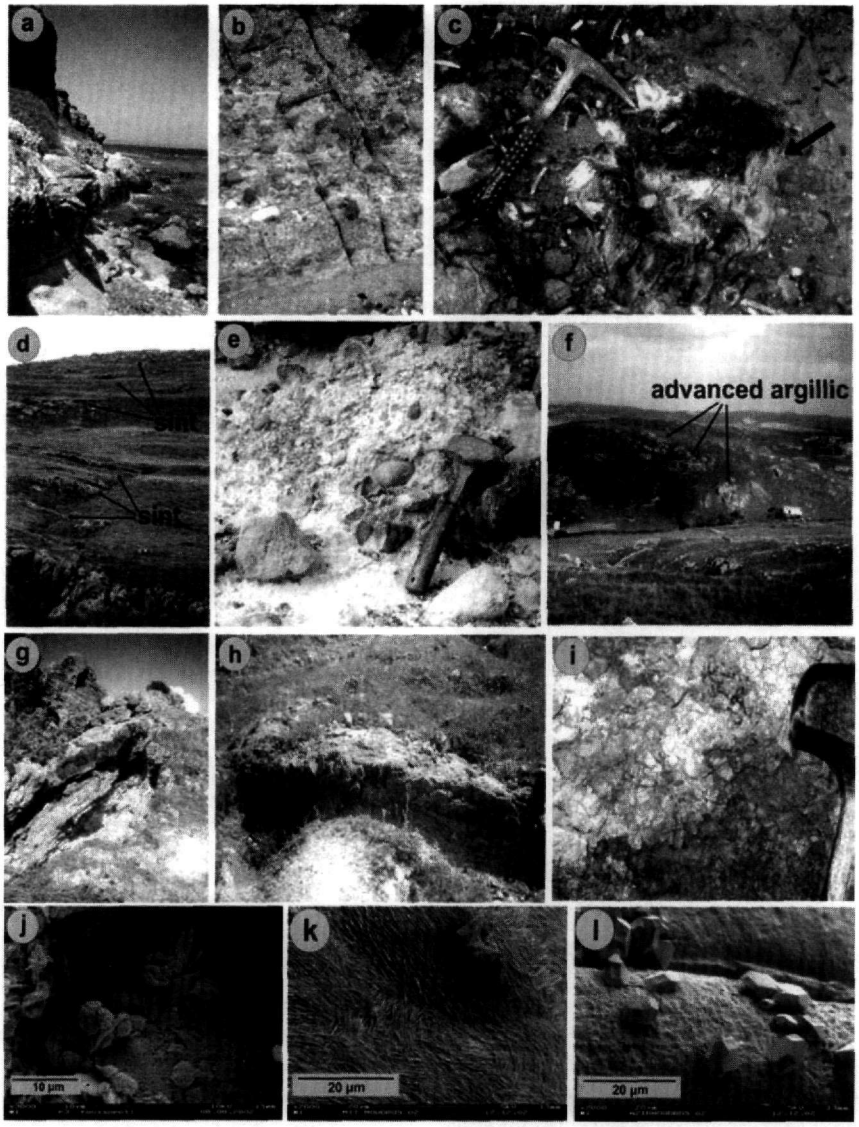

Figure 3 - Portianou locality. (a) A succession from volcano-sedimentary (sandstone like tuffite) to volcaniclastic material made up by angular to subangular andesite-dacite fragments. (b) Close-up to the upper volcaniclastic formation as in Fig. 4a, (c) Silicified wood within the basal tuffite. Moudros-Roussopoulis area: (d) Volcanic agglomerate formation at the base (up to 20m thick) is overlain by pyroclastic flow units. Several fossiliferous opalized "sinter" horizons (sint) are intercalated between relatively fresh volcanics (e) Close-up of the basal volcanic agglomerate formation from previous figure. (f) View towards Roussopouli. Hypogene silicic and advanced argillic alteration zones. (g) Tilted opalized horizon rich in silicified wood overlies alunitized pyroclastics. (h) Opalized horizon including silicified wood overlies pyroclastic material (i) Hydrothermal breccia composed of silicified and alunitized rock fragments within a matrix rich in Fe-oxides. SEM-micrographs of various mineral phases from Roussopouli-Moudros area. (j) Alunite crystals in vugs of advanced argillic altered rocks at Roussopouli (k) Lepispheres of opal-CT recrystallized after amorhous silica (opal-A) in advanced argillic altered hydrothermal breccia, near Moudros (l) Tridymite (?) crystals on silicified wood from Moudros

fluviatile intercalations between the pyroclastic formations and were deposited during erosional periods that lasted between the volcanic activity phases. The pyroclastic hostrocks demonstrate varying degrees of hydrothermal alteration. In some places the fossiliferous horizons overly an alunitic alteration zone and hydrothermal breccias rich in natroalunite (Fig. 5g) whereas the wood occurs as breccia fragments. Usually the opaline horizon is intercalated between fresh rocks. Perfectly preserved leaves indicate quiescent conditions during the fossilization procedure. The fossiliferous silicified horizons are crosscut by later chalcedony veins. Silicification in both the "silica sinter", as well as within the wood material, varies from red and white, to black colour. The white colour resulted of total depletion of iron oxides (see sample M14b, Table 1). In general there is a depletion of major and trace elements in silicified sinter and wood. Elevated Fe_2O_3 content (up to 2.6 wt%) is related to the presence of iron oxides and contributes to the red colour of the silicification (Table 1). XRD-studies indicated mainly quartz as the stable silica phase within the wood. Transformation of amorphous silica to opal-CT and then to quartz is postulated based on XRD and SEM studies (Fig. 5k).

The field observations indicate that there is a close spatial and probably genetic relationship between the silicic-alunitic alteration zones and the fossiliferous silica layers. In any case there is a lateral transition and evolution of the above mentioned alteration zones laterally and upwards in stratiform fossiliferous silicification.

5. Discussion-Conclusions

Recent studies confirmed that the silicification of wood begins as a process of open space filling and not as a replacement of organic material by SiO_2 (Roessler 2001). It seems to be controlled by diffusion of microscopic particles of $Si(OH)_4$, (molecules) within the wood structure. Under this aspect the deposition of SiO_2 could be resulted without destruction of the organic structure of the wood. However in advanced stages of silicification a removal of organic material is also possible (Roessler 2001).

This study demonstrates a close genetic relationship between the silicification processes leading to petrified forests in Evros and Limnos, and the hydrothermal alterations which were developed during the waning stages of volcanic activity. Alterations typical for magmatic-hydrothermal systems cover extended areas in Evros region (Kassiteres-Sapes, Loutros-Pefka, and the Stavros-Gerakina locality northwest of Lefkimi) and Limnos island (Fakos peninsula and the Moudros-Roussopouli areas. These alterations have a mineralogy which indicates reaction of the volcanic rocks with acid sulfate-chloride waters of magmatic-hydrothermal origin, with pH values even smaller than 2 and at elevated temperatures (according to White and Hedenquist 1995). In addition these fluids were generated after condensation of magmatic vapors rich in SO_2 and HCl in groundwater present within the volcanic edifices. The late development of quartz-chalcedony rich veins accompanying a K-feldspar (adularia) alteration of the wall-rocks (Kassiteres, Lykofi-Lefkimi), is characteristic of deposition by more reduced and neutralized geothermal fluids. This indicates an evolution from a reactive magmatic-hydrothermal system dominated by magmatic gases, to a geothermal system that is dominated by meteoric and/or seawater, in common with many other places in the world (Henley and Ellis 1983). Figure 6 shows the depositional environment of silicified wood studied, within a volcanic-hydrothemal framework.

The silicified wood observed south of the Kassiteres area, occurs within argillically altered (kaolinite alteration) tuffs and in close proximity to silicic and advanced argillic alteration zones. Available data indicate that silicification of wood in Kassiteres took place in a two-stage procedure: firstly by slightly acid fluids as they were migrating away from the advanced argillic alteration zone, and secondly by more reduced and neutralized fluids as late quartz-chalcedony veins crosscuting the wood. A similar process has been also described for the silicification of wood in Chemnitz, Germany (Roessler 2001).

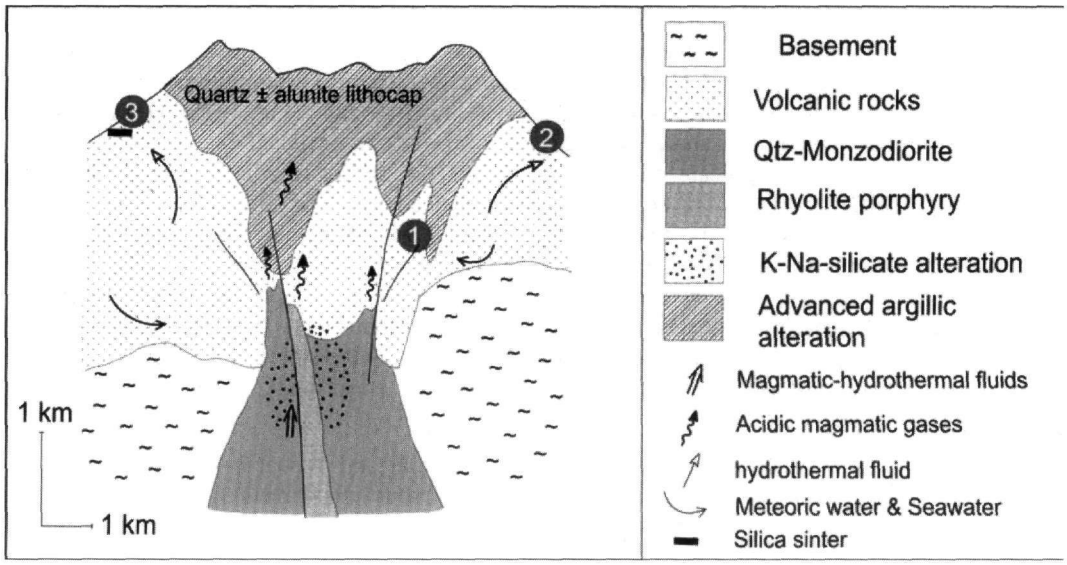

Figure 4 - Hypothetical model demonstrating depositional environment of silicified wood occurrences in Kassiteres (1), Lykofi-Fylakto-Lefkimi (2) and Limnos island (3)

In contrast to Kassiteres area, the fossilized occurrences of Fylakto, Lefkimi, etc., are lying some km away from the supposed highly reactive magmatic-hydrothermal center near Stavros locality. Responsible for the silicification of trees were reduced and near neutral pH fluids as demonstrated by the alteration mineralogy of the broad area (zeolitic alteration). Reduced and near neutral pH fluids were also depositing the abundant quartz-chalcedony veins crosscuting all the formations in the broad Fylakto-Lykofi-Lefkimi area.

In Limnos island, the Fakos peninsula has been recognized as a Cenozoic magmatic-hydrothermal center with characteristics comparable to those of Kassiteres area. The central parts of the volcanic edifice are occupied by silicic and advanced argillic alteration zones of magmatic-hydrothermal origin. The silicified wood occurs in the periphery of Fakos but in very close proximity to large scale fault zones that facilitated the circulation of hydrothermal fluids. Although the petrified trunks found within relatively fresh pyroclastics, could have been formed partly by devitrification processes by near neutral pH fluids, a hydrothermal deposition of silica is established for the wood present in the silicified horizons between Moudros and Roussopouli. The silicified horizons probably correspond to swamp depressions, which were flooded by the upwelling hydrothermal fluids. Field observations indicate a scenario of contemporaneous formation between the horizons and the silicic and advanced argillic alteration zones in a hot spring environment. The horizons probable represent lateral surface manifestations of the above alteration zones. Neutralization was resulted as the fluids migrated away from the acidic outflow zones. Alternatively some of the horizons could represent true silica sinter formations (like the Rhynie chert in Schottland, Rice *et al.* 2002), deposited from near neutral fluids and not directly related to the silicic and advanced argillic alteration zones. This scenario requires distinct periods of formation and is a matter of further investigation. The Evros and the Moudros-Roussopouli areas represent unique natural monuments in Greece, comparable to the Lesvos island petrified forest (Velitzelos *et al.* 2002) and belong to the Greek mineralogical and geological heritage. Ongoing work aims to constrain the details about the mechanisms resulting in the silicification of wood in Evros and Limnos regions.

6. Acknowledgments

Mrs G. Doerfner is especially thanked for the XRD measurements in the University of Ulm.

7. References

Christofides, G., Soldatos, T., Eleftheriadis, G., and Koroneos, A., 1998. Chemical and isotopic evidence for source contamination and crustal assimilation in the Hellenic Rhodope plutonic rocks, *Acta Vulcanologica*, 10, 305-318.

Davis, E., 1960. The volcanic rocks of Lemnos island, *Ann Geol Pays Hellen,* 11, 1-82.

De Boorder, H., Spakman, W., White, SH., and Wortel, MJR., 1998. Late Cenozoic mineralization, orogenic collapse and slab detachment in the European Alpine Belt, *Earth Plan Sc Lett*, 164, 569-575.

Del Moro, A., Innocenti, F., Kyriakopoulos, C., Manetti, P., and Papadopoulos, P., 1988. Tertiary granitoids from Thrace (Northern Greece): Sr isotopic and petro- chemical data, *N Jb Miner Abh,* 159, 113-135.

Fytikas, M., Giuliani, O., Innocenti, F., Manneti, P., Mazzuoli, R., Peccerillo, A., and Villari, L., 1979. Neogene volcanism of the Northern and Central Aegean region, *Ann Geol Pays Hell*, 30, 106-129.

Fytikas, M., Innocenti, F., Manneti, P., Mazzuoli, R., Peccerillo, A., and Villari, L., 1984. Tertiary to Quaternary evolution of volcanism in the Aegean region, In J.E. Dixon and A.H.F. Robertson (eds), *The geological evolution of the eastern Mediterranean, Geol. Soc. Spec. Publ.,* Oxford, 17, 687-699pp.

Henley, R.W., and Ellis, J., 1983. Geothermal systems ancient and modern: A geochemical review, *Earth Sci Rev*, 19, 1-50.

Innocenti, F., Kolios, N., Manetti, O., Mazzuoli, R., Peccerillo, G., Rita, F., and Villari, L., 1984. Evolution and geodynamic significance of the Tertiary orogenic volcanism in northeastern Greece, *Bull Volcanol*, 47, 25-37.

Innocenti, F., Manetti, O., Mazzuoli, R., Pertusati, P., Fytikas, M., and Kolios, N., 1994, The geology and geodynamic significance of the island of Limnos, North Aegean Sea, Greece, *N Jb Geol Palaont Mh*, 11, 661-691.

Kopp, C.O., 1965. Geologie Thraziens III. Das Tertiar zwischen Rhodope und Evros, *Ann Geol. Pays Hell*, 16, 315-362.

Krohe, A., and Mposkos, E., 2001. Structural evolution and exhumation history of the Rhodope UHP-HP metamorphic province (Northern Greece), *Bull Geol Soc Greece*, 34, 75-82.

Kyriakopoulos, K., 1987. A geochronological, geochemical and mineralogical study of tertiary plutonic rocks of the Rhodope massif and their isotopic characteristics. *Unpubl. Ph.D. thesis*, Univ. Athens, 343pp. (in greek)

Melfos, V., Vavelidis, M., Christofides, G., and Seidel, E., 2002. Origin and evolution of the Tertiary Maronia porphyry copper-molybdenum deposit, Thrace, Greece. *Mineral Deposita*, 37, 648-668.

Papadopoulos, P., 1982. *Geological map of Greece, Maronia sheet*, 1:50.000, IGME, Athens.

Papp, A., 1953. Erläuterungen zur Geologie der Insel Lemnos, *Ann Geol Pays Hell*, 1-33.

Pecskay, Z., Eleftheriadis, G., Koroneos, A., Soldatos, T., and Christofides, G., 2003. K/Ar dating, geochemistry and evolution of the Tertiary volcanic rocks (Thrace, northeastern Greece). In D. Eliopoulos *et al.* (eds), *Mineral Exploration and Sustainable Development*, Millpress Publications, Rotterdam. 1229-1232pp.

Pe-Piper, G, Christofides, G., and Eleftheriadis, G., 1998. Lead and neodymium isotopic composition of Tertiary igneous rocks. of northeastern Greece and their regional significance, *Acta Vulcanologica*, 10, 255-263.

Rice, C.M., Trewin, N.H., and Anderson L.I., 2002. Geological setting of the early Devonian Rhynie cherts, Aberdeenshire, Scotland: an early terrestrial hot spring system, *Journal Geol. Society London* 159, 203-214.

Roessler, R., 2001. Der Versteinerte Wald von Chemnitz, *Museum für Naturkunde Chemnitz,* 205pp.

Roussos, N., 1993. *Geological map of Greece, Myrina and Moudros sheets, Limnos island*, scale 1:50.000, I.G.M.E., Athens.

Skarpelis, N., Economou, M., and Michael, K., 1987. Geology, petrology and polymetallic ore types in Tertiary volcanosedimentary terrain, Virini-Pessani-Dadia area, West Thrace (Northern Greece), *Geol. Balc*, 17(6), 31-41.

Velitzelos, E., and Zouros, N., 1997. The petrified forest of Lesvos – Protected natural monument, Engineering Geology and the environment, In P. Marinos, Koukis, Tsiambaos and G. Stournaras (eds), Balkema Publications, 3037-3043pp.

Velitzelos, E., Mountrakis, D., Zouros, N., and Soulakelis, N., 2002. *Atlas of the Aegean geological monuments,* (Ed. Aegean Ministry), 351pp.

Velitzelos, E., Velitzelos, D., Iamandei, S., and Iamandei, E.P., 2006. Tertiary petrified palm trees in Greece, *7th European Paleobotany-Palynology Conference, 6-16 Sept., Prague*, 150p.

Voudouris, P., 1993. Mineralogical, geochemical and fluid inclusion studies on epithermal vein type gold-silver mineralizations at Kassiteres/Sapes, (NE-Greece), *Unpub PhD thesis,* Univ Hamburg, 218pp.

Voudouris, P., and Skarpelis, N., 1998. Epithermal gold-silver mineralizations in Perama (Thrace) and Lemnos, *Bull Geol Soc Greece*, 32(3), 125-135. (in Greek)

White, N.C., and Hedenquist, J.W., 1995. Epithermal gold deposits: Styles, characteristics and exploration, *Soc Econ Geol Newsletter*, 23, 9-13.

Δελτίο της Ελληνικής Γεωλογικής Εταιρίας τομ. XXXX, 2007
Πρακτικά 11ου Διεθνούς Συνεδρίου, Αθήνα, Μάιος 2007

Bulletin of the Geological Society of Greece vol. XXXX, 2007
Proceedings of the 11th International Congress, Athens, May, 2007

THE BASEMENT FAULTS SYSTEM IN THE NORTHWESTERN ARABIAN PLATE, JORDAN

Al-Zoubi A. S.[1]

[1] *Al-Balqa' Applied University, Faculty of Engineering, Surveying and Geomatics Department, Salt, Jordan Al-Salt, 19117 Jordan, aalzoubi@go.com.jo*

Abstract

Gravity and magnetic data are powerful tools utilized to detect the faults (lineaments). In Jordan, still the detailed analyses and reprocessing based on images, would effectively generate shaded relief of second derivative of potential filed, as the contour gravity and magnetic maps itself yield additional faults location. Accordingly new basements faults map focuses on faults crisscrossing Jordan that scrutinize the structural condition of Jordan indicating that the faults belong to distinct groups with different directions. However, these groups are representing a system of an "Orthogonal and Diagonal" network deem to be part of the pragmatic fracture system of the earth. It has been observed that the striking characteristics of these faults expressed by their (1) faults extension relatively extended for long distances and (2) intersection of these systems with each other possibly will help in defining their relative ages. Comparing the results of the current study with those of previous investigations provide an evidence to deem that these known faults in Jordan as supported by the geological or geophysical studies coincide in their positions with faults of linear characteristics as the new interpretation of the potential field maps indicates. However, a single system of this network shows a group of identical characteristics, as each system was formed at the same period of time, yet these different fault systems are concordant with the different phases of the tectonic activities of the region.
Key words: *Potential Field, Dead Sea, Shaded Relief, Pragmatic Fracture.*

Περίληψη

Τα βαρυτικά και τα μαγνητικά δεδομένα αποτελούν ικανά εργαλεία στην ανίχνευση ρηγμάτων. Στην Ιορδανία οι ανάλογες λεπτομερείς αναλύσεις και η επεξεργασία εικόνων παρήγαγαν αποτελεσματικά το σκιασμένο ανάγλυφο. Ο νέος χάρτης υπόγειων ρηγμάτων εστιάζει στα ρήγματα που διατρέχουν Ιορδανία, και διερευνά τις δομικές συνθήκες της περιοχής υποδεικνύοντας ότι τα ρήγματα ανήκουν σε ευδιάκριτες ομάδες με διαφορετικές διευθύνσεις. Αυτές οι ομάδες αντιπροσωπεύουν ένα σύστημα «Ορθογώνιου και Διαγώνιου» δικτύου που αποτελεί τμήμα του πραγματικού συστήματος διάρρηξης της Γης. Έχει παρατηρηθεί ότι, τα ιδιαίτερα χαρακτηριστικά αυτών των ρηγμάτων που εκφράζονται από (1) εκτάσεις μεγάλου εύρους και (2) αλληλοτεμνόμενα συστήματα, πιθανόν να συντελέσουν στον προσδιορισμό των σχετικών ηλικιών τους. Συγκρίνοντας τα αποτελέσματα της παρούσας μελέτης με αυτά προηγούμενων ερευνών προκύπτει ότι τα γνωστά ρήγματα της Ιορδανίας με βάση τις σχετικές γεωλογικές και γεωφυσικές έρευνες, συμπίπτουν με ρήγματα γραμμικών χαρακτηρι-

στικών, όπως υποδεικνύει η νέα ερμηνεία των χαρτών δυναμικών πεδίων. Κάθε σύστημα του δικτύου αποτελεί μία ομάδα με ίδια χαρακτηριστικά, καθώς διαμορφώθηκε σε συγκεκριμένη χρονική περίοδο, ενώ τα διαφορετικά συστήματα σχετίζονται με διαφορετικές φάσεις της τεκτονικής δραστηριότητας στην περιοχή.
Λέξεις κλειδιά: *Δυναμικό Πεδίο, Νεκρά Θάλασσα, Σκιασμένο Ανάγλυφο, Πραγματικός Τεμαχισμός.*

1. Introduction

Jordan is situated at the northwestern side of the Arabian Plate, along the eastern flank of the ancient Tethys Ocean in the western side of the Dead Sea Transform (Fig. 1). Dead Sea Transform extends for more than 1000 km from the northern end of the Red Sea, where the crust is currently extending to the Taurus zone plate collision in Europe (Fig. 1). Eversince the time of its formation, less than 20 My ago, the Dead Sea Transform Fault has undergone about 105 km left-lateral horizontal displacement (Joffe and Garfunkel 1987, Freund *et al.* 1970, Garfunkel 1981, Hatcher *et al.* 1981 Quennel 1958, Girdler 1985), leading to have Jordan situated at the transition zone between the stable part of the Arabian Plate and the unstable area of the Dead Sea Transform Fault. Lovelock (1984) suggested that the crust in the northwestern part of the Arabian Plate (beneath Jordan) has been fragmented into stable blocks separated by mobile zones. While the crystalline basement and sedimentary cover holds a block structure with faults to serve as blocks boundaries. Despite of its significant geodynamic settings, the Jordan block structure and its boundaries has been subjected to limited investigation. Although several studies on the sedimentary basin of Jordan have been conducted, most of these tend to focus on the large basins such as Dead Sea, Al-Azraq, Wadi Sirhan, El Jafer and Risha Basin (Fig. 2) particularly in reference to oil exploration which were largely based on seismic investigation. These studies are still limited and inaccessible to public for further evaluation.

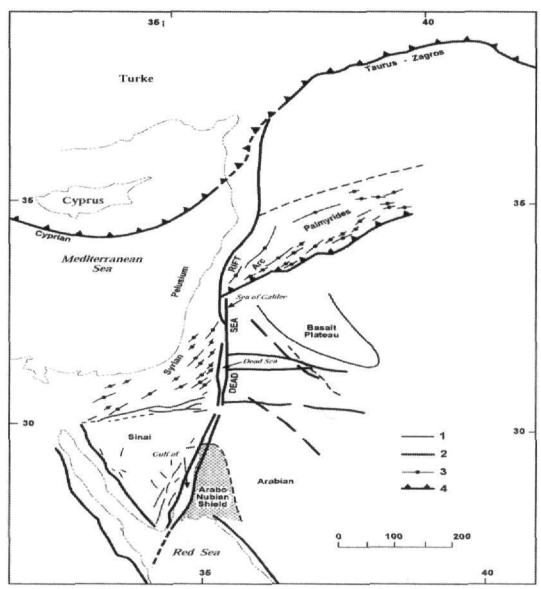

Figure 1 - Generalized tectonic setting of the Middle East showing the Arabian plate, Sinai sub-plate, the Dead Sea Transform (including Gulf of Aqaba, Dead Sea, and Sea of Galilee) and Palmyrides zone. 1—Faults; 2—Main Faults; 3—Fold Axes; 4—Main Thrust Fronts (modified after Ben-Avraham and Grasso 1991, Bender 1974)

The Northwestern Arabian block (Jordan) has been generally regarded as structurally featureless, except for a few well-acknowledged faults. Jordan Geological Map (modified after Bender 1968) displayed only few sets of faults (Fig. 3) trending N-S and NW–SE and E-W striking short faults in the central part of Jordan. The significance of these faults is due to the fact that they control the mineral deposits, oil and gas within several sedimentary basins and groundwater flows. Similarly, there are other natural resources (mineral deposits, hydrocarbon and groundwater flow) scattered at various geologic sites associated with fluid conducting faults.

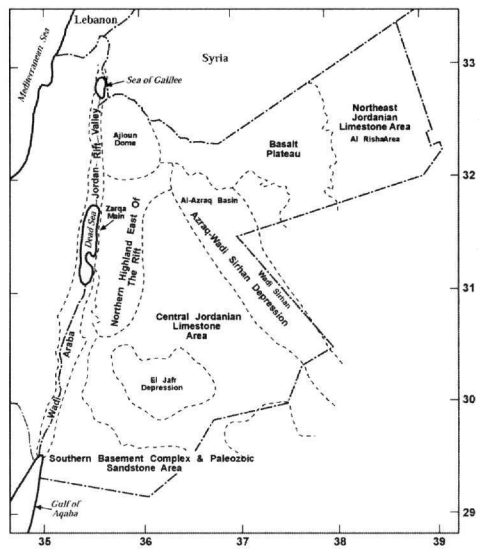

Figure 2 - Geologic–physiographic provinces of Jordan (after Bender 1974)

Therefore in order to detect subsurface faults more precisely, geophysical methods are considered as a powerful tool, i.e., potential methods (gravity and magnetic) or seismic process.

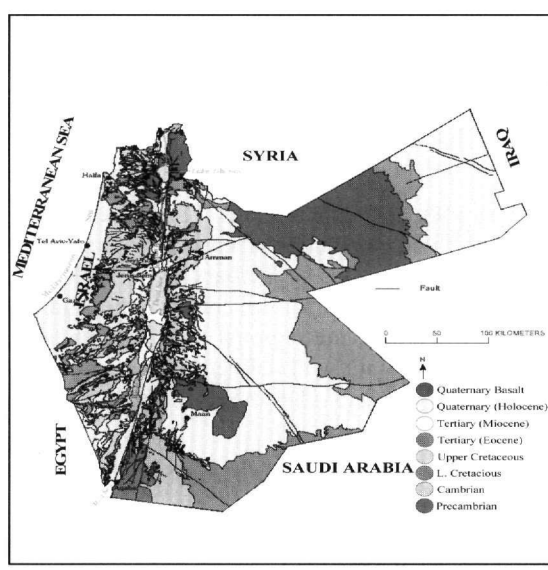

Figure 3 - Regional Geology map of Jordan

The present study utilizes potential field methods over a broad region as an attempt to describe the faults structure of Jordan. The steep basement faults in Jordan platform tends to be more subtle and

exerts a considerable Syn-and Post-depositional influence on the sedimentary cover. However, the faults and fractures are occasionally following the older orogenic basement structures that commonly cut across them. Nevertheless, the steep and straight faults in Jordan are commonly expressed as subtle potential-field lineaments, which might be gradient zones or alignments of separate local anomalies in various types and shapes, or aligned breaks or discontinuities in anomaly pattern.

2. Geological Setting

The oldest known rocks of Jordan, classified as a Pre-Cambrian Aqaba Granite Complex, outcrops in its southwestern part. Since the Pre-Cambrian age the granitic shield is predominantly a land surface ringed by seas receiving sediment from the land. Generally, Jordan tectonic history is divided into three phases: the Gondwana, Syrian Arc, and Rift phases (Dewey *et al.* 1973). During the Gondwana phase (Cambrian – Early Cretaceous), Jordan was on a spot near the northern margin of the Gondwana paleo-continent. Tectonically, the area was relatively stable and the sedimentation was dominantly continental type, interspersed with rather minor but widespread marine incursions. However, the Lower Palaeozoic rocks of Cambrian, Ordovician and Silurian age are outcropping in southern Jordan and on the western side of the Dead Sea-Jordan Rift Valley. Several wells have encountered Upper Carboniferous and Permian rocks of the pre-rift sequence, indicating a variety in depositional environments from continental clastic to shallow marine carbonate. In fact, this general sedimentation pattern continued into the Triassic and Early Jurassic, yet its sedimentation became increasingly more aquatic. The shoreline position from Triassic to Late Cretaceous remained roughly unchanging across central Jordan with the open sea lying to the northwest.

During the Late Cretaceous, it has been noticed that subduction of the Neo-Tethyan oceanic lithosphere was initiated at the north. Whereas, the resulting compression along the southern margin of the Neo-Tethys indicated within locally abducted ophiolites and folding in the Syrian Arc trend. The Syrian Arc portrays a sigmodial trend extending from the northern Sinai northward into Syria (Fig. 1), following to the trend of the Late Cretaceous continental margin. However, the extension within the Arabian Plate during the Late Cretaceous (Bender 1974, Lovelock 1984) caused a series of northwest-trending basins such as Al-Azraq and Wadi Sirhan Basins (Fig.2). At later stages, a strike-slip faulting in the Neogene's have modified the overall configuration and structural style of the Al-Azraq and Wadi Sirhan Basins, then offset and modified the fold geometry of the Syrian Arc trend. Various transgressions from the northwest to the southeast were repeated several times during the Mesozoic. Moreover, between the middle Jurassic and Early Cretaceous the volcanism was active in the western part of Jordan. Likewise a mafic to felsic dykes and sills occurred in the Wadi Araba region are cutting across the Mesozoic sedimentary rocks (Bender 1974).

During the Late Oligocene - Early Miocene, the left lateral movement along the Dead Sea – Jordan Rift Valley was initiated along with coarse lenticular unsorted conglomerates which begin to appear in the section overlying Late Cretaceous or Tertiary units in the eastern Wadi Araba area. However, they show unconformable relationship at several localities indicating uplift and probably tectonic activity (Bender 1974). Therefore, the regional fault system consists of a series of three major west-stepping, en-echelon faults, with well defined pull-apart basins having formed at each of the major offshoots, i.e., the Gulf of Aqaba, Dead Sea Basin and Sea of Galilee Basin (Figs 1, 2).

An apparent total strike-slip displacement along the Dead Sea Rift system estimated at 105 km (Freund *et al.* 1970). Matching the structural and sedimentary features offset across the fault zone, Quennel (1958) considered that the separation took place at two stages; the first stage expanding to 63 km took place during the Miocene, whereas the second stage took place during the late Pleistocene. Furthermore, Garfunkel (1981) and Freund *et al.* (1976, 1970) have reached a similar conclusion through measuring a contemporaneous motion in the adjoining Red Sea. They recommended that the second stage should have taken place 4-5 My ago leading to the Dead Sea Rift

opening whereas more than 3.5 km of evaporites were deposited, probably during the late Miocene to early Pleistocene (Bender 1974). The total basin fill within the Dead Sea basin reaches more than 10 km (Ginzburg and Ben-Avraham 1997). Measurements based on gravity data, and the Dead Sea basin represent a long pull– apart nature of 135 km long, 10-20 km wide (ten-Brink *et al.* 2001, 1999, 1993) and at least 8.5 km deep. Some localities show 7.250 km Pliocene salts (Al-Zoubi and ten-Brink 2001). Consequently, Al-Zoubi and ten-Brink (2001) estimated the thickness of the original salt layer to be not less than 2.3 km.

The deposits of Quaternary age in Jordan reflect a continuous uplifting and retreating of the marine environment, with an extensive mafics volcanic and shallow intrusive activity occur as localized flows and plugs. The plateau flood basalts with primitive chemistry appear to reflect a rapid propagation of fractures into the mantle, followed by rapid extrusion (Barberi *et al.* 1979). Based on the geological history described above and other geological, paleogeographic and stratigraphic evidence, the territory of Jordan can be subdivided into seven major geological-physiographic provinces as given in Figure 2.

3. Geophysical Data

The sedimentary basin in Jordan has been explored and investigated over the last four decades. Numerous land magnetic, gravity and seismic surveys were carried out as a part of oil exploration in the region. Gravity data in Jordan were compiled by the Natural Resources Authority, summarized from various surveys recorded at different times using different parameters, technologies and specifications. Considerably, the gravity-data standards of one station per 4 km are usually maintained in remote areas of Jordan, whereas the lineaments with enough length are detectable with careful anomaly enhancement. In addition, the aeromagnetic survey was completed in the 1981 along grid flight lines in EW and NS directions. The geophysical data in some places were supplemented by borehole data which provided valuable information about a complex architecture of the basins. To refine the techniques of detecting faults we have created a magnetic and gravity maps of Jordan, with the data processed to highlight subtle lineaments. The new maps are correlated with the geological maps (scale 1:50.000) in particular those may be related to brittle faults.

4. Magnetic Map

The aeromagnetic map of Jordan (Fig. 4) is dominated by large amplitude, low frequency anomalies expect in a few areas. Recording a strongly contrasting pattern of short wavelength and high frequency anomalies of low amplitude related to surface mafic rocks (basalt) which are highly magnetic occurring east of the Dead Sea in the northeast Jordan. The central, southeastern and eastern part of Jordan tends to produce mostly broad relatively long wavelength anomalies reflecting the thick sedimentary section.

Apparently, the magnetic map of Jordan has a relatively smooth relief except where it reflect the basalt flow. However, there are some large anomalies located in the southwestern, northwestern and central part of Jordan. The anomaly located in the SW Jordan is sharply terminated to the west and linked to the shallow faulted basement. The series of round to elliptical (high and low) in shape anomaly formed lines which facilitate the process of correlating them with the faults. Similarly, an identical shape occurred along Al Karak–Wadi Fiha fault. In the central part of Jordan the low magnetic anomaly strikes about EW and extends across it. It bifurcates eastward, north and south of a large high magnetic anomaly which terminates in east central Jordan and continues eastward into Saudi Arabia (Phoenix 1981). It is worth mentioning that some local intra-sedimentary anomaly sources could be in relevance to depositional concentrations of magnetic minerals. However, in some clastic rocks or in secondary magnetization of sedimentary rocks derived from the circulating brines or the surface's man-made infrastructure may also cause anomaly.

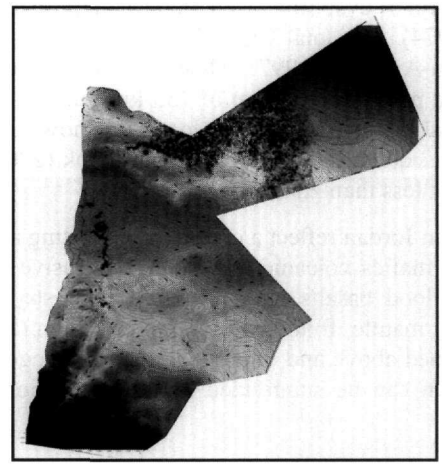

Figure 4 - Total field magnetic map of Jordan (Phoenix 1981). Contour interval is 10 nT

5. Gravity Map

The Bouguer gravity map of Jordan (Fig. 5) outlines large-scale of variations, a difference of 136 mGal was recorded, whereas several trends and anomalies are clearly observed on the Bouguer anomaly map including the followings: (1) north-northeasterly trend gravity anomalies of the order of –20 to –132 mGal were marked at Wadi Araba- Dead Sea- Jordan Valley Rift. The northern parts of the Wadi Araba-Dead Sea-Jordan Valley Rift area dominated by small variations ranging from –20 to –30 mGal, while moderate variations ranging from –50 to –85 mGal were marked in the southern parts. The Bouguer gravity anomaly decreases gradually from both northern and southern parts of the Wadi Araba -Dead Sea- Jordan Valley Rift towards the Dead Sea Basin, suggesting that the Dead Sea Basin sags towards the center (ten-Brink *et al.* 1993, Al-Zoubi and ten-Brink 2002). The lowest Bouguer gravity value was recorded is -134 mGal; (2) the existence of a north-northeasterly trend gravity anomalies, of the order of –35 to +4 mGal are marked the northern Highlands east of the Rift. The anomaly as high as +4 mGal follows the elevated topography of Ajloun uplift. Ajloun uplift is a broad domal structure covered by 4-5 km of predominantly Mesozoic sedimentary strata. However, a model for crust underneath the northern highland shows that the crust is marked with higher density and thicker than that of the transform zone area on the western side. The northeastern plateau on the eastern side indicates that Jordan may have been affected by orogenic processes which have resulted in densification of the crust (Al-Zoubi and Ben-Avraham 2002); (3) a northeast trend of nearly narrow zone high gravity anomalies -40 mGal, is marked the Southern Basement Complex; (4) the high Bouguer gravity anomaly lies in the northwestern part of the Central Jordanian Limestone Area. The anomaly is roughly oval shaped and marked by –18 mGal Bouguer gravity high; (5) a south- southeast negative gradient in regional Bouguer values from –60 mGal to –95 mGal in the southern parts of the Central Jordanian Limestone Area. The negative gradient follows the Tabuk basin in Saudi Arabia; (6) within the area Al-Azraq- Wadi Sirhan Depression, the gravity field ranges from –55 to -80 mGal and maintains a general northwesterly trend; and (7) a northeast positive gradient in regional Bouguer values from –60 mGal in the southern parts of the Northeast Jordanian Limestone Area to -50 mGal in the northeast side and the region northeast of the Basalt Plateau. The positive gradient follows Rutbah uplift in the southeastern parts of Syrian and western Iraq. Remarkably, the Rutbah uplift is a broad domal basement structure covered by 5-6 km of predominantly Palaeozoic sedimentary strata (Al- Zoubi 1992).

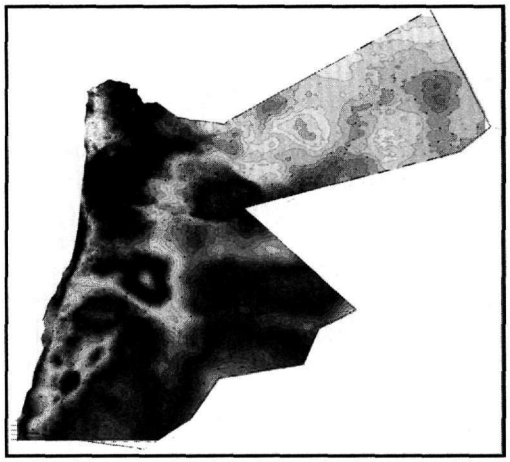

Figure 5 - Bouguer Gravity Map of Jordan (Natural Resources Authority), contour interval 2 mGal

6. Data Preparation

To trace the faults' signatures within a magnetic and gravity maps detailed data processing using a wide variety of anomaly-enhancement techniques and display parameters is essential. The best way is to sort potential anomaly by shape, amplitude, trend and other relevant geological features. However, this is considered as a critical process as some short wave length anomaly produced artificial sources could interfere with geological features. Therefore, the false anomaly (noise) should be suppressed prior to processing. The filtering process or upward data continuation helped to remove the shortwave anomaly and smoothed the data.

The diversity of filtering techniques has been applied to the analyses of potential field data. However the recognition should be to the traditional methods of presentation, principally contour maps, which filter-out much of the original information content of the data connected to geological structure and trend. Therefore, filters have proved effective forms of presentation particularly for regional data. Filters contain data about both anomaly amplitude and anomaly gradient (relief), exploited the inherent ability of the human visual system to interpret intensity and textural information. The latter is significant, particularly as anomaly gradients trend directly to the depth of burial of the causative structures. Nevertheless, the shaded-relief presentations are significance to treat the field as topography illuminated from a particular direction. Possess an additional property of enhancing features which trend roughly perpendicular to the direction of illumination having a sense of enhancing subtle, but often important to lineaments which were not apparent on the original contour maps.

7. Geophysical Fault Detection

The interpretation stage carried out by subdividing Jordan into different zones according to morphology and the level of homogeneity of the magnetic and gravity fields. The magnetic and gravity maps of Jordan shown in (Figs 4, 5) were subdivided into almost homogeneous zones. These zones were sort in accordance with the geological overview of Jordan, particularly with the magnetic contour map (Fig. 4) which clearly shows borders of these zones (Figs 2, 3). The quality of interpretation basically based on the conventional contour maps of the potential field data including total intensity of magnetic map (Fig. 4), Bouguer gravity map (Fig. 5) shaded relief maps of Bouguer gravity (Fig. 6), shaded relief of magnetic map (Fig. 7) and magnetic image map (Fig. 8).

Best visual method to identify lineaments is to view the map in different angles, to view with different orientations. The linear anomaly extends for hundreds of kilometres easily, which could be related to the major faults that are cutting the earth crust. These anomalies are clearly seen at the central, southern and northeastern parts of Jordan (Figs 4-8).

Figure (9) shows the analyses the structural condition of Jordan indicating that these faults are within distinct groups of different directions. These groups signify an orthogonal and diagonal network system that could be considered an integrated part of the regmatic fracture system of earth. Each group of the orthogonal and diagonal network could be subdivided into two systems and consequently results in four sub-systems of main faults as following: (1) N-S direction faults; (2) NW-SE direction faults; (3) E-W direction faults; and (4) NE-SW direction faults. However, the striking characteristics of each of these faults are: (1) an extension of the faults relatively expanding for long distances and (2) intersection of these systems with each other may help in the determining their relative ages.

8. Structural Interpretation

Comparing the results of the current geophysical study with previous investigations indicates that the identified faults in Jordan coincide in their positions with faults of linear characteristics which were defined as a result of the interpretation of potential field maps. A single system of this network displays a group of identical characteristics, taking into account that each system was formed under certain stress of conditions. However, it is possible to be reactivated under different stress fields in different phases of the tectonic activities of the region. Moreover, the distances between faults of a signal system depends on their courses and structures type that intersect them.

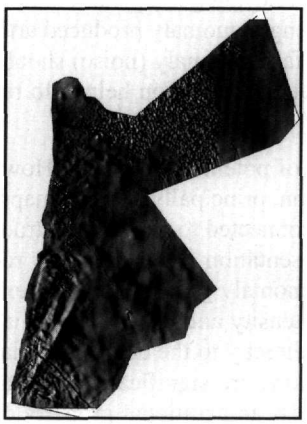

Figure 6 - Bouguer gravity map shaded relief, Jordan

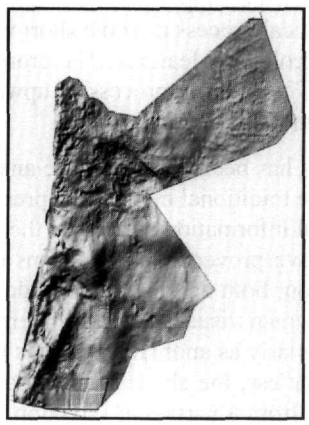

Figure 7 - Magnetic map shaded relief, Jordan

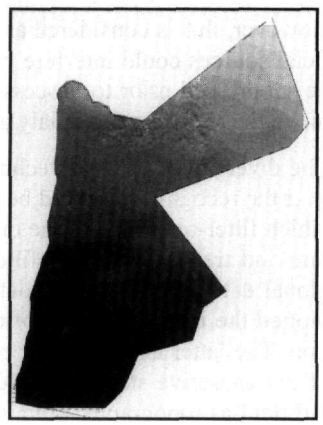

Figure 8 - Image of the total magnetic field map, Jordan

The performed geophysical evaluation of the fault pattern mainly refers to the deformation pattern which exists within the upper rock cover; nonetheless, more than 80% of Jordan is covered by rocks younger than Jurassic age. Indicating that tectonic activities of Cretaceous age up to the Quaternary are responsible for what might be seen on the surface and in outcrops. Although, few structural patterns are tracing pre-existing tectonic elements from the deeper older rock formation, these are not indicating that the pre-existing structures have not affected the recent deformation patterns in the younger sediments. On the contrary, they should have been reactivated due to the younger deformation processes. Presume that the changing of the stress fields may have led to a reactivation impact to completely change the former character of the fault system.

The old even Precambrian structures that are trending NW-SE (Najd fault system), N-S and W-E were reactivated by the extensional forces connected to the opening of the Tethys during the Late

Palaeozoic and Lower Cretaceous. The change from the opening of the Tethys to the sub-deduction of the African-Arabian Plate; below the European-Asian Plate has led to the slightly sigmoid SW-NE trending compressional structure with folds and thrust faults. The last major tectonic deformation is caused by the N-S trending left lateral shear movement of the Arabian Plate with conjugated shear deformation.

8.1. N-S Fault System

This system is considered to be the major among all known fault systems, besides it is the most active system within the study area. However, one of the N-S trending faults came into sight at the eastern and central parts of Jordan which is the most pronounced pattern fitting to this system; is the Aqaba- Dead Sea- Jordan Rift system. Most of these faults are extending beyond the Jordanian territory. The fault system extends in the N-S direction tends to give a first impression of an individual successive fault zones incapacity of 12 km width. The separating distance of the fault zones ranging from 40 to 45 km. Unfortunately, it was impossible to delineate such faults by the geophysical techniques, particularly in areas covered with basalts. Despite the fact that a separation of residual anomalies from regional anomalies was configuration, the lack of gravity survey data and the complexity of the magnetic anomalies map led to hinder interpretation relevant to following up faults.

Consequently, the small elongated basin character of these fault systems led to be interpreted as a continental graben system compared with the Red Sea graben as its northward continuation in a status of nascendi. However, various relevant studies have argued that this whole N-S orientated fault system is a transform structure next to the Arabian Plate that was separated from the African Plate and is moving now in a left lateral shear movement to the north. Thus, the total lateral displacements documented by the parallel offset of typical crossing structures comprehend about 107 km.

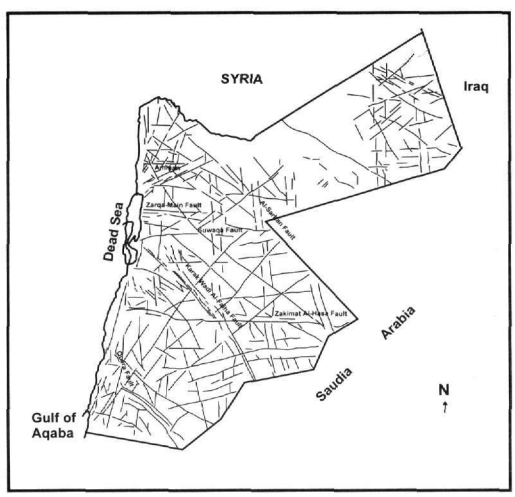

Figure 9 - Faults disruption map, Jordan

The apparent frequent isolated fault segments are belonging to through-going movement track, extending from the Red Sea towards the mountain chain in Turkey. The movement did not occur along one straight line, but jumped from one parallel shear fault to another. It was developed into a shear pattern in a narrow N-S oriented zone before the full separation of the Arabian Plate at the beginning of the shear movement. However, the left lateral movement jump from one fault to the next in the west (left side) has developed a pull-a-part basin. Meanwhile, the jump back to the east or only gradual transition or merging into the next fault in the east formed a transpression zone, where part of the northward moving plate should be squeezed out. This pattern of pull apart basins

and transpression zones which are required from the mechanism of the shear movement along a non-straight slightly undulated line are clearly documented over the entire area from the Gulf of Aqaba with three successive pull apart basins, unbroken in the basins of Wadi Araba, the Dead Sea Basin, the Jordan Valley Basin and the Basin of the Lake Tiberias. Transpressional zones are intercalated for instance in the area of Wadi Araba. However, this is not obvious due to young sediment cover delectable by the geophysical survey as zones with Mesozoic or basement rocks lying on shallow depths of the Wadi Araba-Jordan Rift valley.

The N-S aligned shear faults are accompanied by parallel N-S normal faults and emphasizing the N-S fault pattern. These normal faults exemplify a secondary fault system to the transform system. Therefore, the vertical displacements along the main shear movement and particularly the steep slopes along the pull-apart basins deem to develop gravitational instabilities. This led and still leading to mass movements and vertical displacements along these normal faults pursuing a mass movement towards the Basin, partly developed on the awake of the fault steps, which for example are clearly developed along the Dead Sea.

Furthermore, the age of N-S transform system originally assumed to be a two-stage development following the former assumption of a two-stage ocean spreading in the southern Red Sea (Girdler 1985). However, the first stage with a displacement of 40 km has been assumed in the Eocene–Oligocene, while the second stage pursuing till today should have been started in the Middle Miocene. The Median Peninsula has shown that the transform movement along the Aqaba-Dead Sea-Jordan line was free of the opening of the Red Sea (Red Sea-Suez stage) first stage. It started about 12 My ago (Late Miocene) associated by the opening of the Gulf of Aden which in the course of ocean's spreading along the Ridge Arabia has been pushed northward since that time. Hereafter, it possible to consider that the time of the creation of some other N-S trending faults coincide with that of the Aqaba-Dead Sea-Jordan Rift ever since the late Miocene. This direction is already evident at the Precambrian basement and documented at the ascending lines of Oligocene and Early Miocene volcanism.

In addition to this, the process of quantitative interpretation of the gravity field indicates that the system extends to great depths, and the faults of this system could be considered as open faults. These types of faults are characterized by being subdivided into separate parts affected by the horizontal displacements, particularly in areas of junctions with other fault systems.

8.2. NW-SE Fault System

This system is composed of the NW-SE directed faults that widely distributed all over the structural map of Jordan, and extends even to the neighbouring countries such as Saudi Arabia. The extension of these faults could reach hundreds of kilometres, such as the Karak-Wadi Al-Faiha fault and Al-Sarhan faults. In general, this group of faults parallels the Red Sea Rift and penetrates the earth's crust, reaching the mantle. These faults are characterized by being originated under tensional forces (open faults). This assumption is confirmed by the occurrence of volcanic intrusions along the Karak- Wadi Al- Faiha faults, east of the Dead Sea and the great basaltic rocks covering vast area in Syria, Jordan and Saudi Arabia. The time period at which the faults of this system were originated is considered to be in accordance with the time period of which the Red Sea fault and Najd fault were generated, and mostly it is closely related to the Red Sea rift. This is obvious from the tectonic activity of these systems during the Cenozoic period, i.e., at the time when the Red Sea basin began to expand. Accordingly, it is very definite to indicate horizontal displacements in parts of this fault system that are also clearly demonstrated on the geological map of Jordan.

8.2.1. The E-W fault system

This system includes the E-W directed faults, which have different extensions. However, some are extended even in to Saudi Arabia such as the Zakimat Al- Hasa fault. The average distance between the faults of this system is ranging from 35 to 40 km. However, sometimes there are faults

of relatively limited lengths (geological map of Jordan, scale 1: 500.000) for instance, the fault passes near Amman. Nonetheless, faults of this system could be considered as basement faults even though some of which are recognized on earth surface for a limited distance. It is obvious that the faults of this system have been affected by the horizontal displacement. Therefore, some of which may reach great depths such as the Zakimat Al-Hasa, Suwaqa and Zarqa-Main faults with volcanic eruptions and hydrothermal deposits.

8.2.2. The NE-SW fault system

Faults of NE-SW direction are shown on the geophysical maps mostly as lineaments. These linear breaks are parallel to each other and at the same time they make a curvature in the southwestern part of the country. In general, this system lies perpendicular to the Red Sea fault. In reality, the presence of this system is confirmed by the direction of wadis traces in Jordan.

9. Discussion and Conclusions

Considerably it is difficult to state the true age of these major fault systems in Jordan. On the other hand, scrutinizing the geological map (Fig. 3) and the map of the faults (Fig. 9) constructed in accordance to the final interpretations of the gravity and magnetic data that will allow determining the relative ages of these systems based on the relative period of the tectonic activity of these faults. Precise analyses of locations of the systems intersect in different areas indicates that the location and the intersection of the magnetic and gravity anomalies are of the same type. Whereas, the first major fault system that extends N-S could be considered as an open tension fault which is also subdivided into portions intersected by other fault systems. As the horizontal displacement is also well recognized in many parts of this system, it could be accepted as the oldest system affected by tectonic events. However, faults of the second system NW-SE underwent displacement in some locations and intersected by other fault systems as in the case of central Jordan, i.e., the Al Karak Wadi Fiha fault and the fault lying in the Wadi Sirhan and Al-Azraq Basin. These faults are considered to be open tension faults that intersect the N-S directed faults. Consequently this system could be younger than the previous one. Some elements of this system are intersected by faults of E-W direction within which lie many parts of this system. At the Conclusion, the faults of E-W direction are younger than those of NW-SE direction. The faults with NE-SW direction which were considered as lineaments are intersecting all previously mentioned fault systems. They are not affected by any displacement of its own fault portions whenever intersecting with other systems. Accordingly, this system may be considered the youngest known one as confirmed by the direction of the Wadis in the eastern and central parts of Jordan.

Examining the distribution of the faults at the structural map of Jordan, there are two perpendicular network of faults, i.e., orthogonal and diagonal. As each network consist of two systems perpendicular to each other. Commonly, each of the principal networks is considered to share the same-time-period, indicates the existence of four systems of different relative ages. It is possible to consider the age of each one of these systems only appertains to the time of the fault formation. It is possible to consider the age of the fault formation due to earth planetary jointing system which in the course of geologic times underwent changes due to many factors that were responsible for the formation of a single system within its particular characteristics as mentioned before. Therefore, the main fault systems in Jordan could be assumed as a part of the global system and its planetary characteristics.

The appearance of such systems mainly due to the rotational movement of the earth and the consequential pulses of that movement. Otherwise, it may due the diffusion of internal thermo currents and other factors to be the cause. Accordingly, Jordan presents a significant hint which let us assure two types of faults regarding their origin: (1) Displacement faults may be originated by the rotation-axial movement of earth leading to consequential pulses in stress forces and pressure in the rocks of the earth's crust and (2) Faults originated by the events of internal intrusions took place by various natural processes within the core of the earth.

The principle role in the formation of the main fault systems is due to the changes in the rotational movement of earth and its consequential pulses that faulted the earth crust rocks and form the horizontal displacements which took place in the Afro-Arabian Rift, i.e., the strike slip movements, which in turn influenced the Arabian Plate.

10. Acknowledgments

The author tenure at Karlsruhe University was funded by the Alexander von Humboldt Foundation wish to thank the Jordan Natural Resources Authority of Jordan for their participation by providing accessibility to the records available relevance to this study. Furthermore, would like to extend his thanks to the Karlsruhe University (Applied Geology Department) for using their facilities and for their hospitality. Moreover, the support of Alexander von Humboldt Community is greatly appreciated.

11. References

Al-Zoubi, A., 1992. Deep geological structure of Jordan from geophysical data, *Unpublished D.Sc. and Ph.D. Thesis*, Saint Petersburg Mining Institute, Russia, 179 pp.

Al-Zoubi, A., and Ben-Avraham, Z., 2002. Structure of the earth's crust in Jordan from potential field data, *Tectonophysics*, 346, 45-59.

Al-Zoubi, A., and ten-Brink, U., 2001. Salt diapirs in the Dead Sea Basin and their relationships to Quaternary extensional tectonic, *Marine and Petroleum Geology*, 18, 779-797.

Al-Zoubi, A., and ten-Brink, U., 2002. Lower crustal flow and the role of shear in basin subsidence: an example from the Dead Sea basins, *Earth and Planetary Sciences Letters,* 199, 67-79.

Ben-Avraham, Z., and Grasso, M., 1991. Crustal structure variation and transcurrent faulting at the eastern and western margins of the eastern Mediterranean, *Tectonophysics*, 196, 269-277.

Barberi, F., Capaldi, G., Gasparini, P., Marinelli, G., Santracroce, R., Scandone, R., and Tureil, M., 1979. Recent basaltic volcanism of Jordan and its implication on the geodynamic history of the Dead Sea shears zone, *International Symposium Geodynamic Evol., of the Afro-Arabian Rift System*, Rome.

Bender, F., 1968. *Geology of Jordan,* Supplement edition in English with minor revisions.

Bender, F., 1974. *Geology of Jordan*, Gebrueder Borntraeger, Berlin, 196 pp.

Dewey, J. F., Pitman, C.C., Ryan, W., and Bonnin, J., 1973. Plate tectonics and the evaluation of Alpine System, *Geol. Soc. Am. Bull.* 84, 3137-3180.

Freund, R., Garfunkel, Z., Zak, I., Goldberg, Weissbord, M. T., and Derin, B., 1970. The shear along the Dead Sea rift, Phlilos, *Trans. R. Soc. London*, 267 (A), 107-130.

Freund, R., and Garfunkel, Z., 1976. *Guidebook to the Dead Sea rift*, Hebrew University, Jerusalem, 27 pp.

Garfunkel, Z., 1981. Internal structure of the Dead Sea leaky transform (rift) in relation to plate kinematics, *Tectonophysics*, 80, 81-108.

Ginsburg, A., and Ben-Avraham, Z., 1997. A seismic refraction study of the north basin of the Dead Sea, *Geophysical Research Letters* 24, 2063- 2066.

Girdler, R., 1985. Problems concerning the evaluation of oceanographic lithosphere in the Northern Red Sea, *Tectonophysics* 116, 109-122.

Hatcher, R. D., Zietz, I., Regan, R. D., and Abu-Ajamieh, M., 1981. Sinistral strike- slip motion on the Dead Sea rift: Confirmation from new magnetic data, *Geology*, 9, 458-462.

Joffe, S., and Garfunkel, Z., 1987. Plate kinematics of the circum Red Sea–a revaluation, *Tectonophysics*, 141, 5-22.

Lovelock, S., 1984. A review of the tectonics of the northern Middle East Region, *Geol. Mag.*, 121, 577-587.

Phoenix, 1981. A comprehensive airborne magnetic/ Radiation survey of the Hashemite Kingdom of Jordan, *Final Report to Natural Resources Authority*, Amman.

Quennel, A. M., 1958. The structure and geomorphic evolution of the Dead Sea rift, Q. *J. Geol. Soc.* London, 64: 1-24.

ten-Brink, U., Al-Zoubi, A., and Rybakov, M., 2001. Bouguer gravity map of the Dead Sea fault system, Jordan and Israel, *USGS*, Open files report, 01-216.

ten-Brink, U., Rybakov, M., Al-Zoubi, A., Hassouneh, M., Bataeneh, A., Frieslander, U., Goldschmidt, V., Daoud, M., Rotstein, Y., and Hall, J. K., 1999. The anatomy of the Dead Sea plate boundary: Does it reflect continuous changes in plate motion? *Geology*, 27, 887-980.

ten-Brink, U., Ben-Avraham, Z., Bell, R., Hassouneh, M., Coleman, D., Andreason, G., Tibor, G., and Coakley, B., 1993. Structure of the Dead Sea pull-apart basin from gravity analysis, *Journal of Geophysical Research*, 98 (21), 887-894.

Δελτίο της Ελληνικής Γεωλογικής Εταιρίας τομ. XXXX, 2007
Πρακτικά 11ου Διεθνούς Συνεδρίου, Αθήνα, Μάιος 2007

Bulletin of the Geological Society of Greece vol. XXXX, 2007
Proceedings of the 11th International Congress, Athens, May, 2007

UNIAXIAL COMPRESSIVE STRENGTH, DRY UNIT WEIGHT AND FRACTURE PATTERNS OF ULTRABASIC ROCKS IN OTHRYS MOUNTAIN (CENTRAL GREECE): CORRELATIONS AND EVALUATION.

Diamantis K.[1], Karamousalis Th.[1], Antoniou Vas.[1], and Migiros G.[1]

[1] *Agricultural University of Athens, Department of Sciences, Division of Geological Science and Atmospheric Environment, Laboratory of Mineralogy-Geology, kostasdiam@aua.gr, karamousalis@aua.gr, vantoniou@aua.gr, bagm@aua.gr*

Abstract

Ultrabasic rocks, taken from the Othrys mt. (Central Greece), are studied in this paper. The structural geology and tectonics of the study area are described. Uniaxial Compressive Strength (UCS) and dry unit weight (γ) values are calculated and fracture angles are measured. The results are statistically assessed and empirical relationships (exponential equations) between UCS and γ are presented for the ultrabasic rocks, divided in Peridotites, Serpentinised Peridotites and Serpentinites. Due to the low correlation coefficient of the Serpentinised Peridotites, it was decided that the Serpentinised Peridotites and Serpentinites should be examined together. The correlation coefficient of the combined category is much better than the separate ones.

Furthermore, this paper demonstrates that the majority of the ultrabasic rocks tested were breaking at one angle (φ°), which mainly fluctuated between 75° and 90°. The fracture angles correlate with previously recognised geological (mainly tectonic) structures.

The observed deviations are due to petrographic variety, structural complexity, preferred orientation of olivine and orthopyroxene and internal imprinted tectonic deformation.

Key words: *Rock mechanics, ophiolites, laboratory tests.*

Περίληψη

Στη παρούσα δημοσίευση μελετούνται τα υπερβασικά πετρώματα από την περιοχή της Όθρυος (Στερεά Ελλάδα). Η γεωλογική δομή και η τεκτονική της εξεταζόμενης περιοχής περιγράφοντα συνοπτικά. Οι αντοχές σε ανεμπόδιστη μονοαξονική θλίψη και τα φαινόμενα βάρη υπολογίζονται και οι γωνίες θραύσης μετρούνται. Τα αποτελέσματα αξιολογούνται στατιστικά και παρουσιάζονται εμπειρικές σχέσεις μεταξύ της αντοχής σε μονοαξονική θλίψη και του φαινόμενου βάρους. Εξαιτίας του χαμηλού συντελεστή συσχέτισης στους Σερπεντινιωμένους Περιδοτίτες, αποφασίσαμε οι Σερπεντινιωμένοι Περιδοτίτες και οι Σερπεντινίτες να εξεταστούν μαζί. Ο νέος συντελεστής συσχέτισης είναι πολύ μεγαλύτερος από τον προηγούμενο.

Επιπλέον, στην παρούσα δημοσίευση φαίνεται πως η πλειοψηφία των υπερβασικών πετρωμάτων θραύεται σε μια μόνο γωνία (φ°), η οποία κυμαίνεται κυρίως μεταξύ 75° και 90°, ενώ γίνεται και συσχετισμός των γωνιών θραύσης με την τεκτονική.
Οι όποιες αποκλίσεις παρατηρήθηκαν αποδίδονται στην πετρογραφική ποικιλία, στη δομική πολυπλοκότητα, στον προτιμητέο προσανατολισμό του ολιβίνη και του ορθοπυρόξενου και στην εσωτερικά αποτυπωμένη τεκτονική παραμόρφωση.
Λέξεις κλειδιά: *Βραχομηχανική, οφιόλιθοι, εργαστηριακές δοκιμές.*

1. Introduction

Many attempts have been to correlate the Uniaxial Compressive Strength (UCS), which is undoubtedly the geotechnical property of rocks which is most often quoted, with certain mechanical and physical characteristics. Nevertheless, only few studies have been concentrated on ultrabasic rocks (Koumantakis 1982, Paventi *et al.* 1996, Marinos *et al.* 2006). An opportunity to conduct such investigation came up when the Laboratory of Mineralogy-Geology of the Agricultural University of Athens undertook the geomechanical tests from ERGOSE S.A. for the construction of railway tunnels in Othrys mt.

The study area is located in Othrys (Central Greece) and specifically between the villages of Lianokladi and Domokos (Fig. 1). It belongs to the Sub-Pelagonian geotectonical unit and it is mainly comprised of ultrabasic rock masses (Marinos 1974, Migiros 1990).

A number of boreholes were drilled along a narrow N-S zone, from which 138 representative samples were chosen to be examined.

Uniaxial Compressive Strength and dry unit weight (γ) values were calculated following the international standards. Photographs were taken before and after each test, fracture patterns were drawn, the angles were measured and statistically classified.

Within the framework of the present study, the fluctuations of UCS and γ values and the statistical analysis of the fracture angles are presented. This paper attempts to derive reliable empirical equations between UCS and γ, to correlate them with both fracture angles and depth and to outline the influence of the geological structure.

2. Materials and methods

Drill core samples from the Othrys mt. were investigated for geotechnical purposes (construction of railway tunnels by ERGOSE S.A.) in the Laboratory of Mineralogy-Geology of the Agricultural University of Athens. The boreholes were carried out in a 25 km long N-S direction, from Lianokladi to Domokos villages, perpendicular to the geological and tectonic structures of the area and they were drilled at depths up to 300 m from the surface. The wide range of sample depth along with the quite large numbers of samples, render our results representative for the Othrys ultrabasic rock masses.

The initial choice of the samples and the sequence of tests were decided by the supervising rock mechanics engineer and geologists. At our laboratory a second check was done by taking into account the isotropy and homogeneity of the samples and some were disqualified as inappropriate (about 33 %), mainly due to visible discontinuities, i.e. fractures, reducing the number of samples to 138.

Due to the variable grade of serpentinisation of the peridotite samples, many thin sections were cut and examined under a polarising microscope and some samples were further analysed by the XRD method. Three petrologic types of peridotites were distinguished based on their different physical and mechanical properties.

The Uniaxial Compressive Strength (UCS) tests were carried out in accordance with the ISRM (1981) standard. The core samples, whose diameters were 61, 71 and 83 mm, were carefully prepared keeping an L/D ratio between 2,5 and 3,0. The edges of the samples were cut parallel and smooth. The samples were then oven dried and before every test the samples were weighted with accuracy in order to calculate the dry unit weight. After each test, the pattern of the fractures was drawn and the angles of the fractures were measured.

The data was analysed with the Analysis Tool Pack of Microsoft Excel 2003 and the results were evaluated and then correlated with the geological structures of the area.

3. Geology

The area between the Lianokladi and Domokos villages (Othrys mt.) consists mainly of Alpine formations (Fig. 1) that belong to the Sub-Pelagonian geotectonic unit (Mountrakis *et al.* 1983, Katsikatsos *et al.* 1986). We can distinguish them, from bottom to top, in the following formations (Marinos 1974, Ferriere 1982, Migiros 1990):

(a) A carbonate sequence of Triassic-Jurassic age which constitutes the basement of the area.

(b) A tectonic nappe, mainly ophiolitic (Katsikatsos *et al.* 1986).

(c) An unconformable sequence of Cretaceous limestones which passes upward to flysch.

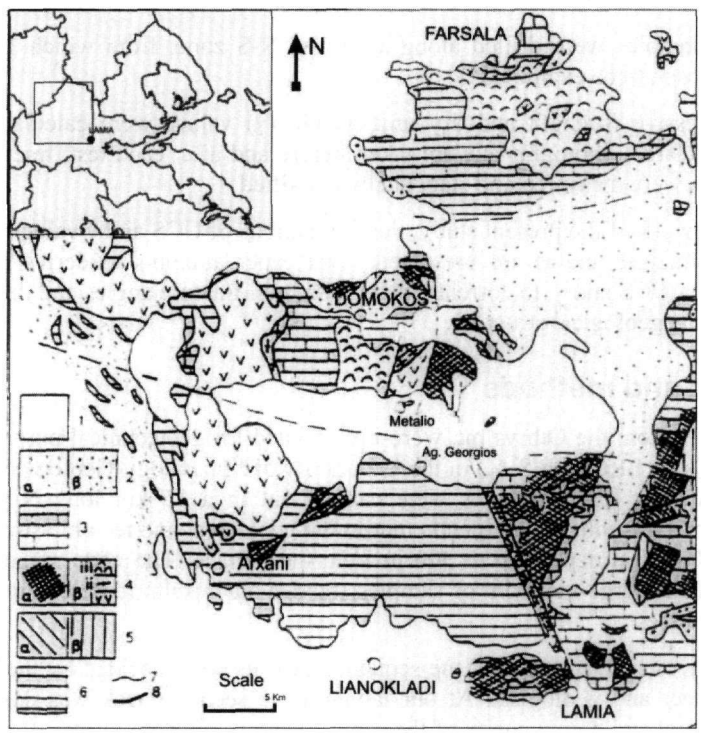

Figure 1 – Geological map of Othrys area (Migiros 1990): 1. Postalpine formations 2. Flysch (α) Paleocene – Eocene (β) Upper Cretaceous 3. Cretaceous formations of eastern and central Othrys 4. Pre-Upper Cretaceous tectonic nappe (α) Undivided (β) Ophiolitic formations (i) tectonites (ii) cumulates (iii) non-cumulites and volcanic sequence 5. Pre-Cretaceous formations (α) eastern (β) central Othrys 6. Western Othrys formations (undivided) 7. Geological boundary 8. Tectonic contact

The ophiolitic formations have thrusted the Triassic-Jurassic carbonate sequence and are consisted of volcano-sedimentary formations, basaltic lavas, basic rocks and ultrabasic masses. The

ultrabasic rock masses are mainly represented by the peridotites whose grade of serpentinisation varies.

In our study we classified the peridotite samples into the following three rock groups taking into account petrological and mineralogical studies:

(a) Peridotites: We refer mainly to lerzoliths, hartzbourgites and plagioclastic peridotites with a grade of serpentinisation less than 30 %.

(b) Serpentised Peridotites: The same rock type but its grade of serpentinisation lies between 30 % and 70 %.

(c) Serpentinites: Ultrabasic rock types, mainly hartzbourgites, whose grade of serpentinisation is more than 70 %.

According to Migiros 1990, the tectonic analysis of the geological formations exhibits the following prominent tectonic features in the ultrabasic rock masses:

(a) Schistosity: NW-SE direction and NE dip less than 30°.

(b) Low thrusts: E-W direction and N dip between 30°-45°.

(c) Thrusts: NW-SE direction and NE dip between 45°-60°.

(d) Faults: E-W, NW-SE, NE-SW directions and dips more than 60°.

4. Laboratory test results

4.1. Dry unit weight (γ)

The dry unit weight was calculated for the total number of 138 ultrabasic samples and their values are illustrated in Figure 2. As seen in Table 1 (statistical analysis), the dry unit weight fluctuates between 22.99 and 33.77 kN/m^3 and the average value is 27.64 kN/m^3.

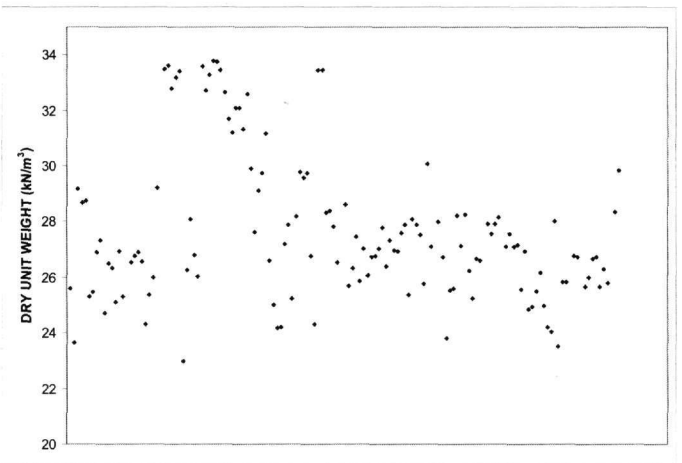

Figure 2 - Dry Unit weight values of the investigated ultrabasic samples

The ultrabasic rocks, based on their dry unit weight and taking into account their petrological studies are divided in Peridotites, Serpentinised Peridotites and Serpentinites.

The dry unit weights of Peridotites range from 29.56 kN/m^3 to 33.77 kN/m^3, those of Serpentinites from 22.99 kN/m^3 to 25.98 kN/m^3 and the values of Serpentinised Peridotites vary from 26.00 kN/m^3 to 29.19 kN/m^3 (Table 2).

From the above mentioned and taking into account the low standard deviations of the groups that were formed petrologically, we conclude that there is also a clear differentiation to the dry unit weight values, as it was expected, which is due to the grade of serpentisation.

Table 1 - Statistical analysis results of the investigated ultrabasic samples

ULTRABASIC ROCKS	
	DRY UNIT WEIGHT (KN/m^3)
MAX	33,77
MIN	22.99
MEAN	27.64
STDEV	2.62

Table 2 - Statistical analysis results of the investigated ultrabasic samples.

		DRY UNIT WEIGHT (KN/m^3)
PERIDOTITES	MAX	33.77
	MIN	29.56
	MEAN	32.04
	STDEV	1.52
SERPENTINISED PERIDOTITES	MAX	29.19
	MIN	26.00
	MEAN	27.29
	STDEV	0.81
SERPENTINITES	MAX	25.98
	MIN	22.99
	MEAN	25.02
	STDEV	0.77

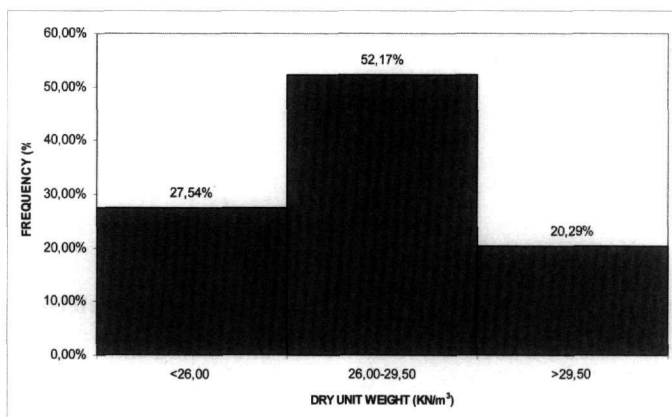

Figure 3 - Dry unit weight histogram

Finally based on the results of the dry unit weight statistical analysis for each petrological group and regarding 29.50 kN/m^3 as the minimum value for Peridotites and 26.00 kN/m^3 as the

maximum value for Serpentinites, a histogram was created (Fig. 3). As can be seen the largest number of samples belong to Serpentinised Peridotites (52.17 %).

4.2. Uniaxial Compressive Strength (UCS)

A scatter diagram of all UCS values is illustrated in Figure 4. The UCS values range from 169.63 to 0.40 MPa exhibiting a great fluctuation. Some very uncommon low values of UCS are due to internal discontinuities, macroscopically undetected. The mean value is 53.62 MPa and the standard deviation is 35.34 MPa (Table 3). The high value of the standard deviation can be attributed to the fact that the majority of the samples belong to the Serpentinised Peridotites group (52.17 %), which exhibit great anisotropy.

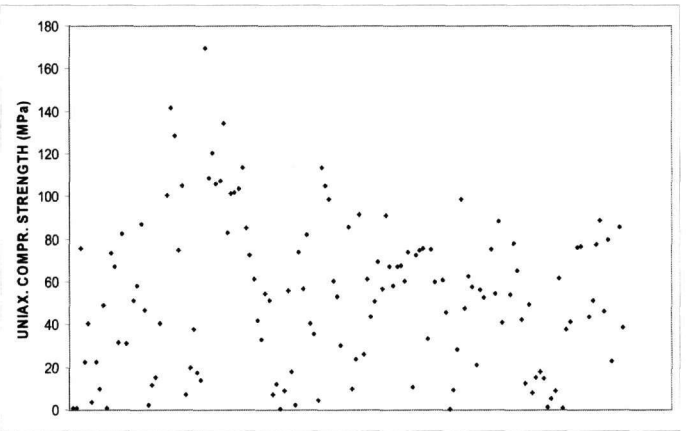

Figure 4 - Uniaxial Compressive Strength values of the investigated samples

Table 3 - Statistical analysis results of the investigated ultrabasic samples

ULTRABASIC ROCKS	
	UNIAXIAL COMPRESSIVE STRENGTH (MPa)
MAX	169.63
MIN	0.40
MEAN	53.62
STDEV	35.34

4.3. Fracture Angles (φ°)

Following the UCS tests, photographs of the samples were taken and fracture patterns were drawn. Of the 138 samples, 86.96% had single dipping fractures, while the 13.04 % was broken in two angles (Fig. 5). These two groups of samples were statistically analyzed separately. After distinguishing four bins ($30°\leq\varphi°<45°$, $45°\leq\varphi°<60°$, $60°\leq\varphi°<75°$, $75°\leq\varphi°\leq90°$), it is shown that both groups were mainly broken in angles between 75° and 90° (Figs 6, 7). In addition, no fracture angle values less than 30° were observed. Detailed statistical analysis is shown in Table 4.

Finally, for each sample the dominant angle was identified. A histogram of the prevalent fracture angles is shown in Figure 8. It is evident that the majority of the samples (60.14 %) had a prevalent fracture angle between 75° and 90°, while only the 2.17 % broke between 30° and 44°.

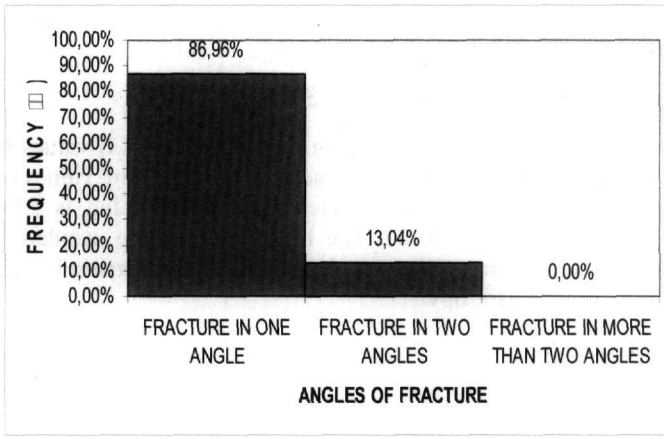

Figure 5 - Frequency of the fracture angles

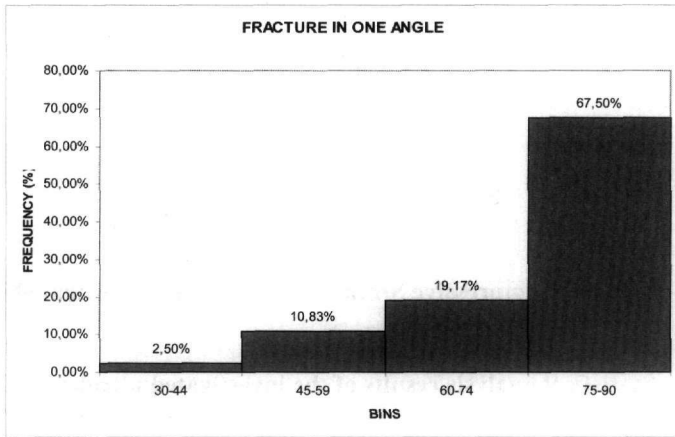

Figure 6 - Frequency of one fracture angle

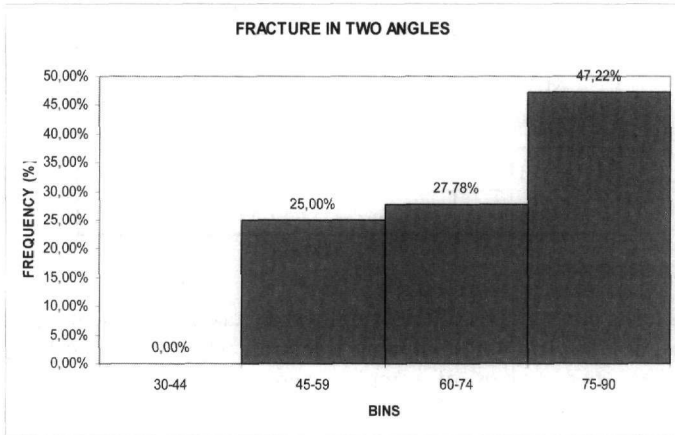

Figure 7 - Frequency of two fracture angles

Table 4 - Statistical analysis results of fracture angles

	FRACTURE IN ONE ANGLE				FRACTURE IN TWO ANGLES			
BINS	30-44	45-59	60-74	75-90	30-44	45-59	60-74	75-90
FREQUENCY	3	13	23	81	0	9	10	17
FREQUENCY (%)	2,50%	10,83%	19,17%	67,50%	0,00%	25,00%	27,78%	47,22%
MEAN	37,33	55,69	67,48	84,15	0	52,00	67,10	82,41
MODE	42	54	70	85	0	50	64	85

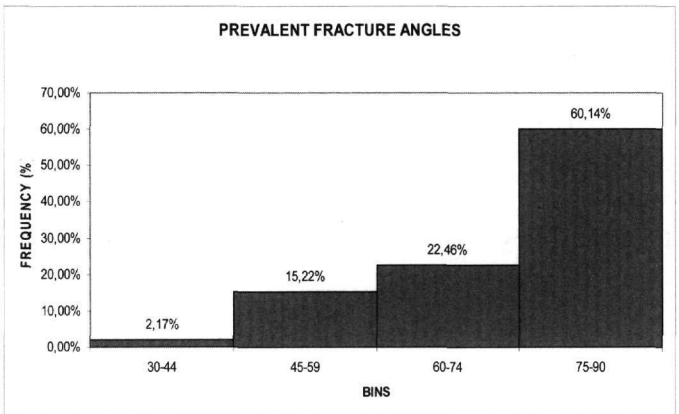

Figure 8 - Histogram of the prevalent fracture angles

5. Results & Discussion

The statistical analysis software used to correlate UCS and dry unit weight was the Analysis Tool Pack of the Microsoft Excel 2003. Figure 9 is a plot diagram of UCS against γ for the total number of the samples. The relationship gives a good correlation coefficient (R=0.66) and is defined by the equation $UCS=0.0063e^{0.3117\cdot\gamma}$. A closer examination of Figure 9 reveals a discrepancy of the normally exponential relationship between dry unit weight and UCS. This is attributed to the anisotropic single-crystal elastic properties and the lattice preferred orientation of olivine and orthopyroxene. Specifically for the Peridotites, the relationship between UCS and γ gives a high correlation coefficient (R=0.78) and is represented by $UCS=0.2067e^{0.1892\cdot\gamma}$ (Fig. 10). The same relationship gives a low correlation coefficient (R=0.26) for Serpentinised Peridotites (Fig. 11) and a good one (R=0.66) for Serpentinites (Fig. 12). Thus it is suggested that Serpentinised Peridotites and Serpentinites should be examined together. The new correlation coefficient is 0.74 and the equation is defined by the $UCS=3\cdot10^{-7}e^{0.6962\cdot\gamma}$ (Fig. 13). Moreover, the deviations are due to the varied grade of serpentinisation, the petrographic variety (hartzburgites, lerzolites, plagioclastic peridotites) and the internal structural complexity due to the tectonic deformation and alteration.

It can be seen from Figures 5-6, that the majority of the ultrabasic samples broke in one angle, which predominately fluctuated between 75° and 90°. When samples fractured in two angles, the percentage of the bins 45°-59° and 60°-74° increased while the percentage of the bin 75°-90° decreased (Fig. 7), which is quite reasonable.

From the aforementioned, it is obvious that the fracture angles of the samples deviate from the expected value of 45°. This is mainly attributed to the internal imprint of tectonic structures; specifically, angles lower than 45° are related to low thrusts, between 45° and 60° to the thrusts and those with angles greater than 60° are correlated to the faults and/or collapse effect.

Finally, there is no obvious relationship between the UCS and the fracture angle as in between the fracture angle and the depth from which the samples were taken. As it is aforementioned, this is attributed to the petrographic variety and/or to the preferred orientation and the internally imprinted tectonic structures.

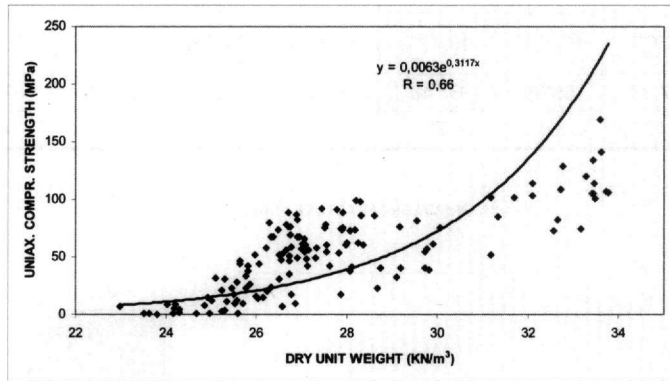

Figure 9 - UCS against Dry unit weight for the total number of ultrabasic samples

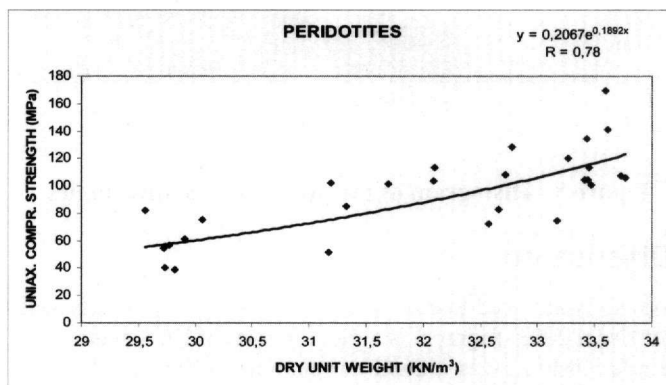

Figure 10 - UCS against Dry unit weight only for the Peridotites

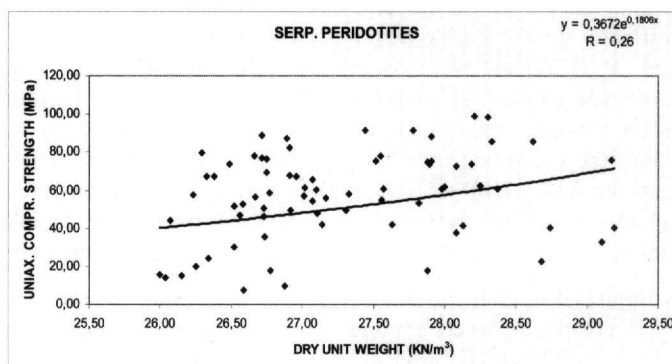

Figure 11 - UCS against Dry unit weight only for the Serpentinised Peridotites

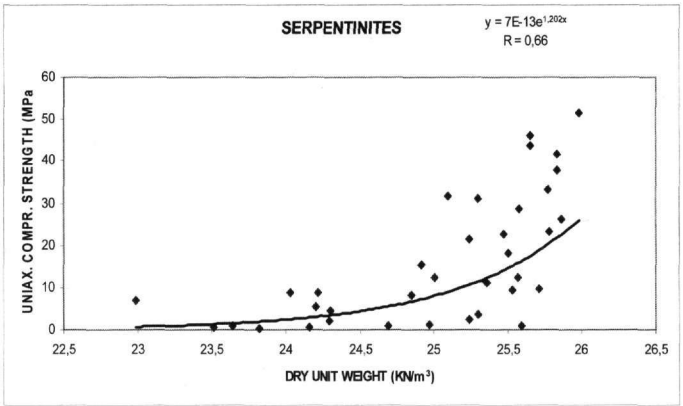

Figure 12 - UCS against Dry unit weight only for the Serpentinites

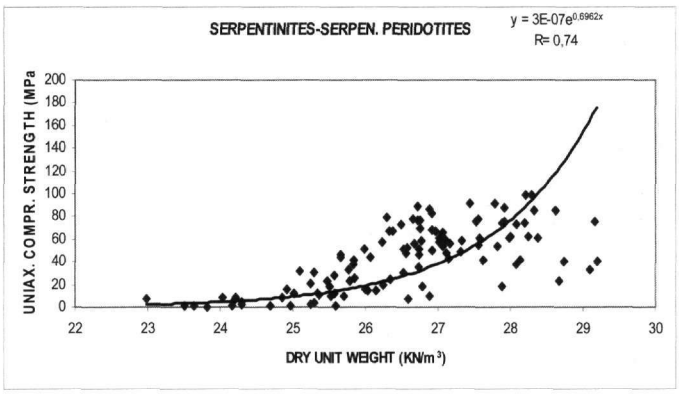

Figure 13 - UCS against Dry unit weight combining Serpentinised Peridotites and Serpentinites

6. Conclusions

Due to the petrographic variety, the grade of serpentinisation, preferred orientation of olivine and orthopyroxene, the structural complexity and the internally imprinted tectonic deformation, ultrabasic rocks were divided in three groups (Peridotites, Serpentinised Peridotites and Serpentinites). Each group presents a wide range of geomechanical and physical properties.

This paper demonstrates that for ultrabasic rocks, the relationship between UCS and γ gives a good correlation coefficient (R=0.66) and is defined by the equation $UCS=0.0063e^{0.3117\cdot\gamma}$. For the Peridotites only, the relationship between UCS and γ gives a high correlation coefficient (R=0.78) and is represented by $UCS=0.2067e^{0.1892\cdot\gamma}$. As far as Serpentinised Peridotites are concerned, the relationship between UCS and γ presents a low correlation coefficient (R=0.26) in contrast to Serpentinites (R=0.66). It was realized that the examination of Serpentinised Peridotites and Serpentinites together provides a good correlation coefficient (0.74) and the new equation is defined by the $UCS=3\cdot10^{-7}e^{0.6962\cdot\gamma}$. It is obvious that the determination of UCS value with an easy and economical way (estimation of γ) can provide an important help to the geotechnical engineers.

Furthermore, the majority of the ultrabasic samples were fractured in one angle, which mainly varied between 75° and 90°. The samples broken in two fractures, presented an increase of the percentage of the bins 45°-59° and 60°-74° while the percentage of the bin 75°-90° got decreased. Moreover, the fracture angles of 30°-44° were mainly correlated with low angle thrusts, the bin of 45°-59° corresponds to the thrusts and that of 60°-90° to the faults or collapse effects.

Finally, there is no apparent relationship between the fracture angle and the depth from which the sample was taken and between the UCS and the fracture angle.

7. References

Ferriere, J., 1982. *Paleogeographies et Tectoniques Superposees dans les Hellenides Internes au Niveau de l' Othrys et de Pelion (Grece),* Univ. des Sciences et Techniques de Lille.

I.S.R.M., 1981. Suggested methods for determining the uniaxial compressive strength and deformability of rock materials, *International Society of Rock Mechanics, Commission on standardization of laboratory and field tests,* 111-116pp.

Katsikatsos, G., Migiros, G., Triantaphyllis, M., and Mettos, A., 1986. Geological structure of internal Hellenides (E. Thessaly-SW Macedonia, Euboea-Attica-Northern Cyclades islands and Lesvos). *I.G.M.E., Geol. and Geoph. Res., Special Issue,* 191-212.

Koumantakis, J., 1982. Comportement des peridotites et serpentinites de la Grece en travaux public. Leur propretes physiques et mechaniques, *Bul IAEG,* 25, 53-60.

Marinos, G., 1974. Geology of Othrys and issues on its ophiolites, *Ann. Geol. Des Pays Hell.,* University of Athens, 118-148.

Marinos, P., Hook, E., and Marinos, V., 2006. Variability of the engineering properties of rock masses quantified by the geological strength index: the case of ophiolites with special emphasis on tunneling, *Bull. Eng. Geol. Env.* 65, 129-142.

Migiros, G., 1990. The lithostratigraphic-tectonic structure of Othris (Central Greece), *Bull. of the Geol. Society of Greece,* XXVI, 107-120.

Mountrakis, D., Sapountzis, E., Kilias, A., Eleftheriadis, G., and Christofides, G., 1983. Paleogeographic conditions in the western Pelagonian margin in Greece during the initial rifting of the continental area, *Canadian Journal of Ear. Sc.*, 20, 1673-1681.

Paventi, M., Scoble, M., and Stead, D., 1996. Characteristics of a complex Serpentinised Ultramafic Rock Mass at the Birchtree Mine, Manitoba. In H. Aubertin, Mitri (ed.), North American Rock Mechanics Symposium, Rotterdam, 339-346pp.

Δελτίο της Ελληνικής Γεωλογικής Εταιρίας τομ. XXXX, 2007
Πρακτικά 11ου Διεθνούς Συνεδρίου, Αθήνα, Μάιος 2007

Bulletin of the Geological Society of Greece vol. XXXX, 2007
Proceedings of the 11th International Congress, Athens, May, 2007

THE MORPHONEOTECTONIC STRUCTURE OF THE TRANSITIONAL ZONE BETWEEN THE GORTYNIA MT. HORST AND THE PYRGOS-OLYMPIA BASIN (CENTRAL - WESTERN PELOPONNESE, GREECE)

Fountoulis I.[1], Mavroulis S.[1], and Theocharis D.[1]

[1] *National and Kapodistrian University of Athens, Faculty of Geology and Geoenvironment, Department of Dynamic Tectonic Applied Geology, fountoulis@geol.uoa.gr, smavroulis@yahoo.gr, dtheocharis@geol.uoa.gr*

Abstract

The present paper aims to the understanding of the neotectonic deformation in areas where no post-alpine sediment occurs. The study area is located at the transitional zone between the horst of Gortynia Mt. (Arcadia) and the Pyrgos-Olympia basin in the central-western Peloponnese and is tectonically and seismically active. The studied neotectonic faults can be distinguished in low to mid angle faults and high angle faults. The majority of them present striation sets with significant horizontal component that causes the change in the direction and plunge of the fold axes of Pindos unit. The younger and with more active characteristics fault zones are the Lefkohori and Ohthia ones.

Key words: *neotectonic, low angle fault, active fault, structural contour map.*

Περίληψη

Στην παρούσα εργασία στόχος είναι η κατανόηση της νεοτεκτονικής παραμόρφωσης σε περιοχές όπου δεν απαντούν μεταλπικές αποθέσεις. Η περιοχή μελέτης ευρισκόμενη στην ΚΔ Πελοπόννησο, στη μεταβατική ζώνη μεταξύ του βυθίσματος Πύργου-Ολυμπίας και των ορέων της Γορτυνίας που είναι μία από τις γνωστές τεκτονικά και σεισμικά ενεργές περιοχές. Τα νεοτεκτονικά ρήγματα που μελετήθηκαν διακρίθηκαν σε μικρής-μέσης κλίσης και μεγάλης κλίσης, στην πλειονότητα των οποίων παρατηρήθηκαν ομάδες γραμμών προστριβής με σημαντική οριζόντια συνιστώσα η οποία έχει ως αποτέλεσμα την αλλαγή στη διεύθυνση και τη βύθιση των αξόνων των πτυχών της Πίνδου. Οι νεότερες με χαρακτηριστικά ενεργών ρηξιγενών ζωνών είναι αυτές του Λευκοχωρίου και της Όχθιας.

Λέξεις κλειδιά: *νεοτεκτονική, ρήγμα μικρής κλίσης, ενεργό ρήγμα, υπεδαφικός τεκτονικός χάρτης.*

1. Introduction

The study of the neotectonic deformation is usually focused in neotectonic grabens that have been filled in with sediments and less in the tectonic horsts.

The study area locating close to the Hellenic Arc system at the central-western part of Peloponnese and constitutes the eastern margin of the Pyrgos-Olympia basin and from the neotectonic point of view is one of the less studied areas. More specifically, is located at the transitional zone between the horst of Gortynia Mt. (Arcadia) and the Pyrgos-Olympia basin (Fig. 1). The broader western Peloponnese is dominated by extensional tectonics as expressed by the E-W oriented normal faults on the northern and southern part (Mariolakos and Papanikolaou 1987).

In order to understand the neotectonic deformation in this area, the geomorphological and morphotectonic features as well as the deformation of the alpine structural features during the neotectonic period were studied. More specifically, our study was based on: (i) mapping of the tectonic structures and especially the active ones and recording of kinematic indicators, (ii) the study of the drainage network as well as the incision it presents, (iii) the spatial distribution of the planation surfaces, (iv) the construction of the structural contour map of the contact between the Pindos geotectonic unit and the Tripolis geotectonic unit in the wider area and (v) the correlation of the seismicity with the faults.

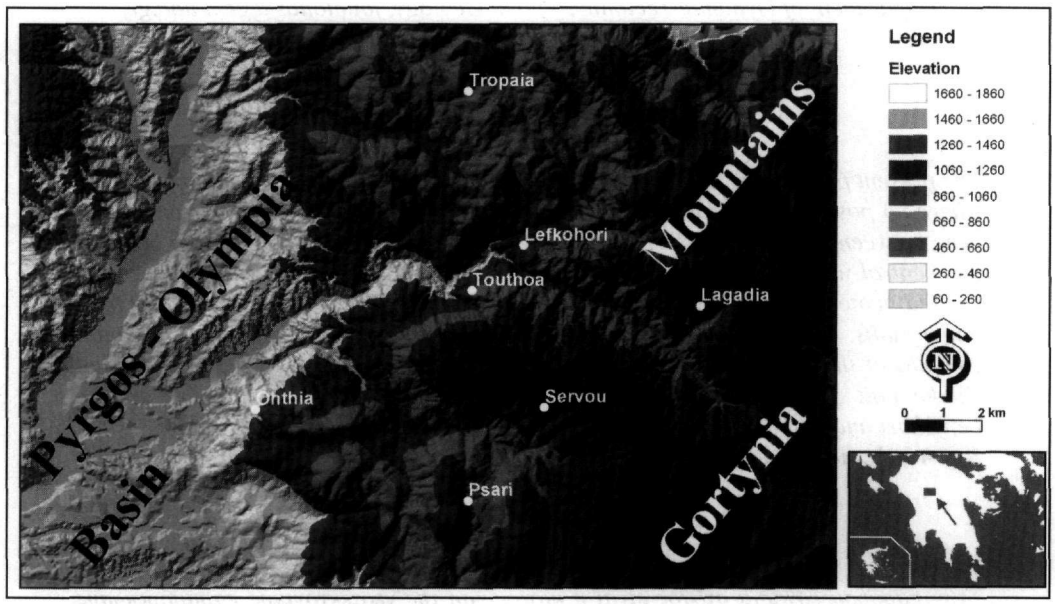

Figure 1 - Gortynia Mts and Pyrgos-Olympia basin as well as the relief of the study area are shown

2. Geological Setting

In the broader area two main alpine units (Pindos and Tripolis) and post-alpine deposits occur (Lalechos 1974, Jacobshagen *et al.* 1978, Katsiavrias 1991, Lekkas *et al.* 1992, Fountoulis 1994).

Pindos unit constitutes a nappe that overthrusts the Tripolis unit. The formations of Pindos nappe can be distinguished into three groups that are clastic sediments of Upper Triassic, Lower Cretaceous and Tertiary age, limestones with pelagic facies of Upper Triassic - Upper Cretaceous age and radiolarites s.l. mainly of Jurassic age. The whole unit is intensively folded and faulted, forming successive thrusts with movement direction from east to west.

Tripolis unit crops out in the form of tectonic windows below the nappe of Pindos unit at the mountains of Gortynia reaching altitudes of 1300 m. The stratigraphic column can be distinguished into two groups; the neritic carbonate sequence from Triassic to Eocene and the flysch at the top mainly of Oligocene age (Papanikolaou 1986).

The post-alpine sediments occur in the broader western part of the study area. They can be distinguished into marine, lacustrine, lagoonal and terrestrial formations lying unconformably on the alpine basement. The present geographic distribution and the relations between these sediments are determined mainly by the ongoing active tectonics. The post-alpine sediments in the broader area are of Quaternary age (Hagemann 1977, Lekkas *et al.* 1992, Lekkas *et al.* 2000):

- Holocene age formations include recent fluvial deposits, talus, scree and terra rossa with pebbles coming mainly from Pindos unit and
- The Erymanthos formation is of Pleistocene age and consists mainly of continental polymictic conglomerates, in a loose fine-grained matrix.

3. Morphotectonics

This neotectonic study is based not only on fault analysis, but also on the analysis of some geomorphic features of the area. More specifically the morphotectonic study was based on the study of: (a) the drainage network and (b) the spatial distribution of the planation surfaces.

Drainage network

Lagadiano River developed in the study area (Fig. 2) consists a part of the of Ladon River drainage network. The Lagadiano River is a 5th order drainage network whose 5th order tributary presents a NW-SE direction and is created by the confluence of three 4th order tributaries, which are Liaporrema, Touthoa and Goura from north to south respectively. In most sites these tributaries are perpendicular to the main faults whereas in few other sites are parallel to the faults. For example, Liaporrema River initially has a NW-SE direction almost perpendicular to Lefkohori fault zone (LFZ) (Fig. 2). Thereinafter, it change abruptly direction to NE-SW and is parallel to Lefkohori fault zone (LFZ).

The incision zones are directly and dynamically related to the tectonic regime of the area and developed mainly perpendicular to fault zones (Fig. 2). An incision zone is located in the area between Lefkohori and Touthoa and especially in the NW-SE trending Touthoa River. This zone is perpendicular to NE-SW striking Lefkohori fault zone (LFZ) forming an impressive canyon. Another interesting incision zone is observed to the south-southeast of Aetorrahi in Goura River. The river and the zone initially have an E-W direction progressively changing to NW-SE direction parallel to Kokkinorrahi – Arapides fault zone (K-AFZ).

These abrupt changes of the stream directions and its relation with the fault zones suggest that the neotectonic deformation affect directly the configuration of the drainage network. These geomorphological structures are the result of intense uplift movements of segments bounded and controlled by the fault zones of the area.

Planation Surfaces

The spatial distribution, the shape and the elevation are elements of the planation surfaces, which are affected by the tectonic movements of a region. The methodology applied for the study of planation surfaces includes the following stages:

(i) Editing of topographic elements (contour lines) from the topographic map sheets TROPAEA and DHIMITSANA (Hellenic Army Geographical Survey) in 1:50.000 scale.

(ii) Construction of Digital Elevation Model (DEM) with 20m-elevation range.

(iii) Construction of planation surfaces map, distinction into destructive and constructive planation surfaces and separation into elevation groups of >0-200 m, 200-400 m, 400-600 m, 600-800 m, 800-1000 m, 1000-1200 m and 1200-1400 m. Surfaces with slope from 0° to 5° considered as destructive planation surfaces.

(iv) Study of air photos in 1:50.000 scale.

(v) Fieldwork and confirmation of the results of the stages above.

Planation surfaces in elevations of >0-200 m, 200-400 m and 400-600 m cover larger areas than the planation surfaces in elevations of 600-800 m, 800-1000 m, 1000-1200 m and 1200-1400 m. This is due to the fact that the planation surfaces in higher altitudes are older structures that have undergone erosion processes for a longer period of time than the planation surfaces in lower altitudes.

The planation surfaces created on Pindos nappe present an arrangement with N-S trending parallel zones and their altitude ranges from 200 to 1000m from southwest to northeast (Fig. 2). This arrangement occurs west of Ohthia, Aetorrahi, Touthoa and Lefkohori fault zones but the altitude range from 400 to 1000m and from northwest to southeast.

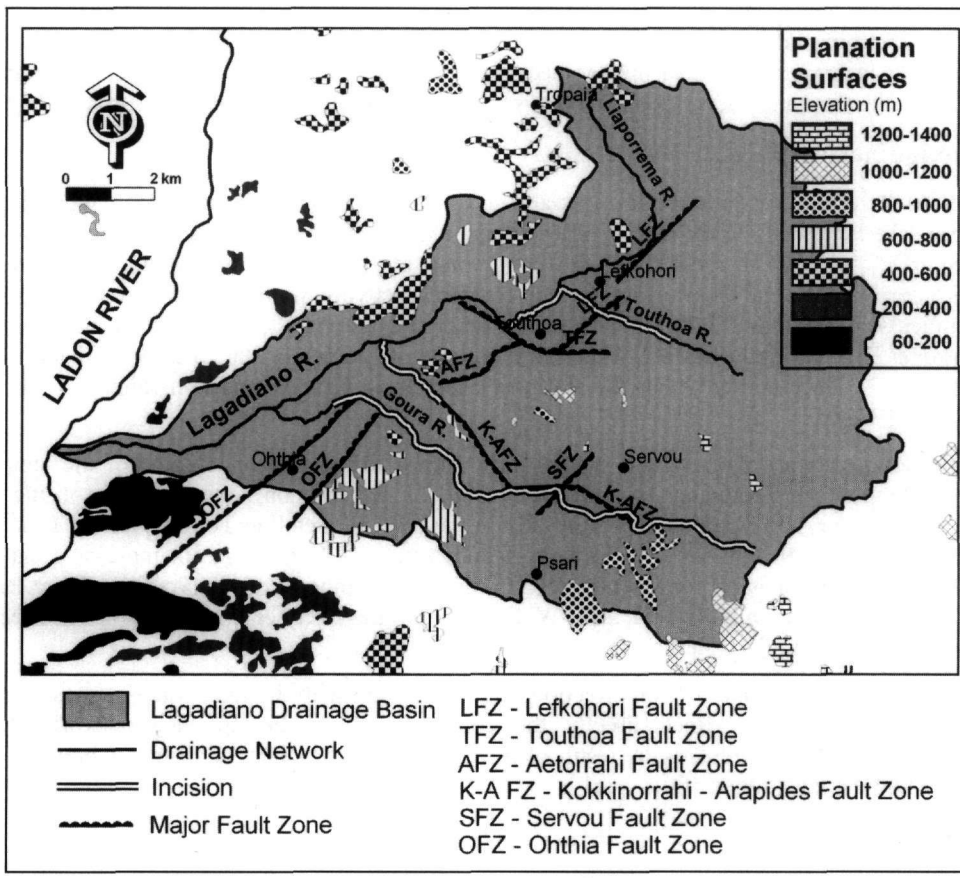

Figure 2 - Map showing the main geomorphic features (planation surfaces, incision zones, and the main tributaries of the drainage network) as well as the major fault zones of the study area

The successive formation of these geomorphological structures is disordered in the west of Ohthia fault zone region. There is an absence of planation surfaces in elevations from 200 to 600 m and an abrupt transition from the group of 60-200 m to the group of 600-800 m.

4. Neotectonics

The tectonic deformation of the area can be distinguished into two main different deformation phases: the alpine and the neotectonic phase. The alpine deformation is characterized by the creation of overthrusts, thrusts and folds and it took place from the Upper Eocene to the Early Miocene. Vertical movements characterize the neotectonic phase. It is the period during which the formation of neotectonic macrostructures (neotectonic grabens and neotectonic horsts bounded by fault zones) takes place. New faults rupture post-alpine and alpine formations or old faults formed during the alpine phase are reactivated. This is the most usual condition and thus traces of reactivations can be observed on the fault surfaces. These are tectonic breccias with different lithologies, different striations sets, tectonic gashes and other types of kinematic indicators with different kinematic character.

The neotectonic structure of W. Peloponnese is characterized by the presence of large neotectonic blocks that correspond either to grabens or horsts (Mariolakos and Papanikolaou 1981, 1987, Lekkas *et al.* 2000). These blocks are bounded by fault zones (Mariolakos *et al.* 1985) striking E-W and NNW-SSE and creating a complex mosaic, with particular neotectonic structural and evolution characteristics in every single part of the area.

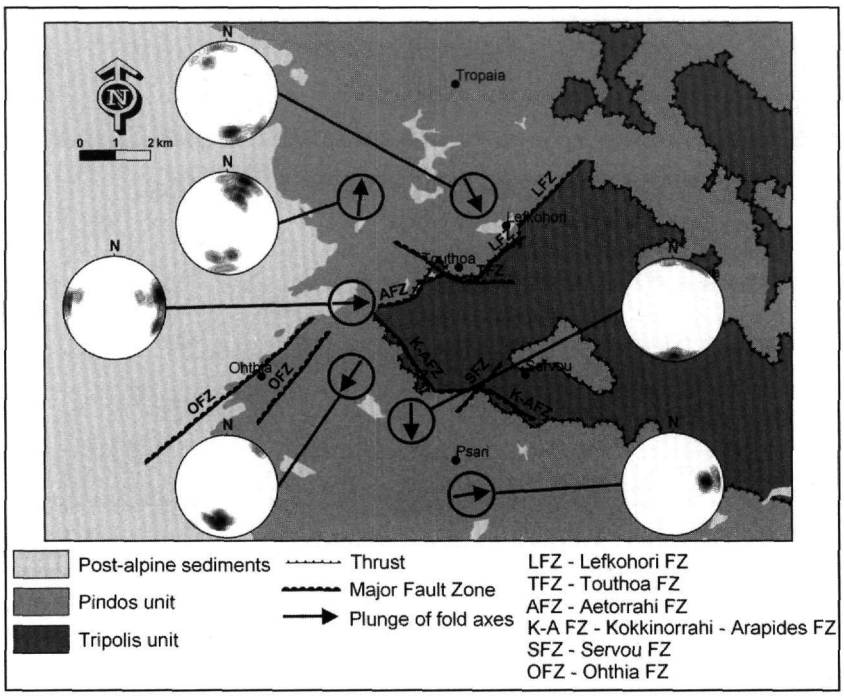

Figure 3 - Structural map showing the tectonic window of Tripolis unit and the main fault zones of the study area as well as the statistical analysis of the fold axes (lower hemisphere, equal area projection) occurring in the Pindos unit formations (see text)

The main neotectonic structures in the study area are the Olympia basin and the Gortynia Mt. horst bounded by major fault zones, which are: Lefkohori fault zone (LFZ), Touthoa fault zone (TFZ), Aetorrahi fault zone (AFZ), Kokkinorrahi-Arapides fault zone (K-AFZ), Servou fault zone (SFZ) and Ohthia fault zone (OFZ) (Fig. 3).

Lefkohori FZ (LFZ) is a NE-SW directed fault zone and constitutes the tectonic boundary between the formations of Tripolis unit and the pelagic carbonates of Pindos unit (Fig. 4A). It forms a large escarpment in the morphology (Fig. 4B) and intense incision transversal to its strike (Fig. 4C). It consists of NW-SE and NE-SW striking faults characterized by a dip-slip kinematics.

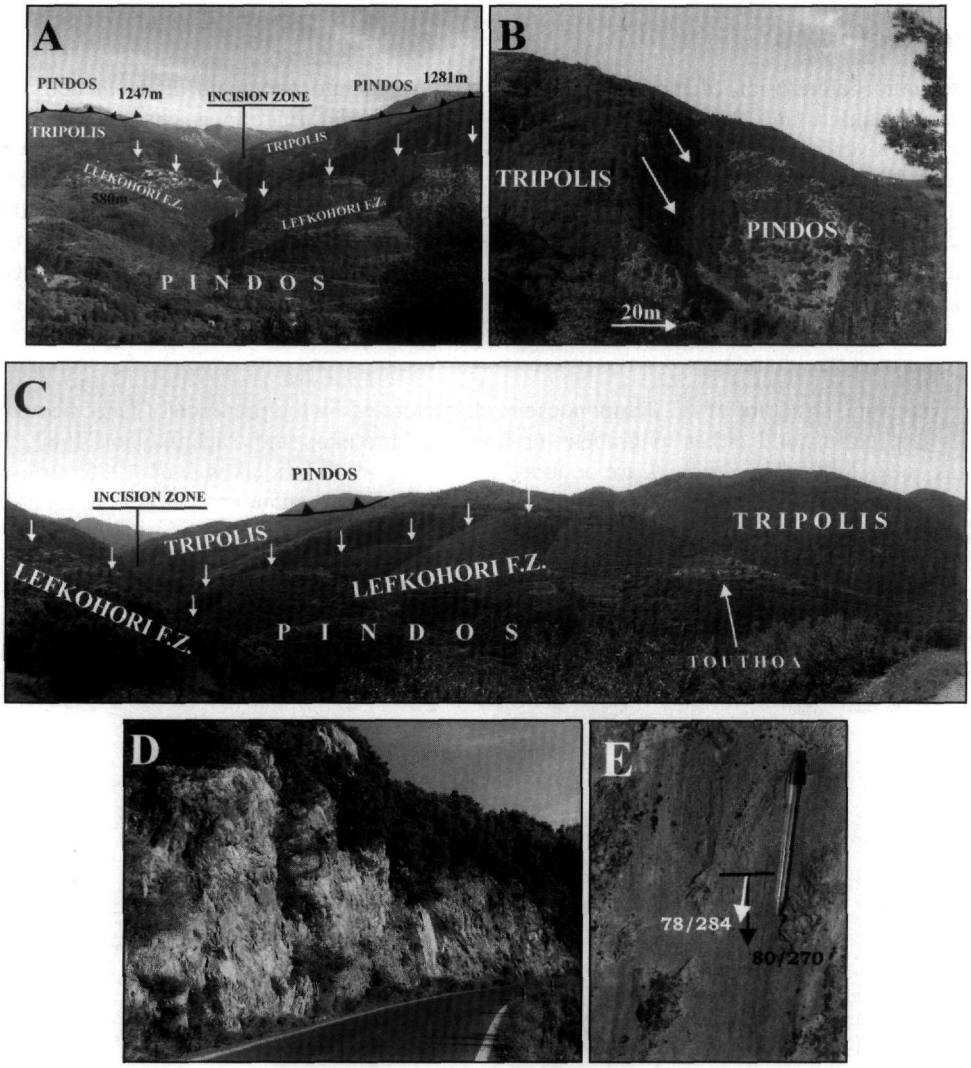

Figure 4 - (A) Partial view of LFZ with incision in the impressive canyon of Touthoa River. The remains of Pindos nappe in Lagadia (left) and Servou (right) indicate a vertical displacement at least 700m for LFZ. (B) LFZ forms a large escarpment in the morphology. (C) Panoramic view of LFZ from northwest. (D) A NW-SE striking fault that cut carbonates of the Tripolis unit and (E) fault surface with dip slip striations

Large remains of Pindos nappe are located in the east and south of Lefkohori FZ in Lagadia and Servou areas respectively. These remains of Pindos unit occur at an altitude of 1241m and they overthrust Tripolis flysch (Fig. 4A). Taking into consideration the occurrence of Pindos formations in the areas of Lefkohori, Lagadia and Servou, the vertical throw of Lefkohori FZ is estimated to be more than 700m.

Touthoa FZ (TFZ) does not present a certain direction (Fig. 5A). In the south and east of Touthoa this fault zone initially has an E-W direction progressively changing to NW-SE in the west of Touthoa. It constitutes the contact between the carbonates and the flysch of Tripolis unit with pelagic limestones and clastic sediments of Pindos unit. It is an E-W striking fault (Fig. 5B) with different striation sets (Fig. 5D).

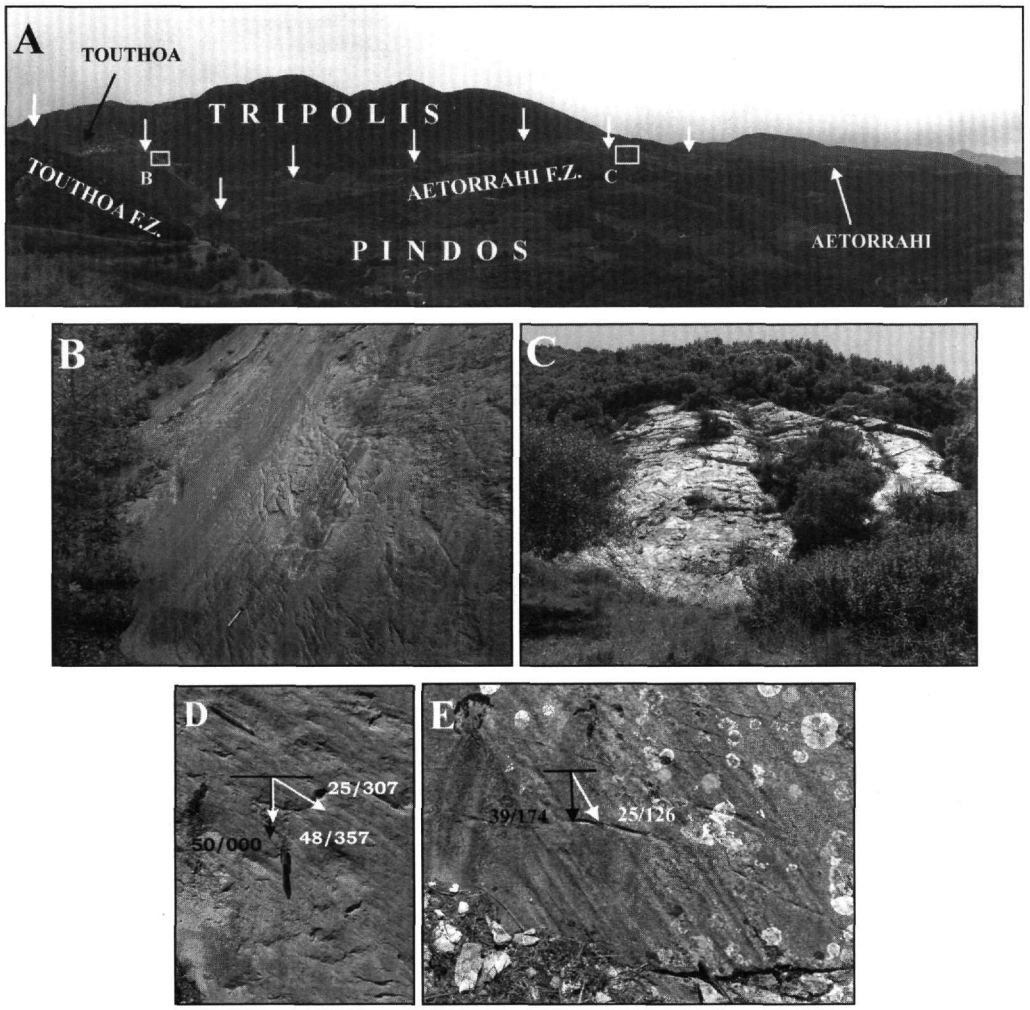

Figure 5 - (A) Panoramic view of Toythoa (TFZ) and Aetorrahi (AFZ) fault zones from northwest. (B) Fault surface of TFZ trending E-W with (D) two sets set of striations. (C) Curved low angle fault surface of AFZ with (E) a set of striations

A large remain of Pindos nappe is located northeast of Touthoa in the region of Servou. The occurrence of Pindos unit that overthrusts Tripolis unit flysch is located at an altitude of 1281 m. Taking into consideration the altitudes that Pindos unit occur in the area of Touthoa (500 m) and Servou (1280 m), the vertical displacement of Touthoa FZ is estimated to be more than 700 m.

Aetorrahi (AFZ) is located in the east-northeast of Aetorrahi village and presents a NE-SW direction (Fig. 5A). It brings to contact the carbonates of Tripolis unit with clastic sediments of Pindos unit. To the east of Aetorrahi a low angle E-W striking fault presents a curved surface dipping 39°/174° (Fig. 5C) and a set of striations plunging 25°/306° (Fig. 5E). The vertical displacement of AFZ is estimated to be at least 650m taking into account the occurrence of Pindos formations in the altitudes of 630 and 1281 m in the Aetorrahi (hangingwall) and Servou (footwall) areas respectively.

Ohthia FZ (OFZ) is NE-SW directed fault zone and consists of two segments in en echelon arrangement. The eastern segment cuts carbonate rocks of Pindos unit (Fig. 6A). On a fault surface of it tectonic breccia and a set of striations is observed (Figs 6A, 6B). The breccia is compact and oligomictic and consists of fragments coming from the Pindos limestones.

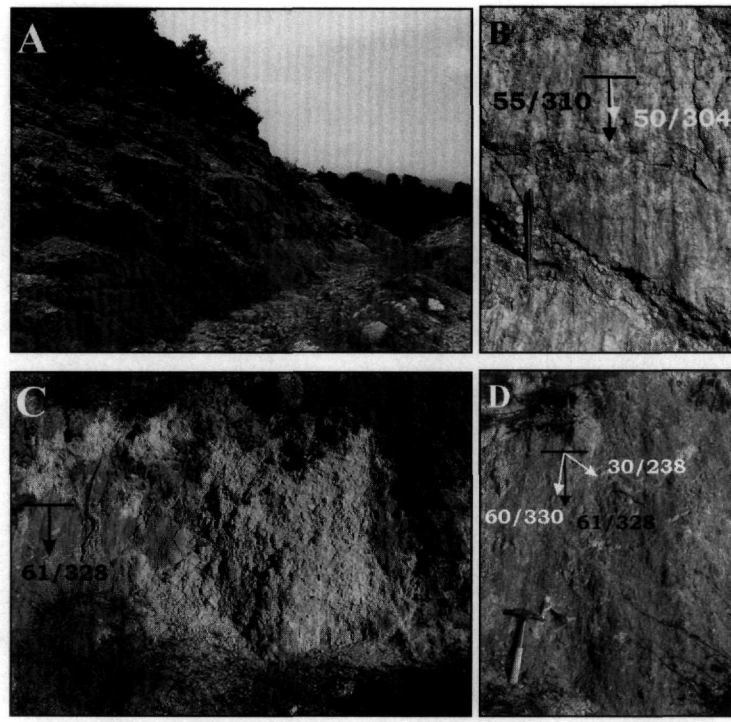

Figure 6 - (A) A NE-SW fault surface of the Ohthia (OFZ) fault zone cutting the limestones of Pindos unit. (B) Tectonic breccia and dip slip striations on it observed on the previous fault surface. (C) A NE-SW fault surface of the same fault zone being the contact between the Pindos limestones and the pleistocene age Erymanthos formation. This surface belongs to the western segment of the OFZ and has (D) two sets of striations

The western segment brings to contact carbonate rocks of Pindos with Erymanthos formation of Pleistocene age (Hagemann 1977, Lekkas *et al.* 1992, Lekkas *et al.* 2000) (Fig. 6C). This segment consists mainly of NE-SW striking faults with two sets of striations and three different types of tectonic breccia taking into account the lithology of the fragments they consist and their relative age (Fig. 6C). The older tectonic breccia consists mainly of fragments coming from Pindos unit and is compact and oligomictic. The intermediate tectonic breccia consists of fragments of Pindos limestones and of Erymanthos formation, as well as from the older breccia and is polymictic and not so compact. The younger tectonic breccia consists of fragments from Erymanthos formation and other breccia and is polymictic and not cohesive. On the fault surface occurring on the younger breccia two sets of striations were observed (Fig. 6D).

Frantzeta Mt. is located west of Servou at an altitude 1240m. Fault zones reactivations cause the uplift of the mountain relatively to the neighboring areas (Fig. 7A). Servou FZ (SFZ) is a NE-SW directed low angle fault zone (Fig. 7B) with surfaces on which three sets of striations as well as iron oxides occur and constitutes the boundary between the neritic limestones and the flysch of Tripolis unit. It. Two of the striation sets show significant horizontal component in the movement as well as dip slip one (Fig. 7C).

Kokkinorrahi - Arapides FZ (K-A FZ) is traced at the northeast of Kokkinorrahi and at the south of Arapides (Fig. 7A). It constitutes the contact between the carbonates and the flysch of Tripolis unit or between the carbonates of Tripolis unit and the clastic sequence of Pindos unit. Eastern of Kokkinorrahi this fault zone initially has an NW-SE direction progressively changing to E-W and again to NW-SE to the south and southeast of Arapides respectively.

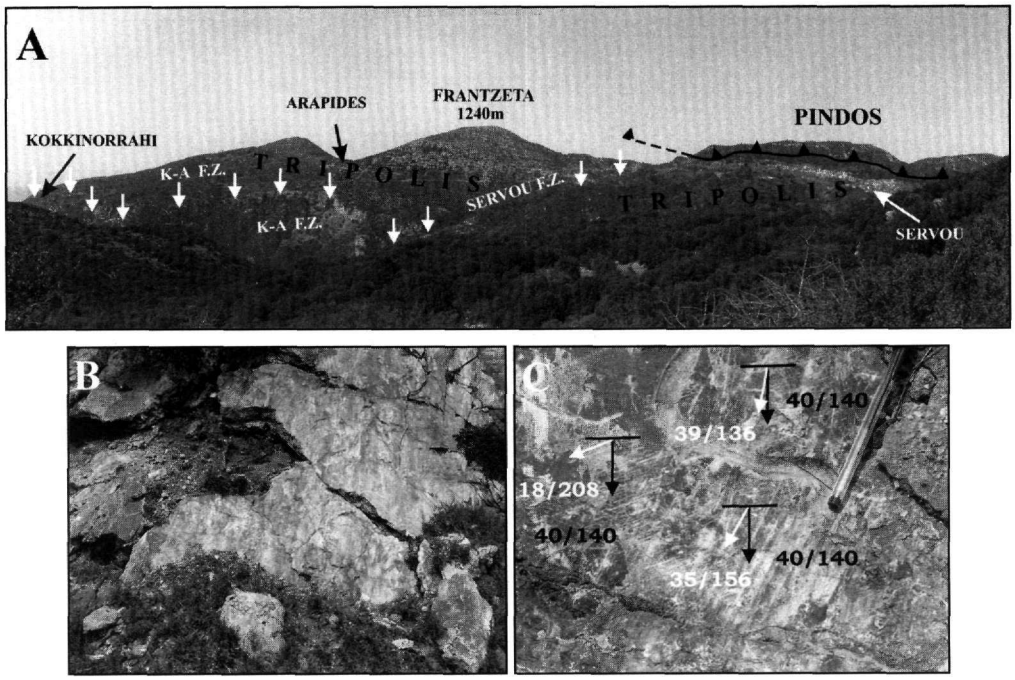

Figure 7 - (A) Panoramic view of Servou (SFZ) and Kokkinorrahi-Arapides (K-AFZ) fault zones with the remains of Pindos nappe in Servou wider area (view from the south). (B) Fault surface of SFZ presenting three sets of striations plunging 35°/156°, 39°/136° and 18°/208° from the older to the younger respectively (C)

In order to understand the kinematics of the area we also studied the deformation of alpine tectonic structure during the neotectonic period. According to the aforementioned, the alpine tectonic structure includes folds and thrusts. Normally, fold axes and thrusts strike N 10-30° W, which is the normal strike of the fold axes and thrusts in the external Hellenides (Mariolakos *et al.* 1985, Mariolakos and Papanikolaou 1987). The strike of the fold axes in the area west of Lefkohori FZ is NNW-SSE and change to E-W in the area west of Aetorrahi area and to N-S in the area northwest of Psari. These changes of the fold axes strike in area close to the fault zones imply that there is an important horizontal component in the Lefkohori, Aetorrahi and Kokkinorrahi - Arapides fault zones (Fig. 3). The effect of the uplift movement of Gortynia Mt. on the alpine tectonic structure of the study area becomes more obvious because of rotations and direction changes of alpine structural elements. The alpine tectonic structure is being deformed during the neotectonic period.

The following comments can be done concerning the construction of the structural contour map of the contact between formations of Pindos geotectonic unit and formations of Tripolis geotectonic unit in the wider area: (i) the general dip direction of the Pindos nappe is towards the west, (ii) the tectonic contact between Pindos unit and Tripolis unit reaches its higher altitudes at the areas of Servou (1100-1200 m) and Lagadia (1200-1300 m), (iii) there are many anticlinal and synclinal structures in the Pindos formations, (iv) the dip direction of the Pindos nappe at the area south-east of Tropaia is towards the west-southwest whereas the dip direction of the Pindos nappe at Touthoa area is towards the northwest, (v) the dip direction of the Pindos nappe at Psari area is towards the south-southwest and (vi) the existence of the faults zones becomes clear near the contact because of the form of the contour lines of structural map (Fig. 8).

The whole structure at the western part present a macro curvature structure of very open anticlinal type with an E-W striking axis in Frantzeta Mt. It has to be noticed that neotectonic macrofolds formed in the post-alpine sediments in different scales have been studied by Mariolakos and Fountoulis (1991) and Fountoulis (1994).

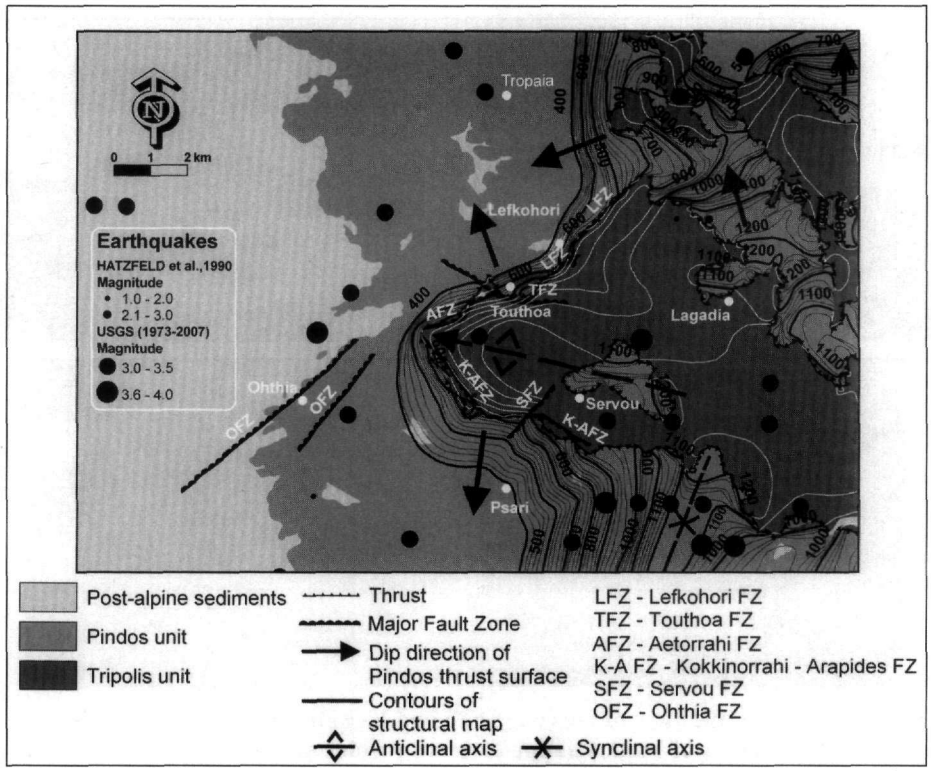

Figure 8 - Structural contour map of the contact between the formations of Pindos and Tripolis geotectonic units and the plot of earthquake epicenters (USGS) in the study area

The earthquake activity in the study area is not so intensive as in the western part of Pyrgos – Olympia basin, but there are several earthquake epicenters. Some of these epicenters could be correlated with the Ohthia fault zone, but it true that there is no seismic evidence that can be correlated with the reactivation of a fault zone.

5. Conclusions -Discussion

Taking into account all the above mentioned we come to the following conclusions:

The endogenic (tectonic) processes control the spatial distribution, the size, the shape, and the elevation of the planation surfaces created on the alpine basement. Furthermore, morphogenetic processes that configure the incision and the geometry of the drainage network are mainly controlled by the neotectonic deformation.

Concerning the activity of all the described neotectonic fault zones, two of them (Ohthia and Lefkohori) are the younger and could be characterized as active due to: (i) the escarpment they present, (ii) the spatial distribution of the planation surfaces created on their footwall and hangingwall blocks, (iii) the incision developed on the footwall transversal to them, and (iv) the reactivation of the faults during the neotectonic period as it is certified by the presence of successive tectonic breccia oligomictic and especially polymictic containing fragments coming from the alpine formations as well as from the Pleistocene age Erymanthos formation. Moreover, the vertical displacement especially of the active fault zones is more than 700 m.

The alpine tectonic structure is intensively deformed during the neotectonic period. This is established by the change of the strike and plunge of the fold axes, especially in the areas close to the studied fault zones.

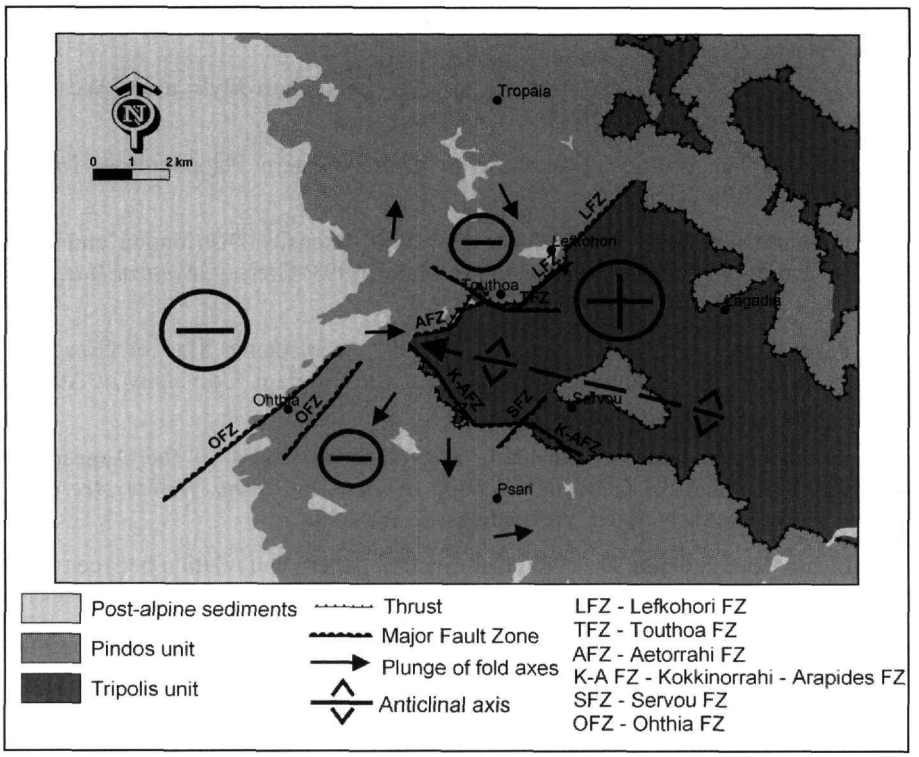

Figure 9 - Map depicting the main neotectonic fault zones of the study area. The symbol (-) corresponds to subsidence and the symbol (+) corresponds to intense uplift

More specifically, it is evident that the geometry of the thrust surface of Pindos tectonic unit has changed considerably, dipping towards NW in the area between Lefkohori - Touthoa and towards SW in the area south of Servou village (Fig. 8) and the fold axes of Pindos unit present a plunge towards south to southwest and in some cases they change plunge towards east (Fig. 8). This change in geometry of the Pindos unit fold axes can be explained taking in to account that the marginal fault zones occurring in the study area and bordering the tectonic horst, present a sinistral strike slip component in the movement causing the dextral rotation of the fold axes especially in the areas close to these fault zones. It has to be mentioned that the observed oblique striations disclose a significant vertical component in the movement.

6. References

Fountoulis, I., 1994. Neotectonic evolution of Central - West Peloponnese, *Thesis*, Sector of Dynamic, Tectonic and Applied Geology, Faculty of Geology, University of Athens, GAIA, **7**, 386pp. (in Greek with abridged English version)

Hagemann, J., 1977. Stratigraphy and sedimentary history of the Upper Cenozoic of the Pyrgos area (W. Peloponnesus, Greece), *Ann. Géol. Pays Hellén.*, 30/2, 441-454. XXVIII, 299-333.

Hatzfeld, D., Pedotti, G., Hatzidimitriou, P., and Makropoulos, K., 1990.The strain pattern in the western Hellenic arc deduced from a microearthquake survey, *Gophys. J. Int.*, 101, 181-202.

Jacobshagen, V., Dürr, S., Kockel, F., Kopp, K.O., Kowalczyk, G., Berckhemer, H., and Büttner, D., 1978. Structure and geodynamic evolution of the Aegean region. In H. Closs, D. Roeder

and K. Schmidt (eds), *Alps, Apennines, Hellenides*, Inter. Union Comm, Geodynamics Sci. Rep. Stuttgart. vol. 38 (1978), 537–564pp.

Katsiavrias, N., 1991. Geological structure of the Lefkochori-Myli area, West - Central Peloponnesus, *Thesis*, 172pp, NTUA. (in Greek)

Lalechos, N., 1974. The geological structure of central-western Peloponnisos, *Thesis*, 94pp., University of Patras. (in Greek)

Lekkas, E., Fountoulis, I., and Papanikolaou, D., 2000. Intensity Distribution and Neotectonic Macrostructure Pyrgos earthquake data (26 March 1993, Greece), *Natural Hazards*, 21, 19-33.

Lekkas, E., Papanikolaou, D., and Fountoulis, I., 1992. Neotectonic Map of Greece, Pyrgos - Tropaia sheet (scale 1:100.000). Applied Scientific Program, University of Athens, Sector of Dynamic, Tectonic and Applied Geology.

Mariolakos, I., and Papanikolaou, D., 1981. The Neogene basins of the Aegean Arc from Paleogeographic and the Geodynamic point of view, Int. *Symp. Hellen. Arc and Trench, Athens, 1981*, Abstracts 65-66, Proceedings, S, 383-399.

Mariolakos, I., and Papanikolaou, D., 1987. Deformation pattern and relation between deformation and seismicity in the Hellenic arc, *Bull. Geol. Soc. Greece*, XIX, 59-76. (in Greek)

Mariolakos, I., and Fountoulis, I., 1991. Neotectonic macrofolds in the area of Filiatra (SW Peloponnese, Greece), *Proceedings 5th Geol. Congress of the Geol. Soc. Greece, May 1990, Thessaloniki, Bull. Geol. Soc. Greece*, XXV/3, 19 – 38. (in Greek)

Mariolakos, I., Papanikolaou, D., and Lagios, E., 1985. A Neotectonic Geodynamic Model of Peloponnesus Based on Morphotectonics, Repeated Gravity Measurements and Seismicity, *Geol. Jb.*, B 50, 3-17.

Papanikolaou, D., 1986. Geology of Greece. 240pp. Athens. (in Greek)

USGS National Earthquake Information Center – NEIC: http://earthquake.usgs.gov/regional/neic

Δελτίο της Ελληνικής Γεωλογικής Εταιρίας τομ. XXXX, 2007
Πρακτικά 11ου Διεθνούς Συνεδρίου, Αθήνα, Μάιος 2007

Bulletin of the Geological Society of Greece vol. XXXX, 2007
Proceedings of the 11th International Congress, Athens, May, 2007

COST Action 625 Results: Monitoring of the Kaparelli fault, 2003-2006

Ganas A.[1], Drakatos G.[1], Bosy J.[2], Petro L.[3], Kontny B.[2], Stercz M.[3], Melis N. S.[1], Cacon S.[2], Papanikolaou M.[1], Pirentis A.[1], and Kiratzi A.[4]

[1] *Institute of Geodynamics, National Observatory of Athens, 11810 Athens, Greece*
aganas@gein.noa.gr

[2] *Institute of Geodesy and Geoinformatics, Agricultural University of Wroclaw, Grunwaldzka 53, 50-357 Wroclaw, Poland*

[3] *Geological Survey of Slovak Republic, Jesenskeho 8, SK-040 01 Kosice, Slovak Republic*

[4] *Department of Geophysics, Aristotle University of Thessaloniki, 54124 Thessaloniki, Greece*

Abstract

Since November 2003 a collaborative group between Greek, Polish, and Slovak colleagues installed a dense network of non-permanent GPS stations and extensometers to monitor active faults in the eastern end of the Gulf of Corinth, central Greece. The network includes eleven GPS stations across the Kaparelli fault and the Asopos rift valley to the east and two TM-71 extensometers that were installed on the Kaparelli fault plane. The motions recorded by the TM-71 instruments show agreement with long-term fault kinematics. The GPS network has been measured in three campaigns (2004, 2005 & 2006) with very good accuracies (1-4 mm in the horizontal plane). Given that the total offset on the Kaparelli fault is small, and the geological data suggesting a segmented character of this fault, we expect in the near future to differentiate fault slip and strain accumulation among segments.

Key words: *Active faults, GPS, TM-71, Kaparelli, Corinth Gulf, earthquakes, strain.*

Περίληψη

Η ευρύτερη περιοχή του Καπαρελλίου Βοιωτίας παρακολουθείται από διεθνή ομάδα γεωεπιστημόνων με σκοπό την μέτρηση της σύγχρονης παραμόρφωσης και την σύγκριση της με τα γεωλογικά δεδομένα από μετρήσεις υπαίθρου και παλαιοσεισμολογικές τομές. Η έρευνα ξεκίνησε το έτος 2003 με χρηματοδότηση κυρίως από το Ευρωπαϊκό πρόγραμμα COST Action 625. Εγκαταστήσαμε στο ενεργό ρήγμα του Καπαρελλίου α) δύο επιμηκυνσιόμετρα τύπου TM-71 για την καταγραφή των κινήσεων πάνω στο επίπεδο του ρήγματος και β) έντεκα (11) σταθμούς GPS για την μέτρηση της παραμόρφωσης του στερεού φλοιού κοντά στο ρήγμα. Τα πρώτα αποτελέσματα είναι πολύ ενθαρρυντικά διότι βασίζονται σε καλής ποιότητας μετρήσεις και συγκρίνονται ευνοϊκά με τα γεωλογικά δεδομένα.

Λέξεις κλειδιά: *Ενεργό ρήγμα, Καπαρέλλι, GPS, TM-71, σεισμοί, παραμόρφωση.*

1. Introduction

Central Greece is one of the most tectonically active and rapidly extending regions in the world. Surface topography and geomorphology are clearly associated with seismic activity along large normal faults (Armijo *et al.* 1996). Extension is mainly directed N-S (Clarke *et al.* 1998) with greater rates towards the west. In February – March 1981 a sequence of three earthquakes with magnitudes greater than 6.3 struck the eastern Gulf of Corinth (King *et al.* 1985, Hubert *et al.* 1996). North-dipping surface breaks were noted the morning after the first two events on the southern side of the Gulf (Perachora Peninsula) and south-dipping ruptures appeared on the northern side of the Gulf (Kaparelli region) as a result of the third event (Fig. 1; data from Jackson *et al.* 1982). In both areas seismic motion occurred along basin-bounding faults bringing in contact Mesozoic limestone and alluvial deposits as well as colluvium. Focal mechanisms of small and shallow earthquakes (data from Ambraseys and Jackson 1990) also show normal faulting with the active fault plane dipping at about 45° for faults at the eastern end of the Gulf of Corinth including Kaparelli. Our group used two (2) TM-71 extensometers to measure fault-motion on a monthly basis and GPS satellite technology to pinpoint the location of survey stations down to a fraction of a centimetre. We set up a pillar-mounted antenna over a survey station and attached a data receiver to the antenna. The antenna picks up GPS satellite signals and stores the information in the data receiver. After two days of observations, the set-up is taken down and we downloaded the data onto computers for processing. After processing, the data is used to determine the station locations and the strain across active faults.

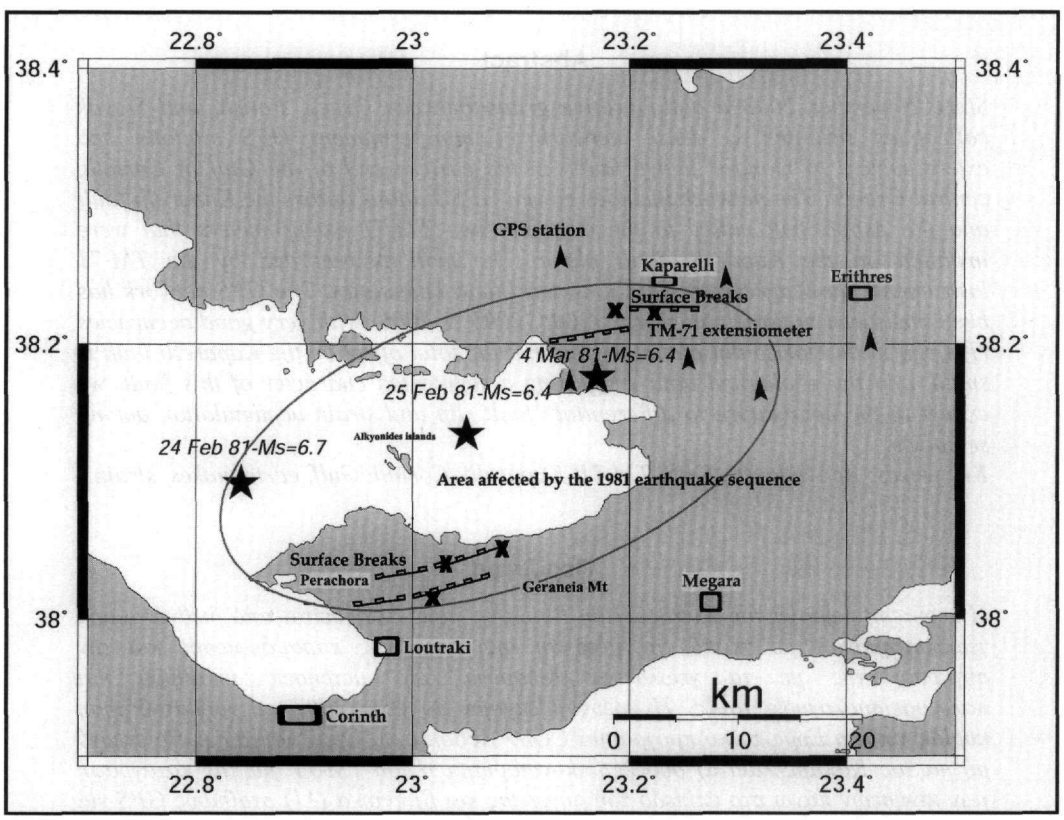

Figure 1 – Map of the study area showing epicentres of the 1981 earthquake sequence (stars). X signs point to TM-71 instrument locations and black arrows indicate locations of non-permanent GPS stations installed during 2003. Lines with barbs indicate normal faults that ruptured during the 1981 earthquake sequence

2. Monitoring the activity of the Kaparelli Fault

The Kaparelli Fault consists of three segments, two of which were ruptured in 1981 (Jackson *et al.* 1982). The two-ruptured segments form left-stepping en echelon geometry, while the third north-western segment of the fault did not rupture (Fig. 2). The fault segments are clearly expressed at the surface by nearly continuous scarps. The footwall elevation is 600 m and lithology is composed of hard, Mesozoic limestone. The hanging wall block forms a small basin and contains approximately 200 m of fluvial-terrestrial deposits of Pleistocene age as well as Holocene alluvium. Recently, three trenches have been excavated across the Kaparelli Fault (Pavlides *et al.* 2003, Kokkalas *et al.* in press). Their stratigraphic record shows at least three events during the Holocene period, with the 1981 event included. The estimated mean slip rate is 0.28 mm/yr. Colluvial tectonostratigraphy and analysis of displacements on key horizons suggests surface rupturing events in the order of 0.7-1 m.

In order to measure the kinematics of deformation in 3-D our group has installed a) a dense GPS network and b) two (2) extensometers. The details of installation of instruments and project rationale are given in Drakatos *et al.* (2005) and Cacon *et al.* (2005). In summary, our group has begun monitoring of the Kaparelli fault area since May 2003. On May 26, 2003 we installed an extensometer of TM-71 type (Kostak and Cruden 1990). At this site the fault strikes N77°E and dips 77° towards the South. A second instrument was installed on July 15, 2004. The TM-71 readings are recorded on a nearly monthly basis by NOA. In addition, a dense GPS network has been installed comprising six (6) stations. The network was deployed on November, 11-12 2003 and its first measurement took place in May 2004. The network was expanded on March 31, 2005. Five (5) new stations were installed inside the Asopos rift valley (see Figure 4 below). Both sub-networks were measured during May 2005 and May 2006.

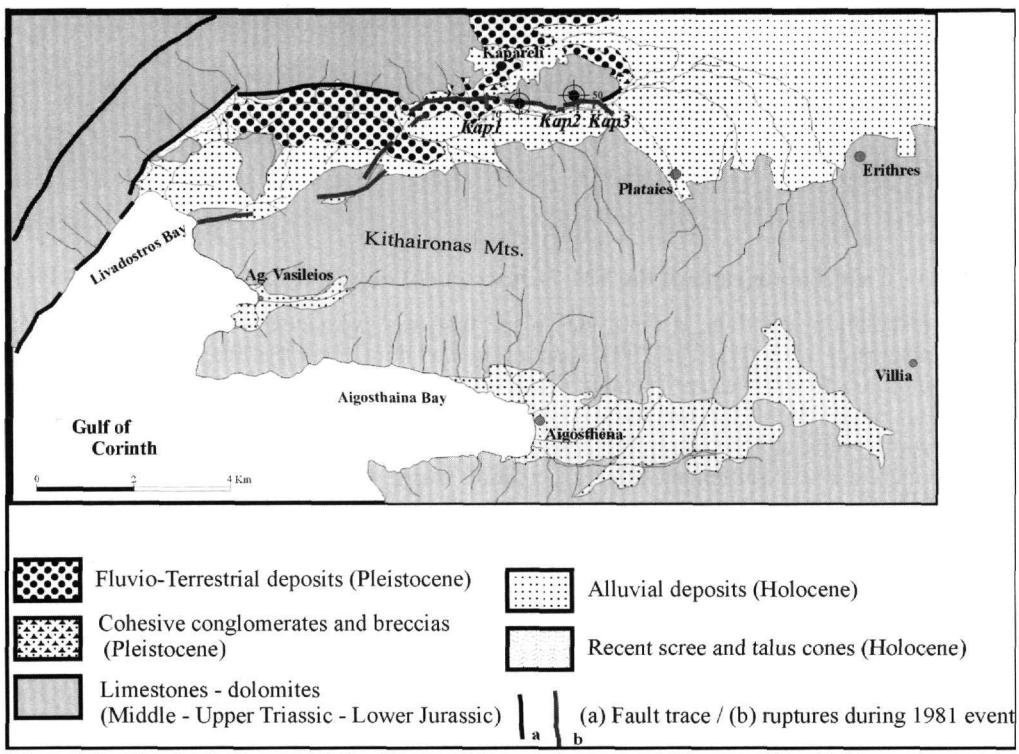

Figure 2 - Geological map of the Kaparelli area in central Greece. The 1981 ruptures are shown in red. Trench positions are denoted by Kap1, Kap2 and Kap3. Circle symbols point to TM-71 installations. Map after Pavlides *et al.* 2003

3. Monitoring fault motion using TM-71 Instruments

The TM-71 is designed to monitor long-term displacements in all three directions in space at millimetre scale. It is capable of recording displacements by producing interference patterns on optical grids (Kostak 1991) in the form of black and white fringes. It mainly consists of two identical indicators consisting of two superimposed glass plates. On each glass plate a grid of equidistant circles and a grid consisting of equidistant parallel lines have been etched. The interference patterns produced by the circular grids consist of a number of symmetrically arranged fringes stretching radially from the centre. The number N of the fringes on one side of the diameter (symmetry axis) provides the length of the displacement vector while the orientation of the symmetry axis provides its direction (Fig. 3). The advantage of this instrument is that, it involves no electromechanical parts and it can be easily installed across active faults by use of steel bars (e.g. Maniatis *et al.* 2003, Drakatos *et al.* 2005).

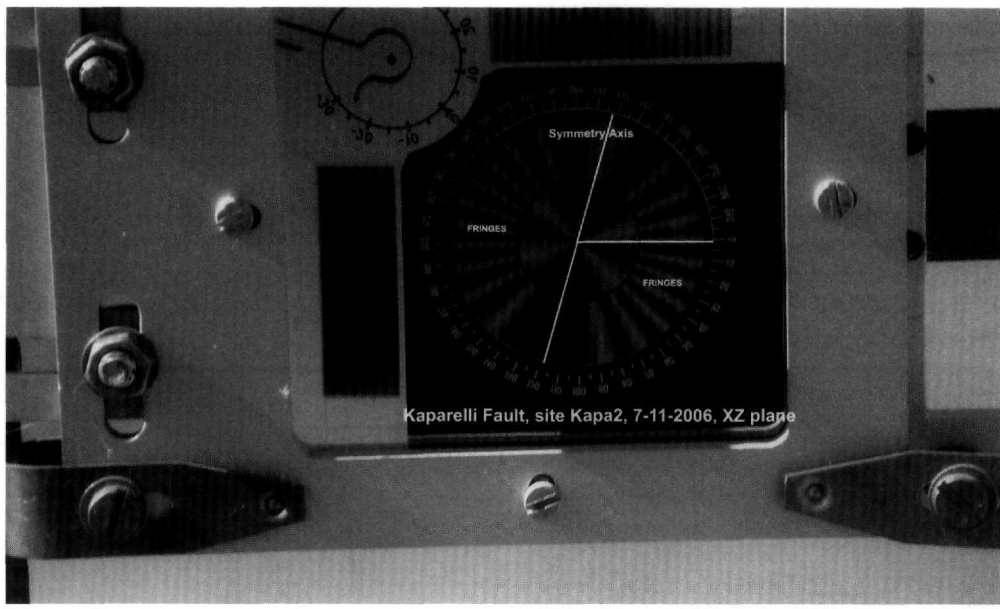

Figure 3 – Field Photograph of the TM-71 instrument on site Kapa2 (7 November 2006)

The 2003 installation was done at the trench Kap2 that was excavated across the Kaparelli fault (Fig. 2; Drakatos *et al.* 2005). The 2004 installation was done against a free surface of the fault plane, about 2 km to the west of locality Kap2, near the asphalt road from Kaparelli to Agios Vasilios. Our observations for site Kapa1 span a period of 3 years so it is possible to make a preliminary interpretation (Fig. 4). Initial change in X-axis (up to the end of 2003) is probably the result of concrete block settlement after its creation inside the trench. Since 2004 we observe opening of the order of 0.2-0.4 mm that is in agreement with average fault slip rate from past earthquakes. We also observe a seasonal effect of opening-closure that is probably related to the temperature variation of the steel bar which is directly exposed to sunlight. Displacement along Z-axis is relatively stable. Along the axis Y (horizontal; along the fault strike) observed motion is dextral oblique slip. A similar pattern is observed in the rotation plot (Fig. 4) for the plane XY (the horizontal plane) which is stable since early 2004. Rotation sense is negative because the near-fault side is compressed due to shear. This dextral shear motion is consistent with the slip vector model of Roberts and Ganas (2000) that predict oblique slip vectors at normal fault tips. In Kapa2 the observation period is shorter (about 2 years) but the fault-normal opening is stable (X-axis; Fig. 4). The signal along the two other axes is less clear. However, the rotation plot shows positive values that indicate sinistral motion on the horizontal plane (XY).

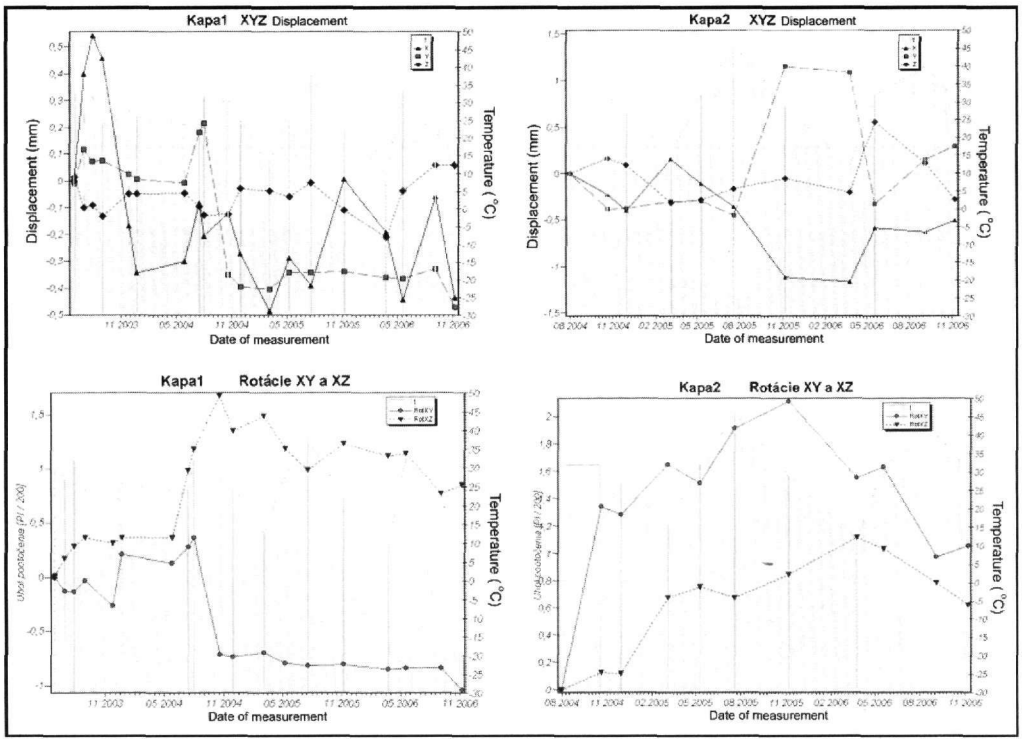

Figure 4 – (Left) Displacement – Time diagram for site Kapa1 along the Kaparelli Fault. (Right) Displacement – Time diagram for site Kapa2. Accuracy of measurements better than 0.1 mm (Stemberk *et al.* 2003). Bottom graphs show rotation of XY (horizontal) and XZ (vertical) planes of the instrument, respectively. Units are in grades (1 circle = 400 grades). The position of the X, Y, and Z axes of the instrument corresponds respectively to: (X) the direction perpendicular to the fault or fault-normal motion, (Y) direction parallel to fault strike or the strike slip motion along the fault surface and (Z) vertical direction or the dip slip component of motion

4. Monitoring regional deformation using GPS Instruments

The motion of crustal blocks in central Greece can be described in a first approximation by a combination of translation and rotation (Goldsworthy *et al.* 2002). Strain accumulation occurs across major rift zones including the Gulf of Corinth and Gulf of Evia (Clarke *et al.* 1998). Strain is not localized uniformly but with noticeable variations both in azimuth and amplitude. This difference could be explained by either along-strike changes in fault behavior or in material properties. Geological data by Roberts and Ganas (2000) indicate the long-term strain patterns along normal faults are not uniform and that a systematic difference exists between the average extension directions in central Greece (Gulf of Corinth vs Gulf of Evia). KAPNET (Fig. 5) was designed with two things in mind: a) to map strain build-up along the Kaparelli fault – Asopos rift valley for better estimating earthquake potential and b) to compare geodetic strain patterns with geological strain patterns. A third objective is to measure local variations in strain rate that might reveal the mechanical properties of earthquake faults.

The KAPNET network spans about 1-5 kilometers on either side of the surface trace of the Kaparelli fault (Fig. 5). Baseline length rates of change from this network can be used to measure the near-fault strain rate. The network was measured for the first time in May 2004 using the ASTHECH receivers of the Polish group. In particular stations ERIT, KAPA and TAPS (Fig. 4)

were surveyed using ASHTECH Zxtreme instruments and ASH701975.01A antennas where remaining stations were surveyed using Z-XII instruments and ASH700718B antennas. Station AGTR (Fig. 5) was used as the base station. The initial network was expanded during 2005 with the installation of five (5) more stations. All NOA stations were measured using Leica 1200 receivers.

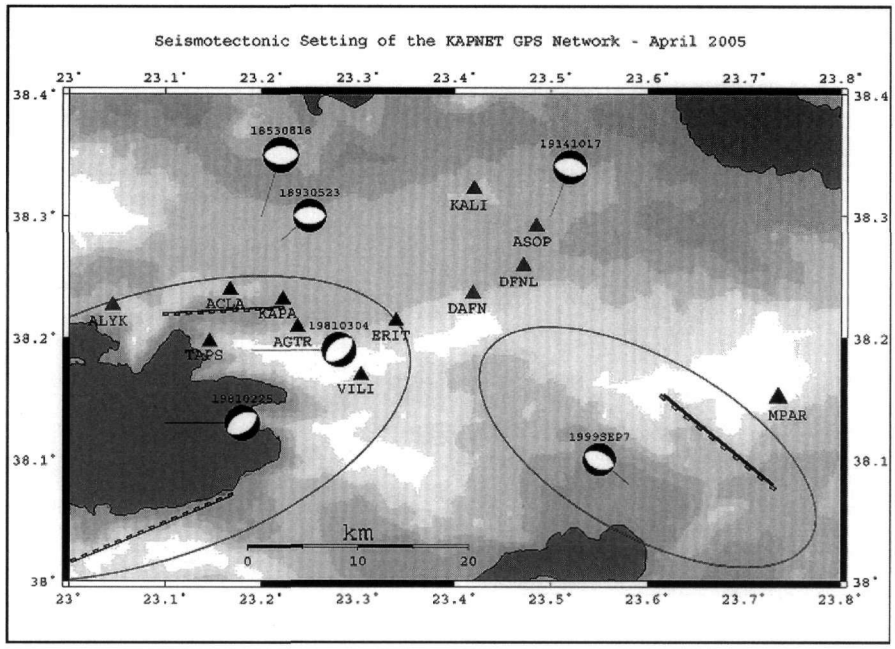

Figure 5 – Elevation map of the study area showing the locations of the GPS stations. Dark red triangles show the 2003 installations. Beachballs represent fault plane solutions of strong, shallow earthquakes

The GPS observations from 2005 and 2006 campaigns were processed with the Bernese GPS post-processing software (version 4.2; Hugentobler *et al.* 2001). The data were combined with regional permanent sites MATE (Italy) and IGD1 (2005), NOA1 (2006; Athens, Greece). The solutions were then transformed into ITRF2000 (Altamini *et al.* 2002; each daily session separately). A special data processing strategy was developed for the local precise network with the following issues and assumptions (Bosy and Kontny 1998, Bosy *et al.* 2003): a) Global ionosphere model CODE for a phase ambiguity resolution b) Antenna phase centres calibrated according to the NGS, c) Troposphere model – the Niell mapping function without a priori model; residual atmosphere zenith delays were estimated for one-hour intervals and d) Precise ephemeris computed by the Centre of Orbit Determination in Europe (CODE) to determine satellite positional data.

All KAPNET positions were resolved with Root-Mean-Square residuals less than 2 mm (on average; Fig. 6). The antenna parameters of the 2005 and 2006 campaigns are given in Table 1. Our first results include coordinates and RMS errors of KAPARELLI local network points for two years 2005 and 2006. They were generated by connecting the daily solutions using the ADDNEQ program (Brockmann 1996, Hugentobler *et al.* 2001). Computed ITRF2000 (observation epoch) φ and λ coordinates, ellipsoidal heights and their RMS errors are collected in Table 2. The accuracy of determined coordinates (φ, λ and h) representing un-weighted RMS values of coordinate residuals taken from each year (comparison of station coordinates from each session with respect to the combined solution in mm) is shown in Figure 6. The un-weighted RMS values computed from repeated observations give more realistic accuracy of stations coordinates. They provide conditions for detecting horizontal movements of the stations at the <5 mm level (maximum) and at <2 mm level (mean value).

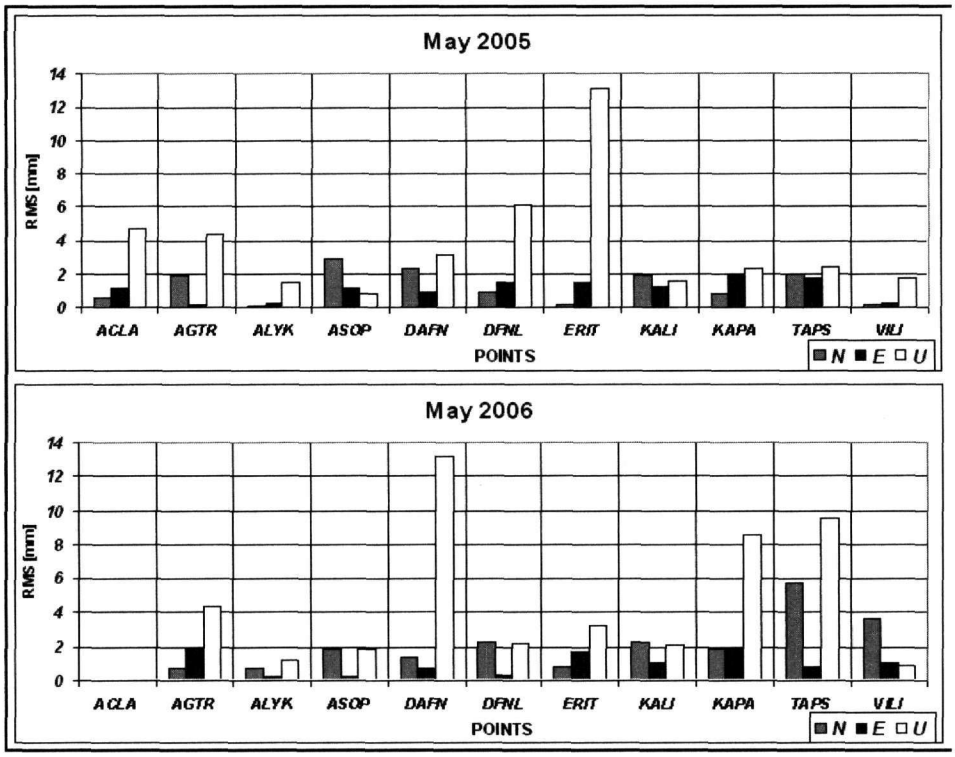

Figure 6 – The un-weighted RMS values with respect to the combined solution in mm

5. Discussion - Conclusions

a) Data from the TM71 instruments along the Kaparelli Fault show fault-normal opening as expected for this normal fault. A seasonal effect is also discernible in the data of Kapa1 instrument (Fig. 4). Also, the shear motion in Kapa1 is dextral in agreement with non-uniform strain patterns along active normal faults (Roberts and Ganas 2000).

b) Three (3) similar instruments have been installed in the Perachora peninsula by Maniatis *et al.* (2003; Fig. 1). Given that Holocene fault slip rates at these localities differ by a factor of five (5) or even more it is important to compare 3-D strain measurements in order to estimate inter-seismic strain accumulation along the two fault zones. Another issue concerns the identification of instrument-induced errors on our measurements and their estimation. The advantage that TM-71 has no electronics parts is counterbalanced by the infinitesimal deformations caused by climatic fluctuations (precipitation, temperature). For example a seasonal effect along the X-axis is visible in the 16-year data series from the Simitli graben in SW Bulgaria (Dobrev and Kostak 2000).

c) The data processing of repeated satellite GPS standards provide conditions for detecting horizontal movements at our stations at 2 mm level (on average). Taking into account the mean fault movement rate of about 0.3 mm/y, indicated by paleoseismology, significant displacement across Kaparelli can be detected by GPS after 4-7 years of observations. With data of such precision we could address two important questions: (1) is there systematic variation along strike in the near-fault strain rate? Variations along strike could be explained by spatial changes in the depth to which the fault is locked in the inter-seismic period, or by variations in the elastic properties of rocks near the fault zone. (2) How well can a single elastic model fit both the near-field and far-field strain observed geodetically?

Table 1 - Parameters of the GPS antennas of the Kaparelli (Greece) research area during the 2005 and 2006 field observation campaigns. Height is in metres

2005							
130				131			
POINT	ANT. TYPE	h-OBS	h-RED	POINT	ANT. TYPE	h-OBS	h-RED
ACLA	ASH700718B	0.8290	0.7654	ACLA	ASH700718B	0.8300	0.7664
AGTR	ASH700936D_M	0.7640	0.7262	AGTR	ASH700936D_M	0.7640	0.7262
ERIT	ASH701975.01Agp	0.7810	0.7380	ERIT	ASH701975.01Agp	0.7830	0.7400
KAPA	ASH701975.01Agp	0.8080	0.7650	KAPA	ASH701975.01Agp	0.8070	0.7640
TAPS	ASH701975.01Agp	0.8140	0.7710	TAPS	ASH701975.01Agp	0.8140	0.7710
VILI	ASH700718B	0.8150	0.7514	VILI	ASH700718B	0.8150	0.7514
ALYK	LEIAT502	0.7230	0.6672	ALYK	LEIAT502	0.7230	0.6672
ASOP	LEIAX1202	0.7500	0.6880	ASOP	LEIAX1202	0.7500	0.6880
DAFN	LEIAX1202	0.7210	0.6590	DAFN	LEIAX1202	0.7210	0.6590
DFNL	LEIAX1202	0.7390	0.6770	DFNL	LEIAX1202	0.7390	0.6770
KALI	LEIAX1202	0.7230	0.6610	KALI	LEIAX1202	0.7230	0.6610
2006							
122				123			
POINT	ANT. TYPE	h-OBS	h-RED	POINT	ANT. TYPE	h-OBS	h-RED
ACLA	ASH700718B	0.8350	0.7714	ACLA	ASH700718B	0.8350	0.7714
AGTR	ASH700936D_M	0.7640	0.7292	AGTR	ASH700936D_M	0.7640	0.7292
ERIT	ASH701975.01Agp	0.7810	0.7380	ERIT	ASH701975.01Agp	0.7810	0.7380
KAPA	ASH701975.01Agp	0.8070	0.7640	KAPA	ASH701975.01Agp	0.8070	0.7640
TAPS	ASH701975.01Agp	0.8120	0.7690	TAPS	ASH701975.01Agp	0.8120	0.7690
VILI	ASH700718B	0.8200	0.7564	VILI	ASH700718B	0.8210	0.7574
ALYK	LEIAT502	0.6910	0.6910	ALYK	LEIAT502	0.6910	0.6910
ASOP	LEIAX1202	0.6910	0.6910	ASOP	LEIAX1202	0.6910	0.6910
DAFN	LEIAX1202	0.6910	0.6910	DAFN	LEIAX1202	0.6910	0.6910
DFNL	LEIAX1202	0.6910	0.6910	DFNL	LEIAX1202	0.6910	0.6910
KALI	LEIAT502	0.6910	0.6910	KALI	LEIAT502	0.6910	0.6910

Table 2 - The ITRF 2000 coordinates of the KAPNET stations

Point	φ			λ			h	RMS φ	RMS λ	RMS h
	[o ' "]			[o ' "]			[m]	[mm]	[mm]	[mm]
ITRF2000 EPOCH: 2005-05-10 23:59:45										
ACLA	38	14	20.457830	23	10	1.655841	473.2161	0.5	0.7	3.7
AGTR	38	12	29.119021	23	14	13.982700	578.4204	0.5	0.7	3.7
ALYK	38	13	34.536100	23	2	42.984761	474.9853	0.7	0.7	4.9
ASOP	38	17	28.851765	23	29	6.323049	321.9817	0.5	0.7	3.7
DAFN	38	14	8.585989	23	25	7.455789	533.3963	0.5	0.7	3.7
DFNL	38	15	31.194095	23	28	16.535688	357.5885	0.5	0.7	3.7
ERIT	38	12	47.859336	23	20	21.377514	474.0419	0.5	0.7	3.9
KALI	38	19	18.825944	23	25	14.223037	395.7988	0.5	0.7	3.9
KAPA	38	13	52.699457	23	13	18.760112	340.7526	0.5	0.7	3.7
TAPS	38	11	47.745238	23	8	45.103563	481.9591	0.5	0.7	3.9
VILI	38	10	7.788711	23	18	11.234132	694.3970	0.5	0.7	3.7
ITRF2000 EPOCH: 2006-05-02 23:59:45										
ACLA	38	14	20.457462	23	10	1.656128	473.2449	0.5	0.5	3.1
AGTR	38	12	29.118592	23	14	13.982988	578.4606	0.3	0.3	2.0
ALYK	38	13	34.535574	23	2	42.985050	475.0196	0.4	0.5	3.0
ASOP	38	17	28.851322	23	29	6.323437	322.0029	0.3	0.4	2.3
DAFN	38	14	8.585571	23	25	7.456152	533.3879	0.4	0.5	2.7
DFNL	38	15	31.193592	23	28	16.535760	357.6028	0.3	0.4	2.1
ERIT	38	12	47.858913	23	20	21.377813	474.0702	0.3	0.4	2.1
KALI	38	19	18.825917	23	25	14.223237	395.8117	0.3	0.4	2.7
KAPA	38	13	52.699048	23	13	18.760358	340.7809	0.4	0.4	2.4
TAPS	38	11	47.744646	23	8	45.103803	481.9939	0.3	0.4	2.1
VILI	38	10	7.788286	23	18	11.234429	694.4191	0.3	0.3	2.0

d) The large E-W faults of the Gulf of Corinth slip fast (1-2 mm/yr) and terminate towards the south of the Kaparelli Fault, while the large normal faults of the Parnitha region to the east slip at about five (5) to ten (10) times less (0.2-0.4 mm/yr; Ganas *et al.* 2004). It is interesting to map this transition in fault slip rates by using the GPS measurements of KAPNET. Our first results (Fig. 6) point to an excellent quality of GPS data that will provide stable solutions. A second point concerns the total offset on the Kaparelli fault that is small (< 200 m), while the geological data suggest that it is segmented. So our GPS measurements will differentiate strain accumulation among the segments. These observations will also shed light into fault growth processes as Kaparelli is an early phase in the development of large normal faults that involves the merging of two or more faults of differing strikes, rather than the steady lengthening of a single fault segment.

e) The results from the GPS observations will help us establish both the magnitude and direction of geodetic strain and compare it with the Holocene faulting record as published in Pavlides *et al.* (2003) and Kokkalas *et al.* (in press). The orientation of the strain axes will be also compared with the configuration of the rupture zones of both the 1981 and the 1999 earthquakes (Fig. 5).

6. Acknowledgments

This research was funded by COST Action 625, the General Secretariat for Research (Greece) and the National Observatory of Athens. We are indebted to our COST colleagues for many stimulating discussions. The NOA GPS poles were constructed at the NESTOR workshop in Pylos. We acknowledge helpful discussions by B. Kostak, George Stavrakakis, Spiros Pavlides, Yannis Koukouvelas, Andrei Gosar, Luigi Piccardi, Emanuele Tondi and Vincenzo Spina. Many thanks are due to Mr. Errikos Skassis for this help with GPS instrumentation. We also thank two anonymous reviewers for comments.

7. References

Altamini, Z., Sillard, P., and Boucher, C., 2002. ITRF2000: A new release of the International Terrestrial Reference Frame for Earth Science applications, *J. Geoph. Res.*, 107 (B10), 2214, doi: 10.1029/2001JB000561.

Ambraseys, N.N., and Jackson, J.A., 1990. Seismicity and associated strain of central Greece between 1890 and 1988, *Geophysical J. Int.*, 101, 663-708.

Armijo, R., Meyer, B., King, G.C.P., Rigo, A., and Papanastasiou, D., 1996. Quaternary evolution of the Corinth Rift and its implications for the Late Cenozoic evolution of the Aegean, *Geophys. J. Int.*, 126, 11–53.

Bosy, J., and Kontny, B., 1998. Strategy of GPS data processing in local geodynamical networks, *Reports on Geodesy* No. 9(39), Warsaw University of Technology, Institute of Geodesy and Geodetic Astronomy, 105-113pp.

Bosy, J., Figurski, M., and Wielgosz, P., 2003. A strategy for GPS data processing in a precise local network during high solar activity, *GPS Solutions*, Volume 7, Number 2 Springer-Verlag, 120–129pp.

Brockmann, E., 1996. Combination of Solutions for Geodetic and Geodynamic Applications of the Global Positioning System (GPS) PhD. dissertation, Astronomical Institute, University of Berne, Berne, Switzerland.

Cacon, S., Kontny, B., Bosy, J., Cello, G., Piccardi, L., Tondi, E., Drakatos, G., and Ganas, A., 2005. Local geodynamic researches in Polish Sudetes and the Mediterranean region, *Reports on Geodesy*, No. 2 (73), 231-244.

Clarke, P.J., Davies, R.R., England, P.C., Parsons, B., Billiris, H., Paradissis, D., Veis, G., Cross, P.A., Denys, P.H., Ashkenazi, V., Bingley, R., Kahle, H.-G., Muller, M.-V., and Briole, P., 1998. Crustal strain in central Greece from repeated GPS measurements in the interval 1989-1997, *Geophys. J. Int.*, 135(1), 195-214.

Dobrev, N., and Kostak, B., 2000. Monitoring tectonic movements in the Simitli graben, SW Bulgaria, *Engineering Geology*, 57(3-4), 179-192.

Drakatos, G., Petro, L., Ganas, A., Melis, N., Kostak, B., Kontny, B., Cacon, S., and Stercz, M., 2005. Monitoring of strain accumulation along active faults in the eastern Gulf of Corinth: Instrumentation and network setup, *Acta Geodyn. Geomater.*, 2, No 1(137), 13–23.

Ganas, A., Pavlides, S. B., Sboras, S., Valkaniotis, S., Papaioannou, S., Alexandris, G. A., Plessa, A., and Papadopoulos, G. A., 2004. Active Fault Geometry and Kinematics in Parnitha Mountain, Attica, Greece, *Journal of Structural Geology*, 26, 2103-2118.

Goldsworthy, M., Jackson, J., and Haines, A.J., 2002. The continuity of active fault systems in Greece, *Geophysical Journal International*, 148, 596-618.

Hubert, A., King, G., Armijo, R., Meyer, B., and Papanastasiou, D., 1996. Fault Re-activation, Stress Interaction and Rupture Propagation of the 1981 Corinth Earthquake Sequence, *Earth & Planet. Sci. Lett.*, 142, 573-585.

Hugentobler, U, Sacher, S., and Fridez, P., 2001. Bernese GPS Software Version 4.2, Astronomical Institute, University of Berne, Switzerland.

Jackson, J.A., *et al.,* 1982. Seismicity, normal faulting and the geomorphological development of the Gulf of Corinth (Greece): the Corinth earthquakes of February and March 1981, *Earth & Planet. Sc. Let.*, 57, 377–397.

King, G.C.P., Ouyang, Z.X., Papadimitriou, P., Deschamps, A., Gagnepain, J., Houseman, G., Jackson, J.A., Soufleris, C., and Virieux, J., 1985. The evolution of the Gulf of Corinth (Greece): an aftershock study of the 1981 earthquakes, *Geophys. J. R. astr. Soc.*, 80, 677-693.

Kokkalas, S., Pavlides, S., Koukouvelas, I., Ganas, A., and Stamatopoulos, L., in press. Paleoseismicity of the Kaparelli fault (eastern Corinth gulf): evidence for earthquake recurrence and fault behaviour, *Bolletino di Geofisica Teoretica ed Applicata.*

Kostak, B., and Cruden, D.M., 1990. The Moiré crack gauges on the crown of the Frank Slide, *Can. Geotech. J.,* 27, 835-840.

Kostak, B., 1991. Combined indicator using Moiré technique, *Proccedings of 3rd International Symposium on Field Measurements in Geomechanics*, Oslo, Norway, 53-60.

Maniatis, G., Lempp, CH., and Heinisch, H., 2003. 3D strain monitoring of onshore active faults at the eastern end of the Gulf of Corinth (Greece), *J. Geodynamics*, 36, 95–102.

Pavlides, S., Koukouvelas, I., Ganas, A., Kokkalas, S., Tsodoulos, I., Stamatopoulos, L., Goyntromichou, C., and Valkaniotis, S., 2003. Preliminary palaeoseismological results from the Kaparelli fault (Central Greece), *Geophysical Research Abstracts*, vol. 5, 07069, European Geophysical Society.

Roberts, G.P., and Ganas, A., 2000. Fault-slip directions in central and southern Greece measured from striated and corrugated fault planes: Comparison with focal mechanism and geodetic data, *Journal of Geophysical Research*, 105 (B10), 23443-23462pp.

Stemberk, J., Kostak, B., and Vilimek, V., 2003. 3D monitoring of active tectonic structures, *Journal of Geodynamics*, 36, 103-112.

Δελτίο της Ελληνικής Γεωλογικής Εταιρίας τομ. XXXX, 2007
Πρακτικά 11ου Διεθνούς Συνεδρίου, Αθήνα, Μάιος 2007

Bulletin of the Geological Society of Greece vol. XXXX, 2007
Proceedings of the 11th International Congress, Athens, May, 2007

THE CORINI ACTIVE FAULT IN SOUTHWESTERN VIOTIA REGION, CENTRAL GREECE: SEGMENTATION, STRESS ANALYSIS AND EXTENSIONAL STRAIN PATTERNS

Ganas A.[1], Spina V.[2], Alexandropoulou N.[1], Oikonomou A.[1], and Drakatos G.[1]

[1] *Institute of Geodynamics, National Observatory of Athens, 11810 Athens, Greece*
aganas@gein.noa.gr

[2] *Earth Sciences Dept, Univ. Camerino, V. Gentile III da Varano, Camerino (MC), Italy*

Abstract

The Corini normal fault is an active structure of Quaternary age in Southwestern Viotia. This is a region of low finite strain, located between the Quaternary rifts of the Gulf of Corinth and the Gulf of Evia. The fault is segmented into several segments with an average strike of N58°E and dip direction to the SE. The architecture of the fault zone is characterized by a 15 cm thick gouge rock, observed along the fault plane on the footwall side. At several localities along strike we observed a well-defined basal strip of un-eroded fault plane that represents the width (uplift) of the last co-seismic slip. The width of the strip ranges 20-30 cm. Slip inversion data show a mean orientation of sigma3 (least principal stress) as N328°E which implies similar kinematics with the active faults of the south coast of the Gulf of Corinth.

Key words: *Strain, active faults, fault slip, stress, Corini.*

Περίληψη

Στην εργασία παρουσιάζονται νέα γεωλογικά δεδομένα για ένα ενεργό ρήγμα της Νοτιοδυτικής Βοιωτίας. Η περιοχή αυτή χαρακτηρίζεται από χαμηλή παραμόρφωση συγκρινόμενη με τις νεοτεκτονικές τάφρους τόσο του Κορινθιακού (προς Δυσμάς) όσο και του Ευβοϊκού (προς ανατολάς). Το κανονικό ρήγμα της Κορύνης αποτελείται από δύο μεγάλα τμήματα και μερικά αρκετά μικρότερα με μέση παράταξη ΑΒΑ-ΔΝΔ (Β58°) και φορά κλίσεως προς ΝΑ. Το ρήγμα έχει συνολικό μήκος 12 km και έχει αναπτυχθεί στο ανθρακικό υπόβαθρο της Υποπελαγονικής. Η αρχιτεκτονική της ρηξιγενούς ζώνης χαρακτηρίζεται από την ύπαρξη ενός τεκτονικού λατυποπαγούς με μέσο πάχος 15 εκατοστών. Στην βάση του καθρέπτη της Κορύνης παρατηρείται λωρίδωση με μικρή έως καθόλου διάβρωση πάχους 20-30 εκατοστών, η οποία αντιπροσωπεύει την τελευταία σεισμική κίνηση του ρήγματος με άνοδο του σταθερού τεμάχους. Αναφορικά με την κινηματική το σημαντικότερο εύρημα έγκειται στο ότι ο ελάχιστος άξονας της κύριας τάσης έχει μέση διεύθυνση Β328°Α, η οποία περίπου ταυτίζεται με αυτή των ενεργών ρηγμάτων της νότιας ακτής της Κορινθιακής τάφρου (χερσόνησος Περαχώρας).

Λέξεις κλειδιά: *Παραμόρφωση, Ενεργό ρήγμα, άνυσμα ολίσθησης, τεκτονική τάση, Κορύνη.*

1. Introduction

Numerous structural and geodetic studies have shown that central Greece is a young, extensional province of the Aegean area and one of the most actively deforming in the world (Jackson *et al.* 1982, King *et al.* 1985, Roberts and Ganas 2000, Briole *et al.* 2001). Surface topography and geomorphology are clearly associated with seismic activity along large normal faults developed during the last 1-3 Ma (million years). Extension is mainly directed N-S with increasing rates to the west (Clarke *et al.* 1998). The main extensional features are a series of Plio-Pleistocene rifts such as the Gulf of Corinth and the Gulf of Evia (Fig. 1; Ganas and Papoulia 2000, Goldsworthy and Jackson 2001). The southern side of the Gulf of Corinth is bound by a series of major north-dipping normal faults, forming a complex asymmetric half graben (Jackson *et al.* 1982, Roberts 1996, Morewood and Roberts 2001). There are E-W striking active normal faults with antithetic dip, i.e. to the south; however, they are visible at the northern edge of the Gulf. Two of these normal faults are the Kaparelli fault that ruptured in 1981 (Jackson *et al.* 1982) and the Corini fault in south-west Viotia. Our work presents new data on strain patterns along the Corini fault including sets of slip vector orientations and other geological observations along a 12-km stretch to the east of Corini village (Fig. 2). We also present detailed 1:5000 maps showing fault segmentation patterns and 32 morphological profiles that can be used a proxy to throw profiles across the fault. Similar data were also collected for the Erithres fault, a large normal fault to the east, including 1:5000 geological maps, stereonets from structural analysis etc. In this paper we focus on the Corini Fault and compare our results with the kinematics of active faults along the south coast.

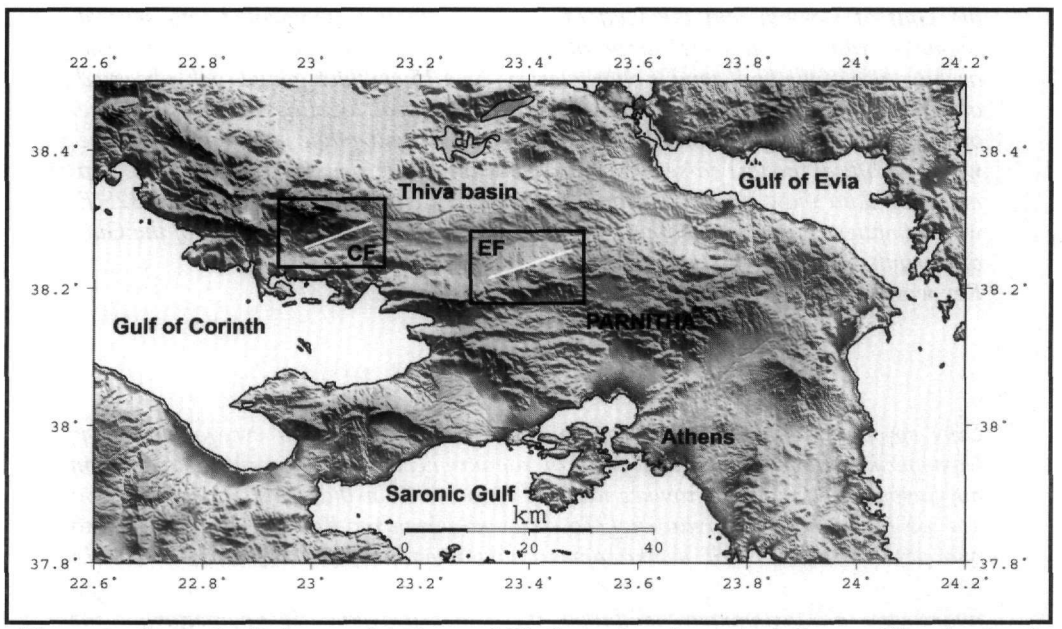

Figure 1 - Shaded relief map of Attica and Viotia regions in central Greece. Illumination is from the north-east. Black rectangles indicate locations of Corini Fault (CF) and Erithres Fault (EF), respectively. Area of rectangle CF is shown in Figure 2, below. Thin white lines indicate linear traces of active faults. Elevation data were provided by the SRTM mission

Our goal was to analyze structural data from active normal faults and to describe their architecture and the structural characteristics. This approach allowed us to constraint the orientation of the stress field and that to determine the direction of extension since Plio-Quaternary time in this sector of the central Greece. In detail, the results include a map of active faults in the area (Fig. 3), analysis of their lengths, cumulative slip (throw) estimates, analysis of dip angles and slip directions, and associated maximum earthquake magnitudes. Detailed mapping has examined the

fault segmentation pattern, which is whether faults aligned along a particular direction form part of the same zone (a segment; e.g. Crone and Haller 1991) or are separate structures. In addition, lineation (striae) data from the main fault planes were collected at various localities. Data from smaller footwall faults were collected, as well. We also examine if the dominant fault-slip direction in our data set does not remain constant along strike, but varies systematically. Our findings can be compared to lineation data sets as suggested by Roberts and Ganas (2000). We will investigate if striations produced by ruptures exhibit converging patterns of slip towards the hangingwall, and how those patterns are distributed along the fault. For example, two lineation sets with different orientations implies rupture of different portions of the same fault segment during successive earthquakes (Roberts and Ganas 2000).

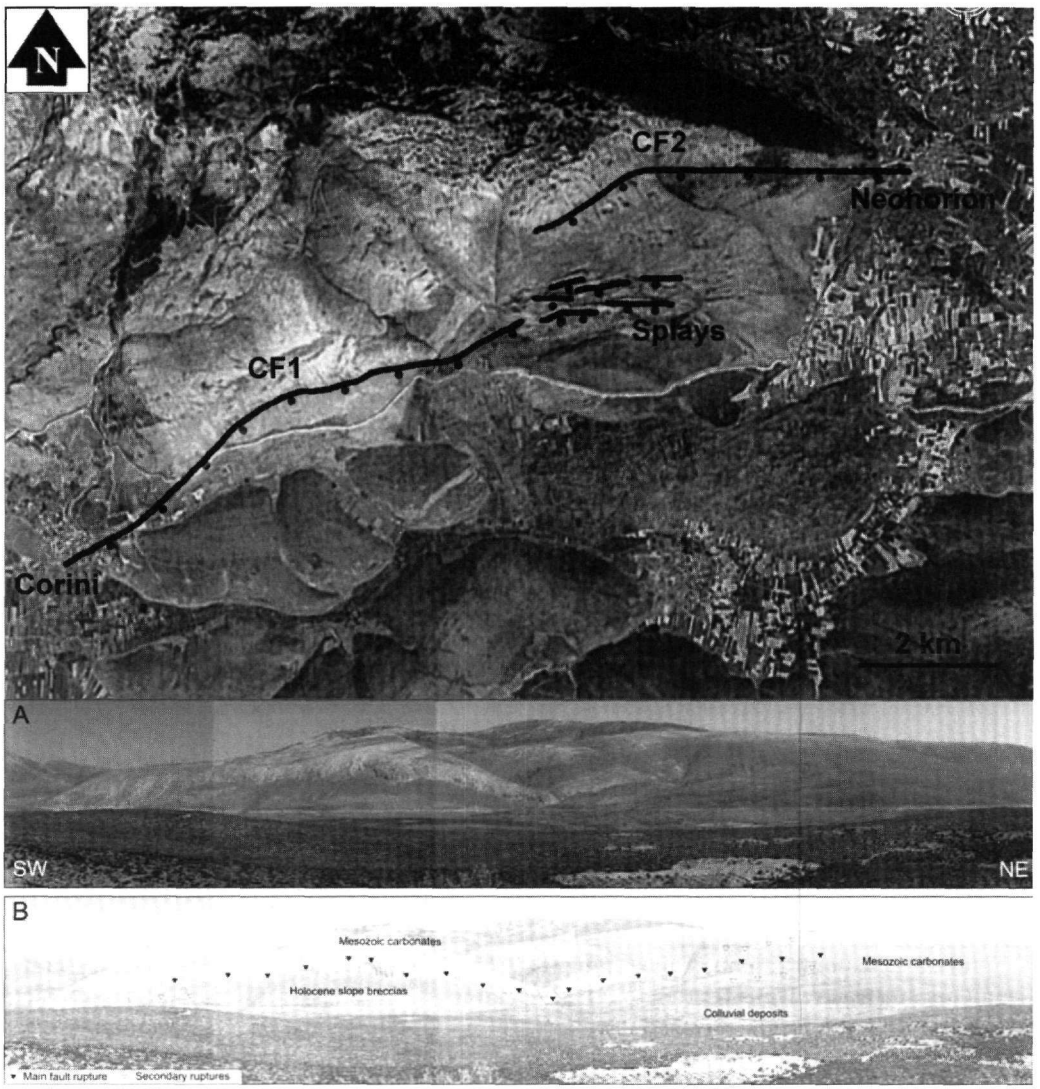

Figure 2 - Satellite image and corresponding field photograph of the Corini normal fault in south-west Viotia region, central Greece. Top: Landsat image with superimposed traces of active faults. Middle: Original picture, Bottom: main fault plane is indicated by a series of black triangles. Secondary planes are shown by the alignment of white triangles. The main rock types are also indicated. The highest altitude of the fault plane is approximately 480 m. View to the Northwest. Photograph taken 14 June 2006

2. Geological Setting

The Corini Fault has developed at high angles to the dominant NW-SE structural trend of the Hellenides. The pre-rift rocks comprise mainly Mesozoic carbonates (limestone and dolomite; Fig. 2). We mapped the faults at high resolution scale (≥1:5000) and created a large data-set by collecting geo referenced structural surveys. The 12 km long Corini normal fault (CF) crops out along the southern slope of the Elikon Mountain (Figs 1, 2). The fault strikes roughly NE-SW, dips toward SE, and it is characterized by a segmented pattern (Fig. 3). The fault is marked by a rectilinear and fresh scarp, brings into contact Mesozoic rocks in the footwall, with reddish coarse grained colluvium and slope deposits of probably Holocene age, in the hanging wall. At the fault termination zones, near Corini and Neohorion villages, we observed in the hanging wall area pelites and reddish marls (syn-rift deposits) of Plio-Pleistocene age (Fig. 3). The architecture of the CF is characterized by two main fault segments; the western segment named here CF1 is shown in the field photograph of Figure 2. The geological map of this area shows that CF1 (Fig. 3), starts from the Corini village extending for almost 8 Km to the east and it is characterized by fifteen (15), shorter fault segments showing both right and left stepping (Fig. 3). CF2 is 4 km long and terminates near the Neohorion village. CF2 was mapped at 1:50000 scale.

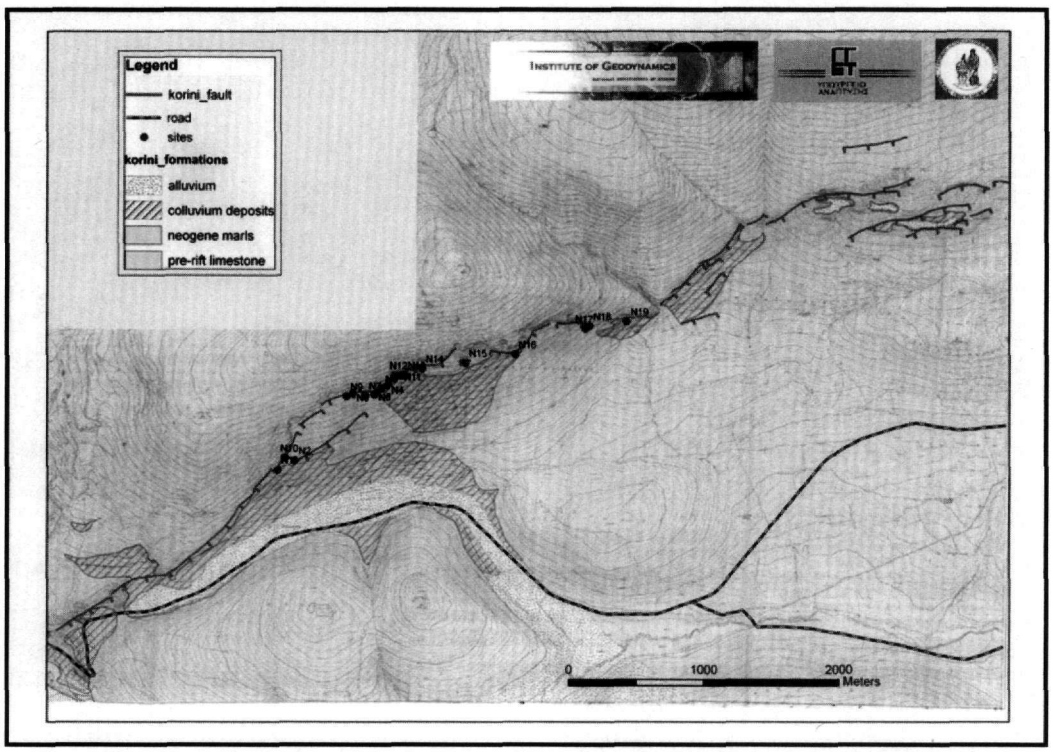

Figure 3 - Geological map of the segment CF1 of the Corini fault showing smaller fault segments and structural sites (N1 to N19). Location of N points was determined in the field with a hand-held GPS (accuracy 5 m). Background topographic map has elevation interval of 4 m

Near Corini village (west end), CF1 crops out at elevations 280 m to 480 m. Here, it is characterized by a 3 m high fault scarp along which we observed an eroded fault plane in carbonate rocks with a basal strip along its base (Fig. 4c) and with associated a damage zone of almost 10-15 m. Also, reddish cemented and striated breccias of variable thickness were observed along the main fault plane (Fig. 4a). Further to the east, CF1 is well exposed along the main slope of Elikon Mountain (Fig. 2), from 400 m to 600 m of elevation, and towards its end it is characterized by overlapping fault strands that depict a complex array (Fig. 3 east of point N19).

We interpret this fault pattern as an "isolated-splay" structure because small normal faults are seen to cluster at the termination of CF1 (Fig. 3) without either an "anastomosing" or a "branching" relationship to it. Between points N9 and N19 CF1 displays an impressive feature with a morphological break up to 31 m; also, 1-2 cm long crystals of calcite were occasionally observed along main fault plane (Fig. 4b). In addition, secondary ruptures, both in the hanging wall and in the foot wall of the CF1, were mapped. The architecture of the fault zone along the entire CF1 is characterized by a 15 cm thick gouge rock, observed along the fault plane on the footwall side. At several localities along strike of CF we observed a well-defined basal strip of un-eroded fault plane that represents the extent (uplift) of the last co-seismic slip (Fig. 4e). The width of the strip is about 20-30 cm.

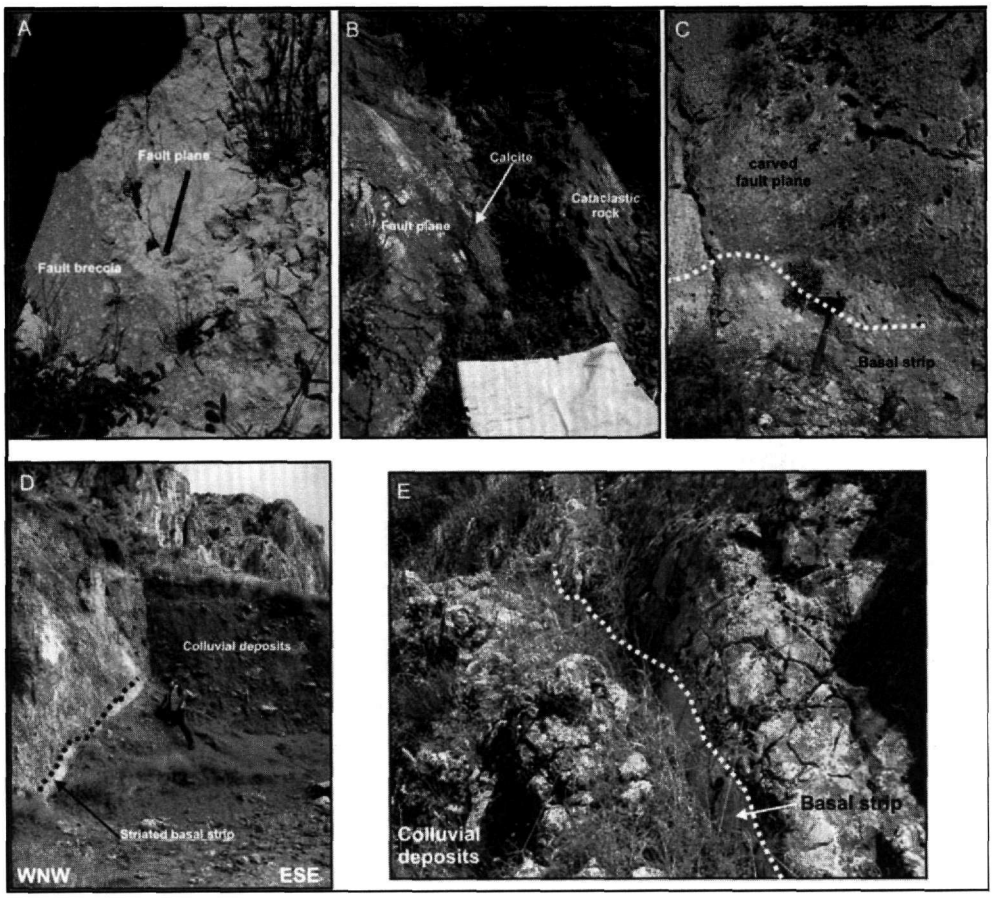

Figure 4 - Field photographs of the Corini active fault showing a) detail of fault plane in contact with fault breccia b) detail of fault plane with calcite crystals c) 30-cm basal strip of equal width indicating last co-seismic slip (hammer for scale) d) Fault plane contact with colluvium (site N1; view to the east) and e) detail of fault surface with basal strip indicated by arrow. All photographs were taken during June 2006

3. Analysis of Structural Data

Along the CF1 segment we performed a systematic surveying in order to collect structural data (e.g. fault orientation, fault striae, and displacement-length profiles). To obtain accurate data concerning the rupture surface, each structural site was marked in the field with a hand-held GPS and it was geo-referenced to the UTM projection with GIS software. The GIS base map originated from a mosaic of 1:5000 maps of the Greek Army that was georeferenced to the UTM projection

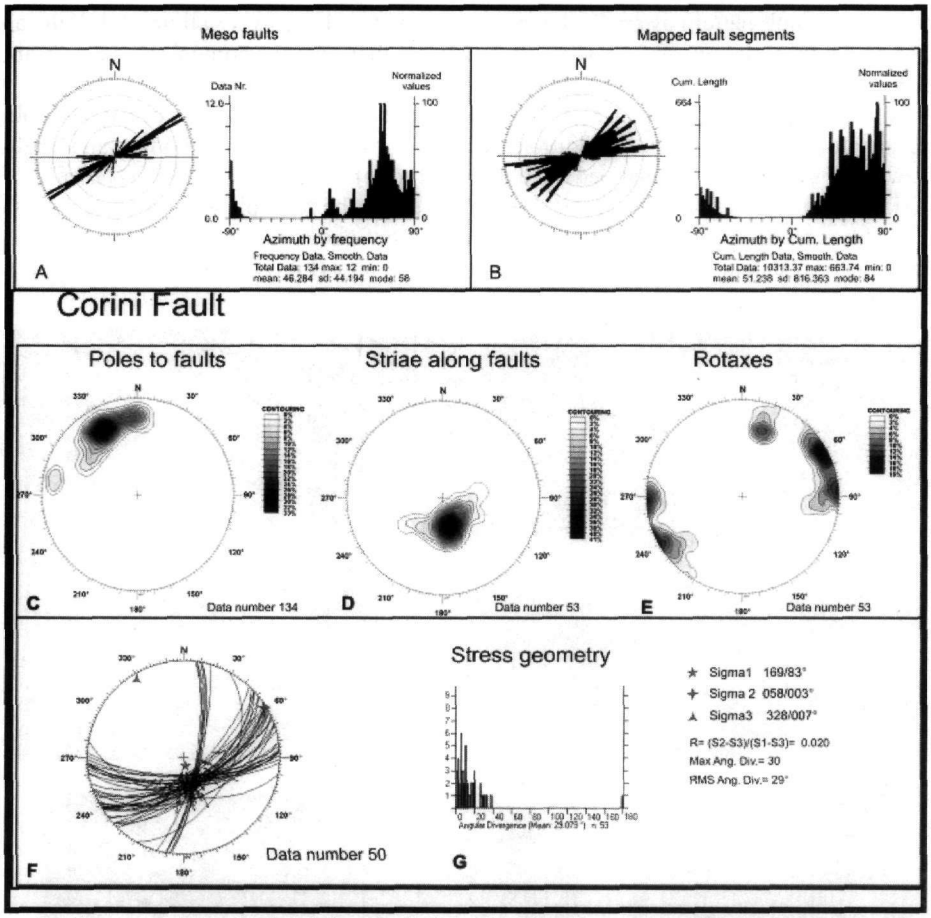

Figure 5 - Structural analysis of the Corini Fault. The data comprise 134 measurements of strike and dip angle and 53 measurements of rake angle on the fault plane. North is marked by "N". A) Data portrayed on rose diagrams: Strike of fault planes and histogram of fault plane orientations (azimuth). B) Histogram of fault segment length vs. fault segment azimuth showing that NE segments are more important in accumulating fault length. C) D) E) Data are portrayed on lower hemisphere equal-area projections (Stereonets). Stereonets portray all data as contoured poles to the strike and dip of planes and trend and plunge of lines. The percent data at the contoured point maximum is indicated to the right of each stereonet. The number of points in the data sets is indicated in the lower right of each diagram. F) & G) Paleostress analysis. Stress axis terminology is as follows: sigma 1 denotes trend and plunge of maximum principal stress, sigma 2 of intermediate stress and sigma 3 of least stress, respectively

using ARC GIS v. 9.1. Fault data are plotted on rose diagrams (Figs 5a, 5b) and stereonets (Figs 5c to f) using the Structural Data Integrated System Analyzer software (DAISY 2.19) by Salvini (2000). The DAISY software uses a Gaussian curve-fitting routine for determining peaks in directional data (Salvini *et al.* 1999) that was first described by Wise *et al.* (1985). This statistical method includes three different and progressive steps: Histogram Analysis, Multiple Gaussian Analysis and Spectral Analysis to filter and show the distribution and frequency data of the selected parameters. In particular, the Transect Analysis allowed us to highlight strike distribution, dip and rake variations of fault planes along a well oriented transect parallel to the fault (Fig. 6). Considering the scale which we collected data, we chose to show the processing of the Multiple Gaussian analysis. The structural data collected were then used to discuss the geometry of the

fault-related stress ellipsoid (Fig. 5g) and the direction of extension associated to the studied faults. The mean strike of fault planes was found N46°E (Fig. 5a), the standard deviation 44.1° and the mode N58°E. In Figure 5c, 5d and 5f we show contour diagrams of poles to fault planes, rake angle of striae (slickensides) along fault planes and rotational axes. The latter represent structural lineations on fault planes orthogonal to the slip vector (corresponding to the direction of the maximum shear stress). Their distribution indicates the intermediate axes of the stress ellipsoid (σ2). The contour diagrams give the statistical distribution of percentage of values in respect to all collected data. For poles of fault planes the best fit is 332/24° (dip direction and inclination), for striations, the best fit is 165/68° (trend and plunge) and for rotaxes, the best fit is 60/6° (trend and plunge).

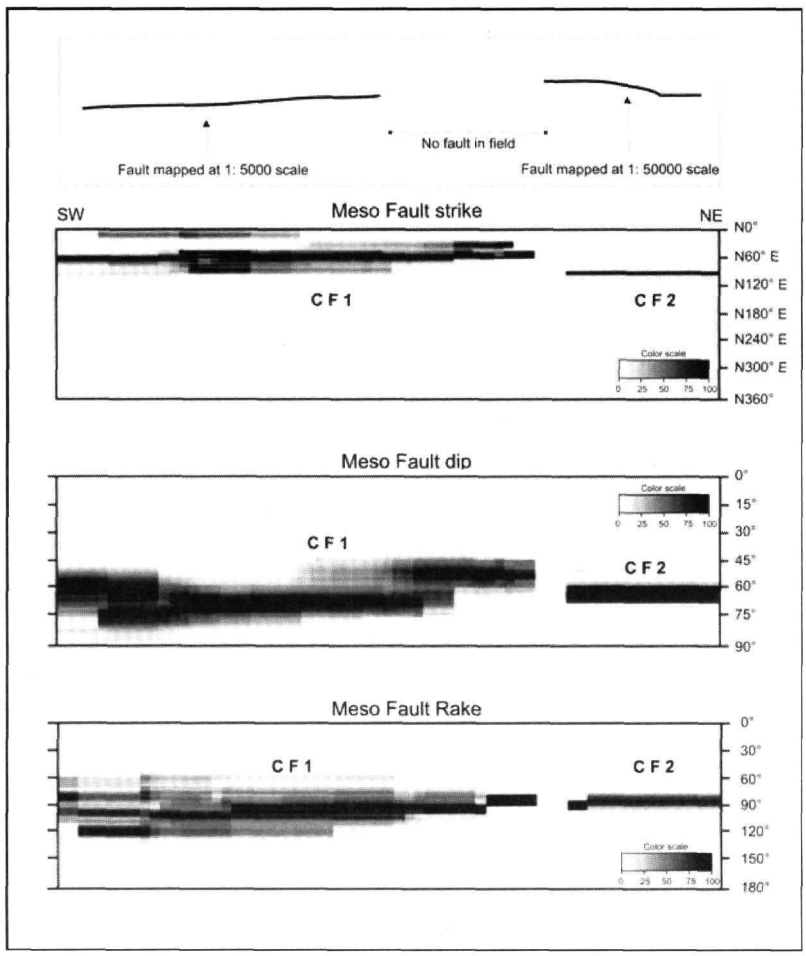

Figure 6 - Transect Analysis of the Corini Fault. Line brightness is proportional to the volume of data collected in the field. It can be seen that segment CF2 strikes N100°E, dips 60°-70° south and rake is almost 90°, i.e. motion is pure dip-slip. However, the rake along the segment CF1 is mostly > 90° indicating right-lateral movement

The analysis of the slip inversion (Fig. 5G) showed that the stress field is extensional with sigma 3 (σ3) oriented N328°E. The maximum angular divergence between the predicted and the actual slip direction is 30° because of fault segmentation along strike. The sigma 3 value from Corini compares well with the mean extension direction (N320°E-N340°E) of the T-axis of the 1981 earthquakes (Taymaz *et al.* 1991), as well as with the mean extension direction defined by the slip vector data of the 1981 surface ruptures (N350°E; Jackson *et al.* 1982). This result implies that

fault kinematics is similar on either side of the Gulf of Corinth. On the contrary fault slip data from Ganas *et al.* (2004) and Roberts and Ganas (2000) show that immediately to the north-east, east and south-east of the Corini Fault area the sigma 3 orientation changes to N7°-N14°E. In addition, the transect analysis method shows that the spatial variation of fault slip vector is constant for segment CF2 but not for segment CF1 (Fig. 6) where it is seen that the oblique-slip component of fault motion is mostly right lateral. A possible explanation for this behaviour is that fault slip patterns have not been developed due to the young age of segmentation or that the western end of the fault is part of a larger structure (a relay ramp) where earthquake ruptures from neighbouring segments can propagate.

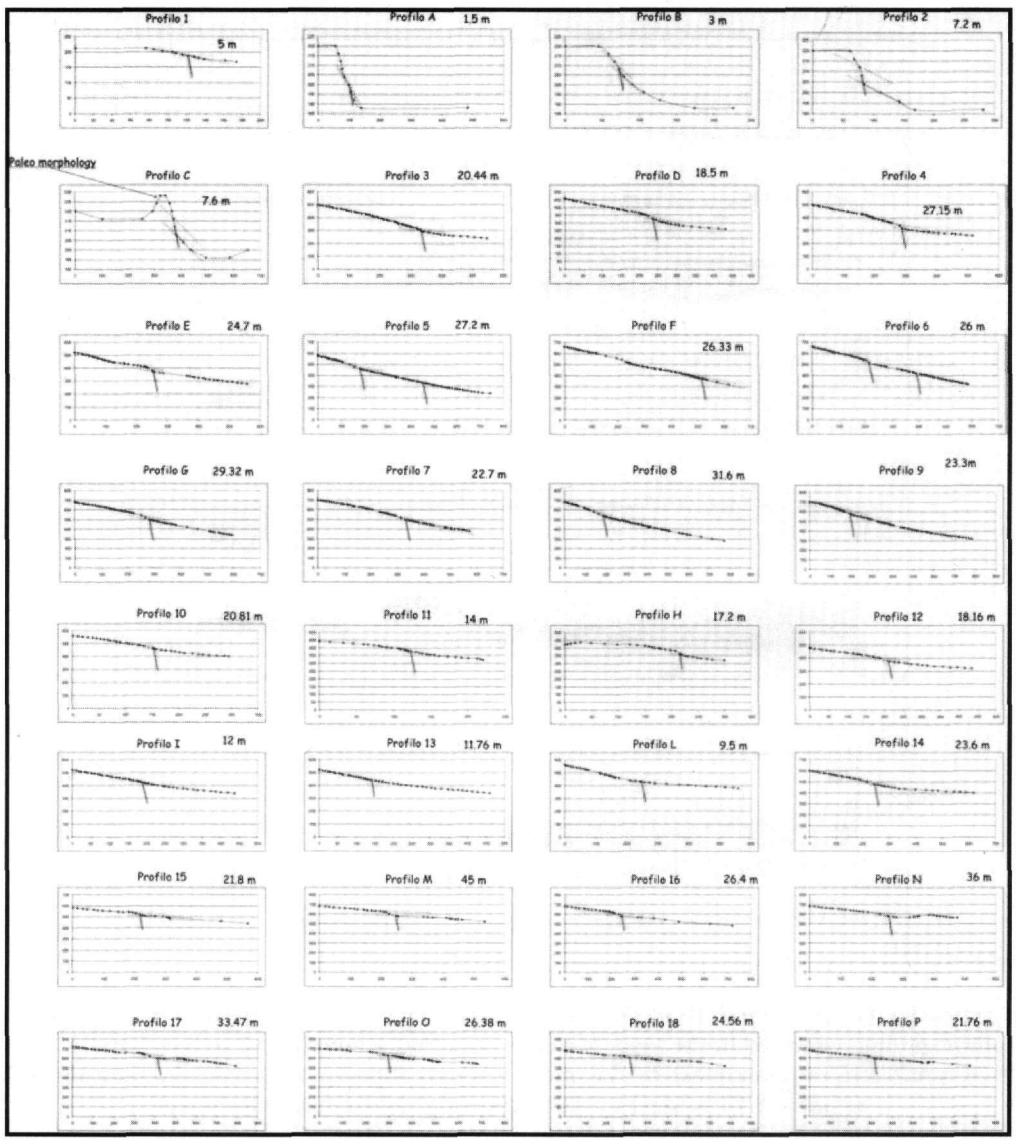

Figure 7 - Topographic profiles across the Corini Fault (segment CF1). All profiles are oriented approximately NNW-SSE. Thin, near vertical line indicates location of fault. The morphological offset equals the height difference between top scarp and bottom scarp and ranges between 5-45 m. Presumable this value represents fault throw since the end of the last glaciation (18 Ka; Roberts and Michetti 2004)

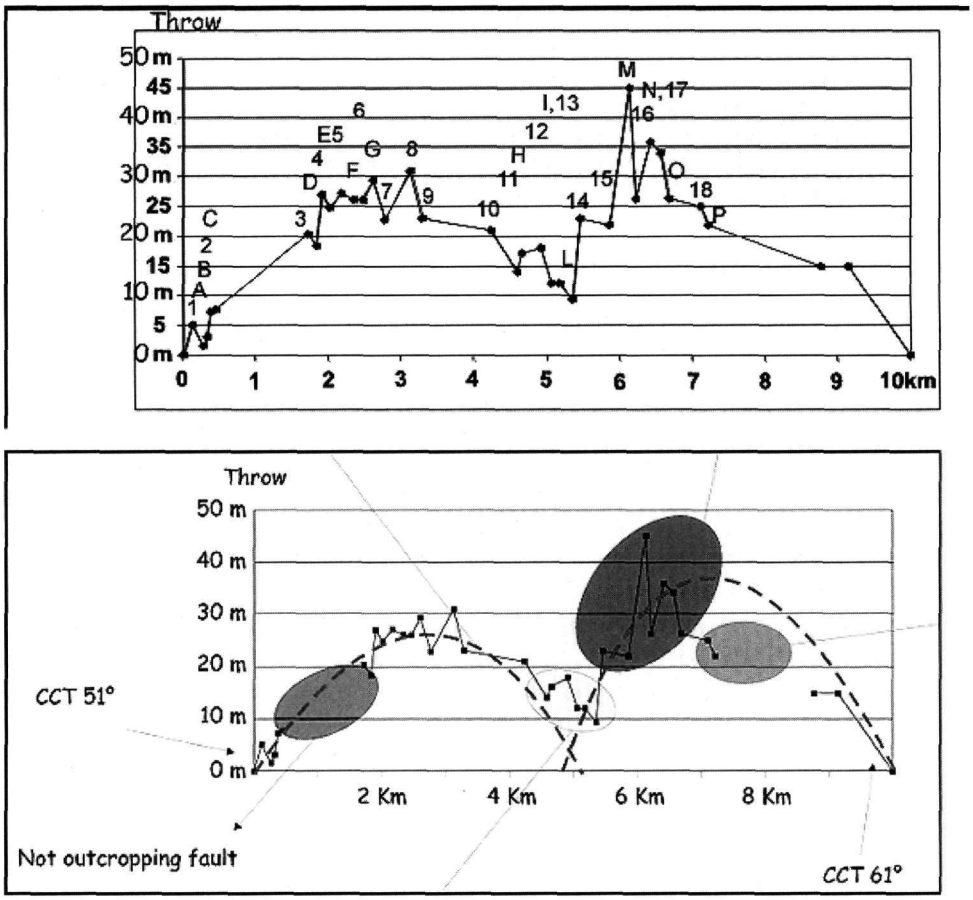

Figure 8 - (Top) Displacement-Length diagrams for the Corini Fault – segment CF1. Data points (black boxes with labels) originate from morphological profiles of Figure 7. We suggest that morphological offset is representative of fault displacement because of similar bedrock lithology and fault dip direction along strike. We observe that the profile does not fit the ideal, elliptical shape but shows two maxima at 2-3 km and 6-7 km, respectively. (Bottom) Sketch for interpretation of top graph. The profile can be split into two parts, each one with almost similar bell-shaped profile. The area between 4 and 6 km shows low throw values which suggest a linkage of two CF1 proto-segments

We could not collect any reliable geological data on throws along the Corini Fault. We can infer that throws are generally small because the NE-SW basin that develops in the hangingwall shows no evidence for thick syn-rift (Fig. 3). The main syn-rift lithology is colluvium and alluvium with minor occurrence of marl and pelite. It is therefore, reasonable to suggest that CF is a young structure perhaps not older that 1000000 (1 Ma) years. One method to study throw variations along strike (throw is the vertical component of the displacement vector) is to draw vertical cross-sections across the main fault plane and measure the morphological offset of the scarp (Fig. 7). The morphological offset we measure along strike can be used as a proxy for geological throw because the bedrock lithology is the same (Mesozoic carbonate) and dip-direction is constant (to the SE). The offset ranges from 5-45 m and shows two maxima along strike (Fig. 8). A possible explanation for this shape asymmetry is that CF1 grew because of linkage of two proto-segments. This is an important observation because in the field we were not able to see this. Also, the 1:50000 topographic map shows that along the Corini fault two large segments are clearly visible. The structural analysis (Figs 5, 6) also supports this interpretation. Strikes of fault planes for CF1

cluster around N60°E but for CF2 are close to N100°E. Rake of fault planes along CF1 is most right-lateral but for CF2 is almost 90° (dip-slip). The segment boundary area between CF1 and CF2 is to the north of CF1 (Figs 2, 3) where fault plane occurrence is lost. If we assume a late Pleistocene age for the reddish breccias occurring along the fault plane (100000 – 20000 years) we can estimate a mean slip rate for this fault. The reddish breccias have been associated with post-glacial weathering of slopes (see Roberts and Michetti 2004). This rough estimate provides mean slip rates in the order 0.2 – 1 mm/yr.

4. Discussion - Conclusions

a) The Corini normal fault shows evidence of recent tectonic activity such as fresh fault planes, axial drainage, linear mountain fronts etc., typical for the Aegean region. It borders an impressive mountain range constituted by Mesozoic carbonates. Geological data on slip vectors from Corini can be used to measure the crustal extension direction because in previous studies Hancock and Barka (1987) and Stewart and Hancock (1988, 1990, 1991) have showed that recently activated or freshly exhumed normal fault planes exhibit kinematic indicators ranging from metre-scale corrugations and gutters to centimetre-scale frictional wear striae. Also, Roberts (1996) and Roberts and Ganas (2000) made use of those indicators to model the non-characteristic growth of normal faults inside juvenile rifts such as those in central Greece.

b) The architecture of the CF is characterized by two main fault segments; the western segment starts from the Corini village extending for almost 8 Km to the east and it is characterized by shorter fault segments (500–1000 m long) showing both right and left stepping (Fig. 3). In addition, the Late Quaternary displacement – length profile (Fig. 8) can be split into two parts, each one with almost similar bell-shaped profile. The area between 4 and 6 km shows low throw values which suggest a linkage of two Corini-fault proto-segments, now comprising CF1.

c) At several localities along strike of CF1 we observed a well-defined, erosion-free basal strip on the fault plane that represents the extent (uplift) of the last co-seismic slip. The width of the strip is 20-30 cm (Fig. 4). This amount is similar to basal stripes found along other normal faults in neighbouring rifts (Fig. 1; Lemeille 1977, Ganas *et al.* 1998, Ganas *et al.* 2004).

d) The dominant fault-slip direction in our data set does not remain constant along strike, but varies from right-lateral oblique-slip (CF1) to almost dip-slip (CF2). No left-lateral striations were found.

e) We can estimate the maximum earthquake from the Corini normal fault using the best established correlation relation which Wells and Coppersmith (1994) have determined for shallow-focus (crustal) continental interplate or intraplate earthquakes on the basis of a rather comprehensive data base of historical events: $Mw = (1.16 \pm 0.07) \log (SRL) + (5.08 \pm 0.10)$. For SRL=12 km we estimate $6.2<Mw<6.5$.

f) The historical seismicity of this fault is unknown. No association can be established with the M>6.0, large earthquakes of the 19th Century near the town of Thiva (18.8.1853 and 23.5.1893; Ambraseys and Jackson 1990).

g) The analysis of the slip inversion data from CF showed that the stress field is extensional with sigma 3 ($\sigma 3$) oriented N328°E. This value compares well with the mean extension direction of the T-axis of the 1981 earthquakes, as well as with the mean extension direction defined by the slip vector data of the 1981 surface ruptures. This result implies that fault kinematics are similar on either side of the Gulf of Corinth

5. Acknowledgments

This work was funded by the PREVIEW IP Project (FP6), the General Secretariat for R&T (Greece) and the National Observatory of Athens. F. Salvini advised us on using the DAISY software for data elaboration. C. Tsimi helped with the use of ARC GIS. Figure 1 was made by the use of GMT software. Satellite image of Figure 2 was obtained from Google Earth™. We thank one anonymous reviewer for comments and Prof Hara Drinia for editorial assistance. We also thank Spiros Pavlides, Emanuele Tondi for discussions and George Stavrakakis for his support.

6. References

Ambraseys, N.N., and Jackson, J.A., 1990. Seismicity and associated strain of central Greece between 1890 and 1988, *Geophysical Journal International*, 101(3), 663–708.

Briole, P., Rigo, A., Lyon-Caen, H., et al., 2000. Active deformation of the Corinth rift, Greece: Results from repeated Global Positioning System surveys between 1990 and 1995, *Journal of Geophysical Research*, 105(B11), 25605-25625.

Clarke, P.J., Davies, R.R., England, P.C., et al., 1998. Crustal strain in central Greece from repeated GPS measurements in the interval 1989-1997, *Geophysical Journal International*, 135(1), 195-214.

Crone, A., and Haller, KM., 1991. Segmentation and the coseismic behavior of Basin and Range normal faults; examples from east-central Idaho and southwestern Montana, U.S.A., *Journal of Structural Geology*, 13, 151–164.

Ganas, A., Roberts, G.P., and Memou, Tz., 1998. Segment boundaries, the 1894 ruptures and strain patterns along the Atalanti Fault, Central Greece, *Journal of Geodynamics*, 26, 2-4, 461 - 486.

Ganas, A, and Papoulia, I., 2000. High-resolution, digital mapping of the seismic hazard within the Gulf of Evia Rift, Central Greece using normal fault segments as line sources, *Natural Hazards*, 22 (3), 203-223.

Ganas, A., Pavlides, S.B., Sboras, S., Valkaniotis, S., Papaioannou, S., Alexandris, A.G., Plessa, A., and Papadopoulos, G.A., 2004. Active fault geometry and kinematics in Parnitha Mountain, Attica. Greece, *J. Structural Geology*, 26, 2103–2118.

Goldsworthy, M, and Jackson, J., 2001. Migration of activity within normal fault systems: examples from the Quaternary of mainland Greece, *Journal of Structural Geology*, 23 (2-3), 489-506.

Hancock, P.L., and Barka, A.A., 1987. Kinematic indicators on active normal faults in western Turkey, *Journal of Structural Geology*, 9, 573-584.

Jackson, J.A., Gagnepain, J., et al., 1982, Seismicity, normal faulting and the geomorphological development of the Gulf of Corinth (Greece): the Corinth earthquakes of February and March 1981, *Earth & Planet. Sc. Let.*, 57, 377– 397.

King, GCP, Ouyang, Z.X., Papadimitriou, P., et al., 1985. The evolution of the Gulf of Corinth (Greece) - an aftershock study of the 1981 earthquakes, *Geophysical J. Royal S.*, 80 (3), 677.

Lemeille, F., 1977. Etudes rnicrotectoniques en Grèce Centrale Nord-Orientale (Eubèe Centrale, Attique, Bèotie, Locride), *Thèse 3eme cycle*, Univ. Paris XI, 173pp.

Morewood, N.C., and Roberts, G.P., 2001. Comparison of surface slip and focal mechanism slip data along normal faults: an example from the eastern Gulf of Corinth, Greece, *Journal of Structural Geology*, 23 (2-3), 473-487.

Roberts, GP, 1996. Non-characteristic normal faulting surface ruptures from the Gulf of Corinth, Greece, *Journal of Geophysical Research*, 101 (B11), 25255-25267.

Roberts, G.P., and Ganas, A., 2000. Fault-slip directions in central and southern Greece measured from striated and corrugated fault planes: Comparison with focal mechanism and geodetic data, *Journal of Geophysical Research*, 105 (B10), 23443-23462.

Roberts, G.P., and Michetti, A.M., 2004. Spatial and temporal variations in growth rates along active normal fault Systems: an example from Lazio-Abruzzo, central Italy, *Journal of Structural Geology*, 26, 339-376.

Salvini, F., 2000. *Structural Data Integrated System Analyzer software (DAISY 2.19),* Dipartimento di Scienze Geologiche, Universita degli Studi di "Roma Tre", Rome, Italy.

Salvini, F., Billi, A., and Wise, D.U., 1999. Strike-slip fault propagation cleavage in carbonate rocks: the Mattinata Fault Zone, Southern Apennines, Italy, *Journal of Structural Geology*, 21, 1731-1749.

Stewart, I.S., and Hancock, P.L., 1988. Normal fault zone evolution and fault scarp degradation in the Aegean region, *Basin Research*, 1, 139-153.

Stewart, I.S., and Hancock, P.L., 1990. Brecciation and fracturing within neotectonic normal fault zones in the Aegean region. In R.J. Knipe and E.H. Rutter (eds), *Deformation Mechanisms, Rheology and Tectonics*, Geological Society Special Publication 54, 105-110pp.

Stewart, I.S., and Hancock, P.L., 1991. Scales of structural heterogeneity within neotectonic normal fault zones in the Aegean region. In P.L. Hancock, R.S. Yeats and D.J. Sanderson (eds), *Characteristics of Active Faults, Journal of Structural Geology*, 13, 191-204pp.

Taymaz, T, Jackson, J.A., and McKenzie, D.P., 1991. Active tectonics of the north and central Aegean Sea, *Geophysical Journal International*, 106, 433-490.

Wells, D.L., and Coppersmith, K.J., 1994. New empirical relationships among magnitude, rupture length, rupture width, rupture are, and surface displacement, *Bull. Seismol. Soc. Am.*, 84, 974–1002.

Wise, D.U., Funiciello, R., Parotto, M., and Salvini, F., 1985, Topographic lineament swarms: Clues to their origin from domain analysis of Italy, *Geological Society of America Bulletin*, 96, 952-967.

Δελτίο της Ελληνικής Γεωλογικής Εταιρίας τομ. XXXX, 2007
Πρακτικά 11ου Διεθνούς Συνεδρίου, Αθήνα, Μάιος 2007

Bulletin of the Geological Society of Greece vol. XXXX, 2007
Proceedings of the 11th International Congress, Athens, May, 2007

LATE- AND POST-ALPINE TECTONIC EVOLUTION OF THE SOUTHERN PART OF THE ATHOS PENINSULA, NORTHERN GREECE

Georgiadis G. A.[1], Tranos M. D.[1], and Mountrakis D. M.[1]

[1] *Aristotle University of Thessaloniki, School of Geology, Department of Geology, 54124 Thessaloniki, Greece, gggk@geo.auth.gr, tranos@geo,auth.gr, dmountra@geo.auth.gr*

Abstract

The boundary between Internal Hellenides and the Hellenic hinterland is exposed in the southern part of the Athos peninsula as a NE-SW trending contact between the Serbomacedonian massif and the Circum-Rhodope Belt. The main tectonic features and deformation of the area during late- and post-alpine times have been investigated in order to understand better the late orogenic processes that led to the present arrangement of this boundary. The field study showed that the prevailing structures in the southern Athos peninsula are an asymmetric, SW-plunging, NW-verging mega-scale antiform and a NE-SW striking left-lateral shear zone. These structures are the result of a transpressional deformation that initiated at least since the Eocene under ductile, syn-metamorphic (low-greenschist facies) conditions and progressively changed during the Oligocene-Early Miocene to brittle conditions with E-W striking reverse faults-thrusts and NNW-SSE striking right-lateral and NE-SW striking left-lateral strike-slip faults. This deformation waned in Middle Miocene changing to transtension with E-W striking, left-lateral strike-slip and NW-SE right-lateral oblique to normal faults. Since the Late Miocene an extensional regime dominates the area with the least principal stress axis (σ_3) orientated NE-SW during Late Miocene – Pliocene and N-S from Early Pleistocene – present.

Key words: *Circum-Rhodope Belt, hinterland, collision, transpression, faulting.*

Περίληψη

Το όριο μεταξύ των εσωτερικών Ελληνίδων και της Ελληνικής ενδοχώρας αποκαλύπτεται στο νότιο τμήμα της χερσονήσου του Άθω ως μια επαφή ΒΑ-ΝΔ παράταξης μεταξύ της Σερβομακεδονικής μάζας και της Περιροδοπικής Ζώνης. Μελετήθηκαν τα κύρια τεκτονικά χαρακτηριστικά και η παραμόρφωση της περιοχής κατά τη διάρκεια της τελική αλπικής ορογένεσης όσο και μετά από αυτήν με σκοπό την καλύτερη κατανόηση των τελικών ορογενετικών διεργασιών που οδήγησαν στην σημερινή διαμόρφωση αυτού του ορίου. Η υπαίθρια έρευνα έδειξε ότι οι κυρίαρχες δομές στο νότιο τμήμα της χερσονήσου του Άθω είναι ένα ασύμμετρο, βυθιζόμενο προς τα ΝΔ, με φορά προς τα ΒΔ μέγα-αντίμορφο και μια ΒΑ-ΝΔ διεύθυνσης αριστερόστροφη διατμητική ζώνη. Αυτές οι δομές είναι αποτέλεσμα μιας transpressional παραμόρφωσης που άρχισε τουλάχιστον από το Ηώκαινο σε πλαστικές, συμμεταμορφικές (χαμηλή πρασινοσχιστολιθική φάση) συνθήκες και σταδιακά άλλαξε κατά το Ολιγόκαινο – Κάτω Μειόκαινο σε θραυσιγενείς συνθήκες με

Α-Δ διεύθυνσης ανάστροφα ρήγματα-επωθήσεις και ΒΒΔ-ΝΝΑ διεύθυνσης δεξιόστροφα και ΒΑ-ΝΔ διεύθυνσης αριστερόστροφα ρήγματα οριζόντιας μετατόπισης. Αυτή η παραμόρφωση σβήνει κατά το Μέσο Μειόκαινο και αλλάζει σε transtension με Α-Δ διεύθυνσης αριστερόστροφα ρήγματα οριζόντιας μετατόπισης και ΒΔ-ΝΑ δεξιόστροφα πλάγια έως κανονικά ρήγματα. Από το Άνω Μειόκαινο ένα εφελκυστικό καθεστώς κυριαρχεί στην περιοχή με τον ελάχιστο κύριο άξονα τάσης (σ3) σε ΒΑ-ΝΔ διεύθυνση κατά το Άνω Μειόκαινο – Πλειόκαινο και σε Β-Ν διεύθυνση από το Κάτω Πλειστόκαινο – σήμερα.
Λέξεις κλειδιά: *Περιροδοπική Ζώνη, ενδοχώρα, σύγκρουση, transpression, ρηγμάτωση.*

1. Introduction

In the Hellenic orogen, the Internal Hellenides are delimited to the east by the Serbomacedonian and Rhodope Massifs that constitute the hinterland of the orogen (Fig. 1). Specifically, this boundary in the area of the former Yugoslavia and Central Macedonia is located between the Serbomacedonian Massif to the East and the Circum-Rhodope Belt to the West and shows a constant NNW-SSE trend. This boundary has been interpreted as a right-lateral transpressional fold-and-thrust belt, the Circum Rhodope Thrust System (CRTS), formed during late collisional deformation (Tranos et al. 1999). The boundary at the SE extremity of the Chalkidiki peninsula makes an abrupt change in trend from NNW-SSE to NE-SW. Because of the sea and the limited study of the area our understanding of this trend change is insufficient. In the southern part of the Athos peninsula, apart from basic geological mapping at 1:100.000 and 1:50.000 scales by Kockel et al. (1977) and Kockel and Mollat (1978) there has been no systematic study of the area and this trend change. As a result, the current view of the geology of the area and the boundary between the internal Hellenides and hinterland is that contained in their work.

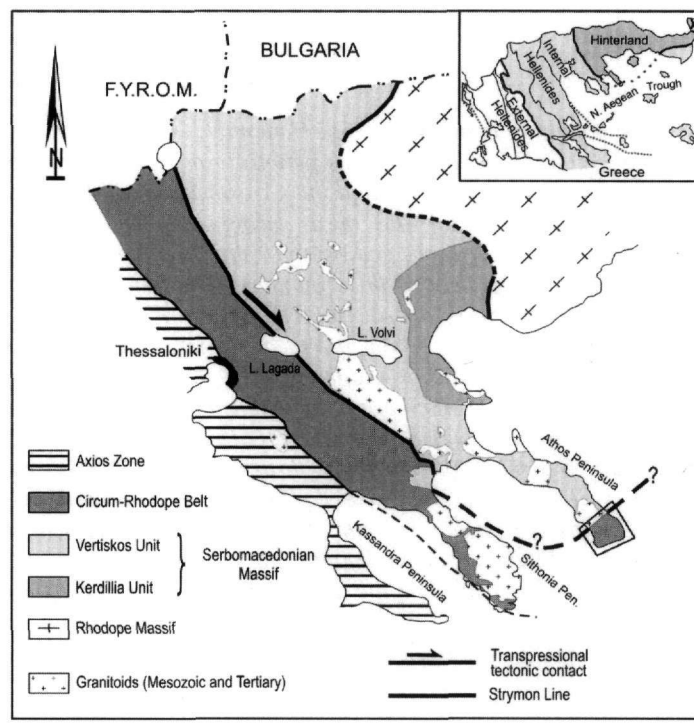

Figure 1 – Geotectonic map of central Macedonia-Chalkidiki peninsula

This paper examines the geology and structural evolution of the southern part of the Athos peninsula, which is the only place where the NE-SW trend of the boundary between Circum-Rhodope Belt and the hinterland can be studied. Thus studying this boundary's trend change contributes to the better understanding of the deformation and the orogenic processes in this part of the Hellenic orogen. In particular, the geometry and kinematics of the ductile and brittle structures

of the area have been studied and integrated with the existing views which suggest a left-lateral transpressional deformation for the region during Tertiary time.

2. Geological setting

The Serbomacedonian Massif (Fig. 1) consists of Paleozoic or older crystalline rocks that are grouped into the upper Vertiskos Unit and the lower Kerdillion Unit (Kockel *et al.* 1977) that consist of migmatites, biotite gneisses, marble horizons, two-mica gneiss and amphibolites. Towards the East, the Serbomacedonian Massif tectonically overlies the Rhodope Massif along the 'Strymon Line' that was considered as a Tertiary thrust fault by Kockel *et al.* (1977), but recent study has shown it to be a low-angle extensional detachment by Dinter and Royden (1993) and by Kilias *et al.* (1999).

The Circum-Rhodope Belt follows the NNW-SSE trend of the Serbomacedonian Massif (Fig. 1) and consists of Upper Paleozoic and Mesozoic meta-sedimentary rocks which have been grouped into the following three units (Kauffmann *et al.* 1976, Kockel *et al.* 1977) that are from East to West:

- the Deve Koran – Doubia Unit with Upper Paleozoic volcanosedimentary rocks and neritic Triassic carbonate rocks,
- the Melissochori – Cholomon Unit with Triassic pelagic carbonate and flysch meta-sediments of Middle Jurassic age, and
- the Aspri Vrisi – Chortiatis Unit with Permo-Triassic clastic rocks and Triassic neritic carbonate rocks in its lower part, and Lower-Middle Jurassic deep-sea sediments and ophiolites in its upper part. From these magmatic rocks the most characteristic rock types are those of mainly quartz-dioritic composition (Sapountzis 1969) that were metamorphosed to greenstones, green-gneisses and green-schists and make up the Chortiatis Magmatic Suite (Kockel *et al.* 1977). The intrusion of these magmatic rocks was attributed to the development of a volcanic arc in the area during the Middle Jurassic (Mussalam and Jung 1986).

The rocks of mainly the Serbomacedonian Massif, and the rocks of the Circum-Rhodope Belt were intruded by granitoids (Fig. 1) in Mesozoic to Tertiary times (Kockel *et al.* 1977, De Wet *et al.* 1989, Christofides *et al.* 1990).

A main orogenic phase that occurred in Middle-Late Jurassic time and affected the hinterland and the Internal Hellenides is attributed to the collision of the Cimmerian continent with Eurasia (Mountrakis 2002). In addition, the region was subjected to the Tertiary alpine orogenic phase that caused the final configuration of the whole Hellenic orogen and which is characterised by NW-SE trends and SW vergence (Dinaro-Hellenic orogenic fabric).

The first orogenic event was associated with an amphibolite facies metamorphism in the Serbomacedonian Massif and a greenschist facies metamorphism in the Circum-Rhodope Belt, followed by a retrograde low-grade greenschist facies metamorphism (Kockel et al. 1977; Dixon and Dimitriadis 1984, Vergely 1984, Chatzidimitriadis *et al.* 1985, Papadopoulos and Kilias 1985, Sakellariou 1989).

The Tertiary orogenic phase was associated with open, E-W trending, asymmetric folds and reverse-faults with south vergence (Sakellariou 1993). A similar NNW-SSE contraction associated with ESE-WSW trending folds, NNW-SSE and NE-SW trending shear zones and E-W trending thrusts faults deformed the Eocene Sithonia granitoid (Tranos *et al.* 1993).

The study of the post-metamorphic structures along the western boundary of the Serbomacedonian Massif (Tranos *et al.* 1999) and the Chalkidiki peninsula (Tranos 1998) suggests that the area underwent a transpressional deformation during the Latest Oligocene-Middle Miocene. This

deformation was the result of a NNE-SSW contraction and its waning stage includes extensional faults that were related to an extension perpendicular to the NNE-SSW contraction (Tranos 1998). This deformational event is generally regional and related to the latest stages of the collision between the Apulian and Eurasian plates, since it has been recognized in SW Bulgaria (Tranos *et al.* 2006), Thrace (Koukouvelas and Doutsos 1990, Karfakis and Doutsos 1995) and the North Aegean Trough (Tranos 2004).

The deformation of central Macedonia since Late Miocene time is a continuous extension with the least principal stress axis ($\sigma 3$) oriented NE-SW during Late Miocene – Pliocene and N-S from Lower Pleistocene to present (Mercier *et al.* 1989).

3. Geology and structural elements of the area

3.1. Geology of the study area

The southern part of the Athos peninsula (Fig. 2) exposes rocks that belong to the Aspro Vrisi – Chortiatis Unit of the Circum-Rhodope Belt. More precisely, the central-northern part of the study area exposes greenstones, green-gneisses and greenschists of the Chortiatis Magmatic Suite, into which intercalations of schists and phyllites and few elongate tectonic slivers of serpentinized ultramafic rocks (ophiolites) are present. In addition, in the eastern part of the mapped area and within the Chortiatis Magmatic Suite, plagioclastic-microclinic gneisses have been mapped that alternate with the green-gneisses (Kockel *et al.* 1977). The central-southern part of the study area is covered by greyish-white and bluish-grey Triassic recrystallized limestones-marbles (Kauffmann *et al.* 1976) that form Mt. Athos. Here the Chortiatis Magmatic Suite is poorly exposed and forms a NE-SW trending narrow strip within the limestones-marbles.

At the NE edge of the study area, the Chortiatis Magmatic Suite is in contact with a NE-SW boundary with the crystalline rocks, i.e. gneisses of the Serbomacedonian Massif. However, the exposure of this boundary has been significantly obliterated, due to the emplacement of the Gregoriou granitoid along it. This granitoid is probably related to the Sithonia granitoid (Tranos *et al.* 1993) and has been recently dated as Eocene (Kontopoulou *et al.* submitted).

Post-alpine, Quaternary scree deposits of significant extent cover at places not only the rocks but their contacts as well.

3.2. Ductile structures

3.2.1. Foliation

The main foliation of the rocks of the Chortiatis Magmatic Suite is a S_1 schistosity. This foliation trends generally NE-SW (Fig. 3a) and is parallel to the primary layering S_0 of the rocks since it is almost parallel with the lithological boundaries in most of the mapped area. The minerals of the S_1 foliation, such as chlorite, albite, actinolite, epidote and biotite, indicate a greenschist facies of metamorphism (Sapountzis 1969, Kockel *et al.* 1977).

At places, a second foliation S_2 is recognized affecting S_1 and forms a crenulation cleavage (Fig. 4a). The orientation of S_2 is constant throughout the study area dipping to SE (Fig. 3b) at moderate angles. S_2 is associated with quartz re-crystallization and locally growth of muscovite and chlorite, indicating low-grade metamorphic conditions (greenschist facies metamorphism).

In the northern part of the study area a NNE-SSW to NE-SW trending mylonitic foliation (S_m) affects the rocks of the Chortiatis Magmatic Suite forming in places with the S_1 a vertical S-C fabric (Fig. 4b). This mylonitic schistosity is associated with minerals similar to those defining the S_2 foliation and thus indicates similar metamorphic conditions.

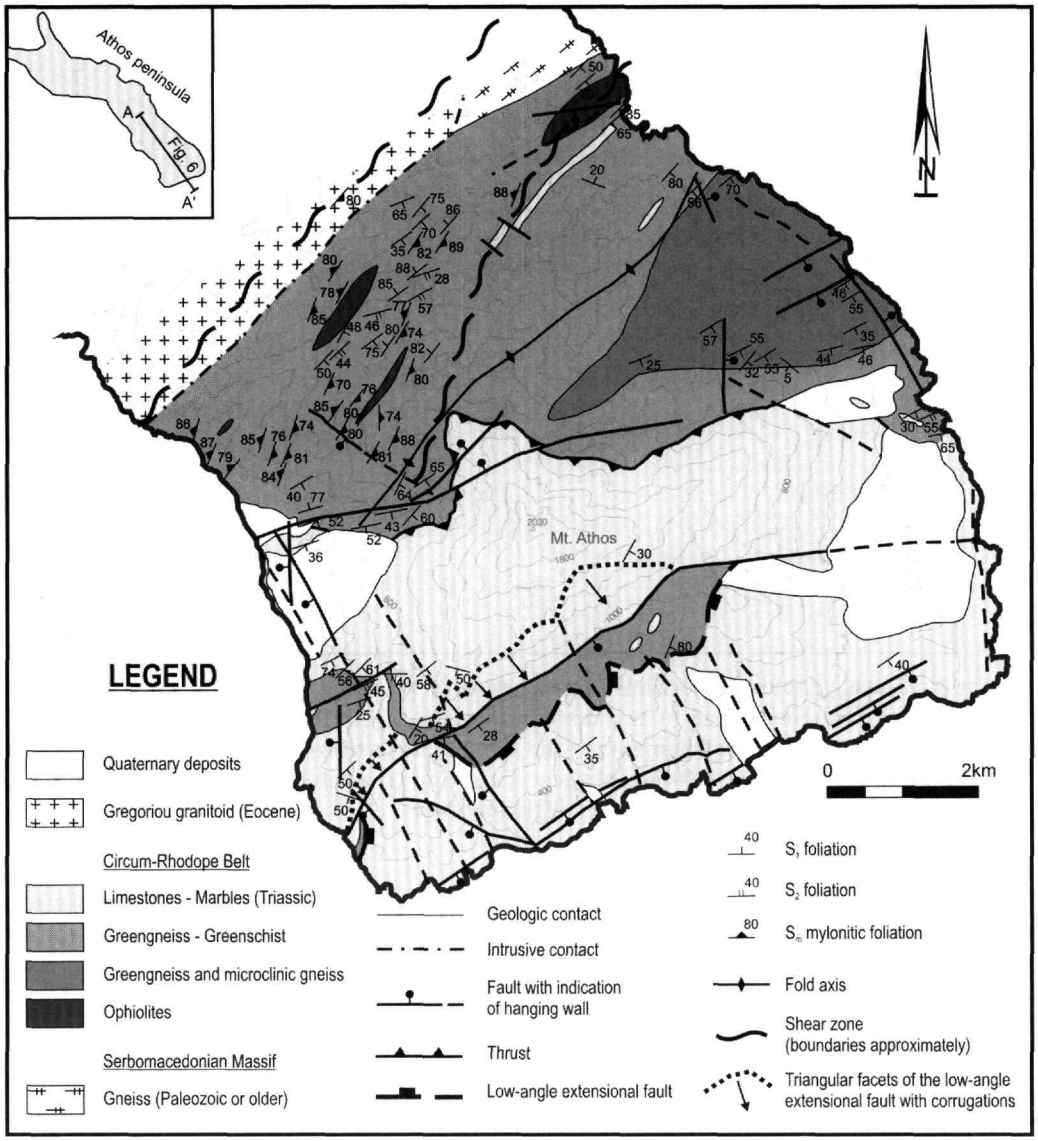

Figure 2 – Geologic map of the study area modified from Kockel *et al.* (1977)

3.2.2. Folding

The fieldwork carried out in the rocks of the Chortiatis Magmatic Suite indicates that the S1 foliation is folded at metre- to decimetre-scale, asymmetric, open-closed to overturned folds that plunge at gentle- to moderate angles (~30°) mainly to the SSW (Figs 3c, 4c). The axial surface of the folds trends NE-SW and dips consistently towards SE at moderate angles. The fact that the S_2 foliation is parallel to the axial surface forming crenulations in the S_1 foliation indicates that it is the axial planar schistosity of these folds. The mapping of S_1 and S_2 indicates that at a map-scale these folds are parasitic folds to a larger antiform of similar attitude and NW-vergence that dominates the southern area (Fig. 3d). In particular, the NNE- to NE-trending limb of the antiform is located north of Mt. Athos and dips at a high-angle to vertical. The other limb trends ENE and dips to the SE at a moderate angle and forms the main part of Mt. Athos and continues to until the southern edge of the peninsula.

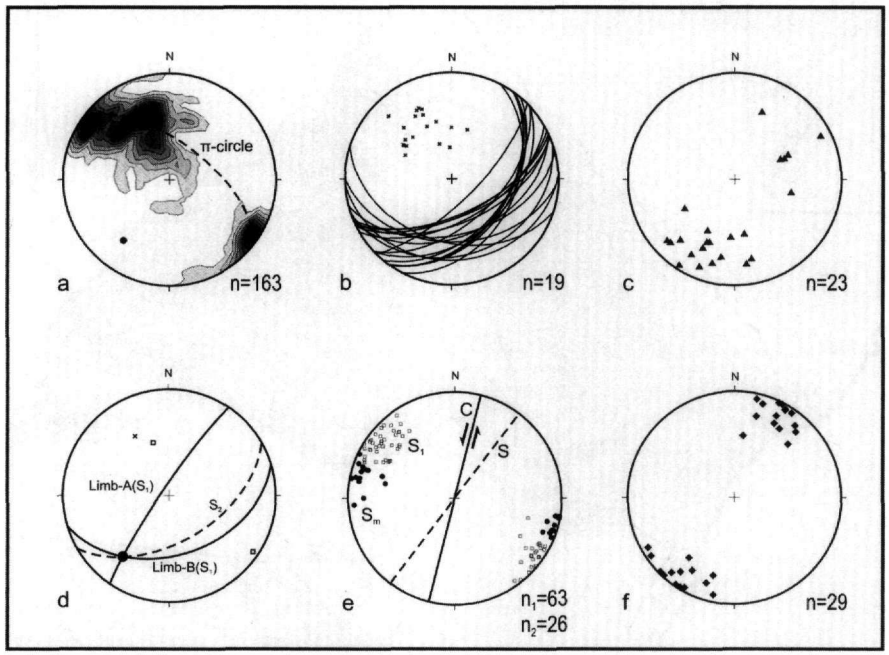

Figure 3 – Stereographic projections (lower hemisphere, equal area): (a) density of S_1, and the π-circle and π-pole defined by this distribution, (b) S_2 foliation, (c) axes of the mesoscale folds, (d) the main structural elements of the large scale antiform, (e) S-C fabric formed by S_1 and S_m indicating the left-lateral shear zone, and (f) stretching lineation on the S_m mylonitic foliation

3.2.3. Shear zone

The mylotitic foliation (S_m) present in the central-northern part of the study area and in the rocks of the Chortiatis Magmatic Suite is the result of semi-ductile shearing that affected the S_1 foliation forming an S-C fabric (Fig. 3e). This mylonitic schistosity trends NNE-SSW (to NE-SW) and is (sub)vertical, in contrast to S_1 that deviates from the vertical. The S-C fabric is associated with a horizontal stretching lineation (Fig. 3f) and the S-C kinematics defines a left-lateral sense-of-shear (Fig. 4b). The varying intensity of the S_m mylonitic foliation and consequently the S-C fabric at different locations implies that the shearing resulted by a heterogeneous shear zone. Due to this heterogeneity and the intense vegetation, the boundaries of the zone are defined approximately. The shear zone also affects the Eocene Gregoriou granitoid, since the later presents close to its contact with the Chortiatis Magmatic Suite a solid-state foliation parallel to S_m (see Kockel *et al.* 1977). The approximate contacts of the mylonitic shear zone are shown in figure 2.

3.3. Brittle structures

Information concerning the geometry and kinematics of the faults in the map area were recorded and analyzed, and information about the cross-cutting relationship and overprinting criteria among the different faults has been also used to define their time succession in order to separate them into different faulting events. The separation of the faults was mainly based on their type, i.e. reverse, strike-slip and normal, and the use of the elaborated distribution of the P and T-axes. The geometry and kinematics of these faults are the follow:

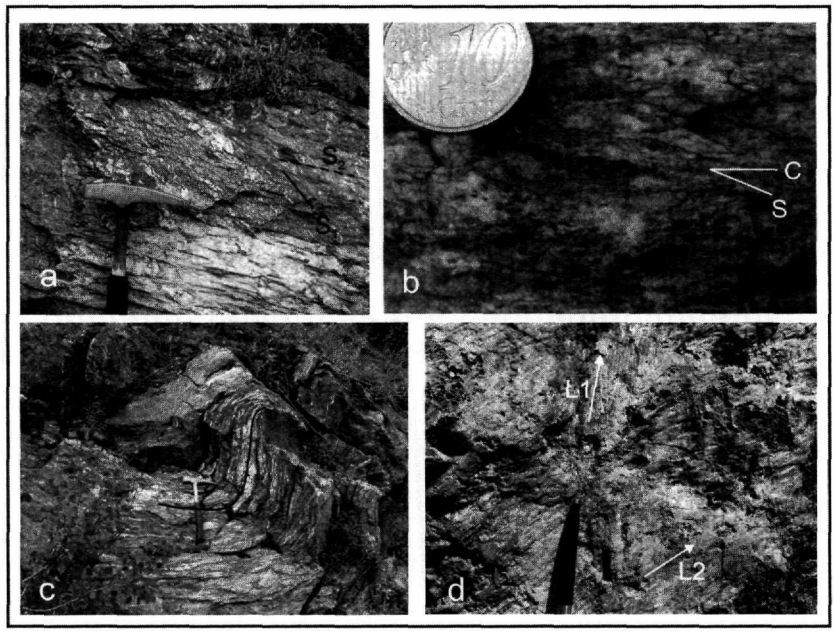

Figure 4 – Field photographs: (a) crenulation cleavage formed by the superpositon of the S_2 foliation on the S_1 (b) S-C mylonitic fabric indicating left-lateral shearing in the green-gneisses, (c) asymmetric fold in the green-gneiss, (d) two generations of slickenlines (L1, L2) present on an E-W striking fault, with L2 (left-lateral strike-slip) overprinting L1 (reverse)

3.3.1. Reverse faults

The reverse faults strike ~E-W and dip at low angles to the south or at high angles to the north (Fig. 5a). Most of them exhibit a quartz coating where fiberlines and fibersteps are recognized defining N-S movements. On the northern slopes of Mt. Athos, N-directed thrusts have been found close to the contact of the Chortiatis Magmatic Suite with the overlying Triassic limestones-marbles.

3.3.2. Strike-slip faults

The strike-slip faults of the area strike NNW-SSE, NE-SW and E-W and dip at high angles both to the north and south (Fig.5). They often exhibit Riedel structures and recrystallized quartz coating on which the formed microstructures (i.e. fiberlines and fibersteps) define the sense of movement. The majority of the NNW-SSE trending faults are right-lateral. In some cases, left-lateral strike-slip faults have been observed and these were attributed to local mechanical response of the rock. The NE-SW strike-slip faults are left-lateral and often they have been found close to the NNW-SSE right-lateral faults. The E-W trending faults are left-lateral and on the fault surfaces the strike-slip slickenlines overprint the dip-slip reverse sense slickenlines (Fig. 4d).

3.3.3. Normal faults

The normal faults strike NW-SE and E-W, while sporadic N-S striking normal faults are also observed. The majority of the NW-SE striking faults are normal to oblique slip and in many cases they reactivated older right-lateral strike-slip faults. These faults cut the afore-mentioned reverse faults. The Mt. Athos is bounded by E-W and ENE-WSW striking faults that dip at high angles forming steep slopes (Fig. 2). The normal fault that diminishes the southern slopes of Mt. Athos affects a low-angle extensional fault dipping 20° SSE that parallels and modifies the contacts of the greenschists with the Triassic marbles forming similarly dipping, huge triangular facets with corrugations on the marble slopes of the footwall (Fig. 2).

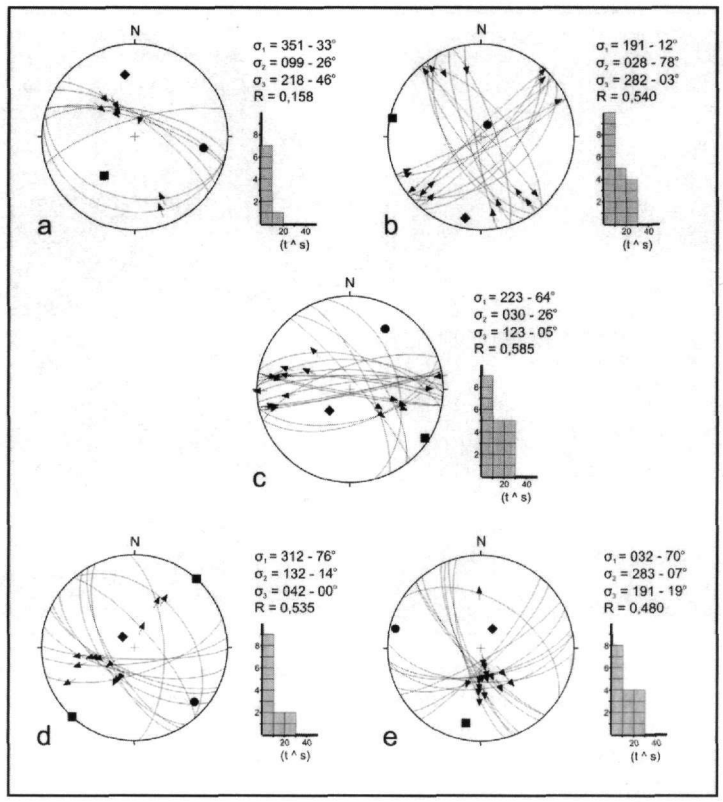

Figure 5 – Paleo-stress diagrams (lower hemisphere, equal area) and the deviation angle between the theoretical and real slip vector as calculated by the stress-inversion program described by Angelier (1990). (a) DA event -reverse faults, (b) DA event - strike-slip faults, (c) DB event - strike-slip and oblique extensional faults, (d) D1 event - normal faults, (e) D2 event - normal faults and oblique normal faults. σ_1= diamond, σ_2= circle, σ_3= square

3.3.4. Dynamic analysis-stress regimes

Based on the discrimination of the faults into different types (reverse, strike-slip and normal), but also their temporal relations as established from fieldwork, the recorded faults were analyzed using the stress inversion program described by Angelier (1990). This program calculates the direction of the principal stress axes (σ_1, σ_2, σ_3) and the ratio $R = [(\sigma_2-\sigma_3)/(\sigma_1-\sigma_3)]$ of the stress ellipsoid. For an acceptable solution, we adopted the condition that the slip vector of the faults should not deviate more than 30° from the theoretical one more than 90% of all the faults. The analysis elaborated five stress ellipsoids that define four deformational events. Due to the lack of stratigraphic criteria that would permit the dating of the deformational events, we correlated these events with the above field cross-cutting criteria and the previously reported regional deformational events.

DA – transpressional event: It is a pure-shear dominated transpressional event with the maximum stress axis (σ_1) oriented N-S. It is determined from the reverse faults and NNW-SSE and NE-SW trending, strike-slip faults (Fig 5a, b). A tectonic event with similar fault geometry and kinematics was reported by Tranos (1998) for the Sithonia peninsula and for the Chalkidiki area, and also further to the north for the SW Bulgaria (Tranos *et al.* 2006) and is dated as Late Oligocene – Early Miocene. This event was also recognized farther to the East by reverse faults in the Thrace area by Koukouvelas and Doutsos (1990). During this event the minimum stress axis (σ_3) varies between vertical and horizontal with a WNW trend with respect to the main faults, e.g. reverse or strike-slip faults at the different locations.

DB – transtensional event: This event is defined by E-W striking left-lateral strike-slip faults and the NW-SE striking right-lateral oblique faults (Fig. 5c). It is characterized by a steeply plunging maximum stress axis (σ_1) bearing SW and a horizontal minimum stress axis (σ_3) bearing WNW-ESE. The elaborated intermediate stress axis (σ_2) plunges gently to the NNE and is also compressive, indicating that contraction in this direction is similar to that in the previous DA event, but seems to wan during the DB event. The DB event was recognised by Tranos (1998) (DB and D1 events) and was dated as Early-Middle Miocene and it was also recognised more regionally (Tranos 2004, Tranos *et al.* 2006).

D1 – extensional event: The D1 event is characterized by NE-SW extension (Fig. 5d) and was dated in the Late Miocene – Pliocene by Pavlides and Kilias (1987), Mercier *et al.* (1989) and Tranos (1998). During this event, large NW-SE striking normal faults were activated and are considered to be the boundary faults to the NW-SE striking basins of the Northern Greece. Similar faults are recognised to form the NW-SE orientated Athos peninsula. It is important to mention that E-W-striking faults activated as left-lateral oblique faults during this event.

D2 – extensional event: The D2 event is characterized by N-S extension that leads to the activation of E-W-striking normal faults and NW-SE-striking left-lateral oblique faults (Fig. 5e). A large E-W-striking normal fault mapped along the north slopes of Mt. Athos is considered to be activated during this event and it is parallel to the large ENE-WSW striking faults that have been recognised offshore of the southern coastline of the peninsula and caused the subsidence along the southern slopes of the Athos peninsula (Papanikolaou *et al.* 2002). This event corresponds to the contemporary stress regime present over a wide region from Early Pleistocene to present and gives rise to the intense seismic activity of the area (Pavlides and Kilias 1987, Mercier *et al.* 1989, Tranos 1998, Mountrakis *et al.* 2006).

4. Discussion – structural interpretation

The geological structure of the southern part of the Athos peninsula is dominated by a SW-plunging antiform with NNW-vergence and a left-lateral heterogeneous shear zone of NE-SW strike (Fig 6). The NE-SW trending mesoscale folds that are related to this antiform, although of different trend, were formed under similar low-grade metamorphic conditions (low greenschist facies) and have a similar style to the E-W trending (Sakellariou 1993) and ENE-WSW trending folds (Tranos *et al.* 1993) that have been reported for the Chalkidiki and Sithonia peninsula respectively. The NE-SW left-lateral shear zone is also associated with low-grade metamorphic conditions (low greenschist facies) and was formed by the same NNW-SSE to N-S contraction. These folds as well as shear zones and thrusts of similar kinematic symmetry have been attributed by the same authors to NNW-SSE to N-S contraction that has been dated in Eocene. Therefore, the folding and the shear zone of the southern part of Athos peninsula should be attributed to a common deformation event that took place at least since Eocene, since it affects the Gregoriou granitoid. The fact that this ductile deformation is of analogous kinematic symmetry and dynamic compatibility with the abovementioned DA brittle event allows us to consider that they both represent a single progressive DA event.

The NE-SW trend of the folds mapped in the southern part of the Athos peninsula that apparently differs from the ENE-WSW to E-W folds mentioned for the other adjacent regions could be explained by a transpressional deformation. More precisely, the folds could have initially formed as ENE-WSW folds normal to the NNW-SSE to N-S contraction and were progressively rotated anticlockwise to their present orientation. This explanation is supported by similar behaviour of folds formed during transpressional deformation as experimentally determined by Tikoff and Peterson (1998). That the NNW-SSE to N-S contraction determined by the left-lateral shear zone forms a high angle with the trend of the large antiform indicates that this event is a left-lateral 'pure shear dominated' transpression.

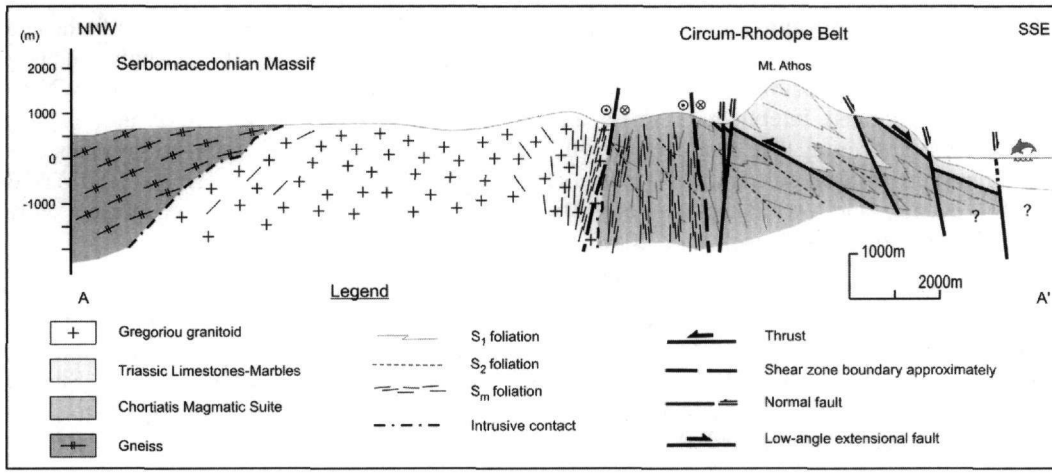

Figure 6 – Schematic cross section of the southern part of the Athos peninsula

The boundaries of the transpressional zone in the southern Athos peninsula defined by our fieldwork are oriented NE-SW, parallel to the boundary of the Serbomacedonian Massif and the Circum-Rhodope Belt and possibly may continue further to NE.

The DA event is a ductile 'pure-shear dominated' transpression that evolved during the Late Oligocene – Early Miocene in more brittle conditions activating reverse and strike-slip faults that also define a similar N-S contraction. This left-lateral transpression could be considered analogous to the NW-SE trending right-lateral transpression along the Circum Rhodope Thrust System (Tranos *et al.* 1999). The DA deformation changed to the DB transtension during the Early-Middle Miocene activating E-W-striking left-lateral strike-slip faults and NW-SE-striking oblique extensional faults that gave rise to a WNW-ESE extension and a NNE-SSW contraction. The activation of the SSE-dipping low-angle extensional fault mapped in the southern slope of Mt. Athos is attributed to the DB because its orientation and kinematics favours the NW-SE extension that characterises this event. Besides, similar low-angle extensional faults have also been reported for the Early-Middle Miocene in the wider area (Tranos 1998, Tranos *et al.* 2006).

Therefore, the studied area, and thus the boundary between the hinterland and the Internal Hellenides was progressively deformed under both ductile and brittle conditions by a transpressional deformation, which is dated as Tertiary and more precisely from at least the Eocene to Middle Miocene. This deformation is attributed to the main and late-orogenic collision between the Apulian – Eurasian plates.

The younger activation of the faults defines NE-SW and N-S extensional regimes that are post-collisional ones and related to the Hellenic subduction zone. These regimes fit well with the already reported extensional regimes since the Late Miocene (Pavlides and Kilias 1987, Mercier *et al.* 1989, Pavlides *et al.* 1990, Tranos 1998, Mountrakis *et al.* 2006). The uplift of the Athos peninsula is attributed to the NE-SW extension, whereas the final configuration of Mt. Athos is mainly attributed to the N-S extension.

5. Acknowledgments

Dr. Uwe Ring and Dr. Clark Burchfiel are thanked for their comments and suggestions.

6. References

Angelier, J., 1990. Inversion of field data in fault tectonics to obtain the regional stress. III. A new rapid direct inversion method by analytical means. *Geophys. J. Int.*, 103, 363-376.

Christofides, G., D'Amico, C., Del Moro, A., Eleftheriadis, G., and Kyriakopoulos, C., 1990. Rb/Sr geochronology and geochemical characters of the Sithonia plutonic complex (Greece), *Eur. J. Mineral.*, 2, 79-87.

Chatzidimitriadis, E., Kilias, A., and Staikopoulos, G., 1985. Nouvi aspetti petrologici e tettonici del massiccio Serbomacedonne e delle regioni adiacenti, della Grecia del Nortd, *Boll. Soc. Geol. It.*, 104, 515-526.

De Wet, A. P., Miller, J. A., Bickle, M. J., and Chapman, H, J., 1989. Geology and geochronology of the Arnea, Sithonia and Ouranoupolis intrusions, Chalkidiki peninsula, northern Greece, *Tectonophysics*, 161, 65-79.

Dinter, D. A., and Royden, L., 1993. Late Cenozoic extension in northeastern Greece: Strymon Valley detachment system and the Rhodope metamorphic core complex, *Geology*, 21, 45-48.

Dixon, J. E., and Dimitriadis, S., 1984. Metamorphosed ophiolitic rocks from the Serbomacedonian Massif, near Lake Volvi, Northeast Greece, *The Geological Evolution of the Eastern Mediterranean*. Geol. Soc. Lond., Spec. Publ., 17, 603-618.

Karfakis, J., and Doutsos, T., 1995. Late orogenic evolution of the Circum-Rhodope Belt, Greece, *N. Jahrb. Geol. Paläont. Mh.*, 5, 305-319.

Kauffmann, G., Kockel, F., and Mollat, H., 1976. Notes on the stratigraphic and paleogeographic position of the Svoula Formation in the Innermost Zone of the Hellenides (Northern Greece), *Bull. Soc. Geol. France*, 7, t. XVIII, n° 2. 225-230.

Kilias, A., Falalakis, G., and Mountrakis, D., 1999. Cretaceous-Tertiary structures and kinematics of the Serbomacedonian metamorphic rocks and their relation to the exhumation of the Hellenic hinterland (Macedonia, Greece), *Int. Journ. Earth Sciences*, 88, 513-531.

Kockel, F., Mollat, H., and Walther, H. W., 1977. Erlauterungen zur Geologischen Karte der Chalkidhiki und angrenzender Gebiete 1:100.000 (Nord-Griechenland). Bundesanstalt fur Geowisseschaften und Rohstoffe, Hannover, 119pp.

Kockel, F., and Mollat, H., 1978. Geologic map of Greece 1:50.000 scale, Athos sheet. *Institute of Geology and Mineral Exploration*, Athens.

Kontopoulou, D. Zananiri, I., Michard, A., Feinberg, H., Atzemoglou, A., Pozzi, J.-P., and Voidomatis, Ph., subm. Neogene tectonic rotations in the vicinity of the North Aegean Trough: New palaeomagnetic evidence from Athos and Samothraki (Greece), *Bull. Geol. Soc. Greece*.

Koukouvelas, I., and Doutsos, T., 1990. Tectonic stages along a traverse cross cutting the Rhodopian zone (Greece), *Geol. Rundschau*, 79, 3, 753-776.

Mercier, J.-L., Simeakis, K., Sorel, D., andVergely, P., 1989. Extensional tectonic regimes in the Aegean basins during the Cenozoic, *Basin Research*, 2, 49-71.

Mountrakis, D., 2002. Tectonic evolution of the Hellenic orogen. Geometry and kinematics of the deformation, *Bull. Geol. Soc. Greece*, vol. XXVIV, 2113-2126 (in Greek with English abstract).

Mountrakis, D., Tranos, M., Papazachos, C., Thomaidou, E., Karagianni, E., and Vamvakaris, D., 2006. Neotectonic and seismological data concerning major active faults, and the stress regimes of Northern Greece. In A. H. F. Robertson and D. Mountrakis (eds), *Tectonic development of the Eastern Mediterranean region.* Geol. Soc. Lond., Spec. Publ. 260, 649-670pp.

Mussalam, K., and Jung, D., 1986. Petrology and geotectonic significance of salic rocks preceding ophiolites in the Eastern Vardar Zone, Greece, *Tschermaks Min. Petr. Mitt.*, 35, 217-242.

Papadopoulos, C., and Kilias, A., 1985. Alterbeziehungen zwischen Metamorphose und Deformation im zentralen Teil des Serbomazedonischen Massivs (Vertiskos Gebirge, Nord-Griechenland), *Geol. Rundsch.*, 74, 77-85.

Papanikolaou, D., Alexandri, M., Nomikou, P., and Ballas, D., 2002. Morphotectonic structure of the western part of the North Aegean Basin based on swath bathymetry, *Marine Geology*, 190, 465-492.

Pavlides, S. B., and Kilias, A. A., 1987. Neotectonic and active faults along the Serbomacedonian zone (SE Chalkidiki, northern Greece), *Ann. Tecton.*, 1, 97-104.

Pavlides, S., Mountrakis, D., Kilias, A., and Tranos, M., 1990. The role of strike-slip movements in extensional area of Northern Aegean, (Greece). A case of transtensional tectonics, *Ann. Tecton.*, 4, 196-211.

Sakellariou, D., 1989. The geology of the Serbomacedonian massif in the northeastern Chalkidiki peninsula, North Greece. Deformation and metemorphism, *PhD thesis*, Univ. Mainz, 177pp.

Sakellariou, D., 1993. Tectonometamorphic evolution of the geotectonic units of the Chalkidiki peninsula, *Bull. Geol. Soc. Greece*, vol. XXVIII, 165-177.

Sapountzis, I., Petrography and geological setting of the greengneisses of Thessaloniki, *PhD thesis*, Univ. Thessaloniki. (in Greek with English summary)

Tikoff, B., and Peterson, K., 1998. Physical experiments of transpressional folding, *J. Struct. Geol*, 20, 661-672.

Tranos, M. D., 1998. Contribution to the study of the neotectonic deformation in the area of Central Macedonia and North Aegean. *PhD thesis*, Univ. Thessaloniki (in Greek with English summary).

Tranos, M. D., 2004. Faulting of the Lemnos Island (northern Greece). In: A. A. Chatzipetros and S. B. Pavlides (eds), *Proceedings of the 5th International Symposium on Eastern Mediterranean Geology,* vol. 1, 205-208pp.

Tranos, M. D., Kachev, V. N., and Mountrakis, D. M., 2006. Transtensional origin of the Simitli basin, SW Bulgaria. In: M. Sudar, M. Ercegovac and A. Grubić, *Proceedings of the XVIIIth Congress of the Carpathian-Balkan Geological Association*, 636-640.

Tranos, M. D., Kilias, A. A., and Mountrakis, D. M., 1993. Emplacement and deformation of the Sithonia granitoid pluton (Macedonia, Hellas), *Bull. Geol. Soc. Greece*, vol. XXVIII, 195-210.

Tranos, M. D., Kilias, A. A., and Mountrakis, D. M., 1999. Geometry and kinematics of the Tertiary post-metamorphic Circum Rhodope Belt Thrust System (CRBTS), Northern Greece, *Bull. Geol. Soc. Greece*, vol. XXXIII, 5-16.

Vergely, P., 1984. Tectonique des ophiolites dans le Hellenides internes. Consequences sur l'evolution des regions Tethysiennes occidentales, *PhD thesis,* University of Paris, Paris.

Δελτίο της Ελληνικής Γεωλογικής Εταιρίας τομ. XXXX, 2007
Πρακτικά 11ου Διεθνούς Συνεδρίου, Αθήνα, Μάιος 2007

Bulletin of the Geological Society of Greece vol. XXXX, 2007
Proceedings of the 11th International Congress, Athens, May, 2007

THE EVOLUTION OF THE STRESS FIELD IN EASTERN MACEDONIA AND THRACE

Gkarlaouni C.[1], Papadimitriou E.[1], Kilias A.[2], Falalakis G.[2], and Gemitzi A.[3]

[1] *Aristotle University of Thessaloniki, School of Geology, Department of Geophysics, hagarl@geo.auth.gr, ritsa@geo.auth.gr*

[2] *Aristotle University of Thessaloniki, School of Geology, Department of Geology, kilias@geo.auth.gr, georgefalalakis@tgm.gr*

[3] *Democritus University of Thrace, Dept. of Environmental Engineering, Laboratory of Ecological Engineering, and Technology, agkemitz@env.duth.gr*

Abstract

Eastern Macedonia and Thrace are characterized by moderate seismicity compared to the adjacent North Aegean area, as it is derived from both historical information and instrumental records. The known strong (M≥6.5) historical earthquakes that occurred during the past three centuries, however, have caused appreciable casualties and for this reason the seismic hazard assessment in the study area is of considerable social importance. These events (Didimoteiho earthquake (M=7.4) in 1752, Komotini earthquake (M=6.7) in 1784 and Drama earthquake (M=7.3) in 1829) are associated with a fault zone that runs the area of interest from west to east, in neighboring faults or fault segments. Their consequential occurrence is examined in the framework of the evolution of the stress field by the calculation of Coulomb stress that is due to their coseismic slips as well as the long term tectonic loading on the regional major faults. Geometry and kinematics of the faults are derived from macroseismic information and the field geologic examination of the active neotectonic structures that dominate in the region. The current pattern of stress changes provide indications of the areas where stress is increased and consequently possible sites for an impeding earthquake due to Coulomb stress transfer.

Key words: *Neotectonic faults, Coulomb stress, Seismic hazard, Northern Greece.*

Περίληψη

Η ανατολική Μακεδονία και η Θράκη με βάση ιστορικές αναφορές όσο και ενόργανες καταγραφές, χαρακτηρίζονται από μέτρια σεισμικότητα συγκριτικά με τη γειτονική σεισμική ζώνη του Β. Αιγαίου. Ωστόσο οι γνωστοί ισχυροί (M≥6.5) ιστορικοί σεισμοί οι οποίοι έγιναν κατά τους τρεις περασμένους αιώνες έχουν προκαλέσει σημαντικές απώλειες καθιστώντας σημαντική την εκτίμηση της σεισμικής επικινδυνότητας στην περιοχή αυτή. Οι ισχυροί αυτοί σεισμοί (Διδυμότειχο (M=7.4), 1752, Κομοτηνή (M=6.7), 1784 και Δράμα (M=7.3), 1829) συνδέονται με μια ζώνη διάρρηξης η οποία διατρέχει την περιοχή μελέτης από τα δυτικά προς τα ανατολικά, σε γειτονικά ρήγματα. Η διαδοχική γένεση των σεισμών αυτών εξετάζεται με βάση την εξέλιξη του πεδίου των τάσεων στην περιοχή, με υπολογισμό των μεταβολών της τάσης Coulomb

που οφείλεται τόσο στις σεισμικές ολισθήσεις όσο και στη μακροπρόθεσμη τεκτονική φόρτιση των σημαντικών ρηξιγενών δομών. Η γεωμετρία και η κινηματική των ρηγμάτων προκύπτουν από μακροσεισμικά δεδομένα και από γεωλογικές παρατηρήσεις στα ενεργά νεοτεκτονικά ρήγματα που κυριαρχούν στη περιοχή. Η παρούσα κατάσταση του πεδίου των τάσεων παρέχει ενδείξεις για πιθανές θέσεις μελλοντικού ισχυρού σεισμού λόγω της μεταφοράς τάσεων μεταξύ γειτονικών ρηγμάτων.
Λέξεις κλειδιά: *Νεοτεκτονικά Ρήγματα, Τάση Coulomb, Σεισμική Επικινδυνότητα, Βόρεια Ελλάδα.*

1. Introduction

The area of eastern Macedonia and Thrace is located north of the North Aegean Trough (NAT), the prolongation of the dextral strike slip North Anatolia Fault (NAF) zone into Aegean Sea, being the boundary between the more stable Eurasia lithospheric plate and fast moving Aegean microplate (Fig. 1). The study area constitutes part of the back arc Aegean region and therefore extension is the dominant pattern of active deformation with the T axis striking almost N–S, although deformation is not as great as in the Aegean sea. Strong earthquakes (M≥6.5) are known to have occurred along a fault zone that is aligned in an E–W direction (Fig. 1).

Although instrumental seismicity is sparse and of lower magnitude when it is compared with the adjacent areas, and in particular with the seismicity along the North Aegean Trough (Fig. 1), strong earthquake occurrence is not of minor importance, thus constituting a major threat for the populated areas. The historical descriptions on the reported damage and affected areas (Papazachos and Papazachou 2002) as well as maps of isoseismals (Papazachos *et al.* 1997) for the three devastating events that occurred in 1752 (Didimoteiho, M=7.4), 1784 (Komotini, M=6.7) and in 1829 (Drama, M=7.3), testify the need for seismic hazard assessment investigation.

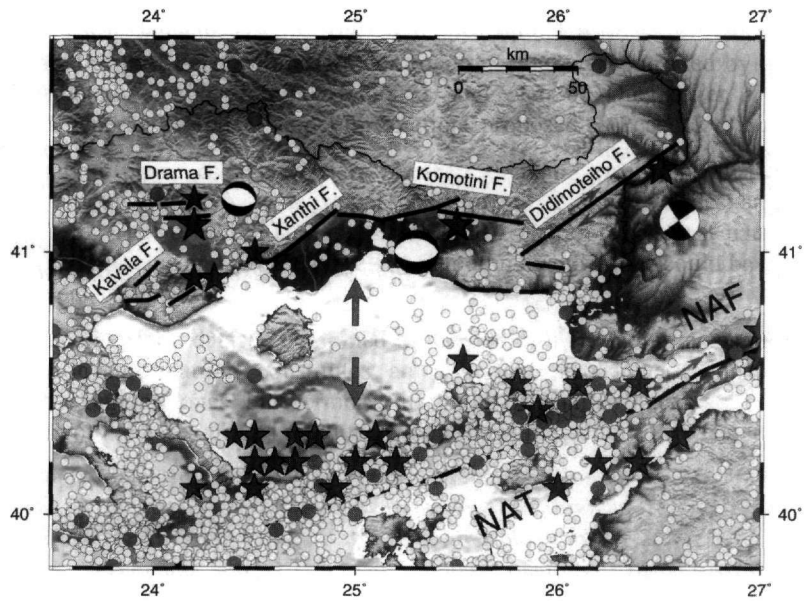

Figure 1 - Spatial distribution of earthquakes with M≥6.0 that occurred in the study area since 1000 A.D. (asterisks), and instrumental seismicity (dark gray circles for events of M≥5.0 since 1911 and light gray circles for events of M≥3.0 since 1981). The known active faults and the main seismotectonic characteristics of the broader area are depicted (NAF: North Anatolian Fault, NAT: North Aegean Trough)

In the present study, we investigate the stress perturbations caused by the stronger earthquakes mentioned above. This involves incorporation of both tectonic loading on the regional major faults and coseismic slip during the main shocks. Therefore, the scope of this research is to define the geometry of the faults associated with the strong earthquakes occurrence and their kinematics, and then by making use of this information to compute the static stress changes for the whole study area. The computations reveal the stress interactions between the faults and are important in determining where the next strong events, might occur. The identification of currently being stress enhanced areas contributes to the assessment of seismic hazard in the study area, as far as possible locations of future strong events are expected in these sites.

2. Geological and Seismotectonic setting

The geological structure of the study area consists of rock formations attributed to the Paleozoic Rhodope massif and to the Mesozoic Circum–Rhodope Belt zone (CRB), as well as Eocene mollasic and Oligocene–Miocene volcanosedimentary sediments (Fig. 2). The Rhodope massif extends through southern Bulgaria and northeastern Greece forming a crystalline unit of Paleozoic or older age, reactivated during Alpine times (Kilias and Mountrakis 1990). The area of Eastern Macedonia and Thrace is a well deformable region affected by several faults that bound the Neogene tectonic basins. Basin sedimentation started during Lutesian with initial deposition of continental sediments followed by marine type deposits (Goranov and Atanassov 1992). Andesitic volcanism characterizes also the initial stages of sedimentation (Kilias *et al.* 2003). Evolution of the basins continues with the deposition of marine and molassic type sediments during Priabonian until Upper Oligocene time, simultaneously with a post continental collision of intense volcanic activity of calc–alkaline to sosonitic composition, migrated progressively southward (Innocenti *et al.* 1984).

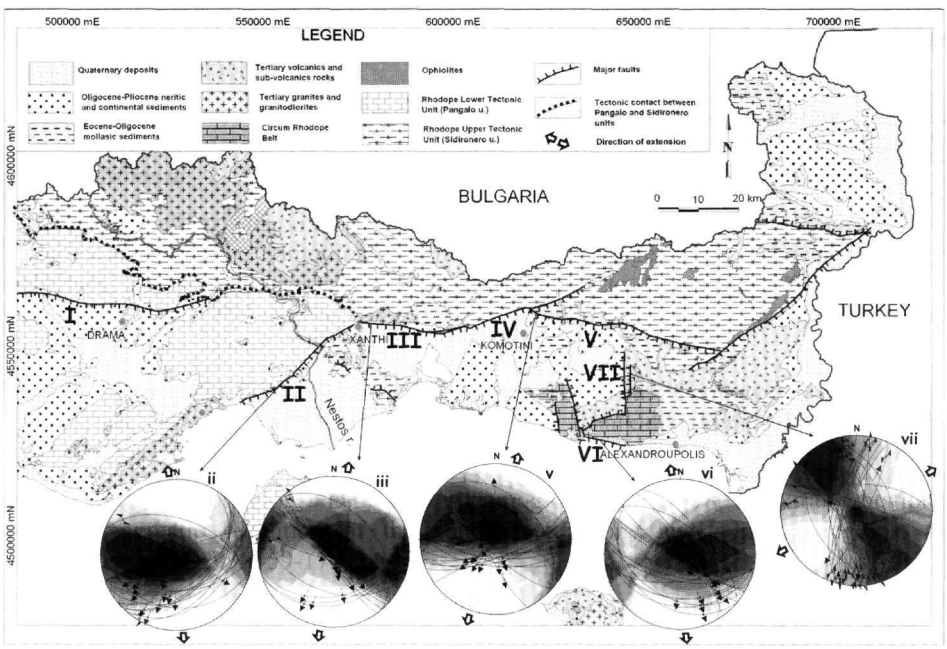

Figure 2 - Simplified geological map of the Eastern Macedonia and Thrace in Greece (modified by Kilias *et al.* 1990) showing the kinematics of the fault segments and the computed principal stress axes using the Right Dihedron method (equal area, lower hemisphere stereographic projection). The numbering is referred to a fault segment as in the text

According to Lyberis (1985) and Mercier et al. (1989) the major faulting events in Thrace are: (i) a NW–SE extension of Upper Miocene age, (ii) a NE–SW extension which resulted in a right lateral strike-slip movement during Pliocene time and (iii) a later N–S extension through Pleistocene, which also had a right lateral component of motion. Koukouvelas and Aydin (2002) as well as Rodoyanni *et al.* (2004) showed the importance of the strike-slip tectonics that controls the northern Aegean basins and fault kinematics. The main active fault zones that are recognized in the area are the following: I. Drama-Prosotsani, II. Chrisoupoli–Xanthi, III. Xanthi–Iasmos, IV. Iasmos–Komotini, V. Komotini–Sapes, VI. Maronia and VII. Sykorachi (Figs 2, 3). According to geological criteria the Maronia and the parallel Petrota–Vrachos faults are characterized as possible active ones (Kilias *et al.* 2003, Mountrakis *et al.* 2006).

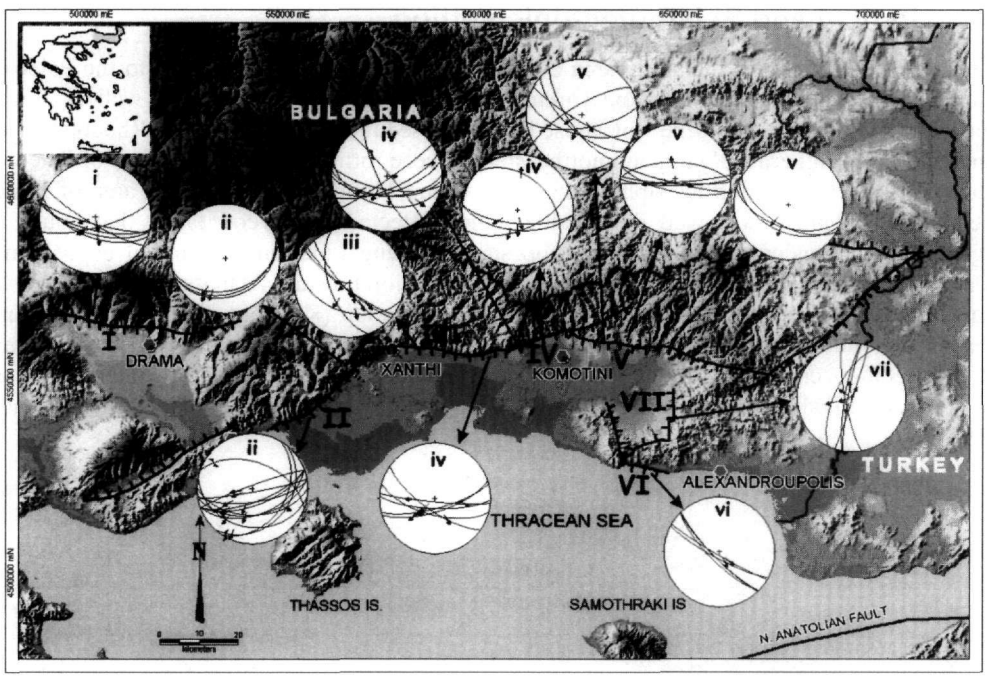

Figure 3 - Digital Elevation Model of the study area indicating the locations of the major faults with their kinematics (data from Kilias *et al.* 2005 and observations during this study) in each site (equal area, lower hemisphere stereographic projection). The numbering is referred to a fault segment as in the text

At the western part of the study area the Drama–Prosotsani (I) fault zone (Fig. 3) bounds the southern slopes of Falakron Mountain and forms a rather complex geometry synthesized of subparallel, interrupted fault strands that dip steeply to the south (Mountrakis *et al.* 2006). All segments develop an E–W strike and they form a right stepping fault geometry covered by an alluvial plain. Mountrakis *et al.* (2006) suggest that the alluvial plain obscures the main fault trace revealing a rather small slip rate for the fault zone, a fact that is in agreement with the geodetic data of Kotzev *et al.* (2006). Along the fault trace outcrops of travertines, springs and fault breccia fanglomerates are found. A normal offset related to north–south extension field is defined (Mountrakis *et al.* 2006). The most important active structure in eastern Macedonia and Thrace is the Kavala–Xanthi–Komotini fault zone (Fig. 3) with a length of more than 120 km, which passes close to these cities, a fact that demands seismic hazard assessment study for the area. This fault zone consists of segments with separate tectonic features whose general strike ranges from NE–SW to WNW–ESE (Mountrakis and Tranos 2004, Kilias *et al.* 2006). The zone is divided in four major parts regarding Chrisoupoli–Xanthi (II), Xanthi–Iasmos (III), Iasmos–Komotini (IV) and Komotini–Sappes (V) segments (Kilias *et al.* 2006, Mountrakis *et al.* 2006). Chrisoupoli–Xanthi

segment is 35 km long, it strikes NE–SW and controls the southern slope of the Lekani Mountain. The fault expression dipping with moderate angle towards SE is exposed well at Paradisos village. Along its surface there are records of three slickenline generations with the older one indicating a strike slip movement and the younger being in accordance with the extension that presently dominates in the area. Xanthi–Iasmos segment is 27 km long, strikes WNW–ESE to E–W and consists of smaller subparallel faults. The younger group of slickenlines marked on its surface reveal an oblique right lateral normal movement. Iasmos–Komotini fault segment is 16 km long, it strikes ENE–WSW and consists of two parallel left stepping and overlapping strands 6 km and 13 km long, respectively. It is characterized by successive reactivations with the last ones being normal. The Komotini–Sappes fault zone has a total length of 30km and a complicated synthetic geometry, it consists of strands <8km in length, striking WNW–ESE, or E–W, and dipping with medium to high angles to the south. The fault zone accommodates right to left lateral oblique normal movement. Further south from Maronia to Alexandroupoli the Maronia (VI) fault zone, 35km in length, is exposed and controls the coastline of the Thracian Sea (Kilias *et al.* 2003, Mountrakis *et al.* 2006). Segmentation gives smaller faults of WNW–ESE and ENE–WSW strike. Tectonic measurements show an oblique normal movement with a small sinistral strike slip component. The geological observations are in accordance with the seismological data. There is an epicenter distribution extending in a WNW–ESE direction along the coastline dipping to the south with a high angle, the fault cuts young sediments in the exit of Paliorema stream and seems to have been uplifted about 1 m (Kilias *et al.* 2003). It consists of parallel segments that dip gradually to the sea. Another fault zone is the Sykorachi (VII) that outcrops the surface in a length of 23 km with NNE–SSW striking and NW dipping (Fig. 3). It is an initially sinistral strike–slip fault with younger activity related with an important dip-slip component of movement.

3. Long–term Slip Rate Constraints on the Major Faults

Various geotectonic models have been proposed to investigate the dominant tensile tectonic pattern in Aegean area. Papazachos and Comninakis (1971) were the first to introduce that the Eastern Mediterranean oceanic plate is subducting under the Aegean, along the Hellenic Arc in association to the Benioff zone defined from the intermediate depth earthquakes. McKenzie (1978) showed that the northward motion of the Arabian plate extrudes the Anatolian microplate laterally to the west after slipping along the dextral strike slip NAF. Anatolia, which forms a distinct microplate, forces the Aegean microplate to perform a southwest movement, as it is bounded from Apoulia plate from the west.

Global Positioning System (GPS) data suggest a southwestward motion of the Aegean plate with respect to the Eurasian Plate (e.g. Reilinger *et al.* 1997). The Anatolian plate is moving westerly relative to the Eurasian plate along the North Anatolian Fault, with an average velocity of about ~24 mm/yr which is accommodated by an additional N–S deformation of ~11 mm/yr in the Aegean, resulting in a total SW motion of ~41 mm/yr of the south Aegean relative to Eurasia. Papazachos (1999) using two types of data, GPS and seismological, showed that the pattern of deformation in the Aegean area cannot be described by a rigid body rotation model that best fits the Anatolian – Eurasian relative motion. The rotation of the Anatolian plate is transferred in the Aegean area as a simple translation, indicated by the subparallel deformational field in this area. This translation occurs along the central and southern part of the coasts of Turkey and the neighbouring Greek islands. The Aegean moves almost uniformly in a SSW direction (~200°–220°) with an average velocity of ~30 mm/yr, which increases from 25 mm/yr in the central and southern part of the western coast of Turkey to 30–35 mm/yr near the southwestern part of the Hellenic arc (Papazachos 1999). This significant increase is due to the strong N–S extension in the Aegean and western Turkey.

The northern boundary of the Aegean extensional regime passes through central Bulgaria, as first suggested by McKenzie (1972) based on limited seismological data. Kotzev *et al.* (2006) after geodetic survey in order to determine kinematics in south and western Bulgaria reconfirms the

previous researcher and present more robust evidence that the region consists the northern boundary of the extensional Aegean domain. They found a mean extensional velocity of 1–2 mm/yr or less with an uncertainty near or below 0.5 mm/yr. These velocities are far less than the ones along the NAT, however they increase while moving from the interior of Bulgaria to the south. In particular, for Thrace and Macedonia they suggest that the region moves to the south with a velocity of 1 mm/yr related to a constant pole in Northern Bulgaria. Since there are not known active faults have been mapped in southern Bulgaria, this movement is considered that it is absorbed entirely from the Kavala–Xanthi–Komotini fault zone (Fig. 3). Based on these motions the long slip rates for these faults are defined approximately, so that they will be in accordance with the above geodetic results. Thus, a long term slip rate equal to 1mm/yr was assigned for the fault segments included in our evolutionary stress model (Table 1).

Table 1 - Information on the properties of the fault segments that are included in the stress evolutionary model

Name	Fault Center		Strike (deg)	Dip (deg)	Length (km)	Depth (km)	Faulting type	Slip Rate, mm/yr
	Latitude °N	Longitude °E						
Chrisoupoli – Xanthi	41.05	24.74	55	50	36.20	0 – 15	N	1
Xanthi – Iasmos	41.13	25.00	90	50	18.10	0 – 15	N	1
Iasmos – Komotini	41.14	25.27	75	80	34.48	0 – 15	N	1
Komotini – Sappes	41.19	25.45	98	53	36.20	0 – 15	N	1
Avantas	40.95	25.93	98	50	16.37	0 – 15	N	1
Maroneia	40.88	25.53	140	60	6.89	0 – 15	N	1
Maroneia – Komotini f1	40.85	25.65	90	60	17.24	0 – 15	N	1
Maroneia –Komotini f2	40.85	25.87	90	50	12.06	0 – 15	N	1
Drama-Prosotsani	41.13	24.04	90	53	58.62	0 – 15	N	1
Kavala f1	40.91	23.95	225	50	15.5	0 – 15	N	1
Kavala f2	40.82	23.93	90	50	15.5	0 – 15	N	1
Kavala f3	40.84	24.12	238	50	12.92	0 – 15	N	1
Didimoteiho	41.20	26.20	54	90	80.00	0 – 15	RS	1

4. Methodology

The methodology introduced by Deng and Sykes (1997) for a stress evolutionary model is applied in the present study. According to this, changes in the stress field are associated with not only the coseismic slip of the stronger events that occur in an area, but also with the tectonic loading on the major faults of this area. For this reason, information on the geometry of the active faults and their corresponding long–term slip rates, as presented in the previous section, along with the geometry of the faults that slipped in strong main shocks and the corresponding coseismic slip are necessary. Since details on the surface rupture and coseismic slip are not available for the events included in our evolutionary model, these are determined by scaling laws derived from global data, and give these parameters as a function of the earthquake magnitude (Papazachos *et al.* 2004). Thus, the fault length, L (km), and coseismic slip, u (cm), were estimated by the equations (1) and (2) for strike–slip and dip–slip faults, respectively:

Equation 1:

$$\log L = 0.59M - 2.3 \qquad \log u = 0.68M - 2.59$$

Equation 2:

$$\log L = 0.50M - 1.86 \qquad \log u = 0.72M - 2.82$$

The changes in the stress field associated with coseismic slips and long–term tectonic loading on the major faults of the study area are calculated, following the approach of Deng and Sykes (1997). The changes in the Coulomb failure function (ΔCFF) depend on both changes in shear stress, $\Delta\tau$, and normal stress, $\Delta\sigma$ [modified from Scholz (2002)]:

Equation 3:

$$\Delta CFF = \Delta\tau + \mu' \Delta\sigma$$

Here μ' is the apparent coefficient of friction.- 327 -Both $\Delta\tau$ and $\Delta\sigma$ are calculated for the fault plane of the next earthquake in the sequence of events, whose triggering is inspected. The change in shear stress, $\Delta\tau$, is positive for increasing shear stress in the direction of relative slip on the observing fault; $\Delta\sigma$ is positive for increasing tensional normal stress. When compressional normal stress on a fault plane decreases, the static friction across the fault plane also decreases. Both positive $\Delta\tau$ and $\Delta\sigma$ move a fault toward failure; negative $\Delta\tau$ and $\Delta\sigma$ move it away from failure. A positive value of ΔCFF for a particular fault denotes movement of that fault toward failure (that is, the likelihood that it will rupture in an earthquake is increased). The stress calculations are performed for an isotropic elastic half space (Erikson 1986, Okada 1992). The shear modulus and Poisson's ratio are fixed as 33 GPa and 0.25, respectively. Small changes in the value of the shear modulus do not alter essentially the calculations, and in most relevant studies dealing with crustal earthquakes, a value of 33GPa (e.g. Deng and Sykes 1997, King *et al.* 1994a), 30GPa (e.g. Toda *et al.* 1998) or 32 GPa (e.g. Parsons *et al.* 1999) is used. The selection of the value of the apparent coefficient of friction, μ', is based on previous results. A value of μ' equal to 0.4 was chosen and considered sufficient throughout the calculations (King *et al.* 1994a, Nalbant *et al.* 1998).

Interseismic stress accumulation between large events is modelled by "virtual negative displacements" along major faults in the entire region under study using the best available information on long–term slip rates. These virtual dislocations are imposed on the faults with sense of slip opposite to the observed slip. The magnitude is incremented according to the long–term slip rate of the fault. This virtual negative slip is equivalent to constant positive slip extending from the bottom of the seismogenic layer to infinite depth. Hence, tectonically induced stress builds up in the vicinity of faults during the time intervals between earthquakes. All computed interseismic stress accumulation is associated with the deformation caused by the time–dependent virtual displacement on major faults extending from the free surface up to the depth at which earthquakes and brittle behavior cease (~15 km).

5. Stress Evolution and Earthquake Triggering

Stress changes since 1752 are computed at a depth of 8km. This depth was chosen to be several kilometers above the locking depth (15 km) in the model. This is in agreement with King *et al.* (1994b) who found that seismic slip peaks at mid–depths in the seismogenic zone. Thus, the depth of the seismogenic layer in our calculations is taken to be in the range of 3–15 km for all of the events we modeled, in agreement with relevant previous studies (e.g. Papadimitriou and Sykes, 2001). The rupture models are approximated by rectangular surfaces with two edges parallel to the Earth's surface. Although the rupture is more complicated and slip varies along its segments, it is believed that the above approximation is sufficient to identify areas of stress changes, when they are computed for distances far from the causative fault. Dark gray regions denote negative changes in CFF and inferred decreased likelihood of fault rupture (stress shadows). Light gray regions represent positive ΔCFF and increased likelihood of fault rupture (stress bright zones) (Harris and Simpson 1993, 1996). It should be mentioned that stress is a tensorial quantity so it depends not only on the source fault geometry and slip, but also on the geometry and rake of the target (receiver) faults that surround the source. Thus shadow zones and bright zones must be viewed in the context of specific styles of fault slip, i.e., strike slip or dip slip faults. Information on the source parameters of the earthquakes included in the stress evolutionary model is given in Table 2.

Earthquake of Didimoteiho, M=7.4 The earthquake of eastern Thrace occurred on 29th July 1752, it was preceded by two foreshocks and followed by a three months lasting aftershock sequence (Papazachos and Papazachou 2002). The whole area suffered from continuous shocks for over a

year, which caused a great catastrophe in buildings of Andrianople and a great part of the city's walls collapsed. Havsa, where the maximum macroseismic intensity is measured (I=IX), Hasoy, as well as Zerna, Kozkoy and Ferecik villages were damaged, and faced casualties and deaths. A displacement of 2.76 m and a fault length of 80 km were estimated from equations (1) and (2). In Figure 4a the coseismic stress changes associated with this main shock are presented. The stress pattern is calculated for a strike slip faulting according to the fault plane solution of the main shock (Table 2) and creates a bright zone at the western edge of the fault where the east–west oriented fault zone of Xanthi is situated, in contrast to the shadow zone that covers the area along the fault's strike.

Table 2 - Information on the source parameters of the earthquakes included in the stress evolutionary model

Date	Epicenter		Location	Rupture Length (km)	u (m)	M	Fault Plane Solution		
	Latitude °N	Longitude °E					Strike (deg)	Dip (deg)	Rake (deg)
1752, July 29	41.31	26.51	Didimoteiho	80.0	2.76	7.4	54	90	177
1783, November 6	41.10	25.5	Komotini	36.2	1.00	6.7	98	53	-93
1829, May 5	41.10	24.2	Drama	58.62	2.73	7.3	90	53	-93

Earthquake of Komotini, M=(6.7) Written references for the occurrence of this event on 6th November 1783, near the city of Komotini are found in a remnant of the monastery of Panagia Eikossifinissa, built in the northern slopes of Pagaeon Mountain (Papazachos and Papazachou 2002), reporting the collapse of 500 buildings. The state of stress just before the occurrence of this main shock is shown in Figure 4b. Both the 31 years constant tectonic loading on major faults since 1752, as well as the coseismic stress changes due to the Didimoteiho earthquake are taken into consideration. The target fault is located inside a stress enhanced area, when the stress field is inverted according to its fault plane solution, i.e. normal faulting dipping to the south. The fault length is equal to 36 km long according to Mountrakis *et al.* (2006), while a mean displacement of 1.0 m was estimated from equation (2).

Earthquake of Drama, M=7.3 The third strong main shock in our study area occurred near Drama on 5th May 1829, following two strong foreshocks on 11th and 13th April. Macroseismic effects result in a possible epicenter westward migration, during the sequence, along the active fault zone (Papazachos and Papazachou 2002). The damage caused by the foreshocks was greater at the eastern part (Xanthi etc.), while the main shock was greatly disastrous for the western part of the epicentral area (Drama etc.). The earthquake was strongly felt up to the coasts of Macedonia and Thrace from Constantinople to Bucharest. The city of Drama as well as the cities of Kavala and Serres suffered a total catastrophe (Papazachos and Papazachou 2002). The inhabitants were forced to evacuate their houses and stayed for over a week in the fields. The fault associated with its occurrence is located in an area with positive ΔCFF (Figure 4c), when the stress changes are calculated according to its faulting type (Table 3). Figure 4d depicts the state of stress up to present, calculated for dip slip faulting striking E–W. The coseismic slips of the three main shocks and the tectonic loading on the major faults that are included in the model are summed together. This Figure evidences that only the faults segments of Xanthi–Komotini are currently in stress enhanced areas.

6. Discussion and Conclusion

The neotectonic investigations in the Eastern Macedonia and Thrace area documented the importance of an Eocene–Oligocene transpressional tectonics followed by a Miocene–Pliocene and Pliocene onward extensional events. The latest event that has a NNE–SSW directed extension is active according to geological criteria and shows a good compatibility to the seismological data.

Information on the faults associated with the occurrence of the strong main shocks as well as the ones which did not slip during the last four centuries, is provided from field investigations.

Therefore, their geometry and sense of slip is defined with a considerable accuracy. This information along with the long term tectonic loading on these faults, derived from geodetic measurements, is used as input for our stress evolutionary model.

In our model the evolution of the stress field was computed for the area of eastern Macedonia and Thrace since 1752, when the first strong main shock with adequate historical descriptions occurred. In order to quantify the static stress changes the tectonic loading on the major faults of the area along with coseismic dislocations of three strong main shocks were taken into consideration and the stress evolutionary model was applied. Although the study area is situated close to the North Aegean Trough where seismicity is high, the mainland is deprived from frequent occurrence of both strong and moderate events. However, the populated areas have repeatedly suffered by severe damage due to the occurrence of the above mentioned strong main shocks, and therefore the regional seismic hazard is appreciable.

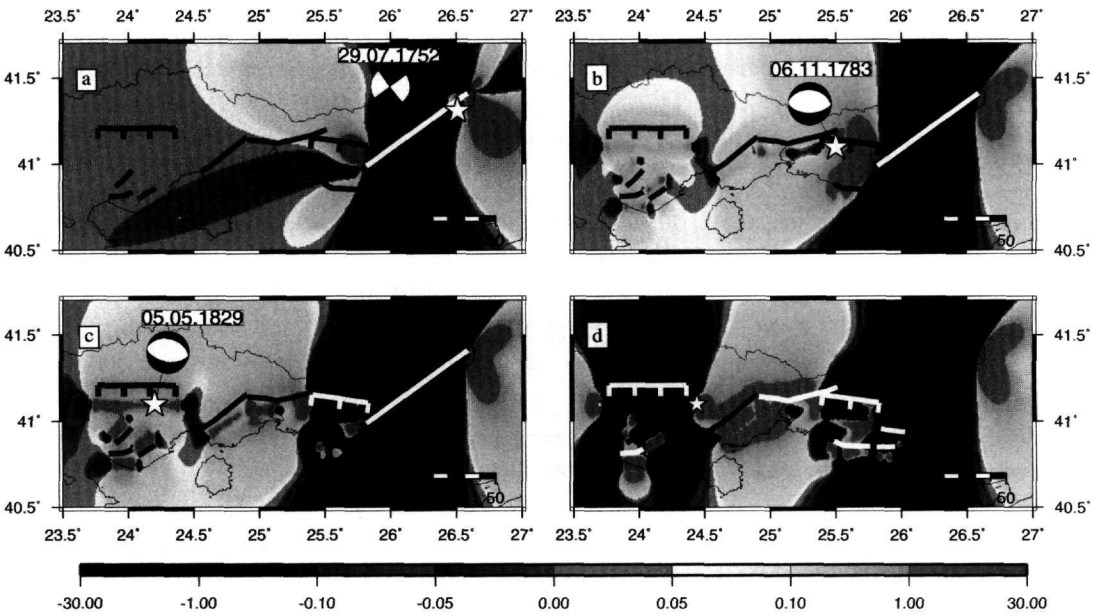

Figure 4 - Stress evolution in Eastern Macedonia and Thrace since 1752. Faults in black represent the target faults according to which the stress changes have been calculated, faults in white represent faults that have slipped in strong earthquakes, and faults in gray are the active ones that still remain unruptured. Fault plane solutions are shown as lower hemisphere equal area projections and main shock epicenters are depicted by a star. A gray scale is used to present schematically the stress changes, measured in bars. (a) Co–seismic Coulomb stress changes associated with the 1752 event. (b) Stress evolution until just before the 1783 event calculated according to its fault plane solution. (c) ΔCFF just before the 1829 main event. (d) State of stress in 2006 computed for the dip slip approximately east–west striking faults

According to our calculations each strong event occurred in an area where the static stress changes had attained relatively high positive values, and indication that they did not inhibited by previous occurrences. On the other hand, the observation that central fault zone that remains inactive during the time period that our data cover, might be explained by the occurrence of past unreported main shocks. This last statement is just a working hypothesis, but in accordance with the long recurrence intervals assigned for the faults in the study area.

7. Acknowledgments

The stress tensors were calculated using the DIS3D code of S. Dunbar, which later improved by Erikson (1986) and the expressions of G. Converse. The GMT system (Wessel and Smith, 1998) was used to plot the Figures. This work was supported by the project "Pythagoras" funded by the EPEAEK II of the Geological and Paleontological Department of the AUTh with the contribution of the Geophysics Department. Geophysics Department contribution 693.

8. References

Deng, J., and Sykes, L., 1997. Evolution of the stress field in Southern California and triggering of moderate size earthquakes: A 200–year perspective, *J. Geophys. Res,* 102, 9859–9886.

Erikson, L., 1986. Users manual for DIS3D: A Three dimensional dislocation program with applications to faulting in the earth, *Masters thesis, Stanford Univ., Stanford, Calif.,* 167pp.

Goranov, A., and Atanassov, G., 1992. Lithostratigraphy and formation conditions of Maastrichtian-Paleocene deposits, Krumovgrad District, *Geol. Balcanica,* 22, 71–82.

Harris, R.A., and Simpson, R.W., 1993. In the shadow of 1857: An evaluation of the static stress changes generated by the M8 Ft. Tejon, California, earthquake, *Eos Trans. AGU,* 74(43), Fall Meet. Suppl., 427.

Harris, R.A., and Simpson, R.W., 1996. In the shadow of 1857: The effect of the great Ft. Tejon earthquake on subsequent earthquakes in southern California, *Geophys. Res. Lett.,* 23, 229–232.

Innocenti, F., Kolios, N., Manetti, P., Mazzuoli R., Peccerillo, A., Rita, F., and Villari, L., 1984. Evolution and geodynamic significance of the Tertiary orogenic volcanism in northeastern Greece, *Bull. Volcanol.,* 47, 25–37.

Kilias, A., and Mountrakis, D., 1990. Kinematics of the crystalline sequences in the western Rhodope massif, *Geol. Balcanica,* 2, 100–116.

Kilias, A., Falalakis, G., and Mountrakis, D., 1999. Cretaceous–Tertiary structures and kinematics of the Serbomacedonian metamorphic rocks and their relation to the exhumation of the Hellenic Hinterland (Makedonia, Greece), *Intern. J. Earth Sciences,* 88, 513–531.

Kilias, A., Mountrakis, D., and Papadimitriou, E., 2003. Neotectonic – Seismotectonic research of the Perama Gold Project area, Evros Pref., 49p (Technical Report).

Kilias, A., Falalakis, G., Gemitzi, A., and Christaras, V., 2005. Faulting and paleostress evolution in the Maronia-Petrota basin. Evidences of active faults (Thrace, Greece), *Proc. of the First International Conference on the Geology of the Tethys, Cairo, 12–14 November 2005.*

Kilias, A., Falalakis, G., Gemitzi, A, Sfeikos, A., Papadimitriou, E., and Garlaouni, H., 2006. Neotectonic synthesis and seismic vulnerability of the Thracean basin (Thrace, Greece), *Proc. of the GV International Conference, Potsdam, 25–29 September 2006,* (Abstract).

King, G.C.P., Stein, R.S., and Lin, J., 1994a. Static stress changes and the triggering of earthquakes, *Bull. Seism. Soc. Am.*, 84, 935–953.

King, G., Oppenheimer, D., and Amelung, F., 1994b. Block versus continuum deformation in the western United States, *Earth Planet. Sci. Lett.*, 128, 55–64.

Kotzev, V., Nakov, R., Georgiev, Tz., Burchfiel, B.C., and King, R.W., 2006. Crustal motion and strain accumulation in western Bulgaria, *Tectonophysics*, 413, 127–145.

Koukouvelas, I.K., and Aydin, A., 2002. Fault structure and related basins of the North Aegean Sea and its surroundings,. *Tectonics,* 21, doi:10.1029/2001TC901037.

Lyberis, N., 1985. Geodynamique du domain egean depuis le Miocene superieur, *These Doct. d' etat,* Univ. Paris VI, 367pp.

McKenzie, D.P., 1972. Active tectonics of the Mediterranean region, *Geophys. J. R. Astron. Soc.*, 30, 109–185.

McKenzie, D., 1978. Active tectonics of the Alpine–Himalayan belt: the Aegean Sea and the surrounding regions, *Geophys. J. R. astr. Soc.*, 55, 217–254.

Mercier, J.–L., Simeakis, K., Sorel, D., and Vergely, P., 1989. Extensional tectonic regimes in the Aegean basins during the Cenozoic, *Basin Res.*, 2, 49–71.

Mountrakis, D.M., and Tranos, M.D., 2004. The Kavala–Xanthi–Komotini fault (KXKF): a complicated active fault zone in Eastern Mediterranean–Thrace (Northern Greece). In A.A. Chatzipetros and S.B. Pavlides (eds), *5th International Symposium of Eastern Mediterranean Geology, Thessaloniki, Greece,* 2, 857–860.

Mountrakis, D., Tranos, M., Papazachos, C., Thomaidou, E., Karagianni, E., and Vamvakaris, D., 2006. Neotectonic and seismological data concerning major active faults, and the stress regimes of Northern Greece, *Geol. Soc. London, Special Publ.,* 260, 649–679.

Nalbant, S.S., Hubert, A., and King, G.C.P., 1998. Stress coupling between earthquakes in northwestern Turkey and the north Aegean Sea, *J. Geophys. Res.*, 103, 24469–24486.

Okada, Y., 1992. Internal deformation due to shear and tensile faults in a half–space, *Bull. Seism. Soc. Am.*, 82, 1018–1040.

Papadimitriou, E., and Sykes, L., 2001. Evolution of the stress field in the Northern Aegean Sea (Greece), *Geophys. J. Int.*, 146, 747–759.

Papazachos, B.C., and Comninakis, P.E., 1971. Geophysical and tectonic features of the Aegean Arc, *J. Geophys. Res.,* 76, 8517–8533.

Papazachos, B., and Papazachou, C., 2002. *The earthquakes of Greece*, Ziti Publications, Thessaloniki, 317pp.

Papazachos, B.C., Papaioannou, Ch.A., Papazachos, C.B., and Savvaidis, A.S., 1997. Atlas of isoseismal maps for strong shallow earthquakes in Greece and surrounding area (426 BC–1995), *Pub. Geophysics Lab., Univ. Thessaloniki,* 176pp.

Papazachos, B.C., Scordilis, E.M., Panagiotopoulos, D.G., Papazachos, C.B., and Karakaisis, G.F., 2004. Global Relations between seismic fault parameters and moment magnitude of Earthquakes, *Bull. Geol. Soc. Greece*, XXXVI, 1482–1489.

Papazachos, C.B., 1999. Seismological and GPS evidence for the Aegean–Anatolia interaction, *Geophys. Res. Lett.*, 26, 2653–2656.

Parsons, T., Stein, R., Simpson, R., and Reasenberg, P., 1999. Stress sensitivity of fault seismicity: A comparison between limited–offset oblique and major strike-slip faults, *J. Geophys. Res.,* 104, 20,183–20,202.

Reilinger, R.E., McClusky, S.C., Oral, M.B., King, R.W., Toksoz, M.N., Barka, A.A, Kinik, I., Lenk, O., and Sanli, I., 1997. Global positioning System measurements of present–day crustal movements in the Arabia–Africa–Eurasia plate collision zone, *J. Geophys. Res.,* 102, 9983–9999.

Rondoyanni, T., Georgiou, C., Galanakis, D., and Kourouzidis, M., 2004. Evidences of active faulting in Thrace region (north–eastern Greece), *Bull. Geol. Soc. Greece*, 36, 1671–1678.

Scholz, C., 2002. The mechanics of earthquakes and faulting, Cambridge University press, Cambridge, 439.

Toda, S., Stein, R., Reasenberg, P., Dieterich, H., and Yoshida, A., 1998. Stress transferred by the1995 M_w = 6,9 Kobe, Japan, shock: Effect on aftershocks and future earthquake probabilities, *J. Geophys. Res.*, 102, 24,543–24,505.

Wessel, P., and Smith, W.H.F., 1998. New, improved version of the Generic Mapping Tools Released, *EOS Trans. AGU, 79*, 579.

Δελτίο της Ελληνικής Γεωλογικής Εταιρίας τομ. XXXX, 2007
Πρακτικά 11ου Διεθνούς Συνεδρίου, Αθήνα, Μάιος 2007

Bulletin of the Geological Society of Greece vol. XXXX, 2007
Proceedings of the 11th International Congress, Athens, May, 2007

CASPIAN SEA GEODYNAMICAL EVOLUTION EFFECT ON THE SEA LEVEL CHANGING ALONG THE QUATERNARY PERIOD

Khoshravan H.[1]

[1] *Head of coastal management group, Caspian Sea research & study center, Water Research Institute, Zaffar Alley, Emam Square, Sari, Mazandaran, Iran, H_khoshravan@yahoo.com*

Abstract

The Caspian Sea as the largest lake in the world has different characteristics considering geosciences (Fig. 1). In fact sea level changing is the most important happening in this region. Annually fluctuation impact on surrounding coastal area has serious damage and human society meet frequent destroyed phenomena. In this paper we are trying to reconstruct rapid Sea level changing in Holocene epoch by use paleontology evidences such as: Mollusks fossil and sedimentary facies record. In this research 254 Quaternary sediment core samples from exploring petroleum wells (M-1, G3-A) have been evaluated considering above mentioned and also more than 130 sea bottom recent sediments on view of biofacies and biostratigraphy studied. Our investigation results show that in the Caspian Sea basin at the Holocene epoch there are many periodic sea level fluctuations and climatologic impact is most important agent for sea level changing in this basin.

Data results are showing that in the studied area there were many periodic rapid sea levels changing during the Quaternary period. The Caspian Sea has several fluctuations along 10,000 years ago and its latest begin about 25 years ago. Finally we can conclude that Caspian Sea level fluctuation could continue at future similar past time and climatologic impact and tectonic movement are important agents for sea level changing in this region.

Key words: *biostratigraphy, gastropod, Caspian Sea, fluctuation, mollusc, Holocene epoch.*

Περίληψη

Η Κασπία Θάλασσα, η μεγαλύτερη λίμνη στο κόσμο, παρουσιάζει ποικίλα χαρακτηριστικά όσον αφορά τις γεωεπιστήμες (Fig. 1), με σημαντικότερο όλων τις διακυμάνσεις στις στάθμης της. Οι ετήσιες διακυμάνσεις της στάθμης έχουν πολλές φορές καταστροφικές επιπτώσεις στις παράκτιες περιοχές και τους πληθυσμούς που κατοικούν εκεί. Στην παρούσα εργασία γίνεται προσπάθεια αναπαράστασης των απότομων μεταβολών της στάθμης κατά το Ολόκαινο με τη βοήθεια απολιθωμένων μαλακίων και ιζηματογενών φάσεων. Αναλύθηκαν 254 δείγματα ιζήματος προερχόμενα από φρέατα εξόρυξης πετρελαίου (M-1, G3-A) καθώς και περισσότερα από 130 δείγματα επιφανειακών ιζημάτων πυθμένα. Σύμφωνα με τα αποτελέσματα της έρευνας, κατά το Ολόκαινο -και εν γένει το Τεταρτογενές- καταγράφονται πολλές περιοδικές διακυμάνσεις της στάθμης της Κασπίας Θάλασσας, οφειλόμενες κατά κύριο λόγω σε μεταβολές του κλίματος. Η τελευταία διακύμανση

που καταγράφηκε ξεκίνησε πριν περίπου 25 χρόνια. Τέλος συμπεραίνουμε ότι, οι διακυμάνσεις αυτές θα συνεχιστούν με παρόμοιο ρυθμό και στο μέλλον, ελεγχόμενες από κλιματικές διακυμάνσεις και τεκτονικές κινήσεις.
Λέξεις κλειδιά: βιοστρωματογραφία, γαστερόποδα, Κασπία Θάλασσα, μαλάκια, Ολόκαινο, διακυμάνσεις στάθμης.

1. Introduction

Currently the use of recent evidences for historic phenomena reconstructing is occurred in the geology science. In the paleocimatology and pale geography studies, fossil and sedimentary petrography records are the best tools for the past events recognition. For instance some faunas which they leave to certain environment like the recent time help us to know about environmental conditions at the previous time. The last research on Middle and Upper Pliocene sediments in the Caspian sea southern basin (Chelken, Agchagile formation) showed that the Caspian sea was a real marine basin and with high biodiversity of molluscs (Mousavi 1994). On the basis of these elements we could recognize the environment conditions of the Caspian Sea at the Quaternary period and its fluctuation reconstructing. Therefore in this research we have used fossils and sediments petrography records for the Caspian Sea level changing evaluation. Among the Quaternary invertebrate fossils, Gastropod species are the most important indicator for environment analysis and pale climatology studies. Because biodiversity of their species is considerably in the Quaternary sediments and their adaptation to new environment considering sea bottom depth increasing and water salinity degree is very sensibility. Usually sedimentation processes in the Caspian Sea basin have regular condition. It means at the sea floor, the size of sediment grains decreased gradually with depth increasing. At the shallow water, the depth between 1 to 10 m sand sediments deposit when sea floor depths increasing, sediments vary to closer material and the percent of clayey matrix gradually increase. In the deep zone of the Caspian Sea, very fine sediment like mud and ooze has developed correctly (Khoshravan 1999). Therefore we could use above mentioned results for pale environment analysis and sea level reconstructing in the Caspian Sea basin.

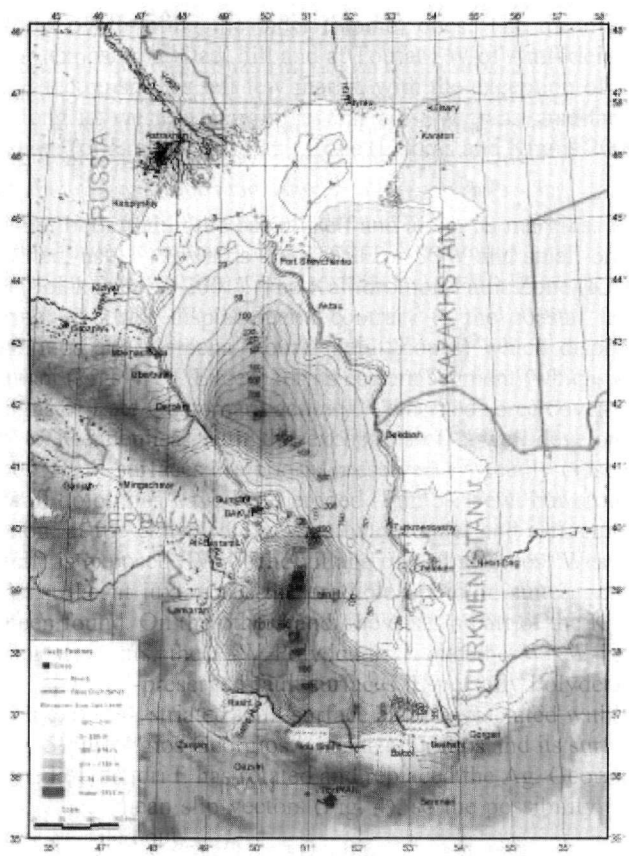

Figure 1 - The Caspian Sea Geographical location map

2. Method

In this research our investigation were programmed in two directions. At the first step we need to know which class of molluscs varied with depth increasing respectively. So we were sampling 130 sea bottom sediments at the 18 stations from shoreline to 400 m depth in the southern coasts of the Caspian Sea (5, 10, 20, 50, 100, 200, 400 and randomly 800 m depth) with grab sampler on the research vessel. After sample preparing stage, fossil determination was beginning. In general we found that gastropod species were most useful indicator for bathymetry of sea depth classification. Therefore with microscopy species determination we could classify the Caspian Sea floor in the southern part to five depth limitations. In fact today there are five assemblage zones of Gastropod species in the southern region of Caspian Sea from depth 5 to 400 m. So we should determine similar Gastropod species in the old sediments. Also we studied core sample from oil exploring wells in the southern coasts plain of Caspian Sea (M-1, G 3-A) (Fig. 2). About 254 core samples have been studied considering stratigraphy and palaeontology indexes. After gastropod fossil species determination and systematic classification we were trying to compare all of them with recent equivalent biota. Therefore with this method pale bathymetry of Quaternary sediments of the Caspian Sea has been done perfectly.

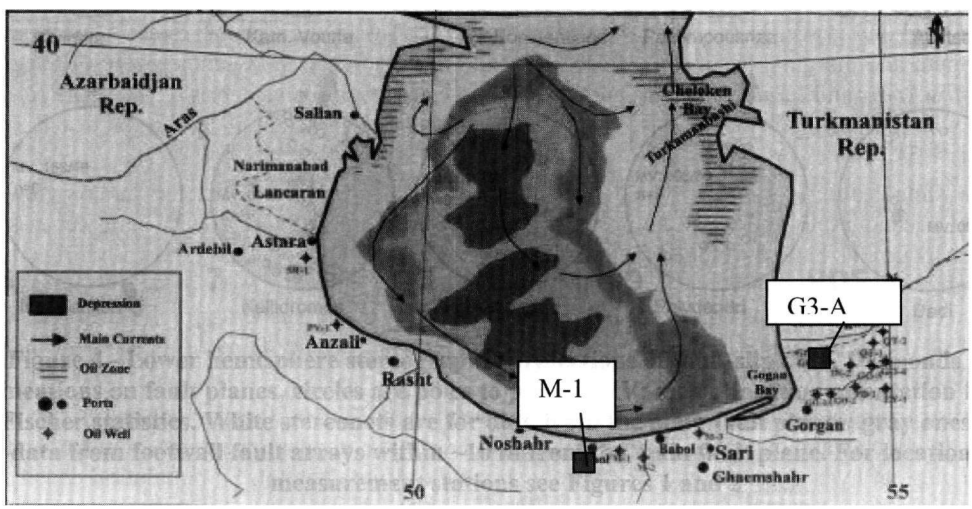

Figure 2 - Mazandaran petroleum exploring wells location map

3. Caspian Sea recent Gastropod assemblages' distribution on depth zone

Gastropods are more abundant than any other group of molluscs at the present day; they also occupy a greeter range of habitat. The majorities are aquatic, and of these most live in shallow seas; they are also widespread in freshwater and on dry land. Modern examples include the marine limpets, winkles and whelks, and the terrestrial snails and slugs.

Gastropods are classified by features of the soft part, but these leave few clues in the empty shell. Accordingly, fossil shells are classified by comparing them with similar modern shells. There are three subclasses: Prosobranchia, Opistobranchia and Pulmonata (Murray 1985). Only the prosobranchs are most important indicator and are discussed in more detail here.

The prosobranchs are fully torted and are divided into three orders: Archeogastropoda (Cambrian-Recent), Mesogastropoda (M. Ordovician-recent), and Neogastropoda (Cretaceous-recent) (Moore 1969). In the Caspian Sea Archeogastropoda and Mesogastropoda species have developed perfectly on the sea floor (Khoshravan 1995). *Theodoxus pallasi* from Archeogastropoda and other species from Mesogastropoda are frequent in this area. The structure of gastropods shell consider-

ing thickness and size in the Caspian Sea vary to other open marine biota. Often they are so small and have very tinny shell. The distributions of several species of gastropods on sea bottom in the Caspian Sea southern basin have been classified to five zones. Each zone contain special fossil of gastropods they are live together at the certain depth on sea bottom (Table 1). Sea bottom substrate sediments composition and biodiversity accumulation of gastropod species change into each zones. So those are introduced as below table.

Table 1 - Caspian Sea bottom depth classification with Gastropod assemblages

Coastal Environment	Depth(m)	Gastropods	Sediments	Indicator index
Beach zone	0	Pulmonata	Sand-Gravel	Without Marine Element
Near shore zone	5-10	Clessionella	Sand-Silty Sand	%Clessionella> Caspiella
Offshore	10-50	Caspiella	Silty Clay-Clay	%Caspiella> Clessionella
Inner Shelf	50-200	Caspia	Clay – Marl-Mud	Caspia> Caspiella%
Outer Shelf	200-400	Micromelania	Ooze-Mud	%Micromelania> Caspia

1- Beach zone: This zone is located in beach zone and corresponding with shoreline, sediments include sand and gravel in the several part of southern coasts of the Caspian Sea. At the near of river mouth and marginal basin some fresh water and dry land gastropod genus live in this region like *Helix*, *Radix* and *Planorbis* genus and always there are much plants debris on the shore line of course without marine elements. Also much rework bivalve shell accumulated on the beach zone (Plate 1: 1-3).

2- Near shore zone: In this zone, the depth of sea water is between 1 to 10 meters and on view of physical oceanography indexes, this position is located in the near shore zone where waves surf and swash currents have developed. Sediments include fine sand to very fine sand with little silt to clay matrix. The most important gastropods fauna in these depths are *Clessionella, Pygohydrobia* species. Often the thickness of their shell is very thin and crystal shape as fragile material. The percent of *Clessionella* and *Pygohydrobia* species population density is more than others in this zone (Plate 1: 4-9).

3- Offshore zone: Offshore environment with the depth between 10-50 m include sediments with sandy silt, silt clay and clayey marl deposit. Usually substrate composition and environment condition on view of hydrodynamic energy are very suitable for biota habitat. So population density of gastropods in this zone is high degree. *Caspiella, Clessionella genuses* are the most important gastropods but they have different abundance on sea bottom. Bio indicator index of Gastropod species determined with the high population of caspiella species ratio others. *Oxypyrgula* and *Clessionella sp.* have low population density (Plate 2: 1-9).

4- Inner Shelf: The depth of water in this zone is between 50-200 m. Sediments contain: Marley clay and carbonate mud with dark color. Gastropods assemblage includes different species of *Caspia* and *Oxypyrgula genuses*. The increasing of *Caspia* species accumulation ratio to *Caspiella sp.* is good indicator for this zone recognition in the old sediment of Quaternary. The shell of gastropods has developed with certain thickness and the number of whorls have been increased (Plate 3: 1-8).

5- Outer Shelf: Several gastropods live at the depth between 200-400 m, Sediments include: carbonate ooze with sulfide minerals (Pyrite and Sphalerit). Anaerobic condition has developed in the deepest sea bottom. The most important gastropods Genus in this zone contain: Planorbis, Micromelania, Abeskunus species. The increasing of Abeskunus and Micromelania species population ratio others is a good indicator for this depth zone finding in the old sediments (Plate 4: 1-6).

Plate 1 - Size scale of each fossil shell ×12. 1-*Planorbis* sp., 2-*Helix* sp., 3-*Radix* sp., 4-*Clessionella martensi*, 5-*Clessionella triton*, 6-*Clessionella variabilis*, 7-*Pygohydrobia eichwaldi*, 8-*Pygohydrobia oviformis*, 9-*Pygohydrobia gemata*

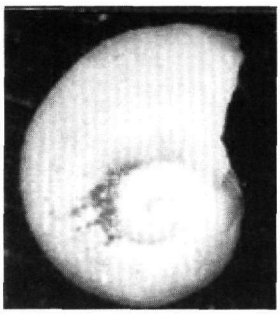

1

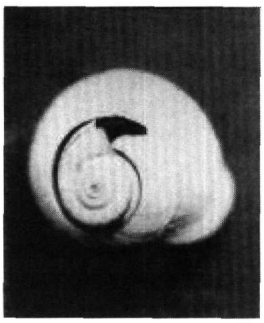

2

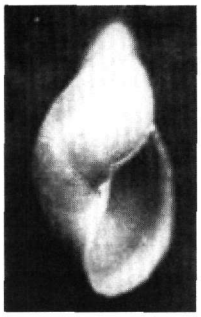

3

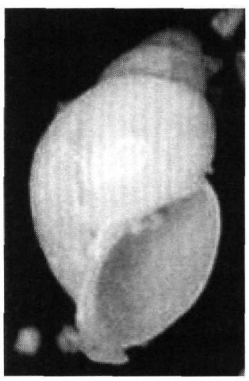

4

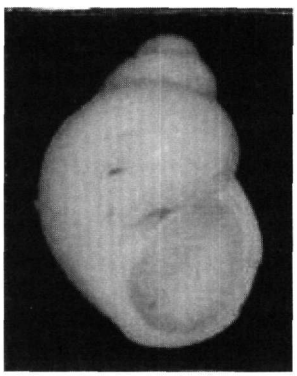

5

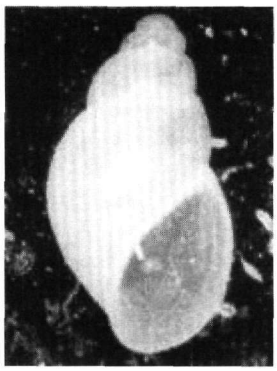

6

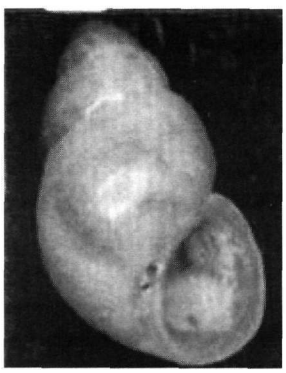

7

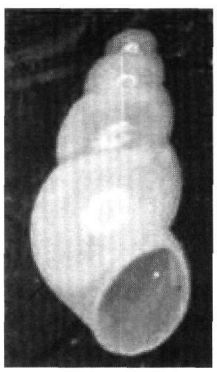

8

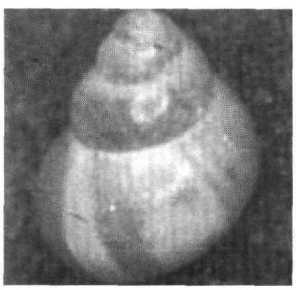

9

Plate 2 - Size scale of each fossil shell ×12. 1-*Caspiella ulski*, 2-*Caspiella laveli*, 3- *Caspiella baeri*, 4- *Caspiella derbentina*, 5- *Caspiella klensnikoviana*, 6- *Caspiella triavilis*, 7- *Caspiella conus*, 8- *Caspiella ovum*, 9- *Caspiella eichwald*



1



2

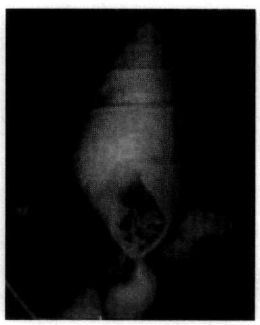

3



4



5



6

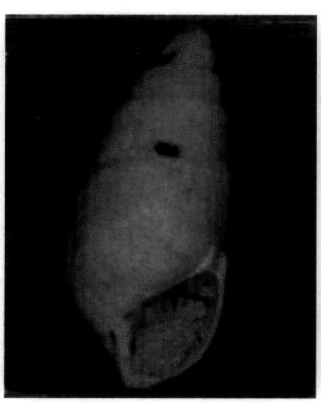

7

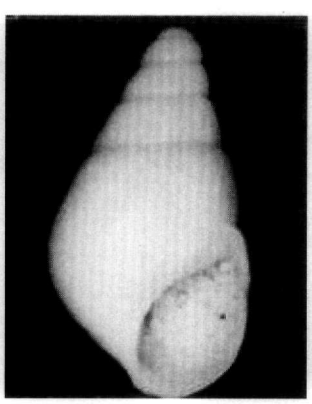

8

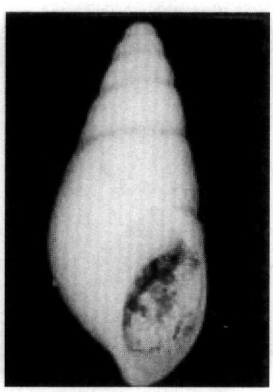

9

On the basis of above mentioned we have five gastropod assemblage indicators in the southern coasts of Caspian Sea which help us to do paleobathyometery evaluating on Quaternary sediments and Caspian Sea level fluctuation reconstructing. Continuously as follow we are trying to investigate Quaternary sediments considering above characteristics and finally we will introduce Caspian Sea level fluctuation at the Quaternary period.

4. Caspian Sea level fluctuations in the Quaternary period

In this research we could recognize Caspian Sea level fluctuation in the Quaternary period with comparing recent bio indicators with similar old fossil and sediment petrography evidences. In the Fig. 3 you can see Caspian Sea levels fluctuation periodically curve that has been reconstructed with use bio indicator. In fact this curve describes sea level changing during Quaternary period about 2.5 million years ago till now. At the X axis, thickness of layers and on the Y axis depth of water is located. So the condition of curve line shows us that there are many sea levels periodically changing with passing of time. For instance at the point A on the curve line at the late Quaternary sediments (Apsheronian Stage) the Caspian Sea at the point station (M-1 Well) has moderate to high depth but with beginning of regression phase rapid sea level changing had been occurred rapidly. Sometimes uncertain agents caused the sea level randomly decrease but this condition in the Bakovian stage changed and depth of water immediately increased and progression phase started (point B). This process continued till lower late khazarian sediments and at the late khazarian stage all at once Caspian Sea level rapidly decreased. In fact this event was beginning of regression phase in the Caspian Sea basin after Bakovian (point C). In the khovalynskian stage progression phase again caused sea level raised and the depth of sea increased (point D). But in the late Neocaspian stage the second fall at the curve line apparent regression phase as all at once and rhythmic fluctuation continued till present time (point E). What we could result from this curve is the presence of three kind of fluctuation rhythms in the Quaternary period. Those were a long time sea level changing, moderate time and short or rapid sea level fluctuation period. But in the Holocene epoch Caspian Sea level fluctuation has Rapid condition. There are many regression and progression phases in that time. In fact at the late Neocaspian stage Caspian Sea has a moderate depth in studied area and periodically sea level change so the depth of water some times increased and some times decreased (Fig. 4). After this time at the early Neocaspian stage Caspian Sea level decrease and regression phase happened. For example from 10000 years ago till now there were so many fluctuations in this basin and now we could feel the last period progression of it.

1- Long time sea level fluctuation

This kind of sea level changing was created with tectonic movements. It has low velocity and unfeeling events. During Quaternary period, The Caspian Sea has two real sea level rises in Bakovian and khovalynskian. Apparently about 400000 years it would be taken and two most important regression phases also in khazarian and Neo Caspian happened. So for this event, tectonic movement is most important factor.

2- Moderate time□sea level fluctuation

This natural changing on sea level has been happened at glacial and interglacial phases. In Quaternary period there were many glacial phases which were effected sea level changing.

3- Short time sea level fluctuation

These processes at the little time and with high velocity cause rapid sea level changing. Climatologic agent was most important for rapid sea level change in the Caspian Sea basin during the early of Quaternary in Holocene epoch.

Plate 3 - Size scale of each fossil shell ×12. 1-*Caspia baeri*, 2- *Caspia pallasi*, 3- *Caspia gemelini*, 4- *Caspia pseudobacuana*, 5- *Caspia pseudodimidiata*, 6- *Oxypyrgula bogatscheviana*, 7- *Laevicaspia eburnean*, 8-*Abeskunus brusiana*

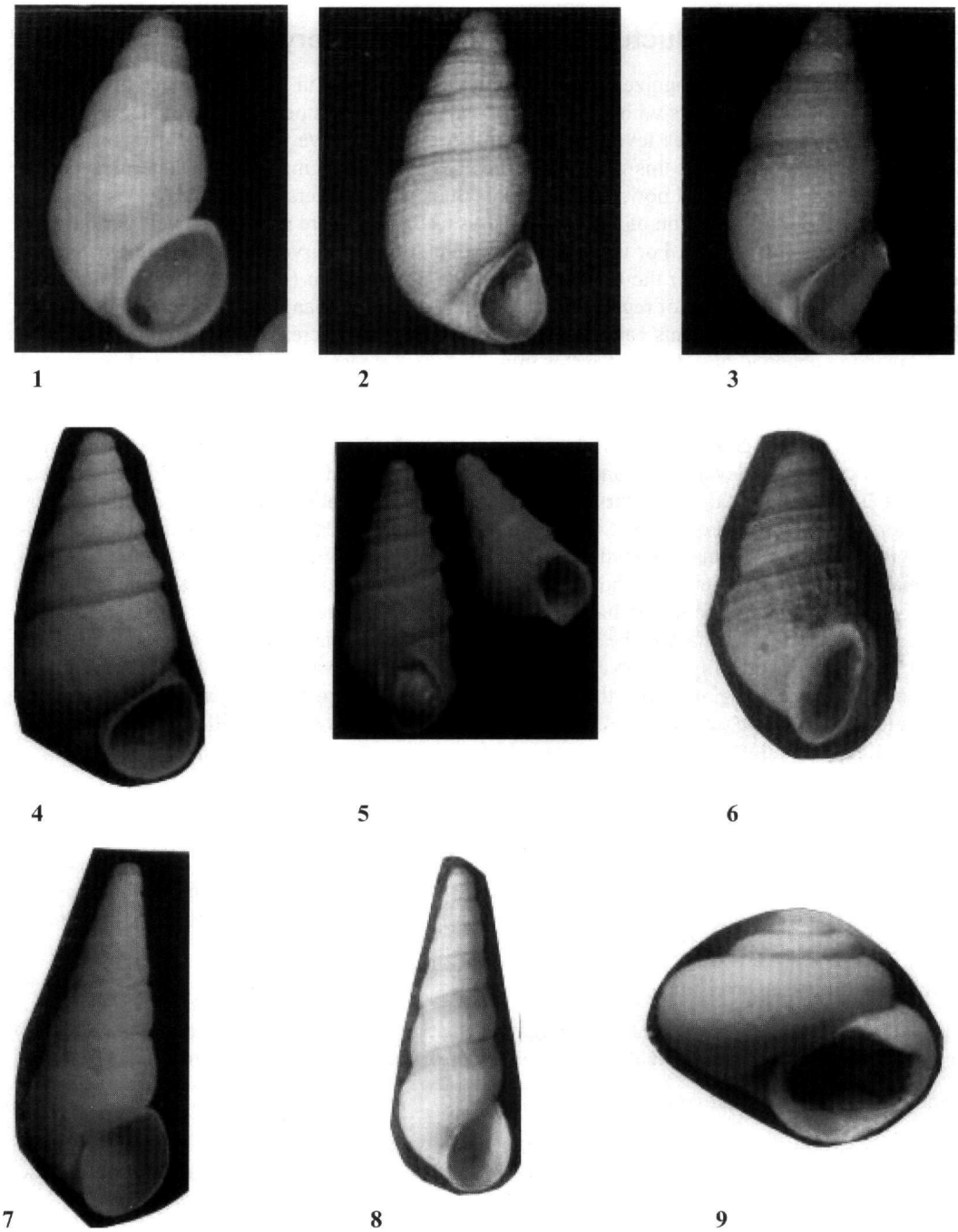

At the present we can observe some sediment sequences at the margin of beach in the southern coasts of Caspian Sea which contain sea level changing record especially at the end time of Quaternary period.

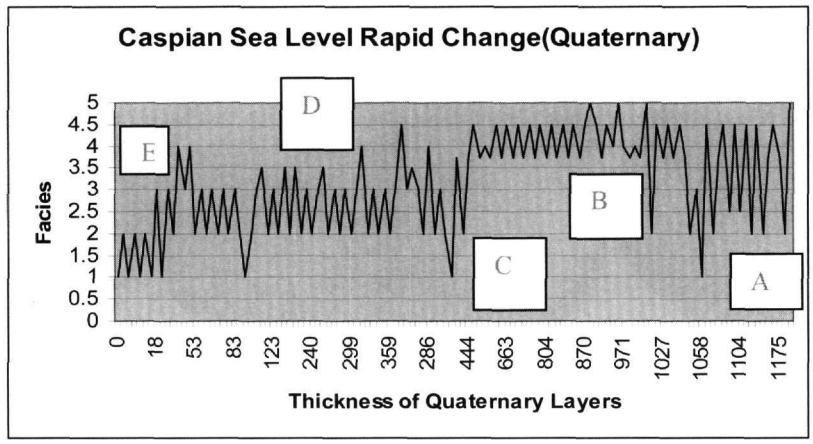

Figure 3 - Caspian Sea level rapid change in the Quaternary period

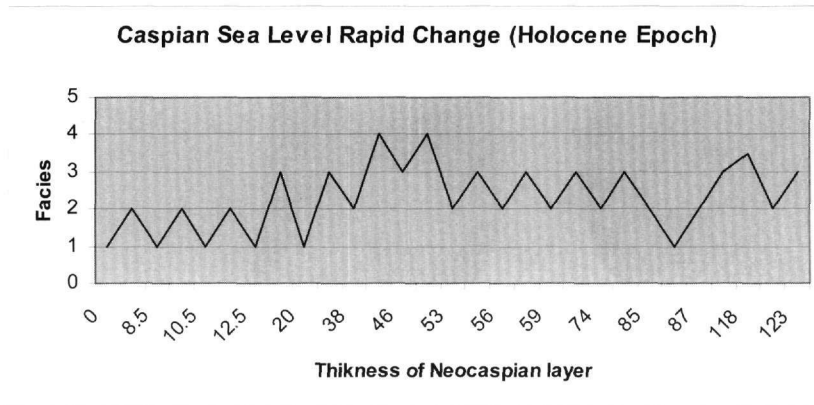

Figure 4 - Caspian Sea level rapid change in the Holocene Epoch

5. Conclusion

1- On the whole during the Quaternary period the Caspian sea basin has periodic sea level changing with different duration(long, moderate, short).

2- At the Holocene epoch most natural changing in the Caspian Sea basin related with climatologic changing and rapid sea level changing happened gradually and alternative phenomena.

3- Bio indicators are useful tool for reconstructing of sea level changing in the Caspian Sea.

4- Gastropod is most important indicator for bio environment recognition and sea level changing analysis.

5- Tectonic movement, glacial activities and climatologic impact are the most important agents for Caspian Sea level fluctuation.

6. Acknowledgements

This work is part of the Caspian Sea national research & study center. We acknowledge the all colleagues who organized and participated to the sea cruise (September 1997), during which the

Plate 4 - Size scale of each fossil shell ×12. 1-*Abeskunus sphaerion*, 2-*Abeskunus depressispira*, 3-*Planorbis djalalus*, 4-*Planorbis eichwaldi*, 5-*Micromelania laticarinata*, 6-*Micromelania turricula*

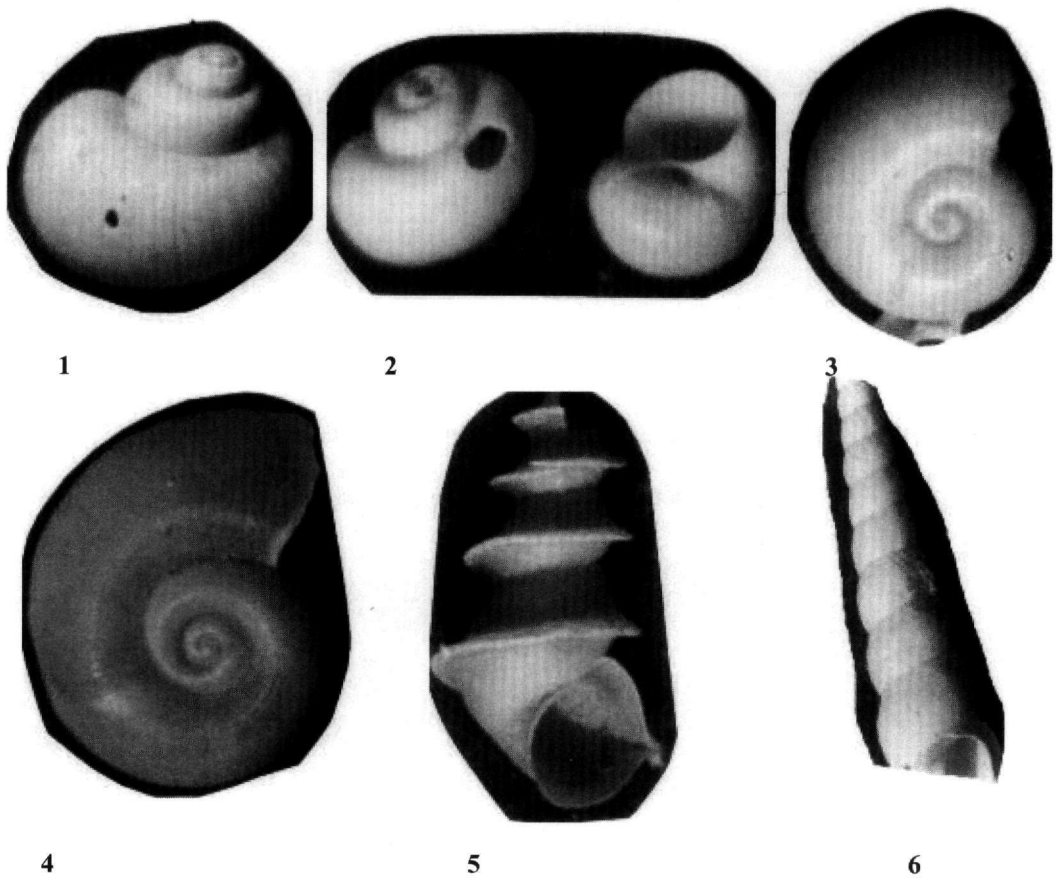

sediment sample was collected by fishery research institute of Iran. The sub-surface sample was made available thanks to Mr Mousavi Rohbakhsh (N.I.O.C). We are grateful to Mr Arsalan Mansouri (Head of CSNRSC) and others for their helpful comments.

7. References

Khoshravan, H., 1995. *The Biostratigraphy and Paleogeography investigation on Quaternary Sediments in the southern Coasts of The Caspian Sea*, Isfahan University.

Khoshravan, H., 1999. *The Biofacies and Biostratigraphy modeling on Quaternary sediments in the southern Coasts of Caspian Sea*, Azad University of Tehran.

Mousavi, R.M., 1994. Caspian Sea Neogene Period bio stratigraphy and palaeontology, *Khazar Oil Company*, Tehran, Iran.

Murray, J.W., 1985. *Atlas of invertebrate macrofossils*, Longman-England.

Moore, R.C., 1969. Treatise on invertebrate paleontology, part 1, Mollusk Gastropods, *Russel Rutter Co.,* New York City, 85-157.

Δελτίο της Ελληνικής Γεωλογικής Εταιρίας τομ.XXXX, 2007
Πρακτικά 11ου Διεθνούς Συνεδρίου, Αθήνα, Μάιος 2007

Bulletin of the Geological Society of Greece vol. XXXX, 2007
Proceedings of the 11th International Congress, Athens, May, 2007

NEOGENE TECTONIC ROTATIONS IN THE VICINITY OF THE NORTH AEGEAN TROUGH: NEW PALAEOMAGNETIC EVIDENCE FROM ATHOS AND SAMOTHRAKI (GREECE)

Kondopoulou D.[1], Zananiri I.[1,2], Michard A.[3], Feinberg H.[3], Atzemoglou A.[4], Pozzi J.-P.[3], and Voidomatis Ph.[1]

[1] *Department of Geophysics, Aristotle University of Thessaloniki, P.O. Box 352-1, Thessaloniki 54124, Greece, despi@geo.auth.gr, izanan@geo.auth.gr*

[2] *I.G.M.E., Mesogion Str. 70, 115 27, Athens*

[3] *Laboratoire de Géologie, UMR 8538, 24 rue Lhomond, 75231 Paris, Cedex 05, France*

[4] *I.G.M.E., Frangon Str. 1, 546 26, Thessaloniki*

Abstract

The present study focuses on two post-orogenic plutons, the Athos (Grigoriou) and Samothraki granites, as well as the Samothraki volcanics, located in the vicinity of the North Aegean Trough. A detailed palaeomagnetic study was carried out, with the aim of constraining the age and mechanism of tectonic rotations. In addition, anisotropy of low-field magnetic susceptibility (AMS) was studied and isothermal remanent magnetization (IRM) and thermomagnetic analyses were performed. Finally, a radiometric age for the Athos granite was obtained (43.3 ± 1.0 Ma K/Ar biotite). The measured declinations indicate clockwise rotations of the Athos (16.6°) and Samothraki (36.3°) blocks. The age of rotation is constrained to be <18 Ma at Samothraki, whereas the much smaller rotation of the Athos block can only be dated as younger than Eocene. Comparing the new palaeomagnetic data to the published dataset for Northern Greece, we suggest that the palaeomagnetically determined rotations in the vicinity of the North Aegean Trough are dominantly of post-Early Miocene age, and are controlled by major strike-slip faults and distributed "small" or minor faults.

Key words: *palaeomagnetism, block rotations, geodynamics, Aegean.*

Περίληψη

Μελετώνται δύο μετα-ορογενείς πλουτωνίτες, ο γρανίτης του Άθω (Γρηγορίου) και της Σαμοθράκης, και τα ηφαιστειακά πετρώματα της Σαμοθράκης, που βρίσκονται στην ευρύτερη περιοχή της Τάφρου του Βορείου Αιγαίου. Πραγματοποιήθηκε λεπτομερής παλαιομαγνητική μελέτη, με σκοπό τον καθορισμό της ηλικίας και του μηχανισμού των τεκτονικών περιστροφών. Επιπλέον μετρήθηκε η ασθενούς πεδίου ανισοτροπία της μαγνητικής επιδεκτικότητας (AMS) και έγιναν πειράματα ισόθερμης παραμένουσας μαγνήτισης και θερμομαγνητικές αναλύσεις. Τέλος, καθορίστηκε ραδιομετρικά η ηλικία του γρανίτη του Άθω (43.3 ± 1.0 Ma K/Ar σε βιοτίτη). Οι μετρηθείσες μαγνητικές αποκλίσεις αναδεικνύουν δεξιόστροφη περιστροφή για τον

Άθω (16.6°) και τη Σαμοθράκη (36.3°). Η ηλικία της περιστροφής εκτιμάται μικρότερη των 18 Μα για τη Σαμοθράκη, ενώ η πολύ μικρότερη περιστροφή του τεκτονικού τεμάχους του Άθω χαρακτηρίζεται νεώτερη από Ηωκαινική. Συγκρίνοντας τα νέα παλαιομαγνητικά αποτελέσματα με τα ήδη δημοσιευμένα για τον ευρύτερο βορειοελλαδικό χώρο, προτείνουμε ότι οι τεκτονικές περιστροφές στην περιοχή της Τάφρου του Βορείου Αιγαίου, που καθορίστηκαν με παλαιομαγνητικές μετρήσεις, χρονολογούνται μετά το Κάτω Μειόκαινο και ελέγχονται από κύρια ρήγματα οριζόντιας μετατόπισης και πληθώρα μικρότερων δευτερευόντων ρηγμάτων.
Λέξεις κλειδιά: *Παλαιομαγνητισμός, περιστροφές τεμαχών, γεωδυναμική, Αιγαίο.*

1. Introduction

The Aegean Sea and surrounding regions are a natural laboratory for the study of continental crust deformation. From the late Middle Miocene to Present, the area underwent dramatic N-S to NE-SW extension and crustal thinning (Mercier *et al.* 1979, Le Pichon and Angelier 1979, Papazachos and Kiratzi 1996). This was coeval with the westward displacement and bulk counterclockwise (CCW) rotation of the Anatolian-Aegean plate, which was accommodated by roll-back of the Hellenic subduction zone (McKenzie 1978, Jolivet *et al.* 1996). The active displacement data derived from focal mechanism solutions (Taymaz *et al.* 1991, Papazachos *et al.* 2000) and GPS or SLR positioning analyses (Le Pichon *et al.* 1995, McClusky *et al.* 2000) show that deformation of the Aegean continental crust strongly differs north and south of the North-Aegean Trough (NAT, Fig. 1). The NAT fault zone forms the boundary between these crustal domains and is a seismically active, ~ 30 km-wide, transtensional dextral fault zone along the western continuation of the North-Anatolian (NAF) fault system (Pavlides *et al.* 1990, Taymaz *et al.* 1991, Roussos and Lyssimachou 1991, Hatzfeld 1999, Laigle *et al.* 2000, McNeill *et al.* 2004).

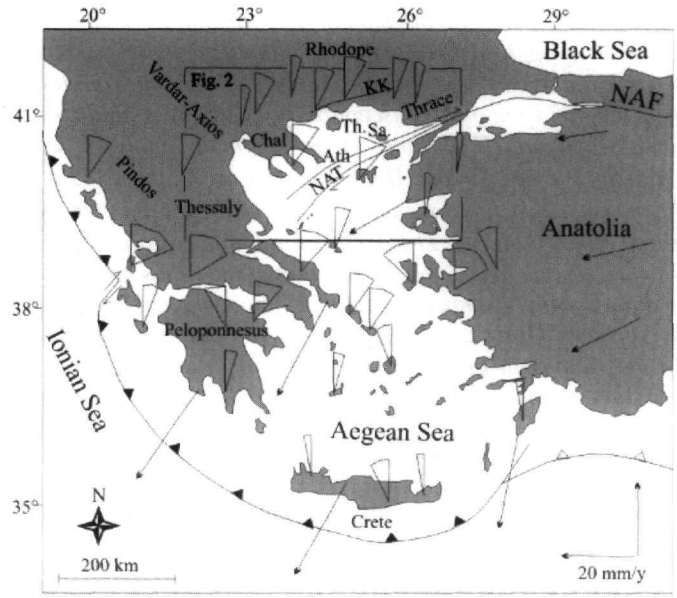

Figure 1 - Location map (framed: Fig 2) showing the regional plate boundaries and geodetic displacements (arrows) after McClusky *et al.* (2000). Pie figures represent previously published palaeomagnetic rotations. Bold line with teeth: thrust faults related to the Aegean subduction. NAF: North-Anatolian fault; NAT: North-Aegean Trough; KK: Kavala-Xanthi-Komotini fault. Ath: Athos peninsula; Chal: Chalkidiki; Sa: Samothraki island; Th: Thasos island

During the last two decades, a large set of palaeomagnetic data (Kissel and Laj 1988, Kondopoulou 2000 and references therein; van Hinsbergen 2005), has been obtained from Cenozoic formations from all over the Aegean area with the aim of constraining the style and timing of crustal deformation. In the last 4 years additional palaeomagnetic data have been obtained in the northern, western and southern Aegean, summarized in van Hinsbergen *et al.* (2005). Palaeomagnetic measurements reveal dominant CW rotations north of the NAT fault zone (Vardar-Axios basin, Chalkidiki peninsula, Rhodope massif) with an apparent systematic increase in magnitude from almost 0° (no rotation) in Thrace to 20°-30° in the Vardar Zone, together with a northward decrease of the rotation angle (Atzemoglou *et al.* 1994 and references therein). However, the timing of the observed rotations and their tectonic interpretation still remain controversial there, as palaeomagnetic data north of the NAT fault zone were mostly deduced from Eocene-Oligocene formations, and only rarely from Miocene-Pliocene ones.

The present contribution aims to constrain the age and mechanism of tectonic rotations in Northern Greece through the palaeomagnetic study of two post-orogenic plutons, the Athos (Grigoriou) and Samothraki granites (Fig. 1), and of the volcanic-sedimentary formations intruded by the latter granite. The particular interest of these study areas is twofold: i) the plutons are of different age, dated as Eocene and Miocene, respectively; and ii) they are located at different distances to the north of the NAT, with the Samothraki granite on the very edge of the easternmost and narrower part of the Aegean trough. Our results suggest a link between block rotation and strike-slip faulting during late Neogene time.

2. Geological setting

The North Hellenic orogen mainly formed at the expense of the Variscan and of Jurassic oceanic crust which is preserved in scattered ophiolitic massifs (Fig. 2). These crustal elements were involved in a protracted Alpine orogeny and the northeastward subduction of the Rhodopian domain under the Eurasian margin during the Late Cretaceous-Eocene (Burg *et al.* 1990, 1996, Michard *et al.* 1994, 1998, Ricou *et al.* 1998, Kilias *et al.* 1999). From the Middle-Late Eocene to the Middle Miocene, the North Hellenic orogen underwent strong post-orogenic extension with coeval emplacement of granodioritic plutons, deposition of clastic sediments and calc-alkaline volcanism in half-graben basins (Maltezou and Brooks 1989, Jones *et al.* 1992, Yanev and Bardintzeff 1997, Harkovska *et al.* 1998, Soldatos *et al.* 2001). Late Miocene-Pliocene to Pleistocene extension eventually occurred in brittle conditions and resulted in graben and half-graben subsidence controlled by NW-SE and E-W trending normal faults (Pavlides and Kilias 1987, Martin and Mascle 1989, Voidomatis *et al.* 1990, Roussos and Lyssimachou 1991). The normal fault array seems broadly controlled by the NAT strike-slip fault zone which progressively changes westward into an extensional horsetail system (Fig. 2).

The ***Athos (Grigoriou)*** granodiorite is a subcircular pluton (Fig. 3a) which intrudes the Serbo-Macedonian unit, i.e. the upper plate of the Rhodope Core Complex. The Athos pluton belongs to a group of calc-alkaline intrusions of southern Chalkidiki, emplaced either within the Serbo-Macedonian unit or the adjoining, lower grade "Circum-Rhodope" units (Sithonia). Prior to the present study, Eocene ages had already been obtained from three out of the five south Chalkidiki granodioritic intrusions: 40-50 Ma at Sithonia (Kondopoulou and Lauer 1984, Vergely 1984, De Wet *et al.* 1989, Christofides *et al.* 1990), 53 Ma at Ierissos (Frei 1996), 44-47 Ma at Ouranopolis (De Wet *et al.* 1989). As shown at Sithonia (Sakellariou 1993, Tranos *et al.* 1993), the emplacement of the south Chalkidiki plutons accompanied the latest stages of ductile deformation of the country rocks, when they were already exhumed at upper crustal levels. The foliation pattern in both the granodiorite and the dioritic screens of the Athos apex (Fig. 3a) suggests syntectonic emplacement, coeval with a normal-dextral throw of the fault which separates the intrusion from the overlying Mount Athos greenschist and marble unit.

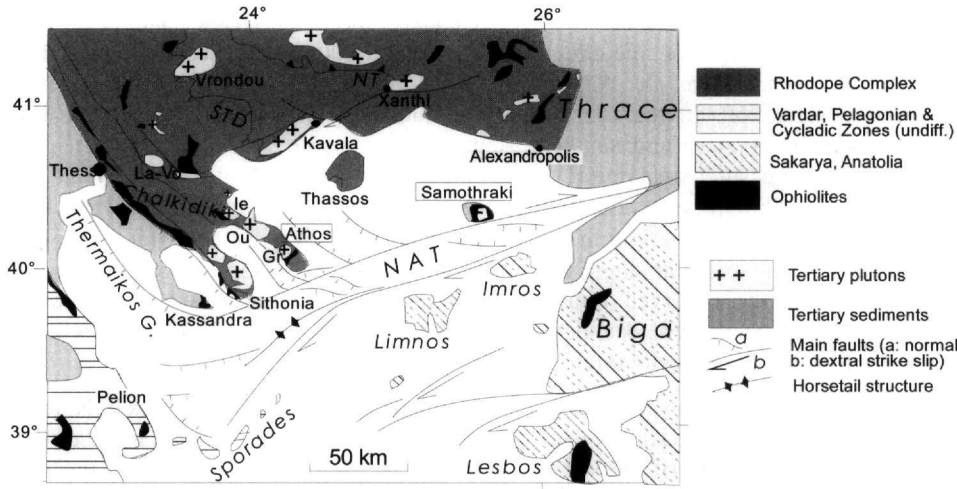

Figure 2 - Structural setting of the Athos and Samothraki study areas. NAT strike-slip and normal fault network after Pavlides *et al.* (1990), Voidomatis *et al.* (1990), Taymaz *et al.* (1991), Roussos and Lyssimachou (1991), Papazachos *et al.* (1999), Laigle *et al.* (2000), McNeill *et al.* (2004). Horsetail structure south of Sithonia after Martin and Mascle (1989). Gr: Grigoriou; Ie: Ierissos; La-Vo: Langada-Volvi graben; NT: Nestos thrust; Ou: Ouranopolis; STD: Strymon-Thassos detachment; Thess: Thessaloniki

Samothraki Island is located in the north-eastern Aegean (Fig.2) and geotectonically belongs to the Circum-Rhodope Belt (Kauffmann *et al.* 1976). From bottom to top, the island consists of, i) a low-grade meta-ophiolitic complex intruded by a calc-alkaline granite; ii) tilted volcano-sedimentary formations of Late Eocene-Early Miocene age; iii) almost horizontal Upper Miocene-Pliocene sediments (Fig. 3b; Tsikouras and Hatzipanagiotou 1998, Christofides *et al.* 2000). The *volcanics* are divided into an older and a younger volcanic rock series (Eleftheriadis *et al.* 1994). The younger volcanics (YVRS; sampled here) consist of latites, trachytes and high-K dacites dated at 22.3-18.9 Ma (K-Ar in biotite and whole rock; Eleftheriadis *et al.* 1994). Their chemical characteristics show that they represent a calc-alkaline volcanic rock series (Eleftheriadis *et al.* 1993). The *Samothraki pluton* emplaced at shallow depth, about 4-5 km according to the Al-in-hornblende barometer, contemporaneously with the youngest overlying volcanics, both being dated at 18.5±0.2 to 18.1±0.2 Ma (Rb-Sr in biotite and whole rock, Christofides *et al.* 2000). The Eocene-Early Miocene formations dip NW and SE in the western and eastern parts of the island, respectively. Their basal contact is no longer an unconformity, but has been reworked by detachment faults which place the granite close to the coeval volcanics (Fig. 3b). Hence, the granite was emplaced and exhumed in extensional conditions (ENE-trending direction of extension), like the coeval Kavala (Symvolon) granite beneath the Strymon Valley detachment (Sokoutis *et al.* 1993, Dinter and Royden 1993, Lips *et al.* 2000). The western part of Samothraki Island shows outcrops of gently folded Upper Miocene-Pliocene sediments. They are separated from the uplifted part of the island by a west-dipping normal fault, related to the recent, North Aegean extensional tectonics.

3. Sampling and laboratory measurements

In the Athos peninsula, 12 sites have been sampled in the Grigoriou batholith (Fig. 3a). Sampling was carried out by core drilling and orientation with standard compass techniques in nine out of the 12 studied sites, whereas 8-10 oriented hand samples, later cored in the laboratory, were taken from sites GR, GS and GT. As each of the neighbouring GR and GS sites yielded an insufficient number of samples, they were grouped together into a GRS site. Therefore we finally have 11 sites

in Athos. By contrast, most of the 13 Samothraki sites (Fig. 3b) were sampled as oriented hand samples. The Athos samples come from a limited range of lithologies (porphyroid granite, granodiorite, dioritic enclaves) within the Grigoriou batholith (Table 1). The Samothraki sites are more varied and include 5 sites in granodiorite (GPA, GPK, GPL, GSA, GSB), 7 sites in the coeval acidic lavas (AUN, AP, ALO-ALN, HO: lower level, HR: upper level, TRL, VRE), and one site (TK) in the Eocene sediments faulted above the plutonic body (Table 2).

A total of 162 standard specimens from the Athos area were measured for both palaeomagnetic analysis and anisotropy of magnetic susceptibility, whereas 109 specimens from Samothraki were measured for palaeomagnetic analyses. Natural remanent magnetizations (NRM) were measured with AGICO JR5 and MOLSPIN spinner magnetometers. Predominantly thermal and in several cases also alternating field (AF) demagnetizations were performed. Directions were analysed on orthogonal plots and selected with a least-square routine (Kirschvink 1980). The variation of magnetic susceptibility with temperature was monitored with a KLY-3 Kappabridge and a Bartington MS2B Meter. Acquisition of isothermal remanent magnetization (IRM) curves were obtained using a ASC pulse magnetizer. Finally, anisotropy of low-field magnetic susceptibility measurements (AMS) were performed with the KLY-3 Kappabridge apparatus. All measurements were carried out in the Palaeomagnetic laboratories of the Ecole Normale Superieure (Paris) and the Aristotle University of Thessaloniki.

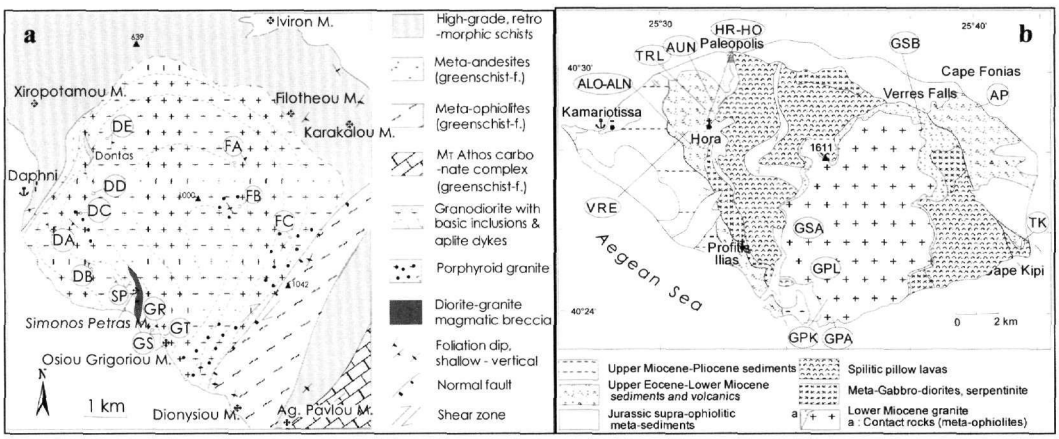

Figure 3 - a)Location of the sites sampled in the Grigoriou pluton of Athos peninsula; geological map modified after Kockel and Mollat (1977), b)Location of the sites sampled in the Samothraki granite and juxtaposed metasediments and lavas; geological map after Tsikouras and Hatzipanagiotou (1998)

4. Results

4.1. Athos peninsula

The nature of the main magnetic carriers varies with lithology at these sites. In the more acidic lithologies, sampled in the Filotheou area (sites FA, FB, FC), the magnetic carriers mainly consist of magnetite, with a smaller amount of haematite, according to the observed thermomagnetic and IRM curves (Fig. 4). By contrast, in the granodioritic parts of the Grigoriou pluton, the main magnetic mineral is likely to be maghemite, with an unquantified amount of pyrrhotite (indicated by unsuccessful AF cleaning of these samples and a drastic drop of magnetic remanence about 350-400 °C: Fig. 5). Two out of 11 sites (DE and SP, not reported here) were rejected after complete demagnetization, due to the absence of stable components of magnetization. The remaining 9 sites yielded stable and reasonably well-grouped palaeomagnetic components (Table 1). Some of the selected sites display a very low temperature (< 200 °C) overprint. At higher temperatures, samples from different lithologies show different behaviour during demagnetization

as follows. The Filotheou "acidic" sites exhibit an intermediate temperature (200-450 °C) unblocking component with a SW declination and a reverse inclination, sometimes followed by NE-directed normal component at 550-580 °C, likely carried by magnetite. The remaining granodioritic sites show a low temperature (150-250 °C) NE-directed normal component, again followed by an intermediate temperature (300-450 °C) SW-directed reverse component (Fig. 5).

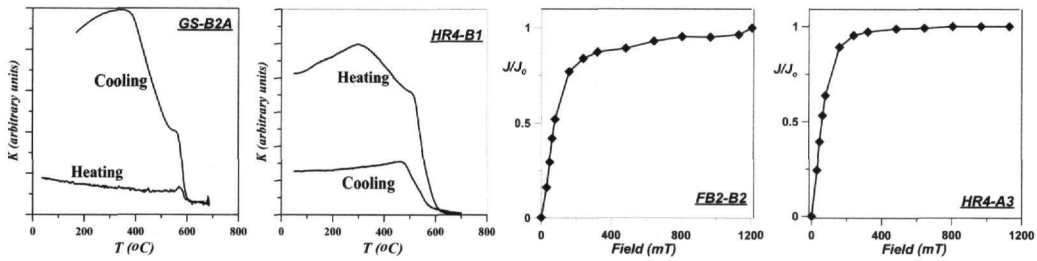

Figure 4 - Representative thermomagnetic curves (left) showing the variation of magnetic susceptibility (k) with temperature and IRM acquisition plots (right) from representative samples from Athos and Samothraki

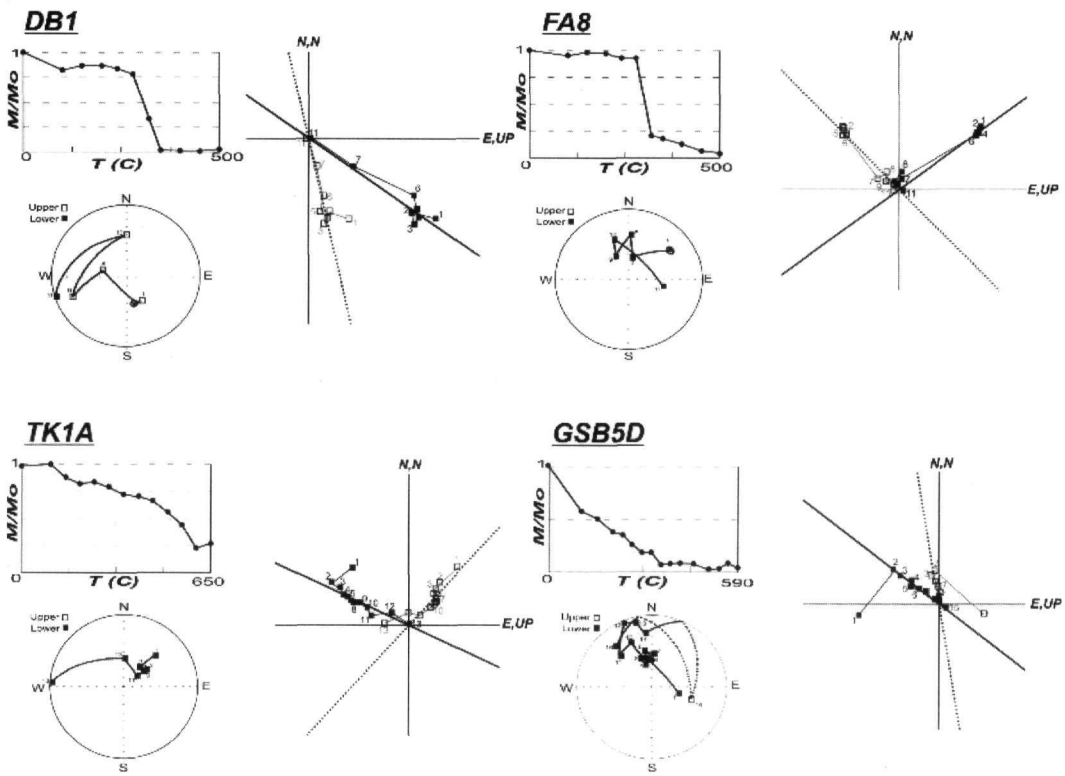

Figure 5 - Representative demagnetization decay curves, lower-hemisphere stereographic projections and orthogonal demagnetisation plots in geographic coordinates, from the Athos granite (DB1 and FA8) and the Samothraki CW (TK1A) and CCW (GPA5) sites

Table 1 - Mean directions of high- and mid-temperature components from the Athos sites. (N/N1=samples used/total, ΔD=confidence limit on the declination, α_{95}=semi-angle of cone of confidence, K=precision parameter)

Site	Rock type	Age	N/N1	Dec ± ΔD	Inc	α_{95}	K
DA	Granodiorite	L. Eocene	11/16	168.5 ± 8.8	-63.6	3.9	135
DB	Granodiorite	L. Eocene	10/10	189.6 ± 17.9	-56.3	9.8	25
DC	Porphyroid granite	L. Eocene	14/17	202.2 ± 22.6	-59.4	11.3	13
DD	Diorite/granite	L. Eocene	5/14	206.5 ± 19.2	-64.0	8.3	85
FA	Granodiorite	L. Eocene	10/12	052.9 ± 9.1	27.0	8.1	36
FB	Porphyroid granite	L. Eocene	7/11	194.1 ± 43.8	-65.0	17.0	14
FC	Leucocratic granite	L. Eocene	10/20	209.4 ± 13.4	-08.2	13.3	14
GRS (GR+GS)	Granodiorite	L. Eocene	10/14	209.4 ± 9.2	-49.2	6.0	59
GT	Granodiorite	L. Eocene	10/14	198.1 ± 25.7	-54.7	14.5	12
Mean (FC excluded - low Inc)			*8/11*	*203.6 ± 21.1*	*-56.4*	*11.5*	*24*

Table 2 - Mean directions of high-temperature components from the Samothraki sites. (N/N1=samples used/total, ΔD=confidence limit on the declination – n.a.=not available, α_{95}=semi-angle of cone of confidence, K=precision parameter)

Site	Rock type	Age	N/N1	Dec ± ΔD	Inc	α_{95}	K
AUN	Lava	L. Miocene	7/7	223.9 ± 23.2	-43.5	16.6	14
GPK	Granite	L. Miocene	9/10	216.3 ± 37.2	-62.0	16.5	11
GSA	Granite	L. Miocene	8/10	230.7 ± 18.1	-45.5	12.6	20
TK	Sediment	U. Eocene	9/10	041.6 ± 13.0	49.6	8.4	39
VRE	Pyroclastic	Eocene	9/11	221.0 ± 7.8	-17.8	7.4	49
HOR (HO+HR)	Lava	L.Miocene	5/9 CW	217.7 ± 19.4	-42.1	14.3	42
			4/9CCW	316.3 ± 56.8	66.0	19.9	22
GPL	Granite	L. Miocene	7/8	212.4 ± 25.3	-16.5	24.2	7
AP	Volcanic	L. Miocene	6/6	323.9 ± 23.7	51.8	14.4	23
GSB	Granite	L. Miocene	5/8	337.3 ± 24.0	43.7	17.1	21
ALO-ALN	Lava	L. Miocene	4/7	157.1 ± n.a.	-79.3	21.9	19
TRL	Lava	L. Miocene	12/13	037.3 ± 12.9	-32.8	10.8	17
GPA	Microgranite	L. Miocene	7/10	224.0 ± 19.1	29.0	16.6	14
Mean (AUN, GPK, GSA, TK, HOR, VRE)			*6/12*	*222.1* ± 17.2	*-43.6*	*12.4*	*30*
Mean (HOR-CCW, AP, GSB, ALO-ALN)			*4/12*	*328.6* ± 41.4	*60.5*	*19.0*	*24*

4.2. Samothraki Island

The main magnetic mineral in both the granitic and dacitic lithologies is mostly magnetite, as the remanence shows a low coercitivity and is completely destroyed at 580 °C (Fig. 5). In the reddish sandstone at site TK, the magnetic carrier consists of fine-grained haematite, as suggested by the demagnetization curve and a lack of success of AF demagnetizations. Thermomagnetic analyses and IRM measurements of volcanics and granites show a clear predominance of magnetite but with small amounts of haematite in some cases (Fig. 4). The granite and lava samples generally show a low temperature (LT) component with normal polarity unblocked at T<300 °C, and a high temperature (HT) component with reverse polarity unblocked between 380-580 °C. The HT component is consistently oriented towards the SSW direction, despite some scattering in both declination and inclination. In contrast, the sandstone samples show a good clustering of a NE-directed normal component, defined between 100-550 °C, with a roughly antiparallel HT

component which only appears above 650 °C. The direction of this HT component cannot be precisely derived, due to its weak intensity. Despite the almost systematic trend of HT components towards a NE-SW direction, a more detailed analysis is needed.A. The three granitic sites (GPK, GPL and GSA), two lava sites (AUN, HOR), the pyroclastic site (VRE) and the sedimentary site (TK) yielded stable high temperature (HT) directions (Table 2), which converge towards the expected direction for the area and for this time-span (Miocene). The mean magnetization for these sites is 222.1/-43.6 (α_{95} = 12.4, K = 30).B. Another group of directions is seen at sites AP and ALN with westward declinations and antipodal polarities, but with a very high inclination and a big scatter for site ALN. Site AP is located in strongly faulted and weathered lavas and yielded components oriented westwards. The same westward declination is seen in five out of eight samples from site GSB, located at the very border of the granitic stock (at about 5 m from the hornfels aureole). We should note that the remaining three samples at this site fit to the directions of the first group. A similar case is represented by sites HO-HR where two main tendencies can be identified; one fitting the first, expected for the area, direction and a second strongly deviated westwards with scattered inclinations.C. Finally, we draw the attention to a peculiar grouping obtained both in volcanics and granites (sites TRL and GPA) with eastward declinations but negative inclinations. Any error of sampling is excluded as these directions have been obtained also by other groups in more than three sites (Beck *et al.* personal communication) and were also reported in volcanics from Lemnos Island (Westphal and Kondopoulou 1993). A specific series of measurements, including paleointensities, is under progress in order to investigate this strange behaviour.

4.3. Inferred age of magnetization

In the framework of the present study, we measured a K/Ar biotite age on a sample from the Grigoriou pluton. The Athos granitoid pluton crossed the 300 °C isotherm around 43 Ma (Table 3). Taking into account that the characteristic component of magnetization is carried by magnetite, we assume an equivalent *Eocene age* for the acquisition of remanence in our samples from Athos, provided that the pluton did not stay long at temperatures above 300 °C.

Table 3 - K/Ar dating of the Grigoriou granite, Athos peninsula (R. Montigny, Laboratoire de Geochimie, EOST Strasbourg)

Sample number and location	Rock type	Mineral	K_2O (wt%)	^{40}Ar rad (10^{-11} mol/g)	$\frac{100\times {}^{40}Ar\ rad}{{}^{40}Ar}$	Calculated age Ma (± 2σ)
G93 168b Grigoriou	granodiorite	biotite	8.90	56.22	91	43.3 ± 1.0
$\lambda_\varepsilon = 0.581 \times 10^{-10}\ a^{-1}$; $\lambda_\beta = 4{,}962 \times 10^{-10}\ a^{-1}$; $^{40}K/K$ total $= 1.167 \times 10^{-4}$ mol/mol						

The Samothraki samples are more varied. Three out of the five sites taken from the granitic intrusion were dated at 19.8 Ma (Christofides *et al.* 2000). Site AUN was sampled in the upper volcanics, coeval with the underlying granite (Christofides *et al.* 2000). In both cases, the magnetic carrier is magnetite, and the magnetization is likely to have an Early Miocene age. The latitic samples from site TRL gave an age of 18.9 ± 0.5 Ma (Eleftheriadis *et al.* 1994). The main magnetic carriers are both magnetite and heamatite, but the origin of this magnetization is not fully understood as it is directed eastward and up. An age of 22.3 ± 0.8 Ma is assigned to the dacitic site of Alonia (Eleftheriadis *et al.* 1994). Its magnetization is carried by magnetite and is directed westward and diverges from the general trend of the other sites. In contrast, the sediments of the site TK are dated as Late Eocene and their main magnetic carrier is haematite. In this case, the magnetization can be either diagenetic and primary, or related to a complete remagnetization due to the granite emplacement at shallow depth. We consider the second hypothesis as more likely (see next sub-section), and retain an Early Miocene age of magnetization.

It can be deduced from the above considerations that the age of magnetization for most volcanic and granitic sites in Samothraki is *Miocene*.

5. AMS measurements

AMS measurements yield the magnitudes of the three principal and mutually orthogonal axes of the AMS ellipsoid ($K_1 \geq K_2 \geq K_3$), as well as their declinations and inclinations with respect to the geographical reference frame. The mean magnetic susceptibility is given by $K_m = (K_1 + K_2 + K_3)/3$. The corrected anisotropy degree $P' = \exp\sqrt{2\left[\left(\ln\frac{K_1}{K_m}\right)^2 + \left(\ln\frac{K_2}{K_m}\right)^2 + \left(\ln\frac{K_3}{K_m}\right)^2\right]}$, and the shape parameter of Jelinek (1981) $T = (lnF - lnL)/(lnF+lnL)$, where $F = K_2/K_3$ and $L = K_1/K_2$, were also calculated. The mean AMS data are presented in Table 4.

Table 4 - Mean AMS measurements for various locations from Athos and Samothraki

Location	Rock Type	Km ($\times 10^{-6}$SI)	P'	T	K_1 (Dec/Inc)	K_2 (Dec/Inc)	K_3 (Dec/Inc)
Athos (West	Granite	271	1.089	-0.184	171/02	242/79	076/10
Athos (East)	Granite	229	1.092	0.237	029/10	263/35	137/01
Athos (South)	Granodiorite	345	1.045	0.117	169/05	065/77	266/12
Samothraki	Lavas	14842	1.043	0.246	016/05	272/31	096/68
Samothraki	Granite	8758	1.109	0.446	081/02	353/12	148/49

In the paramagnetic granitoid of Athos the magnetic susceptibility is quite low, with a mean of 263 μSI. The anisotropy degree shows a high variation from 1.010 to 1.542, with a mean of 1.080 (8 %). The majority of the samples lie in the 1.010-1.200 interval. The magnetic fabric is generally well-defined; the K_1 axes, defining the magnetic lineation are almost horizontal with a mean direction of 356/01, while the magnetic foliation plane is nearly vertical (004/74 E). On the contrary, in Samothraki rocks the magnetic susceptibility is very high, with a mean value of 11800 μSI, indicating the presence of magnetite, which has also been confirmed by other laboratory tests. The anisotropy degree is quite low for the Samothraki volcanics (4 %) while it reaches medium levels within the granitoids (11 %). The magnetic fabric shows a clear trend of the K_1 axes, which in all but one site are almost horizontal. The magnetic foliation, contrary to that of Athos rocks, is steep, ranging from 50-70°.

The magnetic anisotropy in minerals can deviate from the ambient field the direction of thermo- or chemical- remanent magnetization acquired by minerals. This deviation is expected to be negligible for small anisotropy degrees, but can be substantial for larger anisotropies. This problem has been treated at length by Stacey (1960), Uyeda *et al.* (1963), Hrouda (1982), and Stephenson *et al.* (1986). Given that the anisotropy degrees of the present study are relatively low (means of 8% and 4% for Athos and Samothraki respectively) the possible deflections of the palaeomagnetic vectors due to the anisotropy effect can be assumed to be negligible, enhancing thus the reliability of the calculated rotations.

6. Discussion and Conclusions

6.1. Tectonic corrections

Palaeomagnetic directions show rather scattered inclination values, either at the site level (especially in Samothraki; Table 2), or at the regional scale of the massif (Athos; Table 1, Fig. 6). In the latter case, NW-trending normal faults have been observed along the SW and NE sides of the peninsula (Pavlides and Caputo 1994). Such faults may have split the peninsula into tilted fault blocks, and therefore may have caused the shallowing or steepening of inclinations in the NE or

SW blocks, respectively. This working hypothesis was not checked in the field, due to extensive forest cover and poor outcrops, and no angular values could be measured for untilting.

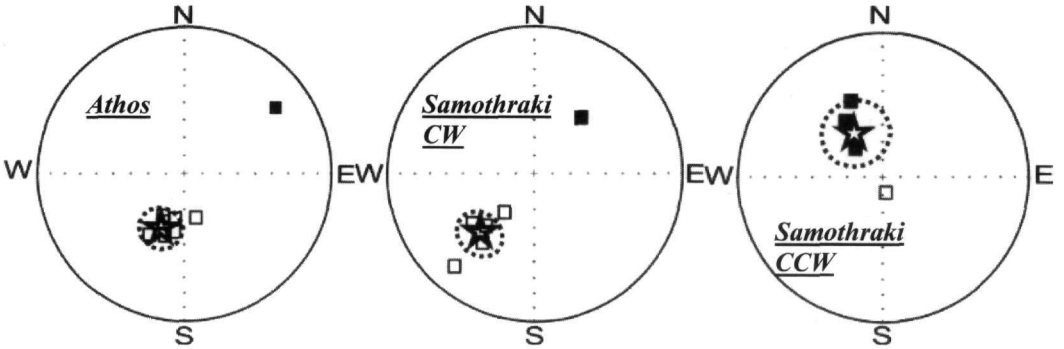

Figure 6 - Site mean directions in geographic coordinates for Athos and Samothraki. Open symbols represent negative inclinations, filled symbols indicate positive inclinations. The star indicates the calculated mean direction; a95 is shown around mean

In Samothraki, the in situ directions show a better cluster after transferring the TK mean direction into the upper hemisphere (Fig. 6). The granitic pluton does not appear to be affected by faulting (except at its very SW border, outside of the sampling area; Fig. 3b). In the sedimentary (TK) and volcanic (AUN, TRLO) sites, indications of the palaeohorizontal are available, with respective strike and dip values N180, 40E, N60, 50NW, and N190, 70. Application of these tectonic corrections results in poorly significant stratigraphic directions (AUN: dec. = 270°, inc. = 37° ;TK: dec. = 341°, incl. = 59°) and scatter increases. In the case of site TK, magnetic mineralogy (haematite) and structural setting suggest a complete remagnetization during Lower Miocene granite emplacement and likely coeval tilting of the Late Eocene rocks.We note here that $TK_{corrected}$ is partly supported by directional group B,but the resolution is very poor in order to conclude about a widely spread remagnetization. At site AUN, the dome-shaped acidic extrusives emplaced on the western slope of the Oligocene-Miocene volcanic centre were affected by further tilting related to the emplacement of the granitic body at shallow depth, likely before complete cooling. This particular setting would explain the lack of significance of the tectonic correction. Accordingly, all results are presented *in situ* (Tables 1, 2).

6.2. Rotation age and mechanisms

The observed declinations indicate clockwise rotations of the Athos and Samothraki blocks around vertical axes. The rotation angle is calculated (Butler 1992) by subtraction of the expected declination given by the reference poles of Westphal *et al.* (1986) and Besse and Courtillot (2002) for the Eocene (7.0°) and Early Miocene (5.8°), respectively. The resulting rotation angles are 16.6°±17.2° for the Athos (Grigoriou) area and 36.3°±14.0° for Samothraki island. The age of rotation is constrained to be <18 Ma at Samothraki, whereas the smaller rotation of the Athos block can only be dated as younger than Eocene. In the same way the corresponding inclination flattenings were calculated: -3.6°±9.6° for Athos and 12.2°±10.2° for Samothraki.

Previous research aiming to establish a chronology of rotations in Northern Greece was hampered by the lack of magnetizations of different ages in a single block, except in the Vrondou block of Central Rhodope, which includes Early Oligocene and Early Miocene intrusions. In that case, Dimitriadis *et al.* (1998) inferred the occurrence of a minor Oligocene CW rotation (8°) followed by additional CW rotation (13°) after the Early Miocene. In the broader area surrounding the Athos peninsula and Samothraki a number of published palaeomagnetic results allow the establishment of a general pattern for the occurrence of rotations after the Eocene (Table 5). For the Symvolo area published data by Atzemoglou (1997), Zananiri (2004) and van Hinsbergen (2005) show moderate angles of CW rotation. For Chalkidiki, including Sithonia (Kondopoulou

and Westphal 1986) and Kassandra (Haubold *et al.* 1997), the rotation angles do not vary significantly between the Eocene (29°-33°) and the Miocene sites (20°-30°). Rotation angles varying between 15°-30° CW have been also measured in Upper Pliocene sediments of Chalkidiki (two sites, one of which is located at the beginning of Athos peninsula; Westphal *et al.* 1991). Therefore, all the rotation angles measured in Athos and Samothraki follow this regional trend of recent (Neogene) rotations, despite their scattered values. The rotation angle for Athos (16.6°) is one of the smallest measured in the area (but converges with the ones in Symvolo), whereas the Samothraki rotation (36.3°) is the largest measured in Miocene formations. Post-Eocene anticlockwise rotation was not observed in the vicinity of the study area.The few and ill-defined CCW directions in four Samothraki sites do not constitute a solid set for valid interpretations. Hence, the weak Athos block rotation points to a contrasting behaviour during the Neogene, not only with Samothraki but with most other studied formations in the surrounding area (except the broader Symvolo region).

Table 5 - Published rotation angles from the vicinity of the North Aegean Trough

Area	Formation	Age	D/I (°)	α^{95}	Rot	Reference
Riza	Sediments	Up. Pliocene	195/-45	8	15°	Westphal et al. 1991
Ierissos	Sediments	Up. Pliocene	212/-17	38	32°	Westphal et al. 1991
Kassandra	Sediments	Miocene	025/54	5	19.5°	Haubold et al. 1997
Lemnos	Volcanics	Miocene	034/48	15	28.5°	Westphal and Kondopoulou 1993
Ouranoupolis	Granite	Oligocene	219/ -24to-58	9	32.8°	Kondopoulou and Westphal 1986
Sithonia	Granite	Oligocene-Eocene	037/31	9	30.8°	Kondopoulou and Westphal 1986
Kassandra	Sediments	Jurassic (post-depositional magnetization, Eocene?)	043/43.6	8.3	36.0°	Feinberg et al. 1994
D_{exp} : Miocene=5.5°, Oligocene=6.2°, Eocene=7.0° (Calculated using the Europe Apparent Polar Wander Path; Besse and Courtillot 2002)						

The difference between the measured Neogene rotations at Athos and Samothraki could be related to the different location of these blocks with respect to the North Aegean Trough (NAT). Samothraki island stands directly on the northern edge of the NAT, close to the Saros basin (Figs 2 and 3). In contrast, the Athos (Grigoriou) block is c. 25 km from the western part of the NAT, i.e. the area where the dextral movement is increasingly distributed. Fault mechanics suggest that before the onset of a concentrated displacement regime along the NAF-NAT fault system a wide dextral shear zone should have accommodated the incipient Anatolia-Europe relative movement, starting at c. 13 Ma (Le Pichon *et al.* 2003). We assume that this early shear zone included the future Samothraki island and caused its large rotation as early as the Late Miocene. The Athos peninsula suffered less rotation at that time since it was more distant from the NAT shear zone, and was already located in the extremity of the extensional horsetail. This scenario seems plausible but one cannot disregard that the Sithonia and Ouranoupolis plutons, which are synchronous in age and with equal distance from the NAT display a rotation angle twice as large as the Athos one, i.e. 30° vs 17°, respectively. The ca. 15 of differential rotation between these peninsulas is likely to originate from the conjugate movements between the Athos and Sithonia fault zones and the southwestward increase of horizontal slip along these faults (Koukouvelas and Aydin 2002). This increase could result in the opening of Sigitikos basin with a small scissor component.An additional evidence for such a pattern is given in Papanikolaou *et al.* (2006).Based on detailed analysis of air gun lithoseismic profiles,the existence of a separate Athos block is clearly shown in

their fig.4,and a gradual increase of opening and deepening of the neighboring basin supports our scenario as exposed in the previous paragraph.

6.3. Regional implications

Geodetic determination of horizontal velocities in a Eurasia-fixed reference frame indicates coherent motion of 30 mm/yr towards the SW in central and southern Aegean, *versus* inhomogeneous motions of 5 to 10 mm/yr towards the S or SW in the coastal area of northern Greece (Chalkidiki, south Rhodope) and adjoining islands (Thassos, Samothraki) (McClusky *et al.* 2000). These domains are separated by the NAF-NAT (Fig. 1).

The tectonic interpretation of the palaeomagnetically observed rotations from Northern Greece, and of their relationship with those observed in central Aegean (south of the NAT active boundary) is still an open issue. Kondopoulou *et al.* (1996) suggested that the area was tectonically similar to the present-day south Aegean subduction zone as early as the Early Tertiary. Based on the trend of ductile stretching lineations in the Aegean basement rocks, as well as on the palaeodeclination pattern, Walcott and White (1998) suggest that Northern Greece, central Aegean, mainland Greece and Peloponnesus altogether belong to a "Central Aegean Block" which sequentially formed at the expense of an Oligo-Miocene, E-W trending orogen, and rotated from ~25 Ma onward. Dimitriadis *et al.* (1998) also claim that parts of the Rhodope massif underwent minor CW rotations during the Late Oligocene, whereas additional CW rotations occurred after the Early Miocene. They propose that at least the post-Early Miocene rotations in Northern Greece were the result of plate tectonic motion in the Aegean, and of brittle crustal detachment, translation and rotation on top of a stretched ductile lithosphere. In contrast, Goldsworthy *et al.* (2002) argue that the rotations observed from Chalkidiki to the central Aegean and mainland Greece could be explained by a model of distributed strike-slip faulting in western Anatolia-Central Aegean, ending in a normal fault system in central-western Greece, i.e. a modified version of the Taymaz *et al.* (1991) "broken slats" model.

Comparing the new palaeomagnetic data to the published dataset for Northern Greece (Kondopoulou 2000), we suggest that the palaeomagnetic rotations in Northern Greece are dominantly related to post-Early Miocene block rotations, and are controlled by major strike-slip faults and distributed "small" or minor faults as suggested by Duermeijer *et al.* (1998) and consistent with a generic theoretical model for rotations proposed by Peacock *et al.* (1998).

During the rotation phase of the western Aegean domain, extension in the Aegean was accommodated among others by extensional detachments of the Cyclades and the Rhodope (Altherr *et al.* 1982, Hejl *et al.* 2002, Lips *et al.* 2000). Therefore, at least part of the rotation difference between Sithonia and Athos, as well as Samothraki and Athos could be explained by the activity of these detachments.

The present palaeomagnetic dataset, combined to the one of surrounding areas and the compiled regional kinematic information, constitutes an important step towards distinguishing local rotations from the regional ones. Furthermore, the limits of smaller blocks are better constrained through the study of the here referred rotations which show interactions between local and regional deformation.

7. Acknowledgments

The present study was accomplished in the framework of a bilateral agreement between France and Greece (PLATON). Sampling in Athos has been possible thanks to the friendly support of the Holy Monasteries of Simonos Petra and Philotheou. Professors G. Christofides and G. Eleftheriadis provided useful information about the complicated Samothraki petrology. Dr. M. Vlachou kindly provided unpublished data on radiometric dating. Dr. A. Morris is thanked for useful comments, suggestions and improvement of English language.. The manuscript greatly

benefited from reviews by Prof.. M. Mattei and an anonymous reviewer. This paper is a Geophysical Laboratory of the Aristotle University of Thessaloniki contribution number 687/2007.

8. References

Altherr, R., et al., 1982. A late Oligocene/Early Miocene high temperature belt in the Attica Cycladic crystalline complex (SE Pelagonian, Greece), *Geol. Jahrb., Reihe E. Geophys.*, 23, 97-164.

Atzemoglou, A., 1997. Palaeomagnetic results from Northern Greece and their contribution to the interpretation of the geodynamic evolution of the area during the Tertiary, *PhD thesis*, Aristotle University of Thessaloniki, Greece. (in Greek with English abstract)

Atzemoglou, A., Kondopoulou, D., Papamarinopoulos, S., and Dimitriadis, S., 1994. Paleomagnetic evidence for block rotations in the western Greek Rhodope, *Geophys. J. Int.*, 118, 221-230.

Besse, J., and Courtillot, V., 2002. Apparent and true polar wander and the geometry of the geomagnetic field over the last 200 Myr, *J. Geophys. Res.*, 107 (B11), 2300, doi:10.1029/2000JB000050.

Burg, J.P., Ivanov, Z., Ricou, L.E., Dimor, D., and Klain, L., 1990. Implication of shear sense criteria for the tectonic evolution of the central Rhodope massif, southern Bulgaria, *Geology,* 18, 451-454.

Burg, J.P., Ricou, L.E., Ivanov, Z., Godfriaux, I., Dimov, D., and Klain, L., 1996. Syn-metamorphic nappe complex in the Rhodope massif. Structure and kinematics, *Terra Nova,* 8, 6-15.

Butler, R.F., 1992. Paleomagnetism: Magnetic Domains to Geologic Terranes. Blackwell Scientific Publications, 238pp.

Christofides, G., D'Amico, C., Del Moro, A., Eleftheriadis, G., and Kyriakopoulos, C., 1990. Rb-Sr geochronology and geochemical characters of the Sithonia plutonic complex, Greece, *Eur. J. Mineral.*, 2, 79-87.

Christofides, G., Eleftheriadis, G., Esson, J., Soldatos, T., Koroneos, A., and Bröcker, M., 2000. The evolution of the Samothraki granitic pluton, N-Aegean Sea, Greece; geochronology, chemical and isotopic constraints for AFC modelling, In I. Panayides, C. Xenophontos,and J. Malpas (eds), *Proceedings of the Third International Conference on the Geology of Eastern Mediterranean,* 193-209.

De Wet, A.P., Miller, J.A., Bickle, M.J., and Chapman, H.J., 1989. Geology and geochronology of the Arnea, Sithonia and Ouranopolis intrusions, Chalkidiki Peninsula, northern Greece, *Tectonophysics,* 161, 65-79.

Dimitriadis, S., Kondopoulou, D., and Atzemoglou, A., 1998. Dextral rotations and tectonomagmatic evolution of the southern Rhodope and adjacent regions, Greece, *Tectonophysics,* 299, 159-173.

Dinter, D.A., and Royden, L., 1993. Late Cenozoic extension in north-eastern Greece, Strymon valley detachment system and Rhodope metamorphic core complex, *Geology,* 21, 45-48.

Duermeijer, C.E., Krijgsman, W., Langereis, C.G., and Ten Veen, J.H., 1998. Post-early Messinian counterclockwise rotations on Crete, implications for Late Miocene to Recent kinematics of the southern Hellenic arc, *Tectonophysics,* 298, 117-189.

Eleftheriadis, G., Esson, J., Soldatos, T., and Christofides, G., 1993. Magmatic evolution of the Tertiary volcanic rocks of the Samothraki Island (Thrace, N. Greece), In *Panagos Honorary Volume*: *Technical University Publications,* vol. A, Athens, 330-349pp.

Eleftheriadis, G., Pe-Piper, G., Christofides, G., Soldatos, T., and Esson, J., 1994. K-Ar dating of the Samothraki volcanic rocks, Thrace, North-Eastern Aegean (Greece), *Bull. Geol. Soc. Greece,* XXX/1, 205-212.

Feinberg, H., Kondopoulou, D., Michard, A., and Mountrakis, D., 1994. Paleomagnetism of some northern Greece ophiolites and associated sediments, *Bull. Geol. Soc. Greece,* XXX/1, 359-370.

Frei, R., 1996. The extent of inter-mineral isotope equilibrium, a systematic bulk U – Pb and Pb step leaching, PbSL, isotope study of individual minerals from the Tertiary granite of Ierissos, northern Greece, *Eur. J. Mineral.,* 8, 1175-1189.

Goldsworthy, M., Jackson, J., and Haines, J., 2002. The continuity of active fault systems in Greece, *Geophys. J. Int.,* 148, 596-618.

Harkovska, A., Marchev, P., Machev, Ph., and Pécskay, Z., 1998. Paleogene magmatism in the Central Rhodope area, Bulgaria – A review and new data, *Acta Vulcanologica,* 10, 199-216.

Hatzfeld, D., 1999. The present-day tectonics of the Aegean as deduced from seismicity, in Durand B, Jolivet L, Horväth F, Séranne M, eds, The Mediterranean basins, Tertiary extension within the Alpine orogen, *Geol. Soc. London spec. Publ.,* 156, 415-426.

Haubold, H., Scholger, R., Kondopoulou, D., and Mauritsch, H.J., 1997. New paleomagnetic results from the Aegean extensional province, *Geologie en Mijnbouw,* 76, 45-55.

Hejl, E., Riedl, H., and Weingartner, H., 2002. Post-plutonic unroofing and morphogenesis of the Attic-Cycladic complex (Aegea, Greece), *Tectonophysics,* 349, 37-56.

Hrouda, F., 1982. Magnetic anisotropy of rocks and its application in geology and geophysics, *Geophys. Surv.,* 5, 37-82.

Jelinek, V., 1981. Characterization of the magnetic fabric of rocks, *Tectonophysics,* 79, T63-T67.

Jolivet, L., Goffé, B., Monié, P., Truffert-Luxey, C., Patriat, M. and Bonneau, M., 1996. Miocene detachment in Crete and exhumation P-T-t paths of high-pressure metamorphic rocks, *Tectonics,* 15, 1129-1153.

Jones, C.E., Tarney, J., Baker, J.H., and Gerouki, F., 1992. Tertiary granitoids of the Rhodope, Northern Greece – Magmatism related to extensional collapse of the Hellenic orogen, *Tectonophysics,* 210, 295-314.

Kauffmann, G., Kockel, F., and Mollat, H., 1976. Notes on the stratigraphic and paleogeographic position of the Svoula formation in the innermost zone of the Hellenides (Northern Greece), *Bull. Soc. Geol. France,* 18, 225-230.

Kilias, A., Falalakis, G., and Mountrakis, D., 1999. Cretaceous-Tertiary structures and kinematics of the Serbomacedonian metamorphic rocks and their relation to the exhumation of the Hellenic hinterland, Macedonia, Greece, *Int. Journ. Earth Sci.,* 88, 513-531.

Kirschvink, J.L., 1980. The least-squares line and plane and the analysis of paleomagnetic data, *Geophys. J. Roy. Astron. Soc.,* 62, 699-718.

Kissel, C., and Laj, C., 1988. The Tertiary geodynamic evolution of the Aegean arc: a palaeomagnetic reconstruction, *Tectonophysics,* 146, 183-201.

Kondopoulou, D., 2000. Paleomagnetism in Greece, Cenozoic and Mesozoic components and their geodynamic implications, *Tectonophysics,* 326, 131-151.

Kondopoulou, D., and Lauer, J.P., 1984. Paleomagnetic data from Tertiary units of the North Aegean zone, In : Dixon, J.E., Robertson, A.H.F. (Eds). The geological evolution of the Eastern Mediterranean, *Geol. Soc. London spec. Publ.,* 17, 681-686.

Kondopoulou, D., and Westphal, M., 1986. Paleomagnetism of the Tertiary intrusives from Chalkidiki (northern Greece), *J. Geophys.,* 59, 62-66.

Kondopoulou, D., Atzemoglou, A., and Pavlides, S., 1996. Palaeomagnetism as a tool for testing geodynamic models in the North Aegean, convergences, controversies and a further hypothesis, In A. Morris and D.H. Tarling, (Eds), Palaeomagnetism and tectonics of the Mediterranean region, *Geol. Soc. London Spec. Publ.* 105, 277-288.

Koukouvelas, I.K., and Aydin, A., 2002. Fault structure and related basins of the North Aegean Sea and its surroundings, *Tectonics,* 21, 5, 1046, doi: 10.1029/2001TC901037.

Laigle, M., Hirn, A., Sachpazi, M., and Roussos, N., 2000. North Aegean crustal deformation, An active fault imaged to 10 km depth by reflection seismic data, *Geology,* 28, 71-74.

Le Pichon, X., and Angelier, J., 1979. The Hellenic arc and trench system. A key to the neotectonic evolution of the eastern Mediterranean area, *Tectonophysics,* 60, 1-42.

Le Pichon, X., Chamot-Rooke, N., Lallemant, S., Noomen, R., and Veis, G., 1995. Geodetic determination of the kinematics of central Greece with respect to Europe. Implications for eastern Mediterranean tectonics, *J. Geoph. Res.,* 100, 12,675-12,690.

Le Pichon, X., Chamot-Rooke, N., Rangin, C., and Sengor A.M.C., 2003. The North Anatolian fault in the Sea of Marmara, *J. Geoph. Res.,* 108, B4, art. no. 2179.

Lips, A.L.W., Stanley, H.W., and Wijbrans, J.R., 2000. Middle-Late Alpine thermotectonic evolution of the southern Rhodope Massif, Greece, *Geodinamica Acta,* 13, 281-292.

Maltezou, F., and Brooks, M., 1989. A geophysical investigation of post-Alpine granites and Tertiary sedimentary basins in northern Greece, *J. Geol. Soc. London,* 146, 53-59.

Martin, L., and Mascle, J., 1989. Structure et évolution récente de la mer Egée, le domaine nord-égéen, *C. R. Acad. Sci.,* 309, 1039-1045.

McClusky, S., Balassanian, S., Barka, A., et al., 28 authors, 2000. Global Positioning System constraints on plate kinematics and dynamics in the eastern Mediterranean and Caucasus, *J. Geophys. Res.,* 105, 5695-5719.

McKenzie, D., 1978. Active tectonics of the Alpine-Himalayan belt, the Aegean Sea and surrounding regions, *Geophys. J. R. Astr. Soc.,* 55, 217-254.

McNeill, L.C., Mille, A., Minshull, T.A., Bull, J.M., and Kenyon, N.H., 2004. Extension of the North Anatolian Fault into the North Aegean Trough: Evidence for transtension, strain partitioning, and analogues for Sea of Marmara basin models, *Tectonics,* 23, TC2016, doi :10.1029/2002TC001490.

Mercier, J.L., Delibassis, N., Gauthier, A., Jarrige, J.J., Lemeille, F., Philip, H., Sébrier, M., and Sorel, D., 1979. La néotectonique de l'Arc Egéen, *Rev. Géol. Dyn. Géogr. Phys.,* 21, 67-92.

Michard, A., Goffé, B., Liati, A., and Mountrakis, D., 1994. Découverte du faciès schiste bleu dans les nappes du Circum-Rhodope, un élément d'une ceinture HP-BT éohellénique en Grèce septentrionale? *C. R. Acad. Sci. Paris,* 318 II, 1535-1542.

Michard, A., Feinberg, H., and Montigny, R., 1998. Supra-ophiolitic formations from the Thessaloniki nappe, Greece, and associated magmatism : an intra-oceanic subduction predates the Vardar obduction, *C. R. Acad. Sci.,* 327, 493-499.

Papanikolaou, D., Alexandri, M., and Nomikou, P., 2006.Active faulting in the North Aegean Basin, *Geol.Society of America,Special Paper,* 409, 189-209.

Papazachos, C.B., and Kiratzi, A.A., 1996. A detailed study of the active crustal deformation in the Aegean and surrounding area, *Tectonophysics,* 253 (1-2), 129-153.

Papazachos, B.C., Karakaisis, G.F., Papazachos, C.B., and Scordilis, E.M., 2000. Earthquake triggering in the north and east Aegean plate boundaries due to Anatolia westward motion, *Geophys. Res. Lett.,* 27, 3957-3960.

Pavlides, S.B., and Kilias, A.A., 1987. Neotectonic and active faults along the Serbomacedonian Zone (Chalkidiki, N. Greece), *Terre Cognite,* EUG IV, 7, 2-3, p. 303, Strasbourg.

Pavlides, S., and Caputo, R., 1994. The North Aegean region – A tectonic paradox, *Terra Nova,* 6, 37-44.

Pavlides, S., Mountrakis, D., Kilias, A., and Tranos, M., 1990. The role of strike-slip movements in the extensional area of Northern Aegean, Greece. A case of transtensional tectonics, *Annales Tectonicae,* 4, 196-211.

Peacock, D.C.P., Anderson, M.W., Morris, A., and Randall, D.E., 1998. Evidence for the importance of "small" faults on block rotation, *Tectonophysics,* 299, 1-13.

Ricou, L.E., Burg, J.P., Godfriaux, I., and Ivanov, Z., 1998. Rhodope and Vardar; the metamorphic and the olistostromic paired belts related to the Cretaceous subduction under Europe, *Geodinamica Acta,* 11, 285-309.

Roussos, N., and Lyssimachou, T., 1991. Structure of the Central North Aegean Trough; an active strike-slip deformation zone, *Basin Res.,* 3, 39-48.

Sakellariou, D., 1993. Tectonometamorphic evolution of the geotectonic units of the Chalkidiki peninsula, *Bull. Geol. Soc. Greece,* 28/1, 165-177.

Sokoutis, D., Brun, J.P., Van den Driessche, J., and Pavlides, S., 1993. A major Oligo-Miocene detachment in southern Rhodope controlling north Aegean extension, *J. Geol. Soc. London,* 150, 243-246.

Soldatos, T., Koroneos, A., Christofides, G., and Del Moro, A., 2001. Geochronology and origin of the Elatia plutonite, Hellenic Rhodope Massif, N Greece, constrained by new Sr isotopic data, *N. Jb. Miner. Abh.,* 176, 179-209.

Stacey, F., 1960. Magnetic anisotropy of igneous rocks, *J. Geophys. Res.,* 65, 2429-2442.

Stephenson, A., Sadikun, S., and Potter, D.K., 1986. A theoretical and experimental comparison of the anisotropies of magnetic susceptibility and remanence in rocks and minerals, *Geophys. J. R. Astr. Soc.,* 84, 185-200.

Taymaz, T., McKenzie, D., and Jackson, J., 1991. Active tectonics of the north and central Aegean area, *Geophys. J. Int.,* 106, 433-490.

Tranos, M.D., Kilias, A.A., and Mountrakis, D., 1993. Emplacement and deformation of the Sithonia granitoid pluton, Macedonia, Greece, *Bull. Geol. Soc. Greece,* 33/5, 5-16.

Tsikouras, B., and Hatzipanagiotou, K., 1998. Petrogenetic evolution of an ophiolite fragment in an ensialic marginal basin, northern Aegean, Samothraki Island, Greece, *Eur J. Mineral.,* 10, 551-567.

Uyeda, S., Fuller, M., Belshe, J., and Girdler, R., 1963. Anisotropy of magnetic susceptibility of rocks and minerals, *J. Geophys. Res.,* 68, 279-291.

van Hinsbergen, D.J.J., Langereis, C.G., and Meulenkamp, J.E., 2005. Revision of the timing, magnitude and distribution of Neogene rotations in the western Aegean region, *Tectonophysics,* 396, 1-34.

Vergely, P., 1984. Tectonique des ophiolites dans les Hellénides internes (déformations, métamorphismes et phénomènes sédimentaires) conséquences sur l'évolution des régions Tethysiennes occidentales, *Thèse, Doct.* D'Etat. Univ. Paris-Sud, 660pp.

Voidomatis, Ph., Pavlides, S., and Papadopoulos, G.A., 1990. Active deformation and seismic potential in the Serbomacedonian zone, northern Greece, *Tectonophysics,* 179, 1-9.

Walcott, C.R., and White, S.H., 1998. Constraints on the kinematics of post-orogenic extension imposed by stretching lineations in the Aegean region, *Tectonophysics,* 298, 155-175.

Westphal, M., and Kondopoulou, D., 1993. Paleomagnetism of Miocene volcanics from Lemnos Island, implications for block rotations in the vicinity of the north Aegean Trough, *Annales Tectonicae,* 7, 142-149.

Westphal, M., Bazhenov, M.L., Lauer, J.P., Pechersky, D.M., and Sibuet, J.C., 1986. Paleomagnetic implications on the evolution of the Tethys belt from the Atlantic Ocean to the Pamirs since the Triassic, *Tectonophysics,* 123 (1-4), 37-82.

Westphal, M., Kondopoulou, D., Edel, J.-B., and Pavlides, S., 1991. Paleomagnetism of late Tertiary and Plio-Pleistocene formations from N. Greece, *Bull. Geol. Soc. Greece,* 25/3, 239-250.

Yanev, Y., and Bardintzeff, J.M., 1997. Petrology, volcanology and metallogeny of Paleogene collision-related volcanism of the Eastern Rhodopes, Bulgaria, *Terra Nova,* 9, 1-8.

Zananiri, I., 2004. Contribution to the study of the geotectonic evolution of the Rhodope Massif, NE Greece, with the aid of magnetic methods (Anisotropy of magnetic susceptibility), *PhD thesis*, Aristotle University of Thessaloniki, Greece. (in Greek with English abstract)

Δελτίο της Ελληνικής Γεωλογικής Εταιρίας τομ. XXXX, 2007
Πρακτικά 11ου Διεθνούς Συνεδρίου, Αθήνα, Μάιος 2007

Bulletin of the Geological Society of Greece vol. XXXX, 2007
Proceedings of the 11th International Congress, Athens, May, 2007

NEOTECTONIC BASIN EVOLUTION IN CENTRAL-EASTERN MAINLAND GREECE: AN OVERVIEW

Kranis H.[1]

[1] *National and Kapodistrian University of Athens, Faculty of Geology and Geoenvironment, Department of Dynamic, Tectonic & Applied Geology, hkranis@geol.uoa.gr*

Abstract

The neotectonic evolution of central-eastern mainland Greece (Sterea Hellas) is documented in the result of local extensional tectonics within a regional transtensional field, which is related to the westward propagation of the North Anatolian Fault. The observed tectonic structures within the neotectonic basins and their margins (range-bounding faults and fault zones, rotation of tectonic blocks) suggest a close relation to the Parnassos Detachment Fault (PDF), which is a reused alpine thrust surface. Lokris basin (LB) occupied a central position in this neotectonic configuration, having received its first sediments in the Uppermost Miocene and subsequently been greatly affected by tectonic episodes, which continue until nowadays. LB is considered to have been separated from the present-day North Gulf of Evia not earlier than the Lower Pleistocene. Voiotikos Kifissos Basin, on the other hand, is tightly related to the activation of PDF, occupying the position of a frontal basin and having developed along the main detachment front.
Key words: *Lokris, detachment faulting, block rotation, North Anatolian Fault.*

Περίληψη

Παρουσιάζεται η νεοτεκτονική εξέλιξη της κεντροανατολικής Στερεάς Ελλάδας, η οποία οφείλεται σε εφελκυστική τεκτονική, στο πλαίσιο ενός ευρύτερου διεφελκυστικού πεδίου, σχετιζόμενου με την προς δυσμάς προέλασης του Ρήγματος της Βόρειας Ανατολίας. Οι παρατηρούμενες δομές, τόσο εντός των νεοτεκτονικών λεκανών, όσο και στα περιθώριά τους, υποδηλώνουν στενή σχέση με το Ρήγμα Αποκόλλησης του Παρνασσού, το οποίο αποτελεί μια επαναδραστηριοποιημένη αλπική επιφάνεια επώθησης. Η Λεκάνη της Λοκρίδας,(ΛΛ) που καταλαμβάνει κεντρική θέση στην περιοχή μελέτης άρχισε να λειτουργεί στο Ανώτατο Μειόκαινο και έχει επηρεαστεί από διαδοχικά τεκτονικά επεισόδια, ενώ παραμένει μια τεκτονικά ενεργή περιοχή. Η εν λόγω λεκάνη θεωρείται ότι διαχωρίστηκε από τον σημερινό Βόρειο Ευβοϊκό κόλπο όχι νωρίτερα από το Κατώτερο Πλειστόκαινο. Η Λεκάνη του Βοιωτικού Κηφισού φαίνεται ότι σχηματίστηκε μετά την ΛΛ, αλλά πλέον δείχνει πολύ λιγότερο ενεργή. Η θέση της ωστόσο, είναι ιδιαίτερα σημαντική, καθώς αποτελεί μια μετωπική λεκάνη που αναπτύχθηκε κατά μήκος του ρήγματος αποκόλλησης.
Λέξεις κλειδιά: *Λοκρίδα, ρήγμα αποκόλλησης, περιστροφές τεμαχών, Ρήγμα Βόρειας Ανατολίας.*

1. Introduction

This paper will review stratigraphic and lithological data that constrain the ages of deformation and structural evolution of central-eastern mainland Greece ("Sterea Hellas"), which lies between two prominent, currently marine, basins in central Greece, namely the Gulfs of Corinth and Evia in the south and north, respectively (Fig.1). It is a tectonically active region, which has been affected by extensional-style tectonics, hosting well-known WNW-ESE tectonic structures, such as the Atalanti, Arkitsa- Agios Konstantinos – Kamena Vourla, and Kallidromon Fault Zones (Philip 1974, Roberts and Jackson 1991, Ganas and White 1996, and others) and others, oblique or transverse to these, as the Hyampolis fault (Palyvos *et al.* 2006) and the Bralos-Oiti Fault zone (Kranis and Lekkas 2000, Tzanis *et al.* 2004). In the last decade or so, it has been realized that central mainland Greece is undergoing mixed horizontal shear and extension (e.g. Taymaz *et al.* 1991, Armijo *et al.* 1996, Goldsworthy *et al.* 2001: Burchfiel 2004).

The core of this study was the Lokris Basin (LB), which is believed to host evidence of the tectonic activity for at least the last 6-8 My, since the Upper - Uppermost Miocene. The location, geomorphological, geological and tectonic characteristics of the LB are witnesses to successive tectonic episodes which are related not only to local but also to regional geodynamic processes. LB is an asymmetric graben, bounded on the south by the Kallidromon Fault Zone (KFZ). Between Mts Kallidromon and Parnassos – Giona lies the Voiotikos Kifissos Basin (VKB) (Fig.1), which owes its existence to tectonic activity on the NE margin of the Parnassos – Giona.

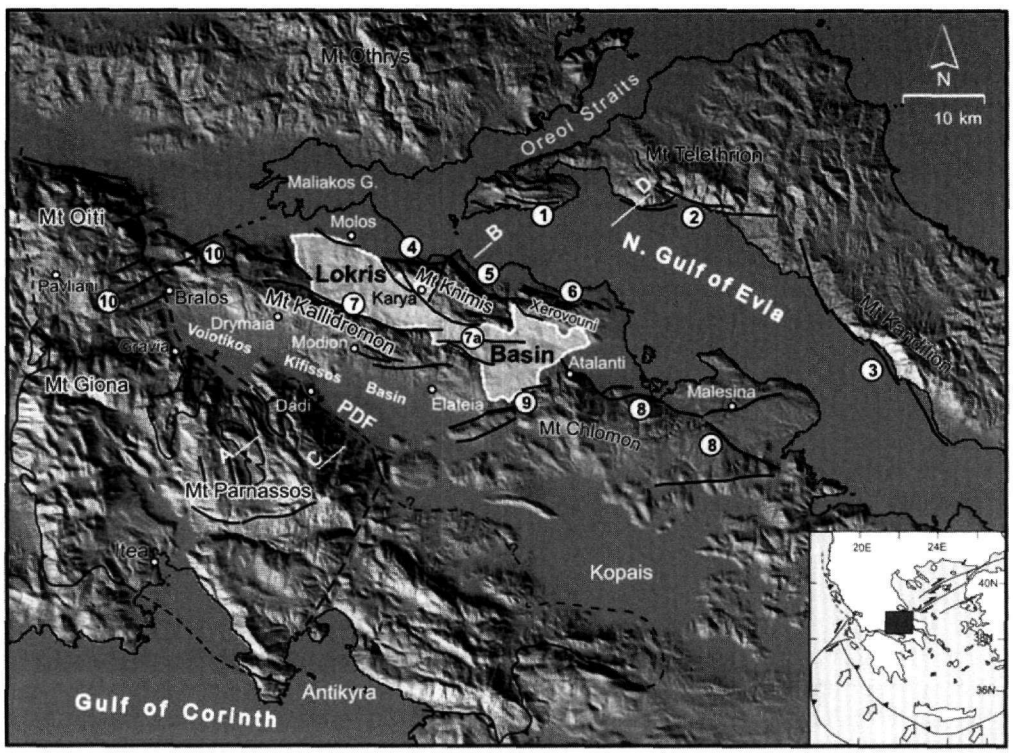

Figure 1 - Hillshaded relief of central-eastern mainland Greece. PDF: Parnassos Detachment Fault; 1: Lichas Fault Zone; 2: Telethrion FZ; 3: Kandilion FZ; 4: Kamena Vourla FZ; 5: Agios Konstantinos FZ; 6: Arkitsa – Longos FZ; 7: Kallidromon GZ; 8: Atalanti FZ; 9: Hyampolis FZ; 10: Bralos-Oiti FZ. Lines AB and CD correspond to the sections of Fig. 6

2. Neotectonic Basins

2.1.Lokris Basin (LB)

Lokris basin (the 'Renginio Basin' of Leeder and Jackson's, 1993) covers an area of 190 km^2 and can be divided into two sub-basins, (Fig. 2), on geomorphological, tectonic and geologic-stratigraphical criteria (see Kranis 1999 for discussion). It has an elongated, WNW-ESE form, with a length of 30 km and a maximum width of 8-9 km. Its southern-southwestern margin, formed by oblique-normal range-bounding fault zones (Kranis 1999), is the Kallidromon mountain complex, which includes Mts Elafovouni, Kallidromon and Sfingio. To the east-southeast it is partially bounded by Mt Chlomon and partially 'open' to the Atalanti plain. The northern boundary is mainly formed by the southern flanks of Mt Knimis and its eastward prolongation (Xerovouni); however, at the northwestern part, the basin is 'open', in the sense that it gives on directly to the alluvial plain of Molos. The basin is drained by a number of –mostly ephemeral- streams that discharge into the Northern Euboikos and Maliakos Gulfs. Many of these streams are deeply incised, cutting through the basin fill.

The sedimentary fill of the LB is or terrestrial (lacustrine and fluvial) origin, with the probable exception of a small outcrop close to the village of Renginion, where Dermitzakis and Papanikolaou (1981) and Dermitzakis (pers. comm.) suggested the occurrence of marine facies. Nonetheless, the basinal facies are not uniformly found throughout the basin and the absence of marker horizons makes the compilation of a single representative stratigraphic column quite difficult. However, the general stratigraphic configuration is as follows (Fig. 2b). (a) The oldest sediments are the Goulemi and the Karya formations, which crop out along the northern margin of the basin, now uplifted by neotectonic faults that mark the southern margin of Mt Knimis. The former is lignite-bearing and has an age of Uppermost Miocene – Early Pliocene, according on fossil mammal remains (*Aceratherium*), studied by Symeonidis (1974); Lemeille (1977) also reported fauna of the same age, but did not give further details. Palynological studies by Celet and Delcourt (1960) from the same area and examination of fossil flora from borehole samples (Ioakim, 1986) also indicated the same age. The Karya formation, composed mainly of multimictic and oligomictic conglomerates and breccias, has an estimated thickness of 150-200 m, presents irregular geometry and it is always found at altitudes higher than 400 m (Fig. 3). Actually, the peak of Mt Knimis, at 940 m a.s.l. is covered by this formation, the exact age of which remains uncertain. Nonetheless, it occupies a stratigraphic position analogous to that of the Goulemi one, that is to say, a basal formation overlain by the main sedimentation of the LB. (b) the area north of the basin axis and south of the aforementioned formations is covered by the Agnandi fm., a thick fluvio-lacustrine sequence of Pliocene to ?Early Pleistocene age. It consists of loose conglomerates alternating with sands, sandstones and silt (Fig. 3). Numerous exploratory boreholes sunk by Institute for Geology and Mineral Exploration (IGME) (Metaxas 1987; 1992; 1994) have given us a crude lithostratigraphic configuration of this formation. Specifically, it comprises (from bottom to top) fine, fossil bearing silt (40-80 m), followed by 20-90 m of clays and sands, 90-120 m of multimictic conglomerates (mainly ophiolitic clasts) and ends with several hundreds of m of oligimictic conglomerates (mainly carbonate pebbles) (c) The youngest one is the Renginion formation, which also contains lignite seams and outcrops south of the basin axis, with considerable surficial extent along the western margin and at the eastern portion of LB; it consists of fine sands, calcareous clays, sandstones and fine conglomerates, with a total thickness more than 300 m (Fig. 3). Philip (1974) mentioned the presence of proboscidean, *Equus, Bos* or *Leptobos* north of Rengini, Kranis (1999) reported the discovery of a Hippopotamus tusk north of Mendenitsa, and Athanassiou (2006) described remains of *Eucladocerus sp* and *Mammuthus* cf. *meridionalis* within these deposits. These findings as well as palynological analyses by Ioakim and Rondoyianni, (1988) from the lignites of Zeli, suggest that the age of this formation is (?)Latest Pliocene - Early Pleistocene.

Flanking the basin, especially along its southern and western margins, are Quaternary scree and talus cones. A formation which belongs in the category of slope breccia is the Mendenitsa formation (Fig. 3), which occupies part of the SW margin of the basin. The topmost member of this formation was recognized by Philip (1974), as a very compact heterometric breccia (it is the main building material of the castle of Mendenitsa), similar to the breccias described by Sorel (2000) for the Kalavryta area, in N. Peloponnesus. The total thickness of the formation is approx 120 m. It significance lies in the fact that it is faulted by the Kallidromon Fault Zone (Kranis 1999), thus providing satisfactory constraints on the activity of the KFZ.

The sediment geometry in the LB seems to follow a predictable pattern. The bedding dips are quite high, being usually around 30°. Very often, and especially in the middle part of the WLB and ELB, dip values are as high as 45°. The distribution of dip directions is in a quasi-amphitheatrical fashion, in the sense that, on average, dip directions in the western, central and eastern sections of the LB are southwesterly, southerly and southeasterly, respectively.

The relief of the basin is quite rough, especially in the WLB, where slope values can be as high as 40 %, while the mean altitude is 350 m. The erosional planation surfaces are few, scattered and usually dipping. Most of them are related to the inclined bedding surfaces and usually coincide with erosion-resistant conglomerate or sandstone banks, forming a 'questa' landscape, particularly in the western portion of LB.

2.2. The coastal landstrip

The narrow landstrip between Mt Knimis and the N. Gulf of Evia can be distinguished in two sectors. The eastern one, around Arkitsa hosts outcrops of lacustrine and brackish facies (sands and fine sandstones (Arkitsa fm.), which Philip (1974) dated as Early- Middle Pleistocene. These sediments are overlain by characteristic argillaceous – silty banks bearing *Viviparus* (*Paludina*) which form a flat headland on the hanging-wall of the Arkitsa Fault; which Dewez (2003) interpreted it as consisting of two flights of terraces having been formed at 125 and 200 ka BP, respectively. The *Viviparus* caprock is generally horizontal, while the underlying strata display gentle dips (most often less than 10°) without systematic orientation. The western sector includes sediments with lithostratigraphic and geometrical characteristics analogous to the Upper Formation of the LB. These are fluviolacustrine conglomerates, silts and sands, with steady S-SW dips in the range of 10-20°. South of Agios Konstantinos, these deposits are overlain by horizontal banks of compact breccia, while towards the west they are covered by recent scree. The limited extent of these outcrops and the scarcity of natural or artificial sections did not allow for more detailed investigation. Nevertheless, their facies and geometry suggest their affinity with the upper members (Pliopleistocene – Early Pleistocene) of the deposits in the LB.

2.3. Voiotikos Kifissos Basin (VKB)

It is a part of the catchment of the Voiotikos Kifissos River and can be divided into two sub-basins, which correspond to the upper and median flow sections of the river. The size of the basin is in the order of 400 km^2, with the two sub-basins covering approximately equal areas. The two sub-basins are divided by a narrow passage close to Amfikleia (Fig. 5), where the alpine basement is exposed and Voiotikos Kifissos River flows through the limestones and dolomites of the Sub-Pelagonian Unit and erodes its Late Quaternary deposits (fluvial terraces).

The relief in both sub-basins is smooth, with a mean altitude of 250 m. and the maximum slope value not exceeding 10 %. A large part of the VKB is an extended alluvial plain, with the Late Pleistocene – Holocene deposits of the river having covered the underlying sediment fill.

The sedimentary fill of the basin has limited thickness, and it mostly consists of Late Quaternary alluvial plain deposits. Especially for the western (upper) sub-basin, the alluvial cover is quite thick, reaching even 100 m. or more, as confirmed by geophysical soundings carried by IGME (Tsioumas 1998, pers. comm.).

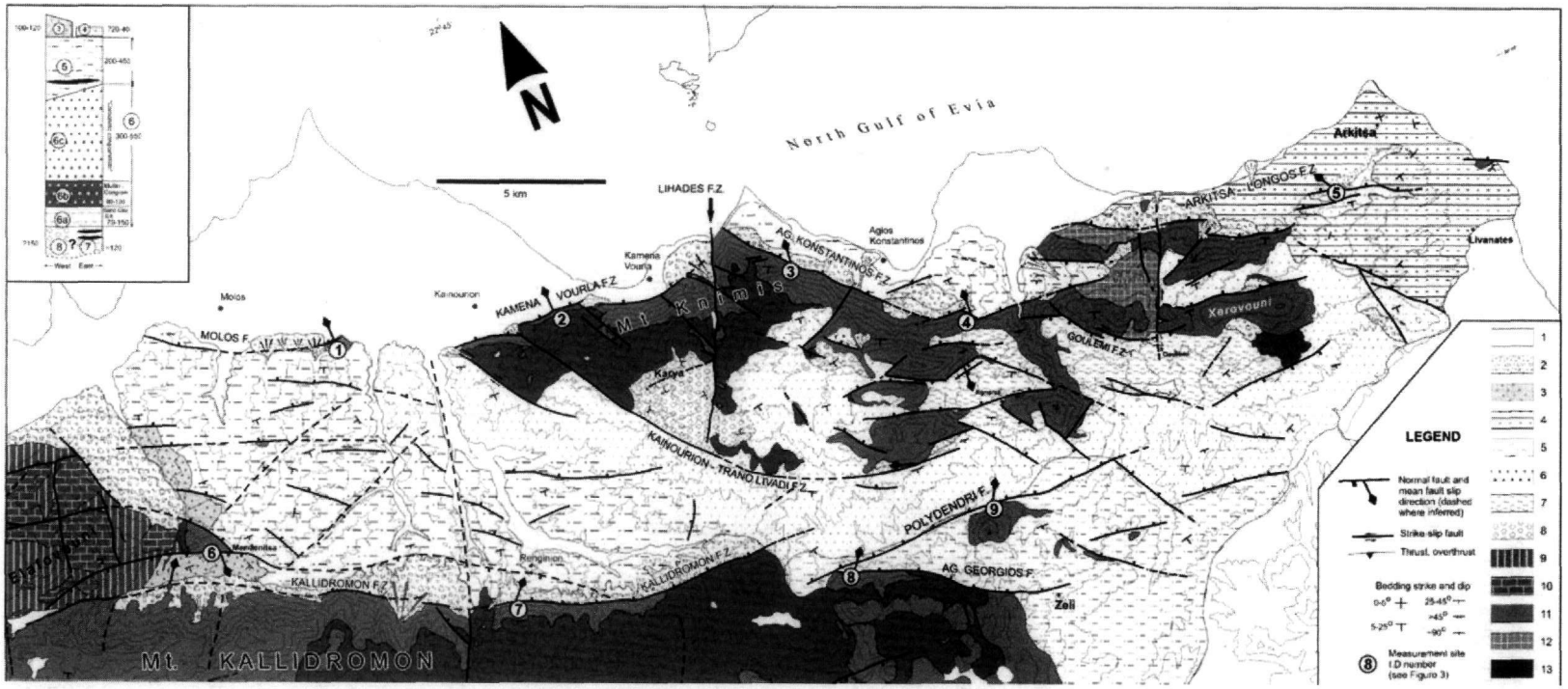

Figure 2 - (a) Simpilfied geological map of the Lokris Basin (after Kranis, 1999). 1: Alluvium and Holocene deposits; 2: Quaternary scree; 3: Mendenitsa formation; 4: Arkitsa fm; 5: Renginion fm; 6 Agnandi fm; 7: Goulemi fm; 8: Karya fm; 9: Late Cretaceous clastics; 10: Late Cretaceous carbonates; 11: Triassic- Jurassic carbonates; 12: Volcaniclastic compex; 13: ophiolite suite. See text for description of lithological units. (b) Schematic stratigraphic column of the LB, based on Metaxas (1987, 1992, 1994) and our own observations. Numbers correspond to the formations mentioned above. Note that Agnandi fm (no 6) appears with its subdivisions (6a, b, and c), which are described in the text, but are not shown in (a) due to the ambiguity in their boundaries

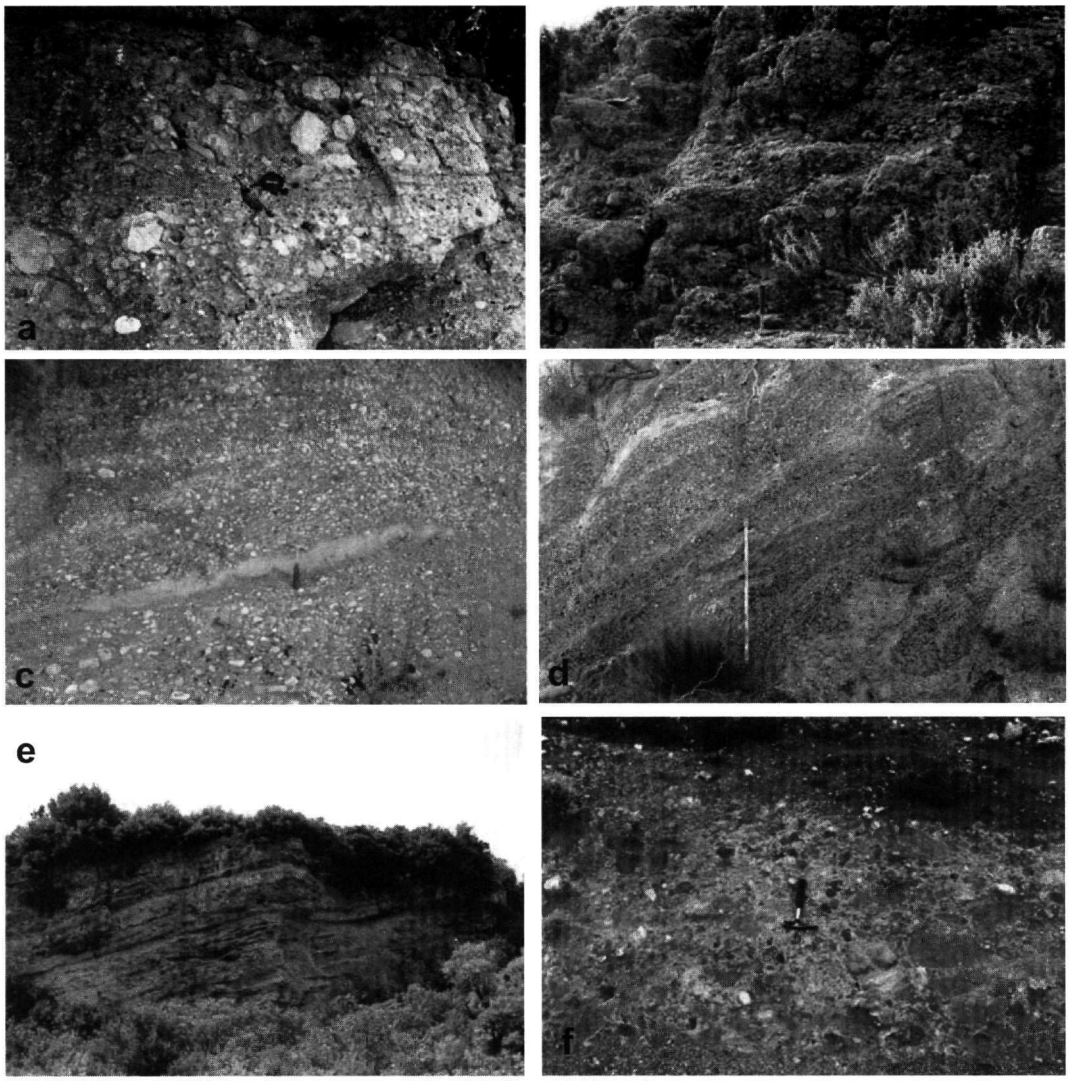

Figure 3 - Field photos from outcrops in Lokris. (a) the basal members and (b) the ologimictic conlomerates of the Karya fm. Lens cap and hammer for scale; (c) typical exposure of the Agnandi fm; (d) The steeply dipping fine conglomerates of the Renginion fm. Dip direction is SSW; (e) the compact carbonate breccias that form the upper member of the Mendenitsa formation; (f) typical exposure of the reddish conglomerates in Drymaia

The age of the oldest sediments, which outcrop at the northern flank of the western sub-basin, close to Drymaia, and the northwestern edge of the eastern sub-basin, close to Modion, remains questionable. These are multimictic conglomerates in reddish clayey matrix, with clasts of various lithological types (sandstones, pelites, calcareous and igneous), with a thickness of approximately 100-150 m at Drymaia and less at Modion (Fig. 3). Based on lithological criteria, Celet (1962) regarded them as molassic remnants, presumably of Oligocene – Miocene age; however, this dating cannot be ascertained. Upon them is deposited a series of fluviolacustrine origin (150 maximum thickness), almost identical in character to the younger (Pliopleistocene- Early Pleistocene) deposits of the LB. However, the surficial outcrops of these deposits are limited a portion of the southern flanks of Mt Kallidromon, close to the village of Modion. The contact between these deposits and the underlying conglomerates can only be seen in a hill NE of Modion, as at other locations it is either covered by recent deposits (i.e. south of Drymaia) or it is faulted.

The outcrops of all these deposits are located north of the basin axis, along the southern flanks of Mt. Kallidromo; the general dip direction is southerly. Towards the south there is no indication for their underlying the alluvial fill and their thickness seems to taper out towards the south. Their dips are generally gentle, not exceeding 10-15°S.

The southern margin of VKB, especially along the foot of Mt Parnassos is covered by extensive scree and talus cones. According to Pope (2000) the most dominant of these alluvial fans, (the Tithorea fan) was initiated in the Upper Pleistocene and developed through the Holocene, in successive episodic stages. The basement of the basin is found at an altitude about at sea level and for the eastern sub-basin is the carbonates of the Sub-Pelagonian Unit, while for the western it is partially a clastic formation, probably corresponding to the flysch of the Parnassos Unit.

2.4. Observations on marginal and interbasinal tectonic structures

Kranis and Papanikolaou (2001) showed that the NE margin of Mt Parnassos corresponds to a large detachment fault (PDF), with the hanging-wall Triassic dolomites of the Subpelagonian Unit overlying a thin slice of the flysch pelites of the Parnassos Unit. PDF is a reused (alpine thrust) surface, with extensional tectonic features overprinting the older (alpine) ones. The mean slip vector, calculated from data from a quarry exposure at Dadi hill and at Toufa, SW of Amfikleia, is oriented NE (Figs 4, 5). Within the VKB tectonism has left few marks, with the exception of the antithetic fault set of Elateia (Fig 1). Along its western margin several NE-SW transverse faults have been located, belonging to the Pavliani (or Bralos-Oiti) Fault Zone (Lekkas and Kranis 2000, Tzanis *et al.* 2004).

LB shows signs of intense tectonic activity, both within the basin itself and along its margins. The sedimentary fill is densely faulted and tilted, usually towards the S, SSE or SSW and small-order horsts have formed within the basin (Mariolakos *et al.* 2001). The Kallidromon Fault Zone (KFZ) displays characteristics of oblique-normal (dextral) displacement, contrary to the coastal fault system (Arkitsa-Longos, Agios Konstantinos and Kamena Vourla Fault Zones) which displays constant sinistral oblique-normal movement (Figs 4, 5). Except for its eastern segment (which will be described later) the KFZ shows no signs of Late Quaternary activity. Cemented scree cover the entire mountain foot, from Renginion to Mendenitsa, with the exception of a well-developed alluvial fan at the village of Kallidromos. Fault surfaces are poorly preserved especially close to Mendenitsa, where the tectonized footwall dolomites have been eroded (Fig. 5). Few, but eroded slickensides are found south of Renginion, at the exit of the new railway tunnel and a fractured zone (but not the main fault surface itself) is exposed SW of the village of Kallidromos. West of Renginio, where the KFZ takes an E-W strike, it juxtaposes the erodible ophiolite suite against loose scree, but no fault surfaces have been found. On the other hand, the eastern part of the KFZ, which is represented by two overlapping segments, the E-W Polydendri f. and the WNW-ESE Agios Georgios f., displays rather "fresh" and well-preserved fault surfaces. Especially Polydendri f., which dips around 40-45° N has a well exposed, striated fault surface and is associated with an impressive, ~250 m high escarpment (Fig. 5); the Agios Georgios f. has gentler dips and its surface is more eroded. One could assume that the Polydendri f. has rotated and replaced the Ag. Georgios f.: both of them however, have almost identical mean slip vectors (Fig. 4), so the possibility that the Ag. Georgios fault is still active cannot be ruled out.

The southern margin of Mt Knimis is partially formed by the Kainourio – Trano Livadi Fault Zone (KTLFZ), which displays 'peculiar' characteristics, the most important of which is that it is found with steep northerly dips northerly dips (instead of southerly, as one should expect), albeit being apparently an antithetic structure to the KFZ. Moreover, its striated fault surface gave a mean displacement vector oriented WNW.

Mt Knimis itself is a highly faulted, elongate 'horst' block, hosting several smaller-order faults (Fig. 2). On the coastal fault system equally important is the NW-SE main segment of the Agios Konstantinos f., which displays dip not higher that 35° and slip vectors invariably oriented towards

the North (Fig. 5). The faults east of west of the AKFZ are the Kamena Vourla F.Z. and the Arkitsa F.Z., respectively and their mean strike is WNW-ESE and dips are considerably higher, around 60°, on average. In other words, the AKf is oblique to the other two coastal fault systems. The same goes for a number of NW-SE, NE- or SW-dipping normal faults, located between the villages of Agnandi and Goulemi. The northernmost of them is the Paliompoukriza f. (location 4 in Fig. 2), which is now linked with the AKf. This NW-SE fault presents two sets of slip vectors. The younger one, oriented N and consistent with the kinematics of the AKf and an older one, which is dip-slip (Fig. 5). Our investigations so far have not brought to light any piece of evidence for an older, dip-slip movement for the AKf itself, despite its proximity and identical orientation with the aforementioned NW-SE fault set.

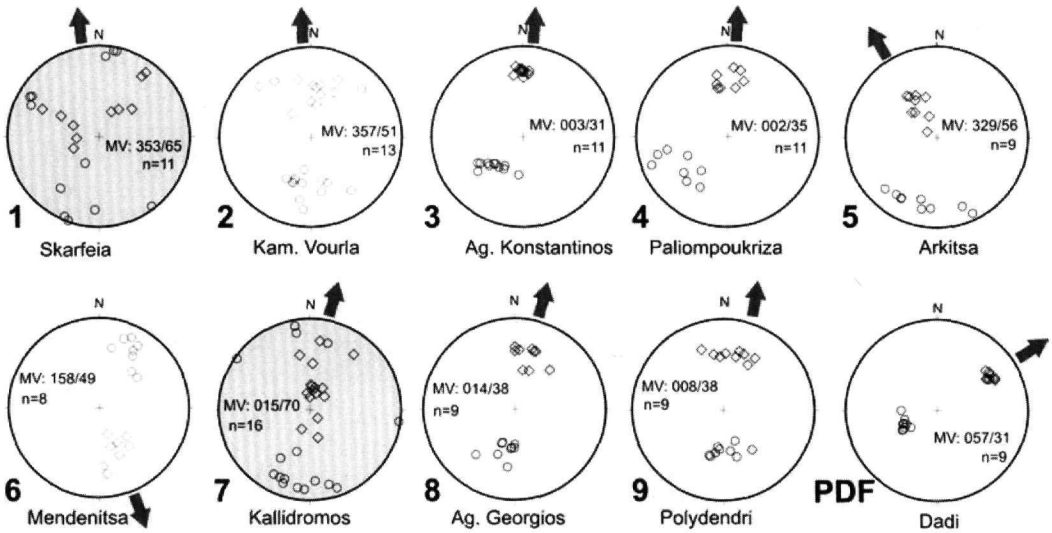

Figure 4 - Lower hemisphere stereographic projections of fault-slip data. Diamonds are lineations on fault planes, circles are poles to planes. MV: mean lineation orientation from Fischer statistics. White stereonets are for data from the main fault planes; gray ones for data from footwall fault arrays within ~10 m from the main fault plane. For location of measurement stations see Figures 1 and 2

The eastern and western boundaries of LB and VKB, seem to be (at least partially) controlled by oblique or transverse fault zones, the kinematics of which are oblique-normal to strike-slip, such as the Hyampolis Fault Zone (Kranis *et al.* 2001, Palyvos *et al.* 2006) and the aforementioned Bralos-Oiti FZ.

3. Discussion and Conclusions

The understanding of neotectonic evolution of the studied area calls for good age constraints; unfortunately, these are, to some degree, lacking, so what follows in this section is a working hypothesis on deformation rates, based the few available biostratigraphical data and lithostratigraphical correlations; further work involving dating can greatly improve this story.

The onset of lacustrine sedimentation is placed at Uppermost Miocene, with typical basal facies in Goulemi – Agnandi. During the same period, lacustrine sediments also started to be deposited in the area of Malesina; however, there is no proof that these two locations formed part of a greater lacustrine system. Deposition was also taking place in Karya, albeit with different litholological characteristics, owing to the difference in bedrock material (ophiolites instead of carbonates).



Figure 5 - (a) Fault surface of the Paliompoukriza f. and (b) close-up at the same location, to show the two sets of striations: oblique-slip postdates dip-slip; (c) striated slickenside of the AKf; (d) the Polydendri f. fault scarp here is ~200 m high; (e) eroded fault surface of the KFZ, west of Mendenitsa; (f) the striated surface of the antithetic fault of KFZ at Mendenitsa. View to NE

Tectonic activity resulted in the uplift of the Uppermost Miocene – Early Pliocene sediments, which are now found at high altitudes, in Karya, Agnandi and Goulemi. The NW-SE set of faults between Agnandi and Goulemi may have also been formed during these early stages. This period also marked the start of the uplift of the coastal mountain range; however this uplift has not been uniform throughout the extent of Mt Knimis and its eastern prolongation, Xerovouni, as will be discussed later.

Whether the Voiotikos Kifissos basin had opened during that period or not cannot be established easily, considering the lack of biostratigraphical information. The age of reddish conglomerates of Drymaia and Modion remains uncertain: this could provide a good lower age limit. What we do know is that there are no lignite-bearing sequences, which could be analogous to the Goulemi fm.,

while the thick conglomerate series of the LB (Agnandi fm.) are also absent. The formations that overlie the reddish conglomerates are lithostratigraphically similar to the Renginion fm. Should this be the case, then the VKB must have been s a small, narrow and elevated (intermontane) basin, above the level of fluvio-lacustrine sedimentation, within an extended mountain mass that corresponded to the current Mts Parnassos and Giona in the south and Kallidromon in the north.

The end of Pliocene –and probably until the Lower-Middle Pleistocene- is characterized be widespread fluviolavustrine sedimentation, albeit of varying depositional environments. These sediments are also found outside the present geomorphological borders of LB, such as (i) in Modion – Elateia, at the southern slopes of Mt Kallidromon, (ii) in Arkitsa (with significantly different lithostratigraphical characteristics); (iii) north of Gravia and covering the Bralos pass, between Mts Kallidromon and Oiti. In other words, the continental sedimentation during this period was extensive, covering the greatest part of the broader Lokris region. The present-day mountain masses were not yet uplifted in their current position, appearing as isolated bedrock salients, half-buried under the thick Early Pleistocene deposits. Jackson (1999) reported the occurrence of granite pebbles at the base of the Renginion formation: the source of these clasts must have been either to the north of the LB, which means, according to the same researcher, that they could not have been transported there if the coastal faults were active then.

Between Middle and Upper Pleistocene, tectonic activity increased significantly to the degree that it resulted in dramatic changes in the Lokridian landscape. Mt Kallidromon almost reached its present form, being a distinct, elongated fault block which underwent rapid uplift, the amount of which may have been smaller in the east than in the west. This suggestion is based both on geomorphological observations (the altitude of the erosional planation surfaces along its ridgeline lowers gradually towards the east (Kranis 1999) and on the basis of the altitude of the ophiolitic nappe, which also diminishes in the same direction. The formation and uplift of the elongated Kallidromon block separated the main bulk of the LB sedimentary fill from the isolated outcrop between Modion and Elateia, at the southern flanks of the mountain.

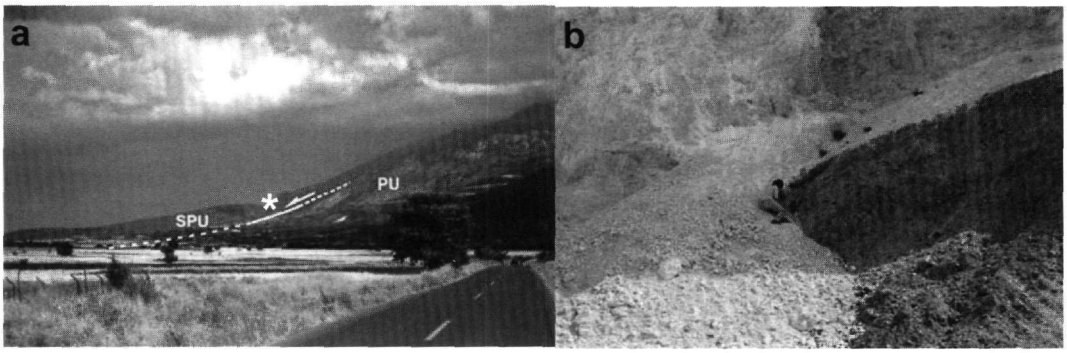

Figure 6 - (a) The Parnassos Detachment Fault (PDF) at Dadi Hill, Amfikleia, on the northern slopes of Mt Parnassos. View to ESE. PU: Parnassos Unit; SPU: Sub-Pelagonian Unit. Dadi hill is a characteristic turtle-back form, located just on the detachment front. Asterisk marks the location of (f): The PDF exposed in an abandoned quarry. The surface dips to the left (N) and away (NE) from the viewer

The LB itself acquired much of its present form, too. The coastal mountain range (Knimis – Xerovouni) was also uplifted as a minor but complex fault block, blocking partially the communication with the basin and the Northern Gulf of Evia. The coastal strip of Pleistocene sediments NW of Agios Konstantinos is a case similar to those in Modion, being cut off from the main body of the fluviolacustrine sequence, as a result of tectonism.

As was also the case of Mt Kallidromon, the uplift of Mt Knimis was not uniform, either, being much higher at the eastern end (Goulemi – Melidoni), where the volcaniclastic base of the

sedimentary platform is exposed, than in the western end (Thronion), where the ophiolite tectonic cover is found at very low altitudes (Kranis 2002). However, the uplift of Knimis may have also been influenced by the set of NW-SE faults mentioned above, which might have caused an initial amount of uplift in the Pliocene, before the formation and the activation of the coastal fault system which gave Knimis its present form. Another observation has to do with the relationship of the NW-SE fault system to the coastal faults and especially the Agios Konstantinos f. The two sets of striations on the Paliompoykriza f, which is now linked with the AKf, may reflect the evolution of this particular structure, in the sense that in its first period of activity moved as a dip-slip normal fault, but its kinematics changed when it became linked with the coastal fault zone.

Tectonically-induced block rotation was has been a striking result of this tectonic phase. This has been confirmed both by observations in the horst-blocks (Mts Kallidromon and Knimis) and within the LB. where all fault blocks have been rotated towards the S-SSW. This block rotation is corroborated by the following observations: (i) in Mt Knimis, uplift has been significantly greated in its eastern part. On top of that, rotation has also taken place around a horizontal WNW-ESE axis, towards the south. This is shown in the very low dip values of the NE-dipping Agios Konstantinos Fault (not exceeding 35°), together with the rotation observed along the southern margin of the mountain, marked by the Kainourio – Trano Livadi Fault Zone (KTLFZ), which Kranis (1999) wrongly interpreted as a reverse fault, as it is a formerly S-dipping fault, now rotated by 25-35° to steep northerly dips. (ii) within the LB, the Agnandi and Renginion formations are found dipping towards the S, SSW and SSE with dip values around 30-35°, reaching even 45° at places. This type of sediments is not expected to be deposited always horizontally, as the fluvial deposits tend to dip away from their source region, which was, in all probability, the elevated mountain ranges in the south. In other words, the sedimentary basin fill may have been rotated more than 35° towards the south. Rotation has also affected the Mendenitsa formation, which is found tilted up to 40-45° S.

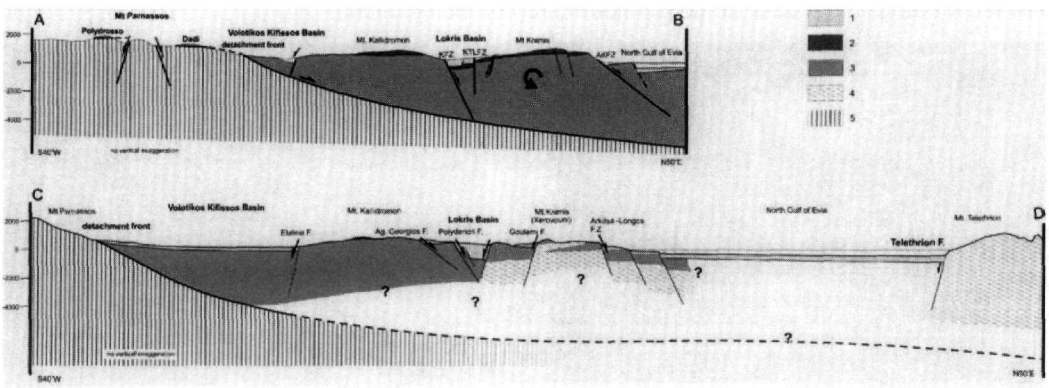

Figure 7 - Interpretative cross-sections through the Lokris and Voiotikos Kifissos Basins (see Fig. 1 for location). 1: Synrift deposits (Pliocene- Quaternary); 2: Ophiolite suite; 3: Sub-Pelagonian Unit; 4: volcaniclastic complex and basement of the SPU; 5: "Lower Plate" formations, which correspond (at least in the western parts) the Parnassos Unit. The formation of both VKB and LB is attributed to the NE-ward sliding on the PDF. Section AB demonstrates the block rotation of Mt Knimis, resulting in the low dips of the AKFZ and the northerly dips of the originally S-dipping KTLFZ. This pattern is confirmed by the systematic southward lowering of the base of the ophiolite nappe. Section CD shows the uplifted volcaniclastic basal complex of the SPU, at the area of Melidoni, which may be linked to the SPU basement, outcropping just across the N. Gulf of Evia, on Mt Telethrion. The suggested shallowing of the detachment surface beneath the Gulf is believed to reflect the crustal thinning observed at this area (Makris *et al.* 2001)

The aforementioned observations and suggestions are in agreement with the general concept of a northward fault migration (Goldsworthy and Jackson 2001) and fault-block rotation. Trying to understand the driving mechanism behind this, we investigated the southernmost extensional structure in the area, which marks the NE NE margin of Mts Parnassos, Giona and Oiti. Kranis and Papanikolaou (2001) called it the Parnassos Detachment Fault (PDF) (Figs 1, 3, 6, 7) and demonstrated that this is a reused (originally a thrust) surface. The timing of activity on this structure cannot be easily established, due to the absence of appropriate stratigraphical markers. It may have been a mobile zone that responded to the propagation of the North Anatolian Fault, on its reaching the Hellenic (present-day) mainland and giving rise to what Sengör (1979) called "Grecian Shear Zone". The fact that the central mainland Greece is undergoing mixed horizontal shear and extension has been shown by GPS surveys (e.g. McClusky *et al.* 2000) and has been reviewed by Burchfiel (2004). In this sense, the PDF is thought to be the northernmost of a series of WNW-ESE to NW-SE transtensional structures that have responded to the NAF propagation, which in combination with the ongoing back-arc dynamics have given rise to extensional structures, including the Gulf of Corinth (Dewey and Sengör 1979, Armijo *et al.* 1996, Burchfiel 2004). However, there are several questions to be answered yet. One is whether the observed neotectonic deformation is indeed confined within this approximately 35-40 km wide NE-SW zone, which includes LB, VKB, and the NW parts of the N. Gulf of Evia and the island itself, or it extends further to the SE (and less possibly to the NW). If the former suggestion is valid, then the observed transverse, NE-SW tectonic structures may exert significant tectonic control in the active tectonics of the region. However, for this to be verified, further research is needed, especially along the SPU alpine thrust front and the related basins (such as the Kopais Basin), for extensional neotectonic overprints.

4. Acknowledgments

Prof. J. Jackson and Dr G. Roberts and are thanked for their highly useful reviews of the manuscript. Professor D. Papanikolaou and colleagues Dr E. Skourtsos and L. Gouliotis are thanked for constructive discussions.

5. References

Armijo, R., Meyer, B., King, G.C. P., Rigo, A., and Papanastassiou, D., 1996.Quaternary evolution of the Corinth Rift and its implication for the late Cenozoic evolution of the Aegean, *Geophysical Journal International*, 126, 11–53.

Athanassiou, A., 2006. Reghinio, a new mammal locality from the Plio-Pleistocene of Central Greece, *N. Jb. Geol. Paläont. Mh.*, 2, 116-128.

Burchfiel, B.C., 2004. New Technology: new geological challenges, *GSA Today*, 14, 4-9.

Celet, P., 1962. Contribution a l'étude géologique du Parnasse-Kiona et d'une partie des régions méridionales de la Grèce continentale, *Ann. Geol. de Pays Hellen.*, XIII, 1-446.

Celet, P., and Delcourt, A., 1960. Les terrains néogènes de Locrides (Grèce orientale moyenne): leur situation géologique et leur age, *Ann. Soc. Geol Nord*, LXXX, 1125-132.

Dermitzakis, M.D., and Papanikolaou, D.J., 1981. Paleogeography and Geodynamics of the Aegean region during the Neogene, *Proc. VIIth Intern. Congress on Mediterranean Neogene, Athens, 27September- 2 October 1979*, 245-289.

Dewey, J.F., and Sengör, A.M., 1979. Aegean and surrounding regions:complec multiplate and co ntinuum tectonics in a convergent zone, *Geol. Soc. Amer. Bull.*, 90, 84-92.

Dewez, T., 2003. Geomorphic markers and digital elevation models as tools for tectonic geomorphology in Central Greece, *Unpubl. PhD Thesis*, Brunel University, 173pp.

Ganas, A., and White, K., 1996. Neotectonic fault segments and footwall geomorphology in Eastern Central Greece from Landsat TM data, *Geol. Soc. Greece Sp. Publ.*, 6, 169-175.

Goldsworthy, M., and Jackson, J., 2001. Migration of activity within normal fault systems: examples from the Quaternary of mainland Greece, *J. Struct. Geol.*, 23, 489-506.

Goldsworthy, M., Jackson, J., and Haines, J., 2001. The continuity of active fault systems in Greece, *Geoph.J. Int.*, 148, 596-618.

Ioakim, C., and Rondoyanni, T., 1988. Contribution à l'étude géologique de la région de Zeli, Locride (Grèce centrale), *Rev. de Micropal.*, 31, 2, 129-136.

Ioakim, Ch., 1986. *Palynological – Stratigraphical study of the L3 borehole in Agnandi, Lokris*, IGME Unpubl Report, Athens, 4p. (in Greek)

Jackson, J., 1999. Fault death: a perspective from actively deforming regions, *J. Struct. Geol.*, 21, 1003 – 1010.

Kranis, H.D., and Papanikolaou, D.I., 2001. Evidence for detachment faulting on the NE Parnassos mountain front (Central Greece), *Bull. Geol. Soc. Greece*, XXXIV/1, 281-287.

Kranis, H.D., and Lekkas, E.L., 2000. The Pavliani fault zone: Evidence for westward propagation of the North Anatolian Fault Zone in Eastern Mainland Greece, *Proc. IESCA 2000 , 25-29.9.2000,* (Abs.) 48p.

Kranis, H.D., Palyvos, N., Livaditis G., and Maroukian, H., 2001. The Hyambolis Zone: geomorphological and tectonic evidence of a transverse structure in Lokris (Central Greece), *Bull. Geol. Soc. Greece*, XXXIV/1, 251-257

Kranis, H.D., 1999. Neotectonic Activity of Fault Zones in central-eastern Mainland Greece (Lokris), *Ph.D. Thesis. GAIA,* 10, 2003, 234pp.

Kranis, H.D., 2002. Kinematics of active faults in Lokris, central Greece – block rotation within a crustal-scale shear zone? In J. Michalik, L. Simon and J. Vozar (eds), *Proc. XVII Congress of the Carpatho-Balkan Geol Ass., Geologica Carpathica*, 53, 157-159.

Leeder, M.R., and Jackson, J.A., 1993. The interaction between normal faulting and drainage in active extensional basins, with examples form the western United States and central Greece, *Bas. Res.*, 5, 79-102.

Lemeille, F., 1977. Études néotectoniques en Grèce centrale nord-orientale (Eubée centrale, Attique, Béotie, Locride) et dans les Sporades du Nord, *Thèse*, Univ. Paris XI.

Makris, J., Papoulia, J., Papanikolaou, D., and Stavrakakis, G., 2001. Thinned continental crust below northern Evoikos Gulf,central Greece, detected from deep seismic soundings, *Tectonophysics*, 341, 225-236.

Mariolakos, I., Kranis, H,. Maroukian, H., and Fountoulis, I., 2001. Tectonically controlled drainage evolution in Lokris, *Bull. Geol. Soc. Greece*, XXXIV/1, 175-782

McClusky, S.C., Balassanian, S., Barka, A., Demir, C., Ergintav, S., Georgiev, I., Gurkan, O., Hamburger, M., Hurst, K., Kahle, H., Kastens, K., Kekelidze, G., King, R., Kotzev, V., Lenk, O., Mahmoud, S., Mishin, A., Nadariya, M., Ouzounis, A., Paradissis, D., Peter, Y., Prilepin, M., Reilinger, R., Sanli, I., Seeger, H., Tealeb, A., Toksoz, M.N., and Veis, G., 2000. Global positioning system constraints on plate kinematics and dynamics in the eastern Mediterranean and Caucasus, *Journal of Geophysical Research*, 105, 5695–5719.

Metaxas, A., 1987. *Geological investigation of Agnandi sub-region, Lokris*, Unpubl. IGME report, Athens. (in Greek)

Metaxas, A., 1992. *Geological research on the lignite occurrence in the southern field of Agnandi Tahtali sub-region (Phtiotis),* Unpubl. IGME report, Athens. (in Greek)

Metaxas, A., 1994. *Results of research for lignite in the area "Tahtali-Rengini – Ag. Haralambos – Mendenitsa" in 1993*, Unpubl. IGME report, Athens, 24pp. (in Greek)

Palyvos, N., Badekas, I., and Kranis, H., 2006. Transverse fault zones of subtle geomorphic signature in northern Evia island (central Greece extensional province): An introduction to the Quaternary Nileas graben, *Geomorphology*, 76, 363-374.

Philip, H., 1974. Etude néotectonique des rivages égéens en Locride et Eubée nord-occidentale (Grèce), *Thèse doc.* sp., Acad. de Montpelier, 86 p.

Pope, R.J., 2000. The application of mineral magnetic and extractable iron (Fe_d) analysis for differ entiating and relatively dating fan surfaces in central Greece, *Geomorphology*, 32, 57-67.

Roberts, S., and Jackson, J., 1991. Active normal faulting in central Greece: an overview, In A.M. Roberts, G. Yielding and B. Freeman (eds), *The Geometry of Normal Faults*, Geol. Soc. Sp. Pub., 56, 125-142.

Sengör, A.M., 1979. The North Anatolian Transform fault: its age, offset and tectonic significance, *J. Geol. Soc. London,* 136, 269-282.

Sorel, D., 2000. A Pleistocene and still-active detachment fault and the origin of the Corinth-Patras rift, Greece, *Geology*, 28, 83-86.

Symeonidis, N., 1974. Ein Bemerkenswerter Wirrbeltierfund aus dem Lignit von Atalanti (Phthiotis, Griechenland), *Ann. Geol. Pays Hell.*, XXVI, 306-314.

Taymaz, T., Jackson, J., and McKenzie, D., 1991. Active tectonics of the north and central Aegean Sea, *Geoph. J. Int.*, 106, 433-490.

Tzanis, A., Chailas, S., and Kranis, H., 2004. Aeromagnetic and topographic constraints on the active tectonics of central Greece, *Proc. 10th GSG Conference, 15-17.4.2004, Thessaloniki*, Ext. Abs., 627-628.

Δελτίο της Ελληνικής Γεωλογικής Εταιρίας τομ. XXXX, 2007
Πρακτικά 11ου Διεθνούς Συνεδρίου, Αθήνα, Μάιος 2007

Bulletin of the Geological Society of Greece vol. XXXX, 2007
Proceedings of the 11th International Congress, Athens, May, 2007

IMPLICATIONS FOR THE CORRELATION OF THE HELLENIC NAPPES IN SW AEGEAN: THE GEOLOGICAL STRUCTURE OF THE ARCHANGELOS REGION, RHODES ISLAND

Lekkas E.[1], Danamos G.[1], and Skourtsos E.[1]

[1] *National and Kapodistrian University of Athens, Faculty of Geology and Geoenvironment, Department of Dynamic, Tectonic and Applied Geology, elekkas@geol.uoa.gr, eskourt@geol.uoa.gr*

Abstract

In the region of Archangelos in central-eastern Rhodes, a nappe sequence from bottom to top consists of: i) Laerma unit, an Oligocene age wild flysch, ii) Archangelos unit, a neritic limestone of Upper Triassic – Mid Eocene age grading through red pelites to a flysch sequence, probably combarable to Ethia unit of Crete, iv) the Profitis Ilias unit, a pelagic sequence of platy limestones and radiolarites of Upper Triassic – Upper Cretaceous age, similar to Pindos Unit and v) the ophiolites. The emplacement of the nappes on the relative autochthonous Laerma unit was carried out in surface conditions and is due to gravitational sliding estimated during Lower Oligocene to Middle – Upper Oligocene.

Key words: *External Hellenides, geotectonic unit, palaeogeography, wild flysch, Rhodes.*

Περίληψη

Στην περιοχή του Αρχαγγέλου στην κεντροανατολική Ρόδο, η καλυμματική στήλη περιλαμβάνει από κάτω προς τα πάνω τις παρακάτω γεωτεκτονικές ενότητες: i) Την ενότητα Λαέρμα, ένας ολιγοκαινικός άγριος φλύσχης, ii) την ενότητα Αρχαγγέλου, μία ασταθή νηρητική ακολουθία ηλικίας Ανωτέρου Τριαδικού – Μέσου Ηωκαίνου που μεταβαίνει μέσω ερυθρών πηλιτών σε μία κλαστική σειρά τύπου φλύσχη, η οποία συγκρίνεται με την ενότητα Εθιάς στη Κρήτη ή την ενότητα Καληλίμνη στην Κάρπαθο, iii) την ενότητα Προφήτη Ηλία, μία πελαγική σειρά από πλακώδεις ασβεστόλιθους και ραδιολαρίτες ηλικίας Ανωτέρου Τριαδικού – Ανωτέρου Κρητιδικού, συγκρίσιμη με αυτή της ενότητας Πίνδου στην Ηπειρωτική Ελλάδα και iv) τους οφιόλιθους. Η τοποθέτηση των καλυμμάτων στην σχετικά αυτόχθονη ενότητα Λαέρμα έλαβε χώρα σε επιφανειακές συνθήκες στο Μέσο – Ανώτερο Ολιγόκαινο και οφείλεται σε βαρυτικές ολισθήσεις.

Λέξεις κλειδιά: *Εξωτερικές Ελληνίδες, γεωτεκτονική ενότητα, παλαιογεωγραφία, άγριος φλύσχης, Ρόδος.*

1. Introduction

The external Hellenides represent an enlogated arched belt located on the Aegean Arc front, extending from Epirus to the Dodecanese islands comprising of alpine rocks classified in various

nappes or geotectonic units. The continuations of those nappes from the northwestern to the southeastern end of the arc although it is easy to be tracked through Epirus, Mainland Greece, Peloponnesus and Crete, in the Dodecanese islands however, controversial suggestions exist. This fact is due to the limited surface outcrop of the alpine formations in this region, due to important stratigraphic variations that a unit can present through its geographical development and continuation along the arc and due to the confirmed post-alpine deformation that has led to the formation of Neogene basins that are presently filled by thick sequences of clastic sediments. The aforementioned have resulted in various suggestions through time, regarding the number of units that compose the Dodecanese islands and their correlation to the existing units in Crete and Mainland Greece. Moreover, the fact that the Dodecanese islands are neighbouring to the southwest Turkey and Taurides, triggers the challenge for the correlation of the alpine rocks with those in Asia Minor.

Rhodes is located in the southwestern section of the Aegean arc, is the largest island of the Dodecanese where the alpine rocks present significant surface outcrop and allow better lithostratigraphical observations, though the extended outcrops of the post-alpine deposits have as a result the alpine formations to outcrop as islets. Therefore, various views and suggestions regarding the number of geotectonic units that outcrop on the island and as a consequence their stratigraphy, their paleogeographical location and their correlation to the existing units of the External Hellenides, have been proposed (e.g. Mutti *et al.* 1970, Aubouin and Dercourt 1970, Aubouin *et al.*1976, Harbury and Hall 1988, Papanikolaou *et al.* 1995).

This paper presents the results of the detailed geological mapping on a section of the island, where the alpine rocks dominate, outcropping in great variety. The new stratigraphic and tectonic data presented are the preliminary results of a detailed and lengthy research and contribute significantly to the understanding of the geological structure of the island and the paleogeographical representation of the southeastern Aegean and the correlation of the Hellenides with the Taurides. Therefore, the aim of this paper is to contribute to the knowledge of the Alpine units that are involved in the islands' structure presenting the results of the detailed geological mapping of the region of Archangelos in the central – eastern section of the island.

2. The Geological Structure of the Island of Rhodes

In the tectonic structure of the island of Rhodes a series of alpine units are involved that are distinguished from bottom to top as follows (Papanikolaou *et al.* 1995, Lekkas *et al.* 2002):

- Lindos Unit. It consists of a cyan to black marble sequence, 400 – 450 m thick that grades to red thin platy marbles (cipolline marbles) and grey calcareous phyllites and finally to metamorphosed flysch consisting of greenish schists and phyllites. This transition is estimated to have taken place during the Upper Eocene – Lower Oligocene. This unit represents the lowermost, relatively autochthonous unit of the island.
- Laerma Unit. It outcrops in the area between Attabiros and Lindos, in the central section of the island and corresponds to a unique clastic formation of wild flysch with alternations of clays, pelites, sandstones and bioclastic limestones. Frequenty interbedded horizons of agglomerates and conglomerates with ophiolite elements and psammitic fragments are observed. Within the unit, olistholiths of green igneous rocks, micritic limestones and agglomerated bioclastic limestones are also recorded. The included fauna within the olistholiths determines a formation age of post – Upper Eocene, possibly Oligocene.
- Attabiros - Akramitis Unit. It consists of a pelagic sequence of thin platy and micro-agglomerated limestones with silex of Upper Jurassic – Middle Eocene age.
- Archangelos Unit. It consists of a thick sequence of massive to thick – bedded limestones and Upper Triassic – Lower Eocene dolomites with Lower Eocene age flysch at the top.

- Profitis Ilias Unit. It consists of thin platy, micritic, and micro-agglomerated limestones with silex and red marls or radiolarites of Upper Triassic – Upper Cretaceous age.
- Ophiolite Unit. Masses of green igneous rocks (gabbro, diabase, serpentinite) that are frequently followed by radiolarites. This unit is considered to tectonically overly either the Archangelos Unit or the Profitis Ilias Unit.

The above alpine units are unconformably covered by thick clastic sequences deposited in the extensional basins formed after the stacking of the nappes during the Upper Oligocene. These structures become even more complicated by the action of faults that are interrupting the formations continuity (Papanikolaou *et al.* 1995).

3. Geological Structure of the Archangelos Region

The study area is located between the villages of Kolimpia, Arhipolis, Malona and Haraki and covers an approximate area of 100 km^2. It includes alpine formations that are attributed to various geotectonic units that are covered by molassic and post alpine sediments (Fig. 1). The results of the detailed geological mapping that was conducted in a 1:10,000 scale are presented in the following paragraphs where the alpine units are described in detail and data are provided regarding the post alpine formations.

3.1. Alpine Nappes

3.1.1. Laerma Unit

Laerma Unit represents the lowermost tectonic unit of the study area on top of which the rest of the units have been emplaced (Figs 1, 2). The largest outcrops of this unit are located in Stegna and Tsagarika, east of Archangelos, in Kavalina location west of Kolimbia and east of the Archipolis. In the area of Laerma (central Rhodes) it exceeds 1000 m in thickness. It corresponds to a clastic formation that comprises of alternations of clay, yellowish-brown to greenish pelites, calcareous sandstones and bioclastic limestones with turbiditic sedimentary structures. At the lower parts of this formation, interbedded conglomerate and agglomerate horizons that do not exceed 3-5 m in thickness exist, including angular ophiolithic elements, psammitic fragments and red pelites. Within this clastic formation, olistholiths are also observed with significant size variability that can reach a few tenths of meters in length and thickness. These olistholiths have probably originated either by green igneous rocks, by gypsum or by marly, micritic, pelagic limestone rich in plangtonic foraminifera (Globigerinidae, Globorotalidae) in horizons that do not exceed 5cm, or by sandstones or finally by clasts and a transferred rich benthonic fauna comprised of *Nummulites*, *Alveolines* etc. The thin platy limestones in the Laerma area seems to represent a calcareous intercalation within the pelitic – psammitic flysch matrix, that presently appears as discontinuous due to intense shearing that resulted in boudinage. The included microfauna determine a post – upper Eocene age, possibly lower Oligocene or Oligocene in general.

3.1.2. Archangelos Unit

The outcrops of the Archangelos Unit are subdivided in two areas since they present differences in their tectonic structure. The first area is located on the hills south and northeastern of the Archangelos settlement and in the greater region of Tsambika. Stratigraphically it can be divided in two sequences (Fig. 2), a lower volcanosedimentary one and an upper calcareous sequence. The lower one corresponds to a volcanosedimentary formation observed as a tectonic wedge within the calcareous sediments of the unit, located approximately 500-600 m southwest of the Archangelos settlement. This formation is known as the Koumouli formation (Mutti *et al.* 1970) named after the homonymous mountain in northern Rhodes studied thoroughly by Lekkas *et al.* (2002). It comprises of two distinct series, a lower one, which is characterized by alternations of pelites, tuffs and rarely sandstones and limestones, within which, bodies of green and purple volcanic rocks are observed in the form of altered pillow lavas, and an upper series which is characterized by

alternations of pelites, sandstones and bioclastic limestones. The density and the thickness of the carbonate intercalations is increasing towards the upper layers until its domination and contains a variety of fossils such as corals, sponges, echinoids, crinoids and brachiopods. These beds according to Lekkas *et al.* (2002) are representing the transitional beds towards the carbonate platform of the unit, which is also confirmed by their age (Middle – Upper Triassic). It appears that the lowermost of the beds were deposited on a shoal environment while the uppermost beds under biothermal conditions (Mutti *et al.* 1970, Harbury and Hall 1988).

The upper section of the unit in the Archangelos area, corresponds to a carbonate platform (Figs 1, 2), with thick-bedded white to grayish-white limestones and dolomites with Dasycladaceae, *Cladocoropsis mirabilis*, corals and fragments of echinoids and gastropods. In the Tsambika hill as well as in the Outhos location, dark grayish-white, pinkish, platy to massive Upper Cretaceous limestones dominate with rudists, Orbitolinidae and Textulariidae.

The second largest exposure of this unit is in the hilly area of Mesovouno, southeast of Arhipolis settlement. The difference with the Archangelos outcrop is that this one comprises of three large thrust sheets. The two lowermost are comprised of carbonate rocks and flysch while the third one is comprised of limestone. These three thrust sheets are located under the Profitis Ilias Unit (Figs 1, 2). In the areas of Mesovouno and Symiako where the lower thrust sheet outcrops, grayish whitish, white and dark massive or thick-bedded limestones are observed of Liassic age that are grading to thin platy filamentous limestones, the lowest part of which is of Toarsian – Oxfordian age (Fig. 3A). Unconformably to these limestones, medium-bedded platy to massive Upper Cretaceous limestones are observed containing fragments of corals, bryozoa, bivalves and algae. Near the top of the Mesovouni, bioclastic limestones are observed, possibly deposited in a shallow water – high energy environment (Harbury and Hall 1988) while the included microfauna such as *Nummulites* sp. *Discocyclina* sp. *Globigerapsis* and Alveolinidae, suggest open marine conditions of deposition. The aforementioned limestones are grading through small en-echelon faults to brown marly limestones and dark reddish siltstones that represent the lowest part of a flysch, the upper part of which is characterized by alternations of grey – greenish sandstones, polymict conglomerates and marls (Fig. 3B). The thickness of the flysch exceeds 120 m and a large percentage of the clastic material has originated by the erosion of an ophiolithic nappe.

The flysch in its turn is overlain by the intermediate thrust sheet which comprises of whitish to pinkish neritic limestones with rudists, algae, and corals. These limestones are grading through normal faults to flysch of greenish pelites and yellowish green sandstones. The upper imbrication presents the characteristics of the upper sections of the carbonate rocks of the first imbrication, however without the presence of flysch. Through a set of low-angle normal faults the upper thrust sheet is in contact with formations that are classified to the Profitis Ilias Unit.

The Archangelos unit seems to represent a shallow water sequence which is typical for a carbonate platform (Harbury and Hall 1988). At the end of the Liassic a change in deposition depth is recorded which seems not to de due to local subsidence of the platform but due to large scale tectonic events, as it has been recorded in neighbouring carbonate sequences such as Karpathos (Davidson 1974, Harbury and Hall 1988). It is interesting that a second subsidence event of the platform is observed during the Cenomanian that in combination with the absence of the Lower Cretaceous in all of the outcrops of the unit is indicative of significant uplift and erosion of platform sections, phenomena related to large scale extensional events (Harbury and Hall 1988).

Most researchers support that the Archangelos Unit can be compared to the Tripolitza Unit (Aubouin and Decourt 1970, Leboulenger and Matesco 1975, Papanikolaou *et al.* 1995) while Aubouin *et al.* 1976, suggest that it can be compared to the outcrops of the Kalilimni units in the island of Karpathos. However, the initiation of the flysch sedimentation in the Middle Miocene (Mutti *et al.* 1970), the presence of dark, reddish transitional beds, the frequent alternations in deposition depth that characterize the carbonate sequence (Harbury and Hall 1988), are indicative of significant differences to the Tripolitza Unit. Moreover, because these formations are

underlying the Profitis Ilias Unit (Pindos), the Archangelos Unit could be correlated either with the transitional units of Ethia type in Crete or with the Kalilimni Unit in the island of Karpathos (Auboin *et al.* 1976).

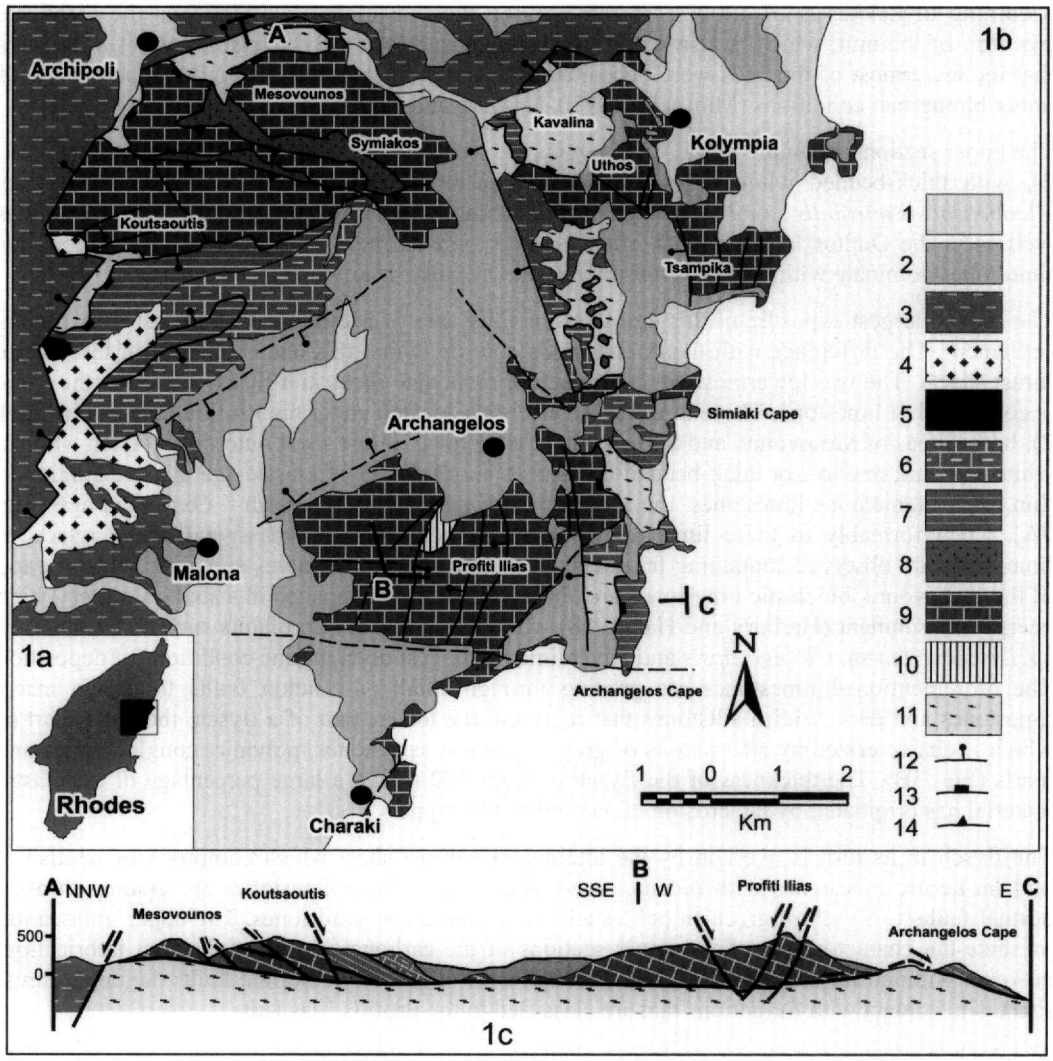

Figure 1 – (1a) The study area is located to the central eastern part of the Rhodes Island. (1b) Geological map of the Archangelos region. 1: Alluvial, 2: Asgourou Fm, 3: Pliocene clastic sediments, 4: Molasse, 5: Ophiolites, 6-7: Profitis Ilias Unit, 6: Upper Cretaceous platy limestones, 7: Platy limestones and radiolarites of Upper Triassic - Upper Jurssic age, 8-10: Archangelos Unit, 8: Flysch, 9: Limestones, 10: Volcanosedimentary sequence, 11: Laerma Unit, 12: High-angle normal fault, 13: Low-angle normal fault, 14: Thrust fault. (1c) Representative geological section of the study area where it is obvious that the upper nappes were emplaced over the Laerma Unit through an horizontal extensional fault

3.1.3. Profitis Ilias Unit

The largest outcrop of this unit is observed north of Malona while smaller outcrops are recorded in many locations as in Tsagarika and Kavalina and on the road from Archagelos towards the Stegna beach (Fig. 1).

It is a pelagic series of Upper Triassic – Upper Cretaceous age, of thin bedded pelagic limestones, radiolarites, pelites and chert nodules (Figs 2, 3D). A full stratigraphic column is recorded north of Malona in the Xerovouno hill where grey, brown-reddish, micritic, platy limestone with nodules and intercalations of greyish to black cherts, are followed by greyish to white, yellowish breccia limestones with intercalations of reddish pelites and dark or reddish chert. Frequently, the breccia limestones contain fragments of echinoderms, shells and algae, possible products of submarine gravitational slumps. This formation in the literature is described as the Elafokambos formation and its lower part in western Rhodes has a Karnian age from *Halobia stryciana* and *Halobia subreticulata* (Guernet 1974, Mutti *et al.* 1970). Above this formation, a sequence of 50 m thick reddish radiolarites with dark redish pelites and rarely marly limestones is found. Within this sequence a Valanginian age horizon with Calpionellidae is recorded. The latter is grading to thin platy grey yellowish or reddish micritic limestones (Fig. 3C) with marly limestone interbeddings, thin beds of greenish and reddish pelites and cherts that form the Senonian age Messaro formation (Mutti *et al.* 1970, Danelian *et al.* 2001)

Another important formation of this unit is located east of Arhangelos, near the coastline where grey to yellowish brown or reddish limestones, interbedded with cherts of Karnian – Lower Liass age (Orompelli and Pozzi 1967, Mutti *et al.* 1970), overlay the flysch sediments of Laerma. Furthermore, important outcrops are located along and towards the north of the road from Archangelos to Stegna where intensely fractured and folded thin platy limestones with chert intercalations of Senonian age are observed.

These outcrops indicate a low energy deposition environment and deep water. The Xerovouno radiolarites were deposited below CCD with depths that exceeded 2 km (Harbury and Hall 1988), while the transition to the carbonate sedimentation with calpionellidae and radiolarian in combination with the increase of carbonate beds during Cretaceous indicates a deepening of CCD level. This unit is considered to represent the eastern extension of the Pindos Unit in mainland Greece and Crete (Aubouin and Decourt 1970, Papanikolaou *et al.* 1995, Lekkas *et al.* 2002, Danelian *et al.* 2001).

3.1.4. Ophiolite unit

It is observed in the western section of the study area between Mesaros and Limnes and presents a limited surface outcrop (Fig. 1). It comprises of altered peridotites followed by reddish green radiolarites and pelites while the whole sequence exhibits intense fracturing. Although Mutti *et al.* (1970), suggest that these ophiolite masses are located under the formations of Profitis Ilias Unit, our mapping data do not confirm such a suggestion.

Geochronology with K-Ar in hornblend within these ophiolites in the northern and western Rhodes suggest ages ranging between 75 – 95 Ma with mean values of 87 Ma (Koepke *et al.* 2003), indicating the lower timescales of the Upper Cretaceous. Similar ages have been suggested for the Taurides ophiolites in southwestern Turkey and more specifically on the metamorphic sole of those nappes and on the doleritic veins included in the ophiolites. Moreover, Rhodes ophiolites exhibit many similarities to the Taurides ophiolites, on the basis of petrography and geochemistry of the trace elements and in their deposition environment. According to the above, Koepke *et al.* (2003) suggested that these ophiolites cannot be compared to the Cretan ophiolites but to the Cretaceous ophiolitic belt of the Taurides.

3.2. Molassic Sediments

These are located on the western and central parts of the study area (Fig. 1). They include greenish sandstones and polymict conglomerates with relatively well rounded clasts that probably have originated by the erosion of an ophiolithic nappe. These sediments lay unconformably on the Profitits Ilias Unit formations and are in contact with post-alpine sediments via normal faults.

3.3. Post-Alpine Formations

3.3.1. Formation of Pliocene Clastic Sediments

These sediments are observed to the north and west of the study area (Fig. 1). They consist of thick polymict conglomerates of terrestrial origin alternating with sandstones and clays. Within the latter, thin lignite horizons are observed. The greatest percentage of the clasts has derived from the erosion of Profitis Ilias nappe and the remaining has derived from the rest alpine units. Its age is considered as Pliocene and is possibly expanding towards the Upper Miocene.

3.3.2. Asgourou Formation

This formation is outcropping in the central and eastern section of the study area (Fig. 1). Its base is composed of medium cohesion mosaics, sandstones and pelites that exhibit significant lithofacial differentiations. The age of this series is Upper Pliocene - Lower Pleistocene. This series is overlaid by bioclastic limestones, marls and clays that were deposited in an open sea environment and have a Pleistocene age (Mutti *et al.* 1970, Meulenkamp *et al.* 1972, Lekkas *et al.* 2000).

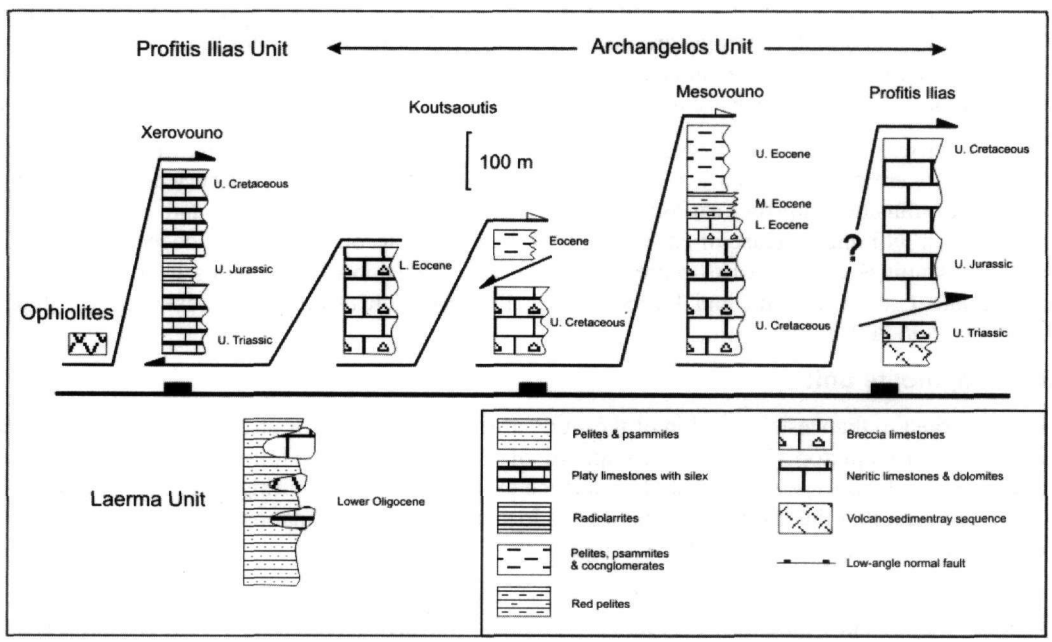

Figure 2 – The stratigraphic coloumns of the geotectonic units that outcrop in the Archangelos region and their tectonic relation

4. Tectonics

The principal characteristics of the tectonic structure of the study area are the following: a) all the aforementioned units tectonically overlay the Laerma unit through a tectonic contact that exhibits low angle or is near horizontal and b) the faults that bring the units in contact have an extensional character (Figs 1, 2, 3E).

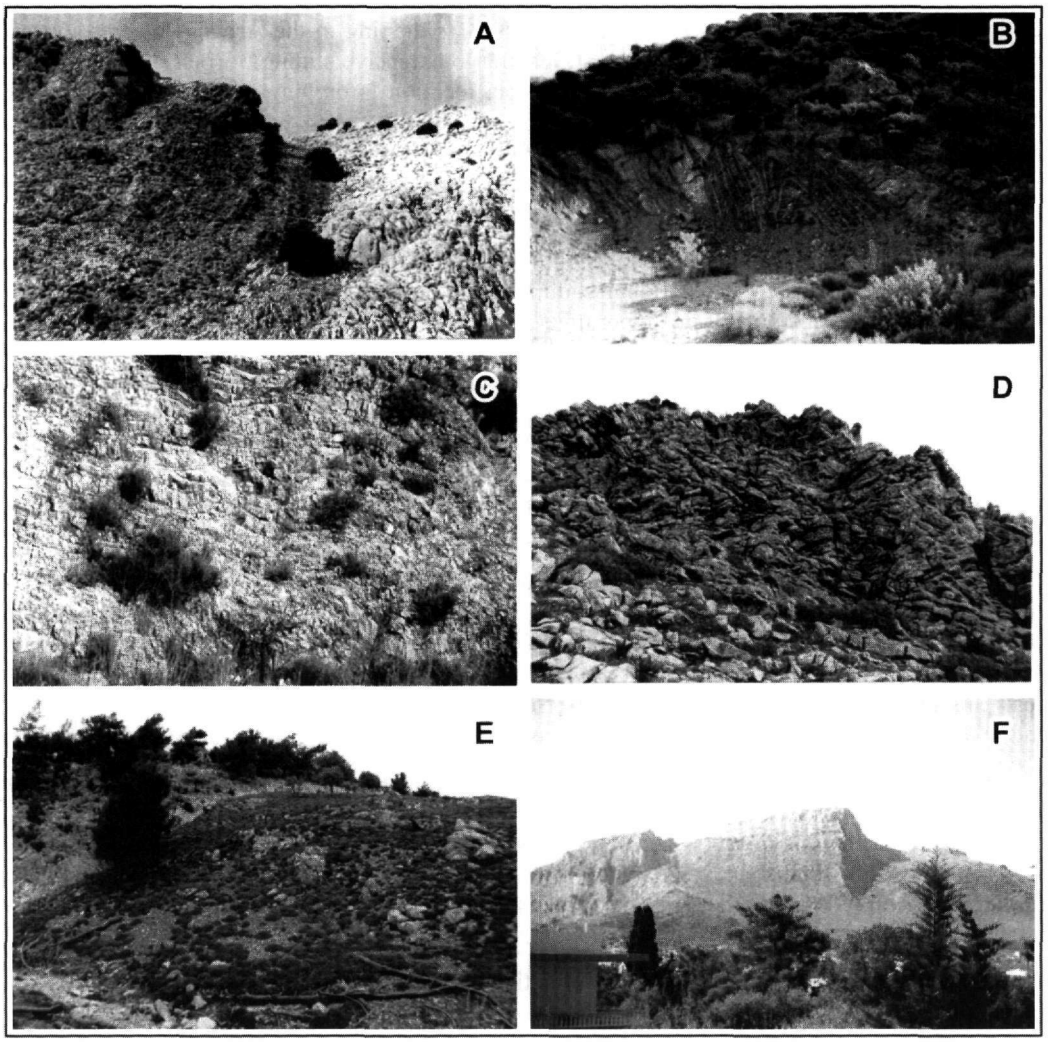

Figure 3 - At the Mesovouno hill, massive limestones of the Archangelos Unit, Liassic in age, are grading to thin platy filamentous limestones, the lowest part of which is of Toarsian – Oxfordian age. Unconformably to these limestones, Upper Cretaceous thick bedded limestones are observed (A). Alternations of greenish sandstones, polymict conglomerates and marls of the upper part of the flysch sequence of Archangelos Unit (B). Platy limestones of Upper Cretaceous in age of the Profitis Ilias (C). Folded Karnian platy limestones of the Profitis Ilias Unit (D). A high-angle normal fault separating the Archangelos Unit from the Profitis Ilias Unit (E). Extensional faults in the Profitis Ilias hill, south of Archangelos settlement (F)

As it can be seen in Fig. 1, the carbonates of Archangelos Unit and the pelagic sediments of Profitis Ilias are emplaced on top of the clastic sediments of Laerma Unit through a surface that has a general horizontal character or presents small dip towards various directions. This can be observed in Arhipolis area where the Archangelos limestones that build up Mesovouni are overlying the Laerma Unit through a tectonic contact that dips gently towards the SW. A similar geometry is recorded in the contact between Profitis Ilias Unit and Laerma flysch to the north of Malona. At Koumelo location, south of Stegna, the pelagic limestones of Profitis Ilias Unit overly the Laerma clastics through a surface with intermediate dip angles towards the east with a sense of shear the top to the east. In the area between Stegna and Arhangelos, the contact between the

neritic limestones of Arhangelos Unit with the flysch, is dipping in the Arhangelos area towards the west and at Stegna area towards the east, leading to extensive sliding of rock masses. Finally, in Kavalina area, this tectonic surface in Kolimbia location is dipping towards the east to SE, allowing the tectonic contact of the clastic sediments of the flysch with the Upper Cretaceous limestones of Archangelos Unit, while in Efta Piges it dips towards the W to SSW allowing the tectonic contact of pelagic limestones of the Profitis Ilias Unit with pelites and sandstones of the flysch.

The above observations lead to the conclusion that the emplacement of the upper nappes onto the Laerma flysch is related to gravitational sliding phenomena. Therefore, these emplaced nappes must be regarded as remnants of the upper units that were emplaced in their present locations after gravity sliding over the clastic sediments of Laerma Unit (Fig. 2). The fact that the age of the uppermost flysch horizons of Laerma Unit is Lower Oligocene and because the base of the molassic sediments has a Middle to Upper Oligocene age, leads to the conclusion that the time interval between Lower Oligocene and Mid – Upper Oligocene is the period when these movements were took place. Regarding the kinematics of this contact, it presents a general direction "the top to the ENE" mainly based on the study of the shear zones within the upper part of the clastics of Laerma Unit directly beneath this tectonic contact.

In the area of Koutsaoutis Mountain, north of Malona settlement, the tectonic contact between the Archangelos Unit and Profitis Ilias Unit is preserved (Figs 1, 3E). It is a high-angle normal fault, of a WSW –ENE strike dipping towards the SSE. Towards its western end it bounds the western limits of the Pleiocene post-alpine basin in the Apollonon area, in the western section of the study area. This fault is dissected by a later NNW-SSE striking fault of high dip angle towards the east that towards the north of Malona is covered unconformably by the Asgouros formation sediments.

An important variation is recorded between the fold axes directions observed within the aforementioned nappes and especially within the formations of Profitis Ilias Unit and those recorded in other regions of the island. It was noted that the principal strike directions were NW-SE to NNW-SSE forming an angle of 60°-90° to those described by Mutti *et al.* (1970) and Harbury and Hall (1988) in other regions of the island. This difference might be due to rotation of the study area during neotectonic deformation.

Another set of folds has a principal N-S direction and is probably related to a compressional deformation phase that was carried out after the deposition of Pleistocene sediments, possibly during Pleistocene. This deformation, created folds with similar directions within the molassic sediments and the Pleistocene formations in the Apollonon basin and the Laerma flysch as it is suggested by the folding of the tectonic contact between the upper units and the parautochtonous Laerma Unit. It is quite possible that this compressional phase could also be responsible for the normal faults with a mean N-S direction that are observed within the carbonates of Archangelos Unit in the Profitis Ilias area (Fig. 3F). These faults give the impression that they were created in order to enable the brittle rocks of the upper units to follow the folding pattern of the more ductile basement (Fig. 1c). As the Pleistocene sediments of Asgourou formation seal the aforementioned faults, we can suggest that these faults were active during the Upper Pliocene – Lower Pleistocene.

The general uplift of the region seems to be due to submarine reverse faults along the southeastern coastlines of the island causing gradual uplift of the area as it is suggested by the fossilized Upper Pleistocene beaches that are presently located in relief that exceed 500 m, e.g. at Profitis Ilias Arhangellou (Pirazzoli *et al.* 1989, Kontogianni *et al.* 2002). An additional result of this deformation could be the reverse fault north of Arhangelos where the carbonates of the Arhangelos Unit are overthrusted on Asouros formation sediments.

5. Discussion - Conclusion

Most researchers agree that the lowest tectonic unit on the island is the metamorphosed unit of Lindos (Aubouin and Decourt, 1970) that corresponds either to the Ionian Unit or the Plattenkalk Unit in Crete (Orombelli and Pozzi 1967, Leboulenger and Matesco 1975, Papanikolaou *et al.* 1995). This unit is tectonically overlain by a "wild flysch" which was named after Papanikolaou *et al.* 1995 and Lekkas *et al.* 2000, as Laerma Wild Flysch or Laerma Unit. This unit has a dominant outcrop in the central part of the island of Rhodes and represents the deepest unit in the study area.

In southwestern Rhodes the unit of Attaviros – Akramiti dominates and according to most researchers the sequence of the lithofacies and biofacies are similar to the Ionian Unit in mainland Greece and Crete (Renz 1929, 1955, Orombelli and Pozzi 1967, Mutti *et al.* 1970, Aubouin and Dercourt 1970, Leboulenger and Matesco 1975). On the contrary, Harbury and Hall (1988), suggested that the paleogeographical region was further inwards from the Archangelos Unit intervening between the latter and the pelagic unit of Profitis Ilias, which was separated from the Pindos Unit suggesting that it comprised a second deep basin further inwards to that of Pindos with the platform of the Archangelos Unit separating the two.

The Archangelos unit comprises of a thick series of massive to thin bedded limestones aged Upper Triassic – Lower Eocene and of a flysch of Middle to Upper Eocene age (Mutti *et al.* 1970, Leboulenger and Matesco 1975). As the previous unit, this unit is also overlying the Wild Flysch of Laerma. Initially Renz (1929, 1955) considered it to belong to the Parnassos- Giona Unit in Mainland Greece. However, Aubouin and Dercourt (1970), Leboulenger and Matesco (1975) and Papanikolaou *et al.* (1995), mentioned that its tectonic location under Profitis Ilias Unit (Pindos unit) and the Eocene age of the upper horizons of the carbonate series allow to suggest that it corresponds to the Gavrovo – Tripolitza unit. In this present paper, we suggest that this unit can be correlated with the transitional units of Ethia type, having a depositional environment near the inner border of the Gavrovo – Tripolitza platform unit which is affected by intense extensional events that are probably related to the opening of the basin of Profitis Ilias, located further inwards.

The Profitis Ilias Unit comprises of exclusively pelagic sediments such as thin platy limestones with chert intercalations, reddish marls and reddish radiolarites of an Upper Triassic – Upper Cretaceous age (Mutti *et al.* 1970), which corresponds to the Pindos Unit. The confirmation of the Upper Jurassic age of the radiolarites and the presence of the carbonate horizon with *Calpionelles* (Danelian *et al.* 2001) appears to support this suggestion.

The uppermost nappe in the island of Rhodes is composed of ophiolithic rocks that are overlying the Profitis Ilias Unit (Aubouin and Dercourt 1970, Leboulenger and Matesco 1975, Papanikolaou *et al.* 1995). On the contrary, Mutti *et al.* (1970) suggested that the ophiolites are located on top of the Arhangelos Unit and under the Profitis Ilias Unit. These ophiolite masses were interpreted as remnants of the Sub-Pelagonian zone nappe (Aubouin and Dercourt 1970) or as remnants of the Pindos Ocean (Papanikolaou *et al.* 1995).

Recent geochronological data suggest that the Rhodes ophiolites are of Upper Cretaceous age and must correlate to the ophiolites that are observed in southwester Turkey in the nappe region of Lycian (Koepke *et al.* 2002). This fact brings to light the necessity for the correlation of the Dodecanese geotectonic units to those in southwestern Turkey and especially the Lycian nappes and the parautochthonous metamorphic masses of Baydaglari and Menderes which will allow the decoding of the tectonic structure and the solution to the palaeogeographical representations problem in this section of the Alpine orogenetic belt.

All these units are emplaced through a low-angle extensional fault on the Laerma flysch Unit dated as Lower Oligocene. The emplacement of the nappes on the relatively autochthonous unit of the study area was performed in upper tectonic levels conditions and might be due to gravitational sliding.

6. Acknowledgments

The authors wish to express thanks to the reviewers for their constructive comments and suggestions.

7. References

Aubouin, J., and Dercourt, J., 1970. Sur la geologie de l' Egee: regard sur le Dodecanese meridional (Kassos, Karpathos, Rhodes), *Bull. Soc. Geol. Fr.,* (7), XII, 455-472.

Aunouin, J., Bonneau, M., and Davidson, J., 1976. Contribution a' la geologie de l' arc egeen: l' ile de Karpathos, *Bull. Soc. Geol. Fr.*, (7), XVIII, 2, 385-401.

Danelian, T., Bonneau, M., Cadet, J.P., Poisson, A., and Vrielynck, B., 2001. Palaeogeographic and palaeoceonographic implications of new and revised bio-chronostratigraphy constraints from the Profitis Ilias unit (Rhodes, Greece), *Bull. Geol. Soc. Greece*, 34, 2, 619-625.

Guernet, C., 1974. Le massif de l'Elaphocampos, l'ile de Rhodes et les Hellenides, *C. R. Acad. Sc. Paris,* 278, Serie D, 813-815.

Harbury, N., and Hall, R., 1988. Mesozoic extensional history of the southern Tethyan continental margin in the SE Aegean, *J. Geol. Soc., London*, 145, 283-301.

Koebke, J., Seidel, E., and Kreuzer, H., 2003. Ophiolites on the Southern Aegean islands Crete, Karpathos and Rhodes: composition, geochronology and position within the ophiolite belts of the Eastern Mediterranean, *Lithos* 65, 183– 203.

Kontogianni, V.A., Tsoulos, N., and Stiros, S., 2002. Coastal uplift, earthquakes and active faulting of Rhodes Island (Aegean Arc): modeling based on geodetic inversion, *Marine Geology* 186, 299-317.

Leboulenger, P., and Matesco, S., 1975. Contribution a l' etude geologique de l' arc egeen: l' ile de Rhodes, *Theses 3e cycle*, Universite P. et M. Curie, Paris.

Lekkas, E., Papanikolaou, D., and Sakellariou, D., 2000. Neotectonic map of Greece, 1:100.000 scale: Sheet Rhodos, *European Center on Prevention and Forecasting of Earthquakes, Earthquaking Planning and Protection Organization.*

Lekkas, E., Danamos, G, Skourtsos, E., and Sakellariou, D., 2002. Position of the Middle Triassic Tyros Beds in the Gavrovo-Tripolis Unit (Rhodes Island,Dodecanese, Greece), *Geologica Carpathica*, 53/1, 37-44.

Meulenkamp, J., Mulder, F., and van de WeerD, A., 1972. Sedimentary history and paleogeography of the Late Cenozoic of the island of Rhodos, *Z. Deutsch. Geol. Ges.,* 123, 2, 541-553.

Mutti, E., Orombelli, G., and Pozzi, R., 1970. Geological Studies of the Dodecanese Islands (Aegean Sea). Geological map of the Island of Rhodes and Explanatory Notes, *Ann. Geol. des Pays Helleniques,* 22, 77-226.

Orombelli, G., and Pozzi, R., 1967. Studi geologici sulle isola del Dodecaneso (Mare Egeo). V-Il Mesozoico nell' isola di Rodi (Grecia), *Riv. Ital. Paleont. Strat.,* 73, 409-536.

Papanikolaou, D., Lekkas E., and Sakellariou, D., 1995. Tectonic units and terrane analysis in Rhodos and adjacent Dodekanese islands, Greece, *XV Congr. Carpatho-Balcan Geol. Assoc., Symp. Tectonostratigraphic Terranes in CB Region, Athens, September 17-20, 1995, Abstracts*, 20.

Pirazzoli, P., Montogianni, L., Saliege, J., Segonzac, G., Thommeret, Y., and Vergnaud-Grazzini, C., 1989. Crustal block movement from Holocene shorelines: Rhodes Island (Greece), *Tectonophysics*, 170, 89-114.

Renz, C., 1929. Geologische Untersuchungen auf den Inseln Cypern und Rhodos, *Prakt. Acad. Athenes*, 4, 301-314pp.

Renz, C., 1955. *Dia vorneogene Stratigraphie der normalsedimentaeren Formationen Griechenlands*, Inst. Geol. Subsurf. Res., 637pp, Athen.

Δελτίο της Ελληνικής Γεωλογικής Εταιρίας τομ. XXXX, 2007
Πρακτικά 11ου Διεθνούς Συνεδρίου, Αθήνα, Μάιος 2007

Bulletin of the Geological Society of Greece vol. XXXX, 2007
Proceedings of the 11th International Congress, Athens, May, 2007

STRESS INTERACTION BETWEEN THRUST FAULTS ALONG THE SW HELLENIC ARC (GREECE)

Messini A. D.[1], Papadimitriou E. E.[1], Karakostas V. G.[1], and Baskoutas I.[2]

[1] *Geophysics Department, University of Thessaloniki, GR54124 Thessaloniki, Greece, anna.messini@gmail.com, ritsa@geo.auth.gr, vkarak@geo.auth.gr*

[2] *Geodynamic Institute, National Observatory of Athens, GR11810 Athens, Greece*

Abstract

The occurrence of strong earthquakes (M≥6.3) and the evolution of the stress field along the southwestern part of the Hellenic arc since 1959 are examined by the calculation of Coulomb stress changes. The study area is characterized by low angle thrust faults and high seismicity as being part of the subduction interface. Coulomb stress changes were calculated assuming that earthquakes can be modeled as static dislocations in an elastic half–space, considering the co–seismic slip during strong events and the slow tectonic stress build–up along major fault segments due to the movements of the tectonic plates. The ruptures are modeled taking into account the strike, dip, and rake appropriate to each event examined. It is evaluated whether the stress changes brought a given earthquake closer to, or farther away from, failure. It was found that the majority of the events (strong and smaller) are located in stress enhanced areas.

Key words: *Coulomb stress, thrust faulting, interaction.*

Περίληψη

Μελετάται η γένεση ισχυρών σεισμών (M≥6.3) και η εξέλιξη του πεδίου των τάσεων από το 1959 στο ΝΑ τμήμα του Ελληνικού Τόξου, υπολογίζοντας τις μεταβολές των τάσεων Coulomb. Η περιοχή μελέτης χαρακτηρίζεται από μικρής γωνίας κλίσης ανάστροφα ρήγματα και υψηλή σεισμικότητα καθώς είναι τμήμα της ζώνης κατάδυσης. Οι μεταβολές των τάσεων Coulomb υπολογίστηκαν θεωρώντας ότι οι σεισμοί προσομοιάζονται ως στατικές εξαρμώσεις σε ελαστικό ημιχώρο, λαμβάνοντας υπόψη τη σειμική ολίσθηση και την αργή τεκτονική φόρτιση των σημαντικών ρηγμάτων που οφείλεται στις κινήσεις των τεκτονικών πλακών. Οι διαρρήξεις προσομοιώνονται με βάση την κατάλληλη παράταξη, κλίση και γωνία ολίσθησης για κάθε σεισμό που εξετάζεται. Εξετάζεται αν οι μεταβολές της τάσης ευνόησαν η εμπόδισαν τη γένεση δεδομένου κάθε φορά σεισμού. Βρέθηκε πως η πλειοψηφία των σεισμών (ισχυρών και μικρότερων) εντοπίζεται σε περιοχές θετικών μεταβολών των τάσεων Coulomb.

Λέξεις κλειδιά: *Τάσεις Coulomb, ανάστροφη διάρρηξη, αλληλεπίδραση.*

1. Introduction

The most prominent feature of the broader Aegean region (Fig. 1) is the Hellenic arc and the associated Benioff zone, formed by the subduction of the Eastern Mediterranean oceanic plate beneath

the Aegean micro–plate (Papazachos and Comninakis 1970). Reliable fault plane solutions allowed a better understanding of the active tectonics in the study area since 1960. Thrust faulting dominates along the arc, with a NE–SW direction of the axis of maximum compression, laterally bounded by the dextral Cephalonia Transform Fault (CTF) to the west and Rhodes sinistral fault to the east (Papazachos 1961). Govers and Wortel (2005) refer to these strike slip faults as Subduction–Transform Edge Propagator (STEP) faults, and suggest that they are formed at the termination of subduction trenches and are a geometric consequence that allows subduction to continue.

The Hellenic subduction zone is characterized by high seismicity along the arc. Historical information evidences the occurrence of large events ($M_s \geq 7.5$) at the southwestern part of the arc around the island of Crete, such as the 62 A.D., 251, 1494, and 1810 events of M7.5, the 1856 event with M7.7, and the 365 A.D. event of M 8.3 (Papazachos and Papazachou 2003). Severe damage both in the natural and constructed environment and loss of life were the consequences of these events occurrence. This high seismic activity necessitates seismic hazard assessment in the study area that is attempted here by resolving the evolution of the stress field and inspecting possible triggering of the next events in a sequence of events.

Earthquakes in sequence generally are not independent but each one is affected both by tectonic loading and stress changes caused by coseismic slip in prior events (Scholz 1990). There is a plethora of studies exploring the phenomenon of triggering of subsequent earthquakes by static or dynamic stress changes during the past decade (see reviews by Harris 1998, King and Cocco 2001). Many researchers focused their studies on strike slip faults such as the San Andreas, North Anatolian and Eastern California Shear zone since the pattern of stress transfer does not vary greatly with depth. The majority of thrust earthquakes on the other hand occur in subduction zones offshore, where seismic and geodetic coverage is often poor. Despite these limitations, previews studies of subduction earthquakes (Dmowska *et al.* 1988, Lin and Stein 2004, among others) pointed out the important role of stress interaction in such tectonic environments.

In this study, we explore the Coulomb stress changes (ΔCFF) associated with strong earthquakes ($M \geq 6.3$) and the evolution of the stress field along the southwestern part of the Hellenic arc since 1959, when more reliable information on earthquake source parameters is available. These earthquakes are included in the stress evolution model along with the long–term tectonic loading on the major thrust faults of the area. We aim to examine if the coseismic and cumulative changes in stress can explain the spatial and temporal occurrence patterns of past strong earthquakes.

2. Method

Static stress changes associated with strong and large earthquakes influence the space–time pattern of the following seismicity (Deng and Sykes 1997, Harris 1998 and references therein). The advantage of using stress changes is that often absolute values of stress are not known, but stress change values can be calculated from information about the geometry and slip of an earthquake rupture. The method introduced by Deng and Sykes (1997) is used in the present study to calculate stress changes associated to all of the events examined. According to this method, stress is considered a tensor quantity that varies in time and space, with the Earth approximated as homogenous elastic half space. Cumulative changes in stress are assumed to arise from tectonic loading generated by the plate motions and displacements on faults associated to strong earthquakes. Interseismic stress accumulation is modeled by introducing "virtual negative displacements" along major faults in the entire region under study, using the best available information on long term slip rates. This virtual dislocation has the same size and orientation as the fault segment in question, but with the opposite sense of slip. The value of slip on the virtual dislocation is incremented in time according to the long–term slip rate along the fault. The fault segment is considered to slip constantly from the bottom of the seismogenic layer to infinite depth. Hence tectonically induced stress builds up in the vicinity of faults during the interseismic periods. Stress buildup is released wholly or in part during the next strong earthquake, with real displacements on given faults that

are considered positive in the model. Changes in stress associated with strong earthquakes are modeled by introducing certain co–seismic displacements on ruptured fault segments in elastic half–space and adding the changes in the components of the stress tensor together as they occur in time.

Earthquakes occur when stress exceeds the fault strength. The closeness to failure is quantified by using the change in Coulomb failure function (ΔCFF) (modified from Scholz 1990). It depends on both changes in shear stress, $\Delta\tau$, and normal stress, $\Delta\sigma$:

Equation 1

$$\Delta CFF = \Delta\tau + \mu'\Delta\sigma$$

Here μ' is the apparent coefficient of friction and its value was chosen to be equal to 0.4 and considered sufficient throughout the calculations (King *et al.* 1994, Lin and Stein 2004). Bird and Kagan (2004) use a value of 49GPa for subduction zones in an effort to encompass the presence of both crust and mantle rocks, which is also adopted in the present study. The change in shear stress, $\Delta\tau$, is positive for increasing shear stress in the direction of relative slip on the observing fault while $\Delta\sigma$ is positive for increasing tensional normal stress. When compressional normal stress on a fault plane decreases, the static friction across the fault plane also decreases. Both positive $\Delta\tau$ and $\Delta\sigma$ move a fault toward failure while negative values of $\Delta\tau$ and $\Delta\sigma$ move it away from failure. Therefore, a positive value of ΔCFF for a particular fault denotes an increased likelihood that it will rupture in an earthquake.

3. Fault plane solutions and major faults

Reliable fault plane solutions (FPS) of the earthquakes that occurred along the southwestern Hellenic arc were collected from previous publications and CMT Harvard solutions (Table 1) and are shown as lower hemisphere equal area projections in Figure 1, which evidences the dominancy of thrust faulting in the study area. Papazachos *et al.* (2001) used seismological and geological data in order to determine the properties of the faults where the known major (M≥6.0) shallow (depth<40 km) earthquakes have occurred since 480 B.C. (shown by their code names in Fig. 1). The belt of low angle thrust faults along the Hellenic arc, strikes from NW to SE parallel to the coastline and dips to the NE following the Benioff zone. Shallow dipping mechanisms are characteristic of subduction zones and are related to the motion of the overriding lithosphere. The axis of maximum compression along the arc has a NE–SW direction (Fig. 1). Information on reliable fault plane solutions and topography as well as the above mentioned information was used in the present study in order to define the location and geometry of the faults associated with each event (indicated by the earthquake occurrence year in Figure. 1) as well as the faults across which the tectonic loading is accommodated (IFS and CFS in Fig. 1).

Table 1 – Information on the available fault plane solutions for events of M≥4.5 that occurred in the study area since 1959. 1. Papazachos and Papazachou (1997), 2. McKenzie (1972), 3. Kiratzi and Langston (1989), 4. McKenzie (1978), 5. Papadimitriou (1993), 6. Taymaz *et al.* (1990), 7. Benetatos *et al.* (2004), 8. CMT Harvard solutions, 9. Louvari (2000)

Origin			Epicenter		Depth		Mechanism (Deg)			Ref
Year	Date	Time	Lat	Lon	km	M	strike	Dip	Rake	
1959	05/14	06:36:56	35.00	24.72	39	6.3	309	35	99	1
1965	04/09	23:57:02	35.13	24.31	39	6.1	301	18	98	1
1969	06/12	15:13:31	34.40	25.00	19	6.1	294	29	105	2
1972	05/04	21:39:57	35.10	23.60	40	6.5	309	18	89	3
1973	01/05	05:49:18	35.72	21.73	42	5.6	306	30	82	4
1973	11/29	10:57:44	35.18	23.75	22	6.0	283	38	97	5

1977	08/18	09:27:41	35.32	23.43	13	5.6	265	13	62	6
1977	09/11	23:19:19	34.90	23.00	16	6.3	295	40	95	5
1979	05/15	06:59:23	34.54	24.50	35	5.7	253	17	65	6
1983	03/19	21:41:39	34.68	25.33	65	5.6	358	39	131	8
1984	06/21	10:43:46	35.40	23.30	40	6.2	322	16	114	5
1985	04/21	08:49:42	35.63	22.01	25	5.2	149	50	78	7
1995	12/07	18:00:53	34.73	23.94	15	5.6	319	6	123	8
1995	12/10	03:27:50	34.76	23.98	17	5.3	289	22	75	8
1997	10/13	13:39:39	36.44	22.16	32	6.4	322	19	108	9
1997	11/05	12:22:53	34.90	24.00	22	5.5	309	6	108	9
1999	04/17	08:17:58	36.03	21.59	27	5.3	172	59	95	7
2000	02/22	11:55:31	34.95	25.38	20	5.0	92	71	68	7
2000	05/24	10:01:44	35.80	21.95	18	5.5	111	80	63	7
2004	03/28	14:54:48	35.57	22.99	55	4.7	310	31	97	8
2004	11/04	06:22:40	35.71	23.03	85	5.2	186	48	58	8

4. Rupture models

Earthquakes of M≥6.3 that occurred since 1959 in the study area are included in the stress evolutionary model. Starting year and cutoff magnitude where selected based on the fact that reliable fault plane solutions derived by waveform modeling exist for earthquakes of M≥6.3 since 1959 in the area of Greece.

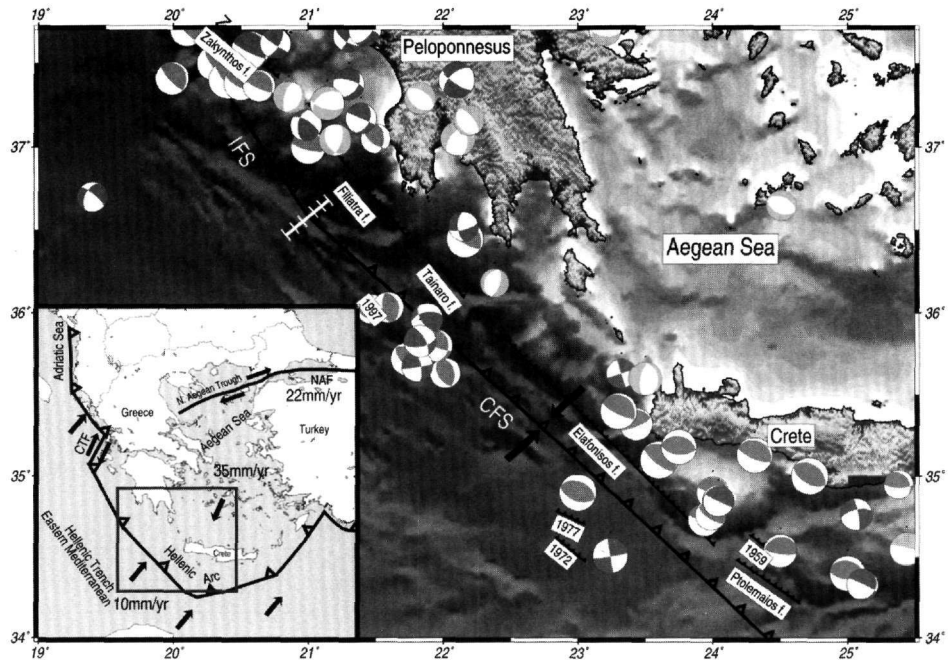

Figure 1 – Major faults along with the focal mechanisms of strong and moderate earthquakes in the studied area. Inset: Seismotectonic properties of the Aegean and surrounding regions. (IFS: Ionian Fault Segment; CFS: Crete Fault Segment; CTF: Cephalonia Transform Fault; NAF: North Anatolian Fault). Arrows indicate relative plate motions (After Papazachos 1999 and McClusky *et al.* 2000)

The rupture zones are simplified and approximated by rectangular planes. Three parameters essential to the model application are fault length, width, and average displacement. Therefore, the cal-

culation of the main rupture dimensions and the average coseismic slip are necessary. The distribution of slip is non–uniform along a fault, but detailed source models are not necessary when calculating the far field stress distributions (King and Cocco 2001). Thus, uniform average slip is adequate for ΔCFF determination, calculated using a scaling law by Papazachos *et al.* (2004) for dip–slip subduction faulting:

Equation 2

$$\log u = 0.64M - 2.56$$

Since all faults are offshore and geological data are not available to determine fault length, it was determined by the equation (3) (Papazachos *et al.* 2004) valid for subduction earthquakes:

Equation 3

$$\log L = 0.55M - 2.19$$

The rupture zones of subduction thrust earthquakes do not propagate all the way to the surface at the trench and their down–dip termination occurs at depths that vary between 40 and 60km (Scholz 1998). For the Hellenic subduction zone rupture terminates at 35 to 50 km (Papazachos *et al.* 2000, Laigle *et al.* 2004, Papadimitriou and Karakostas 2005). For an arc with low seismic coupling, such as the Hellenic arc, earthquakes tend to have small rupture zones and the zones of high moment release are small isolated patches on the subduction interface (Scholz 1990). In an effort to distinguish large and small earthquakes, Scholz (1982) stated that the large ones propagate throughout the brittle crust and they can be represented as a rectangular rupture with one edge at the free surface. Small earthquakes on the other hand can be represented as circular sources in an elastic medium. These observations led us to conclude that a constraint had to be set concerning fault width.

The ability of a thrust earthquake to promote failure along strike depends on its length/width (L/w) ratio (Lin and Stein 2004). Large (M>7) thrust earthquakes become longer along strike because their down–dip extent is limited by the finite depth of the brittle elastic crust, thus L/w>1. All subduction earthquakes in our sample with magnitudes $6.3 \leq M \leq 6.6$ are considered small earthquakes, thus, we set the constraint $L/w \approx 1$. The earthquake source parameters for applying the evolutionary model are given in Table 2.

Table 2 – Source parameters of M≥6.3 earthquakes that are included in the stress evolutionary model [1. Papazachos and Papazachou (1997), 2. Kiratzi and Langston (1989), 3. Papadimitriou (1993), 4. Louvari (2000)]

Date	Lat (N)	Long (E)	Depth (km)	L (km)	W (km)	M	u (cm)	Mechanism			Ref
								Strike	Dip	Rake	
14/05/59	35.00	24.72	39	19	12	6.3	17.8	309	35	99	1
04/05/72	35.10	23.60	40	27	26	6.5	24.0	309	25	89	2
11/09/77	34.90	23.00	16	19	12	6.3	17.8	295	40	95	3
13/10/97	36.45	22.16	32	21	21	6.4	19.9	322	25	108	4

5. Geometry and long term slip rate constraints on major faults

In order to incorporate tectonic loading at the subduction front in our stress evolution model we introduce two major thrust fault segments, along the subduction interface, where we consider the tectonic loading. These are hereafter mentioned as the Ionian Fault Segment (IFS: W part of the arc) and the Crete Fault Segment (CFS: SW part of the arc) and are shown in Figure 1. Assuming that all thrust earthquakes along the arc occur on the plate interface, the distribution of moderate earthquakes (M≥4.5) and their fault plane solutions are used along with local topography in order

to define the geometry of these fault segments. Information from recent publications on the geometry of the subduction zone was also taken into account. Strike and location was constrained by the distribution of M≥4.5 earthquakes and ocean bottom topography. A dip of 25° was assigned to the IFS since most of the fault plane solutions of earthquakes in that area show fault planes with a dip ranging from 17° to 25°. The CFS is shallower than the IFS (Papazachos *et al.* 2000, Laigle *et al.* 2004, Meier *et al.* 2004, Papadimitriou and Karakostas 2005), and its dip is considered equal to 20° (Papadimitriou and Karakostas, 2005), and the faulting type along the plate interface as pure thrust (rake: 90°) on both fault segments (Table 3).

The available information on the kinematics of the Hellenic is used for the definition of the long-term slip constraint. Many models have been proposed concerning the number of plates involved in the formation of the subduction zone and the orientation and proportion of the relative movements (e.g., Taymaz *et al.* 1991). Seismological (fault plane solutions, seismic moment release rates) and geodetic (Global Positioning System–GPS, Satellite Laser Ranging–SLR) data have been used by various researchers in order to determine the direction and the velocity of these movements.

Reference is given briefly in several previous works dealing with the kinematics in this part of the Hellenic Arc, since there is a plethora of published studies and geodetic data that we cannot ignore. We focus on geodetic results with a reference frame fixed on Eurasia.

Kahle *et al.* (1995) obtained a SW–oriented movement of SW Greece with an average velocity of 30mm/yr, the rates being increasing from the area south of the central Ionian Islands to the southwestern tip of Peloponnesus reaching 40mm/yr. Le Pichon *et al.* (1995) suggested that the Aegean moves with a velocity of about 38mm/yr with respect to Africa. Papazachos and Kiratzi (1996) estimated 13 mm/yr crustal shortening along the outer part of the Hellenic arc with the use of seismological data. Davies *et al.* (1997) using GPS measurements observed that trench ward velocity increases towards the Western Hellenic arc from 30 mm/yr in NE Aegean to 50 mm/yr in SW Peloponnesus. Reilinger *et al.* (1997) based on GPS measurements of crustal motions for the period 1988-1994 and available SLR data, and Lundgren *et al.* (1998) along with additional SLR data obtained a convergence velocity at 33 to 36 mm/yr in the southern part of the arc and a velocity of 35 mm/yr in the western Hellenic arc. Papazachos (1999) estimated trench ward velocity equal to 30-35 mm/yr using seismological and geodetic data.

Table 3 – Information on the major fault segments introduced in the stress evolutionary model to incorporate tectonic loading

No	Fault name	Center		Strike deg	Dip deg	Rake deg	L km	Slip mm yr^{-1}
		Lat	Long					
1.	Ionian Fault Segment (IFS)	37.20	20.49	325	25	90	167	13
2.	Crete Fault Segment (CFS)	35.29	22.7	312	20	90	410	4.5

Cocard *et al.* (1999) based on GPS measurements and obtained a maximum rate along the SW part of Peloponnesus of the order of 40mm/yr decreasing to 35mm/yr on the island of Crete. McClusky *et al.* (2000) presented GPS measurements for the period 1988–1997 and concluded that the largest relative motions across plate boundaries occur along the Hellenic Trench at 35±1 mm/yr with respect to Eurasia and Africa moves to the north at 5.4±1 mm/yr with respect to Eurasia. Kreemer and Chamot-Rooke (2004) calculated a continuous velocity and strain rate field using published GPS data and suggested that the Aegean block moves consistently at 33 to 34 mm/yr towards the SW in an Africa-Eurasia reference frame.

It is well recognized that only part of the total amount of tectonic loading due to the plate convergence is released seismically. Some sections of plate boundaries are deficient in their moment release as compared with plate tectonic estimates. The contribution of seismicity to the convergence

of the Aegean and Arabian plates has been found to be small indicating that this subduction is occurring largely aseismically. The western part of the arc seems to have a higher seismic coupling coefficient than the southern part of the arc. The first authors to recognize the aseismic nature of the southern part of the Aegean were Galanopoulos (1967) and Ergin (1966). Jackson and McKenzie (1988) suggest that only 10% of the upper crustal deformation is taken up seismically in the southwestern part of the arc and 30-35 % in the western part. Papazachos and Papazachou (2003), pointed out that 30 % of total convergence rate at 45 mm/yr is seismic, resulting in 13.5 mm/yr of seismic slip. Papazachos and Kiratzi (1996) computed a mean deformation velocity, in terms of seismic energy release, of 12 mm/yr in the western part of the arc. Papadimitriou and Karakostas (2005) constrained seismic coupling to 10 % in the SW part of the arc. Considering these observations we assume seismic slip to be 13 mm/yr in the western part of the arc and 4.5 mm/yr in the southwestern part of the arc.

6. Coseismic stress changes

In Figure 2 the coseismic stress changes associated with four strong events occurred during 1959-2005 are shown. In each part of the figure we show thrust fault plane solutions of all the subsequent earthquakes and plot the ones with differences in strike, dip and rake up to 30° using black color, taking into account the 20° error in the determination of focal mechanisms. The rest of the subsequent thrust fault plane solutions are shown in light gray and the focal mechanism of the next strong event is shown in dark gray. Dark gray regions denote negative changes in CFF and inferred decreased likelihood of fault rupture (stress shadows). Light gray regions represent positive ΔCFF and increased likelihood of fault rupture (stress bright zones). It must be mentioned that stress is a tensorial quantity so it depends not only on the source fault geometry and slip, but also on the geometry and rake of the target (receiver) faults. Thus shadow zones and bright zones must be viewed in the context of specific styles of fault slip, i.e., strike, dip, and rake.

Coulomb stress changes are calculated according to the geometry of the target fault, which is the fault of the subsequent strong earthquake in our sample, and at the appropriate depth. For thrust faulting the stress change is depth–dependent (Lin and Stein 2004) and thus the down–dip geometry of the source fault and the depth of receiver faults become essential to Coulomb analysis. Following King *et al.* (1994) who found that seismic slip peaks at mid–depths in the seismogenic zone we evaluated the mid–depth by studying the depth distribution of all moderate thrust earthquakes of our data set (Table 1). In the SW part of the arc focal depths of thrust events range from 3 to 40 km, thus sampling depth was chosen to 20 km.

Considering this, the coseismic stress changes associated with the 14 May 1959 (*M* 6.3) event are calculated according to the faulting type of the 1972 earthquake (Fig. 2A). One subsequent event with similar fault plane solution was brought closer to failure (April 1965, *M* 6.1) and two events (1969, 1972) were not inhibited. The coseismic stress changes associated with the earthquake on 4 May 1972 (*M* 6.5) are added to the previous ones and calculated according to the faulting of the third earthquake in 1977 (Fig. 2B). All subsequent thrust earthquakes with similar to the target fault focal mechanisms located around the 1972 epicenter, one of them being the next strong earthquake in our sample (September 1977, *M* 6.3), are enhanced. The August 1977 event having a different orientation than the target fault lies in the borders between stress shadow and stress bright zone and the January 1973 event is also not inhibited. In Figure 2C the coseismic stress changes associated with the earthquake of 11 September 1977 (*M* 6.3) are added to the stress changes associated to the previous events and resolved on the fault connected with the fourth strong earthquake in 1997. This earthquake was not inhibited by the accumulated coseismic stress changes, along with four other events (1983, 1985, and two in 1995), while two of the subsequent earthquakes were enhanced (1979 and 1984). Figure 2D shows the coseismic stress changes associated with all four strong shocks computed according to the faulting type of the CFS. Three subsequent earthquakes (1997 and two in 2004) are located in stress enhanced areas, two more are not inhibited to fail (both in 2000), while one event lies in a stress shadow (1999).

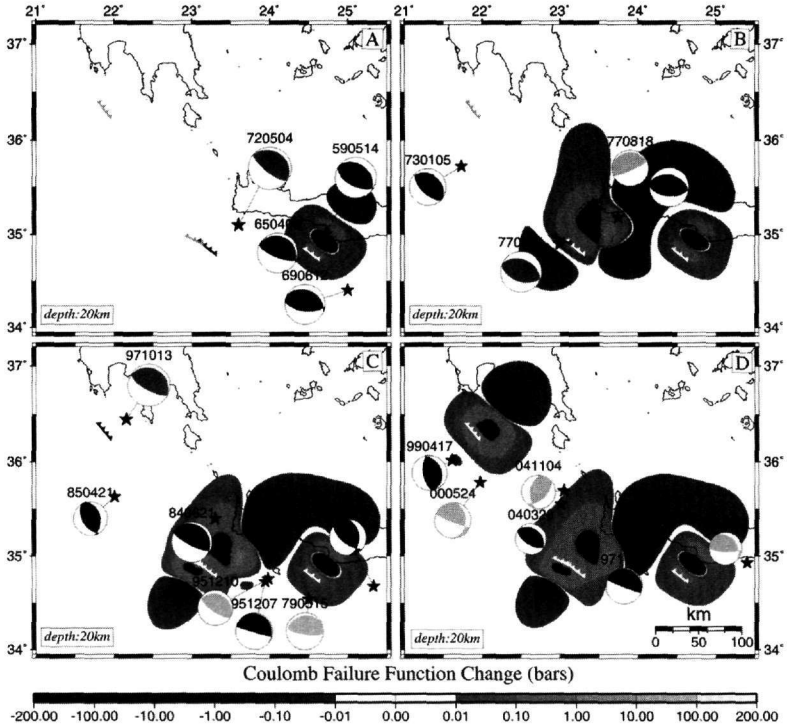

Figure 2 – Coseismic stress changes associated with the occurrence of four strong earthquakes in SW Hellenic arc since 1959. Stress changes are denoted by the scale at the bottom (in bars) and are calculated for thrust faults at 20 km. The stress pattern is calculated according to the fault plane solution of the next strong event. Fault plane solutions are shown as lower-hemisphere equal-area projections and the occurrence date (Year/Month/Day) is given at the top of each focal sphere. Black focal spheres are similar to the fault plane solution of the target event (up to 30° difference in strike, dip and rake),whose focal sphere is in dark gray and its fault is black while the rest thrust fault plane solutions are light gray. Fault traces that have already ruptured are in white and the rest are ingray. Stars denote epicentres of earthquakes and are connected with a thin line to the FPS of the event. (A) Co-seismic Coulomb stress changes associated with the 1959 event imparted on the 1972 rupture zone. (B) Co-seismic Coulomb stress changes associated with the 1959 and 1972 events imparted on the 1977 rupture. (C) Co-seismic Coulomb stress changes associated with the 1959, 1972 and 1977 events imparted on the 1997 rupture. (D) Coulomb stress changes associated with the four strong events imparted on the SW part of the arc

7. Stress evolutionary model

The history of cumulative stress changes, due to both coseismic slip during the strong earthquakes and the tectonic loading on the major faults in the study area, is examined in an attempt to explore the spatial and temporal occurrence patterns of such earthquakes. To this effect, we examine the evolution of the stress field since 1959 and assume stress changes to be zero before that time. We will show that according to the stress evolutionary model, all the larger earthquakes subsequently occurred in bright zones, not in shadow ones. To do this, we only show mechanisms of shocks of similar type of faulting for which the stress calculations are performed (Fig. 3). Most of the moderate thrust shocks with similar fault plane solution (black focal spheres), for which the stress calculations are performed, were located in stress–enhanced zones. In each snapshot, ΔCFF is calculated for a preferred focal mechanism, the one of the next event whose triggering is inspected.

Each snapshot shows the state of the stress field just before the occurrence of the next earthquake included in the stress evolutionary model resolved on its fault plane.

The coseismic stress changes associated with the 1959 event are calculated according to its fault plane solution at a depth of 20 km (Fig. 3A). The accumulated stress changes just before the May 1972 thrust event resolved on its fault plane are shown in Figure 3B. A broad bright zone encompasses the area due to tectonic loading on the CFS. Both the epicentre of this earthquake and the epicentre of a preceding event (April 1965 M 6.1) lie in a stress enhanced area, while the location of one event (July 1969 M 6.1) is in the borders between stress shadow and stress bright zones. In Figure 3C the accumulated stress changes just before the January 1977 event are calculated according to its fault plane solution are shown. The bright zone is more pronounced and encompasses all the thrust earthquakes that occurred during 1972–1977. In Figure 3D the accumulated stress changes just before the October 1997 event are calculated. The model successfully explains the locations of all the thrust earthquakes that occurred in the time period 1977–1997. Figure 3E shows stress accumulated on the CFS in 46 years (1959–2005) and the coseismic stress changes of the strong events included in the evolutionary model. The pattern remains the same though it is more enhanced. All thrust earthquakes that occurred after 1997 up to 2005 are located in stress enhanced regions.

8. Discussion

We explore the Coulomb stress changes (ΔCFF) associated with strong earthquakes (M≥6.3) that occurred along the southwestern part of the Hellenic arc since 1959. The investigation could not be extended to the rest of the Hellenic arc since no strong earthquakes occurred in the SE part of the arc during the study period. We applied a stress evolutionary model in the study area for the period 1959–2005 in order to examine if the history of coseismic and cumulative changes in stress can explain the spatial and temporal occurrence of strong (M≥6.3) and smaller earthquakes.

When considering coseismic stress changes our results suggest that thrust earthquakes interact around CFS, since when a strong shock occurs it changes the conditions for failure in its vicinity. The strong event of September 1977, as well as several of the subsequent earthquakes with similar fault plane solutions, are enhanced by the May 1972 shock.

Stress loading on the Ionian and Crete fault segments modulates the stress acting on nearby thrust faults. When considering the accumulated stress changes our analysis is successful in explaining the location of moderate to strong earthquakes in the study area. It has been shown that all events are located in areas of positive ΔCFF except the June 1969 (M=6.1) event near Crete.

It is well accepted that earthquakes occur in stress enhanced areas The inability of any Coulomb stress model to be consistent with this observation is attributed to the following factors: uncertainties both in location and depth constraints, details on coseismic slip, geodetic analyses for the long term slip rate along the fault and sensitivity of the stress pattern of thrust events to small changes of fault dip and focal depth. In addition, one should consider that subduction earthquakes are patches on the subducting interface rather than ruptures confined in the seismogenic layer and thus the definition of their rupture models include unavoidable uncertainties.

9. Acknowledgments

The stress tensors were calculated using a program written by J. Deng (Deng and Sykes 1997) based on the DIS3D code of S. Dunbar, which later improved (Erikson 1986) and the expressions of G. Converse. The GMT system (Wessel and Smith 1998) was used to plot the figures. The comments of T. Taymaz and an anonymous reviewer helped in the paper improvement. This work was supported by the project "Pythagoras" funded by the EPEAEK. Geophysics Department contribution 690.

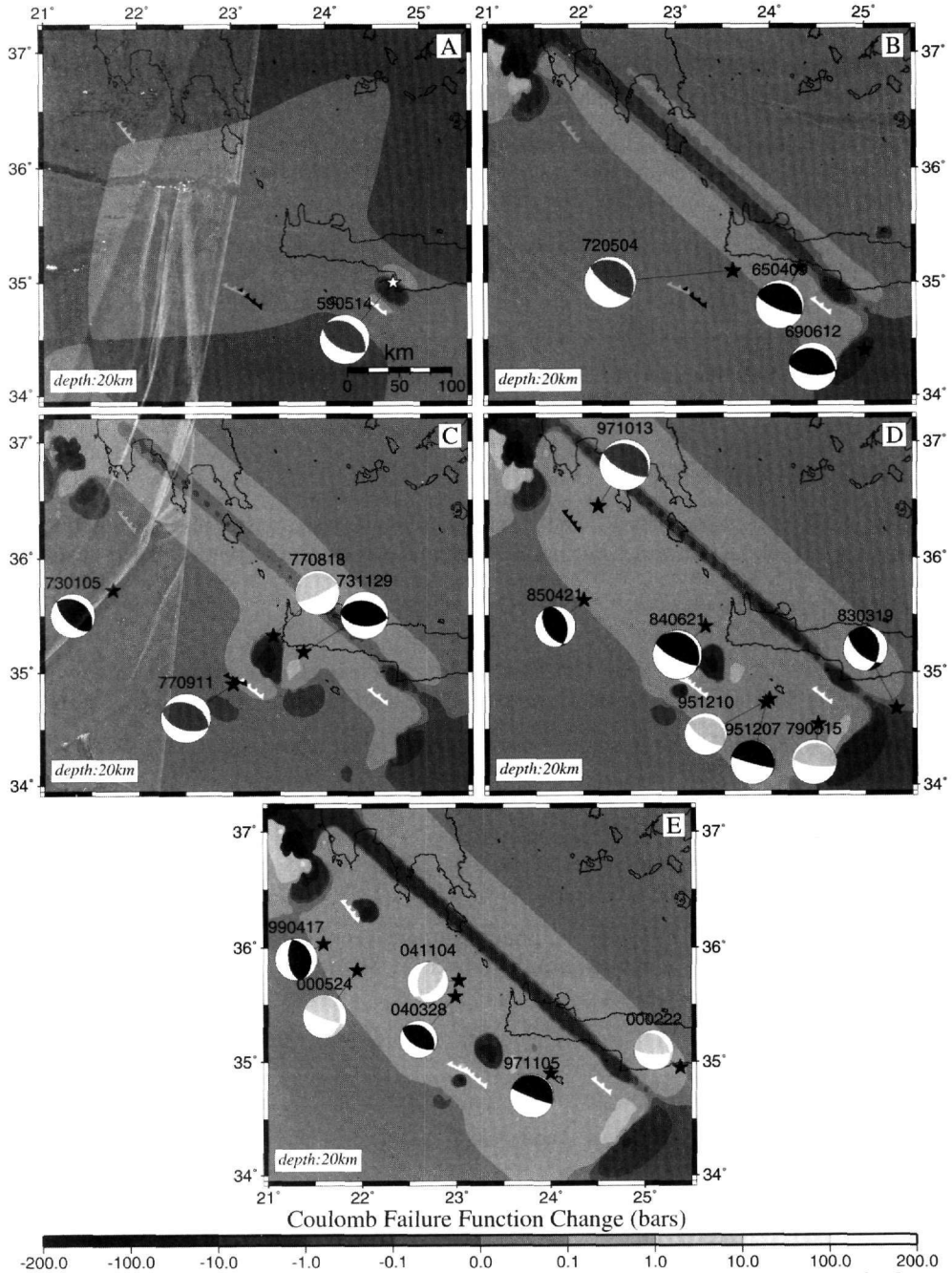

Figure 3 – Stress evolution in SW Hellenic arc since 1959. Fault plane solutions faults and epicentres are denoted as in figure 2. (A) Co-seismic Coulomb stress changes associated with the 1959 event. (B) Stress evolution until just before the 1972 event and thrust focal mechanisms for events during 1959–1972. (C) ΔCFF just before the 1977 main event along with the fault plane solutions of events during 1972-1977. (D) Stress evolution until just before the 1997 shock with FPS of thrust earthquakes during 1977-1997. (E) State of stress in 2005 computed on the subduction interface along with thrust earthquakes that occurred in the period 1997-2005

10. References

Benetatos, C., Kiratzi, A., Papazachos, C., and Karakaisis, G., 2004. Focal mechanisms of shallow and intermediate depth earthquakes along the Hellenic Arc, *J. Geodyn.*, 37, 253–296.

Bird, P., and Kagan, Y.Y., 2004. Plate–Tectonic analysis of shallow seismicity: apparent boundary width, beta, corner magnitude, coupled lithosphere thickness, and coupling in seven tectonic settings, *Bull. Seism. Soc. Am.*, 94, 2380–2399.

Cocard, M., Kahle, H.G., Peter, Y., Geiger, A., Veis, G., Felekis, S., Paradissis, D., and Billiris, H., 1999. New constraints on the rapid crustal motion of the Aegean region: recent results inferred from GPS measurements (1993-1998) across the Hellenic Arc, Greece, *Earth Planet Sci. Lett.*, 172, 39–47.

Davies, R., England, P., Parsons, B., Billiris, H., Paradissis, D., and Veis, G., 1997. Geodetic strain of Greece in the interval 1982-1992, *J. Geophys. Res.*, 102, 24,571-24,588.

Deng, J., and Sykes, L.R., 1997. Evolution of the stress field in southern California and triggering of moderate–size earthquakes: A 200–year perspective, *J. Geophys. Res.*, 102, 9859–9886.

Dmowska, R., Rice, J., Lovinson, L., and Josell, D., 1988. Stress transfer and seismic phenomena in coupled subduction zones during the earthquake cycle, *J. Geophys. Res.*, 98, 7869–7884.

Ergin, K., 1966. On the epicenter map of Turkey and surrounding area, *Turk. Jeol. Kur. Bult.*, 10, 122.

Erikson, L., 1986. User's manual for DIS3D: A three–dimensional dislocation program with applications to faulting in the Earth, *Masters Thesis,* Stanford Univ., Stanford, Calif., 167pp.

Galanopoulos, A.G., 1967. The seismotectonic regime in Greece, *Ann. Geof.*, 20, 109.

Govers, R., and Wortel, M. J. R., 2005. Lithosphere tearing at STEP faults: Response to edges of subduction zones, *Earth Planet. Sci. Lett.*, 236, 505–523.

Harris, R.A., 1998. Introduction to special section: Stress triggers, stress shadows, and implications for seismic hazard, *J. Geophys. Res.*, 103, 24,347–24,358.

Jackson, J., and McKenzie, D., 1988. The relationship between plate motions and seismic moment tensors and the rates of active deformation in the Mediterranean and Middle East, *Geoph. J.*, 93, 45–73.

Kahle, H–G., Müller, M. V., Müller, S., Geiger, A., Danuser, G., Mueller, S., Veis, G., Billiris, H., and Paradissis, D., 1995. The strain field in northwestern Greece and the Ionian Islands: results inferred from GPS measurements, *Tectonophysics*, 249, 41–52.

King, G.C.P., Stein, R.S., and Lin, J., 1994. Static stress changes and triggering of earthquakes, *Bull. Seism. Soc. Am.*, 84, 935–953.

King, G.C.P., and Cocco, M., 2001. Fault interaction by elastic stress changes: New clues from earthquake sequences, *Adv. Geophys.*, 44, 1–38.

Kiratzi, A., and Langston, C., 1989. Estimation of earthquake source parameters of the May 4, 1972 event of the Hellenic arc by the inversion of waveform data, *Physics Earth Planet. Inter.*, 57, 225–232.

Kreemer, C., and Chamot-Rooke, N., 2004. Contemporary kinematics of the southern Aegean and the Mediterranean Ridge, *Geophys. J. Int.*, 157,1377–1392.

Le Pichon, X., Chamot-Rooke, N., Lallemant, S., Noomen, R., and Veis, G., 1995. Geodetic determination of central Greece with respect to Europe: Implications for eastern Mediterranean tectonics, *J. Geophys. Res.*, 100, 12,675–12,690.

Laigle, M., Sachpazi, M., and Hirn, A., 2004. Variation of seismic coupling with slab detachment and upper plate structure along the western Hellenic subduction zone, *Tectonophysics*, 391, 85–95.

Lin, J., and Stein, R.S., 2004 Stress triggering in thrust and subduction earthquakes, and stress interaction between the southern San Andreas and nearby thrust and strike slip faults, *J. Geophys. Res.*, 109, B02303, doi:10.1029/2003JB002607.

Louvari, E., 2000. A detailed Seismotectonic study of the Aegean and neighboring regions based on focal mechanisms of moderate sized earthquakes, *Ph.D. Thesis,* Thessaloniki, University publications, 309pp.

Lundgren, P., Giardini, D., and Russo, R.M., 1998. A geodynamic framework for eastern Mediterranean kinematics, *Geoph. Res. Lett.*, 25, 4007–4010.

McClusky S., Balassanian, S., Barka, A., Demir, C., Ergintav, S., Georgiev, I., Gurkan, O., Hamburger, M., Hurst, K., Kahle, H., Kastens, K., Kekelidze, G., King, R., Kotzev, V., Lenk, O., Mahmoud, S., Mishin, A., Nadariya, M., Ouzounis, A., Paradissis, D., Peter, Y., Prilepin, M., Reilinger, R., Sanli, I., Seeger, H., Tealeb, A., Toksöz, N. M., and Veis, G., 2000. Global Positioning System constraints on plate kinematics and dynamics in the eastern Mediterranean and Caucasus, *J. Geophys. Res.*, 105, 5695–5719.

McKenzie, D. P., 1972. Active tectonics of the Mediterranean region, *Geophys. J. R. astr. Soc.*, 30, 109–185.

McKenzie, D.P., 1978. Active tectonics of the Alpine-Himalayan belt: the Aegean Sea and surrounding regions, G*eophys. J. R. astr. Soc.*, 55, 217–254.

Meier, T., Rische, M., Endrun, B., Vafidis, A., and Harjes, H–P., 2004. Seismicity of the Hellenic subduction zone in the area of western and central Crete observed by temporary local seismic networks, *Tectonophysics*, 383, 149–169.

Papadimitriou, E. E., 1993. Focal mechanism along the convex side of the Hellenic arc, *Bull. Geof. Teor. Appl.*, 35, 401–426.

Papadimitriou, E.E., and Karakostas, V.G., 2005. Faulting geometry and seismic coupling of the southwest part of the Hellenic subduction zone, *Abstract in 33rd IASPEI General Assembly, Santiago, Chile, 2–8 October 2005.*

Papazachos, B.C., 1961. *A contribution to the research on fault plane solutions of earthquakes in Greece, PhD Thesis*, University of Athens, 75pp.

Papazachos, B.C., and Comninakis, P.E., 1970. Geophysical features of the Greek island arc and eastern Mediterranean ridge, *Com. Ren. Des Sceances de la Conference Reunie a Madrid*, 1969, 16, 74–75.

Papazachos, B.C., and Papazachou, C., 1997. *The earthquakes of Greece*, Thessaloniki, Ziti Publications, 289pp .

Papazachos, B.C., and Papazachou, C., 2003. *The earthquakes of Greece*, Thessaloniki, Ziti Publications, 286pp .

Papazachos, B.C., Karakostas, V.G., Papazachos, C.B., and Skordilis, E.M., 2000. The geometry of the Wadati–Benioff zone and lithospheric kinematics in the Hellenic arc, *Tectonophysics*, 319, 275–300.

Papazachos, B.C., Mountrakis, D.M., Papazachos, C.B., Tranos, M.D., Karakaisis, G.F., and Savvaidis, A.S., 2001. The faults that caused the known strong earthquakes in Greece and surrounding areas during 5th century B.C. up to present, *2nd Conf. Earthq. Engin. and Engin. Seism., 28–30 September 2001, Thessaloniki*, 1, 17–26.

Papazachos, B.C., Scordilis, E.M., Panagiotopoulos, D.G., Papazachos, C.B., and Karakaisis, G.F., 2004. Global relations between seismic fault parameters and moment magnitude of earthquakes, *10th Congr. Hellenic Geol. Soc., Thessaloniki, Greece, 14–17 April 2004,* 539–540.

Papazachos, C.B., 1999. Seismological and GPS evidence for the Aegean–Anatolia interaction, *Geoph. Res Lett.*, 26, 2653–2656.

Papazachos, C.B., and Kiratzi, A.A., 1996. A detailed study of the active crustal deformation in the Aegean and surrounding area, *Tectonophysics*, 253, 129–153.

Reilinger, R.E., McClusky, S.C., Oral, M.B., King, R.W., and Toksöz, M.N., 1997. Global Positioning System measurements of present–day crustal movements in the Arabia–Africa–Eurasia plate collision zone, *J. Geophys. Res.*, 102, 9983–9999.

Scholz, C.H., 1982. Scaling laws for large earthquakes: Consequences for physical models, *Bull. Seism. Soc. Am.*, 72, 1–14.

Scholz, C.H., 1990. *The mechanics of earthquakes and faulting*, Cambridge, Cambridge University press, 439pp.

Scholz, C.H., 1998. Earthquakes and friction laws, *Nature*, 391, 37–42.

Taymaz, T., Jackson, J., and Westaway, R., 1990. Earthquake mechanics in the Helenic Trench near Crete, *Geophys. J. Int.*, 102, 695–793.

Taymaz, T., Jackson, J. A., and McKenzie, D., 1991. Active tectonics of the North and Central Aegean Sea, *Geophys. J. Int.-Oxford*, 106, 433–490.

Wessel, P., and Smith, W.H.F., 1998. New, improved version of the Generic Mapping Tools Released. *EOS Trans. AGU* 79, 579pp.

Δελτίο της Ελληνικής Γεωλογικής Εταιρίας τομ. XXXX, 2007
Πρακτικά 11ου Διεθνούς Συνεδρίου, Αθήνα, Μάιος 2007

Bulletin of the Geological Society of Greece vol. XXXX, 2007
Proceedings of the 11th International Congress, Athens, May, 2007

LATE- AND POST-MIOCENE GEODYNAMIC EVOLUTION OF THE MESOGEA BASIN (EAST ATTICA, GREECE): CONSTRAINTS FROM SEDIMENT PETROGRAPHY AND STRUCTURES

Mposkos E.[1], Krohe A.[2], Diamantopoulos A.[1], and Baziotis I.[1]

[1] *National Technical University of Athens, School of Mining and Metallurgical Engineering, Section of Geological Sciences, mposkos@metal.ntua.gr*

[2] *University of Munster, Institute of Mineralogy, Laboratory for Geochronologie, krohe@nwz-uni-muenster.de*

Abstract

In Attica, from the Miocene through the Quaternary, successive generations of detachment faults caused exhumation and denudation of Alpine HP rocks and – later on – formation of sedimentary basins. The Mesogea low angle detachment fault separates the HP rocks exposed at the southern flank of the Penteli Mt from the Late – post-Late Miocene Mesogea basin. Combined sedimentary-petrologic and structural analyses reveal the following: (i) Late Miocene sediments include material from unmetamorphosed source areas suggesting that, until then, parts of the HP rocks were buried under the (largely unmetamorphosed) Pelagonian nappe unit. (ii) Post-Late Miocene sediments exclusively contain clasts from high-P source areas and show downward bending of the layering that accommodates slip along a listric fault surface. Close to the Penteli Mt, within the post-Late-Miocene sediments gravity sliding-blocks of metamorphic rocks occur. All this indicates post-Late Miocene activity along this detachment fault controlled rapid surface uplift/relief formation, denudation and fast erosion of HP rocks in the Penteli Mt.
Key words: *Debris material, gravity-sliding block, detachment, Penteli.*

Περίληψη

Κατά την διάρκεια του Νεογενούς διαδοχικές γενεές ρηγμάτων αποκόλλησης συνέβαλαν στην εκταφή των μεταμορφωμένων πετρωμάτων της Αττικής και στην διαμόρφωση λεκανών πληρωθέντων με ιζήματα. Το ρήγμα αποκόλλησης των Μεσογείων διαχωρίζει τα μεταμορφωμένα πετρώματα του Πεντελικού όρους απο τα άνω μειοκαινικά-μετα μειοκαινικά ιζήματα της λεκάνης των Μεσογείων. Ιζηματολογικά, πετρολογικά και τεκτονικά δεδομένα έδειξαν τα ακόλουθα: (Ι) Ιζήματα άνω μειοκαινικής ηλικίας περιέχουν υλικό τροφοδοσίας, το οποίο προέρχεται απο αμεταμόρφωτα πετρώματα της Πελαγονικής ζώνης, γεγονός που μαρτυρεί ότι τμήματα των μεταμορφωμένων πετρωμάτων καλύπτονταν τουλάχιστον μέχρι τότε, από αμεταμόρφωτα. (ΙΙ) Μετα-μειοκαινικά ιζήματα, που το υλικό τροφοδοσίας τους προέρχεται μόνο από μεταμορφωμένα πετρώματα, παρουσιάζουν μεγάλες κλίσεις στρωμάτων, μαρτυρώντας ολίσθηση κατα μήκος ενός ρήγματος αποκόλλησης. (ΙΙΙ) Στα μετα-μειοκαινικά ιζήματα

της νότιας πλευράς της Πεντέλης, εγκλείονται ολισθόλιθοι μεγάλων διαστάσεων αποτελούμενοι απο μεταμορφωμένα πετρώματα. Όλα αυτά δείχνουν ότι το ρήγμα αποκόλλησης των Μεσογείων ήταν ενεργό μετά το Άνω Μειόκαινο ελέγχοντας την ταχεία ανύψωση της Πεντέλης, το σχηματισμό αναγλύφου και τη διάβρωση των μεταμορφωμένων πετρωμάτων της.
Λέξεις κλειδιά: *Κλαστικό υλικό, ολισθόλιθος, αποκόλληση, Πεντέλη.*

1. Introduction

Formation of sedimentary basins is the surface expression of deformation processes affecting the deep crust. Therefore, sedimentary and structural records of such basins provide clue information on large-scale deformation processes within the crust.

This article is a combined structural and sedimentary study of the Neogene formations of the Mesogea basin in east Attica. A basin and range topography characterizes that area, where insulated mountain ranges – the Penteli and Hymettus Mounts (Mts) confine Neogene-Quarternary basins (Fig. 1). Surface elevation in the Penteli and Hymettus areas and basin formation seem to be correlated processes. Tilted (rotated) Miocene to Pliocene terrestric and lacustrine sediments indicate that tectonic movements associated with the basin formation have continued until recently.

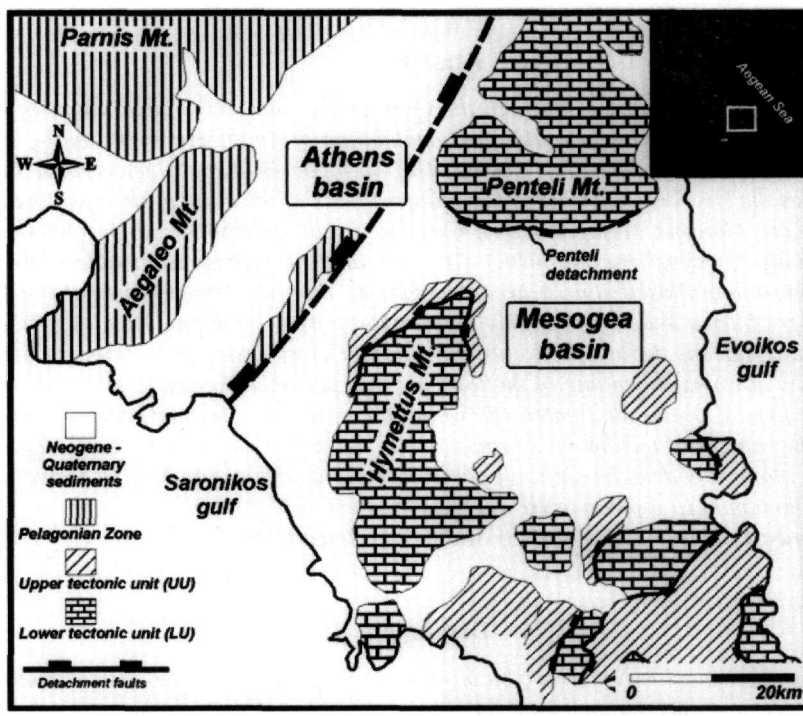

Figure 1 - Simplified tectonic map of Attica (from Katsikatsos *et al.* 1986) showing the Mesogea and Athens basins

2. Tectonic subdivision of Attica

On a broader scale Penteli and Hymettus Mts are part of the Attic – Cycladic metamorphic belt, which in Attica emerges underneath the Pelagonian zone as a tectonic window described as Attica core complex (Diamantopoulos 2006). From the bottom to the top all tectonic units from the Attica area are characterized as follows:

(i) The Attic-Cycladic belt making up NE, E and S Attica (Mts of Penteli, Hymettus, Panion, parts of the Mesogea area and the Lavrion peninsula) comprises two tectonometamorphic units (Marinos and Petraschek 1956, Katsikatsos *et al.* 1986, Lozios 1993) that are themselves separated by low angle detachment surfaces. The lower unit (LU) consists of alternating marbles, calc-schists and metapelites with intercalations of orthogneisses, metamigmatites, metabasic rocks and serpentinites; locally (Hymettus and Panion Mts) a thick dolomite marble series (Pirnari dolomites) occurs. The LU undererwent a high-pressure/low-temperature (HP/LT) metamorphism with peak P-T conditions at 9-11 kbar and ~370 °C followed by decompression to 5-6 kbar combined with heating (Baziotis *et al.* 2006). Katsikatsos *et al.* (1986) argued that the LU is the SW continuation of the Almyropotamos unit exposed within the Olympos window at a similar tectonic position. The upper unit (UU) consists of phyllites, metasandstones, calc-schists, marbles and glaucophane bearing metasediments and metabasites (phyllite nappe according to Marinos and Petraschek 1956; neohellenic nappe according to Katsikatsos *et al.* 1988; allochthon of Penteli according to Lozios 1993). Mineral assemblages from metabasites record a HP/LT metamorphism with peak P-T conditions of ~9 kbar and 350-370 °C followed by decompression combined with cooling suggesting exhumation along a subduction channel (Baziotis *et al.* 2006). According to Altherr and Seidel (2002) the ages of HP/LT and greenschist facies metamorphisms are Eocene and Oligocene-Miocene, respectively.

(ii) Unmetamorphosed rocks of the Pelagonian zone overly the Attic-Cycladic belt in west Attica (Parnitha, Aegaleo and Poikilo Mts). They comprise; i) Late Carboniferous-Early Triassic clastic and carbonate sediments with volcanic intercalations, ii) Triassic-Jurassic platform carbonates, iii) Ophiolites associated with oceanic sediments (shale-chert formation), iv) transgressive Cretaceous limestones that pass upwards into Paleocene flysch.

Presently, only isolated blocks of the Pelagonian nappe are preserved in east Attica. On the Lavrion peninsula, a small isolated block (~50 m in thickness) consisting at the base of serpentinites and chert and at the top of Cretaceous fossiliferous limestones overlies the UU (Katsavrias 1991, Photiadis and Carras 2001). At the eastern slope of Hymettus Mt, 6 Km south of Koropi, also remnants of Eocene-Oligocene "Molasse" sediments tectonically overly the marbles of the LU (Alexopoulos *et al.* 1998). The "Molasse" sediments consist of alternating mudstones, sandstones and limestones; the sandstones contain clasts of quartz, albite, perthitic microcline, biotite, chlorite, chromite and garnet and rock-fragments like limestones, cherts, metabasalts and serpentinite.

On the western slope of Hymettus Mt, equivalents to the Pelagonian nappe are the Athens schists tectonically overlying phyllites of UU and marbles of the LU of the Attic-Cycladic belt. Cherts and limestones of the Pelagonian zone overlay the Athens schists (Akropolis, Lykabettus and Tourkovounia hills, Marinos *et al.* 1971). In north Attica and south Evia a low-angle detachment surface separating the UU from the Pelagonian zone (Diamantopoulos 2006) is exposed.

3. Geology of the Neogene basins

In Attica there are two major basins that contain Late Miocene to recent sediments: The Athens basin being confined to the NNW by the Parnitha, to the NE by the Penteli, to the E by the Hymettus, and to the W by the Aegaleo and the Poikilo Mts and the Mesogea basin being situated S of the Penteli and E of the Hymettus Mts. (Fig. 1). We focus on formation of the Mesogea basin.

Sediments of the Mesogea basin are in tectonic contact with metamorphic rocks of the lower unit of the Attic-Cycladic crystalline belt. The sediments overlay the LU at the southern slope of Penteli Mt (marbles, calc-schists and mica-schists with rare intercalations of orthogneisses and metabasites) and at the eastern slope of Hymettus Mt (marbles with subordinate calc-schists and mica-schists). They overlay the UU at the southern, eastern and western border of the basin (Fig. 2,

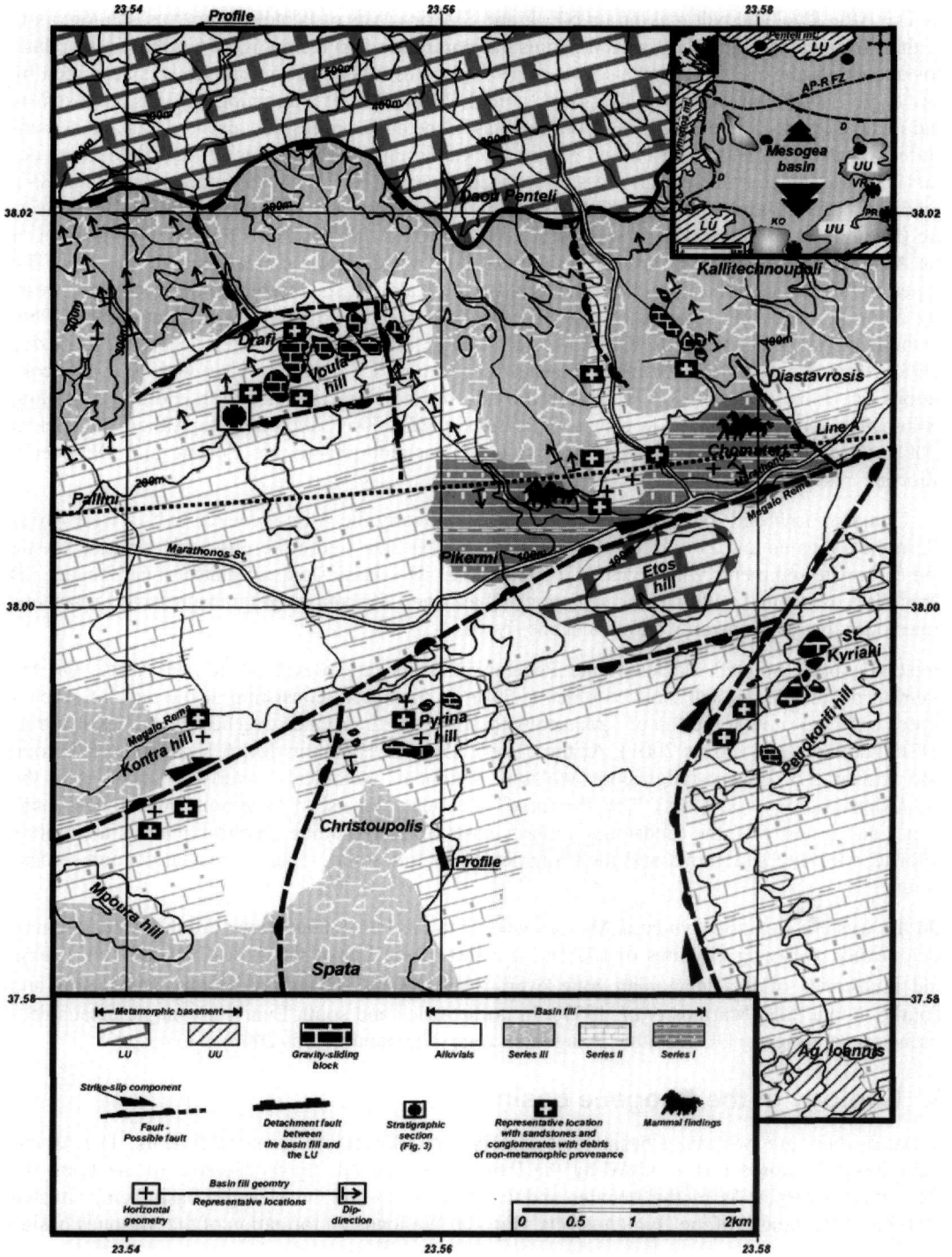

Figure 2 - Geological map of the northern part of Mesogea basin. Inset map: Simplified geological map of the Mesogea basin and surrounding Mts., (modified by Lepsius 1893). Black circles confine the mapped area. AP-R FZ: Agia Paraskevi-Rafina fault zone, VR :Vravronas, PR : Porto Rafti, KO : Koropi, D : Detachment separating UU from LU

insert map) predominantly consisting of marbles, phyllites, calc-schists and metabasites containing blue amphiboles. Those are also common in metasediments of the UU from the Marathon Lake area (western slopes of Penteli Mt, Lozios 1993). Blue amphibole clasts in the basin sediments is thus a positive indicator for the provenance of clastic material from the UU. Major structures confining the Mesogea basin are gently south dipping Penteli detachment to the north (Fig. 2) and a N-S trending high angle normal fault to the west, following the E slope of the Hymettus Mt. A steep post-Miocene fault zone confines isolated topographic highs south of the Rafina-Stavros stripe, where the basement (marbles and schists) emerges on the Etos hill (Fig. 2). The formation of both, the Athens and Mesogea basins is related to Aegean back-arc extension and temporally coincides with denudation of the metamorphic LU in Attica (see below). The sedimentary record gives evidence on the source areas of deposits, and provides thus information on now eroded parts in this area, the paleotopography and synsedimentary tectonic movements.

3.1. Sediments of the basin

Since 18th century many geologists have studied the Mesogea basin (i.e. Lepsius 1893, Papachatzis 1953 Marinos and Symeonidis 1974, Mettos 1992 and references therein). The area attracted great interest from the discovery of fossils of mammals at the famous localities "Megalo Rema" and "Chomateri" near Pikermi. Sediment formations include Late Miocene (Turolian, Mettos 1992, Ioakim *et al.* 2005) fluvioterrestrial and lacustrine sediments. They consist of alternating and laterally changing sandstones, mudstones, conglomerates and limestones. At the southern slope of Penteli post-Late Miocene fluvioterrestrial conglomerates discordantly overlie the Micoene sediments. Mud- and sandstone intercalations are abundant. Lepsius (1893), Papachatzis (1953), Marinos and Symeonidis (1974) described these as Diluvial deposits, while Mettos (1992) and Katsikatsos (2002) included the conglomerates into the Miocene sediments.

Figure 2 shows the distribution of sediments in the northern part of Mesogea basin mainly based on our own field observations, and including the maps of Lepsius (1893), Papachatzis (1953), Marinos and Symeonidis (1974). Field observations combined with petrographic investigations confirm that a large amount of clasts from Miocene conglomerates and sandstones originate from sedimentary and ophiolitic rocks that are notably absent in the mountain ranges now bordering the basin. Clasts include limestones with or without fossils, cherts, radiolarites, silt and sandstones, altered basalts, serpentinite as well as chromite grains. Corresponding source rocks are widely distributed through the Pelagonian zone that overlies the metamorphic rocks in West Attica. Thus, the Pelagonian nappe (now eroded) contributed to Mesogea basin fill. Based on different provenances of the dominant clasts and facies, from the bottom to the top, three sediment series are distinguished. Lateral and vertical transitions from one series to another suggest areal variations in relief and a general increase of relief with time related to denudation of the lower metamorphic unit.

Series I: At the base, it consists of up to 10-15 m thick red to yellow-red sandy-to silty mudstones with intercalations of sandstones and conglomerates. The basement onto which this series deposited does not emerge at the surface thus the thickness of series I is unknown. The mudstones comprise fossils of mammals and micromammals (Marinos and Symeonidis 1974 and references therein) and predominantly consist of quartz, illite, smectite, calcite and dolomite. The sandstones contain rock fragments mainly of muscovite – oxychlorite schists, marbles and quartzites, as well as grains of quartz, albite, more rarely epidote and blue amphibole. Oolites show clasts of quartz, marble, or muscovite schists in the core and shells of micritic calcite (Fig. 4A) indicating deposition in a shallow, near the shore lacustrine environment. Clasts and oolites are cemented with sparitic calcite (50-70 μm grain size). In metapelites and calc-schists of Penteli Mt, muscovite-oxychlorite schists are common. The presence of such clasts in the sandstones of Series I suggests that at the time of their deposition, the LU partly emerged at the surface and was subjected to erosion. The conglomerates contain pebbles of marble, micaschist, chert and limestone.

Series II: This is the most-widespread Late-Miocene to Pliocene fluvio-lacustrine series in the Mesogea basin. It comprises alternating limestones, mudstones, sandstones and conglomerates.

Northeast and west of Chomateri (Fig. 2) marly limestones, sandstones, and conglomerates dominate. The conglomerates contain pebbles of limestones, cherts and sandstones. Sandstones from the Kalitechnoupoli area predominantly contain clasts of fossiliferous and non-fossiliferous limestone, chert, radiolarite, mudstone, serpentinite, diabase and chromite. In these sandstones clastic grains originating from metamorphic rocks of the UU and LU are absent. In the Kontra hill area conglomerates with pebbles of limestones, cherts and sandstones (~1 to 3 cm in size) dominate showing more or less horizontal bedding. In the area of Palini-Drafi, Series II comprises alternating sandstones, mudstones, conglomerates and limestones, dipping with 30-35^0 toward the north.

Figure 3 shows a lithological column of Series II from Voula hill (Fig. 2). Four types of sediments occur showing a rhythmic alternation in the lithological succession.

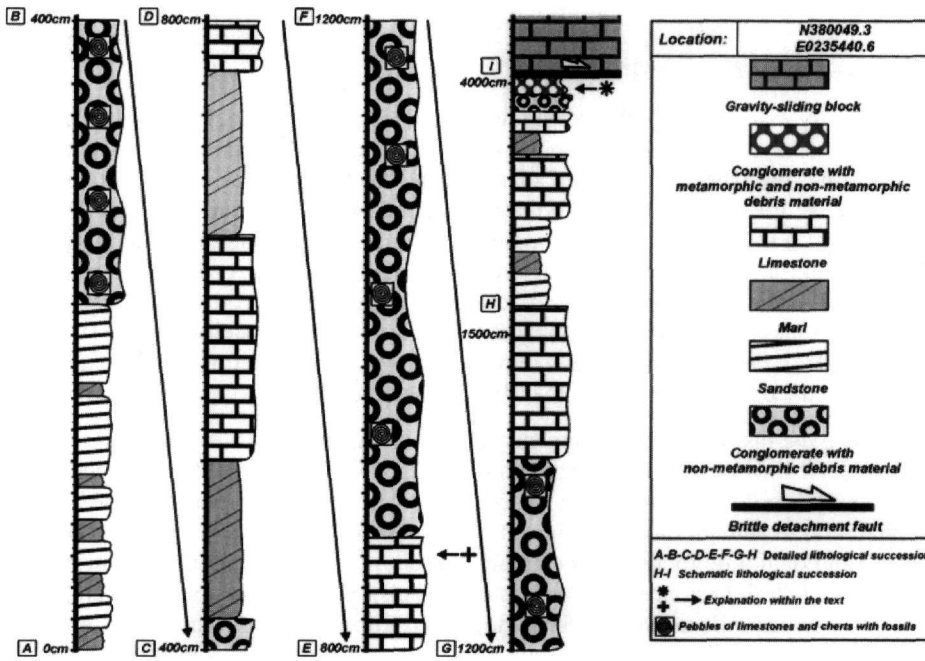

Figure 3 - Lithological column of sediments from Series II in Voula hill

a: Sandstones. The clastic grains of the sandstones comprise rock fragments of micritic limestone, chert, radiolarite, serpentinite, basalt, mudstone, two mica gneiss and grains of quartz, feldspar, calcite, chlorite, muscovite, chromite (predominant in the heavy mineral fraction), garnet and epidote. They are cemented with sparitic calcite.

b: Unconsolidated or loosely consolidated sandy-silty clays. The clay fraction consists of smectite, quartz, calcite and illite. The grains from the sand fraction are similar to those reported above for the sandstone. The grains are well-rounded indicating transport from greater distances or multiple reworking. Neither the sandy-silty clays nor the sandstones contain clastic grains that would indicate provenance from metamorphic rocks typical of the Penteli area.

c: Unconsolidated or loosely consolidated conglomerates. They consist of well-rounded spherical to ellipsoidal pebbles, 2 to 6 cm in size, and a sandy matrix. Dominant are: (i) Pebbles of light grey to white coloured micritic limestones (frequently rich in microfossils (Figs 4b, c), sparitic, oolitic limestones and limestones with spheroidal SiO_2 aggregates. (ii) Pebbles of red to greenish cherts mostly full of radiolaria (Fig. 4d). (iii) Pebbles of sandstones possibly derived from the Eocene-Oligocene "Molasse" sediments with clasts of quartz, plagioclase, microcline, biotite, muscovite, garnet, chromite, rutile, and composite

grains of chlorite-muscovite schist indicating provenance from magmatic, metamorphic and ultramafic rocks, similar to those of the Pelagonian zone.

(iv) Pebbles of metabasalt (diabase Fig. 4e) consisting of augite, plagioclase, magnetite, and of chlorite, calcite and pumpellyite being alteration products of magmatic minerals. Only in upper parts of series II, in the Voula hill (star in Fig. 3), a conglomerate predominantly contains pebbles of chert, metabasalt and of chloritoid bearing chlorite-muscovite schist. As in the metapelites from Penteli Mt, chloritoid-bearing chlorite-muscovite schists are common; this indicates that some clasts originated from metamorphic rocks of the Penteli area.

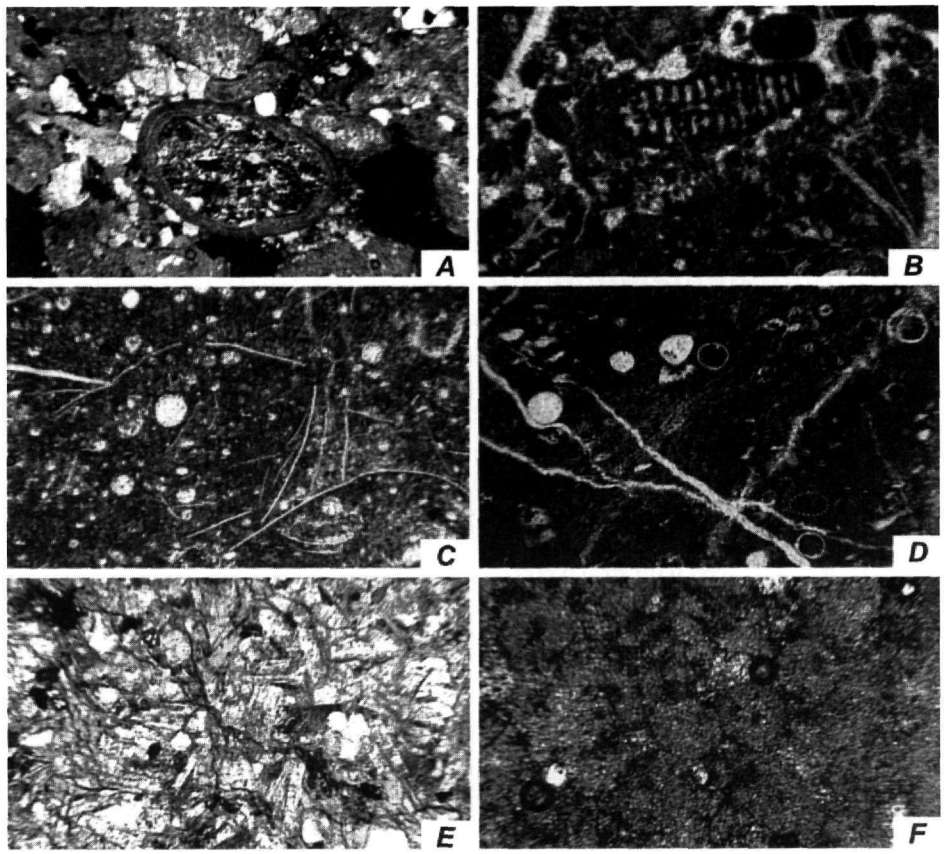

Figure 4 - A) Oolite with muscovite schist core and micritic calcite shell in sandstone of Series I. B) Pebble of limestone with foraminifera. C) Pebble of limestone with radiolaria and algae. D) Pebble of chert with radiolaria. E) Pebble of metabasalt with plagioclases with ophitic texture. F) Oolitic limestone: ooids cemented with sparitic calcite (B-F in conglomerates from Series *II*)

d: Limestones: Four limestone interlayers occur. They vary in thickness from 2 up to 20 meters (Fig. 3) are grey to light brownish and very hard with a flinty fracture. The third limestone interlayer (from the bottom to the top) is oolitic. Oolites consist of coarse-grained sparitic calcite (10-20 μm in size) cemented with isometric calcite crystals 40-50 μm in size (Fig. 4F). This indicates precipitation/recrystallization of calcite in shallow, quite warm water environment. Iron hydroxide impregnation coloured the matrix calcite brownish.

In the Petrokorifi hill area, at the base of Series II, un- or only loosely consolidated conglomerates (> 5m in thickness) crop out that upwardly pass into alternating beds of sand- and mudstones (some cm to dm in thickness). Pebbles in conglomerates consist of cherts, limestones and sand-

stones, while clasts in sandstones are mainly quartz, oxychlorite, muscovite, biotite, epidote, chloritoid, blue amphibole and fragments of muscovite-schists. Locally, the heavy-mineral fraction of the sandstone contains abundant blue amphibole. This suggests that both metamorphic units supplied debris material to the sandstones of Series II in the Petrokorifi hill, as blue amphibole is widespread in metabasites and schists of the UU, chloritioid and oxychlorite in metapelites and calc-schists of the LU. In contrast in Series II sandstones from the Voula hill, Kontra hill and Kallitechnoupoli debris material from unmetamorphosed domains dominate.

In the "Megalo Rema" river, well-cemented conglomerates upwardly grade into alternating mudstones, sandstones and conglomerates (~ 100-120 m thick) that are un- or loosely consolidated. Palynological investigation by Kaouras and Oikonomopoulos (unpublished 2007) in a dark-grey mudstone yielded Pliocene sedimentation age. Well-rounded pebbles and gravels (2 to 15 cm in size) within the conglomerates consist largely of calcite marbles, rarely dolomite marbles, schists and gneisses indicating a metamorphic source area. The presence of blue amphiboles in the sandstones suggests that metamorphic rocks of the UU contributed to the clastic material of this series. The contact to the underlying Series I (red mudstones) is probably tectonic as is indicated by a change of dip directions of the bedding from N in this series (north of the line A in Fig. 2) to S in the underlying Series I (red mudstones).

Series III: Series III unconformably overlies Series I and II reflecting an erosional event before onset of sedimentation of Series III. The clasts indicate a remarkable change in the provenance of the sediments of series III. In the Drafi area, north of the Voula hill (Fig. 1) Series III (> 200 m in thickness) start with silt- and sandstones. The clasts in the siltstones consist of calcite, quartz, while K-mica, chlorite, oxychlorite, chloritoid, albite, epidote and fragments of marble, calcareous schists, chloritoid schists. These are all widespread in the LU of the Penteli Mt. Angular shapes of the calcite and marble grains indicate material transport over only short distances. Sedimentation continues with fluvio-terrestrial conglomerates. These contain large gravels (up to 1 meter in size) consisting of marbles, calc-schists, metapelites and gneisses. This indicates rapid surface uplift / relief formation combined with strong erosion in the Penteli area at that time.

3.2. Gravity-sliding blocks

On the hills Voula near Drafi, near Kallitechnoupoli (both on the slope of Penteli Mt), Petrokorifi, and Pyrina (Fig. 1), isolated blocks of metamorphic rocks overlie the Late Miocene sediments *(Series II).*

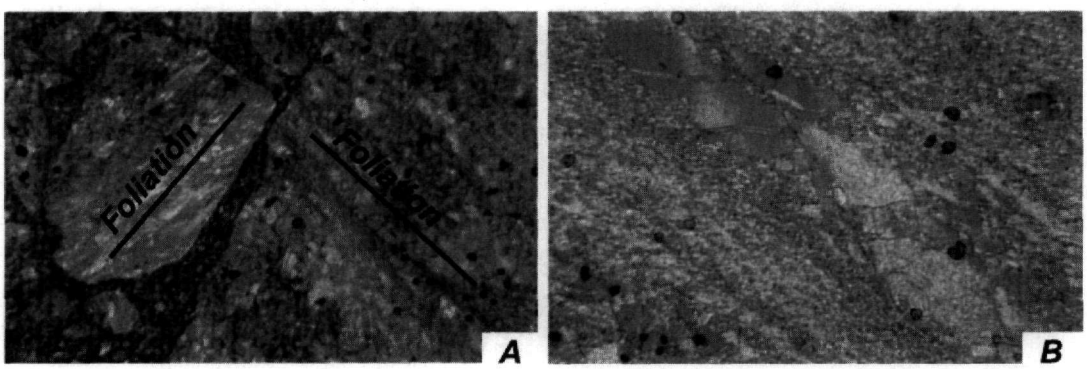

Figure 5 - Gravity-sliding blocks: A) Cataclastic texture in the marble (Voula hill); B) Marble with mylonitic foliation, reflecting polyphase deformation (Pyrina hill)

Such blocks have been alternatively considered as outcrops of basement (blocks of Voula and Kallitechnoupoli hills; Marinos and Symeonidis 1974), as Miocene limestones (blocks of Voula, Petrokorifi and Pyrina, Lepsius 1893) or as olistholites sliding from Penteli marbles within the Miocene sediments (blocks of Voula and Pyrina hills, Mettos 1992).

Field observations and petrography show that the blocks of Voula hill consist of calcite marbles an d light greenish grey phengite orthogneisses. The marble within the block shows a brecciated textu re with mm to cm-sized clasts in the fine-grained matrix (Fig. 5A). The clasts show a well-develop ed mylonitic foliation and lineation defined by elongated grains showing dynamic recrystallizatio n. The blocks of Petrokorifi hill consist of dolomitic marble with intercalations of a metabasite (Agia Kyriaki area), and a calcite marble (farther to the south; Fig. 2). The dolomitic marble is brecciated. Porphyroclasts are mm to cm in size consisting of dolomite single-grains or grain aggregates. The microcrystalline matrix is composed of 10-20 μm large isometric grains. The intercalated metabasite consists of brown hornblende+ albite+chlorite+epidote+actinolite+quartz. Calcite marbles are brecciated showing 20 to 50 cm large, angular blocks. Their mylonitic foliation is randomly oriented indicating clast rotation during brecciation.

The gravity-sliding blocks of Pyrina hill consist of calcite and dolomite marbles respectively overlying unconsolidated conglomerates with pebbles of limestone and chert, and sandstones with clasts of quartz, calcite, oxychlorite, dolomite, blue amphibole, chloritoid, and muscovite schist. The calcite marble is brecciated with up to 10 cm large clasts in a fine-grained matrix. The clasts show well-developed mylonitic foliation. This deformation possibly continued during decreasing temperatures, from the plastic to the brittle regime within discrete zones (μm to mm thick). Elongated ribbons consisting of medium grained, elongated calcite grains showing undulatory extinction alternate with elongated ribbons consisting of a fine-grained, equigranular grain mosaic, that underwent dynamic recrystallization (Fig. 5b). The dolomite marble is brecciated. The clasts consist of more or less isometric dolomite grains without internal deformation.

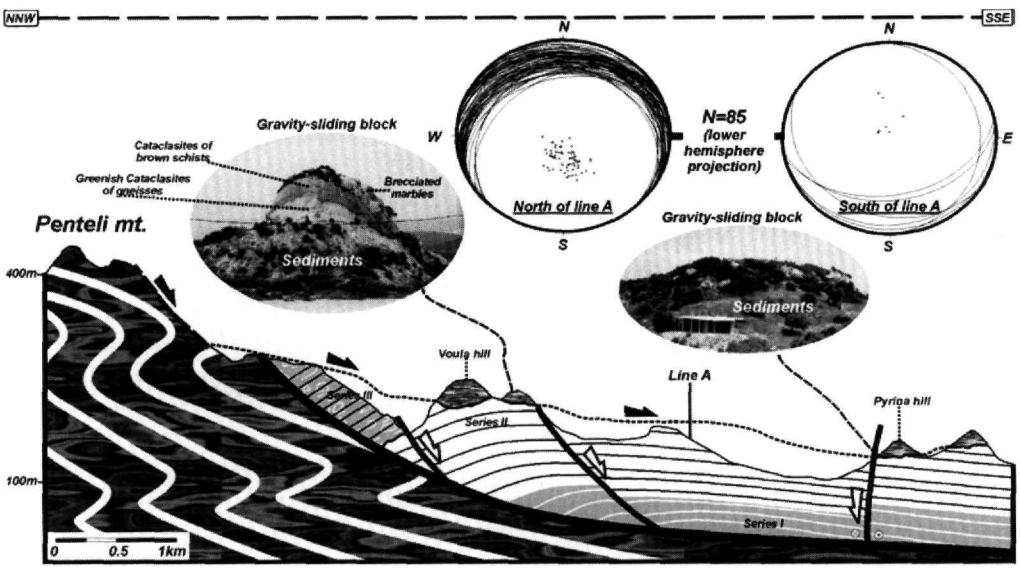

Figure 6 - Geological profile, showing the geometry of the northern part of Mesogea basin (see Fig. 2 for profile location)

The gravity-sliding blocks of Kalitechnoupoli occur at the base of Series III. They comprise quartz-muscovite bearing marble, almost pure calcite marble, and a block of metabasite. The calcite marble shows brecciated texture with mm to cm-sized clasts in a fine grained matrix. The clasts show well-developed mylonitic foliation and lineation imprinted by elongated calcite grains with shape and lattice orientation as shows the observation with the gypsum plate.

4. Structural relationships between Mesogea basin and basement

4.1. Syn-detachment evolution

Syn-detachment-evolution of the basin is suggested by the relationships between the orientation of detachment fault bounding the basin against the Penteli Mt and the orientations of bedding within the basin (block rotation; Fig. 6).

Systematic structural analyses indicate a uniformly north dip of the sedimentary layering in the northern part of the study area, towards the detachment exposed at the southern flank of the Penteli Mt. Also the thickness of the sediments increases towards Penteli Mt. In contrast, to the south of line A (Fig. 2), the bedding is about horizontally oriented. Rotation of the bedding to the north of line A contemporaneously with continuing sedimentation of Series II indicates that this detachment fault controlled the basin evolution implying a listric geometry (Fig. 6). The emplacement of gravity-sliding blocks onto the sediments further suggests that movements along this detachment surface were associated with formation of a steep relief, i.e. doming of the Penteli Mt. Actually en-echelon listric faults occur at the southern slope of the Penteli re-working the ductile structures of the metamorphic basement (Fig. 7). These 2nd order south-dipping listric fault surfaces, determine the present geomorphology. The structural profile in figure 6 shows the structures of the basin fill and of the detachment fault in the study area. Within the basin, steeply inclined secondary normal faults crosscutting the sediments rooting in the major detachment fault determine block rotation in the sedimentary basin (Fig. 6).

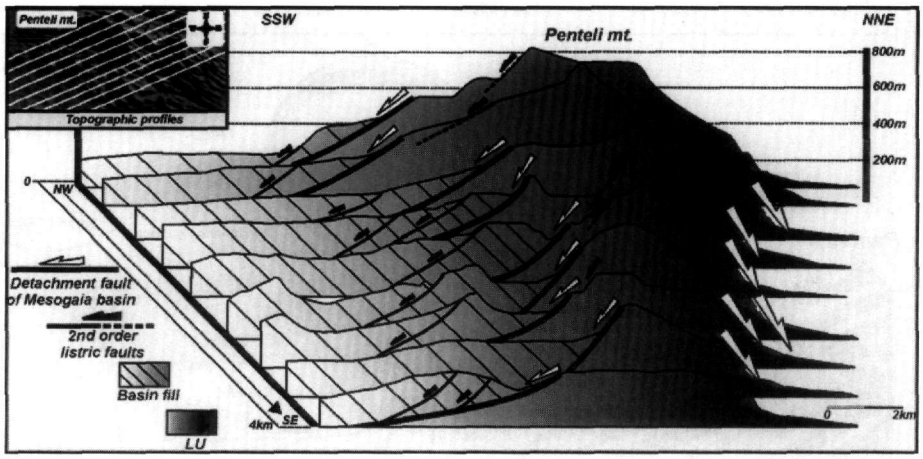

Figure 7 - Topographic profiles through Penteli Mt. showing the detachment fault of Mesogea basin and the 2nd order listric faults

4.2. Polyphase detachment faults: basin evolution and exhumation of the metamorphic rocks

In the Mesogea basin the early sedimentation stages start in the Late Miocene (Mettos 1992, Ioakim *et al.* 2005), after cooling and emplacement of the high-*P* rocks in the brittle upper crust, i.e. after 8 Ma (indicated by intrusion age of the Lavrion granodiorite; Altherr *et al.* 2002). Basin formation and simultaneous denudation of metamorphic rocks are related processes controlled by detachment faults (Diamantopoulos 2006). In detail, our data suggest a complex two-stage tectonic scenario as proposed in Figure 8.

In the earlier sedimentation stages deposits include material from the Pelagonian zone as well as from the metamorphic rocks of the underlying units. This suggests that removal of the Pelagonian nappe from the Attic-Cycladic belt may have already started, by translation along older (Miocene) detachment faults similar to that exposed e.g. in southern Evia.

In a subsequent stage, rapid surface uplift of LU in the Penteli Mt occurs. This is interpreted to be related to a younger (post-Miocene) detachment fault crosscutting the LU as is e.g. exposed at the southern-flank of the Penteli Mt. This detachment controlled sedimentation in the uppermost coarse-grained parts of the Mesogea basin close to the Penteli Mt (Fig. 8). In either stage extension occurred in north-south direction.

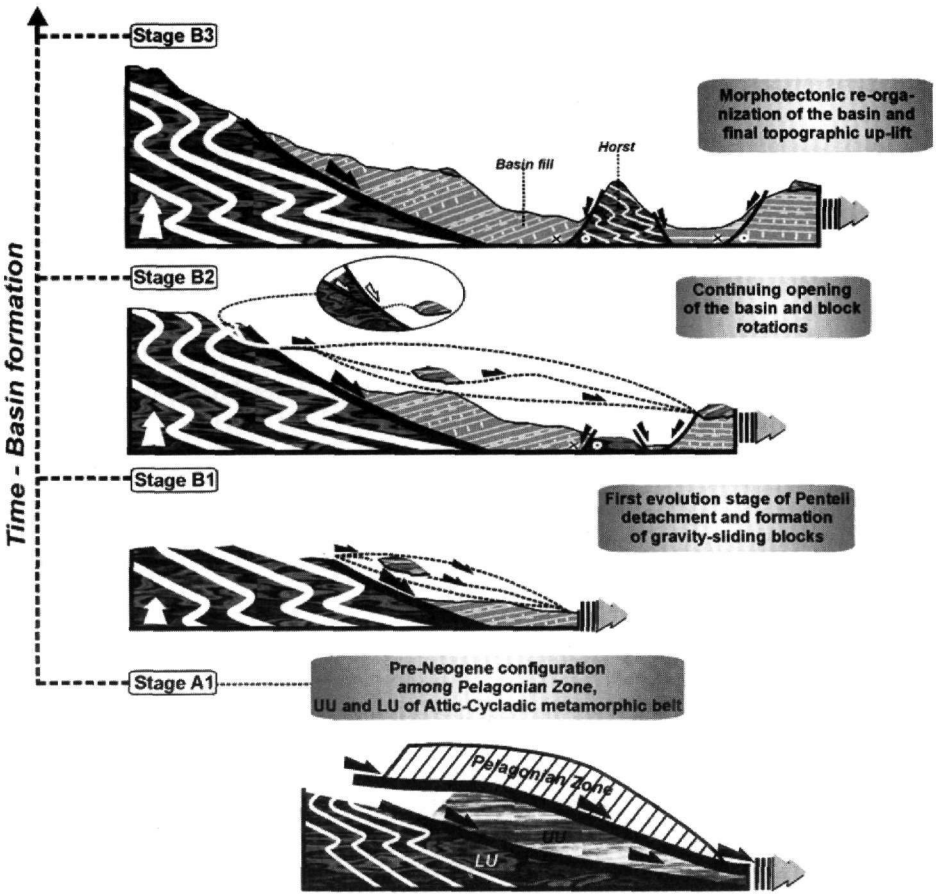

Figure 8 - Tectonic scenario, depicting the pre-Neogene configuration of tectonic units and the evolution of Mesogea basin during and after Late Miocene

5. Discussion and Conclusions

Hymettus and Penteli Mts represent tectonic windows of the Attic-Cycladic HP metamorphic belt in Attica. Structures bounding the metamorphic rocks against the sedimentary basins are either low angle detachment surfaces or steep normal faults reflecting tectonic movements related to denudation of metamorphic rocks and subsequent tectonic stages. Deposition of sediments in the basins, denudation and doming seem to be mutually related processes as is concluded from the sedimentary and structural data. Though decoding the temporal evolution of the deposition environment of the study area is obscured by rather narrow horizontal changes in deposition environments, in sum, field observations and petrography of the sediments from Mesogea basin suggest the following basin evolution and the related tectonic processes:

1: Sediments of the base of Series I are largely pelitic suggesting either material transport over large distance or smooth relief. Intercalations of coarse-grained sediments (sandstones, conglom-

erates) appear rather related to climatic changes than to changes in topography at that time. Calcareous ooids in sandstones typically indicate sedimentation in shallow-water lacustrine conditions.

2: Conglomerates, sandstones and mudstones of Series II document provenance of debris material from unmetamorphosed Pelagonian nappes. In Miocene conglomerates from the Voula hill, the area between Pikermi and Kallitechnoupoli, the Kontra hill, and from the basal series of Petrokorifi hill (Fig. 2), predominant clasts are cherts, sandstones, mudstones and limestones; subordinate are clasts of basalts and serpentinites. Chromite is also frequent. Conglomerates containing pebbles from an unmetamorphosed source region also occur on the road north of Vravrona, in Porto Rafti area and the area east of Koropi (stars in inset map of Fig. 2).

3: Post-Miocene sediments unconformably overlay the deeper series indicating post-Turrolian erosion of the Miocene sediments. The post-Miocene sandstones and mainly fluvial conglomerates of Series III indicate continuing basin formation accompanied with increased relief formation in Penteli area. Fragments of these sediments only originate from the LU of Penteli area (marbles, calcschists, pelitic schists and orthogneisses), being angular, poorly sorted with apparent grain sizes ranging from some mm to more than 1 meter, in line with short transport distances.

4: Gravity-sliding blocks of marbles originating from the LU exposed in the Penteli only occur at a distance of ~1 km to 5 km from the Penteli Mt, and only over the Late Miocene sediments or within the post- Late-Miocene conglomerates, above Series II and within Series III. This is consistent with continuing widening of the basin along with rapid surface uplift and formation of a topographic relief and strong erosion also of the metamorphic LU from the post-Late-Miocene onward. In Petrokorifi and Kallitechnoupoli areas, gravity-sliding blocks mainly consist of mylonitic and cataclastic calcite and dolomite marbles with subordinate metabasites and phengitic orthogneisses (Voula hill) that are all typical for the LU from the Penteli area. Possibly isostatic rebound of the lower plate associated with translation along this detachment initiated post-Late Miocene surface uplift.

5: To the south of line A in figure 2, the bedding is either nearly horizontal or is gently inclined towards the south. 'But to the north of line A, toward the Penteli Mt., the dip of the Miocene and post-Miocene sediments is ~5-40°. Close to the south-dipping detachment surface that broadly forms the southern slope of Penteli, the bedding of Series III sediments dips at 30-40°, toward the north. This configuration is consistent with block rotation within the hanging wall block and downward bending of the hanging wall block above a listric normal fault surface thus indicating continuing translation along the detachment during and after the deposition of the conglomerates

Surface uplift in the Hymettus area also occurred after the Late Miocene time, as is the case in the Penteli area. At the eastern slopes of Hymettus Mt, 6 Km south of Koropi, Eocene-Oligocene "Molasse" sediments are tectonically overlain by a chaotic series (Alexopoulos *et al.* 1998), interpreted as gravity-sliding blocks. This chaotic zone consists of metagabbros, altered serpentinites, hematitic silica rocks and a cataclastic marble containing fragments of marble ultramylonites. A narrow cataclastic zone (~1-2 m in thickness) separating the "Molasse" sediments from the marble contains rounded fragments (pebbles) of fossiliferous limestones, sandstones and cherts typically for clastic components in the Late Miocene conglomerates. This suggests that this chaotic series is a gravity-sliding block evidently emplaced after the deposition of the Late Miocene sediments, similar to the gravity-sliding blocks south of Penteli area.

6. Acknowledgments

We wish to thank L. Royden and an anonymous referee for helpful suggestions that helped to improve the style and content of this article.

7. References

Alexopoulos, A., Lekkas, S., and Moraiti, E., 1998. On the occurrence of a non metamorphic Uppper Eocene – Lower Oligocene clastic sequence, wedged between the allochthon and the relative autochthon system of Attiki (Greece), *Bulletin Geological Society of Greece,* XXXIV/1, 79-84.

Altherr R., and Seidel, W., 2002. I-type plutonism in a continental back-arc setting: Miocene granitoids and monzonites from the central Aegean Sea, Greece, *Contrib Mineral Petrol,* 143, 397-415.

Baziotis, I., Mposkos, E., and Perdikatsis, V., 2006. Reconstruction and correlation of the exhumation history of high-pressure/low-temperature metamorphic rocks from Attica, *NECAM 2006,* Milos island, Greece, 28.

Diamantopoulos, A., 2006. Non-coaxial stretching deformation dominating the Upper Structural Plate of the Metamorphic Core Complex of Attica (Internal Hellenides, Central Greece), *XVIIIth CBGA,* Belgrade, Servia, 101-105.

Ioakim, Ch., Rondoyanni, Th., and Mettos, A., 2005. The Miocene basins of Greece (Eastern Mediterranean) from a paleoclimatic perspective, *Revue de Paleobiologe,* 24, 735-748.

Katsiavrias, N., Solakius, N., and Salaj, J., 1991. The age of the Agios Konstantinos limestone at Lavrion, Southeastern Attica, Greece, *Geologica Carpathica 42,* No 5, 303-309.

Katsikatsios, G., Migiros, G., Triantafillis, M., and Mettos, A., 1986. Geological structure of Internal Hellenides (E. Thessaly – SW. Macedonia, Euboea – Attica – Northern Cyclades Islands and Lesvos), *Geological & Geophysical Research,* Special Issue, 191-212.

Katsikatsios, G., Mettos, A., and Vidakis, M., 2002. Kifisia sheet. *I.G.M.E.* 1/50.000 Scale.

Lepsius, R., 1893. *Geologie von Attika. Ein Beitrag zur Lehre vom Metamorphismus der Gesteine,* Berlin 1983, Translation by Vougiouka G. Library Marasli, 592pp. Athens 1906.

Lozios, S., 1993. Structural analysis of the metamorphic rocks of NE Attica (Greece), *Phd Thesis,* University of Athens, 299pp.

Marinos, G., and Petrascheck, W. E., 1956. Laurium, *Geological and Geophysical Research,* IV, 247.

Marinos, G., Katsikatsios, G., and Mirkou-Peripopoulou, R., 1971. The Athens' schists formation, II. Stratigraphy and structure, *Annales Geologique des Pays Hellenique,* XXV, 183-216.

Marinos, G., and Symeonidis, N., 1974. Neue funde aus Pikermi (Attika, Griechenland) und eine allgemeine geologische Ubersicht palaontologischen Raumes, *Annales Geologique des Pays Hellenique,* XXVI, 1-20.

Mettos, A., 1992. Geological and paleogeographical study of the terrestrial Neogene and Quaternary rocks of NE Attica and of NE Beotia, *Phd Thesis,* Department of Geology, University of Athens, 259pp.

Papachatzis, N. I., 1953. Morphogenetic research of the basin of Mesogaia, *Annales Geologique des Pays Hellenique,* V, 236-260.

Photiades, A., and Carras, N., 2001. Stratigraphy and geological structure of the Lavrion area, *Bulletin Geological Society of Greece,* XXXIV/1, 103-109.

Δελτίο της Ελληνικής Γεωλογικής Εταιρίας τομ. XXXX, 2007
Πρακτικά 11ου Διεθνούς Συνεδρίου, Αθήνα, Μάιος 2007

Bulletin of the Geological Society of Greece vol. XXXX, 2007
Proceedings of the 11th International Congress, Athens, May, 2007

REVIEW AND NEW DATA ON UPLIFT RATES AT THE W TERMINATION OF THE CORINTH RIFT AND THE NE RION GRABEN AREA (ACHAIA, NW PELOPONNESOS)

Palyvos N.[1(*)], Sorel D.[2], Lemeille F.[3], Mancini M.[4], Pantosti D.[1], Julia R.[5], Triantaphyllou M.[6], and De Martini P. M.[1]

[1] *Istituto Nazionale di Geofisica e Vulcanologia, Sez. Sismologia e Tettonofisica, Active Tectonics Group, palyvos@ingv.it, pantosti@ingv.it, demartini@ingv.it*

[2] *Université Paris-Sud, Centre d'Orsay, Faculty of Geology, 91405 Orsay Cedex, sorel@geol.u-psud.fr*

[3] *Institut de Radioprotection et de Surete Nucléaire, Seismic Hazard Division, Fontenay-aux-roses Cedex, francis.lemeille@irsn.fr*

[4] *CNR – Istituto di Geologia Ambientale e Geoingegneria, Roma, marco.mancini@igag.cnr.it*

[5] *Institute of Earth Sciences Jaume Almera, Barcelona 08028, ramon.julia@ija.csic.es*

[6] *National and Kapodistrian University of Athens, Faculty of Geology and Geoenvironment, Department of Hist. Geology - Paleontology, mtriant@geol.uoa.gr*

(*) now at Harokopio University, Geography Department, palyvos@hua.gr

Abstract

We review and present new geochronological data on the uplifted Middle-Late Pleistocene marine deposits at the western termination of the Corinth Rift and the Rion area. Geomorphological and geological observations define the general morphotectonic context of these deposits, which predicts a pattern of differential uplift. Uplift rate estimates based on previous geochronological data (ranging from 0.4 to 6 mm/yr) are discussed in the proposed morphotectonic context of differential uplift, together with estimates from new geochronological data. Based on the data available for post-MIS11 marine deposits, we conclude that time-averaged uplift rates in the last 300-200 ka have been higher than ca. 1.8 mm/yr at the areas of faster uplift (e.g. Profitis Elias, Ano Kastritsi). To define just how higher than 1.8 mm/yr they have been, and to cross-check the validity of very high uplift rate estimates (≥ 4 mm/yr) existing in the bibliography, more datings than those available are required.

Key words: *Tectonic geomorphology, differential coastal uplift, deformation rates, active normal faults, Corinth Gulf.*

Περίληψη

Στην εργασία αυτή γίνεται επισκόπηση υπαρχόντων και παρουσίαση νέων γεωχρονολογικών δεδομένων για τις ανυψωμένες μέσο-άνω πλειστοκαινικές θαλάσσιες αποθέσεις στο δυτικό άκρο του Κορινθιακού κόλπου και την περιοχή Ρίου-Ψαθοπύργου. Γεωμορφολογικές και γεωλογικές παρατήσεις καθορίζουν το γενικό

μορφοτεκτονικό πλαίσιο, το οποίο υποδηλώνει διαφορική ανύψωση με συγκεκριμένα γενικά χαρακτηριστικά. Οι ρυθμοί ανύψωσης που προκύπτουν από προϋπάρχοντα γεωχρονολογικά δεδομένα από διάφορες θέσεις (κυμαινόμενοι από 0.4 έως 6 mm/yr), συζητώνται στα πλάισια του ευρύτερου μορφοτεκτονικού σκηνικού, μαζί με εκείνους από τα νέα δεδομένα. Με βάση χρονολογήσεις θαλάσσιων αποθέσεων νεότερων του ισοτοπικού σταδίου 11, οι μέσοι ρυθμοί ανύψωσης κατά τα τελευταία 300-200 ka είναι μεγαλύτεροι των 1.8 mm/yr στις ταχύτερα ανυψούμενες περιοχές (π.χ. Προφήτης Ηλίας, Άνω Καστρίτσι). Για να προσδιορισθεί το πόσο ακριβώς μεγαλύτεροι είναι ή για την επιβεβαίωση πολύ υψηλών ρυθμών ανύψωσης (≥ 4 mm/yr) που απαντούν στη βιβλιογραφία, απαιτούνται περισσότερα δεδομένα από τα υπάρχοντα.
Λέξεις κλειδιά: *Μορφοτεκτονική, διαφορική ανύψωση ακτών, ρυθμοί παραμόρφωσης, ενεργά κανονικά ρήγματα, Κορινθιακός Κόλπος.*

1. Introduction

The coast of NW Peloponnesos at the westernmost part of the Corinth Gulf Rift and the NE part of the Rion-Patras graben (inset in Fig. 1 top), is characterised by fast active uplift. Geochronological studies of uplifted Middle-Late Pleistocene marine deposits (Doutsos *et al.*1988, Frydas 1991, Doutsos and Poulimenos 1992, Stamatopoulos *et al.* 1994/2004, Frydas *et al.* 1995) have yielded average uplift rate estimates in the range 0.4 to 6 mm/yr (Stamatopoulos *et al.* 1994, Kontopoulos and Zelilidis 1997, Houghton *et al.* 2003, Stamatopoulos *et al.* 2004) for the period since the Middle-Late Pleistocene, and 1.6-1.9 to 2.3 mm/yr (minimum) for the Holocene (Palyvos *et al.* 2006 and subm. paper). In this communication, we review existing data on the geochronology of uplifted Pleistocene marine deposits. Subsequently, we discuss geomorphological and geological observations on the morphotectonic context of the uplifted marine deposits, and we present new U-series dating results / biostratigraphic data on the marine deposits. Afterwards, we discuss all uplift rate estimates the geochronological data translate to, in the frame of the identified morphotectonic context and the pattern of uplift it predicts.

Geomorphological and geological observations were carried out in the field, in aerial photographs of 1:15,000 / 1:30,000 scale and DEMs constructed from 1:5,000 and 1:50,000 HAGS maps. U-series dating was conducted with the total-sample dissolution method following the Bischoff and Fitzpatrick (1991) procedures, and the isotopic composition was determined by alpha spectroscopy. Samples of fine marine deposits were examined at SEM and Light microscope for calcareous nannoplankton content following standard procedures.

2. Review of geochronological results and uplift rate estimates

At the area of the westernmost part of the Corinth Rift and the NE part of the Rion-Patras graben, the lowest formation visible in the uplifted Pleistocene rift fill consists of coarse gravels of Early Pleistocene age (Symeonidis *et al.* 1987), about 200-600 m thick (Doutsos *et al.* 1988). These gravels were deposited in braider river environment and pass laterally to lacustrine/brackish deposits of the Rion-Antirion graben towards the SW (Kontopoulos and Zelilidis 1992, Frydas *et al.* 1995, Kontopoulos and Zelilidis 1997). Above the conglomerate formation, a formation of lacustrine, brackish and marine deposits is found at several locations and at different elevations (e.g. Frydas 1991, Doutsos and Poulimenos 1992, Frydas *et al.* 1995, Kontopoulos and Zelilidis 1997, Stamatopoulos *et al.* 2004).

Frydas (1991) studied diatom assemblages in lacustrine/brackish deposits at the area of Ano Zeria and specified equivalence to biozone MNN20 (270-440 ka, according to Gradstein *et al.* 2004), and an estimate of around 400ka for the age of the formation. Studies of nannoplankton assemblages by Frydas *et al.* (1995) in marine deposits in the broader area between Ano Kastritsi – Patras (Fig. 1 top and farther W), recognised assemblages that suggest a biostratigraphic range from the upper (younger) part of biozone CN14b (equivalent to zone NN20, 440-270 ka) to the

lower (older) part of biozone CN15 (equivalent to NN21, 270 ka to present). Nannofossil analysis by Flotte *et al.* (2005) in marls at the Agios Ioannis (Ano Kastritsi) area, at 585 m above sea level –a.s.l.- (location in Fig. 1), identified nannofossils of biozone NN20, which includes the MIS 9 and 11 highstands (Fig. 2).

Radiometric datings (U-series) of marine macrofauna in the area of Figure 1 have been done by Stamatopoulos *et al.* (1994), Frydas *et al.* (1995, just W of Fig. 1), Houghton *et al.* (2003), Stamatopoulos *et al.* (2004). Stamatopoulos *et al.* (1994) dated corals found at 460 m a.s.l. SW of Ano Kastritsi and obtained an age of ca. 106 ka (MIS 5c) and consequently, an average uplift rate (AUR) of ca. 4 mm/yr. Houghton *et al.* (2003) and Stamatopoulos *et al.* (2004) dated corals at the Drepanon area (Fig. 1), obtaining ages that allow correlation to a small sea-level highstand during MIS 6 and, AURs of 0.7-08 and 0.4 mm/yr, respectively.

Apart from the corals near Drepanon, Stamatopoulos *et al.* (2004) also dated molluscs (*Arca* sp.) at Ano Kastritsi and Agios Georgios areas, at 615 m a.s.l. (Ag. Ioannis) and 451 m a.s.l. (Ag. Georgios), obtaining AURs if 2.8 and 4.8 mm/yr, respectively (locations in Fig. 1 - L. Stamatopoulos, pers. comm.). Whereas unrecrystallised (aragonitic) fossil coral is especially suitable for dating, molluscan shells are less suitable because their U content is of mostly secondary origin, and because there is evidence for post-depositional U loss (Ku, 2000, Jedoui *et al.* 2003, and references therein) and provide "extremely unreliable ages" (quoting McLaren and Rowe 1996). According to McLaren and Rowe (1996), U-series ages from molluscs cannot in isolation (one dating, of one mollusc species) be demonstrated to be correct. Hillaire-Marcel *et al.* (1996) conclude that small differences between true and apparent ages (corresponding to early diagenesis) can be obtained in samples that were quickly cemented (cementation inhibiting further post-depositional U uptake), a condition that is frequently met in littoral environments. The *Arca* sp. dated in our study area did not come from cemented deposits though and, furthermore, in the study of Hillaire-Marcel *et al.* (1996), the mollusc that proved to be most problematic was in fact *Arca,* which showed much later diagenetic uptake of uranium (resulting in even younger apparent ages). Thus, the ages of the *Arca* shells may be minima only and the respective AUR estimates maxima. Whether the apparent ages may be slightly or substantially older than true ages, cannot be estimated.

3. Morphotectonic context

The geomorphic evolution of the study area has been controlled by the migration of fault activity from the basin-bounding faults (Kastritsti and Lakka f.z., Kfz and Lfz in Fig. 1) to parallel structures in the hangingwall of the latter. Namely, to the Rion-Patras, Psathopyrgos and Aigion-Neos Erineos fault zones (RPfz, Psfz and ANEfz in Fig. 1 - Doutsos *et al.* 1985/1988, Poulimenos and Doutsos 1992, Kontopoulos and Zelilidis 1997, Flotte 2003, Flotte *et al.* 2005, Palyvos *et al.* 2005 and references therein). The uplifted Middle-Late Pleistocene marine deposits in the area of interest are found at the parts of the Rion-Patras and Corinth basins that have been uplifting since the Middle-Late Pleistocene as a result of the aforementioned take-over by the presently active faults.

Maps of faults and/or the basin lithologies in the study area (all or parts of it) have been published by Doutsos *et al.* (1985, map of photolineations), Doutsos *et al.* (1988, lithostratigraphic map and map of faults from field mapping and photointerpretation), Doutsos and Poulimenos (1992, lithostratigraphic map and main fault zones only), Kontopoulos and Zelilidis (1997, lithostratigraphic map and map of faults), Koukouvelas and Doutsos (1997, map of faults) Stournaras *et al.* (1998, structural lineaments from remote-sensing), Stamatopoulos *et al.* (2004, revision of Kontopoulos and Zelilidis 1997), Flotte *et al.* (2003/2005, main structures only).

Our purpose being to try to understand the spatial variation of average uplift rates (the pattern of differential uplift) estimated at different locations in the study area, we focused a) on identifying those secondary faults at the footwall of the presently active coastal fault zones that are associated

with geomorphic signatures and geological evidence suggesting activity after the deposition of Middle-Pleistocene marine deposits and, b) in discriminating between major and minor such secondary faults. The faults in the maps in Figure 1 have been drawn from the above view-point, and in the following, we briefly describe features that we consider more important in the morphotectonic setting. We note that several (or most) of the structures exist in the maps of the bibliography cited above, with smaller or larger differences, due to different map scale and different interpretation of observations. Figure 1 does not include faults not associated to substantial displacements in the later part of the Middle-Late Pleistocene (for such faults the reader is referred to maps in the bibliography).

Ano Rodini area. In the area of Figure 1 (top), the best-defined and largest secondary structure is the Ano Rodini fault zone (ARfz), at the footwall of the Psathopyrgos fault zone (partially mapped and shown in cross-section in Doutsos *et al.* 1988, also Stournaras *et al.* 1998). The ARfz trends ENE-WSW and it is located at the projection of the Ano Kastritsi f.z. to the NE The ARfz is not well-exposed in outcrops, but it has a distinct geomorphic expression for ca. 3 km, an escarpment up to 220 m high, at the hangingwall of which brackish and marine deposits are preserved. The existence of the ARfz is also indicated by important contrasts in the bedding trends of the Early Pleistocene gravel formation across it (white stereoplots in Fig. 1), and the strong backtilt of marine deposits close to its trace (light gray stereoplot in Fig. 1). The latter backtilt is not characteristic of the broader area of the ARfz hangingwall. The overall morphology of the (intensely dissected) Ano Rodini plateau in front of the ARfz escarpment, is characterised by systematically decreasing elevations towards the NE, suggesting tilting (ca. 2°) towards the same direction (dashed line in Fig. 3 bottom). This NE-tilting is also suggested by bedding trends away from the ARfz (one example being the area to which the white stereoplot in Fig. 1 refers). We note that close to the Psathopyrgos escarpment, bedding trends in Early Pleistocene gravel formation deviate from the general NE trend identified in the morphology, due to effects of secondary faults - see cross-section in Doutsos *et al.* 1988, where the bedrock occurrence along the Psfz escarpment is considered a horst, with faults also on the southern side (see also Koukouvelas and Doutsos 1997). We do not trace these faults in Fig. 1, because they are not associated with geomorphic signatures indicative of influence in the Middle-Late Pleistocene morphotectonic evolution of the area. The area where the marine deposits are preserved probably corresponds to a shallow graben, bound to the N by a fault secondary to the ARfz.

Zeria, Ano Zeria and Lambiri area. An important secondary structure belonging to the ANEfz is the NW-SE Ziria fault zone (Zfz – Fig. 1 bottom, included in the maps of Doutsos *et al.* 1988, and Stournaras 1998, with some differences). The Zfz corresponds to a dissected, but still very well-defined escarpment, which increases in height from the NW to the SE (up to around 200 m; partial escarpment exhumation is also possible). The fault zone is generally not exposed in outcrops (for one exception, see Pantosti and Palyvos 2007), in which only minor faults sub-parallel to it can be seen or, small faults transverse or oblique to it. Apart from the conspicuous geomorphic discontinuity it corresponds to, the Zfz is also indicated by marked lithological contrast across it, along a significant part of its length. It juxtaposes the stratigraphically lower alluvial fan gravel formation (Kontopoulos and Zelilidis 1997) which occupies its footwall, against finer lacustrine, brackish and marine deposits (Doutsos *et al.* 1988, Frydas 1991, Doutsos and Poulimenos 1992), which are stratigraphically above the gravel (i.e. the Zfz displaces the lacustrine/marine formation). Faults belonging to the Zfz also cause abrupt transitions between the coarser lower part of the gravel formation and its finer upper part (in this area this distinction is possible). The contact between the gravel formation and the lacustrine/brackish/marine formation is a good stratigraphic marker, suggesting that the cumulative displacement hosted by the Zfz after the deposition of the lacustrine/marine formation is increasing towards the SE, in a scissor-like fashion, in accordance with the increasing height of the Ziria escarpment in the same direction. It is probable that the recently active Zfz is part of what was a larger structure in the past, a structure responsible for the abrupt down-stepping of the Pindos bedrock at the escarpment of the

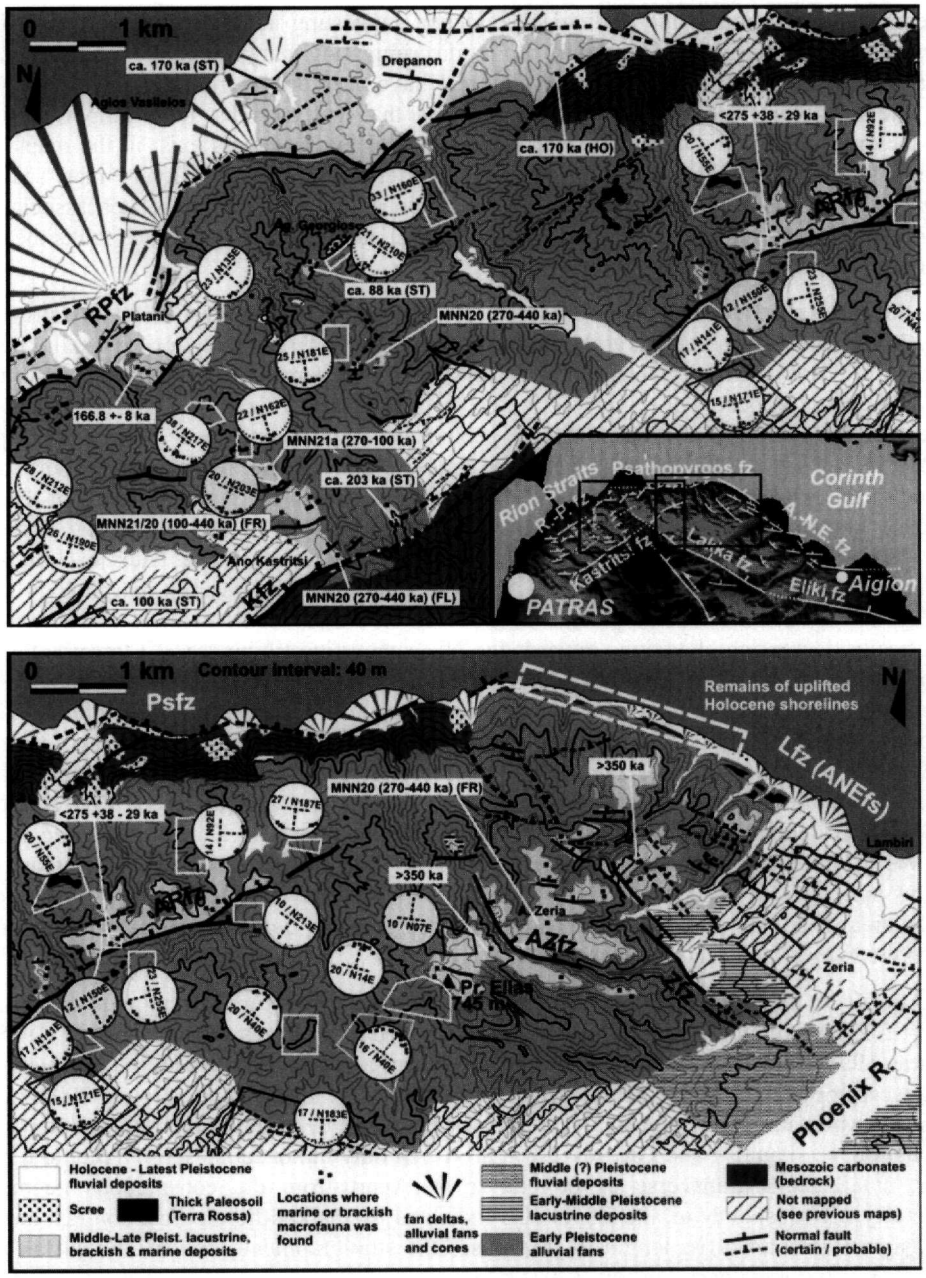

Figure 1 - Map of faults active in the last ca. 300 ka, based on geomorphological and geological observations in the field, DEMs and aerial photographs. Faults active in older periods are not depicted, the map is complementary to previously published maps by Doutsos *et al.* (1988), Doutsos and Poulimenos (1992), Kontopoulos and Zelilidis (1997) and Stamatopoulos *et al.* (2004), which include several (or most) of the fault traces, with differences due to different map scale and due to different interpretations. Line thicknesses are indicative of the amount of fault displacement. Lithological boundaries are from new field mapping (see also earlier maps with more or less small differences, in the works cited above). Stereoplots depict apparent dip measurements (in order to take advantage of measurements on inaccessible cliffs), the resultant true strike/dip estimates indicated by dashed lines

Psathopyrgos fault zone at the exact projection of the Zfz trace in Figure 1, in the area where the Panagopoula landslide complex occurs (see also Pantosti and Palyvos 2007).

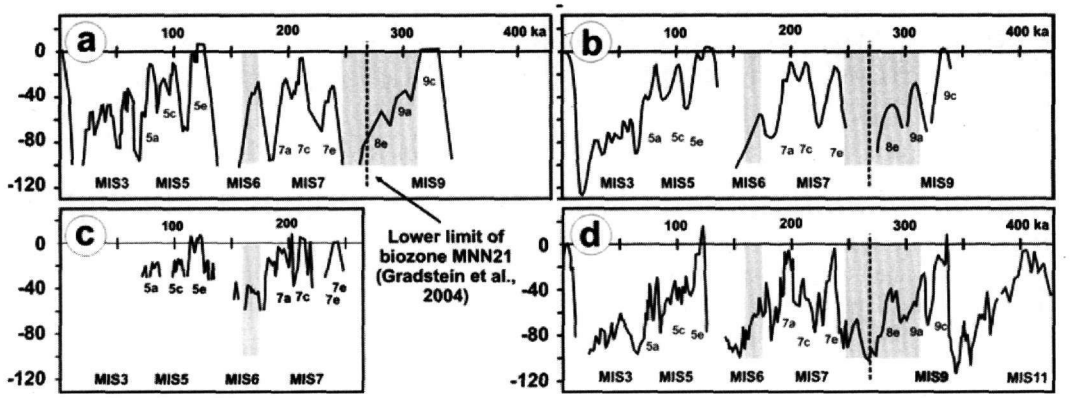

Figure 2 - Different Sealevel curves used in the estimation of average uplift rates. Grey rectangles indicate the age ranges obtained from new U-series datings of coral samples. Sea level curves from: (a) Lajoie *et al.* (1991), (b) Chappell and Shackleton (1986) and Imbrie *et al.* (1984) for MIS 8 and 9, (c) Thompson and Goldstein (2005), (d) Siddall *et al.* (2003). The curves in (a) and (c) come from dated marine terraces in uplifting areas, whereas the other two are based on oxygen isotope records in deep-sea cores

The second most important structure in the area is the Ano Zeria fz (AZfz in Fig. 1 bottom), to the SW of the Zfz, which is associated to an escarpment up to 120-140 m high and clear-cut downstepping of the formation with the marine deposits. In-between the Zfz and the coastal Lambiri f.z, a swarm of NW-SE-trending faults (included in the map and a cross-section in Doutsos *et al.* 1988, some also in Stournaras *et al.* 1998) is indicated by pristine geomorphic signatures, namely linear morphological discontinuities associated with scarps at valley divides and aligned tributary streams on the sides of the main valleys, abrupt lithological changes across them and, in some cases, they can also be observed in outcrops (see DEM from 1:5,000 maps and detailed map of faults in Pantosti and Palyvos 2007). The recognition of the smaller NW-SE faults permits us to avoid misinterpretation of the morphological steps in-between the Ziria and Lambiri fault escarpments, as remains of successive Pleistocene marine terraces. These NW-SE faults accommodate tilting to the SE and down to the NE stepping of the area between the Zfz and Lfz. The SE tilting is suggested by the overall morphology of the latter area (see Pantosti and Palyvos 2007), whereas down-stepping to the SE by NE-SW faults (as mapped by Doutsos *et al.* 1988) may also be superimposed on this general SE tilting trend.

Kastritsi – Agios Georgios area. Doutsos *et al.* (1988) identify a NE to ENE main structural trend in the broader Rio Graben. In the area of Figure 1 (top), the general trend of the main structures, the Kfz and the RPfz (e.g. Doutsos *et al.* 1985, Doutsos and Poulimenos 1992, Kontopoulos and Zelilidis (1997), Flotte *et al.* 2005) is NE-SW. As far as the pattern of secondary faults is concerned, Doutsos *et al.* (1988) mapped faults at various directions, Doutsos and Poulimenos (1992) measured faults with strikes varying from NE-SW to NW-SE (map of the measured faults not included), whereas Kontopoulos and Zelilidis (1997) report a fault pattern consisting of NE-SW normal faults and NW-SE transfer faults. The transfer faults are considered syn-sedimentary with respect to the Early Pleistocene alluvial fan formation, controlling the facies distribution within it (Kontopoulos and Zelilidis 1997). Stournaras *et al.* (1998) do not trace NW-SE faults but several structural lineaments of E-W direction.

As previously specified, the faults in Figure 1 (top) are drawn from a viewpoint of impact on the morphotectonic evolution in the last ca. 300 ka. Thus, they do not include the NW-SE faults in Kontopoulos and Zelilidis (1997) and the prolongation of the Lakka fault zone along the Volinaios

valley traced in Poulimenos and Doutsos (1992), also in order not to mix fault traces drawn with different degrees of generalization. The lengths of the fault traces in Figure 1, in several cases are expected to be underestimates of true fault lengths, due to fault signatures being lost or inconclusive in valleys by erosion and/or landsliding (intense in the area – see Rozos 1991). For the same reasons, we may have missed secondary faults with appreciable displacements in the last 300 ka.

Bibliographic data and our observations regarding the geometry of the RPfz are summarised in Palyvos *et al.* (2007, this volume). As far as secondary structures in-between the RPfz and the Kfz are concerned, in general terms, the available data suggest a pattern consisting of faults parallel to the general direction of the RPfz and Kfz, together with faults oblique to this direction. These faults are indicated by geological evidence and geomorphic discontinuities indicative of activity in the last 300 ka. The oblique faults have been simultaneously active with the NE-SW faults since they also displace the middle – Pleistocene marine deposits (Doutsos *et al.* 1988) and are associated with smaller or larger escarpments. Examples are the oblique faults (ENE-WSW and E-W trending) at the Ano Kastritsi area and to its NW. Direct evidence of recent activity on transverse NW-SE fault zones we identified at the western divide of Volinaios, where in three cases such fault zones are associated to small graben, inside which downthrown marine deposits have escaped erosion.

Bedding in the area between the Kfz and the RPfz, in general dips 20-30° towards the SW-SSW (Flotte *et al.* 2005); locally, steeper or gentler dips can be observed. Stereoplots in Figure 1 (top) include both Early Pleistocene gravel (white) and brackish/marine deposits above them (grey). The fact that both formations show comparably steep dips, indicates that the latter are the result of tilting (i.e. the strong dips of the alluvial fan gravel formation contain only a small component of depositional dip).

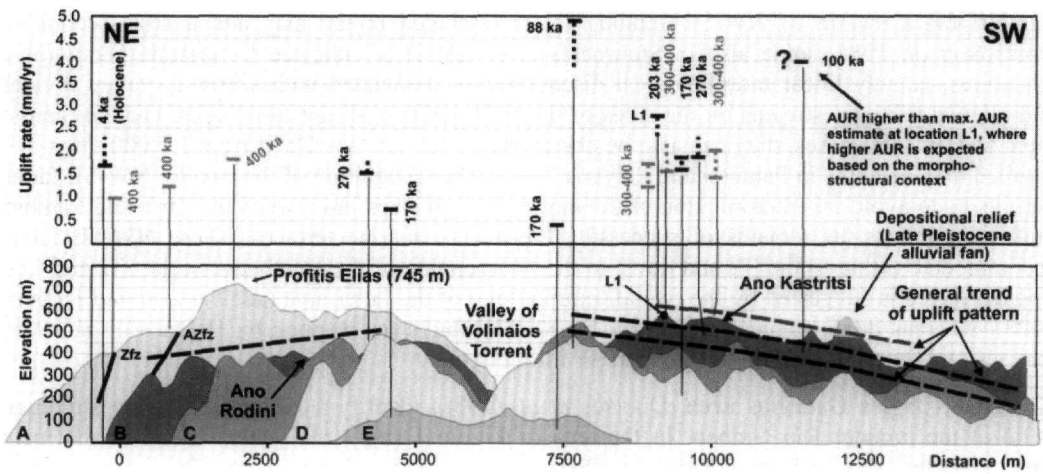

Figure 3 - Bottom: Topographic profiles along the study area (parallel to NE-SW main and secondary fault zones). Exact profile traces in Pantosti and Palyvos (2007). Thick dashed lines indicate the broad-scale pattern of uplift at the hangingwall of the Kastritsi and Ano Rodini fault zones (profiles B, C and D). Profile A is to the SE of the ARfz (passing from the Profitis Elias peak). Profile E crosses a small block at the intersection of the Rion- Patras and Psathopyrgos f.z., the fault zones active at present.

Top: Average uplift rate estimates since different periods of the Middle-Late Pleistocene, from previously available data (Frydas 1991, Frydas *et al.* 1995, Stamatopoulos *et al.* 1994, Houghton *et al.* 2003, Stamatopoulos *et al.* 2004) and new data from this study. Holocene uplift rate estimate from Palyvos *et al.* (2006)

The area between the Kfz and the RPfz has been intensely dissected by fluvial erosion, yet, if the envelope of the relief is considered a "ramp" morphology is identified, with terrain elevations increasing from Patras towards the Volinaios Valley (Fig. 3 bottom). This morphology suggests ca. 2.3° of broad-scale tilting towards the SW. An explanation for the discrepancy between the gentle broad-scale tilting suggested by geomorphology and the much steeper dips of Pleistocene strata (including the marine deposits of the last 300 ka), can be that the steep stratigraphic dips reflect local rotations of small blocks bounded by secondary faults in the area between the Kfz and the RPfz. This hypothesis, requires that transverse faults like those proposed by Kontopoulos and Zelilidis (1997), have had activity also after the deposition of the Early PLeistocene gravel formation.

4. New geochronological data and uplift rate estimates

Corals are indeed rare in most of the studied area and it was only after extensive search that we found some, in relatively few locations. An important point regarding the interpretation of the obtained U-series ages is their geomorphic and stratigraphic context. High rates of coastal uplift have resulted in intense erosion that has eradicated marine terraces in most of the area ("terraces" in a geomorphic sense), whereas ubiquitous faulting does not allow conclusive interpretation of knickpoints at the interfluves as evidence of paleoshorelines. Thus we do not have direct evidence that the sampled deposits are stratigraphically close to marine highstands.

Previous studies have identified that the deposits in the Corinth and Patras Gulfs basins have been alternating between lacustrine, brackish and marine conditions since the Middle Pleistocene (e.g. Keraudren and Sorel 1987, Frydas 1991, Piper *et al.* 1990 and references therein), due to the existence of sills on both the W and E extremities of the basins. In more recent periods (Late Pleistocene) an analogue is the isolation of the still-active parts of the basins by the Araxos and Rion Sills (e.g. Piper *et al.* 1990, Perissoratis *et al.* 2000 and references therein). In view of the above, the discussion in the following will be based on the assumption that the marine deposits should be close to peaks of the Middle-Late Pleistocene eustatic sea-level curve, i.e. we will exclude the lower sea-levels during glacial periods.

Profitis Elias-Ano Zeria area. We dated coral samples (Sorel *et al.* 2005) retrieved at 638 and 405 m a.s.l. from the first marine layer in the formation where Frydas (1991) found diatom assemblages biostratigraphically equivalent to biozone MNN20 (270-440 ka). We obtained ages older than the limit of the U-series method, i.e. "older than 350 ka". As already recognised by Doutsos *et al.* (1988), these deposits are downthrown to successively lower elevations by faults (see next section). Our datings verify the age estimate of "ca. 400 ka" by Frydas (1991) (MIS11 – Fig. 2), in the sense that they exclude the MIS 9 (which is also within biozone MNN20). Assigning the deposits at the Profitis Elias peak (745 m) to the MIS11, we obtain an AUR estimate of ca. 1.8 mm.yr and successively lower ones at down-faulted occurrences of the formation (Fig. 3 top).

Ano Rodini area. At the area of Ano Rodini, we found relatively abundant *Cladocora* sp. corals at three neighbouring locations. A coral sample at ~440 m a.s.l. was dated with the U-series method and gave an age of 275.05 +38.4/-28.8 ka. The $^{230}Th/^{232}Th$ ratio for this sample was below 20 (highlighted in gray in Table 1), indicating contamination with detrital Th. Such contamination results in apparent ages that are older than the true age of a sample. Thus, the obtained age is a maximum-limiting age. Considering that the marine deposits containing the corals most likely should correspond to a period of high sea-level (due to the sill existing farther west), based on the obtained oldest possible age (275+38.4= 313.4 ka), the dated corals should not be older than the MIS 9a highstand (Fig. 2). Assigning them to MIS 9a we obtain a minimum AUR in the range 1.49-1.57 mm/yr. Given that the limit between biozones MNN20 and MNN21a (ca. 270 ka) is close to the obtained age, it would provide a useful constraint on the true age of the deposits from which the corals came from. We carried out nannofossil analyses on two samples of fine nearshore

deposits at 2 different outcrops but, unfortunately both samples were devoid of calcareous nannofossil assemblages.

Ano Kastritsi and Agios Georgios areas. We dated a coral (*Cladocora sp.*) sample retrieved at 252 m a.s.l., obtaining an age of 166.82 +7.7 / -7.2 ka (Fig. 1, Table 1). Micropaleontological analyses identified biozone MNN21a at 480 m a.s.l. (Ano Kastritsi interfluve) whereas a third sample was found to belong to biozone MNN20 (at ca. 492 m a.s.l., Agios Georgios interfluve).

Table 1 - Results of U-series dating of corals from Pleistocene marine deposits. Gray highlight indicates sample slightly contaminated by detrital Th (provides maximum age only)

Sample	Elevation a.s.l. (m)	^{238}U (ppm)	^{232}Th (ppm)	$^{230}Th/^{232}Th$	$^{230}Th/^{234}U$	$^{234}U/^{238}U$	Age (ka)
Profitis Elias (1103)	638	1.88	0.23	31.863 ±1.194	1.14 ±0.03	1.10 ±0.01	≥ **350**
Ano Zeria (1003)	405	1.58	0.31	20.762 ±0.568	1.17 ±0.03	1.11 ±0.01	≥ **350**
Ano Rodini TS (506)	436	2.63	0.80	10.922 ±0.363	0.95 ±0.03	1.13 ±0.02	**275.05** +38/-29
Platani TS (3406)	252	2.1	0.15	34.969 ±1.523	0.79 ± 0.01	1.01 ±0.01	**166.82** +7.7 / -7.2

The only highstand included in the age range obtained for the corals at 252 m, is the MIS6e highstand (Fig. 2). The MIS6e highstand, depending on which eustatic curve is followed, may consist of one or two (shorter-lived) highstands. Using different curves in Figure 2 we obtain AUR estimates in the range 1.61-1.80 mm/yr. We note that if the younger ages in the obtained age range are considered, uplift rate estimates would be higher (also because paleo-sealevel was lower).

The identification of biozone MNN21a provides a maximum-limiting age for the relevant deposits, thus it can be used to estimate minimum values for AUR. The base of MNN21a is placed at around 270 ka (Gradstein *et al.* 2004). If these limits are taken literally, the oldest highstands allowed for would be in MIS 7 (7e), translating to min. AUR in the range 1.99-2.14 mm/yr for the deposits at 480 m a.s.l. (using different curves in Fig. 2). Based on U-series datings and correlation of marine terrace remains at the broader area of Aravonitsa farther E (Pantosti and Palyvos 2007, and paper in prep.), deposits that were found to be marginally within zone MNN21a correlate most probably to the MIS 8e highstand, which is just out of the lower limit of MNN21. Given that the latter limit is not exact (it is associated to an error of several ka) and that works putting it to 285 ka do exist, in order to be on the safe side, we will estimate a minimum AUR assuming that the marine deposits at 480 m correlate to the highstand at MIS8e or younger highstands. This way, we obtain a min. AUR in the range 1.79-1.89 mm/yr.

The presence of MNN20 at 492 m a.s.l. (within a small graben) translates to a min. AUR of 1.23 mm/yr (assigning the deposits to the oldest highstand in MNN20, i.e. the MIS11 at ca. 400 ka) and max. AUR of 1.64-1.78 mm/yr, if assigned to the youngest possible highstand in MNN20 (MIS9a). The MNN20 deposits at the location sampled by Flotte *et al.* (2005) at 585 m a.s.l., translate to a min. 1.46 mm/yr and max. 1.94-2.08 mm/yr AUR with the same reasoning as above (Fig. 3 top). The highest remains of marine deposits in the same area are at about 620 m a.s.l., where Stamatopoulos *et al.* 2004 obtained an age of 203 ka from molluscs (an age that we consider as minimum-limiting, and the respective AUR of 2.8 mm/yr as maximum-limiting). Based on the fact that the oldest purely marine deposits above the Early Pleistocene alluvial fan formation belong to MIS 11 (Frydas 1991 and also the U-series datings herein), these deposits cannot be older than MIS11. Assigning them to MIS11, translates to 1.55 mm/yr minimum AUR (Fig. 3 top).

5. Discussion and conclusions

The obtained average uplift rates (AURs) at different locations (the AUR "field"), should be viewed and interpreted in the context of the identified broad-scale morphotectonic pattern, the changes of rates of activity of the involved main fault systems in the period of interest (i.e. the timing of decrease of activity or death of the Kfz), and in more detail, the pattern of secondary faults and the movements of the smaller fault blocks they define, that are superimposed on this broad-scale deformation. The simplest example of the significance of the above in the study area, concerns the AURs at the Drepanon (Houghton *et al.* 2003, Stamatopoulos *et al.* 2004), which refer to small blocks at the intersection of the Psfz and the RPfz, and not to "the western end of the Gulf of Corinth" (Houghton *et al.* 2003).

The highest remains of marine deposits are found at Profitis Elias (PE) in a formation that dates to the MIS11 (Frydas 1991 and this study) and indicates an AUR of ca. 1.8 mm/yr. They correspond to the first marine incursion in the Corinth Rift during the Middle Pleistocene (as recognised also at the E part of the Rift, by Keraudren and Sorel 1987). The min. AUR at Ano Rodini (1.49-1.57 mm/yr) indicates that at the hangingwall of the ARfz, where we would expect a substantially smaller AUR compared to PE (because the dated marine deposits have been downthrown by the ARfz), we get a comparable min. AUR instead. Also the minimum estimates of Holocene uplift rate in the same area (1.6-2.3 mm/yr Palyvos *et al.* 2006 and paper in prep.) are comparable to the min. AUR at PE. The interpretation we propose is that the AUR at PE, because it is derived from the oldest marine deposits (MIS11), it includes a component of subsidence from the Lakka f.z. (Lkfz), at the hangingwall of which it was deposited. The above is supported by the fact that the dated deposits at PE are not associated to a marine terrace, but a marine intercalation within lacustrine deposits (Frydas 1991, see also Pantosti and Palyvos 2007). Terraces would start forming only after the uplift from the presently active coastal faults superseded the subsidence by the Lfz (causing net uplift above present sea level), due to decrease in the activity or, complete death of the latter. Erosion may have removed a post-MIS11 terrace above them (see Pantosti and Palyvos 2007 for locations of probable post-MIS11 marine deposits in the broader PE area, remnants of younger sequences eroded away).

Given the above, the usual assumption that uplift rate may considered constant through the Middle-Late Pleistocene, is not applicable in our case. Thus, AUR estimates from MIS11 deposits cannot be compared with the AURs from younger deposits, which are expected to be higher (at the same locations, that is). This is observed at Ano Kastritsi, where the AUR from the MNN20 deposits at 585 m a.s.l. (1.46-2.08 mm/yr) is comparable or smaller to AURs estimated from younger marine deposits that have been down thrown substantially by secondary faults (Platani corals and MNN21 at 480 m a.s.l., yielding 1.6-1.8 and min. 1.79-1.89 mm/yr AUR). The uplift rates from post MIS11 deposits at these latter locations is, imply even higher post-MIS11 AURs at the footwalls of the relevant secondary faults (and consequently, also at the areas of the highest occurrences of marine deposits at 585 and 620 m).

Based on a conservative reading of the available data from post-MIS11 marine deposits, we conclude that AURs in the last 300-200 ka have been higher than 1.7-1.8 mm/yr at the faster uplifting areas (Profitis Elias, Ano Kastritsi). For comparison, based on three U-series datings along a transect just to the SE of Figure 1 (bottom), in the Aravonitsa-Selianitika area, AURs in the last 300-200 ka have been of the order of 1.5-1.6 mm/yr or somewhat higher (Pantosti and Palyvos 2007 and paper in prep.). In the area studied herein, defining just how higher than 1.8 mm/yr AURs have been, requires more data than those available. E.g. the 4 mm/yr AUR obtained by Stamatopoulos *et al.* (1994) to the SW of Ano Kastritsi, given the general pattern of differential uplift that predicts increasing AUR towards Ano Kastritsi, it implies even higher AUR at the latter area (Kontopoulos and Zelilidis 1997 estimated 6 mm/yr). Values of 4 and 6 mm/yr being indeed very high and, implying even higher AUR at Profitis Elias, together with a contradiction with the

max AUR of. 2.8 mm/yr obtained at 620 m NE of Kastritsi by Stamatopoulos *et al.* (2004), indicate that more dating of corals at the same and other locations is more than desirable.

Should a more or less well-defined staircase of marine terraces unaffected by faulting had been present, the available data would have been more than enough to constrain the uplift rate at the area of interest, to identify erroneous datings, and to determine the timing of the switch of activity from the Kfz to the Rpfz. The contrary being the case (no terraces, a lot of faults, lack of corals at critical locations), the riddle remains to be resolved by further studies.

6. Acknowledgments

This work was conducted in the frame of the 3HAZ Corinth EU project, and CNRS project GDR Corinthe n. 234. We warmly thank Leonidas Stamatopoulos (University of Patras) for discussion, for giving us details on locations of marine samples dated with the U-series and for pointing out and providing us previous works. We appreciate the constructive review of the submitted manuscript by Gerald Roberts (Birkbeck College - University of London), whom we also thank.

7. References

Bischoff, J.L., Fitzpatrick, J.A., 1991. U-series dating of impure carbonates: an isochron technique using total-sample dissolution, *Geochimica et Cosmochimica Acta*, 55, 543-554.

Chappell, J., and Shackleton, N.J., 1986. Oxygen isotopes and sea-level, *Nature*, 324, 137-140.

Doutsos, T., Kontopoulos, N., and Ferentinos, G., 1985. Das westliche ende des Korinth-Grabens, *N. Jb. Geol. Palaont. Mh.*, H11, 652-666.

Doutsos, T., Kontopoulos, N., and Poulimenos, G., 1988, The Corinth-Patras Rift as the initial stage of continental fragmentation behind an active island arc (Greece), *Basin Research*, 1, 177-190.

Doutsos, T., and Poulimenos, G., 1992. Geometry and kinematics of active faults and their seismotectonic significance in the western Corinth-Patras rift (Greece), *Journal of Structural Geology*, 14 (6), 689-699.

Flotté, N. 2003. Caracterisation structurale et cinematique d'un rift sur detachement: Le rift de Corinthe-Patras, Grece, *These doct.*, 196pp., Univ. de Paris-Sud.

Flotte, N., Sorel, D., Muller, C., and Tensi, J., 2005. Along strike changes in the structural evolution over a brittle detachment faultç example of the Pleistocene Corinth-Patras Rift (Greece), *Tectonophysics*, 403, 77-94.

Frydas, D., 1991. Palaookologische und stratigraphische untersuchugen der diatomeen des pleistozans der N. Peloponnes, Griechenland, *Bull. Geol. Soc. Greece*, XXV/2, 499-513.

Frydas, D., Kontopoulos, N., Stamatopoulos, L., Guernet, C., and Voltaggio, M., 1995. Middle-Late Pleistocene sediments in the northwestern Peloponnesus, Greece. A combined study of biostratigraphical, radiochronological and sedimentological results, *Berliner Gowiss*, E16, 589-605.

Hillaire-Marcel,C., Gariepy, C., Ghaleb, B., Goy, J.-L., Zazo, C., and Barcelos, J.C., 1996. U-Series measurements in Thyrrhenian deposits from Mallorca – further evidence for two last-interglacial high sea levels in the Balearic Islands, *Quaternary Science Reviews*, 15, 53-62.

Houghton, S.L., Roberts, G.P., Papanikolaou, I.D., and McArthur, J.M., 2003. New $234U\text{-}230^{Th}$ coral dates from the western Gulf of Corinth: implications for extensional tectonics, *Geophysical Research Letters*, 30(19), 2013. doi:10.1029/2003GL018112

Jedoui, Y., Reyss, J.-L., Kallel, N., Montacer, M., and Davaud, E., 2003, U-series evidence for two high Last Interglacial sea levels in southeastern Tunisia, *Quat. Sci. Rev.*, 22, 343-351.

Keraudren, B., and Sorel, D., 1987. The terraces of Corinth (Greece) – A detailed record of eustatic sea-level variations during the last 500,000 years, *Marine Geology*, 77, 99-107.

Kontopoulos, N., and Zelilidis, A., 1992. Upper Pliocene lacustrine environments in the intramontane Rio graben basin, NW Peloponnesus, Greece, *N. Jb. Geol. Palaont. Mh.*, H2, 102-114.

Kontopoulos, N., and Zelilidis, A., 1997. Depositional environments of the coarse-grained lower Pleistocene deposits in the Rio-Antirio basin, Greece. In G. Marinos, *et al.* (eds), *Engineering Geology and the Environment*, A. A. Balkema, Rotterdam, 199-204.

Koukouvelas, I., and Doutsos, T., 1997. The effects of active faults on the generation of landslides in NW Peloponnese. In G. Marinos, *et al.* (eds), *Engineering Geology and the Environment*, A. A. Balkema, Rotterdam, 799-804.

Ku, T.-L., 2000. Uranium series methods, In Noller *et al.* (eds), *Quaternary Geochronology – methods and applications*, AGU reference shelf 4, 101-114.

Lajoie, K.R., Ponti, D.J., Powell, C.L., Mathieson, S.A., and Sarna-Wojcicki, A.M., 1991. Emergent marine strandlines and associated sediments, coastal California: a record of Quaternary sea-level fluctuations, vertical tectonic movements, climatic changes and coastal processes, In R.B. Morrison (ed.), *Quaternary Non-Glacial Geology: Conterminous United States: Geological Society of America Decade of North America Geology*, K-2, 190–214pp.

McLaren, S.J., and Rowe, P.J., 1996. The reliability of Uranium-series mollusc dates from the western Mediterranean basin, *Quaternary Science Reviews*, 15, 709-717.

Palyvos, N., Pantosti, D., Stamatopoulos, L., and De Martini, P.M., 2007a. A geomorphological reconnaissance of the Psathopyrgos and Rion-Patras fault systems (Achaia, NW Peloponnesus), *Bull. Geol. Soc. Gr.*, XXXVII. (submitted)

Palyvos, N., Lemeille, F., Sorel, D., Pantosti, D., Pavlopoulos, K., and Philippon, J., 2006. Undocumented uplifted Holocene shorelines at the western termination of the Corinth Gulf Rift: a record of coseismic uplift episodes? *Geophysical Research Abstracts*, vol. 8, 04754.

Palyvos, N., Pantosti, D., DeMartini, P. M., Lemeille, F., Sorel, D., and Pavlopoulos, K, 2005. The Aigion-Neos Erineos normal fault system (Western Corinth Gulf Rift, Greece): Geomorphological signature, recent earthquake history and evolution, *Journal of Geophysical Research,* Vol. 110, No. B9, B09302, 15 pp.

Pantosti, D., and Palyvos, N., (eds), 2007. "3HAZ Corinth" Project Deliverable 30, Maps of active faults, marine terraces and landslides, Unpubl. Report, INGV.

Perissoratis, C., Piper, D.J.W., and Lykousis, V., 2000. Alternating marine and lacustrine sedimentation during the late Quaternary in the Gulf of Corinth rift basin, central Greece, *Marine Geology*, 167, 391-411.

Piper, D.J.W., Doutsos, T., and Stamatopoulos, L., 1990. Quaternary history of the Gulfs of Patras and Corinth, Greece, *Z. Geomorphol.*, 34, 4, 451-461.

Rozos, D., 1991. Engineering geological conditions in Achaia Province – geomechanical characteristics of the Plio-Pleistocene Sediments, *PhD Thesis*, Department of Geology, University of Patras. (in Greek)

Siddall, M., Rohling, E.J., Almogi-Labin, A., Hemleben, C., Meischner, D., Schmelzer, I., and Smeed, D.A., 2003, Sea-level fluctuations during the last glacial cycle, *Nature*, 423, 853-858.

Sorel, D., Pantosti, D., Lemeille, F., Palyvos, N., and De-Martini, P.M., 2005, The step-over between the Eliki and Aigion fault systems: slip transfer and present rates of activity. Unpubl. report for CNRS project GDR Corinthe n° 234, 13pp.

Stamatopoulos, L., Voltaggio, M., and Kontopoulos, N., 1994. ^{230}Th / ^{238}U dating of corals from Tyrrhenian marine deposits and the Palaeogeographic evolution of the Western Peloponnesus (Greece), *Munster. Forsch. Geol. Palaont.*, 76, 345-352.

Stamatopoulos, L., Kontopoulos, N., Voltaggio, M., and Branca, M., 2004. Radiochronological data with U/Th method in lagoonal/marine deposits of the NW Peloponnese, Greece. *Bull. Geol. Soc. Greece*, XXXVI, 1064-1067. (in Greek)

Stournaras, G., Tsimpidis, G., Tsoumanis, P., Yannatos, G., and Guillande, 1998. Instability phenomena in the Neogene deposits of Northern Peloponnesus, Greece, *Bull. Eng. Geol. Env.*, 57, 65-68.

Symeonidis, N., Theodorou, G., Schutt, H., and Velitzelos, E., 1987. Paleontological and stratigraphical observations in the area of Achaia and Etoloakarnania (W Greece), *Ann. Geol. Pays. Hellen.*, 38, 317-353.

Thompson, W.G., and Goldstein, S.L., 2005. Open-system coral ages reveal persistent suborbital sea-level cycles, *Science*, 308, 401-404.

Tsoflias, P., and Loftus, D.L., 1971. Geological map of Greece in 1:50,000– Nafpaktos sheet, IGME, Athens.

Δελτίο της Ελληνικής Γεωλογικής Εταιρίας τομ. XXXX, 2007
Πρακτικά 11ου Διεθνούς Συνεδρίου, Αθήνα, Μάιος 2007

Bulletin of the Geological Society of Greece vol. XXXX, 2007
Proceedings of the 11th International Congress, Athens, May, 2007

GEOLOGICAL, GEOMORPHOLOGICAL AND TECTONIC STRUCTURE OF NE ATTICA AND SEISMIC HAZARD IMPLICATIONS FOR THE NORTHERN EDGE OF THE ATHENS PLAIN

Papanikolaou D.[1], and Papanikolaou I.[1, 2]

[1] *National and Kapodistrian University of Athens, Faculty of Geology and Geoenvironment, Laboratory on Natural hazards, Department of Dynamic, Tectonic and Applied Geology Panepistimioupolis Zografou, 157-84 Athens, Greece, dpapan@geol.uoa.gr*

[2] *University College London, Department of Earth Sciences, Benfield-UCL Hazard Research Centre, Gower Str. WC1E6BT London, UK. E-mail: i.papanikolaou@ucl.ac.uk*

Abstract

A synthesis of geology, geomorphology and tectonics has been compiled regarding the NE part of Attica. This synthesis helps us clarify how old and new structures interrelate and interact to provide the present day setting. Geological, geomorphological maps, and cross-sections are provided to help us depict and extract data. The region of NE Attica forms a tilted tectonic block bounded by the Afidnai fault to the south and the Oropos fault to the north that rotates to the S-SW. This tilt produces southern trending flow directions draining the footwall within the block. Drainage basins are highly asymmetric due to the presence of active normal faults producing a combination of fault parallel and fault perpendicular flow directions. This block is also divided by a NNE-SSW detachment fault that separates the metamorphic units to the east from the unmetamorphic units to the west. It was active in Late Miocene-Early Pliocene and produced several hundred meters of debris-flow deposits. This detachment influences the geometry, style and intensity of deformation, but also the seismicity pattern. In particular, this detachment coincides with the line separating zone I (lowest category of seismic risk) from zone II of the national seismic building code. Finally, the Athens plain is bounded northwards by the active, but low slip-rate E-W trending, 14 km long, Afidnai fault.
Key words: *Detachment, active fault, Afidnai, Oropos, Marathon.*

Περίληψη

Με βάση τη σύνθεση των γεωλογικών, γεωμορφολογικών και τεκτονικών δεδομένων της ΒΑ Αττικής γίνεται διάκριση της αλληλοσυσχέτισης μεταξύ παλαιών και νέων δομών που διαμορφώνουν την παρούσα κατάσταση. Η εξαγωγή δεδομένων βασίστηκε σε γεωλογικούς και γεωμορφολογικούς χάρτες και τομές. Η περιοχή της ΒΑ Αττικής αποτελεί ένα ρηξιτέμαχος το οποίο οριοθετείται από το ρήγμα των Αφιδνών στα νότια και το ρήγμα του Ωρωπού στα βόρεια και περιστέφεται προς τα νότιο-νοτιοδυτικά. Η περιστροφή αποστραγγίζει το υδρογραφικό δίκτυο προς το νότο πάνω στο δάπεδο του ρηξιτεμάχους. Οι λεκάνες του υδρογραφικού δικτύου είναι έντονα ασύμμετρες λόγω

της παρουσίας των ενεργών ρηγμάτων. Οι διευθύνσεις ροής των ρεμάτων λόγω της δράσης των ρηγμάτων είναι είτε παράλληλες είτε εγκάρσιες ως προς τα ρήγματα. Το ρηξιτέμαχος διαιρείται μέσω ενός ΒΒΑ-ΝΝΔ ρήγματος αποκόλλησης σε ένα ανατολικό τμήμα με μεταμορφωμένα πετρώματα και σε ένα δυτικό με αμεταμόρφωτα. Το ρήγμα αυτό ήταν ενεργό κατά το Ανώτερο Μειόκαινο – Κατώτερο Πλειόκαινο και μέσω της δράσης του προκάλεσε την απόθεση πολλών εκατοντάδων μέτρων αδιαβάθμητων ιζημάτων κροκαλο-λατυποπαγών. Το ρήγμα αυτό επηρεάζει τόσο την γεωμετρία, το είδος και την ένταση της παραμόρφωσης όσο και την σεισμικότητα της ευρύτερης περιοχής. Πιο συγκεκριμένα, το ρήγμα αποκόλλησης ταυτίζεται με το όριο που διαχωρίζει την κατώτερη κατηγορία σεισμικότητας Ι, από την ενδιάμεση κατηγορία σεισμικότητας ΙΙ του Ελληνικού Αντισεισμικού Κανονισμού (ΕΑΚ-2003). Τέλος, το Λεκανοπέδιο Αθηνών οριοθετείται προς βορρά από το ενεργό, αλλά χαμηλού ρυθμού ολίσθησης, ρήγμα των Αφιδνών μήκους 14 χλμ.
***Λέξεις κλειδιά**: Ρήγμα αποκόλλησης, Ενεργό ρήγμα, Αφίδνες, Ωρωπός, Μαραθώνας.*

1. Introduction

The northeastern part of Attica forms a complex mosaic of old and new structures. These structures shape the present-day geomorphological, neotectonic and seismicity status. In this paper we: a) try to unravel the geological history of the area since the Late Miocene, b) show how these structures interrelate and interact and c) discuss the implications for seismic hazard assessment.

2. Geological Structure

2.1. Geotectonic Units, Alpine rocks and post-Alpine sediments

Northeastern Attica comprises Alpine basement rocks, both metamorphic and non-metamorphic, and post-Alpine sediments (Fig. 1). The Alpine rocks belong to the metamorphic units of the Northern Cyclades and Almyropotamos that extend from Penteli Mt to the southern Evoikos gulf and to the non-metamorphic unit of Eastern Greece that outcrop in Parnitha Mt (Papanikolaou 1986). The Almyropotamos unit is known from southern Evia, but it crops up also in the area of Marathon. It comprises a thick Mesozoic marble sequence overlain by phyllites representing a metamorphosed Tertiary flysch (Katsikatsos 1969, Dubois and Bignot 1979). The Northern Cyclades unit emerges not only on the northern Cyclades islands, but also in a major part of the southern Evia, where it is known as the Styra unit (Katsikatsos 1979). It consists of thick sequences of mica schists and cipolines grading to siliceous marbles with alternations of greenschists and amphibolites, representing a pelagic volcanosedimentary sequence. More to the south the Northern Cyclades unit is tectonically overlying the relative autochthon unit of Attica (Lozios 1993). The non-metamorphic tectonic unit of Eastern Greece comprises: (i) the SubPelagonian Triassic-Jurassic carbonate platform overlying a volcanosedimentary Permo-Triassic complex and underlying an upper Jurassic schist-hornstein melange formation, (ii) the ophiolite nappe of the Vardar/Axios oceanic basin, and (iii) the upper Cretaceous transgressive sequence made of a shallow-water carbonate platform and a Tertiary flysch. Most part of the Parnitha Mountain consists of the lower group (i). The deformation of the Alpine formations of the above units is post-Late Eocene, as dated from the age of the flysch involved in the tectonic structures and extends up to the Early Miocene as the synmetamorphic deformation shows in the metamorphic rocks of the Cyclades (e.g. Schliestedt *et al.* 1987).

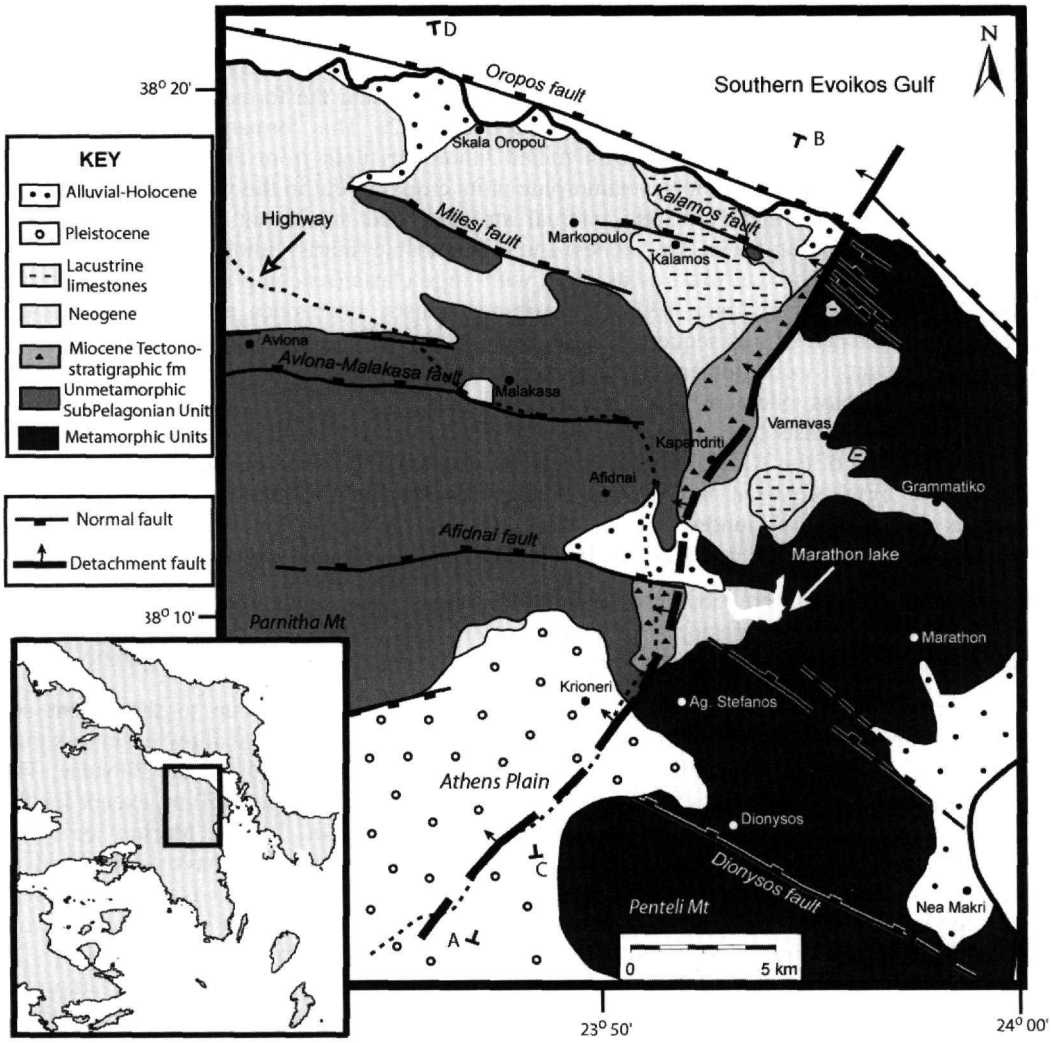

Figure 1 - Geological map of NE Attica

A detachment fault (see below 2.2) separates the metamorphic units from the non-metamorphic units. This detachment passes from the Ochtonia cape in the Aegean coast of Southern Evia (northwards our study area), through Aliveri to Kalamos in northeast Attica and continues to the southwest into the plain of Athens approximately along the Kifissos River (Papanikolaou *et al.* 1999, Xypolias *et al.* 2003). Finally, between the metamorphic and the non-metamorphic units and along strike the tectonic contact there is a narrow zone, where some small outcrops of low-grade metamorphic rocks occur under the post-Alpine sediments that cannot be correlated to either of these two units. These rocks might be correlated to the Alepovouni unit or a similar type of unit observed further south (Papanikolaou *et al.* 2004a), whose lower part comprises a few hundred meters of semi-metamorphic sandstones, schists, and phyllites. The Alepovouni unit is bounded by two detachment faults one separating it from the overlaying unmetamorphic units of Athens and the SubPelagonian and the other detachment from the underlying metamorphic Attica autochthon unit (Papanikolaou *et al.* 2004a).

The post-Alpine sediments of the area comprise Late Miocene – Pliocene continental deposits and minor outcrops of Pleistocene and Holocene alluvial (e.g. Mettos 1992). The older sediments comprise a clastic tectonosedimentary formation that outcrops in the area of Kapandriti, and in the area between Aghios Stefanos and Afidnai (Figs 1, 2, 4). They form a NE-SW zone of debris-flow deposits that are several hundred meters thick (Fig. 3), indicating the formation of a major fault zone in a steep relief during Late Miocene (see below 2.2). This formation consists of large boulders and blocks in a clay matrix with mixed lithologies both from the metamorphic units cropping out in the east and the non-metamorphic units cropping out in the west. In Kapandriti, it is characterized by a complex/chaotic internal structure and significant lateral variations of permeable (sands, conglomerates, sandstones) and impermeable (marls) lithologies. Semi-cohesive breccio-conglomerates prevail towards its base, with large clasts (reaching up to a diameter of 2 meters) sourced from the alpine bedrock involving schists, limestones and cherts (Fig. 4a). Towards the upper part of this sequence, clasts become thinner and finer and at places sandstone beds and less frequently conglomerates are also observed. The same formation outcrops also in the area between Aghios Stefanos and Afidnai and has been evolved laterally to breccio-conglomerates with clasts that are smaller in size (rarely exceed 30-40 cm in diameter). In the immediate footwall of the Afindai fault its thickness exceeds 150 m and the bedding dips 20°-40° towards NNE (Fig. 4b). On top of this breccio-conglomerate formation outcrop lacustrine limestones that are a few hundred meters thick. The top lacustrine limestones are also found unconformably overlying the metamorphic basement in the east around Varnava.

Pleistocene alluvial fans are observed within the Athens plain along the southern slopes of Parnitha Mt and the western slopes of Penteli southwards from the Afidnai and the Aghios Stefanos, uncomformably covering the Neogene sediments (e.g. Papanikolaou *et al.* 2004b).

No outcrops of marine sediments are traced in Northeastern Attica, due to the recent sea transgression in the southern Evoikos gulf. The southern Evoikos gulf is a shallow basin less than 250 m deep that separates Attica from the southern Evia and was formed in Late Pliocene. The thickness of the Plio-Quaternary sediments within the gulf does not exceed 150 m, except for the southeastern area, where they are 250 m thick (Papanikolaou *et al.* 1988a). Marine sediments occur only along the coast of eastern Attica at Rafina area where they have been dated as uppermost Pliocene – lower Pleistocene (Mitzopoulos 1948, Guernet and Sauvage 1970). Finally, recent alluvial sediments are limited in thickness and are observed only in some small narrow bands along the coastline (Oropos, Kalamos, Marathon) and in the Afidnai basin (Fig. 2). Roubanis (1961) reported that in the Afindai plain close to the railway station, the metamorphic basement was drilled at a depth of 47 m and that the Neogene sediments were only 15 m thick, revealing that the Late Pleistocene-Holocene sediments are about 30 m thick. Recent drillings for water in the Plain also showed that the alluvial- Quaternary thickness does not exceed 80 m.

2.2. The role of the detachment fault

The dominant structure is a major NNE-SSW trending detachment, separating the metamorphic units towards the east from the non-metamorphic units towards the west. Moreover, it separates the E-W trending faults in the western part from the NW-SE faults in the eastern part. This detachment caused the downward movement of the non-metarmorphic units and the uplifting of the metamorphic units from the deeper part of the lithosphere where the metamorphism took place in Eocene-Oligocene times. The Miocene tectonosedimentary sequence of debris-flow deposits rests on the hangingwall of the detachment fault and was formed by its activity. This extensional detachment was active throughout Late Miocene times and gradually became inactive during Early Pliocene, when lacustrine deposits have been accumulated all over the area from Varnava and Kapandriti to Kalamos (Fig. 1). The same detachment can be traced further south. In particular, it has subsided the non-metamorphic SubPelagonian unit towards the NNW and uplifted the Alepovouni and the Attica autochthon to the SSE (Papanikolaou *et al.* 2004a).

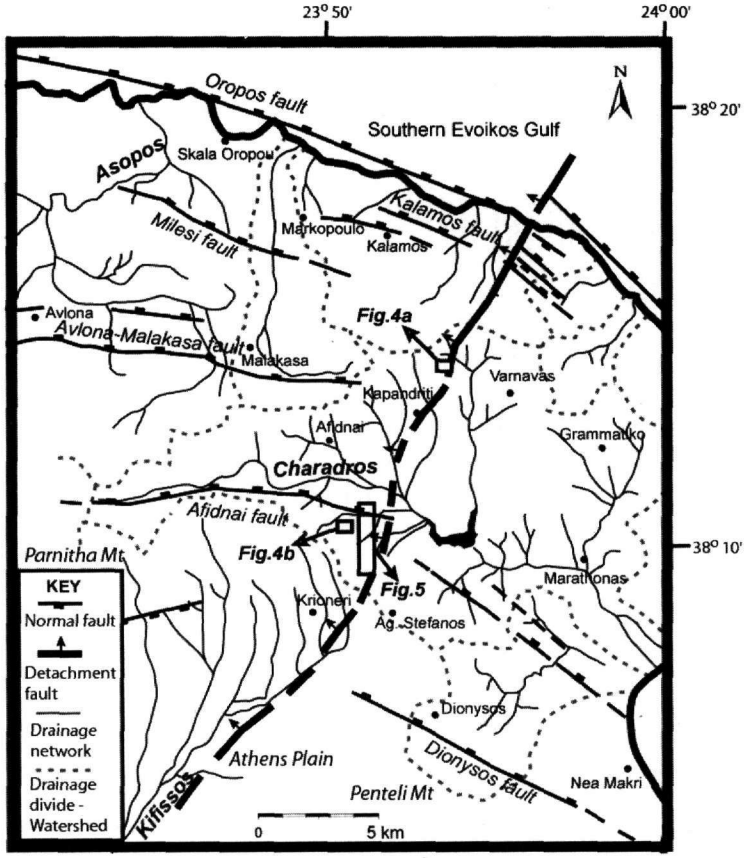

Figure 2 - Drainage network, drainage divide and active faults in NE Attica

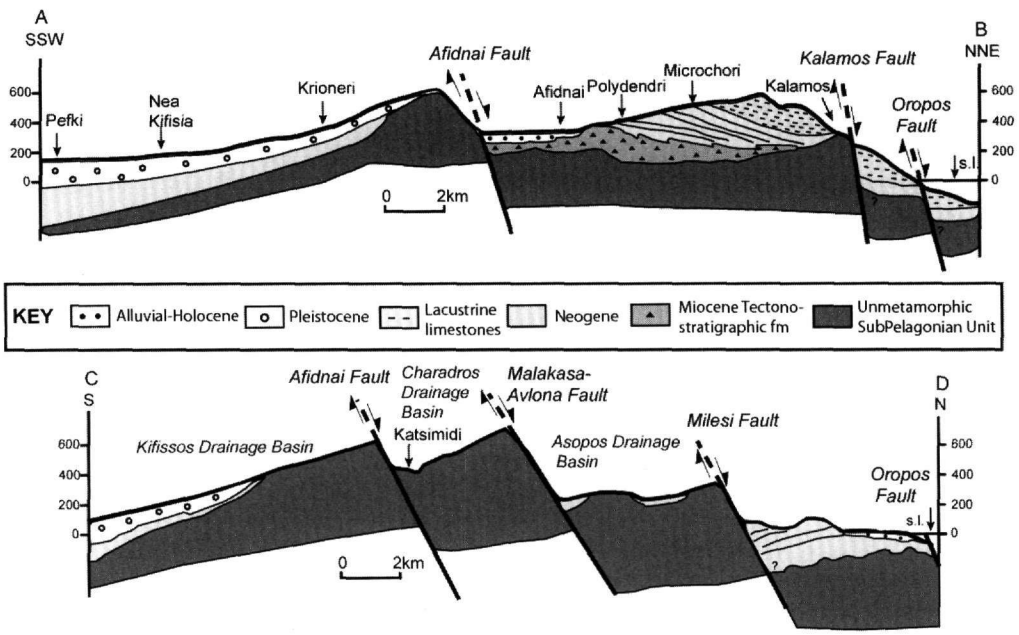

Figure 3 - Cross-sections A-B and C-D (see Fig. 1)

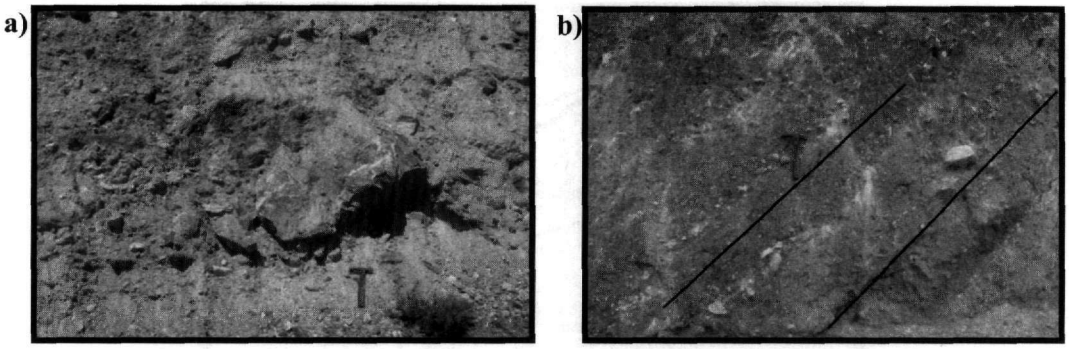

Figure 4 - a) View of the Miocene tectonosedimentary formation of debris-flow deposits in the area of Kapandriti (for location see Fig. 2). Clasts are large (up to a diameter of 2 m), implying that this locality was very close to the detachment trace. b) View of the same formation in the area between Aghios Stefanos and Afidnai in the immediate footwall of the Afindai fault. The bedding plane is nicely revealed, dipping 30°-40° towards NNE. Clasts are relatively small in size rarely exceeding 30-40 cm in diameter, indicating that this locality was less proximal to the detachment

3. Geomorphological and neotectonic structure

The geomorphology of the area is dominated by the Penteli and Parnitha mountains, which border the Athens Plain from the north and the east, respectively. Further north from the southern Evoikos gulf and the coastal zone of Oropos-Kalamos up to the Athens Plain, three major drainage basins are observed: 1) The Kifissos basin in the south with a NNE-SSW flow direction, draining the Athens plain from the southern slopes of Parnitha and the southwestern slopes of Penteli to the Saronic gulf in the southwest. This flow direction is parallel to and near the detachment trace; 2) The Charadros basin with a major W-E flow direction, sourced from the eastern Parnitha highs of about 1200 m up to the lows of the Afidnai plain and the Marathon lake at about 350 m; 3) The Asopos basin towards the northwest which flows northwards, but has a more complex structure due to the existence of the Avlona-Malakasa and the Milesi faults. Finally, some small approximately N-S trending catchments are observed in the area of Kalamos and the Microchori plateau from 500 m elevation up to the coast of southern Evoikos.

Drainage basins are highly asymmetric due to the presence of active normal faults. In particular, there is a combination of fault parallel and fault perpendicular flow that is characteristic of active normal faulting settings (Gawthorpe and Hurst 1993, Eliet and Gawthorpe 1995). The tilted footwall results into fault perpendicular flow directions, which drain the footwall away from the hangingwall (e.g. footwall of the Afidnai fault, footwall of the Oropos-Kalamos fault in the area of Kapandriti; see also cross section Fig. 3). On the other hand, headward erosion within the footwall catchments drain across the fault into the hangingwall producing also fault perpendicular flow directions (e.g. Avlona-Malakasa fault, Afidnai fault, Oropos fault). Finally, several catchments are clearly deflected into a fault parallel flow direction due to hangingwall subsidence (e.g. Afidnai fault, Avlona-Malakasa fault, Milesi fault).

The planation surfaces, both erosional and sedimentary, from 50 m up to 1000 m in altitude, show an E-W preferred orientation and are usually inclined southwards, indicating a tilt around an E-W axis (Papanikolaou *et al.* 1988b). This tilt is nicely illustrated in cross-sections (Fig. 3).

Active faults are trending E-W in the northwestern part and NW-SE in the southeastern part; a common tectonic pattern along the Hellenic arc (Mariolakos and Papanikolaou 1981, 1987). The E-W trending faults are large and known to generate medium to large magnitude earthquakes (1938 Oropos M=6.0, 1981 Alkyonides earthquake sequence M=6.7, M=6.4, M=6.3, 1999 Athens M=5.9), whereas the NW-SE faults occurring in the east are shorter, have lower rates and produce

low to medium magnitude earthquakes (Papanikolaou and Lozios 1990). This neotectonic pattern has been analysed in the northern Attica through morphotectonic observations (Papanikolaou *et al.* 1988b), as well as offshore studies in the Saronikos and the southern Evoikos gulfs (Papanikolaou *et al.* 1988a).

This set of E-W trending north dipping active normal faults in NE Attica consists of: 1) the Oropos-Kalamos fault that is parallel to the coast of the southern Evoikos gulf. It is at least 14 km long and part of it probably ruptured during the M=6.0 event in 1938. The southern Evoikos gulf is a shallow basin less than 250 m deep and the main fault of the Gulf has a throw of 250 m (Papanikolaou *et al.* 1988a), implying that the Oropos-Kalamos zone as a whole is a relatively small structure and of similar importance as the other across strike faults; 2) the ~10 km long Milesi fault, which produces a characteristic bedrock scarp on the Mesozoic limestones that form the footwall and the continental Neogene sediments resting on the hangingwall; 3) the ~ 18 km long Avlona-Malakasa fault that borders the northern slopes of Parnitha Mt. (Papanikolaou *et al.* 1988b, Ganas *et al.* 2004); 4) the 14 km long Afidnai fault, which bounds the Afidnai plain to the south and the Athens Plain to the north (see also Ganas *et al.* 2005).

All these faults have produced a cumulative vertical throw of about 2 km (Fig. 3). The Alpine formations at the top of the Parnitha Mt at about 1400 m are buried several hundred meters beneath the present-day sea level and below the Quaternary and the Neogene sediments near the coast of Oropos. The footwall of the Milesi fault is the northernmost Alpine outcrop observed (Figs 1, 3). These active faults are widely distributed and sharing the strain so that they all exhibit relatively low slip-rates (<0.5 mm/yr). However, they are competitive structures distributed across strike lying on each other's stress shadows (Cowie 1998), implying that in the future one of them will prevail.

It is important that the above set of E-W trending active normal faults in northern Attica is constrained exclusively within the non-metamorphic Alpine units. It is also interesting that these faults taper out to the east as approaching the NNE-SSW trending tectonic contact that separates them from the metamorphic units. These observations are in agreement with the disruption model of the Hellenic arc (see Papanikolaou and Royden 2007) which considers: i) the southern Evia / Northern Attica detachment as the southern boundary of the Central Hellenic Shear Zone activated during Miocene to Early Pliocene and ii) the E-W faults developed to the northwest of the detachment, activated since Late Pliocene. Therefore, this detachment indirectly seems to have a significant effect on the neotectonic structure, influencing the geometry, style and intensity of deformation.

4. The Afidnai fault and the Northern edge of the Athens Plain

4.1. The Athens Plain

In the Late Miocene an E-W trending fault from Attiko Alsos to Kamatero divided the Athens Plain in two sub-basins. The northern part subsided forming a series of lakes throughout Late Miocene-Pliocene, whereas the southern part was tilted to the south with Alpine formations at the northern footwall zone (Attiko Alsos or Tourkovounia) mostly covered by shallow marine sediments in the southern coastal zone of Pireas-Trachones (Papanikolaou *et al.* 2004b). In Early? -Middle Pleistocene the Kifissos river was formed, cutting through the now inactive E-W fault which previously acted as a barrier. As a result, both subbasins were merged into one, producing what is today known as the Athens Plain (Papanikolaou *et al.* 2004b). Overall, since Middle Pleistocene the Athens Plain is very similar to the present-day feature. However, one important modification that occurred since Middle Pleistocene concerns the initiation of activity and/or the speeding up of the Afidnai fault. This fault constrained the northern edge of the Athens plain as well as its drainage basin. Due to the backtilting, most of the footwall area is drained by an extensive channel network that flows southwards down the dip footwall slope, forming the upper part of the Kifissos network. The asymmetry of Kifissos drainage basin, where most channels flow

from Partnitha Mt to the southeast (Fig. 2), illustrates nicely this recent tilt. Also in Middle Pleistocene thick fans and terraces were formed. These planation surfaces observed up to the area south of Krioneri are offset by the Afidnai fault (Fig. 5). As soon as the E-W Kamatero fault became inactive in Middle Pleistocene, the Afidnai fault initiated or took over the extra strain increasing its rate of slip.

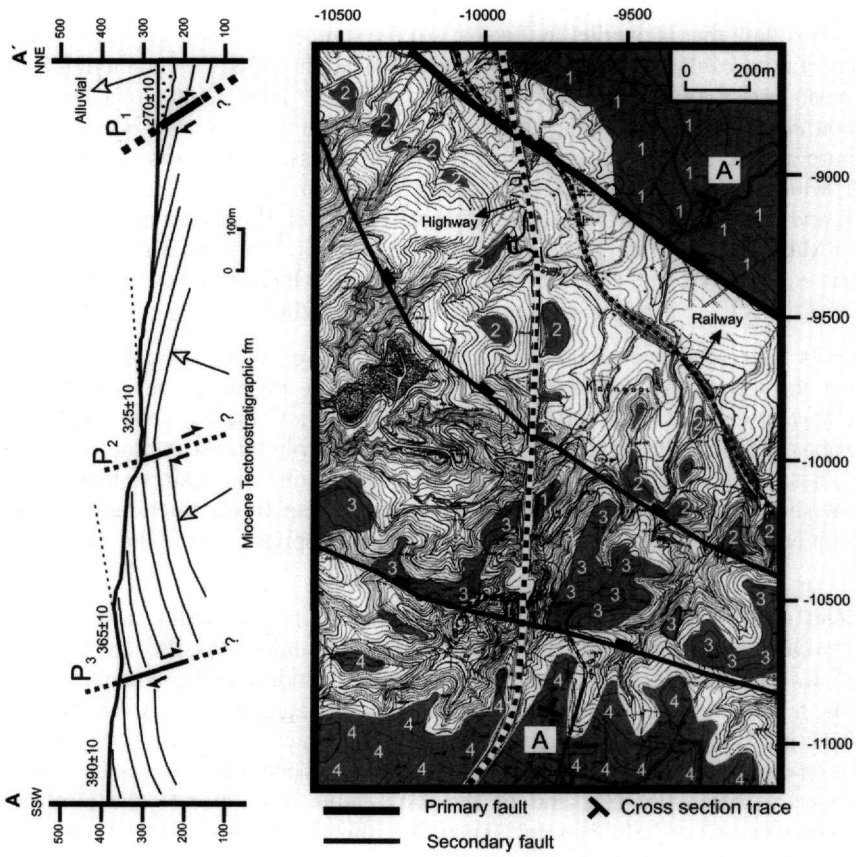

Figure 5 - 1:5000 topographic map (6436/3) and cross-section (A-A') towards the eastern part of the Afidnai fault, showing the traces of the major and the secondary faults and the offset planation surface (for location see Fig. 2)

4.2. The Afidnai fault

The Afidnai fault is a E-W trending normal fault, which downthrows to the north and exhibits all the characteristics of an active structure. This fault does generate an impressive morphological footprint, is oriented perpendicular to the present regional extension direction and bounds the Afidnai Quaternary basin. Even though no post-glacial scarps have been identified, there are signs in the geomorphology and drainage, attesting to its recent activity. In particular, the Charadros river is clearly deflected into a fault parallel flow direction due to the subsidence within the Afidnai hangingwall (Fig. 2). Moreover, the Charadros drainage divide is located only several hundred meters southwards from the Afidnai fault in its footwall, but several kilometers northwards from the fault trace in its hangingwall (Fig. 2). The proximity of the footwall watershed to the fault trace, is due to the tilted footwall that produced southward flow directions, which drain the footwall away from the hangingwall. In conclusion, it is suggested that the fault is active for several reasons such as: i) its geometry (~E-W trending fault parallel to all other major regional active faults, see Mariolakos and Papanikolaou 1981, 1987 and compatible with the

regional ~N-S stress field, Ambraseys and Jackson 1990, Roberts and Ganas 2000, Ganas *et al.* 2004), ii) its morphological expression (Fig. 6), iii) the fact that it bounds Quaternary sediments, and iv) its drainage pattern.

The Afidnai plain is a local base level. The short distance of the drainage divide on the footwall of the Afidnai fault from the fault trace shows that the dominant route for sediments to enter the adjacent basin in the hangingwall is via short, steep footwall catchments. Therefore, the volume of sediment supply into the Afidnai basin is restricted, resulting into a basin of limited extent and thickness. On the other hand, the limited thickness and spatial distribution of the Quaternary sediments also imply that this base level is recently established. The latter indicates that this fault is relatively young (Early? -Middle Pleistocene fault) that is also in agreement with the paleogeography of the Athens Plain.

The rate at which a fault slips fundamentally determines the seismic hazard because average recurrence intervals tend to decrease as slip-rates increase (e.g. Cowie and Roberts 2001). Unfortunately, the lack of characteristic stratigraphic horizons and postglacial scarps limits our ability to calculate accurately the finite throw or the throw-rate. However, the study of geomorphic features, such as terraces/planation surfaces, can provide us with a first order pattern of displacement. The dense vegetation cover of the Parnitha national park and the highly disturbed topography, due to the existing old clay quarries west of the Athens-Thessaloniki highway, severely limit our observation points. Therefore, we focused our terrace mapping mostly east of the highway, where geomorphology is still relatively undisturbed, even though we are aware that we are closer to the eastern tip of the fault, rather than to the center of it. Detailed 1:5000 mapping of the planation surfaces on the northern edge of the Athens Plain revealed the presence of the main fault at the base of the hillside and two secondary faults on the footwall of the main fault. It is unclear whether the secondary faults are still active or that activity may have shifted to the lower major fault following a progressive hangingwall directed migration within the fault zone (Stewart and Hancock 1994). The Afidnai fault separates the major Athens plain from the minor Afidnai-Lake-Marathon Plain. The present day Afidnai basin on the immediate hangingwall of the Afidnai fault lies at 270 ±10 m, whereas the northern edge of the Athens basin is at 390 ±10 m, implying a minimum finite throw of 120 m. Half of this throw is accommodated by the main fault at the base and the other half from the two secondary faults towards the footwall, which are probably linked at depth with the main fault. Considering an Early Pleistocene age (between 1.0 to 1.5 Ma) of the planation surface (see also 4.1), we calculate a long-term throw-rate of 0.08-0.12 mm/yr. However, this rate is extracted from a locality, which is closer to the eastern tip of the fault, rather than to the center of it (Fig. 6). The latter suggests that we may underestimate the rate towards the center of the fault (Papanikolaou and Roberts 2006), because fault slip and slip-rates vary along strike the fault and increase systematically along strike from zero at the fault tips, to maxima towards its center (e.g. Cowie and Scholz 1992). The latter can be nicely observed on the panoramic view of the fault taken from the area of Kapandriti, showing how displacement progressively decreases to minima as approaching the eastern tip of the fault (Fig. 6). Considering that the finite throw towards the center of the fault is about 3 times higher (~360 m, see also Ganas *et al.* 2005 who calculate a 350 m relief based on DEM analysis), the maximum rate is about 0.30 mm/yr. Following the above discussion, we estimate a mean rate of 0.15-0.20 mm/yr for this fault. This value is similar to the value extracted from Ganas *et al.* (2005). They based on DEM morphometry and made an empirical suggestion that slope angle is a function of the long-term fault slip-rate, which varies between 0.13-0.30 mm/yr. For the Afidnai fault they calculated a 0.15-0.19 mm/yr, but using a conservative (4-5 Ma) age constrain. In such a low throw-rate, no postglacial fault scarps or well-shaped bedrock scarps with a free face can be revealed. This occurs because erosion and sedimentation rates are higher and outpace the fault throw-rate.

Even though this fault offsets the Miocene tectonostratigraphic formation, it seems that its eastern tip is located close to the detachment trace, showing once again that the detachment plays a fundamental role in the region (Fig. 1). Further to the east and north from the Dionysos fault, two

NW-SE trending possibly active faults may take over the strain from the Afidnai fault, but no straightforward link to the Afidnai fault can be supported. They leave a rather subtle trace in the morphology and no significant throws can be calculated.



Figure 6 - Panoramic view of the Afidnai fault geometry (photo taken from Kapandriti). Footwall elevation tends to decrease away from the fault centre. Therefore, displacement decreases to minima as approaching the eastern tip of the fault

4.3. Seismic hazard assessment

Following the historical catalogue, no large events (M>6.5) or severe damages have been recorded in NE Attica (Galanopoulos 1955, Papazachos and Papazachou 1997). Only two events have been recorded, the Oropos event in 1938 and another earthquake in 1705. The 1938 Oropos event (Ms=6.0) probably ruptured part of the Oropos offshore fault or the shorter Milesi fault (Fig. 1), generating macroseismic intensity VIII and 18 fatalities (Papazachos and Papazachou 1997). No primary surface ruptures have been observed or documented, but several landslides occurred particularly in the area of Malakasa. As far as the 1705 event (Ambraseys and Jackson 1997) is concerned, there is uncertainty concerning both the magnitude (M~6.4 according to Papazachos and Papazachou 1997) and predominantly the epicentral area. Minor damages were inflicted both to the towns of Athens and Chalkida, so that researchers place the epicenter towards the NE flanks of the Parntitha mountain. It is possible that the Afidnai fault could have ruptured during the 1705 event, however the limited data extracted from the historical record cannot confirm or deny such an interpretation (e.g. it could be also the Malakasa-Avlona fault). The historical record is considered complete for shallow events (h<60 km) for M>6.5 since 1845 and for M>7.3 since 1500 (Papazachos *et al.* 2000). Therefore, it is also possible that an earthquake of M=6.0 to 6.4 could have occurred before the year 1845 and for several reasons has not been recorded.

The worse case scenario implies the rupture of the entire 14 km long Afidnai fault. Based on the equation between Magnitude (M) and surface rupture length (SRL) of the worldwide dataset of Wells and Coppersmith (1994), this fault can generate a M=6.4 event. A similar magnitude (Ms=6.5) is also calculated based on Pavlides and Caputo (2004) empirical relationships from normal faulting events of the Aegean, which may be more representative of the local geotectonic conditions. Ganas *et al.* (2005) estimated the fault as 11 km and calculated a similar Magnitude (Ms=6.4). Considering a mean slip-rate in the order of 0.15-0.20 mm/yr and that all slip is released in earthquakes of the maximum magnitude (M=6.4), therefore assuming a worst-case scenario, we calculate a recurrence interval of about 2000 years.

Taking into account that the completeness of the historical record for such magnitude events covers time periods of a few hundreds years and probably shorter than 500 years (e.g. Papazachos *et al.* 2000), it is evident that the recurrence interval is only a fraction of the completeness period.

Therefore, either this fault has not been activated in historical times or it was activated, but for whatever reason such an event was not recorded in the historical catalogues. Finally, if this fault indeed ruptured in 1705, then the probability for a future event in the near future generated by this source is rather negligible.

5. Discussion-Conclusions

Relief in NE Attica is mainly influenced by fault geometry and fault spacing. Drainage basins are highly asymmetric, producing a combination of fault parallel (E-W) and fault perpendicular (N-S) flow directions. The closely spaced faults produce secondary narrow highs and lows due to the interference between displacement fields, influencing also the drainage divide. The Afidnai fault bounds the northern edge of the Athens Plain and separates it from the secondary Afidnai Plain. It is active, but exhibits a low slip-rate. We have used offset Pleistocene terraces to calculate a long-term throw-rate of 0.1 to 0.3 mm/yr for the Afidnai fault, depending on the actual terrace Pleistocene age estimates and our location along strike the fault. This fault is probably active since Early? -Middle Pleistocene and based on a worst-case scenario, it can generate events of the maximum magnitude (M=6.4), about every 2000 years. Therefore, the completeness of the historical record is much shorter than the mean earthquake recurrence interval of the Afidnai fault.

The NE Attica is also divided by a major NNE-SSW detachment fault that separates the metamorphic units to the east from the unmetamorphic units to the west. This detachment also separates the E-W trending faults towards the western part from the NW-SE trending less active faults towards the eastern part. It was active in Late Miocene-Early Pliocene and produced several hundred meters of debris-flow deposits. It is important that the set of E-W trending active normal faults in northern Attica is constrained exclusively within the non-metamorphic Alpine units and that these faults taper out to the east as approaching the detachment zone. Therefore, this detachment indirectly seems to have a significant effect on the neotectonic structure, influencing the geometry, style and intensity of deformation.

Finally, it is interesting to note that this NNE-SSW trending detachment influences also the seismicity pattern. More precisely, it coincides with the line separating zone I (lowest category of seismic risk) from zone II (intermediate zone) of the national seismic building code (EAK-2003), which have been compiled based on the seismicity level (E.P.P.O.-A.C.E.G., 2001). This is also in agreement with the damage pattern of the 1999 Athens Earthquake, where this detachment further to the south (e.g. inside the Athens Plain) played an important role to the intensity distribution (Papanikolaou *et al.* 1999, Marinos *et al.* 1999), forming a boundary between higher and lower intensities. More precisely, significantly higher damages were produced to sites located both along strike its trace and west from it, within the non-metamorphic units, compared to the sites situated east of the detachment. Therefore, this detachment even though it is inactive, still exerts a significant influence on the present day geological, geomorphological, neotectonic and seismicity pattern, showing how old and new structures interrelate and interact.

6. Acknowledgments

We thank S. Papaspyrou and A. Dovas for their collaboration within the Technopolis-Acropolis Project that gave us the opportunity to study the northern edge of the Athens Plain. Reviews from R. Caputo and E. Vittori improved the manuscript.

7. References

Ambraseys, N.N., and Jackson, J.A., 1990. Seismicity and associated strain of central Greece between 1890-1988, *Geoph. J. Int*, 101, 663-708.

Ambraseys, N.N., and Jackson, J.A., 1997. Seismicity and strain in the Gulf of Corinth (Greece) since 1694, *J. Earth. Eng.*, 1, 663-708.

Cowie, P. A., 1998. A healing-reloading feedback control on the growth rate of seismogenic faults, *J. Struct. Geol.,* 20, 1075-1087.

Cowie, P. A., and Roberts, G. P., 2001. Constraining slip rates and spacings for active normal faults, *J. Struct. Geol.*, 23, 1901-1915.

Cowie, P. A., and Scholz, C. H., 1992. Physical explanation for displacement-length relationship for faults using a post-yield fracture mechanics model, *J. Struct. Geol.,* 14, 1133-1148.

Dubois, R., and Bignot, G., 1979. Presence d' un "hard-ground" nummulitique au sommet de la serie cretace d' Almyropotamos (Eubee meridionale, Grece). Consequences, C.*R. Acad. Sci. Paris*, 289, 993-995.

Eliet, P.P., and Gawthorpe, R.L., 1995. Drainage development and sediment supply within rifts, examples from Sperchios basin mainland Greece, *J. Geol. Soc. Lond.*, 152, 883-893.

E.P.P.O.-A.C.E.G., 2001. Greek Seismic Design Code 2000. Earthquake Planning and Protection organization, Assoc.Civil Engineers, Government Gazette 2184B/20-12-99, Athens, 257pp.

Galanopoulos, A., 1955. Erdbegeographie von Griechenland, *Ann. Geol. Pays Hellen.*, 6, 83-122. (in Greek)

Gawthorpe, R., and Hurst, J., 1993. Transfer zones in extensional basins: their structural style and influence on drainage development and stratigraphy, *J. Geol. Soc. Lond,* 150, 1137-1152.

Ganas, A., Pavlides, S.B., Sboras, S., Valkaniotis, S., Papaioannou, S., Alexandris, G.A., Plessa, A., and Papadopoulos, G.A., 2004. Active fault geometry and kinematics in Parnitha Mountain, Attica, Greece, *J. Struct. Geol.,* 26, 2103-2118.

Ganas, A., Pavlides, S., and Karastathis, V. 2005. DEM-based morphometry of range front escarpments in Attica, central Greece and its relation to fault slip-rates, *Geomorph.,* 65, 301-319.

Guernet, C., and Sauvage, J., 1970. Obervations nouvelles sur le Néogène de la région de Pikermi et Rafina (Attique Grèce), *Bull. Soc. Geol. France,* 12, 241-245.

Katsikatsos, G., 1969. Age of the metamorphic system of S. Evia and its stratigraphic structure, *Praktika Acad. Athinon*, 44, 223-238. (in Greek)

Katsikatsos, G., 1979. La structure tectonique de l' Attique et de l' ile d' Eubee, *Proc. 6th Coll. Geol. Aegean Region,* 1, 211-228.

Lozios, S., 1993. Tectonic analyisis of the metamorphic rocks in NE Attica, *Unpublished Ph.D. thesis*, Department of Geology, University of Athens, 299pp. (in Greek)

Marinos, P., Boukouvalas, G., Tsiambaos, G., Pronotarios, G., and Sabatakakis, N., 1999. Damage distribution in the western part of Athens after the 7-9-99 earthquake, *Newsletter of E.C.P.F.E.*, Counsil of Europe, Issue No 3, 36-39.

Mariolakos, I., and Papanikolaou, D., 1981. The Neogene basins of the Aegean Arc from the Paleogeographic and the Geodynamic point of view, *Proc. Int. Symp. H.E.A.T.*, 383-399.

Mariolakos, I., and Papanikolaou, D., 1987. Deformation pattern and relation between deformation and seismicity in the Hellenic Arc, *Bull. Geol. Soc. Greece*, 19, 59-76.

Mettos, A.I., 1992. Geological and paleogeographical study of the continental Neogene and Quaternary deposits of NE Attica and SE Beotia, *Unpublished Ph.D. thesis*, Department of Geology, University of Athens. (in Greek)

Mitzopoulos, M., 1948. Das Pliozan ron Raphina, *Prakt. Akad. Athinon*, 23, 295-301.

Papanikolaou, D., 1986. *Geology of Greece* (in Greek). Eptalofos Publications, Department of Geology, University of Athens, 240pp.

Papanikolaou, D., Lykoysis, V., Chronis, G., and Pavlakis, 1988a. A comparative study of neotectonic basins across the Hellenic arc: the Messiniakos, Argolikos, Saronikos and Southern Evoikos gulfs, *Basin Research*, 1, 167-176.

Papanikolaou, D., Mariolakos, I., Lekkas, E. and Lozios, S., 1988b. Morphotectonic observations on the Asopos Basin and the coastal zone of Oropos. Contribution on the neotectonics of Northern Attica, *Bull. Geol. Soc. Greece*, 20, 252-267

Papanikolaou, D., and Lozios, S., 1990. Comparative neotectonic structure of high (Korinthia-Beotia) and low rate (Attica-Cyclades) activity, *Bull. Geol. Soc. Greece,* 26, 47-66. (in Greek)

Papanikolaou, D., Lekkas, E., Sideris, C., Fountoulis, I., Danamos, G., Kranis, C., Lozios, S., Antoniou, I.,. Vassilakis, E., Vasilopoulou S., Nomikou, P., Papanikolaou, I., Skourtsos, E., and Soukis, K., 1999. Geology and tectonics of Western Attica in relation to the 7-9-99 earthquake, *Newsletter of E.C.P.F.E.,* Council of Europe, Issue No 3, 30-34.

Papanikolaou, D.I., Lozios, S.G., Soukis, K., and Skourtsos, E., 2004a. The geological structure of the Allochtonous "Athens Schists", *Bull. Geol. Soc. Greece*, 36, 1550-1559.

Papanikolaou, D., Bassi, E, Kranis, H., and Danamos, G., 2004b. Paleogeographic evolution of the Athens basin from upper Miocene to Present, *Bull. Geol. Soc. Greece*, 36, 816-825.

Papanikolaou, D., and Royden, L., 2007. Disruption of the Hellenic arc: Late Miocene extensional detachment faults and steep Pliocene-Quaternary normal faults – or – What happened at Corinth? *Tectonics*, in press.

Papanikolaou, I., and Roberts, G., 2006. Slip-rate variability along strike active faults: Implications for seismic hazard assessment and mapping, *Geoph. Res.* Abstr. 8, 07078, EGU Vienna.

Papazachos, B.C., and Papazachou, C.B., 1997. *The earthquakes of Greece.* Ziti editions, Thessaloniki, 304pp.

Papazachos, B.C., Comninakis, P.E., Karakaisis, G.F., Karakostas, B.G., Papaioannou, C.A., Papazachos, C.B., and Scordilis, E.M., 2000. A catalogue of earthquakes in Greece and surrounding area for the period 550BC-1999, Publ. Geoph. Lab.University of Thessaloniki.

Pavlides, S., and Caputo, R., 2004. Magnitude versus faults' surface parameters: quantitative relationships from the Aegean Region, *Tectonophysics,* 380, 159-188.

Roberts, G. P., and Ganas, A., 2000. Fault-slip directions in central-southern Greece measured from striated and corrugated fault planes: comparison with focal mechanism and geodetic data, *J. Geophys. Res.,* 105, 23,443-23,462.

Roubanis, B.S., 1961. Geological research on the Parnes mountain range, *Annales Geologiques des Pays Helleniques*, 12, 18-104.

Schliestedt, M., Altherr, R., and Matthews, A., 1987. Evolution of the Cycladic crystalline complex: petrology, isotope geochemistry and geochronology. In R. Helgeson (ed.), *Chemical transport in metasomatic processes. NATO Advanced Study Institute Series C*, Reidel, Dordrecht, 218, 389-428pp.

Stewart, I.S., and Hancock, P.L., 1994. Neotectonics. In P.L. Hancock (ed.), *Continental deformation* Pergamon Press, 370-409pp.

Wells, D.L., and Coppersmith, K. J., 1994. New empirical relationships among magnitude, rupture length, rupture width and surface displacement, *Bull. Seism. Soc. America,* 84, 974-1002.

Xypolias, P., Kokkalas, S., and Skourlis, K., 2003. Upward extrusion and subsequent transpression as a possible mechanism for the exhumation of HP/LT rocks in Evia island (Aegean Sea, Greece), *J. Geodyn.*, 35, 303-332.

Δελτίο της Ελληνικής Γεωλογικής Εταιρίας τομ. XXXX, 2007
Πρακτικά 11ου Διεθνούς Συνεδρίου, Αθήνα, Μάιος 2007

Bulletin of the Geological Society of Greece vol. XXXX, 2007
Proceedings of the 11th International Congress, Athens, May, 2007

IDENTIFYING FAULT ACTIVITY IN THE CENTRAL EVOIKOS GULF (GREECE)

Rondoyanni Th.[1], Galanakis D.[2], Georgiou Ch.[2], and Baskoutas I.[3]

[1] *National Technical University of Athens, Faculty of Mining and Metallurgical Engineering, Department of Geological Sciences, 9 Iroon Polytechniou Str.1578,0 Athens, Greece*

[2] *Institute of Geology and Mineral Exploration,. 70 Mesogion Str, 115 27, Athens, Greece*

[3] *National Observatory of Athens, Institute of G eodynamis, Thissio, 11527, Athens, Greece*

Abstract

Geological mapping on a 1:5.000 scale and a tectonic analysis in the wider Chalkida region of the Island of Evia and the adjacent Drossia area of Central Greece, have allowed the identification of a number of active and potentially active normal faults. These faults have been formed or reactivated during the Late Quaternary, since they affect Pleistocene brackish and terrestrial deposits. Some of the faults affect the contact of the limestone bedrock with the Quaternary formations, presenting characteristic polished surfaces. The faults, in places covered by the alluvial deposits of the Chalkida plain, are also detected by geophysical research. Among the identified faults, the most important are considered the Aghios Minas-Chalkida, the Avlida and the Lefkadi active faults. The first one extends from Drossia to the Chalkida area, crossing the sea straights, and has an ENE-WSW direction and a south dip. The other two, are parallel antithetic faults oriented WNW-ESE, and bound the South Evoikos Gulf on the Greek mainland and the Evia Island respectively. The mapping and evaluation of active faults in this region of moderate seismicity, with low topographic relief and consequent absence of morphotectonic features, is especially important from a seismic hazard point of view.
Key words: *Active faults, neotectonic mapping, Chalkida, Central Greece*

Περίληψη

Η περιοχή του κεντρικού Ευβοϊκού κόλπου χαρακτηρίζεται από μέτρια σεισμική δραστηριότητα, ενώ λόγω και της χαμηλής μορφολογίας απουσιάζουν χαρακτηριστικές μορφοτεκτονικές δομές ενεργού τεκτονικής. Εν τούτοις, η γεωλογική χαρτογράφηση σε κλίμακα 1:5.000, η αξιολόγηση των λιθοστρωματογραφικών δεδομένων και η τεκτονική ανάλυση στην ευρύτερη περιοχή της Χαλκίδας και την παρακείμενη περιοχή της Δροσιάς, έκανε εφικτή τη διαπίστωση ύπαρξης ενεργών και δυνητικώς ενεργών ρηγμάτων. Τα ρήγματα αυτά σχηματίστηκαν ή ανέδρασαν κατά τη διάρκεια του Τεταρτογενούς, αφού επηρεάζουν πλειστοκαινικές υφάλμυρες και χερσαίες αποθέσεις. Ορισμένα από τα ρήγματα τα οποία βρίσκονται στην επαφή του προνεογενούς υποβάθρου με τους τεταρτογενείς σχηματισμούς παρουσιάζουν μεγάλου εύρους κατοπτρικές επφάνειες, με γραμμώσεις ολίσθησης και άλλες καθοδηγητικές μικροδομές, που έδωσαν τη δυνατότητα προσδιορισμού του πεδίου των τεκτονικών τάσεων. Η προέκταση των

ρηγμάτων μέσα στις εκτεταμένες αλλουβιακές πεδιάδες επιβεβαιώθηκε με την εκτέλεση γεωφυσικών ερευνών. Μεταξύ των ρηγμάτων που προσδιορίστηκαν θεωρούνται σημαντικότερα τα ενεργά ρήγματα Αγ. Μηνά-Χαλκίδας, Αυλίδας και Λευκαντίου. Το πρώτο, με διεύθυνση ΑΒΑ-ΔΝΔ και νότια κλίση εκτείνεται από τη χερσόνησο της Δροσιάς μέχρι βόρεια από την Χαλκίδα Τα άλλα δύο είναι παράλληλα αντιθετικά ρήγματα με διεύθυνση ΔΒΔ-ΑΝΑ που οριοθετούν το αρχικό τμήμα του Νότιου Ευβοϊκού κόλπου στην Στερεά Ελλάδα και την Εύβοια αντίστοιχα. Η χαρτογράφηση και ο προσδιορισμός ενεργών ρηγμάτων και η επιβεβαίωση τους με γεωφυσικά δεδομένα σε μια περιοχή όπου απουσιάζουν τα εμφανή κριτήρια αναγνώρισης τέτοιων δομών, έχει ιδιαίτερη σημασία κυρίως για την αξιολόγηση της σεισμικής επικινδυνότητας. Επιπλέον, λαμβάνοντας υπόψη τους τελευταίους μεγάλους απρόβλεπτους σεισμούς στην Ελλάδα αλλά και παγκοσμίως, γίνεται φανερή η ανάγκη προσανατολισμού της διεπιστημονικής έρευνας στην μελέτη περιοχών που θεωρούνται μειομένου ενδιαφέροντος από σεισμοτεκτονική άποψη.
Λέξεις κλειδιά: *Ενεργά ρήγματα, νεοτεκτονική χαρτογράφηση, Χαλκίδα, Κεντρική Ελλάδα.*

1. Introduction - The geology of recent deposits

According to a number of published papers concerning seismotectonic researches in the area of the Evoikos Gulf, its Northern part is characterized by very pronounced faulting tectonics, associated with powerful destructive earthquakes (Philip 1974, Lemeille 1977, Ambrasseys and Jackson 1990, Roberts and Jackson 1991, Goldsworthy and Jackson 2001). On the contrary, the Gulf's Central and Southern parts are considered areas of mild tectonic activity and therefore of moderate seismicity (Drakopoulos *et al.* 1984, GeoPro 2006) (Fig. 1). Moreover, this area has a low relief, with no morphotectonic structures characteristic of an active region. The present survey has identified the existence of active faults, capable to produce earthquakes, in the area of the Central Evoikos Gulf (wider Chalkida region). This shows that it is expedient to also conduct studies in areas considered of limited interest from a seismic hazard point of view.

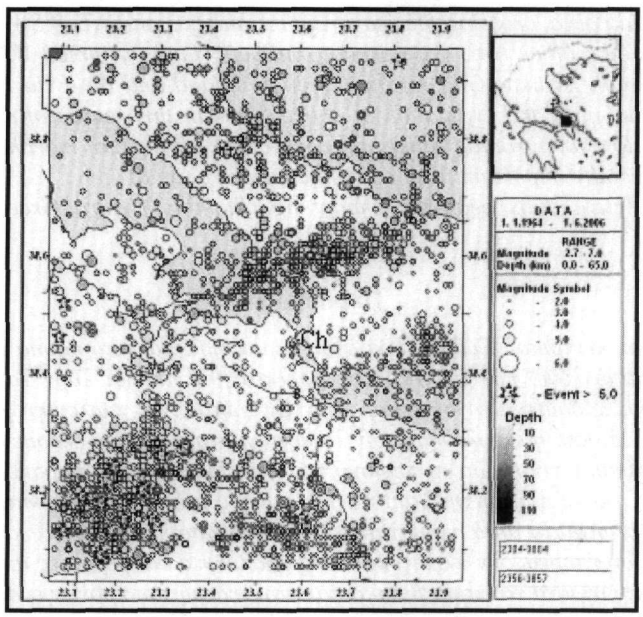

Figure 1 - Map of earthquake epicenters (for 1964-2006 period) of the wider Chalkida (Ch) area. The study area is indicated with the black rectangle in the small map of Greece

After the mapping of the faults, the assessment of their activity was mainly based on stratigraphic and microtectonic data and on a geophysical research that detected faults in the flat areas, while published geophysical data from surveys performed offshore were also evaluated.

The wider region consists of geological formations of the Pelagonian zone, mainly Triassic thick-bedded limestones and dolomites, Jurassic and Cretaceous limestones, chert-schists and ophiolites (Mavrides 2006.) A large area is also covered by Neogene formations, consisting of lacustrine deposits of the Upper Miocene-Pliocene age (Katsikatsos 1999), brackish deposits of the Lower Pleistocene, and clastic deposits of the Middle-Upper Pleistocene covering the larger part of the studied area (Fig. 2).

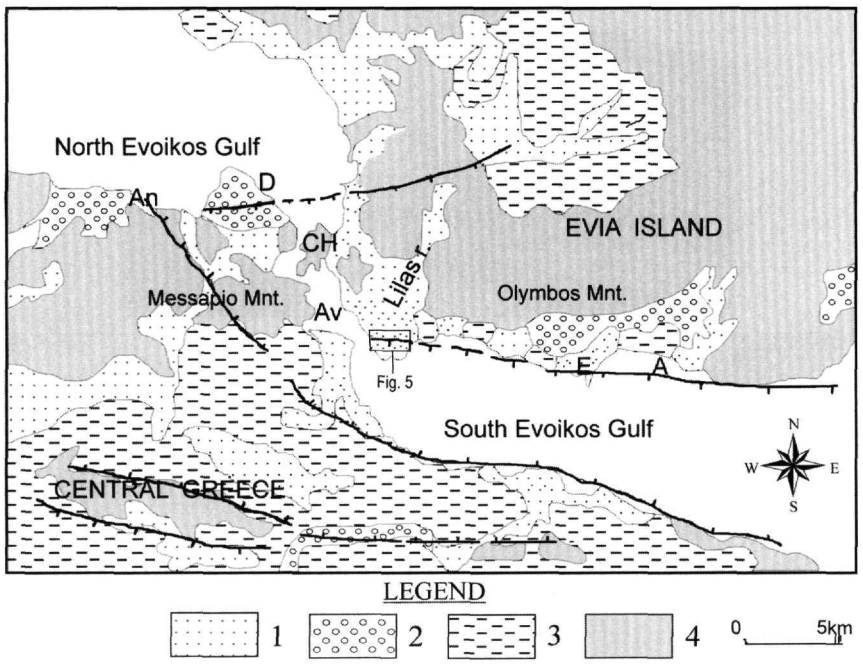

Figure 2 - Simplified geological map of the study area (modified from the geological map of Greece of a scale 1:500.000): 1. Alluvial plains, 2. Pleistocene deposits, 3. Neogene formations, 4: Preneogene basement. (CH-Chalkida, E-Eretria, A- Amarynthos, D- Drossia, An-Anthidona, Av- Avlida)

In particular, the deeper members of the Neogene basins are lacustrine sediments consisting of marls, marly limestones and travertines. Consecutively brown-reddish loams and sands with sandstone and conglomerate intercalations have developed. These deposits, as identified in the Attika-Beotia region, in Central Greece, are of the Upper Miocene age (Mettos 1992). In the Island of Evia, North and South of Chalkida, lacustrine and fluvioterrestrial coarse grained deposits (mainly conglomerates and sandstones) of the Upper Miocene age (Katsikatsos *et al.* 1981) are also outcropping.

Particular attention was paid to the study of the Pleistocene deposits displaying different facies and constituting an important element for the dating of the recent tectonic events that have affected the area (Fig. 3a). The Lower Pleistocene is represented by brackish deposits outcropping mostly in the region of Drossia but also occurring as small-width outcrops along the western coast, up to the bay of Anthidona (Fig. 3b). Their visible thickness is almost 10m and they mainly consist of conglomerates, sandstones and whitish marls including *Adelina elegans, Paludina*, and *Dressensia polymorpha comans* (Rondoyanni 1984). Based on the assessment of the ostracodes found in the region of Drossia, Mavrides (2006) also reports a Pleistocene age.

The deposits of the Middle and Upper Pleistocene are of continental facies, mainly talus cones and scree. The oldest deposits of this type are a limited outcrop of highly cemented limestone breccias in the Eastern slope of the Messapio Mountain (Fig. 3c). They are stratified, fractured and karstified, and appear in the form of grey limestone beds. Based on these characteristics and on their lithostratigraphic relation with the other talus scree mapped in the region, we conclude that they formed during the Middle Pleistocene.

The Northeastern foot of the Messapio Mountain is also covered with medium cemented talus scree. They are limestone breccias with reddish clayey cement, covered by a carbonate crust.

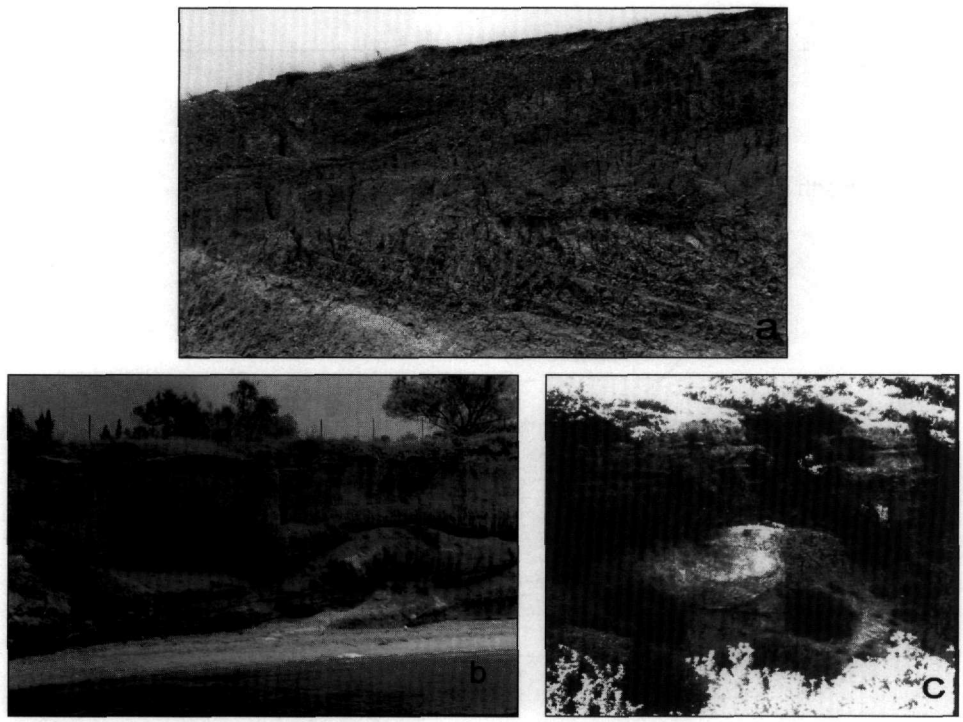

Figure 3 - View of the outcrops of the recent geological formations: a. Pleistocene red clays overlying uncomfortably on the Neogene sediments, b. Pleistocene brackish deposits in Drossia region, c. Consolidated scree on the foothills of Messapio mountain

Based on observations made in the wider area and on their comparison with similar deposits found in Central Greece, the age that may be attributed to these cones is the Upper Pleistocene. Similar deposits are the talus cones and scree found in the Southern foot of the Olymbos Mountain in Evia. Katsikatsos (1999) has reported that they are of the Pleistocene age. In the region of Chalkida the talus scree are more recent and less cemented, with carbonate material.

Holocene deposits outcrop in the regions of Drossia, Chalkida, Eretria and Amarynthos. A study of the Holocene terraces and of the respective neotectonic movements of Evia has been conducted by Genre (1999). In the region of Avlida, according to drilling data, the Holocene deposits are almost 30m thick (Leontaris 1977). Those more extended, are the Late Holocene deltaic deposits associated with the activity of the Lilas River. According to a drilling research in the plain south of Chalkida, the fluvioterrestrial deposits, mainly sands and clays, have a total thickness of almost 20 m (Maroukian and Gaki-Papanastassiou 2002).

2. Active faulting

The main faults that affect the Preneogene and recent geological formations of the study area are normal, oriented WNW-ESE to NW-SE and ENE-WSW to E-W. Detailed mapping and assessment of the activity of these faults gave the following data and considerations.

Two antithetic normal faults with a WNW-ESE direction outcrop in the Avlida region and in the plain of the River Lilas, on the opposite sides of the South Evoikos Gulf (Fig. 4). The Avlida fault, having a northeastern dip, outcrops to the South of the village Avlida and affects the Neogene deposits, as well as the Pleistocene. This fault continues offshore, passing to the North of the village Dilesi, as detected into the recent sediments, by seismic reflection profiles in the Gulf (Perisoratis and van Andel 1991). It has a total length more than 20 km, and forms the southern margin of the Evoikos Gulf.

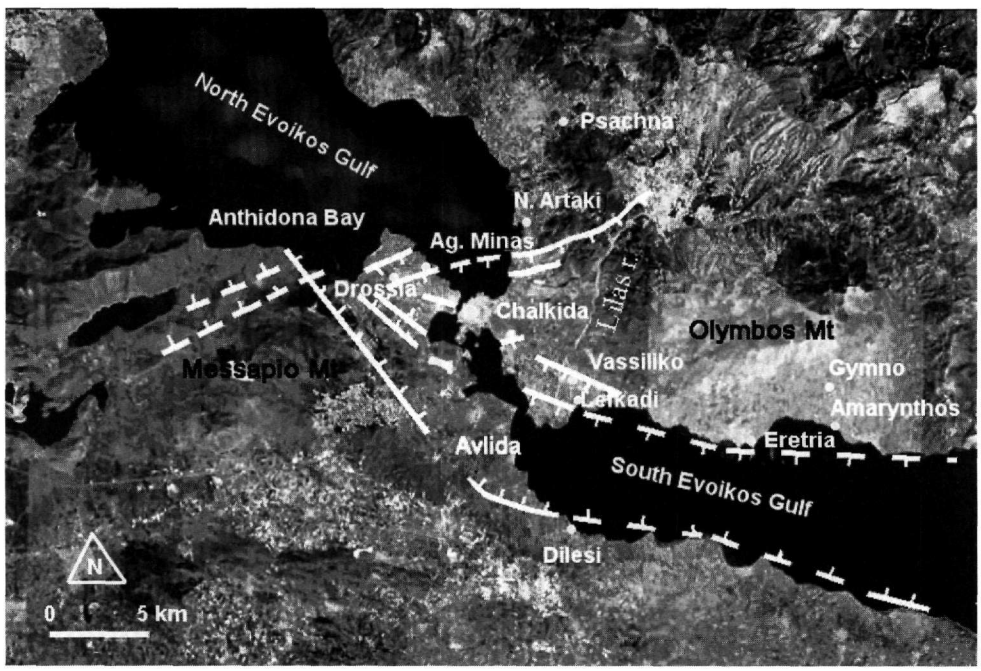

Figure 4 - The active and recent faults in the Central Evoikos area

The Lefkadi fault, dipping to the South, affects the alluvial deposits of the plain of the River Lilas. It continues offshore, for a total length of 25 km, to the South of the village Eretria (Perisoratis and van Andel 1991) and forms the Northern margin of the South Evoikos Gulf. In order to localize the fault trace prolongation into the alluvial plane, a geophysical prospecting, in order to study the variations of rock conductivity in relation to the depth, was conducted in the same area. The quantitative interpretation of 22 geoelectrical soundings, based on an horizontal stratification model, showed the existence of an electrical discontinuity disturbing the Quaternary deposits, which is directly related with the position and the direction of the concerned fault (Fig. 5).

Taking into consideration the thickness of the syn-rift holocene and upper pleistocene sediments in offshore seismic reflection profiles (Perisoratis and van Andel 1991), an average value of the slip rate of the order of 1 mm/yr for the last 150,000 years can be estimated. This slip rate is smaller than that of the faults delimiting the graben of the North Evoikos Gulf, which is of the order of 3mm/yr according to Philip (1974).

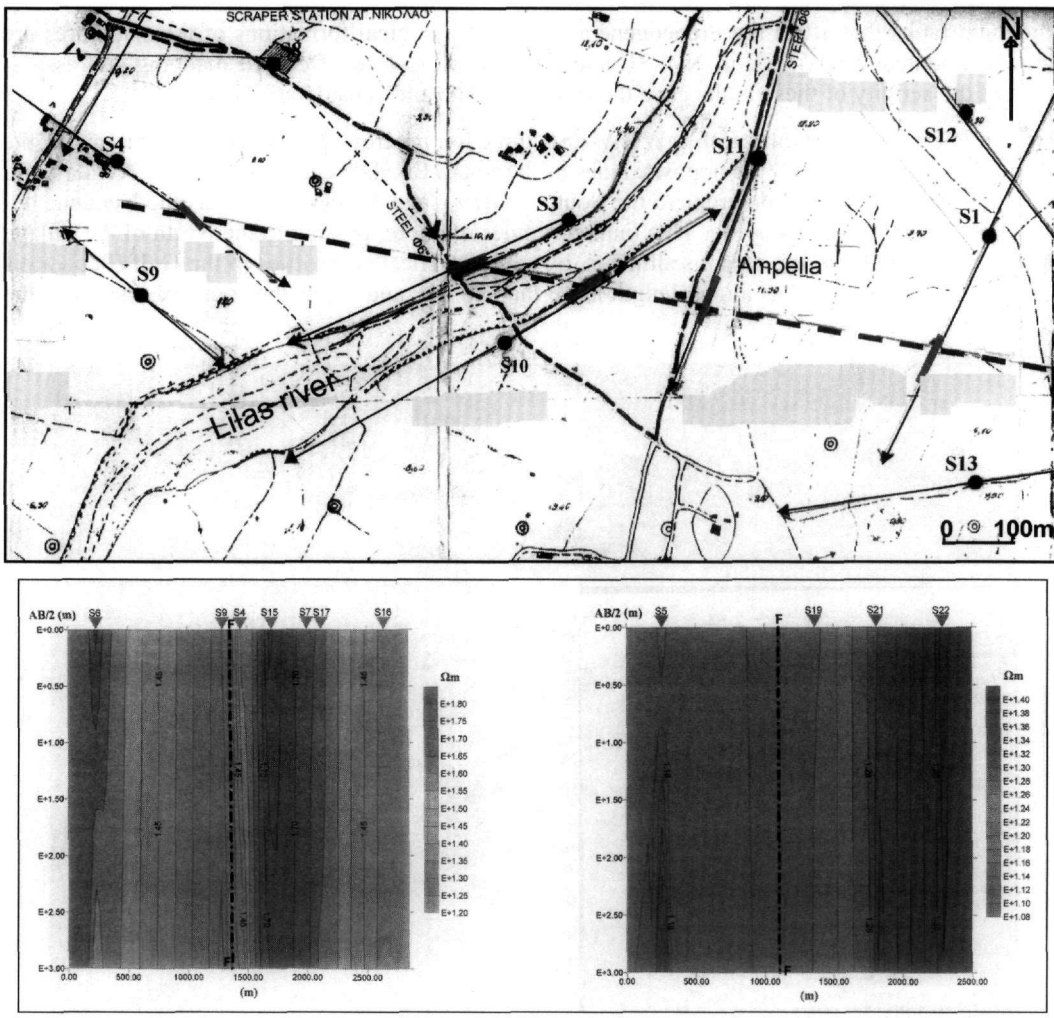

Figure 5 - Map showing the location of the soundings crossing the Lefkadi fault and the corresponding geoelectrical sections, where the recorded fault (F) is noted. The map area is indicated in figure 2

Therefore, within the South Evoikos basin the two antithetic faults of Avlida and Lefkadi, may be considered active, according to the geological and geophysical data, and their evolution is connected with the seismic activity of the area. The larger faults in this region are those associated with the formation of the wider Neogene basin, locating between Evia island and Central Greece. They outcrop at a distance of more than 5 km from the coasts and they have a several hundred meter throw (Mettos *et al.* 1986, 1992).

Numerous smaller faults directed also WNW-ESE to E-W and dipping either to the North or to the South were mapped in the region south of Chalkida. These are faults that affect the Neogene sediments of the area, mainly sandy marls and clays or are detected in their contact with the Preneogene bedrock. The faults have a visible length of 2 to 5 km and a throw of almost 10m, as can be seen from the displacement of characteristic intercalated conglomerate deposits. Among these faults, it is worthwhile mentioning the fault near the village Vassiliko that brings into contact the Triassic-Jurassic marbles and schists with the Neogene sediments and the talus scree as well and has a visible length of 5 km. Based on the measurements of the tectonic striations on the fault sur-

face extensional stresses directed NNW-SSE (σ1: 241°/61°, σ2: 81°/28°, σ3: 346°/8°) are determined, indicating a recent fault reactivation.

Here we should note, that the region farther South, between the villages Eretria and Gymno, presents us with an opposite picture, where the big talus cone of the Upper Pleistocene age at the foot of Mount Olymbos has not been disturbed by recent faults. From a geomorphologic aspect, the normality of the undisturbed slope is obvious and, additionally, from observations of the natural sections along the numerous streams crossing the cone, no faults are detected. Therefore, the cone materials appear to have covered the older faulting surfaces of the Southern slopes of the mountain that created the steep morphology before the deposition of the Quaternary formations.

In the area north of Chalkida, near the village Nea Artaki, a large fault has been mapped, having an ENE-WSW direction and a south dip. The fault affects both the alpine bedrock of Triassic limestones and dolomites, bringing it into contact with the Neogene deposits and the Upper Pleistocene talus scree, which are dislocated by this fault (Figs 6a, b). Two groups of tectonic striations were observed on the fault's very wide polished surface. The measurements of the first (older) group of the striations showed their connection with extensional stresses of a NE-SW direction, related to the Pliocene tectonic phase known in the wider region (Philip 1974, Rondoyanni 1984). The second group of striations also show extensional stresses of a NNW-SSE direction (σ1: 64°/49°, σ2: 277°/36°, σ3: 174°/16°), coinciding with these showed by the fault plane solutions in the wider area.

The exact determination of the fault's continuation into the area covered by alluvial deposits was possible with geophysical soundings. In this area, the interpretation of a number of 7 geoelectrical soundings showed the existence of an electrical discontinuity, coinciding with the continuation of the fault surface and the lowering relief of this area, while a secondary tectonic discontinuity was also detected at a distance of 75 m.

The prolongation of this fault, after it crosses undersea, into the region of Drossia, coincides with the fault observed in the region of Aghios Minas having a polished surface on the limestones. The brackish Pleistocene deposits, in contact with the fault, show characteristic flexures, due to their tectonic displacement (Fig. 6c). In this site there are no younger deposits to allow a more exact identification of the fault's last movement, however its position, as an exact prolongation of the Chalkida fault, as well as their common geometric characteristics strengthen the view that it is the same fault that crosses undersea, has a total length of 15 km and can be considered active.

Moreover, the recent tectonic activity in the area is also established by the presence of faults which, in the peninsula of Drossia, farther North of the Aghios Minas fault, have affected the brackish Pleistocene deposits and the younger strata of red clays (Fig. 7). These are two normal faults having a N70° and N110° direction, a north dip and a few meters throw. The visible length of these faults is almost 5 km, while their undersea continuation is not excluded.

Recent faults are also present in the Eastern part of the Messapio Mountain. The larger one, having a NW-SE direction and presenting a characteristic surface in the bay of Antidona, brings into contact the Preneogene limestones with the cones and screes of the Upper Pleistocene age.

The recent activity of the fault is established by the important displacement of the screes relative to their initial genetic morphologic position, as well as by the existence of subparallel faults within the screes themselves forming small polished surfaces of the order of 100 cm. We may suppose that this fault continues up to the region of Avlida and has a total length of almost 12 km.

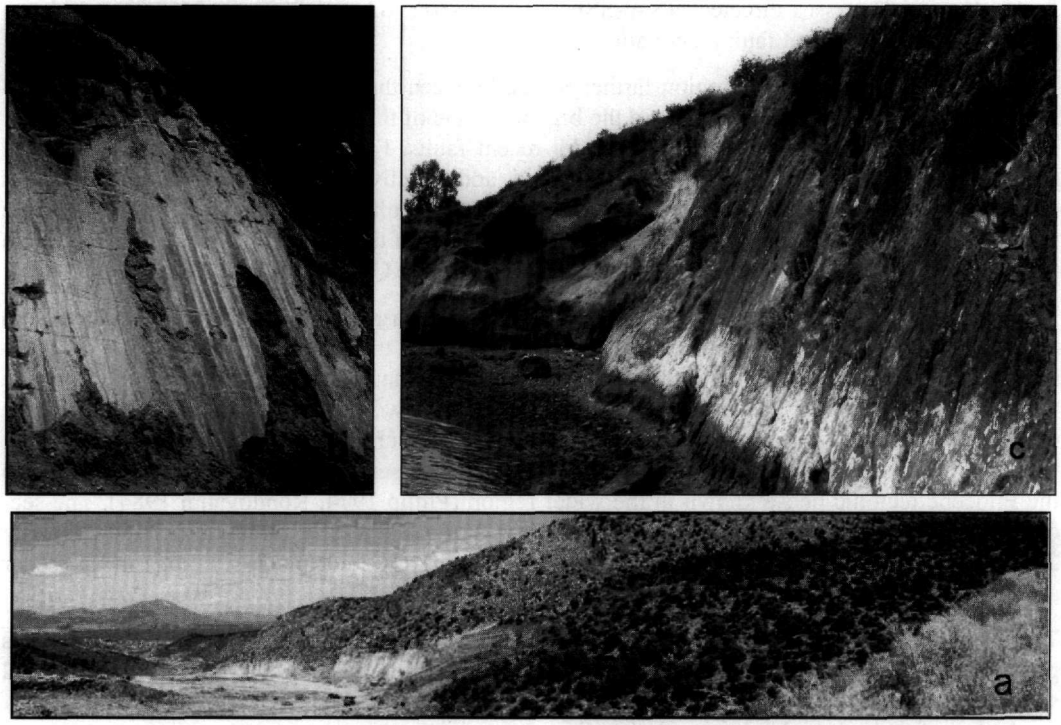

Figure 6 - The Aghios Minas-Chalkida fault: a. General view, b. Detail from the polished fault plane to the North of Chalkida, c. Contact of the limestones with the Pleistocene deposits in Drossia region



Figure 7 - Small faults affecting the Lower Pleistocene deposits in Drossia (a) and Nea Artaki area (b)

However, its probable segmentation south of the Messapio Mountain as well as the fact that its direction forms a small angle with the dominant tectonic stresses, urges us not to consider it of importance for the region.

Here we should stress the difference noted between the region Northwest of Chalkida, were the screes on the Messapio Mountain are strongly tectonized, and the region Southest of Chalkida, where on the Olymbos Mountain, the screes of a similar age appear undisturbed. This is a difference observed in the neotectonics of the wider region between the North and South Evoikos Gulf.

3. Seismicity

In the wider study area and mainly in the North Evoikos Gulf, there are obvious traces of a neotectonic activity continuing to date, with the manifestation of strong earthquakes. Large normal faults delimit the Neogene basins and those same as well as smaller parallel faults interrupt the basins infillings (Philip 1974, Lemeille 1977, Rondoyanni 1984, Ganas *et al.* 2006).

In the region of Central Evoikos there are no large tectonic structures, and the earthquakes are usually of smaller magnitude. Among them, the more recent were the earthquakes of 1853, 1894, 1914 and 1938, which affected both Chalkida and the adjacent region of Eastern Central Greece. The earthquake of 1938 in particular, was a strong surface earthquake, with an epicentre of 38.3° N, 23.8° E and a magnitude of M = 6.0 that caused extended damages in the area of Oropos, where three villages were destroyed and 8.000 people were left homeless. It also caused landslides and liquefaction phenomena on the coastal zone (Galanopoulos 1955, Papazachos and Papazachou 1997).

The latest seismic activity was the Psachna earthquake swarm of 2003, with magnitudes between M=3.0 and M=4.9. The earthquakes hypocentral locations pronounced a southward dip and the focal mechanisms showed an almost N-S extensional stress field. Normal faults with about E-W striking planes were determined, while some faults of an almost N-S direction have also been observed (Benetatos *et al.* 2004).

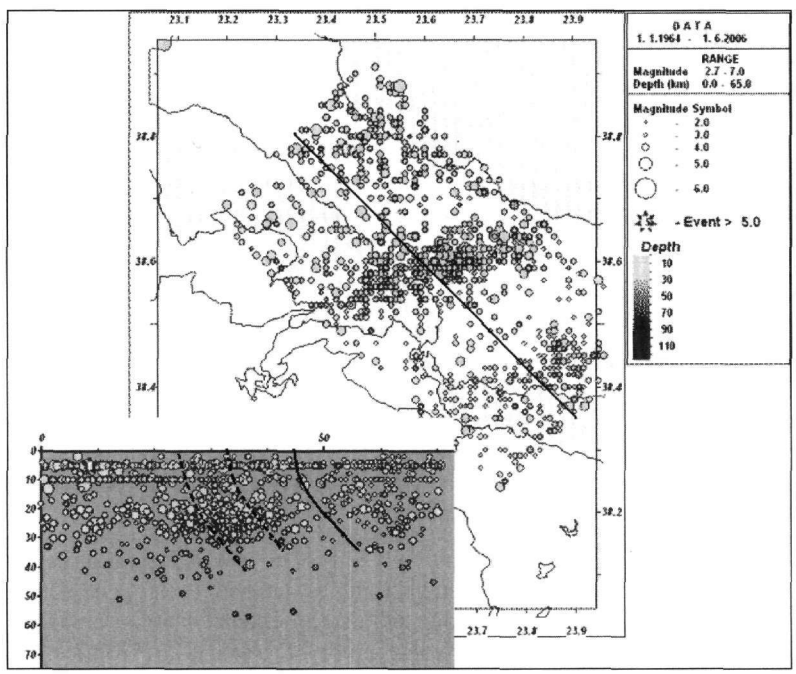

Figure 8 - Seismicity maps and cross section parallel to the axis of the North Evoikos Gulf (noted by solid line). The dashed lines correspond to the traces of inferred faults

On the epicentre map of the wider area, of earthquakes of M=2.7-7.0 magnitude that occurred during the years 1964 to 2006 (from the catalogue of the Geodynamic Institute of the National Observatory of Athens), we see a distribution focusing on the Psachna earthquakes, with an obvious alignment in the ENE-WSW direction. A series of parallel faults, of this direction and dipping south are recognized, on the section made in a direction parallel to the axis of the North Evoikos Gulf (Fig. 8). A second concentration of epicentres is observed in the opening of the South

Evoikos Gulf, where, a section normal to the axis of the Gulf allows us to trace the surfaces of antithetical faults, parallel to these identified by the geological research (Fig. 9).

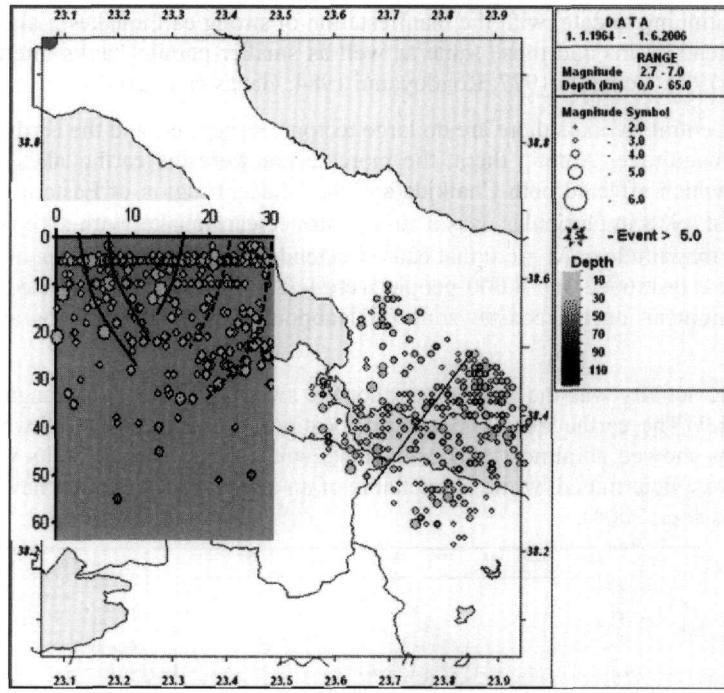

Figure 9 - Seismicity maps and cross section normal to the axis of the South Evoikos Gulf (noted by solid line). The dashed lines correspond to the traces of inferred faults

4. Conclusions

Geological mapping, stratigraphic determinations as well as fault evaluation (based on tectonic and seismological data) in the Central Evoikos region, suggest the presence of a number of active faults, in a region of moderate seismicity. This region is characterized by low elevation morphology, extended alluvial terrains and absence of morphotectonic characteristics indicative of a young tectonism. The identification of the active faults included a geophysical research, conducted to ensure and localize fault continuation into the flat areas, while published data concerning an offshore geophysical research were also evaluated.

The active faults have ENE-WSW to E-W and WNW-ESE to NW-SE main directions and are related to a dominant NNW-SSE extensional stress field, as deduced by tectonic data. Focal mechanisms of the recent Psachna earthquakes indicated also an extension in an almost N-S direction. The most important fault, from a seismotectonic point of view, is the Aghios Minas-Chalkida fault, located close to the Northern part of the town of Chalkida, with a length of 15 km. The Avlida and Lefkadi antithetic faults are of a total length of 20 to 25 km. Located largely offshore, they are responsible for the formation of the Northern part of the South Evoikos Gulf.

Finally, the determination of active faults in a region concerned of low interest from a seismotectonic point of view indicates the usefulness of studying such regions, especially if we take into account the unexpected strong disastrous earthquakes of the last decade, occurring in Greece and other seismic countries.

5. Acknowledgments

We would like to thank G. Skianis, geophysicist of the Institute of Geology and Mineral Exploration, for the time spent together during the fieldwork and the provided geophysical data.

6. References

Ambrasseys, N.N., and Jackson, J.N., 1990. Seismicity and associated strain of central Greece between 1890 and 1988, *Geophysical Journal International*, 101, 663-708.

Benetatos, C., Kiratzi, A., Kementzeridou, K., Roumelioti, Z., Karakaisis, G., Sordilis, E., Latoussakis, I., and Drakatos, G., 2004. The Psachna (Evia island) earthquake swarm of June 2003, *Bull. Geol. Soc. Greece*, XXXVI, 1379-1388.

Bornovas, J., and Rondoyanni-Tsiambaou, Th., 1983. Geological Map of Greece, scale 1:500.000, *IGME*, Athens.

Drakopoulos, I., Makropoulos, K., and Stavrakakis, G., 1984. Junction of Evia - Beotia and Chalkida diversion. Seismological study, *Report for the Greek Ministry of Public Works*, 58pp. (in Greek)

Galanopoulos, A., 1955. Seismic Geography of Greece, *Ann. Geol. Pays Hell.*, VI, 83-121. (in Greek)

Ganas, A., Sokos, A., Agalos, A., Leontakianakos, G., and Pavlides, S., 2006. Coulomb stress triggering of earthquakes along the Atalanti fault, central Greece: Two April 1894 M6 + events and stress change patterns, *Tectonophysics,* 420, *357*-369

Genre, C., 1999. Neotectonics and Late Holocene terraces. The example of Euboea (Central Eastern Greece), *Geomorphologie:relief, processus, environement,* 2, 143-158.

GeoPro, 2006. Geophysical survey in the ooshore zone of the high pressure natural gas pipeline to Aliveri. Microseismicity study. Technical report for the Hellenic Centre for Marine Research, Athens.

Goldsworthy M. and Jackson J., 2001. Migration of activity within normal faults system: examples from the Quaternary of mainland Greece, *Journal of Structural Geology*, 23, 489-506.

Katsikatsos, G., 1999. Geological map of Greece scale 1:50.000, Eretria sheet. *IGME*, Athens

Katsikatsos, G., de Bruijn, H., and van der Meulen, A.J., 1981. The Neogene of the island of Euboea, a review, *Geol. Mijnbouw*, Amsterdam, 60, 509-516.

Lemeille, F., 1977. Etudes néotectoniques en Grèce centrale nord orientale (Eubée centrale, Attique, Béotie, Locride), *Thèse 3me Cycle*, Université de Peris-Sud, 173.

Leontaris, S., 1977. The genesis of the Σχοινέζα – Avlida valley and its relation to the geology of the area, *Min. Met. Chr.*, 33, 34, 21-28. (in Greek)

Maroukian, H., and Gaki-Papanastassiou, K., 2002. Palaeogeographic evolution of the broader area of Lilas river in Central Evia during the Quaternary, *Proc. of the 6th Geographical Symposium*, Thessoloniki, 2, 210-223.

Mavrides, A., 2006 (in press). Geological map of Greece scale 1:50.000, Chalkida sheet. *IGME*, Athens

Mettos, A., 1992. Geological and palaeogeographical study of the continental neogene and quaternary deposits of NE Attica and SE Boeotia, *Rh. D. Thesis., University of Athens*, 259. (in Greek)

Papazachos, B., and Papazachou, C., 1997. The earthquqkes of Greece, Ziti ed.

Perisoratis, C., and van Andel, T.H., 1991. Sea-level changes and tectonics in the Quaternary extensional basin of the South Evoikos Gulf, Greece, *Terra Nova* ,3, 294-302.

Philip, H., 1974. Etude néotectonique des rivages egeenes en Locride et en Eubée nord occidentale (Grèce centrale), *Thèse 3me Cycle*, Université de Monpellier, 90.

Rondoyanni, Th., 1984. Etude néotectonique des rivages occidentaux du canal d' Atalanti (Grece centrale), *Thèse 3e cycle*, Université de Paris - Sud, 190.

Δελτίο της Ελληνικής Γεωλογικής Εταιρίας τομ. XXXX, 2007
Πρακτικά 11ου Διεθνούς Συνεδρίου, Αθήνα, Μάιος 2007

Bulletin of the Geological Society of Greece vol. XXXX, 2007
Proceedings of the 11th International Congress, Athens, May, 2007

TECTONO-SEDIMENTARY STRUCTURE AND LATE QUATERNARY EVOLUTION OF THE NORTH EVIA GULF BASIN, CENTRAL GREECE: PRELIMINARY RESULTS

Sakellariou D.[1], Rousakis G.[1], Kaberi H.[1], Kapsimalis V.[1], Georgiou P.[1], Kanellopoulos Th.[1], and Lykousis V.[1]

[1] *Institute of Oceanography, Hellenic Centre for Marine Research, Anavyssos, Greece, sakell@ath.hcmr.gr, rousakis@ath.hcmr.gr, ekaberi@ath.hcmr.gr, kapsim@ath.hcmr.gr, pgeorg@ath.hcmr.gr, thkan@ath.hcmr.gr, vlikou@ath.hcmr.gr*

Abstract

Systematic single channel seismic and 3.5 kHz profiling, gravity and box coring and ^{210}Pb downcore analyses shed light to the structure and the Late Quaternary evolution of the North Evia Gulf graben. The latter is segmented along its axis in three distinct basins. The shallow, E-W striking western basin displays southward asymmetry. The NW-SE striking, deep central basin and the shallow southeastern one show NE-ward asymmetry and are controlled by the Aidipsos, Telethrion and Kandili fault zones. Sequence stratigraphic data and aragonite crystals in mud layers underlying Holocene deposits verifies that North Evia Gulf was a lake during the last glacial maximum with lake level at about 90m below the present sea level.
Key words: *basin segmentation, tectonic asymmetry, active faulting, lake level.*

Περίληψη

Συστηματική μελέτη του Βόρειου Ευβοϊκού Κόλπου με σεισμικές τομές, τομογραφίες 3,5kHz, πυρηνοληψίες, δειγματοληψίες και αναλύσεις παρέχουν νέα στοιχεία για τη δομή και την εξέλιξη του στο Αν. Τεταρτογενές. Διακρίνονται τρεις επι μέρους λεκάνες: Η ρηχή, δυτική λεκάνη παρουσιάζει διεύθυνση Α-Δ και ασυμμετρία προς Νότο. Η κεντρική λεκάνη και η νοτιοανατολική έχουν διεύθυνση ΒΔ-ΝΑ και ασυμμετρία προς ΒΑ, δηλ. Προς τις ρηξιγενείς ζώνες Αιδηψού, τελέθριου και Κανδηλίου. Από την ερμηνεία των σεισμικών-ακουστικών τομογραφιών και την εύρεση κρυστάλλων αραγωνίτη προκύπτει ότι ο Β. Ευβοϊκός Κόλπος αποτελούσε λίμνη κατά την τελευταία παγετώδη περίοδο με στάθμη περίπου 90 μ. κάτω από την σημερινή.
Λέξεις κλειδιά: *τεκτονική ασυμμετρία, ενεργά ρήγματα, στάθμη λίμνης.*

1. Introduction

The aim of this paper is to explore the neotectonic architecture and the sedimentary fill of the North Evia Gulf active basin and to contribute to the understanding of the deformation and seismic hazard of the area. Furthermore, we present new data on the sea/lake level changes in the Latest Quaternary.

The North Evia Gulf is one of the active rifts/basins, together with the Gulf of Corinth, the Gulf of Patras and other onshore located basins, which overtake the crustal strain in Central Greece region, between the southwestern tip of the North Anatolian Fault and the northeastern tip of the Kefallinia Fault. According to Roberts and Jackson (1991) the area of Central Greece, between Northern Peloponese and Northern Evia has undergone total extension of 20-30 km in NNE-SSW direction and is being presently deformed by a rate of 1 cm/yr (Davies *et al.* 1997). Although a considerable part of this extension may take place in the Gulf of Corinth area (Billiris *et al.* 1991, Armijo *et al.* 1996, Clarke *et al.* 1997), the thinned, only 20 km in thickness, crust below the central North Evia Gulf (Makris *et al.* 2001) is a strong evidence of significant extension too.

The most recent strong earthquake activity dates back to April 1894, when during the Atalanti earthquake sequence the homonymous fault was broken for more than 30km and was followed by tsunami waves, which flooded the low coastal plains of Atalanti Gulf (Pantosti *et al.* 2001, Skouphos 1894, Philippson 1894, Mitsopoulos 1895, Richter 1958, Lemeille 1977, Rondoyianni 1984, Ambraseys and Jackson 1990, Ganas *et al.* 1997).

Despite the surficial sediment map, published by IGME in 1991, few studies of the submarine structure of the North Evia Gulf have been conducted (Van Andel and Perissoratis 2006). Herewith we present results of a systematic survey of the neotectonic basin, conducted in years 2004-2006.

2. Materials and Methods

The marine geological survey in the N. Evia Gulf took place in 2004. A total of 700 km single-channel seismic profiles (Fig. 1a) were acquired using an Air Gun, $10in^3$ air chamber (Bolt USA) simultaneously with a 4-transducer ORE 3.5kHz sub-bottom profiler. Seismic profiling data were acquired both in analog form on an EPC recorder and digitally using Delph Seismic+ software, geo-encoded using Delph Map v. 2.9.6 software and post-processed using SeismicGIS software of Triton Imaging Inc. For the swath bathymetric survey of the gulf a SEABEAM 2120 (20 kHz) system was used (Alexandri *et al.* 2005). Twenty eight gravity cores (using a BENTHOS INS gravity corer) and ten box cores (Fig. 1a) were collected, described macroscopically and analyzed under a Multi Sensor Core Logger for their petro-physical characteristics. Selected samples from the cores were imaged under the scanning-electron-microscope. Actual sedimentation rates (late 0.1 ka) were determined in undisturbed sub-cores from two box cores using the ^{210}Pb method (Appleby and Oldfield 1992, Sanchez-Cabeza *et al.* 1998, Radakovitch 1995).

3. Basin architecture

3.1. Along-axis segmentation

Morphologically and, as it will be shown hereafter, geologically the North Evia Gulf graben can be subdivided along axis into three distinct basins: the western, the central and the southeastern basin (Fig. 1b). The first and the third one are flat bottomed with maximum depth not exceeding 100 m. The central basin is the deepest one, with maximum depth of about 440 m. The boundaries between the three basins are marked by moderately steep slopes along the lines Aidipsos-Arkitsa and Limni-Malesina Peninsula. The Aidipsos-Arkitsa boundary marks the change of the basin's strike from E-W (N90°E) in the western basin to NW-SE (N120°E) in the central and southeastern basins. The steepest slopes in North Evia Gulf occur off North Evia coasts, between Aidipsos and Limni, and form the northeastern margin of the central basin.

3.2. Western Basin

The E-W trending western basin extends from the volcanic Lichadhes islands to the west to the Arkitsa-Aidipsos flexure to the east and constitutes the eastward prolongation of Sperchios valley. On the southern coasts, the Kamena Vourla, Agios Konstantinos and Arkitsa-Logos fault zones

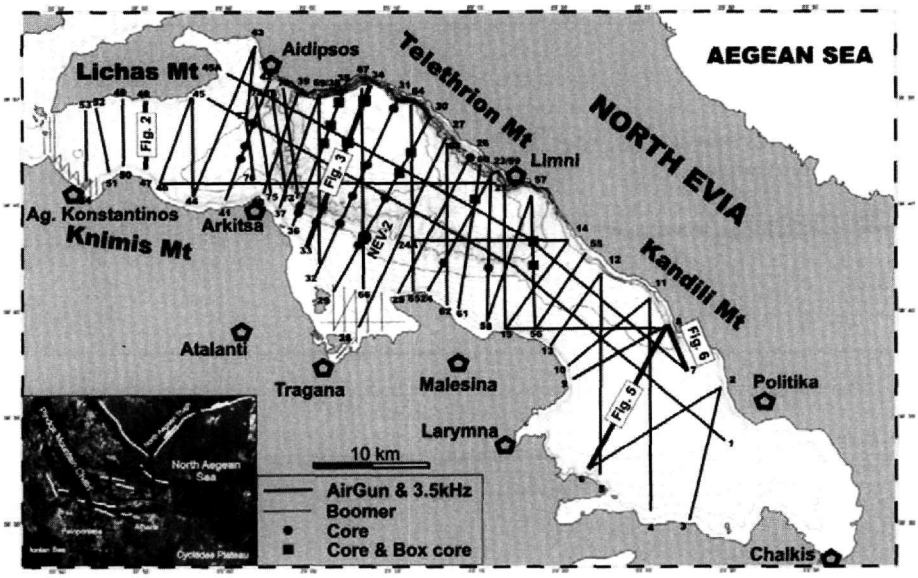

Figure 1a - Location map of AirGun 10in^3 profiles, 3.5 kHz profiles, gravity cores and box cores in the North Evia Gulf. Seismic profiles and gravity/box coring sites presented in this paper are marked on the map. NEV-12 and NEV-13 box cores presented in Fig. 4 are shown as black squares. Inset map shows main tectonic lines in Central Greece

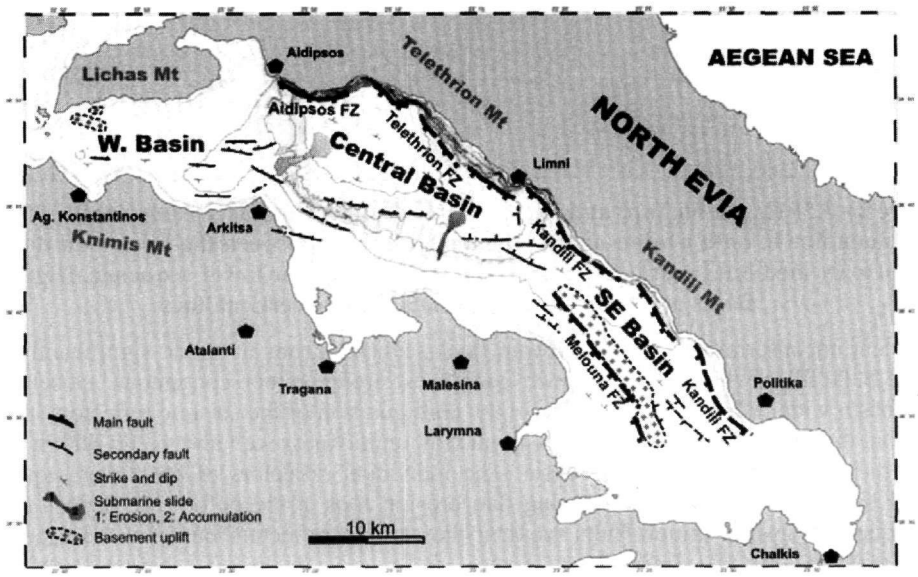

Figure 1b - Tectonic map of North Evia Gulf. Bathymetry from Alexandri *et al.* (2005). The main fault zones are marked as thick black lines. The three, structurally differentiated, basins of the North Evia Gulf are also indicated on the map

(Kranis 1999) form the tectonic boundary between the uplifting alpine basement of Knimis Mt. and the basin. No other marginal fault was imaged on the seismic profiles (Fig. 2) from the western basin, along either the southern or the northern margin.

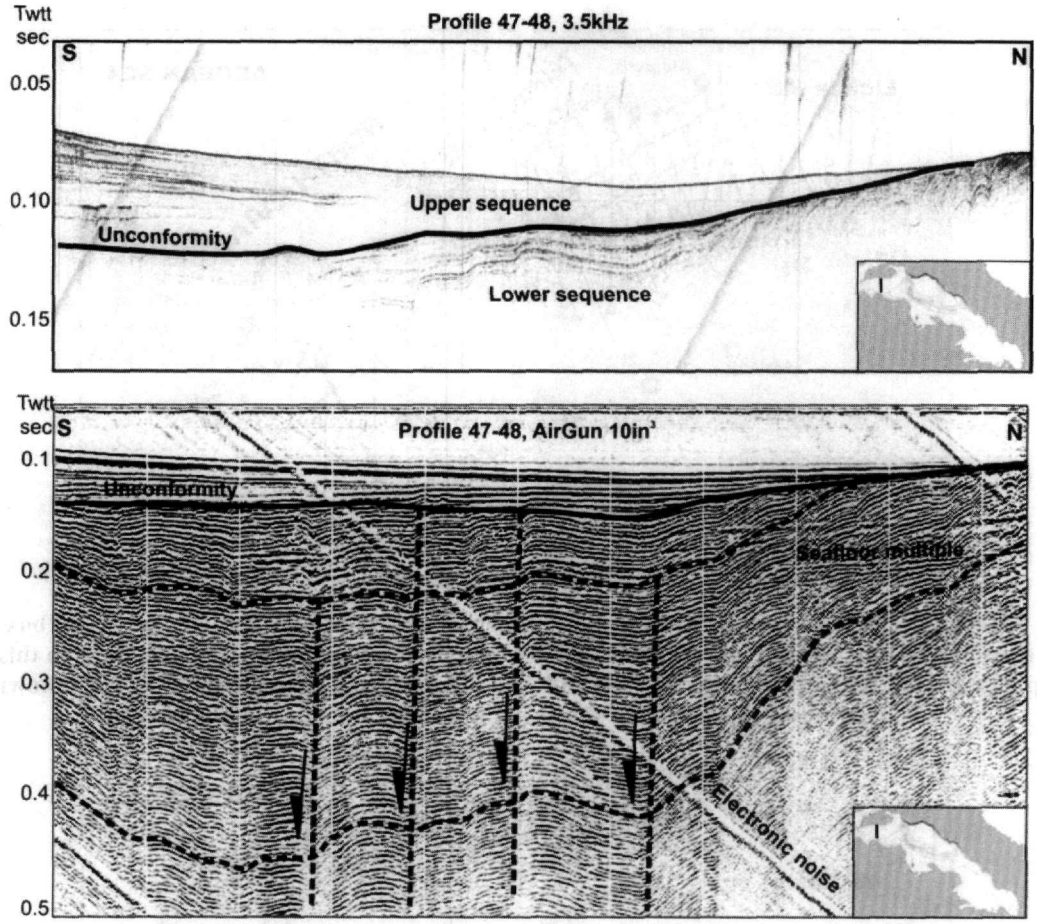

Figure 2 - 3.5kHz profile (up) and Air Gun 10 in^3 single channel seismic profile (down). Thick black line in both profiles marks the unconformity between the lower and the upper sequence. Dashed lines mark the trace of the reflectors of the lower sequence. High angle faults are also shown as dashed, nearly vertical lines

A prominent unconformity separates a lower, thick sequence from an upper, significantly thinner, one. The bulk fill of the lower sequence comprises strong, rather continuous, closely spaced, parallel, basin wide reflectors (Fig. 2). From the configuration of the seismic reflectors it becomes evident that the depocenter of the basin, with maximum thickness well above 300-400 m, lies very close to the southern margin of the basin. The individual reflectors of the lower sequence are truncated by the unconformity, indicating that erosion took place before the deposition of the upper sequence. Several minor faults crosscut the seismic reflectors but they are caped by the unconformity.

The upper sequence displays transparent acoustic character, with wider spaced continuous reflectors, which onlap the underlying unconformity (Fig. 2). Its maximum thickness does not exceed 30-40 m at the southern part of the basin and diminishes towards north. Although no age constrains are available, in analogy with other enclosed areas, like the Gulf of Corinth (Lykousis *et al.* 2006) and the Amvrakikos Gulf (Kapsimalis *et al.* 2005), and on the basis of the acoustic character and the underlying unconformity, we interpret the upper sequence as Holocene marine deposited sediments (see also Van Andel and Perissoratis 2006), derived mainly from the fertile material carried by the torrents, which drain the Knimis Mt. Small outcrops of acoustically opaque

basement at the northwestern edge of the basin may represent volcanic rocks similar to the ones of Lichadhes islands.

3.3. Central Basin

The transition from the shallow, western basin to the deep, central one is marked by a moderately steep slope along the Aidipsos-Arkitsa line, which coincides with a flexure of the deposited sedimentary sequences below it, associated with a series of parallel, N-S trending, minor faults.

Similar configuration is observed along the southern slope of the basin (Fig. 3). The seismic reflectors below the southern shelf and slope dip south- or southwest-wards. The dip direction changes to northeast-wards immediately north of the southern, north-facing faults and remains so throughout the deep basin. The seismic stratigraphy of the basin implies continuous, strong reflectors fanning northwards, indicating thus enhanced subsidence close to the northern margin. The latter is marked by a steep slope and the presence of a large, basin-bounding fault zone, which includes the E-W trending Aidipsos fault and the NW-SE trending Telethrion fault (Figs 1b, 3). Large masses with chaotic acoustic character at the immediate vicinity of the fault surface indicate extensive, gravity-driven deposits, derived from the upper part of the northern slope (Fig. 3). Mass flow deposits occur also along the foot of the southern slope (Fig. 1b).

The overall structure of the central basin is the one of an asymmetric graben with the northeastern tectonic margin being the one which drives the subsidence of the basin throughout its evolution. The northeast-ward fanning configuration of the basin fill supports this interpretation and indicates higher sedimentation rates close to the northern margin. The two main fault zones, Arkitsa and Telethrion, which form the northeastern tectonic boundary of the central basin, have accommodated a cumulative throw well above 1000 m.

Estimation of the actual sedimentation rates, from the ^{210}Pb vertical distribution in very recent sediments from the deep central basin, shows similar pattern. The box cores NEV-12 and Nev-13 were taken from the deep central basin, the latter closer to the northern margin and are composed of mud. Their location is shown on the profile of Fig. 3.

The upper part of box core NEV-12, between 0-7cm bsf. shows strong bioturbation and is thus not taken into consideration for the estimation of the accumulation rate. The supported ^{210}Pb total activity was reached at 30cm bsf. (Fig. 4). The maximum accumulation rate in box core NEV-12 was estimated from the ^{210}Pb profile between 7-30 cm bsf, following the CRS model and was found 0.26 cm/y for the last 100-120 years. The upper 6 cm of box core NEV-13 (Fig. 4) are also bioturbated and were not taken into consideration, while the supported ^{210}Pb total activity was reached at 30 cm bsf. Consequently, following CRS model and the different shape of the ^{210}Pb profile, the maximum accumulation rate for the last 100-120 years was found 0.33 cm/y. This pattern is in accordance with the relative sedimentation rates below the sites of NEV-12 and NEV-13 box cores, as they can be deduced from the geological data of the profile of Fig. 3 and the northeastward thickening of the individual reflectors. A very similar pattern has been observed in box cores taken across the asymmetric Alkyonides basin (Kaberi and Sakellariou 2006).

3.4. Southeastern Basin

A gradual morphological transition and a significant narrowing of the actual basin mark the transition from the central deep basin to the southeastern, shallow and flat basin. The latter displays very different geological structure and basin stratigraphy. A major fault zone, the Melouna one, striking parallel to the long axis and in the middle of the basin, divides it into two parallel, longitudinal subbasins.

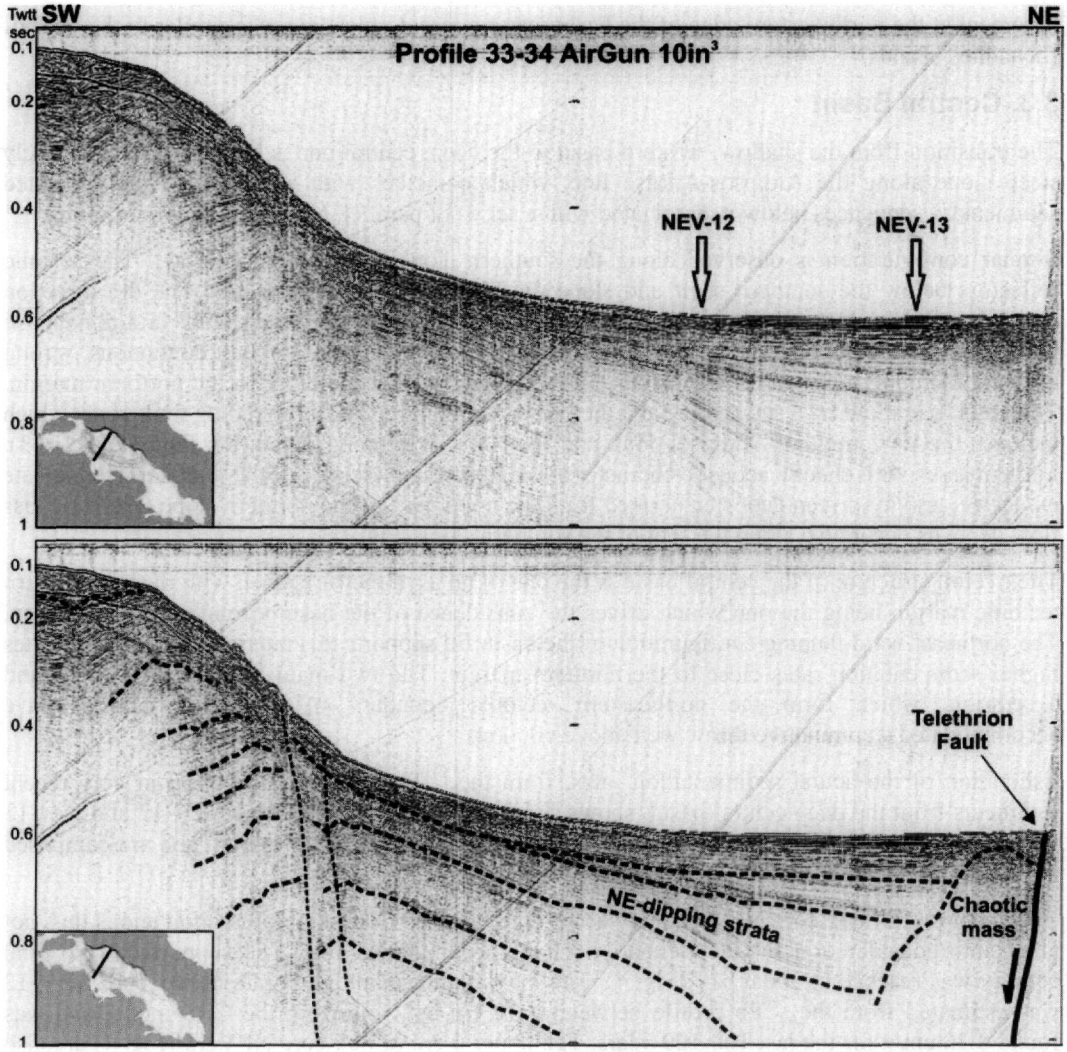

Figure 3 - Air Gun 10in³ single channel seismic profile (up) and interpretation (down). The location of box cores NEV-12 and NEV-13 is shown. The Telethrion Fault is shown as thick black line, arrow indicates sense of movement. Dashed lines mark the trace of the seismic reflectors of the basin fill. Dashed thin lines indicate minor faults at the south slope

Although Melouna fault has little expression on the present seafloor, it seriously affects the basin fill. Three sedimentary sequences are separated by erosional (the lower one) or angular (the upper one) unconformities (Fig. 5). The lower sequence is characterized by rather continuous, strong, curved reflectors, which are being truncated upwards, where they meet the lower unconformity. The latter is being displaced by the Melouna fault by about 80 m in the profile of Fig. 5. The total displacement of the roof of the lower sequence is not constant, but varies significantly along the strike of the fault.

The intermediate sedimentary sequence is characterized by continuous reflectors, which onlap the roof of the lower sequence. It is interesting to note that the individual reflectors of both the intermediate and the lower sequences are bended from both sides towards the Melouna fault (Fig. 5). Moreover, the vertical throw of the fault decreases dramatically upwards. Both aforementioned observations, along with the variable cumulative throw along strike, are evidences that strike-slip movement may be a significant component of the, apparently normal, Melouna fault.

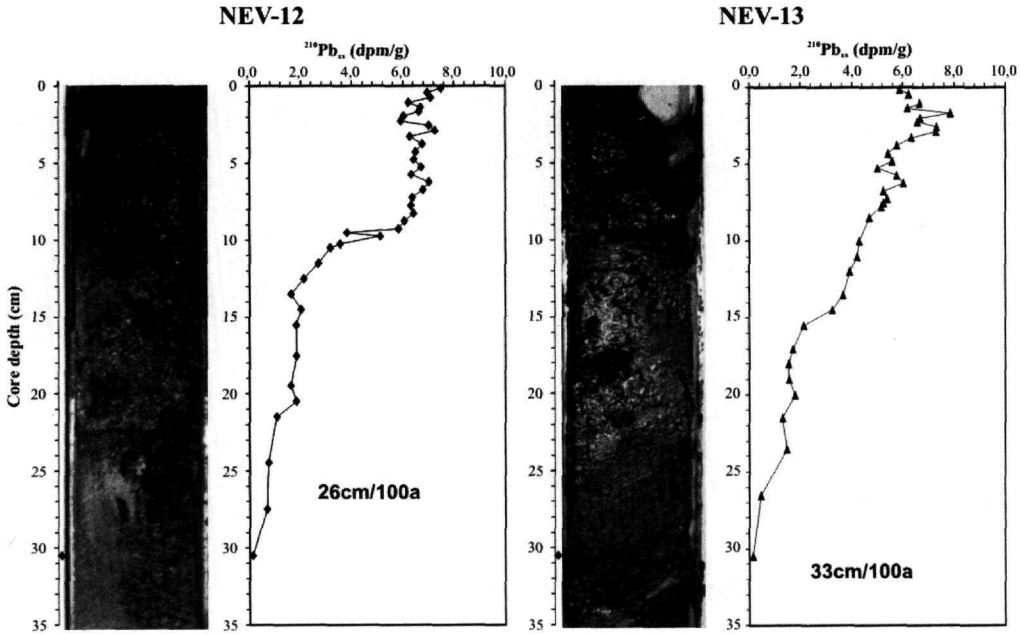

Figure 4 - Photograph of the upper 35 cm and ^{210}Pb activity curves of NEV-12 (left) and NEV-13 (right) box cores taken from the deep central basin of the North Evia Gulf. Estimated maximum, actual sedimentation rates are shown. Location of box cores in Fig. 1a, 3

The updoming of the lower sequence along the central axis of the southeastern basin results to the formation of two parallel trending subbasins, which are expressed in the sedimentary pattern of the intermediate sequence.

The southwestern subbasin, hereafter called Malesina subbasin, reaches maximum thickness of about 350 msecs twtt. (about 300 m) which is being observed either along the middle axis of the subbasin or close to Melouna fault. The boundary of the Malesina subbasin to the Pliocene sequence of Malesina Peninsula is not well imaged. Although no significant fault has been observed on the seismic profiles, the transition from the depocenter to the uplifted peninsula is rather abrupt. According to the seismic data, some parts of the Malesina subbasin display symmetric character, while in other parts subsidence is enhanced close to the Melouna fault.

The depocenter of the northeastern subbasin, hereafter called Kandili subbasin, with maximum thickness of about 500 msecs twtt (about 400 m) lies close to the Kandili fault zone. Similar to the central basin, the individual reflectors of the Kandili subbasin dip northeastwards, toward the Kandili fault zone and they are bended upwards close to the fault surface. The Kandili fault zone forms the tectonic boundary to the alpine basement of North Evia island. The overall configuration of the Kandili subbasin is the one of an asymmetric graben, with the northeastern tectonic margin as the leading role to the subsidence of the subbasin.

No age constrains are available to allow a direct chrono-stratigraphic control of the sedimentary fill of the southeastern basin. Consequently, only assumptions on the possible age of the various sedimentary sequences can be made, on the basis of the existing seismic data and an attempt to correlate the submarine deposits with the post-alpine formations, which outcrop on the adjacent land areas. Thus, we assume that the lower sequence of the southeastern basin may be equivalent to the Pliocene sediments of Malesina Peninsula and North Evia island. If this assumption is true, then a minimum subsidence of 400-500 m can be deduced for the southeastern basin in respect to the adjacent Pliocene land deposits.

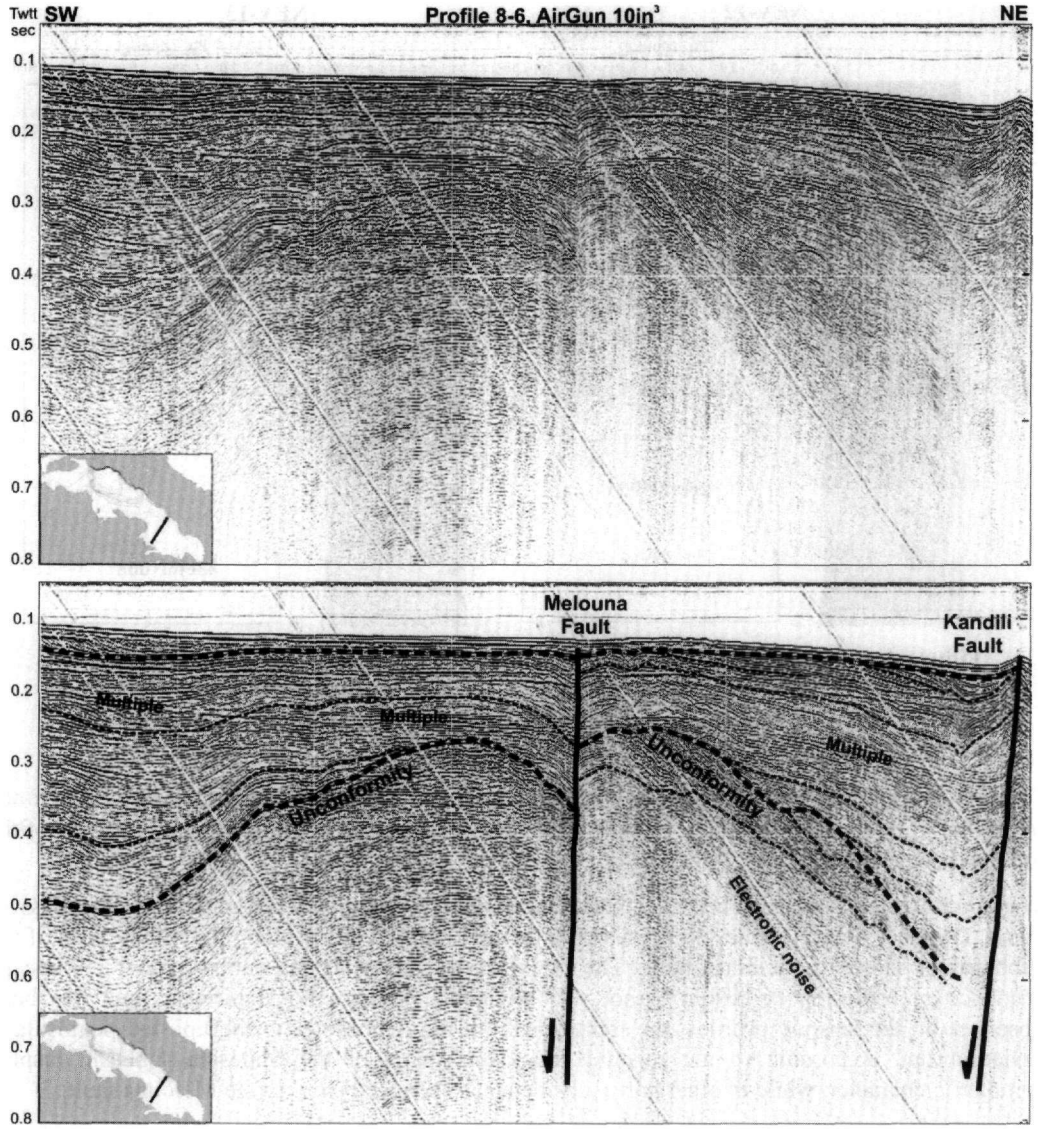

Figure 5 - Air Gun 10in^3 single channel seismic profile (up) and interpretation (down). Kandili and Melouna Fault are shown as thick black lines, arrows indicate sense of movement. Dashed thick lines mark unconformities. Dashed thin lines emphasize the trace of the seismic reflectors of the intermediate and the lower sequences

Consequently, the intermediate sedimentary sequence may have deposited during a certain period in Quaternary. We have no data to define with higher chronological accuracy the onset of the subsidence of the basin and the sedimentation of the intermediate sedimentary sequence.

Despite the rather shallow depth of the basin and the absence of spectacular fault-controlled slopes, like the ones along the northeastern margin of the central basin, it is quite clear that both main fault zones, Melouna and Kandili, show strong evidence of ongoing activity. Slight deepening of the present seafloor and upward bending of the sediment strata close to the Kandili fault support the above conclusion. Further on, the slight displacement of the present seafloor at the trace of Melouna fault, together with the possible strike-slip component of the fault, are also evidences of ongoing activity.

3.5. The North Evia Gulf Pleistocene lake

The systematic survey of the North Evia Gulf with a high resolution, 3.5 kHz sub-bottom profiler, provided a large amount of data on the Latest Quaternary sedimentary deposits and the recent fluctuations of the water level. The Holocene deposits form a variably thick, transparent drape, which covers the older sediments. Maximum thickness of up to 40 m has been observed on the southern shelf, off the outflow of torrents, which drain the mountainous areas of mainland Greece (Fig. 2). In the basins the mean Holocene thickness does not exceed a few meters.

Two well developed submarine terraces occur mainly along the southern slope of the central basin, a shallow one at 90 m and a deeper one at 150m depth. Both terraces are caped by the Holocene transparent drape. In several places around the gulf, but especially at the periphery of the southeastern basin, the Holocene drape overlies a seismic package composed of strong, continuous, parallel reflectors. As shown in Fig. 6 the latter overlie a lower transparent horizon and onlap an irregular, high amplitude reflector, which is interpreted as erosional surface. Following the sequence stratigraphic interpretation shown by Lykousis *et al.* (2006) for similar sequences in the Gulf of Corinth basin, we interpret the upper drape as Holocene deposits and the lower transparent horizon as fine-grain sediments deposited during the previous high sea level stage. Consequently, the intermediate seismic package should represent coarse grain deposits accumulated during the last low sea level stage.

The above described seismic stratigraphy allow drawing some safe conclusions on the water level in the North Evia Gulf during the last glacial stage. The shallowest point where the intermediate seismic package onlaps the erosional surface lies at about 90m (120 msecs) below the present sea level and may with good approximation represent the water level during $^{\delta 18}O$ isotopic stage 2. Note that this depth coincides with the one of the shallow terrace, observed mainly along the southern margin of the gulf. Sedimentological description and SEM analysis of samples from many gravity cores has verified the aforementioned interpretation.

The 217 cm long gravity core NEV-2 was taken from the 150m deep terrace at the southern slope of the Gulf. The upper, 206 cm long, part of the core is dominated by light gray mud/mud turbidites (Fig. 7A). The lower part, between 206-217 cm bsf, is characterized by alternations of mm- to cm-thick light gray, olive gray and grayish white mud layers. This pattern was also observed in long cores recovered from the Gulf of Corinth basin (Lykousis *et al.* 2006) and points out to cyclic changes of redox properties at the water-sediment interface. The transition from the upper to the lower part is marked by gradual increase of the P-wave velocity (from 1520 to 1580 m/sec) and the gamma density, as well as a remarkable decrease of the magnetic susceptibility and the fractional porosity.

Two samples were taken from core NEV-2 and were analyzed under the scanning-electron-microscope. The marine coccolithophorae *Emiliania huxleyi* was abundant in the sample taken from the upper part of the core at 196 cm bsf (Fig. 7B) but was not found in the one taken from the lower part of the core at 212 cm bsf. Aragonite crystals were observed in the latter sample (lower part of the core) but were absent from the sample taken from the upper part of the core (Fig. 7C). *Emiliania huxleyi* was also found in samples taken from the same sedimentary sequence of other cores. The above findings allow assuming that the upper part of NEV-2 was deposited under marine conditions while the lower part of the core may have been deposited under lacustrine conditions during the last low water level stand. Van Andel and Perissoratis (2006), on the basis of high resolution data suggested already, that the North Evia Gulf was isolated from the Aegean Sea during the last glacial stage. This assumption is now confirmed.

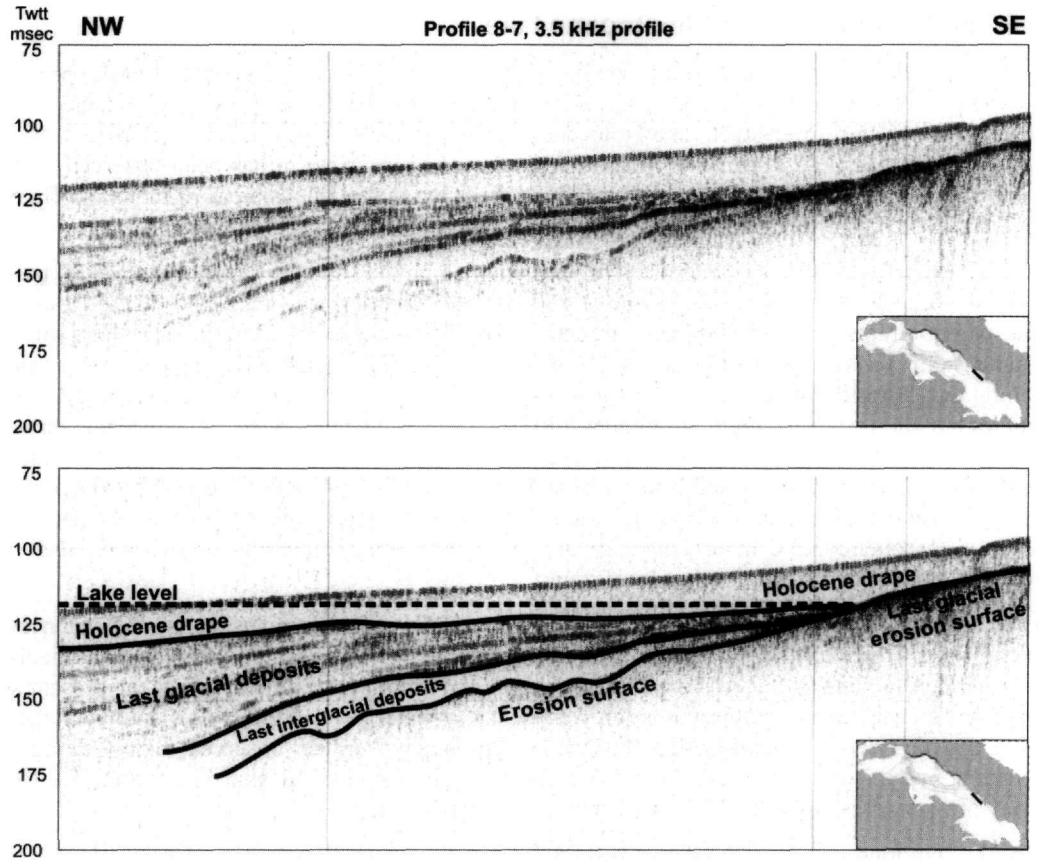

Figure 6 - 3.5kHz subbottom profile (up) and interpretation (down). See text for explanations. Dashed horizontal line indicates last glacial low water (lake) level at about 120 msecs (about 90 m) below present sea level

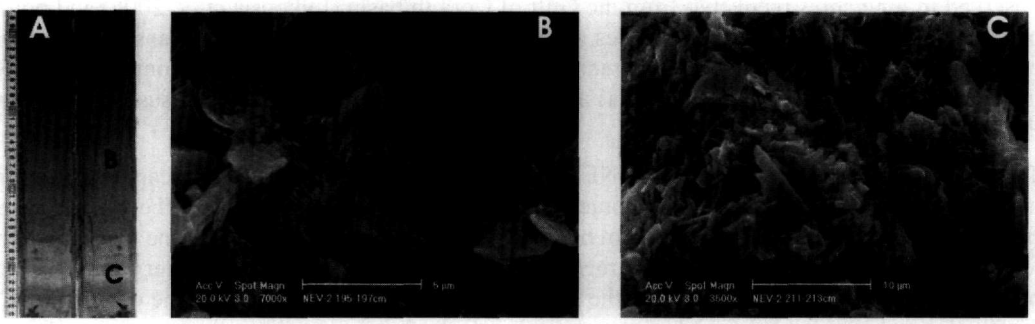

Figure 7 - A) Section of NEV-2 gravity core, between 177-217 cm bsf. B) SEM photograph showing *Emiliania huxleyi* coccoliths found in sample B from the upper, marine part of the core. C) SEM photograph showing aragonite crystals found in sample C from the lower, lacustrine part of the core

4. Conclusions

The North Evia Gulf can be structurally subdivided into three distinct basins, the western, the central and the southeastern one, with different geological and morphological characteristics. Along axis segmentation may be the result of strain partitioning at the southwestern tip of the

North Anatolian Fault superimposed on the inherited alpine structure of Central Greece. Main, basin bounding fault zones strike E-W to NW-SE, parallel to the long axis of the basin. Tectonic lineaments perpendicular to that direction, already observed or inferred in the adjacent land masses, were not clearly imaged on the single channel seismic data.

While the evolution of the western shallow basin is controlled by the large faults along its southern margin, the 440 m deep central basin and the southeastern display northeastward asymmetry, with the Aidipsos, Telethrion and Kandili fault zones, located at the foot of North Evia slope, driving their subsidence.

High resolution subbottom profiles and gravity coring indicate that water level in the North Evia Gulf during the last glacial period was about 90m below the present sea level. Since maximum depth of the Lichades island strait does not exceed 65-70 m, an isolated lake should have developed in the place of the present North Evia Gulf. Lacustrine environment in the Gulf during the last glacial period has been verified with the presence of authigenic aragonite crystals in variably colored mud layers underlying Holocene mud deposits.

5. Acknowledgments

The authors greatly acknowledge I. Pampidis and P. Mantopoulos, both engineers, for their valuable help in operating geophysical equipment during the cruise. Our thanks go also to the officers and the crew of R/V AEGAEO for their valuable support during the cruises. This survey was conducted in the frame of AMPHITRITE project, funded by the General Secretariat of Research & Technology, Greece and coordinated by Dr. I. Papoulia at HCMR.

6. Literature

Alexandri, M., Nomikou, P., Ballas, D., and Papoulia, I., 2005. Submarine topography and morphological regime of Northern Evoikos basin, *Int. Earth. Sci. Coll. Aegean Regions.*

Ambraseys, N.N., and Jackson, J.A., 1990. Seismicity and associated strain of central Greece between 1890 and 1988, *Geophys. J. Int.,* 101/3, 663-708.

Armijo, R., Meyer, B., King, G.C.P., Rigo, A., and Papanastassiou, D., 1996. Quarternary evolution of the Corinth rift and its implications for the late cenozoic evolution of the Aegean. *Geoph. J. Int.*, 126, 11-53.

Appleby, P.G., and Oldfield, F., 1978. The calculation of lead-210 dates assuming a constant rate of supply of unsupported ^{210}Pb to the sediment. *Catena*, 5, 1-8.

Billiris, H., Paradissis, D., Veis, G., England, P., Featherstone, W., Parsons, B., Cross, P., Rands, P., Rayson, M., Sellers, P., Ashkenazi, V., Daavison, M., Jackson, J., and Ambraseys, N., 1991. Geodetic determination of tectonic deformation in Central Greece from 1900 to 1988, *Nature,* 350, 124-129.

Clarke, P.J., Davies, R.R., England, P.C., Parsons, B.E., Billiris, H., Paradissis, D., Veis, G., Denys, P.H., Cross, P.A., Ashkenazi, V., and Bingley, R., 1997. Geodetic estimate of seismic hazard in the Gulf of Korinthos, *Geophys. Res. Lett.*, 24, 1303-1306.

Davies, R.R., England, P.C., Parson, B.E., Billiris, H., Paradissis, D., and Veis, G., 1997. Geodetic strain of Greece in the interval 1892-1992, *J. Geophys. Res.*, 102, 24,571-24,588.

Ganas, A., Roberts, G.P., and Memou, T., 1997. Segment boundaries, the 1894 ruptures and strain patterns along the Atalanti fault, Central Greece, *J. Geodynamics*, 26/2-4, 461-486.

IGME, 1991. Surficial sediment map of the Aegean sea floor (Pagasitikos sheet), Institute of Geology and Mineral Exploration, Athens.

Kaberi, H., and Sakellariou, D., 2006. Active sedimentation rates in the northern Evia Gulf and the Alkyonides basin, *Comparison using the ^{210}Pb method. 8th Hell. Oceanography and Fisheries Symposium, Abstracts*, 179p.

Kapsimalis, V., Pavlakis, P., Poulos, S.E., Alexandri, S., Tziavos, Ch., Sioulas, A., Filippas, D., and Lykousis, V., 2005. Internal structure and evolution of the Late Quaternary sequence in a shallow embayment: The Amvrakikos Gulf, NW Greece, *Mar. Geol.* 222-223, 399-418.

Kranis, Ch., 1999. Neotectonic activity of fault zones in central-eastern Sterea Ellas, Lokris, *Ph.D. Thesis*, Univ. Athens.

Lemeille, F., 1977. Etudes neotectoniques en Grece centrale nord-orientale (Eubee centrale, Attique, Beotie, Locride) et dans les Sporades du Nord (ile de Skiros), *These de Troisieme Cycle*, Univ. Paris XI-Centre Orsay, 173pp.

Lykousis, V., Sakellariou, D., Moretti, I., and Kaberi, H., 2007. Late Quaternary basin evolution of the Gulf of Corinth: Sequence stratigraphy, sedimentation, fault-slip and subsidence rates, *Tectonophysics*, in press.

Makris, J., Papoulia, J., Papanikolaou, D., and Stavrakakis, G., 2001. Thinned continental crust below northern Evoikos Gulf, central Greece, detected from deep seismic soundings, *Tectonophysics,* 341, 225-236.

Mitsopoulos, K., 1895. The great Lokris earthquake of April 1894. National Printing Office, Athens, 40p. (in Greek)

Pantosti, D., De Martini, P.M., Papanastassiou, D., Palyvos, N., Lemeille, F., and Stavrakakis, G., 2001. A reappraisal of the 1894 Atalanti earthquake surface ruptures, Central Greece, *Bull. Seism. Soc. America*, 91/4, 760-780.

Philippson, A., 1894. Das dies jahrige Erdbeben in Lokris, *Zeitschrift Ges. Erdkunde zu Berlin*, 21, 332-334. (in German)

Radakovitch, O., 1995. Étude du transfert et du dépôt du matériel particulaire par le ^{210}Po et le ^{210}Pb. Application aux marges continentales du Golfe de Gascogne (NE Atlantique) et du Golfe du Lion (NW Méditerranée), *PhD. Thesis,* Univ. of Perpignan.

Richter, C.F., 1958. *Elementary Seismology*, Freeman, San Francisco, 768pp.

Roberts, S., and Jackson, J., 1991. Active normal faulting in Central Greece: an overview. In A.M. Roberts, G. Yielding and B. Freeman (eds.), *The Geometry of Normal Faults*, *Geol. Soc. Sp. Publ.* 56, 125-142pp.

Rondoyianni, T., 1984. Etude neotectonique des ravages occidentaux du canal d' Atalanti (Grece Centrale), *These de Troissieme Cycle*, Univ. Paris-Sud-Centre d'Orsay, 193pp.

Skouphos, T., 1894. Die zwei grossen Erdbeben in Lokris am 8/20 und 15/27 April 1894, *Zeitschrift Ges. Erdkunde zu Berlin*, 24, 409-474. (in German)

Sanchez-Cabeza, J.A., Masqué, P., and Ani-Ragolta, I., 1998. ^{210}Pb and ^{210}Po analysis in sediments and soils by microwave acid digestion, *Journal of Radioactivity and Nuclear Chemistry*, 227/1-2), 19-22.

Van Andel, T.H., and Perissoratis, C., 2006. Late Quaternary depositional history of the North Evvoikos Gulf, Aegean Sea, Greece, *Mar. Geol.*, 232, 157-172.

Δελτίο της Ελληνικής Γεωλογικής Εταιρίας τομ. XXXX, 2007
Πρακτικά 11ου Διεθνούς Συνεδρίου, Αθήνα, Μάιος 2007

Bulletin of the Geological Society of Greece vol. XXXX, 2007
Proceedings of the 11th International Congress, Athens, May, 2007

THE TECTONIC SETTING OF THE OCTOBER 8TH 2005 EARTHQUAKE IN KASHMIR, NORTH PAKISTAN

Skourtsos E.[1], and Lekkas E.[1]

[1] *National and Kapodistrian University of Athens, Faculty of Geology and Geoenvironment, Department of Dynamic, Tectonics and Applied Geology eskourt@geol.uoa.gr, elekkas@geol.uoa.gr*

Abstract

On the 8th of October 2005 an earthquake of magnitude 7.6 occurred in northern Pakistan. The earthquake epicenter was located in Pakistan Kashmir, 90 km north of Islamabad, the capital of Pakistan. The focal depth was 26 km triggered by a thrust fault striking NW-SE and of 40o dip angle towards the NE. The mean fault slip was estimated as 4 m. The aftershocks epicenters were located northeastwards of the Indus – Kohistan Seismic Zone. The structures that trace the activated fault were distributed along the southwestern limb of the Muzaffarabad anticline and grouped as structures of flexural-slip folding, structures that are correlated to folding and normal faults. The latter may represent overturned segments of the seismic fault on the high-angle limb of the Muzaffarrabad anticline. This anticline is located on the hanging wall of a thrust fault with geometry and kinematics characteristics similar to those of the Indus – Kohistan Seismic Zone. This zone, from the Hazara – Kashmir Syntaxis to the Swat River represents a blind thrust under the metamorphosed rocks of the Lower Himalayas, while in the region of Sub– Himalayas becomes a distinct structure. This thrust fault is linked in depth to the Main Himalaya Thrust through which, the cratonic basement of India is subducting under its sedimentary cover.

Key words: *Himalayan, main boundary thrust, thrust fault, Kashmir, flexural slip structures, Muzaffarabad fault.*

Περίληψη

Την 8η Οκτωβρίου 2005 σεισμός μεγέθους 7.6 έλαβε χώρα στο βόρειο Πακιστάν. Το επίκεντρό του τοποθετείται στο Κασμίρ, 90 km βόρεια του Islamabad, πρωτεύουσας του Πακιστάν. Το εστιακό βάθος του ήταν 26 km και οφείλεται στη δράση ενός επωθητικού ρήγματος διεύθυνσης ΒΔ-ΝΑ και κλίσης 40ο προς τα ΒΑ, ενώ η μέση ολίσθηση ήταν 4 m. Τα επίκεντρα της μετασεισμικής ακολουθίας εντοπίστηκαν βορειοανατολικά της Σεισμικής Ζώνης Ινδού – Κοχιστάν. Οι δομές που σχετίζονται με το ρήγμα παρατηρήθηκαν κατά μήκος του νοτιοδυτικού σκέλους του αντικλίνου του Muzaffarabad και επρόκειτο για πτυχωσιγενείς δομές ολίσθησης, παραμόρφωση των παλαιών πλευρικών κορημάτων και αλλουβιακών ριπιδίων με ταυτόχρονη δημιουργία νέων και κανονικά ρήγματα μεγάλης κλίσης, τα οποία πιθανά να αντιπροσωπεύουν ανεστραμμένα ή κατακόρυφα τμήματα του σεισμικού ρήγματος στο μεγάλης κλίσης σκέλος του αντικλίνου του Muzaffarabad. Το αντίκλινο αυτό βρίσκεται στο πάνω τέμαχος ενός

επωθητικού ρήγματος με γεωμετρία και κινηματική συγκρίσιμη με αυτή της Σεισμικής Ζώνης Ινδού – Κοχιστάν. Η τελευταία συνιστά από τη Hazara – Kashmir Syntaxis μέχρι τον Ποταμό Swat ένα τυφλό επωθητικό ρήγμα κάτω από τα μεταμορφωμένα πετρώματα των Χαμηλών Ιμαλάϊων, ενώ στην περιοχή των Υπο-Ιμαλάϊων είναι μία διακριτή δομή. Στο βάθος συνδέεται με την Κύρια Επώθηση των Ιμαλάϊων, όπου το κρατονικό υπόβαθρο της Ινδίας υποβυθίζεται κάτω από το ιζηματογενές επικάλυμμά του.
Λέξεις κλειδιά: *Ιμαλάια, κύρια περιθωριακή επώθηση, Κασμίρ, δομές πτυχωσιγενούς ολίσθησης, ρήγμα Muzaffarabad.*

1. Introduction

On the 8th of October 2005 and at 8:50 AM local time (03:50:38 UTC), an earthquake of magnitude 7.6 R hit northern Pakistan. The earthquake epicenter, which is the strongest earthquake in the history of the country since 1935, was located near the capital of the Kashmir, Muzaffarabad, and except northern Pakistan, the earthquake also affected northern India and northeastern Afghanistan. The local authorities of Pakistan recorded over 87,000 casualties and at least a fivefold number of injuries, while according to the United Nations the homeless were estimated to nearly four million. Important damages and at least 1,300 casualties were also recorded in northwestern India.

Although it is not the first time that the Himalayas generate such earthquakes – many earthquakes of magnitude >8 R have been recorded in the past – this was the most catastrophic earthquake recorded on the Himalayan Arc. Major earthquake events recorded during the past century include the Kanga earthquake in 1905 with 19,000 casualties, the Bihar earthquake with 11,000 casualties and the Quetta earthquake with 30,000 casualties (Khattri 1987, Billham 2004). An interesting element is that for the aforementioned earthquakes but also for other historical earthquakes, no primary surface ruptures were recorded, a fact that led Seeber and Ambruster (1981) to suggest that those earthquakes were occurred by the activation of blind thrust faults and that the stresses were released through fold growth of anticline structures rather than primary surface rupturing (Kumar *et al.* 2006 and references therein). However, recent research is controversial to the above suggestions presenting new data on the surface expression of large thrust structures during earthquake events of significant magnitude (Kumar *et al.* 2006).

Similar suggestions were also derived from the first reports on the 8th October 2005 earthquake, which mention large scale landslides along a zone that must correspond to the activated fault and accept that the propagation of the fault rupture have stopped before reaching the earth surface, (e.g. EERI reports, http://www.eeri.org/lfe/clearinghouse/kashmir/observ1.php), as in previous earthquakes.

In this paper, besides the tectonic setting of October 8th 2005 earthquake, we present field data indicative of the surface expression of the activated fault. We believe that these data will provide important information for the behaviour of thrust faults on the earth surface, not only for the Himalayan mountain belt but for similar tectonic settings around the world.

2. Tectonic Setting

2.1. The Himalayas

The Kashmir region represents a section of the Himalayan orogenic chain. This orogen extends from central Afghanistan to the west and to southeastern China to the east, with a length approaching 4,000 km and width varying from 500 to 2,000 km (Fig. 1). It comprises a complex tectonic structure formed by multiple thrusting and stacking of continental terrains and island arcs on the southern margin of Eurasia, a procedure that was initiated during the Upper Paleozoic and continues in our days with the increment of the Indian tectonic plate (Hodges 2000).

This orogenic chain comprises of six tectonic zones that can be observed along its length (Fig. 1a). From north to south these zones are the following (Butter *et al.* 1989, Hodges 2000, Najman *et al.* 2000, 2001. 2002, 2004) (Figs 1, 2): The Trans-Himalayan with batholiths that it is suggested that they represent an Andean type north Tethyan margin. 2) The Indus Suture Zone that comprises of marine sediments, ophiolites, volcanic rocks and mélange. It represents the collision trace between the Indian and the Eurasian plates. 3) The North Himalaya or Tethyan Himalaya or Tibetan Himalaya, comprising of sedimentary and post- sedimentary rocks, of Upper Precambrian – Lower Paleozoic age and of Permian – Cretaceous thick marginal sequences. 4) The crystalline rocks of the Greater Himalaya that comprise of Upper Proterozoic – Lower Cambrian sedimentary, granite and volcanic rocks, metamorphosed during the Tertiary. 5). The Lower Himalaya that represents the lower tectonic nappe and comprises of post-sedimentary, sedimentary and volcanic rocks of Middle Proterozoic and granite rocks of Cambrian – Ordovician age. 6) The Thrust and Fold Belt also referred to as Sub-Himalaya. It represents the Neogene and Quaternary forearc basin section between the Lower Himalaya and the active thrust front of the orogen, the Main Frontal Thrust – MFT, (Fig. 2). This belt is the result of the subduction of the Indian cratonic block under its Phanerozoic sedimentary cover (Najman *et al.* 2001, 2002).

The aforementioned zones are bounded by great Cenozoic normal or thrust faults with a general dip direction towards the north (Figs 1b, 2): (i) the Main Frontal Thrust – MFT or Himalayan Frontal Thrust – HFT, (ii) the Main Boundary Thrust – MBT, (iii) the Main Central Thrust – MCT and (iv) the South Tibetan Detachment System – STDS, (Najman *et al.* 2004 and references therein). All the thrust structures can be observed throughout the mountain chain and it is believed that are linked to a large scale detachment the Main Himalayan Thrust – MHT.

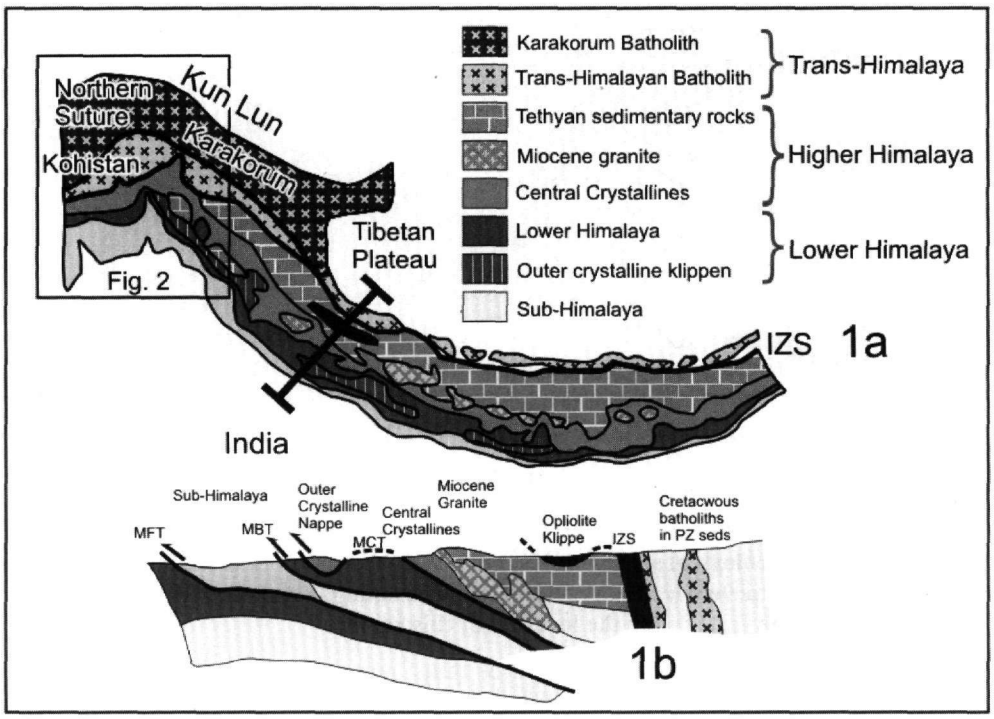

Figure 1 – Geotectonic map of Himalaya orogenic belt (1a) and representative geological section of the belt (1b)

It is estimated that since the Upper Cretaceous approximately 2000–3000 km of convergence has been leveled along this margin (Molnar and Tapponier 1977). GPS measurements indicate that the convergence between India and Eurasia continues in our days with a rate that approaches 40–50

mm/year (DeMets *et al.* 1994, Banerjee and Bürgmann 2002). The 10–20 mm/year are attributed to the sliding on the HFT (Wesnousky *et al.* 1999). Seeber and Ambruster (1981) observed that most of the earthquake epicenters and disasters related to historical earthquakes were concentrated in a region that is bounded to the north by the MCT and to the south by the HFT and suggested that these large earthquakes have caused the activation of the Main Himalayan Thrust south of the Greater Himalaya up to the HFT.

2.2. The Hazara – Kashmir Syntaxis

The earthquake epicenter of the October 8th 2005 was located in Pakistan Himalayas and specifically within the Hazara – Kashmir Syntaxis (Figs 2, 3). The latter represents a tectonic structure that was formed during the progressive penetration of the northwestern end of Indian plate in Asia which caused right lateral rotation of the thrust direction by 75° relative to the India cratonic block, (Critelli and Garzanti 1994, Najman *et al.* 2001, 2002).

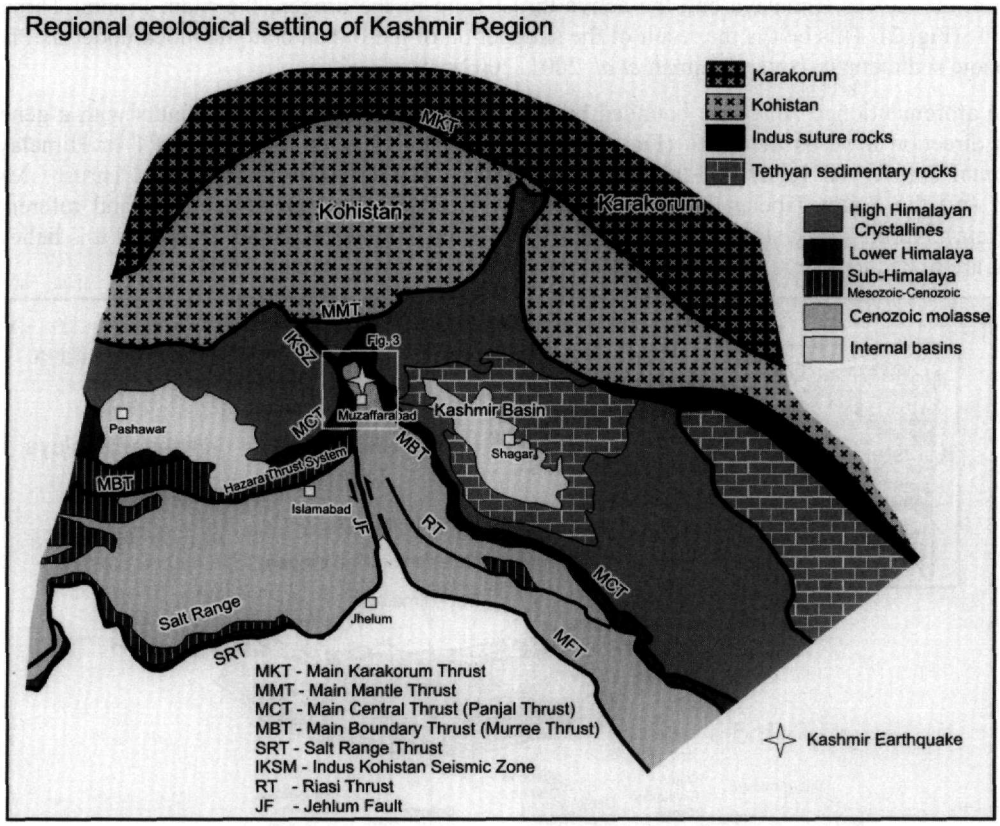

Figure 2 – Regional geological setting of Kasmir, western section of the Himalaya orogenic belt (modified from http://www.albany.edu/geosciences/nangap/paksuc97.html). See figure 1 for the location of this region

The formations located on the footwall of Murree thrust represent a part of the Thrust and Fold belt of the Indian foreland (Baker *et al.* 1988, Jaune and Lillie 1988, Bossart *et al.* 1990). The stratigraphy of the belt is the following from older to younger: (i) The Precambrian basement of metamorphosed and volcanic rocks of the Indian shield, (ii) the Cambrian Salt Range formation of evaporates and sediments with a dominant hyalite phase, that compose the detachment zone of the Fold and Thrust Belt, (iii) Cambrian to Eocene platform sediments with large unconformities at the base of Permian and Paleocene and finally (iv) Miocene - Pleistocene molassic sediments laying unconformably over the platform sediments that can be distinguished in two groups, the

Rawalpindi Group and the Siwalik Group. The Murree formation is considered as part the Rawalpindi Group.

The footwall of the Murree thrust which corresponds to the MBT of India is characterized by the Muzaffarabad anticline (Fig. 3). In the core of the anticline between Balakot and Muzaffarabad, the Abbottabad formation outcrops which comprises of carbonate rocks with chert intercalations and of Upper Precambrian – Cambrian stromatolithic limestones (Bossart *et al.* 1988). This formation is underlying unconformably the 400 m thick Paleocene, shallow water, Lockhart limestones. The latter is grading to the Patala formation which consists of clastic sediments with marly limestone intercalations of Paleocene – Lower Eocene age. These beds are grading to the Murree formation of red clayish beds, with biolclastic limestones and benthic fossils of Lower Eocene age at its base. Latest data from the Balakot formation, the stratigraphic base of Murree formation, indicate that these beds are younger than 37 Ma and that the aforementioned contacts are of tectonic origin and more specifically are thrust faults with a sense of shear "the top to the southwest" (Najman *et al.* 2002). The thrust that emplaces the carbonate rocks over the molassic sediments is known as the Muzaffarabad Fault or Balakot – Bagh Fault (Avouac *et al.* 2006 and reference therein).

3. The October 8th 2005 Earthquake

3.1. Seismological Analysis

The earthquake epicenter of the 8th of October event is located in Pakistan Kashmir, 10 km northeast of Muzaffarabad, the capital of Pakistan Kashmir, and approximately 105 km north of the capital of Pakistan, Islamabad. The earthquake magnitude was recorded as 7.6 R and was located in geographical latitude of 34,493 and longitude of 73,629 (Figs 2, 3). The focal depth of the earthquake was only 26 km, the activated thrust fault had a NW-SE strike (N333°), with 29° dip towards the NE and with a rake of 140° (USGS 2005). The Harvard CMT solution indicates a fault with a N133°E strike, 40° dip towards the NE and a rake of 123° (http://www.seismology.harvard.edu/CMTsearch). The fault displacement was originally estimated that was ranging from 1-6 m, while the displacement dimensions were estimated as 90-100 km X 35-50 km (Chen 2005). Avouac *et al.* (2006) used sub-pixel correlation of ASTER images to calculate the ground deformation and seismic waveforms modeling to suggest that the ground rupturing was continuous for a distance of 75 km with mean offset of 4 m and maximum offset of 7 m to the northwest of Muzaffarabad. The corresponding seismic moment was estimated as 2.94 x 1020 N m.

The main seismic event was followed by a large number of aftershocks. Over a 100 aftershocks had a magnitude that exceeded 5.0 during the first 20 days after the main shock. During the first day, 147 aftershocks were recorded while during the first 15 days over 12 aftershocks had a magnitude that exceeded 5.5 and three had a magnitude that exceeded 6.0. The strongest aftershock had a 6.3 magnitude and was recorded three days after the main shock. Furthermore, 978 aftershocks had a magnitude over 4.0 (USGS 2005). An interesting element of the aftershock sequence is that its concentration is located approximately 50 km northwest of the main shock epicenter.

3.2. Field Observations

A series of structures that are directly related to the activated fault were recorded throughout a distance of 70 km, between the towns of Balakot and Bagh (Fig. 3). This region is characterized by steep slopes with many small and a few large valleys and many alluvial fans and river terraces, overlying by an unconformity the Murree formation and the foreland carbonate rocks. The observed structures are distributed within a zone of width of several tenths of meters along the west – southwestern limb of the Muzaffarabad anticline. The structures include flexural slip folding observed in alluvial fans and river terraces, where sufficient deposits unconformably cover

the alpine basement, tension cracks most of which are located on the crests of the flexural-slip folding structures, landslides and normal faults. The latter were distributed in a zone, a few tenths of meters wide, where the southwest limb of the Muzaffarabad anticline joins the MBT (Fig. 3).

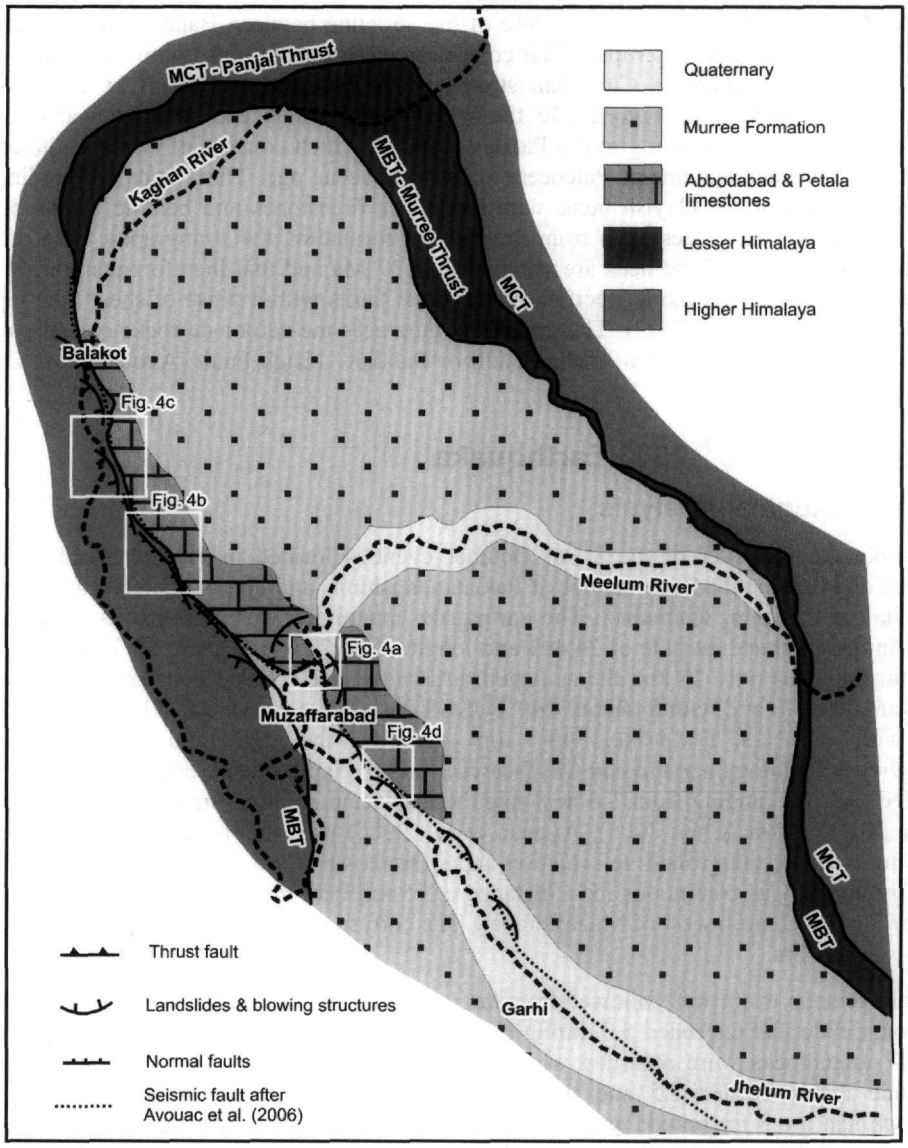

Figure 3 – Geological map of the Hazara – Kasmir Syntaxis modified from Bossart and Ottiger (1990), where we have add our field observations. Notice that between Balakot and Muzaffarabad the seismic fault is identified with the MBT

Between the towns of Balakot and Bagh and along the western and southwestern slopes of the mountains, many new alluvial fans were recorded, formed by depris flow during the main earthquake. Many of these fans were still evolving for days after the main event. The mature fans on the contrary, present deformational characteristics of folding to a buckling extent. The alluvial fans body exhibits extensional faults many of which have listric geometry (Figs 3, 4c). The majority follows the slope geometry and has displacements up to 2 m, while the rest of them develop laterally or at an angle to the aforementioned (Fig. 4c).

Moreover, extensional faults of high dip angles towards the SW were also recorded in this region having a strike similar to that of the activated fault and offset ranging between 0.5 – 4.5 m (Figs 4d, e). Most of these faults develop along the contact between the carbonate rocks and the red pelites of the Murree formation. These faults could be interpreted as slumps but could also represent a surface expression of the seismic fault. Since the geological formations are folded, local stresses develop on their convex surfaces and these formations are lengthened. On the other hand, their concave surfaces are shortened. This has as a result the formation of normal faults on the convex surfaces and reverse faults on the concave surfaces. In the case of Muzaffarabad anticline, the southwestern limb present high dip angles towards the SW and the rupture of the activated fault could have propagated towards the contact between the two aforementioned geological formations resulting in an overturned structure. This led to the surface expression of the reverse fault as a normal fault and not as a thrust fault. It is interesting that this expression is running along the southwestern segment of the MBT of the Hazara – Kashmir Syntaxis which has high-angle dips to the SW (Fig. 3).

To the northern limits of Muzaffarabad town, the homonymous fault caused serious damages on the road network, which is parallel to the Jhalum River. More specifically, the road followed the deformation of the geological basement and was uplifted approximately 2.0 m (Fig. 4b). The uplift can be observed in a 30-35 m wide zone. For the first 20 m the deformation takes place without surface rupturing while for the rest 15 m, tension cracks with N100°E strike was recorded. These cracks are open with a width of 15-40 cm, vertical to the road, are parallel to one another and have a vertical throw of 20-40 cm. They formed on the crest of the flexural-folding of the road asphalt and its geological basement and reach 1m in depth. On the western slope of the road fractured Cambrian limestones were observed with recent fractures having NW to WNW strike and a 50-65° dip towards the NE, that do not always accompanied by slip. In front of this exposure, an unfinished building of concrete pillars was noted. The base of the construction in its southern part was detached from the rest of the building, with a southward sense of motion, suggesting a simultaneous extension in an NE-SW direction and uplift. This section of the building was located on the trace of the extensional cracks of the road towards the west.

Similar structures to those observed on the road, were recorded further to the east on terraces of the Jhelum River, which are significantly more impressive (Fig. 4a). In this area two river terraces can be distinguished, separated by a 12- 15 m high morphological discontinuity. The lower one develops nearly 1-4 m over the present river level while the second one develops 20 m higher from the river level. The morphological discontinuity that separates those two terraces is located on the eastern projection of the extensional cracks described in the previous paragraph and therefore we believe that this discontinuity can be a fault scarp attributed to the Muzaffarabad fault. Along the fault trace, the terrace is interrupted by a 12-15 m high morphological escarpment. The resulting structures exhibit clear characteristics of flexural slip folding. The clasts that compose the terrace have undergone rotation and sliding, while the existing vegetation in this area has followed the folding pattern of the geological basement. The crest sections of the structure are dominated by open tension cracks responsible for the total collapse of the constructions founded on the terrace to a southward direction. The length of these cracks is ranging from 3-30 m, while the width is measured to 5 -30 cm and the depth exceeds one meter. The fact that the height of the morphological discontinuity of the terrace is nearly three times the throw observed on the road and of the calculated throw generated by the earthquake indicates that the fault must have been reactivated during the recent past, since the terrace has a Holocene age. This indication is also supported by the existence of two smaller morphological breaks, in front of the fault front with a height of approximately 1.5 m suggesting past reactivations.

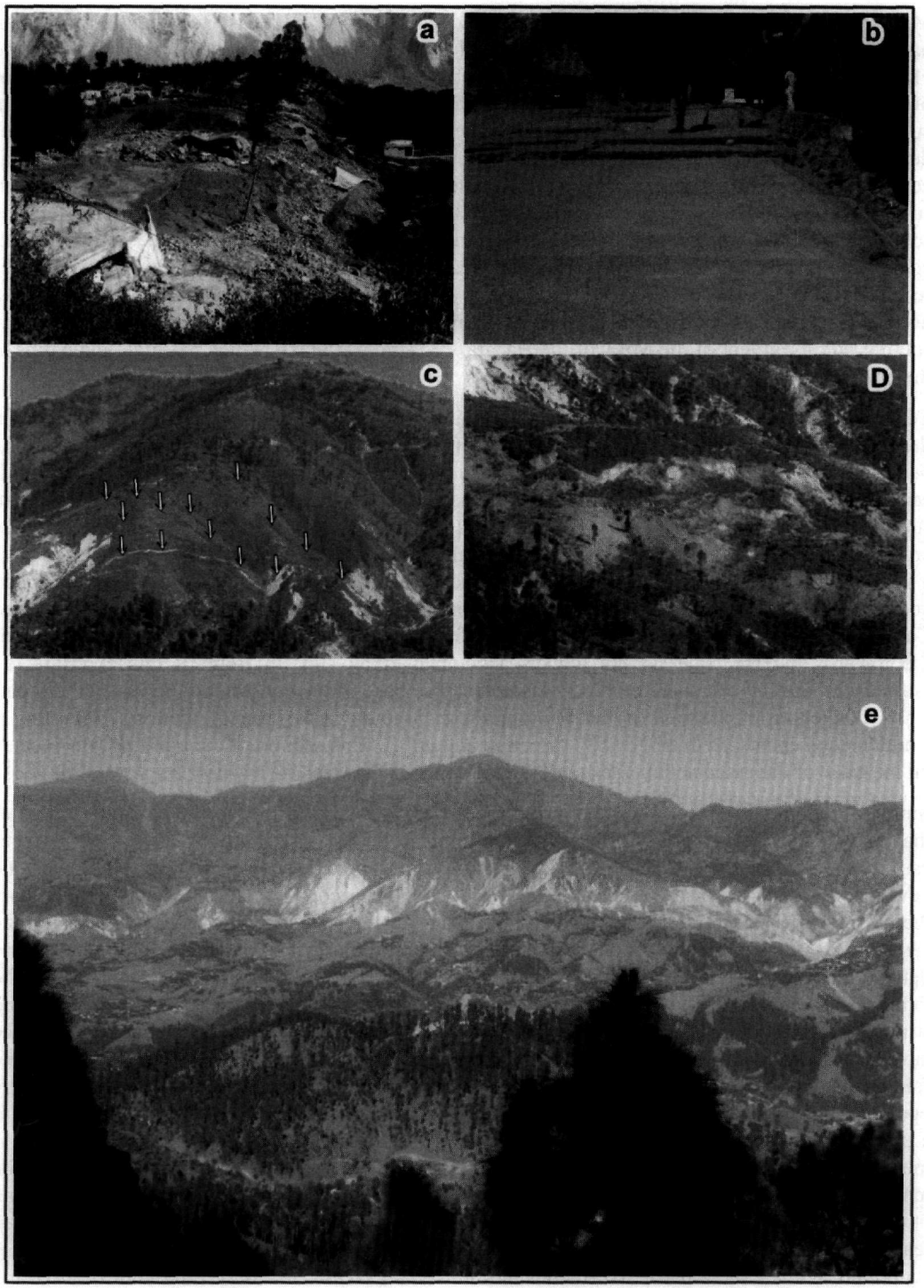

Figure 4 –Flexural folding accompanied with tension cracks on the river terrace (a) and on a road (b) north of Muzaffarabad. Normal faults formed along the trace of the Muzaffarabad fault because of the blowing of the alluvial fans and the Murree formation (c). The activation of the Muzaffarabad fault causes the formation of a normal fault along the vertical limb of the Muzaffarabad anticline (d, e)

4. Discussion

The continuous convergence between India and Eurasia, besides the uplift of Himalaya, has also resulted in the development of great earthquakes along the orogeneic front. Based on previous and historical earthquakes it was suggested that some sections of the Main Himalayan Thrust have not generated large earthquakes till now (Khattri 1987). Such sections are referred to as seismicity gaps. At the western end of the mountain front, the Kashmir area located west of the 1905 earthquake epicenter in Kangra area is considered as a seismicity gap, (Seeber and Ambruster 1981, Khatri 1987, Gahalout 2005).

Based on the aforementioned data it is suggested that the seismically active region of the Himalaya is a 100 km wide zone along the mountain front, bounded by MCT to the north and HFT to the south. To the west, that is in Kashmir area, this zone becomes significantly narrower since both MCT and MBT thrusts are verging close to one another. Additionally, Seeber and Gornitz (1983) studied the stream gradient of the main rivers in the region and concluded that the values were relatively high and could be attributed to the short distance between those active structures.

Since the epicenter of the main shock of October 8th 2005 was located near MBT and important controversies existed regarding its location (e.g. USGS 2005 and Harvard), the first reports on the seismic fault were suggesting that MBT was responsible for the earthquake (e.g. Galahaut 2005). However, the epicenter is located on the Syntaxis core and the focal solution of the earthquake, as given by USGS and Harvard, correspond to a NW direction reverse fault, that dips towards the NE and presents right lateral slip suggesting that the earthquake cannot be attributed to the main fault systems of the region, that is MBT and MCT, since the epicenter area belongs to the Sub – Himalaya, that constitutes the footwall of the MBT.

Furthermore, the aftershock epicenters are located to the northwest of the Syntaxis and to the northeast of a seismic zone indicated by Armbruster *et al.* (1978) during a microseismic research known as the Indus – Kohistan Seismic Zone (Fig. 2). The Indus – Kohistan Seismic Zone has a width of 20 – 40 km and a length of 100 km extending from the Kagar River to the#southeast, to the Swat River to the northwest. This zone runs through Indus River, forming a kink towards the east and a deep gorge within mountains that approach 3,000 m in altitude. These mountains are part of a linear topographic front that forms the Pir Panjal mountain chain extending from Kashmir to Swat River. The topographic front coincides to the uplifted block of MBT along Kasmir and to the Indus – Kohistan Seismic Zone to the northwest of the Syntaxis. This seismic zone along with the high mountains, form a linear projection of the MBT to the northwest of Kashmir which develops around of the Syntaxis and is coupled to the Hazara Thrust Fault System. However, these two structures cannot be correlated since their tectonic evolutions are completely different (Armbruster *et al.* 1978).

Various earthquakes of intermediate depth have been recorded in the Seismic Zone, the most disastrous being that of the 28th of December 1974, with a magnitude 6.0 near Pattan, at its northern end (Gahalaut 2005). The earthquake generation mechanism and other six intermediate magnitude earthquakes since 1976, indicate a reverse motion character on a surface that dips towards the northeast, with a slight right lateral slip, a mechanism relative to that of the 8th of October 2005 seismic event. This seismic zone is characterized by dip angles of the order of 30-50°.

From the distribution of the damages, the greatest percentage of disasters is located along a zone striking NW-SE, from Uri at the borders of India – Pakistan to the eastern end of the Indus – Kohistan Seismic Zone where it correlates to the aftershock epicenters. This is indicative that the ruptures during the main event were distributed along the southwestern limb of the Muzaffarabad anticline, in an area where carbonate rocks of the foreland are outcropping, while the seismic activity migrated to the northwest towards the Indus – Kohistan Seismic Zone. Practically, this means either that the south-eastward extension of the Indus – Kohistan Seismic Zone is not the

MBT but the Muzaffarabad fault or that the main earthquake of the 8th of October 2005 caused the activation of the Indus – Kohistan Seismic Zone. If the first suggestion is true then this zone, from the Syntaxis to the Swat River, appears to constitute a blind thrust under the metamorphosed rocks of the Lower Himalayas while in the Sub-Himalayas ceases to be blind and represents a distinct structure responsible for the formation and the growth of the Muzaffarabad anticline. The second case supposes a strong structural control between those two tectonic structures.

Bendick *et al.* (2007) presented a kinematic model combined the main rupture with a wedge thrust. Based on the data of Seeber and Armbruster (1979), aftershock distributions, and aftershock focal mechanisms infer that the 8 October 2005 earthquake appears to have ruptured the surface between Balakot and Bagh in a reverse fault with strike 331° and dip 29° and mean slip of ~5.1 m, with an additional 1.8 m of slip on the dipping plane of a wedge thrust in the northwest, and centimeters of slip on parts of its weak flat-roof detachment.

We believe that because the geometry and the kinematics of the dipping segment of the Bendick *et al.* (2007) thrust wedge and the Muzaffarabad fault are the same; it confirms the suggestion that the Indus – Kohistan Seismic Zone is the north-westwards extension of the Muzaffarabad fault. The flat segment of the thrust wedge may corresponds either to the detachment of the Murree Formation from their carbonate substratum or to the MBT that is now works as a normal fault because of the deformation and the uplift of its footwall.

We also suggest that the Muzaffarabad thrust fault is linked to the Seeber et al (1981) detachment which seems to extend under and to the north of the Hazara – Kashmir Syntaxis. Seeber *et al.* (1981) proposed the existence of a main thrust, which separates the low-angle and seismically active detachment under the External and Lower Himalaya, from the high-angle and seismically inactive thrust under the Greater Himalaya. Further to the north, under the Himalaya, it extends under the Syntaxis and links to the Indus – Kohistan Seismic Zone.

5. Conclusion

The 8th of October 2005 earthquake in Pakistan Kashmir, was located in the core of the Hazara – Kashmir Syntaxis and was caused by a fault that its hanging wall is represented by the Muzaffarabad anticline. In the core of the anticline, Pre – Cambrian and Paleocene limestones outcrop, while on either side red molassic sediments of the Murree formation are observed. The fault on its deepest projection is linked to a primary thrust comprising a large detachment surface where the sedimentary cover of the Indian foreland is sliding over its metamorphic basement. This blind fault aligns with the Indus – Kohistan Seismic Zone to the northwest which also exhibits similar characteristics.

The surface expression of the fault is not that of a thrust fault. In most locations along its trace, landslides of alluvial debris were recorded. Debris flows, buckling and fractural deformation of older alluvial fans, flexural slip structures in river terraces and frequently normal faults along the contact of Abbotabad and Murree formations were observed. The latter could be the expression of the thrust fault responsible for the 8th of October 2005 earthquake, which near the surface became overturned following the geometric characteristics of the contact between the carbonate rocks and the molassic sediments or the geometry of the MBT.

The earthquake was the result of the progressive movement of the continental plate of India towards the north and its collision with the Eurasian plate. This collision, besides the uplift of Himalaya has as a result catastrophic earthquakes, developed mainly along the mountain chain front that extends for over 2,500 km. This earthquake is suggested to have filled a section of the seismic gaps that have been recorded on this front (Gahalaut 2005). According to recent studies (Billham *et al.* 2001, Billham and Ambraseys 2004), in the following years similar or greater magnitude earthquakes should be expected in this region. This suggestion in combination to the population increase observed in neighbouring to the Himalaya countries and the insufficient

seismic hazard education, increase significantly the earthquake vulnerability of the Himalayan region.

6. Acknowledgments

The authors wish to express thanks to the reviewers for their constructive comments and suggestions. This mission was supported by E.L.K.E. of the National and Kapodistrian University of Athens.

7. References

Armbruster, J., Seeber, L., and Jacob, K.H., 1978. The Northwestern termination of the Himalayan Mountain Front: Active tectonics from microearthquakes, *Journal of Geophysical Research*, 83, B1, 269-282.

Avouac, J.-P., Ayoub, F., Leprince, S., Konca, O., and van Helmberger, D., 2006. The 2005, Mw 7.6 Kashmir earthquake: Sub-pixel correlation of ASTER images and seismic waveforms analysis, *Earth and Planetary Science Letters*, 249, 514-528.

Baker, D.M., Lillie, R.J., Yeats, R.S., Johnson, G.D., Yousouf, M., and Zamin, A., 1988. Development of the Himalayan frontal thrust zone: Salt Range, Pakistan, *Geology*, 16, 3-7.

Banerjee, P., and Bürgmann, R., 2002. Convergence across the northwest Himalaya from GPS measurements, *Geophysical Research Letters*, 29, no. 13, doi: 10.1029/2002GL015184.

Bendick, R., Bilham, R., Asif Khan, M., and Faisal Khan, S., 2007. Slip on an active wedge thrust from geodetic observations of the 8 October 2005 Kashmir earthquake, *Geology*, 35, 267-270, doi: 10.1130/G23158A.1

Bilham, R., 2004. Earthquakes in India and the Himalaya: tectonics, geodesy and history, *Annals of Geophysics*, 47(2), 839-858.

Billham, R., and Ambraseys, N., 2004. Apparent Himalayan slip deficit from the summation seismic moments for Himalayan earthquakes, 1500-2000, *Current Science*.

Bilham, R., Gaur, V.K., and Molnar, P., 2001. Himalayan Seismic Hazard, *Science*, 293, 1442-1444.

Bossart, P., Ottiger, R., and Heller, F., 1990. Rock magnetic properties and structural development in the core of the Hazara-Kashmir Syntaxis, NE Pakistan, *Tectonics*, 9(1), 103-121.

Butler, R.W.H., Prior, D.J., and Knipe, R.J., 1989. Neotectonics of the Nanga Parbat Syntaxis, Pakistan and crustal stacking in the northwest Himalayas, *Earth and Planetary Science Letters*, 94, 329-343.

Chen, J., 2005. Finite-fault slip model. Preliminary result for the 05/10/08 Pakistan earthquake, http://earthquake.usgs.gov.

Critelli, S., and Garzanti, E., 1994. Provenance of the Lower Tertiary Murree redbeds (Hazara-Kashmir Syntaxis, Pakistan) and initial rising of the Himalayas, *Sedimentary Geology*, 89, 265-284.

DeMets, C., Gordon, R.G., Argus, D.F., and Stein, S., 1994. Effect of recent revisions to the geomagnetic reversal time scale on estimates of current plate motions, *Geophys. Res. Lett.*, 21, 2191-2194.

Gahalaut, V., 2005. Did 2005 Kashmir earthquake occur in Kashmir Himalaya seismic gap? http://freewebs.com/vkgahalaut/pakistankashmirearthquake.htm.

Hodges, K.V., 2000. Tectonics of the Himalaya and southern Tibet from two perspectives, *Geological Society of America Bulletin*, 112, no. 3, 324-350.

Jaumé, S.C., and Lillie, R., 1988. Mechanics of the Salt-Range-Potwar Plateau, Pakistan: A fold-and-thrust belt underlain by evaporates, *Tectonics*, 7(1), 57-71.

Khatri, K.N., 1987. Great earthquakes, seismicity gaps and potential for earthquakes disaster along the Himalaya plate boundary, *Tectonophysics*, 138, 79-92.

Kumar, S., Wesnousky, S., Rockwell, T., Briggs, R., Thakur, V., and Jayangondaperumal, R., 2006. Paleoseismic evidence of great surface rupture earthquakes along the Indian Himalaya, *Journal of Geophysical Research*, 111, B03304, doi:10.1029/2004JB003309.

Molnar, P., and Tapponier, P., 1977. The collision between India and Eurasia, *Scientific American*, 236, 30-41.

Najman, Y., Bickle, M., and Chapman, H., 2000. Early Himalayan exhumation: Isotopic constraints from the Indian foreland basin, *Terra Nova*, 12, 28-34.

Najman, Y., Johnson, K., White, N., and Oliver, G., 2004. Evolution of the Himalayan foreland basin, NW India, *Basin Research*, 16, 1-24.

Najman, Y., Pringle, M., Godin, L., and Oliver, G., 2001. Dating of the oldest continental sediments from the Himalayan foreland basin, *Nature*, 410, 194-196.

Najman, Y., Pringle, M., Godin, L., and Oliver, G., 2002. A reinterpretation of the Balakot formation: Implications for the tectonics of the NW Himalaya, Pakistan, *Tectonics*, 21, no. 5, doi: 10.1029/2001TC001337.

Seeber, L., Armbruster, J.G., and Quittmeyer, R.C., 1981. Seismicity and continental subduction in the Himalayan arc. In *Zagros, Hindukush, Himalaya, Geodynamic evolution*, Geodynamic Series, Maurice Ewing Series 3, American Geophysical Union, Washington D.C., 215-242.

Seeber, L., and Armbruster, J.G., 1981, Great detachment earthquakes along the Himalayan Arc and long-term forecasting. In D.W. Simpson and P.G. Richards (Eds), *Earthquake prediction; an international review*, Maurice Ewing Series, American Geophysical Union, Washington, DC, United States, 259-277.

Seeber, L., and Gornitz, V., 1983, River profiles along the Himalayan arc as indicators of avtive tectonics, *Tectonophysics*, 92, 335-367.

Wesnousky, S.G., Kumar, S., Mohindra, R., and Thakur, V.C., Uplift and convergence along the Himalayan Frontal Thrust of India. *Tectonics*, 18, no. 6, 967-976.

U.S. Geological Survey, National Earthquake Information Center, 2005. Magnitude 7.6 – Pakistan, 2005 October 8 03:50:40 UTC, Preliminary Earthquake Report. http://earthquake.usgs.gov.

Yeats, R.S., and Hussain, A., 1987. Timing of structural events in the Himalayan foothills of northwestern Pakistan, *Geological Society of America Bulletin*, 99, 161-176.

Δελτίο της Ελληνικής Γεωλογικής Εταιρίας τομ. XXXX, 2007
Πρακτικά 11ου Διεθνούς Συνεδρίου, Αθήνα, Μάιος 2007

Bulletin of the Geological Society of Greece vol. XXXX, 2007
Proceedings of the 11th International Congress, Athens, May, 2007

TECTONO-SEDIMENTARY EVOLUTION AND RATES OF TECTONIC UPLIFT OF THE SFAKIA COASTAL ZONE, SOUTHWESTERN CRETE

Skourtsos E.[1], Pope R.[2], and Triantaphyllou M. V.[1]

[1] *National and Kapodistrian University of Athens, Faculty of Geology and Geoenvironment, Panepistimioupolis Zografou, 154 21, eskourt@geol.uoa.gr, mtriant@geol.uoa.gr*

[2] *Geographical Sciences, University of Derby, Derby, DE22 1GB, UK, R.J.Pope@derby.ac.uk*

Abstract

Sfakia lies within a narrow coastal zone at the southwestern foothills of the Lefka Ori Mt. Here a segment of the South Cretan margin is preserved onshore, a structure that represents a neotectonic structure with continuous activity since the Upper Miocene. This segment is characterized by a steep, E-W striking and south facing morphological escarpment that constitutes numerous E-W and ESE-WNW striking normal faults. Since the Late Miocene, marine sequences of Tortonian, Early Pliocene and Lower Pleistocene age were deposited along the coastal zone. Since the Middle Pleistocene multiple, coalescent alluvial fans covered both the alpine basement and the marine sediments. Fault-kinematic- and stratigraphic data combined with recently published palaeobathymetry reconstructions allow us to make relable estimates of both the uplift rates of fault blocks in the study area and the period that the faults that demarcate them were active. The results show that the study area is experiencing uplift already since the Middle Pliocene and that the uplift rates of the mountainous parts are higher than those of the coastal zone. The general uplift of the coastal zone seems to be controlled by offshore normal faults, south of Sfakia.
Key words: *active crustal deformation, normal fault, extension, Pleistocene, Lefka Ori, Sfakia.*

Περίληψη

Η περιοχή των Σφακίων είναι μία στενή παράκτια ζώνη στο νοτιοδυτικό τμήμα των Λευκών Ορέων, στο οποίο διασώζεται τμήμα του Νότιου Κρητικού περιθωρίου. Πρόκειται για μία μακρόχρονη νεοτεκτονική δομή που άρχισε τη δράση της στο Ανώτερο Μειόκαινο και συνεχίζεται μέχρι σήμερα. Χαρακτηρίζεται από μία απότομη μορφολογική ασυνέχεια διεύθυνσης Α-Δ, που σχηματίστηκε από ρήγματα διεύθυνσης Α-Δ και ΑΝΑ-ΔΒΔ προκαλώντας εφελκυσμό Β-Ν. Από το Ανώτερο Μειόκαινο μέχρι το Κατώτερο Πλειστόκαινο αποτέθηκαν θαλάσσια, ενώ ακολούθως η ιζηματογένεση συνεχίστηκε με την απόθεση μεγάλου πάχους αλλουβιακών ριπιδιών, διαδικασία που συνεχίζεται μέχρι σήμερα. Η καλύτερη στοιχειοθέτηση της ηλικίας των θαλάσσιων ιζημάτων σε συνδυασμό με πρόσφατα δημοσιεύματα σχετικά με το βάθος απόθεσης τους και με τη χαρτογράφηση των ρηγμάτων της περιοχής, έδωσε τη δυνατότητα να προβούμε σε σημαντικές διαπιστώσεις σχετικά με τους μακροχρόνιους ρυθμούς ανύψωσης των ρηξιτεμαχών της περιοχής, όπως και για το χρονικό διάστημα που τα ρήγματα που ορί-

ζουν αυτά τα ρηξιτεμάχη ήταν ενεργά. Από το Μέσο Πλειόκαινο όλη η περιοχή υπόκειται σε ανύψωση με τις εσωτερικές περιοχές να έχουν ρυθμούς έως και διπλάσιους από εκείνους της παράκτιας ζώνης. Η γενική ανύψωση φαίνεται να ελέγχεται από ρήγματα υποθαλάσσια νότια της περιοχής μελέτης.
Λέξεις κλειδιά: *ενεργή παραμόρφωση, κανονικό ρήγμα, εφελκυσμός, Πλειστόκαινο, Λευκά Όρη, Σφακιά.*

1. Introduction

Active extensional tectonics in the Aegean is accommodated by normal faulting and regional uplift producing new topography at rates higher that those of erosion and deposition (Leeder and Jackson 1993). The lateral extent of the normal faults and their associated tilted fault blocks perform a major control on the distribution of sedimentary facies in these extensional basins. This control is more obvious where the normal faults occur near sea level, which provides a reference point for the vertical motions of footwalls and hanging walls (e.g. Goldworthy and Jackson 2000, D'Agostino *et al.* 2001). The island of Crete is one of the best examples to examine the upper crustal deformation of the outer Aegean domain as the geological data show evidence of a multistage tectonic evolution of the island, since the Upper Oligocene (e.g. Fassoulas *et al.* 1994, ten Veen and Postma, 1999a, 1999b; Fassoulas, 1999, 2001, Peterek and Schwarze 2004, van Hinsbergen *et al.* 2006).

Crete occupies a fore-arc position above the north-vergent subduction zone of the Hellenic Arc along which the Africa plate is consumed under the southern edge of the Eurasian plate. Between the Upper Oligocene and Lower Miocene, the collision of the Apulian micro-continent culminated in the stacking of a thick (>10 km) pile of nappes (Bonneau 1984). The lowermost units were buried at a depth of about 20-30 km and were overptinted by HP-LT metamorphism (Siedel *et al.* 1982, Jolivet *et al.* 1994, 1996, Kilias *et al.* 1996, Fassulas *et al.* 1994). In response to roll-back of the subduction zone (Thomson *et al.* 1999) and the continuous underplating (Jolivet *et al.* 1996), the high pressure rocks were uplifted and, within a very short time span, exhumed along low-angle normal or detachments faults during N-S extension. The rapid uplift of the lower metamorphic nappes is constraint by geochronological data (Thomson *et al.* 1998, 1999) and sedimentary rocks of Middle Miocene age, which unconformably overly the high pressure rocks (Meulenkamp 1979).

After the Middle Miocene, Crete was transformed into a mosaic of asymmetrical horsts and grabens due to both temporally and spatially different modes of vertical movements (Meulenkamp *et al.* 1988). The Neogene to Quaternary sedimentary record provides clear evidence of repeated, dramatic changes in the paleogeographic configuration. In most cases these changes coincided with major tectonic events, although different ideas exist about the evolution of the stress field during that period. The complex interplay of tectonics and sedimentation resulted in a large variety of sediment types and in rapid lithological changes in both a lateral and vertical sense (Meulenkamp 1979, ten Veen and Postma 1999a, 1999b, Fassoulas 1999, 2001, Peterek and Schwarze 2004).

Most of the research concerned with the Neogene and Quaternary structural evolution of Crete focused on the extensional basins of central and eastern parts of the island (e.g. ten Veen and Postma 1999a, 1999b, Fassoulas 1999, 2001). However, research focusing on the Quaternary evolution of those areas is limited to the Messara and Ierapetra basins (e.g. ten Veen and Postma 1999a ten Veen and Kleinspehn 2003, Peterek and Schwarze 2004), due to the absence of complete sedimentary records in other areas. Our study focuses on the Sfakia region south of the Lefka Ori massif, where a segment of the South Cretan margin is preserved in a narrow coastal plain. Unexpectedly, the Midle Miocene to Holocene evolution of this segment has been characterized by multiple phases of normal faulting and episodic sedimentation. On the basis of tentative ages derived from synrift sediments, detailed mapping of the normal faults and on

recently published chronometric data we describe the tectono-sedimentary evolution for the Sfakia segment of the South Cretan margin and present new long-term rates of tectonic uplift for the area.

2. Geological Setting

Western Crete is mainly formed by the Lefka Ori (White Mountains), which reach a maximum height of 2452 metres. The Lefka Ori consists predominantly of carbonate rocks with intense karstic erosion, which is mainly fault-controlled. The highlands of Omalos and Askifou are characteristic karst forms that are covered by Quaternary continental deposits. The southern flanks of the Lefka Ori are drained by numerous streams that run through deep north-south trending canyons at Samaria, Tripiti, Klados and Imbros that extend southwards towards the sea.

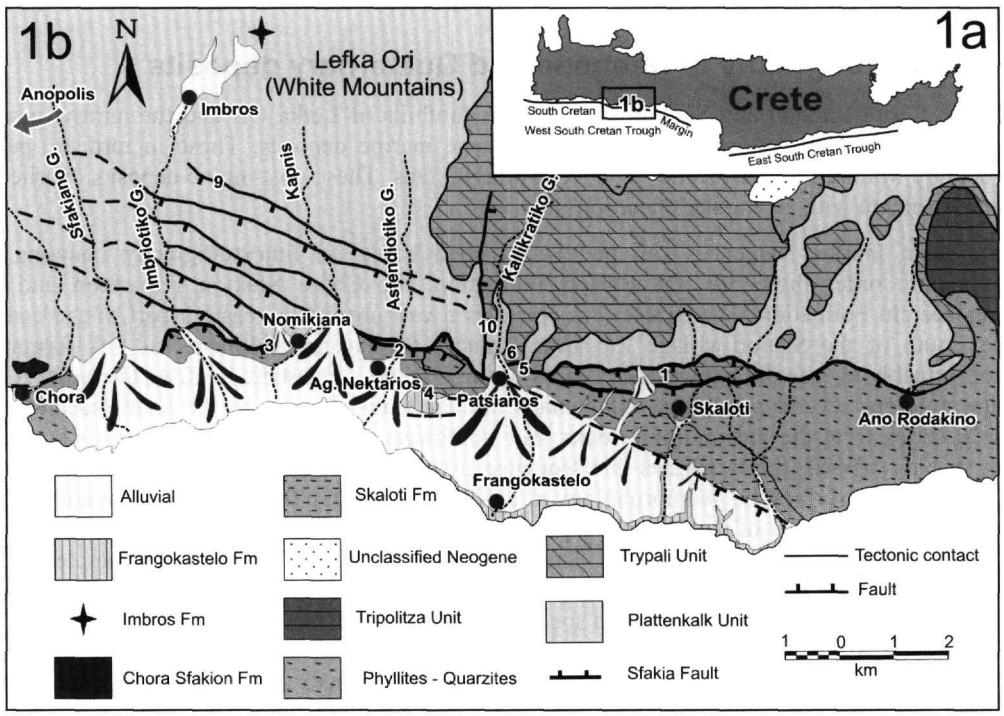

Figure 1 – a) Geological map of the study area modified from I.G.M.E. (1982, 1987). b) The Sfakia coastal zone represents an onshore segment of the South Cretan margin (modified from Alves *et al.* 2007)

Within the Lefka Ori the lowermost Plattenkalk unit is underlain by the lithologically equivalent Trypali unit. Until recently, the Trypali unit was described as a massive complex of dolomitic and calcite marbles with partially tectonic breccia formations, aged Upper Triassic (Pomoni and Karakitsios 2002). Furthermore, Krahl and Kauffman (2004) revealed that the Trypali unit is a sequence of carbonate breccia, cherty marbles, meta-siliclastic sediments and massive marbles of Upper Triassic to Upper Cretaceous in age. This sequence is tectonically overlain by nummulite-bearing plated marbles of the Plattenkalk unit (Alexopoulos *et al.* 2000). Along the western flanks of the Lefka Ori, the Plattenkalk unit is overlain by mica scist, quartzite and some marble intercalations that define the Phyllites – Quartzites unit. At the southeastern foothills of the Lefka Ori, the Tripolitza and the Pindos unit are overlain the previous unit (Karakitsios 1979).

Deformation of the Plattenkalk and Trypali units was attributed to subduction related processes (Fassoulas *et al.* 2004). Variations in the magnitude and style of deformation were lithology-driven. Large, open to tight folds deform the entire stratigraphic section. In places these folds appear to be overturned, locally inverting the stratigraphy and forming large synclines and

anticlines, with fold axes trending east-west and axial planes dipping gently northward. The age of folding is constrained to the Late Oligocene – Early Miocene, as the detachment faulting separating the lower units from the non-metamorphosed upper nappes, clearly overprinted the fold structures (Fassoulas *et al.* 2004).

Since the Middle Miocene, continued exhumation of the metamorphic rocks of the lower units and the uplift of the Lefka Ori, seems to be accompanied the formation of E-W, NW-SE and NE-SW high-angle normal faulting. These faults also formed a series of asymmetrical Neogene basins within which thick sedimentation occurred. To the east of the study area, fluvio-lacustrine to shallow marine sedimentation occurred in the Plakia Basin (Meulenkamp 1979, Angelier 1979). It is suggested that these deposits are Upper Seravallian – Lower Tortonian in age and belong to the Tefelion Group (Meulenkamp 1979).

3. Lithostratigraphy of Neogene and Quaternary deposits

Between Chora Sfakion and Skaloti, the southern foothills of Lefka Ori and the narrow coastal zone are covered by Neogene to Lower Pleistocene marine deposits. These in turn are partly covered by Middle (?) Pleistocene - Holocene alluvial fans. These post-alpine deposits overlie the alpine basement with an angular unconformity.

Three main marine sequences can be distinguished based on lithostratigraphy mapping. In stratigraphic order these are: the Skaloti Formation, the Chora Sfakion Formation and the Frangokastelo Formation. The Skaloti Fm occupies a vast area at the eastern part of the coastal zone, south of the Skaloti village. In several places the basinal sediments of this formation unconformably overlie the high pressure rocks of the Phyllite – Quartzite Unit. At the western end of the outcrop, several small syn-sedimentary normal faults dipping to the south separate the basinal series from the metamorphic rocks. The southwestern border of the outcrop is a normal fault striking NW-SE that separates this sequence from another marine series, the Frangokastelo Fm. This fault describes the geomorphology of this area, separating the small hills that are built up by the marine sediments of the Skaloti Fm, from the flat area that built up by the Late Quaternary alluvial fans and the Francokastello Fm. The Skaloti Fm. consists of sands, conglomerates, marls and shallow marine limestones building a continuous series of ~170 m thick with bedding that is slightly inclined to the south. Based on a specimen of *Clypeaster* that has not been observed in the Pliocene, van Hinsbergen *et al.* (2006) placed the shallow marine deposits of Skaloti Fm. in the Upper Miocene Tefelion Group of Meulenkamp (1979). Our analysis of calcareous nannofossils strongly supports the fact that deposition occurred within a shallow marine environment during the Tortonian and thus corroborates the previous age estimates.

The Chora Sfakion Fm. is observed immediately northeast of Chora village and comprises a 5 m thick sandy deposit of Lower Pliocene age, which overlies coarse conglomerates of unknown age or marbles of the Plattenkalk Unit. It has been suggested that this small outcrop of deep marine deposits is Lower Pliocene in age (van Hinsbergen 2004) and is equivalent to Finikia group of Meulenkamp (1979).

The Frangokastelo Fm. occupies the central part of the coastal zone. According to Sissingh (1972), this formation comprises two distinct sedimentary sequences. First, immediately east of Frangokastelo, a coastal cliff exposes a 35 m thick marine sequence comprising blue-green clays and limestones. Second, close to the village of Agios Nektarios, a sequence comprises of limestones with pebbles, both rounded and angular, with intercalations of clays and clayed marls (Meulenkamp 1969, Sissingh 1972, Driever 1984). According to Meulenkamp (1969) both formations have features that are very different from other marine formations outcropping to the east of the study area or to the central and northern parts of the island of Crete. Although the stratigraphic position of the formation is uncertain, it has been tentatively placed in the Middle Pliocene by Meulenkamp (1969). The same outcrops were dated Late Pliocene by Hinsbergen *et al.* (2006).

Due to uncertainties regarding the age of the Frangokastelo Fm., we made an attempt to date these marine sequences using calcareous nannofossils. Our results show that both outcrops of the Frangokastelo Fm are much younger than previous age estimates. The sequence close to Agios Nektarios is assigned to the Lower Pleistocene [biostratigraphic zones MNN19c and MNN19d which provide an age range of 1.66-1.25 Ma (Lourens *et al.* 2004)]. In comparison, the sequences close to Frangokastelo is assigned to biostratigraphic zones MNN19d and MNN19e, providing an age range of 1.62-0.97 Ma (Lourens *et al.* 2004)]. Thus, the data strongly suggest a Early Pleistocene age for the Frangokastelo Fm. The deposition of the blue-green marls took place under open marine conditions. The Agios Nektarios sequence has low-angle dips to the east, whereas the bedding of the Frangokastelo show dips to the west.

Marine sediments are not only found in the foothills of the Lefka Ori, but also occur in the main mountain zone at altitudes in excess of 1000 m. These sediments occur as isolated outcrops of lithified limestones and conglomerates with shallow marine faunas, which are separated from the Plattenkalk and Trypali units by normal faults. Van Hinsbergen (2004) proposes that these marine sediments closely resemble those exposed in southwestern Crete and probably correspond to the Serravalian – Tortonian Topolia Fm. of the Prina Group (Meulenkamp 1979). Alexopoulos and Marcopoulou-Diakantoni (1996) described also Lower Pleistocene marine fauna in a residual outcrop a few km northeast of Imbros (Imbros Formation).

The alluvial fan zone occupies essentially the whole of the coastal piedmont between Chora Sfakion and Skaloti, and comprises multiple coalescent fan complexes which together form an extensive bajada (Fig. 1). Those fan systems occupying the western half of the piedmont are classically telescopic in planform, with low gradient distal segments nested within increasingly steeper medial segments. In comparison, the eastern piedmont fans display both limited telescopic segmentation and radial segmentation. Irrespective of the style of segmentation, all fans share two distinctive attributes. First, the fan head zone is permanently entrenched. Second, with the exception of the youngest fan deposits and recent channel fills, an immature soil has formed on the majority of fan surfaces (Nemec and Postma 1993).

The exposed marine sequences located stratigraphically beneath the earlier stages of the fans have been assigned to Biozones MNN19c-e (1.66-0.97 Ma). Consequently, the basal debris flow deposits are likely to have been emplaced no earlier than the later part of the early Pleistocene. Optically Stimulated Luminescence dating of coarse silts and fine sands provide maximum ages of c.143 ka BP for the stage 2A surfaces of the Sfakia fan and c.94 ka and c.70 ka for the basal and middle stage 2C of the Patsianos fan (Pope *et al.* in press). Besides, archaeological data strongly suggests that the stage 3 mudflows exposed within the distal portion of the Patsianos fan were emplaced during the pre-historical period [5.5 to 3.0 ka BP (Sphakia Survey 2002)]. Finally, Venetian artefacts contained within the stratigraphically higher fine-grained hyperconcentrated flows suggest that these deposits were emplaced c.1.0 ka BP (Pope and Wilkinson unpublished data).

3.1. Geometry of Normal Faults

3.1.1. Sfakia Fault

The morphology of the study area is dominated by a morphologically well-expressed fault scarp (termed the Sfakia Fault), which forms a steep south-facing escarpment (Fig. 2). The fault represents the eastern onshore segment of the South Margin Fault that forms the southwestern coastline of Crete (Fig 1). The length of this fault is more than 15 km with its western tip close to Ano Rodakino. Two segments can be recognized: First, a 7 km long western segment between Chora and Agios Nektarios village. Second, a 8 km eastern segment between Patsianos and Ano Rodakino. The segment between Agios Nektarios and Patsianos looks to represent a significantly bend of the Sfakia fault.



Figure 2 – The Sfakia fault expressed as a steep south-facing, morphological discontinuity striking E-W and separating a narrow coastal zone from the eastern foothills of the Lefka Ori massif. View to the east

The main feature of the hanging wall of the western segment is the presence of thick alluvial fans, which cover the metamorphic rocks of the Phyllite-Quartzite Unit. The gravels of the younger alluvial fans have been deposited over the high-pressure rocks of the Phyllites – Quartzite Unit in the hanging wall of the fault and the marbles of the Plattenkalk Unit that form the footwall. These gravels are unfaulted and therefore most probably seal the Sfakia fault. On the contrary, the debris flows of the first stage of the westernmost fan (Sfakia fan) that has been deposited directly above intensely fractured marbles of the Plattenkalk Unit have small internal faults that are parallel to the strike of the Sfakia fault. If such faults were not produced by gravity sliding, it is possible that they reflect fault activity during deposition. Studies of the kinematics of the individual faults that formed within this segment indicate an N-S to NNE-SSW direction of extension (Fig. 3, locations 2-4).

The eastern segment of the Sfakia fault is more linear than the western and its damage zone is noticeably wider, reflecting the presence of intensely faulted carbonate breccias of the Trypali unit along its trace. Two parallel faults define the thickness of the damage zone. The southern one is a low-angle normal fault with an eroded fault scarp juxtaposing the Phyllites – Quartzite Unit and the Trypali Unit. The northern one is a high-angle normal fault that juxtaposes the latter unit and Upper Cretaceous marbles of the Plattenkalk Unit. The difference in the dip angle of these two faults is believed to owe to antithetic block rotation of the southern fault block. The analysis of the slickenside lineations of both faults indicates the predominance of N-S directed extension (Fig. 3, location 1). At the western tip of it (or what) (location 5 in Fig. 1), where two faults strike NW-SE and NNE-SSW, fault kinematic data indicate NE-SW extension (Fig. 3).

3.1.2. Frangokastello Fault

The Frangokastelo fault is observed in the hanging wall of the Sfakia fault, northeast of Frangokastelo. The position of the fault is marked by a morphological discontinuity running NW-SE that separates the Skaloti fm in the northeast from the Frangokastelo Fm in the southwest. Its presence is also reinforced by borehole data from the Eggion Veltioseon Service of the Chania Prefecture. Fault displacement at the Frangokastello Fault led to the creation of the accommodation that was filled by the Frangokastelo Fm. Close to the expected trace of the fault; high-angle normal faults offset the Skaloti Fm beds and tilted pebbles and gravels beds within conglomerate units, reveal its normal character.

The topography of the hanging wall of the fault is flat where thin alluvial deposits unconformably overlie the Early Pleistocene marine deposits of the Frangokastelo Fm. The Patsianos fan formed at the mouth of the Kalliktatiko gorge and shows evidences of marine and aeolian sands interfingering with the alluvial deposits. The maximum ages provided by OSL dating of those sands are c.94 ka and c.70 ka.

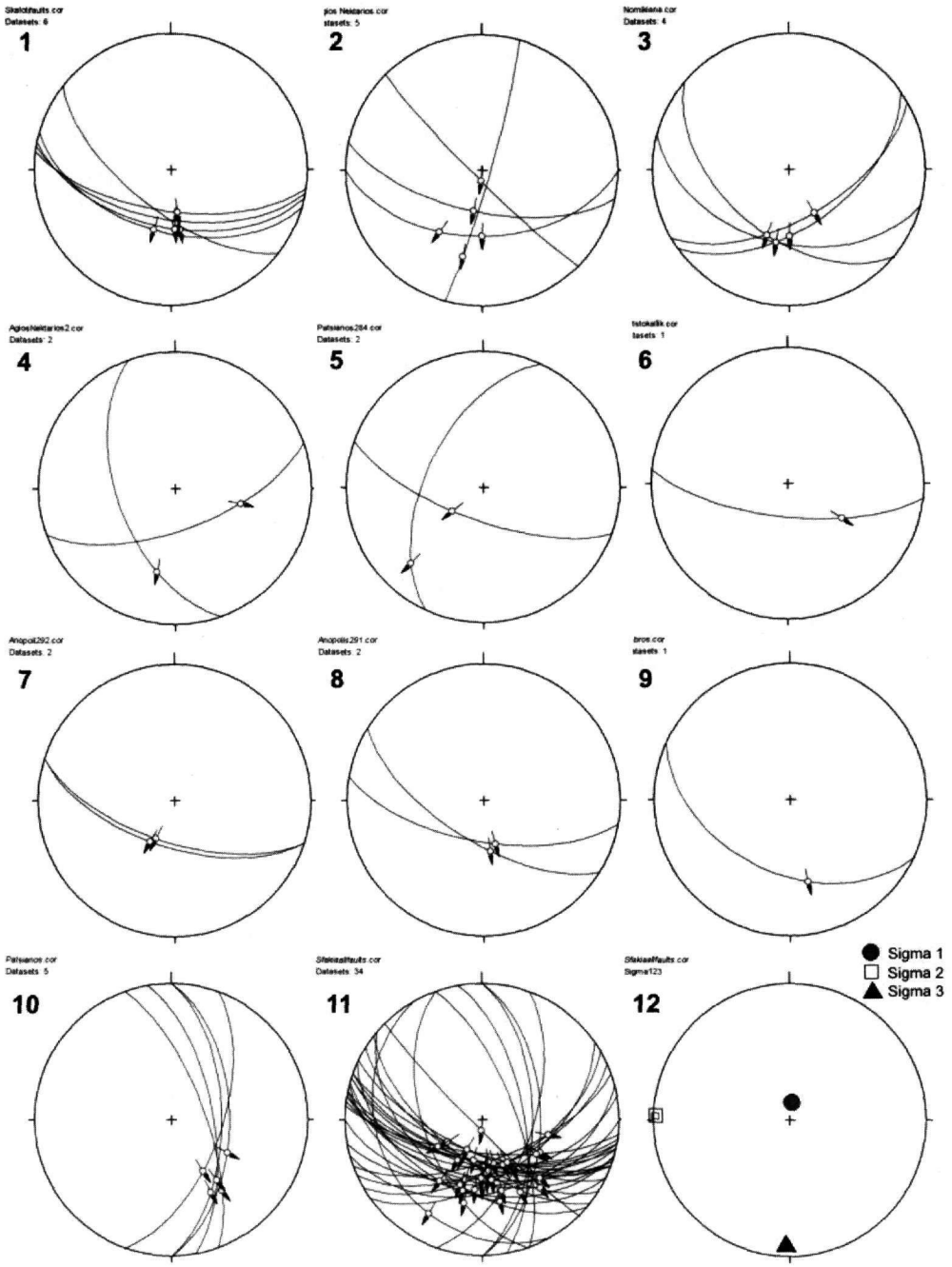

Figure 3 – Fault-slip analysis (P/T method, program Tectonics FP 1.159) performed on kinematic data. Numbers represent the measurements localities, which can be seen in figure 1. The locations 7 and 8 are north of the Anopolis settlement, northwest of Chora. Number 11 shows all the measurements that were used to calculate the mean stress axes of number 12.

3.1.3. Patsianos Fault

The Patsianos fault is a distinctive structure on the footwall of the Sfakia fault running parallel to the Kallikratiko gorge. It strikes N-S and has an high-angle dip to the east. It is a normal right-slip fault that has caused the subsidence of the eastern fault block by 300 m, as shown by the offset of the tectonic contact between the Trypali and Plattenkalk Units. The fault truncates the E-W and NW-SE trending faults that are observed at the southern tip of it. The analysis of the fault-kinematic data indicates an NW-SE directed extension (Fig. 3, location 10).

3.1.4. Faults on the Footwall of the Sfakia Fault

On the footwall of the Sfakia fault a series of parallel normal faults can be observed up to the north of Anopolis (NOT ON THE MAP), striking NW-SE to WNW-ESE and having high-angle dips to the south forming southwest facing, 40-100 m high escarpments. At their base, these escarpments show fault planes with slickensides and juxtaposition of thin collouvial wedges. It is interesting to note that their throw seems to decrease towards the south-east, where these faults tend to link with the Sfakia fault. In the hanging wall of these two faults, antithetic faults were formed at 50-200 m distance from those. These have higher dips than the main faults and demarcate small hanging-wall grabens. The presence of deep valleys normal to these grabens allows to see that the rocks between the antithetic faults is intensevely fractured by near vertical small faults, as if the grabens had been formed by collapse. The study of the fault-kinematic data shows that they are either pure-normal or normal-left-slip faults (Fig. 3, locations 7-9).

4. Uplift Rates

Stratigraphic and tectonic data emerging from our research coupled with recent palaeobathymetric reconstructions (cf. van Hinsbergen *et al.* 2006), allow us to reconstruct the post-Early Miocene geological history of the Sfakion coastal piedmont.

The Upper Miocene sediments that are found at altitudes of ~200 m at the eastern domain of the coastal zone, unconformably overly metamorphic rocks of the Phyllites – Quartzites Unit. Furthermore, van Hinsbergen *et al.* (2006) proposed that given the relationship between depth and %P [fraction of planktonic foraminifera among the total foraminiferal population (cf. van der Zwaan *et al.* 1990)], the deposition depth for this formation is 59 m. The Lower Pliocene sands of the Chora Sfakion were deposited at a depth of 800 m according to the method of van Hinsbergen *et al.* (2006). By comparison, the Frangokastelo Fm. formed at depths of 500-750 m based upon the method of van der Zwaan *et al.* (1990). Today these formations are found at altitudes of ~50 and 120 m, respectively. The presence of the Early Pleistocene (Calabrian) marine fossils northeast of the Imbros settlement at attitudes of 1000 m (cf. Alexopoulos and Marcopoulou-Diakantoni 1996), indicates that the mountainous domain has been uplifted ~1100 m since the Calabrian given that these organisms lived in waterdepths of 30-100 m. This gives an uplift rate of 80cm/ka for this fault block.

It is interesting to note that the Skaloti Fm contains the oldest marine sediments, yet appears to have been uplifted just 300 m to reach its present position. In comparison, younger formations appear to have been uplifted by more than 600 m. This suggests that following the deposition of the Skaloti Fm, subsidence of the study area during the latest Miocene – Lowest Pliocene was of the order of 700 m, and was coincident with activity along the Sfakia Fault (Fig. 4A-B). This in turn led to the exposure of the fault scarp where the sands of Chora Sfakion Fm. were deposited on the alpine basement (Fig. 4B). During the Middle Pliocene to Early Pleistocene, gradual uplift of the order 50-300 m occurred, after which the Frangokastelo Fm. was deposited (Fig. 4C). Although the sediments at Imbros and Chora Sfakion were both deposited on the footwall of the Sfakia fault, differential uplift (600 – 900 m uplift at Chora and 1100 m uplift at Imbros) probably reflects the accumulated offsets of the NW-SE faults observed in the north of the Sfakia fault. Moreover, comparison of the Lower Pleistocene sediments indicates that deposition of the

Frangokastelo Fm occurred at depths of 500-750 m, while sedimentation at Imbros occurred at depths of 30-100 m (Fig. 4C). Consequently, at the time of deposition there was a height difference of 400-720 m. However, their present height difference is 900-950 m, indicating that this difference has increased by 180-500 m after the Early Pleistocene (Fig. 4D). The lowest value of this difference (180 m) can be explained by activity of the NW-SE faults between the outcrops of the Early Pleistocene marine deposits alone. For the highest value (500 m) displacement on the Sfiaka fault must have occurred too.

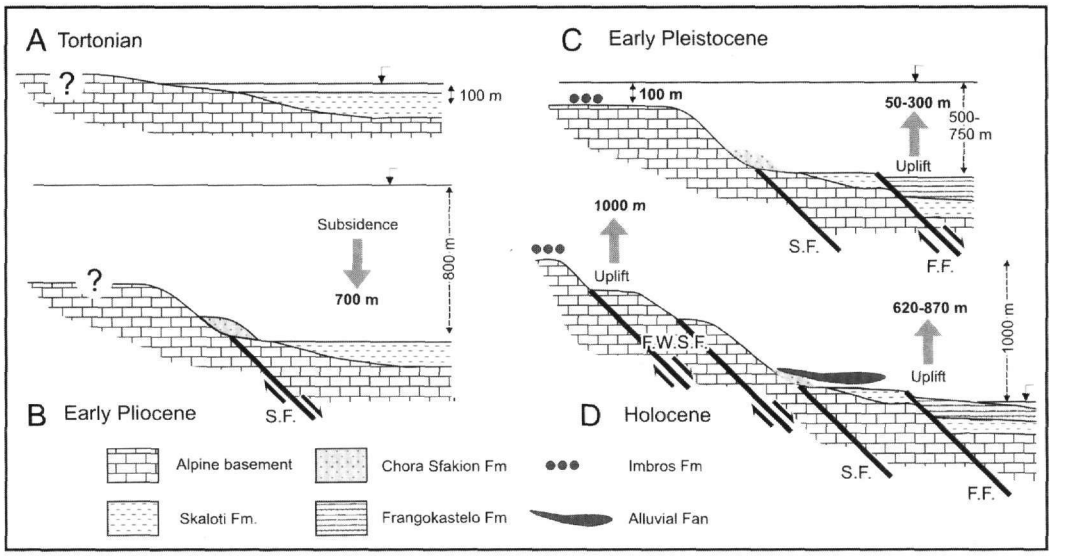

Fig. 4 – Schematic cross sections representing the evolution of the study area after the Tortonian

Useful uplift estimates can also be based on the uplift rates of the Sfakia fault blocks from the Late Pleistocene onward. According to van Hinsbergen *et al.* (2006) the deposition of the Fragokastelo Fm took place at depths of 500 - 750 m, whereas today it is found at altitudes of up to 120 m. This suggests that the uplift rate of the hanging wall of the Sfakia fault is 46 – 64 cm/ka since the Early Pleistocene. This means that the hanging wall is uplifted with a rate that is 1/2 to 4/5 of the rate of footwall uplift. The difference between the uplift rates is due to the presence of the faults that are located in the north of the Frangokastelo Fm, including the Sfakia fault. Therefore, the whole study area has experienced uplift since the Middle Pliocene, but an increase in the rate of uplift is observed between the southern coastal regions and the northern mountainous areas of the Lefka Ori massif. This increase is mostly due to the NW striking faults, and much less due to the Sfakia fault, at least for the period after the Middle Pleistocene, as the materials of the alluvial fans seem to seal this fault. Such suggestions of uplift rates have been proposed for central Crete, where some parts have been uplifted 1000-2000 m since the Late Pliocene (Meulenkamp *et al.* 1994).

5. Discussion - Conclusions

The study area is characterized by the presence of a steep south-facing morphological discontinuity striking E-W that separates a narrow coastal zone from the eastern foothills of the Lefka Ori massif. This steep escarpment is interpreted as a normal fault that represents the eastern and onshore segment of the south fault margin of Lefka Ori mountain range. As testified by (post-alpine) marine sediments deposited on the hanging wall, the Sfakia Fault is a major and long-lived neotectonic structure that invoked the subsidence of the Skaloti Fm and which became active after the Tortonian and remained active until the late Pleistocene.

The Sfakia Fault and other faults, found both in the footwall and hanging wall, show that the deformation was caused by extension in a N-S to NNE-SSW direction, i.e., normal to the long axes of the arc and parallel to the main direction of the compression stresses in that part of the outer Aegean Arc. Although, the majority of faults are normal, some faults (e.g. the Patsianos Fault) exhibit a significant horizontal slip component, which may indicate the presence of wrench tectonics. Alternatively, it is possible that such faults are formed by the same tectonic regime responsible for differential uplift parallel to the mean strike of the South Cretan Margin, including the Sfakia Fault. It is clear that most faults in the southeastern foothills of the Lefka Ori Mountain have kinematic data indicative of N-S to NNE-SSW extension at least from the Late Pliocene to the present. This observation is consistent with the results of Papazachos and Papazachos (2000) and Doutsos and Kokkalas (2002) who suggested NNE-SSW extension in central western Crete.

As far as the palaeogeographic evolution is concerned, the stratigraphic data show the deposition of marine sediments during the whole post nappe extension until the Lower Pleistocene. After the Lower Pleistocene a significant proportion of the hanging wall of the Sfakia fault was emerged and deposition of the first alluvial fans commenced. Nemec and Postma (1993) described the development of the alluvial fans in three stages concurrent with profound climate changes during the Quaternary: an earlier Late Pliocene to Late Pleistocene stage, a mid-Pleistocene stage and a later Holocene stage. The presence of Lower Pleistocene marine deposits underlying the alluvial fans proves that the oldest stage of the alluvial fans development took place sometime in the Middle Pleistocene, while the second stage of the Sfakia fan deposition is tentatively dated to around 143ka (Pope *et al.* in press).

The evolution that is described in the previous section shows that after the Upper Miocene the study area is progressively sliced into numerous faults blocks (Fig. 4) as if the area suffers gravitational collapse. The normal faults that define the numerous fault blocks cause N-S extension while the general uplift of south-western Crete is due to offshore normal faults, in the south of the study area. This collapse seems to be caused by compression perpendicular to the arc taking place in the medial and lower crust from the intense resistance of the subducted plate (Le Pichon *et al.* 1982, 1995, Mascle *et al.* 1998, Peterek and Schwarze 2005).

6. Acknowledgments

The authors wish to express thanks to the reviewers for their constructive comments and suggestions. We also thank Alexopoulos Apostolos (University of Athens) for briefing Emmanuel Skourtsos on the geology of Crete, Andrew Murray (University of Aarhus) for undertaking the OSL analysis. Permission to undertake fieldwork in Crete was granted by the Institute for Geological and Mineral Exploration. Richard J.J. Pope also acknowledges the University of Derby and the British Society for Geomorphology for providing funding towards the fieldwork.

7. References

Alexopoulos, A., and Marcopoulou-Diakantoni, A., 1996. La presence du Calabrien au plateau Impros (Crete occidentale, Grece) et sa signification pour l'evolution tectonique de Crete, *Rev. Paleobiol.*, 15(2), 349-355.

Alexopoulos, A., Hang, H., and Krahl, J., 2000. First Nummulites from the "Plattenkalk" sequence in the Lefka Ori, west Crete, *Ann. Geol. Pays Hell.*, 38, 117-121.

Alves, M. T., Lykousis, V., Sakellariou, D., Alexandri, S., and Nomikou, P., 2007. Constraining the origin and evolution of confined turbidite systems: southern Cretan margin, Eastern Mediterranean Sea (34°30–36°N), *Geo-Marine Letters,* 27, 41-61.

Angelier, J., 1979. Recent quaternary tectonics in the Hellenic arc: Examples of geological observations on land, *Tectonophysics*, 52, 267-275.

D' Agostino, N., Jackson, J.A., Dramis, F., and Funiciello, R., 2001. Interaction between mantle upwelling, drainage evolution and active normal faulting: an example from the central Apennines (Italy), *Geophys. J. Int.*, 147, 475-497.

Bonneau, M., 1984. Corellation of the Hellenic nappes in the south-east Aegean and their tectonic reconstruction. In J.E. Dixon and A.H.F. Robertson (eds), *The geological evolution of the Eastern Mediterranean*, Geological Society of London, 517-527pp.

Doutsos, T., and Kokkalas, S. 2001. Stress and deformation patterns in the Aegean region, *Journal of Structural Geology,* 23, 455-472.

Driever, B., 1988. Calcareous nannofossils biostratigraphy and paleoenviromental interpretation of the Mediterranean Pliocene, *Ultrecht Micropal. Bull.*, 36, 248.

Fassulas, C., 1999. The structural evolution of central Crete: insight into the tectonic evolution of the south Aegean (Greece), *Journal of Geodynamics,* 27, 23-43.

Fassoulas, C., 2001. The tectonic development of a Neogene basin at the leading edge of the active European margin: the Heraklion basin, Crete, Greece, *Journal of Geodynamics,* 31, 49-70.

Fassoulas, C., Kilias, A., and Mountrakis, D., 1994. New data about the pre-Oligocene structural evolution of Crete (Greece), *Bull. Soc. Geol. Greece,* 30(2), 67-81.

Fassulas, C., Rahl, J.M., Ague, J., and Henderson, K., 2004. Patterns and conditions of deformation in the Plattenkalk nappe, Crete, Greece: A preliminary study, *Bull. Geol. Soc. Greece,* 36, 1626-1635.

Goldsworthy, M., and Jackson, J., 2000. Active normal fault evolution in Greece revealed by geomorphology and drainage patterns, *Journal of the Geological Society, London* 157, 967-981.

van Hinsbergen, D., and Meulenkamp, J., 2006. Neogene supradetachment basin development on Crete (Greece) during exhumation of the South Aegean core complex, *Basin Research*, 18, 103-124.

Institute of Geological and Mineral Exploration [I.G.M.E.], 1982. *Geological map of Sellia (1:50000 scale)*, Institute of Geological and Mineral Exploration, Athens.

Institute of Geological and Mineral Exploration [I.G.M.E.], 1987. *Geological map of Vrisses (1:50000 scale)*, Institute of Geological and Mineral Exploration, Athens.

Jolivet, L., Goffe, B., Monie, P., Truffert, C., Patriat, M., and Bonneau, M., 1996. Miocene detachment in Crete and exhumation P-T-t paths of high pressure metamorphic rocks, *Tectonics*, 15, 1129-1153.

Karakitsios, V., 1979. Contribution a l'étude géologique des Hellenides: Étude de la region de Sellia (Crète moyenne-occidentale, Grèce). Les relations lithostratigraphiqueset structurales entre la série des Phyllades et la série de Tripolitza, *These 3eme cycle*, University Pierre et Marie Curie, Paris.

Krahl, J., and Kauffman, G., 2004. New aspects for a palinspastic model of the External Hellenides on Crete, *Proceedings of the 5th International Symposium on Eastern Mediterranean Geology, Thessaloniki, April 2004*, 119-122.

Le Pichon, X., 1982. Land-locked oceanic basins and continental collision: the Eastern Medittarenean as a case example. In K. Esu (ed.), *Mountain building processes,* Academic Press, London, 201-211.

Le Pichon, X., Chamot-Rooke, N., Lallemant, S., Noomen, R., and Veis, G., 1995. Geodetic determination of the kinematics of central Greece with respect to Europe: Implications for eastern Mediterranean tectonics, *Journal Of Geophysical Research* 100(B7), 12675-12690.

Leeder, M.R., and Jackson, J.A., 1993. The interaction between normal faulting and drainage in active extensional basins, with examples from the United States and central Greece, *Basin Research*, 5, 79-102.

Lourens, L.J., Hilgen, F.J., Laskar, J., Shackleton, N.J., and Wilson, D., 2004. Chapter 21: The Neogene period. In F.M. Graistein, J.G. Ogg and A.G. Smith (eds), *A Gelogical Time Scale 2004*, Cambridge University Press, Cambridge, 409-440pp.

Mascle, J., and Chaumillon, E., 1998. An overview of Mediterranean Ridge collisional accretionary complex as deduced from multichannel seismic data, *Geo-Marine Letters* 18, 81-89.

Meulenkamp, J. E., 1979. *Field guide to the Neogene of Crete*, Puplications of the Department of Geology & Paleontology Series A, No 32, 32.

Meulenkamp, J. E., M. J. R. Wortel, W. A. van Wamel, W., Spakman, E., and Hoogerduyn Strating, 1988. On the Hellenic subduction zone and the geodynamic evolution of Crete since the late middle Miocene, *Tectonophysics*, 146, 203-215.

Meulenkamp, J. E., van der Zwann, G. L., and van Wamel, W. A. 1994. On late Miocene to recent vertical motions in the Cretan segment of the Hellenic Arc, *Tectonophysics,* 234, 53-72.

Nemec, W., and Postma, G., 1993. Quaternary alluvial fans in southwestern Crete: sedimentation processes and geomorphic evolution. In M. Marzo and C. Puigdefábregas (eds), *Alluvial Sedimentation*. Special Publication of the International Association of Sedimentologists, 17, 235-276pp.

Papazachos, B. C., Papaioannou, C. A., Papazachos, C. B., and Savvaidis, A. S., 1999. Rupture zones in the Aegean region, *Tectonophysics*, 308, 205-221.

Peterek, A., and Schwarze, J., 2004. Architecture and Late Pliocene to recent evolution of outer-arc basins of the Hellenic subduction zone (south-central Crete, Greece), *Journal of Geodynamics*, 38, 19-55.

Pomoni-Papaioannou, F., and Karakitsios, V., 2002. Facies analysis of the Trypali carbonate unit (Upper Triassic) in central-western Crete (Greece): an evaporite formation transformed into solution-collapse breccias, *Sedimentology,* 49, 1113-1132.

Pope, R., Skourtsos, E., Wilkinson, K., Murray, A., Triantaphyllou, M., and Ferrier, G., in press. Clarifying stages of alluvial fan evolution along the Sfakian piedmont, southern Crete: new evidence from analysis of post-incisive soils and OSL dating, *Geomorphology*.

Sissingh, W., 1972. Late Cenozoic ostracoda of the south Aegean island arc, *Utrecht Micropal. Bull.*, 6, 187.

ten Veen, J.H., and Kleinspehn, K.L., 2003 Incipient continental collision and plate-boundary curvature: Late Pliocene - Holocene transtenstional Hellenic forearc, Crete, Greece, *Journal of the Geological Society*, 160, 1-21.

ten Veen, J. H., and Postma, G., 1999a. Neogene tectonics and basin fill patterns in the Hellenic outer-arc (Crete, Greece), *Basin Research,* 11(3), 223-241.

ten Veen, J. H., and Postma, G., 1999b. Roll-back controlled vertical movements of outer-arc basins of the Hellenic subduction zone (Crete, Greece), *Basin Research,* 11(3), 243-266.

Thomson, S., Stöckhert, B., and Brix, M., 1998. Thermochronology of the high-pressure metamorphic rocks of Crete, Greece:Implications for the speed of tectonic processes, *Geology*, 26(3), 259-262.

Thomson, S., Stöckhert, B., and Brix, M., 1999. Miocene high-pressure metamorphic rocks of Crete, Greece: rapid exhumation by buoyant escape. In U. Ring, M. T. Brandon, G. S. Lister and S. D. Willett (ed.), *Exhumation Processes: Normal faulting, Ductile flow and Erosion*, Special Puplications 154. Geological Society of London, 87-107pp.

Van Der Zwann, G.J., Jorissen, F.J., and De Stigter, H.C., 1990. The depth dependency of planktonic/benthonic foraminiferal ratios: constraints and applications, *Marine Geology*, 95, 1-16.

Δελτίο της Ελληνικής Γεωλογικής Εταιρίας τομ. XXXX, 2007
Πρακτικά 11ου Διεθνούς Συνεδρίου, Αθήνα, Μάιος 2007

Bulletin of the Geological Society of Greece vol. XXXX, 2007
Proceedings of the 11th International Congress, Athens, May, 2007

A NEW CONSIDERATION ABOUT THE ALMOPIA-PAIKON BOUNDARY BASED ON THE GEOLOGICAL MAPPING IN THE AREA OF NEROSTOMA-LAKKA (CENTRAL MACEDONIA, GREECE)

Tranos M. D.[1], Plougarlis A. P.[1], and Mountrakis D. M.[1]

[1] *Aristotle University of Thessaloniki, School of Geology, Department of Geology, GR-54124 Thessaloniki, Greece, tranos@geo.auth.gr, aplougar@geo.auth.gr, dmountra@geo.auth.gr*

Abstract

Geological mapping along the boundary of Almopia and Paikon zone in the 'Nerostoma' region, NNW of Lakka village defines mafic volcanogenic rocks, meta-pelites and radiolarites, thick-bedded to massive micritic limestones and flysch meta-sediments that dip mainly towards SW. Middle-Late Cretaceous fossiliferous limestones overlie unconformably the flysch meta-sediments and are characterised only by a primary foliation S0 that dips at shallow angles to the NNW-N. Secondary foliations S1 (sub-parallel to S0) and S2 are observed in the meta-clastic rocks. A D1 event caused F1 and progressively F2 folds to which S2 is the axial plane schistosity dipping to SW. This event which has not affected the fossiliferous limestones is related to an oblique convergence or inclined transpression during the Late Jurassic-Early Cretaceous. A D2 event dated in Early Tertiary caused an intense NE-thrusting and S-C cataclastic fabric defining top-to-the NE sense-of-shear. At many parts, the unconformity contact between the fossiliferous limestones and the underlying flysch is obliterated by this thrusting event. As a result, the boundary between Almopia and Paikon zones as paleo-geographically defined in this area seems to be meaningless for the Jurassic-Cretaceous times.

Key words: *Internal Hellenides, Axios zone, transpression, Greece.*

Περίληψη

Η γεωλογική χαρτογράφηση κατά μήκος του ορίου των ζωνών Αλμωπίας και Πάικου στη θέση 'Νερόστομα', ΒΒΔ του χωριού Λάκκα προσδιόρισε μαφικά ηφαιστειογενή πετρώματα μεταπηλίτες και ραδιολαρίτες παχυστρωματώδεις έως μαζώδεις μικριτικούς ασβεστόλιθους και φλυσχικά μετα-ιζήματα, τα οποία κλίνουν προς τα ΝΔ. Απολιθωματοφόροι ασβεστόλιθοι Μέσου-Άνω Κρητιδικού επικάθονται επικλυσιγενώς των φλυσχικών μετα-ιζημάτων και χαρακτηρίζονται από πρωτογενή φύλλωση S0, η οποία κλίνει ελαφρά προς τα ΒΒΔ-Β. Δευτερογενείς φυλλώσεις S1 (υποπαράλληλη στην S0) και S2 αναγνωρίζονται στα μετα-κλαστικά πετρώματα. Ένα D1 γεγονός προκάλεσε F1 και προοδευτικά F2 πτυχές, στις οποίες η S2 είναι η αξονική σχιστότητα με κλίση προς τα ΝΔ. Το γεγονός αυτό, που δεν επηρεάζει τους απολιθωματοφόρους ασβεστόλιθους, συνδέεται με μια πλάγια σύγκλιση ή επικλινή transpression στο Άνω Ιουρασικό-

Κάτω Κρητιδικό. Ενα D2 γεγονός, το οποίο χρονολογείται στο Κάτω Τριτογενές προκάλεσε μια έντονη λεπίωση προς τα ΒΑ και S-C κατακλαστική υφή προσδιορίζοντας κίνηση του υπερκείμενου προς τα ΒΑ. Η ασυμφωνία ανάμεσα στους απολιθωματοφόρους ασβεστόλιθους και τον υποκείμενο φλύσχη σε αρκετές θέσεις εξαλείφεται εξαιτίας της λεπίωσης αυτής. Το όριο των ζώνων Αλμωπίας και Πάικου, όπως προσδιορίστηκε παλαιογεωγραφικά στη περιοχή από προγενέστερες έρευνες δεν φαίνεται να έχει έννοια για την περίοδο Ιουρασικού-Κρητιδικού.
Λέξεις κλειδιά: *Εσωτερικές Ελληνίδες, Ζώνη Αξιού, transpression, Ελλάδα.*

1. Introduction

In the Internal Hellenides, at the east of the Pelagonian zone (Fig. 1a), the Axios zone divided from east to west into the zones of Peonia, Paikon and Almopia (Mercier 1968) documents the Mesozoic-Early Cenozoic evolution of several small oceanic basins and a complex history of terrane assembly. For this reason, it has concentrated the interest of many geoscientists (Mercier 1968, Mountrakis 1979, Vergely 1984, Stais 1993, Stais and Ferriere 1994, Sharp and Robertson 1993, Brown and Robertson 1994, Vergely and Mercier 2000, Ferriere *et al.* 2001, Brown and Robertson 2003, etc.). As a result, several arguments and questions about the Mesozoic and Cenozoic evolution not only for the zone itself, but also for the Internal Hellenides have been raised. One of the most arguable subjects is the boundary between the Almopia and Paikon zones, since different interpretations have been given to its geometry and kinematics. In particular, this boundary had been initially interpreted as a WSW-directed thrust through which the Paikon zone overthrusted the Almopia zone (Fig. 1b) (Mercier 1968, Mercier and Vergely 1984), but later as a thrust with opposite transport direction (Fig. 1c) (Sharp and Robertson 1993, Stais 1993). In this paper, we carried out a detail geological and tectonic mapping in scale 1:5.000 in the area 'Nerostoma', which is located approximately 3km NNW of Lakka village (Fig. 1), with the purpose to re-examine the nature of the Almopia-Paikon boundary and its deformational history. Based on this work, we present new data about the geology of the region and redefine the boundary between the zones of Almopia and Paikon.

2. Geological Setting

The Almopia zone and the Peonia zone (which will not be considered in detail here) to the west and east of Paikon zone, respectively, comprise contrasting Mesozoic–Early Tertiary lithologies, including Mesozoic ophiolitic rocks, which are absent from the Paikon zone. The Almopia zone in the west is widely seen as the site of an Early Mesozoic oceanic basin termed the Almopia Ocean (Stais, 1993, Stais and Ferriere, 1991, Sharp and Robertson, 1998). It comprises many units which are characterized by various lithologies and internal thrust deformation. From these units the easternmost one, the Krania Unit, comprising volcanogenic, deep-sea sediments and flysch sediments comes in contact with rocks of the Paikon zone (Fig. 1a).

The Paikon zone (Fig. 1c) is subdivided into two main sequences (Brown and Robertson 2004): (a) The Lower Sequence that consists, from bottom to top, of metamorphosed Triassic?-Jurassic, mixed carbonate-clastic sequence (Gandatch Formation), Jurassic volcanosedimentary rocks (Livadia and Kastaneri Formations) and Lower Cretaceous flysch (Grammos Formation), (b) The Upper Sequence that consists of Cretaceous transgressive limestones that pass upwards to Upper Cretaceous buff pelagic limestones and Lower Tertiary flysch (Tsouka flysch).

The boundary of the Paikon zone with the Almopia zone as has been firstly defined by Mercier (1968) presents NNW-SSE trend from the Greek/former Yugoslavia borders as south as the Yannitsa basin, where it disappears beneath the Quaternary sediments. Close to the borders, in the Pinovo Mt., it coincides with the WSW-directed thrusting of the Upper Cretaceous limestones

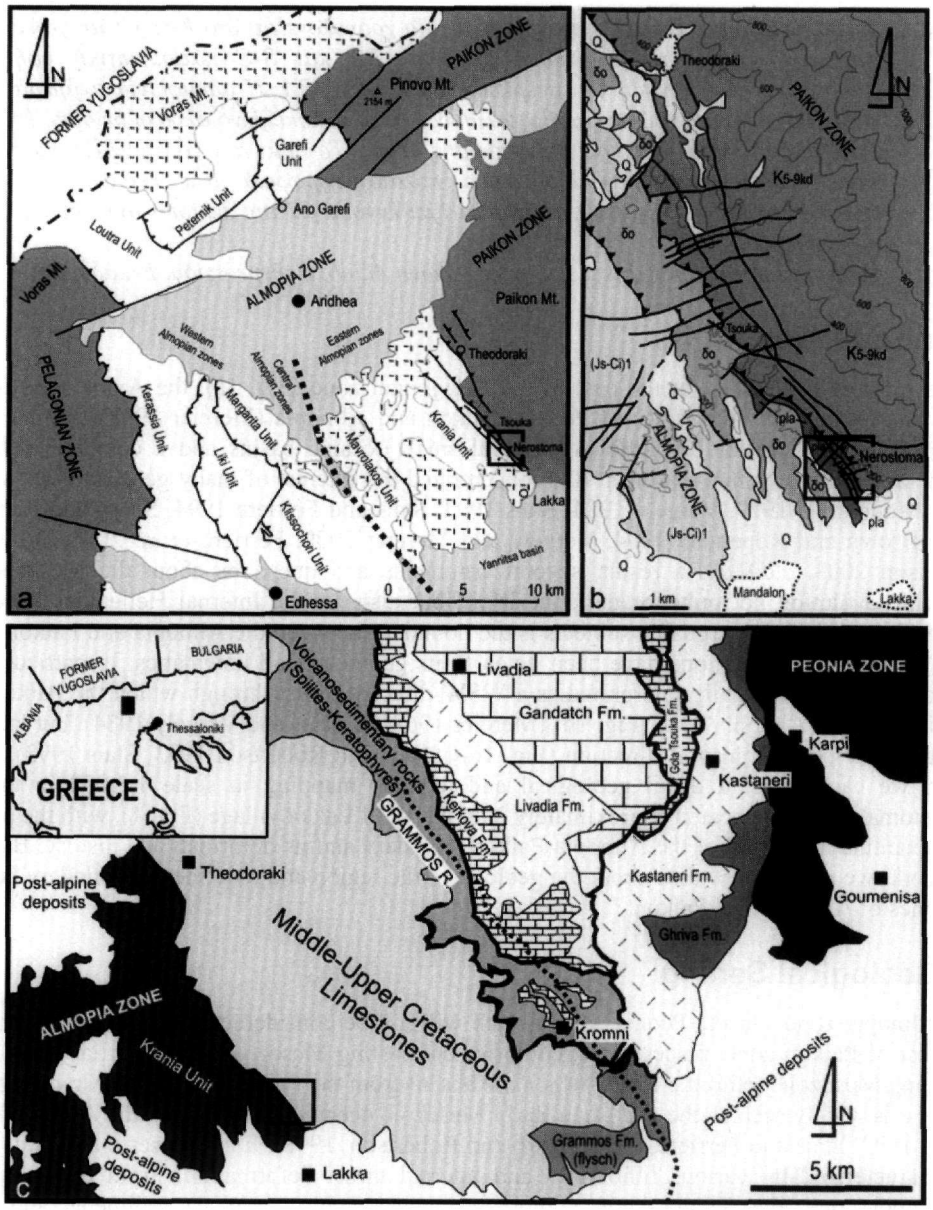

Figure 1 - General geological sketch maps of the wider study area: (a) The Almopia zone and its eastern boundary with Paikon zone (modified from Mercier 1968), (b)The Almopia-Paikon boundary as shown in geological map Edhessa sheet, (Js-Ci)1: volcanosedimentary rocks, δo: dolerites, pla: hyaloclastites (modified from Mercier and Vergely 1984), (c) The tectono-stratigraphic division of the Paikon zone based on previous studies (modified from Vergely *et al.* 2000). The study area is shown with square frame

over the Garefi ophiolitic rocks of the Almopia zone (Fig. 1a). Further to the south, the boundary is located along the western pediments of the Paikon Mt. passing through the Theodoraki village, Sharp and Robertson (1993) and Stais (1993) suggest that this boundary is a thrust with opposite transport direction through which the rocks of the Krania Unit were placed either onto the Upper Cretaceous fossiliferous limestones or their stratigraphically overlying Campanian-Maastrichtian

flysch sediments of the Paikon zone. Since then, many different aspects concerning the boundary and the evolution of the Paikon zone have come in light.

Ricou and Godfriaux (1995) accepting Sharp and Robertson's (1993) interpretation, proposed that the Paikon Mt. is a large anticlinal tectonic window with a core of crystalline rocks from Pelagonian massif. These rocks outwards and upwards are tectonically overlain by the rocks of Paikon zone as a result of large W-directed thrusting. This thrusting took place after the deposition of the Upper Cretaceous limestones, which in turn are tectonically overlain by Almopia and Peonia zones to the west and east, respectively, of the Paikon Mt.

A slightly different view is presented in the cross-section carried out by Ferriere *et al.* (2001). In particular, they show that the rocks of the Almopia zone thrust over a thin carbonate horizon ('Tsouka imbricates' of Sharp and Robertson (1993)) that belongs to the Lakka Unit of the Paikon zone. This horizon stratigraphically overlies Campanian-Maastrichtian flysch sediments. In addition, according to them, the Lakka Unit also comprises, to the bottom, Cretaceous limestones, Lower Cretaceous flysch and Jurassic volcanogenic rocks.

It is clear that Sharp and Robertson (1993) and Ferriere *et al.* (2001) assign a Campanian-Maastrichtian age to the flysch exposed at/or close to the Almopia/Paikon boundary. However, the first authors assigned this age based on the fauna of this age found by Mercier (1968) in similar lithologies. In addition, the second authors admitted that there is a paleontological problem with the faunas and the rocks of the area, since the Globotruncanas found on the roof of the carbonate rocks assign Campanian-Maastrichtian age to these rocks, whereas the Radiolarian fossils found in the overlying flysch sediments assign Turonian or Cenomanian-Turonian or even earlier age.

The deformation of the area has been firstly described by Mercier (1968) who recognized that the Paikon massif had been folded into a broad N-S anticline in post-Upper Cretaceous times and later by Vergely (1984) who proposed three distinct deformational phases to describe the regional deformation of the area:

JE1 – Upper Jurassic: a syn-metamorphic phase of compression causing cm- to m- scale, E-W trending isoclinal folds.

JE2 – Lower Cretaceous: syn-metamorphic phase of compression with large folds (10m – 100 m) with ESE to E vergence.

CT1-2 – Tertiary: series of compressional phases with westward vergence.

More recently Brown and Robertson (1994) distinguished the following events:

D1: This is similar in structures and age with the JE1 of Vergely (1984) and includes E-W-trending tight isoclinal folds with axial planar cleavage and an axis parallel intersection lineation.

E1: This is an inferred extensional event during the Cretaceous because of the hiatus observed in Cenomanian-Turonian times within the Paikon zone representing extension of the crust.

D2: It is a Post-Maastrichtian event that causes a NE-directed fold-and-thrust belt in the western part of the Paikon Mt. D2 structures are NNW-SSE chevron folds.

D3: This event, although is referred for the whole Paikon zone is mostly observed and defined in the eastern part of the mountain as a transpressive event that is associated with a mylonitic fabric with the top-to-the-SW sense-of-shear and a pervasive stretching lineation which plunges consistently toward SW.

E4: This is the Neogene and Quaternary extensional event that is well observed in the whole area of Macedonia (Mercier *et al.* 1989, Mountrakis *et al.* 2006).

A significant difference of the afore-described events is that the JE2 event reported by Mercier (1968) and Vergely (1984) is not sustained by Brown and Robertson (1994). Furthermore, Sharp

and Robertson (1993) who studied the Almopia-Paikon boundary in the area between the Theodoraki and Lakka villages mentioned only one Early Tertiary event that caused folds and thrusts with ENE-vergence.

3. Description of map units (in the Nerostoma region)

Our mapping in the 'Nerostoma' region, NNW of Lakka village indicates that the mapped rocks present a constant NNW-SSE trend. The larger part of the area (Fig. 2), i.e. the central and eastern one, is covered by carbonate rocks, whereas the western part is covered by NNW-SSE trending narrow strips of different lithologies. In particular, we distinguished the following map units from west to east (Fig. 2):

(a) *Matrix-supported volcaniclastic rocks*: They are horizontally bedded post-alpine volcaniclastic rocks formed by the volcanic activity of the Voras volcanic center that took place in Pliocene-Quaternary times (Mercier 1968, Eleftheriadis 1977, Vougioukalakis 1994). They cover the uppermost parts of the NNW-SSE trending hill range with the characteristic toponym 'Korifi tou Dimitri' and rest unconformably onto the mafic volcanogenic rocks. In addition, some very small remnant exposures have been also observed as outliers on the fossiliferous limestones, but without any mapping significance.

(b) *Mafic volcanogenic rocks*: Mainly green-colored dolerites, laves, hydrothermally altered pink colored hyaloclastites (quartz, albite, epidote) and schistose tuffites. They are generally massive, but foliated in places, volcanogenic rocks that dip toward SW with angles 30-60°. They made up the NNW-SSE trending 'Korifi tou Dimitri' hill range, and on the uppermost part of this hill range, are capped by the Pliocene-Quaternary matrix-supported volcaniclastic rocks. They could be correlated with the volcanogenic rocks of the Krania Unit as the latter described by Stais (1993).

(c) *Meta-pelites and radiolarites*: Violet-colored, foliated, fine-grained clastic rocks, i.e., pelites interbedded with violet- or black-colored radiolarites. Within them at places, some few ochre-colored thin horizons of schistose tuffites are intercalated. In addition, some small NW-SE trending bodies of mafic volcanogenic rocks have been also observed within them. They indicate intense foliation parallel to the bedding because of the low-grade metamorphism (greenschist facies). They could be correlated with the Upper Jurassic-Lower Cretaceous deep-sea sediments of the Krania Unit.

(d) *Thick-bedded to massive dark grey-colored micritic limestones*: They form discontinuous lenses that outcrop along the contact between the meta-pelites to the west and the next described flysch meta-sediments to the east. They are massive- to thick-bedded, partly dolomitic, micritic limestones of bluish-grey to dark grey colour that dip as the meta-pelites and the flysch meta-sediments toward SSW. However, no fossils could be found into these limestones in the field.

(e) *Flysch meta-sediments*: Brown-colored to greenish-brown turbidites, which have been subjected to low-grade metamorphic conditions (greenschist facies) and they exhibit intense secondary foliation (Fig. 3a). They consist of poorly sorted, coarse-grained lithic sandstones, siltstones and mudstones with lenses of polymictic pebble conglomerates. Within the flysch meta-sediments, we have also locally observed: (a) lenses of thinly foliated pelagic limestones of pinkish-white colour and thinly foliated to laminated light beige-grey-colored marly limestones, (b) violet-colored meta-pelites similar with the previous referred map unit of meta-pelites and radiolarites, and (c) some channelized clast-supported foliated cobble conglomerates with clasts of mainly volcanic and schist rocks. They could be correlated with the Upper Jurassic-Lower Cretaceous flysch meta-sediments of the Krania Unit.

(f) *Fossiliferous limestones*: They are light to dark grey-colored massive- to thick-bedded neritic carbonate rocks (Fig. 3b) into which plenty of fossils have been recognized and these fossils have

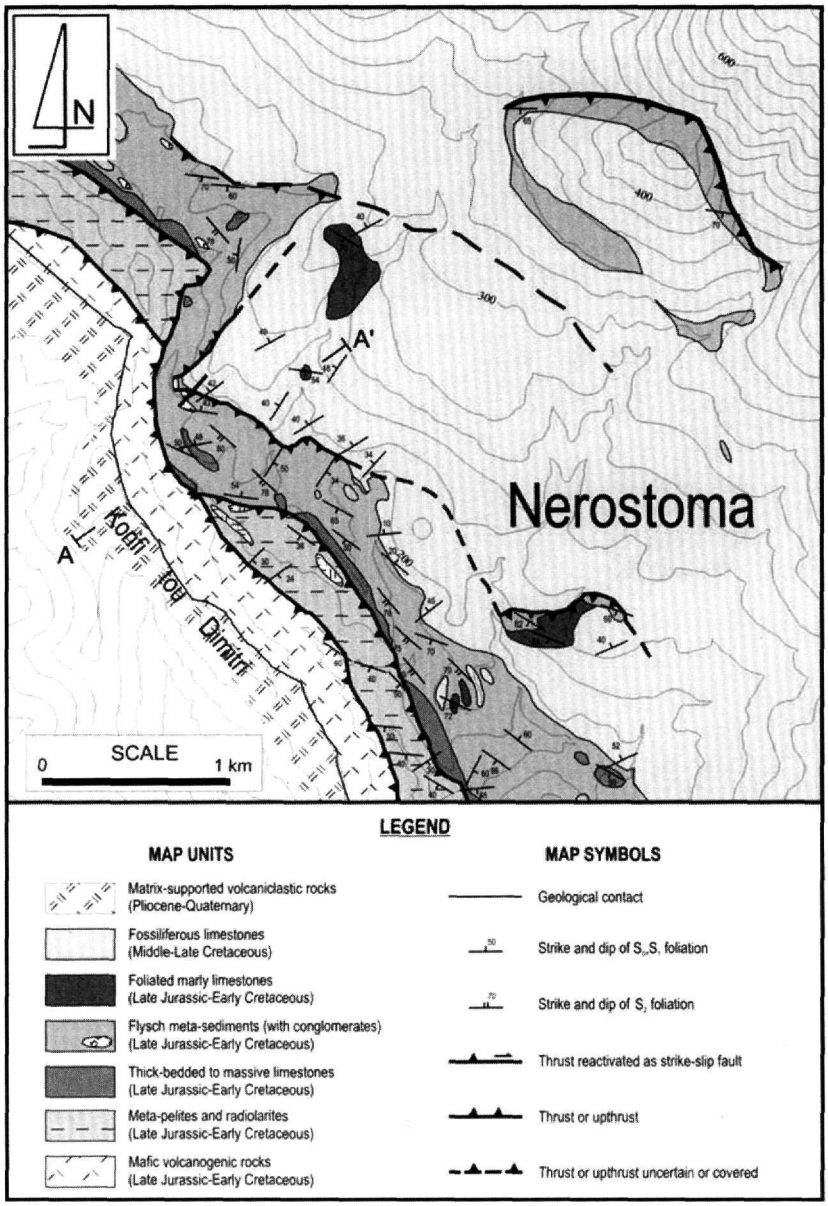

Figure 2 – Geological map of the Nerostoma, Lakka region

been already described by previous workers (Mercier 1968, Ferriere *et al.* 2001). They represent a carbonate platform with milliolid, peloidal and oolite-rich carbonates with local rudist-rich horizons (Sharp and Robertson 1993), which has been dated from these fossils in Cenomanian-Turonian. These fossiliferous carbonate rocks overlie: (a) the Upper Jurassic volcanosedimentary rocks (spilites, keratophyres), (b) the Upper Jurassic-Lower Cretaceous carbonate rocks (Kerkova Fm, Vergely *et al.* 2000) that outcrop more eastwards (outside the map area) in the central Paikon Mt. along the Grammos River, and south of the Kromni village the Lower Cretaceous flysch (Grammos Fm, Sharp and Robertson 1993) (Fig. 1c). Our mapping shows that these limestones also overlie unconformably the flysch meta-sediments exposed in the Nerostoma area (Fig. 3c).

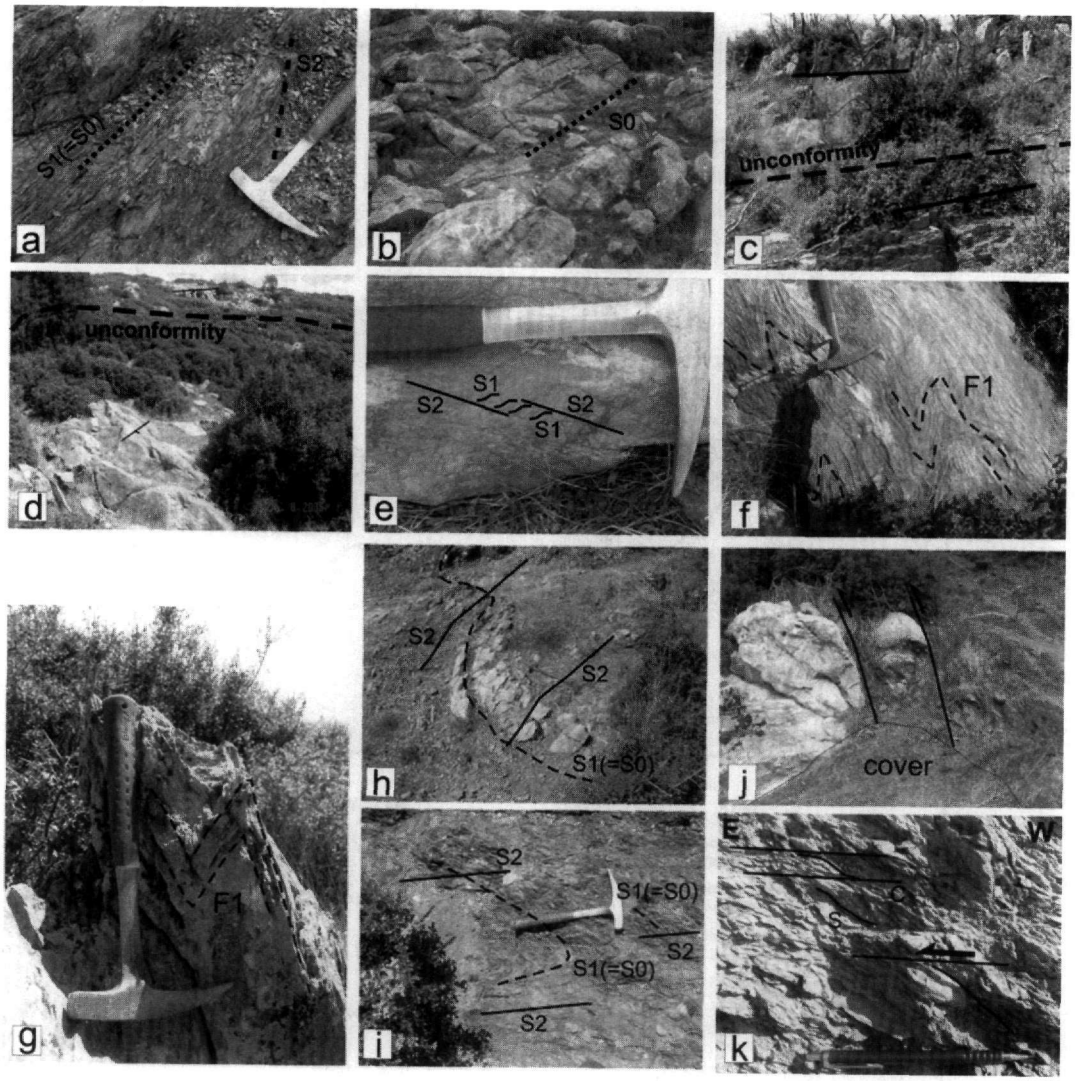

Figure 3 - Field photographs of the rocks and the structures mapped in the Nerostoma region (Lakka). (a) Flysch meta-sediments with S1(=S0) and S2 foliation, (b) Primary region (Lakka). (a) Flysch meta-sediments with S1(=S0) and S2 foliation, (b) Primary foliation S0 in the Upper Cretaceous fossiliferous limestones, (c) Steeply-dipping flysch meta-sediments underlie unconformably the gently dipping toward NNW Upper Cretaceous fossiliferous limestones, (d) inlier of marly thinly foliated limestones exposed to underlie unconformably the Upper Cretaceous massive to thick-bedded fossiliferous limestones, (e) S1, S2 foliations with the limestones that interbedded the flysch meta-sediments, (f) and (g) small-scale F1-folds in the limestones underneath the Upper Cretaceous fossiliferous limestones, (h) and (i) F2-folding and the S1, S2 foliations in the flysch meta-sediments, (j) Thrust contact between the flysch meta-sediments and the fossiliferous limestones, (k) S-C fabric in flysch meta-sediments indicating the top to the NE sense-of-shear

It is worth mentioning that within the outcrop of the fossiliferous limestones, inliers of lithologies similar with the flysch meta-sediments as well as the thinly foliated marly limestones they include

have been found and mapped (Figs 2, 3d). The rocks of the inliers dip constantly toward SSW and underlie unconformably the fossiliferous limestones (Fig. 3d).

4. Structural data

4.1. Foliation

Apart from the post-alpine volcaniclastic rocks that present a horizontal primary foliation, i.e. bedding, the underlying alpine rocks are characterized by a no horizontal either primary or secondary foliation (Fig. 4a).

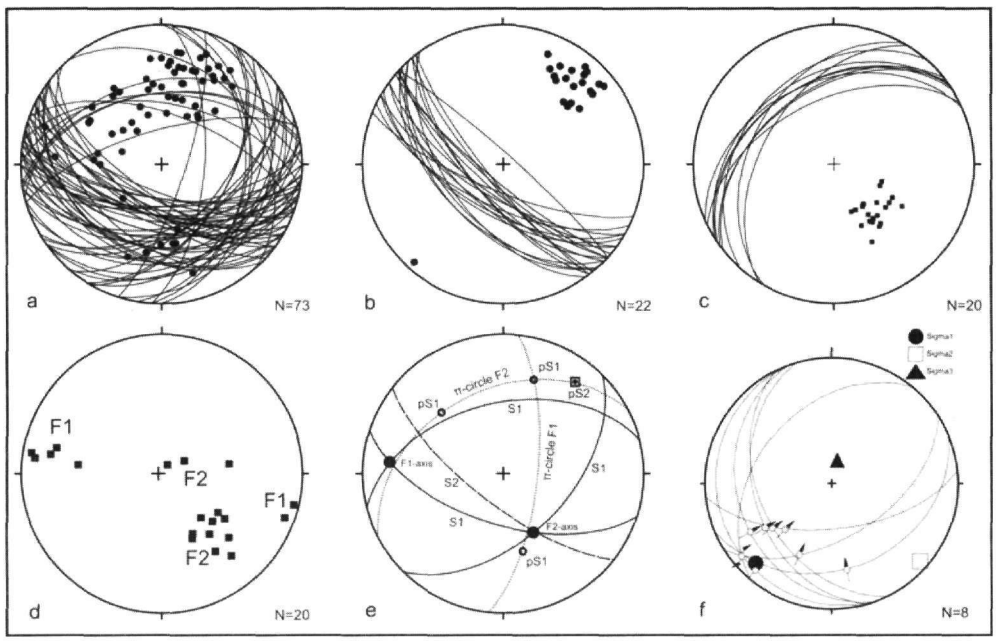

Figure 4 – Stereographic projections (lower hemisphere, equal area). (a) S0, S1 foliation of the alpine map units (fossiliferous limestones not included), (b) S2 foliation of the same map units as in (a), (c) S0 foliation of fossiliferous limestones, (d) Fold axes of mesoscopic F1 and F2 folds, (e) main structural elements of the map units (except fossiliferous limestones), (f) thrust and reverse faults in the area and the paleo-stress determination with the use of the TectonicsFP software

The dolerites are characterized by an S1 secondary foliation that dips generally toward SSW, whereas the hyaloclastites are relatively massive because of their origin (hydrothermal activity). The meta-pelites and radiolarites and the flysch meta-sediments are characterized by an S0 primary foliation which dips at medium to high angles toward SSW, and a secondary S1 foliation (slaty cleavage). The S1 foliation, is the dominant one and trends (sub)parallel to S0 dipping mainly toward SSW (Fig. 3a). A younger S2 foliation (axial plane schistosity) dips constantly toward SW (Fig. 4b) and affects the S1 and S0, forming crenulation cleavage.

It is interesting to mention that the pelagic limestones that have been found within the flysch-sediments as well as the marly limestones that form inliers within the fossiliferous limestones also exhibit the above mentioned S1 and S2 secondary foliations (Fig. 3e).

In addition, an even younger S3 foliation (spaced or fracture cleavage) has been observed locally in the meta-pelites and radiolarites map unit and the thick-bedded to massive dark grey colored micritic limestones mapped between the former and the flysch meta-sediments.

On the other hand, a not so easily observed primary foliation S0 characterizes the fossiliferous limestones; mainly the parts that are not massive (Fig. 3b). This foliation constantly dips gently (~30°) toward NNW to N (Fig. 4c).

4.2. Folding

Two main type of folding have been recognized to affect the above-mentioned alpine rocks except for the fossiliferous limestones. The first F1-folding causes WNW-ESE (~100°) trending large-scale, open to close, steeply inclined to inverted, asymmetric horizontal folds with vergence toward NNE (Figs 3f, g, 4d). The next F2-folding event causes asymmetric moderately plunging folds (Figs. 3h, I, 4d), i.e. the axes of these folds plunge with ~30°-40° toward SE. The F2-folds, which are of metre- to decimetre-scale are smaller in size in comparison to the F1-folds. Because of the F2 folding, the large modal limb dips toward SSW, whereas the smaller modal limb dips toward SE to E.

Both the F1 and F2-folds are associated with the afore-mentioned S2 axial crenulation cleavage, which in general dips at high angles (~70°-80°) toward SW. This fact indicates that the F1 and F2 folds are pene-contemporaneous with the former to precede the later. The main elements of the rocks are indicated in Fig. (4e).

4.3. Thrusting

As shown in the geological map (Fig. 2), most of the contacts are of tectonic nature and they are NE-directed thrusts and upthrusts. This is implied by the fact that the NW-SE trending contacts are not parallel to the S0 primary foliation and that they do not exhibit the geometrical case of a simple separation between two map units. This thrusting event has also affected the contact between the flysch meta-sediments and the fossiliferous limestones (Fig. 2). More precisely, the contact between the fossiliferous limestones and the flysch meta-sediments at many parts is a NE-directed thrust (Fig. 3j) that obliterates the previously formed stratigraphic contact of unconformity through which the fossiliferous limestones had deposited onto the flysch meta-sediments.

The analysis of the mesoscopic thrusts found in the field, with the use of the widely accepted TectonicsFP software, defines a NE-SW compression with sub-vertical least principal stress axis ($\sigma 3$) (Fig. 4f). These faults are associated with cataclastic flow and the formation of S-C cataclastic fabric (Fig. 3k) that defines top to the NE sense-of-shear.

5. Discussion and structural interpretation

The 'Nerostoma' mapped area represents a complicated region where different geological interpretations have been already applied. These interpretations have direct implications on the boundary between the Almopia and Paikon zones.

The most critical issue of the geology of the area is the interpretation of the age and the relationship of the exposed rocks. Especially, to assign the correct age to the flysch meta-sediments and to find out the relationship of this map unit with (a) the elongate narrow limestone lenses that have been mapped along the contact with the meta-pelites and radiolarites, and (b) the fossiliferous limestones

Our geological mapping indicates the following:

(a) The exposed rocks are mafic volcanogenic rocks, pelites and radiolarites, and flysch sediments that are characterized by a low-grade (greenschist facies) metamorphism and the formation of secondary foliation.

(b) The elongate narrow limestones that have been mapped here with the map unit 'Thick-bedded to massive dark grey colored micritic limestones' are of similar appearance with the fossiliferous

limestones. However, they do not reveal fossils in meso-scale and dip as the flysch meta-sediments, in contrast to the fossiliferous limestones that dip constantly toward NNW at gentle angles.

(b) The fossiliferous limestones cap the flysch meta-sediments as indicated by the inliers of flysch meta-sediments and/or thinly foliated marly limestones that have been mapped within the outcrop of the fossiliferous limestones and which underlie unconformably the later (Fig. 5).

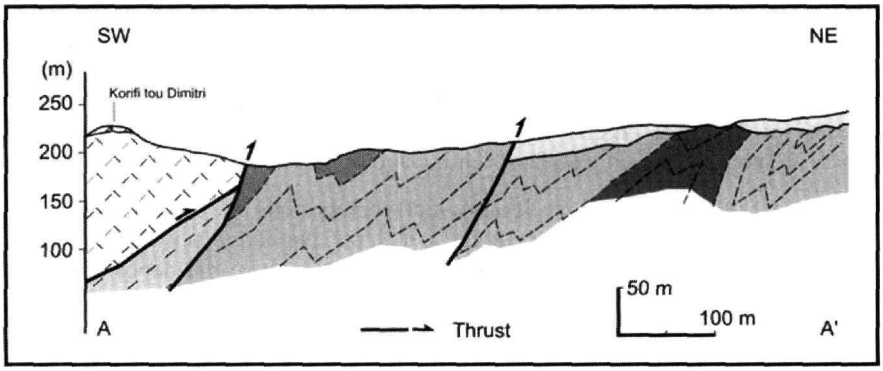

Figure 5 – Geological cross section A-A' (position and symbols as in Figure 2)

(c) The fossiliferous limestones neither exhibit any secondary foliation S1, S2 nor any F1- or F2-folds.

(d) The fossiliferous limestones have been affected by NE-directed thrusts, and only because of such NE-directed thrust, we observe the flysch meta-sediments to overlie these limestones (Fig. 5).

The geological formations up to the Lower Cretaceous flysch meta-sediments have been subjected to a D1 deformation event that includes the F1- and the progressive F2-folding. This event could be correlated with the Upper Jurassic-Lower Cretaceous JE1 and JE2 event mentioned by Vergely (1984). The progressive change from the F1- to F2-folds as well as the consistent s-form geometry and the moderately plunge of the F2-folds toward SE imply that the D1 event might was related to a left-lateral oblique convergence or an inclined pure-shear dominated transpression, into which the contacts dipping toward SSW form an acute angle and not a normal one with the NE-SW contraction (assuming that the S2 foliation forms more or less normal to the maximum strain axis).

In addition, the fact that the NE-directed thrusting is recognized to all the rock units including also the Upper Cretaceous fossiliferous limestones, suggests that a D2 deformation event giving rise to the thrusting toward NE dominated the area in the Early Tertiary times as has already described by Sharp and Robertson (1993). The absence of the Upper Cretaceous carbonate rocks from the Krania Unit could be explained due to D1 deformational event and/or to D2 thrusting event.

The fact that the Upper Cretaceous fossiliferous limestones overlie unconformably the meta-flysch which is syn-metamorphosed and deformed in similar manner with the mafic volcanogenic rocks, the meta-pelites and radiolarites suggest that the later are of older age than the Late Cretaceous and therefore could be correlated with the Jurassic-Lower Cretaceous formations of the easternmost Krania Unit of the Almopia zone as the latter described by Stais (1993). They could also be correlated with the Late Jurassic-Lower Cretaceous formations of the Paikon zone exposed in the central part of the Paikon Mt. and in the eastern part of the Upper Cretaceous carbonate cover. As a result, the area seems to represent no any significant boundary between the zones of Almopia and Paikon in the Jurassic-Early Cretaceous times. Therefore, there was palaeogeographic continuity between the Paikon zone and the Krania Unit in that time. It is clear that the meta-flysch represent the most crucial formation for the paleogeographic reconstruction and since the eastern Almopian Units (Krania and Mavrolakos Units) also include this formation along with the meta-pelites-radiolarites and the mafic volcanogenic rocks, then the boundary between the Almopia and Paikon zones should be traced between the eastern and central Almopian Units.

6. Conclusions

Our geological mapping suggests that the formations exposed in the Nerostoma-Lakka are mafic volcanogenic rocks, pelites and radiolarites and flysch sediments that are metamorphosed and deformed before the Middle-Late Cretaceous, because they are overlain unconformably by the Upper Cretaceous fossiliferous limestones. These rocks are of Late Jurassic-Early Cretaceous age and could be correlated with the formations of the eastern Almopian Units and the Upper Jurassic-Lower Cretaceous formations exposed in the central part of the Paikon Mt. Therefore, the flysch meta-sediments are the most crucial formation for the paleogeographic reconstruction of that period and they are not of Campanian-Maastrichtian age as previously assigned.

The fact that the meta-flysch are of Late Jurassic-Early Cretaceous age and has been also found in the eastern Almopian Units (Stais 1993) suggest that the boundary between the Almopia and Paikon zones should be traced to the west of the study area, where the deposition of the flysch could be traced, that is between the eastern and western Almopian Units.

7. References

Brown, S., and Robertson, A., 1994. New structural evidence from the Mesozoic – Early Tertiary Paikon unit, northern Greece, *Bulletin of the Geology Society of Greece,* XXX/1, 159-170

Brown, S., and Robertson, A., 2003. Sedimentary geology as a key to understanding the tectonic evolution of the Mesozoic – Early Tertiary Paikon massif, Vardar suture zone, N Greece, *Sedimentary Geology*, 160, 179-212

Brown, S., and Robertson, A., 2004. Evidence for Neotethys rooted within the Vardar suture zone from the Voras Massif, northernmost Greece, *Tectonophysics*, 381, 143-173.

Eleftheriadis, G. E., 1977. Contribution to the study of the volcanogenic rocks of the South Almopia, *PhD thesis*, University of Thessaloniki. (in Greek with English summary)

Ferriere, J., Bonneau, M., Caridroit, M., Bellier, J.P., Gorican, S., and Kollmann, H., 2001. Les nappes tertiaires du Paikon (zone du Vardar, Macédoine, Grèce): arguments stratigraphiques pour une nouvelle interprétation structurale, *C. R. Acad Sci.*, Paris 332, 695-702.

Mercier, J., 1968. Etude géologique des zones Helleniques en Macédoine centrale (Grece), *Ann. Geol. Pays Hell.* 20, 792 pp.

Mercier, J-L., Simeakis, K., Sorel, D., and Vergely, P., 1989. Extensional tectonic regimes in the Aegean basins during the Cenozoic, *Basin Research*, 2, 49-71.

Mountrakis, D., 1979. Contribution in the knowledge of the geology of the north boundary of the Axios and Pelagonian zones in the K. Loutraki-Orma area (Almopia), *PhD thesis*, University of Thessaloniki. (in Greek with English summary)

Mountrakis, D., Tranos, M., Papazachos, C., Thomaidou, E., Karagianni, E., and Vamvakaris, D., 2006. Neotectonic and seismological data concerning major active faults, and the stress regimes of Northern Greece, *Geological Society, London, Special Publications*, 260, 649–670, 0305-8719/06

Ricou, L.E., and Godfriaux, I., 1995. Mise au point sur la fenêtre multiple du Paikon et la structure du Vardar en Gréce, *C. R. Acad. Sci.* Paris 321 IIA, 601-608.

Sharp, I.R., and Robertson, A.H.F., 1993. Evidence for Turonian rift-related extensional subsidence and eastward Early Tertiary thrusting, western Paikon zone. Northern Greece, *Bulletin of the Geology Society of Greece,* XXVIII/1, 99-100.

Sharp, I.R., and Robertson, A.H.F., 1998. Late Jurassic-lower Cretaceous oceanic crust and sediments of the easter Almopias zone, NW Macedonia (Greece); implications of the evolution of the eastern "internal" Hellenides, *Bulletin of the Geology Society of Greece,* XXX/1, 47-61.

Stais, A., and Ferriére, J., 1991. Nouvelles données sur la paléogeographie Mésozoique du domaine Vardarien: Les bassins d'Almopias et de Péonias (Macedoine, Hellénides internes septentrionales), *Bulletin Geology Society of Greece,* XXVI/1, 491-507

Stais, A., 1993. Evolution geodynamique des bassins mesozoiques vardariens: Domaines de Péonias et d' Almopias (Hellénides internes, Macédoine centrale, Gréce), *PhD thesis*, University of Lille, 247 pp.

Stais, A., and Ferriére, J., 1994. Péonias (Axios-Vardar oriental; Hellenides): Donnée nouvelles sur les séries Ante-Cretacé et interprétations géodynamiques. *Bulletin of the Geology Society of Greece,* XXX/1, 121-132

Vergely, P., 1984. Tectoniques des ophiolites dans les Hellénides Internes (déformation, métamorphisme et phénomènes sedimentaires). Conséquences sur l' évolution des regions Téthysiennes Occidentales, *PhD thesis*, University Paris-Sud, Orsay.

Vergely, P., and Mercier, J., 2000. Données nouvelles sur les chevauchements d'âge post-Cretacé supérieur dans le massif du Paikon (zone de l'Axios-Vardar, Macédoine, Grèce): un nouveau modèle structural, *C. R. Acad. Sci. Paris,* 330, 555-561.

Vougioukalakis, G., 1994. The Pliocene volcanites of the Voras mountain, Central Macedonia, Greece. *Bulletin of Geological Society of Greece,* XXX/1, 223-240.

Δελτίο της Ελληνικής Γεωλογικής Εταιρίας τομ. XXXX, 2007
Πρακτικά 11ου Διεθνούς Συνεδρίου, Αθήνα, Μάιος 2007

Bulletin of the Geological Society of Greece vol. XXXX, 2007
Proceedings of the 11th International Congress, Athens, May, 2007

MORPHOTECTONICS OF THE PSATHOPYRGOS ACTIVE FAULT, WESTERN CORINTH RIFT, CENTRAL GREECE

Tsimi Ch.[1], Ganas A.[1], Soulakellis N.[2], Kairis O.[3], and Valmis S.[3]

[1] *Institute of Geodynamics, National Observatory of Athens, 11810 Athens, Greece*
aganas@gein.noa.gr

[2] *Department of Geography, University of the Aegean, University Hill, 81100 Mytilene, Greece*

[3] *Agricultural University of Athens, Iera Odos 75, 118 55 Athens, Greece*

Abstract

The study area is located on the western part of the Gulf of Corinth which is considered as a paradigm of an active rift system in Greece. This rift was formed by normal slip on big faults which extend the crust of the Earth in the N-S direction. The morphotectonic indices (hypsometric curve, hypsometric integral, drainage basin asymmetry, ratio of valley floor width to valley height) have been estimated using the 20-m digital elevation model of this area and the ARC software. The normal faults of the study area have been extracted by use of a DEM mosaic of 20-m pixel size, satellite images from Landsat 7 ETM+ and SRTM 90m. Our results highlight the recent activity of the Psathopyrgos normal fault on the basis of a series of morphotectonic evidence and suggest the existence of a single fault segment for a distance of 16 km.

Key words: *Morphotectonics, Corinth rift, Psathopyrgos, active faults.*

Περίληψη

Η περιοχή μελέτης είναι στο δυτικό άκρο του Κορινθιακού ανοίγματος. Ο Κορινθιακός κόλπος αποτελεί χαρακτηριστικό παράδειγμα νεοτεκτονικού βυθίσματος στον Ελληνικό χώρο. Το βύθισμα αυτό δημιουργήθηκε από την δράση μεγάλων ρηγμάτων τα οποία ανοίγουν τον φλοιό κατά την διεύθυνση B-N. Με βάση το ψηφιακό υψομετρικό μοντέλο της περιοχή,ς υπολογίστηκαν τέσσερις μορφοτεκτονικοί δείκτες (υψομετρικό ολοκλήρωμα, ασυμμετρία λεκάνης απορροής, λόγος πλάτους κοιλάδας προς ύψος, και ο δείκτης κλίσης). Επίσης χρησιμοποιώντας το ψηφιακό μοντέλο εδάφους, δορυφορικές εικόνες από τον σαρωτή ETM+ του δορυφόρου Landsat 7 και δεδομένα SRTM, έγινε η ψηφιοποίηση των ρηγμάτων της περιοχής μελέτης. Στην συνέχεια, η μελέτη της τεκτονικής γεωμορφολογίας της περιοχής έγινε με χρήση θεματικών χαρτών, οι οποίοι απεικόνιζαν την χωρική κατανομή των δεικτών. Στην εργασία αυτή μελετήθηκε ιδιαίτερα το κανονικό ρήγμα του Ψαθόπυργου το οποίο λειτουργεί ως μία ενιαία, ενεργή δομή μήκους 16 χιλιομέτρων.

Λέξεις κλειδιά: *Μορφοτεκτονική, Κορινθιακό Άνοιγμα, Ψαθόπυργος, ενεργό ρήγμα.*

1. Introduction

The main aim of this work is the understanding of long-term tectonic processes in the Psathopyrgos area of the western Corinth Rift area through the construction of a series of digital maps showing the spatial distribution of the main morphotectonic indices. The morphotectonic analysis helps to identify tectonic processes at the surface (Keller and Pinter, 1996). Our objectives are a) the mapping of the spatial distribution of the morphotectonic indices over a total area of 19.74 square kilometres (km^2, Fig. 1), b) the spatial relationship between the slip rate of the Psathopyrgos active fault and particular indices and c) the creation of a digital database of the geomorphology characteristics in the study region. In this paper we will present a fraction of our results around the Psathopyrgos area that have been validated in the field.

In central Greece, large, shallow earthquakes (M>6) are found to rupture pre-existing fault scarps such as the 1981 earthquakes in the eastern end of the gulf of Corinth (Jackson *et al.* 1982). Every large earthquake creates a permanent deformation at the Earth's surface (Stein *et al.* 1988), resulting in the uplift of the footwall area and the subsidence of the hangingwall area, respectively. The key factor in shaping the landscape in such areas is the relation of the fault slip rate to the erosion rate, in other words in areas deformed by fast-moving faults the geomorphological signal will be much different from areas with slow-moving faults.

The spatial criteria for the recognition of active normal faults are (Jackson and Leeder 1994, Ganas 1997) a) the alignment of fault scarps along the base of mountain fronts b) the elliptical shape of the footwall area as observed in along-fault strike profiles c) the development of axial drainage in the hangingwall area and d) the development of trellis-type drainage in the footwall area with discharge of footwall catchments at both ends of segments. In this work we used a combination of techniques including use of orthorectified Landsat 7 image, a 20-m DEM mosaic and its by-products (slope map, contours, TIN, shaded relief), a 90-m SRTM elevation model, geological data published in the literature and our own field work.

2. The study region

The study area is the western part of the Gulf of Corinth which is considered to be a paradigm of an active rift system in Greece (Fig. 1; De Martini *et al.* 2004, Pavlides *et al.* 2004, Pantosti *et al.* 2004, Bernard *et al.* 2006). This rift was formed by normal slip on large, E-W striking faults which extend the crust of central Greece in the N-S direction. The length of Corinth rift is 130 km and the width is 20-40 km. The major depth is ~900 m and the major height of the mountains around the Gulf of Corinth is ~2500 m. The south coast of the Corinth rift is uplifting whereas the north part is subsiding. From space geodesy we know that the Peloponnesus (southern part) moves faster towards southwest than the Greek mainland (Clarke *et al.* 1998). The result from this movement is that these two areas move away from each other with an average speed of 1 cm/year and increasing from east to west. The bedrock lithology is mainly limestone and the syn-rift rocks are Pliocene - Quaternary age sedimentary rocks such as marls, sandstones, conglomerates and alluvial fan deposits.

In the study region, the active faults have normal kinematics. The area includes some of the most active faults in Greece that have already been studied by many researchers. For example, the Eliki Fault, which is approximately 40 km long ruptured during two important catastrophic earthquakes in 373 BC and in 1861 (Schmidt 1879). Moreover the study area has rugged relief, several major rivers flowing in the general N-S direction (Fig. 1), many narrow valleys and a lot of other interesting landforms. Within our study area the drainage is organized in fifty six (56) catchments. The catchments developed in the footwall area of the Psathopyrgos normal fault amount to fourteen (14). The morphotectonic data for all catchments are presented in Table 1.

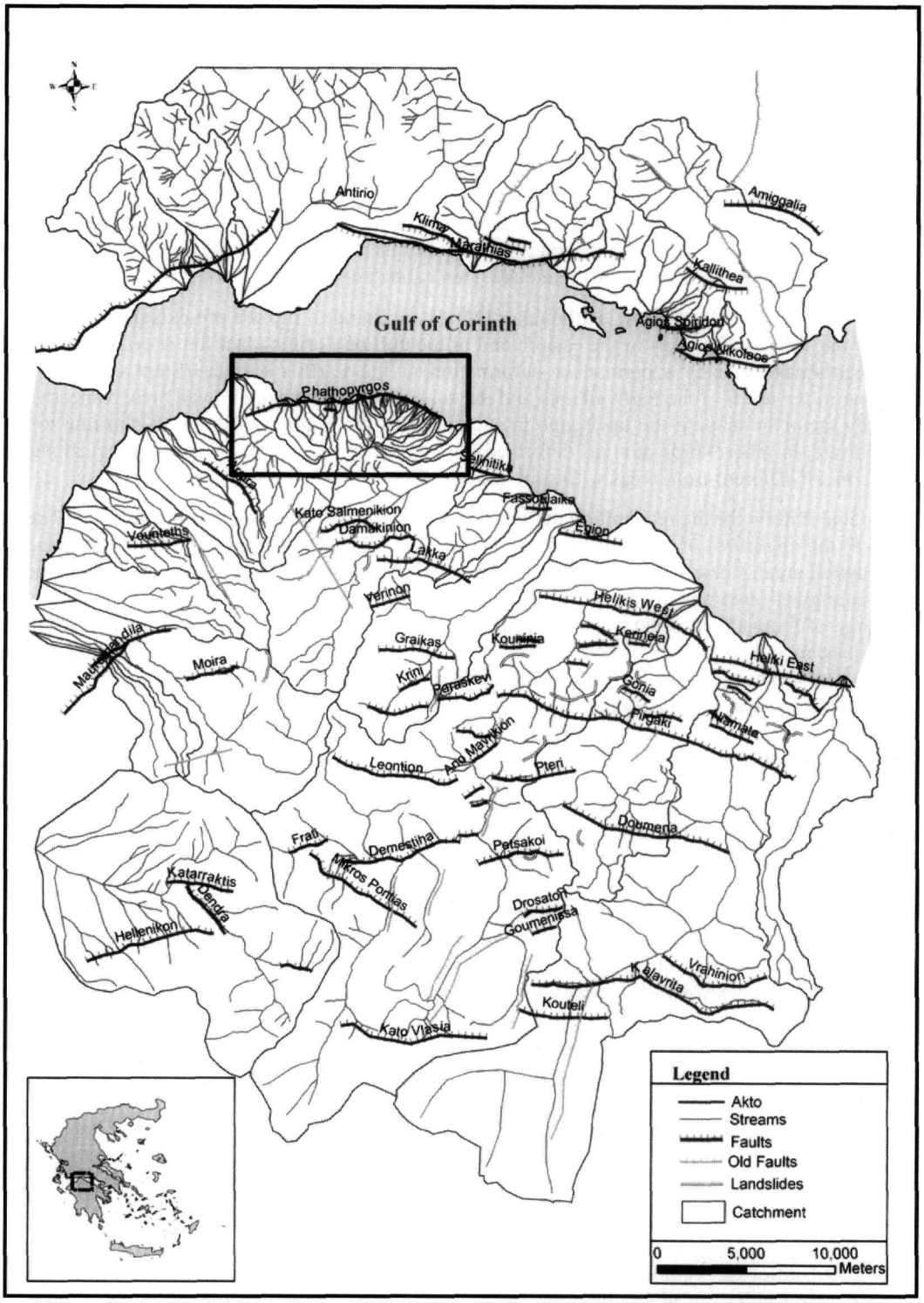

Figure 1 – Map of the study area in Western Peloponnesus and Sterea Hellas. Numbers indicate main catchments. Note the E-W orientation of active faults and the N-S orientation of major rivers. Names of faults are after published literature or by the nearest village/town. Square box indicates the Psathopyrgos fault area

3. Materials and Methods

The software that was used was *ArcGIS™ v.8.1* for Windows. From the available to us digital data, we digitized a) the catchments (56), b) the streams c) the landslides, d) the triangular facets developed on the footwall area of the large, normal faults and e) the normal faults as mapped by Doutsos and Poulimenos (1992), Roberts and Koukouvelas (1996) and by our own field work. The faults were located precisely by collecting fault plane coordinates using field GPS. The feature "active fault" includes 5 fields (attributes) namely the name of the fault, the length, the strike, the distance to the watershed (D to Divide) and the relief of each of them H_{max} - H_{min} (where H_{max} is the maximum elevation in the footwall of the fault and Hmin is the minimum elevation in the hangingwall).

The estimated morphometric indices of this study are the following:

- Hypsometric curve and hypsometric integral *(HI)*

$$HI = \frac{H_{mean} - H_{min}}{H_{max} - H_{min}} \quad (1)$$

where H_{mean}, H_{max} and H_{min} are the mean, maximum and minimum elevation, respectively.

- Drainage basin asymmetry *(AF)*

$$AF = 100 * (Ar/At) \quad (2)$$

where *Ar* is the size of area in the right sub-catchment of main river and *At* is the area of whole catchment.

- Ratio of valley floor width to valley height *(V)*

$$V = \frac{2V_{fw}}{(h_1 - h_3) + (h_2 - h_3)} \quad (3)$$

where V_f is the width of the valley floor, h_1 and h_2 are the elevation of the right and left drainage basic line and h_3 is the elevation of the valley floor.

In this paper we will present the results concerning the spatial distribution of the hypsometric integral (relation 1), the basin asymmetry index (relation 2), and the variation of the slope of the triangular facets along the fault. We also discuss the implications of the above morphotectonic indices and in particular the Valley Height-width ratios (relation 3) for the Psathopyrgos fault.

4. Results and Discussion

Our results are presented in tabular form below (Tables 1, 2) and as maps (Fig. 2 and so on). Table 1 summarises the selected morphotectonic indices for all catchments in Figure 1. Figure 2 presents the spatial distribution of hypsometric integrals and Figure 3 the basin asymmetry, respectively. The map of the hypsometric integral (relation 1) shows very high values in the catchments where their main rivers pour out in the Psathopyrgos and Marathias hangingwall regions (Fig. 2, catchments 13 to 29 and 46 to 50). The Psathopyrgos normal fault strikes E-W and its footwall catchments show values ranging from HI=0.5 to 0.7. The Marathias normal fault also strikes E-W and its footwall catchments range from HI=0.35 – 0.60. This means that these regions have a high mean topography which results from high rates of tectonic activity as demonstrated by the rapid uplift of the footwall of Psathopyrgos fault (0.7-0.8 mm/year; Houghton *et al.* 2003). Also, the hypsometric integral has a relatively high value in the catchments 1 to 5, which have been developed in the footwall area of the Eliki fault. The uplift rate of the footwall area has been determined by De Martini *et al.* (2004) as 1.0- 1.25 mm/year for the East and West Eliki Fault respectively. There is no geological data for uplift rates along the Marathias normal fault.

Table 1- Selected morphotectonic indices of the catchments of the area shown in Figure 1. Shaded rows indicate the catchments of the Psathopyrgos fault

Catchments	Area (m^2)	Af	Vr	Hypsometric Integral	Mean Slope
1	47811930	56.3	0.56	0.48	19.39
2	241417496	43.3	0.29	0.44	19.55
3	84056971	44.7	0.55	0.49	20.96
4	5094981	35.3	0.52	0.39	16.84
5	364478057	53.0	0.34	0.44	18.27
6	64762857	32.2	3.73	0.43	15.45
7	6815984	48.5	1.23	0.31	11.69
8	15683779	27.6	1.38	0.28	13.90
9	2348542	53.7	2.80	0.46	16.59
10	87350558	31.3	4.43	0.40	17.59
11	3121492	44.6	1.21	0.32	10.84
12	1791911	35.3	1.68	0.32	11.05
13	1804260	48.1	1.11	0.49	17.91
14	1359765	48.9	0.43	0.55	17.16
15	699527	38.8	1.15	0.50	18.75
16	1104390	42.6	1.02	0.65	20.17
17	222091	50.7	1.80	0.56	22.27
18	263749	45.7	1.65	0.56	21.86
19	782921	49.2	1.31	0.55	21.20
20	216557	34.0	6.55	0.59	20.64
21	378501	44.7	1.70	0.65	19.85
22	1496489	42.5	1.23	0.61	20.97
23	1632240	58.2	0.41	0.54	26.30
24	3524198	56.7	1.04	0.61	17.46
25	1471935	42.4	1.23	0.65	16.28
26	2623371	60.8	0.66	0.54	19.40
27	3970058	53.6	0.56	0.62	17.79
28	28548291	28.3	0.47	0.35	16.61
29	1033524	23.9	1.04	0.55	18.62
30	2074864	48.2	15.8	0.48	16.25
31	10365813	53.1	1.58	0.42	17.17
32	18112766	58.6	0.64	0.27	13.94
33	21327503	55.9	3.22	0.49	18.07
34	3613023	50.1	-	0.30	8.74
35	13484145	41.8	1.23	0.32	12.18
36	25993049	72.5	1.23	0.27	12.89
37	78844225	67.9	0.61	0.47	16.56
38	11397941	54.7	1.95	0.26	14.12
39	12495250	45.5	0.82	0.57	17.23
40	174732155	-	-	0.29	14.70
41	34297310	40.4	0.90	0.27	15.67
42	876311	46.8	1.38	0.36	17.16
43	1392420	38.3	1.79	0.32	19.13
44	32693871	48.9	3.97	0.45	22.36

45	2901191	47.8	2.22	0.20	6.37
46	143503704	-	-	0.39	19.09
47	31518661	42.1	0.12	0.50	22.17
48	19166567	67.2	0.73	0.55	25.07
49	4367131	42.5	0.67	0.47	21.21
50	13226043	48.1	0.21	0.40	18.41
51	9986878	54.6	1.39	0.40	21.64
52	2878776	35.7	1.26	0.51	22.90
53	1379537	39.2	0.96	0.49	24.33
54	4694924	45.5	0.97	0.46	18.80
55	3191160	41.7	2.23	0.53	20.10
56	71315140	58.5	3.29	0.45	19.67

The map of the Basin Asymmetry factor (AF; relation 2) shows the catchments along the Psathopyrgos fault follow the long-term slip rate distribution, i.e. catchments 14 to 22 show values less than 50 % indicating tilt to the right (east). Catchments 17 and 19 show AF values near 50 indicating the transitional "signal" between the two tilt directions along strike. On the other hand, catchments 23 to 27 show values greater than 50 indicating tilt to the left (west). This result allows us to suggest that Psathopyrgos is a mechanically isolated normal fault, so its footwall profile follows an elliptical shape, therefore tilt direction switches from east to west along strike. Along the Marathias fault the tilt is generally to the west with the exception of catchment 48 (Sergoula stream) which is tilted to the east. Along the Eliki Fault the distal catchments (1 and 5) show values greater than 50 (tilt to the right – east) while the proximal catchments (2, 3 and 4) are tilted to the left (west). As the hinterland of the Eliki fault is also deformed by other, parallel normal faults it is difficult to interpret this tilt pattern. The step over area between the two Eliki segments (Fig. 1) belongs to the catchment of river Kerinitis and shows a moderate tilt to the west (45).

The mean slope map of catchments shows that catchments in the footwall area of Psathopyrgos and Marathias faults have the highest values. Catchment slopes along Psathopyrgos range from 16.2°-26.3° and those along Marathias from 18.4°-25°, respectively. The catchment of Kerinitis river shows the highest mean slope (20.9°) in the footwall area of the Eliki fault.

The Psathopyrgos normal fault at the westernmost end of the Gulf of Corinth (Fig. 1) has been studied in more detail as it shows the characteristic elliptical profile of footwall elevations (Fig. 5). The footwall catchments have been analysed and four morphotectonic indices have been calculated, namely the Hypsometric integral, the mean slope, the valley width-to-height ratio and the basin asymmetry factor. All values are given in Table 3 below.

The footwall area of the Psathopyrgos normal fault is dissected by a dozen of streams with N-S flow. Stream downcutting has developed a series of characteristic erosional landforms along the mountain front, the triangular facets (Fig. 3). Facet slope varies along strike from 15.3° (east end) to 25.8° (west end) with highest values towards the west (slope > 30°; Fig. 4). This data support a weak correlation between mountain front lithology and mean slope of facets. Also, the high mean slope values are characteristic of active faulting (e.g. Ganas *et al.* 2005). A second important observation concerns the east-west distribution of the asymmetry factor (Fig. 6). The catchment asymmetry shows a flip in the tilt direction at about 5 km along strike (from eastward to westward) which is in agreement with the elevation change seen on the footwall profile (Fig. 5). A third observation concerns the distribution of the valley width-to-height ratio. We calculate this ratio upstream of the mountain front for all fourteen catchments along the Psathopyrgos fault (Table 3). The ratio plot (Fig. 6) shows values > 1 at distances 2000-7000 m along strike which is in disagreement with values <1 at both fault ends and towards the middle. This discrepancy is not due to a lack of tectonic uplift and the development of U-shaped valleys in this area but to the

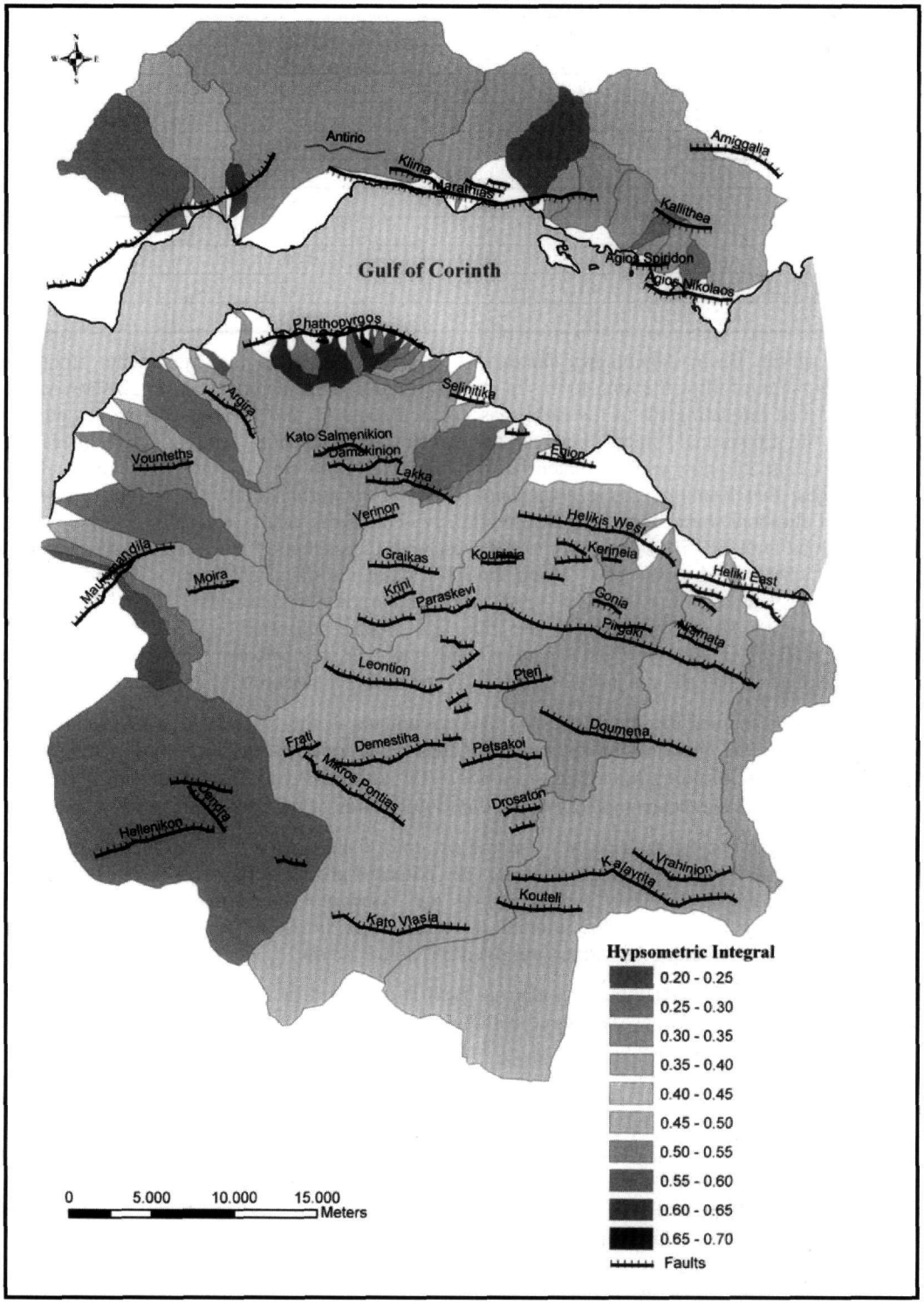

Figure 2 - Map showing the spatial distribution of the hypsometric integral for every catchment. The dark color indicates a high mean topography, while the light color indicates a low topography

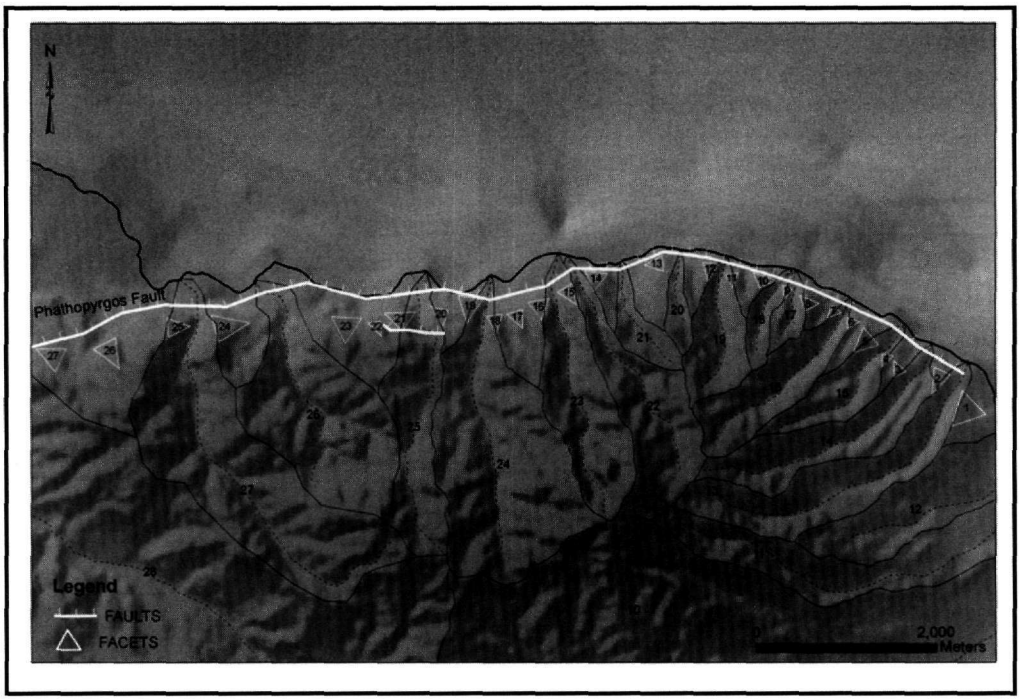

Figure 3 - Map of the Psathopyrgos fault area showing the catchments and triangular facets on its footwall. Integers inside triangles indicate facet numbering along strike

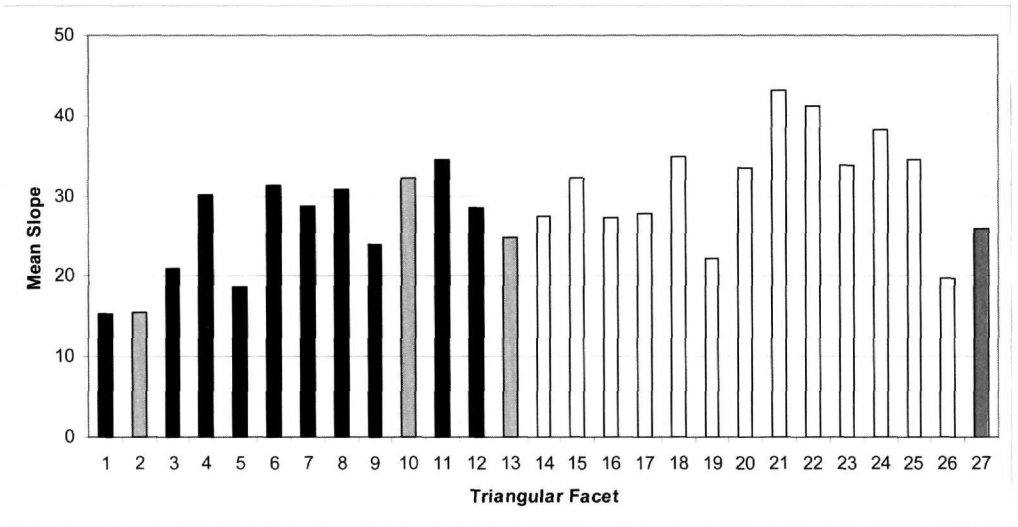

Figure 4 – Bar graph showing the mean slope of the triangular facets along the Psathopyrgos normal fault. Facet colour is according to lithology (Table 2). Facet number is shown in Figure 3

Table 2 – Size (area) and mean slope for each of the triangular facets in the footwall area of the Psathopyrgos Fault. Facet numbering is shown in Figure 3

Number of the Triangular Facets	Area (m^2)	Mean slope (°)	Lithology
1	67500	15.34	Syn-rift (conglomerate)
2	28800	15.45	Syn-rift (scree)
3	12600	20.88	Syn-rift (conglomerate)
4	8100	30.16	Syn-rift (conglomerate)
5	36000	18.71	Syn-rift (conglomerate)
6	8100	31.40	Syn-rift (conglomerate)
7	9000	28.68	Syn-rift (conglomerate)
8	16200	30.85	Syn-rift (conglomerate)
9	8100	24.03	Syn-rift (conglomerate)
10	18000	32.14	Syn-rift (scree)
11	11700	34.48	Syn-rift (conglomerate)
12	19800	28.44	Syn-rift (conglomerate)
13	16200	24.85	Syn-rift (scree)
14	28800	27.44	Pre-rift (limestone)
15	50400	32.22	Pre-rift (limestone)
16	18000	27.28	Pre-rift (limestone)
17	16200	27.89	Pre-rift (limestone)
18	38700	34.84	Pre-rift (limestone)
19	17100	22.17	Pre-rift (limestone)
20	37800	33.53	Pre-rift (limestone)
21	13500	43.16	Pre-rift (limestone)
22	47700	41.18	Pre-rift (limestone)
23	60300	33.77	Pre-rift (limestone)
24	27900	38.18	Pre-rift (limestone)
25	43200	34.44	Pre-rift (limestone)
26	37800	19.76	Pre-rift (limestone)
27	48600	25.87	Syn-rift (marly lim.-scree)

influence of the relatively weak lithology (syn-rift conglomerates). This lithology is more susceptible to hillslope erosion, upstream of the mountain front. Low Vr values (<1) indicate strong incision by streams due to tectonic uplift. For example such values are observed along the Eliki Fault (Verrios *et al.* 2004) where the 1861 earthquake ruptures were observed (Schmidt 1879).

We analysed the elevation profile of the footwall in order to examine if it can be fit by an elliptical line in accordance with other profiles along isolated, normal fault segments in central Greece (Ganas *et al.* 2005). Figure 5 shows the graph showing the footwall elevations along the Psathopyrgos active fault. We observe that the overall elliptical shape is maintained with high confidence as R^2 values range between 0.84 (quadratic fit) and 0.90 (cubic fit).

5. Conclusions

a) We studied the morphotectonics of the western Gulf of Corinth and focused our attention to the Psathopyrgos normal fault. This fault strikes E-W and its footwall catchments show values ranging from HI=0.5 to 0.7. This means that this region has a high mean topography which results from high rates of tectonic activity.

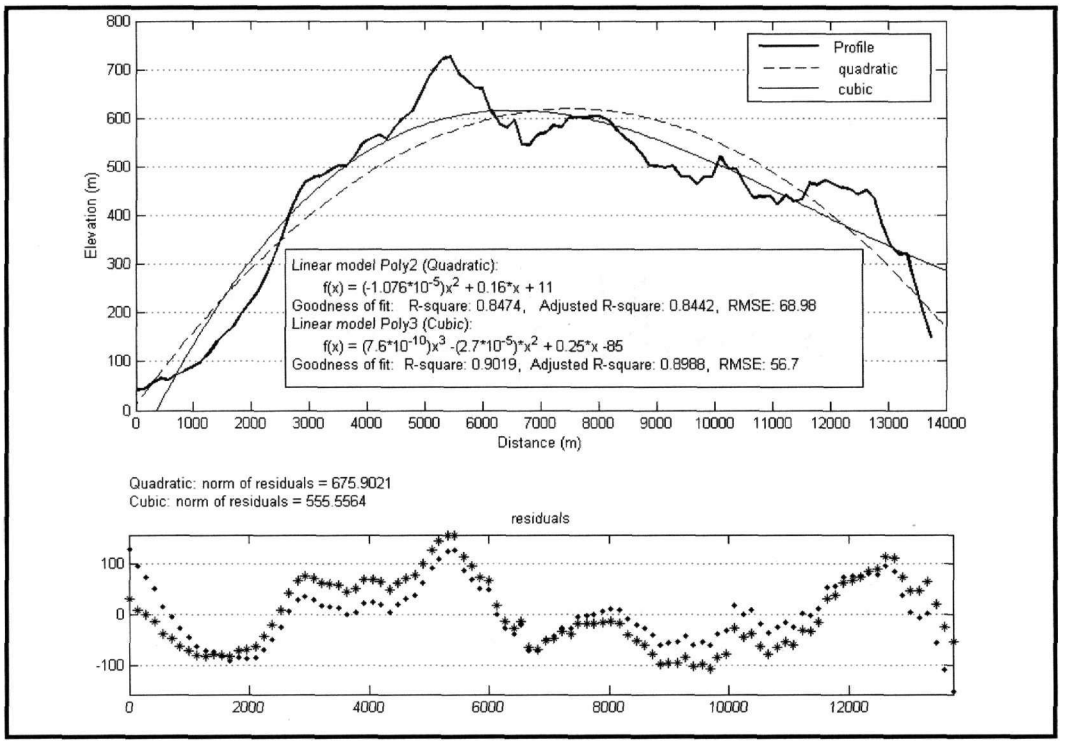

Figure 5 – (Top) Graph showing the footwall elevations along the Psathopyrgos active fault. Also drawn are best-fit curves for quadratic (dashed line) and cubic polynomials (solid line). Vertical exaggeration times 10. (Bottom) Graphs showing goodness of fit along footwall distance. In most cases the cubic fit (dots) is better

Table 3 - Morphotectonic indices along the Psathopyrgos normal fault. The ratio Vr is measured upstream from the mountain front and its distance is given in m

Distance (m)	H. Integral	Mean Slope/rad	Valley (Vr)-Distance to Fault	As/100
468.30	0.55	0.30	0.43 – 1284	0.49
863.29	0.50	0.33	0.98 – 477	0.39
1531.38	0.65	0.35	0.94 – 723	0.43
2148.50	0.56	0.39	1.44 – 282	0.51
2305.50	0.56	0.38	1.20 – 404	0.46
2971.90	0.55	0.37	1.30 – 241	0.49
3474.08	0.59	0.36	1.50 – 464	0.34
4172.08	0.65	0.35	1.40 – 642	0.45
4729.70	0.61	0.37	1.07 – 763	0.43
5018.40	0.54	0.46	0.41 - 623	0.58
5775.60	0.61	0.30	0.97 – 267	0.57
7318.78	0.65	0.28	1.18 – 268	0.42
10611.98	0.54	0.34	0.66 – 689	0.61
14684.12	0.62	0.31	0.56 - 513	0.54

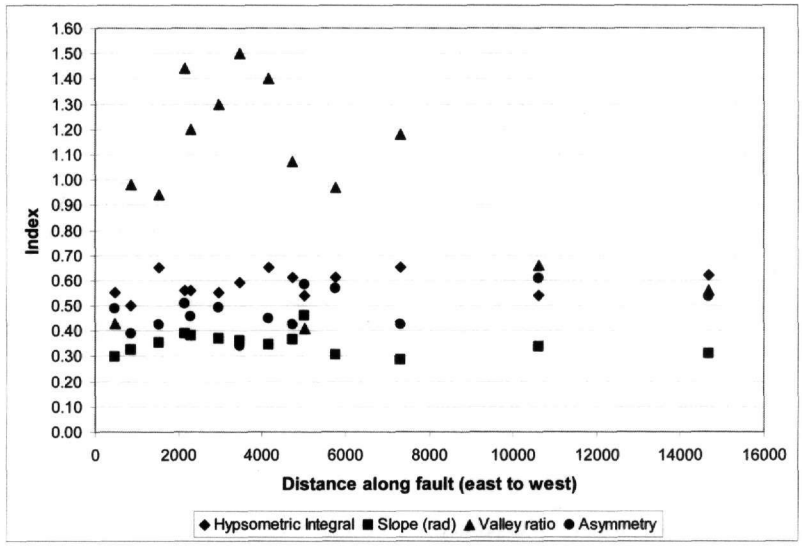

Figure 6 - Graph showing the distribution of morphotectonic indices along the Psathopyrgos Fault. Values of indices are presented in Table 2. In order to maintain a similar Y-axis in this plot the mean slope of catchments is given in radians and the basin asymmetry index is divided by 100

b) The Psathopyrgos fault is a mechanically isolated normal fault, because its footwall elevation profile follows an elliptical shape (Fig. 5) and its footwall tilt direction switches from east to west along strike. The footwall best-fit curve is a cubic polynomial.

c) Mean values of triangular facets are high indicating active faulting. A weak correlation is observed between the mean slope of facets and the lithology of the footwall. Facets developed on limestone have high values (> 30°).

d) The variation of Vr ratio along the Psathopyrgos fault shows values > 1 at distances 2 – 7 km away for the east end. This is not the result of lack of tectonic uplift but it is due to the existence of relatively weak lithology of the syn-rift (conglomerates). Vr values < 1 exhibit valleys developed on bedrock (limestone). In fact, the lowest values of Vr exist at both ends of the fault where long-term slip rates are expected to be the lowest. This observation may suggest that these areas have experienced very recent uplift and intense down-cutting as a result of bi-directional fault growth.

6. Acknowledgments

We thank Professor Pavlides for reviewing the paper and Prof. Hara Drinia for editorial assistance. Sotiris Sboras helped with ARC processing. The 90-m SRTM data set was provided by NASA free of charge. The 20-m DEM mosaic was provided by GEOINFO ltd.

7. References

Bernard, P., Lyon-Caen, H., Briole, P., et al., 2006. Seismicity, deformation and seismic hazard in the western rift of Corinth: New insights from the Corinth Rift Laboratory (CRL), *Tectonophysics,* 426 (1-2), 7-30.

Clarke, P.J., Davies, R.R., England, P.C,. Parsons, B., Billiris, H., Paradissis, D., Veis, G., Cross, P.A., Denys, P.H., Ashkenazi, V., Bingley, R., Kahle, H.-G., Muller, M.-V., and Briole, P., 1998. Crustal strain in central Greece from repeated GPS measurements in the interval 1989-1997, *Geophys. J. Int.,* 135(1), 195-214.

De Martini, P.-M., Pantosti, D., Palyvos, N., Lemeille, F., McNeill, L., and Collier, R., 2004. Slip rates of the Aigion and Eliki faults from uplifted marine terraces, Corinth Gulf, Greece, *C.R.Geoscience,* 336/4-5, 325-334, doi:10.1016/j.crte.2003.12.006.

Doutsos, T., and Poulimenos, G., 1992. Geometry and kinematics of active faults and their seismotectonics significance in the western Corinth - Patras rift (Greece), *Journal. Structural Geology,* 14 (6), 689-699.

Ganas, A., 1997. Fault Segmentation and Seismic Hazard Assessment in the Gulf of Evia Rift, central Greece, *Unpublished PhD thesis,* University of Reading, 369pp.

Ganas, A, Pavlides, S, and Karastathis, V., 2005. DEM-based morphometry of range-front escarpments in Attica, central Greece, and its relation to fault slip rates, *Geomorphology,* 65, 301–319.

Ganas, A., Shanov, S., Drakatos, G., Dobrev, N., Sboras, S., Tsimi, C., Frangov, G., and Pavlides, S., 2005. Active fault segmentation in southwest Bulgaria and Coulomb stress triggering of the 1904 earthquake sequence, *Journal of Geodynamics,* 40(2-3), 316-333.

Houghton, S., Roberts, G., Papanikolaou, I., McArthur, J. and Gilmour, M., 2003. New ^{234}U-^{230}Th coral dates from the western Gulf of Corinth: Implications for extensional tectonics, *Geophysical Research Letters,* 30(19), art. no. 2013.

Jackson, J.A., Gagnepain, J., Houseman, G., King, G.C.P., Papadimitriou, P., Soufleris, C., and Virieux, J. 1982. Seismicity, normal faulting, and the geomorphological development of the Gulf of Corinth (Greece): the Corinth earthquakes of February and March 1981, *Earth planet Sci. Lett.,* 141, 377–397.

Jackson, J.A., and Leeder, M., 1994. Drainage systems and the evolution of normal faults: an example from Pleasant Valley, Nevada. *Journal of Structural Geology*, 16, 1041-1059.

Keller, E., and Printer, N., 1996. *Active Tectonics: Earthquakes, Uplift and Landscape*, Prentice Hall, New Jersey.

Pavlides, S.B., Koukouvelas, I.K., Kokkalas, S., Stamatopoulos, L., Keramydas, D., and Tsodoulos, I., 2004. Late Holocene evolution of the East Eliki fault, Gulf of Corinth (Central Greece), *Quaternary International,* 115-116, 139-154.

Pantosti, D., De Martini, P.M., Koukouvelas, I., Stamatopoulos, L., Palyvos, N., Pucci, S., Lemeille, F., and Pavlides, S., 2004. Palaeoseismological investigations of the Aigion Fault (Gulf of Corinth,Greece), *Comptes Rendus – Geoscience,* 336, 335-342.

Roberts, G. P., and Koukouvelas, I., 1996. Structural and seismological segmentation of the Gulf of Corinth Fault System: implications for models of fault growth, *Annali di Geofisica,* XXXIX, 619-646.

Schmidt, J., 1879. Studien über Erdbeben, *Carl Schottze, Leipzig,* 68–83pp.

Stein, R., King, G.C.P., and Rundle, J., 1988. The growth of geological structures by repeated earthquakes: 2 Field examples of continental dip-slip faults, *Journal of Geophysical Research,* 93(B11),13319-13331.

Verrios, S., Zygouri, V., and Kokkalas, S., 2004. Morhotectonic analysis in the Eliki fault zone (Gulf of Corith, Greece). Bulletin of the Geological Society of Greece, *Proceedings of the 10th International Congress, Thessaloniki, April 2004,* vol. XXXVI, 1706-1715.

Δελτίο της Ελληνικής Γεωλογικής Εταιρίας τομ. XXXX, 2007
Πρακτικά 11ου Διεθνούς Συνεδρίου, Αθήνα, Μάιος 2007

Bulletin of the Geological Society of Greece vol. XXXX, 2007
Proceedings of the 11th International Congress, Athens, May, 2007

MAGMA INTRUSION IN 'PROTO-CALDERA CALDERA' SYSTEMS: EXAMPLE FROM THE NISYROS VOLCANO

Zouzias D.[1], and St. Seymour K.[2]

[1] *Department of Geology, University of Patras, Rion Patras 26500 GR, kstseymr@upatras.gr, dizouzias@upatras.gr*

[2] *Departments of Chemistry, Geography, Concordia University, Montreal H4B 1R6 CA*

Abstract

The interdependence of volcanism and tectonism has been focused upon in the last decade as a result of previously accumulated evidence, as well as, due to the application of remote sensing techniques in both these fields. Volcanoes depend on tectonic features such as faults for their positioning and operation and on petrotectonic environment for the chemistry of their magmas. Faults provide the plumbing system for magma ascent and therefore volcano localisation and distribution in space greatly depends on the tectonic pattern of an area. On the other hand, volcanoes locally imprint their volcanotectonic features such as radial and ring faults which result from cycles of magma replenishment (inflation) and evacuation (deflation) of magmatic reservoirs (magma chambers).

Under this light, the area in the easternmost extremity of the Aegean Arc is being reconsidered. Our main preliminary findings of ongoing research in the area, using field and remote sensing methods indicate localization of volcanic activity on Kos and on the Datca Peninsula of Asian Minor since Miocene due to the north-bounding faults of the Datca Graben. Localisation of volcanic vents and calderas in the Kos-Nisyros area follows intersection of a major tectonic line of north-northwesterly trending faults the 'Kos-Nisyros-Tilos Line' with N50°E, N30°E and N20°W trending faults. On the well-preserved volcano of Nisyros the architecture of the volcanic edifice has significantly been affected by 'trap-door' volcanotectonics of a major volcanic infrastructure in the area namely the Kos-Caldera.

Key words: *volcanotectonics, trapdoor, apical graben, Kos-Datca Graben.*

Περίληψη

Στην αμοιβαία σχέση ηφαιστειότητας και τεκτονικής έχει εστιαστεί η προσοχή των ερευνητών την τελευταία δεκαετία λόγω του αυξανομένου όγκου ηφαιστειοτεκτονικών εργασιών και εφαρμογής τεχνικών τηλεπισκόπησης και στα δύο αυτά πεδία της γεωλογικής έρευνας. Τα ηφαίστεια εξαρτώνται από τεκτονικά φαινόμενα όπως είναι τα ρήγματα για την θέση τους, την λειτουργία τους και από το πετροτεκτονικό περιβάλλον για την χημεία των μαγμάτων τους. Τα ρήγματα παρέχουν το 'υδραυλικό σύστημα' για την άνοδο του μάγματος και ως εκ τούτου η θέση και η χωρική κατανομή των ηφαιστείων εξαρτάται από την τεκτονική δομή μιας περιοχής. Από την άλλη πλευρά, τα ηφαίστεια τοπικά εντυπώνουν τα δικά τους ηφαιστειοτεκτονικά στοιχεία σε μία περιοχή όπως τα ακτινωτά και τα δακτυλοειδή

ρήγματα που προκύπτουν από κύκλους επανατροφοδοσίας με μάγμα (διαστολής) και εκκένωσης (συστολής) των μαγματικών θαλάμων.
Με αυτή την προοπτική επανεξετάστηκε το πιο ανατολικό άκρο του Τόξου του Αιγαίου, τα κύρια πρόδρομα αποτελέσματα της συνεχιζόμενης έρευνας που διεξάγουμε στην περιοχή χρησιμοποιώντας συνδυασμό μεθόδων πεδίου και τηλεπισκόπησης, δείχνουν ότι η ηφαιστειότητα στην Κω και στην απέναντι ακτή της Μικράς Ασίας από την εποχή του Μειοκαίνου επικεντρώνεται στα ρήγματα που ορίζουν το βόρειο όριο του Graben της Datca. Ο γεωμετρικός τόπος των ηφαιστειακών πόρων και καλδερών στην περιοχή της Κω-Νισύρου ορίζεται από μια μεγάλη τεκτονική γραμμή, την γραμμή 'Κω-Νίσυρος-Τήλος' με κατεύθυνση γύρω στα B320° και τις τομές αυτής της γραμμής με B50°A, B30°A and B20°Δ κατευθυνόμενα ρήγματα. Η αρχιτεκτονική του καλά διατηρημένου ηφαιστειακού οικοδομήματος της Νισύρου έχει σημαντικά επηρεαστεί από την ηφαιστειοτεκτονική 'trap-door' μιας μεγάλης ηφαιστειακής υποδομής της περιοχής, της καλδέρας της Κω.
Λέξεις κλειδιά: *ηφαιστειοτεκτονική, trapdoor, apical graben, Κως-Datca Graben.*

1. Introduction

The intimate relationship between tectonics and volcanism has been rather underplayed in scientific works investigating subjects of either discipline. However, where, how and when volcanoes erupt and to a considerable extend what type of volcanic edifice they construct is mainly controlled by their local and regional tectonic framework and the *tectonic-volcanic* forces active within it. The basic prerequisite for magma to rise to the surface is a conduit, provided by a discontinuity such as a fault; it is within this perspective that the field of *volcanotectonics* has developed at a very fast rate in the last decade.

In this paper, we will try to show, using the example of Nisyros volcano, how the *tectonic-volcanic* elements i.e. the fault systems of this stratovolcano relate to the volcanic-tectonic elements such as apical block protocalderas, trapdoor calderas and feeder systems of Nisyros and of the larger area (Kos-Nisyros volcanic complex) and the conjugate history of evolution of volcanism-tectonism in the overall area of *Gòkova-Kos Graben* since Miocene times.

2. The Volcanic Stratigraphy of Nisyros

Nisyros has a structure typical of stratovolcanoes: the non-exposed volcanic stratigraphy displayed in the cores of test drillholes for geothermal energy (P.P.C. unpublished data) consists of intercalations of andesitic lavas with andesitic pyroclastic deposits bound by feeder systems of sills and dykes of similar composition. The exposed stratigraphy begins with pillowed basaltic andesite and pillow breccia and evolves towards more felsic volcanism with rhyodacitic post-caldera domes at the end (St. Seymour 1996). The more recent caldera is a well-defined circular topographic feature with a diameter of 4km, a presently flat caldera floor intercepted by phreatic craters characterized by a drop in the order of ~300m. The highest point is the top of the St. Helias post caldera dome (698 m) (Fig. 1). The oldest age in the exposed stratigraphy is ~160.000 years (Di Paola 1974) and the most recent phreatic eruption took place in 1867 A.D. (Marteli 1917). The recent caldera-forming eruption created a tephra dated c.a. 46.000 yrs BP equivalent to the Y/ tephra horizon identified in sea sediments (Margari 2004).

Mapping of the volcanic stratigraphy comprising 10 units was initially done by Di Paola (1974) and more detailed work was done more recently by Vougioukalakis (1989) establishing 24 units. In this paper we separate these 24 units into four cycles using combined analysis of volcanic stratigraphy along with structural observations. The volcanic stratigraphy of Nisyros shown in Figs 1, 3 is simplified according to the tectonic elements which appear to govern the emplacement and exposure of volcanic products in three dimensions during the evolution of the volcano.

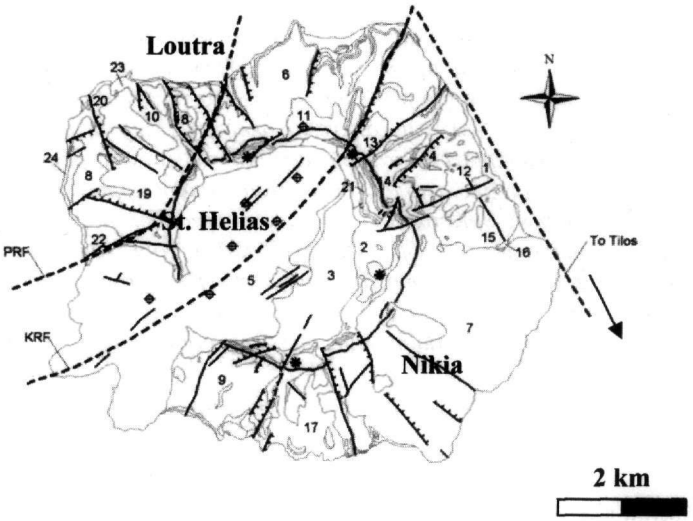

Figure 1 - Geological map of Nisyros island (Modified after Vougioukalakis 1989): Circles embounding cross indicate the highest points of rhyodacitic post-caldera domes (*see St. Helias*), Stars indicate remnants of feeder systems (volcanic necks) and tick-lines represent local grabens (*see Nikia-Loutra Graben*). Dashed lines KRF (*Kos Ring Fault*) and PRF (*Perigussa Ring Fault*) represent the 'sagging fault' and 'trapdoor fault' respectively and the main northwesterly trending fault zone to Tilos island. The volcanic stratigraphy is indicated by numbers (1-24) which are explained on the stratigraphy column on Fig. 3

3. Nisyros Volcano Fault Systems

3.1. Regional Tectonic Elements

Our fault array data (Fig. 2), recent geological structure of the volcano and remote sensing data of other workers have identified four major and two secondary fault systems on the Kos-Nisyros-Yali area (Papanikolaou *et al.* 1991, Vougioukalakis 1993, Papanikolaou and Nomikou 2001, Lagios *et al.* 2005).

- Major Fault Systems

I. The *f1 fault system* trends in a northeasterly direction (N50°E, Fig. 2) with an easterly subvertical dip (70°-80°) and a maximum throw at 100m. This is part of the horst-graben structure that passes from Kandeliousa-Yali-Datca Peninsula.

II. The *f2 fault system* trends at N30°E, i.e. it is rotated 20°-25° counter-clockwise relative to f1 it dips subvertically (70°-80°) westerly-northwesterly and displays a maximum throw of ~120 m. These faults have been traced also in the boreholes for geothermal energy on the caldera floor.

III. The *f3 fault system* trends at N40°W or N320° and dips subvertically. It is a major fault system which has localized many of the main volcanic vents in the area (St. Seymour *et al.* 2006a). Its trend runs from easterly Tilos, Nisyros through the volcano of Yali and into Kos island and parallel to it from the NW part of Tilos, crosscuts the island of Nisyros along the western part of Yali and runs into Kos island (Fig. 7). This is a long-lived fault system affecting on Nisyros pre-caldera, as well as, post-caldera lithologies. It has extensional characteristics with downfaulted displacements reaching 70m and subvertical dips (70°-80°) change along its strike. The *f3 fault system* can be related to the *f4 fault system* by a 20°-25° counter-clockwise rotation.

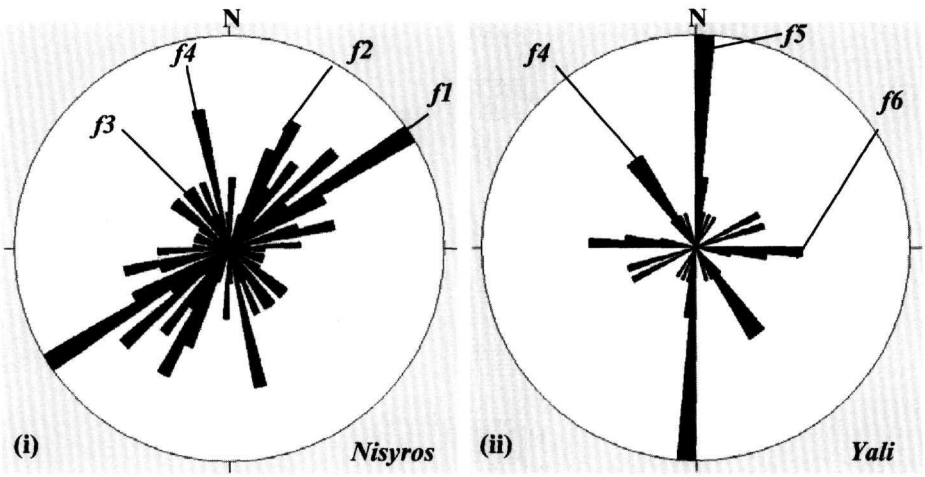

Figure 2 - Rose diagrams of Nisyros (i) and Yali (ii) islands: *Four major* tectonic systems (*f1*, *f2*, *f3* and *f4*) and a radial fault system are clearly displayed on Nisyros island. *Two secondary* fault systems are visible on Yali island which might represent the conjugate sets of *f1* and *f2* fault systems. (*i-5o classes/n=60, ii-5o classes/n=30*)

IV. The *f4 fault system* comprises major faults trending N20°E or N340° and dip 70°-80° towards the west and east forming that way *horst-graben* structures on the volcano of Nisyros. Strands of these faults begin from the Stefanos phreatic crater and extend to the southeast resulting in a graben depression characterised by throws in the order of 40-50 m drop (Fig. 1; Nikia region).

- Secondary Fault Systems

V. The *f5 fault system* and

VI. The *f6 fault system* might represent the conjugate sets of f1, f2 fault systems. Our data show a preponderance of f5, f6 on Yali. Lagios *et al.* (2005) based on bathymetry report a N-S oriented graben between Yali and Strongyli and in the Kefalos peninsula of Kos.

3.2. Volcanotectonic Elements

On the 'rose-diagram' of Fig. 2 the volcanotectonic element of Nisyros island are clearly displayed. These consist mainly of the caldera radial faults with directions spanning 0° to 360° of the Rose-diagram. The f1 (N50°E) and f3 (N40°W or N320°) faults on the northern part of Nisyros island are tangential and bounding to the Perigussa Ring Fault (PRF) 'trapdoor fault' discussed here (Fig. 1). Horizontal and vertical deformation along this fault and clear definition of it because of the applied colour contouring for vertical displacement in Figure 4 of Lagios *et al.* (2005). The other major volcanotectonic feature related to the ring fault of the Kos depression/sagging (St. Seymour *et al.* 2006a) is marked as Kos Ring Fault (KRF) on Fig. 1.

4. Fracturing during volcanic activity: Magma ascent and formation of proto-caldera - caldera system

Doming over an inflated subvolcanic magma chamber produces an apical flattening and subsequently a polygonal apical graben (Fig. 4) i.e. a *protocaldera* (Komuro 1987, Marti *et al.* 1994, Walter and Troll 2001). The intrusion of magma through fractures (conduits) produces inflation of the overlying surface and extension of the conduits along the fault planes as dykes propagating in a radial mode. This results in the creation of *radial faults*, subordinate *concentric (ring) reverse faults*, sub-perpendicular to the radial faults, followed by encircling or *horse-shoe*

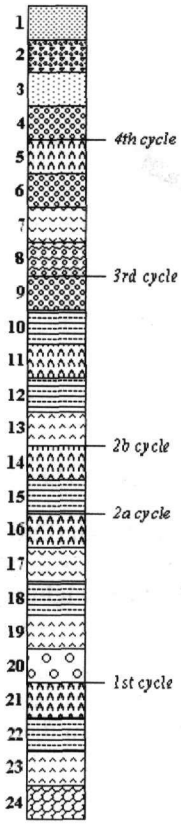

Figure 3 - The volcanic stratigraphy of Nisyros volcano and the *four major volcanic cycles* indicated by the presence of felsic volcanics at the top of each of the four volcanic cycles: 24-submarine andesitic lavas and pyroclastics, 23-lower andesite lava flows, 22-lower basic pyroclastics, 21-lower dacite lava flows (*1st cycle*), 20-Kastro conglomerate, 19-middle andesite lava flows, 18-middle basic pyroclastics, 17-middle rhyolite domes and lava flows of Avlaki, 16-dacite lava flows of Pachia Ammos (*2a cycle*), 15-Pyroclastic formation of Panayia Kyra, 14-dacite lava flows rich in inclusions (*2b cycle*), 13-upper andesite lava flows, 12-upper basic pyroclastics, 11-dacite domes and lava flows of Emporios, 10-block and ash flows of Emporios domes, 9-lower pumice unit (*3rd cycle*), 8-reworked lower pumice, 7-domes and lava flows of Nikia rhyolite, 6-upper pumice unit, 5-post-calderadacite domes and lava flows (*4th cycle*), 4-upper pumice of Yali, 3-hydrothermal explosion products and lacustrine intracalderic deposits, 2-scree and tectonic breccias, 1-beach deposits

shaped faults (Fig. 5). The horse-shoe shaped faults define the *apical graben* which usually has a mean diameter approximately half of that of the subvolcanic reservoir (Walter and Troll 2001). Due to the strongest extension occurring in the apical graben, slumping of large blocks and subsidence takes place which may produce pressure jumps in the underlying magma chamber triggering large scale *ash-flow* eruptions (Gudmundsson 1998). The intersection of radial faults with the edges of the apical block, which represents the imprint of the pressure of the upper part of the magma chamber, define the conduits for magma ascent, extrusion to the surface and initiation of erection of the volcanic edifice. Continuation of the volcanic activity will cause a moderate evacuation of the magma chamber and subsidence due to a combination of apical graben displacement and ring-fault subsidence. The caldera ring-fault is a bell shaped fault with a diameter ca. 1.5 times larger than the diameter of the apical block for shallow magma chambers (Fig. 5). Sagging produces wedges in the outermost periphery and an arrangement of sub-horizontal faults above the magma chamber followed by steep bell-shaped (main) ring-faults

(Walter and Troll 2001). During resurgence existing radial faults reopen, supplementary steepening occurs, peripheral faults close due to magma chamber volume increase and reactivation of ring faults results in additional fracturing. Faults may remain active during and following magma chamber evacuation until their expression reaches the surface, implying that collapse subsidence is (i.e. *caldera formation*) slightly delayed. In conclusion, magma chamber inflation results in radial fractures and dyke injection, an expansion of the flanks and an apical block (*proto-caldera*). Evacuation collapse is characterized by outward-dipping ring faults whilst widespread radial structures are not formed at this stage. Multistage caldera volcanoes are recognized by a network of intersecting radial and concentric structures (dykes and faults) in the central caldera basin and the caldera's periphery. Peripheral relaxation during evacuation forms circumferential en echelon faults in normal and reverse sense and *horst and graben* structures in-between (Walter and Troll 2001; Fig. 5).

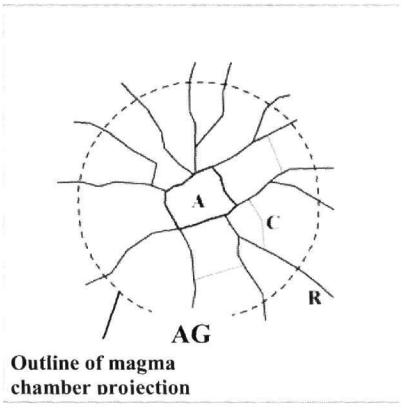

Figure 4 - Ground plan of doming over an inflated subvolcanic magma chamber producing a polygonal apical graben (AG), radial faults (R) and concentric (*ring*) reverse faults (C) adapted from *Walter and Troll, 2001*. Dashed line indicates the outline of magma chamber projection on surface

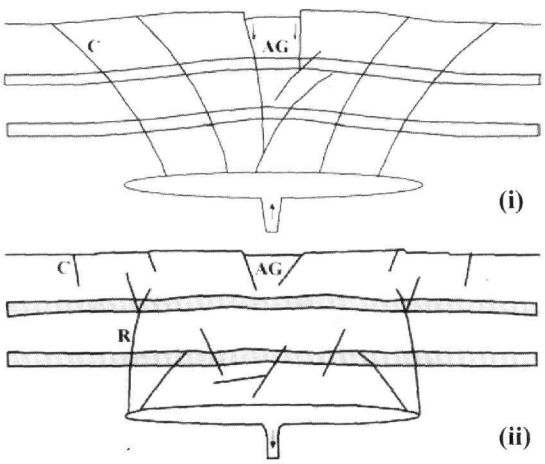

Figure 5 - Fracturing during inflation (i) and evacuation (ii) of the magma chamber adapted from *Walter and Troll, 2001*. *Inflation* (i) results in the creation of radial faults, concentric (*ring*) reverse faults (C) followed by horseshoe-shaped faults. The latter define the apical graben (AG). *Evacuation* (ii) of the magma chamber results in the creation of a bell-shaped fault (*caldera ring fault* - R) and circumferential en echelon faults in normal and reverse sense and horst-graben structures in between. Arrow indicates the feeder (i) or the evacuation system (ii)

5. Volcanotectonic Evolution of Nisyros Volcano

Test drilling for geothermal energy investigation in the 1980's indicated the presence of a subvolcanic magma chamber under the caldera of Nisyros, hosted in the limestone, at a depth of c.a. 2 km from the caldera floor (P.P.C. unpublished data).

5.1. Andesitic Stratocone Proto-Caldera

The Nisyros protocone consisted of *pillowed basaltic andesite* and *andesite* in the form of subaqueous pillow lavas and hyaloclastites succeeded by massive flows, dykes, sills and mafic pyroclastic rock of andesitic composition (St.Seymour and Vlassopoulos 1991).

Since the present caldera is the topographic expression on the ground of the partly evacuated subvolcanic magma chamber we will extrapolate the argument that the topography of the first subaerially emerged andesitic stratocone (proto-Nisyros) reflected mainly the volcanotectonic elements propagated by inflation-magma feeding-deflation and partial magma chamber collapse cycles. Inflation of magma chamber resulted in a *radial fault* network on the crust overlying the magma chamber and an *apical block* due to maximum extension at its center. Intrusion of magma through fault planes would create *radial* and reverse *concentric* (*ring*) faults, as well as, *horseshoe-shaped* faults (Fig. 5).

Feeders for the erupted materials of andesitic basaltic andesite composition would lie in the intersections of the major apparently regional northeasterly fault systems with volcanotectonic elements such as radial and concentric faults or apical block borders. Intersection of these conduits would assume initially the simplified '*star shape*' forms shown in Fig.6. Furthermore lubrication, inflation and partial erosion and widening of the leading faults (conduits) by the ascending magma can endeavour more the role of fault intersection. As mentioned above, this whole fault and apical block geometry would also be imprinted on the Nisyros protocone and the localization of its feeder systems. Remnants of one of these feeders (andesitic volcanic neck) has been unroofed in the north-northwestern part of the caldera floor near the caldera wall (Fig. 1) and probably represents the intersection of a radial fault with an apical block boundary. Partial evacuation of the magma chamber would have formed a *proto-caldera* due to a combination of apical graben displacement and ring fault subsidence. From the location of this neck and assuming that the size of Nisyros magma chamber remained more or less the same over the last ~160.000 years, we can calculate the size and location of the Nisyros proto-caldera suggesting also locations of other, similar to the aforementioned, feeder systems (volcanic necks) (Fig. 1). That is, a caldera diameter represents almost half the diameter of the magma chamber and if the main ring fault is 1.5 times larger than the diameter of the apical block then the proto-caldera of the Nisyros cone was 2-2.6 km in width and was located in the northwestern portion of the present caldera and near the inner caldera wall (Fig. 1). Tilting or slumping of the apical block could produce pressure jumps in the magma chamber, localized concentration of volatiles and ash-flow, (in the case of Nisyros 'scoria-flow' eruptions) (Gudmundsson 1998). This might be related to the emplacement of the lower and middle mafic pyroclastic formations (Figs 1, 3). Periodic closing and stagnation of the magma chamber is indicated by the presence of felsic volcanics at the top of each of the four volcanic cycles (from mafic to felsic) indicated in the volcanic stratigraphy of Nisyros (Fig. 3). Progressive stagnation of the system is reflected by the increase in the volume of felsic volcanic products in the upper two cycles. Opening of the chamber and ensuing magma mixing between resident andesitic and felsic magma end-members is indicated by the presence of dacite in the uppermost position of the volcanic cycles (St. Seymour and Vlassopoulos 1989) (Fig. 3).

5.2. The precursor caldera

On the Nisyros 1:25.000 geological map by I.G.M.E. (Vougioukalakis 1989) (Fig. 1) the feeder necks of units 19, 17, 11, 7 and also the feeder system of unit 6 (St. Seymour unpublished data) are closely proximal to the bounding ring fault of the recent caldera. Since these units are emplaced at

times which cover the total time spectrum in which the subaerial edifice was built, we propose here that this bounding ring fault was long-lived. Since for shallow chambers, as that of Nisyros, the position of the chamber beneath the surface influences the distribution of all concentric structures, bounding ring fault included (Roche *et al.* 2000), we propose that the Nisyros subvolcanic chamber occupied a rather permanent position and therefore the precursor caldera or calderas of Nisyros were occupying the same position. The geometries of these calderas might have been different to accommodate than the recent caldera geometry, taking into account the effects of edifice morphology indicated by the experiments of Walter and Troll (2001).

6. A 'Bird's Eye View' of Nisyros: The effect of Kos Trap-door Caldera Tectonics

St Seymour *et al.* (2006a) and Zouzias and St. Seymour (2006) have given an interpretation of volcanic depressions (calderas) in the Kos-Nisyros area, the localization of which results from the intersection of a major tectonic line intercepting the east coast of Tilos, Nisyros, Yali and passing through Kos with other major crustal discontinuities such as the western extension of the Gòkova Graben (Fig. 7). In figure 7 the larger structure, an approximately 20 km partly submerged caldera, represents the caldera of the 160.000 yrs major eruption of the Kos Plateau Tuff (KPT) and this closely coincides with the interpretation given by Allen (2001) based on physical volcanology arguments. The southeastern portion of the bounding ring faults of the KPT caldera (KRF; Fig. 1) and Perigussa depression (PRF; Fig. 1) cut the western and central part of the Nisyros edifice (Fig. 1). We will discuss here the effects of these volcanotectonic features on the evolution of Nisyros volcanic edifice. Both of these faults seem to follow the general tectonic NE-SW direction, however, since they represent arcs of large extensive bounding ring faults the are gently curved towards the northwest (Fig. 7).

6.1. The effect of Perigussa Ring Fault (PRF) on the Nisyros Edifice

- The intersection of this fault with the bounding fault of the apical block of proto-Nisyros and/or with a radial fault could have provided the passageways necessary (Fig. 6) for the ascent of the andesitic magma which erected the subaerial portion of the Nisyros stratocone.
- '*Trap-door*' rotating motion on the PRF could alternatively submerge or emerge the northwestern portion of the island. Such a rotating motion has presently emerged basaltic andesite pillow lavas and pillow breccias under the old castle wall near Mandraki. Submerging motion in the past would account for the lack of units at the high and medium positions of the volcanic stratigraphy, resulting in exhumation and exposure of unit 19 which has constructed the main body of the subaerial Nisyros protocone.

In multistage caldera volcanoes peripheral relaxation forms circumferential *en-echelon* faults in normal and reverse sense and *horst and graben* structures (Walter and Troll 2001), a few of which are indicated in Fig. 5. Rotation and submergence of the northwestern part of the island and inundation of the local grabens (Fig. 1) would account for the fault-bound exposures and reworking by water of the pumices of unit 8 and the fault-bound conglomerate of unit 20.

6.2. The Effect of the KPT Ring Fault on the Nisyros Edifice

This is a long-lived structure which appears to intersect the subvolcanic magma chamber of Nisyros since it has provided the more efficient feeder passageway for the emplacement of the six post-caldera dacite-domes of Nisyros (unit 5), than the recent caldera bounding ring fault (Fig. 1). A casual examination may identify this portion of the KPT ring fault as a simple regional tectonic northeasterly structure; however, upon closer examination of the spatial distribution of the apices of the six domes of unit 5 and the apex positioning of the dome of unit 11 may reveal its westerly curvature.

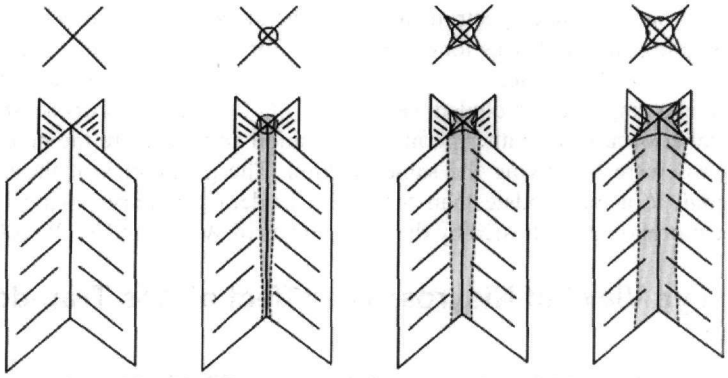

Figure 6 - Intersection of leading faults providing conduits which would assume initially the simplified '*star shape*' form due to inflation and partial erosion and widening of these leading faults. The intersection of these faults with the bounding faults of the apical block of the proto-caldera and/or with radial faults could provide passageway for magma to ascent

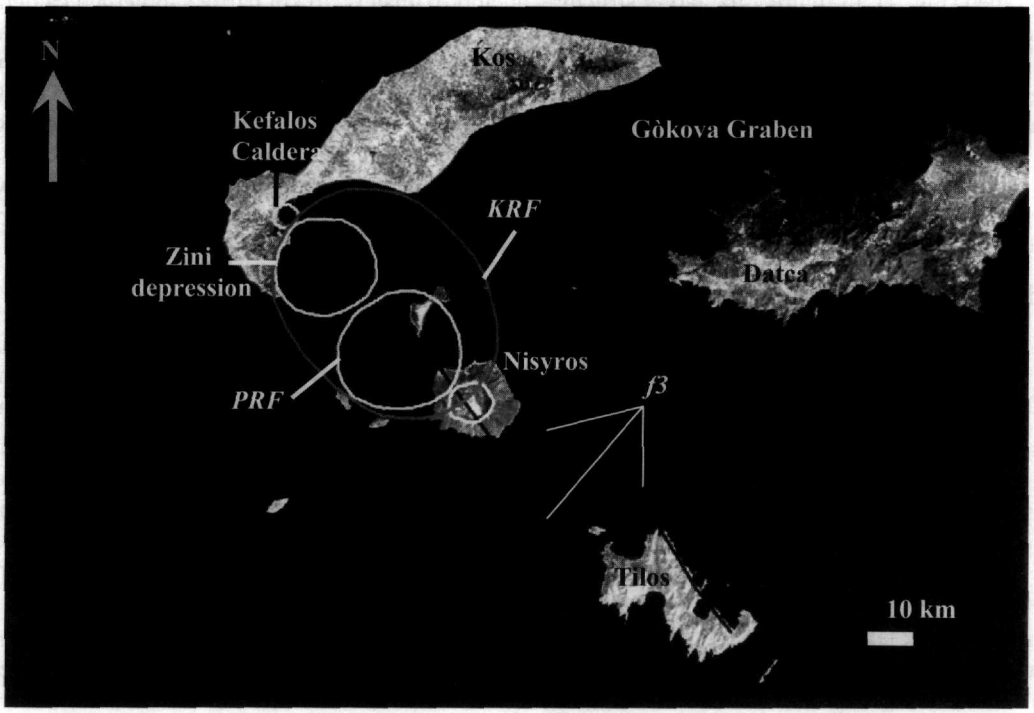

Figure 7 - Landsat-TM image of Kos-Yali-Nisyros-Tilos-Datca area. The *f3 fault system* localizes the main volcanic centers of the area characterized of major discontinuities such as the Gòkova Graben. The KRF and the PRF faults seem to follow the general tectonic NE-SW direction, representing arcs of large extensive bounding ring faults. An interpretation of volcanic depressions (calderas) in the Kos-Nisyros caldera complex is shown, such as Nisyros caldera, Kefalos caldera, Zini and Perigussa depressions, hosted in the sagging caldera of Kos (St. Seymour *et al.* 2006)

The formation of Panayia Kyra entails many surge deposits which indicate infusion of moisture in the magmatic conduit system. It can be speculated for Panayia Kyra surges may have been located in the Nikia-Loutra Graben (Fig. 1) which has presently confined the positions of all the phreatic craters in the recent caldera floor. We trust, that the doctoral research presently underway

investigating this formation (Vougioukalakis personal communication 2006), will provide definite answers to the above considerations.

7. Evolution of volcanism in the Gòkova-Kos Graben

Submarine active tectonism in the southeastern Aegean Sea-southwestern Anatolia (Gulf of Gòkova, reported here as Gòkova-Kos Graben) was investigated by Kurt *et al.* (1999) with multichannel seismic reflection methods. These workers concluded that the opening of the graben was initiated in late Miocene. Boger (1978) reports that normal faults commencing in Late Miocene on Kos island may heralt the opening of the Gòkova-Kos Graben. The southern part, towards the mouth of the graben is bound by a major east-west trending listric fault, the Datca Fault, whereas an antithetic, major, normal fault defines the northern boundary of the graben. However, due to its low dip angle the Datca Fault was decelerated since Early Pleistocene and continuing extension was uptaken by the faults in the northern boundary of the Gòkova Gulf which shows high seismic activity even in the Present. A moderate earthquake in 1968 (magnitude 5.5) in the gulf south of Kos island is attributed to this fault array (Kurt *et al.* 1999). We propose here that the intersection of the continuation of these faults in the Kos-Nisyros area with major northwesterly faults such as the 'Tilos-Nisyros-Kos' Fault have provided access for magma ascent and volcanism in the area.

8. Acknowledgments

We would like to thank Dr. Ioannis Koukouvelas for the review of an early version of this work and Dr. George Vougioukalakis for the scientific discussions on the volcanology of Nisyros.

9. References

Allen, S.R., 2001. Reconstruction of a major caldera-forming eruption from pyroclastic deposit characteristics: Kos Plateau Tuff, eastern Aegean Sea, *J. Volcanol. Geotherm. Res.*, 105, 141-162.

Boger, H., 1978. Sedimentary history and tectonic movements during the late Neogene. In H. Closs, D. Roeder and K. Schmidt (eds), Alps, Appenines, Hellenides, Schweizerbart, Stuttgart, 225-255pp.

Di Paola, G.M., 1974. Volcanology and petrology of Nisyros island (Dodecanese, Greece), *Bulletin of Volcanology*, 38, 944-987.

Gudmundsson, A., 1998. Formation and development of normalfault calderas and the initiation of large explosive eruptions, *Bull Volcanol*, 60,160–170.

Komuro, H., 1987. Experiments on cauldron formation: a polygonal cauldron and ring fractures, *J Volcanol Geotherm Res*, 31,139–149.

Kurt, H., Demirbag, E., and Kuscu, I., 1999. Investigation of the submarine active tectonism in the gulf of Gokova, southwest Anatolia-southeast Aegean Sea, by multi-channel seismic reflection data, *Tectonophysics*, 305, 477-496.

Lagios, E., Sakkas, V., Parcharidis, Is., and Dietrich, V., 2005. Ground deformation of Nisyros volcano (Greece) for the period 1995-2002: Results from DInSAR and DGPS observations, *Bull Volcanol*, 68, 201-214.

Margari, V., 2004. Late Pleistocene vegetational and environmental changes on Lesvos Island, Greece, *Ph.D. 663 Thesis*, University of Cambridge, Cambridge, UK.

Martelli, A., 1917. Il gruppo eruttivo di Nisyros nel mare Egeo, *Mem. Soc. Geol. Ital. Sc. (detta dei XL)*, Serie 3a, vol. XX.

Marti, J., Ablay, GJ., Redshaw, LT., and Sparks, RSJ., 1994. Experimental studies of collapse calderas, *J Geol Soc London,* 151, 919–929.

Papanikolaou, D., Lekkas, E., and Sakellariou, D., 1991. Geological structure and evolution of Nisyros volcano. Bulletin of the Geological Society of Greece, XXV/1, 405-419.

Papanikolaou, D., and Nomikou, P., 2001. Tectonic structure and volcanic centers at the eastern edge of the Aegean volcanic arc around Nisyros island, *Bull Geol Soc Greece*, XXXIV, 12891296pp, *Proc. 9th Intern. Congress, Athens, Sept. 2001.*

P.P.C., unpublished data, 1982. Geology and petrography report on the Geothermal Well NISYROS 1 and Petrography Report on the Geothermal Well NISYROS 2 by Vichos G. and Chlaboutakis M.

Roche, O., Druitt, T., and Merle, O., 2000. Experimental study of caldera formation, *J Geophys Res,* 105, 395–416.

St. Seymour, K., and Vlassopoulos, D., 1989. The potential for future explosive volcanism associated with dome growth at Nisyros, Aegean volcanic arc, Greece, *J. Volcanol. Geother. Res.,* 37, 351-364.

St. Seymour, K., and Vlassopoulos, D., 1991. Magma Mixing at Nisyros volcano, as inferred from incompatible trace-element systematics, *Journal of volcanology and Geothermal Research,* 50, 273-299.

St. Seymour, K., 1996. Geochemistry of the Yali volcano rhyolites and their relationship to the volcanic products of Nisyros, Aegean volcanic arc, *N. Jb. Miner. Mh.,* H.2, 57-72.

St. Seymour, K., Kouli, M., Zouzias, D., Papaioannou, G., and Vamvoukakis, C., 2006a. Identifying Calderas in Aegean Sea, Hellas, Using Remote Sensing Techniques, *European Congress on Regional Geoscientific Cartography and Information Systems Earth and Water*, 13th June 2006, Barcelona, Spain.

St. Seymour, K., unpublished data. Localization of the feeder intersection point of the Upper Unit Pumices on Nisyros Volcano.

Vougioukalakis, G., 1993. Volcanic stratigraphy and evolution of Nisyros island, *Bull. Gel. Soc. Greece*, 28 (2), 239-258.

Vougioukalakis, G., 1989. Geologic map of Nisyros island. 1:25,000, IGME.

Walter, TR., and Troll, VR., 2001. Formation of caldera periphery faults: an experimental study, *Bull Volcanol,* 63, 191–203

Zouzias, D., and St. Seymour, K., 2006. Geochemical Evidence for the Coeval Relationship of the Kos Plateau Tuff (KPT) and Tilos Pumices, Aegean Volcanic Arc, Greece, Submitted in *Neues Jahrbuch für Mineralogie.*

ΕΥΡΕΤΗΡΙΟ ΣΥΓΓΡΑΦΕΩΝ / AUTHORS INDEX

Agalos, A.	1032
Agelopoulou, O.	1710
Aggelopoulos, A.	1749
Agiadi-Katsiaouni, K.	85
Albrich, S.	14
Alexandropoulou, N.	297
Alexiou, J.	560
Alexopoulos, A.	616
Alexopoulos, J.D.	1207, 1892
Alexouli–Livaditi, A.	1513
Alikaj, P.	1925
Al-Zoubi, Ab.S.	251
Antonakos, A.	523, 616
Antonarakou, A.	39, 209, 225
Antoniadis, P.	906
Antoniou, M.	1566
Antoniou, Vas.	264
Antonov, D.	1397
Argyraki, A.	1331
Arikas, K.	1343
Arvanitis, A.	1162
Asvesta, A.	1421
Athanasiou, E.	1045
Athanassiou, A.	201
Atzemoglou, A.	343
Aurisicchio, C.	641
Baltatzis, E.	676
Barbu, O.	21, 666
Bartolomei, A.	641
Baskoutas, I.	386, 439, 1055
Bathrellos, G.D.	1354, 1365, 1759, 1904
Baziotis, I.	399, 653
Bedelean, H.	21, 666
Bedini, E.	1916
Bellas, S.	1
Benetatos, C.	1125
Benissi, M.	1986
Beqiraj, A.	1925
Berástegui, X.	14
Bernaus, J.M.	14
Boev, B.	1377
Bogomolov, Yu.I.	1485
Boix, C.	14
Bortolotti, V.	182
Bosy, J.	287
Boudi, D.	676

Brusca, L. 712
Buckman, J. 1421
Cacon, S. 287
Callen, M. 1499
Çanga, B. 1925
Carras, N. 182
Caus, E. 14
Chailas, S. 1063, 1207
Charalambous, S. 1934
Chatziangelou, M. 1634
Chatziapostolou, A. 191
Chatzitheodoridis, E. 676, 736
Chianese, D. 1080
Cholakova, Z. 1397
Chousianitis, K. 2070
Christanis, K. 191
Christaras, B. 1634
Christidis, G.E. 690, 759
Christofides, G. 700, 984, 1491
Chrysanthaki, I. 1759
Clarke, P. 2032
Clegg, P. 1959
Codrea, V. 21, 666
Conte, G. 1080
D'Alessandro, W. 712
Daci, A. 1387
Damiata, B. 2070
Danamos, G. 374
Danelian, T. 31
Daskalaki, E. 1074
Dassenakis, M. 1892
De Martini, P.M. 412, 1586
Deda, T. 1387
Dermitzakis, M.D. 209, 225
Di Fiore, B. 1080
Diamantis, I. 536
Diamantis, K. 264
Diamantopoulos, A. 399
Dibenedetto, A. 1080
Dierckx, H.M.C. 1768
Dilalos, S. 1892
Dimitrova, D. 1397
Dimiza, M. 209
Dimopoulos, G.C. 1652
Douveas, N. 1644
Drakatos, G. 287, 297, 1257
Drakoulis, A. 723, 769, 775
Drinia, H. 39, 225
Drosopoulou, E. 1304
Efthimiou, G. 1833
Elefanti, P. 1874
England, P. 2032
Fakiris, E. 1947

Falalakis, G. 321
Fassoulas, C. 1780
Fazzuoli, M. 182
Feinberg, H. 343
Ferentinos, G. 64
Ferentinou, M. 1710
Fermeli, G. 1819
Fernández-Turiel, J.L. 1491
Filippidis, A. 723, 769, 775, 1491
Floyd, M. 2032
Foumelis, M. 2020
Fountoulis, I. 275, 1207, 1621, 1973
Foutrakis, P. 1522
Fritsch, E. 794, 805
Frydas, D. 1
Gadjanov, P. 1499
Gaki-Papanastasiou, K. 1552
Gaki-Papanastassiou, K. 1538
Galanakis, D. 439
Galoyan, G. 31
Gamaletsos, P. 736
Ganas, A. 287, 297, 500, 1257
Garcia-Guinea, J. 1769
Gemitzi, A. 321
Georgakopoulos, A. 1491
Georgiadis, G.A. 309, 1652
Georgiadis, I.K. 747, 1022
Georgiou, Ch. 439
Georgiou, P. 451
Gerolymatos, E. 1749
Getsos, K. 53
Ghionis, G. 1530, 1892
Giannoulopoulos, P. 1409
Giaourtsakis, I. 201
Gimeno, D. 1491
Giouri, A.N. 1022
Gkarlaouni, C. 321
Godelitsas, A. 736, 1331
Gonsalvesh, L. 1499
González-Fernández, Án. 829
Goulty, N. 1207
Goumas, G. 1207, 1892
Grammatikopoulos, T. 781
Greco, E. 1080
Hämäläinen, J. 859
Hatzipanagiotou, K. 781, 816, 947
Hoti, S. 1387
Iatrou, M. 64
Iliopoulos, G. 1780
Iordanidis, A. 1421, 1769
Jäntti, T. 859
Jones, R.R. 1959
Julia, R. 412

Kaberi, H. 451
Kadetova, A.V. 1433, 1440
Kairis, O. 500
Kakali, G. 972
Kaklis, T. 560
Kalafati, K. 759
Kalaitzidis, S. 191
Kalfountzos, D. 560
Kallergis, G. 523, 616
Kallioras, A. 536
Kambouris, P. 1207
Kanellopoulos, Th. 451
Kantiranis, N. 723, 769, 775
Kaouras, G. 906
Kapsimalis, V. 451
Kapsiotis, A. 781
Karadassi, S. 1741
Karageorgiou, D.E. 161
Karakatsanis, S. 76
Karakitsios, V. 39, 85
Karakostas, V.G. 386, 1055, 1091, 1187, 2008
Karamanos, C.K. 1091
Karamitrou-Mentesidi, G. 1769
Karamousalis, Th. 264, 1530
Karampelas, S. 794, 805
Karanassiou, S. 1710
Karastathis, V. 1207
Karetsos, G. 1833
Karfakis, J. 1703
Karipi, S. 781, 816
Karlis, D. 1199
Karymbalis, E. 1538
Kassaras, I. 1103, 1150, 1207
Kassoli-Fournaraki, A. 747, 1491
Kati, M. 101
Katsikopoulos, D. 829
Kavadia, D. 1644
Kaviris, G. 1103, 1114
Kaza, G. 1387
Kerestedjian, T. 1397
Keupp, H. 1
Khak, V.A. 1449, 1469
Khoshravan, H. 333
Kilias, A. 321, 2008
King, M. 2032
Kiomourtzi, P. 839
Kiratzi, A. 287, 1125, 1279
Kitsopoulos, K. 851
Kokinou, E. 1138
Kokkalas, S. 1959
Kolaitis, A. 1150
Kolios, N. 1162
Kollios, A. 1505

Kondopoulou, D. 343
Konstantopoulos, P. 113, 154, 173
Konstantopoulou, G. 1664, 1741
Kontakiotis, G. 39, 209
Kontny, B. 287
Kontogianni, V. 1733
Kontopoulos, N. 1578
Kontou, A. 1552
Korkaris, K. 1986
Koroneos, A. 700, 984
Kosiari, S. 1674
Koskeridou, E. 121
Kostakis, K. 972
Kostopoulos, D. 676, 736, 2060
Kostopoulos, D.S. 134
Kotis, Th. 161
Kotsev, T. 1397
Kotsopoulos, S. 560
Koufos, G.D. 134
Kougoulis, Ch. 1162
Kougoulis, J.-S. 1162
Koukis, G. 1683, 1695, 1722
Koukouzas, N. 76, 859, 872
Kouli, K. 209
Kouskouna, V. 1318
Koutles, T. 775
Koutsinos, S. 1162
Koutsouveli, A. 1819
Kozyreva, E.A. 1433, 1449
Kral, J. 700
Kranis, H. 360
Krassilov, V. 142
Krohe, A. 399
Kyriakopoulos, K. 641, 712
Labaki, O. 1880
Ladas, I. 1973
Lagios, E. 1063, 1207, 1219, 2070
Lainas, S. 1683
Lamaj, M. 1925
Lambrakis, N. 523, 570
Lavallée, D. 2032
Leka, G. 1925
Lekkas, E. 374, 463, 2020
Lemeille, F. 412
Liati, A. 700
Livaditis, G. 1365, 1513, 1522
Loperte, A. 1080
Louis, F. 1103
Loupasakis, C. 1703, 1808
Lozios, S. 1267
Lykoudi, E. 629, 1566
Lykousis, V. 209, 451
Magganas, A. 641, 884, 1103

Makedon, T.K. 1652
Makropoulos, K. 1103, 1114, 1150, 1177, 1032
Mancini, M. 412
Maravelis, A. 113, 154, 173
Marcopoulou-Diakantoni, A. 225
Margaritopoulos, M. 712
Marinos, P.G. 1986
Marinos, V. 1986
Marinov, S.P. 1499
Mariolacos, K. 899
Mariolakos, D. 1457
Mariolakos, I. 1973
Marnelis, F. 959
Maroukian, H. 1522, 1530, 1538, 1552
Martsoukou, M. 1609
Mastral, A. 1499
Matziaris, V. 1710
Mavroulis, S. 275
Mazaeva, O.A. 1469
McCaffrey, K.J.W. 1959
Meléndez, G. 1819
Melis, N.S. 287
Mertzanis, A. 1833
Messini, A.D. 386
Metaxas, A. 161
Michard, A. 343
Michas, G. 712
Michopoulos, K. 1859
Migiros, G. 264
Mimides, T. 1476
Mitta, V.V. 1485
Mladenova, V. 1397
Mortyn, G. 209
Moshou, A. 1177
Mountrakis, D.M. 309, 488
Mouzaliotis, A. 536
Mposkos, E. 399, 653
Muceku, Y. 1925
Nikas, K. 523
Nikolaidou, D. 113
Nikolakopoulos, G.K. 1998, 2048
Nikolaou, K. 959
Nikolaou, N. 1808
Nikolintaga, I. 1187
Novack, M. 1986
Oikonomopoulos, I. 906
Oikonomou, At. 297
Orfanogiannaki, K. 1199
Pagonas, M. 76, 1578
Pakos, T. 959
Palikari, S. 653
Palyvos, N. 412, 1586
Panagiotakis, C. 1138

Panagiotopoulos, P. 1947
Panagoulia, D. 629
Panayides, I. 201
Panopoulou, G. 1187
Panteliadou, M. 1986
Pantopoulos, G. 113, 154, 173
Pantosti, D. 412, 1586
Papadakis, G. 712
Papadimiriou, P. 1114, 1150, 1177, 1322
Papadimitriou, E.E. 321, 386, 1055, 1091, 1187, 2008
Papadimitriou, P. 1032, 1114, 1177
Papadopoulos, A.A. 1022
Papadopoulos, G.A. 1055, 1074, 1199
Papadopoulos, T.D. 1207, 1892
Papadopoulou, K. 1599
Papadopoulou, L. 984
Papadopoulou, P. 1644
Papageorgiou, E. 1219
Papanakli, S. 1695
Papanikolaou, D. 425, 859
Papanikolaou, G. 161
Papanikolaou, I. 425
Papanikolaou, M. 287
Papastergios, G. 1491
Papathanassiou, G. 1226
Papatheodorou, G. 64, 1947
Papavassiliou, C.T. 918
Papazachos, C. 2060
Papouli, D. 1986
Papoulis, D. 936
Paradisopoulou, P.M. 2008
Paragamian, K. 1780
Paraskevopoulos, K.M. 805, 984
Parcharidis, I. 2020
Parpodis, K. 570
Parsons, B. 2032
Pasadakis, N. 839
Pavlides, S. 1226, 1279
Pechlivanidou, S. 1513
Pehlivanoglou, K.G. 1609
Peirce, C. 1207
Perraki, M. 653
Perraki, T. 906
Petro, L. 287
Petrou, P. 1257
Photiades, A. 182
Piper, D.J.W. 64
Pirentis, A. 287
Pirli, M. 1207, 1234, 1246
Pirlis, E. 1234, 1892
Plakaki, A. 1331
Pliakas, F. 536
Plougarlis, A.P. 488

Ploumidis, M. 161
Pomoni-Papaioannou, F. 53
Pomonis, P. 947
Pope, R. 475
Poulos, S. 1522, 1530, 1892
Poulovassilis, A. 1409
Pozzi, J.-P. 343
Prieto, M. 829
Principi, G. 182
Prophitis, E. 676
Psomiadis, E. 1476
Pyrgiotis, L. 1722
Renaut, R.W. 972
Rigakis, N. 959
Rigopoulos, I. 947
Rolland, Y. 31
Rondoyanni, Th. 439
Rontogianni, S. 2032
Roumelioti, Z. 1125, 1257
Rousakis, G. 451
Roussiakis, S.I. 201
Rybchenko, A.A. 1433, 1440
Sabatakakis, N. 1683, 1695, 1722
Sachpazi, M. 1091
Sakellariou, D. 451, 1845
Sakellariou, M. 1710, 1934
Sakkas, V. 1219, 2070
Sambaziotis, E. 1621
Schweitzer, J. 1246
Segou, M. 39, 1267
Serpetsidaki, A. 1257
Shuklina, A. 142
Siavalas, G. 191
Sideris, G. 548
Skianis, G.A. 1998, 2048
Skilodimou, H.D. 1365, 1759, 1904
Sklavounos, S. 794, 805
Skourtsos, E. 101, 374, 463, 475
Smyrni, V. 1833
Sofikitis, E. 191
Sokos, E. 1257
Soldatos, T. 794
Sorel, D. 412
Sosson, M. 31
Sotiriadis, M. 560
Sotiropoulos, P. 548
Soulakellis, N. 500
Soulios, G. 560
Spachos, T. 580
Spina, V. 297
St. Seymour, K. 512, 996
Stamatakis, G. 972
Stamatakis, M.G. 723, 769, 972

Stamatis, G. 570
Stamatopoulos, L. 1586
Stamoulis, K. 605
Stampolidis, A. 580, 1279
Stefanova, M. 1499
Stercz, M. 287
Stiros, S. 1733
Stoumpos, G. 1986
Theocharis, D. 275
Theodorou, G.E. 201
Theodosoglou, E. 984
Thewald, U. 238
Tomara, V. 1892
Tombros, S. 996
Tourunen, A. 859
Tranos, M.D. 309, 488, 1652
Triantafyllou, A.G. 1421
Triantaphyllou, M.V. 209, 412, 475
Trikili, I. 1476
Tripsanas, E. 64
Trontsios, G. 747
Trzhcinsky, Yu.B. 1449
Trzhtsinsky, Yu.B. 1440
Tsaparas, N. 39, 225
Tsatsanifos, C. 1733
Tsikouras, B. 781, 816, 947, 1768
Tsimi, Ch. 500
Tsipoura-Vlachou, M. 1009, 1859
Tsirambides, A. 747, 1022
Tsivilis, S. 972
Tsokas, G. 1045, 1279
Tsourlos, P. 580, 605, 1045, 2060
Typou, I. 872
Tzamos, E. 723, 769, 775
Tzanis, A. 548, 1063, 1292, 1304
Vacondios, I. 1664, 1741
Vaiopoulos, D.A. 1998, 2048
Valiakos, I. 1880
Valkaniotis, S. 1226
Vallianatos, F. 1138, 1187
Valmis, S. 500
Vargemezis, G. 580, 593, 605, 1045, 1749, 2060
Varvarousis, G. 161
Vassilakis, E. 1892
Vassilopoulou, S. 1219, 2070
Velitchkova, N. 1397
Velitzelos, D. 238
Velitzelos, E. 238, 1880
Verikiou-Papaspiridakou, E. 1365
Villalonga, R. 14
Vitti, P. 1080
Voidomatis, Ph. 343
Voudouris, C. 580

Voudouris, K. 560, 616
Voudouris, P. 238
Voulgaris, N. 1207, 1234, 1032, 1892
Vouta, S. 775
Vouvalidis, K. 1513
Voza, O. 1080
Vriniotis, D. 1599
Zachariadis, P. 676
Zagana, E. 570
Zakinthinos, G. 1833
Zamba, I. 1318
Zambetakis-Lekkas, A. 101, 1874
Zananiri, I. 343
Zarris, D. 629
Zelilidis, A. 53, 76, 113, 154, 173, 839
Ziafetis, A.A. 1022
Ziock, H. 872
Ziogou, F. 872
Ziveri, P. 209
Zorba, T. 805, 984
Zotiadis, V. 1505
Zouros, N. 1880
Zouzias, D. 512
Tsaparas, N. 39, 225

ΧΟΡΗΓΟΙ

Η Οργανωτική Επιτροπή του 11ου Διεθνούς Συνεδρίου της Ελληνικής Γεωλογικής Εταιρίας ευχαριστεί θερμά τους παρακάτω χορηγούς που στήριξαν οικονομικά το Συνέδριο και συνέβαλαν σημαντικά στην οργάνωση και πραγματοποίησή του.

ΒΟΥΛΗ ΤΩΝ ΕΛΛΗΝΩΝ

ΥΠΟΥΡΓΕΙΟ ΕΘΝΙΚΗΣ ΠΑΙΔΕΙΑΣ & ΘΡΗΣΚΕΥΜΑΤΩΝ

ΥΠΟΥΡΓΕΙΟ ΠΟΛΙΤΙΣΜΟΥ

ΕΘΝΙΚΟ & ΚΑΠΟΔΙΣΤΡΙΑΚΟ ΠΑΝΕΠΙΣΤΗΜΙΟ ΑΘΗΝΩΝ

ΑΤΤΙΚΟ ΜΕΤΡΟ Α.Ε.

ΛΑΤΟΜΕΙΑ ΚΥΡΙΑΚΟΥ

ΤΙΤΑΝ Α.Ε.

ΕΡΓΟΣΕ

ΕΛΛΗΝΙΚΟΣ ΟΡΓΑΝΙΣΜΟΣ ΤΟΥΡΙΣΜΟΥ ΕΟΤ

ΕΤΑΙΡΕΙΑ ΓΕΩΛΟΓΙΚΩΝ ΜΕΛΕΤΩΝ «ΓΕΩΣΚΟΠΙΟ ΑΤΕ»